A P P E N D I X F

OF

F I N A L R E P O R T

ON

CONTRACT NO. CPR-11-5851

Entitled

TEST AND EVALUATION

OF

VEHICLE ARRESTING, ENERGY ABSORBING, AND IMPACT ATTENUATION SYSTEMS

For

U. S. Department of Transportation

Federal Highway Administration

By

Texas Transportation Institute

Texas A&M Research Foundation

College Station, Texas

November 30, 1971

TABLE OF CONTENTS

FOR

APPENDIX F

FOREWORD

Appendix F is a compilation of the twenty three (23) technical memoranda prepared on Research and Development Contract No. CPR-11-5851 entitled "Test and Evaluation of Vehicle Arresting, Energy Absorbing, and Impact Attenuation Systems". These technical memoranda were prepared and submitted to the Federal Highway Administration during the course of this four and one-half year project. In general, a technical memorandum was prepared to report the results of a series of crash tests conducted on a given highway safety barrier. In general, the significant results presented in these twenty three technical memoranda are summarized in the main body of the final report.

The accuracy and reliability of the electronic accelerometer and strain gage data presented in Technical Memoranda 505-1S, 505-2, 505-2S, 505-4, 505-6, 505-8, 505-9, 505-10, and 505-11 are questionable since these data were gathered using a "hard-line" carrier system for sensor excitation. The excitation source and the resultant crash test data were fed through a cable of considerable length (approximately 1000 ft.). The cable was frequently tangled, bent and cut causing, in some cases, significant changes in resistance and capacitance which produce zero and phase shifts in the electronic data.

All other electronic data were gathered by use of an extremely reliable telemetry system described in Appendix D.

TECHNICAL MEMORANDUM 505-1

Texas Transportation Institute
Texas A&M Research Foundation

BARREL PROTECTIVE BARRIER

A Tentative Progress Memorandum on Contract No. CPR-11-5851, U. S. Dept. of Transportation, Federal Highway Administration, Bureau of Public Roads

by

T. J. Hirsch, Research Engineer and Principal Investigator
Structural Research Department
Texas Transportation Institute

July 31, 1968

On March 28, 1968, a very successful vehicle crash attenuation test using 55-gallon drums as a barrier was conducted. This technical memorandum is being written to provide some of the technical information and design details of this vehicle crash attenuation system. Also included is a summary of the high-speed film data taken of this test giving the vehicle impact velocity, average deceleration, peak deceleration, stopping distance, etc. This system, using 55-gallon tight-head universal drums, appears to be a most effective, economical, and practical vehicle crash attenuation device.

Figures 1 through 6 show the crash vehicle and barrel protective barrier before and after the 60 mph vehicle impact. Table 1 presents a summary of the high-speed film crash test data. The vehicle weighed

3,200 lbs. and was a 1964 Dodge four-door sedan. Its initial velocity before impact was 60.2 mph. The vehicle penetrated the barrier 13.3 ft. before coming to a complete stop. The average deceleration force on the vehicle was 9.1 g's. The peak deceleration on the vehicle was 12.7 g's. As can be seen from the photographs, only minor damage was inflicted on the vehicle. One of the four headlights was broken, and the front bumper and grillwork were mashed in approximately 4 in. The vehicle was in running condition immediately after the impact.

Table 3 presents a comparison of this barrel barrier crash test with a "rigid" barrier crash test. If this vehicle had struck a "rigid" barrier, the maximum deceleration would have been approximately 54.2 g's and the average deceleration would have been approximately 34.6 g's. Using these rigid barrier decelerations, the deceleration obtained from the barrel barrier can be compared by taking a ratio which is defined as an Attenuation Index. The Attenuation Index for this barrel barrier test indicates that the impact was only 1/4 as severe as a rigid barrier crash.

Table 2 presents a complete tabulation of the high-speed film data showing time after impact in milliseconds, vehicle displacement, vehicle velocity and deceleration. The total duration of the impact was 0.346 seconds. Figure 7 shows a plan and side view of the barrier as installed. The barrier was constructed as shown by Figure 7 with the exception that only one 8WF17 backup beam was used instead of the two shown on the drawing. The barrier consisted of twenty-nine 55-gallon drums of 16-gage steel. There were 9 rows of three drums, with two drums on the nose, making a total of 29 drums altogether. The total length of the barrier was approximately 19 ft. The vehicle penetrated the barrier 13.3 ft. indicating approximately 70% of the

energy capacity of the barrier was used up. The vehicle had 387,000 ft.-lbs. of kinetic energy.

The dotted lines on the drawing indicate 1/2 in. cables which were tied to the simulated bridge pier and threaded between the rows of barrels, supported on the rolling hoops, and tied off to a reinforced concrete anchor shaft located flush with the ground in front of the nose of the barrier. The 1/2 in. cables were designed to give the barrier lateral stability in case of an angle hit by a vehicle. These cables also hold the barrels on the ground during vehicle impact. The barrels must not be attached to the cable in any manner. They must remain free to slide down the cable during vehicle impact. Additional tests are needed on this system in order to verify the lateral stability of this barrier when struck by a vehicle at angles other than head on.

Figure 8 shows the detail of how the top and bottom of the drums were welded together at all points of contact between adjacent barrels. A piece of No. 5 reinforcing bar 2 in. long was placed between the barrel rims and fillet welded to each barrel. Figure 8 also shows how the tops and bottoms of the barrels were cut and metal removed in order to reduce the crush strength of a barrel down to the desired level. Four elliptical holes were cut in the top and bottom of each barrel leaving an almost square piece of metal in the top and bottom intact and joined to the rim.

Figure 9 shows the static force-deformation curves for the 55-gallon 16-gage steel drums used to construct this barrier.

The top curve on this figure indicates a peak crush force of approximately 20,000 lbs. for a 55-gallon drum with the top and bottom left intact. When the elliptical shape holes are cut in the top and bottom as shown in Figure 8, the crush strength is shown by the lower curve on Figure 9. A peak crush force of approximately 8,000 lbs. was developed under this static test. Figure 9 indicates the importance of removing some of the metal from the top and bottom of the drum in order to reduce the crush strength of the barrel. The uncut barrels will generate approximately three times as much stopping force as the barrels cut as shown.

Figure 10 shows an idealized barrier force-deformation curve under vehicle impact. From an analysis of the high-speed film data it was apparent that the crush strength of the total barrel system welded together was somewhat larger than that obtained from the sum of the individual barrels. This increase in the total barrier force can be attributed to cable friction, ground friction, and lateral support provided to the barrels by adjacent barrels. Additional laboratory tests on barrel crush strengths are now being conducted in order to better establish the barrel strength characteristics.

A descriptive appendix is included to show the American Standard Specifications for 55-gallon tight-head universal drums which were used to construct this barrel protective barrier. Fifty-five-gallon drums can be fabricated with various gage metals from gage No. 12 to gage No. 24. In the very near future, laboratory tests will be conducted on barrels of 18- through 24-gage

metal. Such barrels will be much lighter in weight and could feasibly have the desired crush strength without the requirement of cutting and removing metal from the tops and bottoms.

Figure 11 shows some typical hazards where barrel protective barriers could be effectively employed. Several locations in the state of Texas of this type are now being considered for possible employment of this protective system. Figures 12 and 13 show some other possible configurations which could be used in the employment of 55-gallon drums as an energy absorption barrier.

Summary and Conclusions

This barrel protective barrier appears to be a very effective, economical and practical vehicle crash attenuation device. Based on the single test conducted to date the impact behavior of the system appears very good. The system appears very economical, since the cost of barrels delivered from a barrel factory will range from $6 to $7 each. Second hand barrels can be purchased for as little as $2 each. The system fabricated and tested here was made of second hand barrels costing a total of $58 ($2 each). The cables, steel plates, 8 in. wide flange backup beam, etc. were very minimum in cost.

The system can be fabricated and installed by semi-skilled laborers. Maintenance and reliability of the system also appears good. The system should behave satisfactorily under extremely high or low temperature conditions in either a wet or dry condition. After such a barrier is struck by a vehicle, it will probably

prove very feasible to replace the whole barrel system with a spare or replacement system which could be stored in a highway department maintenance yard. Since the barrels are all welded together and are tied down by the anchor cable it is believed the system will behave satisfactorily under angle impact. The stability of this system under angle impact, however, needs verification by further impact tests which are anticipated in the near future.

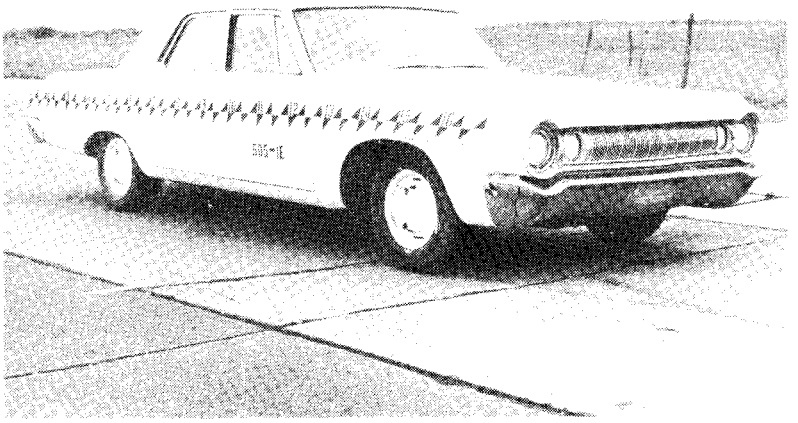

Figure 1. Crash Vehicle before Test

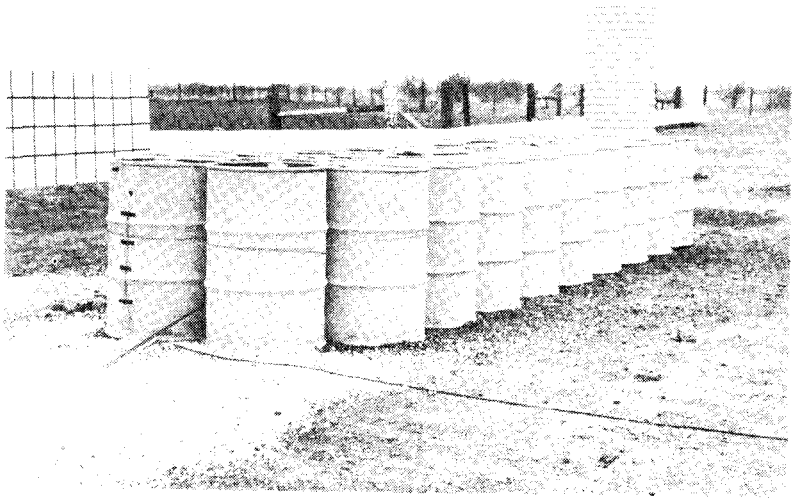

Figure 2. Barrel Protective Barrier Installed in Front of 20 in. Diam. simulated Bridge Pier

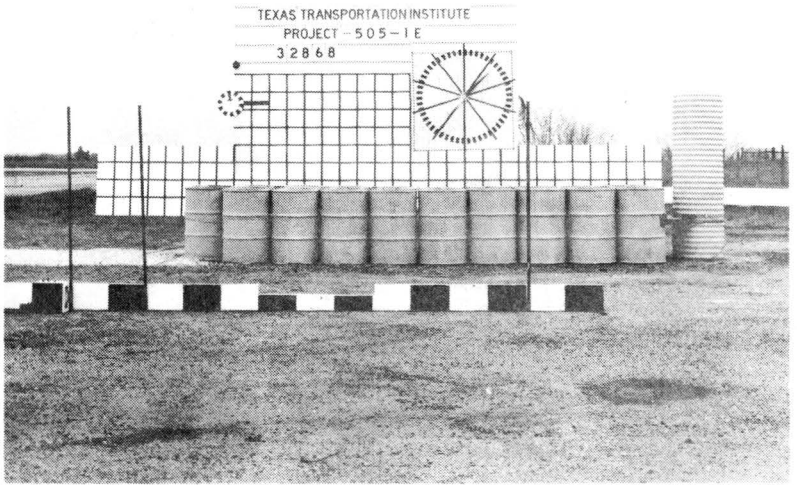

Figure 3. Side View of Barrel Protective Barrier in Front of 30 in. Diam. Simulated Bridge Pier

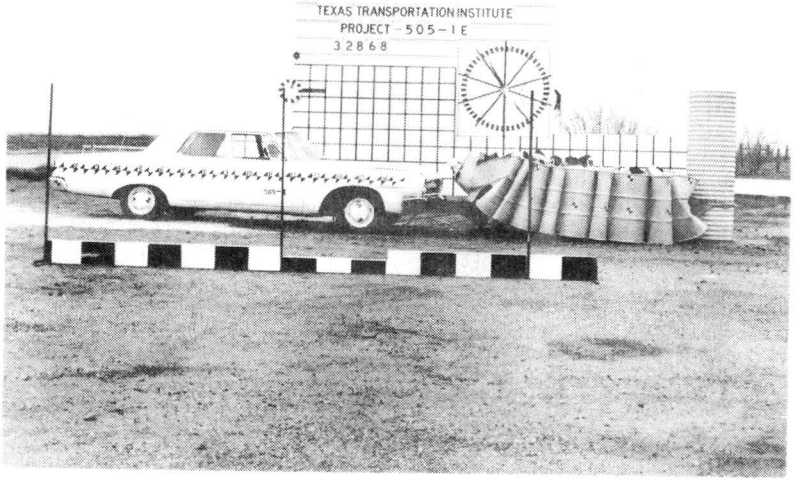

Figure 4. View of Barrel Protective Barrier and Test Vehicle After Impact. Initial Vehicle Velocity 60 mph. Stopping Distance 13.3 ft., Average Vehicle Deceleration 9.1 g's

Figure 5. View of Minor Vehicle Damage. Only one of four headlights was broken. Bumper and Grill deformed approximately 4 in.

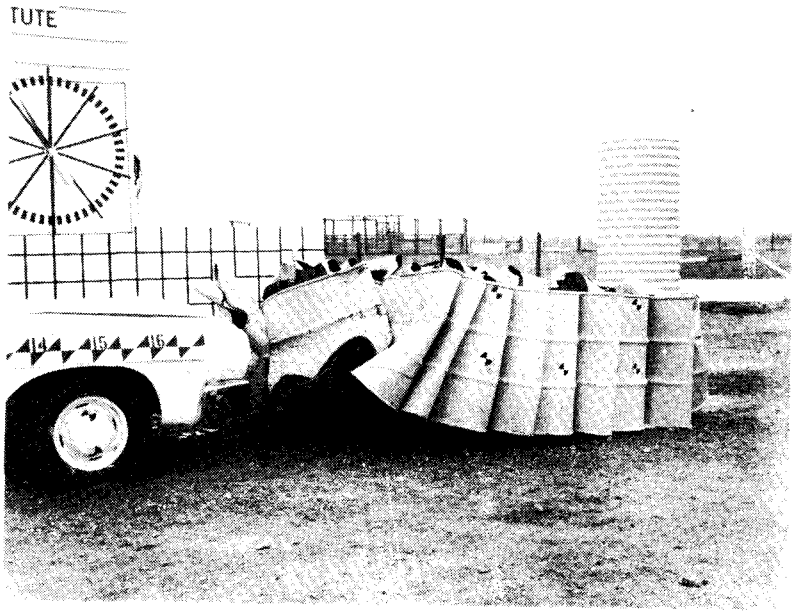

Figure 6. View of Vehicle and Barrier After Impact

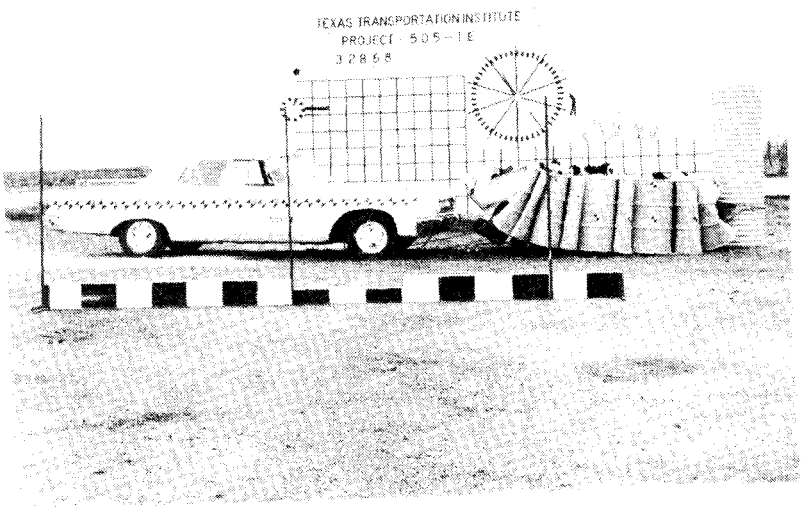

TABLE 1.
Summary of High-speed Film Crash Test Data

Test 505-1E — 55 Gallon Drums with Tops and Bottoms Cut, 3 Drums Wide by 10 Drums Deep, Protecting 2 1/2 ft. diameter Simulated Bridge Pier

Vehicle Weight = 3200 lb. (1964 Dodge, 4-door)

Vehicle Velocity = 60.2 mph or 88.3 fps

Change in Velocity = 60.2 mph or 88.3 fps

Average Deceleration = 9.1 g's

Peak Deceleration = 12.7 g's

Duration of Impact = 0.346 sec.

Stopping Distance = 13.3 ft.

Remarks: Very minor damage to vehicle. One of four headlights broken.

TABLE 2. HIGH-SPEED FILM DATA

TEST RF505-1E

55 Gal. Drums with Tops and Bottoms Cut
3 Drums Wide by 10 Drums Deep
High-Speed Film Data

	Time Milliseconds	Displacement ft	Velocity ft/sec	Deceleration ft/sec^2	Deceleration g's
	0	0		0	0
	6.3	0.57		0	0
			88.3		
	16.8	1.50		0	0
Impact	*27.3	*2.41		0	0
			82.4		
	48.3	4.14		-271.4	-8.4
			76.7		
	69.3	5.75		-409.5	-12.7
			68.1		
	90.3	7.18		-247.6	-7.7
			62.9		
	111.3	8.50		-295.2	-9.2
			56.7		
	132.3	9.69		-319.0	-9.9
			50.0		
	153.3	10.74		-295.2	-9.2
			43.8		
	174.3	11.66		-181.0	-5.6
			40.0		
	195.3	12.50		-247.6	-7.7
			34.8		
	216.3	13.23		-228.6	-7.1
			30.0		
	237.3	13.86		-271.4	-8.4
			24.3		
	258.3	14.37		-114.3	-3.5
			21.9		
	279.3	14.83		-295.2	-9.2
			15.7		
	300.3	15.16		-90.5	-2.8
			13.8		
	321.3	15.45		-204.8	-6.4
			9.5		
	342.3	15.65		-247.6	-7.7
			4.3		
	363.3	15.74		-114.3	-3.5
			-1.9		
	384.3	15.70		-204.8	-6.4
			-2.4		

Time Milliseconds	Displacement ft	Velocity ft/sec	Deceleration ft/sec^2	g's
405.3	15.65		-133.3	-4.1
		-5.2		
426.3	15.54		0	0
		-5.2		
447.3	15.43			

TABLE 3. COMPARISON OF TEXAS BARREL PROTECTIVE BARRIER CRASH TEST WITH RIGID BARRIER IMPACT.

	Barrel Barrier Impact Test 505-1E	Rigid Barrier Impact
Vehicle Weight (W)	3200 lb	3200 lb
Vehicle Velocity (V)	60.2 mph	60.2 mph
Max. Deceleration	12.7 g's	54.2 g's*
Avg. Deceleration	9.1 g's	34.6 g's*
Attenuation Index		
$AI_{(max)} = \frac{G(max.barrels)}{G(max.\ rigid)}$	0.23	
$AI_{(avg)} = \frac{G(avg.barrels)}{G(avg.\ rigid)}$	0.26	

*Note: Estimated Rigid Barrier Impact Deceleration

Determined by G(max.) = 0.9 V

G(avg.) = 0.574 V

Where V is in mph; from Emori, Richard I., "Analytical Approach to Automobile Collisions," SAE Paper 680016, Auto. Engr. Congress, Detroit, January 8, 1968.

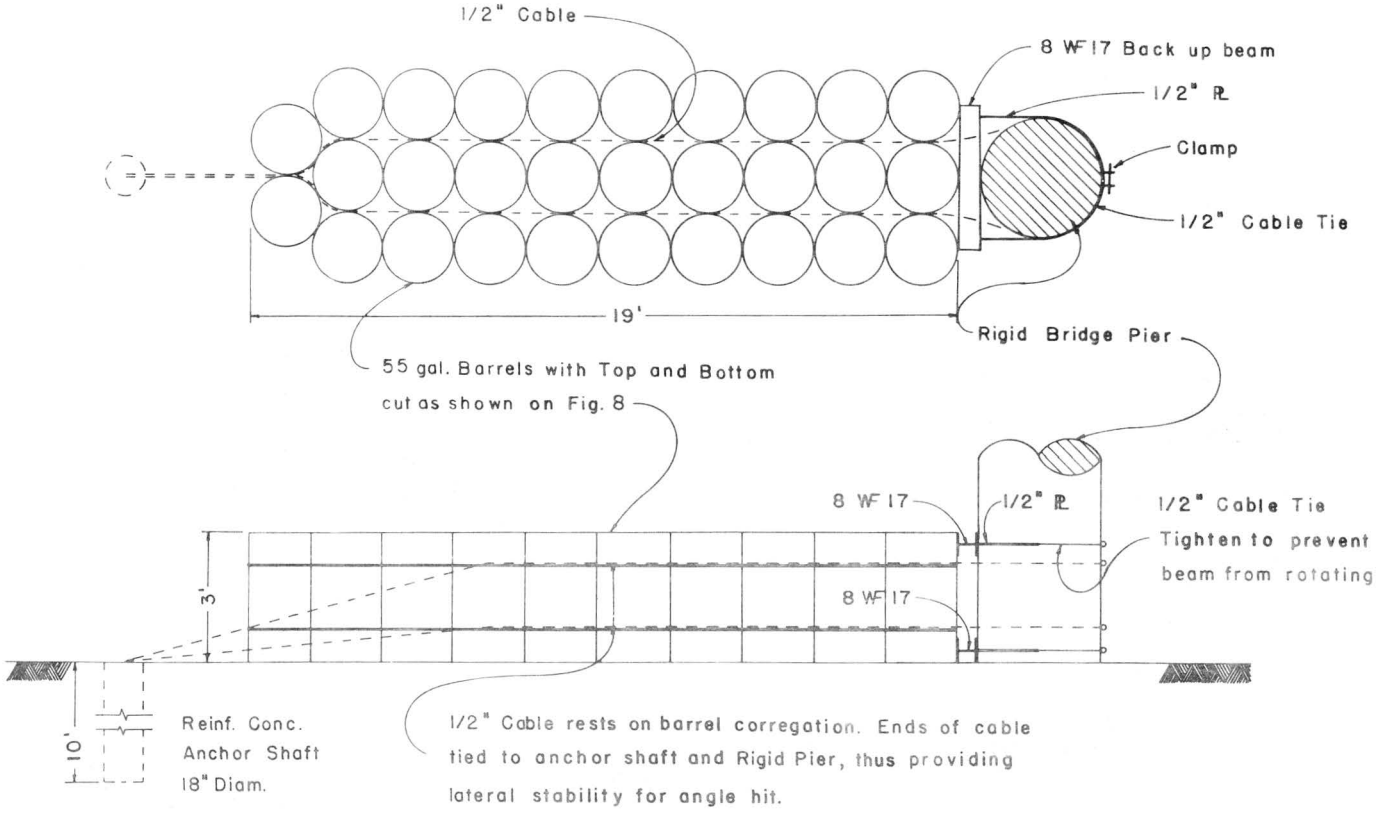

FIG. 7 BARREL PROTECTIVE BARRIER

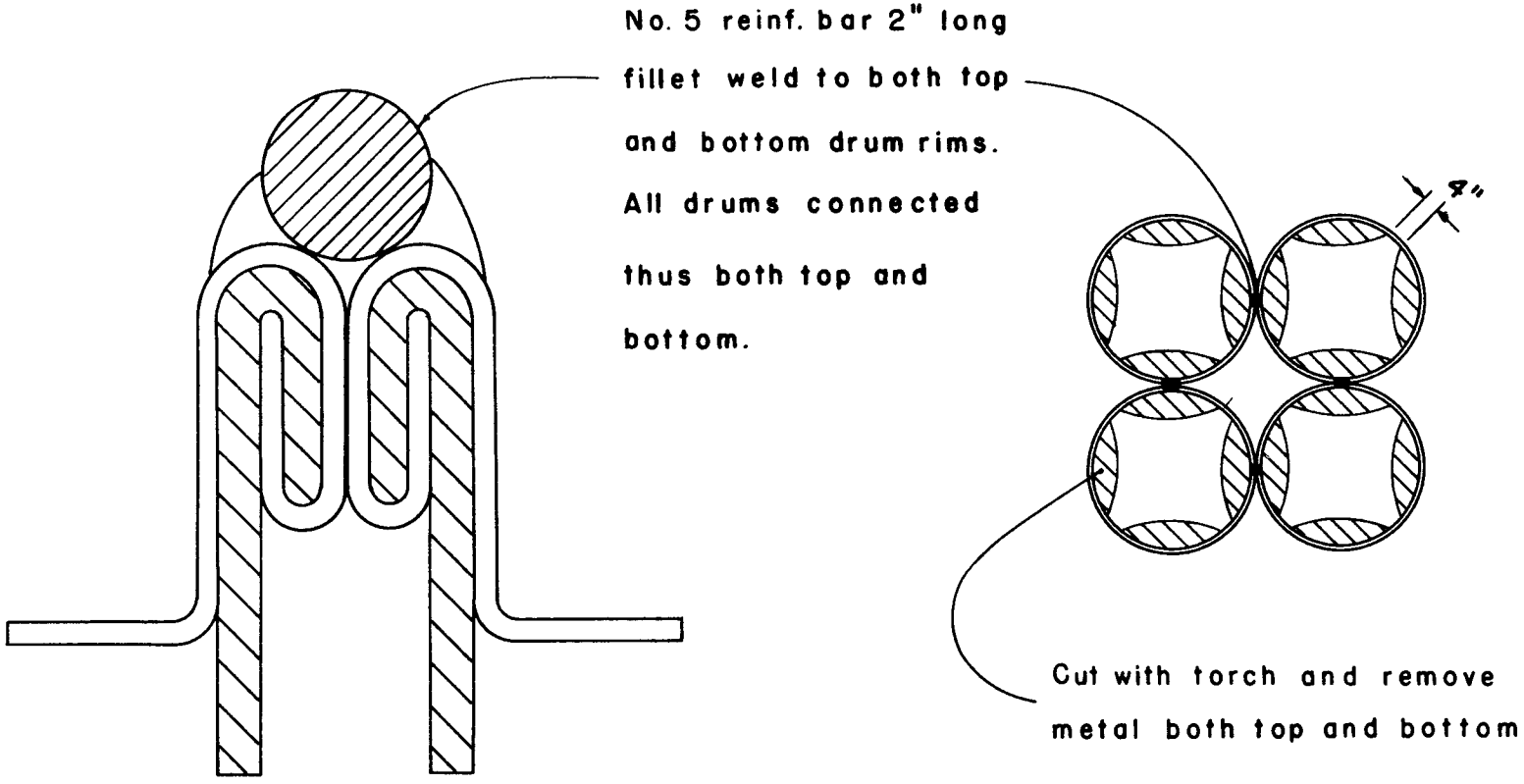

FIG. 8 Detail of Top or Bottom of 55 gal. Tight-Head Univ. Drum, 16 gage steel

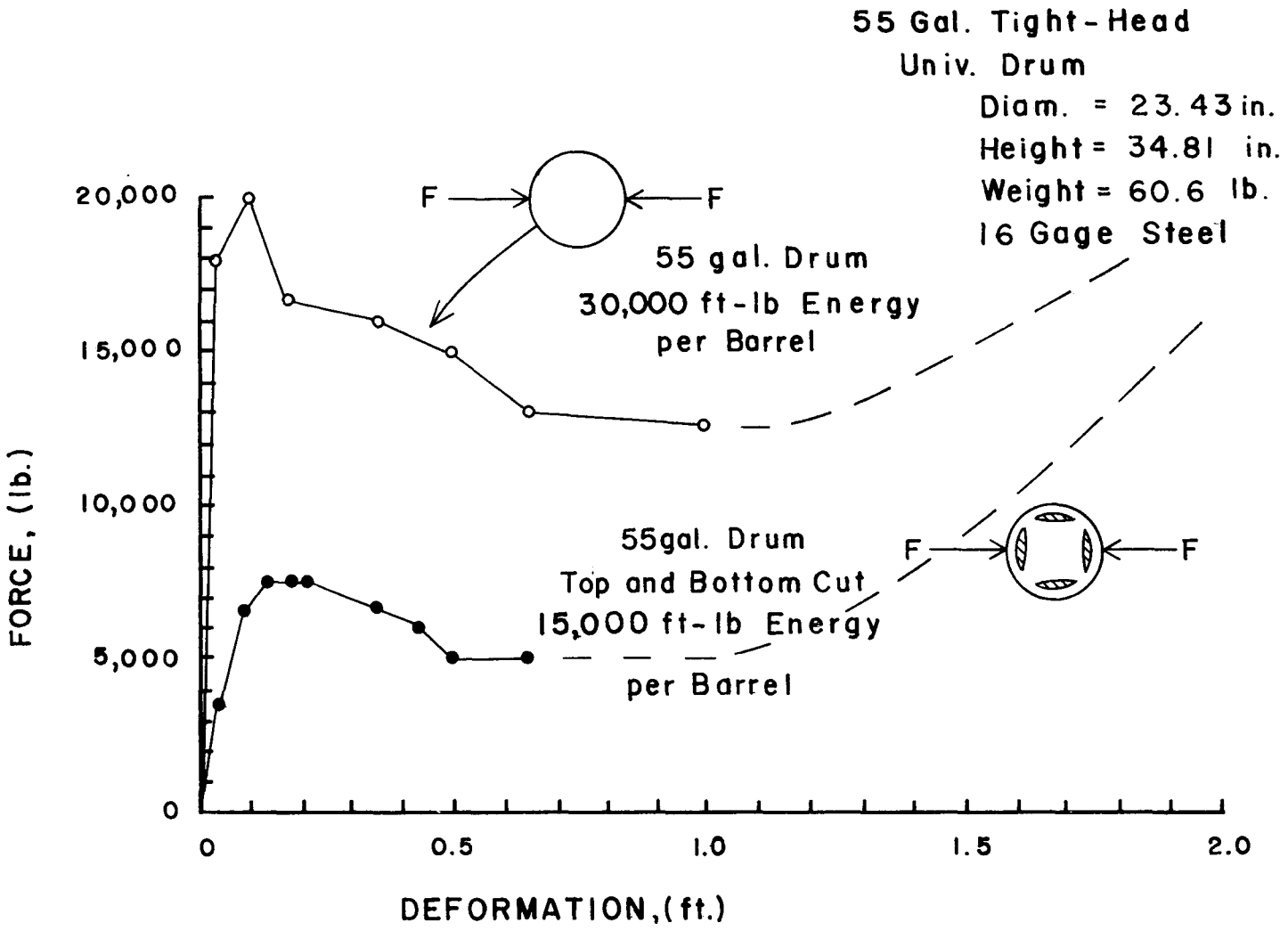

FIG.9 Force-Deformation Curve for 55 gal. Drums

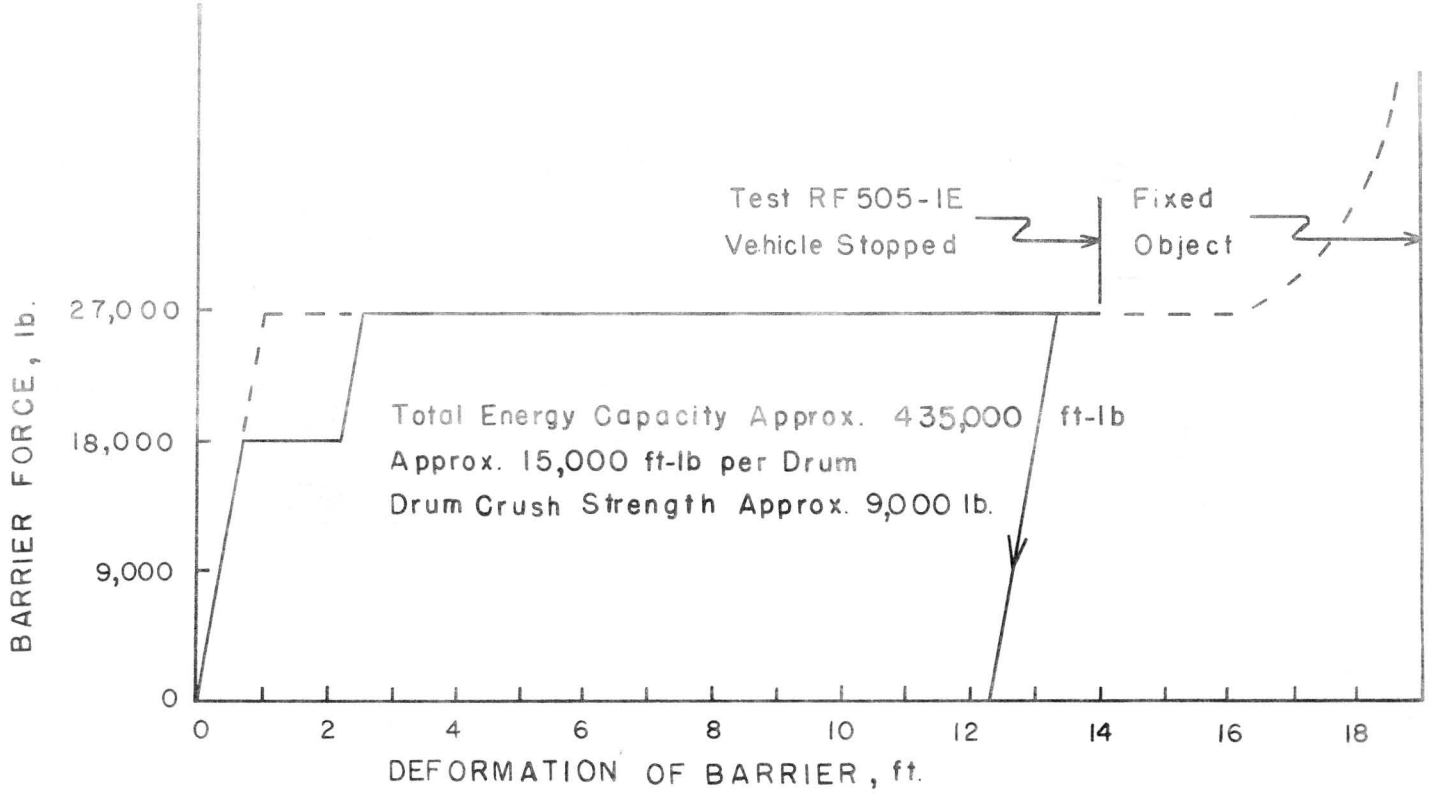

FIG. 10 Idealized Barrier Force-Deformation Curve Under Vehicle Impact (includes drum crush strenght, cable friction, ground friction, etc.)

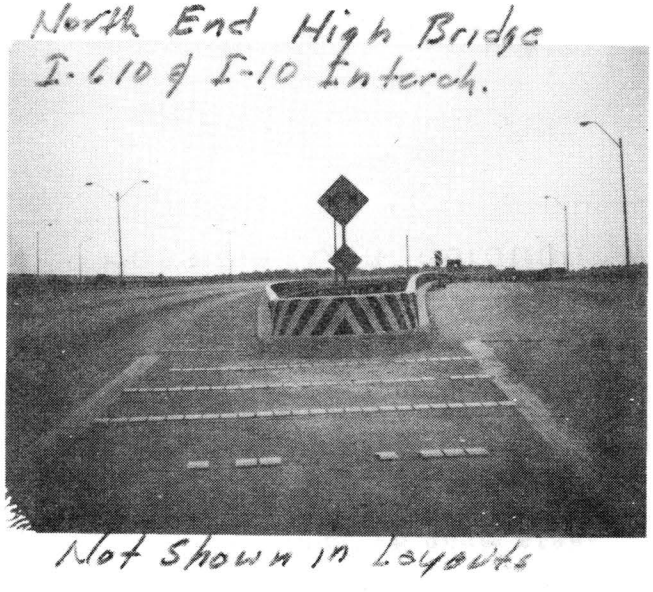

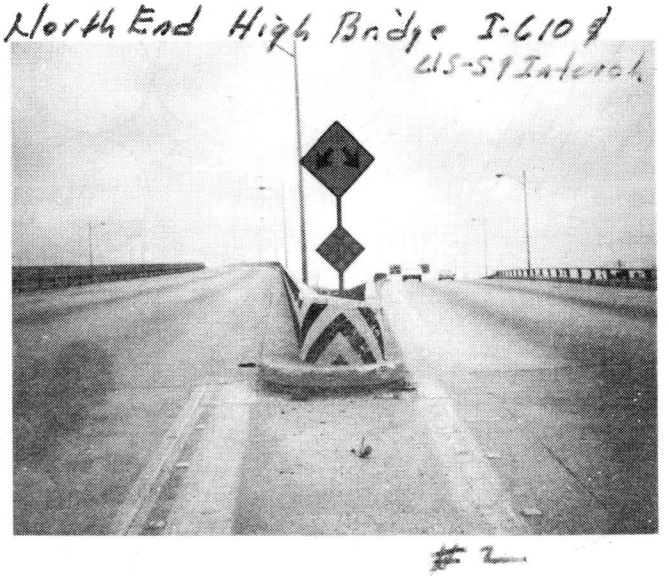

Figure 11. Typical Hazardous Locations Where Barrel Protective Barriers Could be Employed

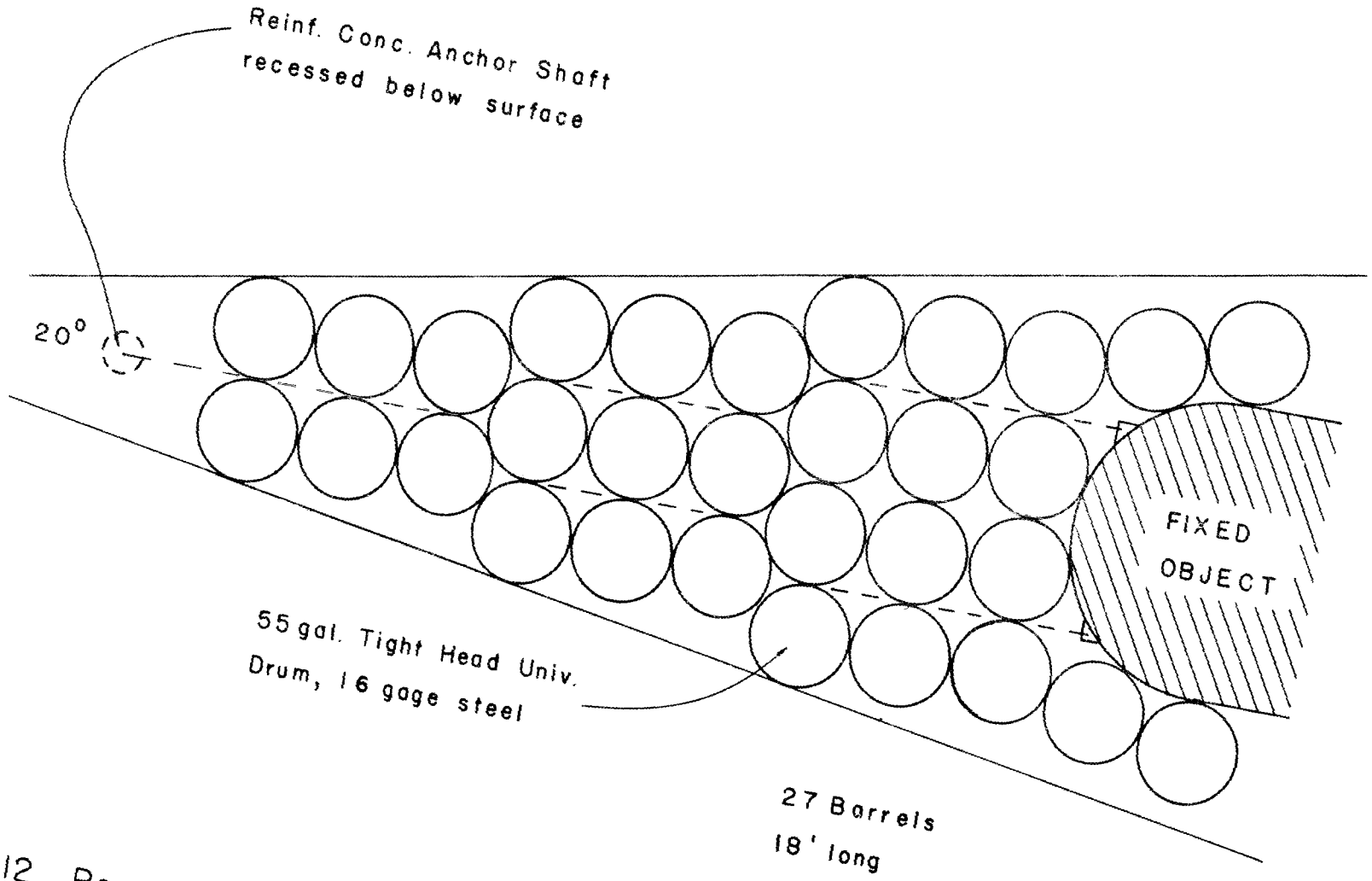

FIG 12 Possible Configuration which could be used

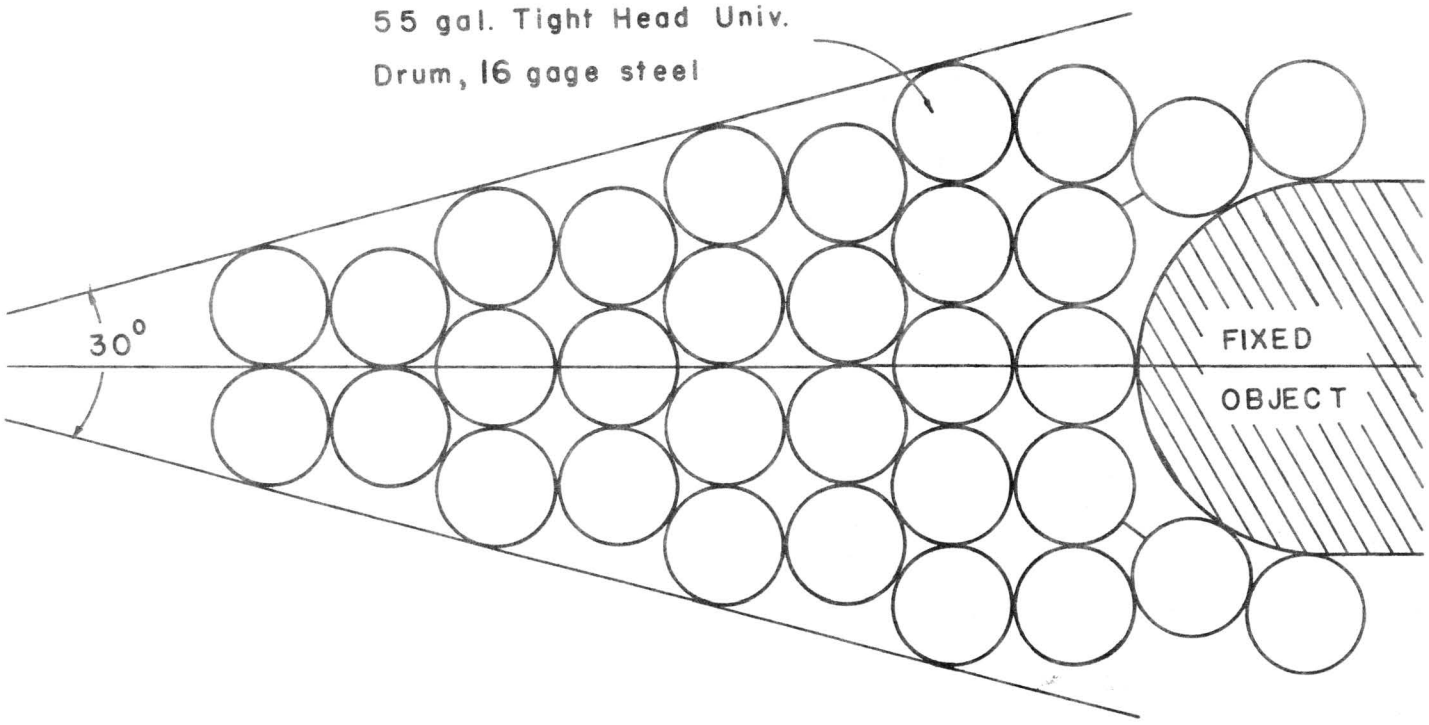

FIG. 13 Possible Configuration which could be used

A P P E N D I X

STANDARD SHIPPING CONTAINERS
TIGHT HEAD DRUMS

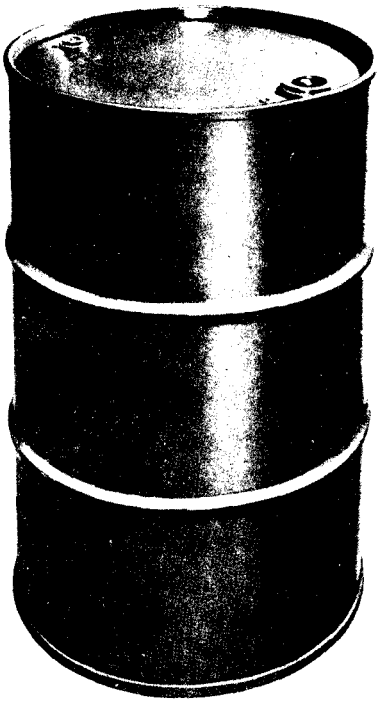

Used for shipping or storing such products as chemicals, paints, petroleum and food – for both domestic and export markets. Extra and special openings will be provided as requested. All ICC drums which are displayed throughout this catalogue are manufactured in accordance with government specifications and are submitted to rigid testing and inspection. Each drum receives a leakage test and there are periodic drop and hydrostatic pressure tests of drums selected at random from our production lines.

Each drum bearing the U.S.S. embossment along with appropriate ICC markings can be filled with maximum confidence.

Can be furnished: Painted—black or other standard colors • Decorated • Lined • Galvanized – hot-dip • Tinned—hot-dip • Stainless • Embossing as requested – names, numbers, trademarks, symbols.

Constructed of 16 to 20-gauge steel to meet all legal requirements.

ICC Spec.	Capacity Gallons	Gauge Body	Gauge Head and Bottom	Inside Diameter	Inside Height	Overall Height	Diameter Over Rolling Hoops	Approx. Tare Weight	Ocean Cube	Approx. No. Per Carload	
										40′	50′
—	57	18	18	22-1/2	34-11/32	35-15/16	23-7/16	49.7	11/0	300	370
17C	55	16	16	22-1/2	33-5/32	34-3/4	23-7/16	60.6	10/9	300	370
17E	55	18	18	22-1/2	33-5/32	34-3/4	23-7/16	48.6	10/9	300	370
17E	55	20	18	22-1/2	33-5/32	34-3/4	23-7/16	40.1	10/9	300	370
—	33	19	19	18-1/4	30-1/32	31-5/8	19-3/16	31.2	6/8	430	540
—	33	18	18	18-1/4	30-1/32	31-5/8	19-3/16	35.6	6/8	430	540
17E	30	20	20	18-1/4	27-9/32	28-7/8	19-3/16	25.3	6/1	570	670
17E	30	19	19	18-1/4	27-9/32	28-7/8	19-3/16	29.3	6/1	570	670
17C	30	18	18	18-1/4	27-9/32	28-7/8	19-3/16	33.5	6/1	570	670
—	30	16	16	18-1/4	27-9/32	28-7/8	19-3/16	41.7	6/1	570	670
—	16	22	22	13-15/16	25-27/64	26-7/8	14-7/8	14.3	3/6	1040	1250
—	16	20	20	13-15/16	25-27/64	26-7/8	14-7/8	17.0	3/6	1040	1250

TECHNICAL MEMORANDUM 505-1S

SUPPLEMENT TO 505-1

Texas Transportation Institute
Texas A&M Research Foundation

THE MODULAR CRASH CUSHION

A Tentative Progress Memorandum on Contract No. CPR-11-5851

U.S. Department of Transportation
Federal Highway Administration

by

T. J. Hirsch
Research Engineer

Gordon G. Hayes
Physics Research Associate

and

Don L. Ivey
Associate Research Engineer

These crash tests and evaluations were conducted under the Office of Research and Development, Structures and Applied Mechanics Division's Research Program on Structural Systems in Support of Highway Safety (4S Program). The opinions, findings, and conclusions expressed in this report are those of the authors and not necessarily those of the Federal Highway Administration.

August 1970

INTRODUCTION

The Modular Crash Cushion was developed under a contract with the Federal Highway Administration as an expedient measure to reduce the number of fatal automobile collisions with rigid obstacles in or near highway rights-of-way.[1*] Additional modifications and tests were sponsored by the Texas Highway Department in cooperation with the Federal Highway Administration.[2] The crash test program and subsequent field experience indicated that this system was more than an expedient measure and that it functioned very well as an impact attenuator from both the performance and economic points of view.[3,4] As part of its program on Structural Systems in Support of Highway Safety (4S Program), the Federal Highway Administration sponsored further research to improve the basic Modular Crash Cushion design.

One constraint that is placed on most impact attenuators is the geometry of the site. A crash cushion protecting a rigid wall at an elevated freeway gore, for example, cannot be much wider than the wall itself without constricting the adjacent traffic lanes. Therefore, in angled collisions toward the rear of the cushion (near the rigid wall) the distance and energy absorbing materials are usually insufficient to stop the vehicle safely before it contacts the rigid wall. In such collisions it is usually better to cause the colliding vehicle to redirect, thereby missing the rigid wall. The provisions for redirection must be such that the cushion has lateral stability, while maintaining the "soft" characteristics during head-on impacts. The results of some of the efforts to satisfy these conditions are presented in this report.

---

*Superscript numerals refer to corresponding numbers in the Selected References.

SYSTEMS TESTED

The three crash cushion designs which were tested used 20-gage steel tight-head drums as the basic energy absorbing modules.

The first configuration is shown in Figure 1. The columns of modules were separated by plywood inserts, and the two support cables ran between the columns of drums in a path as shown in Figure 1. Overlapping redirection panels were attached to the sides of the crash cushion. These panels were made of 3/4" plywood covered with fiber glass which was coated with a polyester resin. This gel coat was used to give more smoothness to the panel surfaces and to improve the appearance of the barrier. The front edges of the panels were hinged so that the back edges could telescope or swing out, allowing free crushing of the barrier during head-on collisions.

The second barrier which was tested is shown in Figure 2. The basic drum arrangement was the same as before, but the support cables were moved to run in a straight line between the outer modules and the redirection panels to reduce vehicle pocketing. A "truss" composed of steel straps was welded to the tops of the modules to increase the lateral strength and stiffness of the crash cushion.

The final system constructed for testing is shown in Figure 3. Steel angle spacers were used here, and the module arrangement was modified to reduce the stopping force at the onset of the collision. This modification is especially desirable when the colliding vehicle is small and lightweight. Also, the rear of the barrier was widened to provide a cushion between the end redirection panels and the rigid wall. Again, cables inside the redirection panels were used to give lateral stability without rigidity.

Photographs of each of the cushions accompany the individual test descriptions.

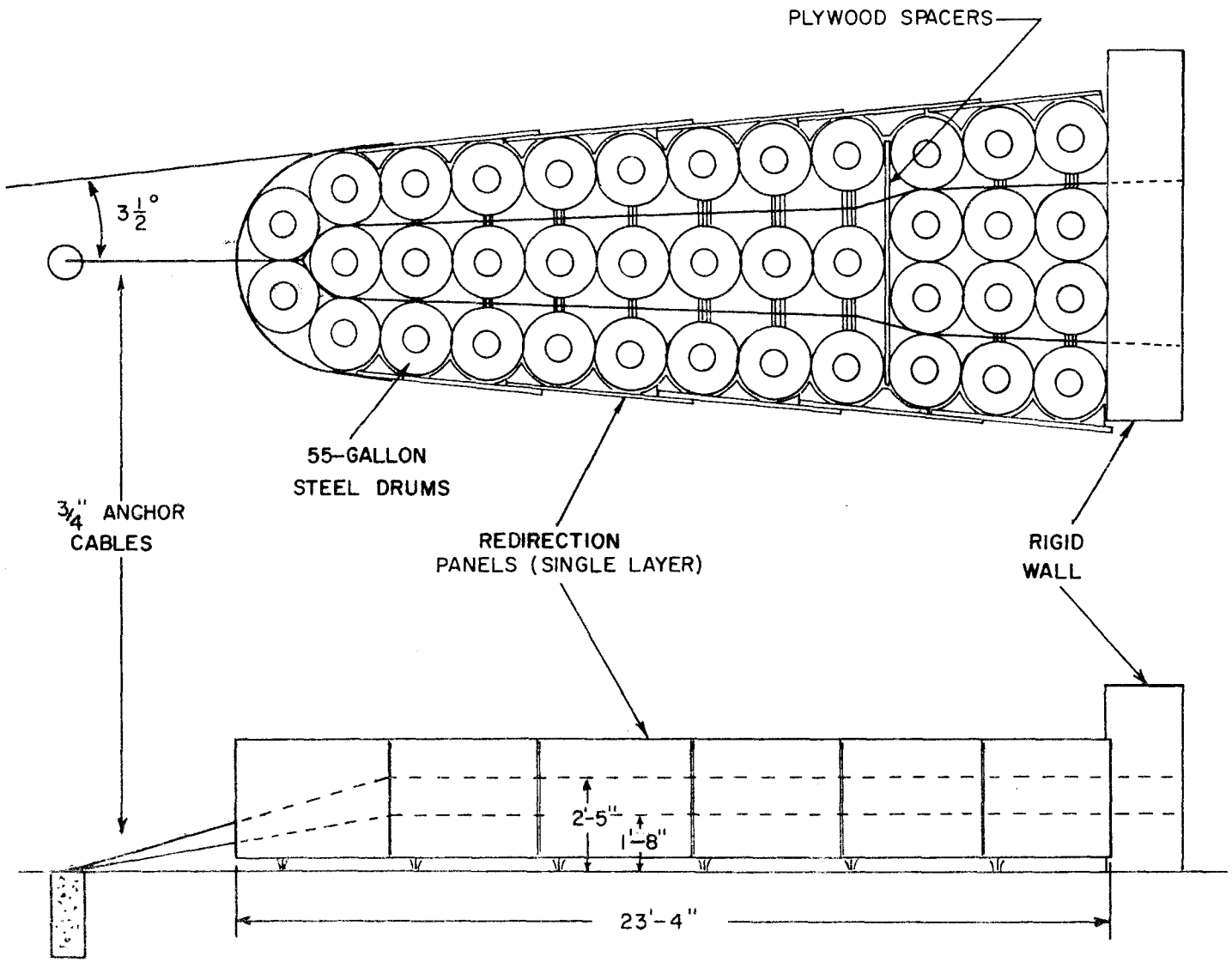

FIGURE 1, CONFIGURATION USED IN TEST 505B-A (BARRIER TYPE I)

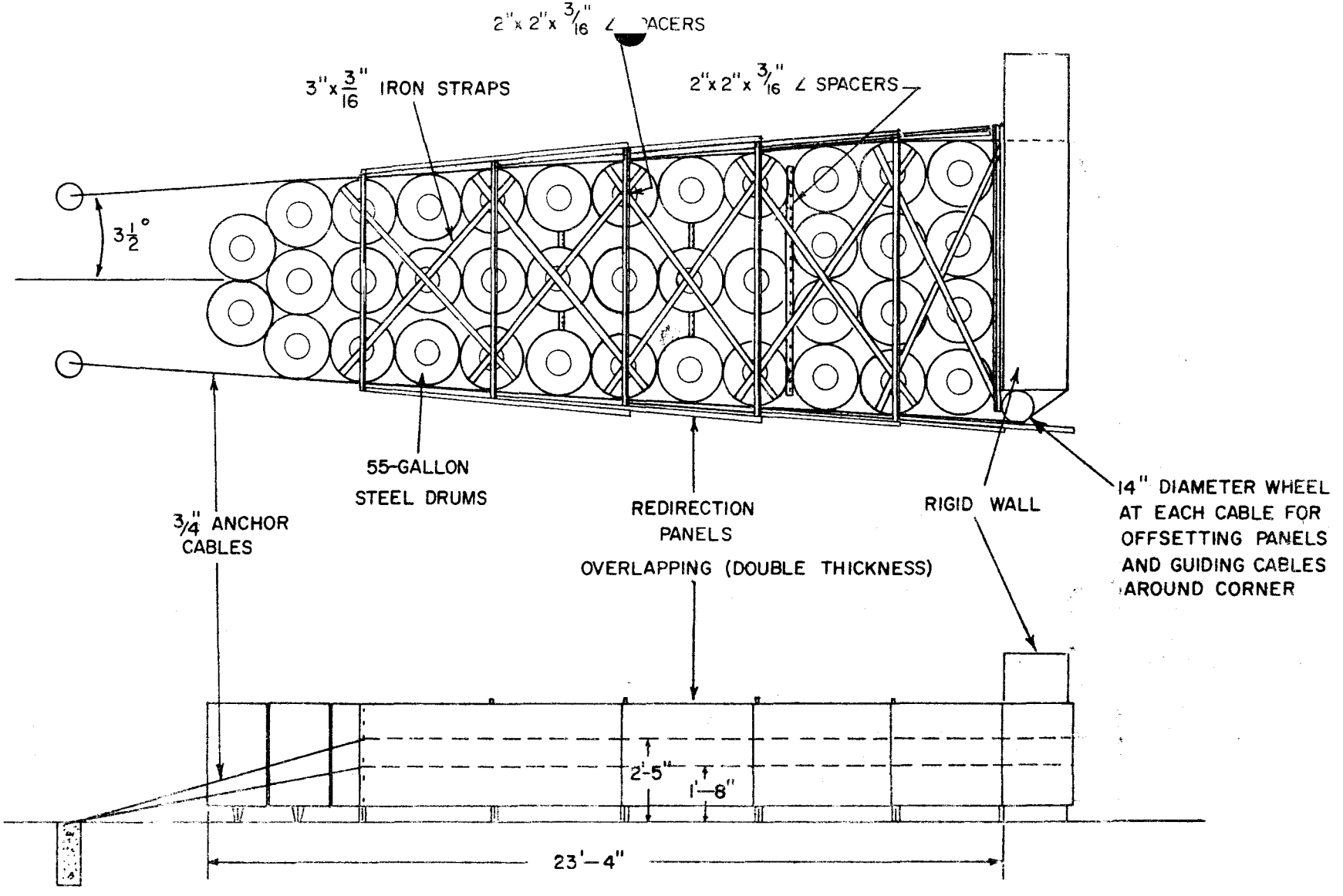

FIGURE 2, CONFIGURATION USED IN TESTS 505B-B AND 505B-C (BARRIER TYPE 2)

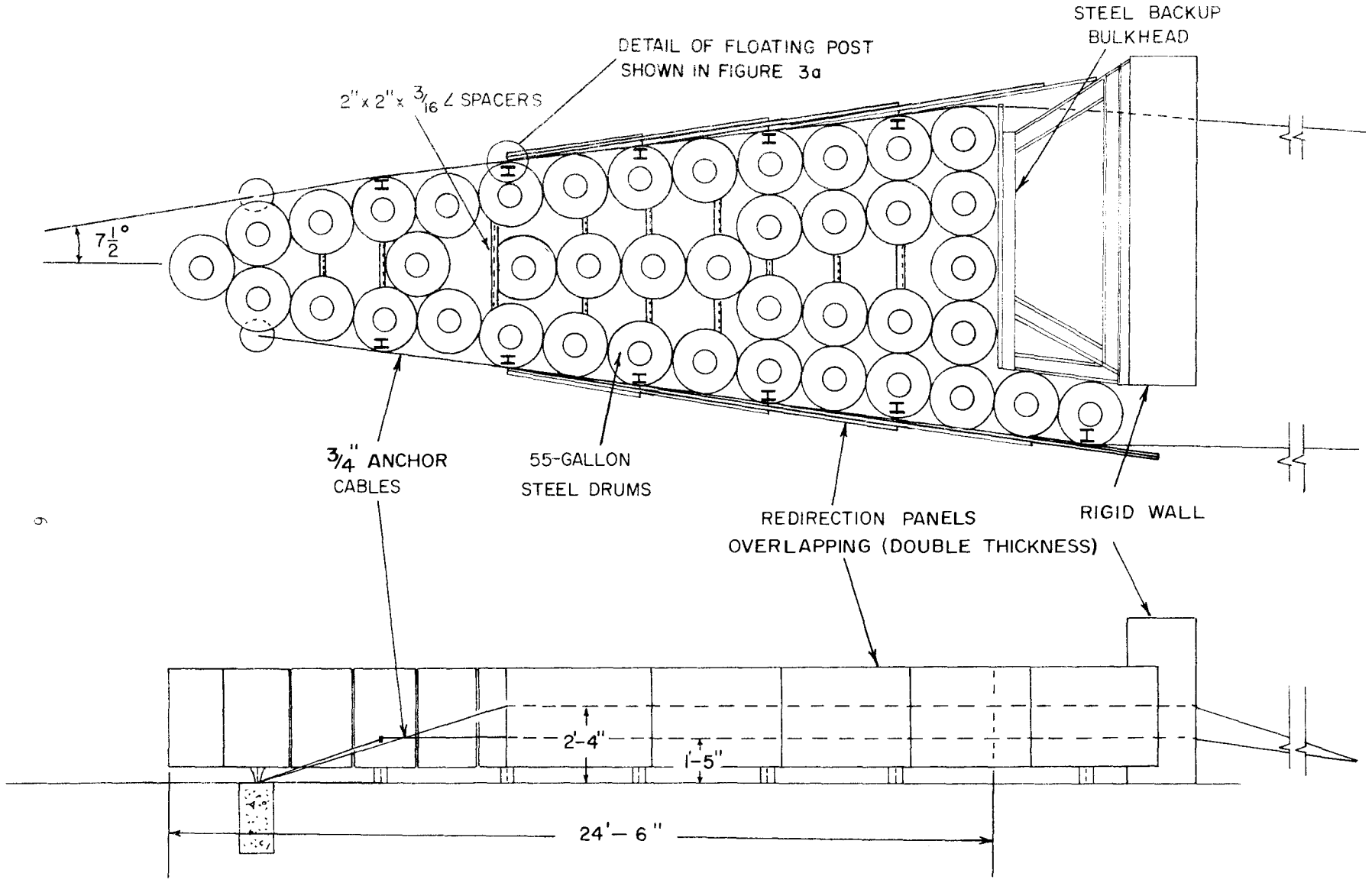

FIGURE 3, CONFIGURATION USED IN TESTS 505B-D AND 505B-E (BARRIER TYPE 3)

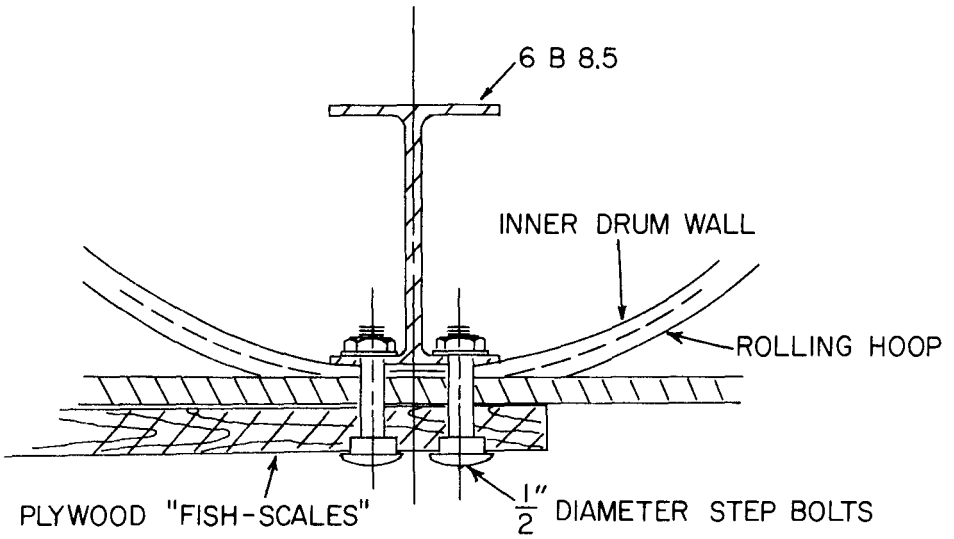

SECTION A-A

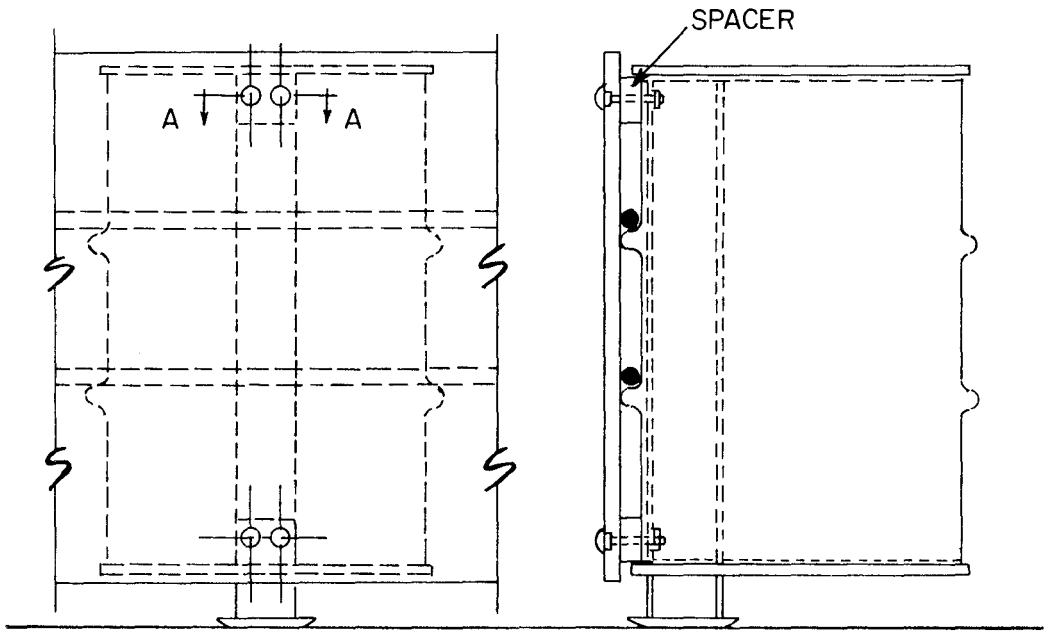

FIGURE 3a DETAIL OF FLOATING POST

TEST PROGRAM

Five full-scale crash tests were run in this series: one oblique impact on the first barrier configuration, and both an oblique and a head-on test on the other two configurations.

The tests were photographed using high-speed motion picture cameras and conventional documentary cameras. Time-displacement data was obtained from the high-speed films. The vehicles were equipped with electro-mechanical accelerometers attached to the longitudinal frame members. In addition, a mechanical Impact-O-Graph was mounted in the trunks as a secondary source of acceleration data. In tests A and E, an anthropometric dummy simulating a driver was secured with a seat belt attached to a load cell for sensing seat belt force. The signals from these transducers were transmitted by multiconductor shielded cable to recording devices. Tape switches activated by the wheels of the approaching vehicle provided a means of checking the initial speeds obtained from the high-speed films.

A typical-instrumentation summary is given in Table 1. Time-displacement data from the high-speed films and reproductions of the accelerometer traces and seat belt force curves are given in the Appendix.

Table 2 is a summary of pertinent test data. For the head-on tests, the average decelerations from the high-speed film data are considered more reliable because initial speed and stopping distance can be measured accurately by this method. The average deceleration in G's is given by $\bar{a} = V_i^2/2gS$, where V_i is the initial speed and S is the stopping distance.

The average deceleration from film data for tests in which the vehicle was redirected is given by $\bar{a} = (V_i^2 - V_f^2)/2gS$, where V_f is the speed of the vehicle at loss of contact with the barrier.

The average decelerations from the accelerometer data are obtained by integrating the area under the analog trace (Appendix) and dividing by the length (time). The deceleration times from the accelerometer traces do not coincide with the times in contact from the films because loss of contact with the barrier does not require that all forces go to zero, even though the vehicle-barrier interaction is completed.

TABLE 1

TYPICAL VEHICLE CRASH TEST INSTRUMENTATION

DEVICE	LOCATION	PURPOSE
CAMERAS:		
1 Hycam (500 frames per sec)	Perpendicular to initial path of vehicle	Initial speed
1 Hycam (500 fps)	Perpendicular to barrier	Entire event
1 Photosonics (500 fps)	Directly above barrier	Overhead view
1 Bell & Howell (128 fps)	Oblique to barrier	Documentary
1 Cine Special (64 fps)	Perpendicular to barrier	Documentary
ACCELEROMETERS:		
1 Statham* and 1 CEC**	Right vehicle frame member	Longitudinal and Transverse acceleration
1 Statham* and 1 CEC**	Left vehicle frame member	Longitudinal and Transverse acceleration
1 Impact-O-Graph	Trunk of vehicle	Triaxial accelerations
OTHER:		
1 Pair of Tape Switches	About 16 ft. before impact	Initial speed
1 Tape Switch	At impact point on barrier	Time of impact
1 Tape Switch and Flash Bulb	On vehicle	Indicate impact visually
1 Seat Belt Strain Gage	Attached to seat belt	Seat belt force on Alderson articulated anthropo-metric dummy

*Strain gage type
**Piezoelectric type

TABLE 2

SUMMARY OF TEST DATA

TEST	A	B	C	D	E
Barrier Type	1	2	2	3	3
Vehicle, Year Make	1963 Valiant	1963 Valiant	1960 Pontiac	1963 Buick	1959 Renault
Vehicle Weight, lbs	3000	3080	4180	4350	1500
Impact Angle, deg	20	20	0	20	0
FILM DATA					
Initial Speed, mph ft/sec	56.9 83.4	59.3 87.0	46.6 68.4	56.8 83.3	58.2 85.4
Average Longitudinal Deceleration, g's	6.8	7.4	6.2	4.0	9.1
Distance in Contact*, ft	16.0	12.6	11.7	24.2	12.4
Time in Contact, sec	.290	.210	.365	.624	.280
Final Speed, mph ft/sec	0 0	26.7 39.1	0 0	19.0 27.8	0 0
ACCELEROMETER DATA					
Longitudinal					
Max. Deceleration, g's	53.0	15.9	7.0	11.3	14.1
Avg. Deceleration, g's	10.8	8.0	3.7	4.6	7.6
Time, sec	.358	.226	.414	.452	.403
Transverse					
Max. Deceleration, g's	3.8	7.3	--	4.3	--
Avg. Deceleration, g's	1.1	3.2	--	0.6	--
Time, sec	.360	.226	--	.292	--

*For Tests A, C, and E, this is the stopping distance.

Test 505 B-A

In this first test, a 1963 Valiant weighing 3000 lbs impacted the Modular Crash Cushion at 56.9 mph. The vehicle centerline made a 20° angle with the centerline of the barrier at impact. The barrier is shown in Figure 4. The redirection panels consisted of 3/4" plywood with two layers of heavy fiber glass roving followed by one layer of gel coat. These panels overlapped approximately 11 inches. Between the columns of barrels were smaller sections of plywood.

After initial contact, the lateral stability of the redirection panels was not sufficient to prevent the vehicle from "pocketing" and crushing several barrels before impacting the edge of the rigid wall. This was the reason for the high maximum longitudinal deceleration of 53 g's. Duration of this high deceleration was about 80 msec, as can be seen from Figures A1 and A2. Contact with the rigid wall occurred about 240 msec after impact, at which time the g level on the accelerometer traces begins to rise sharply (see Figures A1 and A2 in the Appendix).

Analysis of the accelerometer traces showed the average deceleration to be 10.8 g's longitudinally and 1.1 g's laterally. Damage to the vehicle was rather severe due to the impact with the rigid wall (see Figure 6).

This redirection system did not perform as intended. The undesired behavior was attributed to lack of lateral attenuation space at the rear of the barrier adjacent to the edge of the rigid wall. In addition, the barrier had insufficient lateral stability due to the anchor cable positions and to insufficient overlapping of the redirection panels. Subsequent test cushions incorporated design changes which resulted in better redirection capabilities.

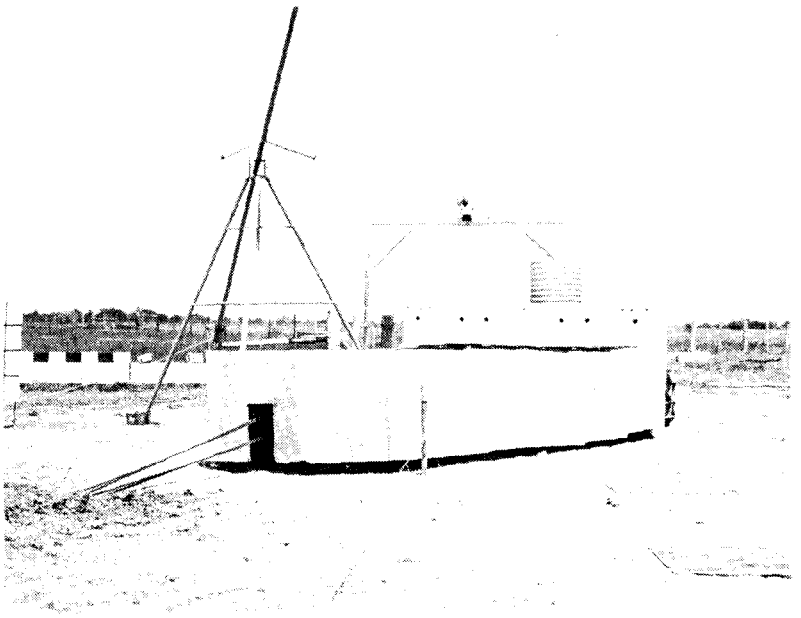

Figure 4, Modular Crash Cushion Before Test 505 B-A.

Figure 5, Vehicle Before Test 505 B-A.

Figure 6, Vehicle After Test 505 B-A.

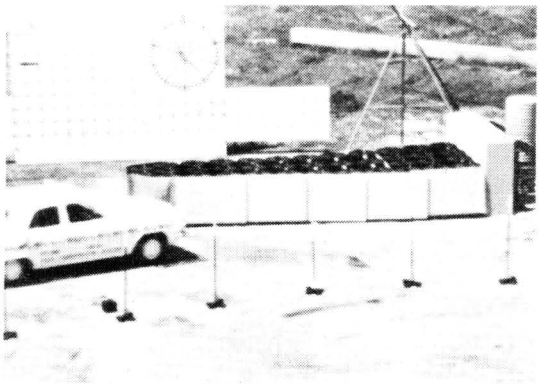

1

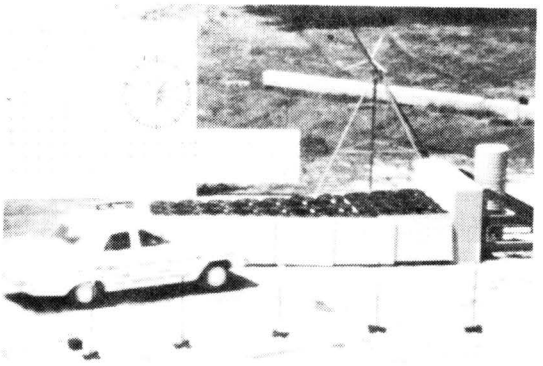

2

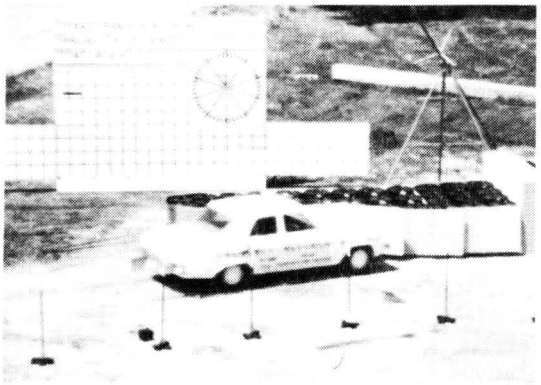

3

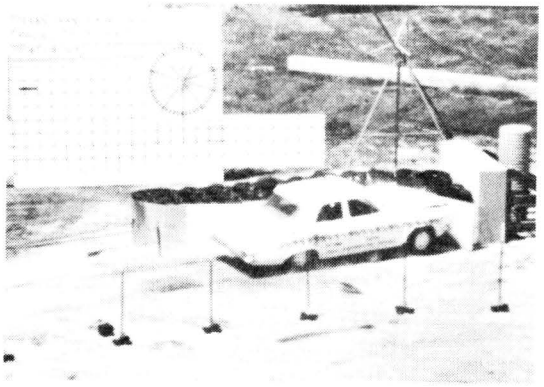

4

5

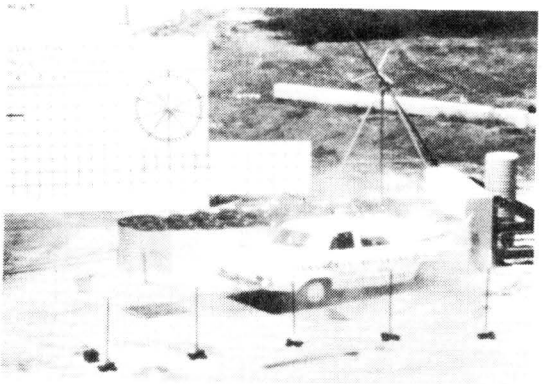

6

Figure 7, Sequential Photographs of Test 505 B-A.
(Side View)

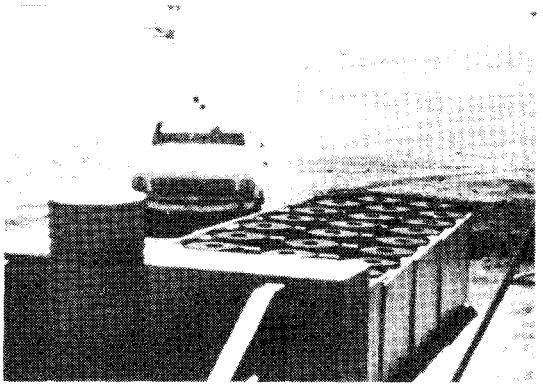

1

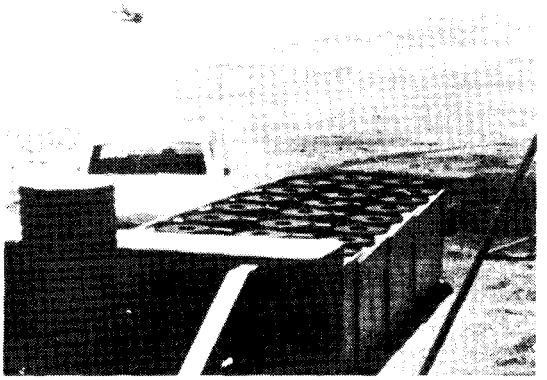

2

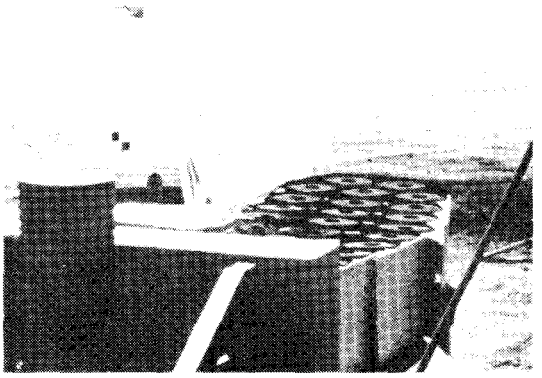

3

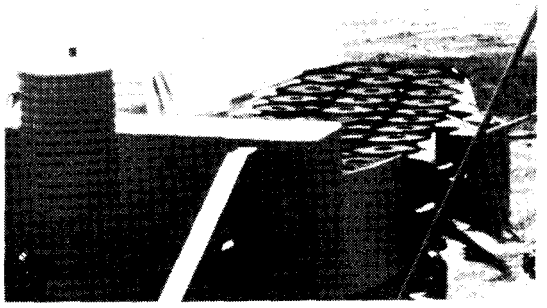

4

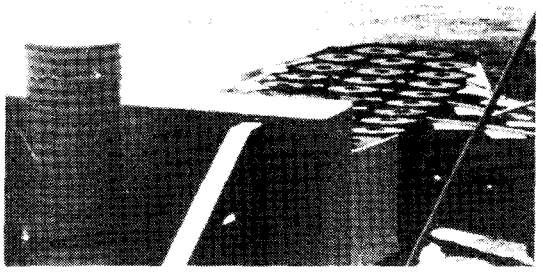

5

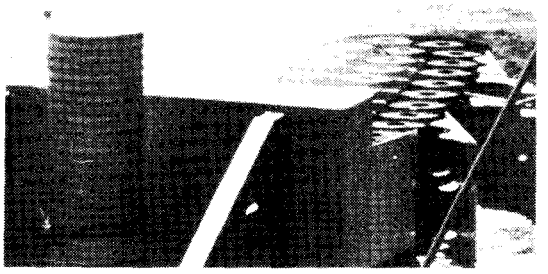

6

Figure 8, Sequential Photographs of Test 505 B-A.

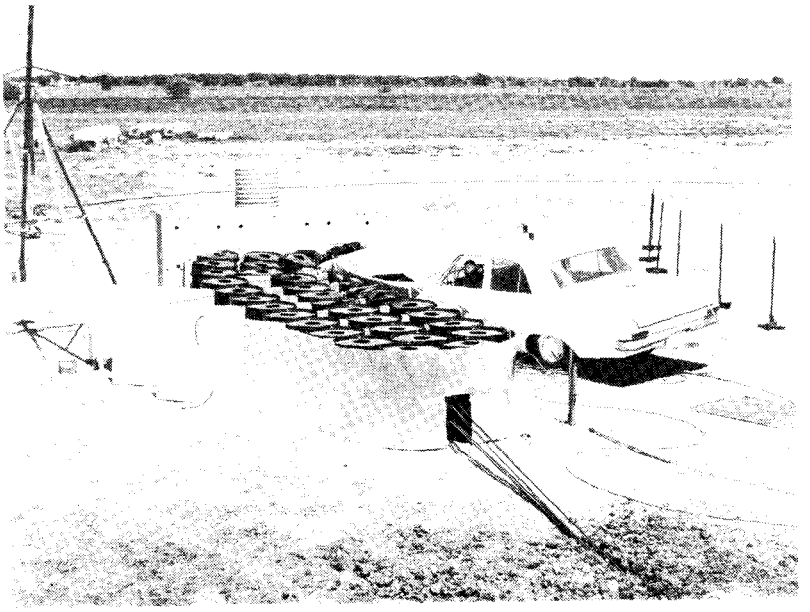

Figure 9, Crash Area After Test 505 B-A.

Test 505 B-B

In order to provide acceptable redirection capabilities, the basic system previously tested was modified. Instead of the plywood spacers between the barrels, metal straps were welded across the top of the barrels as shown in Figure 12. In addition, the anchor cables were placed just inside the deflection panels and were aligned straight and taut. This was done to increase the lateral stability of the system during angle hits for better vehicle redirection. Also, the redirection panels were positioned to overlap each other 4 feet, creating a double thickness of plywood along the impact area.

A 3080 lb Valiant impacted the barrier about 11 ft in front of the rigid wall. The vehicle at contact made an angle of 20° with the center-line of the barrier, and was traveling at 59.3 mph. The vehicle was redirected, leaving the barrier at 26.7 mph after 210 msec. The average longitudinal deceleration during this time was 7.4 g's, and the average transverse deceleration was 3.2 g's.

The left front end of the vehicle was permanently deformed about 1.5 ft. Damage to the barrier was slight. Since only a few barrels were crushed, as seen in Figure 15, the barrier was easily repaired before the next test. This test was considered successful in that the vehicle was redirected as intended, with deceleration levels well within acceptable human tolerances.[5]

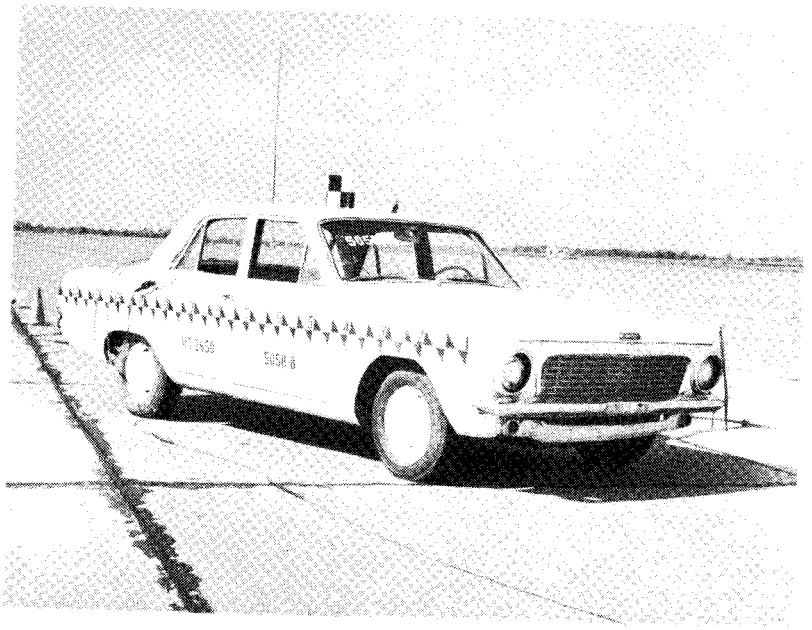

Figure 10, Vehicle Before Test 505 B-B.

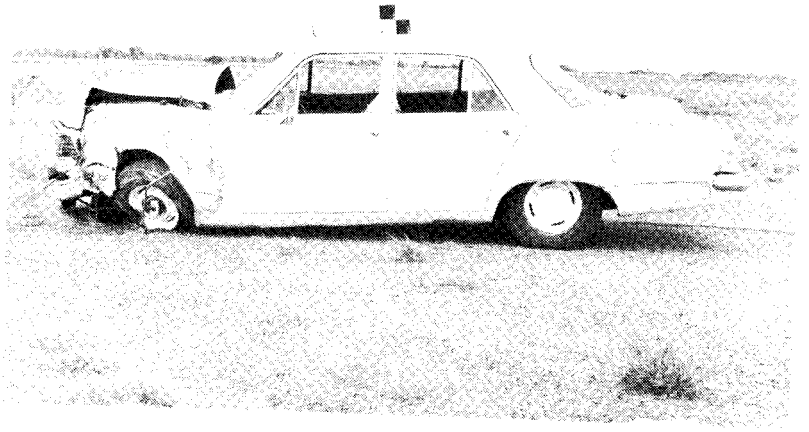

Figure 11, Vehicle After Test 505 B-B.

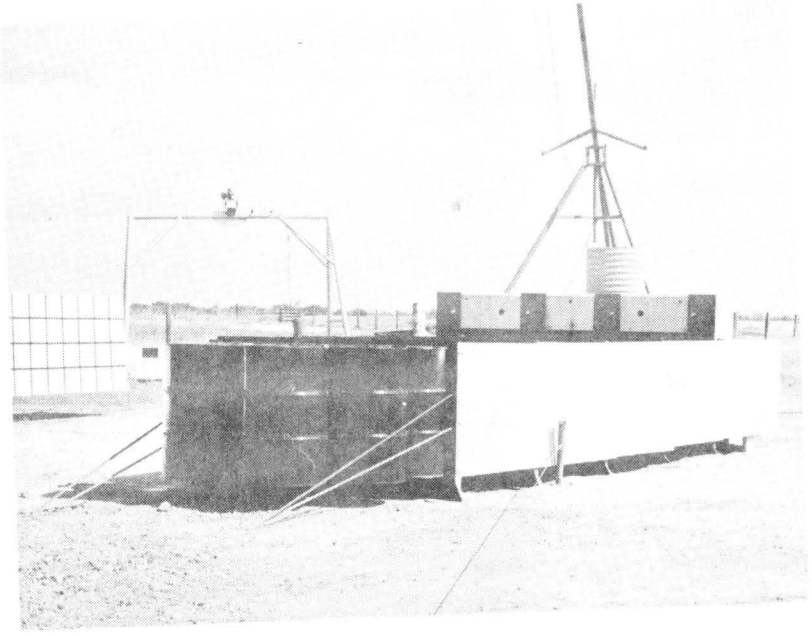

Figure 12, Modular Crash Cushion Before Test 505 B-B.

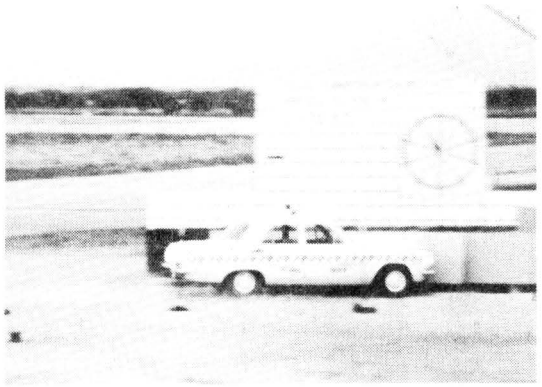

1

2

3

4

5

6

Figure 13, Sequential Photographs of Test 505 B-B.
(Side View)

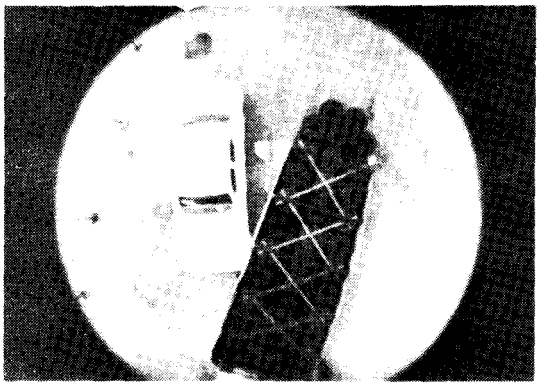

1

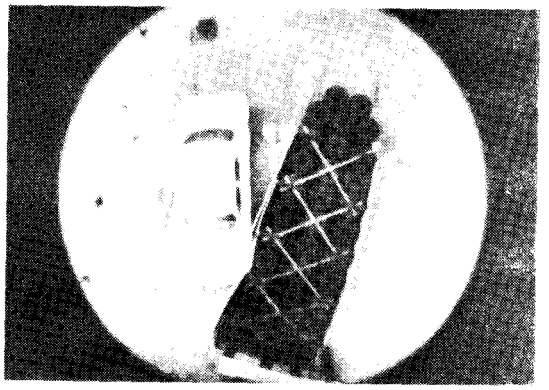

2

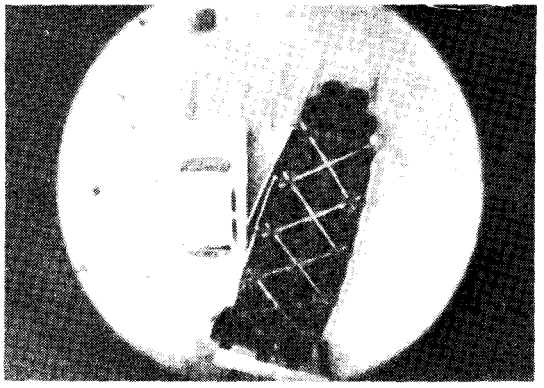

3

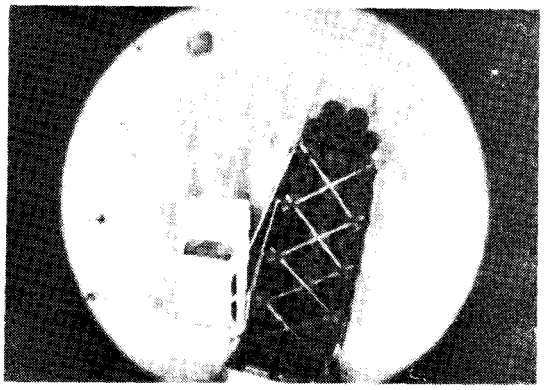

4

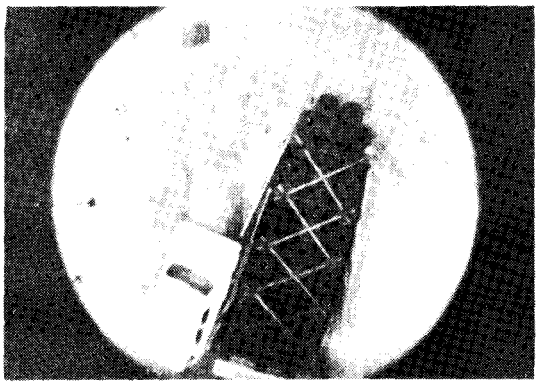

5

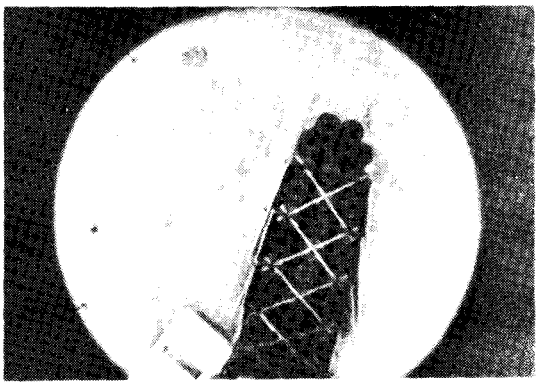

6

Figure 14, Sequential Photographs of Test 505 B-B.
(Overhead View)

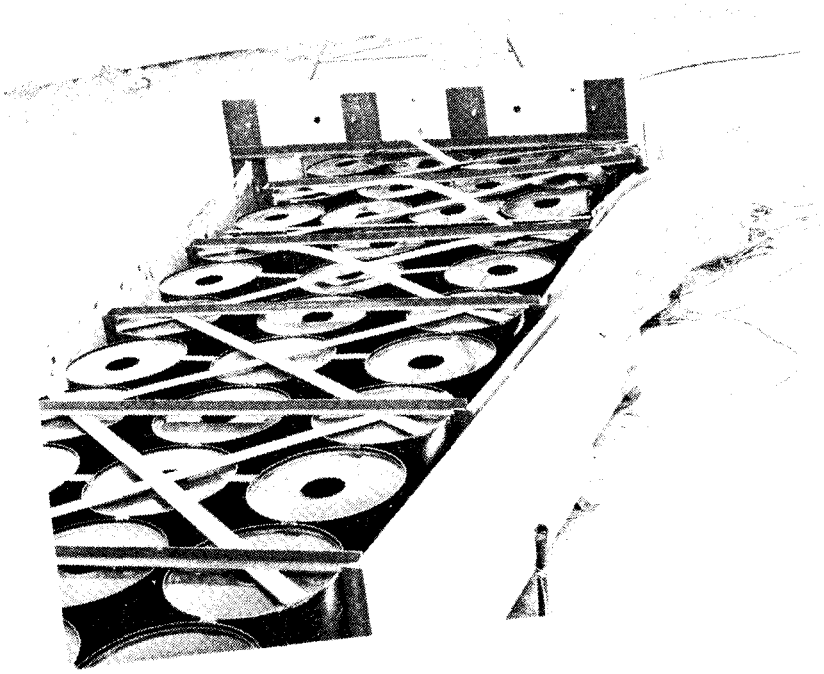

Figure 15. Impact Area After Test 505 B-B.

Test 505 B-C

After a few minor repairs were made, the same crash cushion used in Test B was subjected to a head-on crash test. The purpose of this test was to evaluate the longitudinal response of the modified barrier to a head-on collision. Lateral strength and stiffness had been built into the crash cushion for safe redirection of vehicles impacting at an angle. At the same time, however, this system had been designed to maintain its relatively soft, crushable characteristics for head-on impacts.

The barrier stopped the 4180 lb Pontiac, which was traveling 46.6 mph, in 11.7 ft with an average longitudinal deceleration of 6.2 g's. Deceleration levels were well within the limits considered tolerable to properly restrained humans.[5]

The system performed as designed. The vehicle damage was very minor as shown in Figure 17. Permanent vehicle front end deformation was only 2 inches. The headlights of the vehicle were not broken.

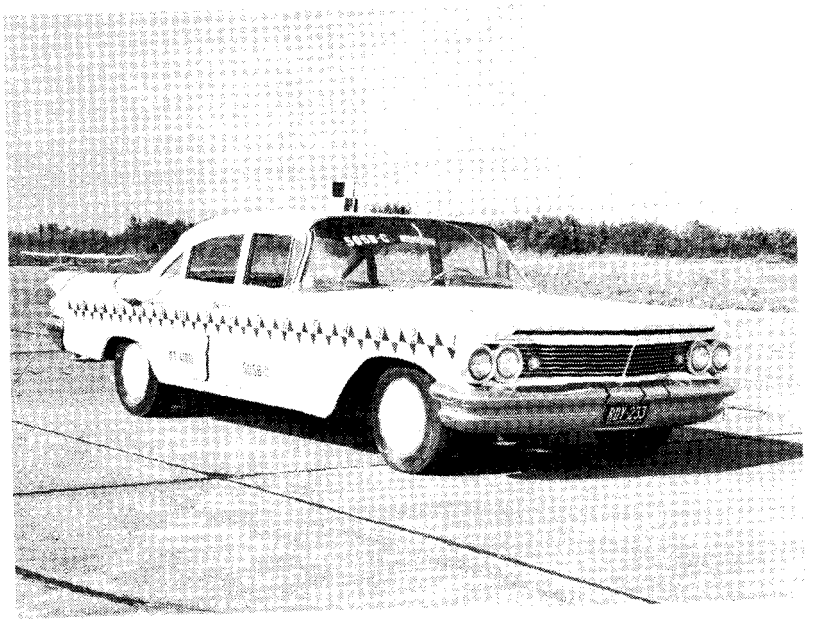

Figure 16, Vehicle Before Test 505 B-C.

Figure 17, Vehicle After Test 505 B-C.

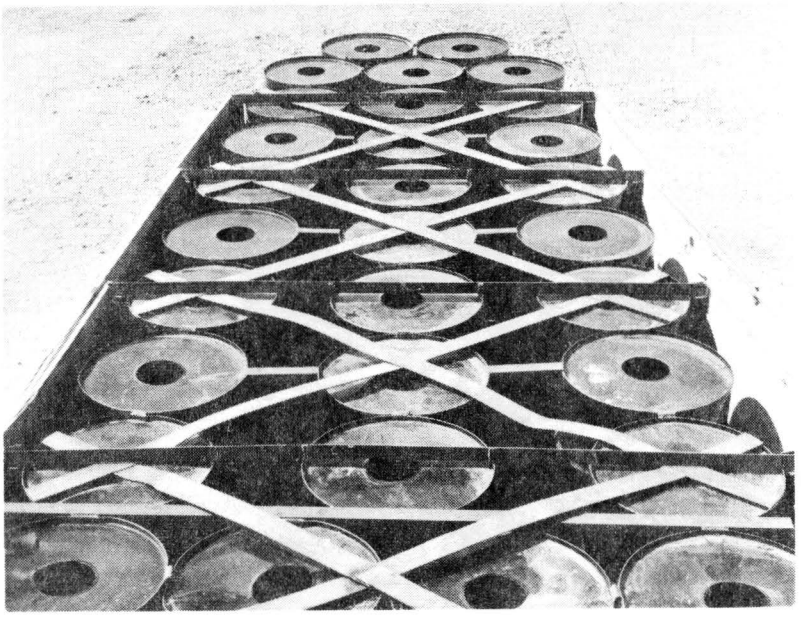

Figure 18, Repaired Modular Crash Cushion
Before Test 505 B-C.

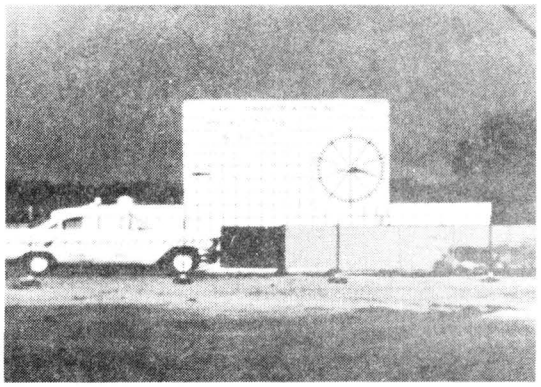

1

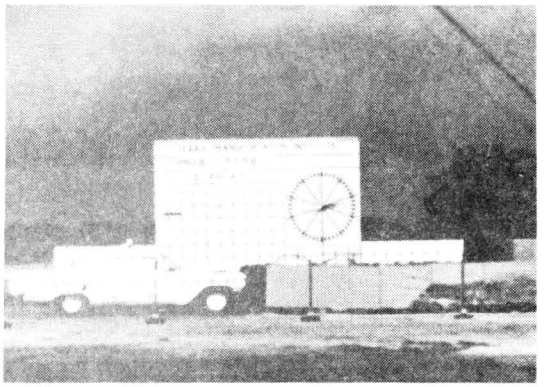

2

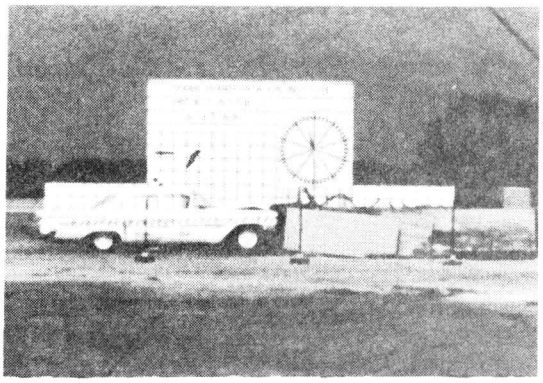

3

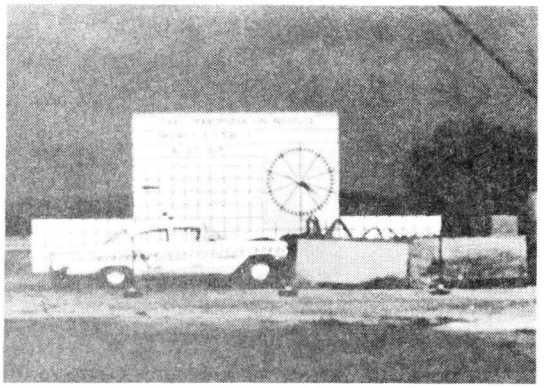

4

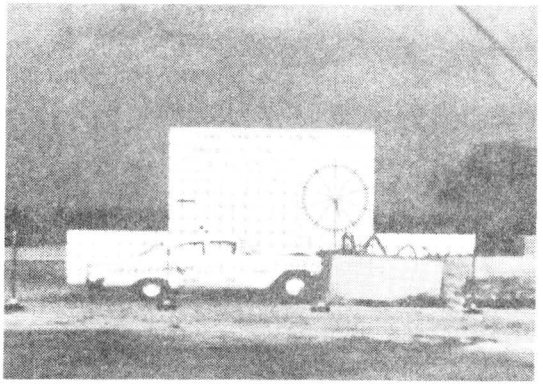

5

Figure 19, Sequential Photographs of Test 505 B-C.
(Side View)

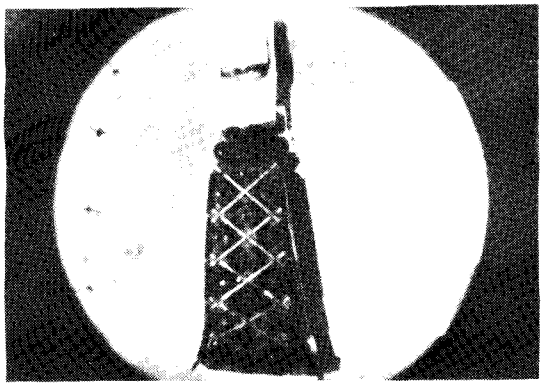

1

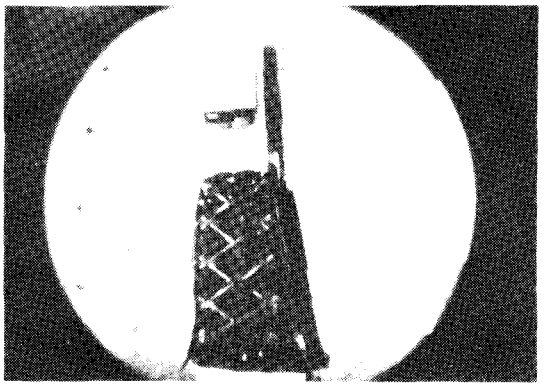

2

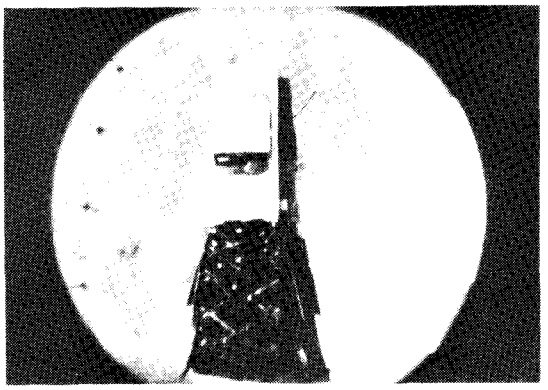

3

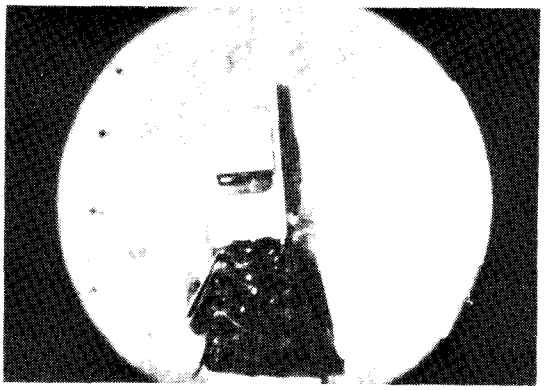

4

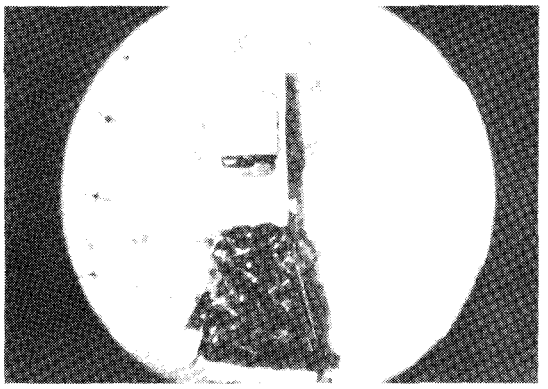

5

Figure 20, Sequential Photographs of Test 505 B-C.
(Overhead View)

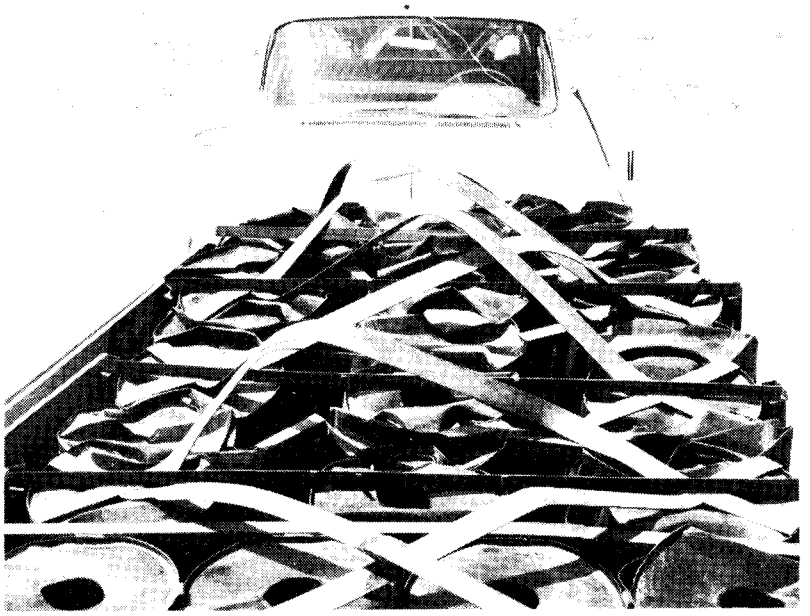

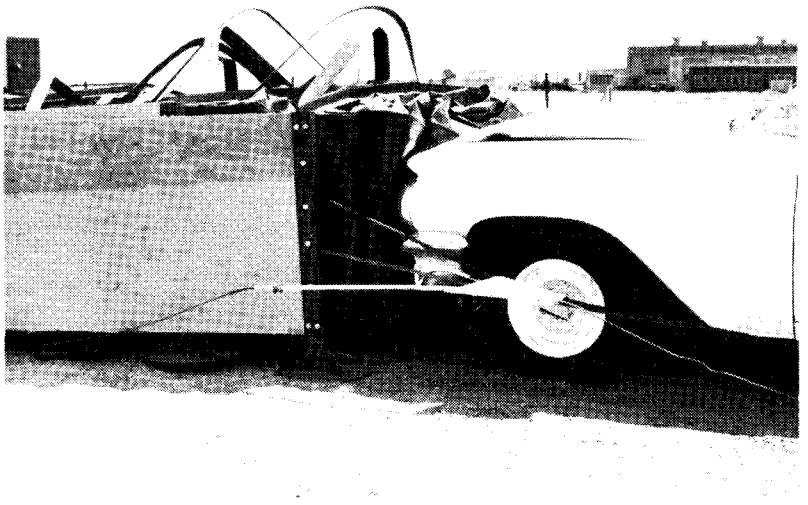

Figure 21, Vehicle and Crash Cushion After Test 505 B-C.

Test 505 B-D

Two modifications were made in the crash cushion used for this test. The rigid back-up wall was modified to simulate a tapered concrete retaining wall at an elevated freeway gore. This type of retaining wall makes it feasible to extend modules of the crash cushion along its sides. The configuration which was tested had modules extending along only the side which was hit, as modules along the opposite side would have been superfluous for the purposes of these tests. The straight, taut cables and overlapping plywood panels were believed to be sufficient for redirecting a vehicle without the use of the metal "truss" as used in tests B and C. In addition, the barrel modules were arranged in a more triangular shape to provide a softer nose for better head-on attenuation of small, lightweight vehicles.

A 20° angle side impact was conducted using a 1963 Buick which weighed 4350 lbs. The initial speed of the vehicle was 56.8 mph, and the vehicle remained in contact with the barrier for 624 msec. The average longitudinal deceleration from the accelerometer traces was 4.6 g's. Average lateral deceleration was 0.6 g's from the same source. A "ramping" tendency was observed; that is, the vehicle climbed up the side of the cushion to a height of about two feet due to a vertical component of force at the left front of the vehicle. However, the test vehicle remained upright throughout the test. A possible cause of the ramping may have been that the upper support cable, being longer than the lower cable, had more potential to displace transversely, allowing the deflection panels to lean slightly inward at the top.

During the time in contact, the cushion demonstrated sufficient lateral stability to prevent "pocketing" and to redirect the test vehicle. The barrier was damaged moderately, and the left front end of the vehicle was permanently deformed 3.25 ft (see Figures 23 and 27).

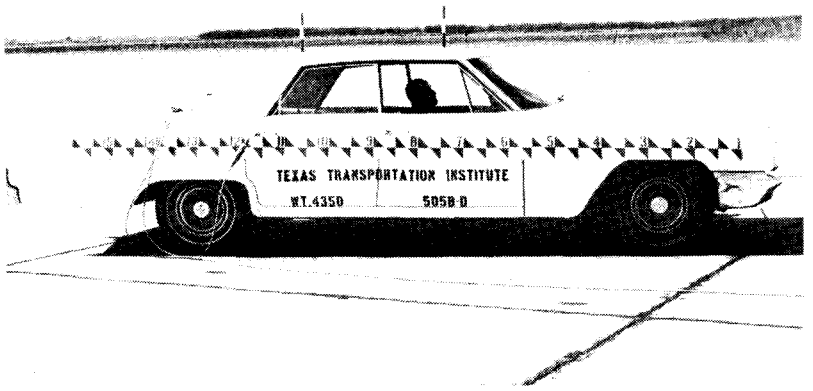

Figure 22, Vehicle Before Test 505 B-D.

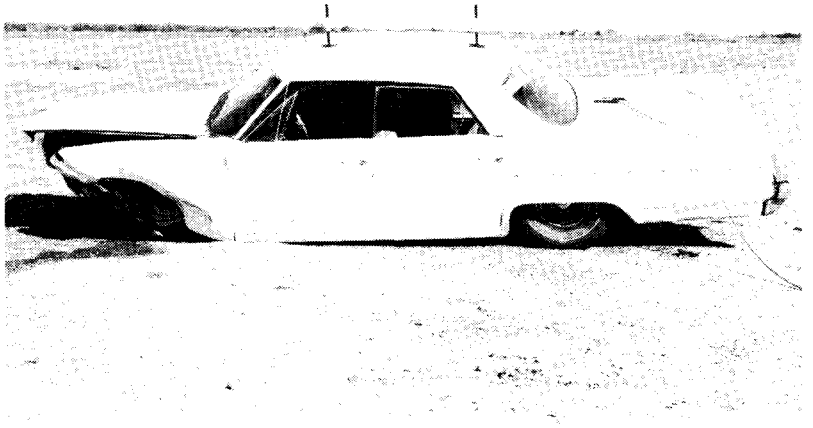

Figure 23, Vehicle After Test 505 B-D.

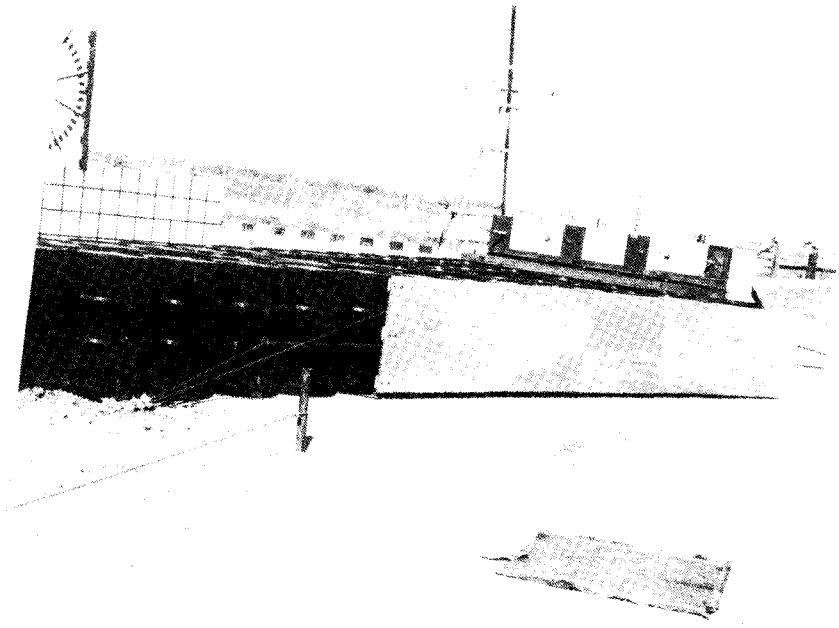

Figure 24, Modular Crash Cushion Before Test 505 B-D.

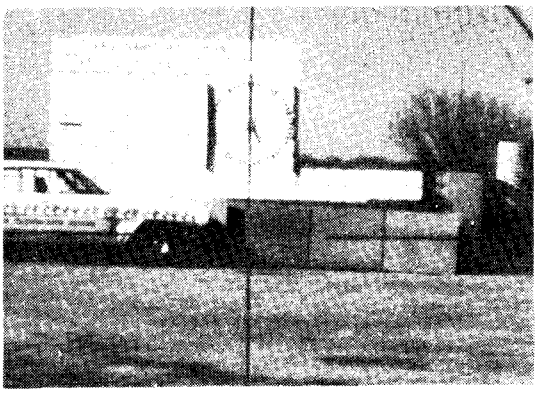

1

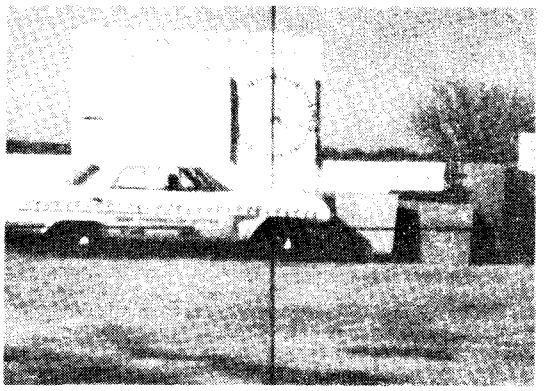

2

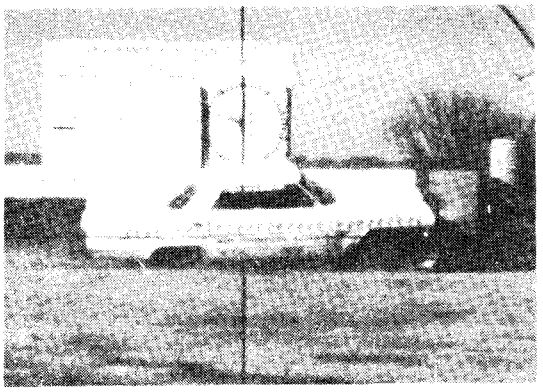

3

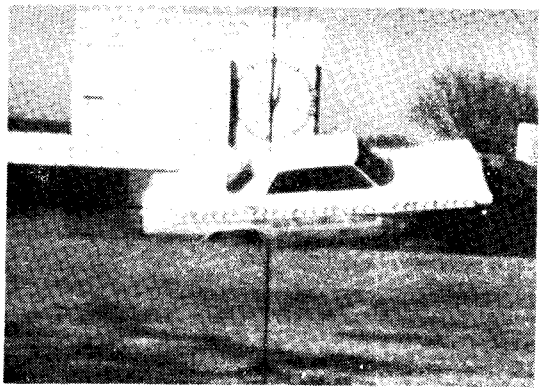

4

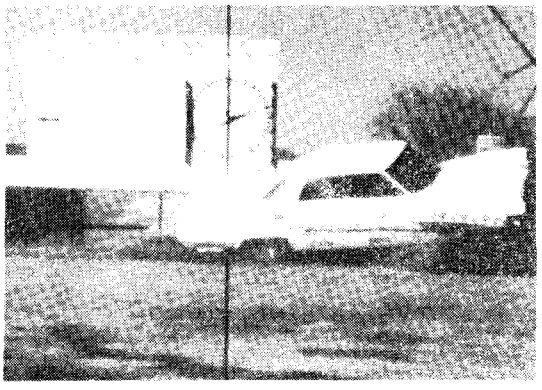

5

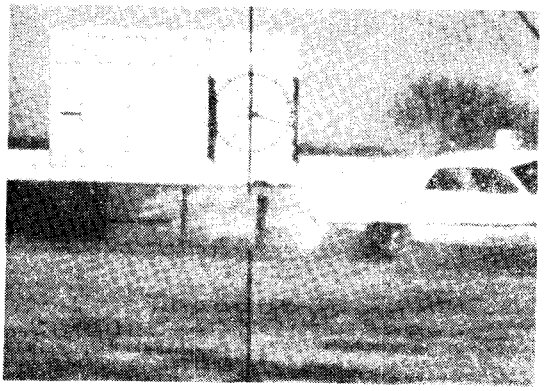

6

Figure 25, Sequential Photographs of Test 505 B-D. (Side View)

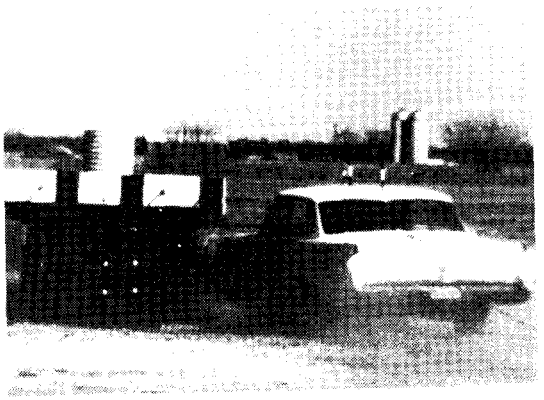

1

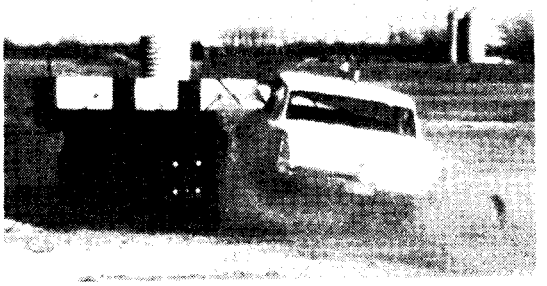

2

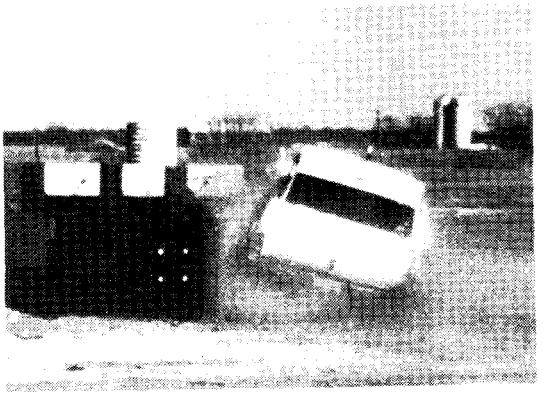

3

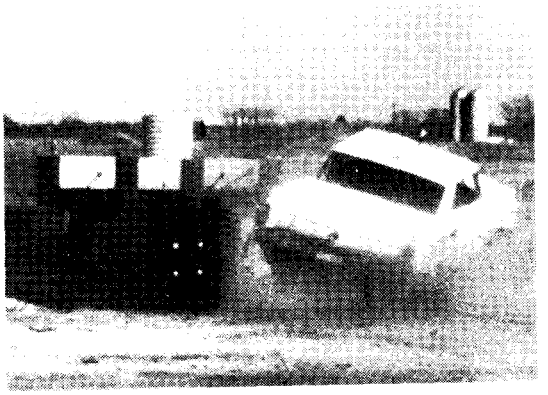

4

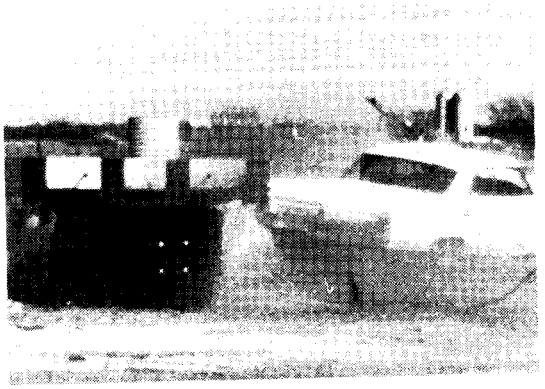

5

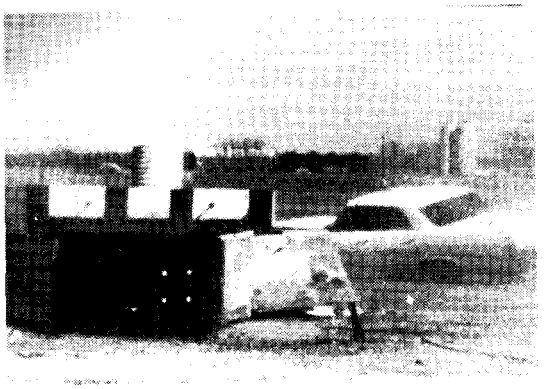

6

Figure 26, Sequential Photographs of Test 505 B-D.
(End View)

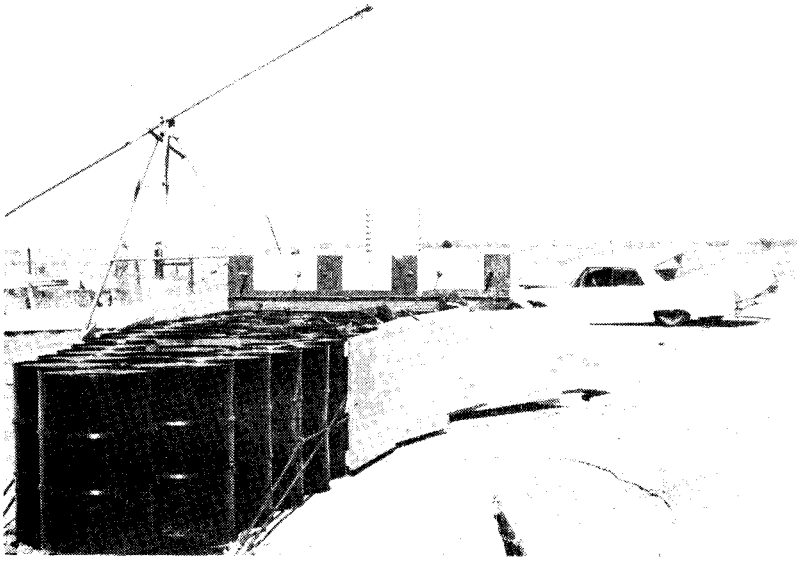

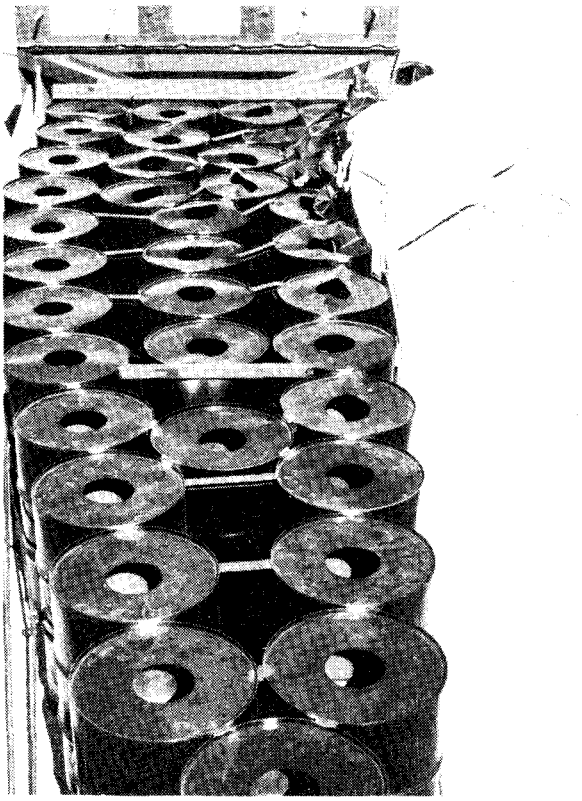

Figure 27, Modular Crash Cushion After Test 505 B-D.

Test 505 B-E

The purpose of this test was to evaluate the effectiveness of the previous barrier in head-on impacts with small vehicles. After minor repairs, the same cushion used in Test 505 B-D was hit by a 1959 Renault at 58.2 mph. This lightweight vehicle (1500 lbs) was stopped in 12.4 ft with an average longitudinal deceleration of 9.1 g's. The sheet metal portion of the front end of the vehicle was severely buckled, which would be expected in a lightweight, low front profile, rear-engine vehicle. The vehicle was stopped smoothly, without tendency to roll or spin.

The deceleration encountered by the lightweight vehicle (9.1 g's) was well below the FHWA Program criteria of 12 g's for research and development testing.[6]

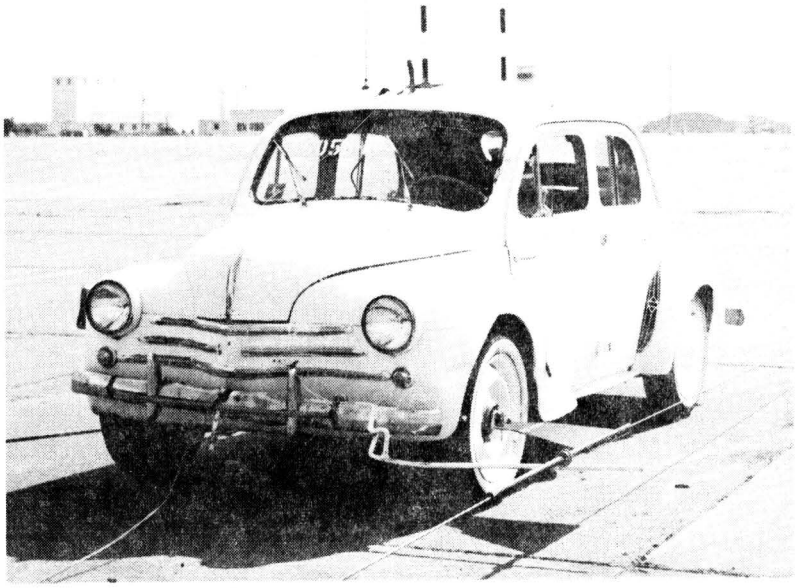

Figure 28, Vehicle Before Test 505 B-E.

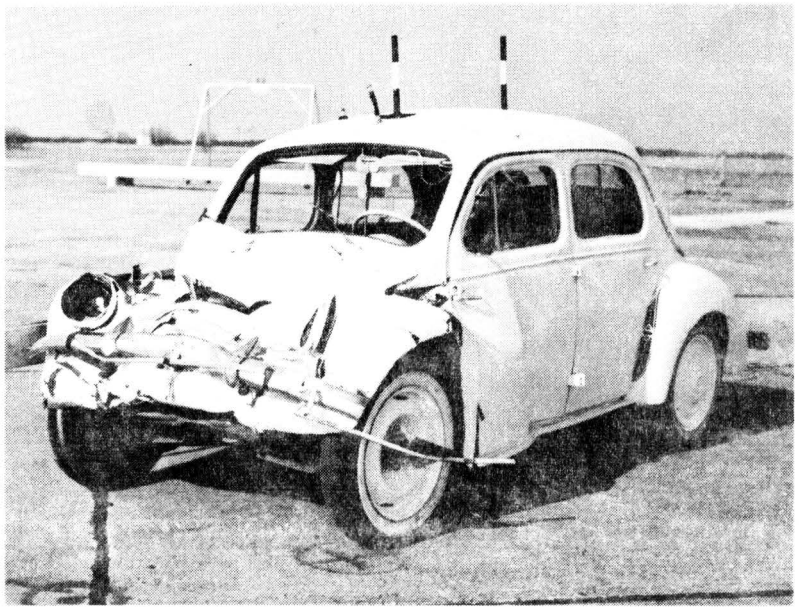

Figure 29, Vehicle After Test 505 B-E.

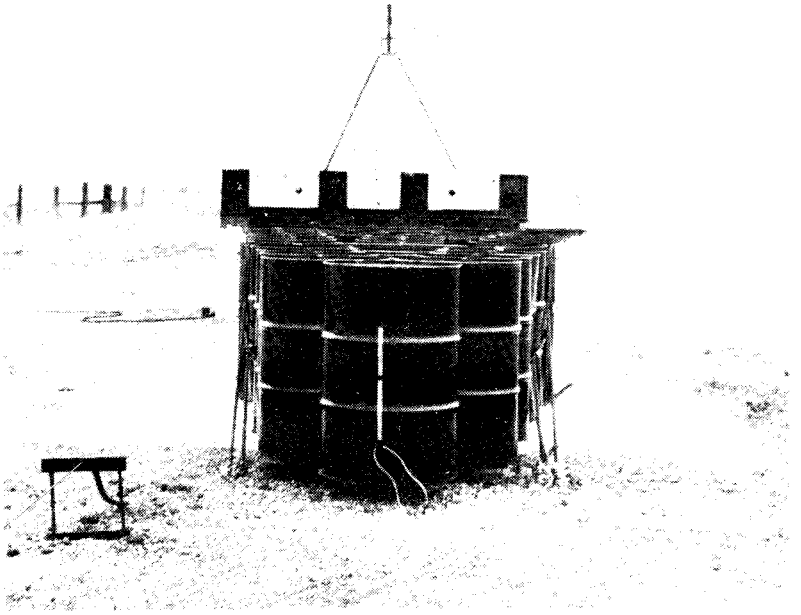

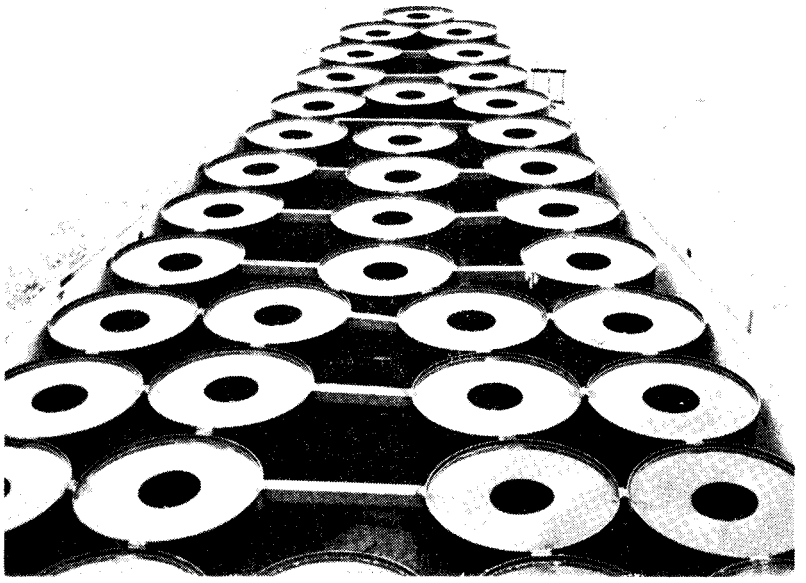

Figure 30. Modular Crash Cushion Before Test 505 B-E.

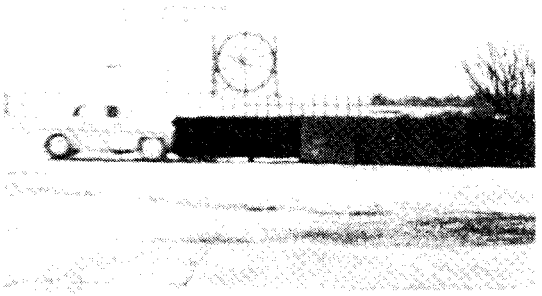

1

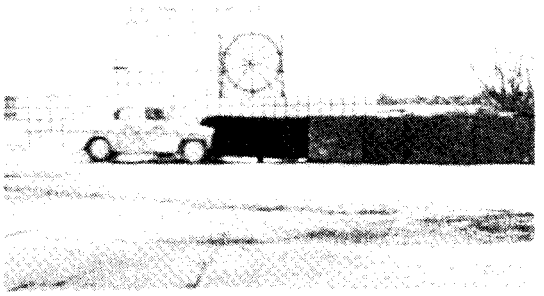

2

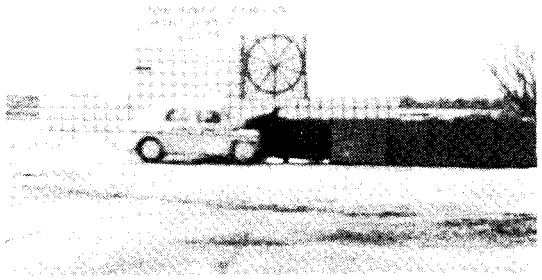

3

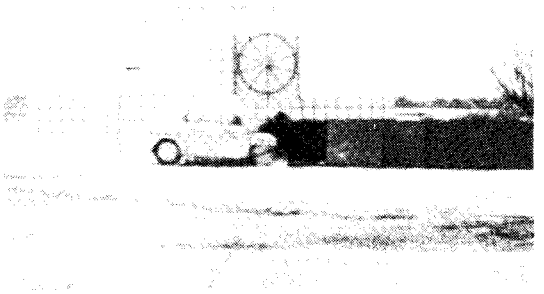

4

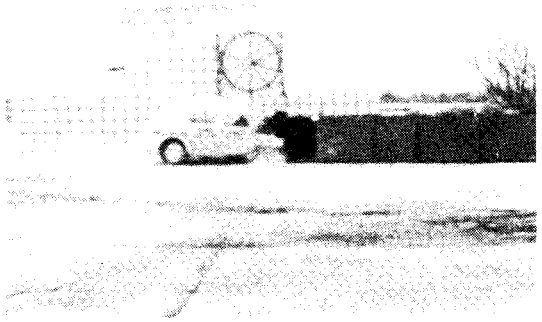

5

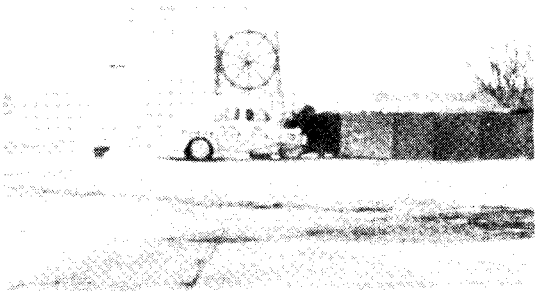

6

Figure 31, Sequential Photographs of Test 505 B-E.
(Side View)

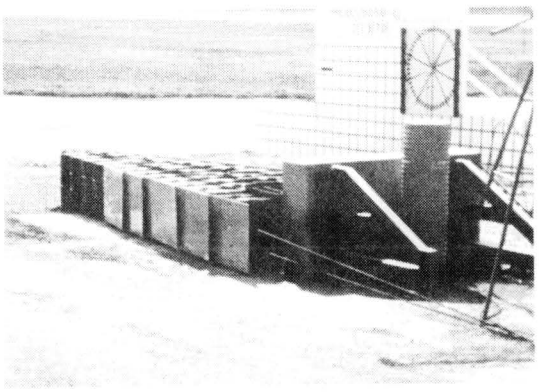

1

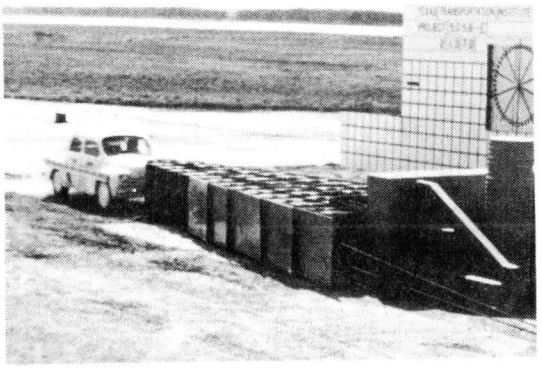

2

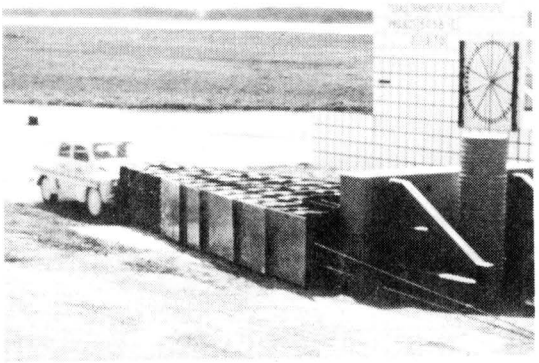

3

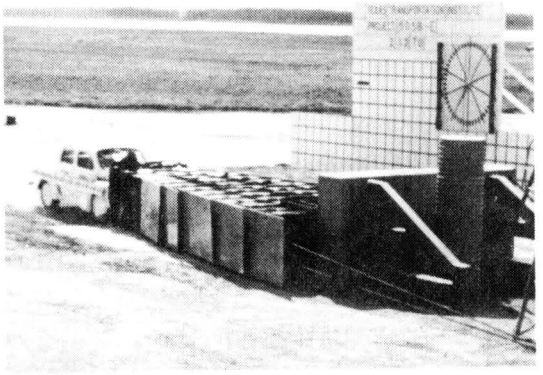

4

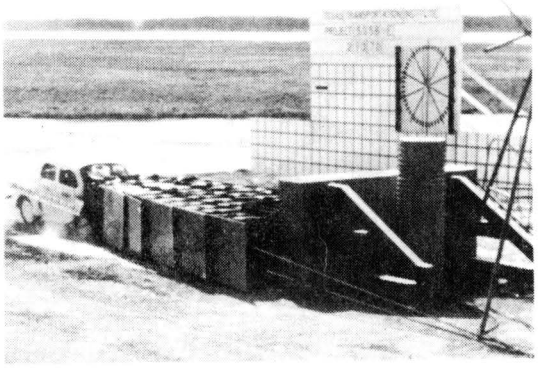

5

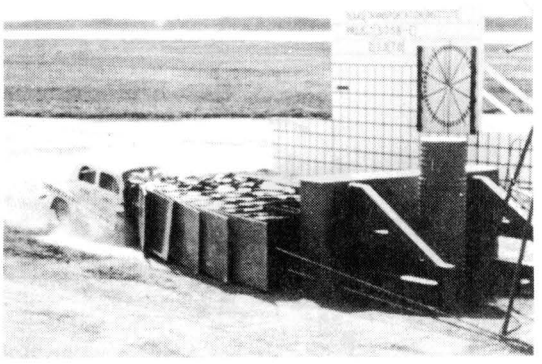

6

Figure 32, Sequential Photographs of Test 505 B-E.
(Oblique View)

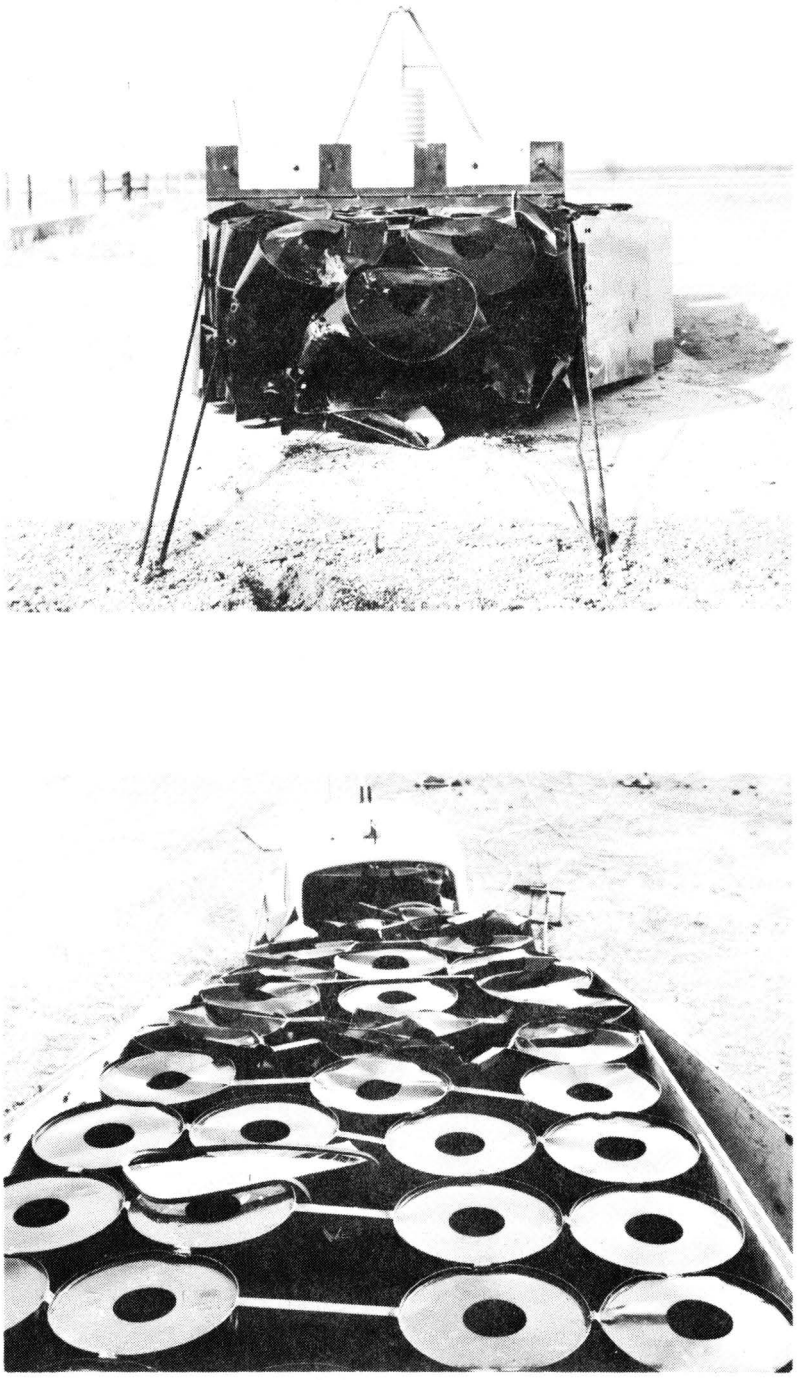

Figure 33, Modular Crash Cushion After Test 505 B-E.

DISCUSSION AND CONCLUSIONS

In order to redirect a vehicle which strikes the crash cushion at an angle and prevent it from contacting a rigid obstacle, the crash cushion must have lateral stability, present a smooth side surface, and be rather "hard" in the lateral direction to prevent vehicle pocketing. The more the side of the cushion is allowed to deform, the greater the angular redirection must be in order to prevent contact with the rigid backup wall. At the same time, the attenuator must not be constrained in the longitudinal direction in order to be acceptable for head-on or near head-on impacts in which all the vehicle kinetic energy must be absorbed.

The first attenuator tested in this series presented an acceptable redirectional surface, but because of the insufficient interior support by the anchor cables and because of the crushable plywood module spacers, it did not provide the necessary lateral strength or stability for redirection of the vehicle.

The second crash cushion design tested had sufficient lateral stability and strength, as well as a smooth redirectional surface, and the test vehicle was redirected without contacting the rigid wall. The redirection over a short time interval causes significant damage to the vehicle, somewhat comparable to the damage which would result from a guardrail or bridge rail collision. The forces measured were considered tolerable or acceptable for properly restrained passengers.

The subsequent head-on test on the repaired cushion showed that a relatively soft, crushable behavior was retained for head-on collisions.

The third crash cushion configuration also successfully redirected the vehicle during the angle impact. However, the absence of the "truss" on barrier type 3 reduces the weight of the structure and permits easier and more economical construction and maintenance.

The head-on test of the third crash cushion prototype utilized a lightweight, rear-engine vehicle. Although the damage to the vehicle's front end was severe, it was expected in this case since the engine was in the rear and only a light, sheetmetal luggage compartment protected the front end. Actually, this crushing too is part of the attenuation process. The passenger compartment was not penetrated. The g levels were not excessive considering the weight and speed of the test vehicle. The vehicle maintained a stable posture throughout the impact, with no overturning tendency.

It appears from this series of tests that for the Modular Crash Cushion lateral support adequate for vehicle redirection can be accomplished without sacrificing longitudinal attenuation. This can be achieved by using well anchored cables running in a straight line along the outside of the modules, with overlapping, hinged plywood panels outside these cables to provide the required lateral strength and stability. A similar redirectional system is in use on the HI-DRO Cushion and has performed satisfactorily on that type of barrier.[7]

SELECTED REFERENCES

1. Hirsch, T. J., "Barrel Protective Barrier", Technical Memorandum 505-1, Texas Transportation Institute, Texas A&M Research Foundation, a progress memorandum on Contract No. CPR 11-5851, U.S. Department of Transportation, Federal Highway Administration, Bureau of Public Roads, June 1968.
2. Hirsch, T. J. and Ivey, Don L., "Vehicle Impact Attenuation by Modular Crash Cushion," Research Report No. 146-1, Texas Transportation Institute, research study number 2-8-68-146 sponsored by The Texas Highway Department in cooperation with the U.S. Department of Transportation, Federal Highway Administration, Bureau of Public Roads, June 1969.
3. Hirsch, T. J., Ivey, Don L., and White, Monroe C., "The Modular Crash Cushion--Research Findings and Field Experience," *Highway Safety, Special Report 107*, Highway Research Board, Washington, D. C., 1970, pp. 140-148.
4. White, Monroe C., Ivey, Don L., and Hirsch, T. J., "In-Service Experiences on Installations of Texas Modular Crash Cushions," Research Report 146-2, Texas Transportation Institute, research study number 2-8-68-146 sponsored by the Texas Highway Department in cooperation with the U.S. Department of Transportation, Federal Highway Administration, Bureau of Public Roads, July 1970.
5. Damon, Albert; Stoudt, Howard W.; and McFarland, Ross A., *The Human Body in Equipment Design*, Harvard University Press, Cambridge, Massachusetts, 1966.

6. Tamanini, F. J. and Viner, John G., "Structural Systems in Support of Highway Safety." ASCE Meeting Preprint 930, July 21-25, 1969.

7. Hayes, Gordon G., Ivey, Don L. and Hirsch, T. J., "Performance of the 'HI-DRO Cushion' Vehicle Impact Attenuator," Technical Memorandum 505-11, Texas Transportation Institute, Texas A&M University, August 1970.

A P P E N D I X

TABLE A1

TEST 505 B-A

High-Speed Film Data

Time (milliseconds)	Displacement (feet)	Time (milliseconds)	Displacement (feet)
-48.0	-4.0	(continued)	
-36.0	-3.0	200.0	13.6
-24.0	-2.0	250.0	14.6
-12.0	-1.0	300.0	16.0
0 Impact	0	350.0	15.8
20.0	1.6	400.0	15.6
50.0	4.0	450.0	15.3
60.0	4.7	500.0	15.1
80.0	6.2	600.0	14.6
100.0	7.6	700.0	14.1
120.0	8.9	800.0	13.7
140.0	10.2	900.0	13.3
160.0	11.4	1000.0	13.1
180.0	12.6	1400.0	13.0

TABLE A2

TEST 505 B-B

High-Speed Film Data

Time (milliseconds)	Displacement (feet)	Time (milliseconds)	Displacement (feet)
-30.0	-2.6	(continued)	
-20.0	-1.7	160.0	10.9
-10.0	-0.9	180.0	11.7
0 Impact	0	200.0	12.3
10.0	0.9	220.0	13.0
20.0	1.8	240.0	13.7
30.0	2.6	260.0	14.5
40.0	3.4	280.0	15.2
50.0	4.2	300.0	16.0
60.0	5.0	320.0	16.8
70.0	5.7	340.0	17.6
80.0	6.4	360.0	18.4
90.0	7.1	380.0	19.2
100.0	7.7	400.0	20.0
120.0	8.9	420.0	20.9
140.0	10.0		

TABLE A3

TEST 505 B-C

High-Speed Film Data

Time (milliseconds)	Displacement (feet)	Time (milliseconds)	Displacement (feet)
-50.8	-3.4	(continued)	
-40.6	-2.8	101.5	6.0
-30.4	-2.1	121.8	6.9
-20.3	-1.4	142.1	7.8
-10.2	-0.7	162.4	8.5
0 Impact	0	182.7	9.1
10.2	0.7	203.0	9.7
20.3	1.4	223.3	10.2
30.4	2.0	243.6	10.6
40.6	2.7	263.9	11.0
50.8	3.3	284.2	11.2
60.9	3.9	304.5	11.5
71.0	4.4	324.8	11.6
81.2	5.0	345.1	11.7
91.4	5.5	365.4	11.7

TABLE A4

TEST 505 B-D

High-Speed Film Data

Time (milliseconds)	Displacement (feet)	Time (milliseconds)	Displacement (feet)
-49.7	-4.1	(continued)	
-41.4	-3.4	216.7	14.4
-33.2	-2.7	236.4	15.2
-24.9	-2.1	256.1	15.8
-16.6	-1.4	275.8	16.2
- 8.3	-0.7	295.5	16.7
0 Impact	0	315.2	17.2
9.8	0.8	334.9	17.6
19.7	1.5	354.6	18.0
29.6	2.3	374.3	18.3
39.4	3.1	394.0	18.8
49.2	3.8	413.7	19.2
59.1	4.6	433.4	19.7
69.0	5.3	453.1	20.1
78.8	6.1	512.2	21.6
88.6	6.8	571.3	23.1
98.5	7.5	630.4	24.8
118.2	8.8	689.5	26.4
137.9	10.2	748.6	28.0
157.6	11.4	807.7	29.7
177.3	12.5	866.8	31.3
197.0	13.5	925.9	32.7

TABLE A5

TEST 505 B-E

High-Speed Film Data

Time (milliseconds)	Displacement (feet)	Time (milliseconds)	Displacement (feet)
-48.6	-4.1	(continued)	
-36.4	-3.1	97.2	7.2
-24.3	-2.1	121.5	8.6
-12.2	-1.0	145.8	9.7
0 Impact	0	170.1	10.6
12.2	1.0	194.4	11.2
24.3	2.0	218.7	11.7
36.4	3.0	243.0	12.1
48.6	3.9	267.3	12.3
60.8	4.7	291.6	12.4
72.9	5.6	315.9	12.3
85.1	6.4	340.2	12.2

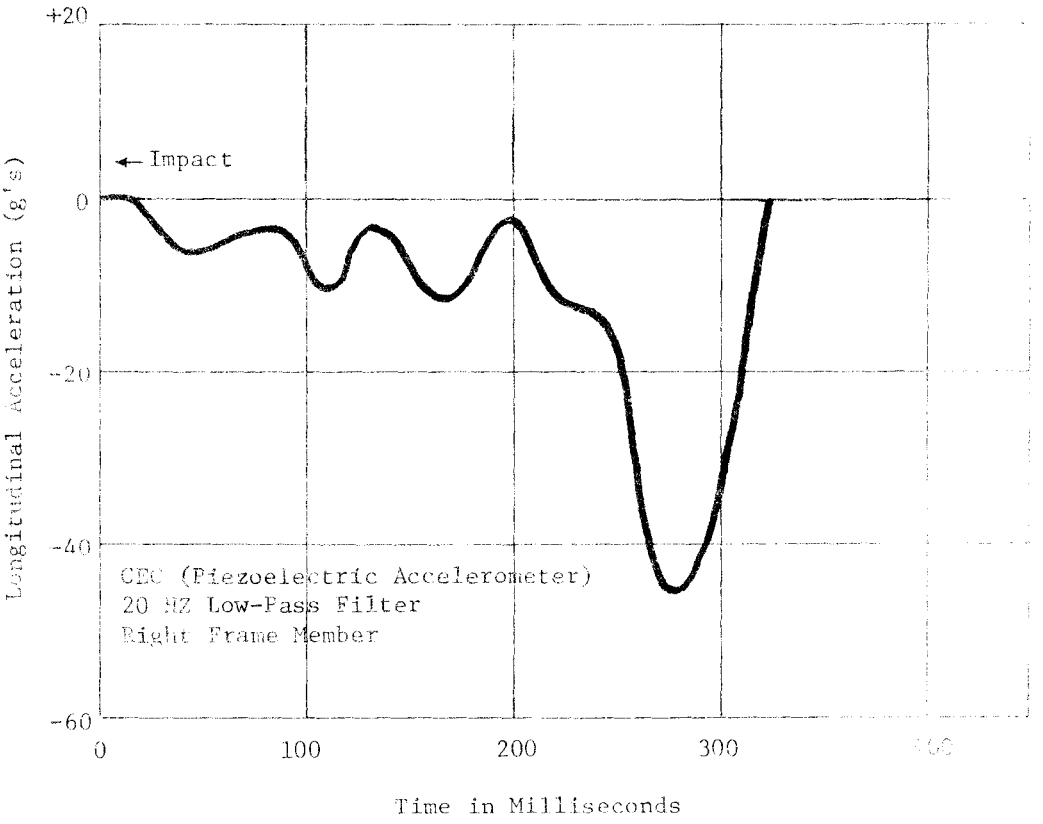

Figure A1, Longitudinal Accelerometer Data, Test 505 R-A

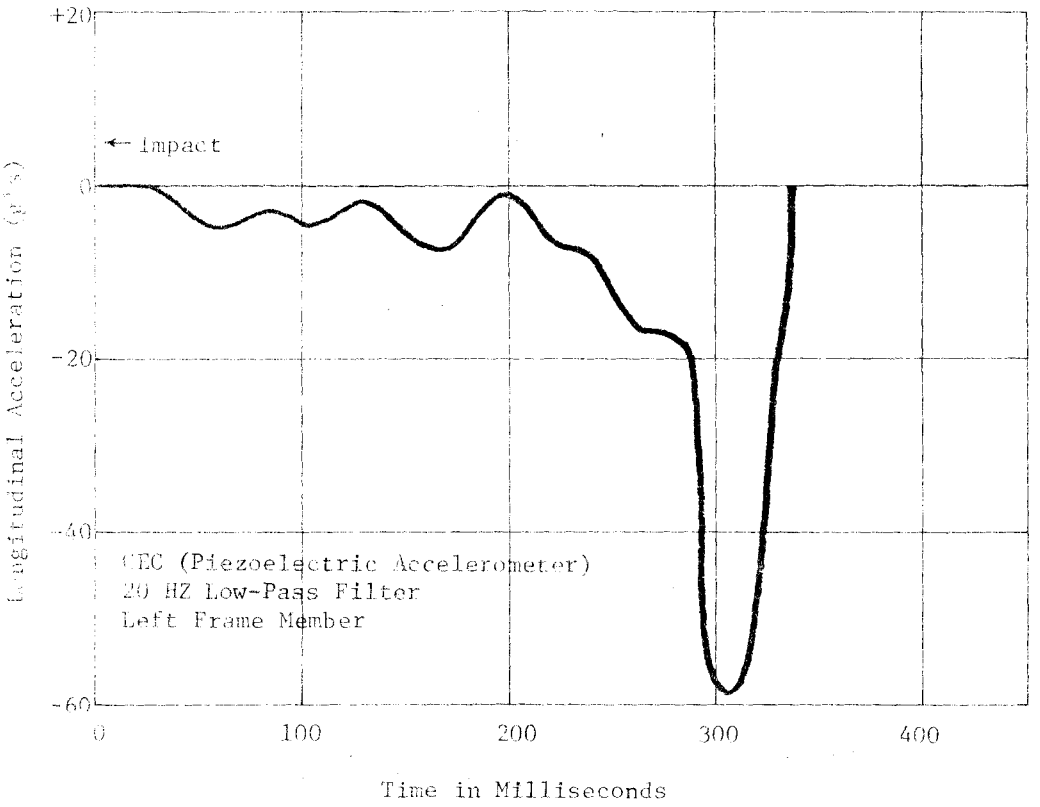

Figure A2, Longitudinal Accelerometer Data, Test 505 B-A.

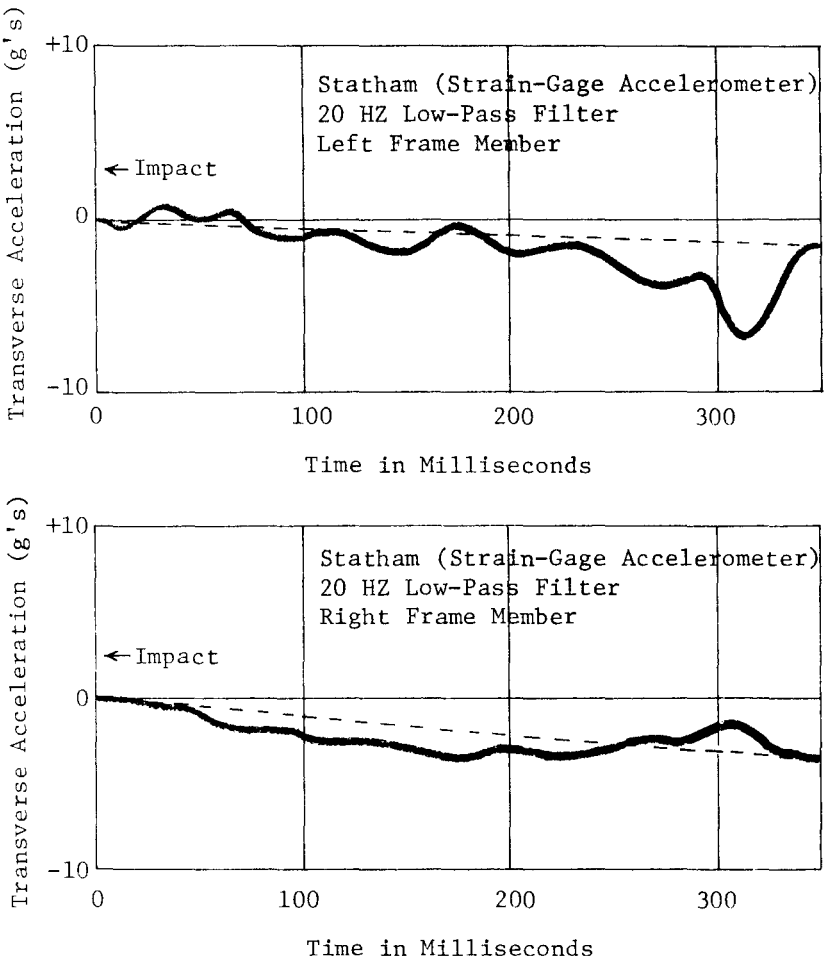

Figure A3, Transverse Accelerometer Data, Test 505 B-A.

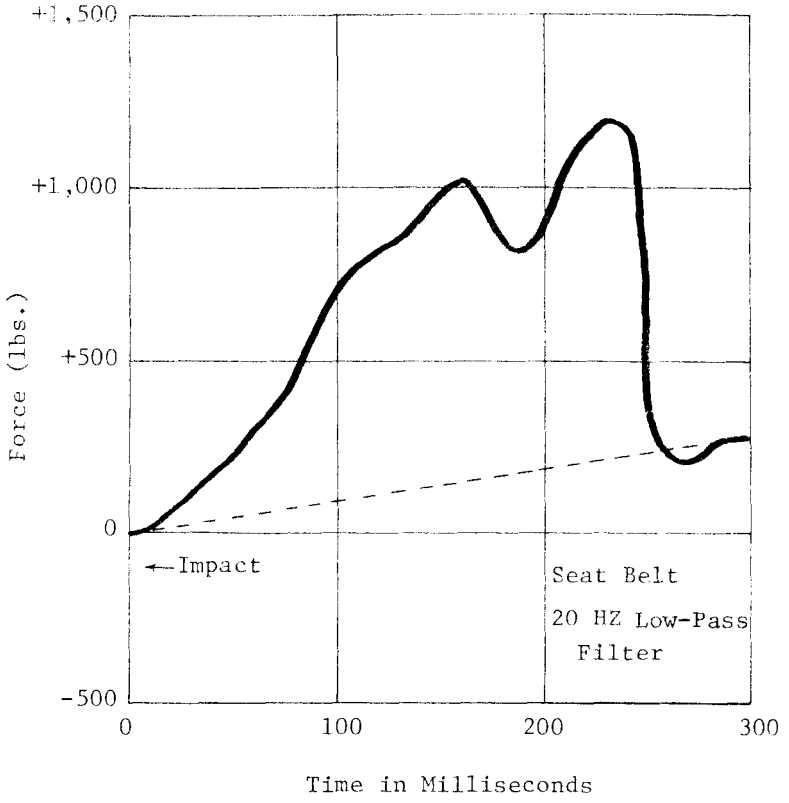

Figure A4, Seat Belt Data, Test 505 B-A.

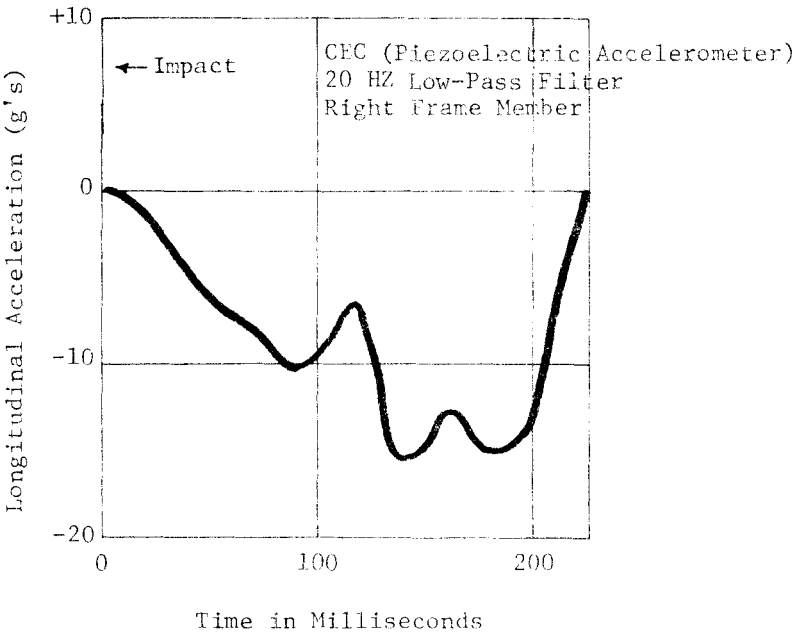

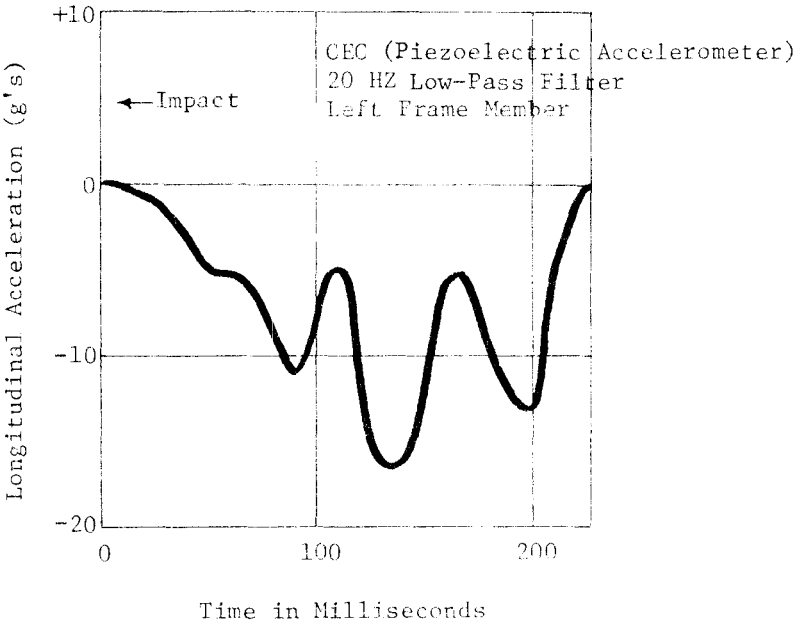

Figure A5, Longitudinal Accelerometer Data, Test 505 B-B.

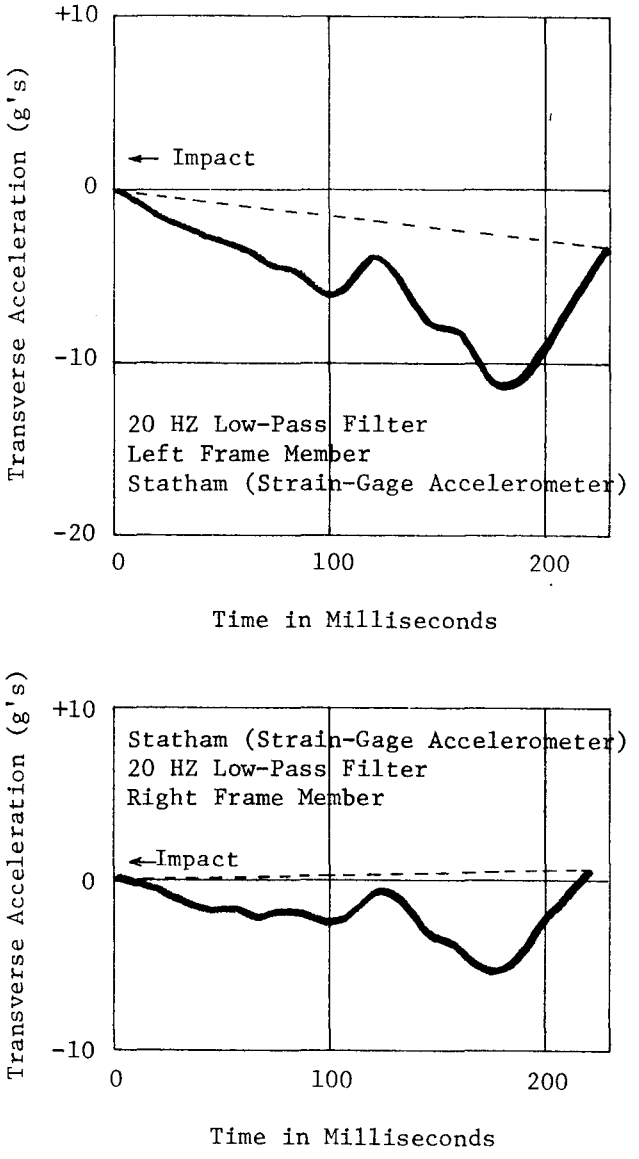

Figure A6, Transverse Accelerometer Data, Test 505 B-B.

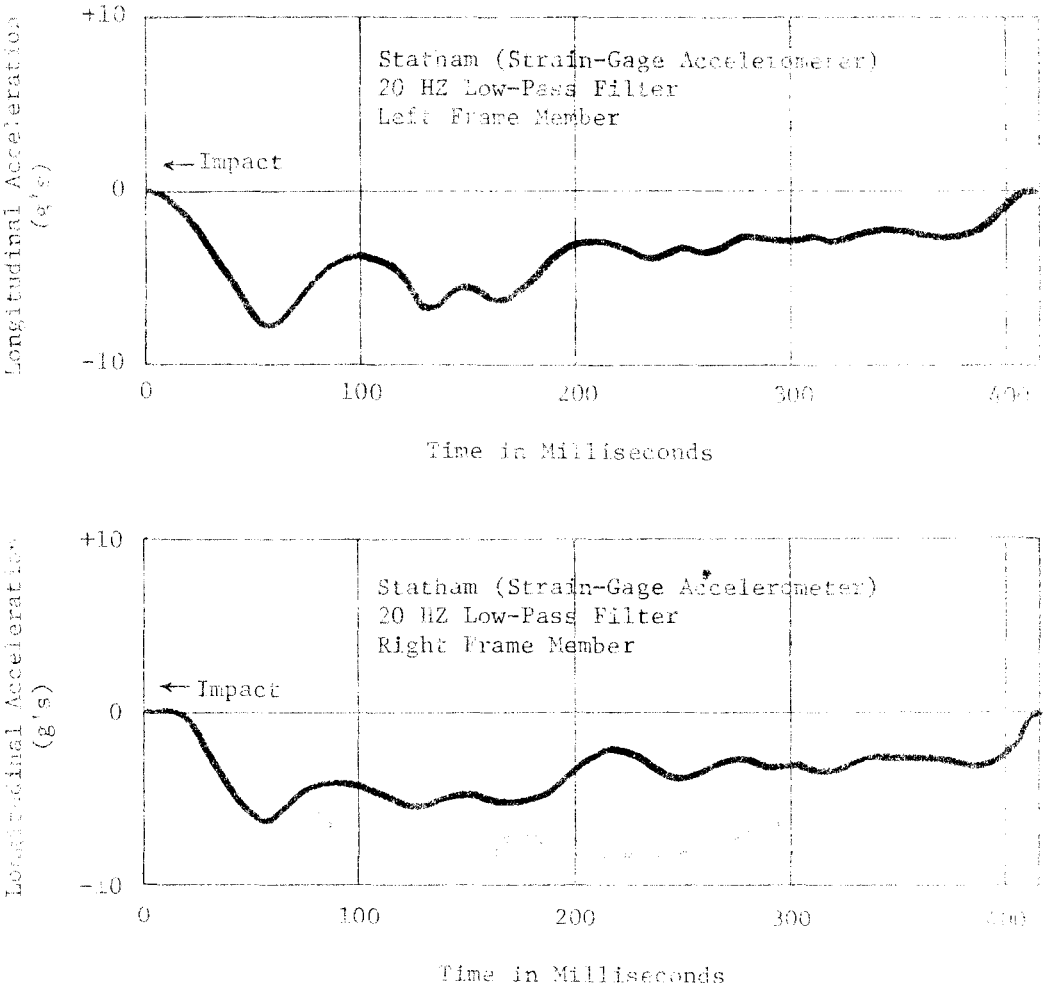

Figure A7, Longitudinal Accelerometer Data, Test 30[illegible]

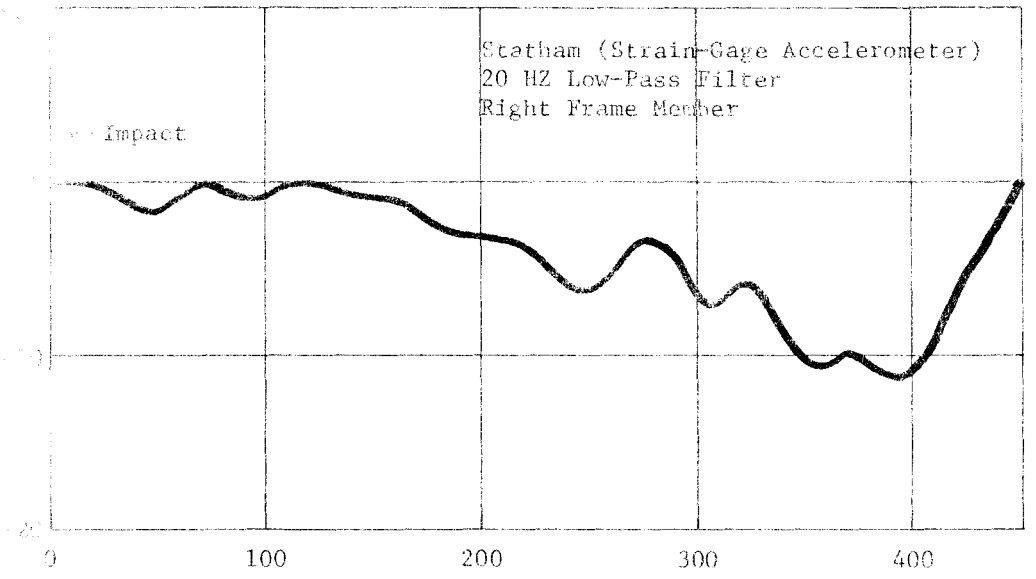

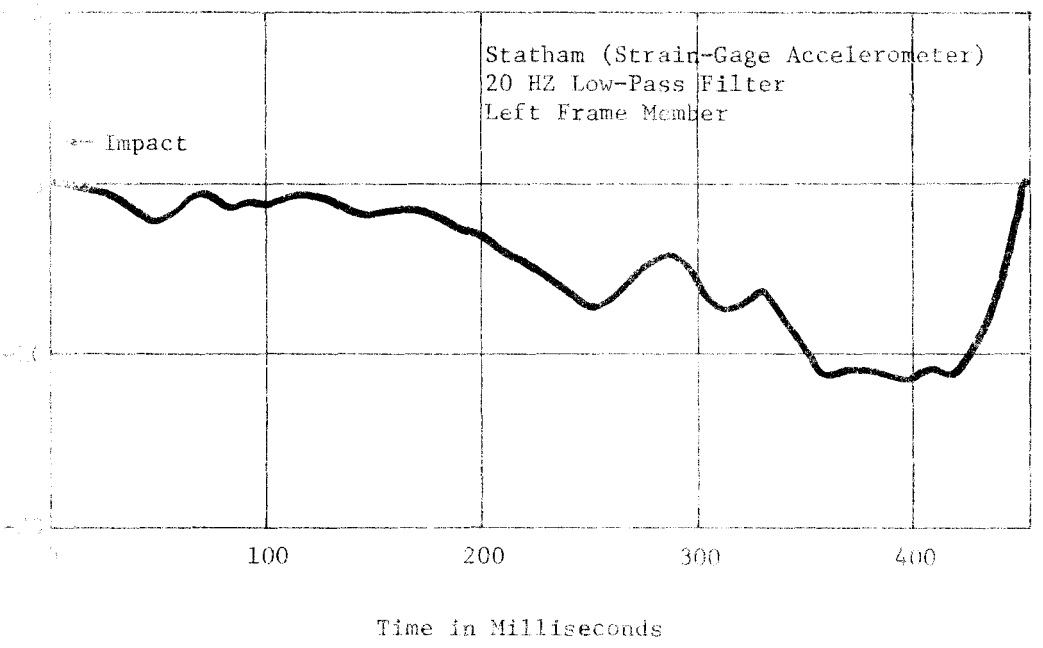

Figure A8, Longitudinal Accelerometer Data, Test 505 B-D.

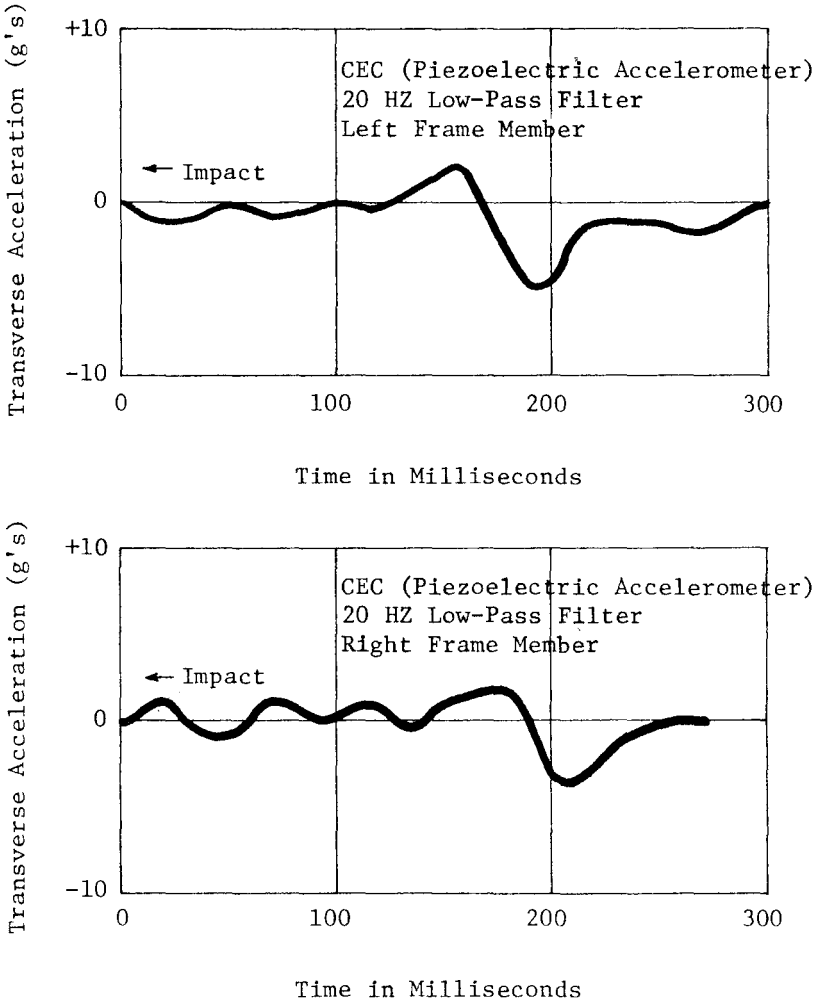

Figure A9, Transverse Accelerometer Data, Test 505 B-D.

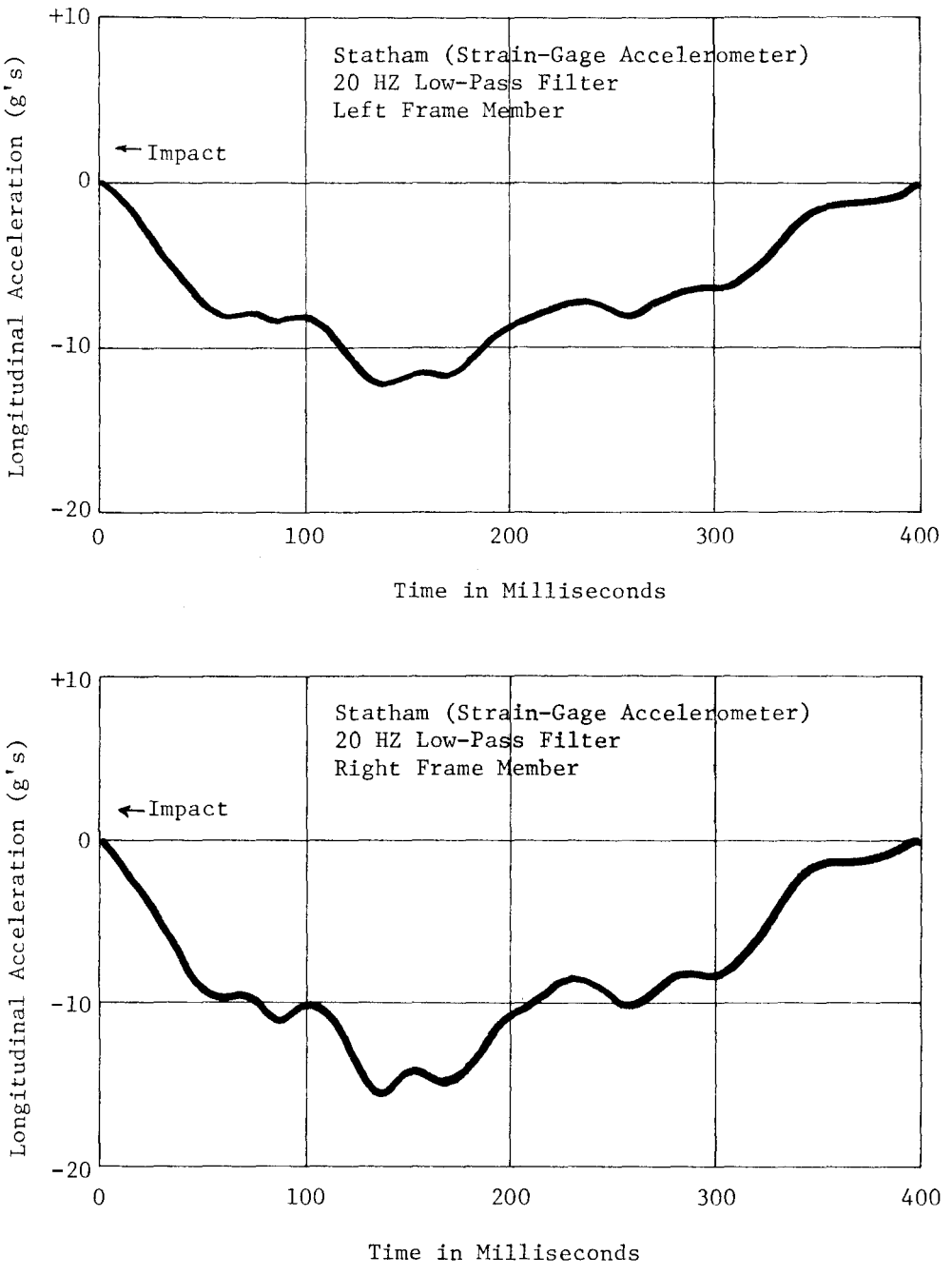

Figure A10, Longitudinal Accelerometer Data, Test 505 B-E.

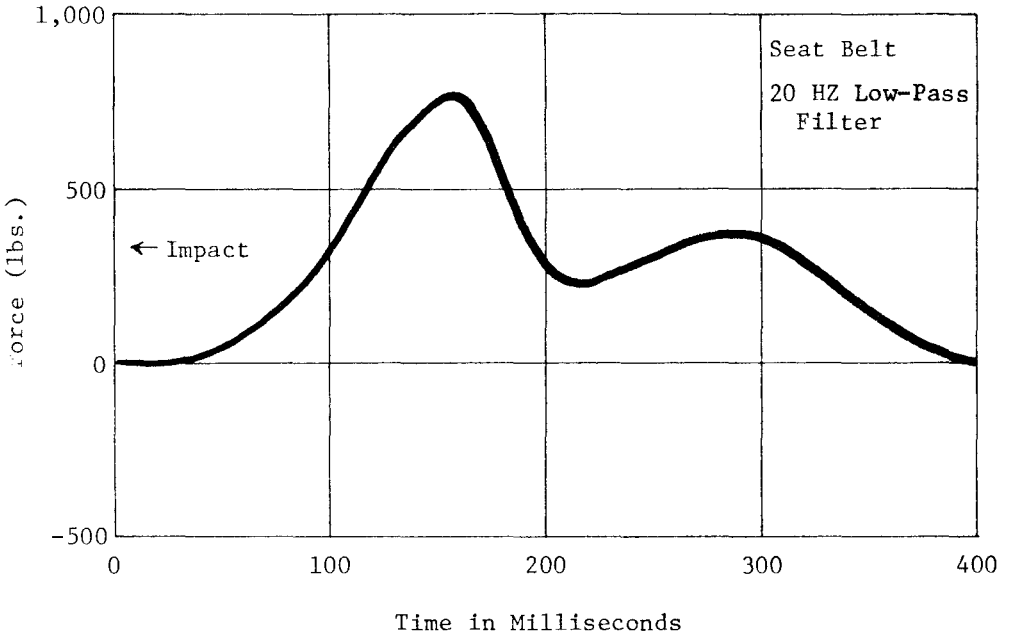

Figure All, Seat Belt Data, Test 505 B-E.

TECHNICAL MEMORANDUM 505-2

Texas Transportation Institute
Texas A&M Research Foundation

TOR-SHOK ENERGY ABSORBING PROTECTIVE BARRIER

A Tentative Progress Memorandum on Contract No. CPR-11-5851, U. S. Dept. of Transportation, Federal Highway Administration, Bureau of Public Roads

by

T. J. Hirsch, Research Engineer and Principal Investigator
Structural Research Department
Texas Transportation Institute

July 31, 1968

INTRODUCTION

From November 14, 1967 to January 10, 1968, the Texas Transportation Institute conducted four full-scale vehicle crash tests on the TOR-SHOK energy absorbing highway protective system which was developed by Aerospace Research Associates (ARA), Inc., of 2017 West Garvey Avenue, West Covina, California. This Technical Memorandum is being written to provide some of the technical information and crash performance of this vehicle impact attenuation system.

Included are photographs of the vehicle and barrier before and after each of the four crash tests. Also included is a summary of the high

speed motion picture film data taken of the tests, giving the vehicle impact velocity, average deceleration, peak deceleration, stopping distance, etc. (see Appendix B). In addition, a summary of the electromechanical instrumentation data which was collected during the tests is included (see Appendix B).

BARRIER DESCRIPTION

The TOR-SHOK energy absorbing barrier was developed by ARA, Inc. under a contract with the Bureau of Public Roads. The barrier was fabricated, delivered, and installed by ARA, and the vehicle crash tests were conducted by personnel of the Texas Transportation Institute. This highway protective system (see Figure 1) is constructed of high strength, lightweight steel tubes which are supported from the fixed object by a number of TOR-SHOK attenuators (detailed description given in Appendix A). At impact, the protective barrier tubes transmit the impact forces axially to the cylindrical TOR-SHOK arms which contain a large number of stainless steel "torus" elements that are squeezed between two cylindrical tubes. At impact these "torus" elements absorb the energy by rolling between the cylinders. Eight of the twelve TOR-SHOK arms are acting in tension while four others are acting in compression. These TOR-SHOK arms exert a stopping force on the vehicle as the barrier deforms under the vehicle collision.

Supplementary data on the TOR-SHOK energy absorbing system is presented in Appendix A. This information was provided by ARA, Inc. Drawings B1450 and B1449 in Appendix A show the dimensions and configuration of the barrier tested. Table 1 in Appendix A gives a summary

of the characteristics of the TOR-SHOK barrier. The barrier tested by TTI had a nose angle of 15°, a nose radius of 31 in., and the weight of the tubular nose was 845 lbs.

TEST PROGRAM

A brief description of the four crash tests conducted is given in Table 1. Test 2A was a head-on impact with a 4600 lb vehicle going at a relatively slow speed, 34 mph. Tests 2B and 2C were both head-on impacts at relatively high speeds, 54 mph and 60 mph, respectively. In Test 2B, a lightweight vehicle weighing 2520 lbs was used, while in Test 2C a heavy vehicle weighing 4940 lbs was used. Test 2D was impacted at an angle of 30° with the longitudinal axis of the barrier with a heavy vehicle weighing 5000 lbs and traveling at a speed of 50 mph.

TEST 2A RESULTS

Figures 1 through 4 show the vehicle and barrier before and after impact for Test 2A. Figure 5 shows an idealized stopping force which the TOR-SHOKs will exert on the impacting vehicle during a head-on collision for various barrier deformations. This force-deformation curve was developed using data presented in Appendix A. Table 2 presents a brief summary of the test results for the head-on impact. It can be seen that the 4600 lb vehicle in Test 2A deformed the barrier 4.48 ft. The maximum TOR-SHOK stopping force was thus approximately 48 kips. From Table 2, it can be seen that the TOR-SHOKs absorbed 163 kip-ft of the vehicle kinetic energy (approximately 91%). The

average deceleration during this impact was 6.6 g's, and the maximum significant deceleration was approximately 13 to 14 g's. This average deceleration was obtained from an analysis of the high speed movies. A more complete summary of the crash test data gathered from the high speed film and electromechanical devices is presented in Appendix B, Table 1B.

An analysis of the crash test results and the photographs presented in Figures 1 through 4 indicate the following conclusions concerning Test 2A:

1. The ARA TOR-SHOK barrier performed as designed.
2. The vehicle damage was relatively minor.
3. The barrier damage was relatively minor. Minor maintenance was required; however, the barrier nose and TOR-SHOKs were reusable.
4. The deceleration level was considered moderate.

Table 3 presents a comparison of the ARA TOR-SHOK impact performance with a "rigid" barrier impact. If the 4600 lb vehicle used in Test 2A had struck a "rigid" wall, the estimated maximum deceleration would have been 30.8 g's; and the estimated average deceleration, 19.6 g's. Using these maximum and average decelerations of a "rigid" barrier impact, the maximum and average decelerations from the ARA TOR-SHOK impact can be compared by taking a ratio which will be defined as Attenuation Index (AI). From Table 3, it can be seen that the Attenuation Index for Test 2A ranged from 0.34 to 0.44 for the average and maximum deceleration, respectively. This Attenuation Index is presented

TABLE 1.

BRIEF DESCRIPTION OF TEST PROGRAM

ON ARA TORSHOK BARRIER

Test Number	2A	2B	2C	2D
Angle of Attack	Head-on	Head-on	Head-on	30°
Vehicle Weight (w)	4600 lb.	2520 lb.	4940 lb.	5000 lb.
Speed (V)	34.1 mph	53.5 mph	59.4 mph	49.9 mph
Kinetic Energy of Vehicle (K.E.)	179 Kip-ft	242 Kip-ft	582* Kip-ft	418 Kip-ft

*Note: The ARA Torshok Barrier was designed to stop a 4000 lb vehicle traveling at 60 mph (88 fps). The max. design kinetic energy was thus 482 Kip-ft. The vehicle in test 2C exceeded this design energy by 21%.

for comparative purposes only. It in no way indicates whether the vehicle crash was survivable or would inflict minor or severe injuries to the occupants of the vehicle. This Index indicates that this collision was about 34 to 44% as severe as a rigid barrier impact.

TEST 2B RESULTS

Figures 6 through 9 show the TOR-SHOK barrier and 2520 lb vehicle before and after the 53.5 mph collision. The test results presented in Table 2 show that the barrier deformed 5.33 ft. Referring to Figure 5, it can be seen that the maximum TOR-SHOK stopping force exerted on the vehicle was 69.6 kips. The total energy absorbed by the TOR-SHOKs was approximately 210 kip-ft (87% of the vehicle kinetic energy). The average deceleration during this impact was 12.3 g's. The maximum significant deceleration on the vehicle was 26 to 27 g's as shown in Table 2.

The conclusions which can be drawn from this test are as follows:

1. The ARA TOR-SHOK barrier performed as designed.
2. The vehicle damage was severe (note Figures 7 and 9).
3. The barrier damage was minor, and the nose element and TOR-SHOKs were reusable.
4. The deceleration level produced on this lightweight vehicle was considered severe.

Referring to Table 3, we can compare this ARA TOR-SHOK impact performance with a rigid barrier impact. If the vehicle in Test 2B had hit a rigid barrier, the maximum deceleration would have been about 48.5 g's, and the average deceleration about 31.0 g's. Comparing

TABLE 2. BRIEF SUMMARY OF TEST RESULTS

TEST NUMBER	2A	2B	2C	2D
Angle of Attack	Head-on	Head-on	Head-on	30° Angle of Impact
Vehicle Weight (W)	4600 lb	2520 lb	4940 lb	5000 lb
Vehicle Velocity (V)	50.0 fps	78.8 fps	87.1 fps	73.3 fps
Vehicle Deformation	1.42 ft	1.88 ft	1.75 ft	1.83 ft
Barrier Deformation	4.48 ft	5.33 ft	11.12 ft	12.13 ft
Max. TOR-SHOK Stopping Force (F)	48 kips	69.6 kips	69.6 kips	--
Energy Absorbed by Torshoks	163 kip-ft (91%)	210 kip-ft (87%)	361 kip-ft (62%)	--
Max. Significant Deceleration	13 to 14 g's	26 to 27 g's	20 to 21 g's	28 to 30 g's
Avg. Deceleration (film) ($\Delta V \div Tg$)	6.6 g's	12.3 g's	9.9 g's	8.1 g's
Remarks: 1.	Performed as Designed	Performed as Designed	Performed as Designed	Unsatisfactory Performance
2.	Vehicle Damage Minor	Vehicle Damage Severe	Vehicle Damage Moderate	Vehicle Damage Severe
3.	Barrier Damage Minor, Reusable	Barrier Damage Minor, Reusable	Barrier Damage Severe, Most Torshoks not Reusable, Major Repairs Required	Barrier Damage Severe, Almost Total Loss
4.	Deceleration Level Moderate	Deceleration Level Severe	Deceleration Level Moderate	Deceleration Level Severe

TABLE 3. COMPARISON OF ARA TORSHOK IMPACT PERFORMANCE WITH RIGID BARRIER IMPACT

Test Number	2A	2B	2C	2D
Vehicle Weight	4600 lb	2520 lb	4940 lb	5000 lb
Vehicle Velocity	34.1 mph	53.5 mph	59.4 mph	49.9 mph
Comparative Rigid Barrier Impact				
Estimated Maximum Deceleration* (G_{max})	30.8 g's	48.5 g's	53.5 g's	44.8 g's
Estimated Average Deceleration* (G_{avg})	19.6 g's	31.0 g's	34.1 g's	30.6 g's
Attenuation Index				
$AI_{max} = \frac{G\ max\ Torshoks}{G\ max\ Rigid}$	.44	.55	.38	.65
$AI_{avg} = \frac{G\ avg\ Torshoks}{G\ avg\ Rigid}$	.34	.40	.29	.27

*Estimated Maximum Deceleration = 0.9 V

Estimated Average Deceleration = 0.574 V, where V is in mph.

Reference: Emori, Richard I., "Analytical Approach to Automotive Collisions," SAE Paper 680016, Auto. Engr. Congress, Detroit, January 8, 1968.

these figures with those obtained in Test 2B yield an Attenuation Index of 0.55 considering the maximum g forces, and an Attenuation Index of 0.40 considering the average g forces. This comparison shown in Table 3 indicates that the impact forces in Test 2B were from 40 to 55% as severe as those that would have been obtained if the vehicle had struck a rigid barrier.

TEST 2C RESULTS

Test 2C was a head-on collision by a 4940 lb vehicle which was traveling at 59.4 mph. In this test, the vehicle kinetic energy exceeded the design energy of the ARA TOR-SHOK barrier by 21% (see Table 1). Since the kinetic energy of the vehicle in Test 2C was 580 kip-ft, it was anticipated that the energy absorbing capacity of the TOR-SHOK arms (361 kip-ft) would be used up; and consequently the arms would be broken or buckled, and the vehicle would penetrate far into the barrier. Figures 10 through 13 show the TOR-SHOK barrier and vehicle before and after the collision.

From Table 2C, it can be seen that the barrier deformed 11.12 ft. The maximum TOR-SHOK stopping force was 69.6 kips. The energy absorbed by the TOR-SHOKs was 361 kip-ft (about 62% of the vehicle kinetic energy). The additional energy of the vehicle was absorbed by breaking and buckling the TOR-SHOK arms and by the vehicle deformation during the collision. The maximum significant vehicle deceleration was approximately 20 to 21 g's. The average vehicle deceleration was 9.9 g's.

In summary, the following conclusions can be drawn concerning this test:

1. The barrier performed as designed.
2. The vehicle damage was moderate (see Figures 11 and 13).
3. Damage to the TOR-SHOK barrier was considered severe. Most of the TOR-SHOKs were buckled and bent, and consequently not reusable. Major repairs and replacement of components were required.
4. The deceleration level was considered moderate.

To compare this ARA TOR-SHOK impact performance with a rigid barrier impact, refer once again to Table 3. If the vehicle used in Test 2C had struck a rigid barrier, it can be seen that the estimated maximum deceleration would have been 53.5 g's, and the average deceleration 35.1 g's. Computing the Attenuation Index yield 0.38 and 0.29, respectively. This indicates that the severity of the TOR-SHOK barrier impact was from 29 to 38% as severe as that which would have resulted from striking a rigid barrier.

DISCUSSION OF HEAD-ON TESTS

To further analyze the head-on impact performance of the ARA TOR-SHOK barrier, Figure 14 presents a comparison of the Attenuation Index with the vehicle weight. From Figure 14, it can be seen that for heavy vehicles around 5000 lbs the Attenuation Index varies from about 0.29 to 0.38. For a 2500 lb vehicle, a lightweight car, the Attenuation Index is seen to vary from about 0.40 to 0.55. This comparison indicates that the TOR-SHOK barrier is more effective as an impact attenuator for heavy vehicles than it is for lightweight or compact vehicles.

TEST 2D RESULTS

In Test 2D, a 5000 lb vehicle struck the ARA TOR-SHOK barrier at an angle of 30° from the longitudinal axis at a speed of 49.9 mph. Figures 15 through 19 show the vehicle and TOR-SHOK barrier before and after the collision. Under this collision, the nose of the TOR-SHOK barrier rotated from the path of the vehicle and allowed the vehicle to strike the rigid post. The TOR-SHOK arms were not activated properly, and consequently they absorbed very little of the vehicle kinetic energy. The impact with the backup post was extremely severe. The maximum deceleration was approximately 28 to 30 g's (from the vehicle accelerometer data, Appendix B). The average deceleration, on the other hand, was approximately 8.1 g's. The vehicle traveled 14.0 ft after striking the nose angle before coming to a complete stop against the vertical backup post.

The following conclusions can be drawn from the results of this test:

1. The barrier did not perform in a satisfactory manner under this 30° angle of impact.
2. The vehicle damage was very severe (see Figures 16, 18, and 19).
3. Damage to the TOR-SHOK barrier was quite severe. Most all the TOR-SHOKs were damaged beyond repair and were not reusable. The TOR-SHOK nose piece was almost totally destroyed.
4. The deceleration level was quite severe.

Table 3 compares the rigid barrier maximum deceleration of 44.8 g's to the approximately 29 g's obtained in Test 2D. It can be seen that

the Attenuation Index is about 0.65 when the maximum values are compared. The Attenuation Index based on the average g's is seen to be about 0.27. This average g Attenuation Index may be misleading since an analysis of the high speed film data shows that the vehicle was still traveling at about 40 mph when the nose angle and vehicle bottomed out and collided with the vertical backup post. This severe impact near the end of the crash is what caused most of the damage to the vehicle and was very severe (about 65% as severe as a rigid barrier collision).

SUMMARY AND CONCLUSIONS

The following general conclusions can be drawn from these four vehicle crash tests:

Head-On Collisions

(1) For head-on collisions, the ARA TOR-SHOK barrier performed as anticipated by the design. (2) Reasonable impact attenuation can be realized when the barrier is struck by heavy vehicles (say 4000 lb or more in weight). (3) Quite severe deceleration levels will be obtained when the barrier is struck by lighter weight and compact vehicles. (4) When the kinetic energy of the vehicle exceeds about 425,000 ft-lb, considerable damage to the barrier and TOR-SHOKs can be anticipated.

Angle Collisions

(1) For the angle collision used in these tests, the performance of the TOR-SHOK barrier was unsatisfactory. Modification of the barrier design to minimize or correct this deficiency is being made by the designers. Angle impact tests on the modified design are anticipated in the near future.

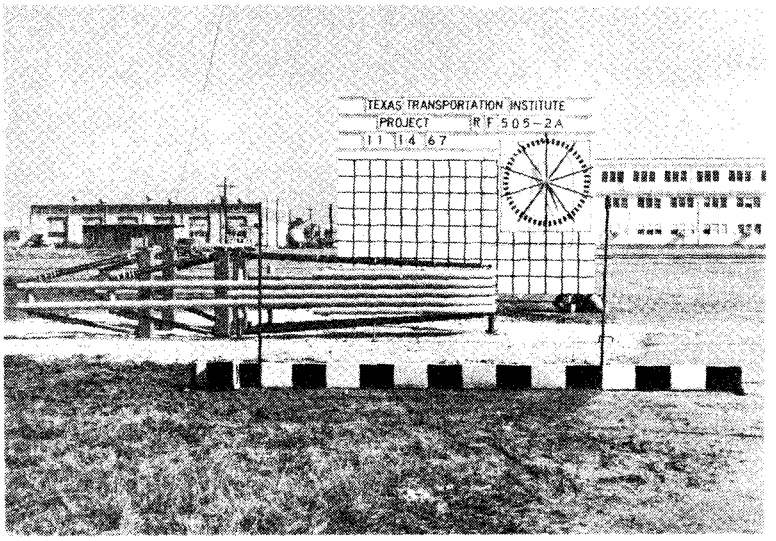

FIGURE 1. TORSHOK BEFORE COLLISION.
TEST 2A.

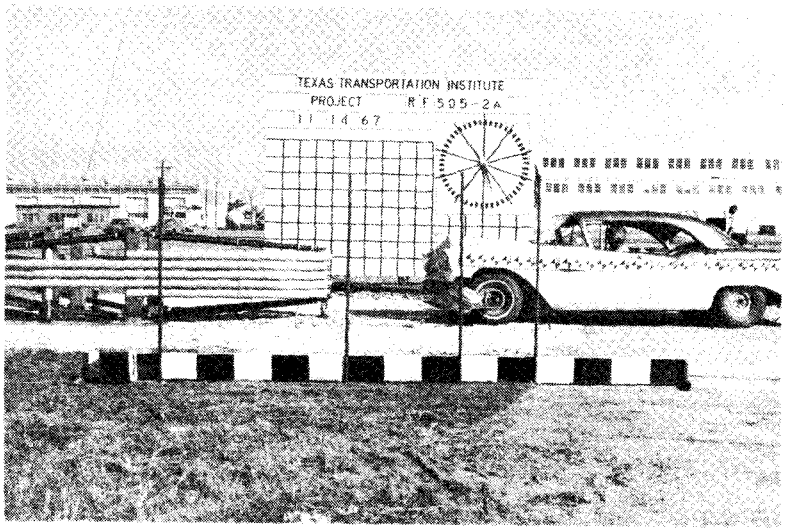

FIGURE 2. TORSHOK AND VEHICLE AFTER COLLISION.
INITIAL VEHICLE VELOCITY 34.1 MPH,
STOPPING DISTANCE 5.9 FT., AVERAGE
VEHICLE DECELERATION 6.6 G'S.
TEST 2A, HEAD-ON IMPACT.

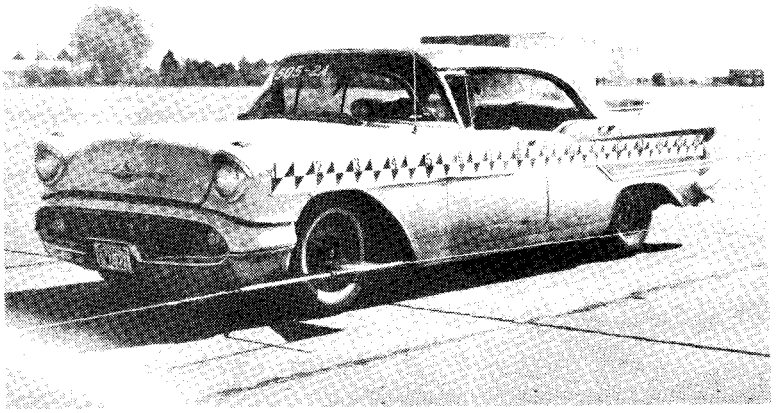

FIGURE 3. VEHICLE BEFORE COLLISION, TEST 2A.
1957 OLDS, WEIGHT 4600 LB.

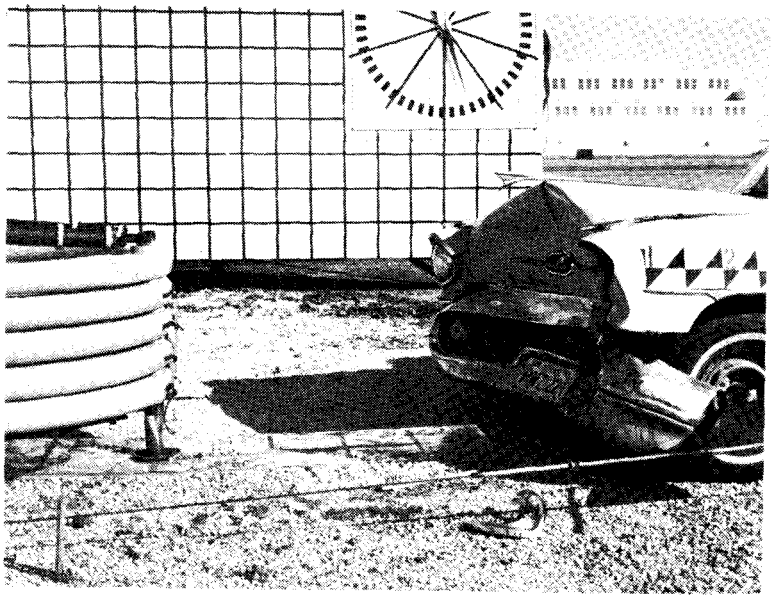

FIGURE 4. VEHICLE DAMAGE. TEST 2A.
VEHICLE DEFORMATION 1.42 FT.,
BARRIER DEFORMATION 4.48 FT.

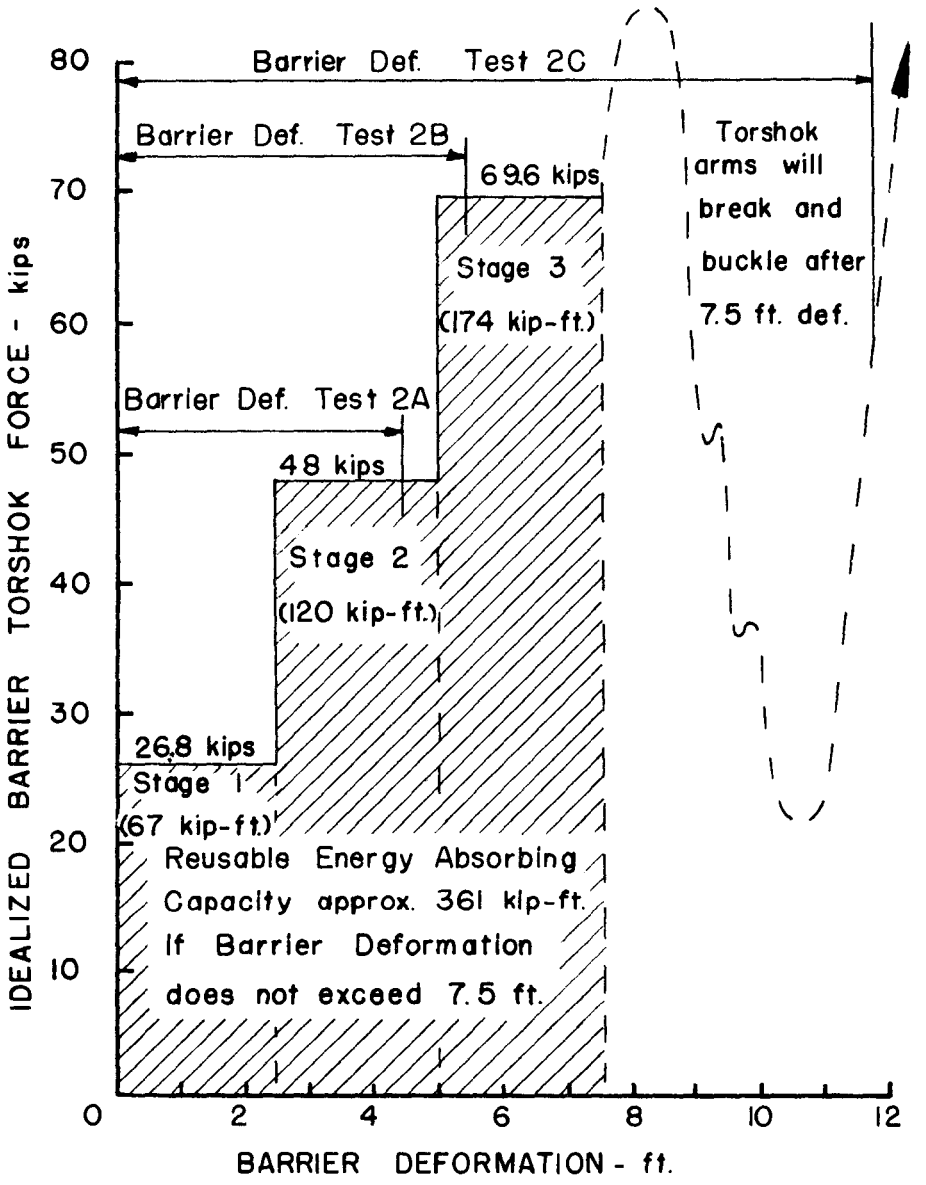

FIGURE 5. IDEALIZED ARA BARRIER TORSHOK FORCE-DEFORMATION CURVE FOR HEAD-ON VEHICLE IMPACT

(Skid friction forces and inertia forces are not included. Curve developed from data presented in Appendix A.)

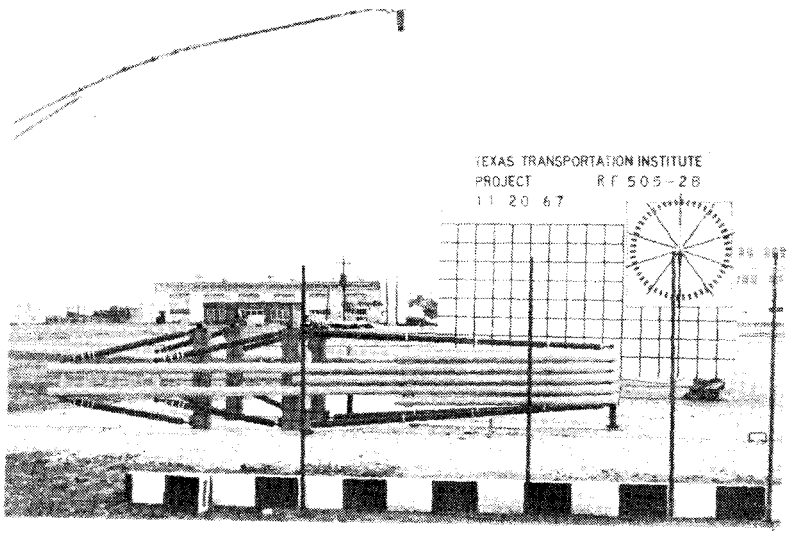

FIGURE 6. TORSHOK BEFORE COLLISION. TEST 2B.

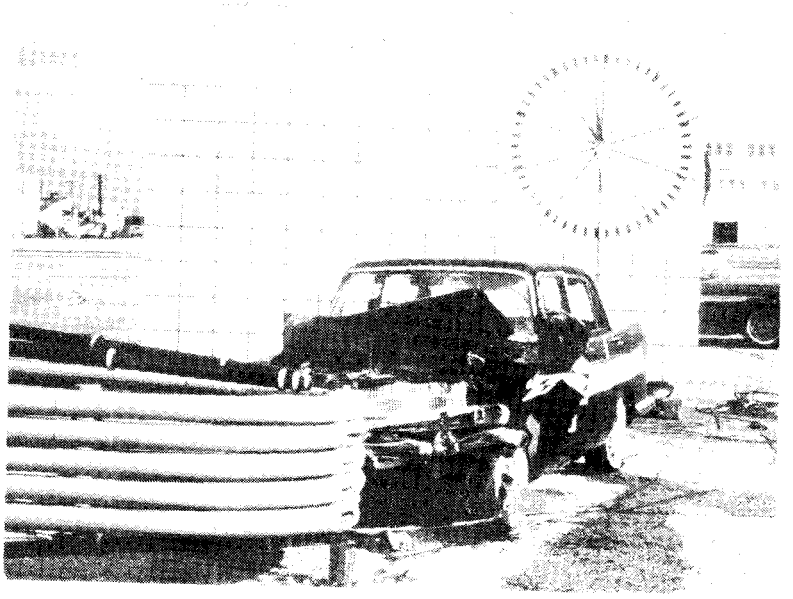

FIGURE 7. TORSHOK AND VEHICLE AFTER COLLISION. INITIAL VEHICLE VELOCITY 53.5 MPH., STOPPING DISTANCE 7.2 FT., AVERAGE VEHICLE DECELERATION 12.3 G'S. TEST 2B, HEAD-ON IMPACT.

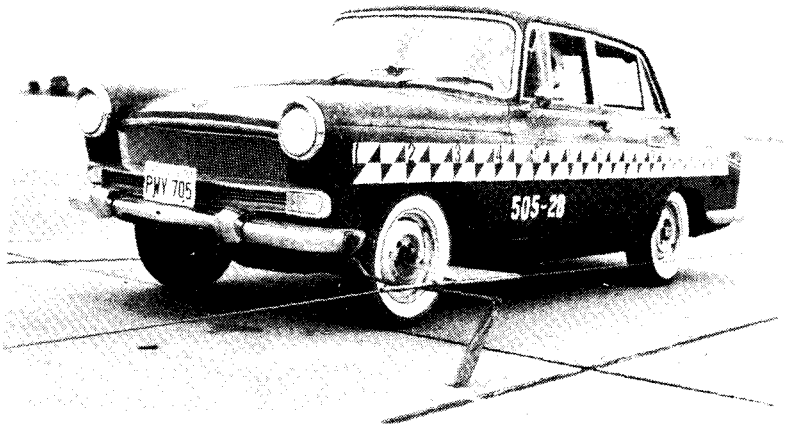

FIGURE 8. VEHICLE BEFORE COLLISION.
TEST 2B, 1957 AUSTIN,
WEIGHT 2520 LB.

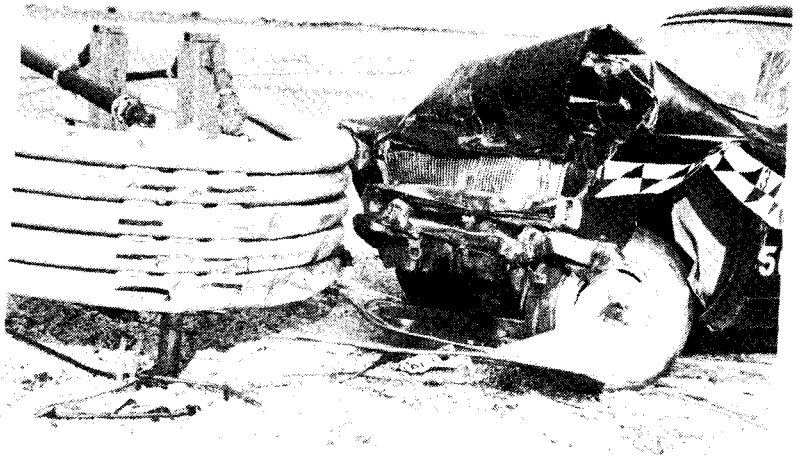

FIGURE 9. VEHICLE DAMAGE.
VEHICLE DEFORMATION 1.88 FT.,
BARRIER DEFORMATION 5.33 FT.
TEST 2B.

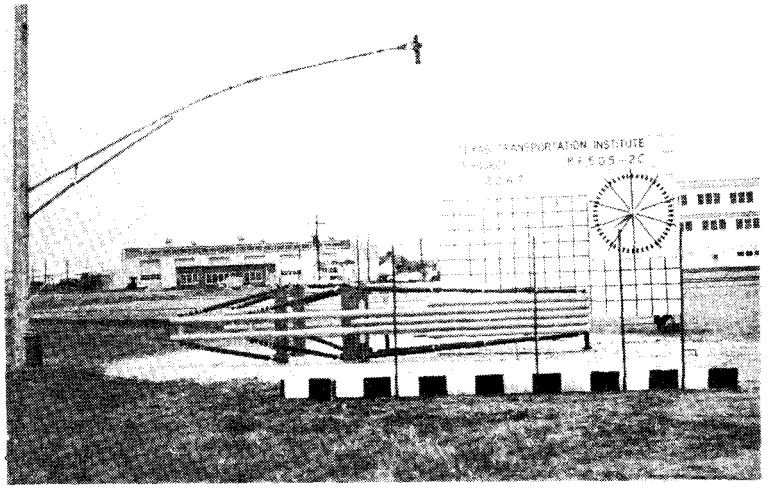

FIGURE 10. TORSHOK BEFORE COLLISION.
TEST 2C.

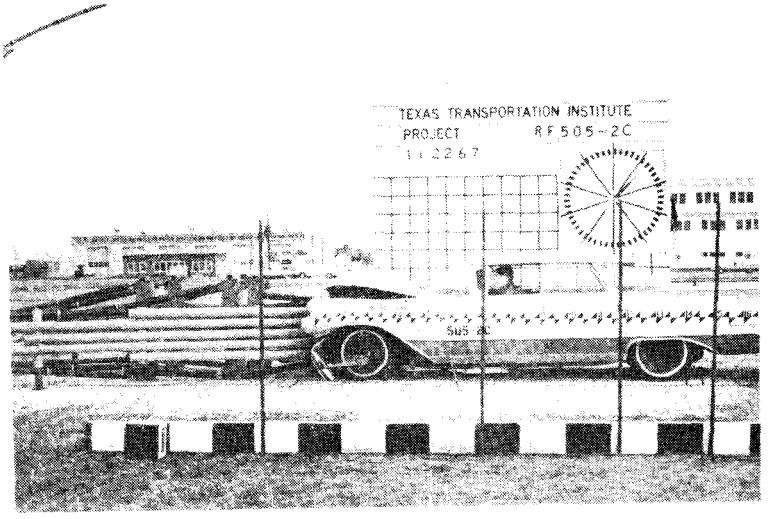

FIGURE 11. TORSHOK AND VEHICLE AFTER COLLISION.
INITIAL VEHICLE VELOCITY 59.4 MPH,
STOPPING DISTANCE 12.9 FT., AVERAGE
VEHICLE DECELERATION 9.9 G'S.
TEST 2C, HEAD-ON IMPACT.

FIGURE 12. VEHICLE BEFORE COLLISION.
TEST 2C, 1960 BUICK,
WEIGHT 4940 LB.

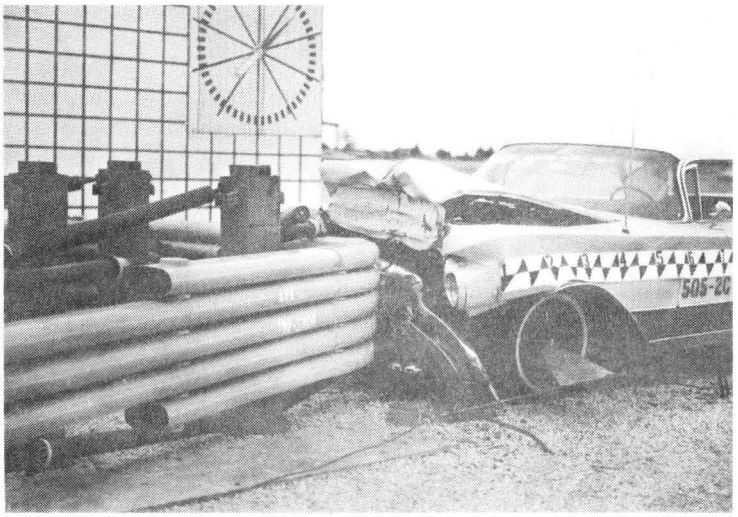

FIGURE 13. VEHICLE DAMAGE. VEHICLE
DEFORMATION 1.75 FT.,
BARRIER DEFORMATION 11.12 FT.
TEST 2C.

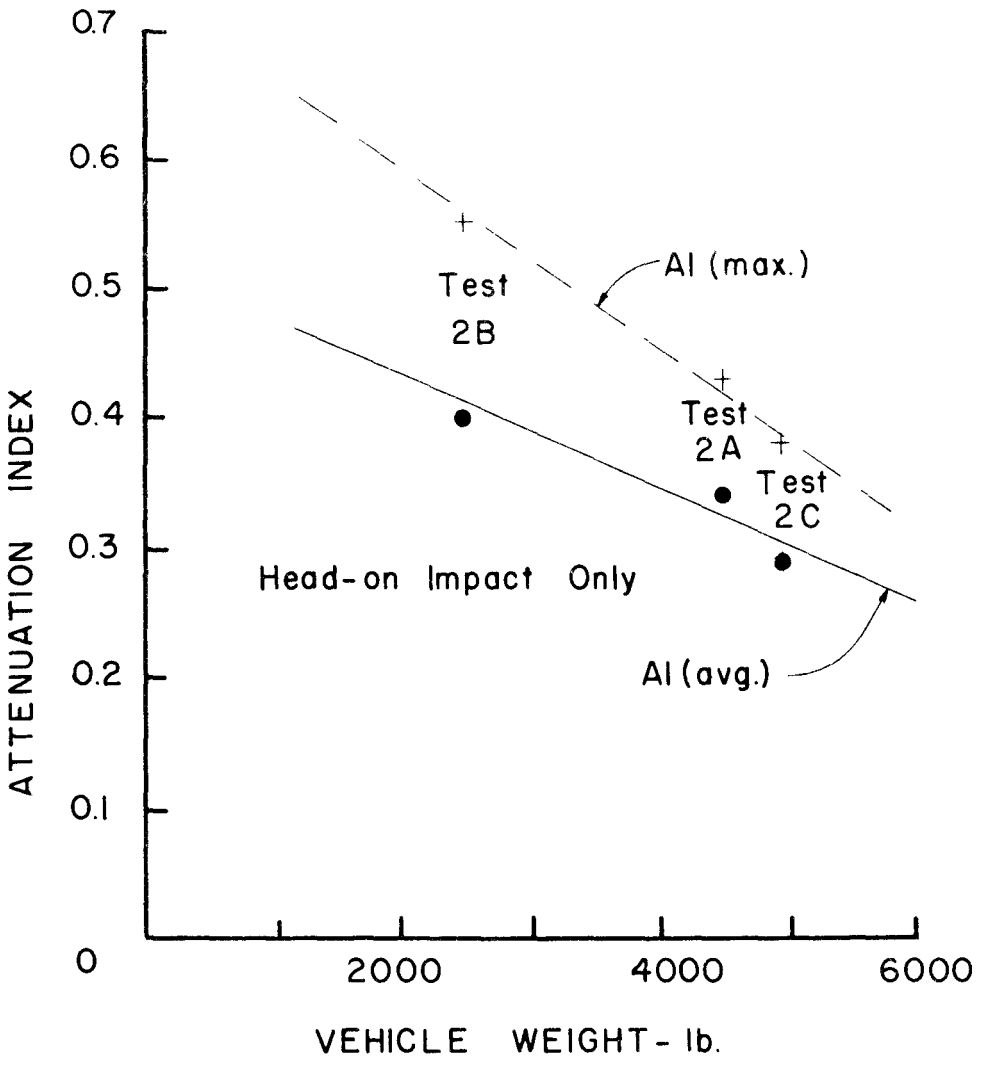

FIGURE 14. COMPARISON OF ATTENUATION INDEX OF ARA TORSHOK BARRIER WITH VEHICLE WEIGHT.

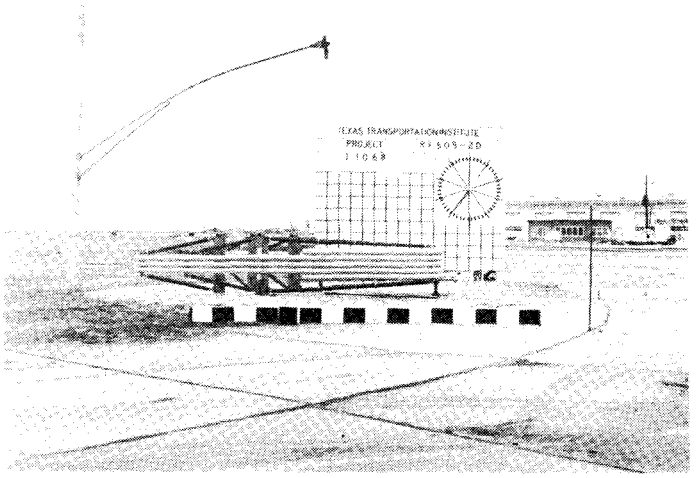

FIGURE 15. TORSHOK BEFORE COLLISION.
TEST 2D.

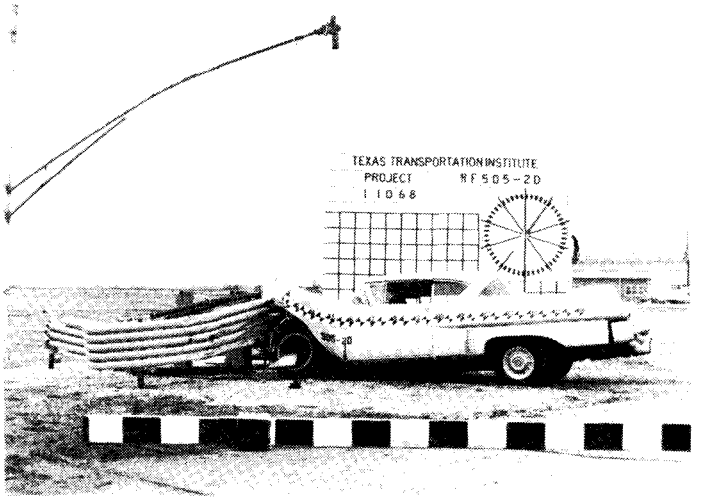

FIGURE 16. TORSHOK AND VEHICLE AFTER COLLISION.
INITIAL VEHICLE VELOCITY 49.9 MPH,
STOPPING DISTANCE 14.0 FT.,
AVERAGE VEHICLE DECELERATION 8.1 G'S.
TEST 2D, 30° ANGLE IMPACT.

FIGURE 17. VEHICLE BEFORE COLLISION.
TEST 2D. 1957 CAD.,
WEIGHT 5000 LB.

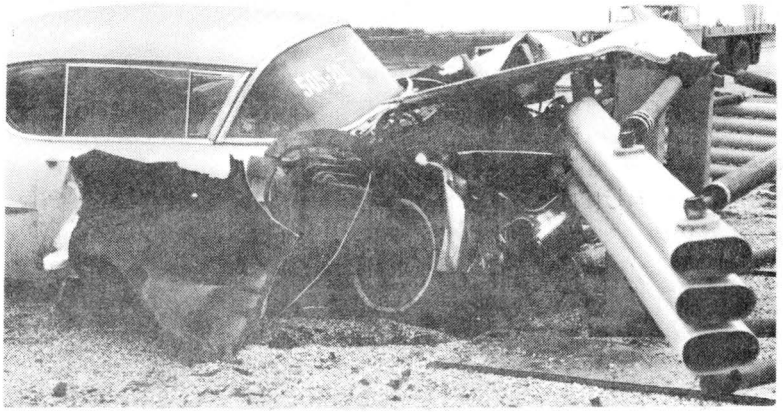

FIGURE 18. VEHICLE DAMAGE. VEHICLE DEFORMATION 1.83 FT.,
BARRIER DEFORMATION 12.13 FT.

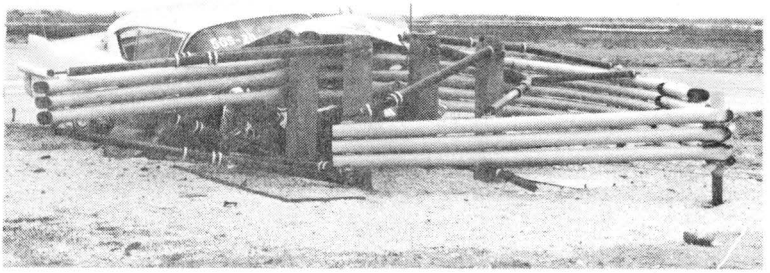

FIGURE 19. BARRIER DAMAGE. BARRIER DEFORMATION 12.13 FT., BARRIER ALMOST TOTAL LOSS.
TEST 2D, 30° ANGLE IMPACT.

APPENDIX A

Supplementary Data on TOR-SHOK
Reusable Energy Absorbing
Highway Protective System

Recently, ARA, Inc. has designed, fabricated, and crash tested an improved TOR-SHOK barrier for the Bureau of Public Roads. In addition, a systematic parametric variation of TOR-SHOK dimensions to meet fixed object abutment dimensions was also made. The purpose of this brief brochure is to provide you with the results of this valuable study.

GENERAL DESCRIPTION OF TOR-SHOK BARRIER

A detailed design drawing of a typical TOR-SHOK barrier which has recently been tested successfully at Texas A & M University is provided in Figures 1 and 2. Basically, the barrier consists of a series of elliptical tubing (4" x 7") with a wall thickness of .065". The barrier is connected with 4" round tubing which, as vertical members, transmit the loads from the elliptical tubing to a set of TOR-SHOKs that provide the principal source of energy absorption. For the configuration shown in Figures 1 and 2, twelve TOR-SHOKs are used. Four are used in front (in compression) and eight are used in the rear (in tension). This arrangement has been found to be desirable for reducing the bending moments in the elliptical guard-rail tubing as well as providing rotational stability of the barrier when the impact is not head-on. Each TOR-SHOK consists of four telescoping tubes which provide three different but successive loading conditions. The lowest load experiences initial movement and strokes until the stage is completely bottomed out at which time the next stage initiates its stroke; finally, the barrier displaces until all three stages are completely bottomed out.

In order to provide a smooth planing surface, the barrier is supported by three skids as shown in Figures 1 and 2. These skids also make use of the TOR-SHOK principle such that for relatively rough surfaces, the barrier strokes downward on the skids rather than destroying the skids due to excessive bending moments caused by the large coefficients of friction between the skid and the ground surface.

Although in Figures 1 and 2, use is made of four posts to simulate the fixed abutment, the abutment itself can be used to react against the twelve TOR-SHOKs. The location of the four posts consequently represent the critical dimensions of the abutment for determining the compatability of the TOR-SHOK barrier geometry.

The main parameter of the abutment appears to be its width since its height and length can invariably be accommodated by an adapter frame which must be required to transmit the loads from the TOR-SHOK's "ball joint" fittings to the fixed abutment. Consequently, a detailed parameter analysis of TOR-SHOK barrier

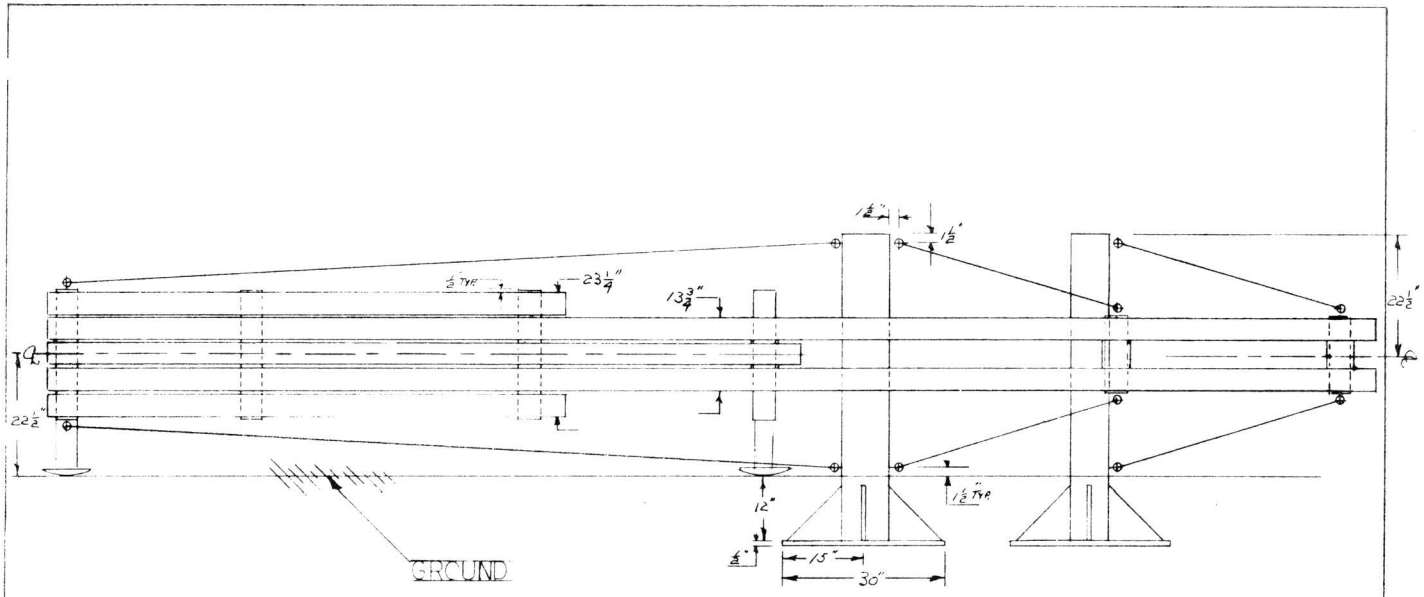

SIDE VIEW

ARA, inc.
West Covina California

ELLIPTICAL TUBE BARRIER
15°31"R HIGH STRESS

DO NOT SCALE DRAWING

Scale	3/4" = 1'	Date	
Drwn	HALT	8-28-67	
Engr	HALT	8-28-67	
Appd	S. R. LIN	10-2-67	
File No.	D-0037	Issued	

B-1450

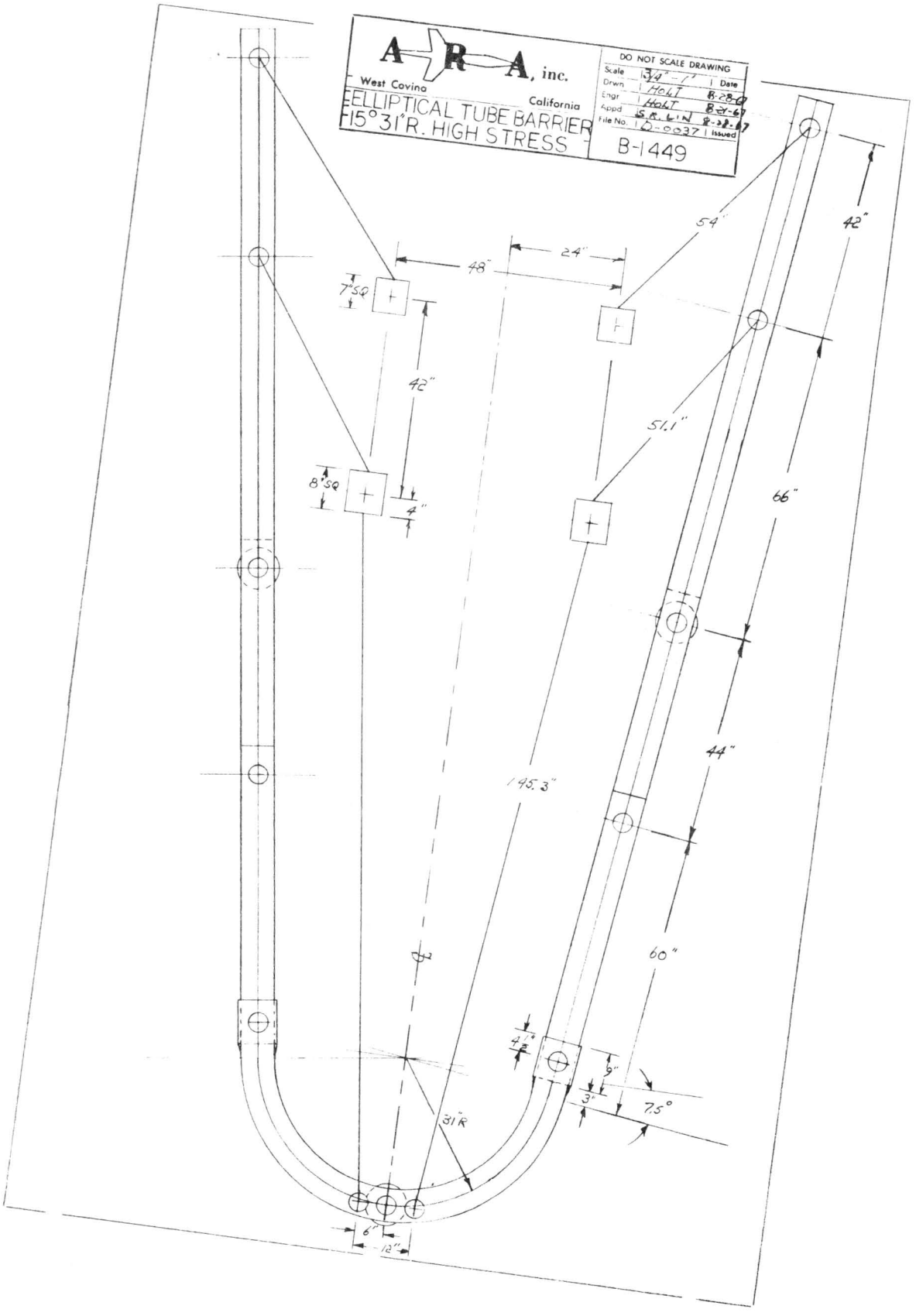
A R A, inc.
West Covina California
ELLIPTICAL TUBE BARRIER
F15°31'R. HIGH STRESS
DO NOT SCALE DRAWING
Scale 3/4" / 1' Date
Drwn HOLT 8-28-67
Engr HOLT 8-28-67
Appd S.R.L.N 8-28-67
File No. 10-0037 Issued
B-1449
54"
42"
48"
24"
7" SQ
42"
51.1"
8" SQ
4"
66"
44"
145.3"
60"
4 1/2"
6"
3"
7.5°
31"R
6"
12"

A3

configurations was made as a function of fixed abutment width for a given attachment distance of 48" from the front of the fixed abutment.

PARAMETRIC DESIGN DATA FOR TOR-SHOK BARRIER

The configuration studies for the TOR-SHOK barrier were made based on using elliptical type tubing having a minimum yield strength of 100,000 psi. This material is available at low cost and provides for a light-weight TOR-SHOK barrier. Since it is difficult to establish the types of abutments that are most applicable, ARA, Inc. has taken it upon itself to develop a detailed parametric analysis of the TOR-SHOK barrier over a range of nose angles which would be acceptable not only from a configuration standpoint, but also from a manufacturing point of view. All of the calculations for the preliminary analysis were based on a 31" nose radius which can be manufactured readily and satisfies most configuration requirements. The details of the calculations are not provided herein, but their results are clearly shown in Figures 3A through 3F, inclusive, wherein nose angle variations were made from 0° to 25°. For all of the cases considered, the number of tubes were varied from the nose to the rear section of the guard-rail (as shown in the figures) to accommodate the variation in bending moment such that the stresses remain reasonably constant. From an analysis of the results shown in Figures 3A to 3F, it is clear that there are many factors to be considered in selecting the optimum design or the optimum configuration for a particular application. In order to provide additional details of the performance characteristics of the TOR-SHOK barrier, TABLE I was prepared. The calculations are made on the basis that the input energy is equivalent to arresting a 4,000 pound vehicle impacting at 60 mph. It must also be understood that for this condition a certain amount of energy will be absorbed by the vehicle since it cannot remain completely intact during the impact. Based on the crash tests conducted under CPR-11-4629, the barrier absorbed approximately 72% of the energy. The results of TABLE I indicate that variations in abutment width can best be accommodated by varying the nose angle for a given nose radius of 31 inches. It is also clear that the energy absorption remains fairly constant over the range of nose angles from 0° to 25°. However, the weight of the barrier has a definite tendency to increase as the nose angle is increased beyond 10° to 15°. The primary reason for this requirement, is that as the nose angle is increased, the inertia loading becomes greater in a direction to cause severe bending moments in the nose section of the barrier which must be accommodated by increasing the structural capability of the barrier tubes and consequently the weight of the barrier. Review of TABLE I also indicates that the loading in each of the TOR-SHOK attenuators are consistent for the front, middle, and rear attenuators, as well as for the first, second and third stages. Note, however, that as the nose angle increases the length of the TOR-SHOKs for the middle and the rear become quite large in order to retain reasonable stresses in the nose section of the elliptical tubes. The additional cost due to an increase in TOR-SHOK lengths is far less than the cost for higher yield strength elliptical barrier tubes.

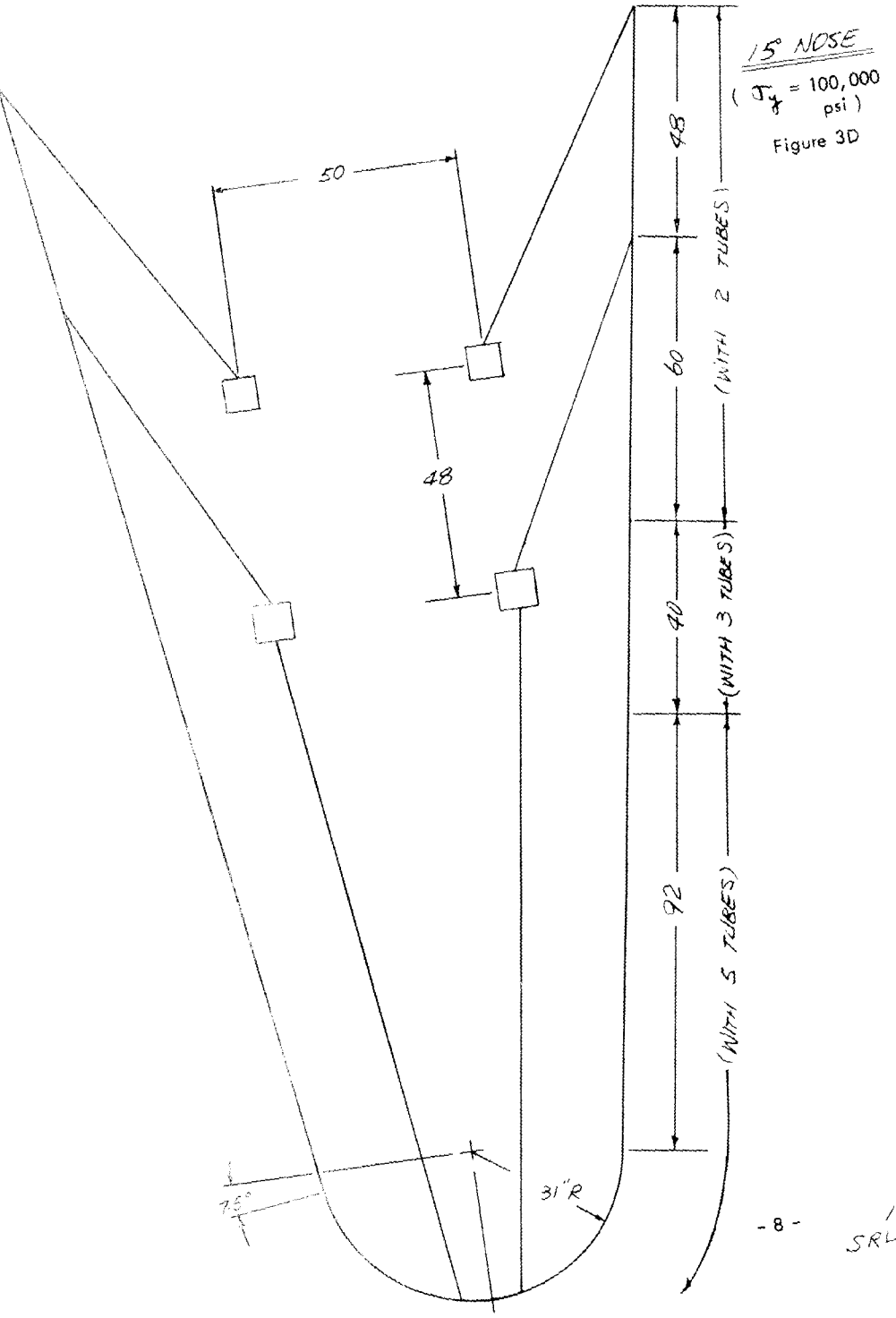

Figure 3D

10-2-67
SRL. YU

In order to illustrate the significant results of the detailed information given in TABLE I, Figure 4 was prepared to summarize the results of the parametric study involving the total weight of the barrier, its relative cost, and the energy absorption capability of the barrier. The results are shown in Figure 4 for the case of an elliptical tubing with a yield strength of 100,000 psi, as well as for comparison purposes, barrier tubes with a yield strength of 150,000 psi. (For the preliminary design shown in Figures 1 and 2, the configuration is noted to be a high-stress nose section which for this case corresponds to the yield stress of 150,000 psi.) Examination of Figure 4 indicates that in general, the energy absorption capability of the barrier remains fairly constant; however, the relative cost tends to increase slightly up to approximately a 20° nose angle. Beyond this nose angle, the weight and the relative cost start to increase rather rapidly. If the weight is a problem beyond 25°, it is recommended that in order to keep the weight below a prescribed value, say 800 pounds, then a high-stress material for the barrier tubes must be used. To illustrate this effect, a weight comparison is shown in Figure 4 at approximately 15° and 25° nose angles for the two yield strength barriers selected. Although the advantages of a high yield stress are obvious, the addendant increase in cost is also obvious as shown in Figure 4. Thus, it appears that up to 25° of nose angle, it is recommended that unless unusual circumstances are warranted, the TOR-SHOK barriers can be designed adequately with elliptical type tubing having a yield stress of approximately 100,000 psi.

TABLE I A

SUMMARY OF PERFORMANCE CHARACTERISTICS
FOR TOR-SHOK BARRIER (NOSE SECTION)
FOR 4000 LB. VEHICLE AT 60 MPH

(σ_y = 100,000 psi)

						SYSTEM TESTED		
NOSE ANGLE (DEGREE)			0	5	10	15	20	25
ABUTMENT WIDTH (INCHES)			24	36	46	50	52	54
INITIAL LENGTH (INCHES)		Front	144.25	143.75	141.25	141.25	140.75	140.75
		Middle	51.50	52.125	52.50	76.00	91.875	92.875
		Rear	52.00	53.25	55.00	78.00	94.375	95.25
ATTENUATOR FORCE, LB.	FIRST STAGE	Front	1600	1600	1500	1500	1500	1500
		Middle	2600	2600	2500	2600	2500	2500
		Rear	2600	2600	2500	2600	2500	2500
	SECOND STAGE	Front	2600	2600	2500	2600	2500	2500
		Middle	4200	4400	4800	4700	4000	4500
		Rear	4200	4400	4800	4700	4000	4500
	THIRD STAGE	Front	4200	4400	4800	4700	4000	4500
		Middle	5900	6700	7400	6350	6450	6800
		Rear	5900	6700	7400	6350	6450	6800
STROKE IN.	FIRST STAGE	Front	33.00	32.00	32.00	31.00	30.00	30.00
		Middle	31.00	28.625	31.125	29.75	28.75	27.75
		Rear	31.25	29.50	30.125	29.25	28.375	27.50
	SECOND STAGE	Front	32.00	32.00	32.00	31.00	31.00	31.00
		Middle	31.50	32.50	30.75	29.875	28.875	25.375
		Rear	31.50	31.50	29.625	29.375	27.875	24.375
	THIRD STAGE	Front	30.50	31.00	28.125	30.50	31.00	31.00
		Middle	29.375	31.00	29.625	31.875	32.875	35.375
		Rear	29.25	30.75	29.75	31.875	32.875	35.375
STAGE LENGTH, IN.	FIRST STAGE	Front	111.25	111.75	109.25	110.25	110.75	110.75
		Middle	82.50	80.75	83.625	105.75	120.625	120.625
		Rear	83.25	82.75	85.125	107.25	122.75	122.75
	SECOND STAGE	Front	79.25	79.75	77.25	79.25	79.75	79.75
		Middle	114.00	113.25	114.375	135.625	149.50	146.00
		Rear	114.75	114.25	114.75	136.625	150.625	147.125
	THIRD STAGE	Front	48.75	48.75	48.75	48.75	48.75	48.75
		Middle	143.375	144.25	144.00	167.50	182.375	181.375
		Rear	144.00	145.00	144.50	168.50	183.50	182.50
ENERGY ABSORPTION (%)			72.9	77.2	79	76.6	76.5	76.5
TOTAL WEIGHT (LB.)			798	794	794	845	897	1122

Fig. (4) Parametric Study of TOR-SHOK Barrier (Nose Section)
for 4000 lb. Vehicle at 60 mph

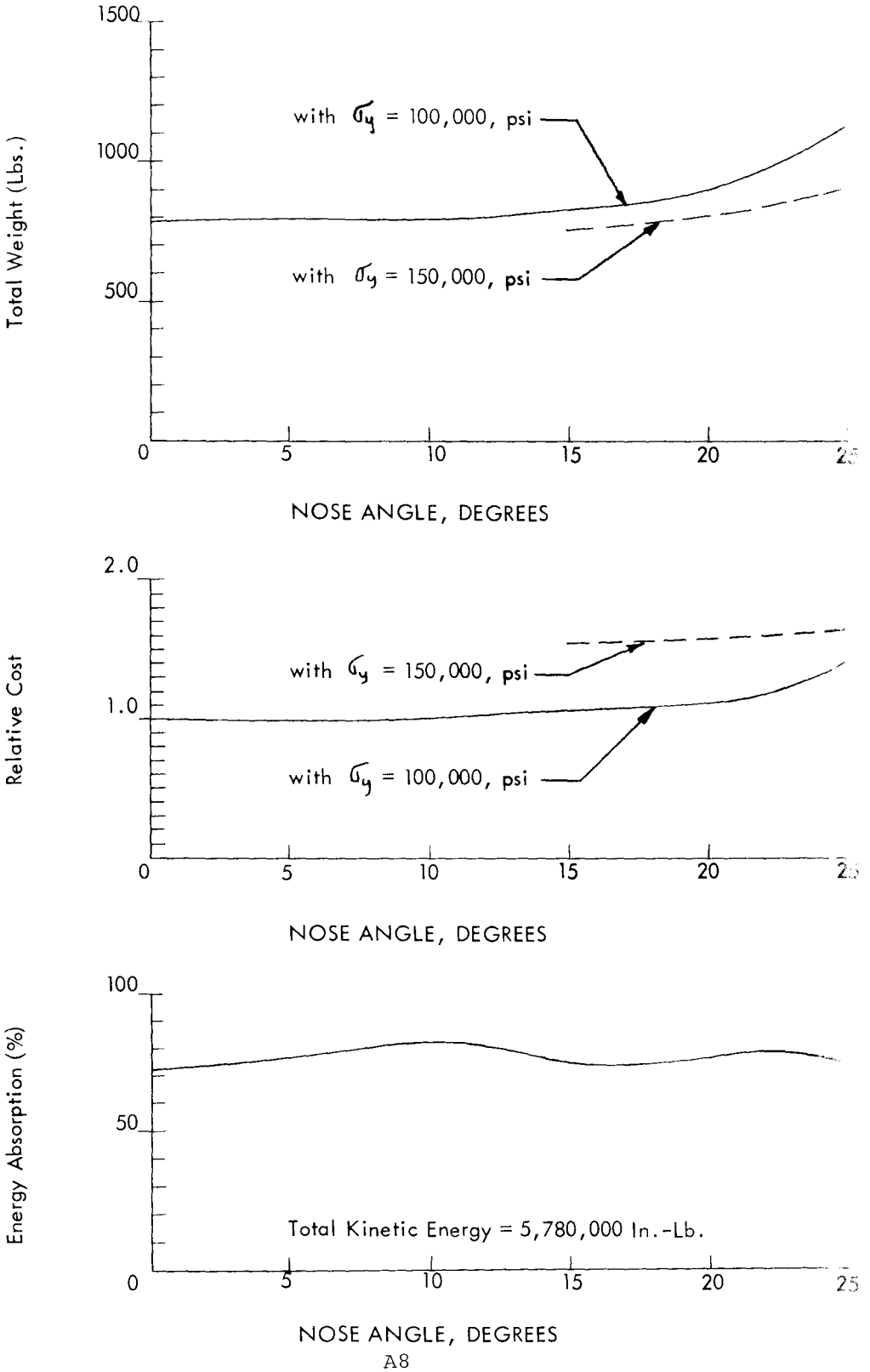

TABLE 1B.- SUMMARY OF CRASH TEST DATA FROM HIGH-SPEED FILM AND ELECTROMECHANICAL DEVICES FOR ARA TORSHOK BARRIERS, RF505-2A, 2B, 2C, and 2D.

TEST NUMBER	A	B	C	D
VEHICLE	1957 Olds. 4dr. Sed., 4600 lbs.	1957 Austin 4dr. Sed., 2520 lbs.	1960 Buick 4dr. Sed., 4940 lbs.	1957 Cad. 2 dr. Hdtp., 5000 lbs.
ANGLE OF IMPACT	0°	0°	0°	30°
FILM DATA				
Velocity (mph)	34.1	53.5	59.4	49.9
Velocity (fps)	50.0	78.8	87.1	73.3
Velocity Change (mph)	34.1	53.5	59.4	49.9
Velocity Change (fps)	50.0	78.5	87.1	73.3
Average Deceleration (g's)	6.6	12.3	9.9	8.1
Peak Deceleration (g's)	29.4	42.1	30.3	60.7
Duration of Impact (sec.)	0.218	0.198	0.273	0.280
Stopping Distance (ft.)	5.9	7.2	12.9	14.0
ELECTROMECHANICAL DATA				
Peak Deceleration (g's)				
Frame Accelerometer	13-14 (long.)	26-27 (long.)	20-21 (long.)	28-30 (long.)
Dummy Accelerometer	12-13 (long.)	33 (long.)	20 (long.)	28-30 (long.)
	11-12 (vert.)	10 (vert.)	19 (vert.)	8 (vert.)
	2-3 (trans.)	4-6 (trans.)	4-6 (trans.)	14-16 (trans.)
Peak Seatbelt Force (lbs.)	No Data	2000	1400	No Data
Duration of Impact (sec.)	0.257	0.242	0.343	0.300
OBSERVATIONS				
Vehicle Deformation (ft.)	1.42	1.88	1.75	1.83
Barrier Deformation (ft.)	4.48	5.33	11.12	12.13
Vehicle Damage	Minor	Severe	Moderate	Severe
TORSHOK Damage	Re-usable	Re-usable	Severe	Severe

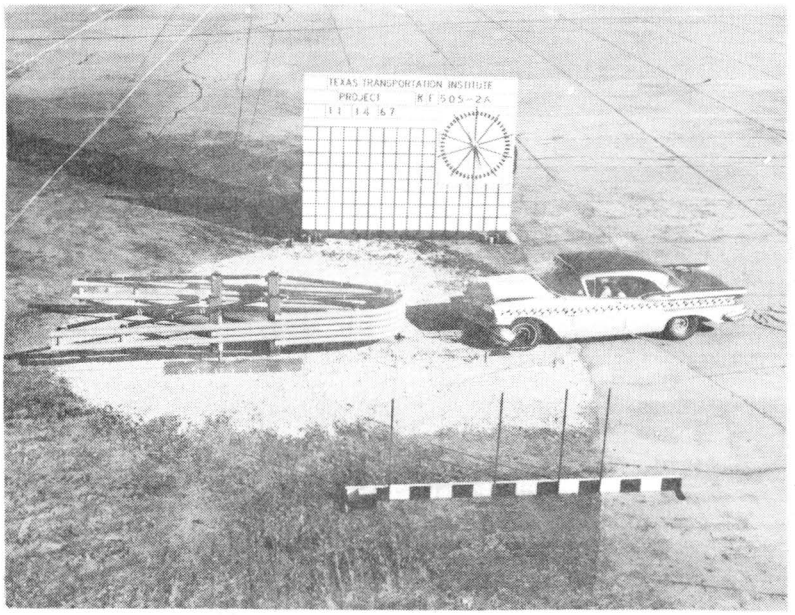

CONDITIONS AFTER TEST (VEHICLE STRUCK BARRIER HEAD-ON)

TABLE 2B.
Summary of High-speed Film Crash Test Data

Test 505-2A ARA Torshok Barrier 15° Nose Angle

Vehicle Weight = 4600 lb. (1957 Olds, 4 dr. Hdtp.)

Vehicle Velocity = 34.1 mph or 50 fps

Change in Velocity = 34.1 mph or 50.0 fps

Average Deceleration = 6.6 g's

Peak Deceleration = 29.4 g's (7.28 msec.)

Duration of Impact = 0.218 sec.

Stopping Distance = 5.9 ft.

Remarks: Minor Damage to Vehicle, behavior was very good.

Vehicle Deformation 1.42 ft. Barrier Deformation 4.48 ft.

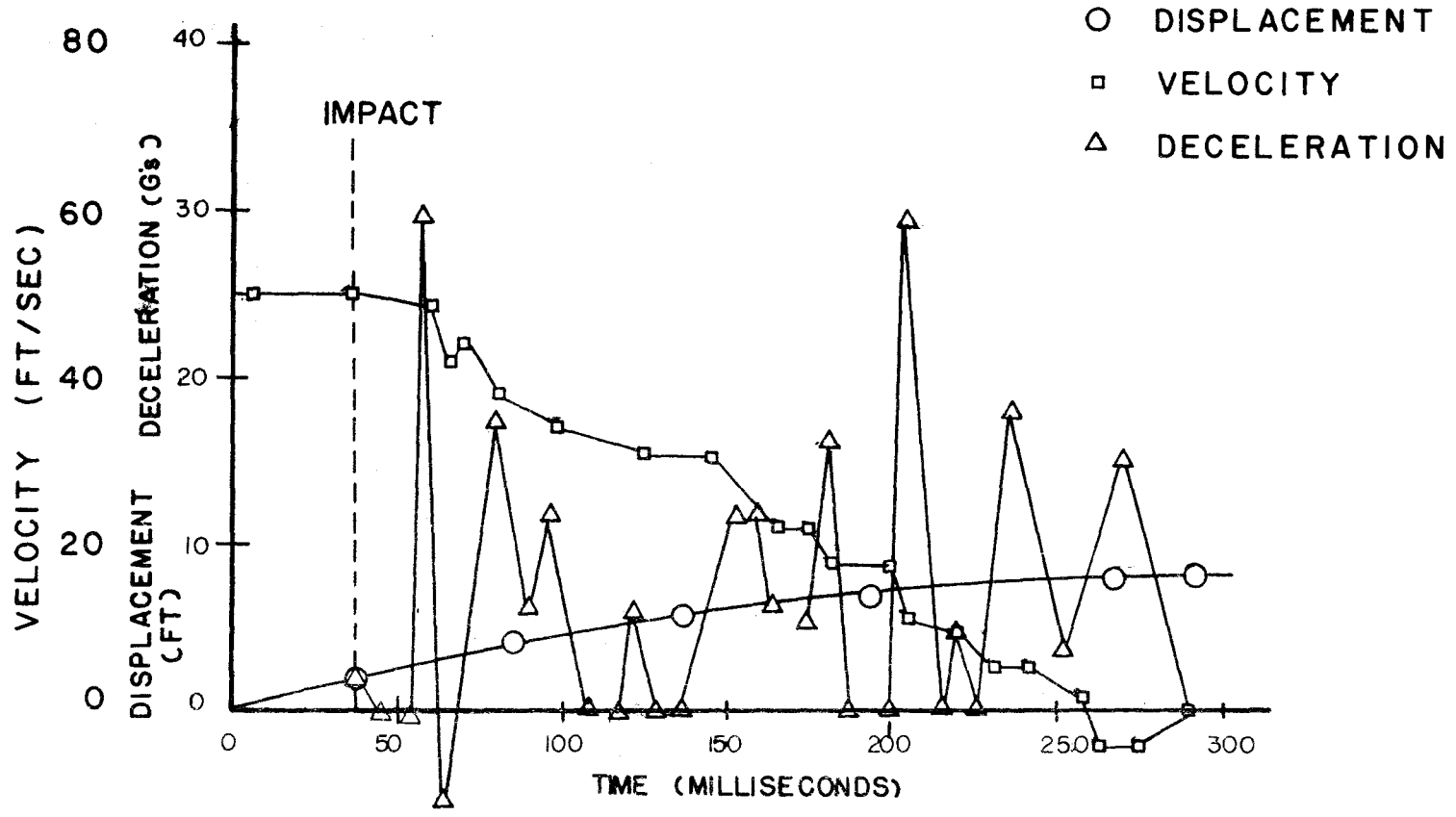

FIGURE IB. DISPLACEMENT, VELOCITY, AND DECELERATION VS. TIME CURVES FOR TEST 505-2A

TABLE 3B.

TEST RF 505-2A

ARA TORSHOK BARRIER 15° NOSE ANGLE

1957 OLDS., 4 DOOR HARDTOP, 4600 LB.

HIGH SPEED FILM DATA

Time Milliseconds	Displacement ft	Velocity ft/sec	Deceleration ft/sec^2	g's
0	0		0	0
		49.5		
7.28	0.36		0	0
		49.5		
14.56	0.72		0	0
		49.5		
21.84	1.08	50.0 avg.	0	0
		50.8		
36.40 Impact	1.82		69	2.1
		49.5		
43.68	2.18		0	0
		49.5		
50.96	2.54		0	0
		49.5		
58.24	2.90		948	29.4
		42.6		
65.52	3.21		-179	-5.6
		43.9		
72.80	3.53		179	5.6
		42.6		
80.08	3.84		563	17.5
		38.5		
87.36	4.12		192	6.0
		37.1		
94.64	4.39		385	12.0
		34.3		
101.92	4.64		179	5.6
		33.0		
109.20	4.88		0	0
		33.0		
116.48	5.12		0	0
		33.0		
123.76	5.36		192	6.0
		31.6		
131.04	5.59		0	0
		31.6		
138.32	5.82		0	0
		31.6		
145.60	6.05		192	6.0
		30.2		
152.88	6.27		371	11.5
		27.5		

(continued on next page)

TABLE 3B.

TEST RF 505-2A (continued)

Time Milliseconds	Displacement ft	Velocity ft/sec	Deceleration ft/sec^2	g's
160.16	6.47		385	12.0
		24.7		
167.44	6.65		192	6.0
		23.3		
174.72	6.82		179	5.6
		22.0		
182.00	6.98		563	17.5
		17.9		
189.28	7.11		0	0
		17.9		
196.56	7.24		0	0
		17.9		
203.84	7.37		948	29.4
		11.0		
211.12	7.45		0	0
		11.0		
218.40	7.53		134	4.2
		9.9		
227.50	7.62		0	0
		9.9		
236.60	7.71		604	18.8
		4.4		
245.70	7.75		361	11.2
		1.1		
254.80	7.76		121	3.8
		0		
263.90	7.76		483	15.1
		-4.4		
273.00	7.72		0	0
		-4.4		
282.10	7.68		0	0

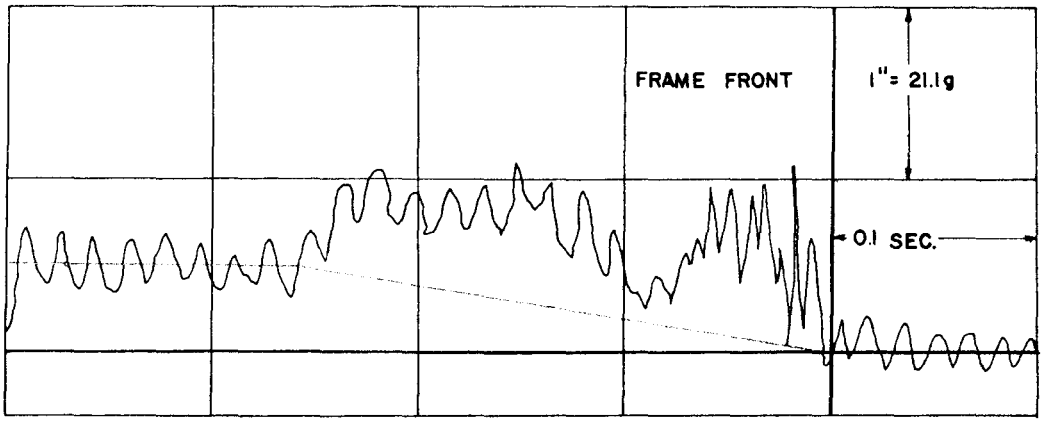

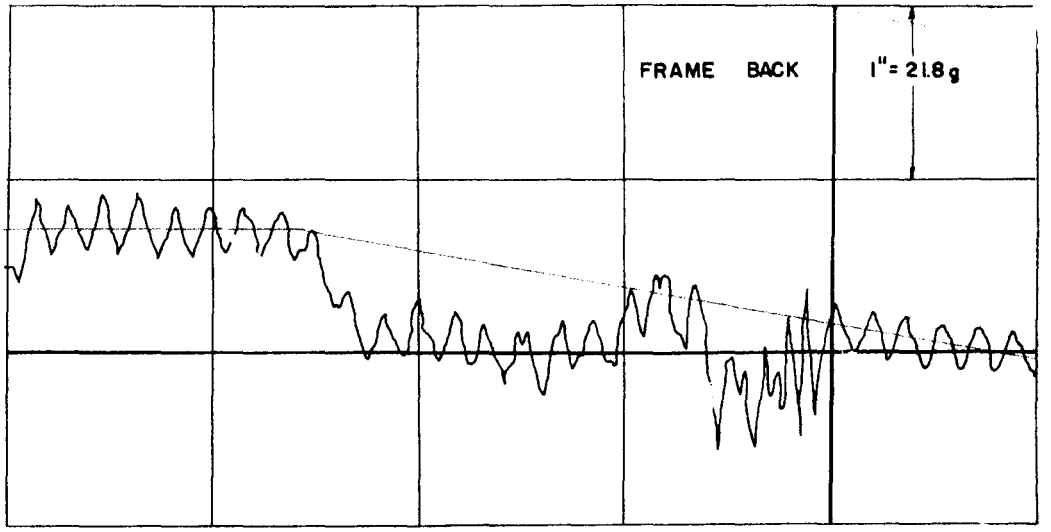

			NO USEABLE DATA	
			SEAT BELT FORCE	

FIGURE 2B. TEST 505 2A FRAME ACCELEROMETER DATA & SEAT BELT FORCE

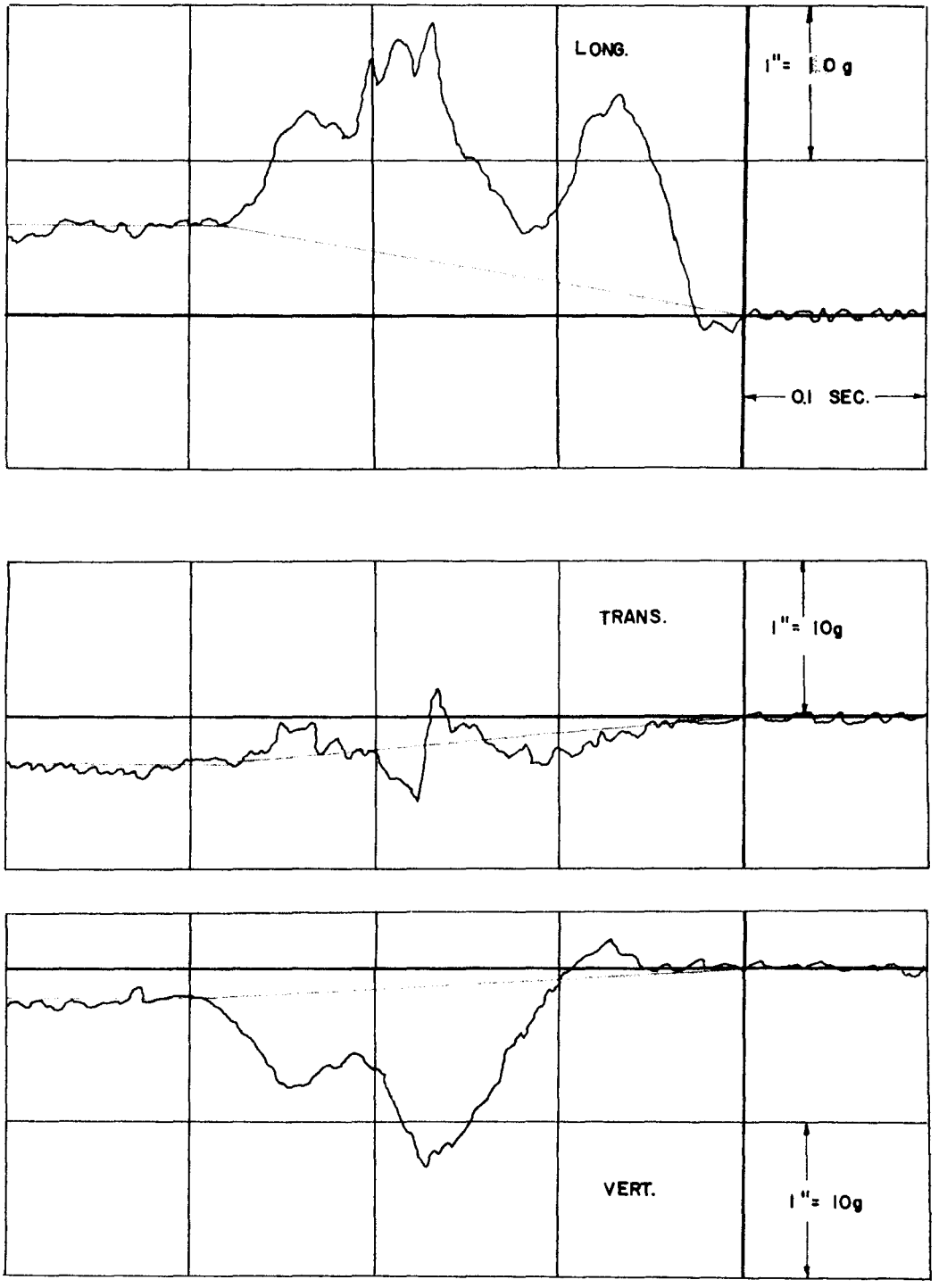

FIGURE 3B. TEST 505 2A DUMMY ACCELEROMETER DATA

CONDITIONS AFTER TEST (VEHICLE STRUCK BARRIER HEAD-ON)

TABLE 4B.
Summary of High-speed Film Crash Test Data

Test 505-2B ARA Torshok Barrier 15° Nose Angle

Vehicle Weight = 2520 lb. (1960, Austin, 4-Door Sedan)

Vehicle Velocity = 53.5 mph or 78.5 fps

Change in Velocity = 53.5 mph or 78.5 fps

Average Deceleration = 12.3 g's

Peak Deceleration = 42.1 g's (9 msec.)

Duration of Impact = 0.198 sec.

Stopping Distance = 7.2 ft.

Remarks: Damage to Vehicle Severe. Vehicle Deformation 1.88 ft.

Barrier Deformation 5.33 ft.

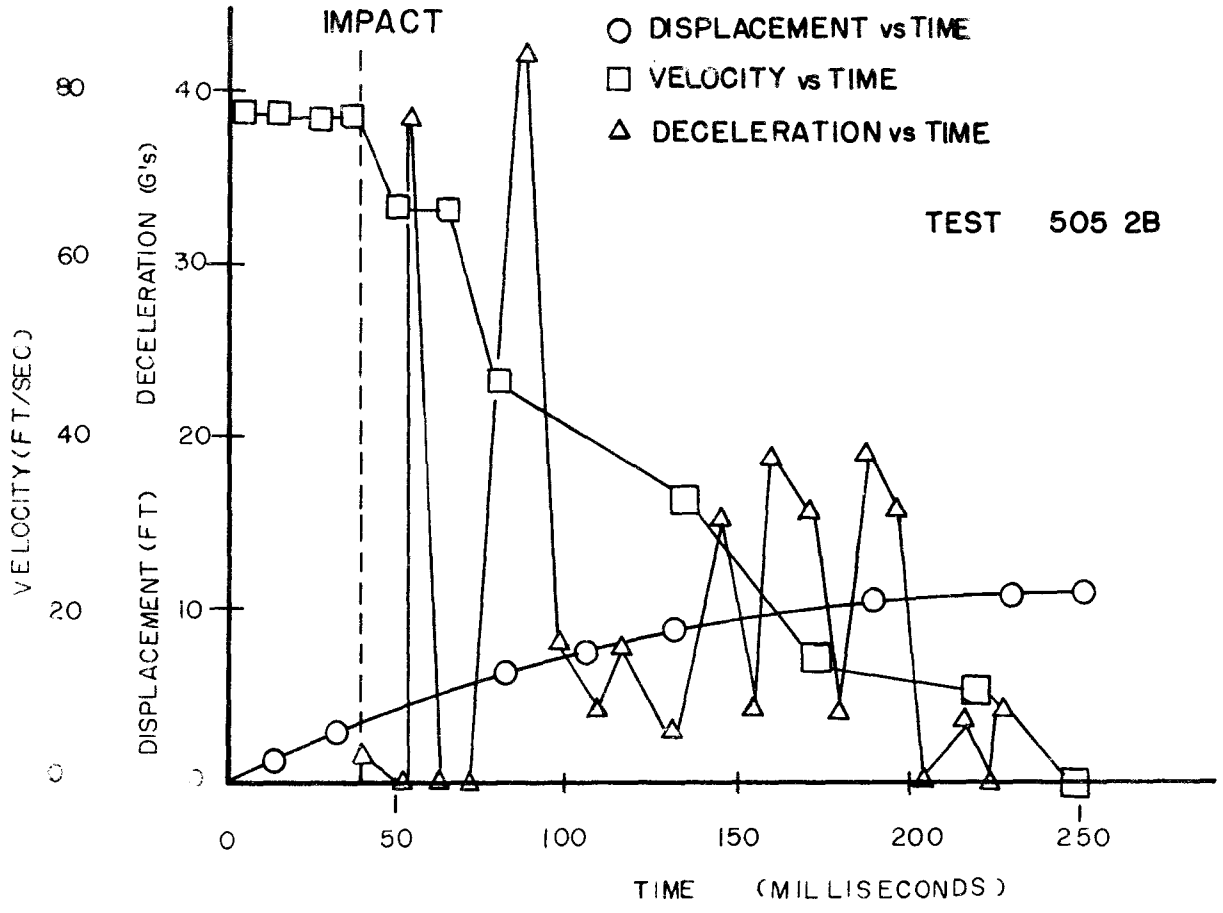

FIGURE 4B. DISPLACEMENT, VELOCITY, AND DECELERATION VS. TIME FOR TEST 505-2B

TABLE 5B.

TEST RF 505-2B

ARA TORSHOK BARRIER 15° NOSE ANGLE

1960 AUSTIN, 4 DOOR SEDAN, 2520 LB.

HIGH SPEED FILM DATA

Time Milliseconds	Displacement ft	Velocity ft/sec	Deceleration ft/sec^2	g's
0	0		0	0
		78.9		
9.0	.71		0	0
		78.9		
18.0	1.42	78.5 avg.	0	0
		77.8		
27.0	2.12		0	0
		78.9		
36.0	2.83		0	0
		77.8		
45.0 Impact	3.53		78	2.4
		77.8		
54.0	4.23		1232	38.3
		66.7		
63.0	4.83		0	0
		66.7		
72.0	5.43		0	0
		66.7		
81.0	6.03		867	26.9
		58.9		
90.0	6.56		1355	42.1
		46.7		
99.0	6.98		256	8.0
		44.4		
108.0	7.38		122	3.8
		43.3		
117.0	7.77		245	7.6
		41.1		
126.0	8.14		122	3.8
		40.0		
135.0	8.50		122	3.8
		38.9		
144.0	8.85		489	15.2
		34.5		
153.0	9.16		133	4.1
		33.3		
162.0	9.46		612	19.0
		27.8		
171.0	9.71		500	15.5
		23.3		
180.0	9.92		122	3.8
		22.2		
189.0	10.12		612	19.0
		16.7		
198.0	10.27		500	15.5
		12.2		

(continued on next page)

TABLE 5B.

TEST RF 505-2B (continued)

Time Milliseconds	Displacement ft	Velocity ft/sec	Deceleration ft/sec^2	g's
207.0	10.38		0	0
		12.2		
216.0	10.49		122	3.8
		11.1		
225.0	10.59		0	0
		11.1		
234.0	10.69		612	19.0
		5.6		
243.0	10.74		622	19.3
		0		
252.0	10.74		0	0

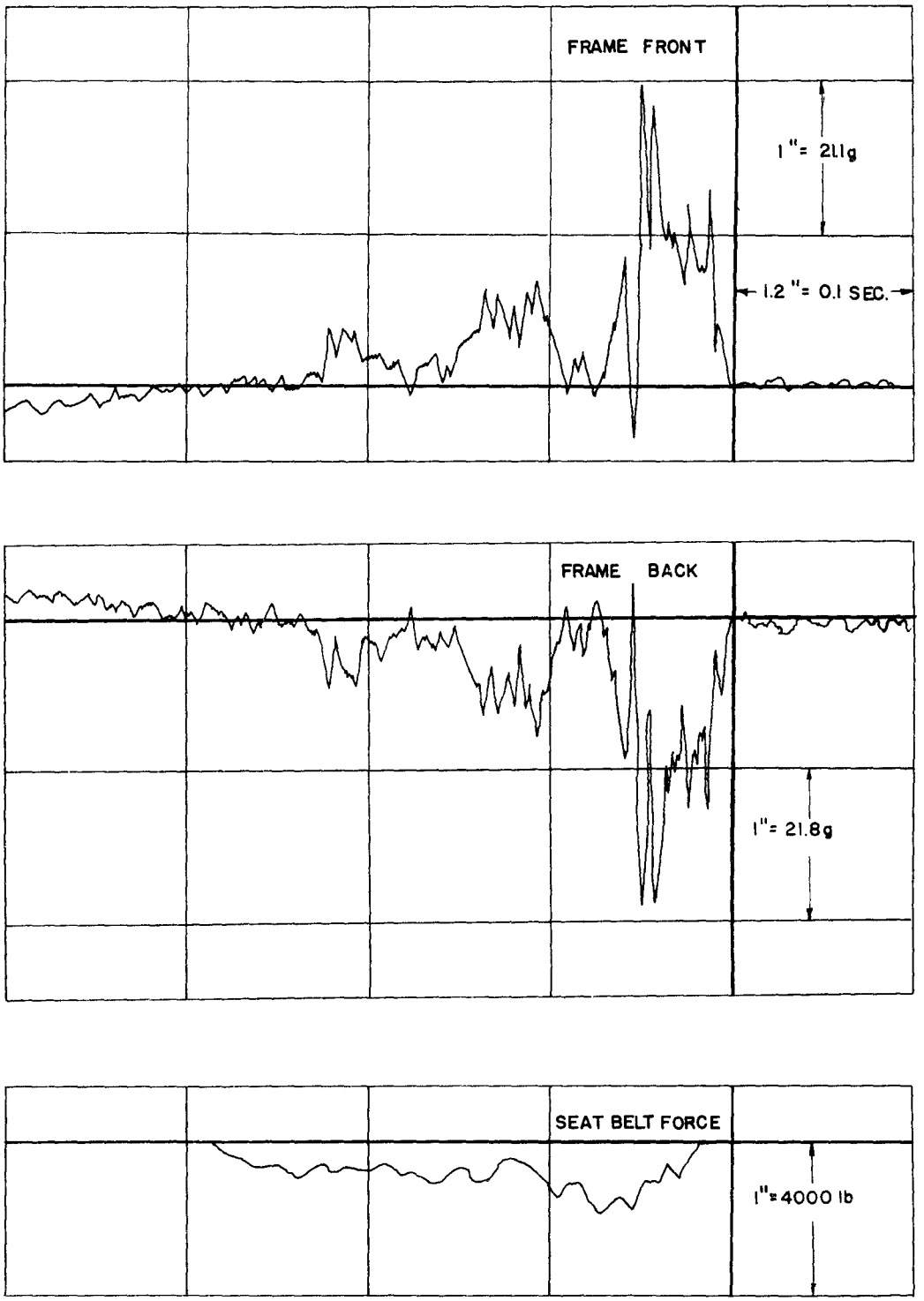

FIGURE 5B. TEST 505 2B FRAME ACCELEROMETER DATA & SEAT BELT FORCE

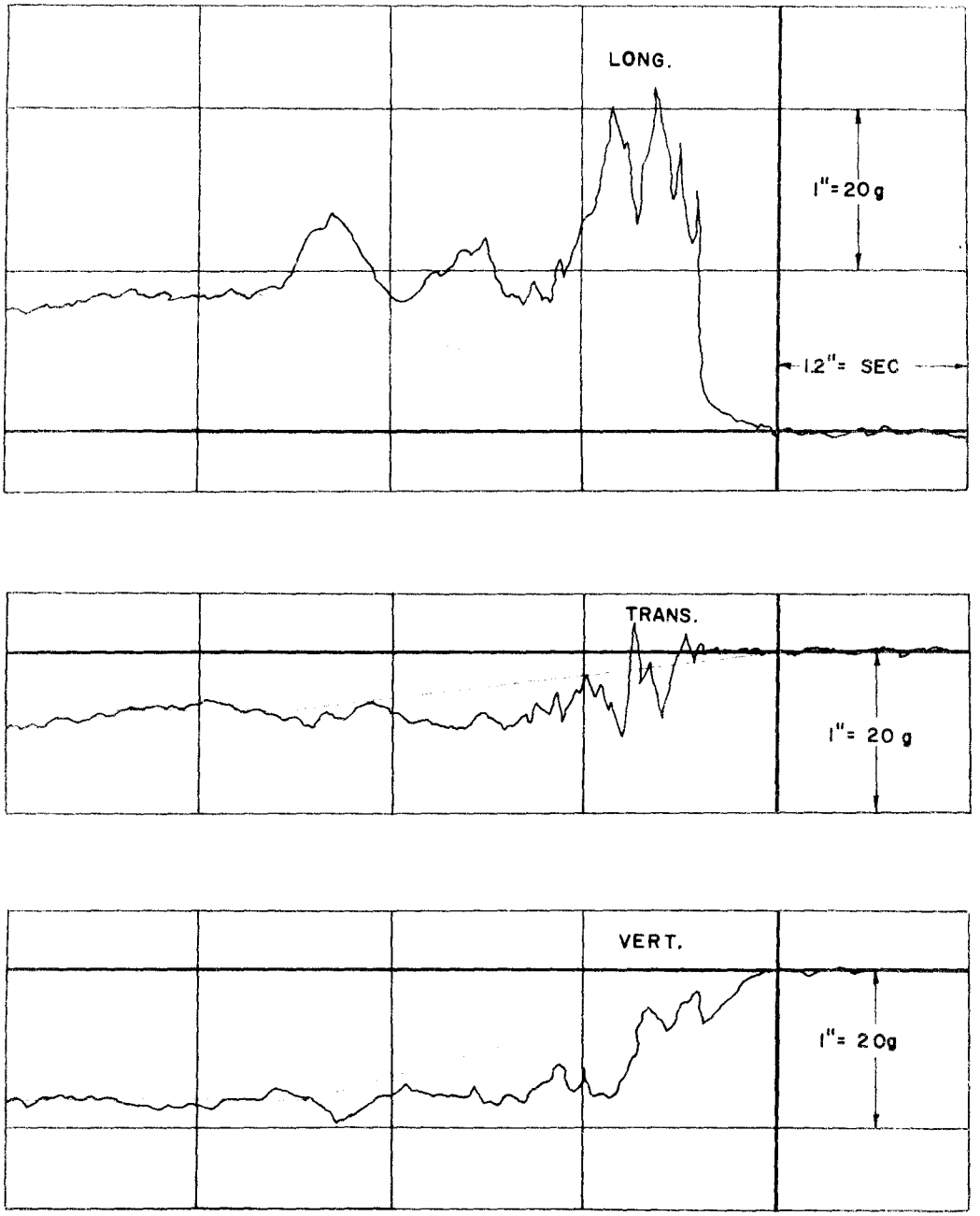

FIGURE 6B. TEST 505 2B DUMMY ACCELEROMETER DATA

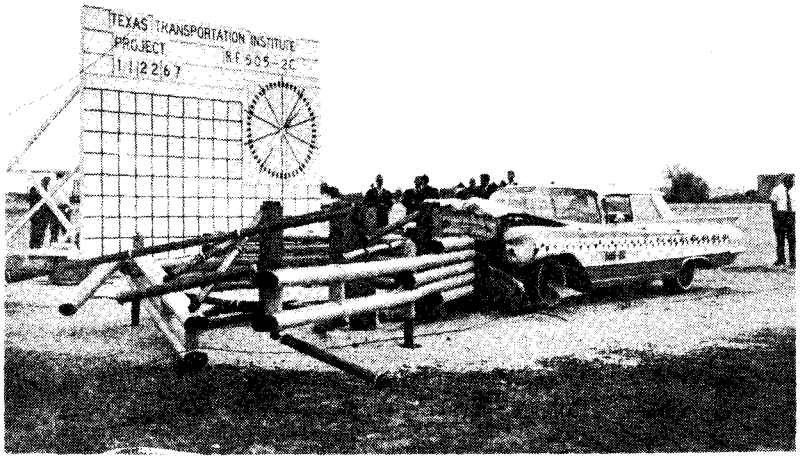

CONDITIONS AFTER TEST (VEHICLE STRUCK BARRIER HEAD-ON)

TABLE 6 B.
Summary of High-speed Film Crash Test Data

Test 505-2C ARA Torshok Barrier 15° Nose Angle

Vehicle Weight = 4940 lb. (1960 Buick, 4-Door Sedan)

Vehicle Velocity = 59.4 mph or 87.1 fps

Change in Velocity = 59.4 mph or 87.1 fps

Average Deceleration = 9.9 g's

Peak Deceleration = 30.3 g's (12.4 msec.)

Duration of Impact = 0.273 sec.

Stopping Distance = 12.9 ft.

Remarks: Damage to Vehicle Moderate. Vehicle Deformation 1.75 ft.
Barrier Deformation 11.12 ft. Barrier Severely Damaged.

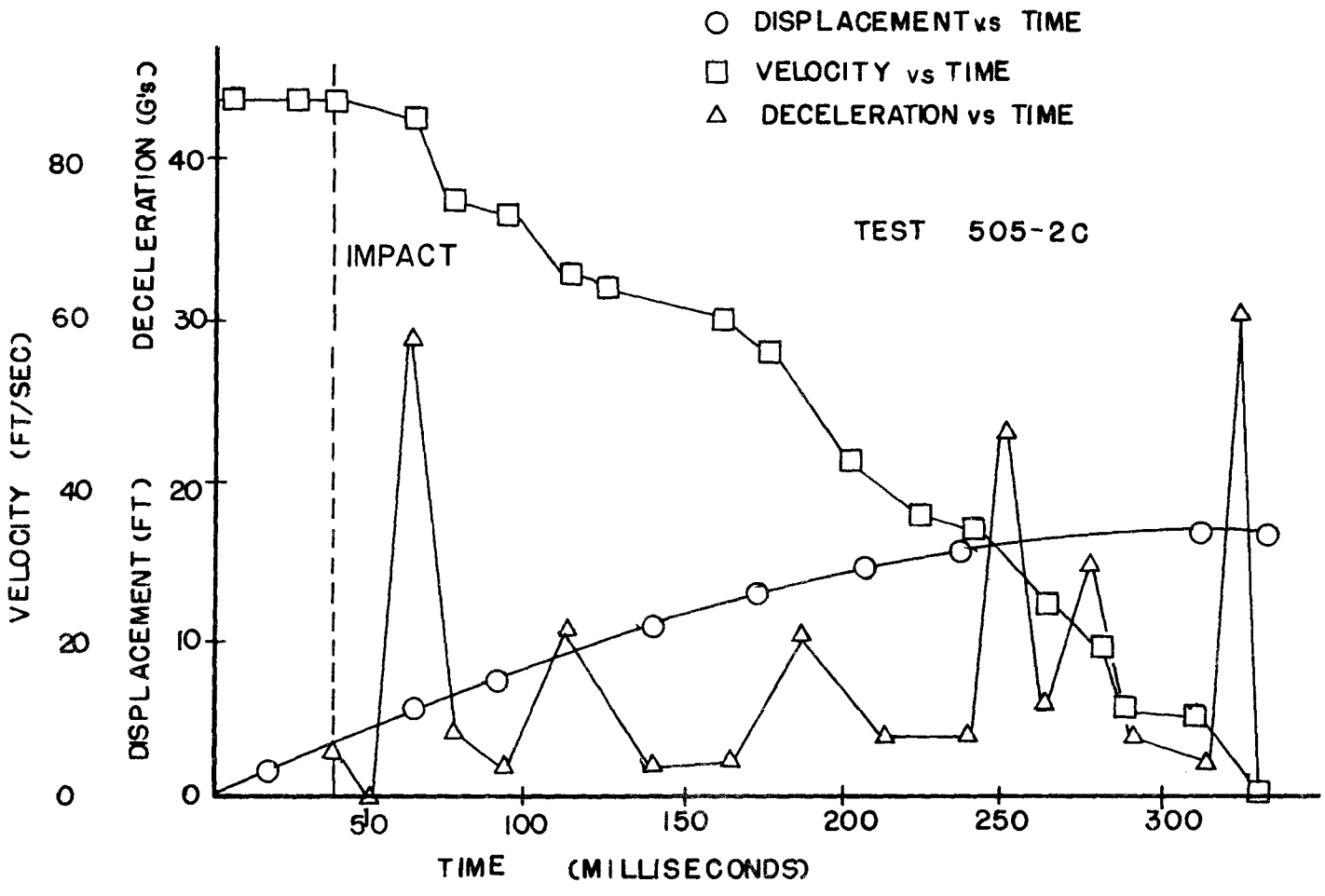

FIGURE 7B. DISPLACEMENT, VELOCITY, AND DECELERATION VS. TIME FOR TEST 505-2C

TABLE 7 B.

TEST RF 505-2C

ARA TORSHOK BARRIER 15° NOSE ANGLE

1960 BUICK, 4 DOOR SEDAN, 4940 LB.

HIGH SPEED FILM DATA

Time Milliseconds	Displacement ft	Velocity ft/sec	Deceleration ft/sec^2	g's
0	0		0	0
		87.1		
12.4	1.08		0	0
		87.1		
24.8	2.16		9	0
		87.1		
37.2 Impact	3.24		137	4.3
		85.4		
49.6	4.30		0	0
		85.4		
62.0	5.30		902	28.0
		74.2		
74.4	6.28		129	4.0
		72.6		
86.8	7.18		65	2.0
		71.8		
99.2	8.07		177	5.5
		68.6		
111.6	8.92		331	10.3
		64.5		
124.0	9.72		258	8.0
		61.3		
136.4	10.48		65	2.0
		60.5		
148.8	11.23		387	12.0
		55.7		
161.20	11.92		73	2.3
		54.8		
173.60	12.60		226	7.0
		42.0		
186.0	13.12		331	10.3
		37.9		
198.4	13.59		194	6.0
		35.5		
210.8	14.03		129	4.0
		33.9		
223.2	14.45		129	4.0
		32.3		
235.6	14.85		653	20.3
		24.2		
248.0	15.15		194	6.0
		21.8		
260.4	15.42		460	14.3
		16.1		
272.8	15.62		129	4.0

(continued on next page)

TABLE 7B.

TEST RF 505-2C (continued)

Time	Displacement	Velocity	Deceleration	
Milliseconds	ft	ft/sec	ft/sec^2	g's
		14.5		
285.2	15.80		129	4.0
		12.9		
297.6	15.96		65	2.0
		12.1		
310.0	16.11		975	30.3
		0		
322.4	16.11		0	0
		0		
334.8	16.11		0	0

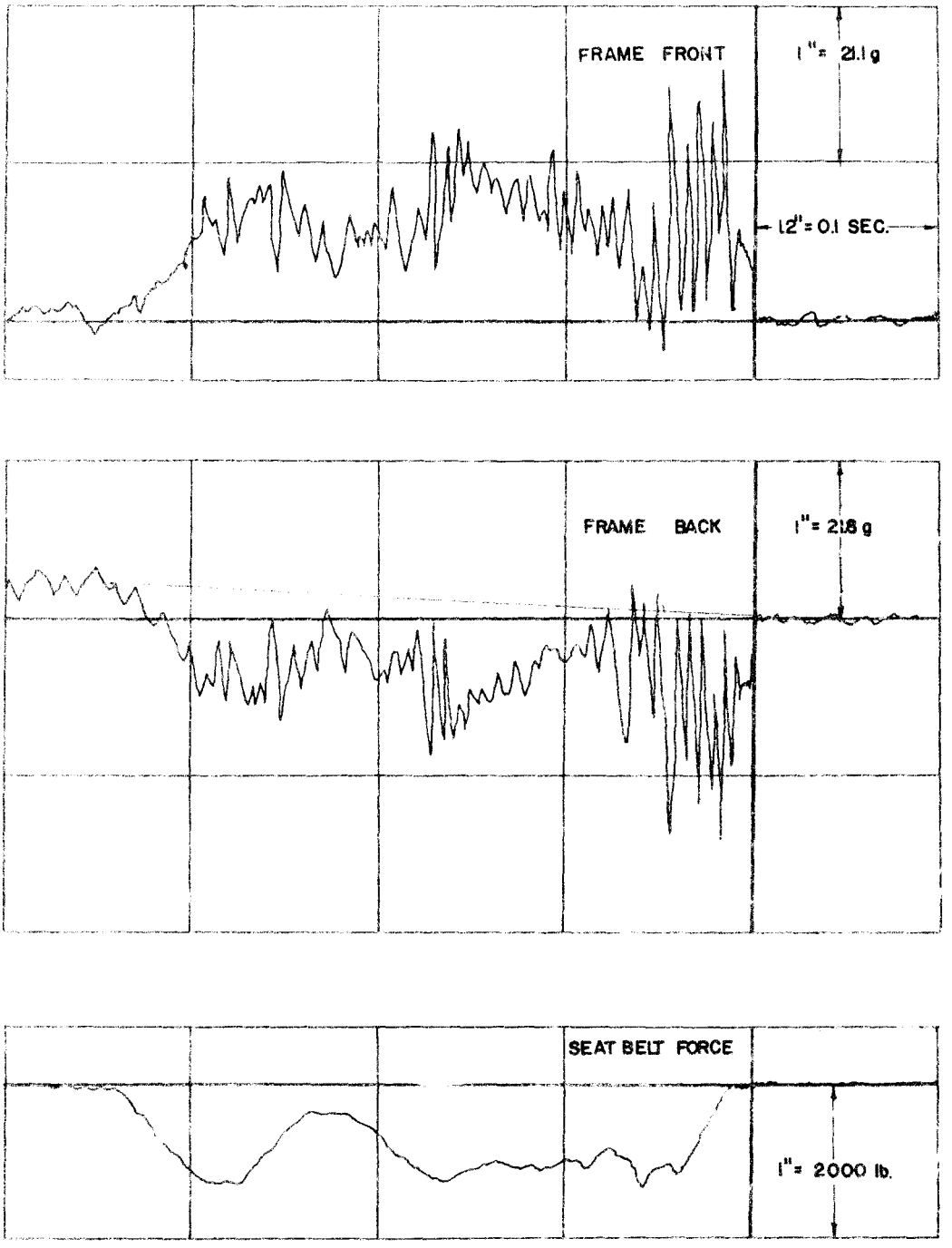

FIGURE 8B. TEST 505 2C FRAME ACCELEROMETER & SEAT BELT FORCE

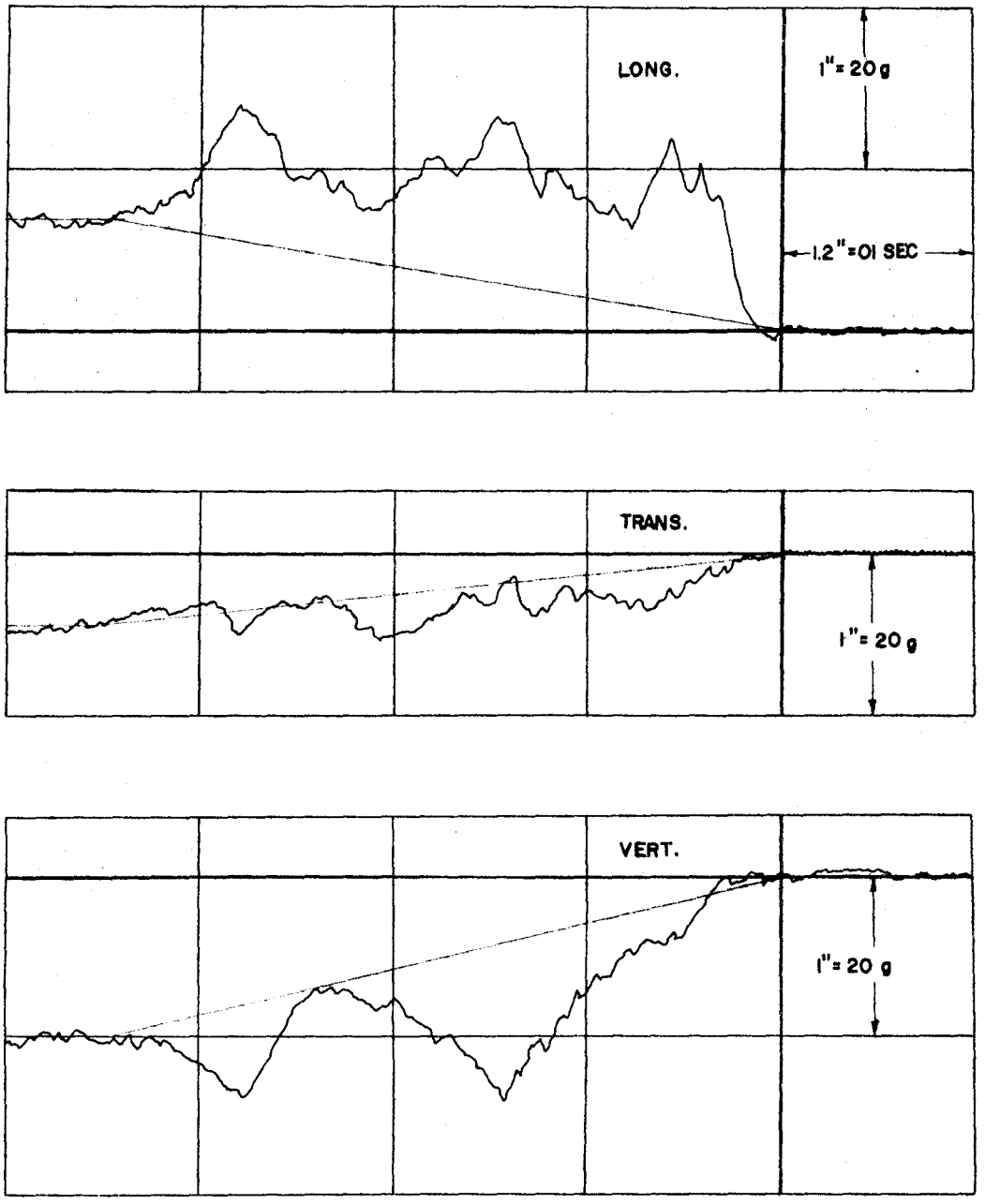

FIGURE 9B. TEST 505 2C DUMMY ACCELEROMETER DATA

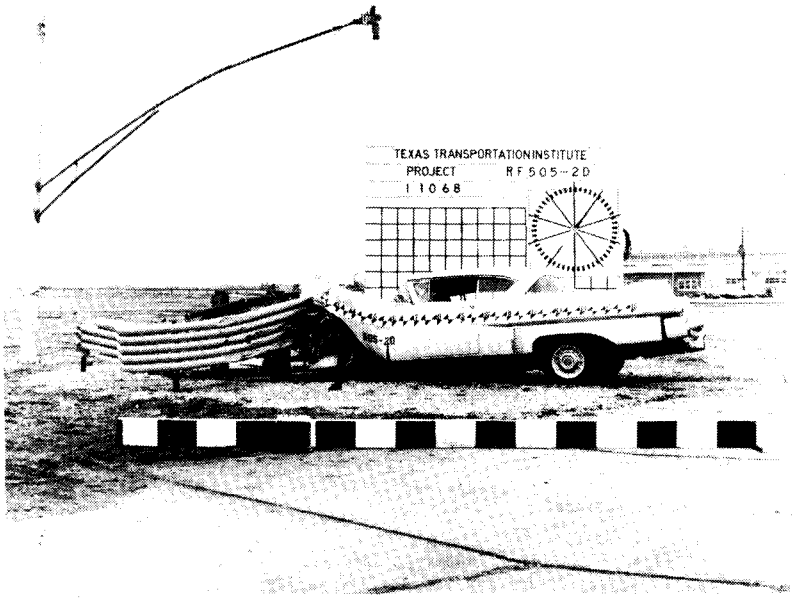

CONDITIONS AFTER TEST (ANGLE OF IMPACT = 30°)

Table 8B.
Summary of High-speed Film Crash Test Data
Test 505-2D ARA Torshok Barrier 15° Nose Angle

Vehicle Weight = 5000 lb. (1957 Cadillac, 2 door hardtop)

Vehicle Velocity = 73.3 fps or 49.9 mph

Change in Velocity = 73.3 fps or 49.9 mph

Average Deceleration = 8.1 g's

Peak Deceleration = 60.7 g's (9.35 msec.)

Duration of Impact = 0.260 sec.

Stopping Distance = 14.0 ft. (Longitudinal movement of vehicle)

Remarks: Damage to Vehicle Severe. Vehicle Deformation 1.83 ft.
Barrier Deformation 12.13 ft. Barrier Almost Total Loss.

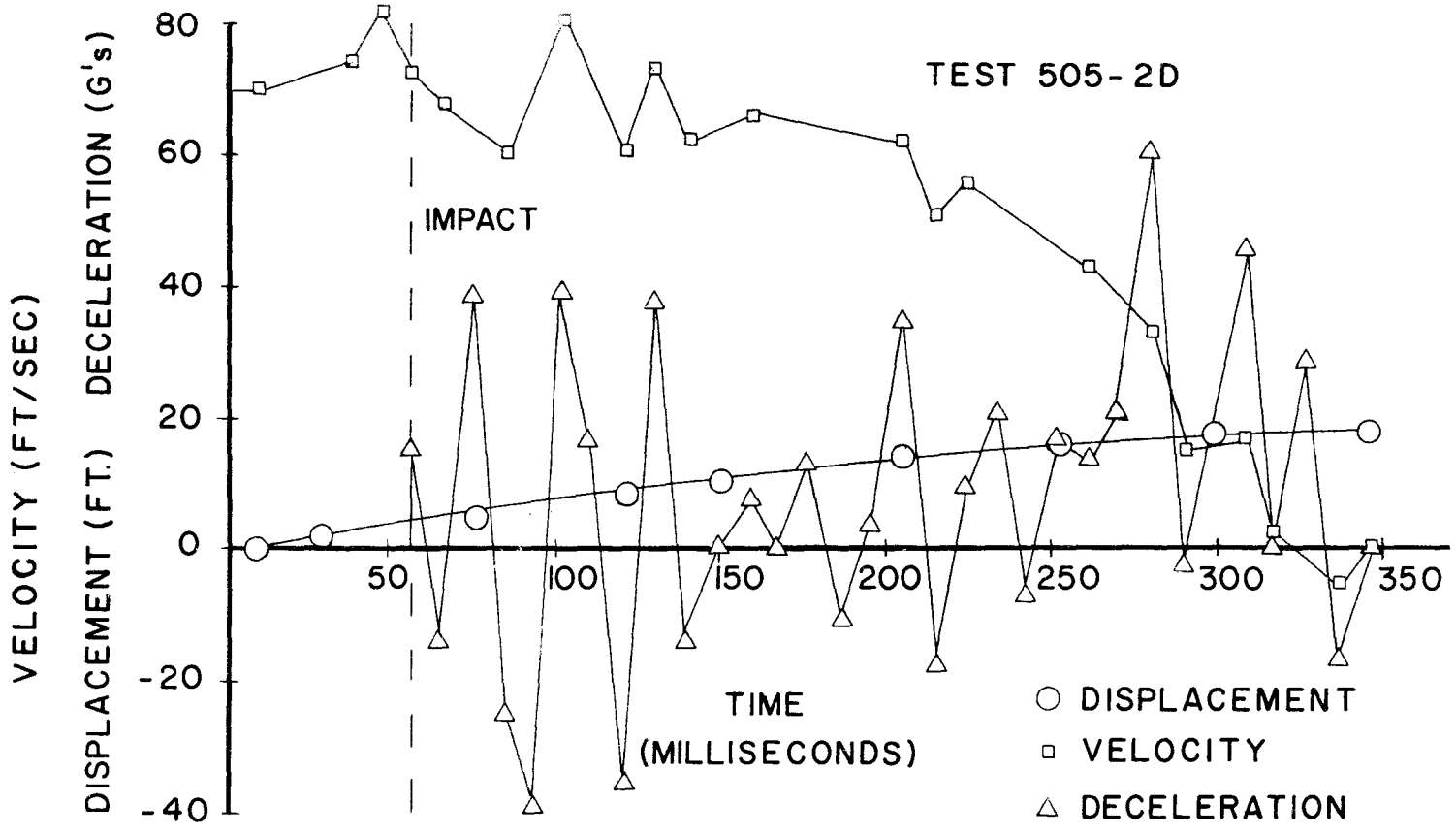

FIGURE 10B. DISPLACEMENT, VELOCITY, AND DECELERATION VS. TIME FOR TEST 505-2D

TABLE 9B.

TEST RF 505-2D

ARA TORSHOK BARRIER 15° NOSE ANGLE

1957 CADILLAC, 2-DOOR HARDTOP, 5000 LB.

HIGH SPEED FILM DATA

Time Milliseconds		Displacement ft	Velocity ft/sec		Deceleration ft/sec^2	g's
			70.6			
9.35		0.66				
			69.5			
18.70		1.31				
			69.5			
28.05		1.96		73.3		
			74.9	Avg.		
37.40		2.66				
			82.5			
46.75		3.43			0	0
			72.8			
56.10	Impact	4.11			514	16.0
			68.5			
65.45		4.75			-460	-14.3
			72.8			
74.80		5.43			1273	39.6
			60.9			
84.15		6.00			-814	-25.3
			68.5			
93.50		6.64			-1262	-39.2
			80.3			
102.85		7.39			1262	39.2
			68.5			
112.20		8.03			568	17.6
			63.2			
121.55		8.62			-1134	-36.2
			73.8			
130.90		9.31			1250	38.9
			62.1			
140.25		9.89			-460	-14.3
			66.4			
149.60		10.51			0	0
			66.4			
158.95		11.13			235	7.3
			64.2			
168.30		11.73			0	0
			64.2			
177.65		12.33			460	14.3
			59.9			

(continued on next page)

TABLE 9B.

TEST RF 505-2D
(Continued)

Time	Displacement	Velocity	Deceleration	
Milliseconds	ft	ft/sec	ft/sec^2	g's
187.00	12.89		-353	-11.0
		63.2		
196.35	13.48		128	4.0
		62.0		
205.70	14.06		1145	35.6
		51.3		
215.05	14.54		-578	-17.9
		56.7		
224.40	15.07		342	10.6
		53.5		
233.75	15.57		685	21.3
		47.1		
243.10	16.01		-225	- 7.0
		49.2		
252.45	16.47		578	17.9
		43.8		
261.80	16.88		450	14.0
		39.6		
271.15	17.25		685	21.3
		33.2		
280.50	17.56		1950	60.7
		15.0		
289.85	17.70		-107	-3.3
		16.0		
299.20	17.85		-129	-4.0
		17.2		
308.55	18.01		1500	46.6
		3.2		
317.90	18.04		0	0
		3.2		
327.25	18.07		910	28.3
		-5.3		
336.60	18.02		-568	-17.6
		0.0		
345.95	18.02		0	0
		0.0		
355.30	18.02		0	0

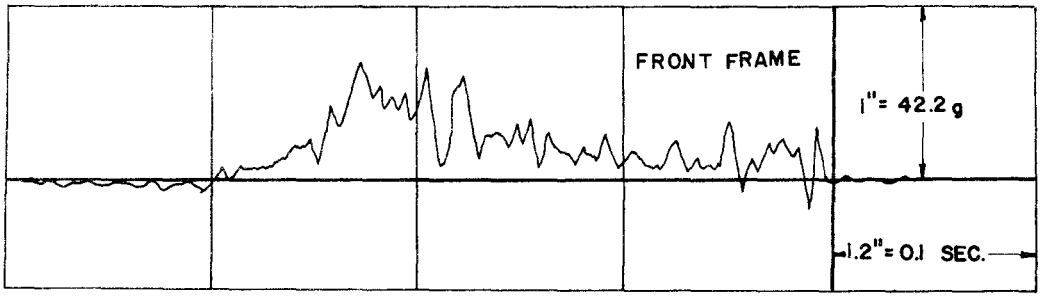

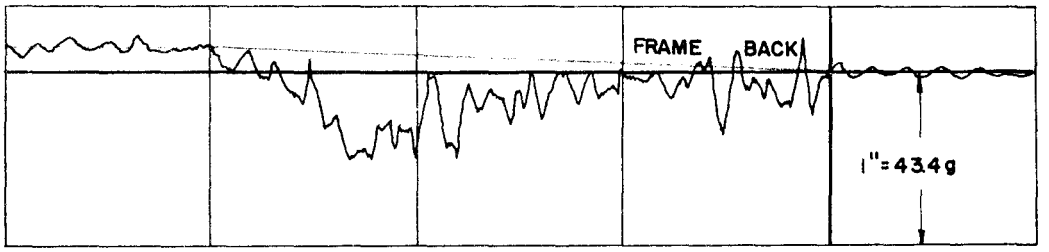

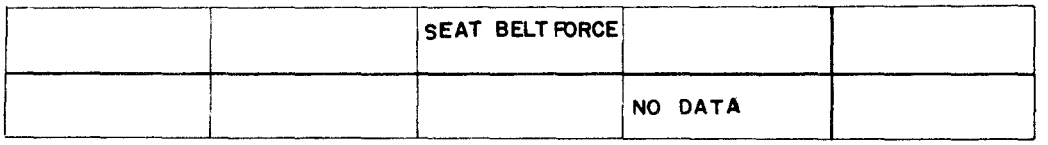

FIGURE IIB. TEST 505 2D FRAME ACCELEROMETER DATA & SEAT BELT FORCE

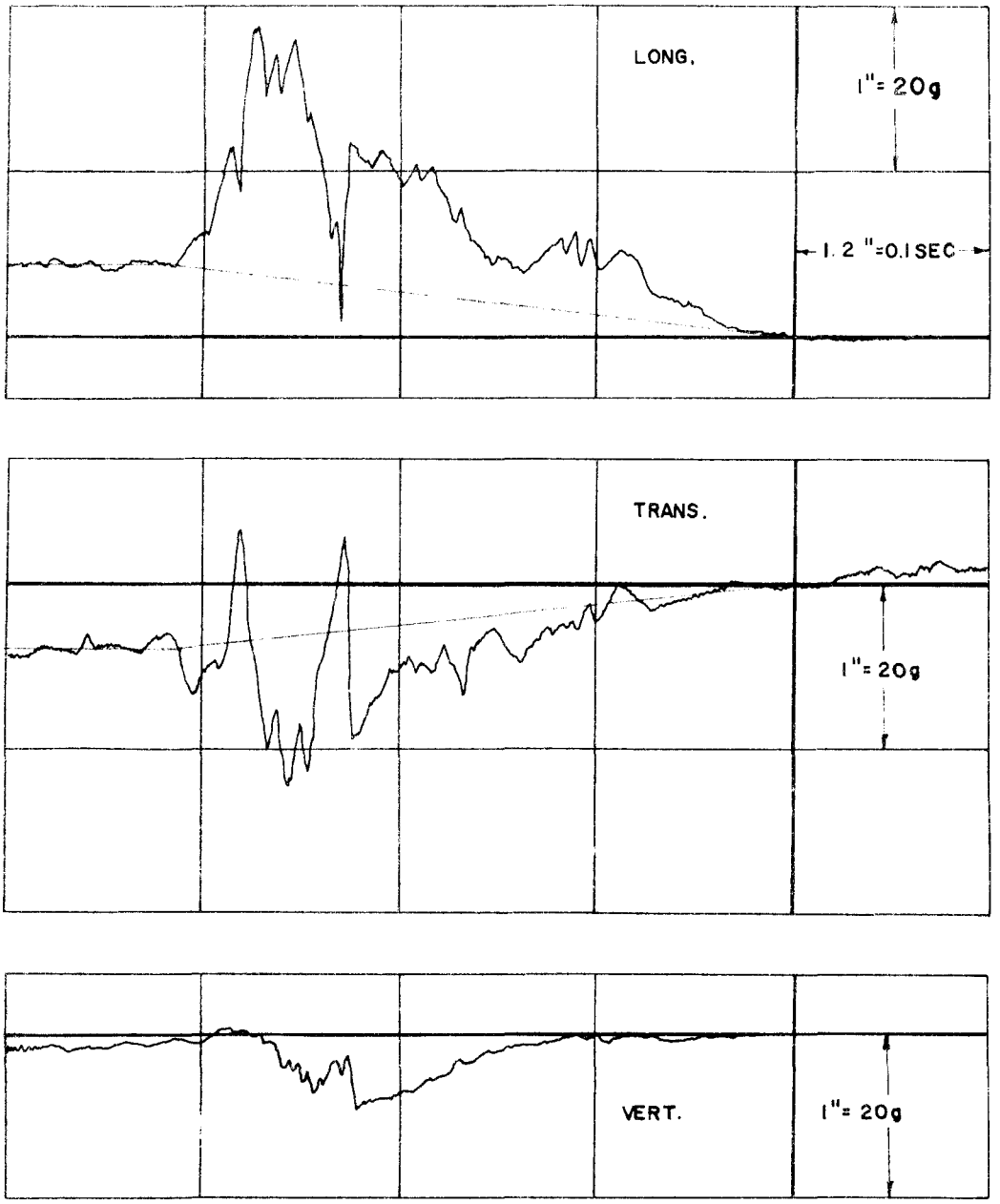

FIGURE 12B. TEST 505 2D DUMMY ACCELEROMETER DATA

TECHNICAL MEMORANDUM 505-2S

SUPPLEMENT TO 505-2

Texas Transportation Institute
Texas A&M Research Foundation

TOR-SHOK AND ROTO-SHOK ENERGY ABSORBING PROTECTIVE BARRIERS

A Tentative Progress Memorandum on Contract No. CPR-11-5851

U. S. Department of Transportation
Federal Highway Administration
Bureau of Public Roads

by

T. J. Hirsch
Research Engineer and Principal Investigator

Harry L. Smith
Engineering Research Associate

and

Don L. Ivey
Associate Research Engineer

Crash tests and evaluations were conducted under the Office of Research and Development, Structures and Applied Mechanics Division's Research Program on Structural Systems in Support of Highway Safety (4S Program). The opinions, findings, and conclusions expressed in this report are those of the authors and not necessarily those of the Bureau of Public Roads.

January 31, 1969

INTRODUCTION

Technical Memorandum 505-2 (July 1968) described three full-scale head-on vehicle crash tests with the ARA TOR-SHOK Energy Absorbing Protective Barrier and one vehicle crash test where the trajectory of the vehicle was at a 30° angle with the barrier centerline. The three head-on crash tests were successful in that the TOR-SHOK barrier performed as intended by the designers. The 30° angle crash test was considered unsatisfactory. The nose piece, that part of the TOR-SHOK barrier consisting of a radial nose section and straight side elements, rotated away from the path of the vehicle and allowed the vehicle to strike the rigid vertical support posts. Since these tests were conducted, the TOR-SHOK barrier has been modified to stabilize the nose piece and prevent it from rotating. In addition to this modification of the TOR-SHOK, a new ROTO-SHOK Energy Absorbing Barrier has been developed.

From December 4, 1968 to December 6, 1968, the Highway Safety Research Center of the Texas Transportation Institute conducted two full-scale vehicle crash tests on the modified TOR-SHOK and new ROTO-SHOK Energy Absorbing Highway Protective Barriers which were developed by Aerospace Research Associates (ARA), Inc., of 2017 West Garvey Avenue, West Covina, California. A detailed description of these tests is provided by this memorandum. These tests and evaluations were conducted under the Office of Research and Development, Structures and Applied Mechanics Division's, Research Program on Structural Systems in Support of Highway Safety (4S Program).

Integral to the evaluation of the two crash tests are photographs of the vehicle and barrier before and after each test, a summary of the high-speed motion picture film data taken of the tests, and a collection of the electromechanical instrumentation data obtained during the tests (see Appendix S-B).

DESCRIPTION OF BARRIERS

The TOR-SHOK Energy Absorbing Barrier which was used in Test 505-2E is detailed on pages B12 and B13 of ARA Report No. 96*. This barrier had a nose angle of 15°, a nose radius of 31 in., and an elliptical tubular nose weighing 845 lbs. The idealized function of this system is described in Report No. 96* and also in TTI Technical Memorandum 505-2**.

The ROTO-SHOK Energy Absorbing Barrier was developed by ARA, Inc. under a contract with the Engineering Division, Office of Traffic Operations, Bureau of Public Roads. The barrier was fabricated and delivered by ARA and was installed and tested by personnel of the Texas Transportation Institute. The ROTO-SHOK protective system is designed to perform as shown in Figure S-1. It consists of a series of straight sections of elliptical tubes rigidly supported from the ROTO-SHOKs by another system of elliptical tubes. Detailed drawings of this mechanism are given in Appendix S-A. Figures S-2 and S-3 show the installation which was tested. The ROTO-SHOKs are mounted by their inner drums on posts (Figure S-3). When the vehicle impacts the series of straight sections (Figure S-2), the protective barrier tubes transmit the impact forces to the elliptical tubes which initiate the angular dissipation of energy in the ROTO-SHOKs. The ROTO-SHOKs contain small diameter tubes positioned with an interference fit in the annulus of two concentric drums. At impact, the rotation of the drums relative to one another provides the energy absorption mechanism

---

* "A Reusable Energy Absorbing Highway Protective System for Median Areas", Aerospace Research Associates, Inc., ARA Report No. 96, June, 1968.

** Hirsch, T. J., "TOR-SHOK Energy Absorbing Protective Barrier", Technical Memorandum 505-2, Texas Transportation Institute, Texas A&M Research Foundation, July 31, 1968.

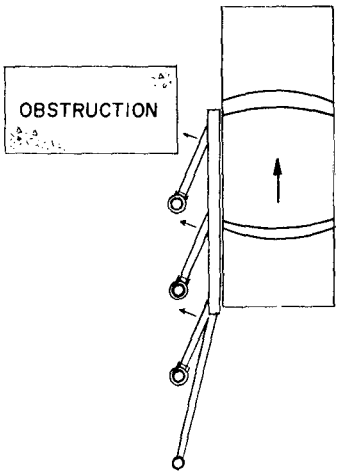

(3) VEHICLE IS REDIRECTED TO MISS OBSTRUCTION

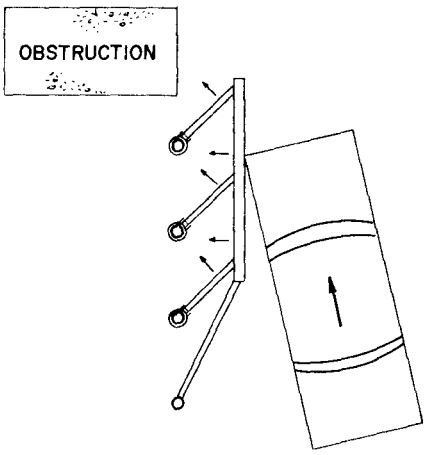

(2) ROTO-SHOK ROTATES AND BEGINS REDIRECTING VEHICLE

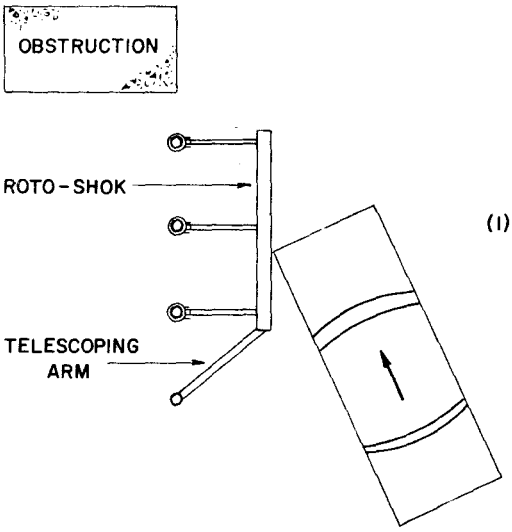

(1) VEHICLE CONTACTS ROTO-SHOK

FIGURE S-1, IDEALIZED FUNCTION OF ROTO-SHOK

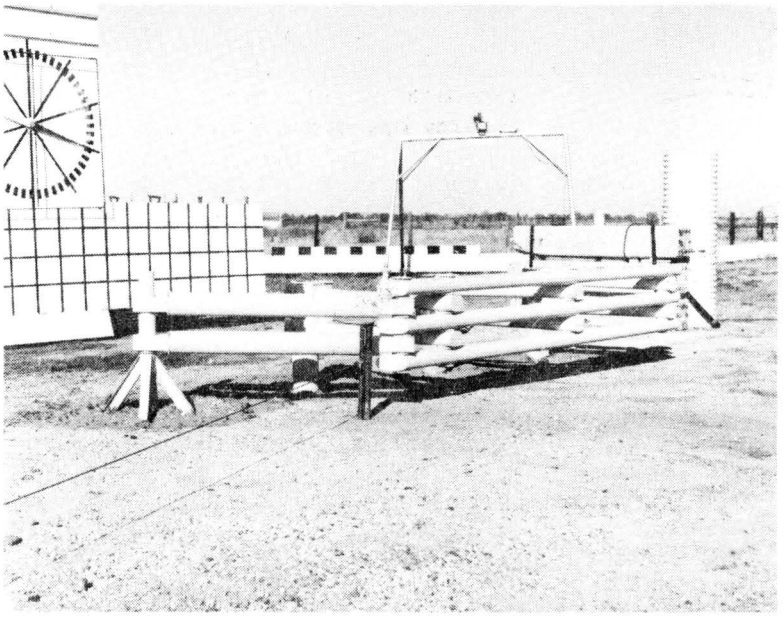

Figure S-2, ROTO-SHOK Viewed From The Line Of Vehicle Trajectory

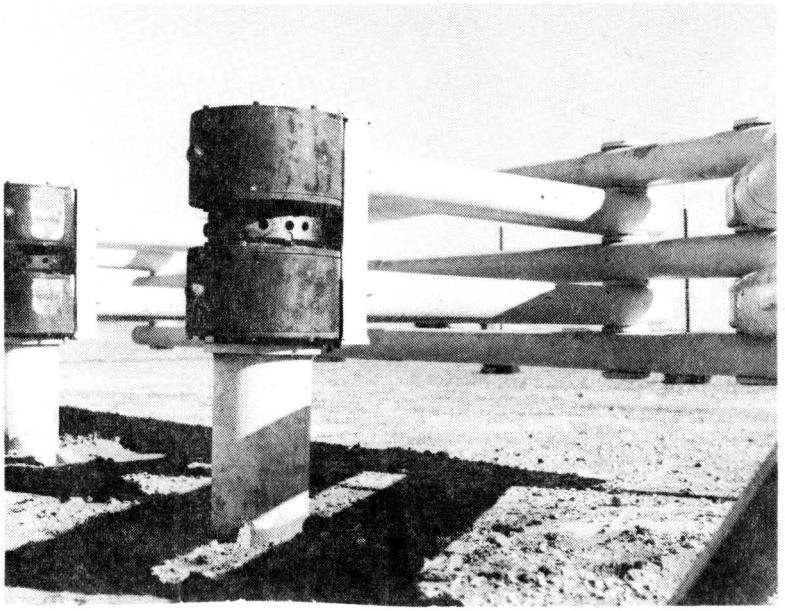

Figure S-3, Details Of ROTO-SHOK From Rear

in terms of cyclic bending strain around the circumference of the small diameter tubes. The resistance to torque provided by the ROTO-SHOK exerts a resisting force on the vehicle as the barrier deforms. This rotation of the ROTO-SHOK arms, and resulting lateral translation of the impact section, allows the vehicle to be redirected with nominal transverse decelerations.

TEST 2E RESULTS, TOR-SHOK BARRIER

Figures S-4 and S-5 show the vehicle and barrier at various stages of Test 2E. The 3600 lb. vehicle struck the ARA TOR-SHOK barrier at an angle of 25° with the barrier longitudinal axis at a speed of 53.0 mph. The vehicle slid down the nose piece, finally pocketing and striking the rigid vertical support post. The intended redirection of the vehicle was not achieved and impact with the back-up post was extremely severe. The maximum longitudinal deceleration was approximately 26 g's (from the vehicle accelerometer data, Appendix S-B). The average longitudinal deceleration was approximately 8.5 g's*. The vehicle traveled 10.9 feet after striking the nose angle before resting against the vertical back-up post.

The following conclusions can be drawn from Test 2E:

1. The barrier did not redirect the vehicle.
2. The vehicle damage was severe (see Figures S-8 and S-9).

---

* Average g values were calculated from the change in vehicle velocity and the longitudinal movement of the vehicle c.g. from its position at first contact with the barrier to its position at maximum penetration into the barrier.

3. Damage to the TOR-SHOK barrier was severe. Many TOR-SHOKs were damaged beyond repair.
4. The deceleration level was severe.

Comparing the rigid barrier maximum deceleration of 47.7 g's* to the approximately 26 g's obtained in Test 2E, it can be seen that the Attenuation Index is about .55.

$$A.I._{max} = \frac{G_{(max\ TOR\text{-}SHOK)}}{G_{(max\ rigid)}}$$

Analysis of the high-speed film data shows, however, that the vehicle was still traveling about 37 mph when collision with the rigid vertical support post occurred. The severe impact with this post is what caused most of the damage to the vehicle. In the last 1.5 feet of vehicle longitudinal movement, the average deceleration (from photographic data, Table S-B1) was 21.4 g's.

---

* Estimated Maximum Rigid Barrier Deceleration = 0.9 V, where V is in mph.
Estimated Average Rigid Barrier Deceleration = 0.574 V, where V is in mph.

Emori, Richard I., "Analytical Approach to Automobile Collisions," SAE Paper 680016, Engineering Congress, Detroit, January 8, 1968.

Summary, Test 2 E

Conditions after test (vehicle struck barrier at angle of 25°)

Table S-1

Test 505-2E ARA TOR-SHOK Barrier 15° Nose Angle

Vehicle Weight = 3600 lbs. (1961 Ford, 4-dr.)
Impact Angle = 25°
Vehicle Velocity = 53.0 mph or 77 fps.
Average Deceleration = 8.5 g's (longitudinal)
Peak Deceleration = 26 g's (30 msec) (longitudinal)
Duration of Impact = 0.212 sec
Stopping Distance = 10.9 ft.

Remarks: Damage to both the TOR-SHOK and vehicle was severe.
Vehicle deformation, 3.5 ft. - Barrier deformation, 3.1 ft.

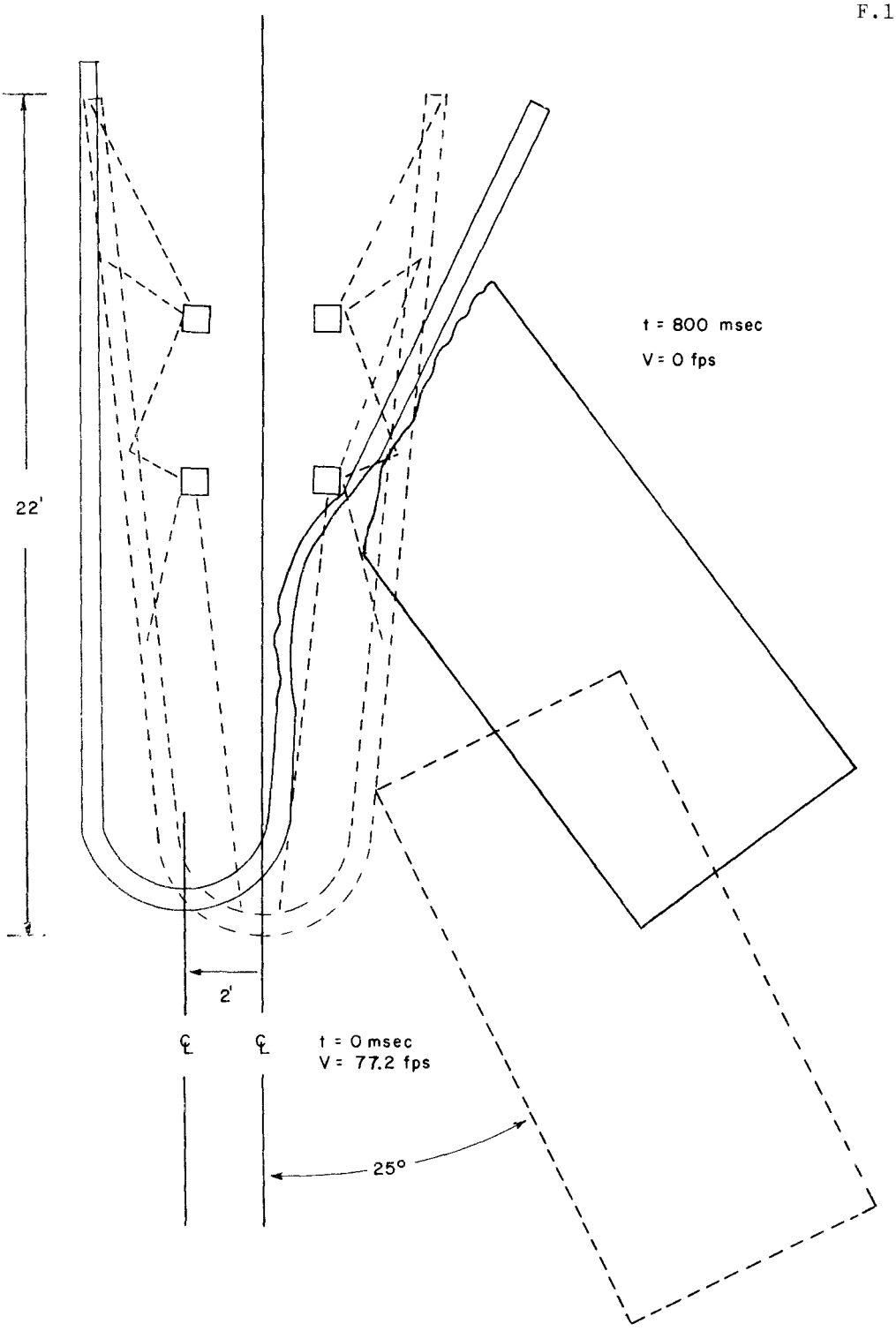

FIGURE S-4, TOR-SHOK POSITION TIME DIAGRAM, TEST 505-2E

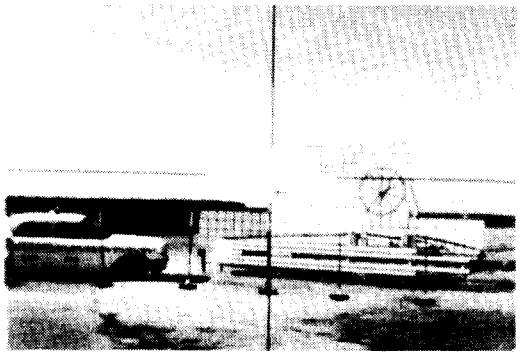

1

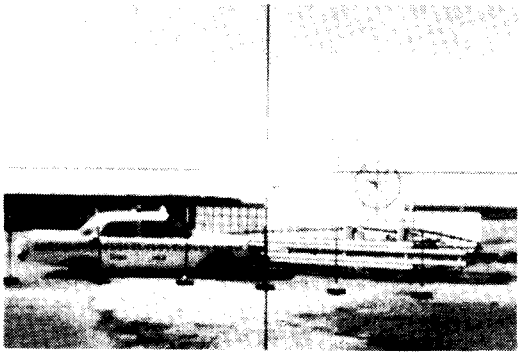

2

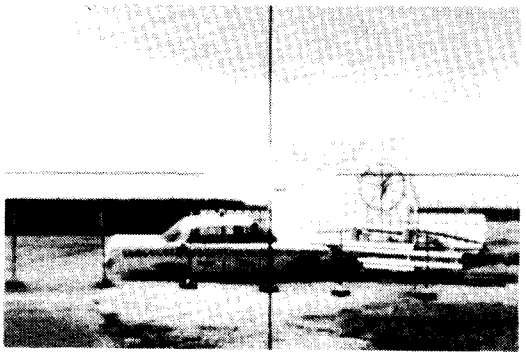

3

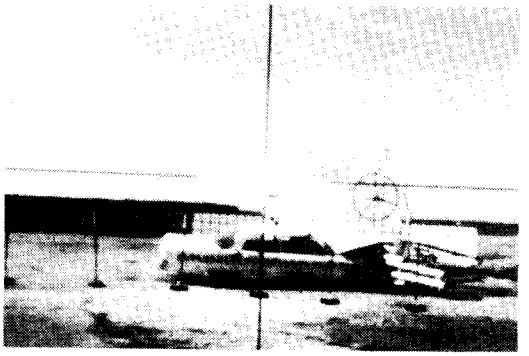

4

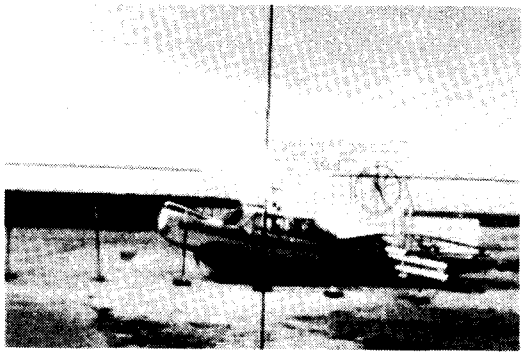

5

6

Figure S-5, Sequential Photographs Of TOR-SHOK, Test 2E

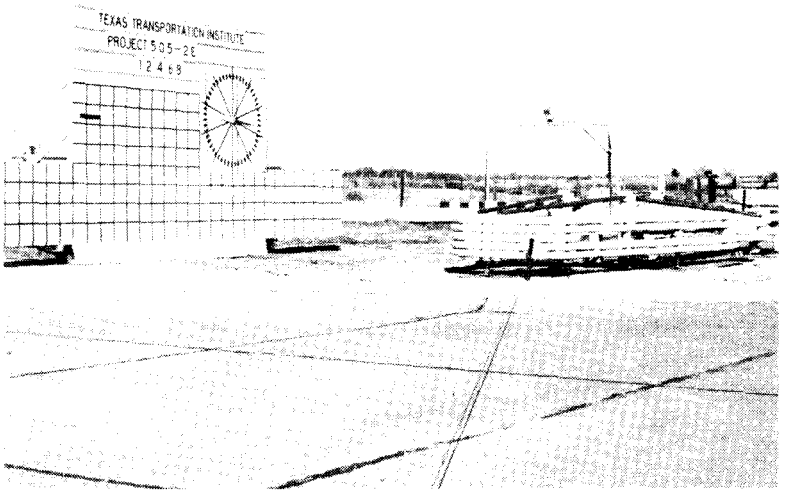

Figure S-6, TOR-SHOK Before Collision, Test 2E

Figure S-7, Vehicle Before Collision, Test 2E

Figure S-8, Damage To Left Front Of Vehicle

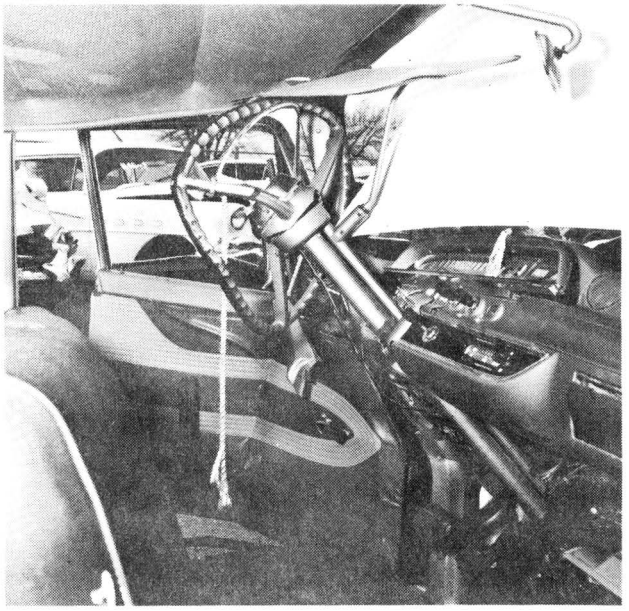

Figure S-9, Intrusion Of Steering Column Into Passenger Compartment

TEST 2F RESULTS, ROTO-SHOK BARRIER

Test 2F was a 25° angle impact by a 4290 lb. vehicle traveling 46.0 mph. The vehicle struck the ROTO-SHOK barrier as shown in Figures S-10 and S-11. After impact, the vehicle was redirected with a velocity of 34.6 mph. Total energy absorbed by the ROTO-SHOK was approximately 118 kip-ft (40% of the vehicle kinetic energy). The maximum vehicle longitudinal deceleration shown using the 10 HZ Filter, was approximately 5 g's. The average vehicle longitudinal deceleration was 1.1 g's while in contact with the ROTO-SHOK.

In summary, the following conclusions can be drawn from Test 2F:

1. The barrier performed as designed.
2. The vehicle damage was superficial (Figures S-11 and S-13).
3. Damage to the ROTO-SHOK was moderate. Much of the elliptical tubing in the straight section needed to be replaced. (Figure S-15).
4. The deceleration level was moderate.

Summary, Test 2 F

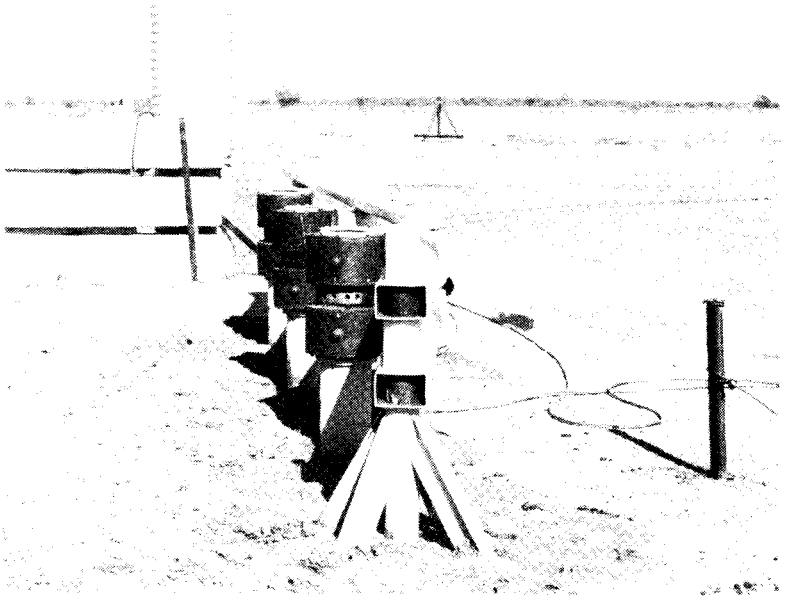

Conditions after test (vehicle struck barrier at angle of 25°)

Table S-2

Test 505-2F ARA ROTO-SHOK Barrier

Vehicle Weight = 4290 lbs. (1959 Lincoln, 4-dr.)
Impact Angle = 25°
Vehicle Velocity = 46.0 mph or 67 fps.
Change in Velocity = 11.4 mph. or 16.3 fps. (longitudinal)
Average Deceleration = 1.1 g's (longitudinal)
Peak Deceleration = 5 g's (40 msec) (longitudinal)
Duration of Impact = 0.500 sec.

Remarks: Damage to ROTO-SHOK was moderate. Vehicle damage was superficial.
Vehicle Deformation, .83 ft. - Barrier Deformation, 4 ft.

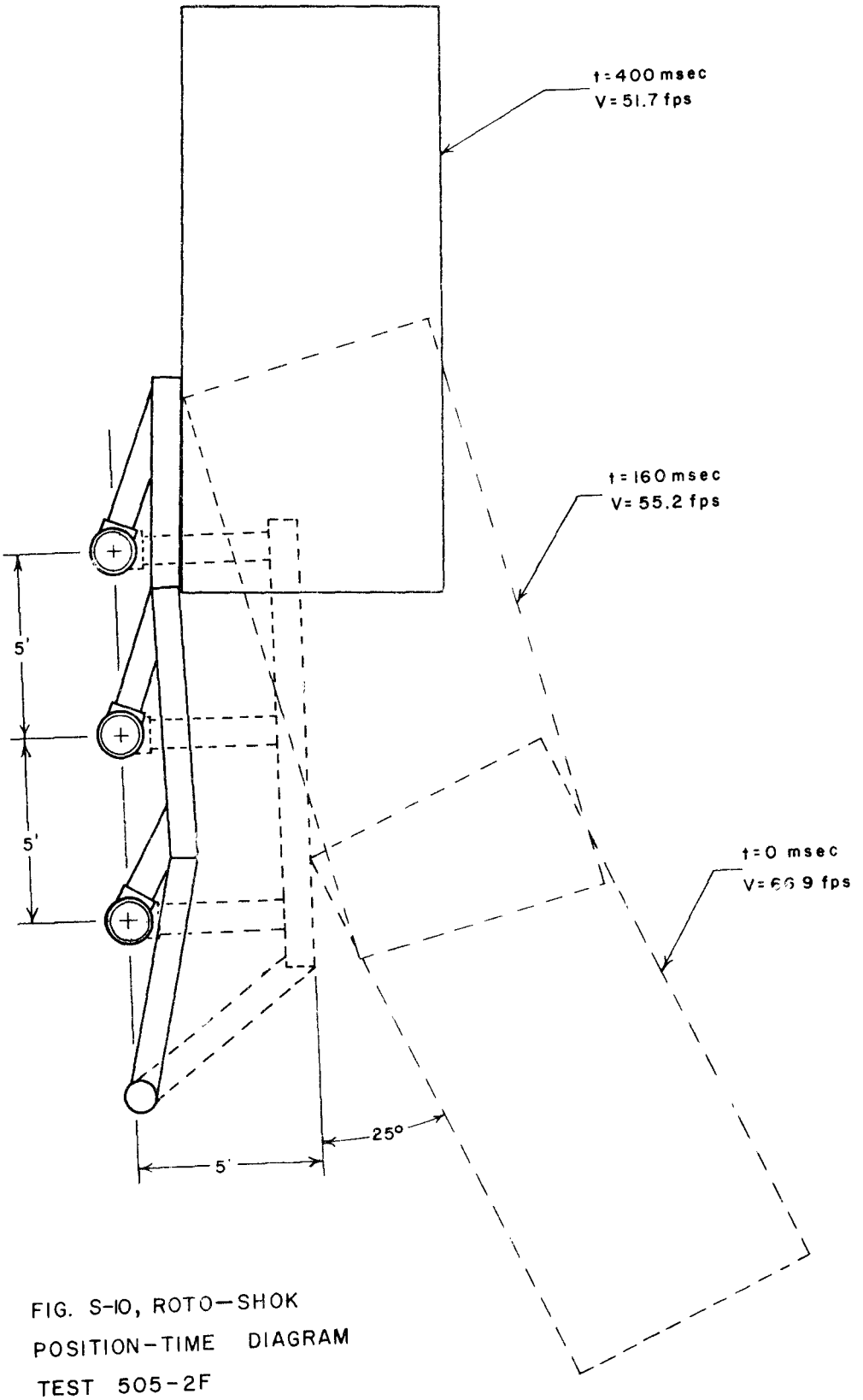

FIG. S-10, ROTO-SHOK
POSITION-TIME DIAGRAM
TEST 505-2F

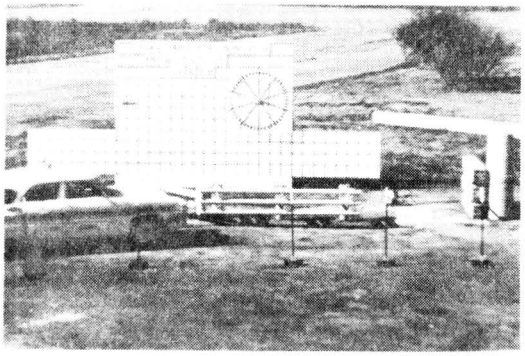

1

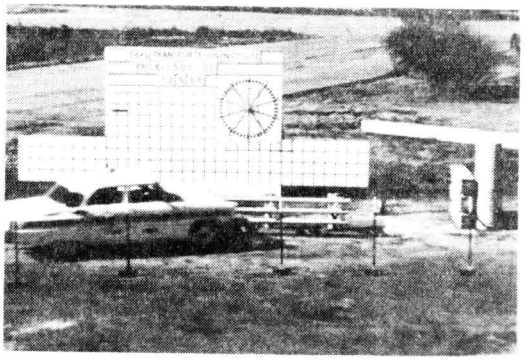

2

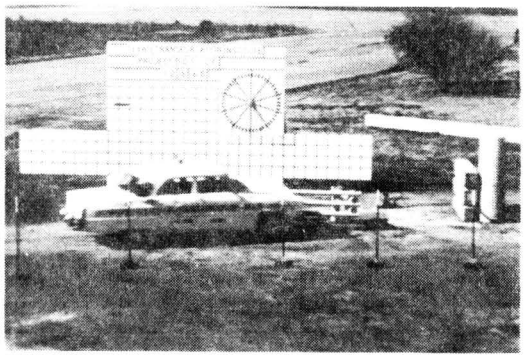

3

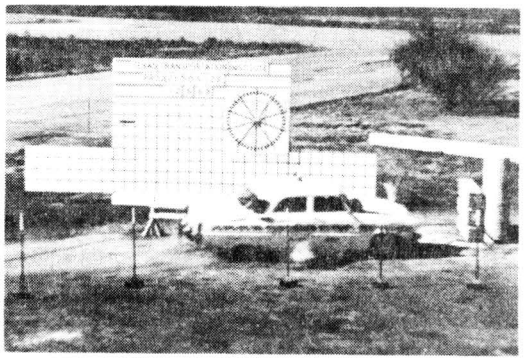

4

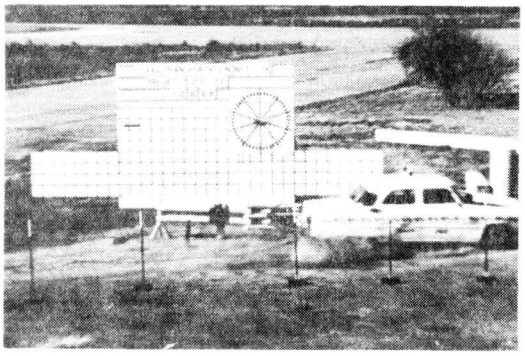

5

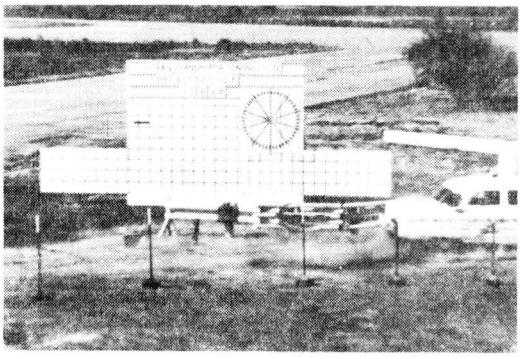

6

Figure S-11, Sequential Photographs ROTO-SHOK, Test 2F

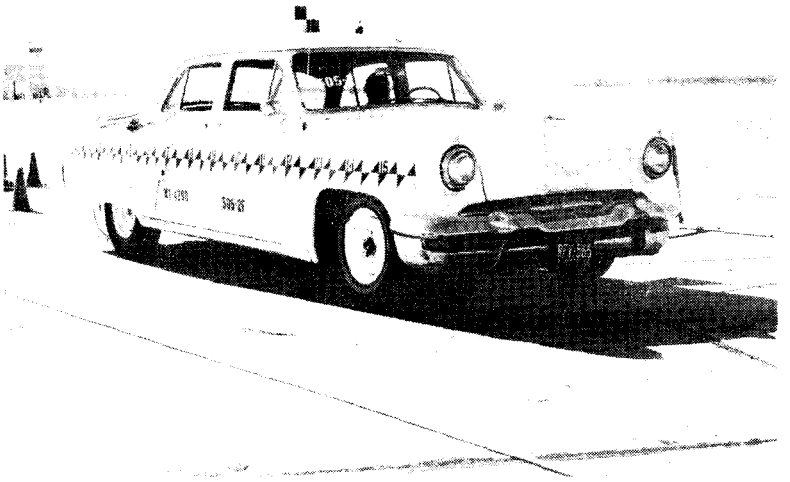

Figure S-12, Vehicle before Collision, Test 2F

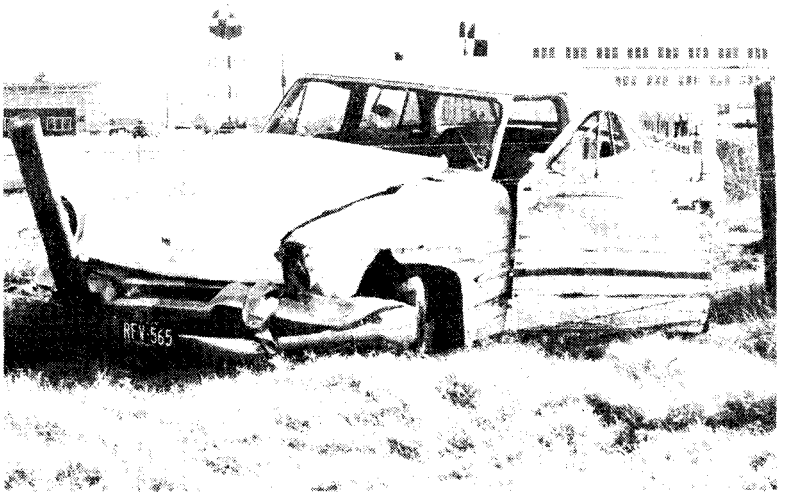

Figure S-13, Vehicle Damage, Test 2F

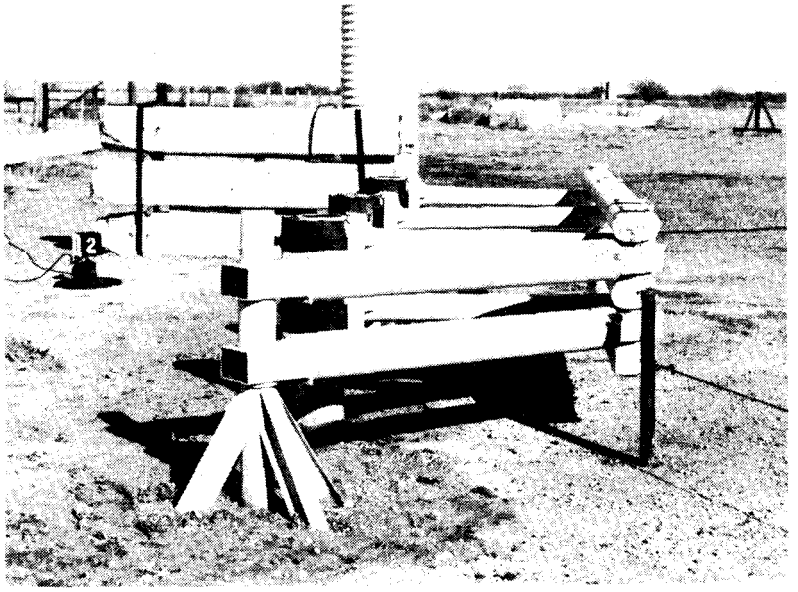

Figure S-14, ROTO-SHOK Before Collision, Test 2F

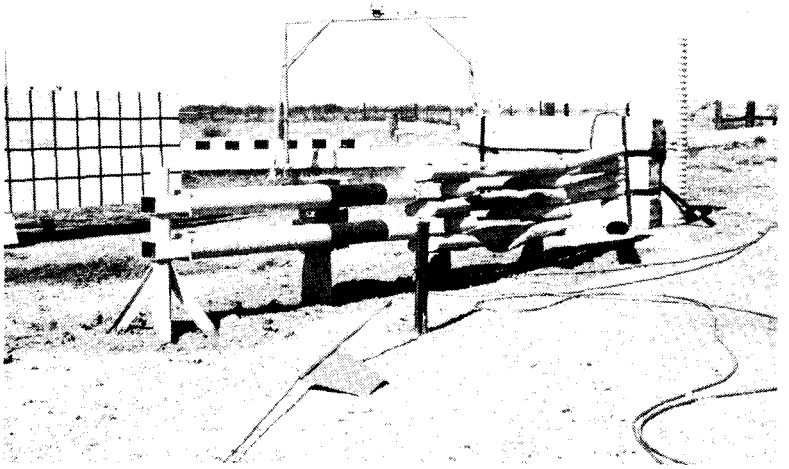

Figure S-15, ROTO-SHOK After Collision, Test 2F

SUMMARY AND CONCLUSIONS

A full-scale vehicle crash test was performed on the modified ARA TOR-SHOK Energy Absorbing Barrier. The nose piece was constructed of elliptical tubes. For a detailed description see ARA Report No. 96*, pages B12 and B13.

The 3600 lb. vehicle struck the barrier at an angle of 25° with the longitudinal barrier axis and at a speed of 53 mph. The barrier did not redirect the vehicle as intended. Instead, the vehicle slid down the nose piece, pocketed, and came to a sudden and severe stop. The designers are now in the process of making further modifications.

Also included are the results of a full-scale vehicle crash test on the ARA ROTO-SHOK Energy Absorbing Barrier system which is described in ARA Report No. 96*, pages C2 and C3. The 4290 lb. vehicle struck the barrier at an angle of 25° and at a speed of 46 mph. The barrier performed as intended and redirected the vehicle with only superficial damage to both.

---

* "A Reusable Energy Absorbing Highway Protective System for Median Areas", Aerospace Research Associates, Inc., ARA Report No. 96, June, 1968.

APPENDIX S-A

DESIGN DRAWINGS OF

TOR-SHOK AND ROTO-SHOK

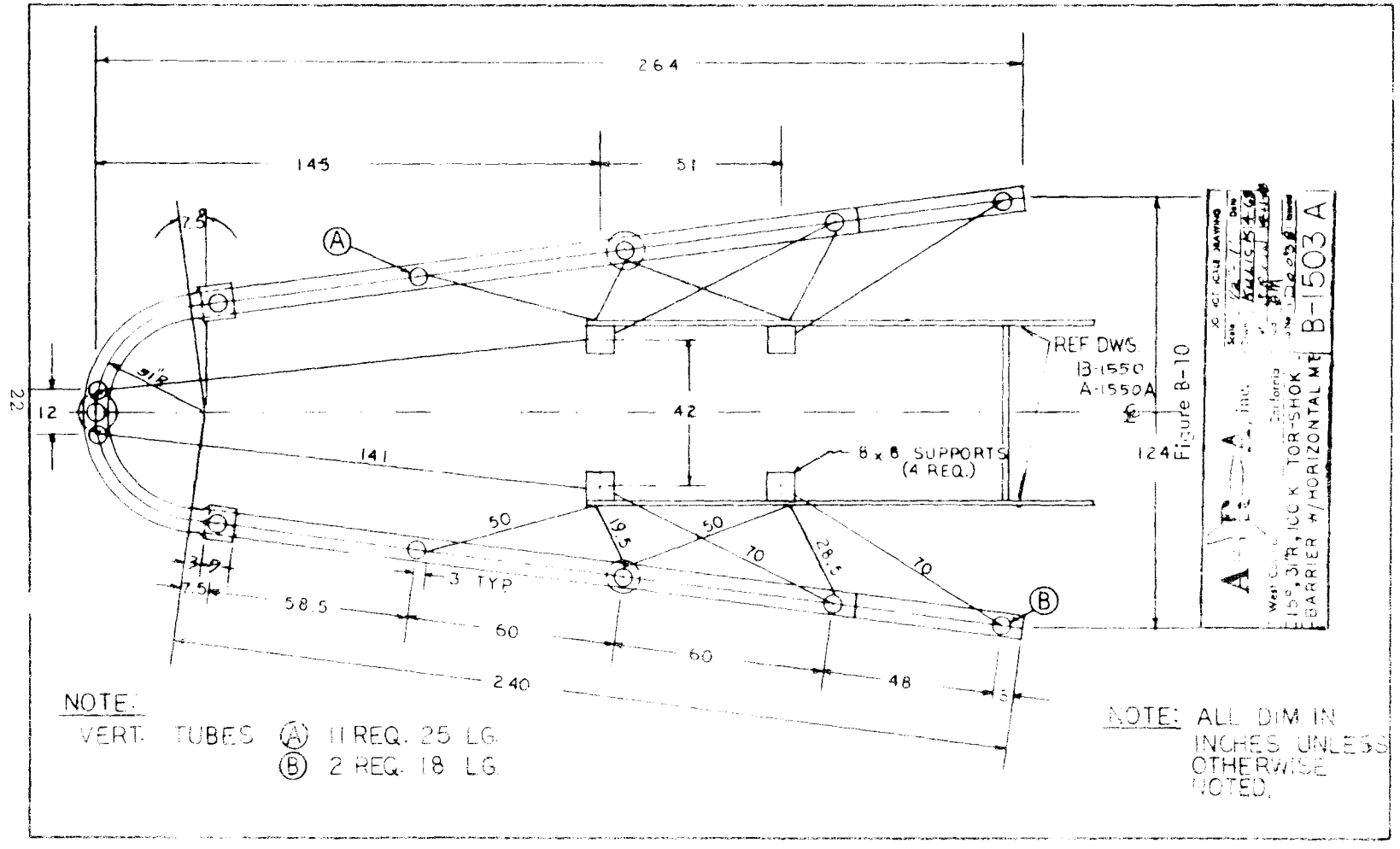
264
145
51
7.5
A
91/2
12
42
141
REF DWS
B-1550
A-1550A
6 x 6 SUPPORTS
(4 REQ.)
124
Figure B-10
50
19.5
50
70
28.5
70
3 TYP
7.5
58.5
60
60
48
240
B
B-1503 A
15°, 3/R, ROCK TOR-SHOK
BARRIER W/HORIZONTAL MT
NOTE:
VERT. TUBES (A) 11 REQ. 25 LG.
(B) 2 REQ. 18 LG.
NOTE: ALL DIM IN INCHES UNLESS OTHERWISE NOTED.

ELLIPTICAL TUBES	
AMT. REQ.	LGTH.
4 EA.	237"
4 EA.	189"

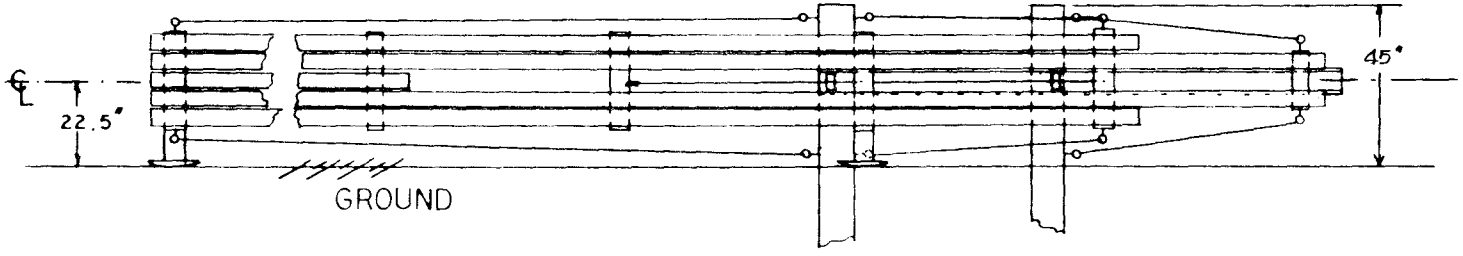

SIDE VIEW

Figure [illegible]-11

A R A, inc. West Covina California	DO NOT SCALE DRAWING
15°-31'R-100K — TOR-SHOK BARRIER	B-1502A

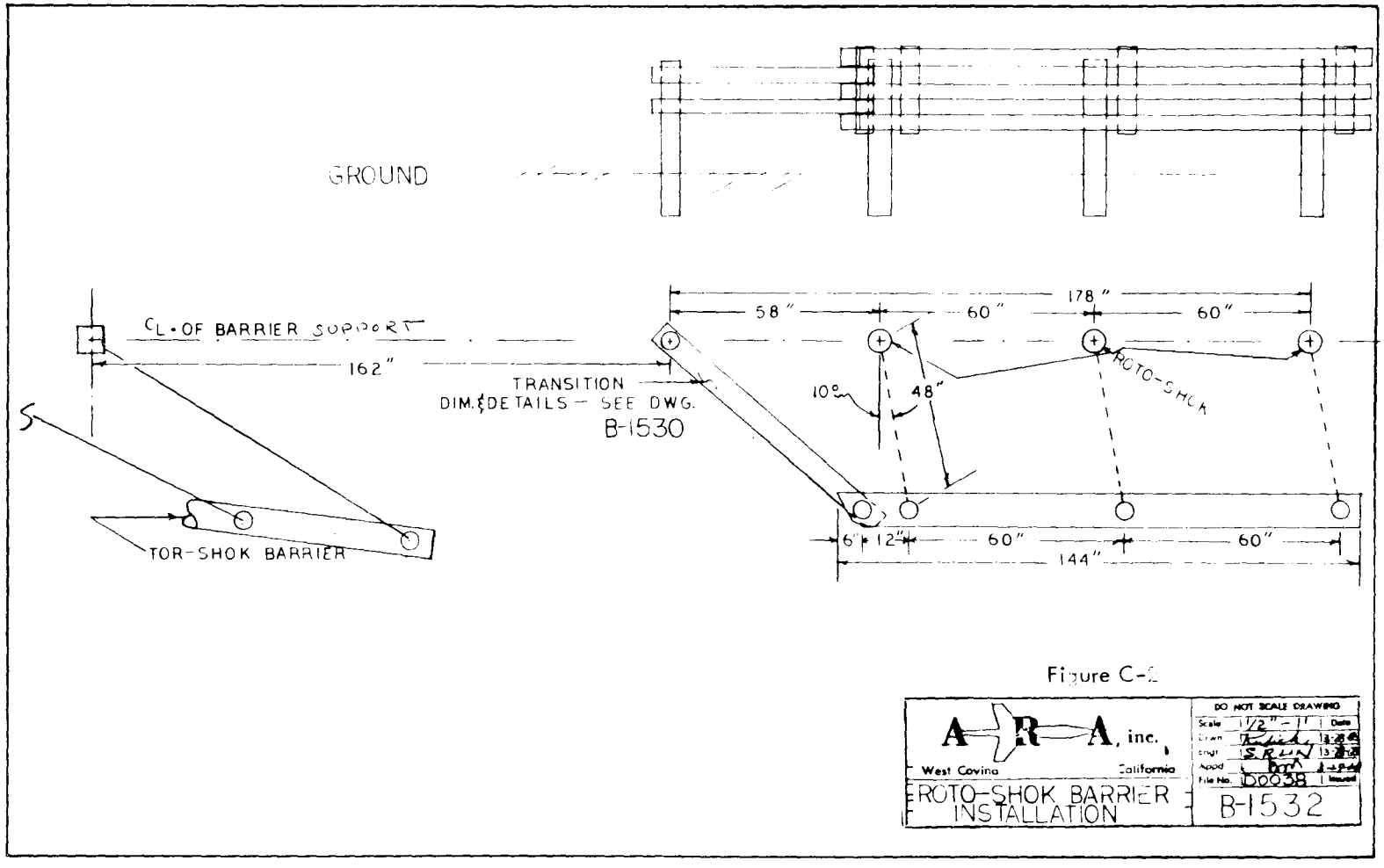
GROUND
CL OF BARRIER SUPPORT
162"
TRANSITION
DIM. & DETAILS — SEE DWG.
B-1530
TOR-SHOK BARRIER
58"
60"
178"
60"
10°
48"
ROTO-SHOK
6"
12"
60"
60"
144"
DO NOT SCALE DRAWING
A R A, inc.
West Covina
California
Scale 1/2" = 1'
Drawn
Engr
Appd
File No. D0038
ROTO-SHOK BARRIER INSTALLATION
B-1532

Figure C-2

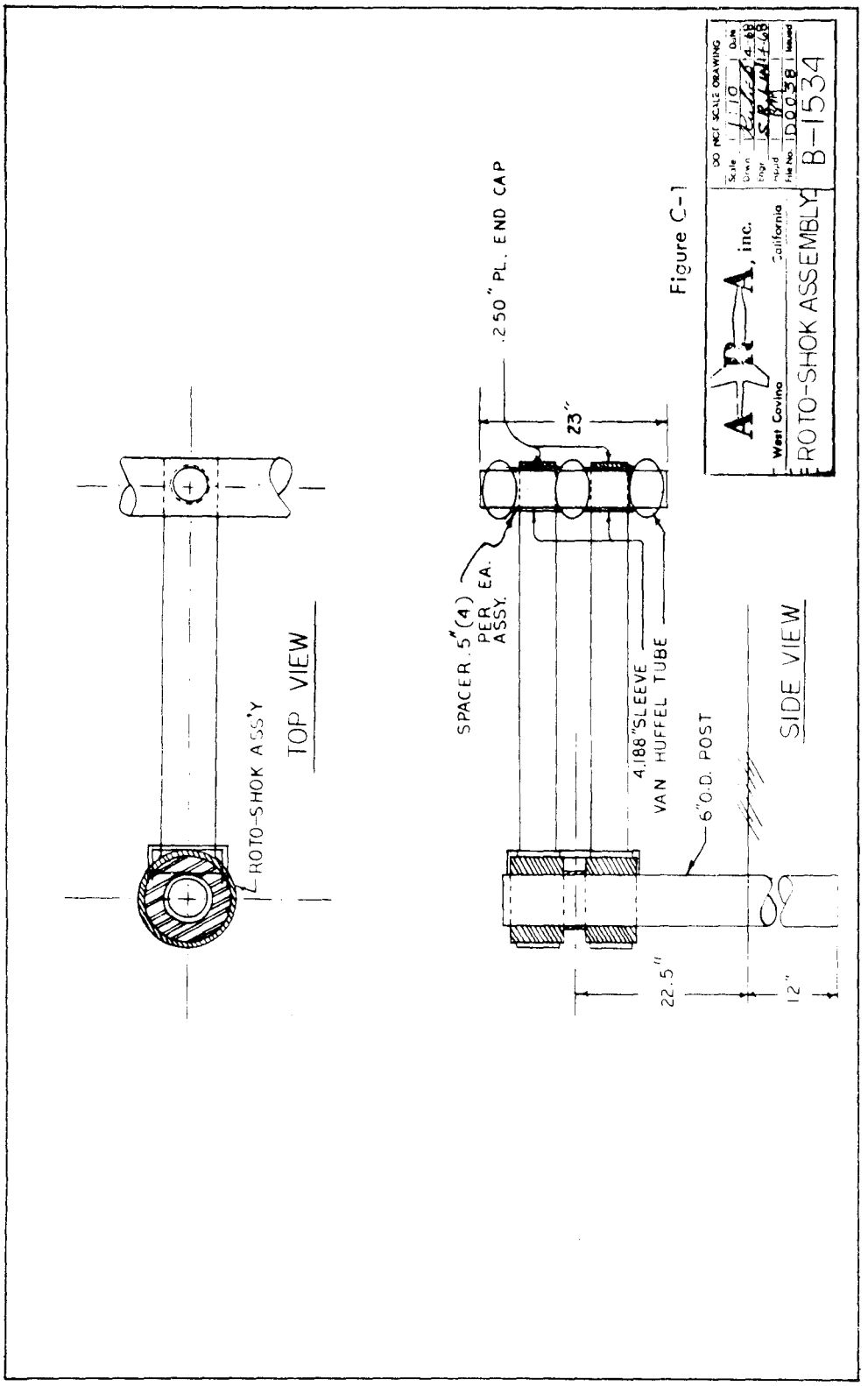
TOP VIEW
ROTO-SHOK ASS'Y
SIDE VIEW
SPACER .5" (4) PER EA. ASSY.
.250" PL. END CAP
23"
4.188" SLEEVE VAN HUFFEL TUBE
6" O.D. POST
22.5"
12"
DO NOT SCALE DRAWING
Scale 1/10
Date 4-68
Drawn
Engr
Appd
File No. ID0038
Issued
A-R-A, inc.
West Covina California
ROTO-SHOK ASSEMBLY
B-1534

Figure C-1

APPENDIX S-B

PHOTOGRAPHIC AND ACCELEROMETER DATA

TABLE S-B1

Test 505-2E

Tor-Shok

High-Speed Film Data

Time Milliseconds		Displacement ft	Velocity ft/sec	
0		0		
			77.3	
10.08		.779		
			79.1	
20.16		1.576		
			80.2	
30.24		2.384		
			72.1	77.2 Avg.
40.32		3.111		
			79.9	
50.40		3.916		
			73.9	
60.48		4.661		
			77.6	
70.56	Impact	5.443		
			76.5	
80.64		6.214		
			74.7	
100.80		7.720		
			72.3	
120.96		9.177		
			68.9	
141.12		10.567		
			64.0	
161.28		11.857		
			64.9	
181.44		13.166		
			56.8	
201.60		14.312		
			48.4	
221.76		15.287		
			34.7	
241.92		15.987		
			14.9	
262.08		16.288		
			2.8	
282.24		16.344		
			-4.6	
302.40		16.251		

TABLE S-B1

Test 505-2E (continued)

Time Milliseconds	Displacement ft	Velocity ft/sec
		-2.0
342.72	16.169	
		-4.1
383.04	16.002	
		-4.4
423.36	15.825	
		-4.0
463.68	15.665	
		-4.0
504.00	15.503	
		-6.2
544.32	15.255	
		-1.9
584.64	15.177	
		-5.1
624.96	14.970	
		-6.4
665.28	14.710	
		-4.0
705.60	14.550	
		-0.6
745.92	14.524	
		-3.6
786.24	14.379	

Vehicle is at rest

TABLE S-B2

Test 505-2F

Roto-Shok

High-Speed Film Data

Time Milliseconds		Displacement ft	Velocity ft/sec	
0		0		
			68.6	
10		.686		
			70.3	
20		1.389		
			64.8	
30		2.037		
			70.3	
40		2.740		
			65.9	
50		3.399		66.9
			72.0	Avg.
60		4.119		
			66.4	
70		4.783		
			61.5	
80		5.398		
			62.6	
90		6.024		
			67.0	
100	Impact	6.694		
			65.2	
140		9.303		
			63.7	
180		11.853		
			53.0	
220		13.971		
			57.2	
260		16.261		
			53.2	
300		18.390		
			53.1	
340		20.514		
			54.0	
380		22.675		
			53.2	
420		24.805		
			52.0	
460		26.886		
			52.3	
500		28.978		

TABLE S-B2

Test 505-2F (continued)

Time Milliseconds	Displacement ft	Velocity ft/sec
		50.8
540	31.010	
		51.0
580	33.052	
		48.4
620	34.990	
		51.6
660	37.055	
		50.9
700	39.091	
		47.9
740	41.007	
		51.2
780	43.055	
		52.3
820	45.147	
		49.4
860	47.124	
		50.0
900	49.122	

Vehicle moves out of view

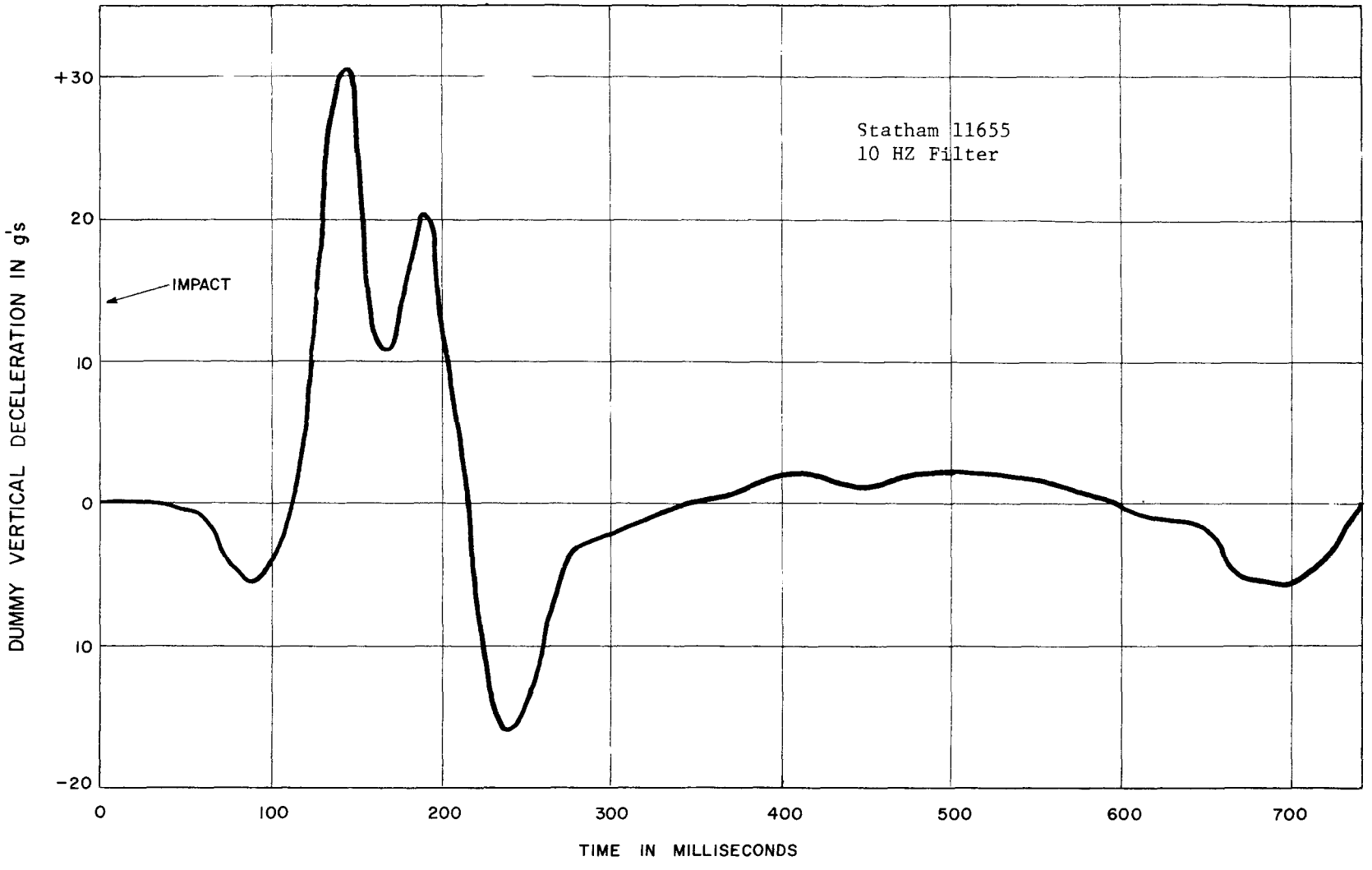

FIGURE S-BI, DUMMY VERTICAL ACCELEROMETER DATA, TEST 505-2E

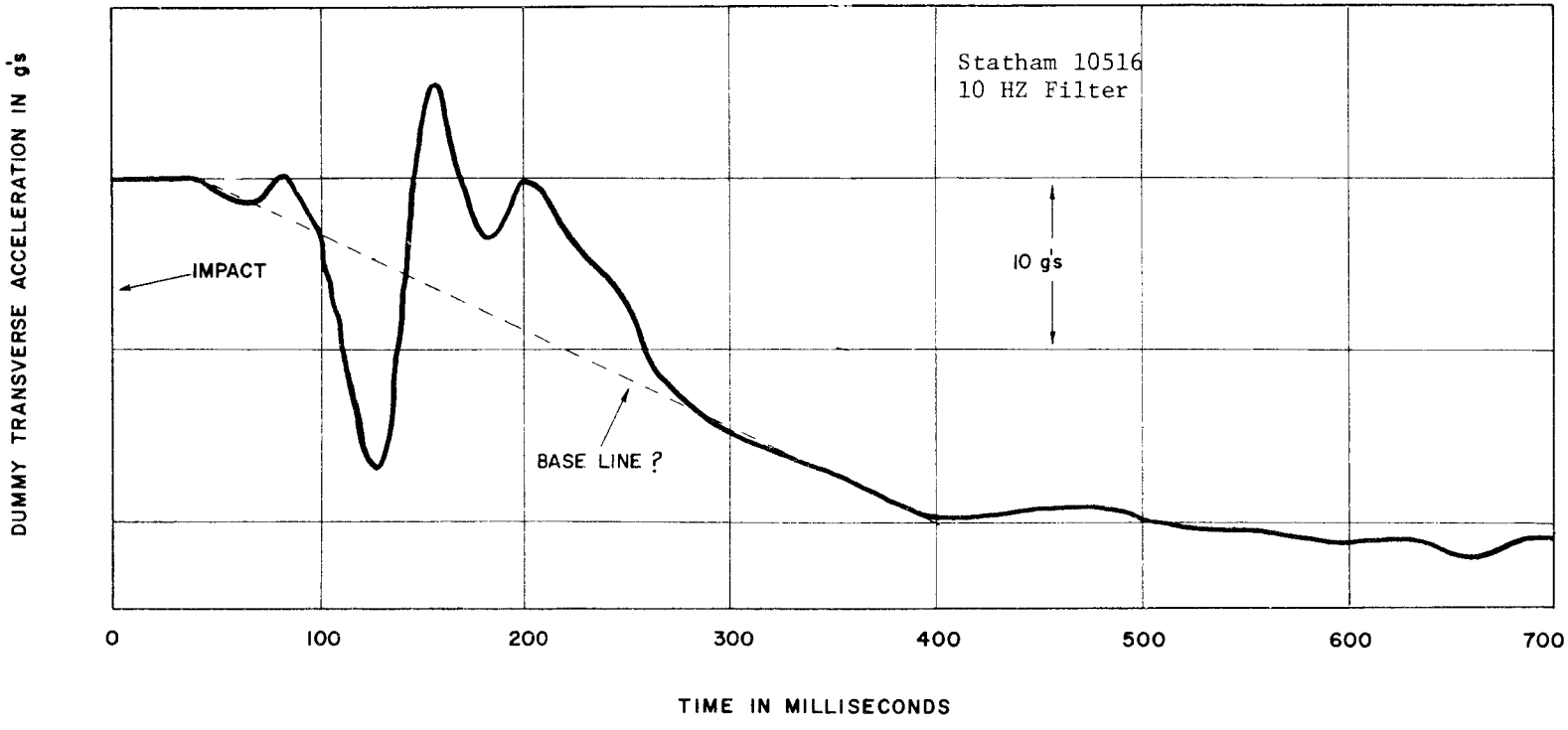

FIGURE S-B2, DUMMY TRANSVERSE ACCELEROMETER DATA, TEST 505-2E

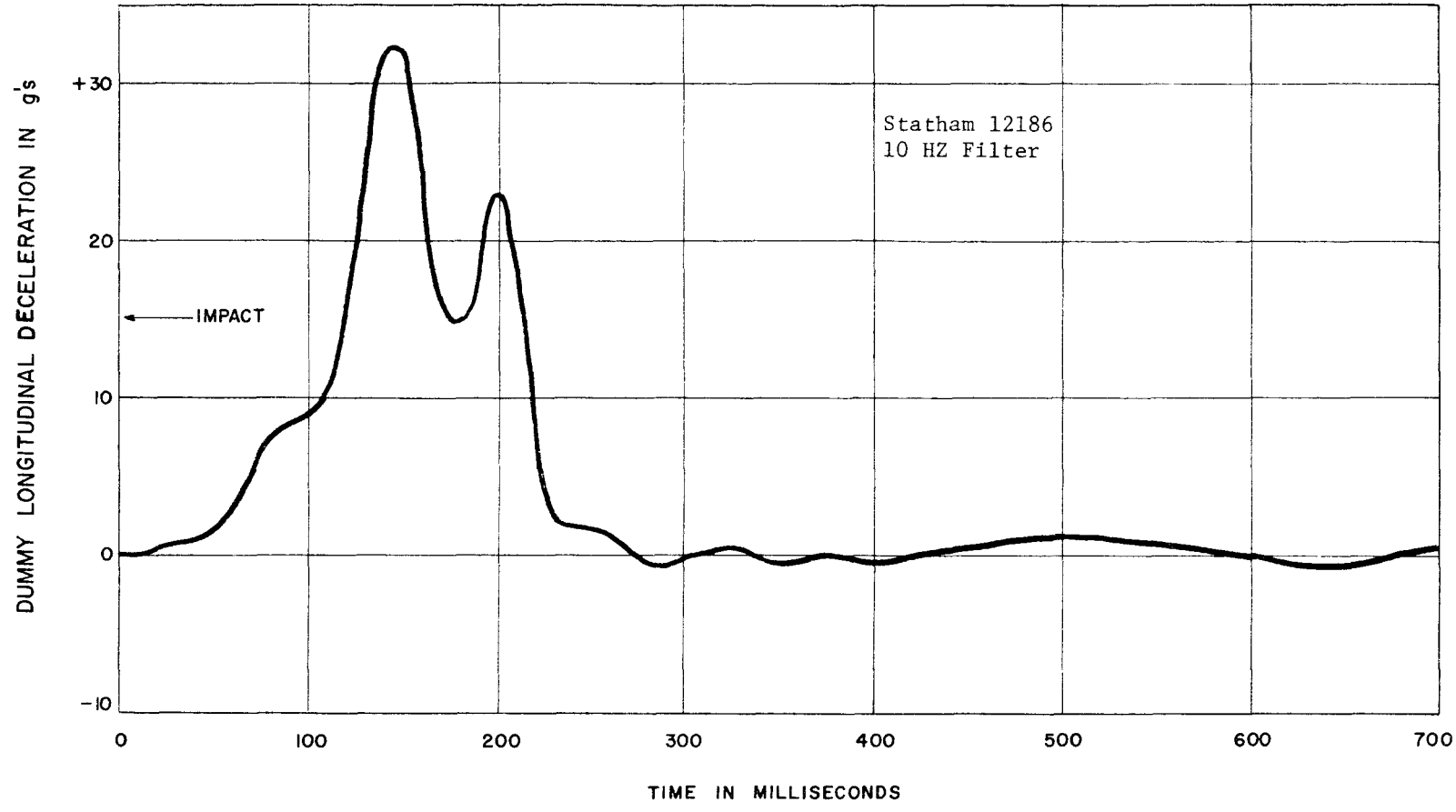

FIGURE S-B3, DUMMY LONGITUDINAL ACCELEROMETER DATA, TEST 505-2E

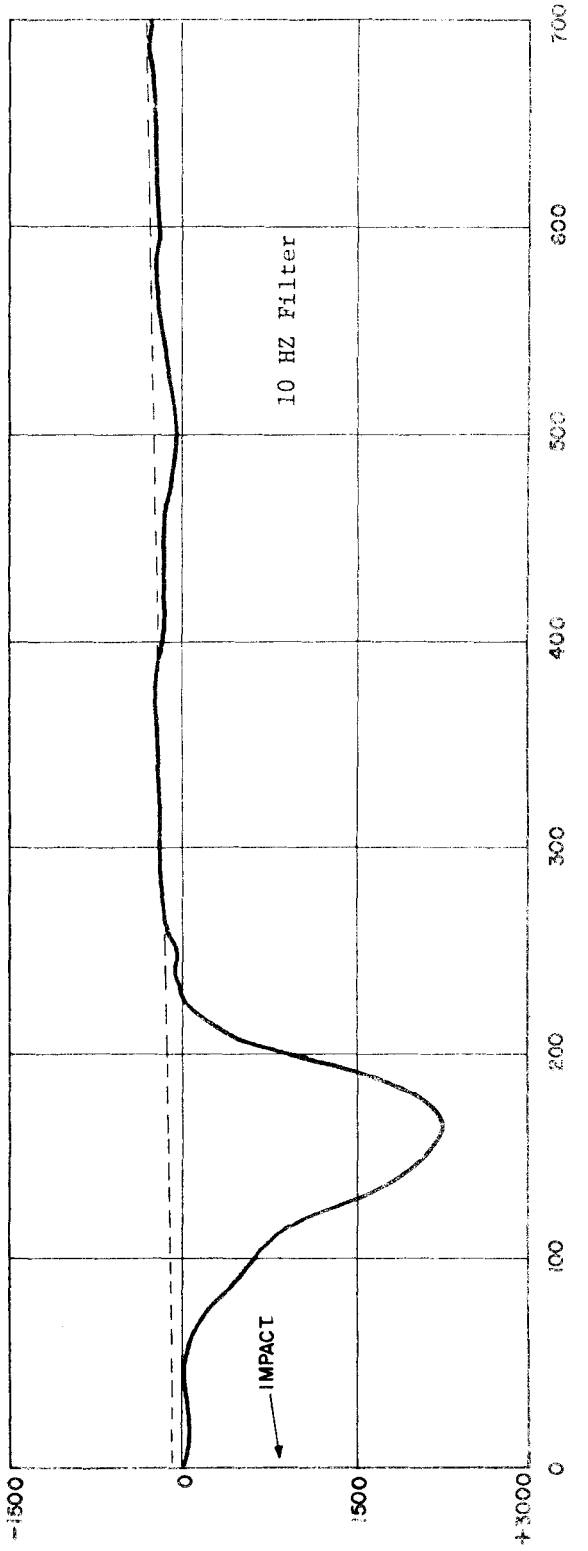

FIGURE S34, DUMMY SEATBELT DATA, TEST 305-2E

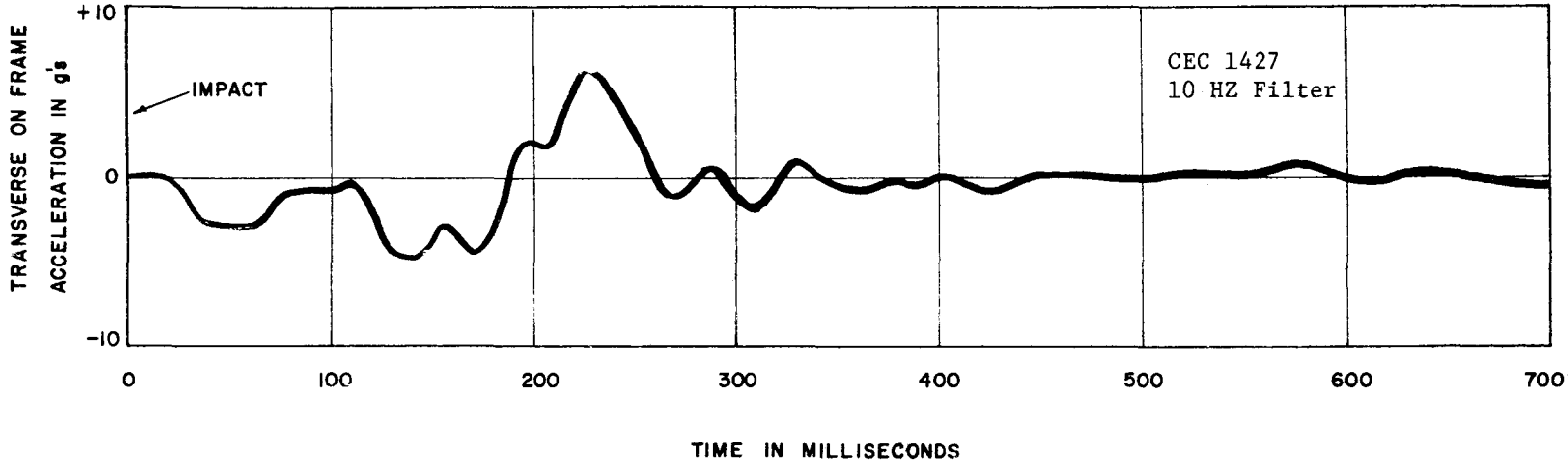

FIGURE S-B5, FRAME TRANSVERSE ACCELEROMETER DATA, TEST 505-2E

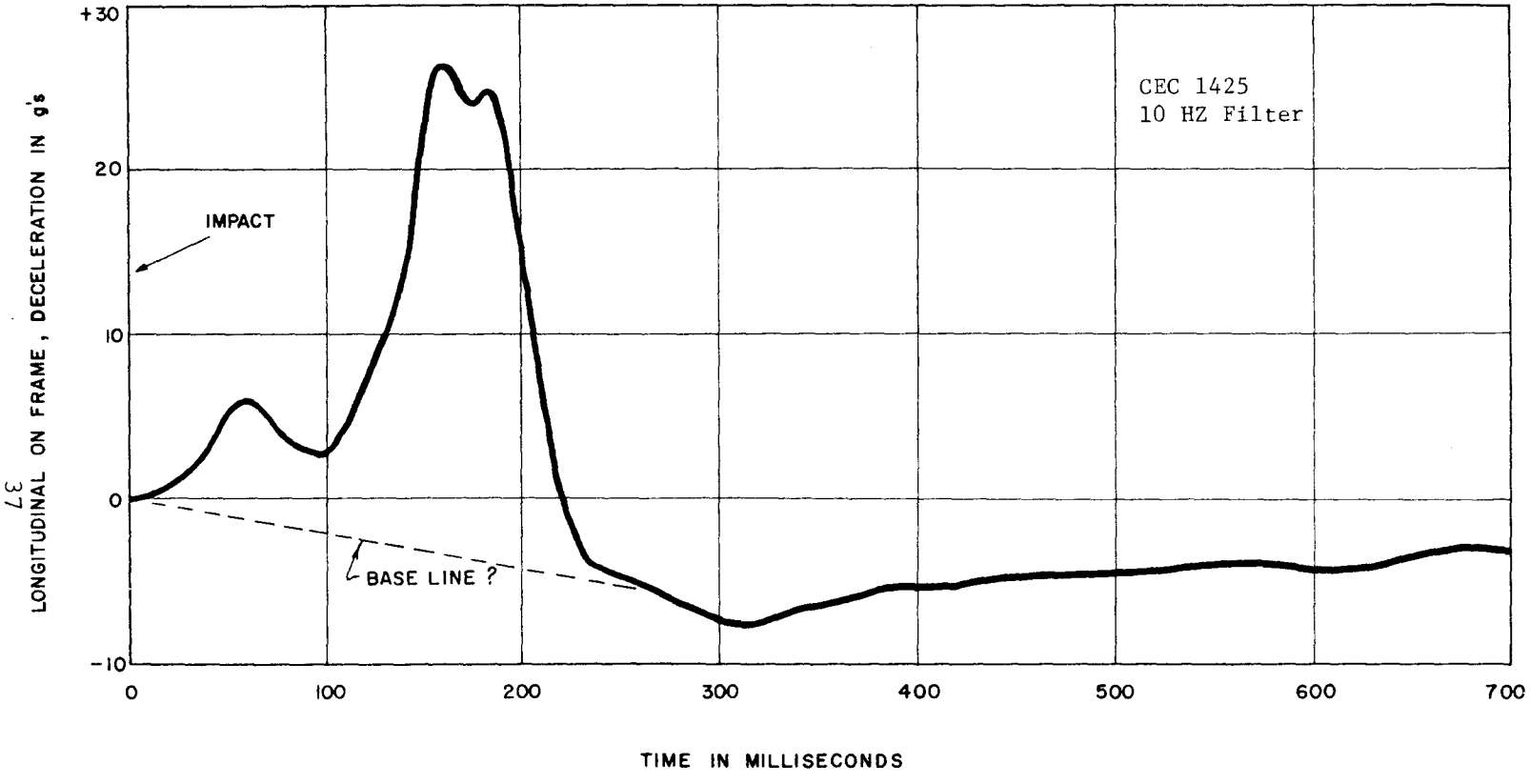

FIGURE S-B6, FRAME LONGITUDINAL ACCELEROMETER DATA, TEST 505-2E

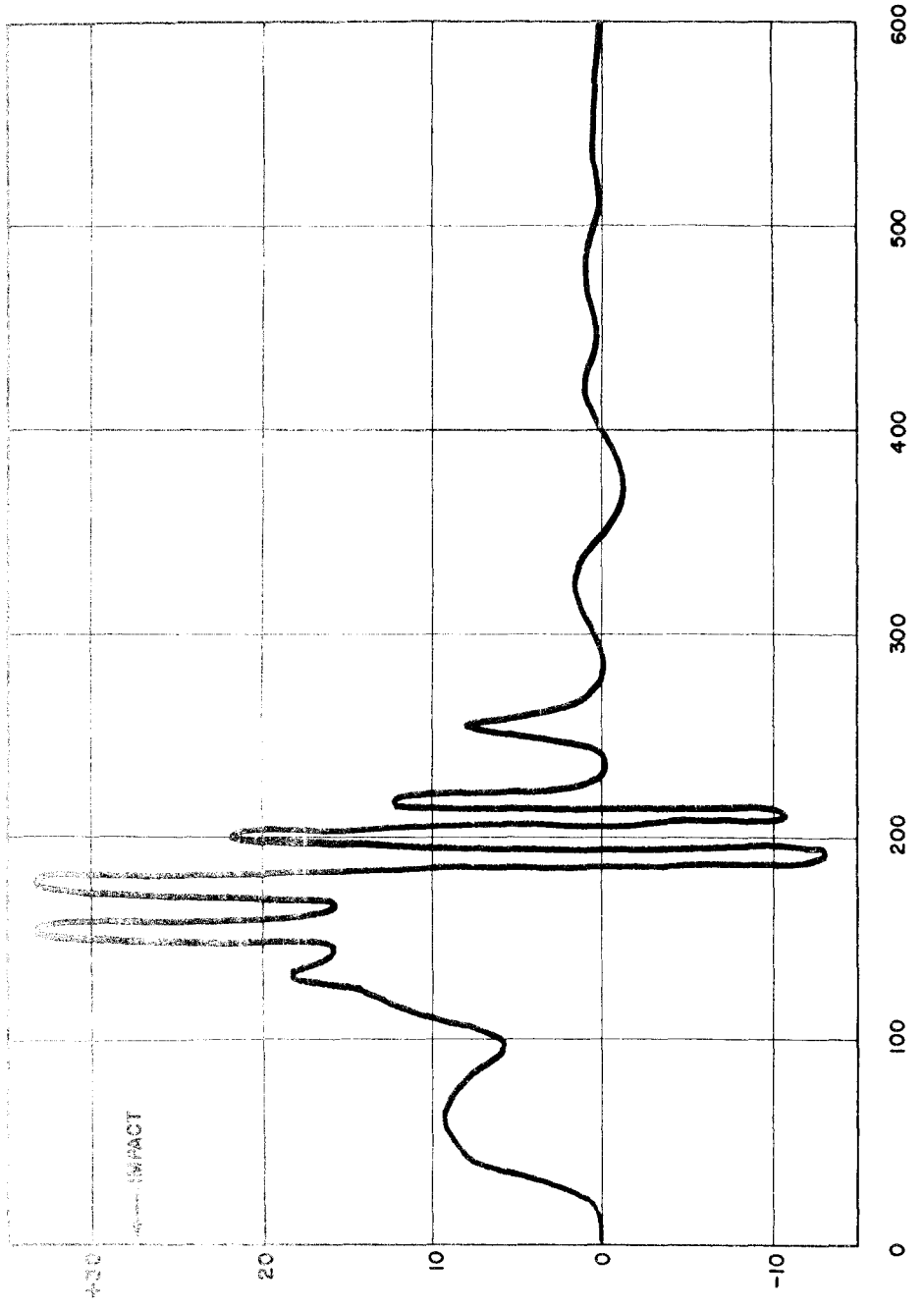

FIGURE S-B7, LONGITUDINAL IMPACT-O-GRAPH DATA, TEST 505-2E

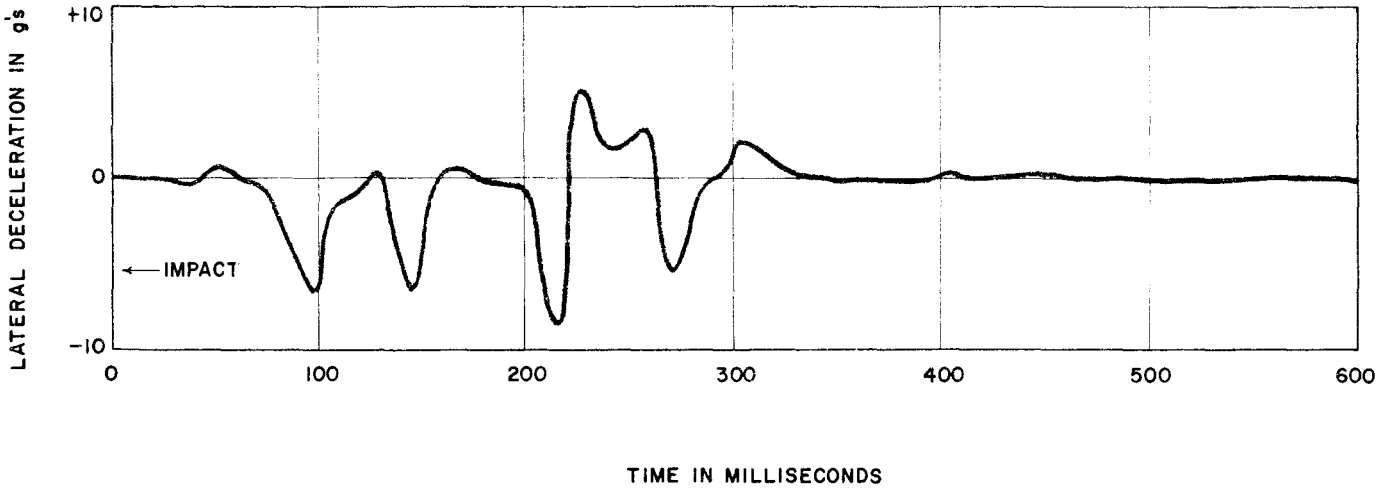

FIGURE S-B8, LATERAL IMPACT-O-GRAPH DATA, TEST 505-2E

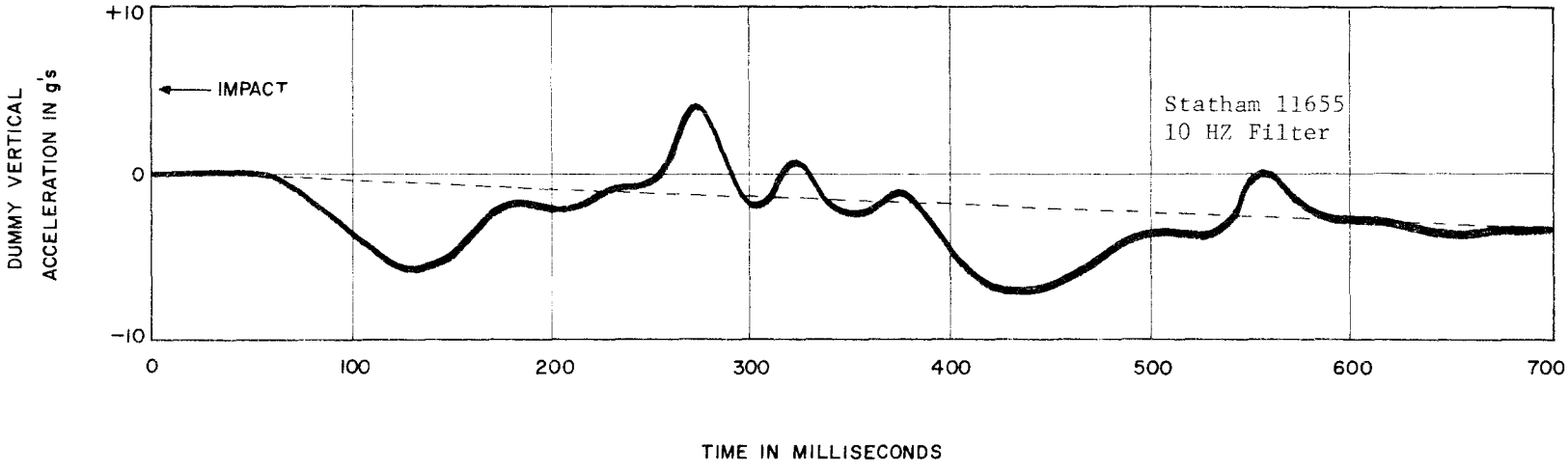

FIGURE S-B9, DUMMY VERTICAL ACCELEROMETER DATA, TEST 505-2F

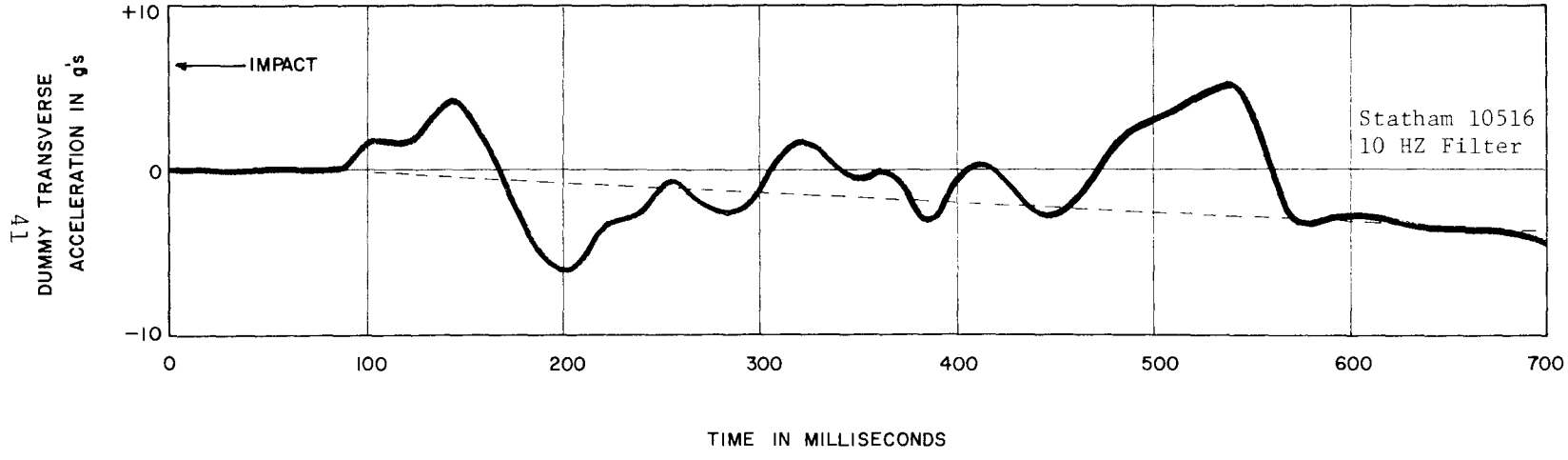

FIGURE S-B10, DUMMY TRANSVERSE ACCELEROMETER DATA, TEST 505-2F

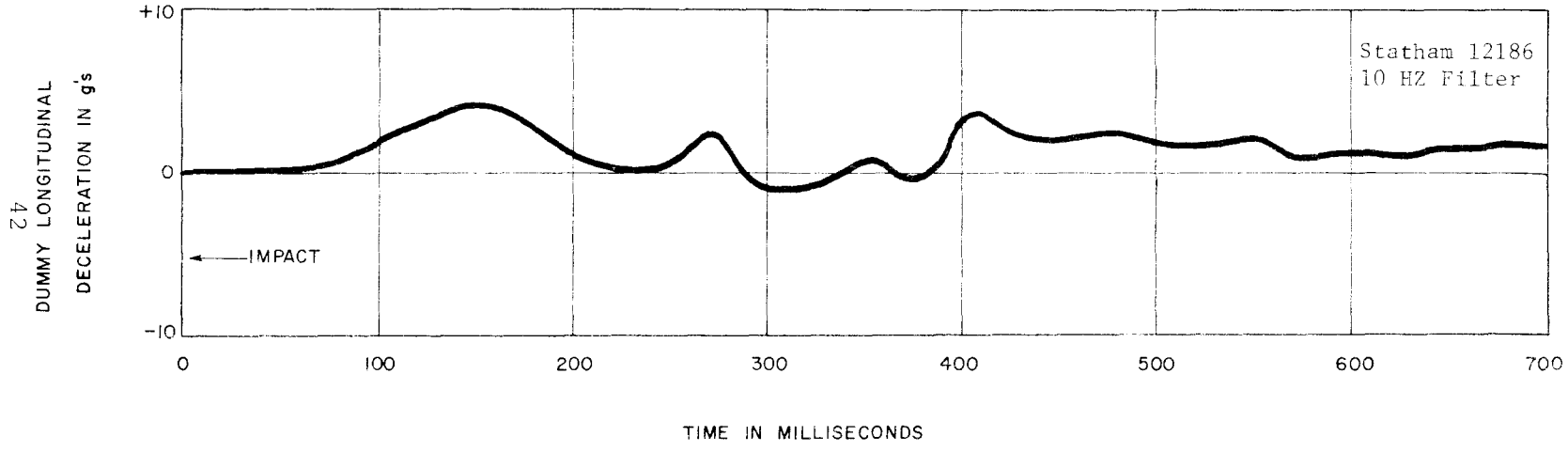

FIGURE S-BII, DUMMY LONGITUDINAL ACCELEROMETER DATA, TEST 505-2F

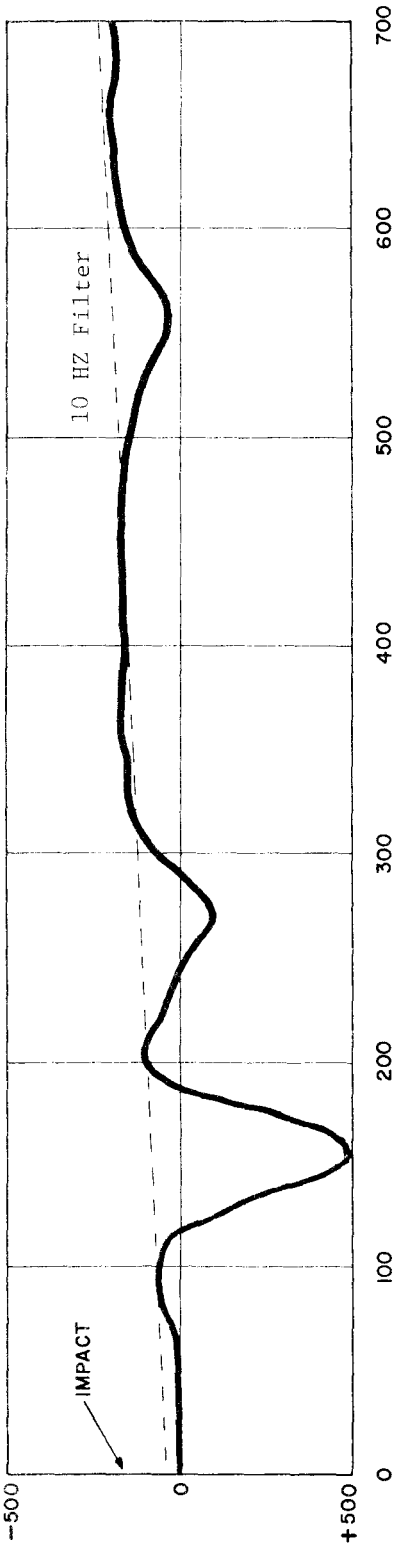

FIGURE S-B12, DUMMY SEATBELT DATA, TEST 505-2F

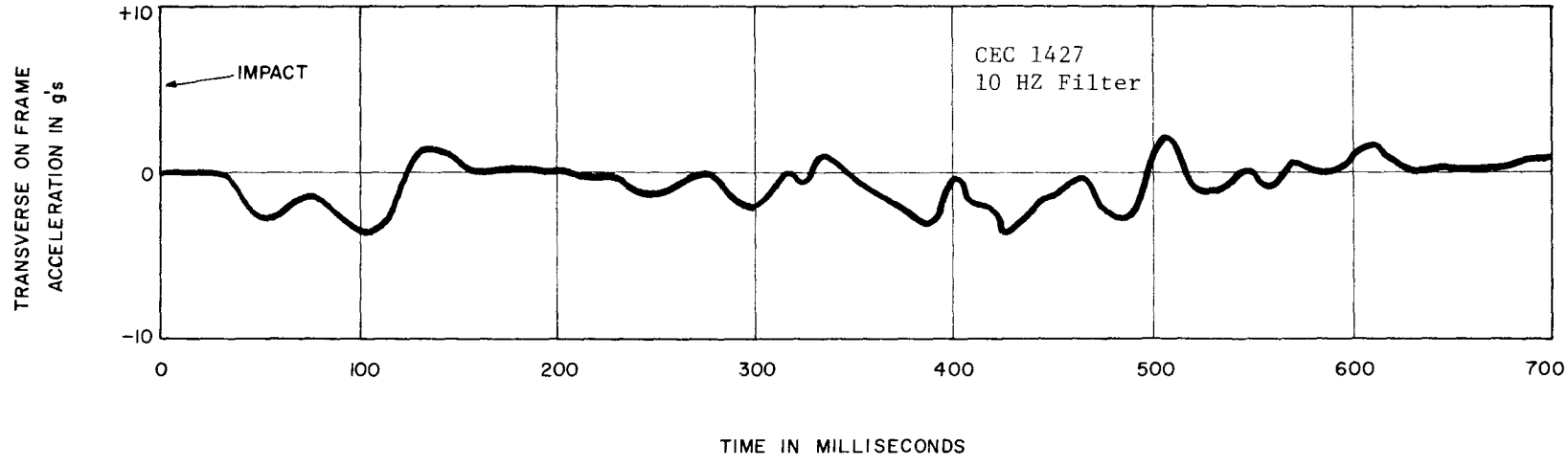

FIGURE S-B13, FRAME TRANSVERSE ACCELEROMETER DATA, TEST 505-2F

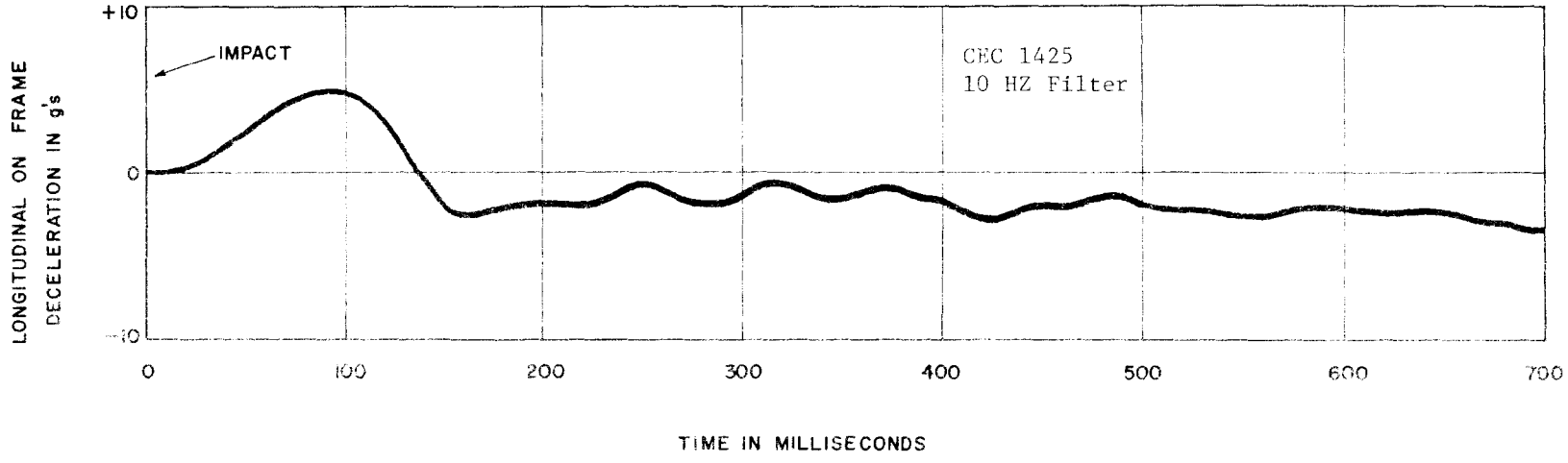

FIGURE S-B14, FRAME LONGITUDINAL ACCELEROMETER DATA, TEST 505-2F

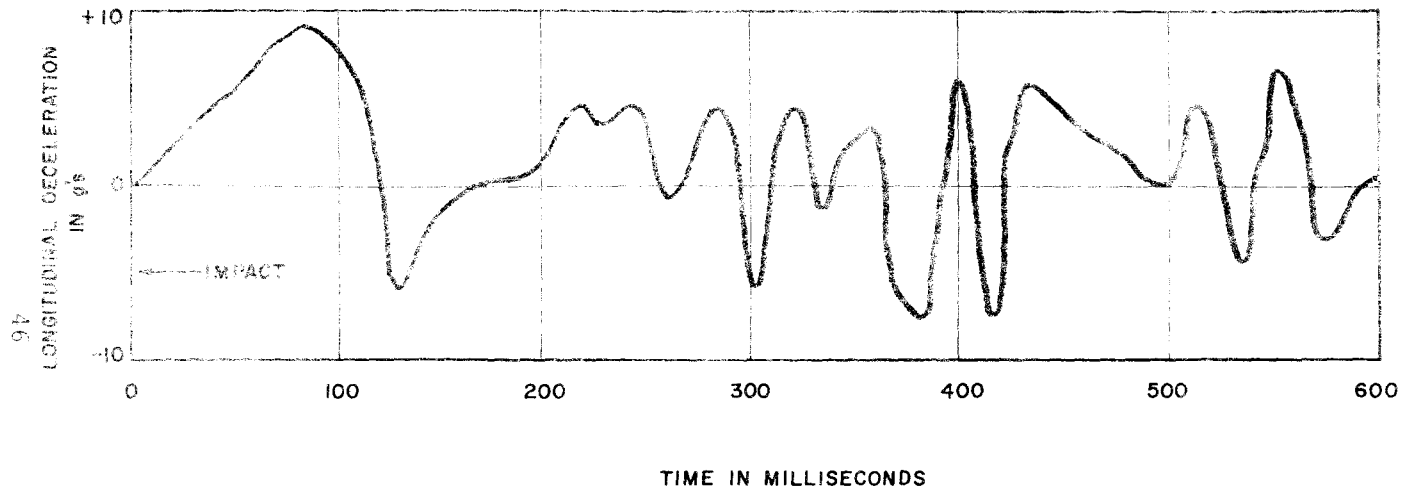

FIGURE S-B 15, LONGITUDINAL IMPACT-O-GRAPH DATA, TEST 505-2F

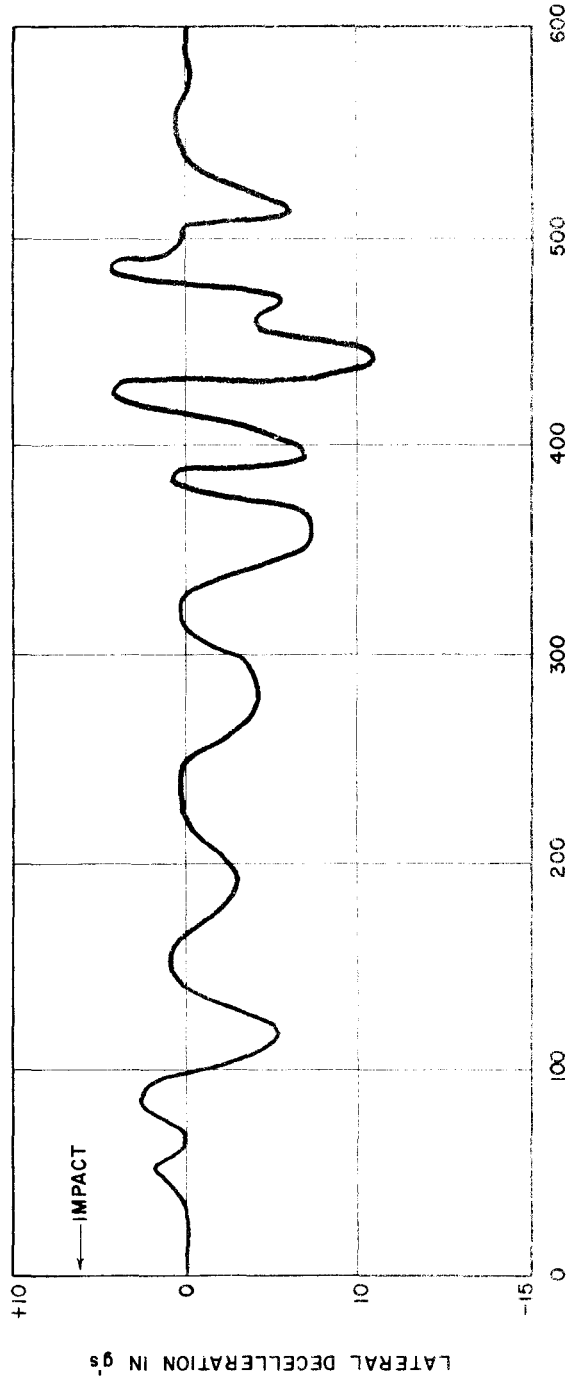

FIGURE S-B16, LATERAL IMPACT-O-GRAPH DATA, TEST 505-2F

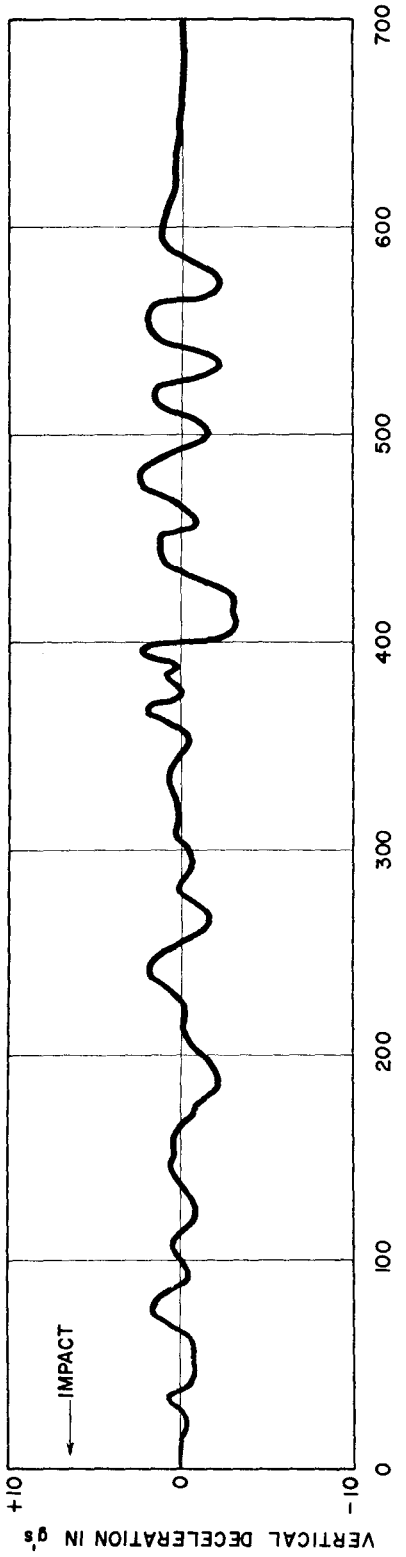

FIGURE S-B17, VERTICAL IMPACT-O-GRAPH DATA, TEST 505-2F

TECHNICAL MEMORANDUM 505-3

Texas Transportation Institute
Texas A&M Research Foundation

ONE-WAY GUARDRAIL INSTALLATION

A Tentative Progress Memorandum on
Contract No. CPR-11-5851, U.S. Dept.
of Transportation, Federal Highway
Administration, Bureau of Public
Roads

by

Don L. Ivey
Associate Research Engineer

and

T. J. Hirsch
Research Engineer
and Principal Investigator

January, 1969

INTRODUCTION

From January 18, 1968 to September 12, 1968 the Texas Transportation Institute conducted four full-scale tests of the vehicle arresting system proposed by the Martin Marietta Corporation, Baltimore, Maryland. This arresting system, called the One-Way Guardrail, is a means of preventing vehicles that go out of control from crossing a highway median by entrapping the vehicle in the median. This entrapment prevents them from encountering oncoming traffic or returning to the roadway from which they came.

Included in this technical memorandum are photographs of the vehicle and barrier at the various stages of each test. High-speed motion picture film was analyzed to give vehicle velocities and average decelerations as each test transpired. The movement of the vehicle during each test is shown by a position-time diagram.

Barrier Description

The One-Way Guardrail vehicle arresting system was developed by the Martin Marietta Corporation under a contract with the Bureau of Public Roads. The arresting system was fabricated and delivered by Martin Marietta to the Highway Research Center of Texas Transportation Institute. The system was installed on the A&M Research Annex and the vehicle crash tests were conducted by personnel of the Texas Transportation Institute Highway Research Center. The system consists of two continuous parallel lengths of guardrail which would be installed approximately 12 feet apart on a highway median. The function of the installation is shown by Figure 1. The guardrail was composed of the standard W-section guardrail on the inward side and a 12 gauge bumper plate on the outward side. These W-section beams and bumper plates were bolted to 4-inch wide flange posts which were installed so that the entire guardrail leaned at an angle of 15^{o} toward the middle of the median. The webb and outward flange of each post was precut at the ground line so that it would bend inward under a rather minimal force. Details of these components are given in Figures 2 and 3. This allows a vehicle which is out of control to lay down the first guardrail it encounters when driving into the median. Once the vehicle crosses the first guardrail, it is trapped between the rigid faces of guardrail on both sides and cannot re-enter the highway it has left or cross the median strip into the opposing traffic.

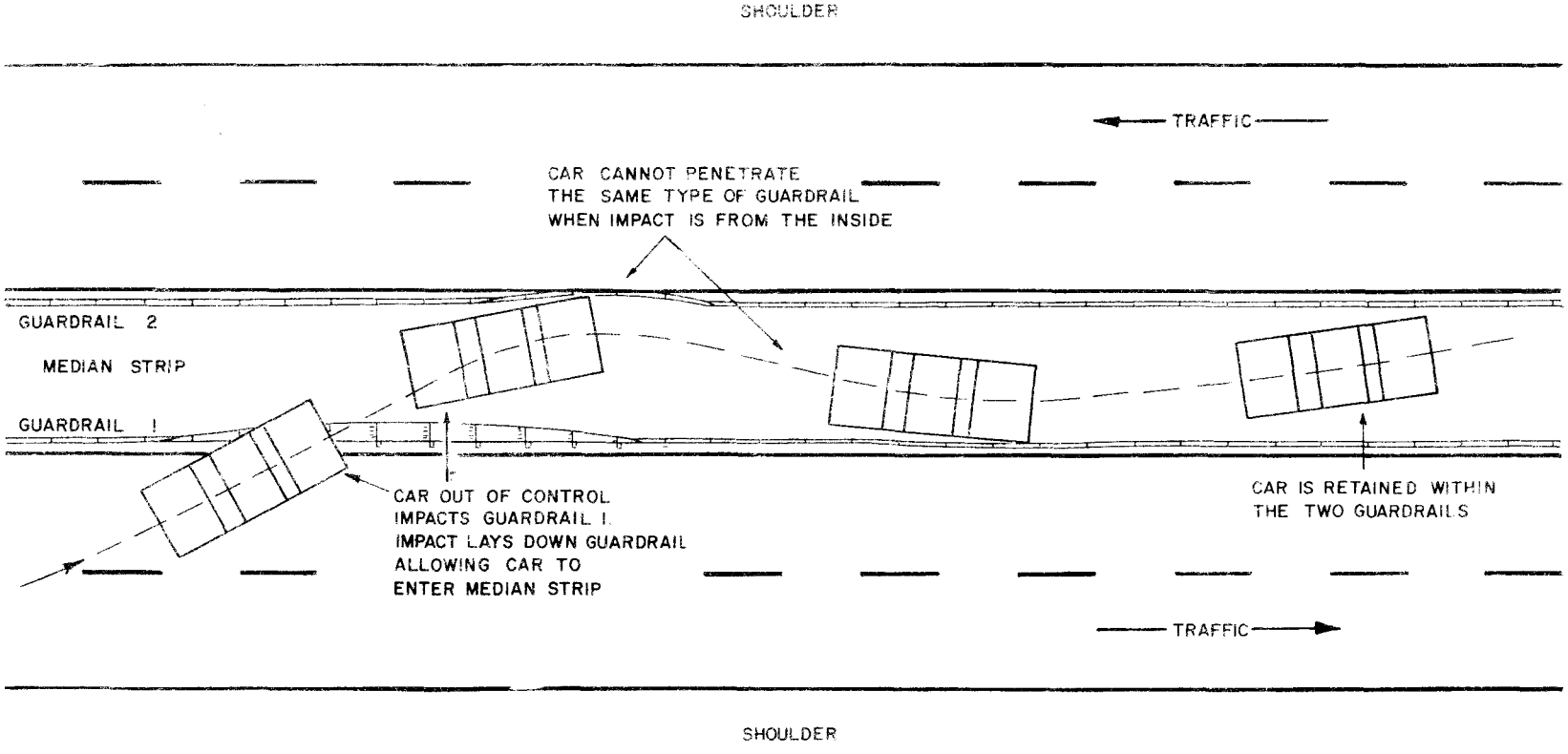

FIGURE 1, IDEALIZED FUNCTION OF ONE-WAY GUARDRAIL INSTALLATION

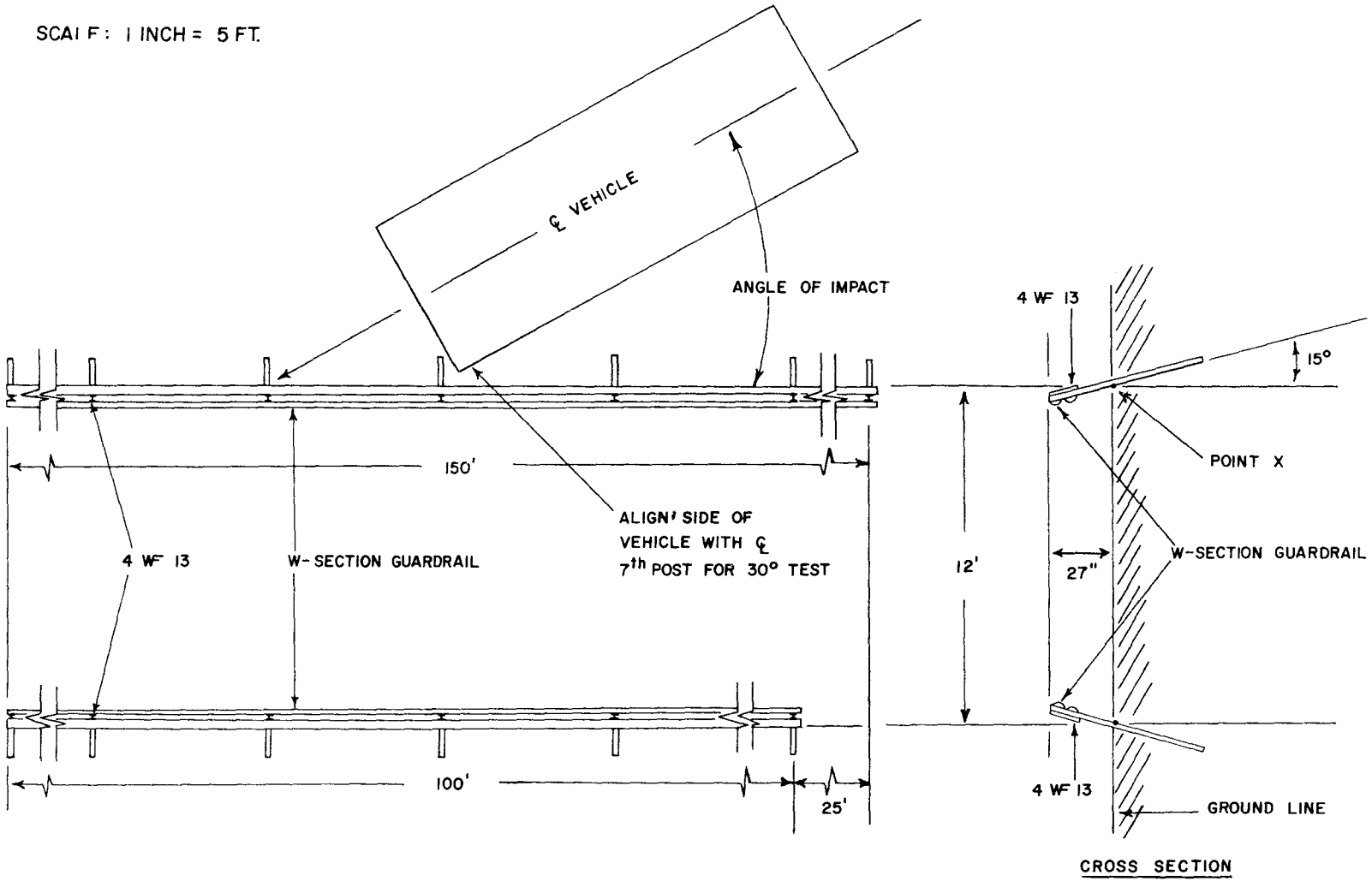

FIGURE 2, PLAN VIEW OF ONE-WAY GUARDRAIL ARRESTING SYSTEM

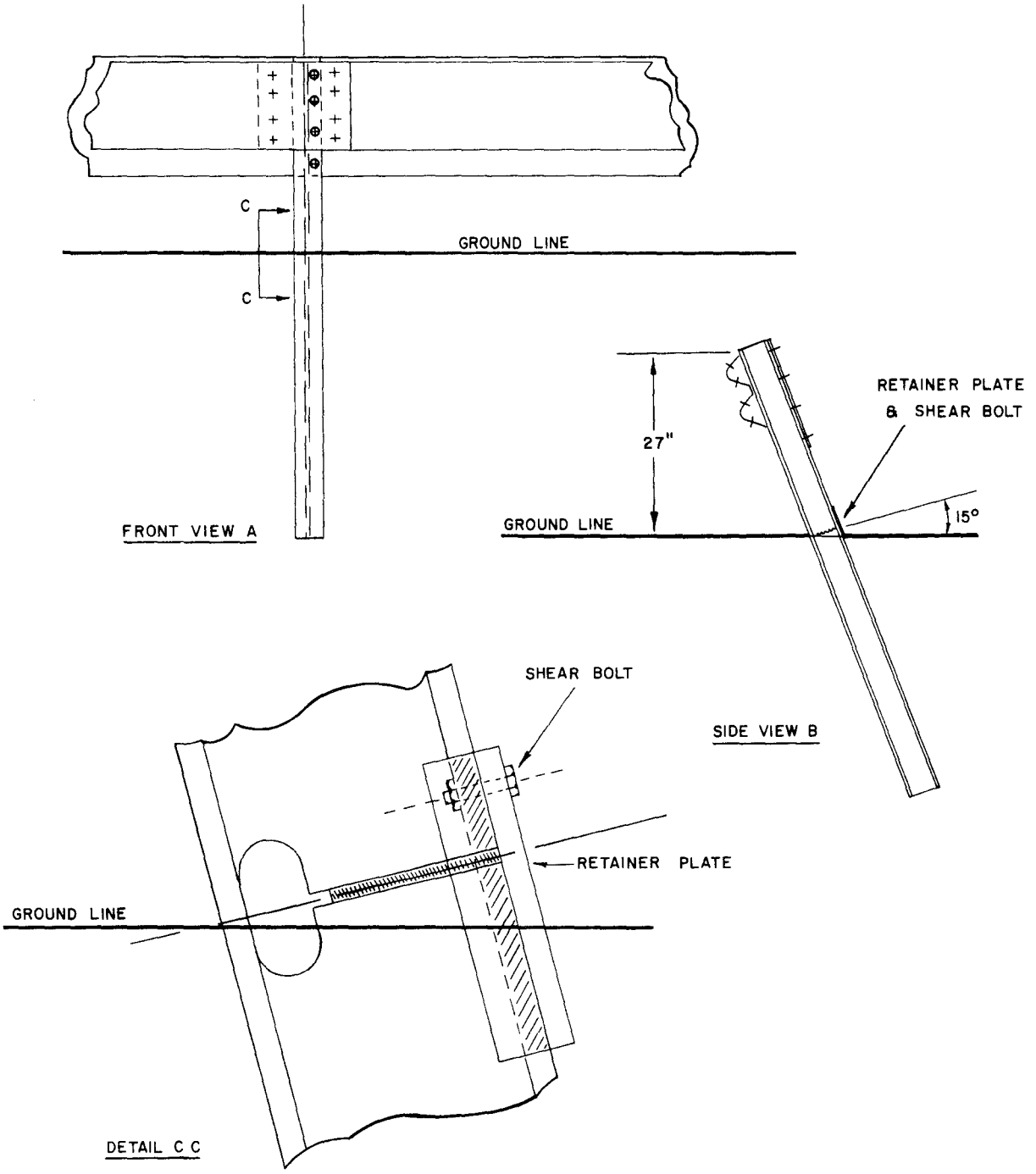

FIGURE 3, DETAIL OF ONE-WAY GUARDRAIL SYSTEM

Additional information and design data on this vehicle arresting system is given by the Operation and Maintenance Manual provided by the Martin Marietta Corporation.

DESCRIPTION OF TESTS

General

Four guardrail crash tests were conducted in this phase of the program. The vehicles ranged in weight from 1600 to 4400 lbs. Angles of attack* which were used on the One-Way Guardrail vehicle arresting system varied from 10^{o} to 30^{o}. The desired vehicle test velocity was 60 mph.

Two Hycam high-speed motion picture cameras, operating at 500 frames per second, and several documentary cameras, running at approximately 110 frames per second, were used to record the tests. One Hycam was used to photograph the vehicle during and immediately preceeding impact with the first guardrail, while the other was positioned to record subsequent vehicle movement. One documentary camera was mounted at one end of the guardrail installation to record the entire test sequence transverse to the arresting system.

Impact velocities were determined electronically as well as photographically. A pair of tape switches were placed so that they would be crossed by the right front wheel of the vehicle just before impact with the first guardrail. The time between actuation of the first and second switch was measured electromechanically, permitting the speed to be calculated.

---

*The angle of attack as used in this report is defined as the angle between the initial trajectory of the vehicle and the line of the guardrail. For example, 30^{o} as shown in Figure 4.

The description of each test includes photographs of the vehicle and arresting system before the test, sequence photographs of the test in progress, and photographs of the vehicle and system after the test. A drawing of the path which the vehicle traveled in relation to the arresting system provides a summary of the test. Deceleration levels are given in relation to the vehicle frame throughout this report.

Test 7A

A small vehicle, weighing 1600 lbs. was directed into the guardrail arresting system at an attack angle of 30^{o} and a velocity of 47 mph. The arresting system performed as designed, redirecting and containing the vehicle. A comparison of the vehicle and guardrail before and after the test indicates that the damage to both was minor. Figure 10 shows the point of impact with the first guardrail, and demonstrates proper performance of the "one-way" design.

Calculated average decelerations in the longitudinal and transverse directions were below 2.2 g's throughout the test, an extremely acceptable level.

Test 8A

A full-size automobile weighing 4300 lbs. impacted the guardrails at an angle of 30^{o} and a velocity of 61 mph. The arresting system failed to contain the vehicle. This was the only test in which the arresting system failed to perform as designed. The kinetic energy of the vehicle perpendicular to the guardrail was 267 Kip-ft, the largest value encountered in the four tests which were conducted.

SCALE: 1 INCH = 10 FEET

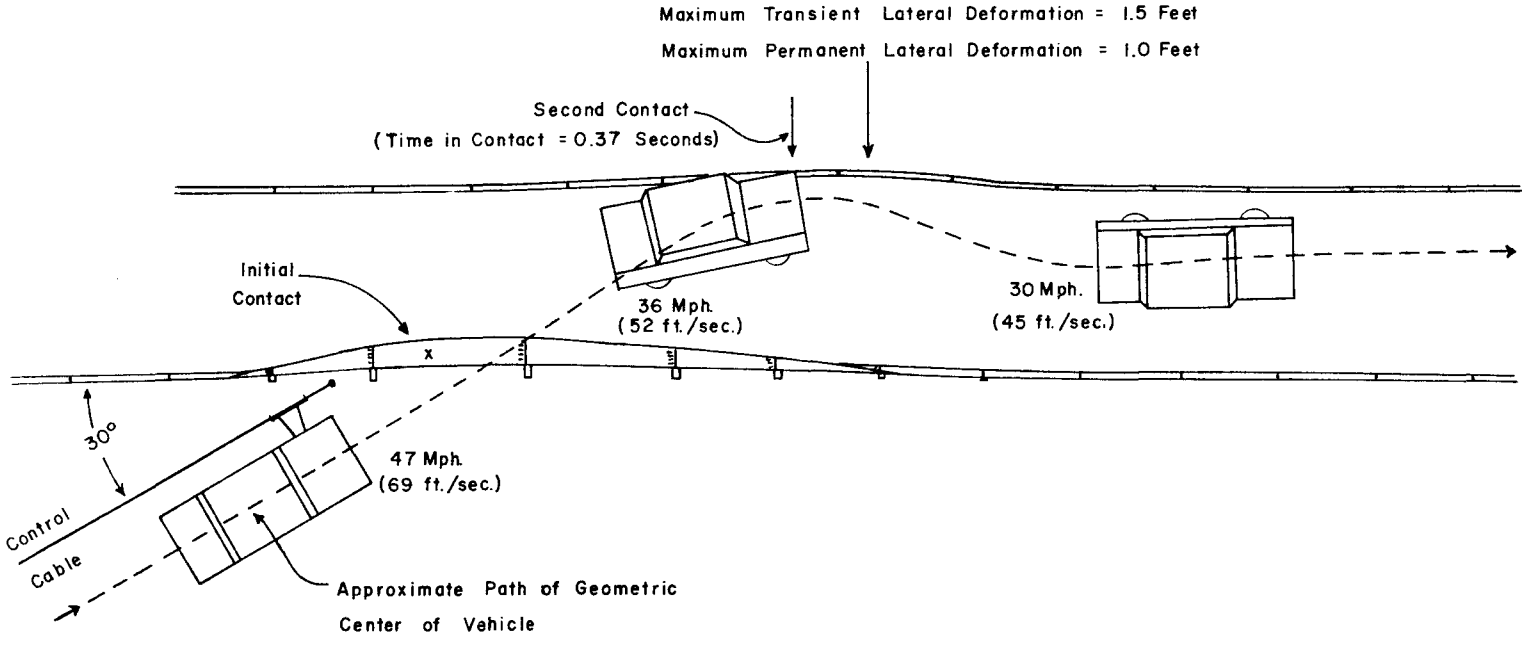

FIGURE 4, SUMMARY OF TEST 505-7A

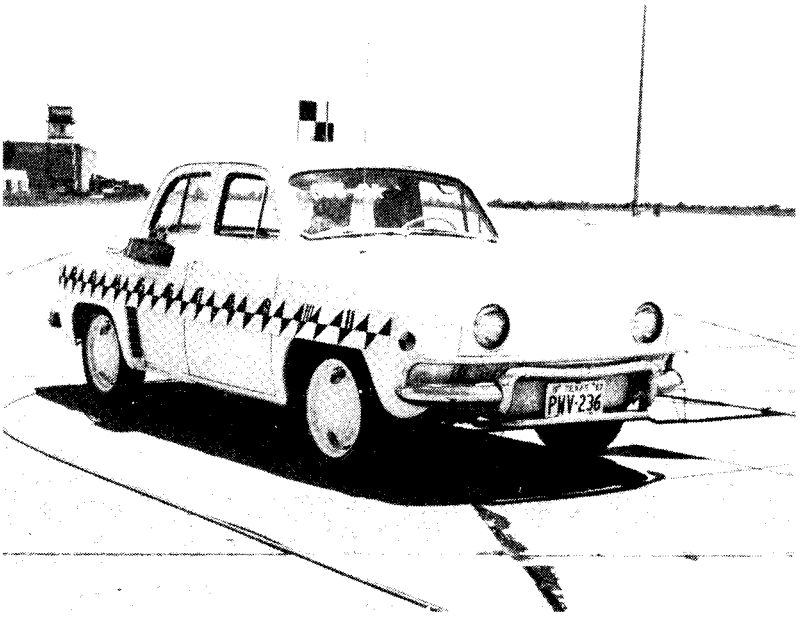

Figure 5, Vehicle Before Test (505-7A)

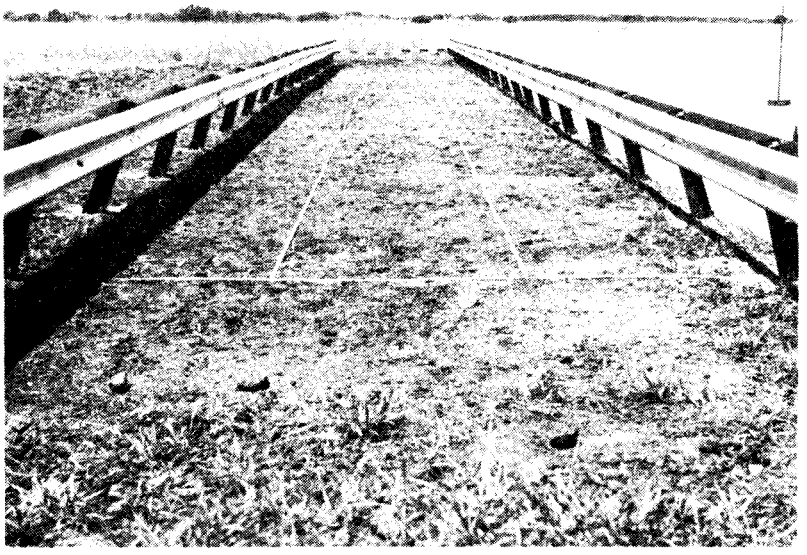

Figure 6, Guardrail Installation Before Test (505-7A)

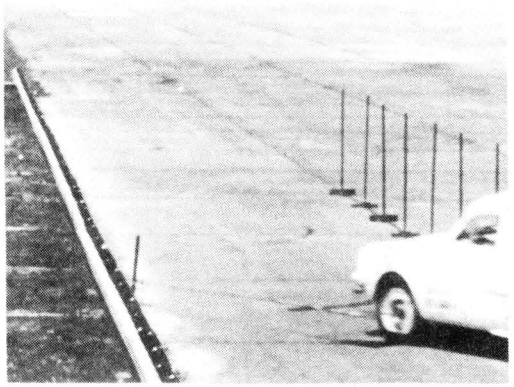

1

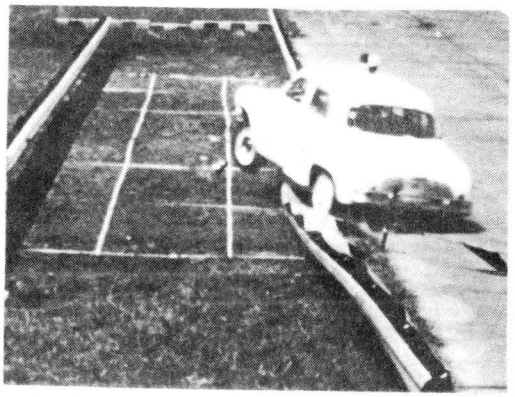

2

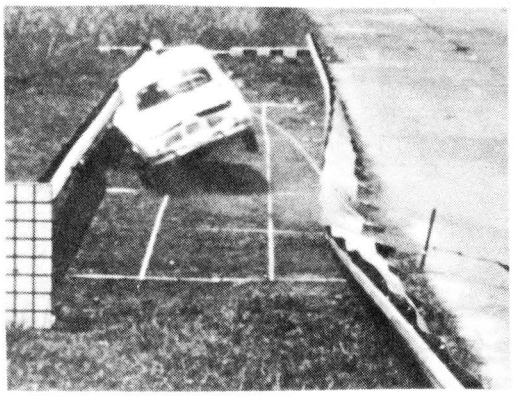

3

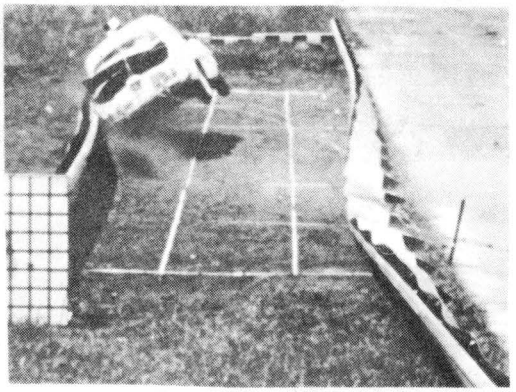

4

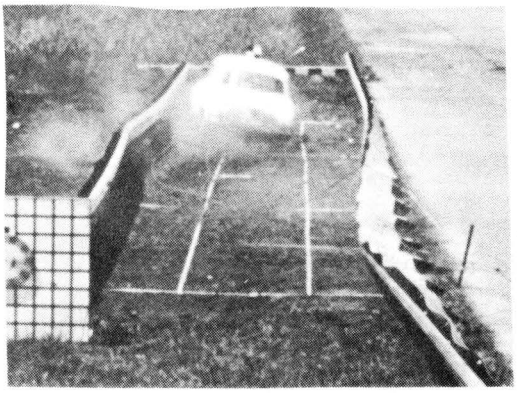

5

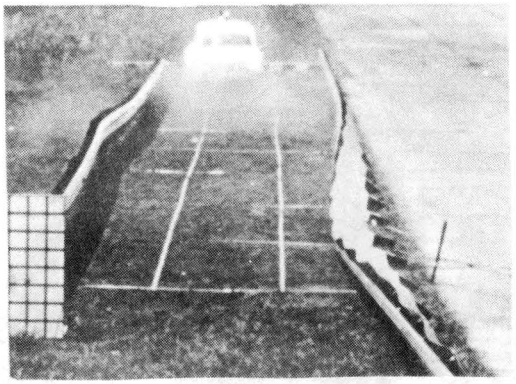

6

Figure 7, Sequential Photographs of Test 505-7A

Figure 8, Vehicle After Test (505-7A)

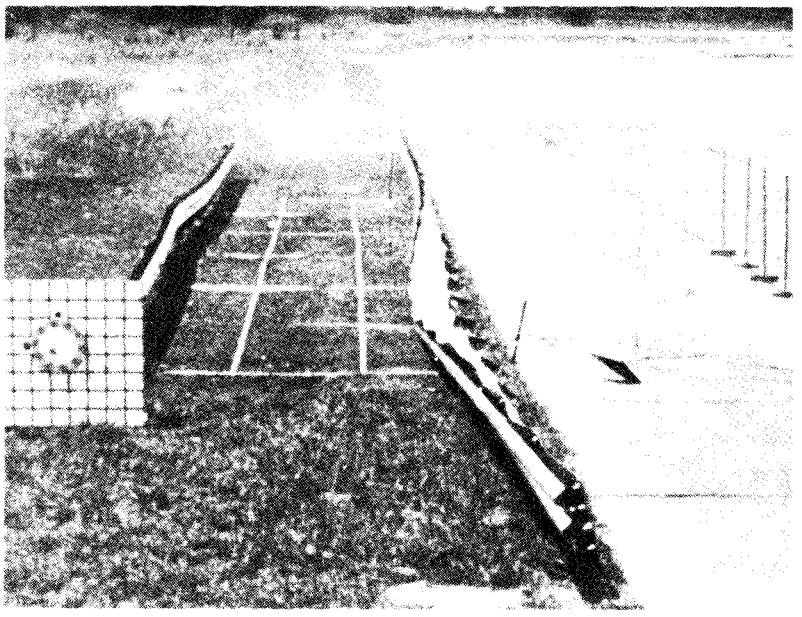

Figure 9, Guardrail Installation After Test (505-7A)

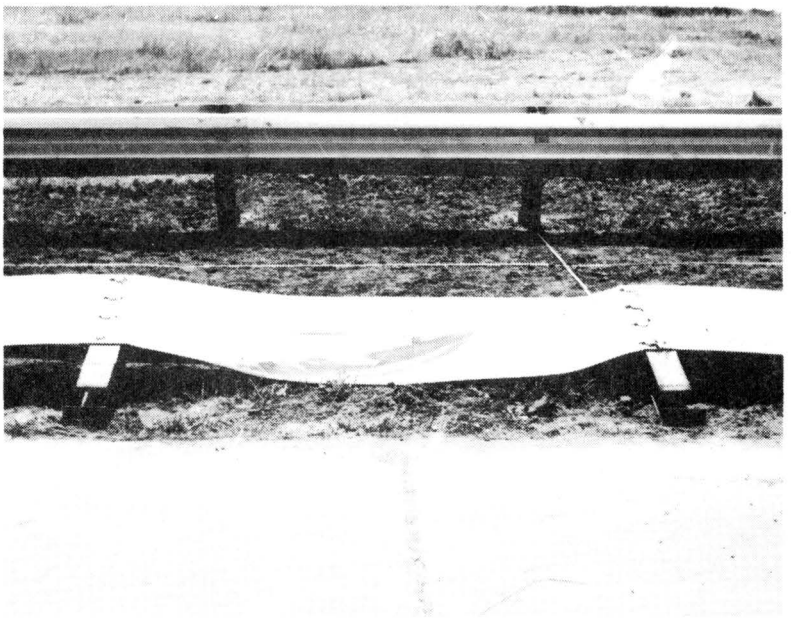

Figure 10, First Guardrail Was Laid Down As Design Predicted (505-A). Tread Mark Shows Point of Vehicle Contact.

The first guardrail collapsed inward as designed, but the vehicle ramped on the second rail after deforming it severely. As shown in Figure 17, the rail suffered heavy local damage. After striking the second guardrail, the car became airborne for approximately 36 feet. The vehicle came to rest upside down after rolling over one and one-half times.

The deceleration levels were moderate but the vehicle sustained heavy damage while rolling after the impact with the second rail.

Test 9A

In this test, the 4180 lb. vehicle, traveling at 64 mph, had slightly more total kinetic energy than the vehicle used in Test 8A. However, the impact angle was reduced to 20^{o}, which reduced the kinetic energy perpendicular to the guardrail to 197 Kip-ft. and allowed the vehicle to be successfully contained. The vehicle recontacted the first guardrail from inside of the system after being redirected by the second guardrail. The critical point was during contact with the second guardrail. The sequence photographs of Figure 21 indicate that the vehicle came very close to jumping the second guardrail. Considerable damage was done to the vehicle suspension at that point.

The left front of the vehicle contacted the ground when the first guardrail was recontacted. This probably contributed significantly to the decelerations experienced at that point.

The average decelerations at the various contact points were all below 2.3 g's, which is a very moderate level.

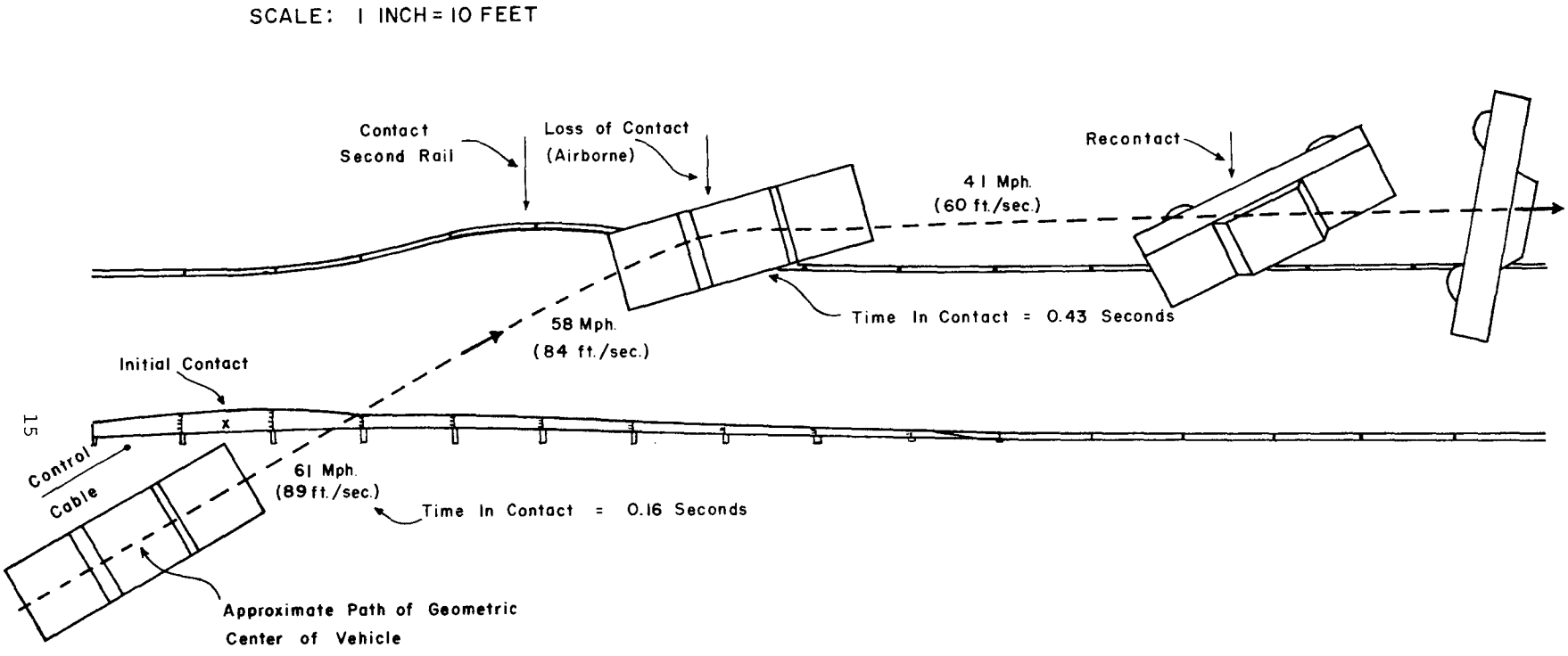

FIGURE 11, SUMMARY OF TEST 505-8A

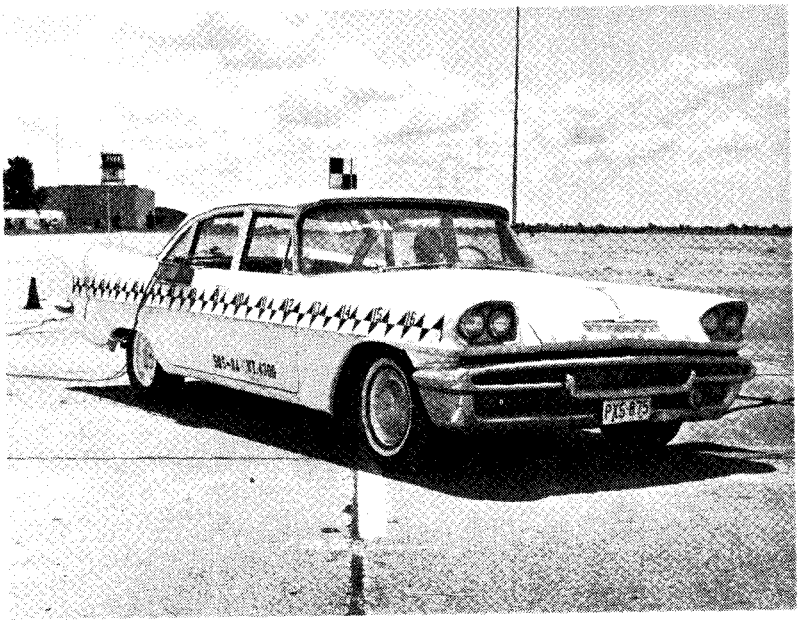

Figure 12, Vehicle Before Test (505-8A)

Figure 13, Vehicle After Test (505-8A)

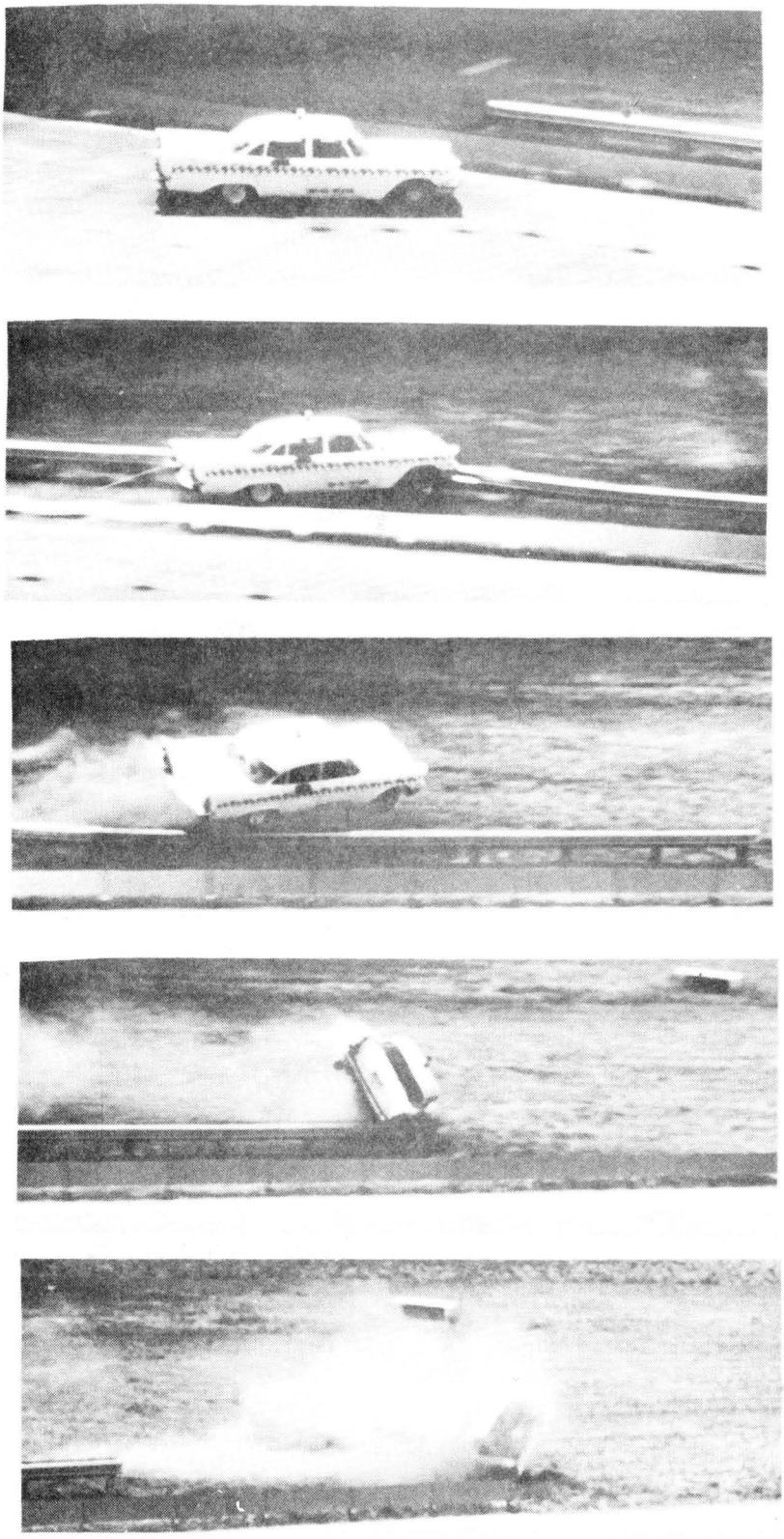

1

2

3

4

5

Figure 14, Sequential Photographs of Test (505-8A, Overhead Camera).

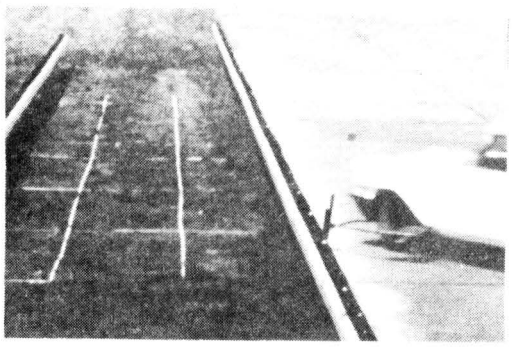

1

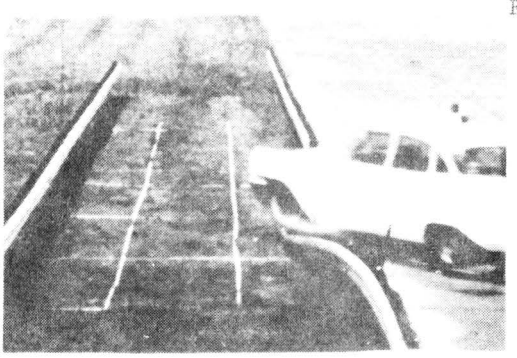

2

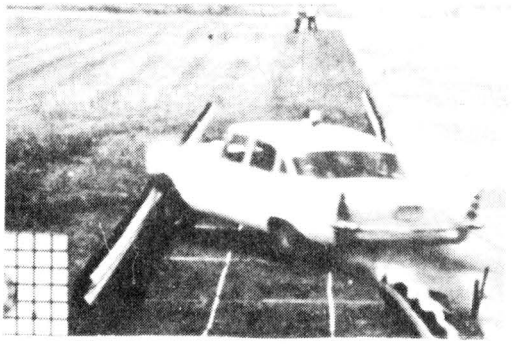

3

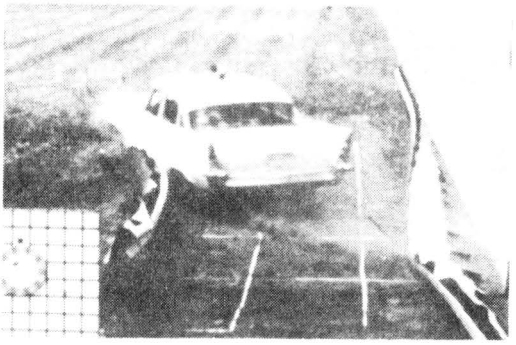

4

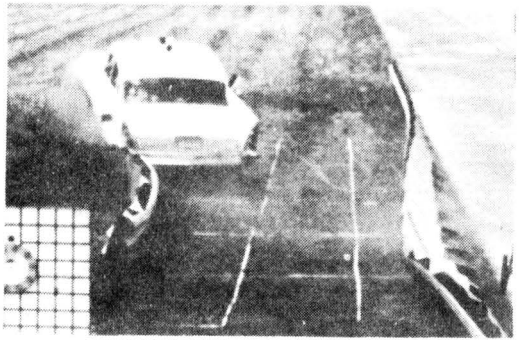

5

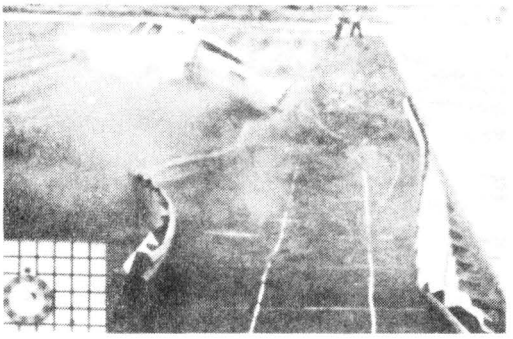

6

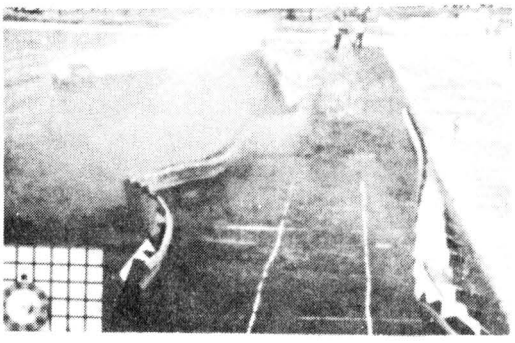

7

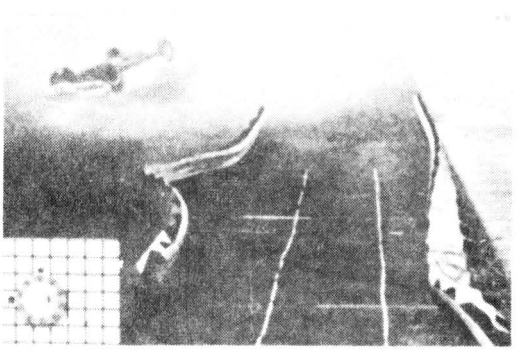

8

Figure 15, Sequential Photographs of Test (505-8A)

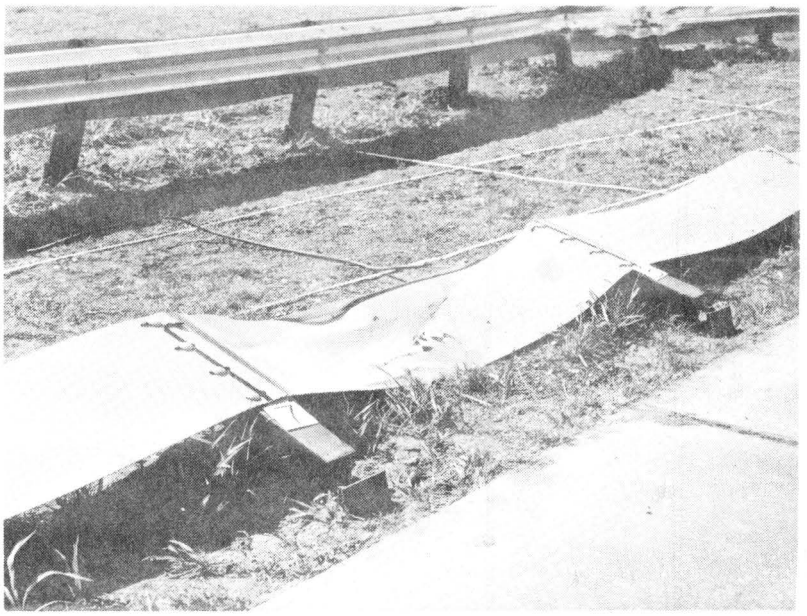

Figure 16, First Guardrail After Test (505-8A)

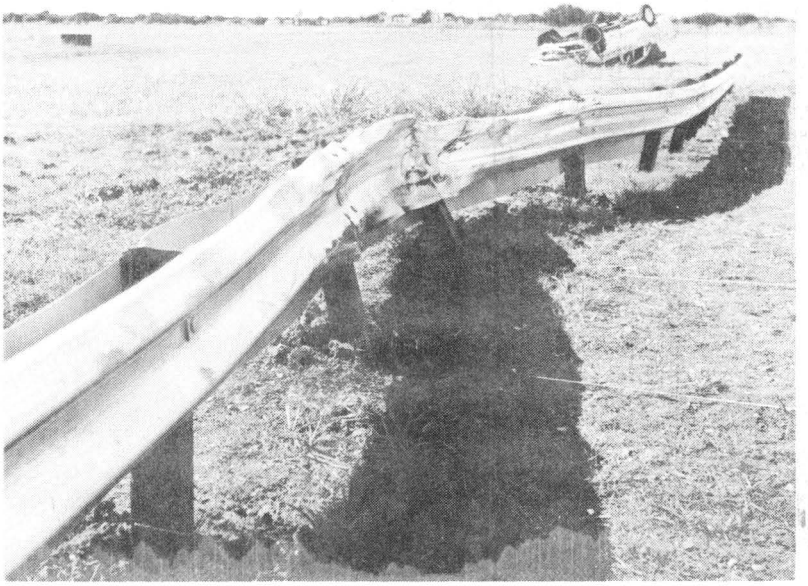

Figure 17, Second Guardrail After Test (505-8A)

SCALE: 1 INCH = 10 FEET

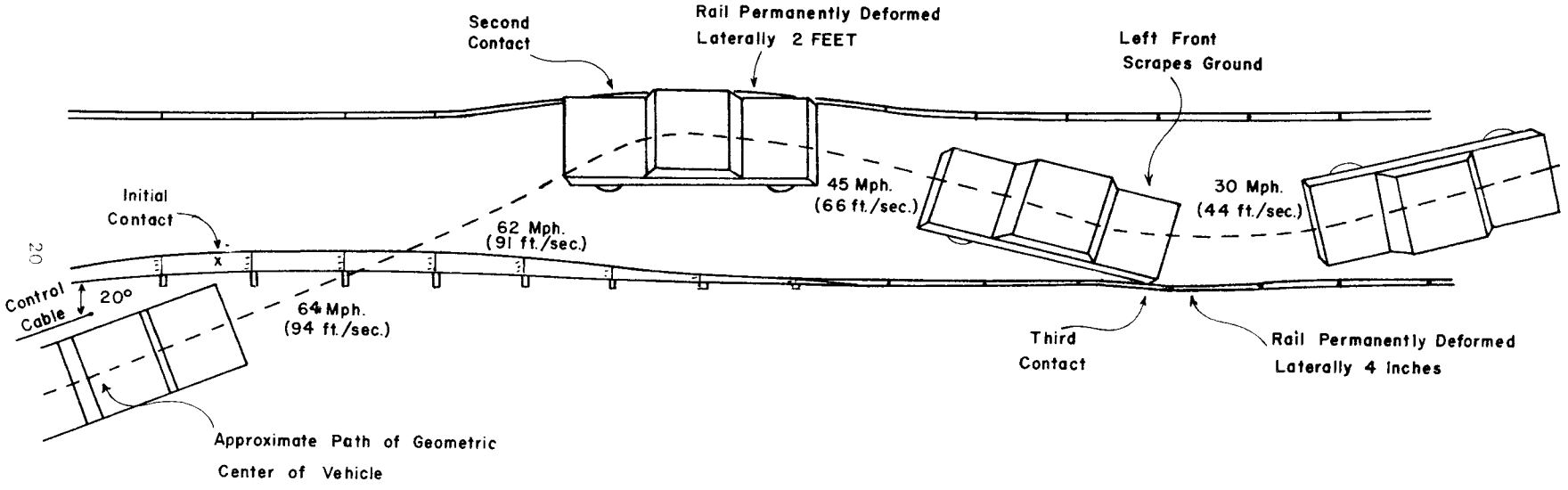

FIGURE 18, SUMMARY OF TEST 505-9A

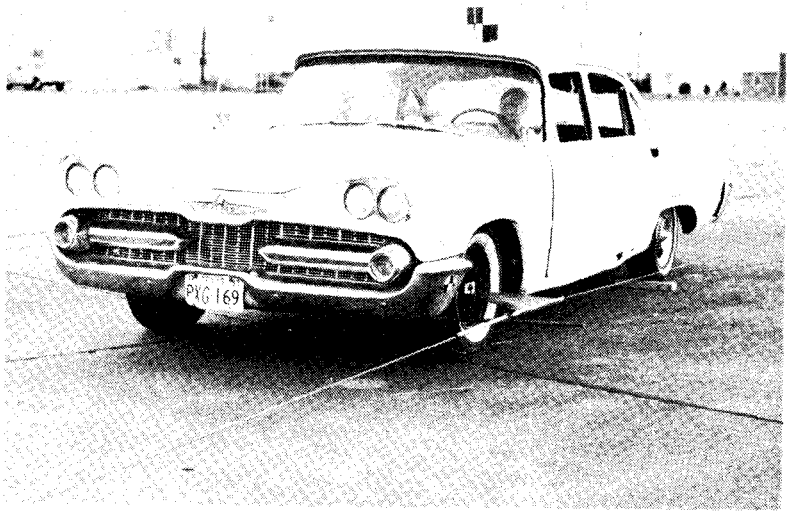

Figure 19, Vehicle Before Test (505-9A)

Figure 20, Vehcile After Test (505-9A)

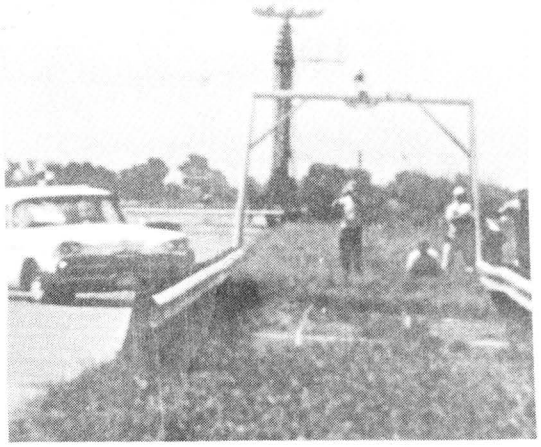

1

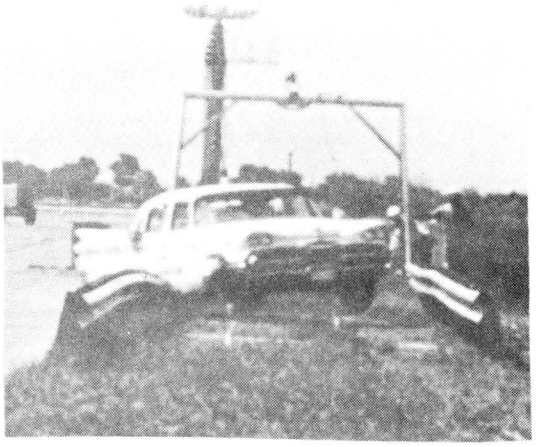

2

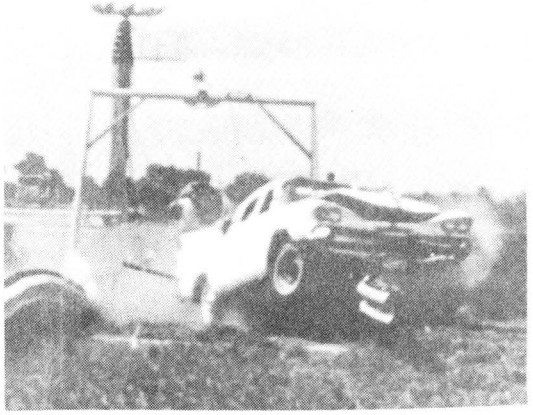

3

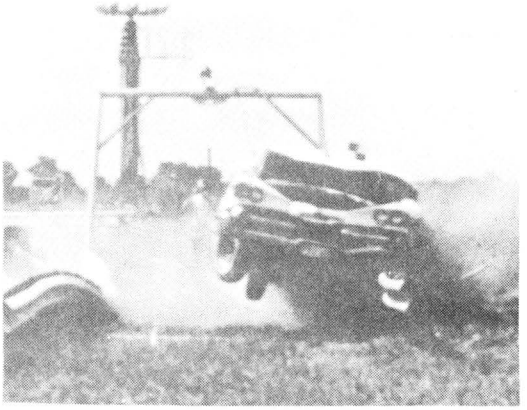

4

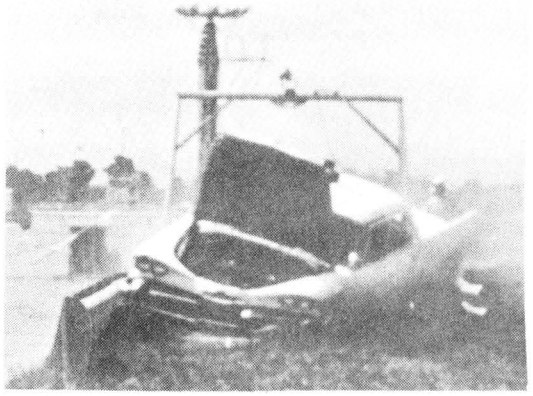

5

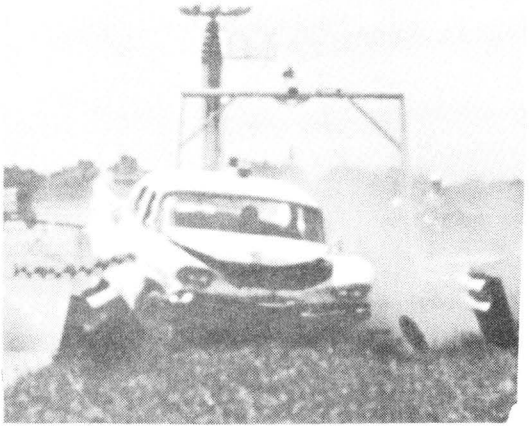

6

Figure 21, Sequential Photographs, Front View (505-9A)

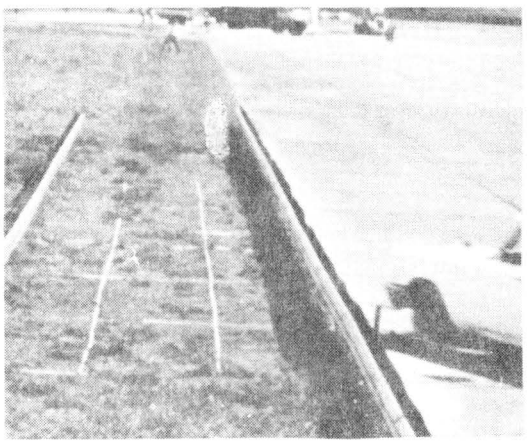

1

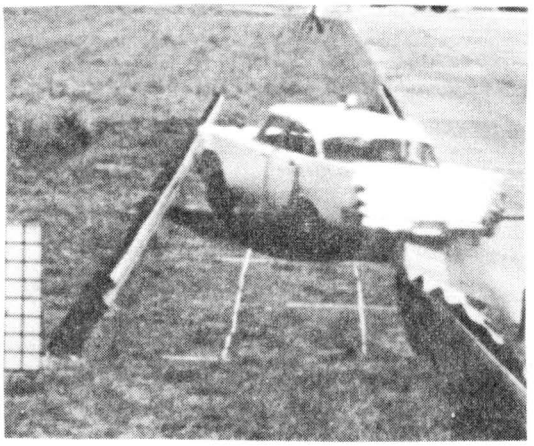

2

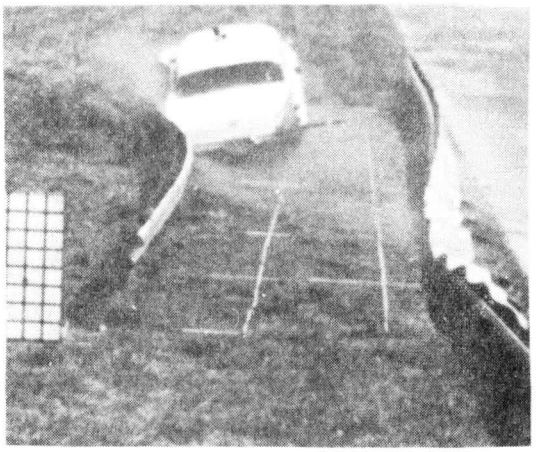

3

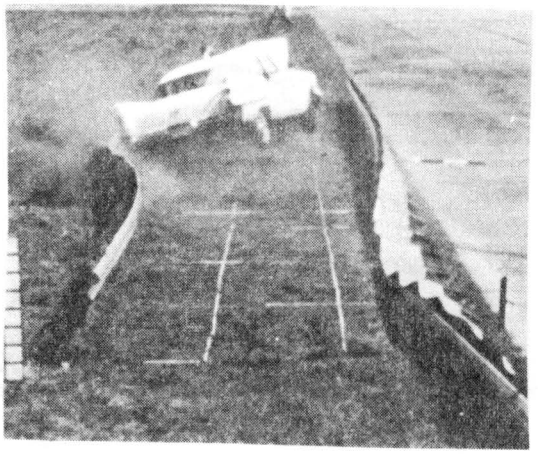

4

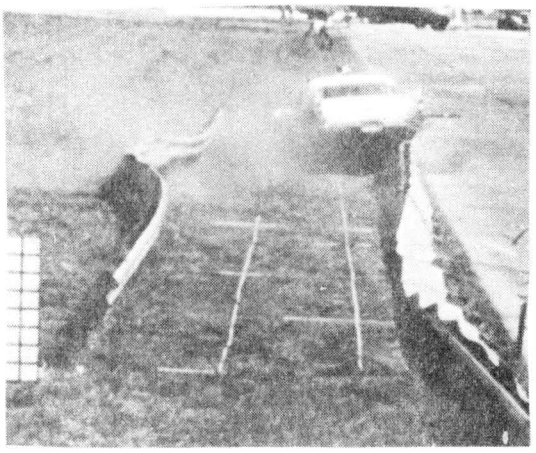

5

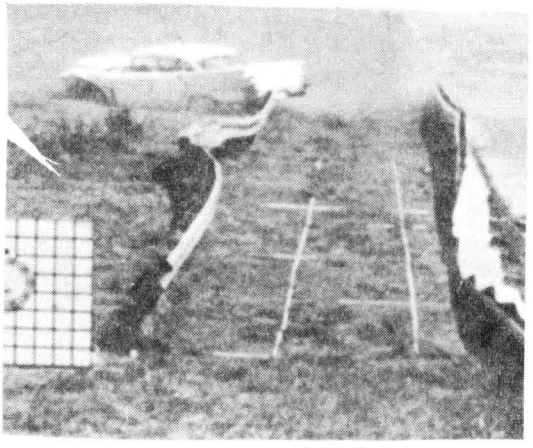

6

Figure 22, Sequential Photographs, Rear View (505-9A)

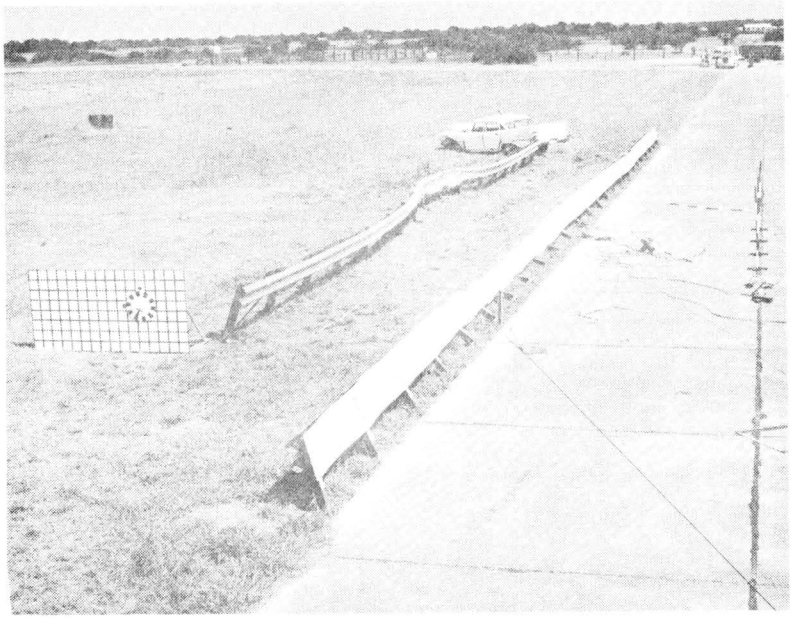

Figure 23, Impact Area After Test (505-9A)

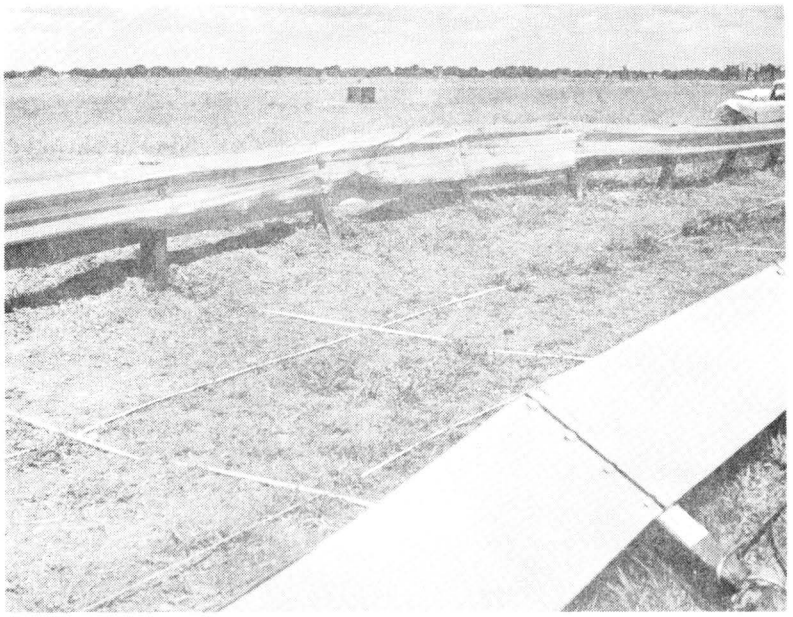

Figure 24, Damage To Second Guardrail (505-9A)

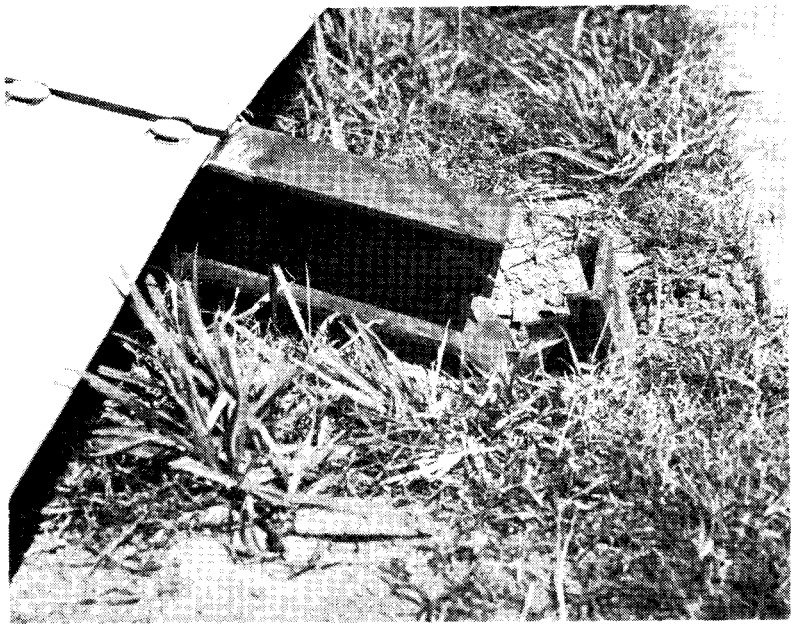

Figure 25, W-in First Guardrail Bent Over at Weakened Section Shear Pin is Still in Place (505-9A)

Figure 26, Guardrail Installation After Test (505-9A)

The strength of the soil has a definite influence on these tests. It is possible that if the soil was much softer or significantly stronger than the condition tested, different results might have been obtained.

Test 10A

The arresting system performed as designed in this test, which was conducted with a low (10^{o}) angle of attack. The 4400 lb. vehicle, moving at 59 mph, was subjected to minor decelerations, the largest of which was 1.7 g's. This deceleration occurred during contact with the second guardrail and was in a transverse direction relative to the vehicle. The car did not severely deflect the second guardrail as in the two previous tests. During the test, the left front tire blew out, which may have contributed to the vehicle damage. This damage was confined to the left front suspension and fender area, as,shown in Figure 32.

SCALE: 1 INCH = 20 FEET

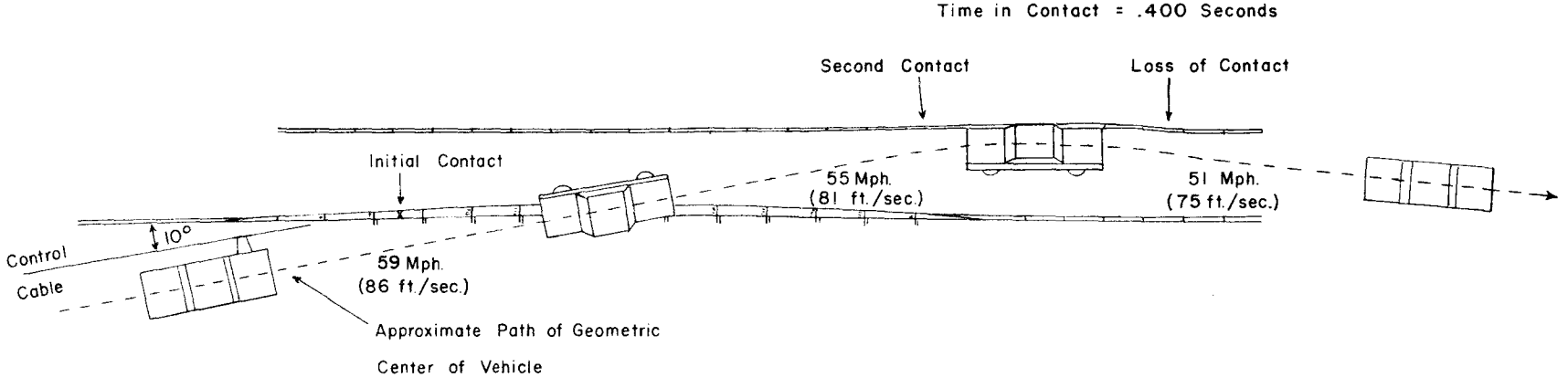

FIGURE 27, SUMMARY OF TEST 505-10A

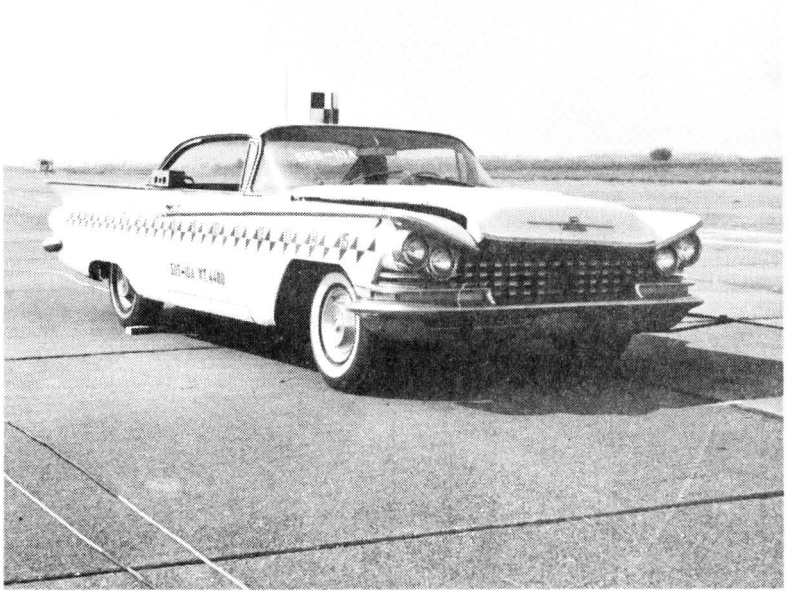

Figure 28, Vehicle Before Test (505-10A)

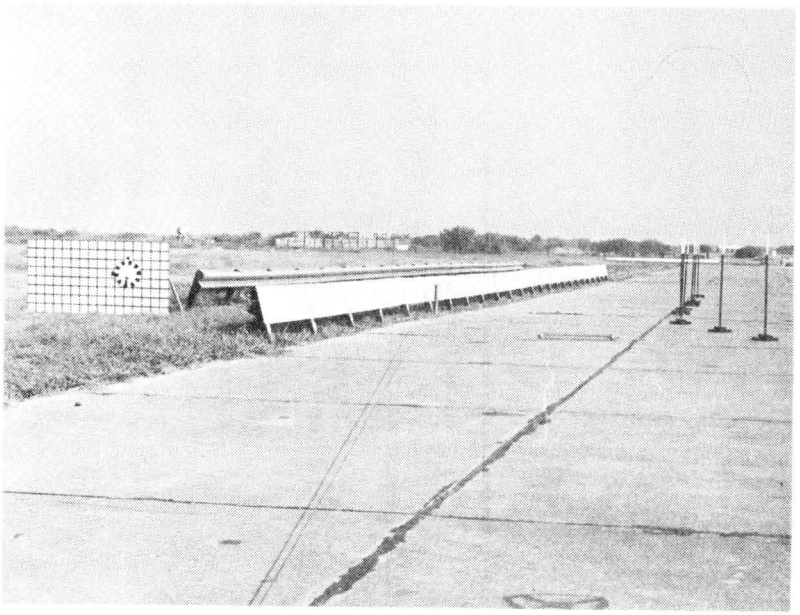

Figure 29, Guardrail Installation Before Test (505-10A)

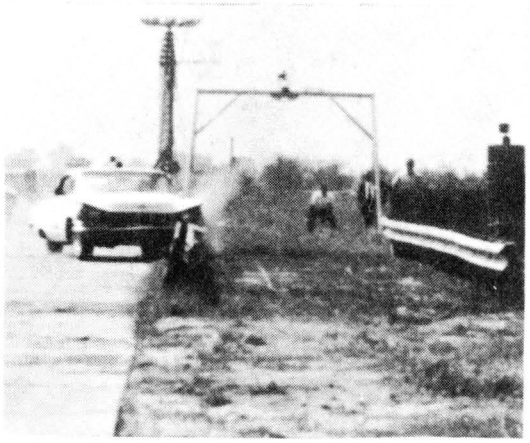

1

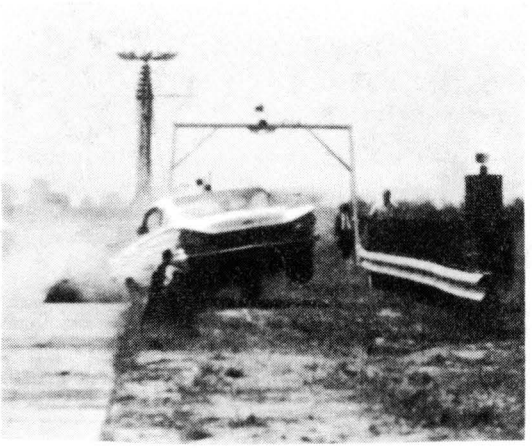

2

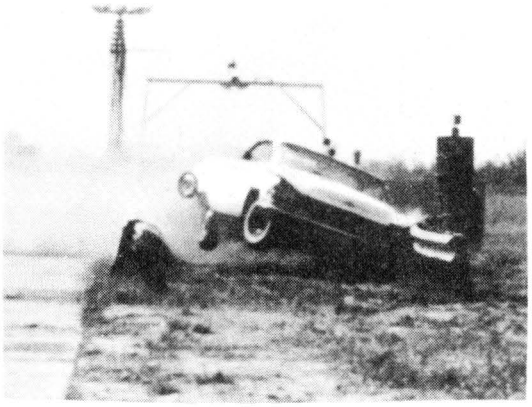

3

4

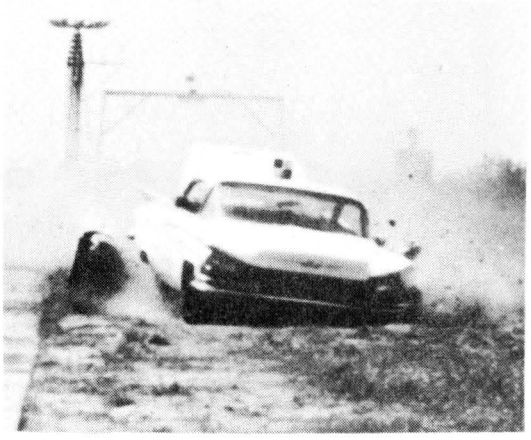

5

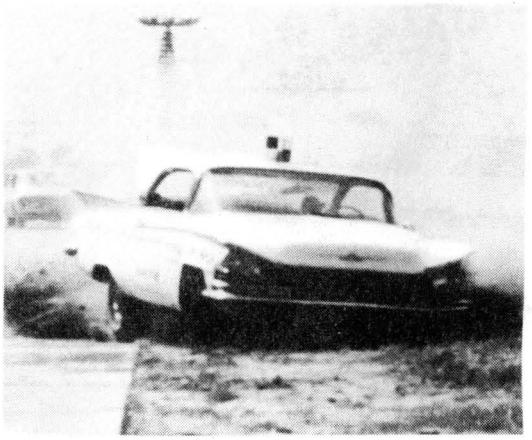

6

Figure 30, Sequential Photographs, Front View (505-10A)

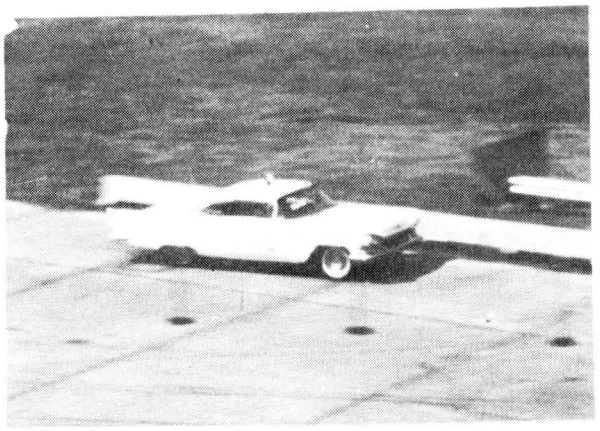

1

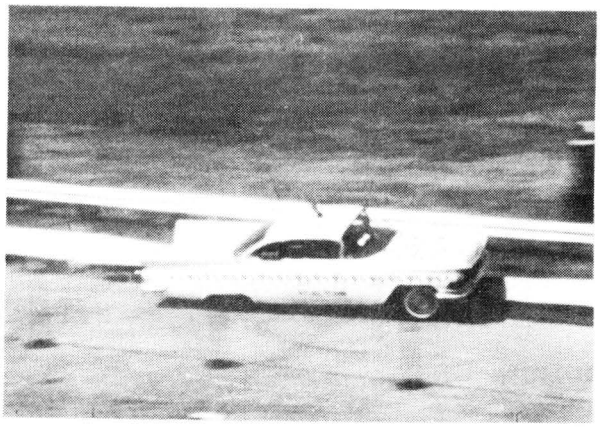

2

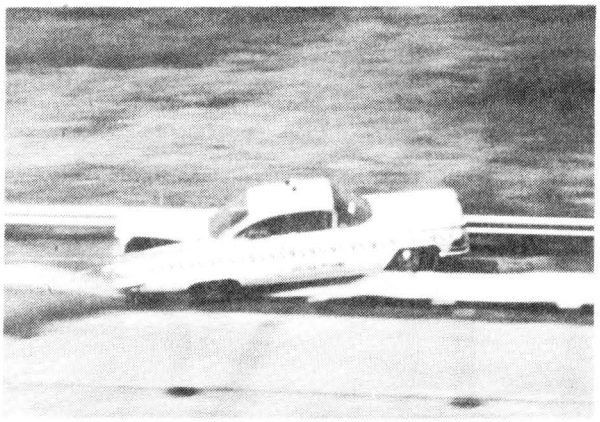

3

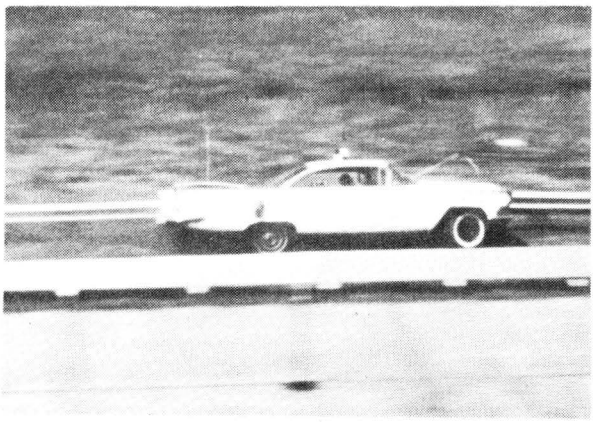

4

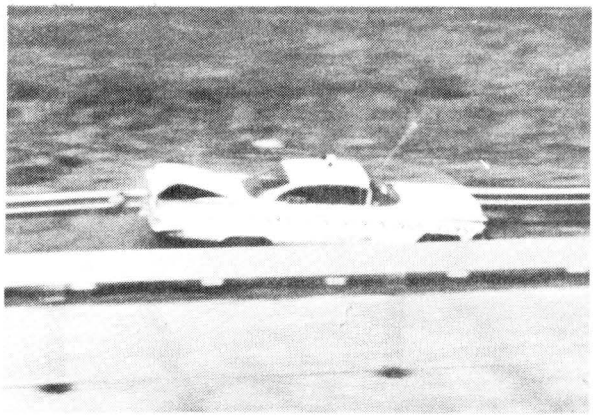

5

6

Figure 31, Sequential Photographs of Test (505-10A, Overhead Camera)

Figure 32, Vehicle After Test (505-10A)

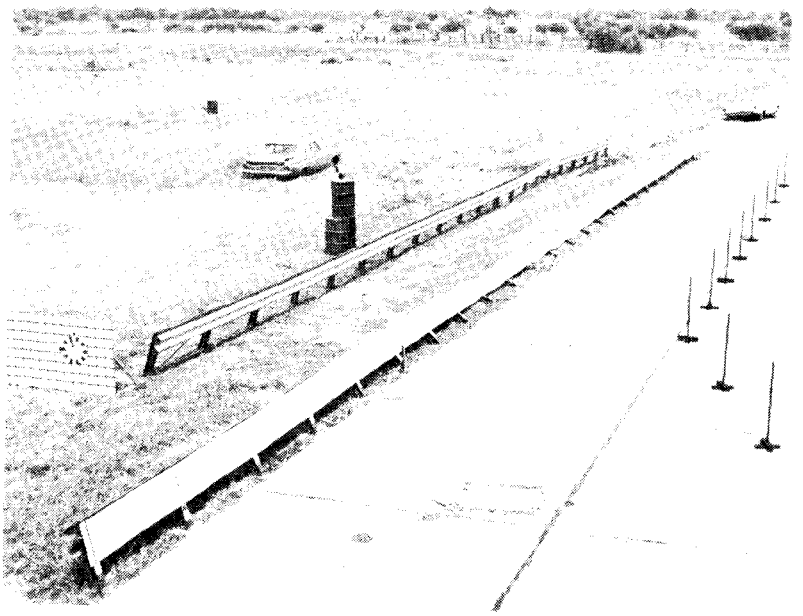

Figure 33, Impact Area After Test (505-10A)

SUMMARY

The full-scale tests which were conducted in this study are summarized in Table 1. The vehicles ranged in weight from 1600 to 4400 lbs. Angles of attack which were used on the One-Way Guardrail vehicle arresting system varied from 10^{o} to 30^{o}. The desired vehicle test velocity was 60 mph. In three of the four tests the actual velocity achieved ranged from 61 to 64 mph. In Test 7A of the compact vehicle, a velocity of only 47 mph was achieved. In three of the four tests, the One-Way Guardrail arresting system performed as designed--redirecting the vehicle and containing it within the two guardrails in the area which would be the median strip in a highway or tunnel application. In Test 8A, that of a 4300 lb. vehicle with a velocity of 61 mph and an attack angle of 30^{o}, containment was not achieved. This was the test in which the vehicle had the maximum kinetic energy in a direction perpendicular to the guardrail installation.

Table 2 summarizes the average g levels which were sustained by the vehicle during contact with the first and second guardrail. The maximum average longitudinal g level, 2.2 g's, was encountered in Test 8A during contact with the second guardrail. The maximum average transverse g level encountered in these tests was the 2.2 g's in Test 9A. These deceleration levels for vehicle arresting guardrails and median barrier systems could easily be tolerated by a properly restrained passenger.* For vehicle speeds slightly less than 60 mph or attack angles slightly less than 30^{o}, the One-Way Guardrail vehicle arresting system would seem to be an effective or adequate device.

---

*The Human Body in Equipment Design, Damon, Albert; Stoudt, Howard W.; and McFarland, Ross A. Harvard University Press, Cambridge, Mass., 1966.

TABLE 1

Brief Description of Test Program

on One-Way Guardrail

Test Number	7A	8A	9A	10A
Angle of Attack	30^{o}	30^{o}	20^{o}	10^{o}
Vehicle Weight	1600 lb.	4300 lb.	4180 lb.	4400 lb.
Impact Speed	47 mph	61 mph	64 mph	59 mph
Kinetic Energy of Vehicle	118 Kip-ft	533 Kip-ft	576 Kip-ft	513 Kip-ft
Kinetic Energy Perpendicular to Guardrail	59 Kip-ft	267 Kip-ft	197 Kip-ft	89 Kip-ft

TABLE 2

Average Vehicle Decelerations*
(From Film)

	Contact with First Guardrail	Contact with Second Guardrail	Recontact with First Guardrail
Test 7A			
Longitudinal	2.1 g's	1.5 g's	---
Transverse	0.6 g's	2.0 g's	---
Test 8A			
Longitudinal	0.5 g's	2.2 g's	---
Transverse	0.0 g's	1.8 g's	---
Test 9A			
Longitudinal	0.3 g's	2.1 g's	1.9 g's
Transverse	0.0 g's	2.2 g's	1.5 g's
Test 10A			
Longitudinal	0.2 g's	0.7 g's	---
Transverse	0.0 g's	1.7 g's	---

* Decelerations are given relative to the orientation of the vehicle's frame at impact.

The importance of the soil in which this arresting system is installed should be emphasized. The installations which were tested at the A&M Research Annex were placed in soil which had a cohesion of approximately 2000 lbs. per square foot.* This allowed a significant deflection of the guardrail support posts during the main collision with the second guardrail. Had the soil been extremely hard, with a very high cohesion, it is possible that test results could have been significantly different. Differences in test results might also have been obtained had the soil been significantly softer. In order to illustrate the probable effect of variations in the physical properties of the soil, the equations shown in Table 3 were derived from the theory presented in Research Reports 105-1** and 105-2*** and the WF post rotations which are shown in Figure 34. In deriving these equations the following energy losses were accounted for: energy required to accelerate guardrail mass; energy required to slip guardrail joints; and the energy required to bend bumper plate and W section in torsion. The longitudinal strain energy that could be put into the system after the W sections and bumper plates slip was neglected.

Examination of the coefficients of these equations will yield the following conclusions, based on the assumption that the soil in the

---

* "Design Procedure Compared to Full Scale Tests of Drilled Shaft Footings," Ivey, Don L. and Dunlap, Wayne A., Research Report No. 105-3, Texas Transportation Institute, February, 1969.

** "Theory, Resistance of a Drilled Shaft Footing to Overturning Loads," Ivey, Don L., Research Report No. 105-1, Texas Transportation Institute, August, 1967.

*** "Resistance of a Drilled Shaft Footing to Overturning Loads, Model Tests and Correlation with Theory," Ivey, Don L., Koch, Kenneth J., and Raba, Carl F. Jr., Research Report No. 105-2, Texas Transportation Institute, July, 1968.

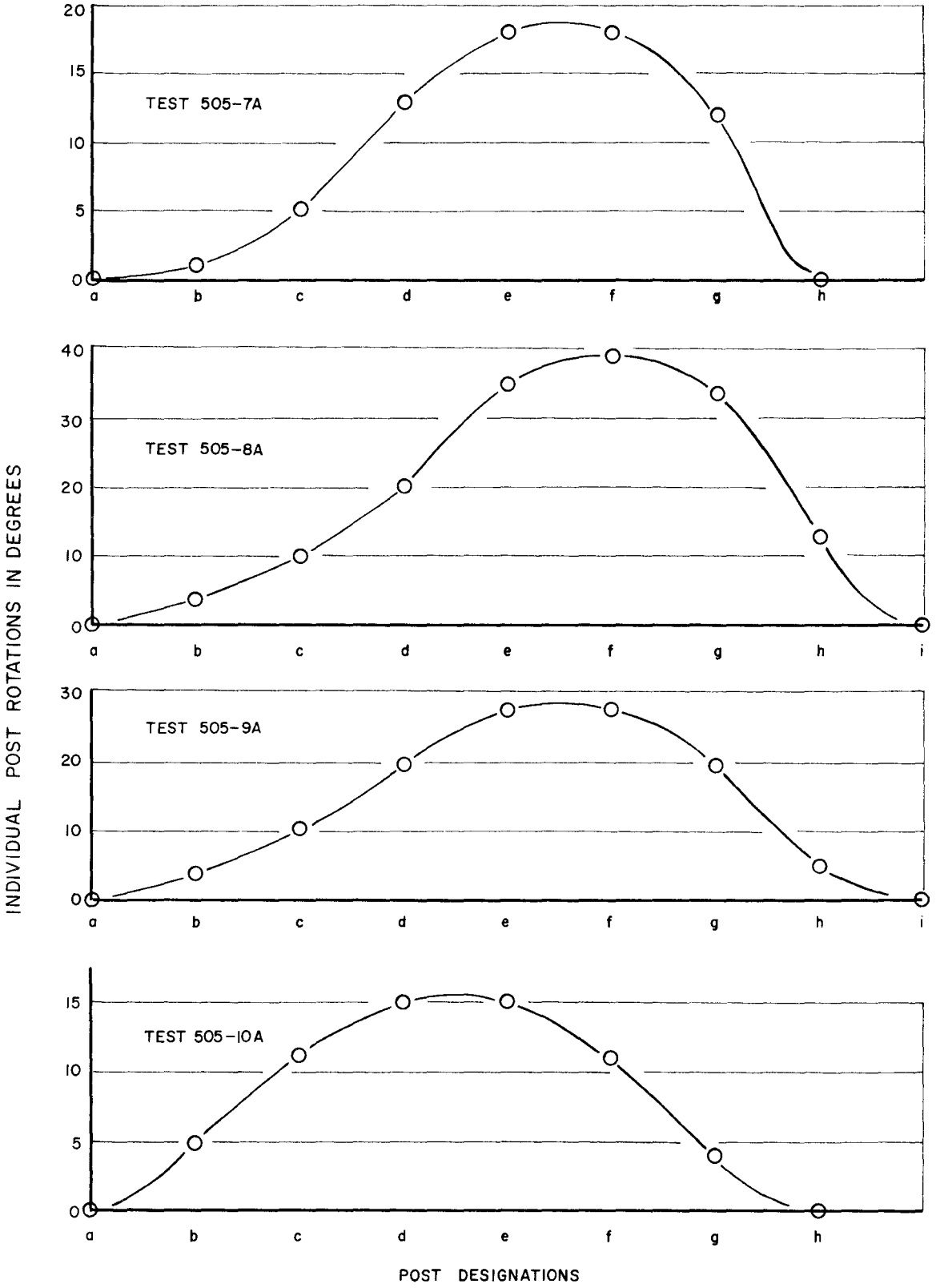

FIGURE 34, INDIVIDUAL POST ROTATIONS FOR INDICATED TESTS (FOR IMPACT WITH SECOND GUARDRAIL)

Assumed Soil Condition	Energy Dissipated, E_p (Good for $\theta > 5^o$) (θ in Degrees)
c = 1000 PSF $\phi = 5^o$	$E_p = 1.03 + 0.34\ (\theta - 5^o)$, Kip-ft
c = 2000 PSF $\phi = 5^o$	$E_p = 2.15 + 0.65\ (\theta - 5^o)$, Kip-ft
c = 5000 PSF $\phi = 5^o$	$E_p = 6.19 + 1.85\ (\theta - 5^o)$, Kip-ft

Table 3, Equations for the Energy Dissipated by Individual Posts for Different Soil Conditions

test program had a cohesion, c, of 2000 PSF and an angle of shear resistance, ϕ, of 5^{o}.

(1) If the guardrail system was installed in a soil with a cohesion of 5000 PSF, and an angle of shearing resistance of 5^{o}, the rotations of the posts in the second guardrail would have decreased by a factor of approximately 3, resulting in a corresponding increase in the average lateral g level.* This increased lateral g level would still be within the tolerance limits of restrained humans.

(2) If the guardrail system was installed in a soil with a cohesion of 1000 PSF and an angle of shearing resistance of 5^{o}, the rotations of the posts in the second guardrail would have increased by a factor of approximately 2. Although the equations would not be accurate in this range of excessive rotations, it does illustrate that in the critical test of a 4000 lb. vehicle traveling 60 mph with an attack angle of 30^{o}, the large rotations would almost certainly result in ramping of the vehicle on the second guardrail. This situation could be remedied by increasing the embedment length of the post or increasing their bearing area by placing concrete around them.

---

*"Bridge Rail Service Requirements as a Basis for Design Criteria," Olson, Robert M., Discussion of Findings of NCHRP Project 12-8, Paper presented at the Annual Meeting of the American Society of State Highway Officials, Minneapolis, Minnesota, 1968.

CONCLUSIONS

The One-Way Guardrail vehicle arresting system performed as designed in three of the four tests conducted. The system should be effective for vehicle velocities somewhat less than 60 mph or angles of attack slightly less than 30^{o}. All tests where the vehicle was contained show deceleration levels well within the tolerance limits of restrained humans.

It should be emphasized that the functioning of this system is dependent to some degree on the properties of the soil surrounding the guardrail support posts. If a low cohesion soil is not avoidable in a given location, the guardrail system could be made to function properly by increasing the imbedment length or the bearing area or by placing concrete around the WF support posts.

A P P E N D I X

TABLE 1A

TEST RF 505-7A

MARTIN MARIETTA GUARDRAIL 30° INCIDENCE ANGLE

1955 RENAULT, 2-DOOR SEDAN, 1600 LB.

HIGH-SPEED FILM DATA

Time Milliseconds	Displacement ft	Velocity ft/sec	
0	0		
		68.0 ┐	
10.29	0.70		
		68.0	
20.58	1.40		
		69.0	
30.87	2.11		
		70.0	68.6
41.16	2.83		Avg.
		68.0	
51.45	3.53		
		69.0	
61.74	4.24		
		68.0 ┘	
72.03 Impact	4.94		
		62.2	
82.32	5.58		
		61.2	
102.90	6.84		
		61.7	
123.48	8.11		
		55.9	
144.06	9.26		
		58.8	
164.64	10.47		
		56.4	
185.22	11.63		
		61.7	
205.80	12.90		
		56.4	
226.38	14.06		
		57.3	
246.96	15.24		
		57.3	
267.54	16.42		
		58.5	
308.70	18.83		
		57.3	
349.86	21.19		
		60.4	
391.02	23.68		
391.60*	---		

*Lost contact with first guardrail.

TABLE 1A

TEST RF 505-7A (continued)

Time Milliseconds		Displacement ft	Velocity ft/sec	
			51.0	
432.18		25.78		
			54.9	
473.34		28.04		52.3
			48.8	Avg.
514.50		30.05		
			54.4	
555.66	Impact #2	32.29		
			53.9	
596.82		34.51		
			47.6	
637.98		36.47		
			50.7	
679.14		38.56		
			40.0	
720.30		40.21		
			49.8	
761.46		42.26		
			40.3	
802.62		43.92		
			49.8	
843.78		45.97		
			44.4	
884.94		47.80		
			45.4	
926.10*		49.67		
			44.7	
967.26		51.51		

Vehicle moved out of view.

*Lost contact with second guardrail.

TABLE 2A

TEST RF 505-8A

MARTIN MARIETTA GUARDRAIL 30° INCIDENCE ANGLE

1956 DE SOTO, 4-DOOR SEDAN, 4200 LB.

HIGH-SPEED FILM DATA

Time Milliseconds	Displacement ft	Velocity ft/sec	
0	0		
		90.9	
10.67	0.97		
		88.1	
21.34	1.91		
		89.0	
32.01	2.86		
		89.0	89.1
42.68	3.81		Avg.
		89.0	
53.35	4.76		
		87.2	
64.02	5.69		
		90.9	
74.69 Impact	6.66		
		90.9	
85.36	7.62		
		87.6	
106.70	9.49		
		89.5	
128.04	11.40		
		85.7	
149.38	13.23		
		82.9	
170.72	15.00		
		89.0	
192.06	16.90		
		86.7	
213.40	18.75		
		85.3	
234.74	20.57		
		84.3	
256.08	22.37		
		85.8	
277.42	24.18		84.4
		83.0	Avg.
320.10*	27.81		
		83.4	
352.11 Impact #2	---		
362.78	31.37		

*Lost contact with first guardrail.

TABLE 2A

TEST RF 505-8A (continued)

Time Milliseconds	Displacement ft	Velocity ft/sec
		75.4
405.46	34.59	
		71.7
448.14	37.65	
		66.5
490.82	40.49	
		56.9
533.50	42.92	
		61.4
576.18	45.54	
		63.3
618.86	48.24	
		61.4
640.20	49.55	
		60.0~Final Velocity
780.00 Airborne	---	

Further analysis not feasible.

TABLE 3A

TEST RF 505-9A

MARTIN MARIETTA GUARDRAIL 20° INCIDENCE ANGLE

1959 DODGE, 4-DOOR SEDAN, 4180 LB.

HIGH-SPEED FILM DATA

Time Milliseconds	Displacement ft	Velocity ft/sec	
0	0		
		96.2	
10.39	1.00		
		90.5	
20.78	1.94		
		94.3	
31.17	2.92		
		96.2	
41.56	3.92		
		93.4	
51.95	4.89		93.9
		91.4	Avg.
62.34	5.84		
		95.3	
72.73	6.83		
		91.4	
83.12	7.78		
		95.3	
93.51	8.77		
		95.3	
103.90 Impact	9.76		
		93.4	
124.68	11.70		
		93.8	
145.46	13.65		
		91.0	
166.24	15.54		
		90.0	
187.02	17.41		
		90.5	
207.80	19.29		
		92.9	
228.58	21.22		
		88.5	
249.36	23.06		
		90.5	
270.14	24.94		
		87.1	
290.92	26.75		
		83.2	
311.70	28.48		

Vehicle went out of view.

TABLE 4A

TEST RF 505-10A

MARTIN MARIETTA GUARDRAIL 10^{o} INCIDENCE ANGLE

1957 BUICK, 2-DOOR HARDTOP, 4400 LB.

HIGH-SPEED FILM DATA

Time Milliseconds	Displacement ft	Velocity ft/sec	
0	0		
		81.6	
12.25	1.00		
		81.6	
24.50	2.00		
		85.7	
36.75	3.05		86.4
		98.0	Avg.
49.00	4.25		
		89.0	
61.25	5.34		
		82.4	
73.50 Impact	6.35		
		91.8	
98.00	8.60		
		85.3	
122.50	10.69		
		89.8	
147.00	12.89		
		89.4	
171.50	15.08		
		87.8	
196.00	17.23		
		86.5	
220.50	19.35		
		87.8	
245.00	21.50		
		87.8	
269.50	23.65		
		83.3	
294.00	25.69		
		87.3	
318.50	27.83		
		88.6	
343.00	30.00		
		89.4	
367.50	32.19		
		90.6	
392.00	34.41		
		88.2	
416.50	36.57		

Transferred to other camera film for remainder of tracking.

TABLE 4A

TEST RF 505-10A (continued)

Time Milliseconds		Displacement ft	Velocity ft/sec	
439.42		38.55		
			86.9	
460.26		40.36		
			83.0	
481.10		42.09		
			84.0	
501.94		43.84		
			80.1	
522.78		45.51		
			84.0	
543.62		47.26		
			83.0	
564.46		48.99		
			78.7	
585.30		50.63		
			87.8	
606.14		52.46		
			82.1	
626.98		54.17		
			81.1	
647.82		55.86		
			86.9	
668.66		57.67		
			76.8	
689.50		59.27		
			79.2	
710.34		60.92		
			82.1	
731.18		62.63		
			81.6	
752.02		64.33		
			84.5	
772.86		66.09		
			79.7	
793.70		67.75		
			81.1	
814.54		69.44		
823.50*		---		
			81.1 ┐	
835.38		71.13		
			81.6	81.1
856.22	Impact #2	72.83		Avg.
			80.6 ┘	
877.06		74.51		
			78.2	
897.90		76.14		

*Lost contact with first guardrail.

TABLE 4A

TEST RF 505-10A (continued)

Time Milliseconds	Displacement ft	Velocity ft/sec
		89.3
918.74	78.00	
		77.7
939.58	79.62	
		85.9
960.42	81.41	
		76.3
981.26	83.00	
		85.4
1002.10	84.78	
		78.2
1022.94	86.41	
		79.2
1043.78	88.06	
		81.6
1064.62	89.76	
		81.6
1085.46	91.46	
		77.3
1106.30	93.07	
		76.3
1127.14	94.66	
		76.8
1147.98	96.26	
		78.7
1168.82	97.90	
1256.00*		

*Lost contact with second guardrail.

TECHNICAL MEMORANDUM 505-4

Texas Transportation Institute
Texas A&M Research Foundation

DRAGNET VEHICLE ARRESTING SYSTEM

A Tentative Progress Memorandum on Contract No. CPR-11-5851

U. S. Department of Transportation
Federal Highway Administration
Bureau of Public Roads

by

T. J. Hirsch
Research Engineer and Principal Investigator

Gordon G. Hayes
Engineering Research Associate

and

Don L. Ivey
Associate Research Engineer

Crash tests and evaluations were conducted under the Office of Research and Development, Structures and Applied Mechanics Division's, Research Program on Structural Systems in Support of Highway Safety (4S Program). The opinions, findings, and conclusions expressed in this report are those of the authors and not necessarily those of the Bureau of Public Roads.

Note: For the reader who is interested in gaining a general idea of the value of this particular arresting system and not in the details necessary to document the technical aspects of this study, the authors recommend reading pages 2 and 5 and scanning the photographs in this report.

February 28, 1969

INTRODUCTION

Six crash tests of a "dragnet" vehicle arresting system were conducted by the Texas Transportation Institute under a contract with the Bureau of Public Roads as part of their program on Structural Systems in Support of Highway Safety. This "dragnet" system uses Metal Bender energy absorbing devices developed by Van Zelm Associates, Inc., of 1475 Elmwood Avenue, Providence, Rhode Island. Descriptions include photographs of the vehicle and arresting system before, during and after each individual test.

DESCRIPTION OF ARRESTING SYSTEM

This system consists of a net made of steel cables attached at each end to Metal Bender energy absorbing devices as shown in Figure A1. The Metal Benders, which are supported on rigid steel posts, are steel boxes containing a series of rollers around which the metal tape is bent back and forth as it is pulled through the case. Each end of the net is attached to one end of the metal tape extending from a Metal Bender. The Metal Benders are designed so that a specified force will be necessary to pull the metal tape through the case. This force is relatively independent of velocity and environmental conditions and depends on the size of the tape used. By varying tape size a number of different tape forces are available.

Supplementary construction and installation data on this system were provided by Van Zelm Associates, Inc.* and are presented in Appendix A. Photographs of the arresting system used in these tests are shown in Figures 2 and 3.

---

* Jackson, M. and Montanaro, L., "Arresting System for Snagging a Vehicle Leaving the Roadway Near Fixed Highway Obstacles," Van Zelm Associates, Inc., A Division of Entwistle Mfg. Corp., May 8, 1967.

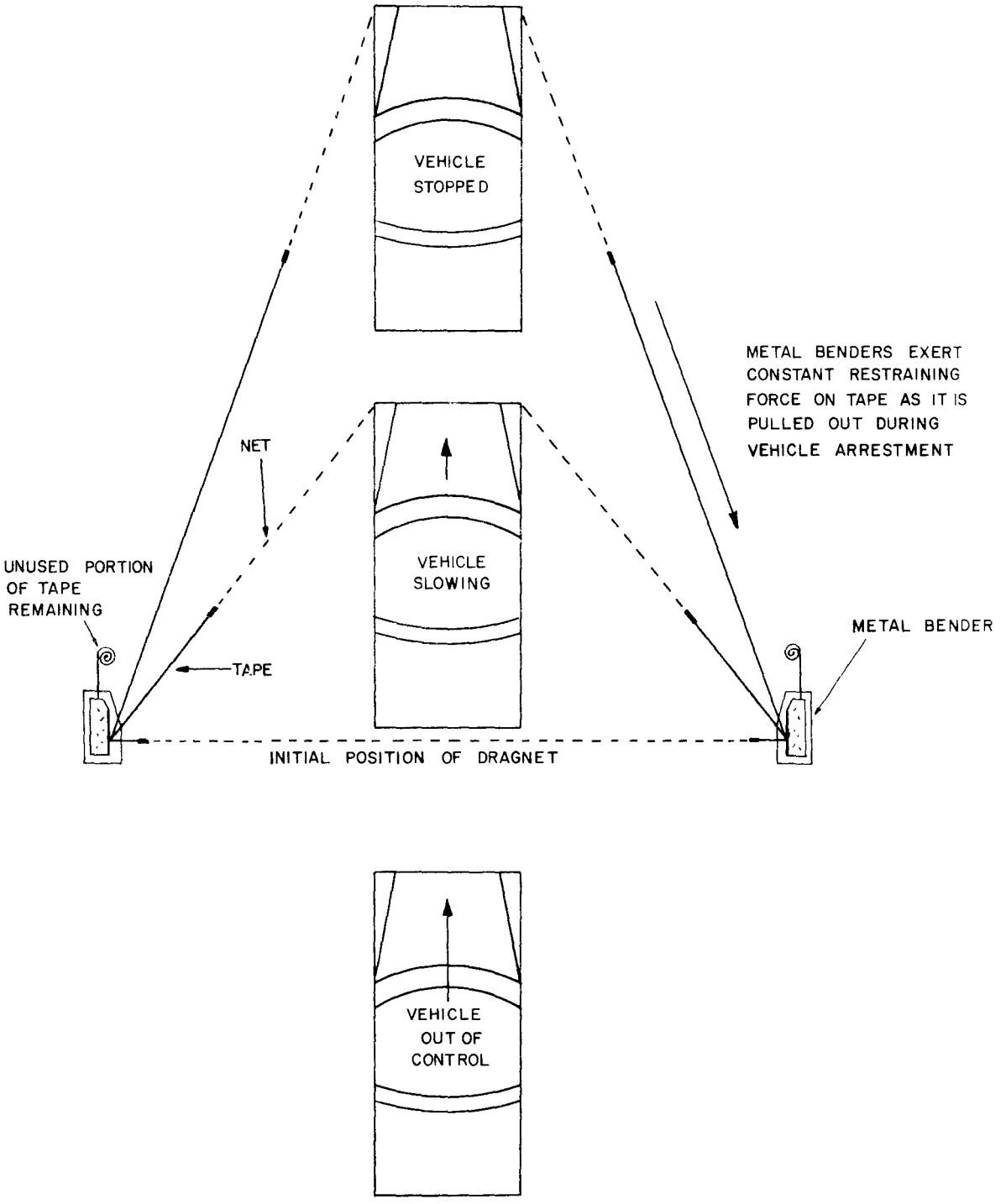

FIGURE 1, IDEALIZED FUNCTION OF DRAGNET ARRESTING SYSTEM

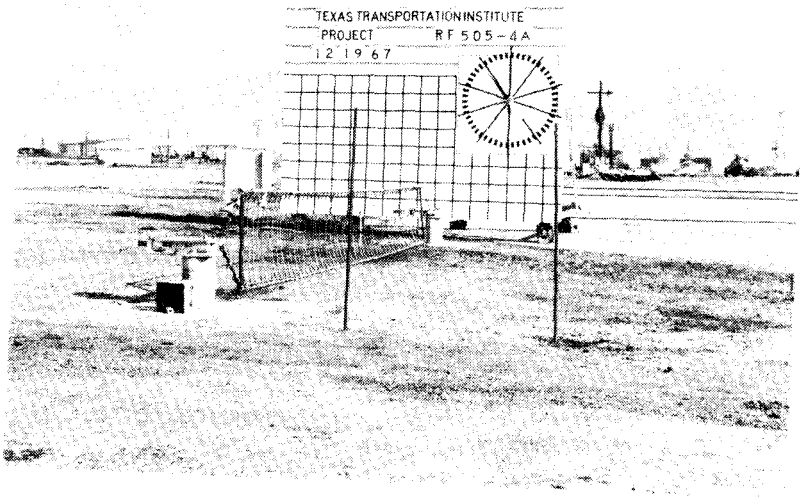

Figure 2, Dragnet Arresting System Before Test 505-4A.

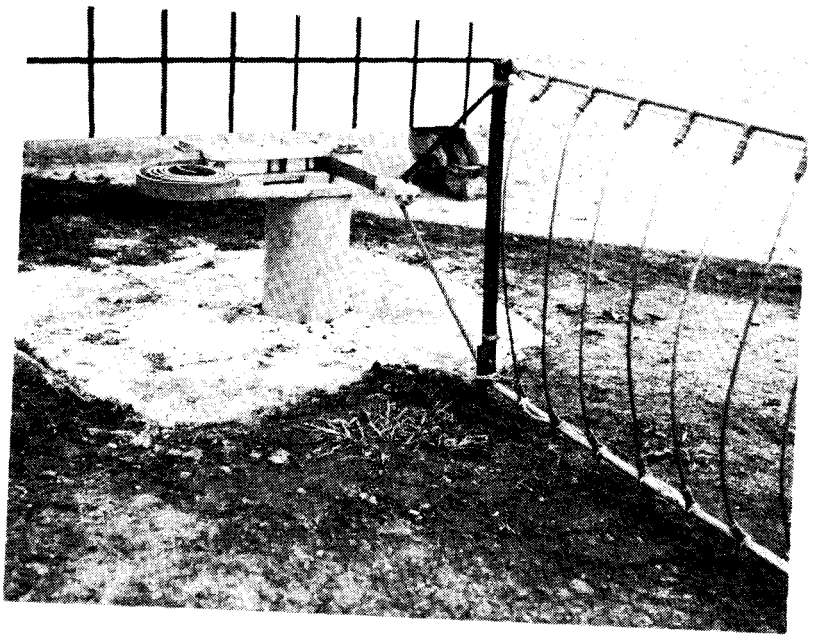

Figure 3, Metal Bender with 25,000 lb. Tape Attached to Net.

CONCLUSIONS

The Van Zelm dragnet vehicle arresting system performed basically as designed in all tests. The performance of the system was very good in four of the six tests. In Test 4D the dragnet was engaged too low on the front of the vehicle, which resulted in the vehicle's rear end vaulting the net after most of the longitudinal deceleration had occurred. In Test 4F the performance of the dragnet system was ideal until one of the tapes ran out. Had this tape been long enough to continue applying load until the vehicle was completely stopped, the performance probably would have been excellent. Deceleration levels were reduced to a small fraction of those which would be expected in rigid barrier impacts. Increasing design tape load results in shortening the stopping distance, increasing the deceleration level and increasing vehicle damage. For any given application of the dragnet system, the longer the allowable stopping distance, the more desirable are the deceleration characteristics of the system because a smaller tape load can be used.

The height of the net was shown to be an important factor in the performance of the system. The net should be positioned so that it completely entraps the front of the entering vehicle. If it is too low, a less desirable performance may be expected, as was found in Test 4D. Good performance was found when the lower main cable of the net was positioned four inches above the ground.

No permanent damage was sustained by the dragnet system during any of these tests. All major components were reusable except for the expendable metal tapes. The system can be applied to a variety of situations by varying the Metal Bender tape tension, the tape length, and the geometry

of the installation. A variety of Metal Bender tape tensions are available, some of which are given in Appendix A.

This series of tests has shown that reasonably accurate predictions of vehicle stopping distance and deceleration levels can be obtained using the equations developed in Appendix B.

RECOMMENDATIONS

The "dragnet" vehicle arresting system is an effective, practical, and economical system for safely stopping vehicles which are out of control at certain highway sites. Some obvious sites for its employment are:

1. Protecting highway medians at bridge overpasses,
2. As a barrier at "dead ends" of highways or roads,
3. As a "dead-end" barrier at ferry landings or as a barrier to close off entrance and exit ramps of freeways,
4. As a barrier to protect certain rigid obstacles in highway rights-of-way.

It is recommended that the height of the arresting net be increased to approximately 4 ft. The net used in the tests was 3 ft. high, and in several tests (notably Test 4D) failed to completely entrap the vehicle's front end. It is desirable that the upper net cable clear the top of the car hood in order to more securely entrap the vehicle.

The lowest Metal Bender tension force which is compatible with the available stopping distance should be selected. In general, Metal Bender tension forces of 12,500 lb. or less are recommended. The behavior of these "dragnet" systems can be predicted very well with the mathematical analysis presented in Appendix B.

It is the opinion of the authors that with Metal Bender tension forces of 8,000 lbs. or less, acceptable stopping characteristics would be achieved with the Metal Benders mounted flush with the ground, thus removing the hazard of the protruding anchor post or pier. Metal Benders of 4,000 lbs. or less can be mounted on single 6 to 8 inch diameter timber posts embedded 3 ft. or more in the ground unless the ground is extremely soft. The top of the timber post should not extend over 20 inches above the ground. These single timber posts would normally not be a significant hazard if struck by a vehicle.

TEST PROGRAM

Six vehicle crash tests of the "dragnet" arresting system were conducted during the period of December 19, 1967 to November 21, 1968. A summary of this testing program is given by Table 1. Both compact and full-size vehicles were directed into the system. Tests 4A through 4D employed Metal Benders with 25,000 pound tape loads. These tape loads were reduced to 12,500 pounds for Tests 4E and 4F.

Each test was recorded using high-speed motion picture cameras. This film was analyzed to give detailed time-displacement data. Lower speed motion picture cameras were placed at selected points to provide a qualitative record of the test in progress. Still photographs of the vehicle before and after each test and photographs of various details of the arresting system were obtained.

Accelerometer transducers were attached to the frames of the vehicles to determine deceleration levels during each test. Deceleration traces are presented in Appendix C. Maximum decelerations under specified filtering techniques were determined from these accelerometer traces, while average decelerations were calculated on the basis of initial speed and stopping distance.

An Alderson articulated anthropometric dummy weighing 161 pounds was used to simulate a human driver in each test. A seat belt securing the dummy was equipped with strain guages which permitted the measurement of seat belt force. Variation in this seat belt force during the progress of each test is presented in Appendix C.

TABLE 1

Summary of Test Program

On Van Zelm "Dragnet" Arresting System

Test No.	4A	4B	4C	4D	4E	4F
Angle of Attack	Head-On	Head-On	30^{o}	30^{o}	Head-On	30^{o}
Tape Arresting Load (Kips)	25.0	25.0	25.0	25.0	12.5	12.5
Vehicle Weight (lbs.)	1460	4300	1620	4520	3760	3880
Vehicle Speed (mph) (fps)	42 61.8	60 87.4	48 69.7	54 78.7	56 82.6	62 91.9
Vehicle Kinetic Energy (Kip-ft)	87.1	513.	123.	437.	401.	512.

TEST 4A

A Renault Dauphine weighing 1460 pounds was directed head-on into the dragnet at a speed of 42 mph. The tape force for each Metal Bender was 25,000 pounds. All components of the system performed as designed and the vehicle was stopped after penetrating 10.2 feet. Stopping distance is defined as the distance the center of gravity of the vehicle travels after the car contacts the net. The Metal Bender strap pullout accounted for 63% of the vehicle's initial kinetic energy of 87.1 kip-ft. The remaining energy was expended in stretching the net, crushing the vehicle (see Figure 5), and increasing the vehicle's potential energy due to raising the center of gravity. The amount expended in increasing gravitational potential energy was only about one kip-ft.

The damage to the front of the vehicle was severe. The maximum longitudinal deceleration, shown in Figure C1, was 16 g's. The average deceleration was 5.8 g's over 0.245 seconds.

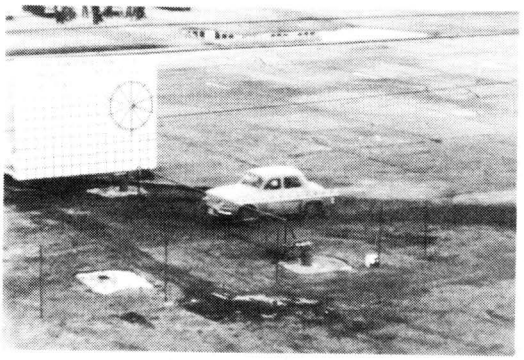

1

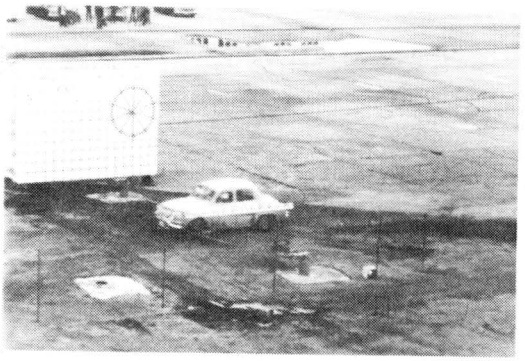

2

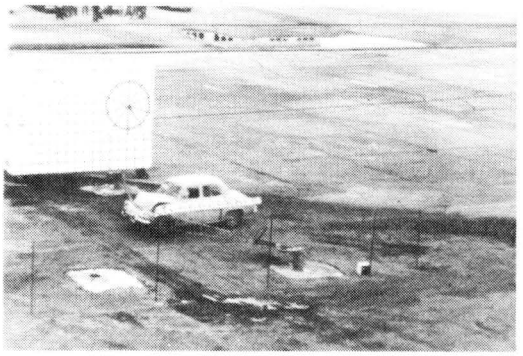

3

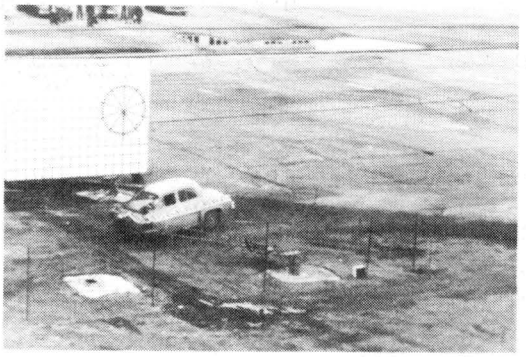

4

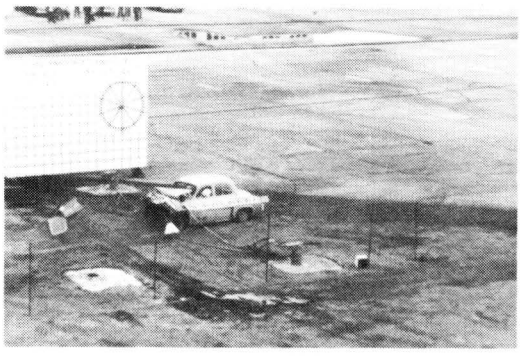

5

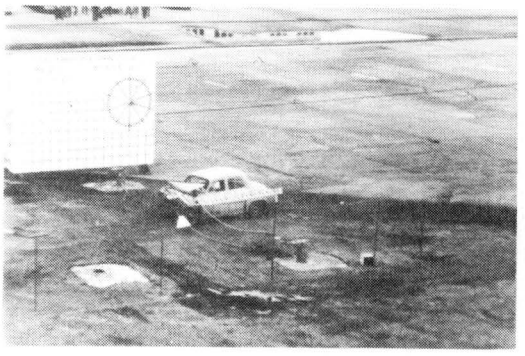

6

Figure 4, Sequential Photographs of Test 505-4A

Figure 5, Vehicle and Dragnet after Test 505-4A.

TEST 4B

A 4300 pound Mercury sedan traveling 60 mph was directed head-on into the arresting system. The dragnet, which was equipped with 25,000 pound tape tension Metal Benders performed as designed. The vehicle was brought to a stop in 19.4 feet and tape pullout expended 58% of the vehicle's energy. The front of the vehicle was pulled down to the ground which caused some frictional energy losses. The change in potential energy due to the elevation of the center of gravity was estimated to be about 17 kip-ft, or 3.3% of the initial energy.

The damage to the front of the vehicle, shown in Figure 9, includes a downward bending of the front of the vehicle's frame. This was due to the net applying pressure to the lower portion of the vehicle's front end. The maximum significant deceleration, shown by Figure C3, was 16 g's, and the average deceleration was 6.1 g's.

Figure 6 , Vehicle Before Test 505-4B.

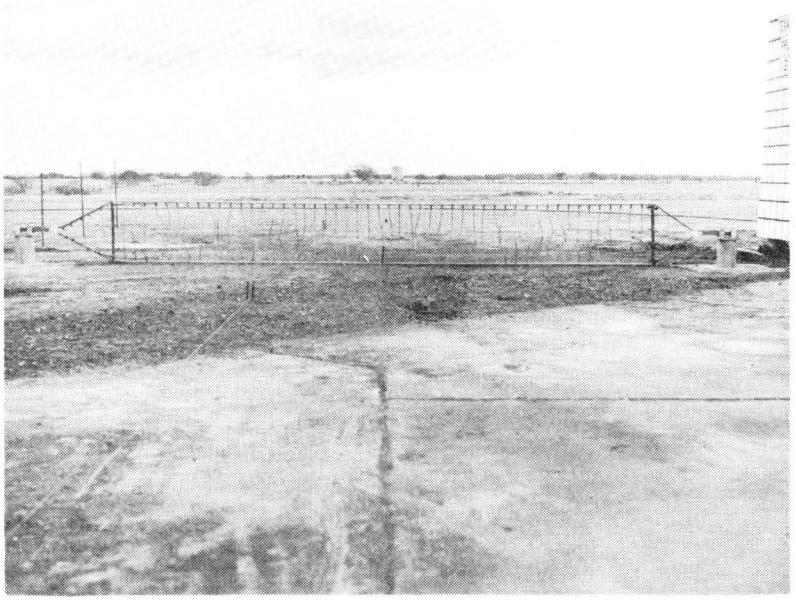

Figure 7 , Arresting System Before Test 505-4B.
(Looking Along Path of Vehicle)

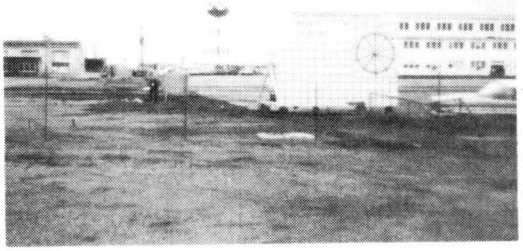

1

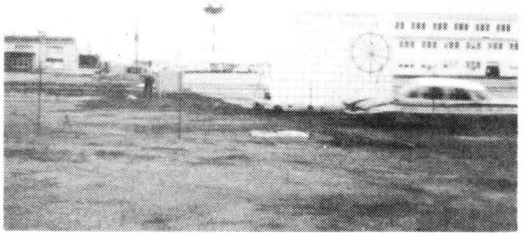

2

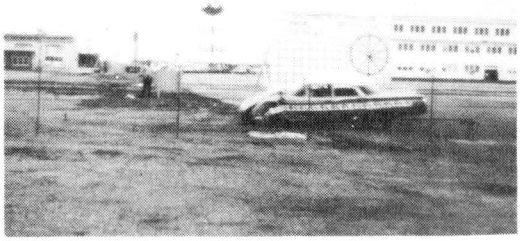

3

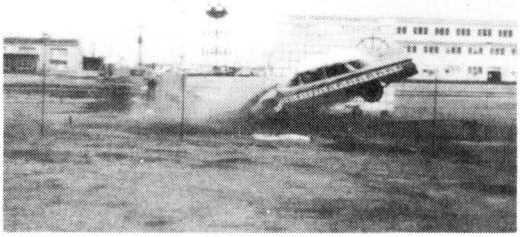

4

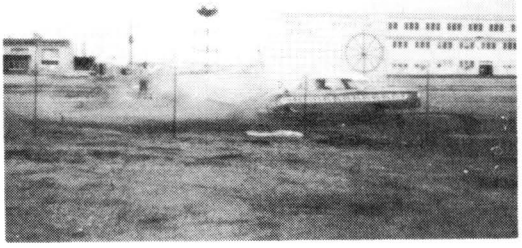

5

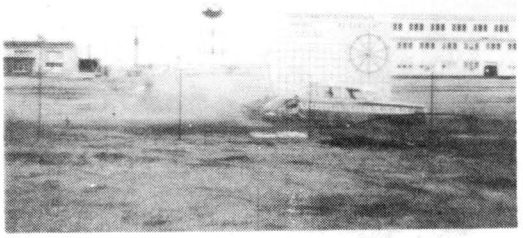

6

Figure 8, Sequential Photographs of Test 505-4B.

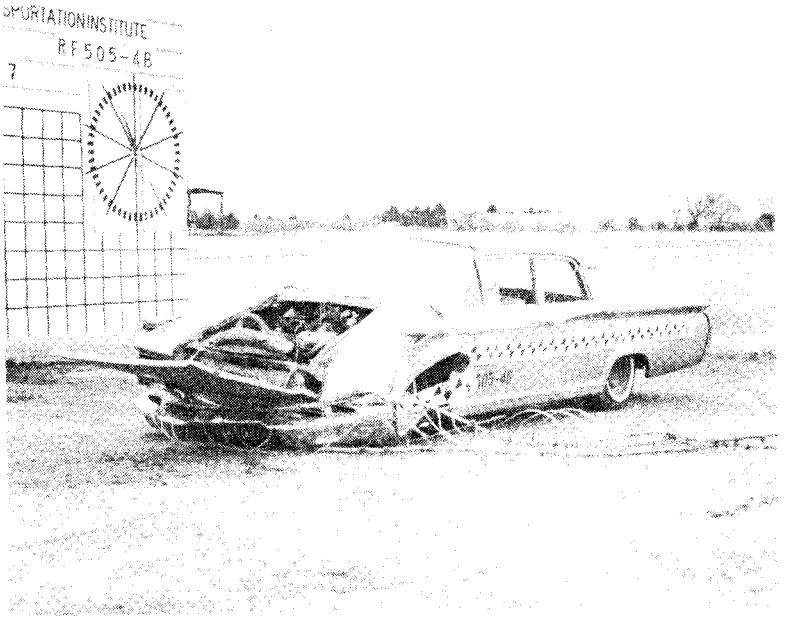

Figure 9, Vehicle After Test 505-4B.

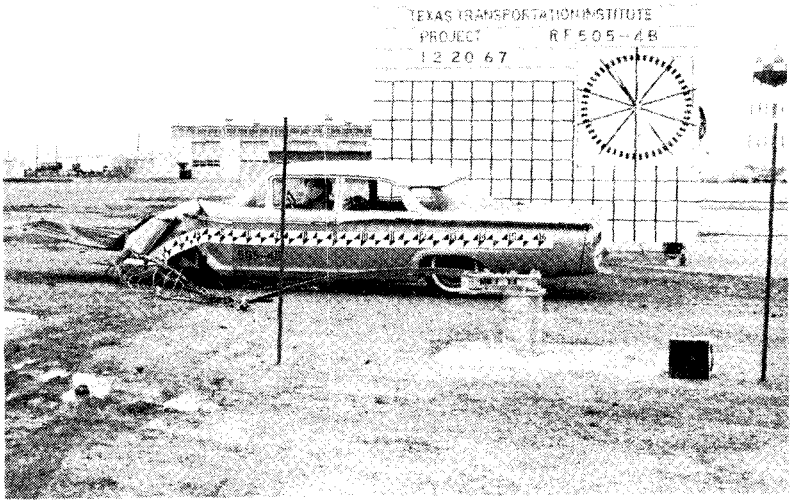

Figure 10, Vehicle and Left Metal Bender After Test 505-4B.

TEST 4C

A 1620 pound Volkswagen traveling at 48 mph entered the arresting system at an angle of 30° with a perpendicular to the net. All subsequent angle tests will be defined on this basis. The vehicle was stopped in 13.8 feet, and pulled a total of 3.4 feet of tape out of the 25,000 pound Metal Benders. This tape pullout consumed 70% of the vehicle's kinetic energy. The estimated energy necessary to impart a horizontal rotation, or spin, to the vehicle and to elevate its center of gravity was about 3 kip-ft. These energy levels are defined at the time during the test when the tapes stop pulling out of the benders. The average deceleration level was 5.5 g's while the maximum deceleration, shown by Figure C5 is about 13 g's. The vehicle damage shown in Figure 12 was moderate.

Figure 11, Vehicle Before Test 505-4C

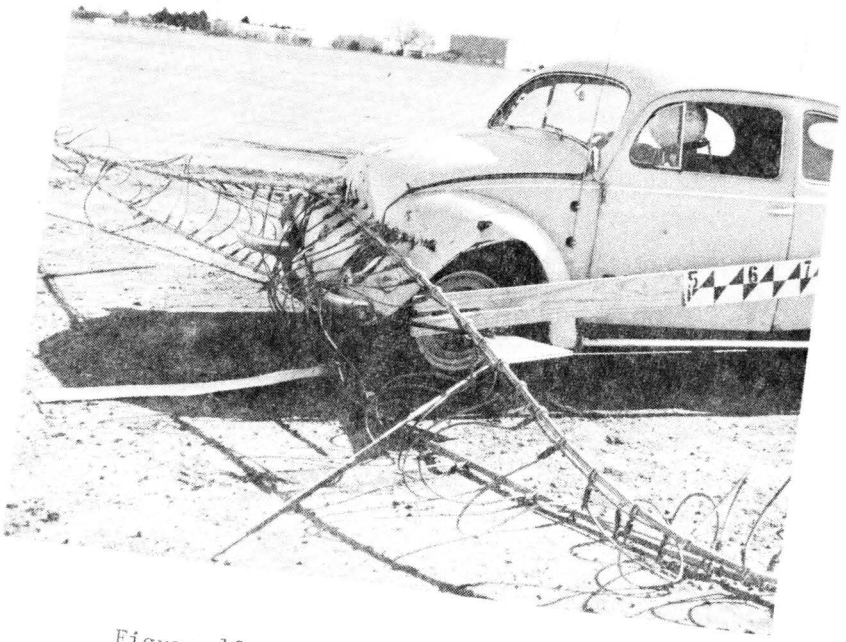

Figure 12, Vehicle After Test 505-4C

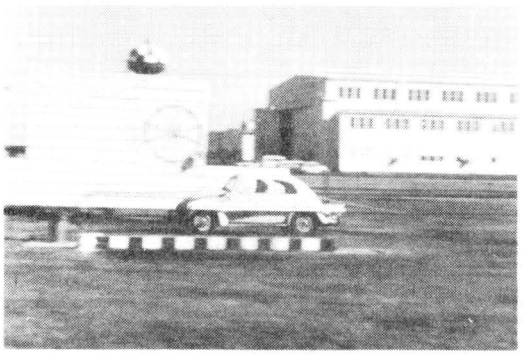

1

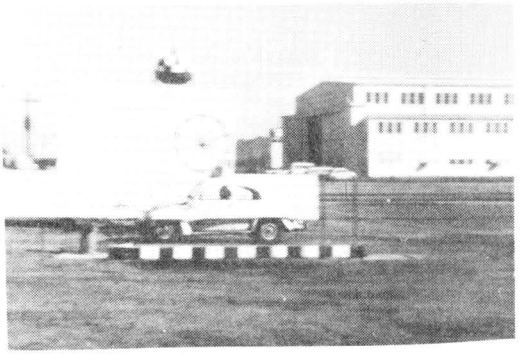

2

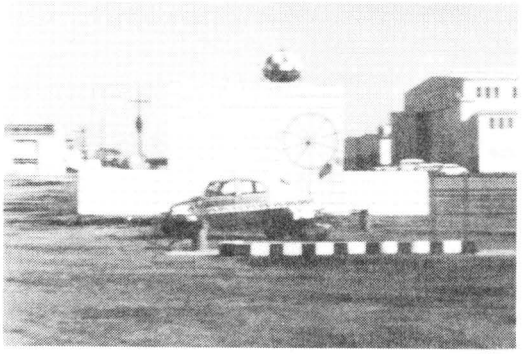

3

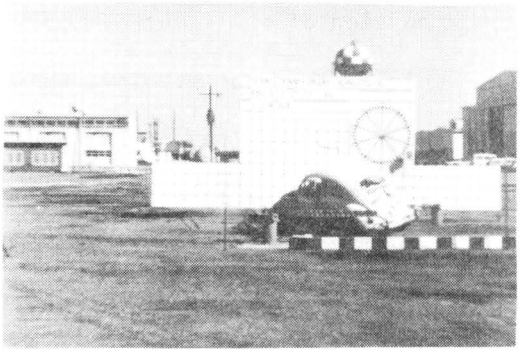

4

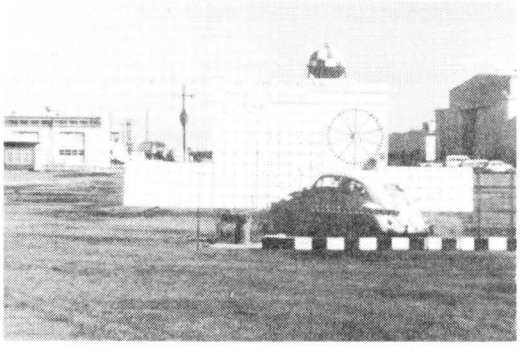

5

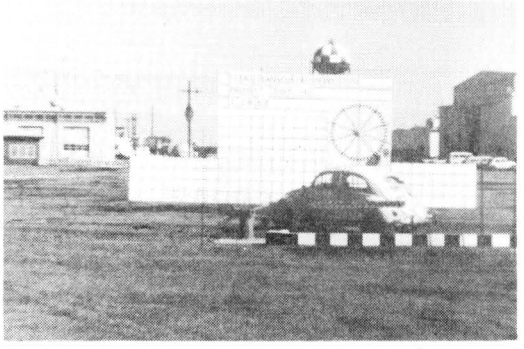

6

Figure 13, Sequential Photographs of Test 505-4C.

TEST 4D

In Test 4D a 4520 pound Oldsmobile sedan, traveling 54 mph, impacted the net on an initial trajectory of 30°. The high-speed films show a maximum travel of 23.5 feet after impact. The 25,000 pound Metal Benders allowed 8.6 feet of metal tape to be pulled through, accounting for 50% of the initial kinetic energy. When the maximum tape pullout had occurred, the vehicle was estimated to have 36 kip-ft of rotational energy and 11 kip-ft of gravitational potential energy. The net entrapped only the lower portion of the front of the vehicle. As the front pulled down below the vehicle center of gravity, the unbalanced inertia force resulted in the vehicle's rotation about the restrained point (see Figure 17). The vehicle was completely off the ground and the rear end went over and outside of the restraining net after the tapes had stopped pulling out. When the vehicle fell back to the ground, it came very close to rolling. The average and maximum significant longitudinal decelerations were 4.1 and 8 g's respectively. Figure C7 shows the accelerometer trace used to determine this maximum deceleration.

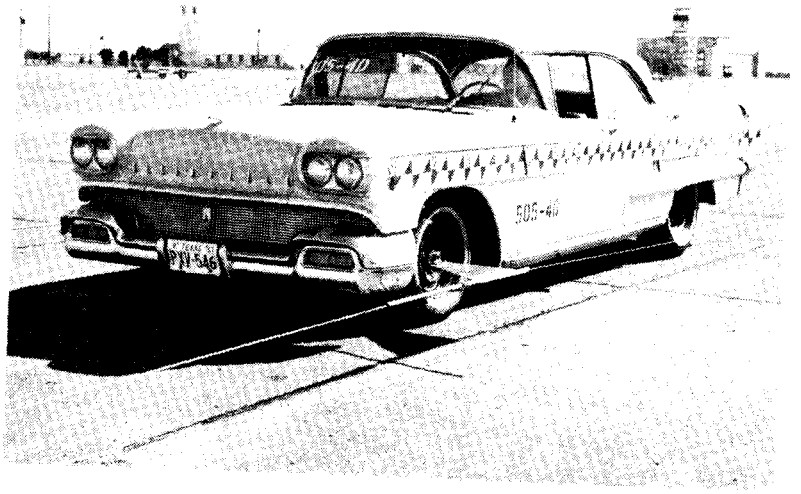

Figure 14, Vehicle Before Test 505-4D.

Figure 15, Vehicle and Right Metal Bender After Test 505-4D.

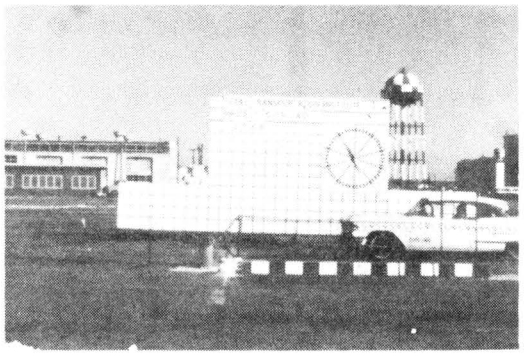

1

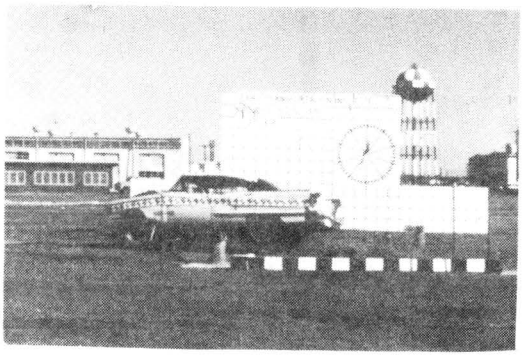

2

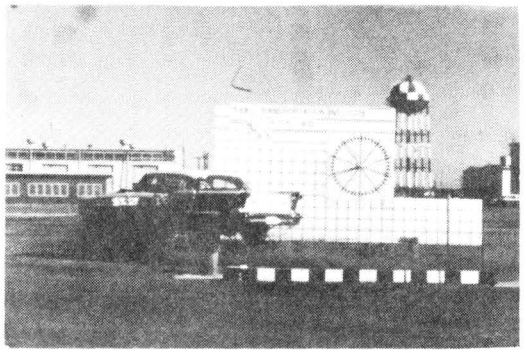

3

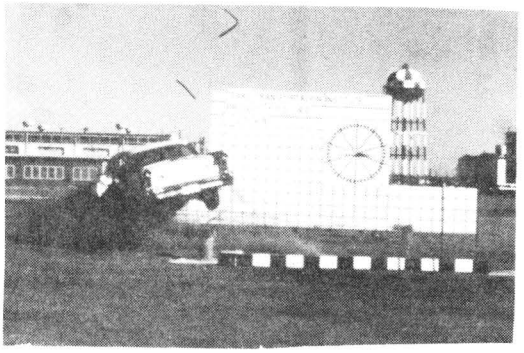

4

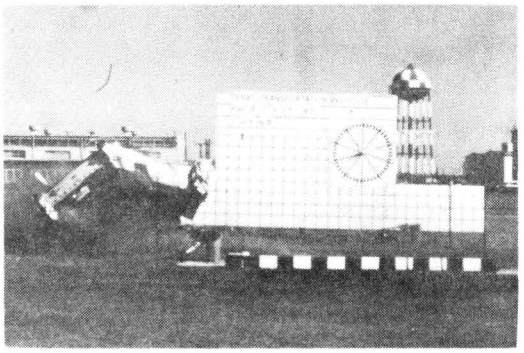

5

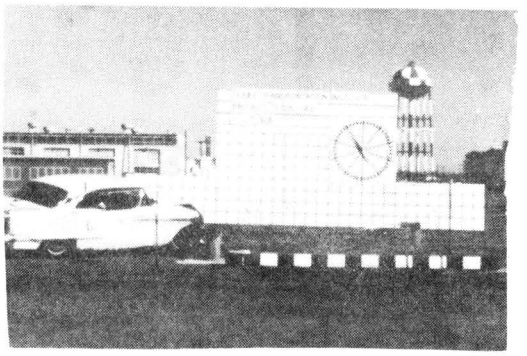

6

Figure 16, Sequential Photographs of Test 505-4D.

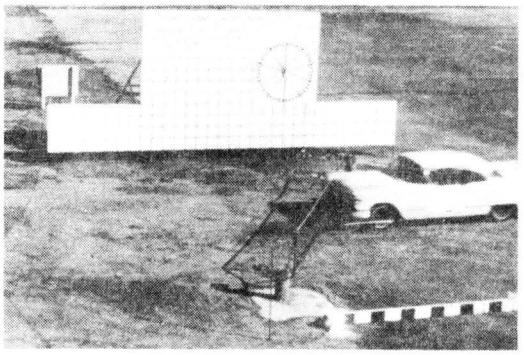

1

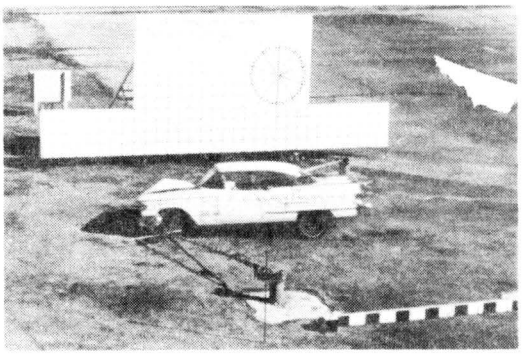

2

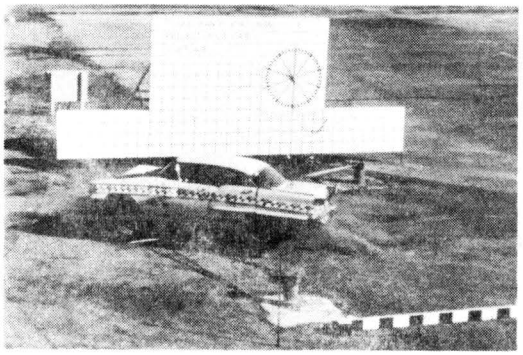

3

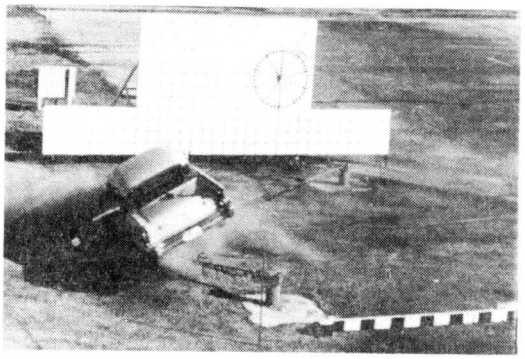

4

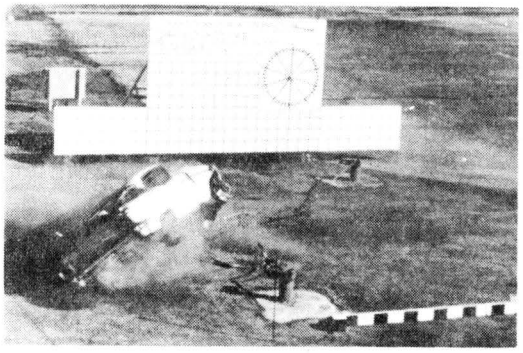

5

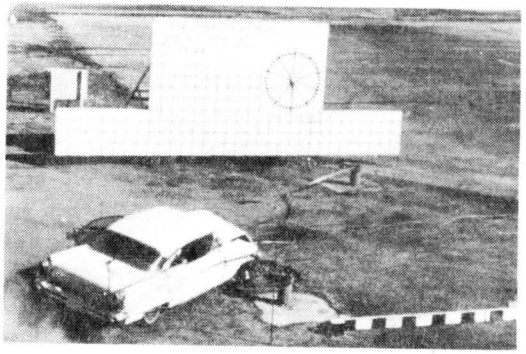

6

Figure 17, Sequential Photographs of Test 505-4D Showing Behavior of Net During Arrestment.

TEST 4E

This test was similar to Test 4B in that a heavy car, a 3760 lb. Dodge sedan, was directed head-on into the dragnet at a velocity of 56 mph. However, in this and the following test the Metal Bender tape load was decreased to 12,500 lbs. and the net was raised about 4 inches off the ground to better entrap the front of the vehicles.

The vehicle was stopped in 26.3 feet and pulled out a total of 30.7 feet of tape, which is equivalent to 384 kip-ft, or 96% of the vehicle's kinetic energy. The vehicle had no significant rotational energy at maximum penetration, but had gained about 7 kip-ft of gravitational potential energy.

The vehicle damage was minor,as would be expected since the maximum deceleration was only 7.0 g's, and the average deceleration was 4.0 g's.

Figure 18, Vehicle Before Test 505-4E.

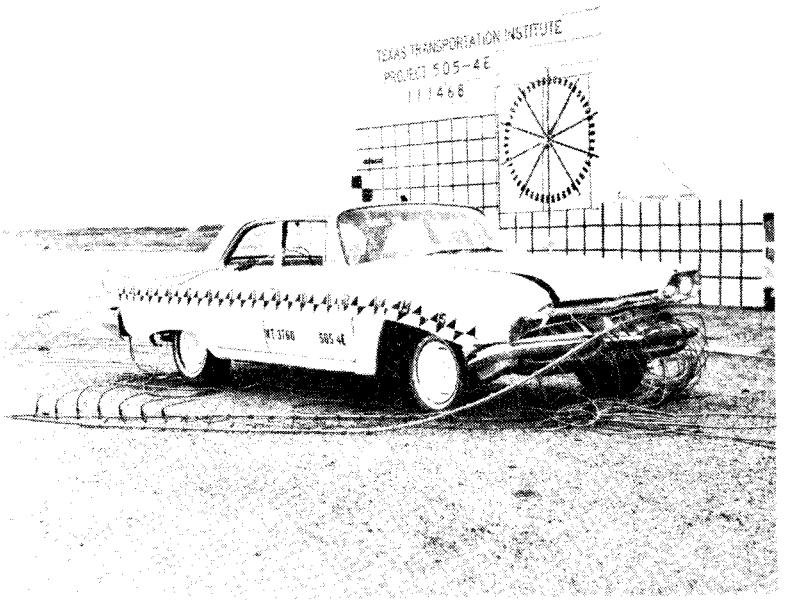

Figure 19, Vehicle After Test 505-4E.

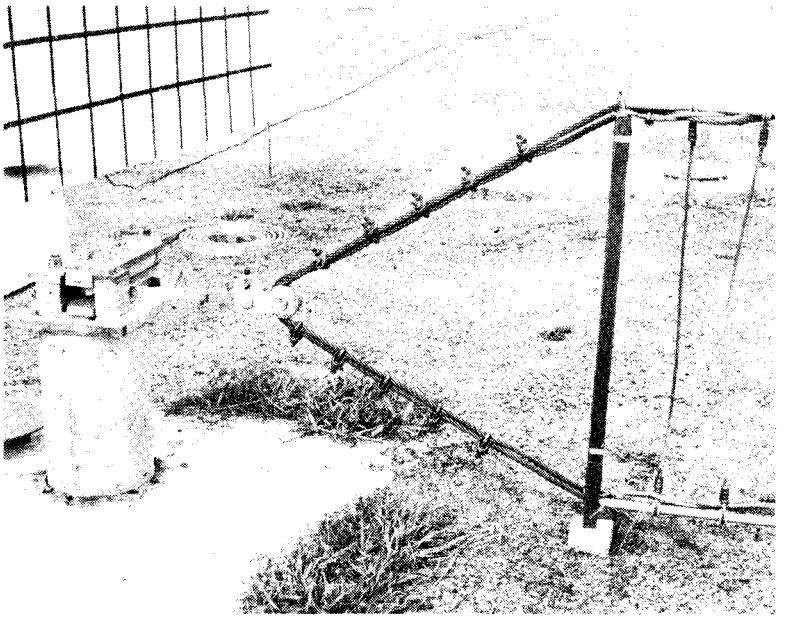

Figure 20, 12,500 Pound Metal Bender Before Test 505-4E.
(Note smaller metal tape)

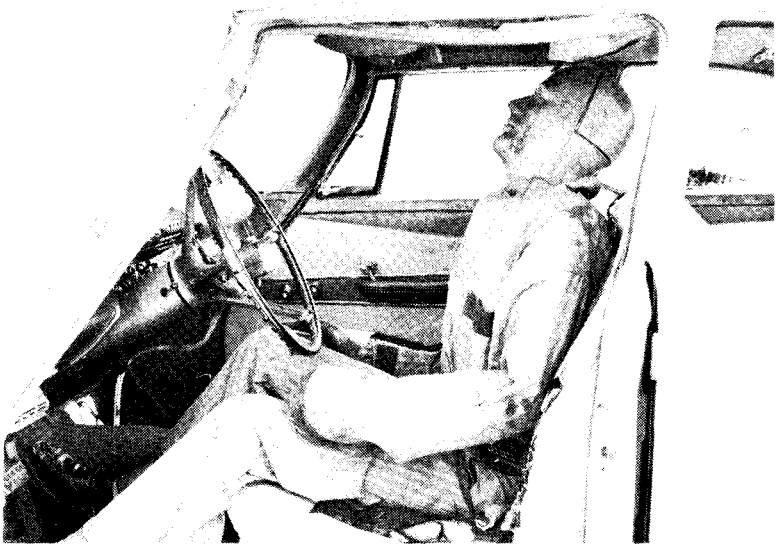

Figure 21, Dummy Used In All Tests
To Simulate Human Driver.

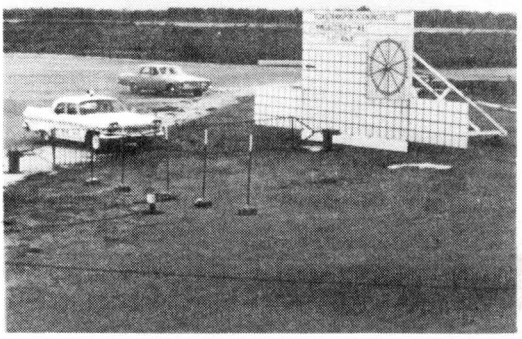

1

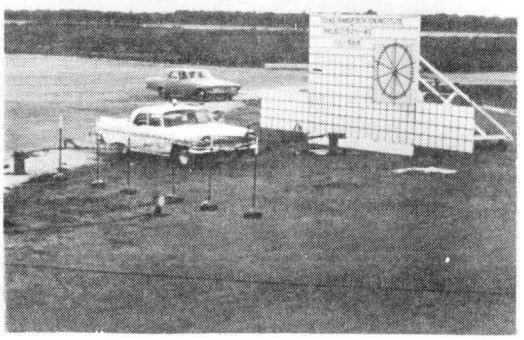

2

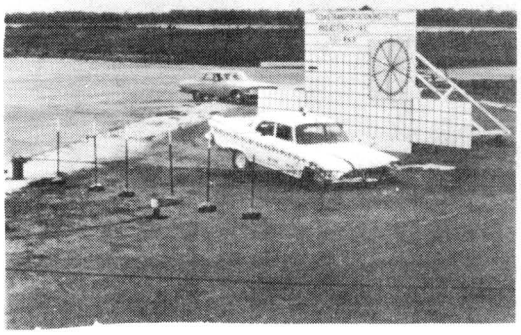

3

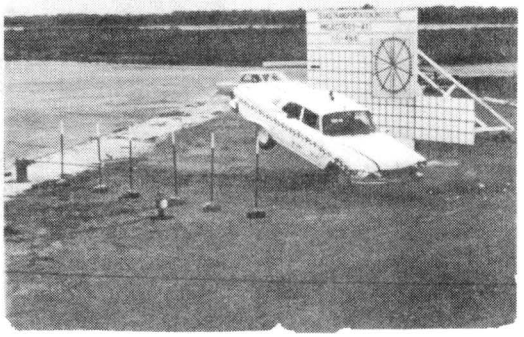

4

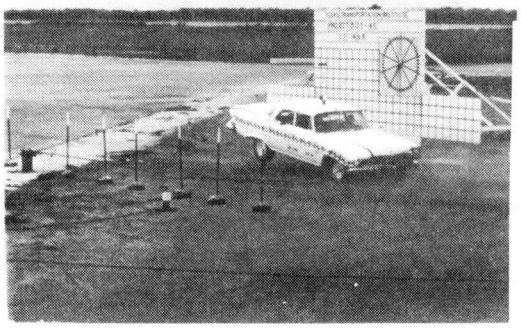

5

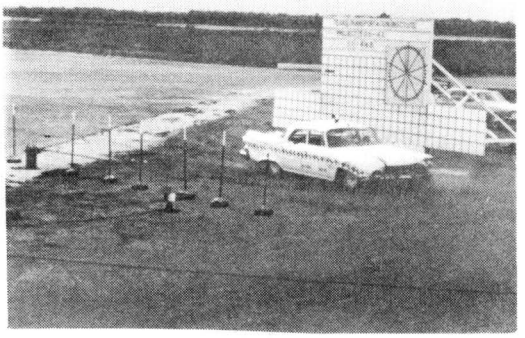

6

Figure 22, Sequential Photographs of Test 505-4E.

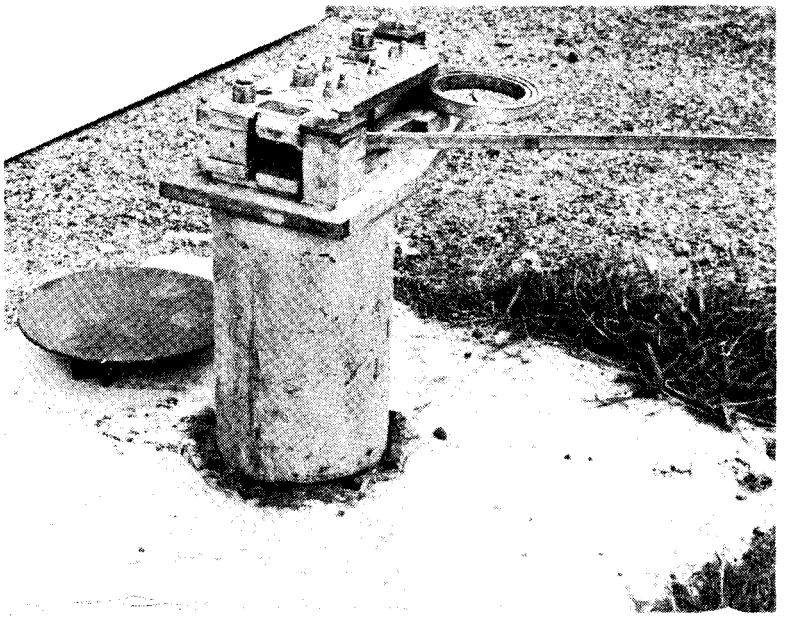

Figure 23, Metal Bender After Test 505-4E.
(Approximately the same amount
of tape remained on each bender)

TEST 4F

As the final test in this series a 3880 pound Ford sedan traveling 62 mph collided with the dragnet at an impact angle of 30°. As in the previous test, 12,500 pound Metal Bender tapes were used.

The tape on the right side was expended and pulled free of the Metal Bender before the vehicle had been brought to a stop. The system performed as designed up to the point of tape pullout. The net, which was still attached to one Metal Bender, caused the car to spin through an angle of about 120 degrees after pulling out the right tape before coming to rest.

The total tape pullout when the right tape pulled free was 32.9 feet, which accounts for 89% of the kinetic energy lost up to that point. The high-speed films indicate that the vehicle had lost about 91% of its initial energy at this point and that the speed was down to about 17 mph.

The total tape pullout of 38.5 feet at full stop accounts for 94% of the vehicle's initial energy. Comparisons of actual and theoretical values are made up to the point of tape expenditure.

The deceleration levels of 5.0 g's (maximum) and 4.1 g's (average) are tolerable to restrained humans.*

---

* Damon, Albert; Stoudt, Howard W.; and McFarland, Ross A., The Human Body in Equipment Design, Harvard University Press, Cambridge, Massachusetts, 1966.

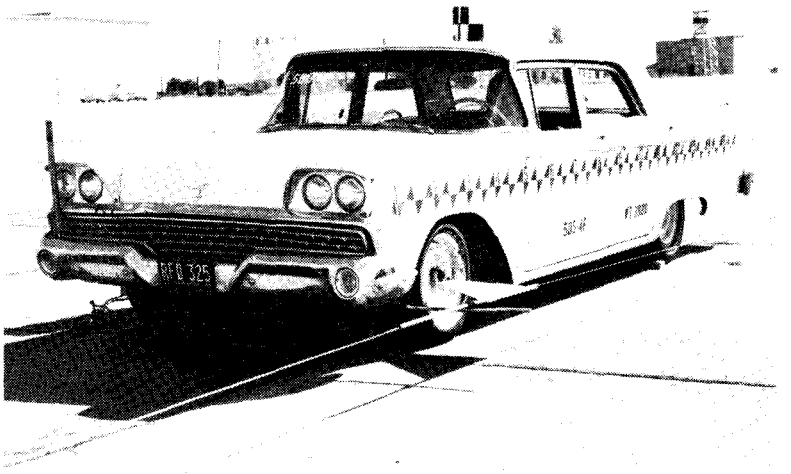

Figure 24, Vehicle Before Test 505-4F.

Figure 25, Vehicle After Test 505-4F.

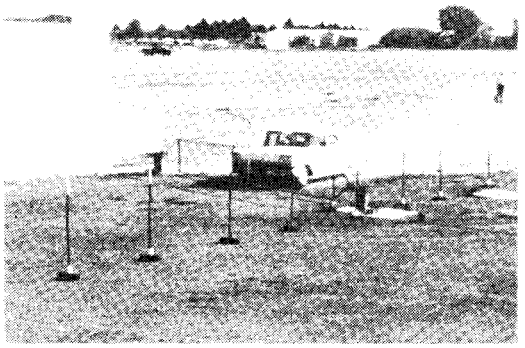

1

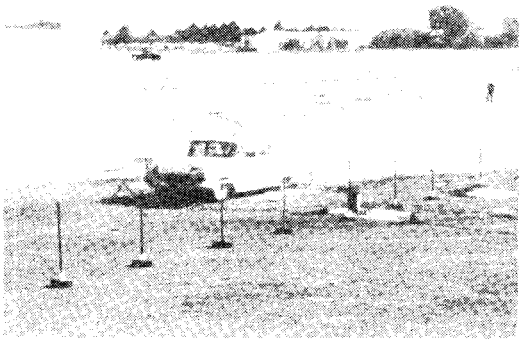

2

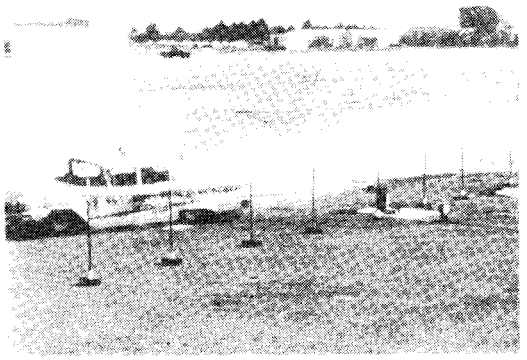

3

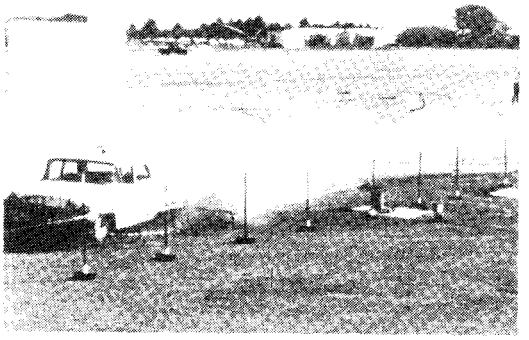

4

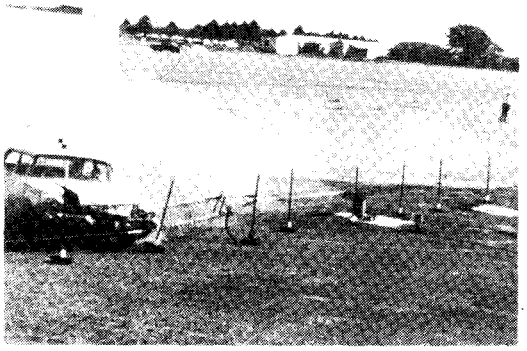

5

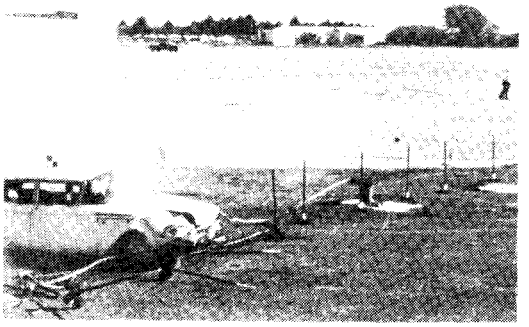

6

Figure 26, Sequential Photographs of Test 505-4F.

DISCUSSION

The complete test series which was conducted on the Van Zelm dragnet is summarized by Table 2. The vehicles used ranged in weight from 1460 lbs to 4520 lbs. All test vehicles impacted the dragnet at its center. Tests 4A, 4B, and 4E were head-on tests, while Tests 4C, 4D, and 4F were 30° angle tests. This means that the initial trajectory of the vehicle made an angle of 30° with a perpendicular to the original position of the dragnet. Tapes producing a 25 kip pull were used in Tests 4A through 4D, while in Tests 4E and 4F this tape force was reduced to 12.5 kips.

The energy absorbed by the Metal Benders ranged from 50% to 70% of the vehicle's initial kinetic energy for the first four tests which used the 25 kip tape loads. In Tests 4E and 4F the percent of energy absorbed by the Metal Benders ranged from 89% to 96%. Inspection of Table 3 will show several reasons for this difference. At the end of Metal Bender tape pullout, which corresponds approximately to zero longitudinal velocity, significant amounts of energy may remain in the form of gravitational potential energy and rotational kinetic energy. In most impacts there is some gravitational potential energy gain due to the tendency of the net to pull the vehicle down in front and for the rear end to rise. This results in an increase in the elevation of the vehicle's center of gravity. The total vehicle weight times this increase in elevation, E_p, is designated the gravitational potential energy at the end of tape travel. In the case of angle tests, there may be present a significant amount of horizontal rotational energy, E_{RV}, which is equal to one-half the product of the vehicle mass moment of inertia (about the vertical axis through the vehicle's center of gravity) times the square of the vehicle's angular

TEST NO.	4A	4B	4C	4D	4E	4F
Angle of Impact	Head-On	Head-On	30°	30°	Head-On	30°
Vehicle Weight (lbs)	1460	4300	1620	4520	3760	3880
Vehicle Velocity (mph)	42	60	48	54	56	62
Metal Bender Tape Load (kip)	25.0	25.0	25.0	25.0	12.5	12.5
Vehicle Deformation (ft)	1.8	1.0	0.9	1.5	0.3	0.5
Vehicle Stopping Distance (ft)	10.2	19.4	13.8	23.5	26.3	29.5*
Total Metal Bender Tape Pullout (ft)	2.2	11.8	3.4	8.6	30.7	32.9*
Energy Absorbed by Metal Bender (kip-ft)	54.8 (63%)	296 (58%)	86 (70%)	214 (50%)	384 (96%)	411 * (89%)
Max. Significant Deceleration (g's) (Electromechanical curves)	16	16	13	8	7.0	5.0
Avg. Deceleration (g's) (Film - $V^2/2gX_{max}$)	5.8	6.1	5.5	4.1	4.0	4.1*

* Up to point tape expended.

TABLE 2. SUMMARY OF TEST RESULTS

TABLE 3

TEST NO.	4A	4B	4C	4D	4E	4F*
E_{KI}	87	513	123	437	401	512
E_{MB}	55	296	86	214	384	481
E_P	1	17	2	11	7	0
E_{RV}	0	0	1	34	0	0
E_{RL}	0	0	0	2	0	0
E_M	31	200	34	176	10	31

E_{KI} = Initial vehicle kinetic energy

E_{MB} = Energy expended in Metal Bender tape pullout

E_P = Gravitational potential energy at end of tape travel

E_{RV} = Horizontal rotational energy (around vertical axis) at end of tape travel

E_{RL} = Transverse rotational energy (around longitudinal axis) at end of tape travel

E_M = Miscellaneous energy expenditure (cable stretch, vehicle deformation, contact with ground, etc.)

$$E_M = E_{KI} - (E_{MB} + E_P + E_{RV} + E_{RL})$$

* Note the fact that these energy levels are up to the point of tape pullout only.

velocity about this axis. Also present may be transverse rotational energy, E_{RL}, which is defined in the same way as the horizontal rotational energy except that the mass moment of inertia and angular velocity is about the longitudinal vehicle axis. Other energy expenditures, E_M, may be accounted for by the axial strain energy which goes into the cable and tapes, the vehicle deformation, and frictional losses such as contact of rigid portions of the vehicle with the ground. This last energy expenditure was prevalent in Test 4B. It can be concluded, at least within the range of tape forces tested, that the lower the tape force the greater the percentage of energy dissipated in the Metal Benders. If the extreme example of a tape with infinite load capacity is considered, almost all of the kinetic energy of the vehicle would be expended in vehicle deformation, rolling, etc.

A convenient way of indicating the relative desirability of dragnet arrestments is to compare the deceleration levels determined by these tests with the decelerations that would be encountered during a collision with a rigid barrier. The Attenuation Index is defined as the ratio of decelerations during an attenuated arrestment (for example by dragnet) with those estimated decelerations during a rigid barrier impact.* Both maximum and average Attenuation Indices (AI_{max} and AI_{avg}), which compare maximum and average deceleration levels, are presented in Table 4.

Tests 4E and 4F, using 12,500 pound Metal Benders, have smaller Attenuation Indices than the first four tests. This is the obvious result of cutting the stopping force in half. This reduction in stopping force significantly reduces the vehicle damage. The relatively large

---

* Emori, Richard I., "Analytical Approach to Automobile Collisions," SAE Paper 680016, Engineering Congress, Detroit, January 8, 1968.

TABLE 4 . COMPARISON OF VAN ZELM "DRAGNET" PERFORMANCE WITH RIGID BARRIER IMPACT

Test No.	A	B	C	D	E	F
Metal Bender Tape Load (Kip)	25.0	25.0	25.0	25.0	12.5	12.5
Vehicle Weight (lb.)	1460	4300	1620	4520	3760	3880
Vehicle Velocity (mph)	42	60	48	54	56	62
*Maximum Deceleration (G_{max})						
Dragnet	16	16	13	8	7.0	5.0
Rigid Barrier	37.8	54.0	43.2	48.6	50.4	55.8
**Average Deceleration (G_{avg})						
Dragnet	5.8	6.1	5.5	4.1	4.0	4.1
Rigid Barrier	24.1	34.4	27.6	31.0	32.1	35.6
Attenuation Index						
$AI_{max} = \frac{G_{max}\ Dragnet}{G_{max}\ Rigid}$	0.42	0.30	0.30	0.17	0.14	0.09
$AI_{avg} = \frac{G_{avg}\ Dragnet}{G_{avg}\ Rigid}$	0.24	0.18	0.20	0.13	0.12	0.12

*G_{max} Dragnet is from frame accelerometer data.

G_{max} Rigid = 0.9 (vehicle velocity in mph)***

**G_{avg} Dragnet = $\frac{V^2}{2gX_{max}}$ from film data.

G_{avg} Rigid = 0.574 (Vehicle velocity in mph)***

***Emori, Richard I., "Analytical Approach to Automobile Collisions," SAE Paper 680016, Engineering Congress, Detroit, January 8, 1968.

energy differences between tape energy and initial kinetic energy in Tests 4A through 4D are the result of large energy expenditures on vehicle deformation.

In Appendix B is a theoretical treatment which algebraically relates vehicle weight, velocity, tape force and stopping distance. The error induced by considering the vehicle to have no finite width is approximately compensated for by the fact that after impact the "spreaders" at the ends of the net buckle, increasing the effective length of the net. Due to the fact that the main net cables loop over and under the front of the vehicles, and that the vehicles are deformed differently, some inaccuracy is expected, especially in arrestments with short stopping distances. It is also assumed in the calculations that the vehicle continues along its original path during arrestment, which is only a rough approximation in angled or non-centric hits.

Figure 27 is a plot of dragnet force on the vehicles against distance traveled after contact. The data used for this plot is taken from the theoretical calculations in Appendix B. A comparison of the calculated energy expenditures is shown in Table 5. The theoretical Metal Bender energy expenditures are obtained using the equations presented in Appendix B. As expected, the theory shows the greatest percent error for Test 4A, which had the shortest stopping distance and greatest relative deformation.

From the theoretical treatment a plot of total Metal Bender tape pullout against X_{max}, the theoretical stopping distance, was made for head-on 30° angled impacts. Neglecting other energy dissipation modes, the initial vehicle kinetic energy divided by the Metal Bender tape

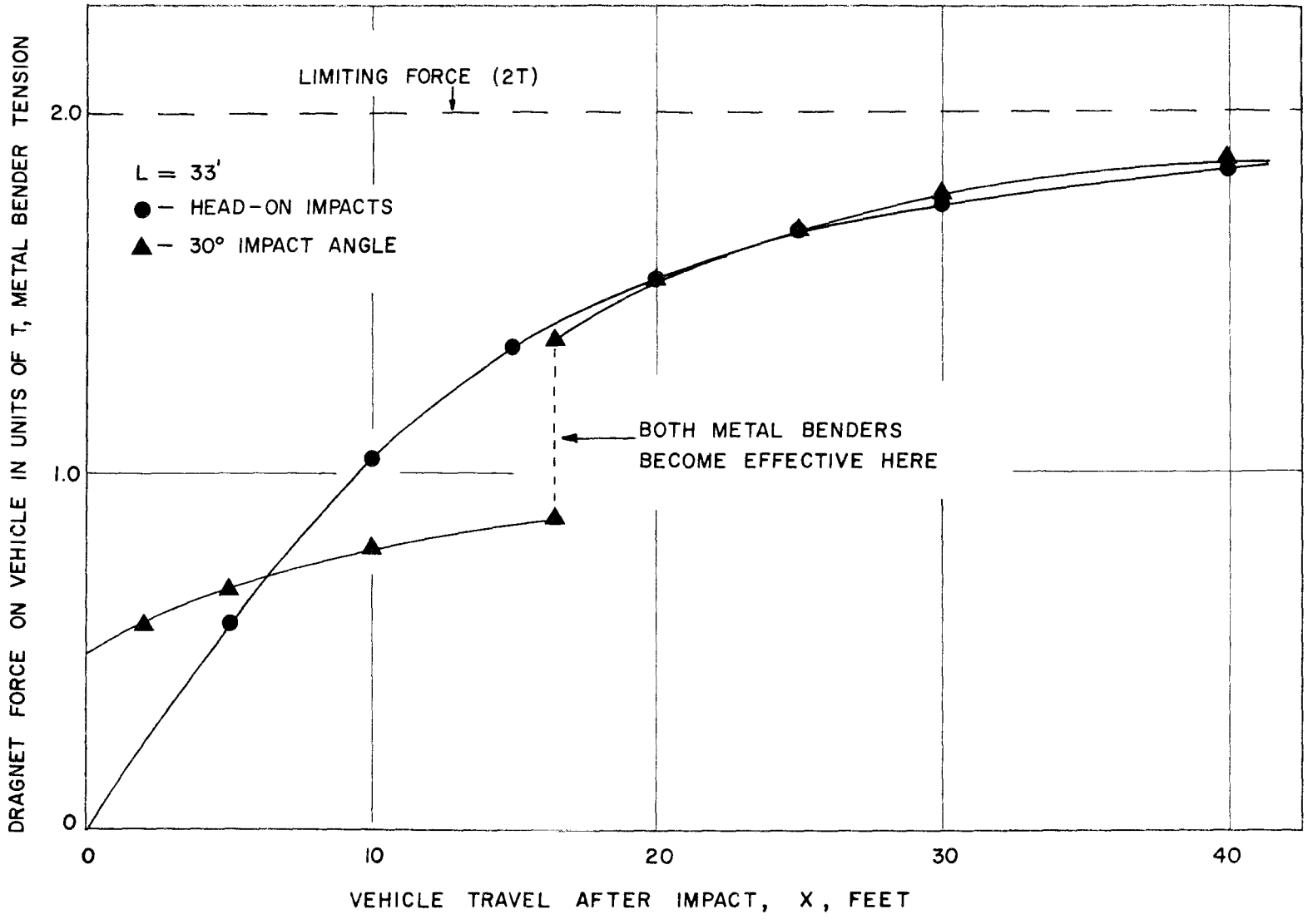

FIGURE 27, THEORETICAL STOPPING FORCE — DISPLACEMENT CURVES FOR CENTRIC IMPACTS

TABLE 5

Comparison of Vehicle Kinetic Energies
with Calculated Energy Expenditures
(in Kip-ft)

Test No.	4A	4B	4C	4D	4E	4F
Initial Kinetic Energy of Vehicle	87.1	513	123	437	401	464*
Energy Expended by Metal Benders (from measured tape pullout)	54.8	296	85.5	214	384	411*
Energy from area under Force-Displacement curve in Figure 27. (Stopping distance from high speed films)	140	450	105	440	365	330*

* To expenditure of tape in right hand Metal Bender.

tension should equal the total tape pullout. By taking the initial velocity, determined from the high-speed films, and calculating initial kinetic energy, and by knowing the Metal Bender tape tensions, we can calculate the theoretical total tape pullout. Using this value and Figure 28, we can determine theoretical stopping distance. The theoretical stopping distances so determined are compared with actual stopping distances from the high-speed film data in Table 6. In this comparison, the measured stopping distance is the measured stopping distance of the vehicle's center of gravity minus the vehicle's deformation. (This is the distance traveled by the vehicle's front end after contacting the net.)

Again the percentage difference between actual and theoretical values is greater for short stopping distances (high Metal Bender tensions). An examination of the high-speed films indicates that in Test 4C the combination of the low, narrow front end of the vehicle and the collapse of the end net spreaders, which occurred in every test, delays application of the main stopping force until the vehicle has traveled about four feet beyond initial contact. This is a considerable portion of the total stopping distance, and explains the large difference between measured and calculated stopping distance. For this vehicle's initial energy, the calculated total tape pullout is 4.9 feet. This compares favorably with the actual measured tape pullout of 3.4 feet. The theoretical calculations are applied to an example design problem in Appendix B.

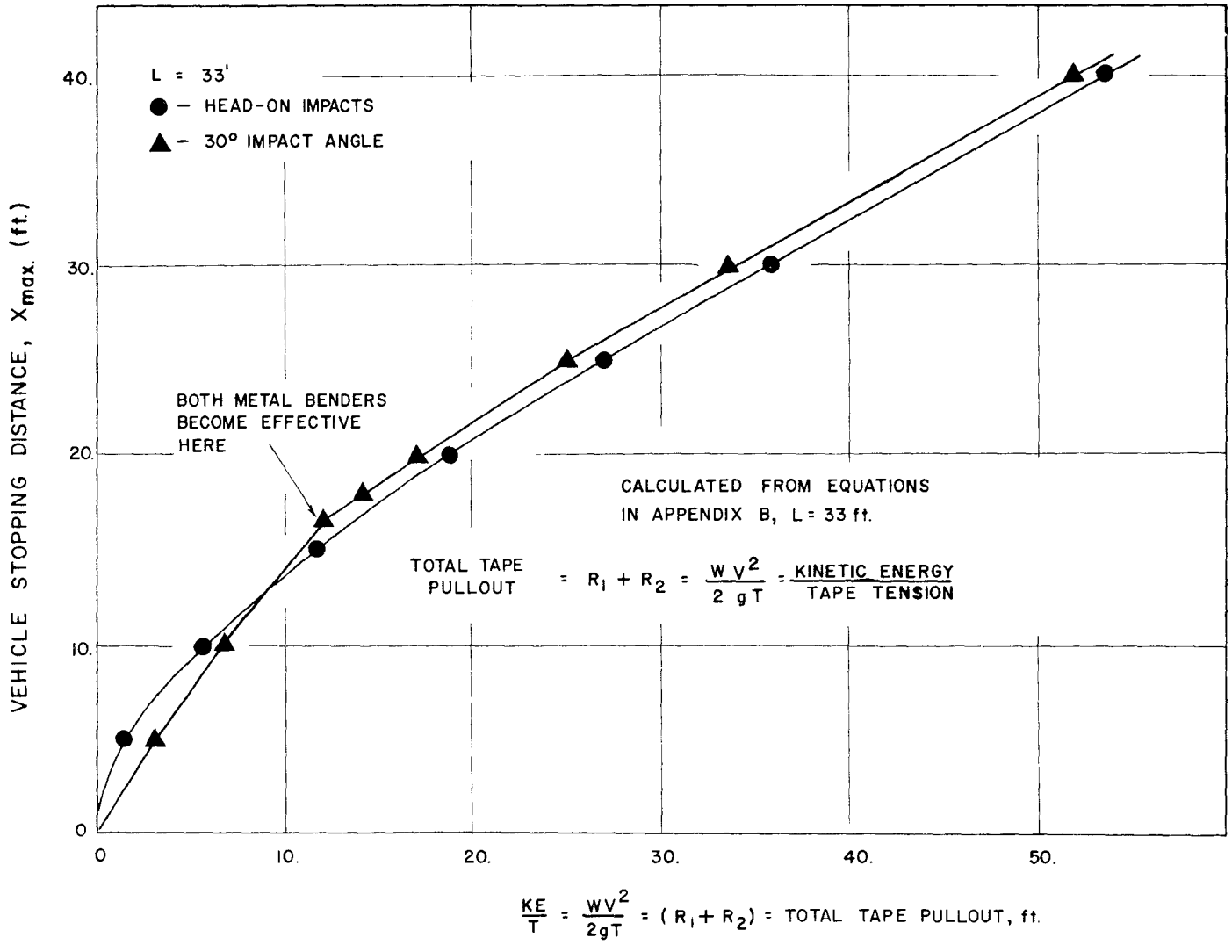

FIGURE 28, STOPPING DISTANCE VS. TOTAL TAPE PULLOUT

TABLE 6

Comparison of Computed Stopping Distances
with Measured Stopping Distances

Test No.	4A	4B	4C	4D	4E	4F
$(X_{max})_M$ (ft) **	8.4	18.4	12.9	22.0	26.0	29.0*
$(X_{max})_C$ (ft) ***	7.8	21.0	7.6	20.2	27.7	29.5*
$\{ (X_{max})_C - (X_{max})_M \}$ (ft)	-0.6	+2.6	-5.3	-1.8	+1.7	+0.5*

* Calculated up to point metal tape was expended.

** Measured stopping distance from film minus vehicle deformation.

*** Calculated stopping distance from initial vehicle velocity and theoretical treatment in appendix.

A P P E N D I X A

Design and Installation

Data

VAN ZELM Associates INC.
DEVELOPMENT ENGINEERS

1475 ELMWOOD AVENUE
PROVIDENCE, RHODE ISLAND 02907
TEL. (401) 781-3500

May 13, 1968
Serial Number S-305

Mr. T. J. Hirsch
Head, Structural Research Department
Texas A&M University
College of Engineering
College Station, Texas 77843

Dear Mr. Hirsch:

This letter supplements the previous information transmitted to you by our letter of April 29, 1968 and answers your telephone request of May 1.

Van Zelm has several Metal Bender Units which have been developed and tested and are adaptable for highway use. These units, with their pertinent physical and operational characteristics are presented below.

Torture Chamber Mod. No.	Tape Size	Tape Load	Tape Nominal Runout	Max. Runout Possible
Std. Dragnet-MBP-1	1-1/4X.050	2500#	200 Ft.	500 Ft.
" " -MBP-2	2" X .050	2000# or 4000#	400 Ft.	1000 Ft.
Texas A&M Config.	2" X 3/8	25,000#	12.3 Ft.	18.7 Ft.
" " "	1-1/2"X3/8	18,500#	18.7 Ft.	18.7 Ft.
" " "	1 X 3/8	12,500#	18.7 Ft.	18.7 Ft.*

Units may be combined to produce a desired tape load which falls between the loads produced by the basic units. For example two 4000 lb. units may be combined to produce an 8000 lb. load or a 4000 lb. unit and a 2500 lb. unit a 6500 lb. load.

Also attached is one copy of Van Zelm drawing 1E-2909 detailing the dragnet test installation at T.T.I.

Very truly yours,

L. Montanaro

LM:lt

* The tapes used in Tests 4E and 4F were 25 feet in length.

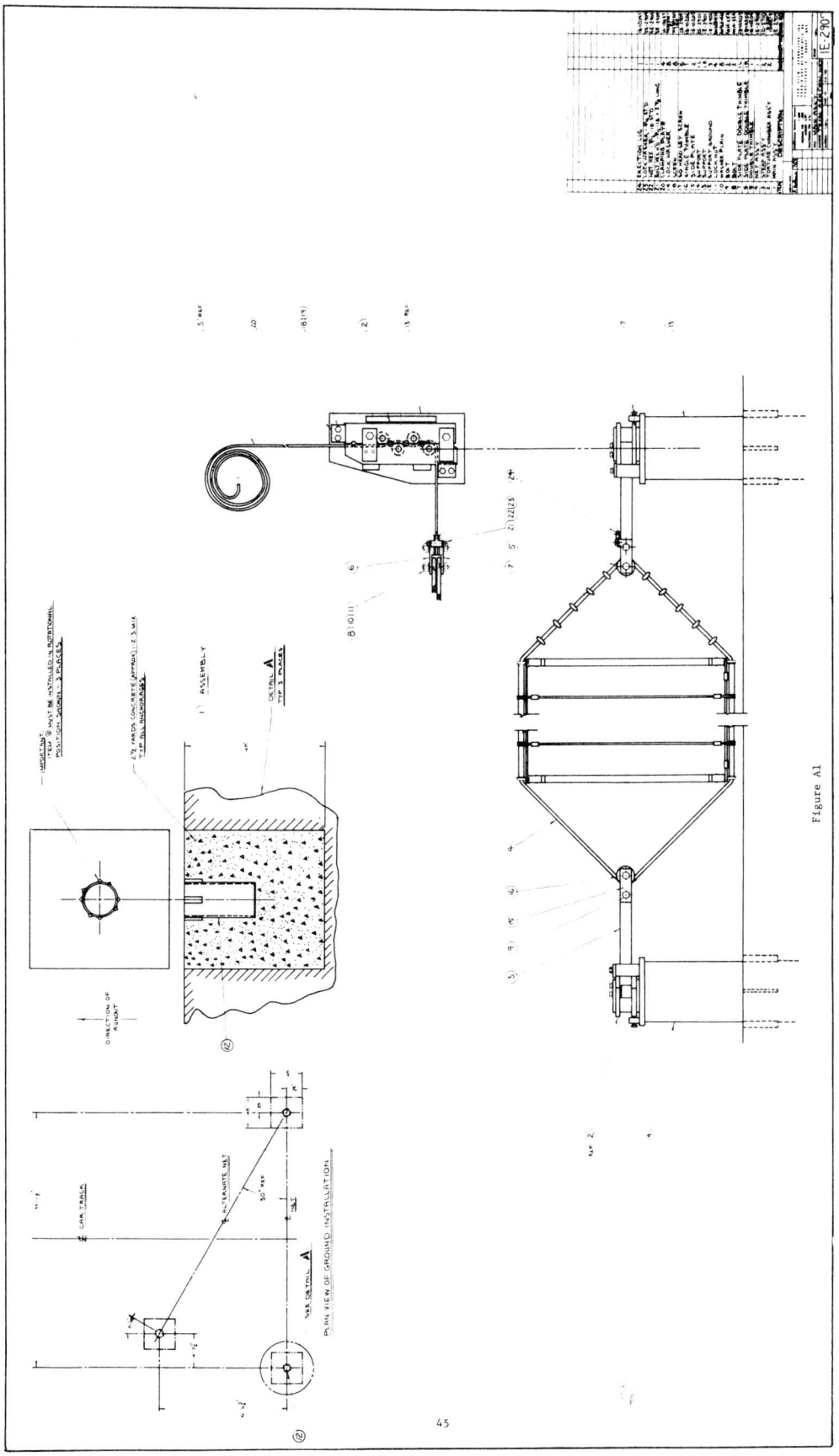

Figure A1

A P P E N D I X B

Theory and Design

Example

EQUATIONS FOR ANALYSIS OF VAN ZELM METAL BENDER DRAGNET SYSTEM

HEAD-ON CENTRIC VEHICLE COLLISION

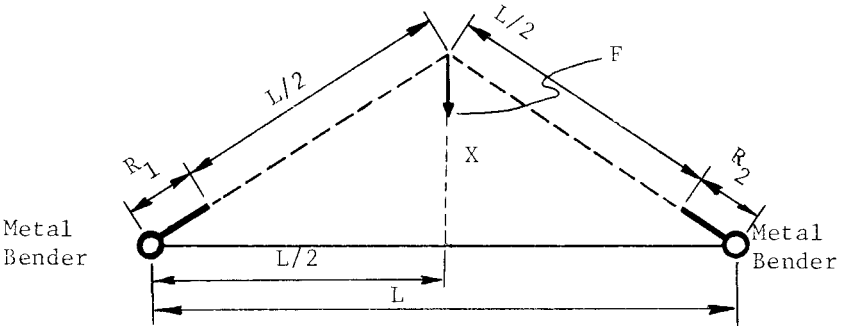

Figure B1

L = length of net, ft.

T = metal bender tape tension force, lb.

R = R_1 = R_2 = run out of metal bender tape (assuming all energy is absorbed by tape), ft.

X = travel distance of vehicle after engaging net, ft.

X_{max} = stopping distance, ft.

F = stopping force component on vehicle, lb.

W = weight of vehicle, lb.

V = initial velocity of vehicle, ft/sec.

g = acceleration due to gravity, 32.2 ft/sec^2.

Relatively simple equations will now be developed which will aid in selecting a desirable metal bending tape tension force (T) and length (R_{max}) in order to stop a given vehicle of weight (W) and speed (V).

Van Zelm now has available metal tapes and metal benders (sometimes called "torture chambers") which provide tape tension forces (T) of 2,500 lb., 4,000 lb., 12,500 lb., 18,750 lb., and 25,000 lb. Two of the 4,000 lb. metal benders can be stacked on top of each other to provide a tape tension force of 8,000 lb.

For these tape tension forces, we can compute the minimum required length of tape (R), the stopping distance required (X_{max}), the maximum and average g forces on the vehicle as follows:

$$\text{Kinetic Energy of Vehicle} = \frac{WV^2}{2g}$$

Assuming all energy is absorbed by metal tape will yield the energy absorbed by metal bender tape = 2TR

Because of symmetry $R = R_1 = R_2$

$$\text{so} \quad 2TR_{max} = \frac{WV^2}{2g}$$

The maximum tape run out is then

(1) $$R_{max} = \frac{WV^2}{4Tg} \quad \text{and} \quad R_{max} = R_{1max} = R_{2max}$$

since system is symmetrical in this case.

From Figure B1,

(2) $$X = \sqrt{\left(R + \frac{L}{2}\right)^2 - \left(\frac{L}{2}\right)^2}$$

(2b) $$X_{max} = \sqrt{R_{max}^2 + R_{max} L}$$ Where X_{max} is the stopping distance required for head-on collision.

The stopping force component on the vehicle is,

(3) $$F = 2T \left(\frac{X}{R + \frac{L}{2}} \right)$$

(3b) $$F_{max} = 2T \left(\frac{X_{max}}{R_{max} + \frac{L}{2}} \right)$$ Maximum vehicle stopping force for head-on collision.

The maximum G force on the vehicle is,

(4) $$G_{max} = \frac{F_{max}}{W}$$

The average G force on the vehicle would be,

(5) $$G_{avg} = \frac{V^2}{2gX_{max}}$$

A graph of F vs. X would be as shown below

$$F = 2T \left(\frac{X}{R + \frac{L}{2}} \right)$$

From Equation 2,

$$R = \frac{1}{2} \sqrt{L^2 + 4X^2} - \frac{L}{2}$$

so

(6) $$F = 2T \left(\frac{1}{\sqrt{\left(\frac{L}{2X}\right)^2 + 1}} \right)$$

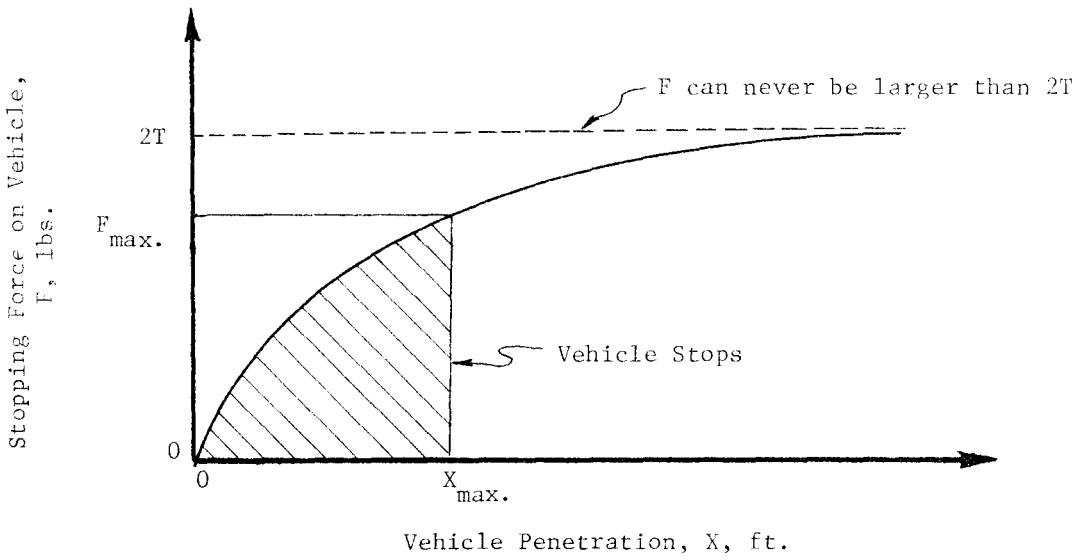

Figure B2, Idealized Vehicle Stopping Force vs. Stopping Distance

The preceding analysis applied to the special case of the "Dragnet" system being struck by a vehicle head-on and in the center. When the vehicle strikes the "Dragnet" at an angle, the mathematics becomes a little more complicated. An analysis of this problem will now be presented.

Idealized analysis of Van Zelm Metal Bender Dragnet Arresting System for centric vehicle collisions at any angle θ.

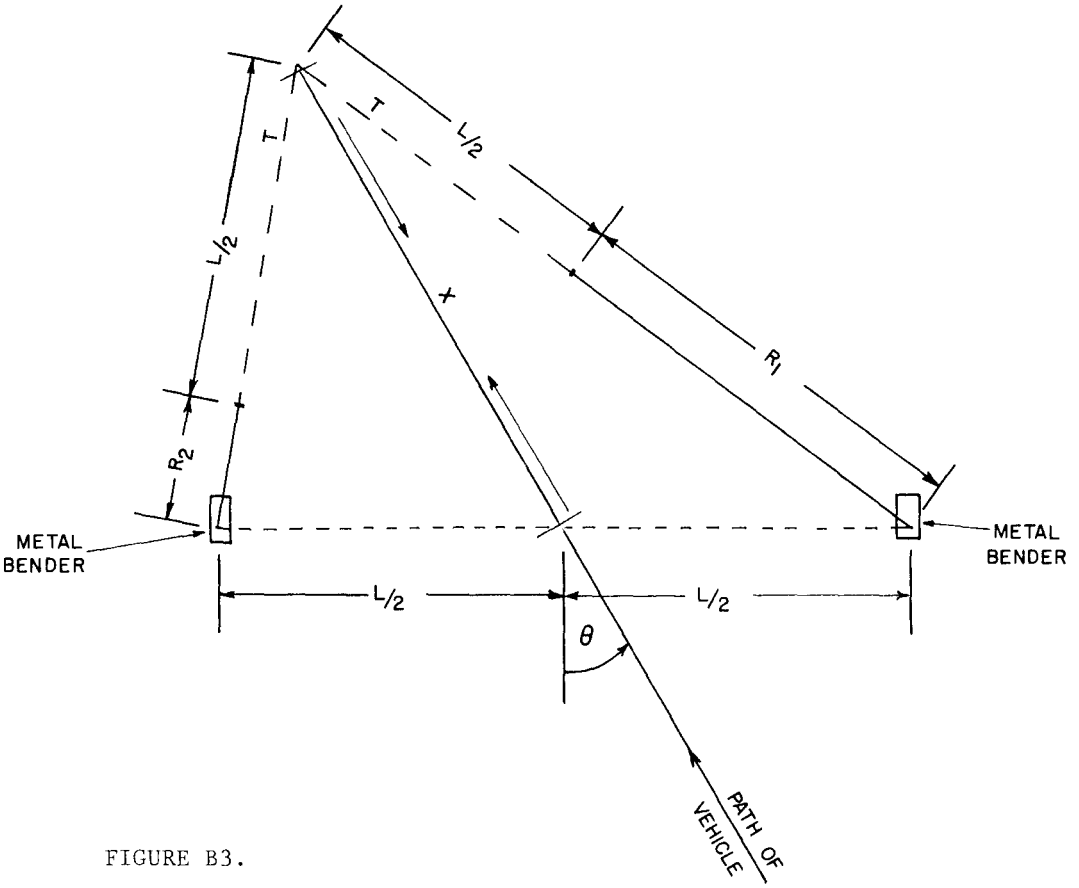

FIGURE B3.

L = Initial length of net and tape between Metal Benders, ft.

T = Metal Bender tape tension, Kip.

R_1 and R_2 = Metal Bender tape runouts, ft.

X = Travel of vehicle along original path after contacting the net, ft.

Xmax = Stopping distance after contacting net, ft.

F_x = Stopping force componet along X, Kip.

W = Weight of vehicle, Kip.

V = Speed of vehicle at impact, ft/sec.

g = Acceleration due to gravity, 32.2 ft/sec^2.

θ = Impact angle, degrees.

Note: It is assumed that $R_2 = 0$ for $X \leq L \sin \theta$. (Derived from Law of Sines.)

Referring to Figure B3, the Pythagorean Theorem gives:

$$\left(R_1 + \frac{L}{2}\right)^2 = \left(\frac{L}{2} + X\sin\theta\right)^2 + \left(X\cos\theta\right)^2$$

This reduces to:

$$(7) \qquad R_1 = \left(\frac{L^2}{4} + X^2 + L\,X\sin\theta\right)^{1/2} - \frac{L}{2}$$

Similarly,

$$(8) \qquad R_2 = \left(\frac{L^2}{4} + X^2 - L\,X\sin\theta\right)^{1/2} - \frac{L}{2} \qquad (\text{for } X > L\sin\theta)$$

$$R_2 = 0 \qquad (\text{for } X \leq L\sin\theta)$$

Equations 7 and 8 can be solved for X in terms of R_1 or R_2:

$$(9) \qquad X = \left(\frac{L^2}{4}\sin^2\theta + R_1^{\,2} + L\,R_1\right)^{1/2} - \frac{L}{2}\sin\theta$$

or $$X = \left(\frac{L^2}{4}\sin^2\theta + R_2^{\,2} + L\,R_2\right)^{1/2} + \frac{L}{2}\sin\theta \qquad (\text{for } X > L\sin\theta)$$

The vehicle kinetic energy is related to the theoretical total strap pullout by:

$$(10) \qquad KE = \frac{WV^2}{2g} = T\,(R_{1_{max}} + R_{2_{max}}) \qquad (\text{when } \theta \text{ not equal to zero})$$

or $$KE = \frac{WV^2}{2g} = 2TR_{max} \qquad (\text{for } \theta = 0°)$$

since $R_{1_{max}} = R_{2_{max}} = R_{max}$ because of symmetry of the system when $\theta = 0°$

The component of Metal Bender stopping force along X due to R_1 is:

$$(11) \qquad F_{R_1} = T\left(\frac{X + \frac{L}{2}\sin\theta}{R_1 + \frac{L}{2}}\right) = T\left(\frac{X + \frac{L}{2}\sin\theta}{\sqrt{\frac{L^2}{4} + X^2 + LX\sin\theta}}\right)$$

Similarly,

$$(12) \qquad F_{R_2} = T\left(\frac{X - \frac{L}{2}\sin\theta}{R_2 + \frac{L}{2}}\right) = T\left(\frac{X - \frac{L}{2}\sin\theta}{\sqrt{\frac{L^2}{4} + X^2 - LX\sin\theta}}\right)$$

The total stopping force along X is: (for $X > L\sin\theta$),

$$(13) \qquad F_T = F_{R_1} + F_{R_2} = T\left(\frac{X + \frac{L}{2}\sin\theta}{\sqrt{\frac{L^2}{4} + X^2 + LX\sin\theta}} + \frac{X - \frac{L}{2}\sin\theta}{\sqrt{\frac{L^2}{4} + X^2 - LX\sin\theta}}\right)$$

$$(14) \qquad F_T = F_{R_1} = T\left(\frac{X + \frac{L}{2}\sin\theta}{\sqrt{\frac{L^2}{4} + X^2 + LX\sin\theta}}\right) \qquad (\text{for } X \leq L\sin\theta)$$

If all the vehicle's kinetic energy is absorbed by the Metal Bender tape pullout, then

$$KE = \frac{WV^2}{2g} = \int_0^{X_{max}} F_T\, dx$$

$$= T\int_0^{X_{max}} \left(\frac{X + \frac{L}{2}\sin\theta}{\sqrt{\frac{L^2}{4} + X^2 + LX\sin\theta}}\right) dx + T\int_{L\sin\theta}^{X_{max}} \left(\frac{X - \frac{L}{2}\sin\theta}{\sqrt{\frac{L^2}{4} + X^2 - LX\sin\theta}}\right) dx$$

(for $X > L\sin\theta$)

Let $\left(\frac{L^2}{4} + X^2 + L\,X\sin\theta\right) = u$, and $\left(\frac{L^2}{4} + X^2 - L\,X\sin\theta\right) = v$

Then $du = (2X + L\sin\theta)dx$, and $dv = (2X - L\sin\theta)dx$

Therefore,

$$KE = \frac{WV^2}{2g} = \frac{T}{2}\int_{u_i}^{u_f} u^{-1/2}\,du + \frac{T}{2}\int_{v_i}^{v_f} v^{-1/2}\,dv$$

$$= \frac{T}{2}\left(2u^{1/2} + 2v^{1/2}\right)_{\text{initial}}^{\text{final}}$$

$$= T\left(\sqrt{\frac{L^2}{4} + X^2 + L\,X\sin\theta}\,\Big|_0^{X_{max}} + \sqrt{\frac{L^2}{4} + X^2 - L\,X\sin\theta}\,\Big|_{L\sin\theta}^{X_{max}}\right)$$

$$= T\left(\sqrt{\frac{L^2}{4} + X_{max}^2 + L\,X_{max}\sin\theta} + \sqrt{\frac{L^2}{4} + X_{max}^2 - L\,X_{max}\sin\theta} - \frac{L}{2} - \frac{L}{2}\right)$$

Or,

(15) $$KE = \frac{WV^2}{2g} = T\left(\sqrt{\frac{L^2}{4} + X_{max}^2 + L\,X_{max}\sin\theta} + \sqrt{\frac{L^2}{4} + X_{max}^2 - L\,X_{max}\sin\theta} - L\right) \quad (\text{for } X_{max} > L\sin\theta)$$

(16) $$\frac{WV^2}{2g} = T\left(\sqrt{\frac{L^2}{4} + X_{max}^2 + L\,X_{max}\sin\theta} - \frac{L}{2}\right) \quad (\text{for } X_{max} \leq L\sin\theta)$$

Note that the expression for total energy obtained by integration of $F_T dx$ (Equation 15) is equal to $T(R_1 + R_2)$ using Equations 7 and 8.

For $\theta = 30°$ (Tests 4C, 4D and 4F), Equations 7, 8, 9, 15 and 16 become, respectively,

(17) $$R_1 = \left(\frac{L^2}{4} + X^2 + \frac{L\,X}{2} \right)^{1/2} - \frac{L}{2}$$

(18) $$R_2 = \left(\frac{L^2}{4} + X^2 - \frac{L\,X}{2} \right)^{1/2} - \frac{L}{2}$$

(19) $$X = \left(\left(\frac{L}{4}\right)^2 + R_1^{\,2} + L R_1 \right)^{1/2} - \frac{L}{4} \qquad \text{(in terms of } R_1\text{)}$$

or $$X = \left(\left(\frac{L}{4}\right)^2 + R_2^{\,2} + R_2\, L \right)^{1/2} + \frac{L}{4} \qquad \text{(in terms of } R_2 \text{ if } X > \frac{L}{2}\text{)}$$

(20) $$\frac{WV^2}{2g} = T \left(\sqrt{\frac{L^2}{4} + X_{max}^2 + \frac{L\,X_{max}}{2}} + \sqrt{\frac{L^2}{4} + X_{max}^2 - \frac{L\,X_{max}}{2}} - L \right) \qquad \left(\text{for } X > \frac{L}{2}\right)$$

(21) $$\frac{WV^2}{2g} = T \left(\sqrt{\frac{L^2}{4} + X_{max}^2 + \frac{L\,X_{max}}{2}} - \frac{L}{2} \right) \qquad \left(\text{for } X \leq \frac{L}{2}\right)$$

For $\theta = 0°$ (Tests 4A, 4B and 4E), Equations 7 and 8 become,

(22) $$R_1 = R_2 = R = \left(\frac{L^2}{4} + X^2 \right)^{1/2} - \frac{L}{2}$$

And Equation 15 becomes,

(23) $$\frac{WV^2}{2g} = 2T \left(\sqrt{\frac{L^2}{4} + X_{max}^2} - \frac{L}{2} \right)$$

From Equation 23,

$$X_{max}^2 = \left(\frac{KE}{2T} + \frac{L}{2} \right)^2 - \frac{L^2}{4} = \left(\frac{KE}{2T} \right)^2 + \left(\frac{KE}{2T} \right) L$$

(24) $$X_{max} = \sqrt{\left(\frac{WV^2}{4gT} \right) \left(\frac{WV^2}{4gT} + L \right)}$$

For head-on impacts, theoretical X_{max} can be determined from Equation 24. For 30° angled impacts, see Figure 27.

AN EXAMPLE OF HOW THESE EQUATIONS CAN BE APPLIED TO
THE DESIGN OF AN ARRESTING SYSTEM USING
VAN ZELM METAL BENDER ENERGY ABSORBING DEVICES

Given: Design factors dictate that the arresting system must stop vehicles with weights up to 4500 pounds and speeds up to 60 mph after en ering the system at angles of up to 20° with the perpendicular to the net. Geometric factors limit the distance between the end anchor posts to 30 feet and the maximum stopping distance to 30 feet.

Problem: What is the required minimum Metal Bender tape tension and tape lengths.

Solution: (See formulas on pages 51 through 54). The total tape pullout, for a particular energy and tension, is about the same regardless of the angle of impact. However, a preliminary calculation, using Equations 7, 8, and 9, shows that the stopping distance is greatest for $\theta = 20°$. Therefore use $\theta = \theta_{max} = 20°$ as a limiting case.

The critical design factors are:

$\theta_{max} = 20°$ $\quad (\sin \theta_{max} = 0.342)$

$X_{max} = 30$ feet

$L = 30$ feet

Using these values in Equations 7 and 8:

$$R_{1max} = \left(\frac{L^2}{4} + X^2_{max} + L X_{max} \sin\theta \right)^{1/2} - \frac{L}{2}$$

$$= \left(225 + 900 + 308 \right)^{1/2} - 15$$

$$= 37.9 - 15 = 22.9 \text{ feet}$$

$$R_{2max} = \left(\frac{L^2}{4} + X^2_{max} - L X_{max} \sin\theta \right)^{1/2} - \frac{L}{2}$$

$$= \left(225 + 900 - 308 \right)^{1/2} - 15$$

$$= 28.6 - 15 = 13.6 \text{ feet}$$

The minimum tape length is R_{1max} = 23 feet, (approximately)

Total tape pullout = (22.9 + 13.6)feet = 36.5 feet.

The maximum vehicle kinetic energy is:

$$\frac{WV^2}{2g} = \frac{(4500)\ (88)^2}{64.4} \text{ foot-pounds} = 542{,}000 \text{ foot-pounds}$$

From Equation 10,

$$T_{min.} = \left(\frac{WV^2}{2g} \right) \left(\frac{1}{R_{1max} + R_{2max}} \right)$$

$$= \frac{542{,}000}{36.5} \text{ pounds} = 14{,}850 \text{ pounds}$$

Theoretically the minimum Metal Bender tape tension is 14,850 pounds and the minimum length of tape required for runout in each Metal Bender is about 23 feet. The Metal Bender tape tension should now be chosen on the basis of the available tape tensions, including some excess tape length as a safety factor.

A P P E N D I X C

Photographic and Electromechanical Test Data

TABLE C1

TEST RF 505-4A

VAN ZELM METAL BENDER, HEAD-ON

1958 RENAULT, 4 DOOR SEDAN, 1460 LB.

HIGH SPEED FILM DATA

Time Milliseconds		Displacement ft	Velocity ft/sec
0		0	
			59.8
11.70		0.70	
			57.3
23.40		1.37	
			68.4
35.10	Impact	2.17	
			59.0
46.80		2.86	
			63.3
58.50		3.60	
			63.3
70.20		4.34	
			55.6
81.90		4.99	
			59.8
93.60		5.69	
			56.4
105.30		6.35	
			55.6
117.00		7.00	
			55.6
128.70		7.65	
			55.6
140.40		8.30	
			44.4
152.10		8.82	
			47.8
163.80		9.38	
			47.1
175.50		9.93	
			37.6
187.20		10.37	
			38.5
198.90		10.82	
			33.4
210.60		11.21	
			24.8
222.30		11.50	

TABLE C1

TEST RF 505-4A (continued)

Time Milliseconds	Displacement ft	Velocity ft/sec
		25.6
234.00	11.80	
		18.8
245.70	12.02	
		11.1
257.40	12.15	
		8.6
269.10	12.25	
		6.0
280.80	12.32	
		0.0
292.50	12.32	

TABLE C2

TEST RF 505-4B

VAN ZELM METAL BENDER, HEAD-ON

1960 MERCURY, 4 DOOR SEDAN, 4300 LB.

HIGH SPEED FILM DATA

Time Milliseconds		Displacement ft	Velocity ft/sec
0		0	
			86.2
13.00		1.12	
			90.0
26.00		2.29	
			86.2
39.00	Impact	3.41	
			83.0
52.00		4.49	
			87.7
65.00		5.63	
			83.9
78.00		6.72	
			86.2
91.00		7.84	
			80.7
104.00		8.89	
			78.5
117.00		9.91	
			78.5
130.00		10.93	
			73.1
143.00		11.88	
			73.1
156.00		12.83	
			70.0
169.00		13.74	
			66.1
182.00		14.60	
			64.6
195.00		15.44	
			65.4
208.00		16.29	
			56.2
221.00		17.02	
			57.0
234.00		17.76	
			54.6
247.00		18.47	
			46.2
260.00		19.07	

TABLE C2

TEST RF 505-4B (continued)

Time Milliseconds	Displacement ft	Velocity ft/sec
		46.2
273.00	19.67	
		43.9
286.00	20.24	
		38.5
299.00	20.74	
		33.9
312.00	21.18	
		28.5
325.00	21.55	
		23.1
338.00	21.85	
		20.8
351.00	22.12	
		16.1
364.00	22.33	
		12.3
377.00	22.49	
		12.3
390.00	22.65	
		6.2
403.00	22.73	
		3.8
416.00	22.78	
		2.3
429.00	22.81	
		0.0
442.00	22.81	

TABLE C3

TEST RF 505-4C

VAN ZELM METAL BENDER, 30° ANGLE

1955 VOLKSWAGEN, 2 DOOR, 1620 LB.

HIGH SPEED FILM DATA

Time Milliseconds		Displacement ft	Velocity ft/sec
0		0	
			70.8
12.00		0.85	
			69.2
24.00		1.68	
			69.2
36.00	Impact	2.51	
			65.8
48.00		3.30	
			70.8
60.00		4.15	
			69.2
72.00		4.98	
			65.8
84.00		5.77	
			65.8
96.00		6.56	
			68.2
108.00		7.38	
			67.4
120.00		8.19	
			64.1
132.00		8.96	
			65.8
144.00		9.75	
			64.1
156.00		10.52	
			59.1
168.00		11.23	
			60.8
180.00		11.96	
			46.6
192.00		12.52	
			45.0
204.00		13.06	
			46.6
216.00		13.62	
			44.2
228.00		14.15	
			41.6
240.00		14.65	

TABLE C3

TEST RF 505-4C (continued)

Time Milliseconds	Displacement ft	Velocity ft/sec
		37.5
252.00	15.10	
		26.6
264.00	15.42	
		26.6
276.00	15.74	
		15.0
288.00	15.92	
		17.5
300.00	16.13	
		8.3
312.00	16.23	
		5.8
324.00	16.30	
		0.0
336.00	16.30	

TABLE C4

TEST RF 505-4D

VAN ZELM METAL BENDER, 30° ANGLE

1958 OLDSMOBILE, 4 DOOR, 4520 LB.

HIGH SPEED FILM DATA

Time Milliseconds		Displacement ft	Velocity ft/sec
0		0	
			78.2
11.90		0.93	
			82.4
23.80		1.91	
			74.8
35.70		2.80	
			82.4
47.60		3.78	
			75.6
59.50	Impact	4.68	
			80.7
71.40		5.64	
			79.0
83.30		6.58	
			77.3
95.20		7.50	
			74.8
107.10		8.39	
			77.3
119.00		9.31	
			73.1
130.90		10.18	
			78.1
142.80		11.11	
			71.5
154.70		11.96	
			79.8
166.60		12.91	
			68.8
178.50		13.73	
			73.1
190.40		14.60	
			70.6
202.30		15.44	
			69.8
214.20		16.27	
			65.6
226.10		17.05	
			60.5
238.00		17.77	

TABLE C4

TEST RF 505-4D (continued)

Time Milliseconds	Displacement ft	Velocity ft/sec
		68.1
249.90	18.58	
		55.5
261.80	19.24	
		57.2
273.70	19.92	
		54.6
285.60	20.57	
		50.4
297.50	21.17	
		51.2
309.40	21.78	
		42.8
321.30	22.29	
		46.3
333.20	22.84	
		34.5
345.10	23.25	
		40.3
357.00	23.73	
		31.9
368.90	24.11	
		37.8
380.80	24.56	
		21.0
392.70	24.81	
		31.1
404.60	25.18	
		23.5
416.50	25.46	
		29.4
428.40	25.81	
		26.9
440.30	26.13	
		25.2
452.20	26.43	
		18.5
464.10	26.65	
		26.1
476.00	26.96	
		23.5
487.90	27.24	
		23.5
499.80	27.52	

TABLE C4

TEST RF 505-4D (continued)

Time Milliseconds	Displacement ft	Velocity ft/sec
		16.8
511.70	27.72	
		28.6
523.60	28.06	
		10.9
535.50	28.19	
		0.0
547.40	28.19	

TABLE C5

TEST RF 505-4E

VAN ZELM METAL BENDER, HEAD-ON

1961 DODGE, 4 DOOR, 3760 LB.

HIGH SPEED FILM DATA

Time Milliseconds		Displacement ft	Velocity ft/sec
0		0	
			90.8
12.59		1.143	
			82.7
25.18		2.184	
			88.3
37.77		3.296	
			77.8
50.36		4.276	
			75.4
62.95		5.225	
			81.9
75.54		6.256	
			81.0
88.13	Impact	7.276	
			80.2
100.72		8.286	
			75.6
125.90		10.189	
			78.6
151.08		12.168	
			77.1
201.44		16.050	
			67.4
251.80		19.443	
			63.0
302.16		22.616	
			56.1
352.52		25.443	
			47.7
402.88		27.846	
			37.5
453.24		29.734	
			29.7
503.60		31.230	
			21.6
553.96		32.317	
			15.1
604.32		33.078	

TABLE C5

TEST RF 505-4E (continued)

Time Milliseconds	Displacement ft	Velocity ft/sec
		8.6
654.68	33.512	
		2.1
705.04	33.619	
		0.3
755.40	33.634	
		-2.6
805.76	33.501	
		-1.9
856.12	33.404	
		-3.2
906.48	33.241	
		-3.5
956.84	33.063	
		-3.2
1007.20	32.901	
		-3.0
1057.56	32.748	
		-4.0
1107.92	32.544	
		-4.5
1158.28	32.315	
		-3.4
1208.64	32.142	
		-3.6
1259.00	31.958	
		-6.4
1309.36	31.637	
		-4.0
1359.72	31.438	
		-5.2
1410.08	31.178	
		-5.4
1460.44	30.908	
		-3.0
1510.80	30.755	
		0.0
1561.16	30.755	

TABLE C6

TEST RF 505-4F

HIGH SPEED FILM DATA

Time Milliseconds		Displacement ft	Velocity ft/sec
0		0	
			90.5
10.06		.910	
			91.6
20.12		1.832	
			90.0
30.18		2.738	
			95.6
40.24	Impact	3.700	
			87.3
60.36		5.456	
			88.5
80.48		7.236	
			85.3
100.60		8.952	
			80.5
120.72		10.572	
			81.9
140.84		12.220	
			78.3
160.96		13.795	
			77.5
181.08		15.355	
			75.0
201.20		16.863	
			68.7
221.32		18.245	
			69.5
241.44		19.643	
			66.5
261.56		20.981	
			62.3
281.68		22.235	
			61.9
301.80		23.481	
			56.4
321.92		24.615	
			54.2
342.04		25.705	
			53.4
362.16		26.779	
			48.4
382.28		27.753	

TABLE C6

TEST RF 505-4F (continued)

Time Milliseconds	Displacement ft	Velocity ft/sec
		46.8
402.40	28.695	
		41.4
422.52	29.529	
		40.8
442.64	30.351	
		37.5
462.76	31.105	
		32.5
482.88	31.759	
		34.1
503.00	32.445	
		28.5
523.12	33.018	
		28.1
543.24	33.583	
		25.4
563.36	34.095	
		19.7
583.48	34.491	
		24.5
603.60	34.984	
		22.7
623.72	35.440	
		18.3
643.84	35.808	
		22.1
663.96	36.252	
		17.7
684.08	36.608	
		19.9
704.20	37.008	
		16.1
724.32	37.332	
		18.5
744.44	37.704	

Vehicle moved out of view

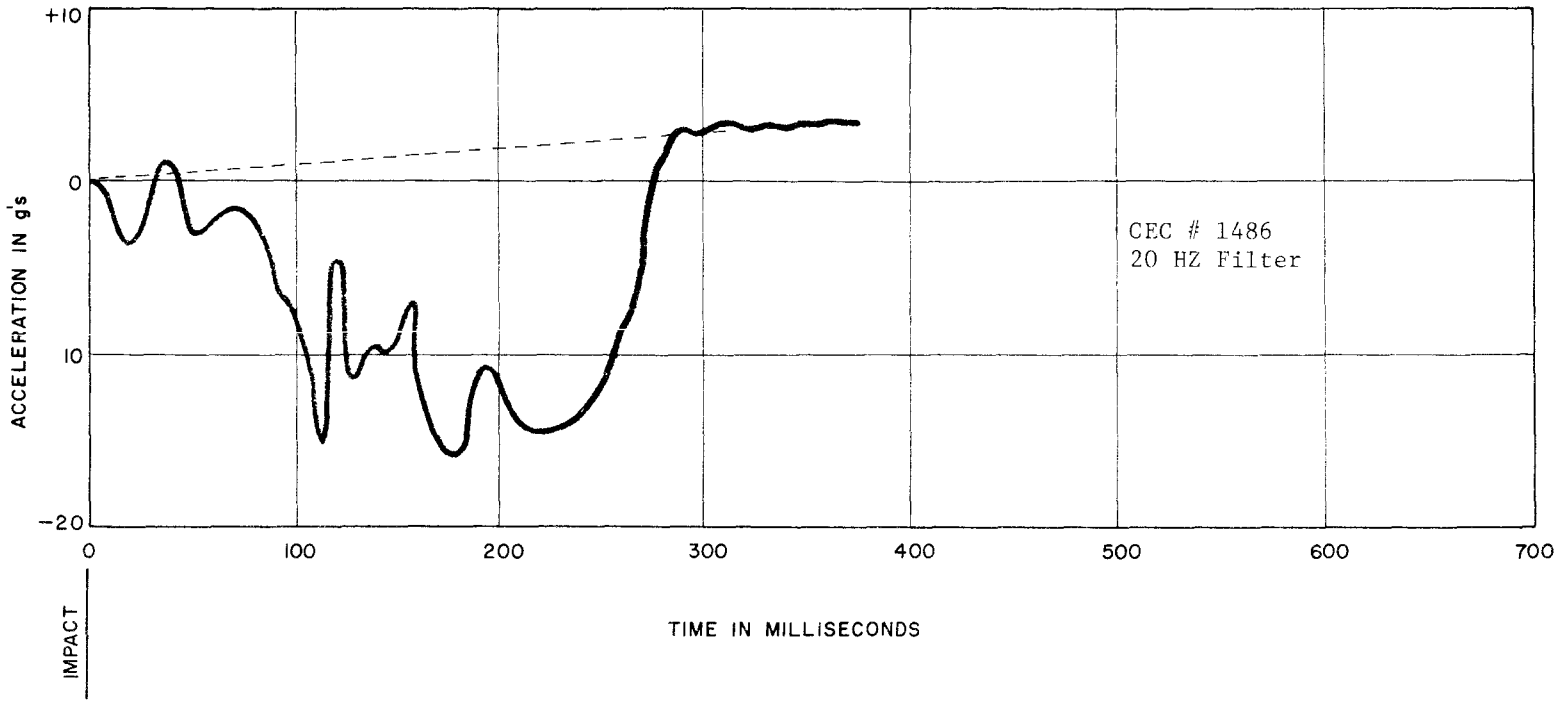

FIGURE C1, VEHICLE FRAME ACCELEROMETER DATA (LONGITUDINAL), TEST RF505-4A

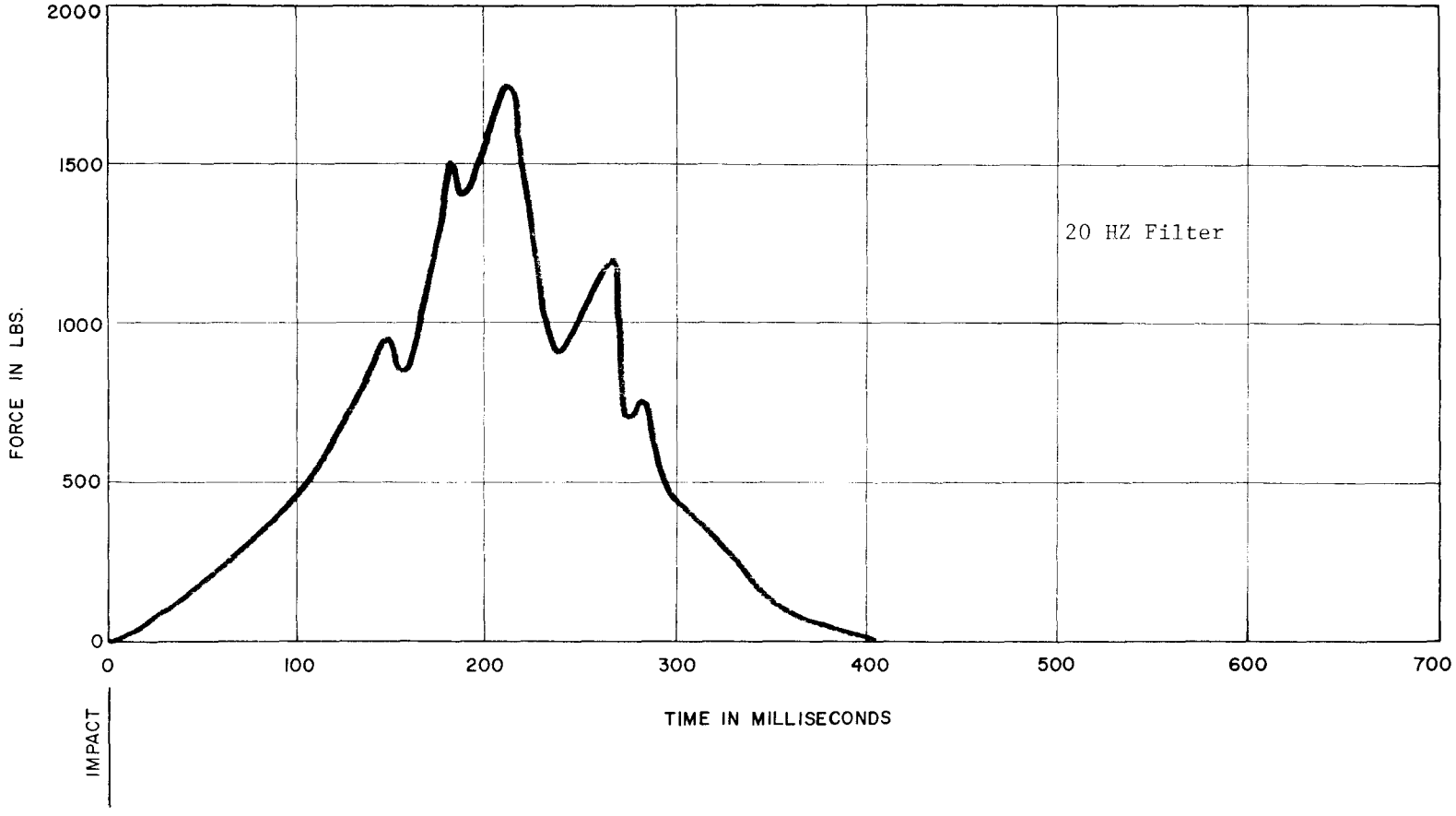

FIGURE C2, DUMMY SEATBELT FORCE DATA, TEST RF 505-4A

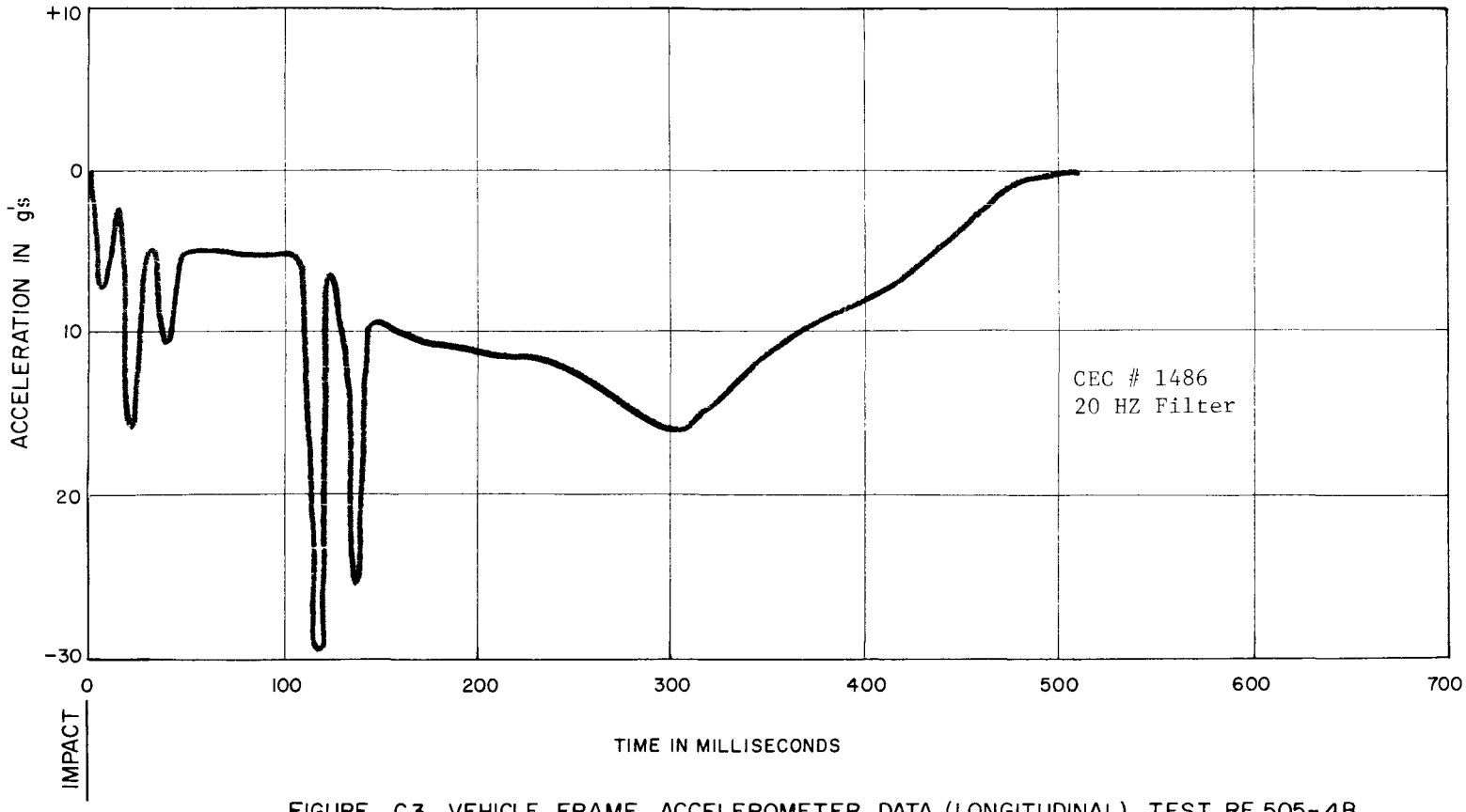

FIGURE C3, VEHICLE FRAME ACCELEROMETER DATA (LONGITUDINAL), TEST RF 505-4B

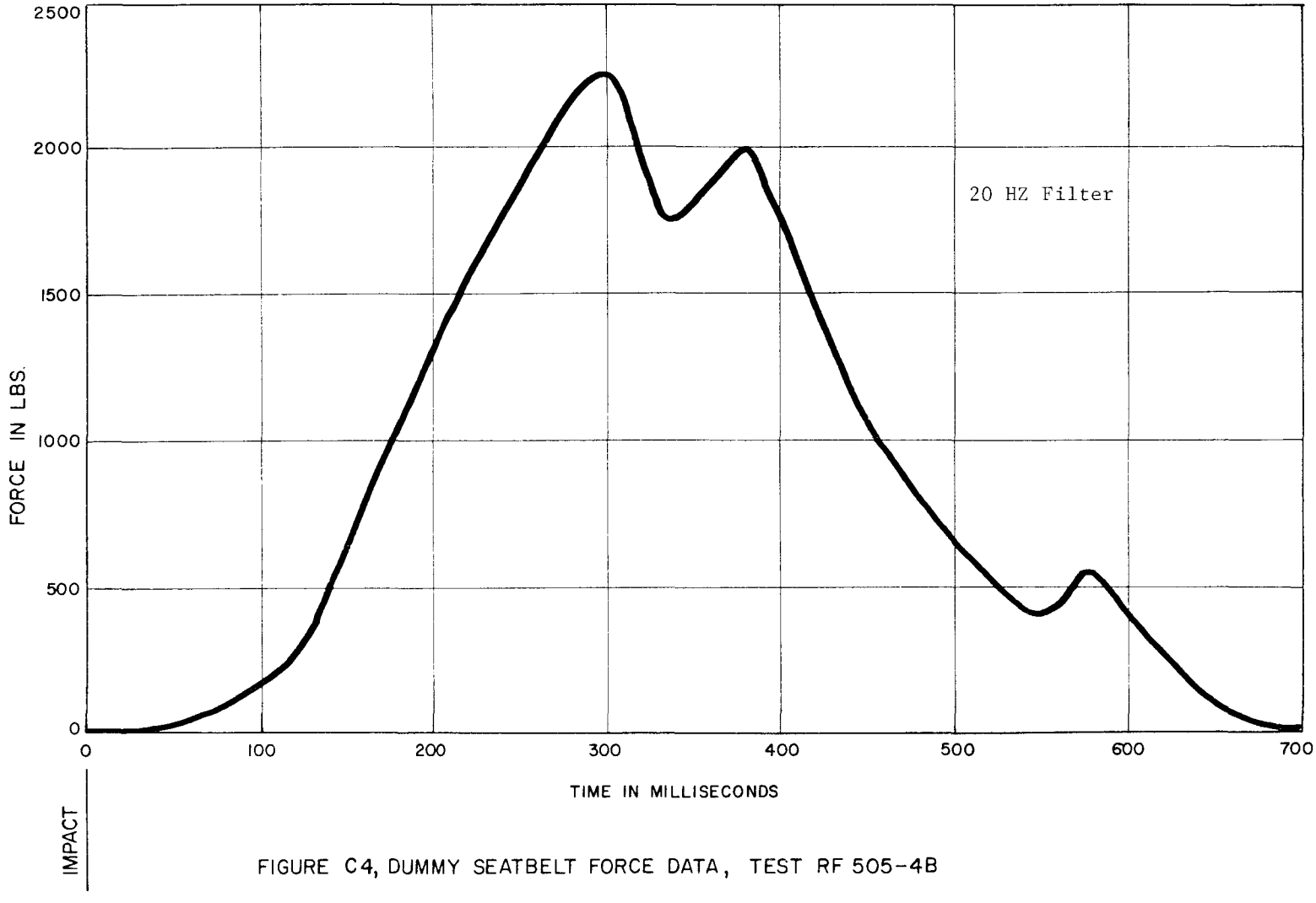

FIGURE C4, DUMMY SEATBELT FORCE DATA, TEST RF 505-4B

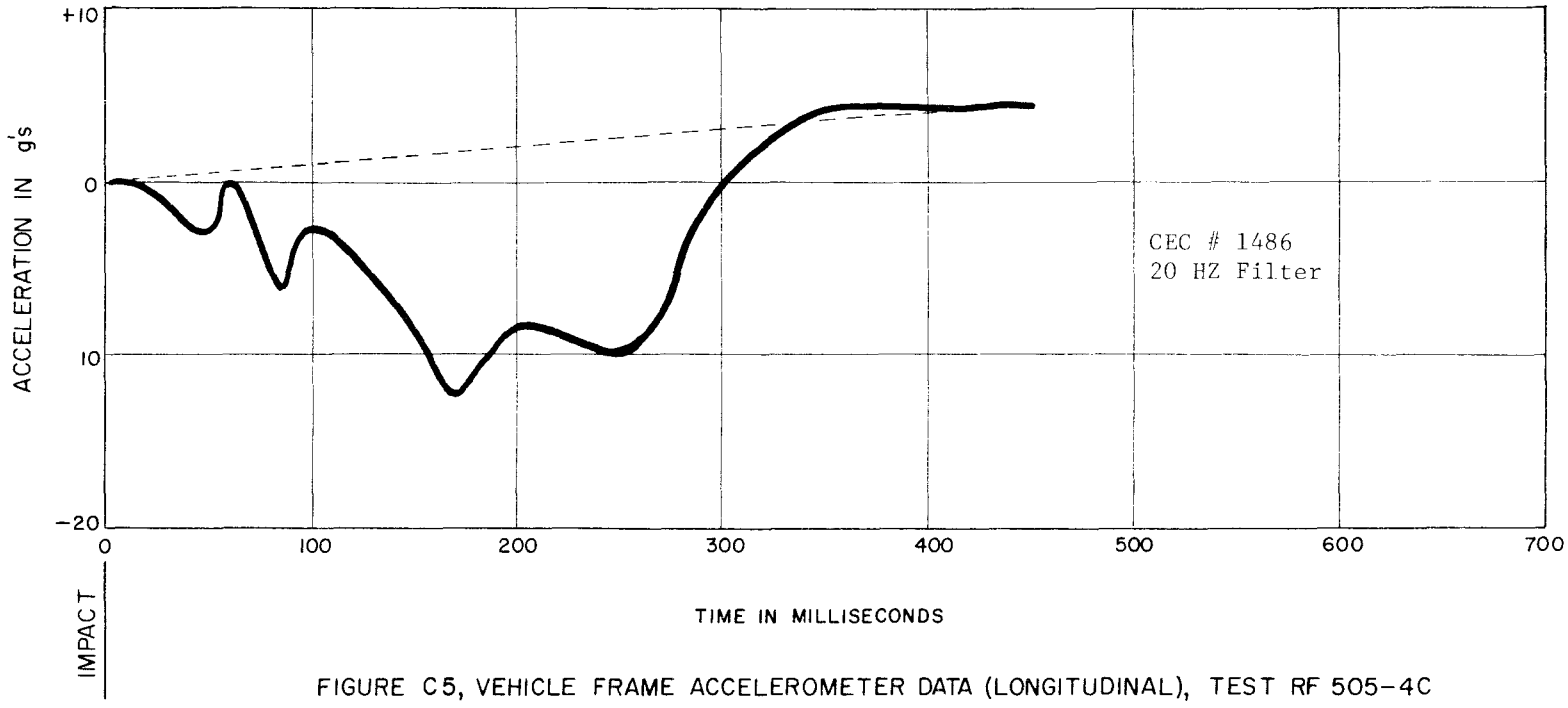

FIGURE C5, VEHICLE FRAME ACCELEROMETER DATA (LONGITUDINAL), TEST RF 505-4C

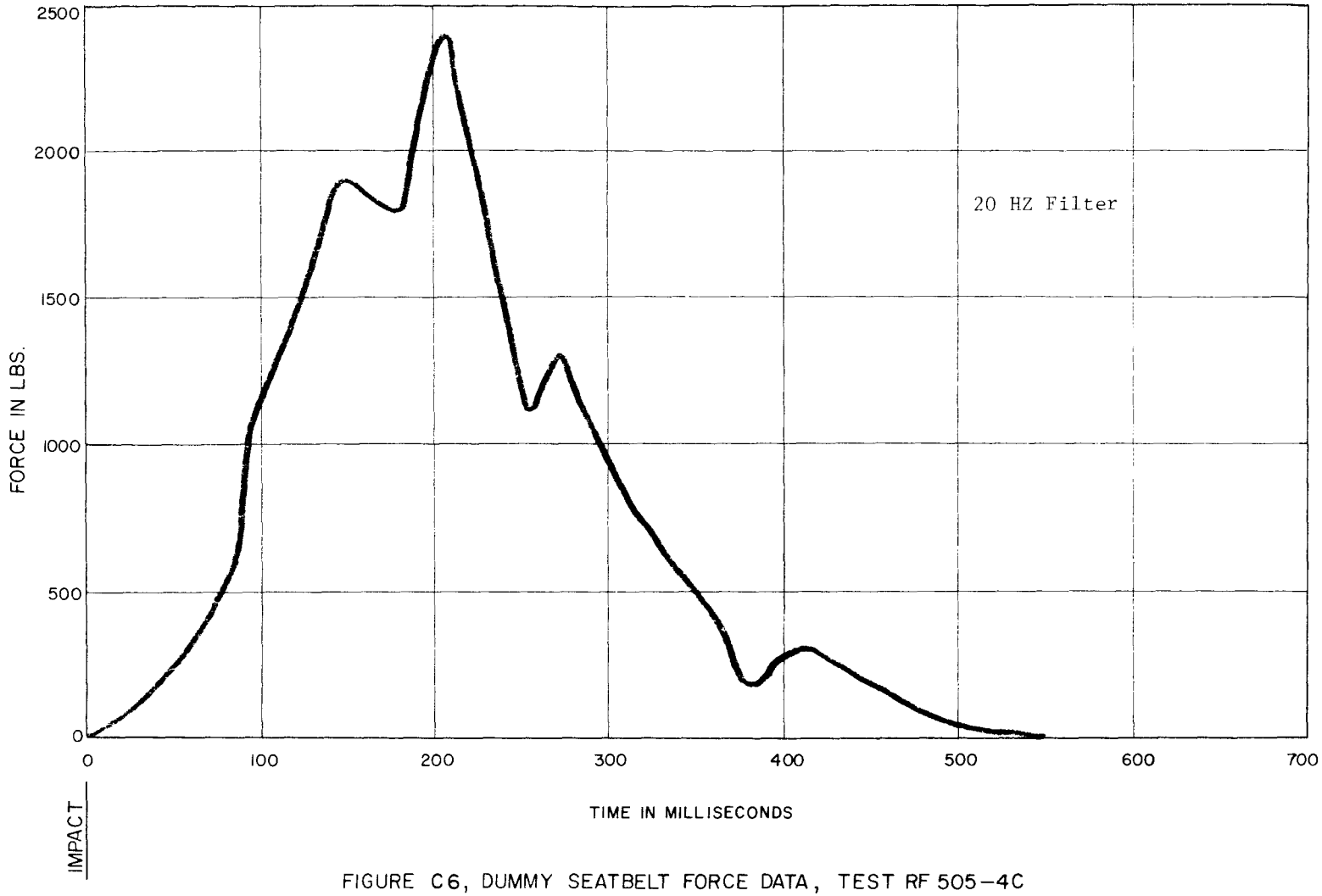

FIGURE C6, DUMMY SEATBELT FORCE DATA, TEST RF 505-4C

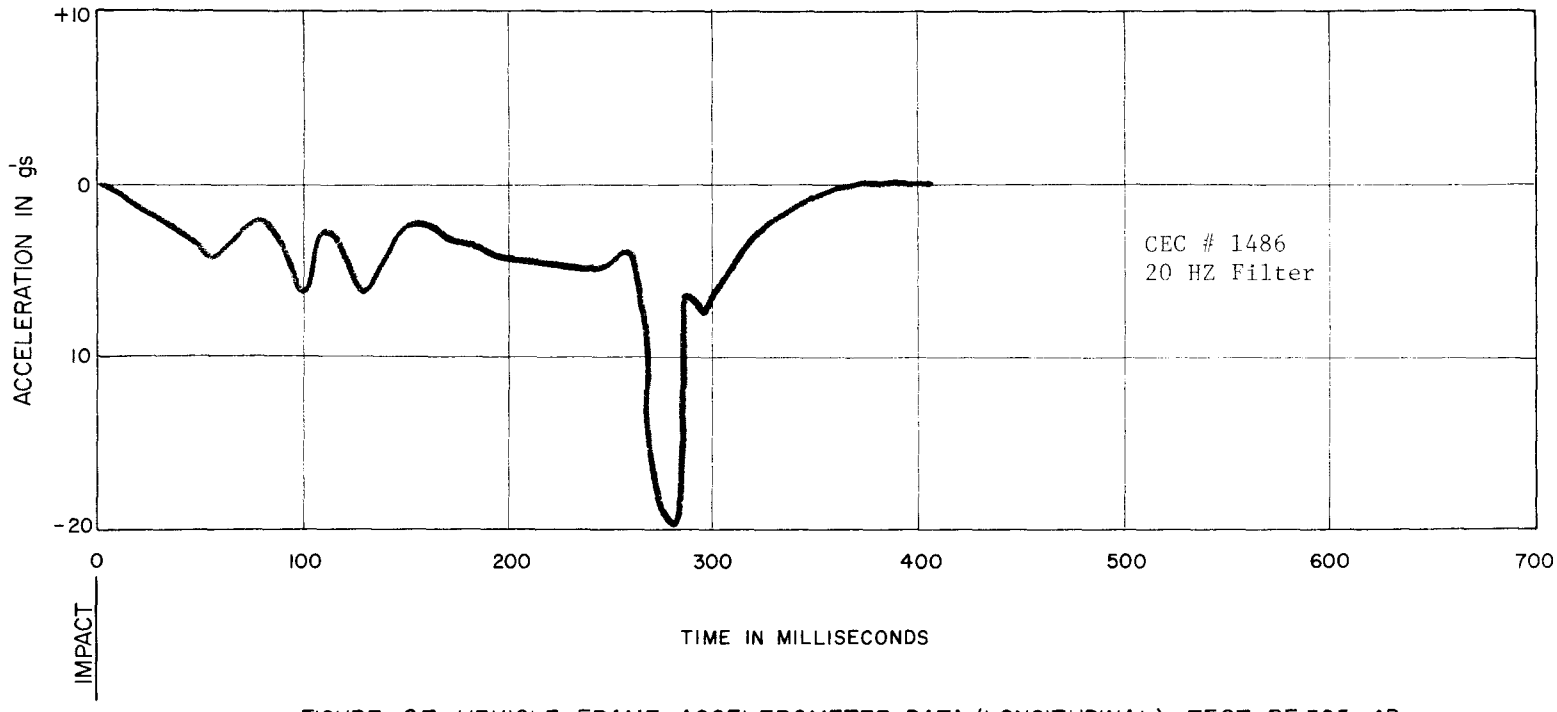

FIGURE C7, VEHICLE FRAME ACCELEROMETER DATA (LONGITUDINAL), TEST RF 505-4D

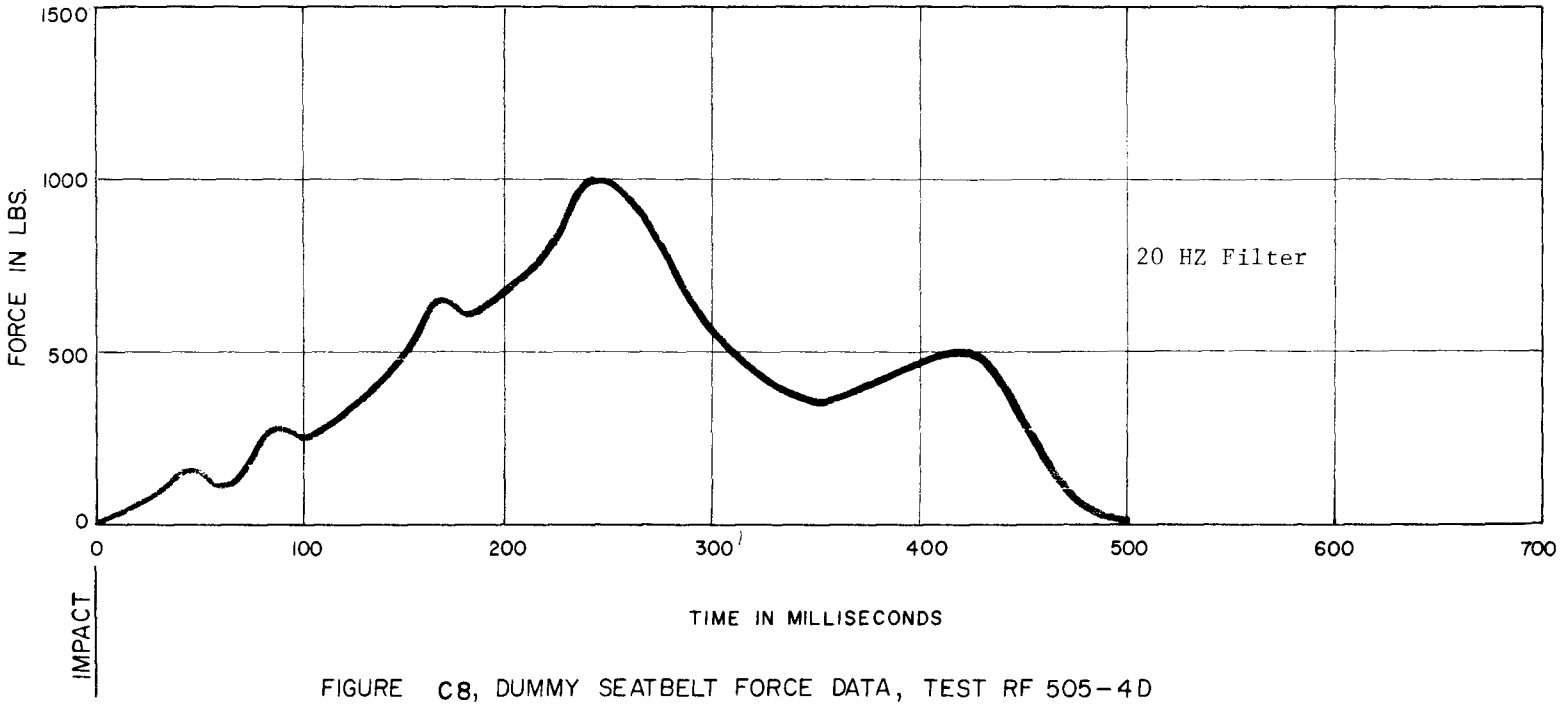

FIGURE C8, DUMMY SEATBELT FORCE DATA, TEST RF 505-4D

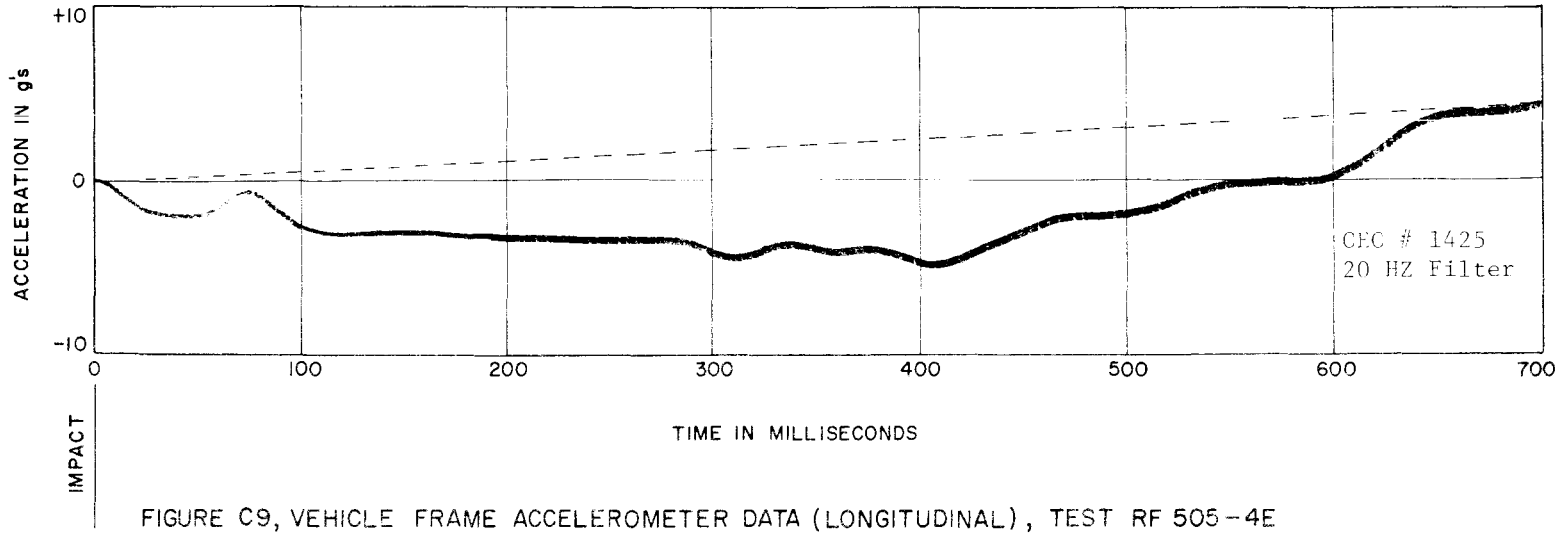

FIGURE C9, VEHICLE FRAME ACCELEROMETER DATA (LONGITUDINAL), TEST RF 505-4E

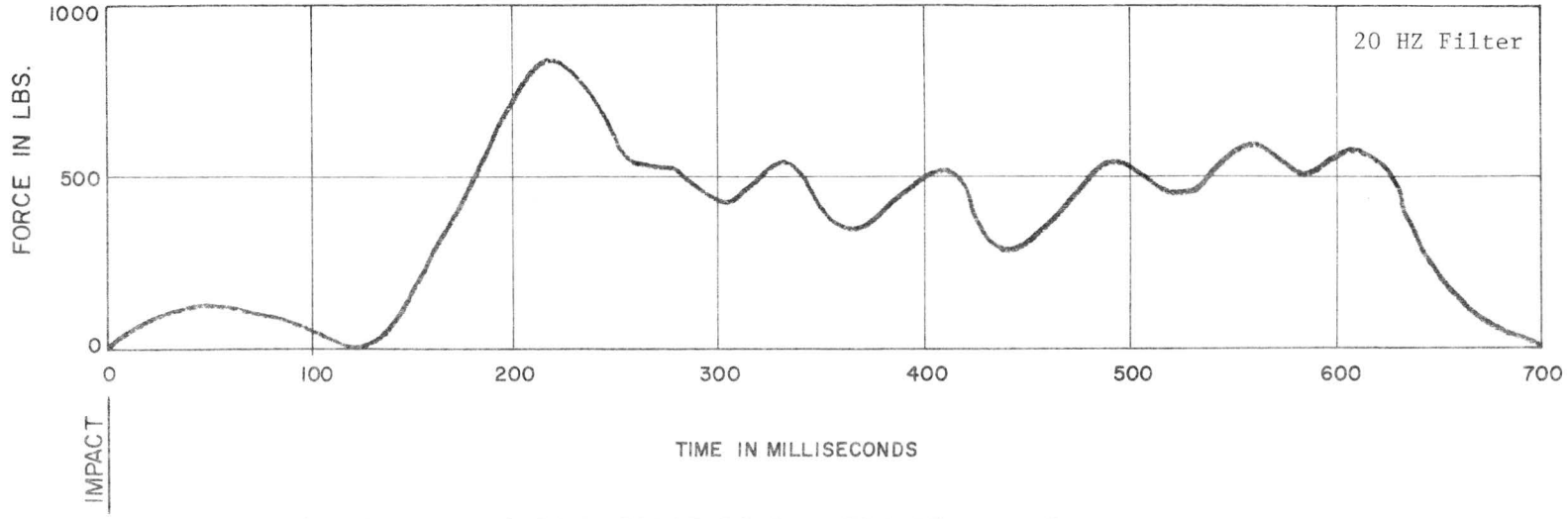

FIGURE C 10, DUMMY SEATBELT FORCE DATA, TEST RF 505-4E

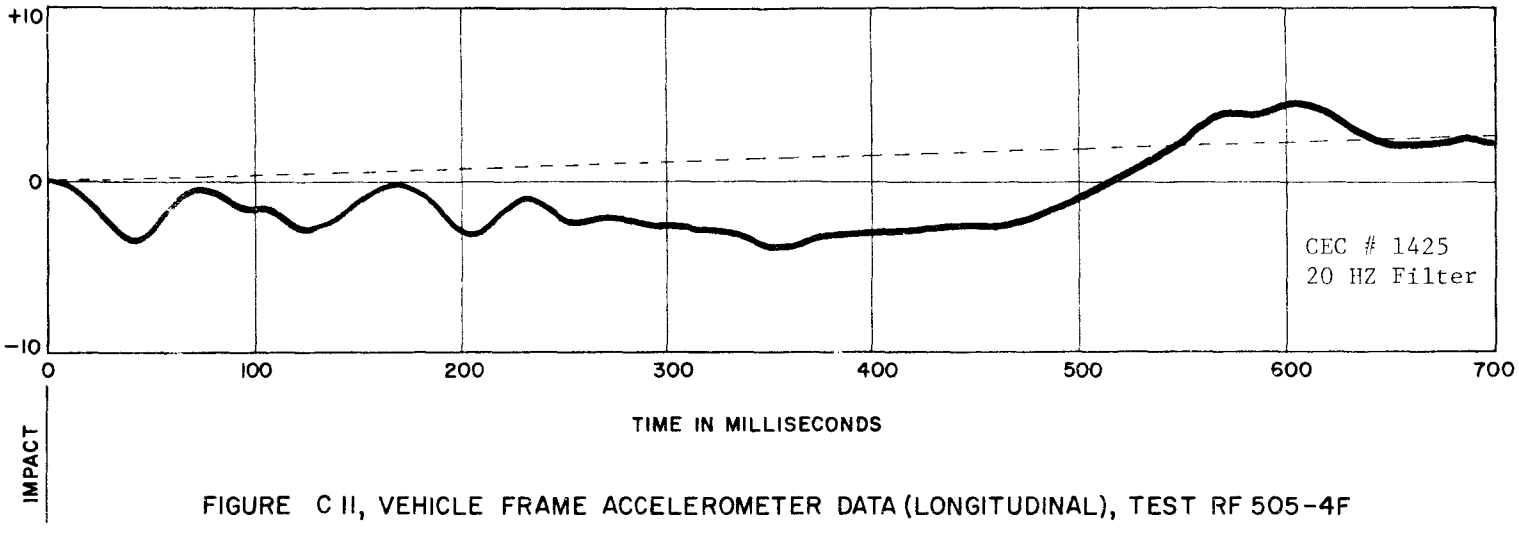

FIGURE C II, VEHICLE FRAME ACCELEROMETER DATA (LONGITUDINAL), TEST RF 505-4F

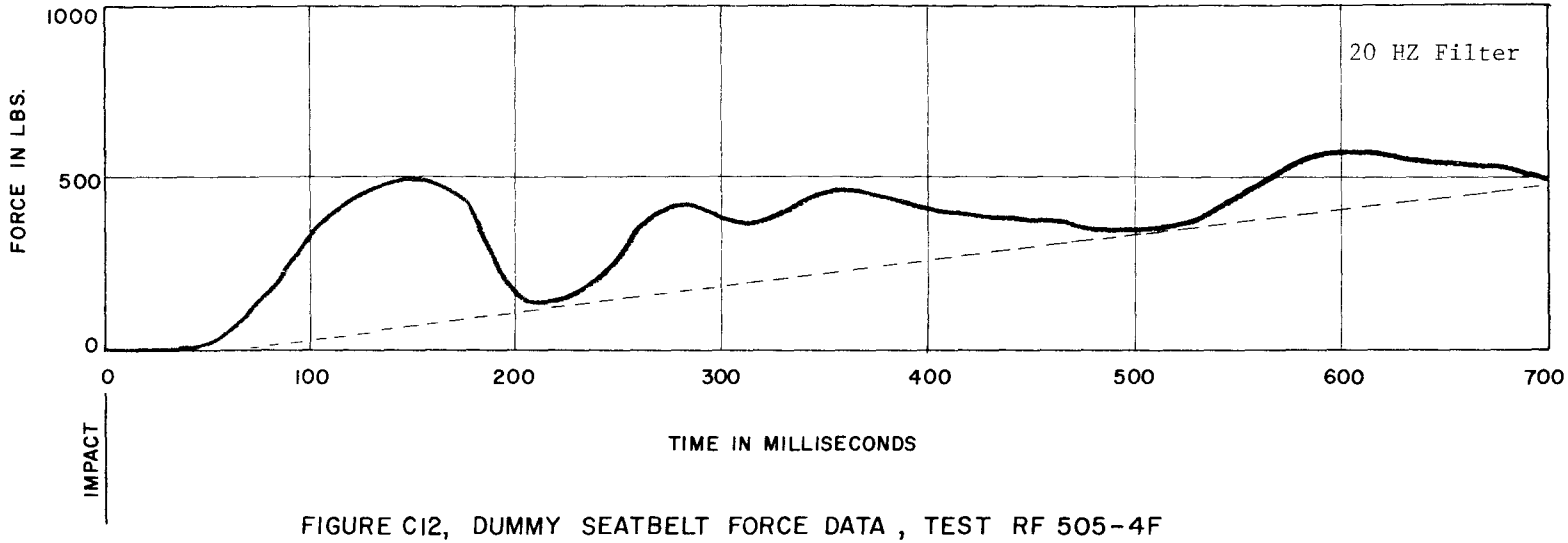

FIGURE C12, DUMMY SEATBELT FORCE DATA , TEST RF 505-4F

TECHNICAL MEMORANDUM 505-5

Texas Transportation Institute
Texas A&M Research Foundation

TIMBER POST ENERGY ABSORBING PROTECTIVE BARRIER

A Tentative Progress Memorandum on Contract No. CPR-11-5851
U.S. Department of Transportation
Federal Highway Administration
Bureau of Public Roads

by

T. J. Hirsch
Research Engineer

Harry L. Smith
Engineering Research Associate

and

Don L. Ivey
Associate Research Engineer

This crash test and evaluation was conducted under the Office of Research and Development, Structures and Applied Mechanics Division's Research Program on Structural Systems in Support of Highway Safety (4S Program). The opinions, findings, and conclusions expressed in this report are those of the authors and not necessarily those of the Bureau of Public Roads.

April 30, 1969

INTRODUCTION

On March 15, 1968, the Texas Transportation Institute conducted a full-scale vehicle crash test of a timber post energy absorbing protective barrier. The purpose of the timber post barrier was to stop vehicles at low levels of deceleration. Included are photographs of the vehicle and barrier before and after the test and a summary of the high speed motion picture film data.

BARRIER DESCRIPTION AND FUNCTION

The timber post barrier was proposed in the final report of Project HPR-2(104), Contract No. CPR-11-3550 concerning Highway Sign Support Research. This barrier was designated System III in Volume 3 of the final report entitled "A Feasibility Study of Impact Attenuation or Protective Devices for Fixed Highway Obstacles."

The timber post energy absorbing protective barrier consisted of 49 creosoted timber posts, 6 inches in diameter by 6 feet long. The posts were embedded 3 feet in clayey soil. Behind the array of posts was a 2 foot diameter concrete post surrounded by a 3 foot thick shell of polyurethane foam. Figure 1 gives a description of the barrier which was tested, and Appendix A shows a proposed application of this protective barrier. At impact, the bending over of successive posts in the soil is intended to absorb the kinetic energy of the vehicle. The resistance provided by each timber post bending over in the soil exerts a stopping force on the vehicle. The cumulative effect of these forces provided by the posts was intended to decelerate the vehicle to the final condition of zero velocity.

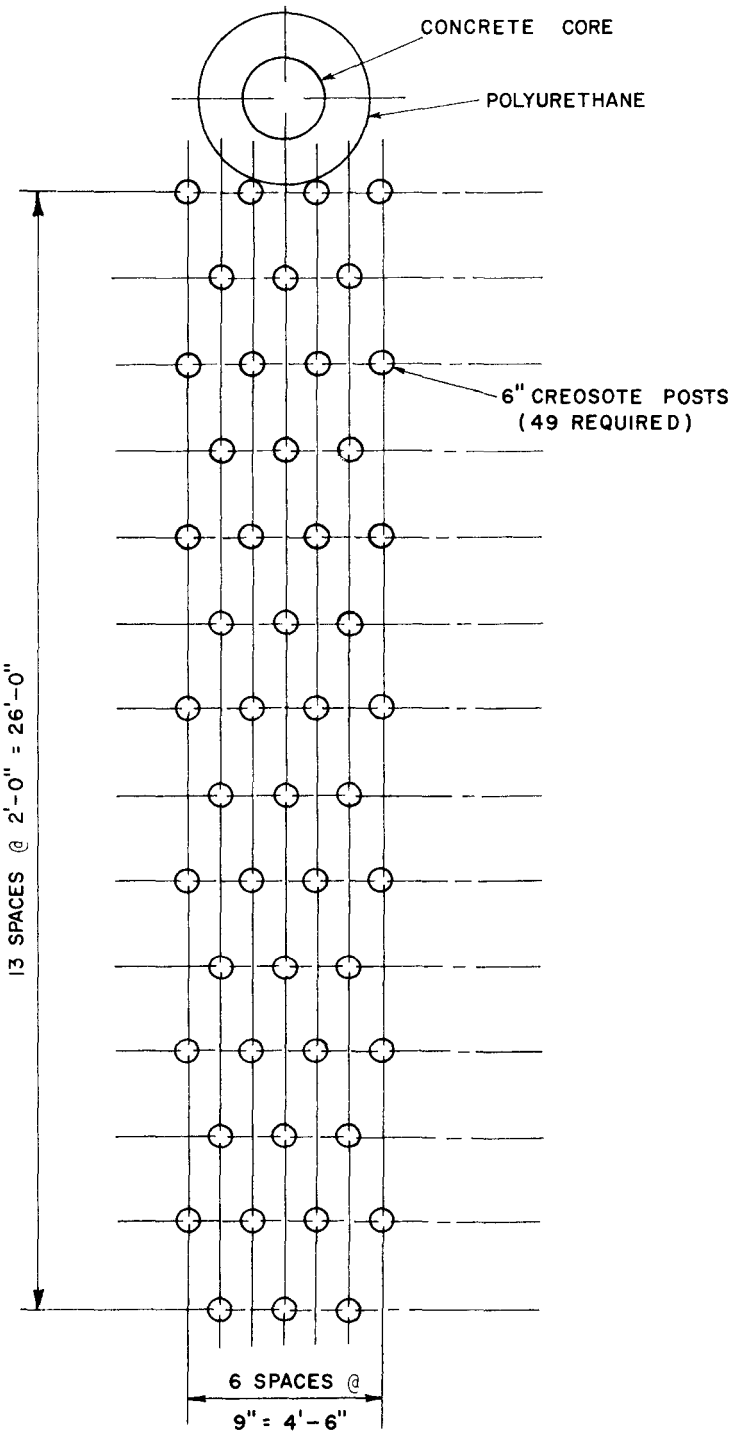

FIGURE 1, TIMBER POST ENERGY ABSORBING PROTECTIVE BARRIER

1/4" = 1'-0"

TEST RESULTS

Figure 2 shows the vehicle and barrier at various stages of their interaction. The 3880 lb. vehicle struck the timber post barrier head-on at a speed of 54.5 mph. The vehicle ramped on the posts and became airborne approximately 350 milliseconds after initial contact. The change in velocity at this time was 41.7 mph. The average longitudinal deceleration over the initial 352 millisecond interval was 5.4 g's; the peak longitudinal deceleration was 20 g's. The vehicle remained airborne for 960 milliseconds (0.96 seconds), coming to rest on top of the posts.

The following conclusions can be drawn from Test 505-5A:

1. The barrier did not function as intended.
2. The vehicle damage was severe (see Figures 5 and 6).
3. Damage to the timber post barrier was moderate. The first three rows of posts were pushed over.
4. The deceleration level was severe.

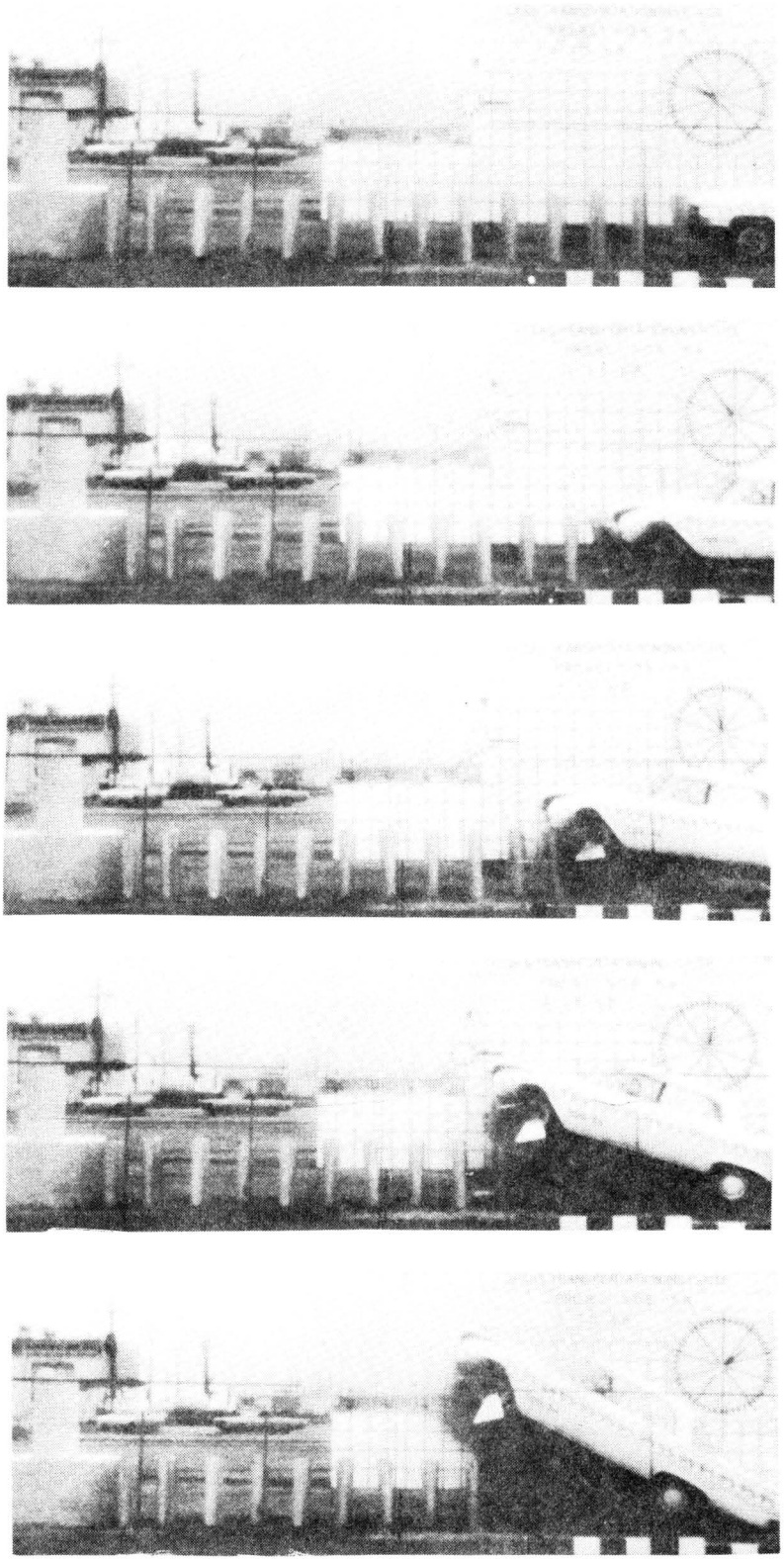

Figure 2. Sequential Photographs of Timber Post Barrier Test.

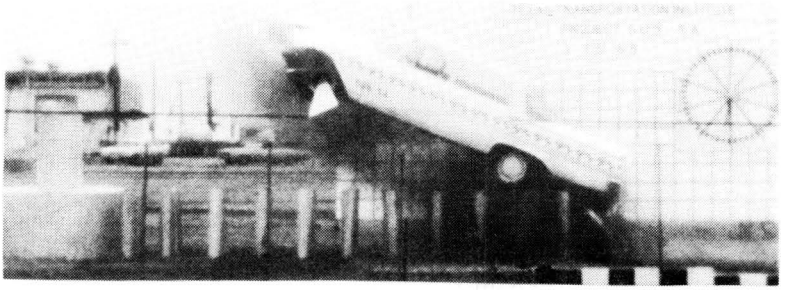

6

7

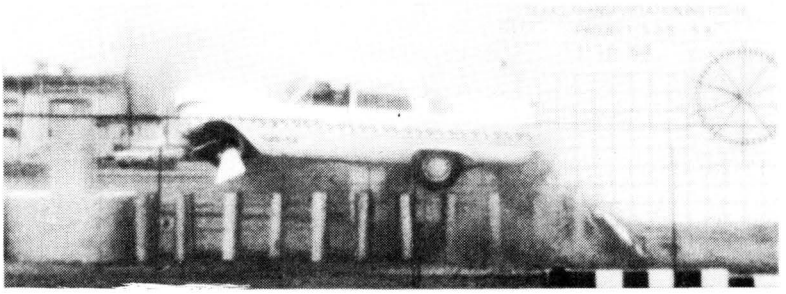

8

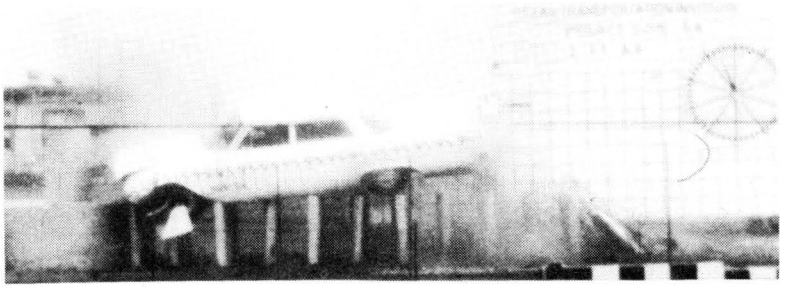

9

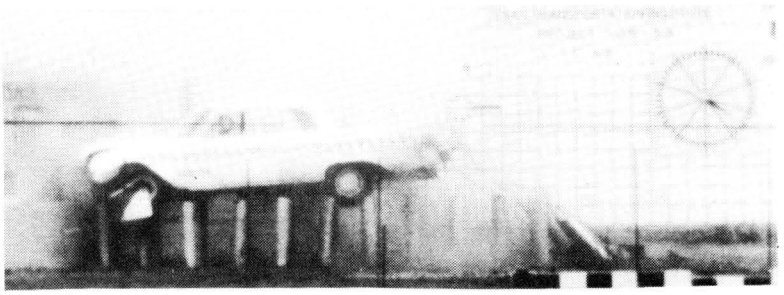

10

Figure 2 (continued).

TABLE 1. COMPARISON OF POST BARRIER IMPACT PERFORMANCE WITH RIGID BARRIER IMPACT

TEST NUMBER	5A
VEHICLE WEIGHT (lb)	3880
VEHICLE VELOCITY (mph)	54.5
MAXIMUM DECELERATION (G max) POST BARRIER RIGID BARRIER*	 20 g's 49.1 g's
AVERAGE DECELERATION (G avg.) (over first 352 msec after impact) POST BARRIER RIGID BARRIER*	 5.4 g's 31.3 g's
ATTENUATION INDEX $AI_{(max.)} = \frac{G_{max\ Post}}{G_{max\ Rigid}}$	0.41
$AI_{(avg.)} = \frac{G_{avg\ Post}}{G_{avg\ Rigid}}$	0.17

* Estimated Maximum Deceleration = 0.9V, where V is in mph.
Estimated Average Deceleration = 0.574V, where V is in mph.

Emori, Richard I., "Analytical Approach to Automobile Collisions," SAE Paper 680016, Engineering Congress, Detroit, January 8, 1968.

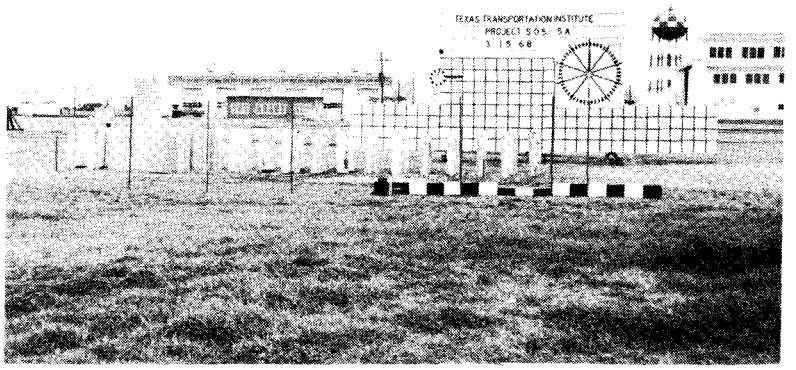

FIGURE 3. WOODEN POSTS BEFORE COLLISION

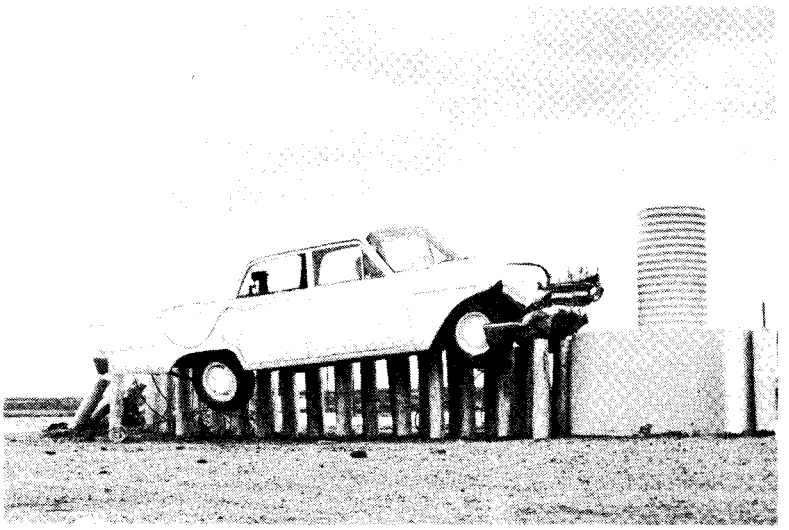

FIGURE 4. POSTS AND VEHICLE AFTER COLLISION
INITIAL VEHICLE VELOCITY 54.5 mph
STOPPING DISTANCE 27.3 FT.,
AVERAGE VEHICLE DECELERATION 5.4 g's
(over first 352 msec following contact).

TABLE 2. SUMMARY OF CRASH TEST DATA FROM HIGH-SPEED FILM FOR CREOSOTED TIMBER POSTS. RF 505-5A

TEST NUMBER	5A
VEHICLE	1961 Ford, 2 Dr. Sed., 3880 lb.
FILM DATA	
Velocity (mph)	54.5
Velocity (fps)	79.9
Velocity Change (mph)	54.5
Velocity Change (fps)	79.9
Average Deceleration (g's)	5.4 (over first 352 msec following contact)
Peak Deceleration (g's)	20
Duration of Impact (sec.)	1.313
Stopping Distance (ft.)	27.3
OBSERVATIONS	
Vehicle Deformation (ft.)	1.37
Barrier Penetration (ft.)	8.39
Vehicle Damage	Severe
Barrier Damage	Moderate

DISCUSSION AND SUMMARY

A full-scale vehicle crash test was conducted on a timber post energy absorbing protective barrier. The objective of the timber post barrier was to stop the vehicle at low levels of deceleration. The barrier consisted of 49 creosoted timber posts, 6 inches in diameter and 6 feet long. Behind the array of posts was a 2 foot 1 inch diameter simulated bridge pier surrounded by a 3 foot thick cushion of polyurethane foam.

The results of Test 505-5A show that low decelerations were not achieved. From the photographic analysis, it appears that impact with the front three rows of timber posts resulted in an energy transfer of larger magnitude than anticipated. Previous research work by Deleys and McHenry, "Highway Guardrails - A Review of Current Practice," Cornell Aeronautical Laboratory, indicated such posts would absorb approximately 15,000 ft.lbs. of energy. The posts in this installation which were overturned by the vehicle apparently absorbed about three times this much energy. Analysis of the high speed films reveals that the front rows of posts were pushed over as intended, but these "pushed-over" posts formed a ramp which resulted in the vehicle becoming airborne. The soil surrounding the timber posts and the depth of embedment has a great effect on the mode of energy transfer and also on the magnitude of the decelerations. The post spacing also appears to be a significant factor.

Additional information is needed to establish the proper post embedment and post spacing for different types of soils so that the vehicle ramping problem can be overcome. Reducing the post cross-section so it will break is not desirable because the energy absorption characteristic

will also be greatly reduced. Consequently a very large number of posts would be required. The importance of the soil in the post-soil interaction was discussed at length in Technical Memorandum 505-3*. Dynamic tests which may aid significantly in the design of this type of barrier are now being conducted by the Texas Transportation Institute as part of Research Study 4105, sponsored by the Texas Highway Department and the Bureau of Public Roads. The authors believe that additional research on the application of these principles to the design of protective barriers could result in a workable system.

CONCLUSION

The full-scale vehicle crash test on a timber post energy absorbing protective barrier revealed that the embedment of the timber post, the spacing and the soil condition are decisive factors in the proper operation of the barrier as a vehicle attenuation device.

Although the crash test did not yield the desirable feature of low deceleration levels, modifications of this timber post barrier design and an awareness of the soil influence on the failure mode and magnitude of energy absorption may result in an effective timber post energy absorbing protective barrier.

---

* "One-Way Guardrail Installation", Don L. Ivey and T. J. Hirsch. Texas Transportation Institute, Technical Memorandum 505-3, January, 1969.

TABLE 3.

SUMMARY OF CRASH TEST DATA

Test 505-5A 6 in. diam. creosoted Timber Posts 6 ft. long, embedded 3 ft. in clayey soil. All posts spaced 2 ft. center to center. 14 rows of 3, 4, 3, 4, etc., posts in each row.

Vehicle Weight = 3880 lb. (1961 Ford, 2 door)

Vehicle Velocity = 54.5 mph or 79.9 fps

Change in Velocity = 54.5 mph or 79.9 fps

Average Deceleration = 5.4 g's (over initial post contact time interval, 352 msec)

Peak Deceleration = 20 g's

Duration of Impact - 1.313 sec.

Stopping Distance = 27.3 ft.

Remarks: Severe damage to vehicle. Vehicle ramped on posts and was launched into the air 352 milliseconds after impact. The change in velocity at this time after impact was 61.1 fps. The average deceleration over this 352 milliseconds was 5.4 g's. The peak deceleration was 20 g's.

FIGURE 5. VEHICLE BEFORE COLLISION.
1961 FORD, WEIGHT 3880 LB.

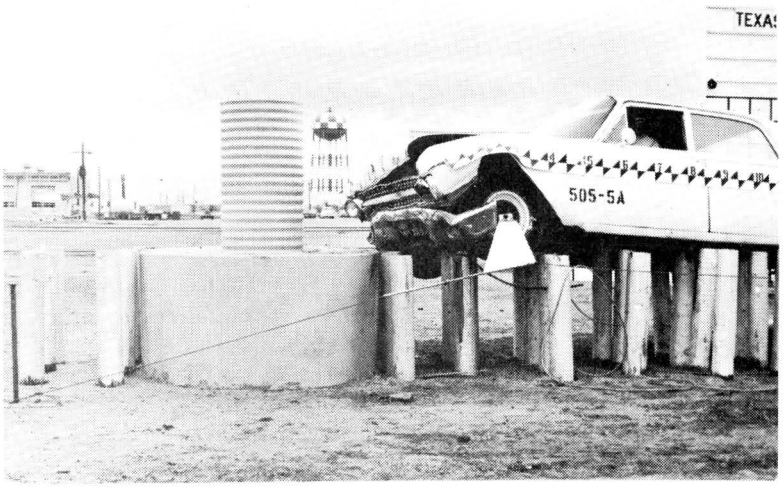

FIGURE 6. VEHICLE DAMAGE.
VEHICLE DEFORMATION 1.37 FT.
BARRIER DEFORMATION 8.39 FT. (measured in terms of rows of damaged posts).

A P P E N D I X A

Design Drawing of Timber Post

Energy Absorbing Protective Barrier

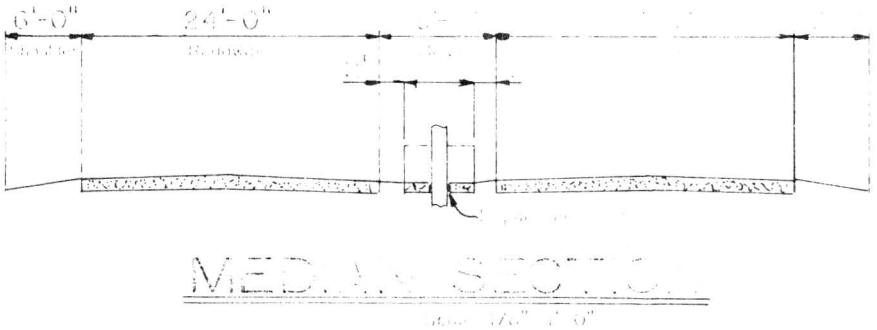

MEDIAN SECTION

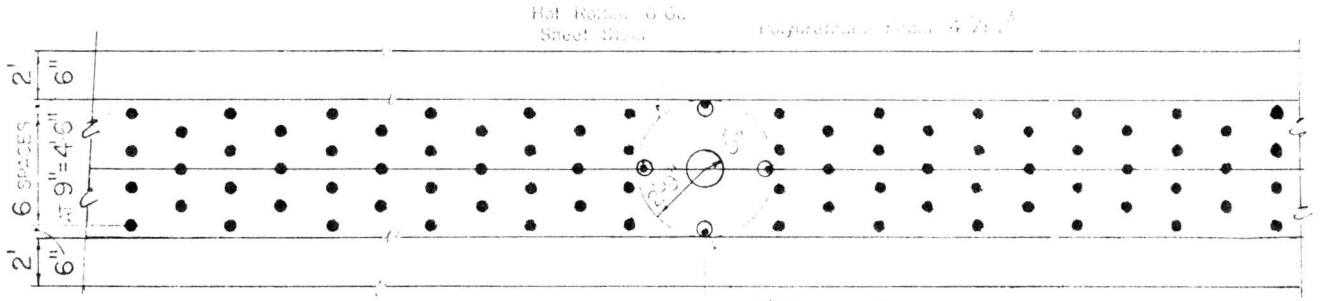

PLAN

Scale 1/4"=1'-0"

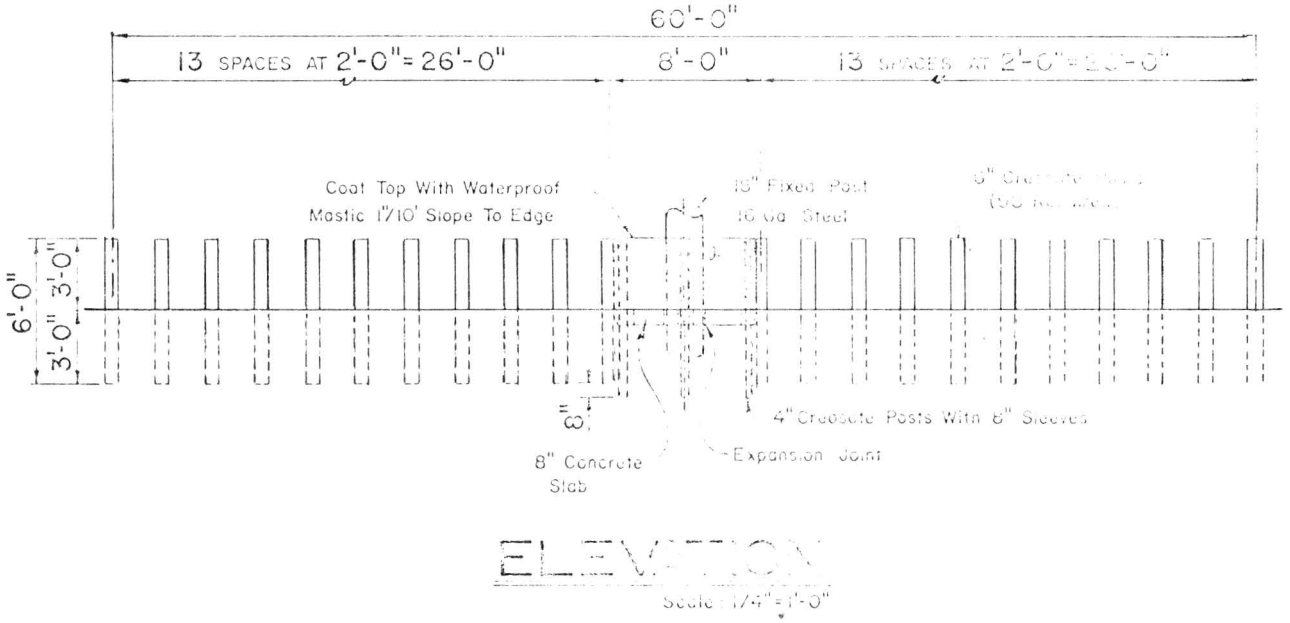

ELEVATION

Scale 1/4"=1'-0"

Design Drawing of Timber Post Energy Absorbing Protective Barrier.

A P P E N D I X B

Photographic Data

TEST RF505-5A

6 in. Diam. Creosoted Timber Posts 6 Ft Long, Embedded 3 Ft in Clayey Soil. All Posts Spaced 2 Ft Center to Center. 14 Rows of 3, 4, 3, 4, etc., Posts in Each Row.

Time Milliseconds	Displacement ft	Velocity ft/sec	
0	0		
		79.2	
20.20	1.60		
		79.2	79.9 avg.
40.40	3.20		
		81.1	
*60.60	*4.84		
		72.8	
80.80	6.31		
		73.3	
101.00	7.79		
		60.3	
121.20	9.01		
		52.0	
141.20	10.06		
		44.1	
161.60	10.95		
		31.7	
181.80	11.59		
		31.2	
202.00	12.22		
		23.8	
222.20	12.70		
		26.2	
242.40	13.23		
		19.8	
262.60	13.63		
		16.8	
282.80	13.97		
		24.2	
303.00	14.46		
		14.9	
323.20	14.76		
		19.3	
343.40	15.15		
		20.3	
363.60	15.56		
		19.3	
383.80	15.95		
		21.3	

Time Milliseconds	Displacement ft	Velocity ft/sec
404.00	16.38	
**		18.8
424.20	16.76	
		19.8
444.40	17.16	
		21.8
464.60	17.60	
		16.3
484.80	17.93	
		18.3
505.00	18.30	
		20.3
525.20	18.71	
		21.2
545.40	19.14	
		20.3
565.60	19.55	
		18.8
585.80	19.93	
		17.8
606.00	20.29	
		15.4
626.20	20.60	
		20.3
646.40	21.01	
		21.3
666.60	21.44	
		13.9
686.80	21.72	
		13.4
707.00	21.99	
		23.8
727.20	22.47	
		16.3
747.40	22.80	
		15.8
767.60	23.12	
		10.4
787.80	23.33	
		21.8
808.00	23.77	
		17.8
828.20	24.13	
		16.8
848.40	24.47	
		17.8
868.60	24.83	
		14.9
888.80	25.13	
		19.8

Time Milliseconds	Displacement ft	Velocity ft/sec
909.00	25.53	
		12.9
929.20	25.79	
		16.3
949.40	26.12	
		17.8
969.60	26.48	
		13.9
989.80	26.76	
		17.4
1010.00	27.11	
		13.9
1030.20	27.39	
		19.3
1050.40	27.78	
		14.4
1070.60	28.07	
		16.3
1090.80	28.40	
		12.4
1111.00	28.65	
		14.3
1131.20	28.94	
		20.8
1151.40	29.36	
		12.9
1171.60	29.62	
		12.9
1191.80	29.88	
		15.8
1212.00	30.20	
		14.8
1232.20	30.50	
		12.9
1252.40	30.76	
		16.3
1272.60	31.09	
		12.9
1292.80	31.35	
		15.3
1313.00	31.66	
		10.4
1333.20	31.87	
		8.4
1353.40	32.04	
		3.9
***1373.60	32.12	
		-1.9
1414.00	32.04	
		-8.2

Time Milliseconds	Displacement ft	Velocity ft/sec
1454.40	31.71	
		-3.2
1494.80	31.58	
		-6.7
1535.20	31.31	
		-4.9
1575.60	31.11	
		-3.0
1616.00	30.99	
		-5.2
1656.40	30.78	
		-5.9
1696.80	30.54	
		-1.2
1737.20	30.49	
		-2.2
1777.60	30.40	

*Impact.

**Vehicle launched into air vel. approx. 20 fps.

***Vehicle stops on posts.

TECHNICAL MEMORANDUM 505-6

Texas Transportation Institute
Texas A&M Research Foundation

POLYURETHANE FOAM IMPACT ATTENUATION BARRIER

A Tentative Progress Memorandum on Contract No. CPR-11-5851

U. S. Department of Transportation
Federal Highway Administration
Bureau of Public Roads

by

T. J. Hirsch
Research Engineer

Gordon G. Hayes
Engineering Research Associate

and

Don L. Ivey
Associate Research Engineer

This crash test and evaluation was conducted under the Office of Research and Development, Structures and Applied Mechanics Division's Research Program on Structural Systems in Support of Highway Safety (4S Program). The opinions, findings, and conclusions expressed in this report are those of the authors and not necessarily those of the Bureau of Public Roads.

July 1969

INTRODUCTION

On May 7, 1968, a vehicle crash test was conducted by the Texas Transportation Institute to evaluate a polyurethane foam impact attenuation barrier. This report, which describes the results of that test, includes photographs of the vehicle and barrier before and after the test, sequential photographs of the test in progress, and data from electromechanical instrumentation.

DESCRIPTION OF BARRIER

The polyurethane foam barrier was proposed in the final report of Project HPR-2(104), Contract No. CPR-11-3550 concerning Highway Sign Support Research. This barrier was designated System I in Volume 3 of the final report entitled "A Feasibility Study of Impact Attenuation or Protective Devices for Fixed Highway Obstacles."

The barrier, which was used to protect a simulated rigid concrete pier, consisted of a mass of polyurethane foam surrounded by a sheet of 16 gage sheet steel (see Figure 1A, Appendix A, for details). The barrier was held in place by four-inch diameter wood posts. The entire barrier rested flush with the ground. Blocks of polyurethane foam were placed in the sheet steel form, and the upper surface was coated with water-proof mastic. The density of the foam in the front half of the barrier was approximately two pounds per cubic foot, while that of the foam in the rear half was approximately three pounds per cubic foot. Figure 2 is a photograph of the barrier prior to the crash test.

Figure 1, Vehicle Before Test 505-6A.

1959 Simca, Weight 2060 pounds.
(Note Cable Guidance System and Stadia Board)

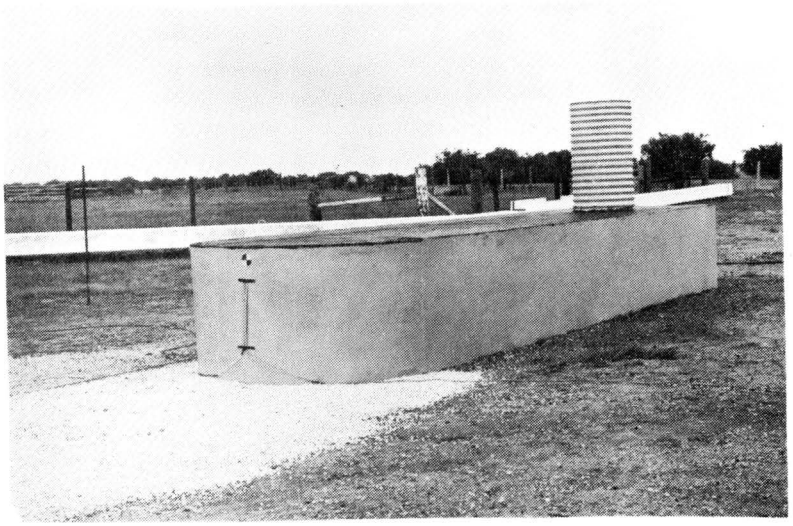

Figure 2, Polyurethane Barrier Before Test 505-6A.

Polyurethane Foam - Nose, 1.94 lbs/ft^3; Crush Strength approx. 20 psi
Rear, 2.72 lbs/ft^3; Crush Strength approx. 35 psi
Barrier - 36" high x 66" wide x 20' long
Surrounded by 16 gage Sheet Steel

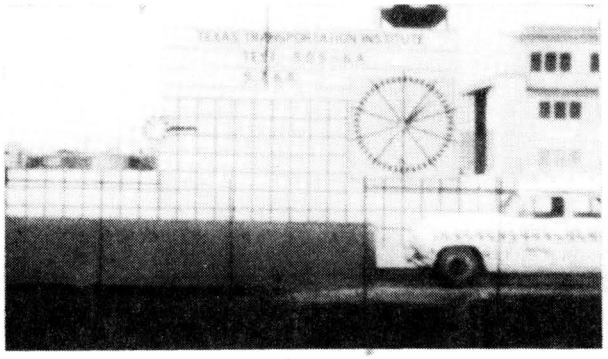

1

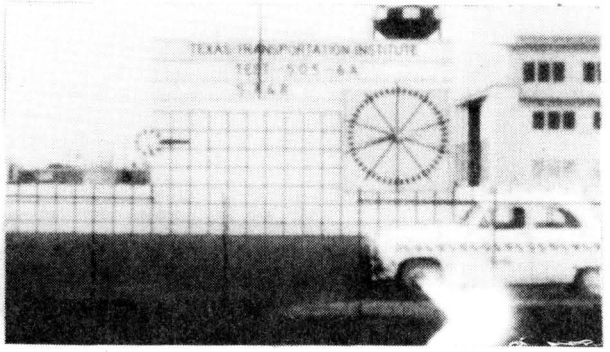

2

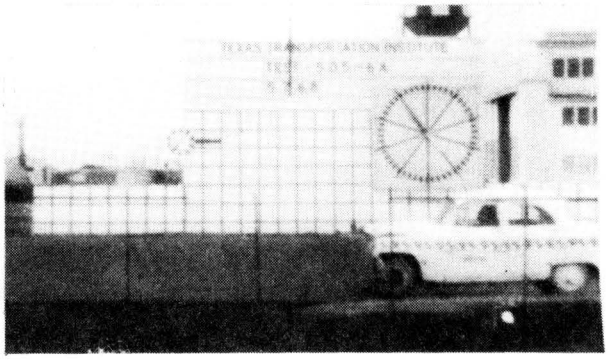

3

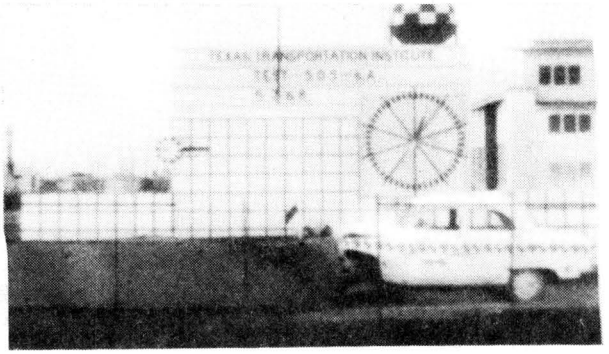

4

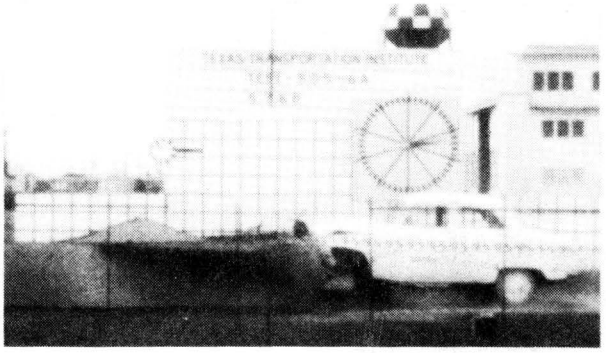

5

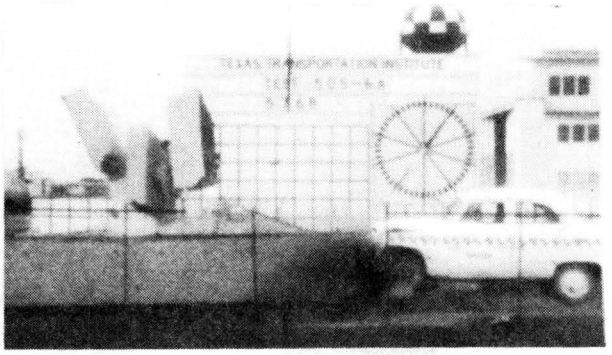

6

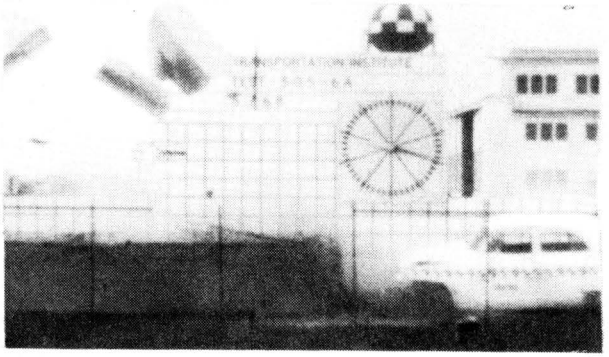

7

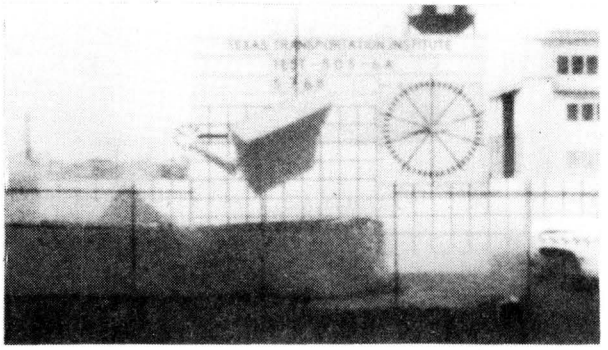

8

Figure 3, Sequential Photographs of Test 505-6A.

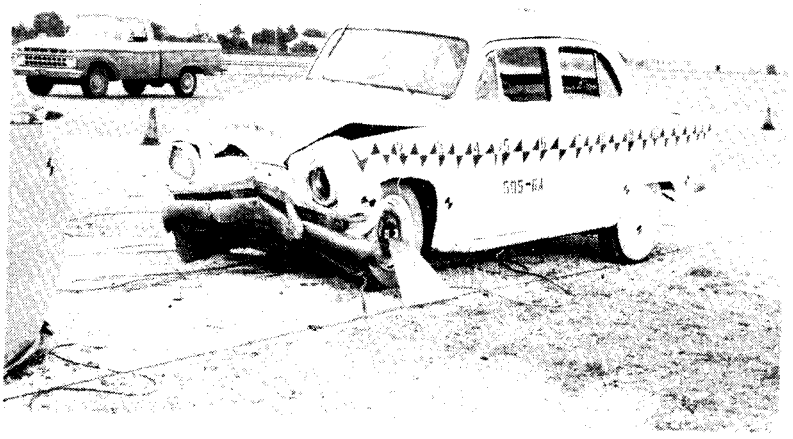

Figure 4, Vehicle After Test 505-6A.

Vehicle Deformation - 1.24 ft.
Stopping Distance - 4.0 ft.

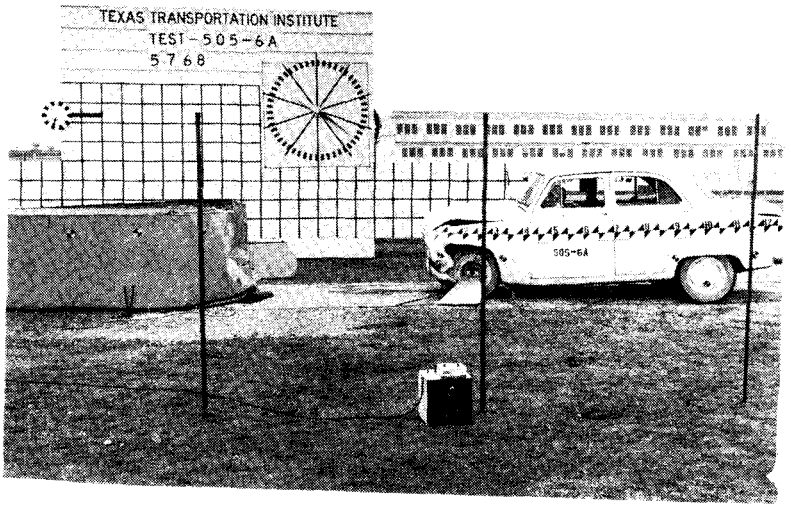

Figure 5, Vehicle and Barrier After Test 505-6A.

Initial Velocity = 70.6 ft/sec = 48.1 mph
Average Deceleration = 19.4 g's

Stopping Distance = 4.0 ft.
Stopping Time = 0.119 sec.

DESCRIPTION OF TEST

A 1959 Simca 4-door sedan weighing 2060 pounds was directed into the barrier head on (along the barrier's longitudinal axis) with an initial speed of 48.1 mph. The vehicle was accelerated under its own power, and directional control was by means of a cable guidance device attached to the left front wheel (see Figure 1).

Two Hycam high speed cameras, operated at 500 frames per second, recorded the test for subsequent time-displacement analysis (Table 1B). In addition, a 128 frame per second Bell & Howell camera and a Bolex 24 frame per second camera provided qualitative photographic data.

Longitudinal vehicle deceleration was recorded from two CEC accelerometer transducers attached to the vehicle's frame, one in front of and one behind the transverse vertical plane through the center of mass. Figure 2B is a reproduction of the traces obtained from these devices.

An Alderson articulated anthropometric dummy weighing 161 pounds was used to simulate a human driver. The dummy, which was secured by a seat belt anchored to a Strainsert strain gage, was equipped internally with three Statham accelerometers mounted orthogonally. Due to an equipment malfunction, the only interpretable data was from the accelerometer mounted sternumward in the dummy. This data is shown in Figure 3B.

A stadia board was mounted on the vehicle to facilitate photographic displacement measurements.

DISCUSSION

A summary of test data is shown in Table 1. The initial energy of the vehicle was 159 kip-ft. The vehicle was stopped four feet after impact, resulting in an average deceleration of 19.4 g's.

The barrier was deformed about 2.75 feet, while the vehicle deformed about 1.25 feet. Precise measurement of the magnitude of deformation in the two bodies was difficult because the deformations were not confined to a plane perpendicular to the direction of motion. However, the damage to the front of the vehicle, as shown in Figure 4, is considered severe. The vehicle's steering wheel was bent by the upper portion of the dummy.

During the collision the vehicle's wheels lost contact with the ground, and the front portion of the barrier was slightly lifted. The wooden post in the barrier at the point of impact was completely severed, while four other posts were displaced by varying amounts. During the test, several large pieces of the polyurethane foam were propelled up and out of the barrier (see Figure 3). The high speed films show that this disintegration occurred just before the vehicle had been brought to a stop, and therefore it is unlikely that it had a significant effect on the outcome of this test.

Figure 6 shows a comparison of the force-displacement curve obtained experimentally from the high speed films with that from the theoretical treatment in Appendix C. A theoretical stopping distance of 4.15 feet compares favorably with the actual stopping distance of 4.0 feet. The

theory is an idealized treatment which neglects the effect of the posts in the barrier. This may partly account for the high estimate. However, in view of the assumptions made in the theoretical treatment, more tests would be required to establish the accuracy of predictions made from the theory.

TABLE 1

SUMMARY OF TEST DATA

Test Number	505-6A
Vehicle Weight	2060 lbs.
Data From High Speed Films:	
Initial Velocity	70.6 ft/sec (48.1 mph)
Initial Kinetic Energy	159 Kip-ft
Stopping Distance*	4.0 ft
Stopping Time	0.119 sec
Average Deceleration	19.4 g's
Vehicle Deformation	1.24 ft
Barrier Deformation	2.75 ft
Data From Electromechanical Devices:	
Average Deceleration	16.0 g's
Stopping Time	0.120 sec

* Defined as the distance the undamaged portions of the vehicle travel forward after impact.

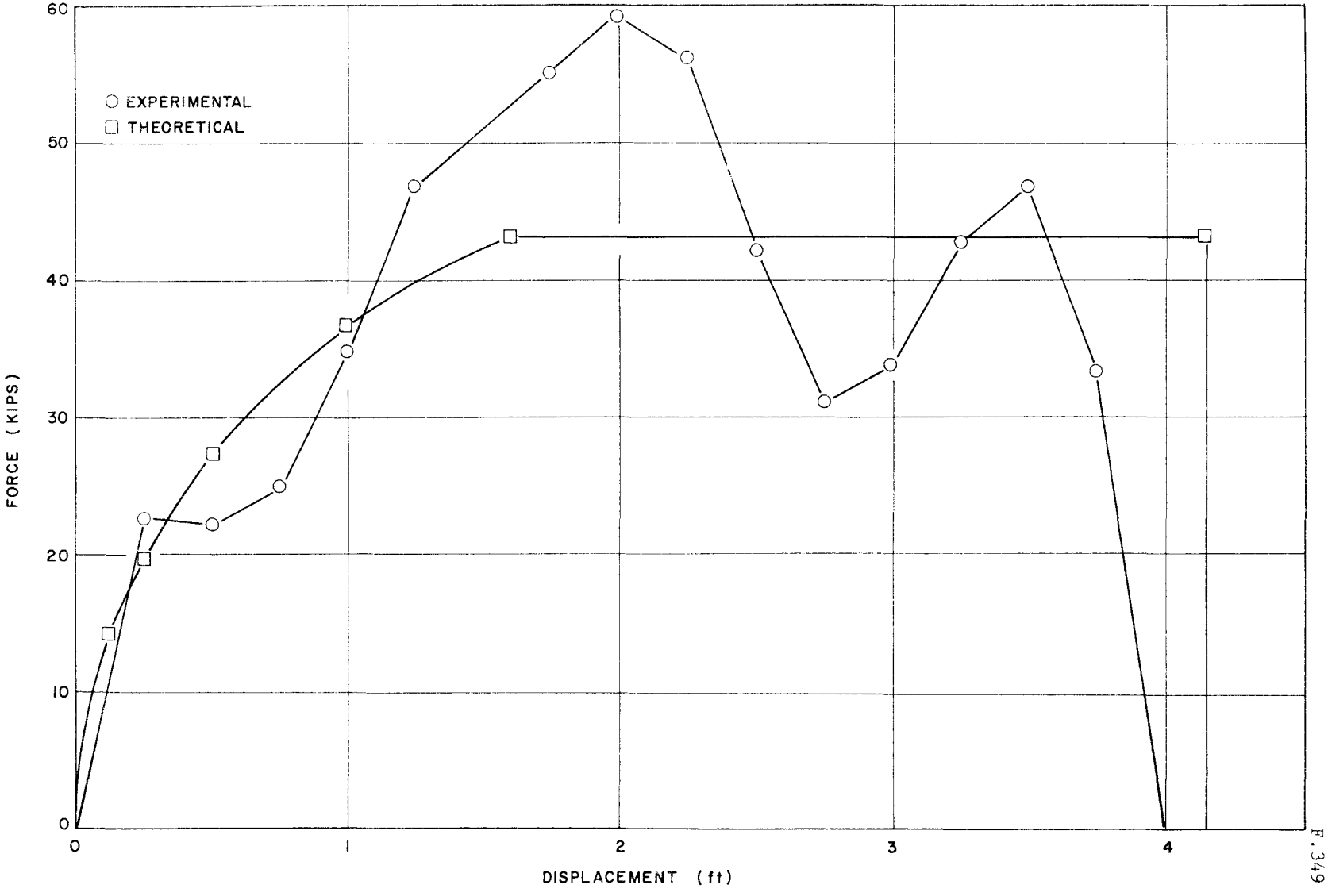

FIGURE 6, EXPERIMENTAL AND THEORETICAL FORCE-DISPLACEMENT CURVES FOR TEST 505-6A

CONCLUSIONS

This particular barrier design was not satisfactory, especially for light vehicles, due to the excessive stopping force and consequently high deceleration levels that it produces. The post at the nose of the barrier seems to contribute significantly to the damage sustained by the vehicle, since the force exerted by the post is concentrated on a small area of the vehicle's front end.

The authors believe that certain modifications to this type of barrier could result in an adequate impact attenuator. The following modifications should be considered:

1. Decrease the strength of the barrier by decreasing the strength of the polyurethane foam, reducing frontal area of the foam, or by incorporating voids in the barrier. The latter approach has been used on masonry attenuators by inserting vertical cylindrical cardboard tubes of appropriate diameters to form the voids.
2. Omit the stabilizing posts and use a cable anchorage system. This would remove the semi-rigid areas from the periphery of the barrier. The cable system should provide the barrier with lateral stability for side or angled impacts, but have little effect on the longitudinal properties of the barrier.
3. Pour the polyurethane foam continuously using the sheet steel covering as the form. This should reduce or eliminate the tendency for large blocks to fly out during impact.
4. Elevate the barrier, or increase its overall height, to reduce the tendency of the vehicle to "ramp" during head-on collisions.

The following are possible advantages of using this type of barrier:

1. The barrier could be simply and quickly fabricated or repaired *in situ*; or it could be fabricated elsewhere and then moved to the desired site in one or more pieces.
2. The barrier would be very light (2 lbs/ft^3 or less) which decreases the initial deceleration of the vehicle due to barrier inertia.
3. The sides of the barrier are flat, reducing the tendency of a glancing vehicle to pocket into the barrier.
4. The barrier could be easily molded into any shape consistent with the geometrical limitations of the site.
5. The polyurethane foam is not subject to corrosion.

A P P E N D I X A

Design Data For Polyurethane Foam Impact Attenuation Barrier

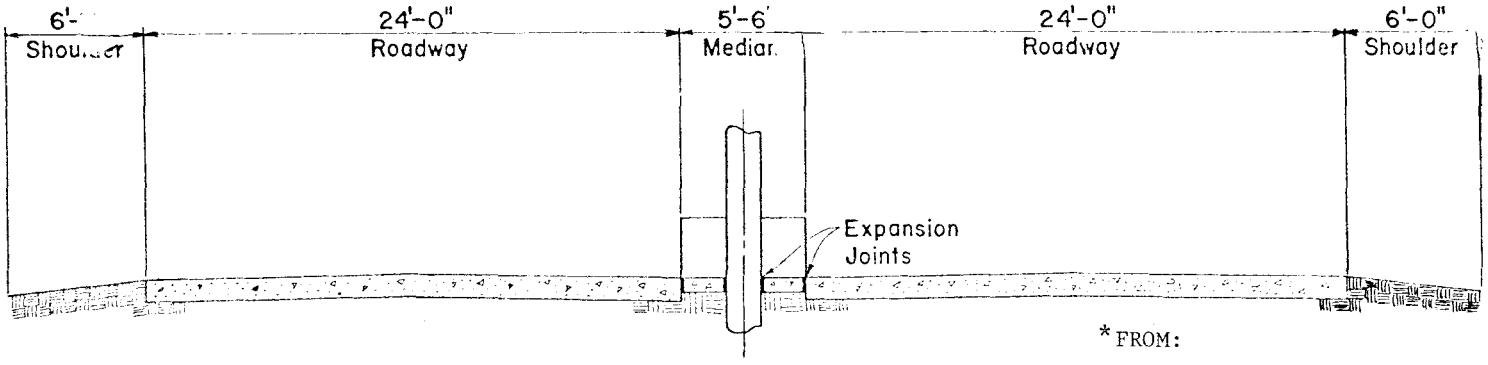

MEDIAN SECTION

Scale: 1/4" = 1'-0"

*FROM:

"Highway Sign Support Structures--Volume 3", Final Report, Texas Transportation Institute, Texas A&M University, January 1967.

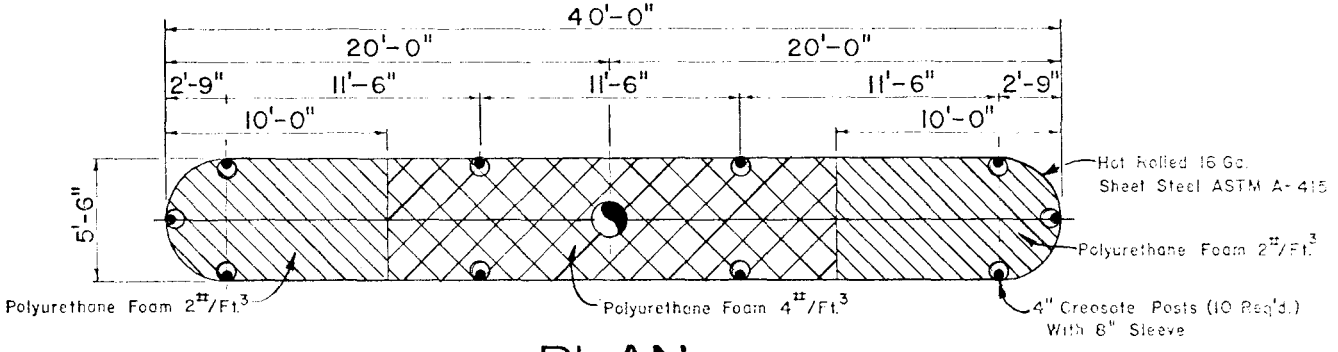

PLAN

Scale: 1/4" = 1'-0"

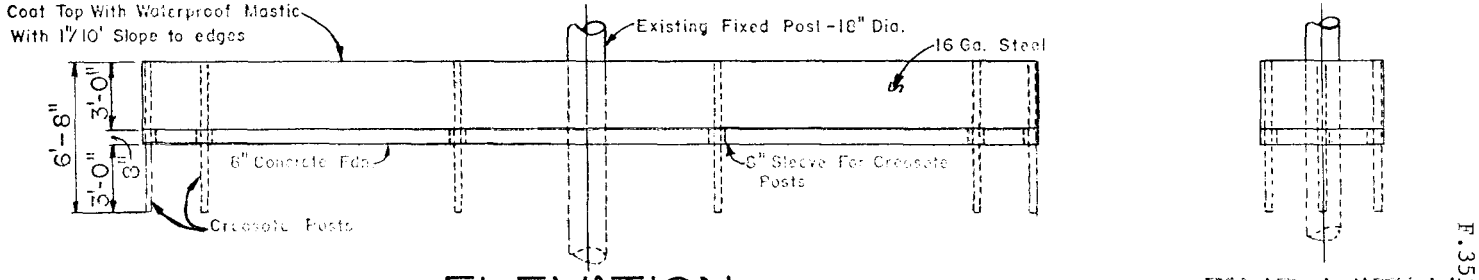

ELEVATION

Scale: 1/4" = 1'-0"

END VIEW

Scale: 1/4" = 1'-0"

* FIGURE IA DETAILS OF POLYURETHANE FOAM BARRIER

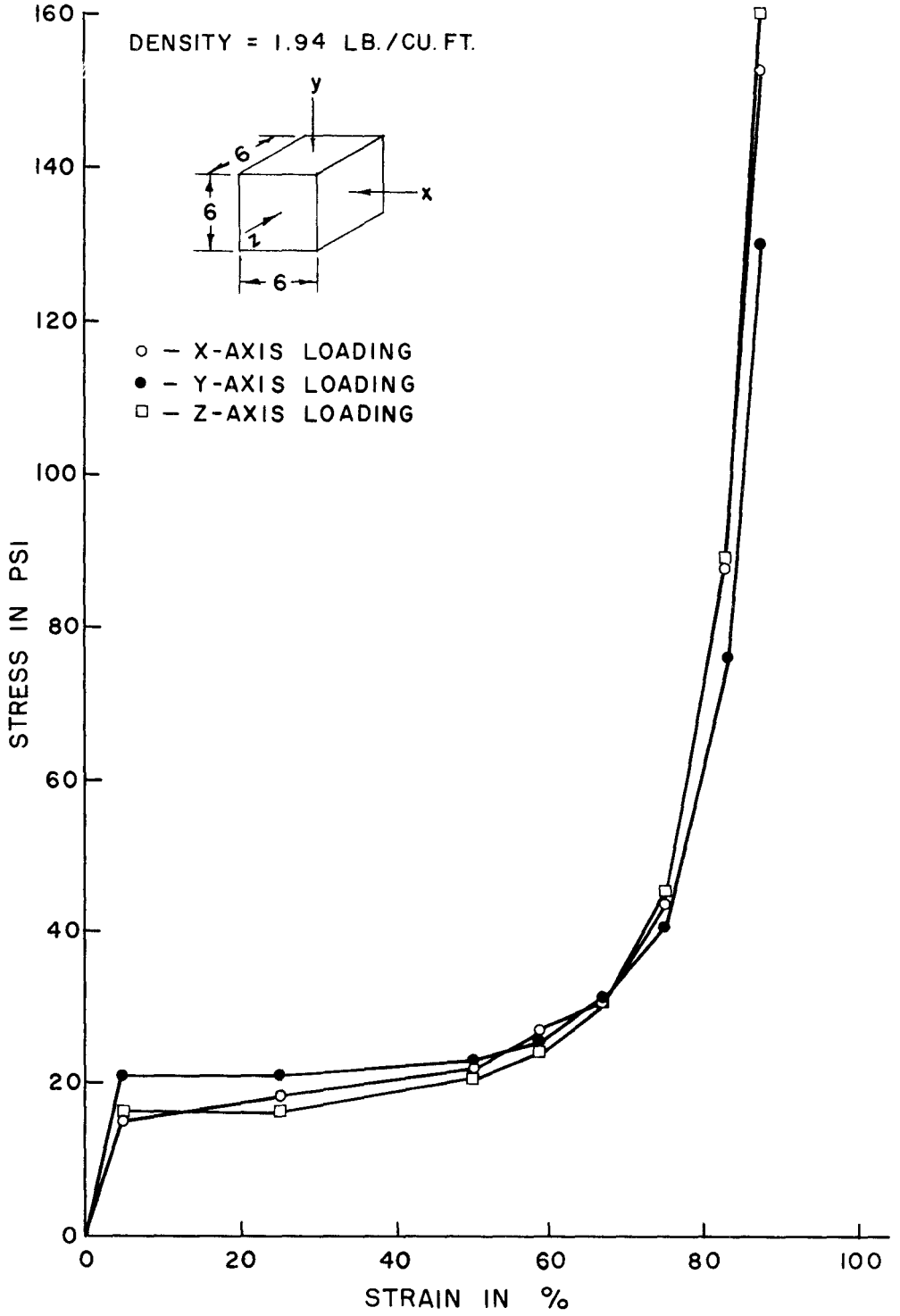

FIGURE 2A STRESS-STRAIN CURVES FOR POLYURETHANE FOAM USED IN FRONT HALF OF BARRIER

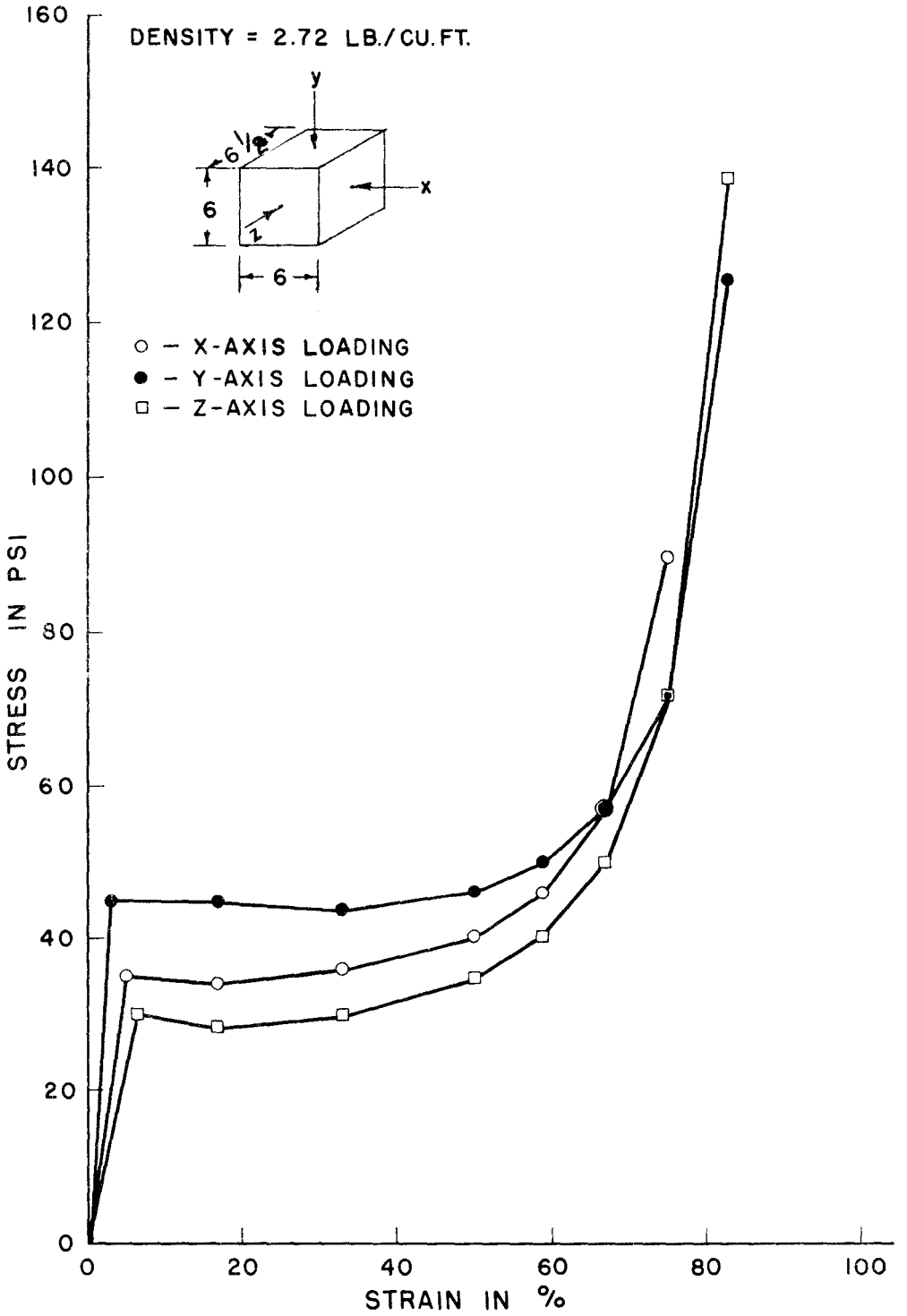

FIGURE 3A STRESS-STRAIN CURVES FOR POLYURETHANE FOAM USED IN REAR HALF OF BARRIER

A P P E N D I X B

Photographic and Electromechanical

Test Data

TABLE 1B

HIGH SPEED FILM DATA

Time milliseconds		Displacement ft	Average Velocity ft/sec	
-39.8		-2.81		
			70.6	
-29.8		-2.11		
			70.9	70.6 Avg.
-19.9		-1.40		
			69.3	
-10.0		-0.71		
			71.6	
0	Impact	0		
			68.3	
+10.0		+0.68		
			65.0	
19.9		1.33		
			57.8	
29.8		1.90		
			48.5	
39.8		2.38		
			39.8	
49.8		2.78		
			35.1	
59.7		3.13		
			29.5	
69.6		3.42		
			21.5	
79.6		3.64		
			14.0	
89.6		3.78		
			11.3	
99.5		3.89		
			8.7	
109.4		3.98		
			1.5	
119.4		3.99		
			0	
129.4		3.99		
			-5.0	
139.3		3.94		
			-5.0	
149.2		3.89		
			-7.1	
169.2		3.75		
			-8.2	
179.1		3.67		
			-9.2	
189.0		3.58		
			-8.7	
199.0		3.49		

(Rebounds total of 7.5 feet)

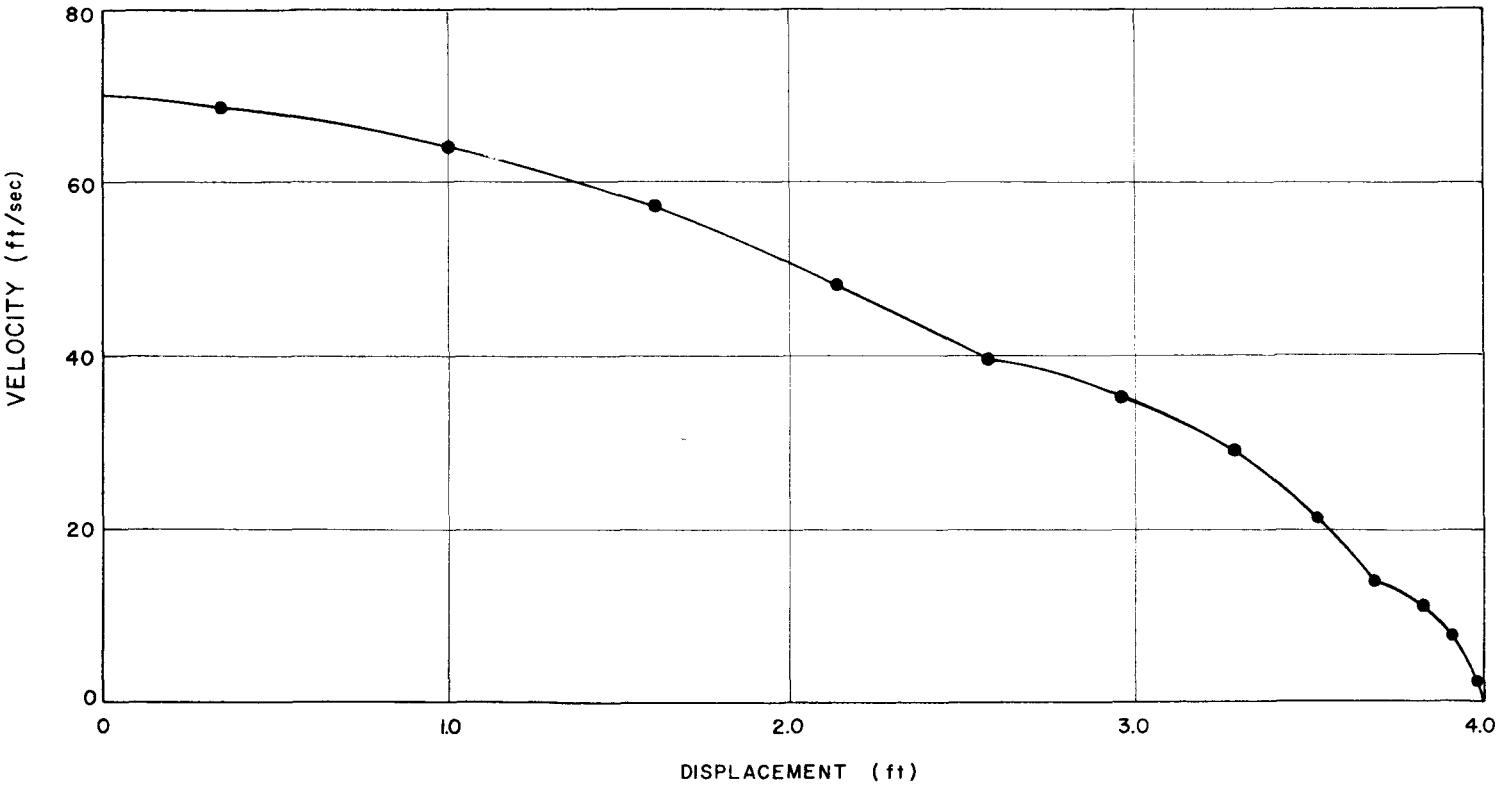

FIGURE 1B, VELOCITY–DISPLACEMENT CURVE FOR TEST 505–6A

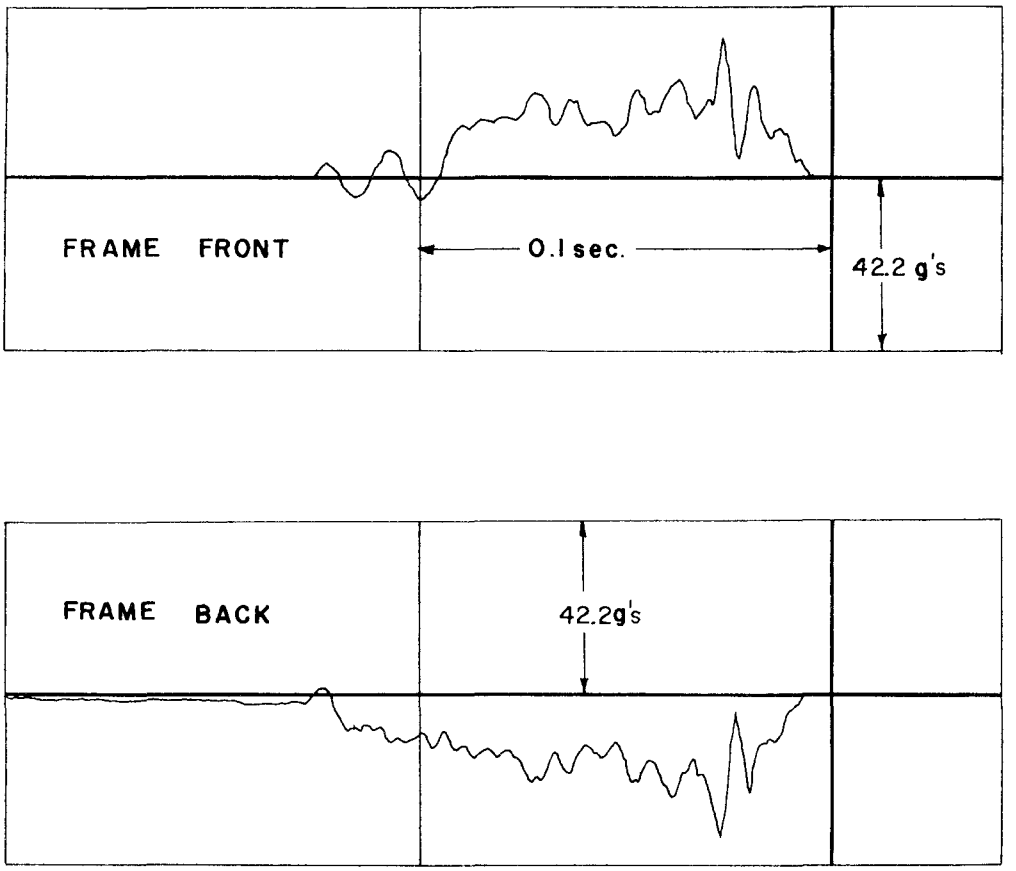

FIGURE 2B TEST 505-6A FRAME ACCELEROMETER DATA

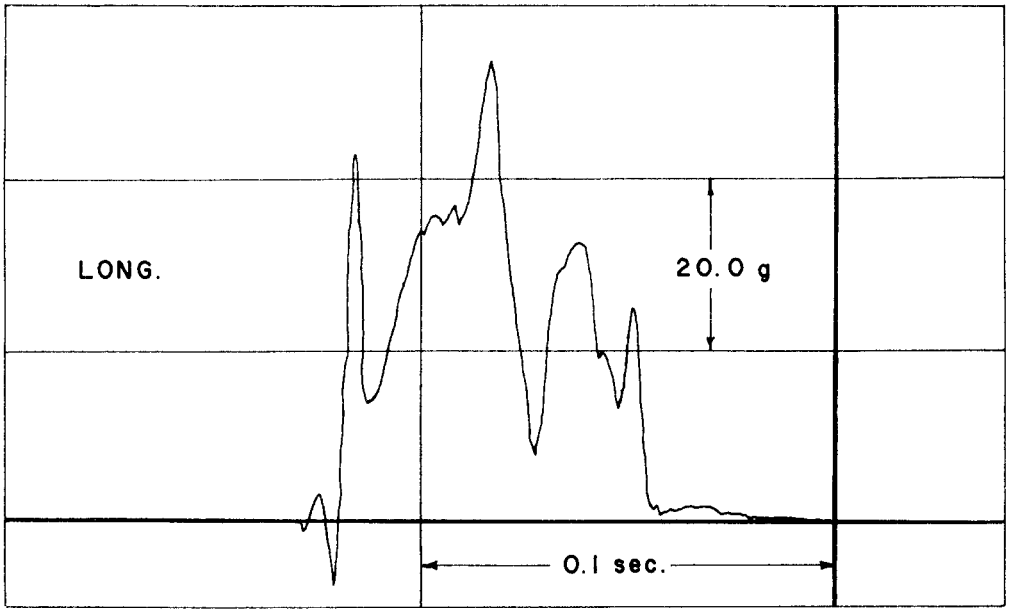

FIGURE 3B TEST 505 - 6A
DUMMY ACCELEROMETER DATA

A P P E N D I X C

Idealized Theory
Used in Predicting Stopping Distance
For Head-On Impact

IDEALIZED THEORETICAL CALCULATIONS FOR HEAD-ON COLLISIONS WITH POLYURETHANE FOAM IMPACT ATTENUATION BARRIER

First, some approximations will be made to simplify the calculations. Keep in mind that these approximations do not represent real events, but may permit predictions of acceptable accuracy.

Simplifying approximations:

1. The vehicle-barrier interface is a plane rectangle of height, h, perpendicular to the direction of motion.
2. The rectangular interface attains a maximum width, d, the width of the vehicle.
3. The crush strength of the barrier is the average stress of the polyurethane foam up to a strain of about 50%, taken from Figure 2A. (Assuming the foam is deformed 50% or less.)
4. The sheet steel covering and the stabilizing posts are neglected in the calculations.
5. The inertia forces required to accelerate and decelerate the foam and covering are neglected.

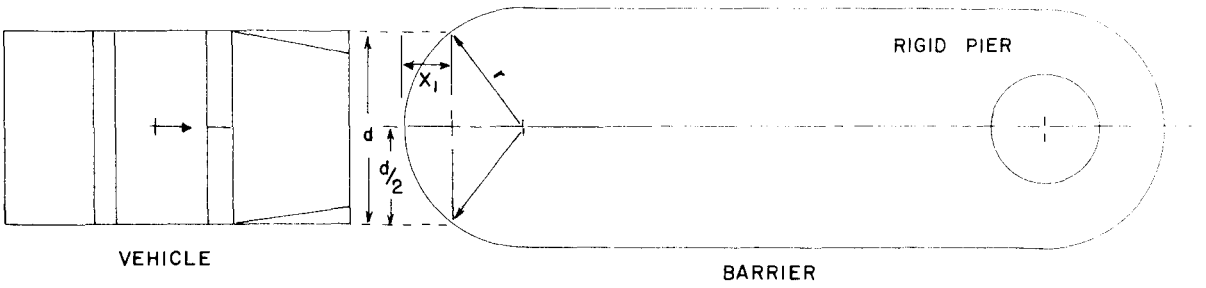

d = Width of vehicle, ft.

r = Radius of curvature of barrier nose. ft

h = Height of barrier, ft.

X = Penetration from ititial contact, ft.

X_1= Penetration when barrier contacts all of vehicle's nose, ft.

X max = Maximum penetration (stopping distance), ft.

S = Crush strength of polyurethane foam being crushed, Kips/ft^2.

F_x = Restraining force on vehicle, Kips.

E_1 = Energy absorbed up to penetration of X_1, Kip-ft.

E_2 = Energy absorbed from X_1 to X, Kip - ft.

$E = E_1 + E_{2_{max}}$ = Total energy absorbed, Kip-ft.

W = Weight of vehicle, Kip.

V = Initial velocity of vehicle, ft/sec.

g = Acceleration due to gravity, 32.2 ft/sec^2.

When $X < X_1$, $\left(X_1 = r - \sqrt{r^2 - \frac{d^2}{4}}\right)$

Area of interface = $A = 2h\sqrt{r^2 - (r - X)^2} = 2h\sqrt{2rX - X^2}$

When $X \geqslant X_1$,

$A = dh$

Force = (stress)(area) = SA

(1) $F_x = 2Sh\sqrt{2rX - X^2}$, for $X < r - \sqrt{r^2 - \frac{d^2}{4}}$

$= Shd$, for $X \geqslant r - \sqrt{r^2 - \frac{d^2}{4}}$

If $X_{max} > X_1$, the energy absorbed is:

(2) $E = E_1 + E_2$

where

(3) $E_1 = \int_0^{X_1} F_x \, dX = 2Sh \int_0^{r - \sqrt{r^2 - \frac{d^2}{4}}} \sqrt{2rX - X^2} \, dX$

and

(4) $E_2 = F_x (X - X_1) = Shd \left(X - r + \sqrt{r^2 - \frac{d^2}{4}}\right)$

(We have assumed that $2r \geqslant d$.)

$E_{2_{max}} = Shd \left(X_{max} - r + \sqrt{r^2 - \frac{d^2}{4}}\right)$

Integrating the right side of Equation 3,

$$E_1 = 2Sh\int_0^{X_1} (2rX - X^2)^{1/2}\, dX = 2Sh\int_0^{X_1} \left[r^2 - (X - r)^2\right]^{1/2} dX$$

$$= 2Shr\int_0^{X_1} \left[1 - \left(\frac{X - r}{r}\right)^2\right]^{1/2} dX$$

Let $\left(\frac{X - r}{r}\right) = \cos\theta$, then $\left[1 - \left(\frac{X - r}{r}\right)^2\right]^{1/2} = \sin\theta$

and $X = r(\cos\theta + 1)$, $dX = -r\sin\theta\, d\theta$

Putting these values in the equation,

$$E_1 = -2Shr^2\int_0^{X_1} \sin^2\theta\, d\theta = -Shr^2\int_0^{X_1} (1 - \cos 2\theta)\, d\theta$$

$$= -Shr^2\left[\theta - \frac{1}{2}\sin 2\theta\right]_0^{X_1} = Shr^2\left[\sin\theta\cos\theta - \theta\right]_0^{X_1}$$

But $\cos\theta = \left(\frac{X - r}{r}\right)$ and $\sin\theta = \frac{\sqrt{r^2 - (X - r)^2}}{r} = \frac{\sqrt{2rX - X^2}}{r}$

So

$$E_1 = Shr^2\left[\left(\frac{X - r}{r^2}\right)\sqrt{2rX - X^2} - \cos^{-1}\left(\frac{X - r}{r}\right)\right]_0^{X_1}$$

$$= Sh\left[(X - r)\sqrt{2rX - X^2} - r^2\cos^{-1}\left(\frac{X - r}{r}\right)\right]_0^{r - \sqrt{r^2 - \frac{d^2}{4}}}$$

Putting in the limits and simplifying,

$$(5) \qquad E_1 = Sh\left[r^2 \cos^{-1}\left(\frac{\sqrt{r^2 - \frac{d^2}{4}}}{r}\right) - \frac{d}{2}\sqrt{r^2 - \frac{d^2}{4}}\right]$$

Combining Equations 4 and 5, we have an expression for the total energy absorbed as a function of X. (for $X > r - \sqrt{r^2 - \frac{d^2}{4}}$)

$$(6) \qquad E = E_1 + E_2 = Sh\left[r^2 \cos^{-1}\left(\frac{\sqrt{r^2 - \frac{d^2}{4}}}{r}\right) - \frac{d}{2}\sqrt{r^2 - \frac{d^2}{4}} + d\left(X - r + \sqrt{r^2 - \frac{d^2}{4}}\right)\right]$$

The energy absorbed for $X \leq r - \sqrt{r^2 - \frac{d^2}{4}}$, as a function of X, is:

$$(7) \qquad E = Sh\left((X - r)\sqrt{2rX - X^2} - r^2 \cos^{-1}\left(\frac{X - r}{r}\right)\right)$$

The theoretical stopping distance of a vehicle in head-on impact can be calculated from the initial kinetic energy as follows (for $X_{max} > r - \sqrt{r^2 - \frac{d^2}{4}}$)

$$\frac{WV^2}{2g} = KE = E = E_1 + E_{2_{max}} = Sh\left(r^2 \cos^{-1}\left(\frac{\sqrt{r^2 - \frac{d^2}{4}}}{r}\right) - \frac{d}{2}\sqrt{r^2 - \frac{d^2}{4}}\right) +$$

$$Shd\left(X_{max} - r + \sqrt{r^2 - \frac{d^2}{4}}\right)$$

or, solving for X_{max},

$$(8) \qquad X_{max} = \frac{\frac{WV^2}{2gSh} - \left[r^2 \cos^{-1}\left(\frac{\sqrt{r^2 - \frac{d^2}{4}}}{r}\right) - \frac{d}{2}\sqrt{r^2 - \frac{d^2}{4}}\right]}{d} + r - \sqrt{r^2 - \frac{d^2}{4}}$$

For Test 505-6A,

$W = 2.06$ kips

$V = 70.6$ ft/sec

$S = 3.88$ kip/ft^2

$r = 2.75$ ft

$d = 5.0$ ft

$h = 3.0$ ft

$$X_{max} = \frac{\frac{(2.06)(70.6)^2}{(2)(32.2)(2.88)(3.0)} - \left[(2.75)^2 \cos^{-1}(0.415) - 2.5(1.14)\right]}{5.0} + 2.75 - 1.14$$

$$= \frac{18.4 - 8.62 + 2.85}{5.0} + 1.61 = 4.15 \text{ ft.}$$

The stopping distance determined experimentally is

X_{max} (Experimental) = 3.99 ft.

The barrier itself did not deform 3.99 ft., but rather 3.99 ft. minus vehicle deformation. However, the barrier is assumed to exert its estimated force during vehicle deformation. For large penetrations, the vehicle deformation should become a much smaller fraction of the total travel.

TECHNICAL MEMORANDUM 505-7

Texas Transportation Institute
Texas A&M Research Foundation

THE EFFECT OF VEHICLE COLLISION WITH ALUMINUM ROADSIDE SIGN STRUCTURES MOUNTED ON FRANGIBLE BASES

A Test and Evaluation Report on Contract No. CPR-11-5851
U.S. Department of Transportation
Federal Highway Administration
Bureau of Public Roads

by

J. E. Martinez
Assistant Research Engineer

T. J. Hirsch
Research Engineer

Yuce Baskurt
Research Assistant

and

J. J. Jumper
Research Assistant

This memorandum presents the results of the mathematical simulation of vehicle collision with aluminum roadside sign structures mounted on frangible bases. This work was conducted under the Office of Research and Development, Structures and Applied Mechanics Division, Research Program on Structural Systems in Support of Highway Safety (4S Program). The opinions, findings, and conclusions expressed in this report are those of the authors and not necessarily those of the Bureau of Public Roads.

January 9, 1970

THE EFFECT OF VEHICLE COLLISION WITH ALUMINUM ROADSIDE SIGN STRUCTURES MOUNTED ON FRANGIBLE BASES

INTRODUCTION

An efficient modern highway requires having roadway signs that relay information to the motorist in a clear and concise manner, and current highway design concepts for multilane facilities have resulted in the installation of sign supports near the edge of the traffic lane. Due to their location, these signs constitute a safety hazard, and collisions with these signs have caused serious injury and fatalities.

An obvious solution to the problem is relocation of the support. This approach is sometimes not feasible, and the engineer must resort to other means to alleviate the dilemma. A design that has already shown considerable merit is the slip base type breakaway support that, upon impact, disengages the post from the foundation. This generally accepted design limits impact forces, but regard must be given to the possibility of the structure falling on the vehicle and creating a hazardous secondary situation for the vehicle occupants.

The purpose of this investigation was to evaluate the crash-dynamic behavior of various aluminum sign post structure configurations mounted on frangible bases having different impact characteristics. The base force-deformation behavior was obtained from laboratory pendulum tests performed by the Texas Transportation Institute, and the results used in the study are presented in the Appendix. The dynamic response of the vehicle and the structure was obtained with the aid of a mathematical model.

DESCRIPTION OF SIGN POST STRUCTURE

The aluminum signs and sign support configurations evaluated in this study are typical of roadside sign structures proposed by the State of Maine. These structures are depicted in Figs. 1 and 2 and the complete post and sign description is given in Table 1.

In the mathematical simulation it was assumed that the frangible bases deform by the amounts indicated in Figs. 3-6. These deformations were obtained from accelerometer test data and represent the distance the impacting ram used in the base fracture test moved after initial contact with the base. This force-deformation idealization makes the peak forces encountered in the larger bases quite great since the energy for all bases must be dissipated for a relatively small value of base deformation. The idealized curves also shown in Figs. 3-6 represent the same base fracture energy as the experimental curves and were necessary to obtain the input to the computer coding which assumes a piecewise linear variation of base shear force.

MATHEMATICAL SIMULATION

Two mathematical models were employed in the study. The model that yields the dynamic response of the single support structure assumes four degrees of freedom and is basically a planer version of the three-dimensional model that was employed in the analysis of luminaire support structures.*(1)* This more recent model was coded in order to reduce the computer time associated with the solution of a problem. A Runge-Kutta numerical integration scheme*(2)* has also been added, making the program more efficient.

The model used to predict the behavior of the dual support structure assumes two degrees of freedom and idealizes the structure as being hinged at the center of the sign and capable of having only a rotation about this point. The effects of the sign and the support that is not impacted are lumped into a torsional spring constant as shown in Fig. 2.

The vehicle is represented as a single-degree-of-freedom spring-mass system having a spring of variable stiffness. The rigid mass and its velocity simulate the momentum of the vehicle and the energy absorbed is determined from the spring force-deformation relationship. In the study it was assumed that the spring constant was a function of the vehicle weight. The collisions were considered to take place for a vehicle approach angle of zero.

VERIFICATION OF MATHEMATICAL MODEL

In order to verify the mathematical models, a full-scale crash test was performed at the Texas Transportation Institute Research Annex. The test employed a 1959 Ford sedan weighing 3550 lbs and the sign 1A. The impact velocity was 29 mph. Additional data is given on page 37.

Table 2 and Fig. 7 present a comparison of model and crash test results and indicate good agreement. It is anticipated that the model will predict very satisfactory results for most cases where the peak force encountered in fracturing the base is not extremely large.

DISCUSSION OF RESULTS

Single Support Structures

The study revealed that for impacting velocities up to 45 mph, the single support structure does not clear the vehicle. The sign 1B, being

taller and having a higher mass-center position than the sign 1A, has a greater tendency to clear the vehicle and will probably do so at the higher velocities. Figure 8 shows the response of sign 1B when it is subjected to a 45 mph collision. Collisions by the lightweight (2500 lbs) vehicles traveling at slow speeds (15 mph or less) may be considered hazardous as they cause the support structure to strike the windshield area of the vehicle in a majority of the cases. This is due to the fact that at the slower speeds the post has a greater tendency to translate and ride the front of the vehicle before falling on it. The effect is more pronounced for collisions with the supports mounted on bases having a high base fracture energy.

The results further revealed that a lightweight vehicle traveling at speeds below 15 mph may be stopped when it collides with supports mounted on bases having fracture energies of 10 ft-kips or greater. This large change in velocity may have a severe effect on the vehicle occupants, and such collisions could be interpreted as hazardous.

Collisions that cause the sign post to strike the top of the vehicle will normally not be hazardous unless the structure is quite massive or the contact is made near the windshield area. If contact is initially made in the windshield area, then it is conceivable that, depending upon the rotation of the post, a secondary impact with the hood or windshield by some other point on the post could occur.

Dual Support Structures

The results of the study of dual support structures disclose that, for the cases investigated, only the slow moving vehicle encounters a

secondary collision with the post. This secondary collision occurs in the area of the windshield of the vehicle and may be interpreted as hazardous. The deceleration rates and velocity changes at these slow speeds are less than those obtained for the single support structures impacted at the same velocity. This is due to the dual support structure idealization and the high position of the assumed center or rotation.

Collisions at the higher vehicle velocities cause the post to clear the vehicle. This is due to the large angular velocity that is acquired by the relatively light support as a result of the vehicular impact. The response of sign post structure 1C following impact by a medium size vehicle at various velocities is depicted in Fig. 9.

Comparison

The results presented in the tables in the Appendix show that the impact behavior of signs 1A and 1B is very similar. The higher center of mass of sign 1A gives it more of a tendency to rotate and, as a result, the rotation angle of the structure is greater when it rotates and strikes the vehicle. In general, it can be said that lowering of the center of mass of the structure will give the support more of a tendency to translate horizontally and will increase the vehicular change in velocity.

Signs 1C and 1D behave in much the same manner. The stiffer torsional spring employed for sign 1C gives the structure a greater rotational stiffness and its effect becomes more pronounced for collisions of light vehicles with supports requiring the larger base fracture energies. In the case of a heavier vehicle impacting at a

low velocity the stiffer torsional spring of sign 1C causes the support to encounter a secondary collision in the hood or windshield area, whereas sign 1D has its support strike the top of the vehicle.

A comparison of the single and dual support structures indicates that greater vehicular velocity changes and deceleration rates will be experienced when similar collisions involve the sign employing the single support. This can partially be attributed to the different sign geometric and inertia properties and the constraints imposed on the idealized structure. They produce the effect of causing the single support to stay in longer contact with the vehicle, thus accounting for the larger velocity changes.

GENERAL CONCLUSIONS

The general conclusions stated here will be based on the cases investigated and a criteria that uses a vehicular velocity change of 11 mph as one that causes passenger injury.*(3)*

The conclusions may be summarized as follows:

Single Support Structures

1. Collisions by vehicles traveling up to 45 mph cause the supports investigated to strike the vehicle.
2. Collisions of a light weight vehicle traveling at speeds of approximately 15 mph may cause a hazardous condition[1] when they impact the large diameter support posts. This is based on vehicular velocity changes of approximately 11 mph.
3. Medium and high speed collisions will cause the support to

---

[1] A hazardous condition is interpreted as one that could cause passenger injury.

strike the top or trunk areas of the vehicle. These cases are not usually hazardous.

Dual Support Structures

1. For the cases investigated, velocity changes remain below the criteria established for a hazardous condition.
2. Low speed collisions (15-20 mph) will normally give rise to a secondary collision in the vicinity of the hood or windshield area. However, these collisions are not necessarily hazardous as the post will not come through the windshield after the secondary collision takes place.
3. Medium and high speed collisions cause the post to clear the vehicle and the vehicular velocity changes remain within tolerable limits.

It should be emphasized that the assumption of the post and sign remaining fastened together during impact has been made. If the connections are not rigid enough, it is possible for the post and the sign to detach and possibly create an additional hazard as secondary collisions with both the post and sign would be encountered.

REFERENCES

1. Martinez, J. E. An Investigation of the Impact Behavior of a Rigid Body. Doctoral Dissertation, Department of Mechanical Engineering, Texas A&M University, August, 1967.

2. McCormick, J. M., and Salvadori, M. G. Numerical Methods in Fortran, Prentice-Hall, Inc., Englewood Cliffs, New Jersey, 1964, p. 242.

3. Patrick, L. M., et al., Knee, Chest, and Head Impact Loads. Proceedings of the 11th Stapp Car Crash Conference, Anaheim, California, October 10-11, 1967, p. 116.

APPENDIX

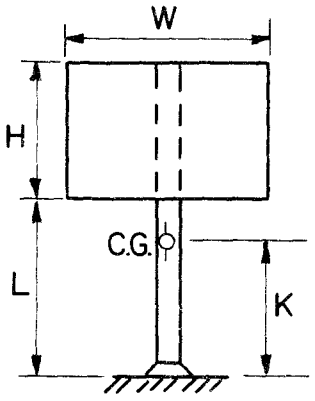

SIGN 1A

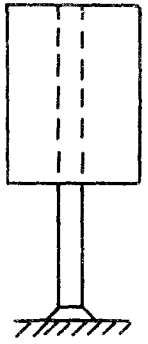

SIGN 1B

SIGN	1A	1B
W (FT.)	6.0	4.0
H (FT.)	5.0	10.0
L (FT.)	7.0	6.0
WEIGHT (LBS.)	93.2	124.0

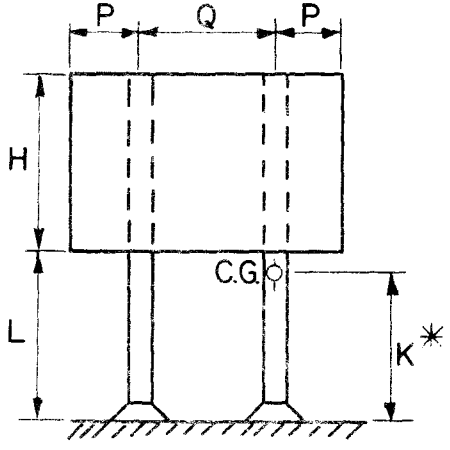

SIGN 1C

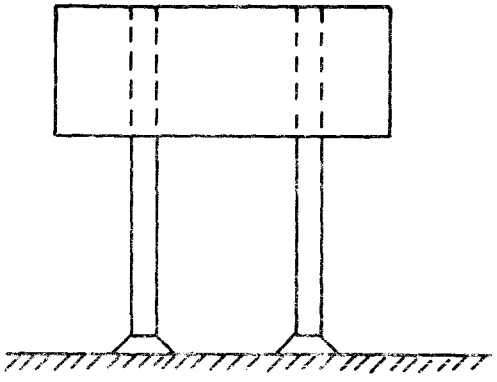

SIGN 1D

SIGN	1C	1D
P (FT.)	2.0	2.5
Q (FT.)	6.0	8.0
H (FT.)	9.0	6.0
L (FT.)	7.0	7.0
WEIGHT* (LBS.)	111.6	93.0

*FOR IDEALIZED SIGN (FIG. 2)

FIGURE 1. SIGN CONFIGURATIONS USED IN STUDY

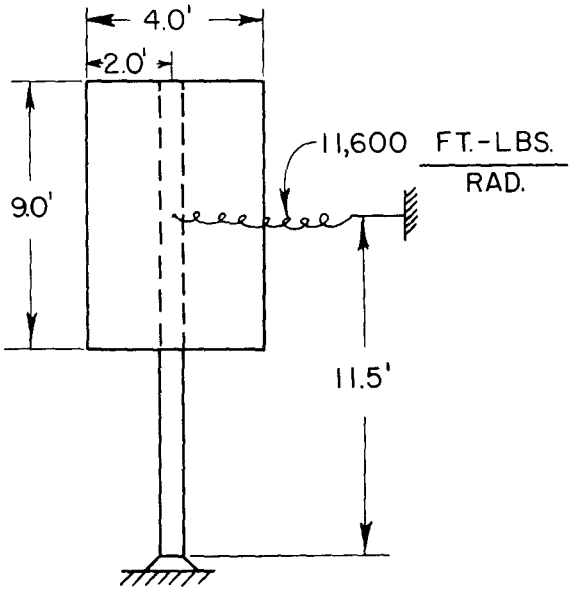

SIGN IC

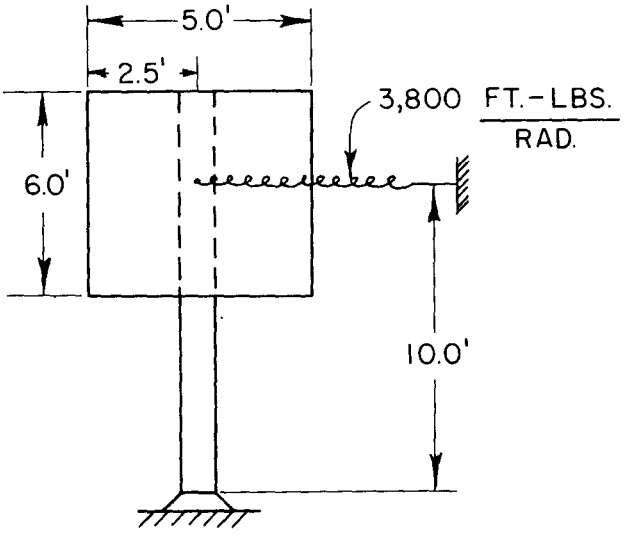

SIGN ID

FIGURE 2. IDEALIZATIONS OF SIGNS IC AND ID

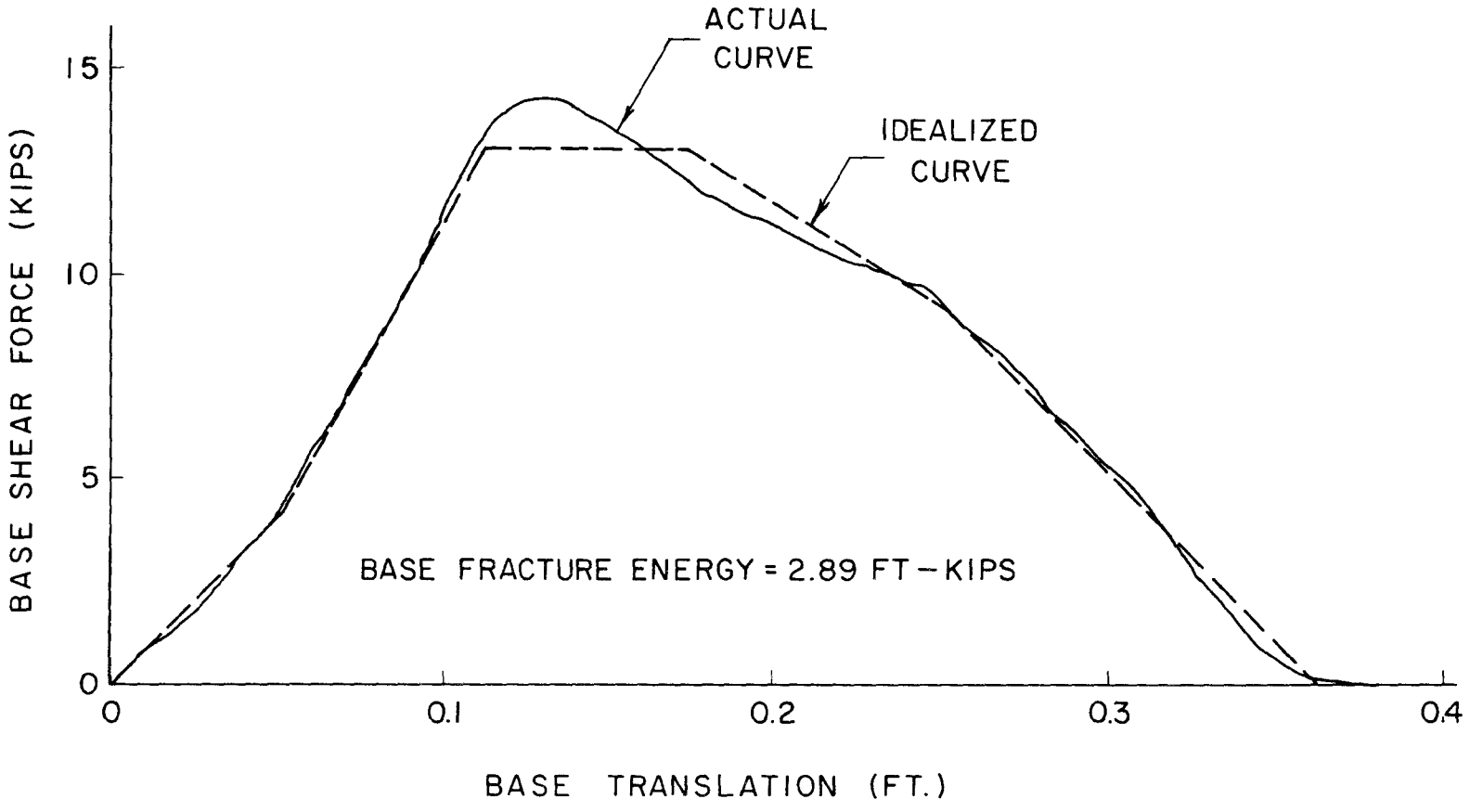

FIGURE 3. BASE FRACTURE ENERGY CURVE FOR 6 "x 3/16" POST

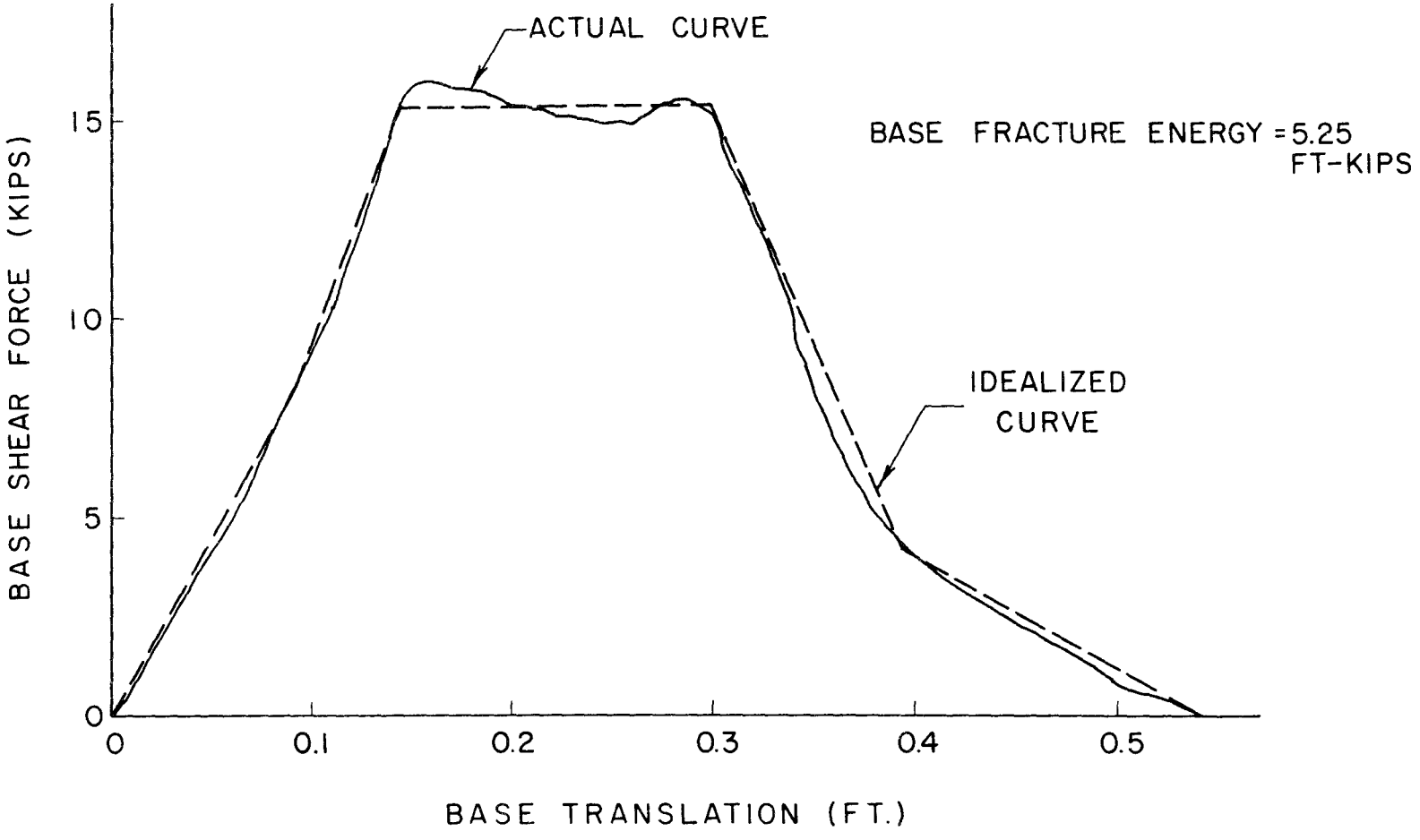

FIGURE 4. BASE FRACTURE ENERGY CURVE FOR 8" x 1/4" POST

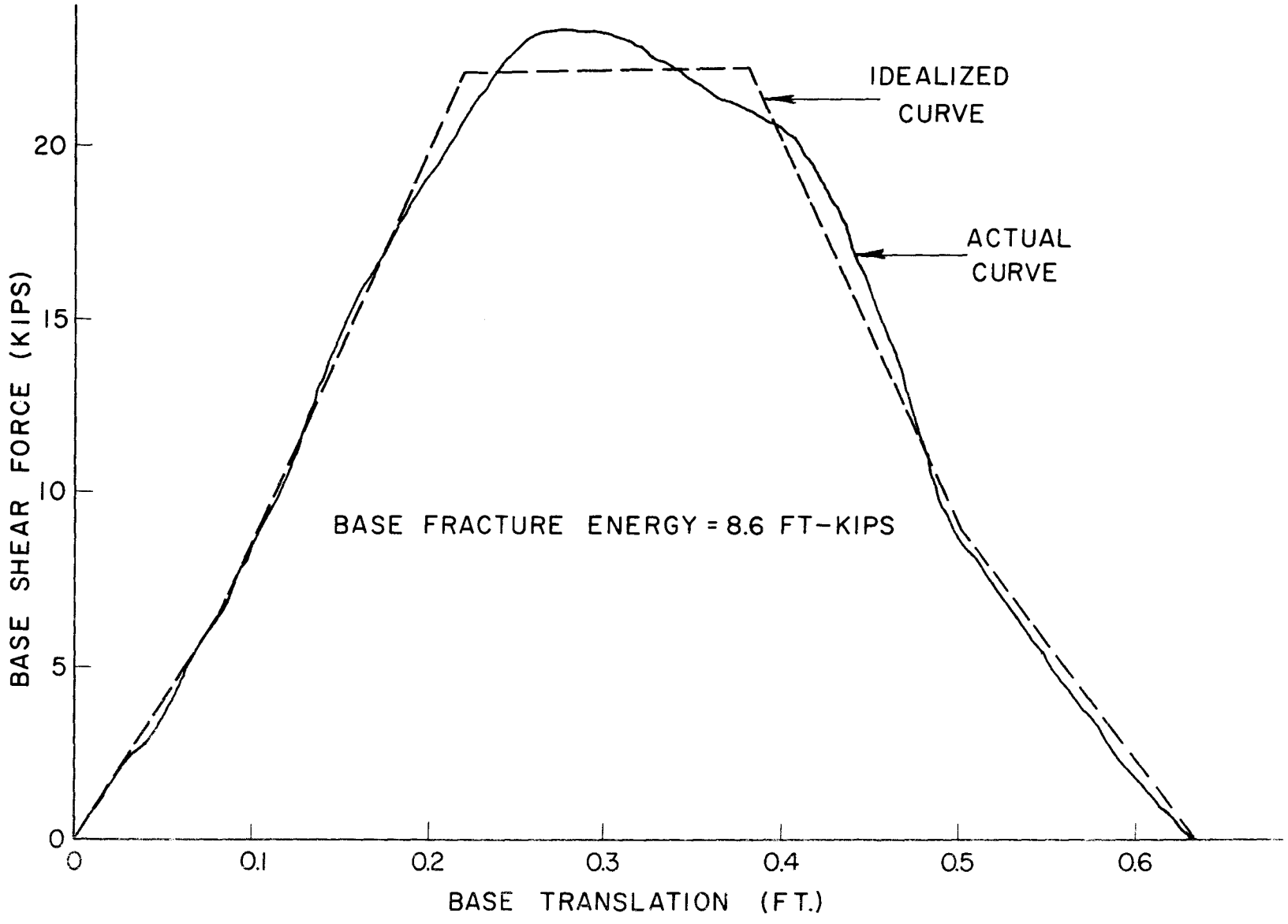

FIGURE 5. BASE FRACTURE ENERGY CURVE FOR 10" x 1/4" POST

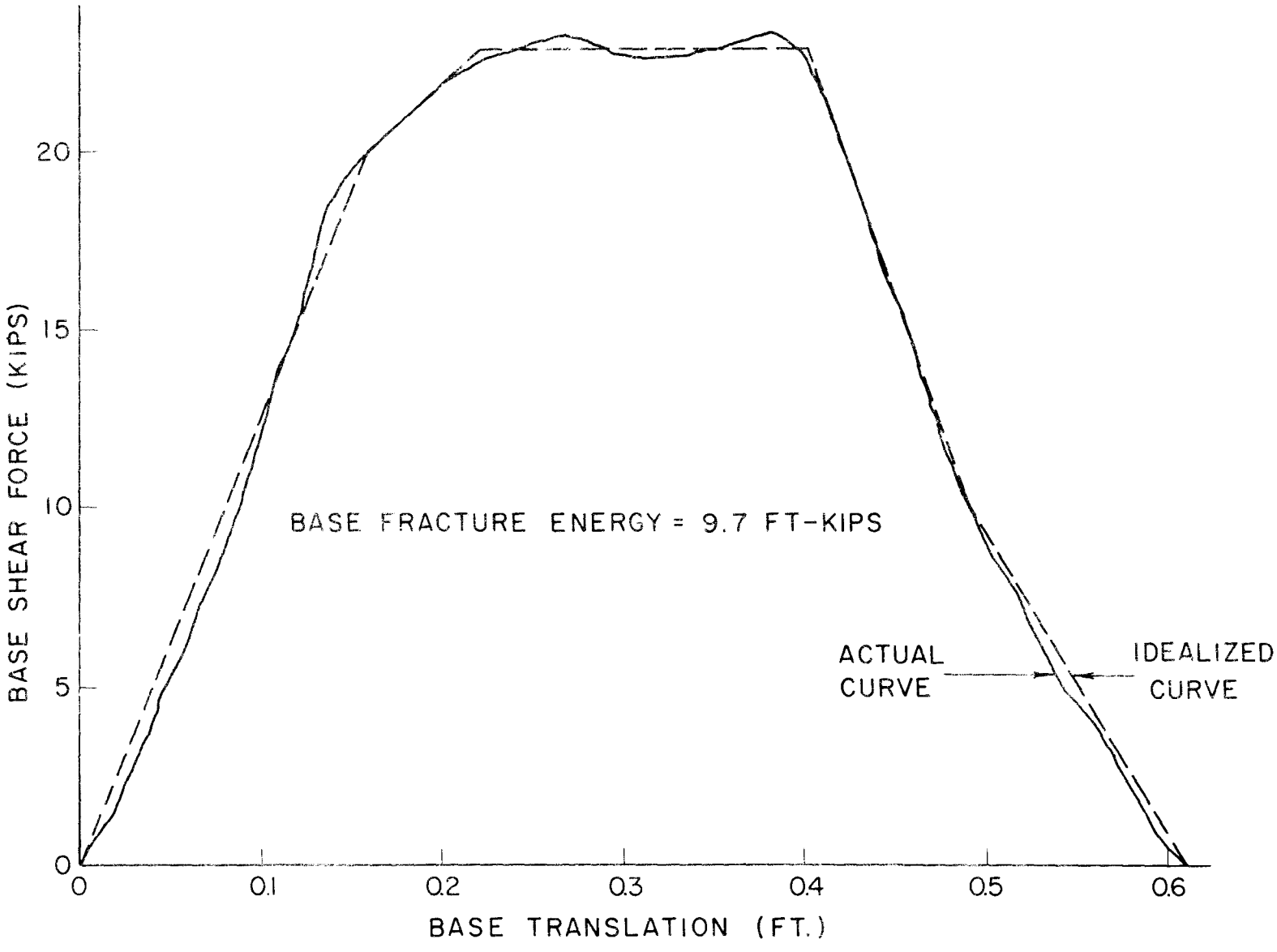

FIGURE 6. BASE FRACTURE ENERGY CURVE FOR 12" x 1/4" POST

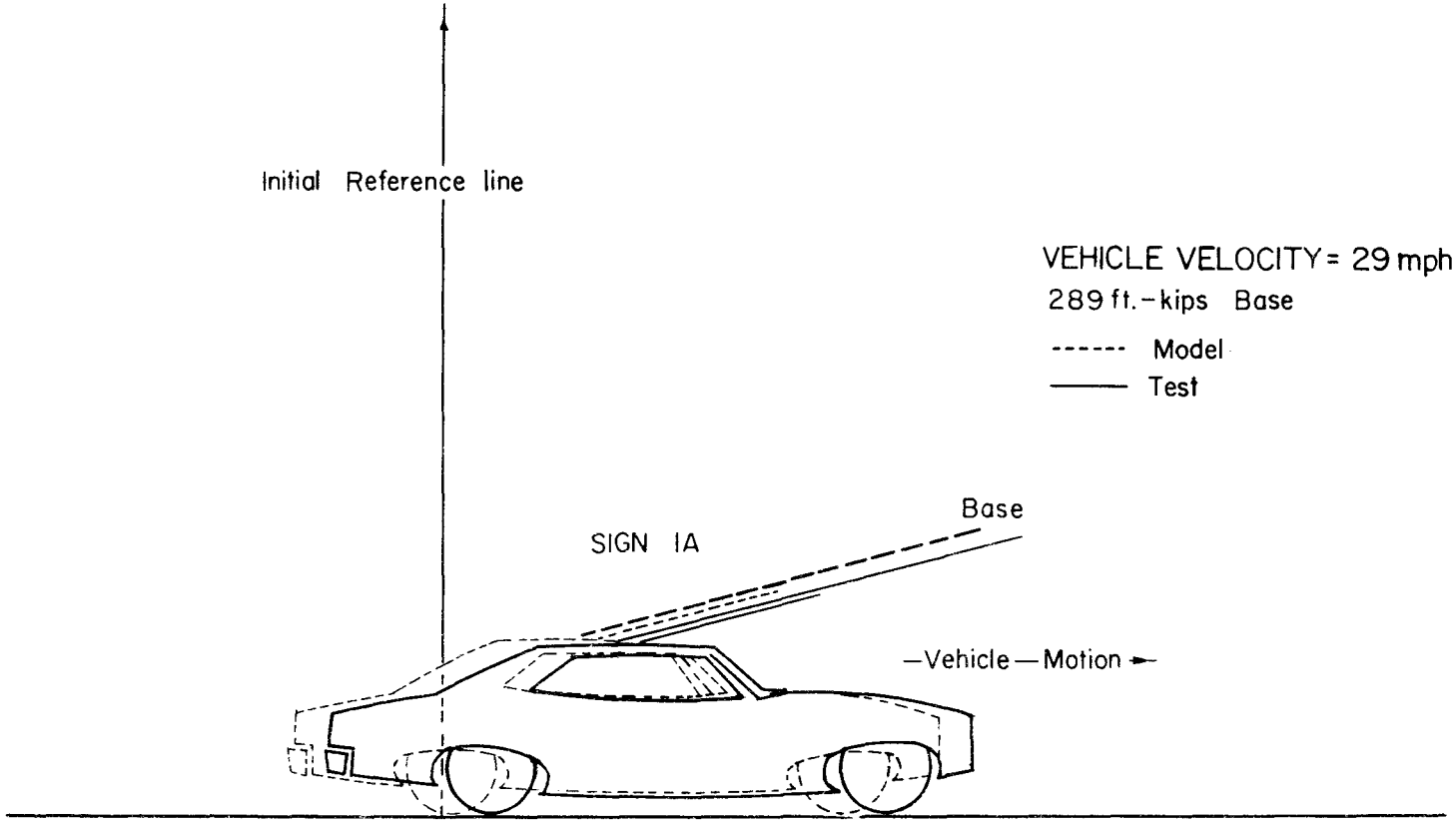

FIGURE 7. COMPARISON OF MODEL AND CRASH TEST RESULTS

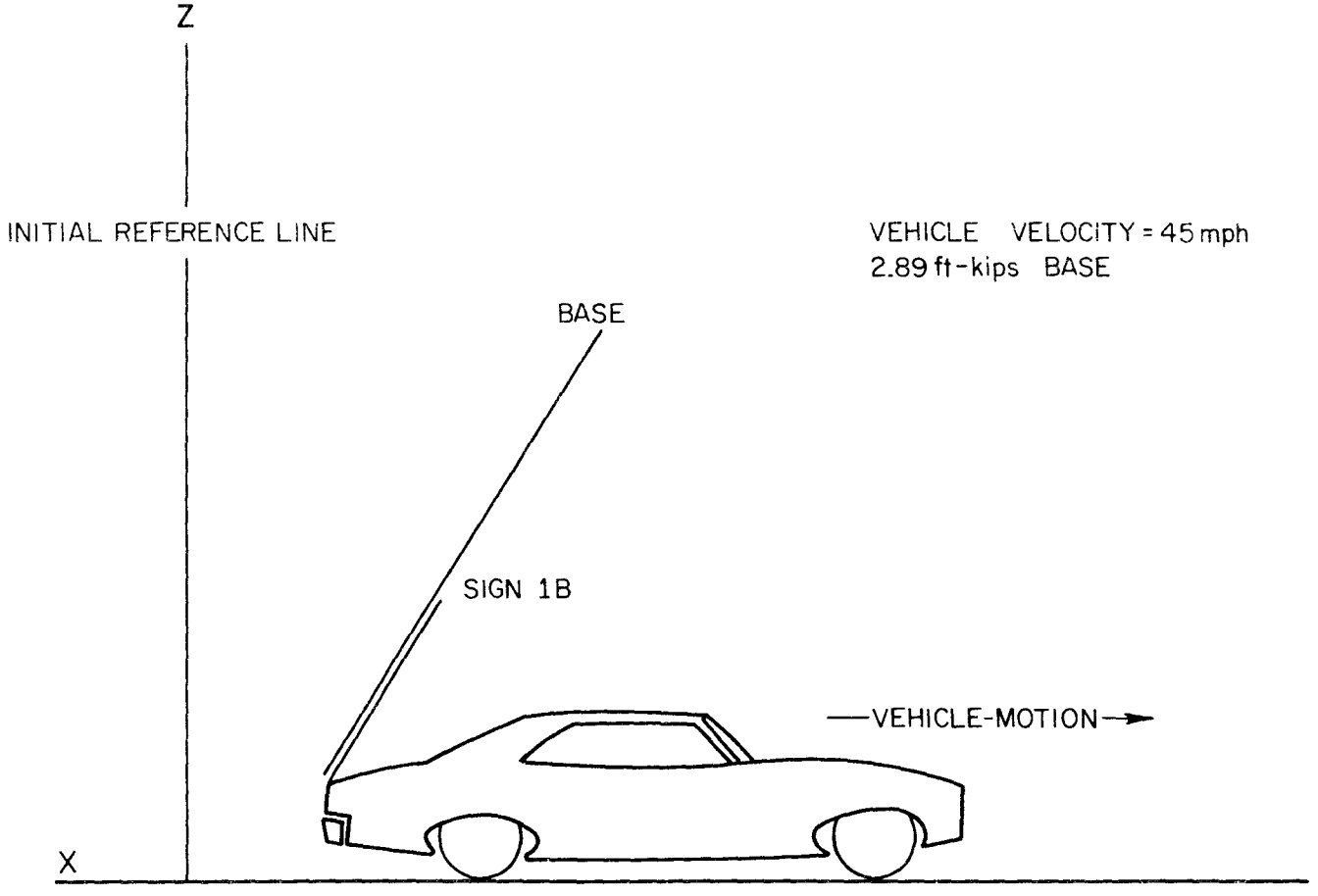

FIGURE 8. TYPICAL IMPACT RESPONSE OF SIGN POST STRUCTURE

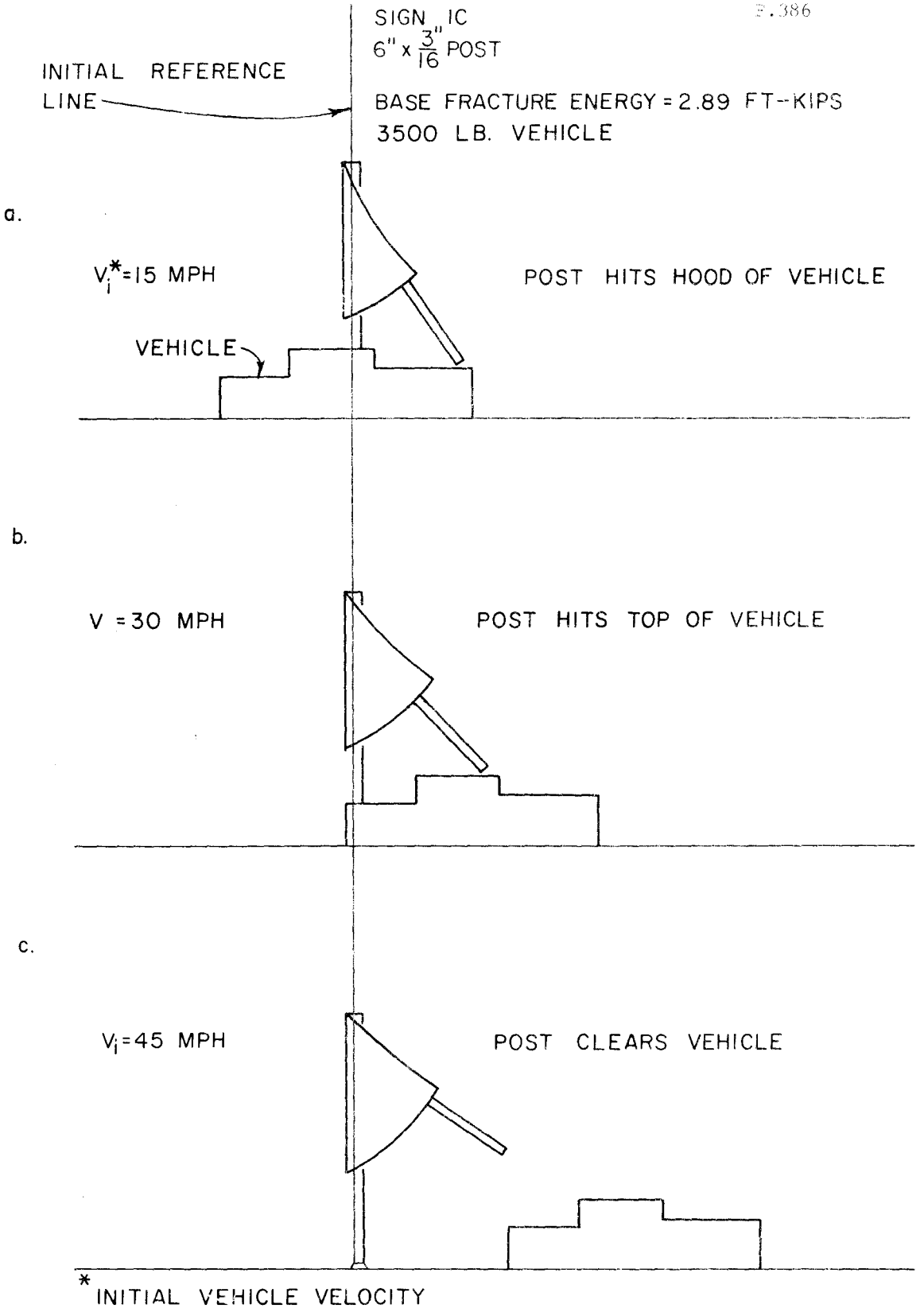

FIGURE 9. TYPICAL IMPACT RESPONSE OF SIGN POST STRUCTURE

SIGN 1A

Post	6" x 3/16"+	8" x 1/4"	10" x 1/4"	12" x 1/4"
Post Height (ft)	12.0	12.0	12.0	12.0
Post Weight (lbs)	52.5	93.1	110.3	132.9
K* (ft)	8.2	7.7	7.6	7.4
Base Fracture Energy (ft-kip)	2.89	5.25	8.6	9.7

SIGN 1B

Post	6" x 3/16"	8" x 1/4"	10" x 1/4"	12" x 1/4"
Post Height (ft)	16.0	16.0	16.0	16.0
Post Weight (lbs)	70.0	124.1	147.1	177.2
K* (ft)	9.9	9.5	9.4	9.2
Base Fracture Energy (ft-kip)	2.89	5.25	8.6	9.7

SIGN 1C

Post	6" x 3/16"	8" x 1/4"	10" x 1/4"	12" x 1/4"
Post Height (ft)	16.0	16.0	16.0	16.0
Post Weight (lbs)	70.0	124.1	147.1	177.2
K+ (ft)	11.5	11.5	11.5	11.5
Base Fracture Energy (ft-kip)	2.89	5.25	8.6	9.7

SIGN 1D

Post	6" x 3/16"	8" x 1/4"	10" x 1/4"	12" x 1/4"
Post Height (ft)	13.0	13.0	13.0	13.0
Post Weight (lbs)	56.9	101.0	119.5	144.0
K+ (ft)	10.0	10.0	10.0	10.0
Base Fracture Energy (ft-kip)	2.89	5.25	8.6	9.7

*For center of gravity of post and sign (Fig. 1)

+For assumed center of rotation of idealized structure (Fig. 2)

+Pipe diameter and wall thickness, respectively

TABLE 1. POST PROPERTIES FOR SIGNS USED IN STUDY

	Initial Velocity (mph)	Change in Velocity (mph)	Post-Vehicle Contact Time (sec)	Average Vehicle Deceleration (g's)	Remarks
TEST	29.0	2.7	0.084	1.47	Sign post rotates 105° and hits top of vehicle 10.75 ft from front bumper. Total time of the event is .338 sec.
MODEL	29.0	2.5	0.084	1.33	Sign post rotates 105° and hits top of vehicle 10.25 ft from front bumper. Total time of the event is .318 sec.

Table 2. Comparison of Model and Crash Test Results

Vehicle Weight (lbs)	Initial Vehicle Velocity (mph)	Change in Vehicle Velocity (mph)	Duration of Collision (sec)	Average Vehicle Deceleration (G's)	Remarks
2500	15	5.0	0.121	1.9	Post hits top of vehicle. L = 6.8 ft[a]
2500	30	2.9	0.091	1.4	Post hits top of vehicle. L = 10.9 ft
2500	45	2.3	0.080	1.3	Post hits top of vehicle. L = 12.6 ft
3500	15	3.4	0.124	1.3	Post hits top of vehicle. L = 7 ft
3500	30	2.5	0.084	1.3	Post hits top of vehicle. L = 10.4 ft
3500	45	2.1	0.069	1.4	Post hits top of vehicle. L = 12.2 ft
5000	15	1.9	0.098	0.9	Post hits top of vehicle. L = 7.3 ft
5000	30	1.3	0.072	0.8	Post hits top of vehicle. L = 10.5 ft
5000	45	1.1	0.066	0.7	Post hits top of vehicle. L = 12.4 ft

(a) L is the distance from front bumper of vehicle to point where support hits

TABLE 3. RESULTS FOR SIGN 1A WITH BASE
FRACTURE ENERGY OF 2.89 FT-KIPS
FOR 6 INCH POST

Vehicle Weight (lbs)	Initial Vehicle Velocity (mph)	Change in Vehicle Velocity (mph)	Duration of Collision (sec)	Average Vehicle Deceleration (G's)	Remarks
2500	15	5.7	0.199	1.3	Post hits windshield area of vehicle.
2500	30	4.7	0.053	4.0	Post hits top of vehicle. L = 9.5 ft[a]
2500	45	4.4	0.039	5.2	Post hits top of vehicle. L = 10 ft
3500	15	3.7	0.146	1.2	Post hits top of vehicle. L = 7 ft
3500	30	3.5	0.099	1.6	Post hits top of vehicle. L = 10 ft
3500	45	3.6	0.037	4.4	Post hits top of vehicle. L = 11.5 ft
5000	15	3.4	0.132	1.2	Post hits top of vehicle. L = 7.5 ft
5000	30	2.3	0.094	1.1	Post hits top of vehicle. L = 10.2 ft
5000	45	2.6	0.036	3.3	Post hits top of vehicle. L = 12 ft

(a) L is the distance from front bumper of vehicle to point where support hits

TABLE 4. RESULTS FOR SIGN 1A WITH BASE FRACTURE ENERGY OF 5.25 FT-KIPS FOR 8 INCH POST

Vehicle Weight (lbs)	Initial Vehicle Velocity (mph)	Change in Vehicle Velocity (mph)	Duration of Collision (sec)	Average Vehicle Deceleration (G's)	Remarks
2500	15	8.8	0.130	3.1	Post hits windshield area of vehicle.
2500	30	5.0	0.111	2.0	Post hits top of vehicle. L = 9 ft[a]
2500	45	5.9	0.048	5.6	Post hits top of vehicle. L = 9 ft
3500	15	7.4	0.127	2.6	Post hits top of vehicle. L = 6.8 ft
3500	30	4.4	0.098	2.0	Post hits top of vehicle. L = 10 ft
3500	45	3.5	0.099	1.6	Post hits top of vehicle. L = 11 ft
5000	15	5.4	0.140	1.8	Post hits top of vehicle. L = 7 ft
5000	30	3.5	0.091	1.7	Post hits top of vehicle. L = 10 ft
5000	45	2.9	0.086	1.5	Post hits top of vehicle. L = 11.8 ft

(a) L is the distance from front bumper of vehicle to point where support hits

TABLE 5. RESULTS FOR SIGN 1A WITH BASE FRACTURE ENERGY OF 8.6 FT-KIPS FOR 10 INCH .POST

Vehicle Weight (lbs)	Initial Vehicle Velocity (mph)	Change in Vehicle Velocity (mph)	Duration of Collision (sec)	Average Vehicle Deceleration (G's)	Remarks
2500	15	9.2	0.153	2.7	Post hits windshield area of vehicle.
2500	30	7.0	0.057	5.6	Post hits windshield area of vehicle.
2500	45	6.8	0.044	7.0	Post hits top of vehicle. L = 7.0 ft[a]
3500	15	7.7	0.136	2.6	Post hits windshield area of vehicle.
3500	30	5.1	0.057	4.0	Post hits top of vehicle. L = 7.0 ft
3500	45	4.7	0.040	5.4	Post hits top of vehicle. L = 7.6 ft
5000	15	6.0	0.150	1.8	Post hits top of vehicle. L = 7.0 ft
5000	30	3.7	0.058	2.9	Post hits top of vehicle. L = 9.0 ft
5000	45	3.8	0.038	4.6	Post hits top of vehicle. L = 10.0 ft

(a) L is the distance from front bumper of vehicle to point where support hits

TABLE 6. RESULTS FOR SIGN 1A WITH BASE FRACTURE ENERGY OF 9.7 FT-KIPS FOR 12 INCH POST

Vehicle Weight (lbs)	Initial Vehicle Velocity (mph)	Change in Vehicle Velocity (mph)	Duration of Collision (sec)	Average Vehicle Deceleration (G's)	Remarks
2500	15	5.5	0.129	1.9	Post hits top of vehicle. L = 9.8 ft[a]
2500	30	3.1	0.086	1.7	Post hits trunk area of vehicle.
2500	45	2.6	0.084	1.4	Post hits trunk area of vehicle.
3500	15	3.8	0.131	1.2	Post hits top of vehicle. L = 10.2 ft
3500	30	2.7	0.092	1.3	Post hits trunk area of vehicle.
3500	45	2.1	0.079	1.2	Post hits trunk area of vehicle.
5000	15	1.9	0.104	0.8	Post hits top of vehicle. L = 10.7 ft
5000	30	1.3	0.076	0.7	Post hits trunk area of vehicle.
5000	45	1.2	0.074	0.7	Post hits trunk area of vehicle.

(a) L is the distance from front bumper of vehicle to point where support hits

TABLE 7. RESULTS FOR SIGN 1B WITH BASE FRACTURE ENERGY OF 2.89 FT-KIPS FOR 6 INCH POST

Vehicle Weight (lbs)	Initial Vehicle Velocity (mph)	Change in Vehicle Velocity (mph)	Duration of Collision (sec)	Average Vehicle Deceleration (G's)	Remarks
2500	15	6.4	0.140	2.1	Post hits top of vehicle. L = 9.0 ft[a]
2500	30	5.0	0.055	4.1	Post hits top of vehicle. L = 12.0 ft
2500	45	4.7	0.040	5.4	Post hits trunk area of vehicle.
3500	15	4.0	0.153	1.2	Post hits top of vehicle. L = 10.0 ft
3500	30	3.9	0.062	2.9	Post hits trunk area of vehicle.
3500	45	3.9	0.038	4.6	Post hits trunk area of vehicle.
5000	15	3.8	0.137	1.3	Post hits top of vehicle. L = 10.0 ft
5000	30	2.4	0.093	1.2	Post hits trunk area of vehicle.
5000	45	2.6	0.038	3.1	Post hits trunk area of vehicle.

(a) L is the distance from front bumper of vehicle to point where support hits

TABLE 8. RESULTS FOR SIGN 1B WITH BASE FRACTURE ENERGY OF 5.25 FT-KIPS FOR 8 INCH POST

Vehicle Weight (lbs)	Initial Vehicle Velocity (mph)	Change in Vehicle Velocity (mph)	Duration of Collision (sec)	Average Vehicle Deceleration (G's)	Remarks
2500	15	9.7	0.162	1.6	Post hits windshield area of vehicle.
2500	30	6.4	0.073	4.0	Post hits top of vehicle. L = 10.3 ft[a]
2500	45	6.5	0.050	5.9	Post hits top of vehicle. L = 10.5 ft
3500	15	8.1	0.162	1.2	Post hits top of vehicle. L = 9.0 ft
3500	30	4.7	0.106	2.0	Post hits trunk area of vehicle.
3500	45	5.0	0.049	4.7	Post hits trunk area of vehicle.
5000	15	5.5	0.157	1.6	Post hits top of vehicle. L = 10.0 ft
5000	30	3.6	0.105	1.6	Post hits trunk area of vehicle.
5000	45	3.6	0.055	3.0	Post hits trunk area of vehicle.

(a) L is the distance from front bumper of vehicle to point where support hits

TABLE 9. RESULTS FOR SIGN 1B WITH BASE FRACTURE ENERGY OF 8.6 FT-KIPS FOR 10 INCH POST

Vehicle Weight (lbs)	Initial Vehicle Velocity (mph)	Change in Vehicle Velocity (mph)	Duration of Collision (sec)	Average Vehicle Deceleration (G's)	Remarks
2500	15	10.0	0.168	2.7	Post hits windshield area of vehicle.
2500	30	7.5	0.059	5.8	Post hits top of vehicle. L = 7.5 ft[a]
2500	45	7.4	0.046	7.4	Post hits top of vehicle. L = 8.5 ft
3500	15	8.5	0.162	2.4	Post hits windshield area of vehicle.
3500	30	5.8	0.058	4.5	Post hits top of vehicle. L = 11.0 ft
3500	45	5.3	0.042	5.8	Post hits top of vehicle. L = 12.0 ft
5000	15	6.2	0.157	1.8	Post hits top of vehicle. L = 8.0 ft
5000	30	4.2	0.065	2.9	Post hits trunk area of vehicle.
5000	45	4.1	0.040	4.7	Post hits trunk area of vehicle.

(a) L is the distance from front bumper of vehicle to point where support hits

TABLE 10. RESULTS FOR SIGN 1B WITH BASE FRACTURE ENERGY OF 9.7 FT-KIPS FOR 12 INCH POST

Vehicle Weight (lbs)	Initial Vehicle Velocity (mph)	Change in Vehicle Velocity (mph)	Duration of Collision (sec)	Average Vehicle Deceleration (G's)	Remarks
2500	15	3.2	0.116	1.3	Post hits hood area of vehicle.
2500	30	2.0	0.075	1.2	Post hits windshield area of vehicle.
2500	45	2.3	0.075	1.4	Post has cleared the vehicle.
3500	15	2.3	0.120	0.9	Post hits hood area of vehicle.
3500	30	1.5	0.081	0.8	Post hits top of vehicle.
3500	45	1.7	0.071	1.1	Post has cleared the vehicle.
5000	15	1.6	0.094	0.8	Post hits hood area of vehicle.
5000	30	1.1	0.069	0.7	Post hits top of vehicle.
5000	45	1.2	0.067	0.8	Post has cleared the vehicle.

TABLE 11. RESULTS FOR SIGN 1C WITH BASE FRACTURE ENERGY OF 2.89 FT-KIPS FOR 6 INCH POST

Vehicle Weight (lbs)	Initial Vehicle Velocity (mph)	Change in Vehicle Velocity (mph)	Duration of Collision (sec)	Average Vehicle Deceleration (G's)	Remarks
2500	15	4.4	0.126	1.6	Post hits hood area of vehicle.
2500	30	2.6	0.050	2.4	Post has cleared the vehicle.
2500	45	3.2	0.040	3.7	Post has cleared the vehicle.
3500	15	3.0	0.134	1.0	Post hits hood area of vehicle.
3500	30	1.9	0.056	1.5	Post has cleared the vehicle.
3500	45	2.3	0.038	2.7	Post has cleared the vehicle.
5000	15	2.2	0.127	1.0	Post hits hood area of vehicle.
5000	30	1.3	0.085	1.0	Post has cleared the vehicle.
5000	45	1.6	0.038	1.9	Post has cleared the vehicle.

TABLE 12. RESULTS FOR SIGN 1C WITH BASE FRACTURE ENERGY OF 5.25 FT-KIPS FOR 8 INCH POST

Vehicle Weight (lbs)	Initial Vehicle Velocity (mph)	Change in Vehicle Velocity (mph)	Duration of Collision (sec)	Average Vehicle Deceleration (G's)	Remarks
2500	15	5.7	0.150	1.7	Post hits hood area of vehicle.
2500	30	3.6	0.065	2.5	Post has cleared the vehicle.
2500	45	4.1	0.045	4.2	Post has cleared the vehicle.
3500	15	4.0	0.145	1.3	Post hits hood area of vehicle.
3500	30	2.6	0.090	1.3	Post has cleared the vehicle.
3500	45	3.0	0.044	3.1	Post has cleared the vehicle.
5000	15	2.8	0.142	1.0	Post hits hood area of vehicle.
5000	30	1.8	0.091	1.0	Post has cleared the vehicle.
5000	45	2.1	0.050	2.0	Post has cleared the vehicle.

TABLE 13. RESULTS FOR SIGN 1C WITH BASE FRACTURE ENERGY OF 8.6 FT-KIPS FOR 10 INCH POST

Vehicle Weight (lbs)	Initial Vehicle Velocity (mph)	Change in Vehicle Velocity (mph)	Duration of Collision (sec)	Average Vehicle Deceleration (G's)	Remarks
2500	15	9.5	0.152	2.5	Post hits hood area of vehicle.
2500	30	5.2	0.055	4.3	Post has cleared the vehicle.
2500	45	5.2	0.045	5.3	Post has cleared the vehicle.
3500	15	5.2	0.156	1.5	Post hits hood area of vehicle.
3500	30	3.8	0.053	3.3	Post has cleared the vehicle.
3500	45	3.8	0.040	4.3	Post has cleared the vehicle.
5000	15	3.6	0.144	1.1	Post hits windshield area of vehicle.
5000	30	2.7	0.060	2.0	Post has cleared the vehicle.
5000	45	2.7	0.040	3.1	Post has cleared the vehicle.

TABLE 14. RESULTS FOR SIGN 1C WITH BASE FRACTURE ENERGY OF 9.7 FT-KIPS FOR 12 INCH POST

Vehicle Weight (lbs)	Initial Vehicle Velocity (mph)	Change in Vehicle Velocity (mph)	Duration of Collision (sec)	Average Vehicle Deceleration (G's)	Remarks
2500	15	2.9	0.109	1.2	Post hits windshield area of vehicle.
2500	30	1.6	0.082	1.0	Post has cleared the vehicle.
2500	45	1.7	0.072	1.1	Post has cleared the vehicle.
3500	15	2.0	0.112	0.8	Post hits windshield area of vehicle.
3500	30	1.3	0.076	0.8	Post has cleared the vehicle.
3500	45	1.2	0.062	0.9	Post has cleared the vehicle.
5000	15	1.5	0.088	0.8	Post hits windshield area of vehicle.
5000	30	0.9	0.065	0.6	Post has cleared the vehicle.
5000	45	0.9	0.060	0.7	Post has cleared the vehicle.

TABLE 15. RESULTS FOR SIGN 1D WITH BASE FRACTURE ENERGY OF 2.89 FT-KIPS FOR 6 INCH POST

Vehicle Weight (lbs)	Initial Vehicle Velocity (mph)	Change in Vehicle Velocity (mph)	Duration of Collision (sec)	Average Vehicle Deceleration (G's)	Remarks
2500	15	4.7	0.179	1.2	Post hits hood area of vehicle.
2500	30	1.9	0.050	1.7	Post has cleared the vehicle.
2500	45	1.8	0.038	2.2	Post has cleared the vehicle.
3500	15	3.2	0.130	1.1	Post hits windshield area of vehicle.
3500	30	1.4	0.090	1.0	Post has cleared the vehicle.
3500	45	1.3	0.037	1.6	Post has cleared the vehicle.
5000	15	2.3	0.119	1.0	Post hits windshield area of vehicle.
5000	30	1.0	0.086	0.5	Post has cleared the vehicle.
5000	45	1.0	0.036	1.2	Post has cleared the vehicle.

TABLE 16. RESULTS FOR SIGN 1D WITH BASE FRACTURE ENERGY OF 5.25 FT-KIPS FOR 8 INCH POST

Vehicle Weight (lbs)	Initial Vehicle Velocity (mph)	Change in Vehicle Velocity (mph)	Duration of Collision (sec)	Average Vehicle Deceleration (G's)	Remarks
2500	15	5.9	0.115	2.3	Post hits hood area of vehicle.
2500	30	2.9	0.100	1.3	Post has cleared the vehicle.
2500	45	2.5	0.042	2.7	Post has cleared the vehicle.
3500	15	4.1	0.112	1.7	Post hits hood area of vehicle.
3500	30	2.1	0.085	1.1	Post has cleared the vehicle.
3500	45	1.8	0.085	1.0	Post has cleared the vehicle.
5000	15	2.9	0.125	1.1	Post hits windshield area of vehicle.
5000	30	1.5	0.082	0.8	Post has cleared the vehicle.
5000	45	1.2	0.077	0.7	Post has cleared the vehicle.

TABLE 17. RESULTS FOR SIGN 1D WITH BASE FRACTURE ENERGY OF 8.6 FT-RIPS FOR 10 INCH POST

Vehicle Weight (lbs)	Initial Vehicle Velocity (mph)	Change in Vehicle Velocity (mph)	Duration of Collision (sec)	Average Vehicle Deceleration (G's)	Remarks
2500	15	7.5	0.136	2.5	Post hits hood area of vehicle.
2500	30	5.2	0.052	4.5	Post has cleared the vehicle.
2500	45	3.6	0.041	4.0	Post has cleared the vehicle.
3500	15	5.1	0.123	1.9	Post hits hood area of vehicle.
3500	30	3.7	0.052	3.2	Post has cleared the vehicle.
3500	45	2.6	0.040	3.0	Post has cleared the vehicle.
5000	15	3.5	0.135	1.2	Post hits windshield area of vehicle.
5000	30	2.6	0.053	2.2	Post has cleared the vehicle.
5000	45	1.8	0.038	2.1	Post has cleared the vehicle.

TABLE 18. RESULTS FOR SIGN ID WITH BASE FRACTURE ENERGY OF 9.7 FT-KIPS FOR 12 INCH POST

TEST 505 SS-A

This test of a frangible aluminum sign support was conducted on November 25, 1969. A 1959 Ford weighing 3550 lbs impacted the sign head on. The sign rotated through approximately 105° before striking the top of the vehicle. The following data has been compiled:

Vehicle Data

Make and model = 1959 Ford sedan

Weight = 3550 lbs

Residual deformation
- Front = 8 in.
- Top = 2 in.

Sign Data

Pole diameter = 6 in.

Pole height = 12 ft

Sign width = 6 ft

Sign height = 5 ft

Overall height = 12.1 ft

Location of cg = 4.1 ft from top of sign

Overall weight = 148 lbs

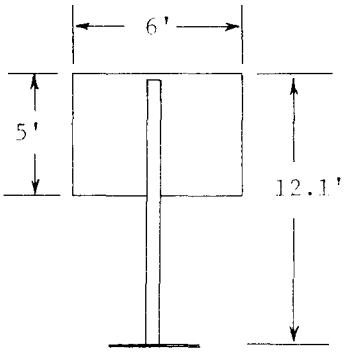

Film Data

Initial speed = 29.0 mph

Final speed = 26.3 mph

Time in contact = 0.084 sec

Distance in contact = 3.32 ft

Energy lost during contact = 17.9 Kip-Ft

Pole horizontal 2 feet above roof, 0.304 seconds and 11.7 feet after impact.

Pole recontacts vehicle (roof), 0.338 seconds and 13.0 feet after impact (after rotating through 105°).

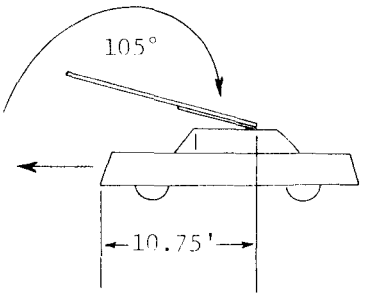

Accelerometer Data

Peak deceleration
- Left frame = 4.1 g's
- Right frame = 4.8 g's

Average deceleration (over 0.071 seconds)
- Left frame = 2.0 g's
- Right frame = 2.1 g's

TECHNICAL MEMORANDUM 505-8

Texas Transportation Institute
Texas A&M Research Foundation

ENERGY-ABSORBING BRIDGE RAIL

(FRAGMENTING TUBE)

A Tentative Progress Memorandum on Contract No. CPR-11-5851

U. S. Department of Transportation
Federal Highway Administration
Bureau of Public Roads

By

T. J. Hirsch
Research Engineer and Principal Investigator

Arthur J. Stocker
Assistant Research Engineer

and

Don L. Ivey
Associate Research Engineer

Crash tests and evaluations were conducted under the Office of Research and Development, Structures and Applied Mechanics Division's Research Program on Structural Systems in Support of Highway Safety (4S Program). The opinions, findings, and conclusions expressed in this report are those of the authors and not necessarily those of the Bureau of Public Roads.

February 1970

INTRODUCTION

Personnel of the Texas Transportation Institute conducted a series of four vehicle crash tests to evaluate an energy-absorbing bridge rail which was designed in a joint effort by engineers of the Bureau of Public Roads and those of the Southwest Research Institute. It is possible to design a backup rail to retain a selected heavy vehicle. However, this was not attempted in the bridgerail which was constructed and, for convenience, the basic components of the Texas T1 bridgerail were used for the backup rail.

This energy-absorbing system is a blocked-out six by six box beam guardrail, attached to 6 WF 25 support posts as shown in Figures 1 and 3. The blocking out of the box beam is accomplished at each WF support point by a guide tube and a fragmenting (energy-absorbing) tube[1]. The thin aluminum fragmenting tube is rigidly connected to the six by six box beam. It is not rigidly connected to the WF post, but fits into a die which is attached to the post. Under lateral load, the fragmenting tube is forced onto the die and progressively breaks into small segments at a predictable load level. The bridge guide tube acts to prevent movement of the box beam in a longitudinal and vertical direction, but slips through its support on the WF post to allow lateral movement of the box beam. The box beam is then capable of lateral deformation (up to a distance of approximately 18 inches) under the loads imposed by an impacting vehicle. After 18 inches of lateral movement, the box beam comes into contact with the rigid WF support posts which develop a high level of lateral restraint.

---

[1] Superscript numbers refer to corresponding numbers in Selected References.

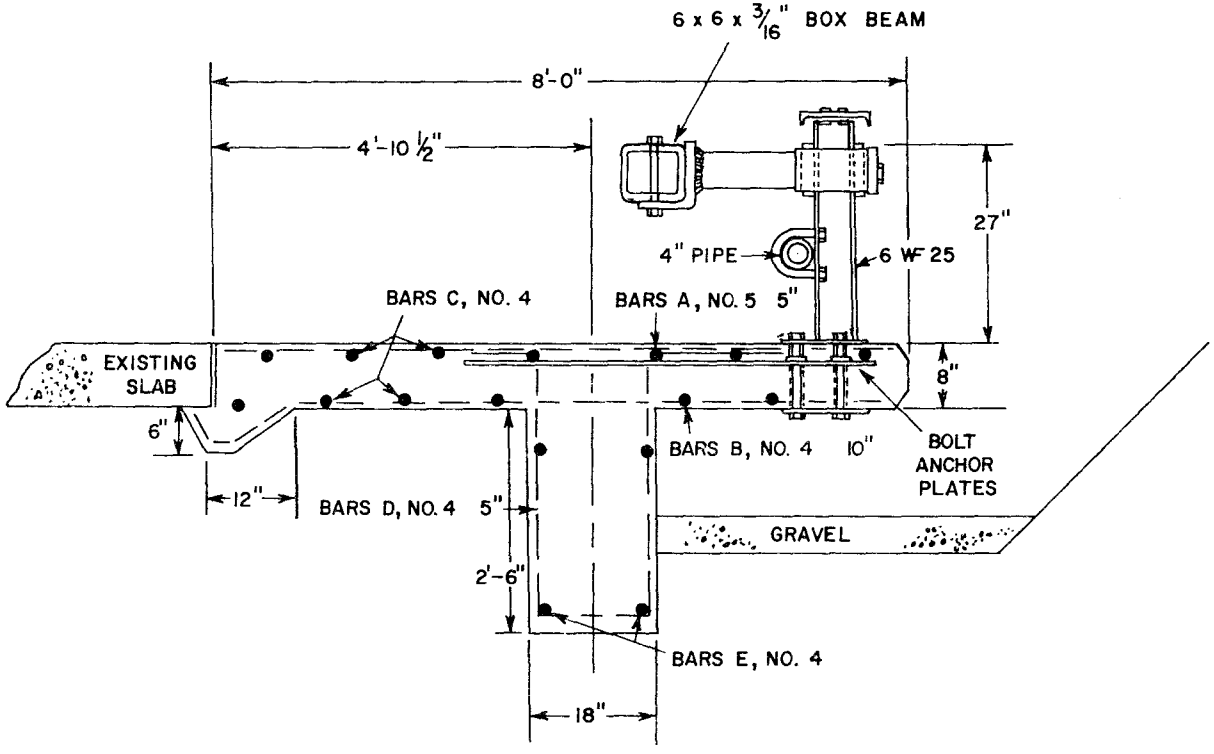

FIGURE 1, CROSS SECTION OF BRIDGE DECK AND BRIDGE RAIL

TEST PROGRAM

General

Four tests were conducted to determine the capabilities of this bridge rail-guardrail system. Three of the tests were against the box beam rail at a post point or between posts with vehicles varying in weight from 1560 lbs to 4720 lbs. A fourth crash was made at a point in the guardrail section to test the transition area between the guardrail and bridge rail. Vehicle weight for the fourth test was 3270 lbs. A plan view of the test installation and summary of the four tests are given by Figure 2.

For the purpose of documentation and data reduction, a total of seven (7) cameras was used. One Hycam motion picture camera, operating at 500 frames per second, photographed the impact point perpendicular to the vehicle line of approach; while a second, similar camera was focused on the impact point perpendicular to the bridge rail. A Fastax camera, operating at 500 frames per second, was positioned in line with the rail at one end to record vehicle deflection parallel to the rail and to record rail deformation. An overhead, high-speed Photosonics camera gave a view of the vehicle movement at impact on tests A and D. Documentary cameras, operating at from 32 to 128 frames per second, provided documentary coverage of each test.

Impact velocities were determined electronically as well as photographically. A pair of tape switches was placed so that they would be crossed by the right front wheel of the vehicle just before impact with the bridge rail. The time between actuation of the first and second switch was measured electromechanically, permitting the speed to be calculated.

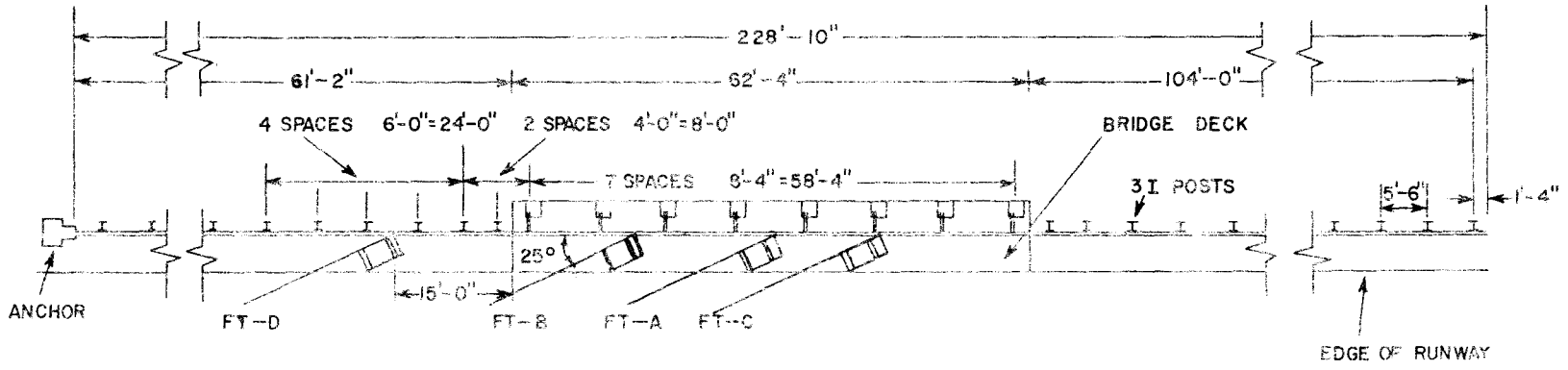

TEST NUMBER	FT-A	FT-B	FT-C	FT-D
ANGLE OF ATTACK	25°	25°	25°	25°
VEHICLE WEIGHT	3200 LBS.	4720 LBS.	1560 LBS.	3270 LBS.
IMPACT SPEED	58.3 mph	54.8 mph	46.1 mph	61.8 mph
INITIAL KINETIC ENERGY (KIP-FT)	363.	474.	111.	418.

FIGURE 2, LOCATION OF VEHICLE IMPACTS

Accelerometer data and time-displacement tables from the high-speed films can be found in the Appendix. The accelerometer traces shown were obtained through a 20 HZ low-pass filter to eliminate the effects of "ringing" and other noise. The unfiltered data is available.

Bridge Rail-Guardrail Details

Figure 1 shows a cross-section through the bridge deck. The following is a parts listing of the hardware in the system, with basic dimensions of each, and overall bridge rail dimensions.

Bridge Rail

Box beam rail	3/16" x 6" x 6"
Fragmenting tube (2024T3 aluminum)	3" O.D. x 0.120 wall
Guide tube	1/4" x 2" x 3"
Post	6 WF 25
Post base plate	1" x 9-1/2" x 10"
Post to slab bolts	7/8"
Plate under slab	1/4" x 8" x 9"
Top of post channel	8"-11.5 lb
Rub rail	4" SCHD 40 pipe
Bridge deck to top of box beam	27"
Bridge deck to top of channel on post	29-9/16"
Front of post to front of box beam	26"
Fragmenting tube length	19"

Guardrail

Box beam rail	3/16" x 6" x 6"
Line post	3" I 5.7 lb
Line post stabilizing plate	1/4" x 8" x 24"
Ground to top of box beam	27"

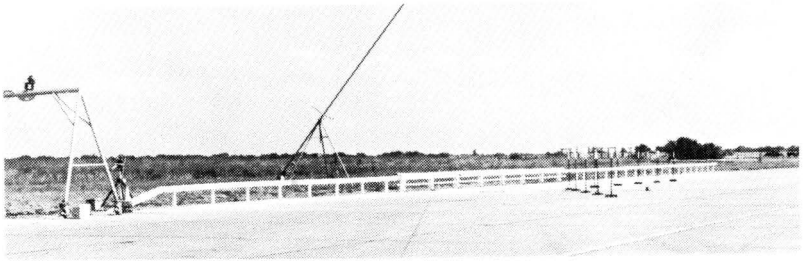

1.

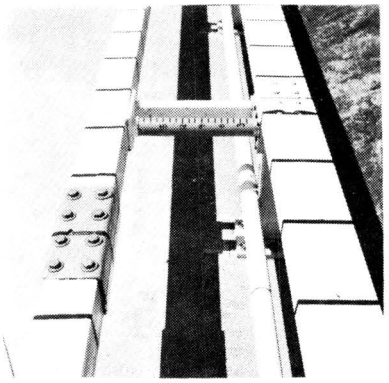

2.

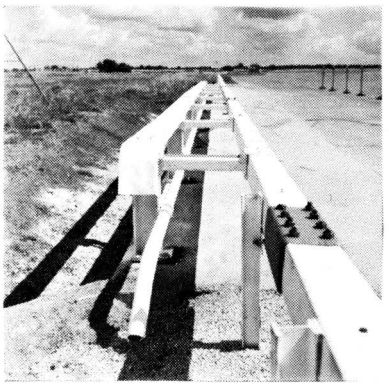

3.

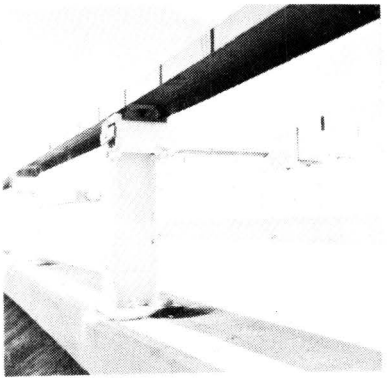

4.

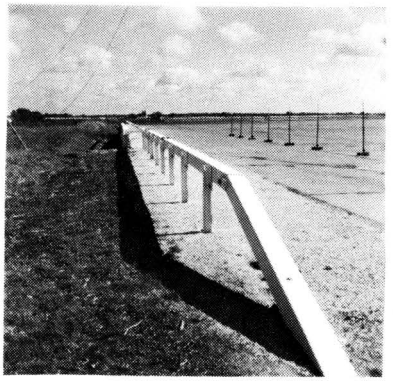

5.

Figure 3, Detail Views of Bridge Rail and Guardrail

Test FT-A

The first test in the series of four was conducted June 5, 1969 with a 3200 lb, 1963 4-door Plymouth. The angle of attack was 25° and impact velocity was 58.3 mph. The impact point for the left front bumper was chosen between two posts in an effort to test the weakest point of the box beam and exert maximum force on the first fragmenting tube downstream from the point of impact.

Figures 4 and 5 show the vehicle condition before and after the test. The vehicle was redirected by the rail and followed closely to the box beam for approximately 75 feet before recontact occurred. This return to the guardrail was caused by drag of the damaged left front wheel. Four guardrail posts were knocked down and the vehicle wedged in the guardrail turn-down. Vehicle passenger compartment encroachment was negligible.

Prior to Tests FT-B, C, and D, the end anchorage was eliminated on the downstream end and an additional length of guardrail installed so that vehicle damage would not be increased by contact with the guardrail anchorage area. The test series was intended to evaluate the bridge area, and was not primarily concerned with the effects of turn-downs or anchorages.

Figure 4 Vehicle Before Test (FT-A)

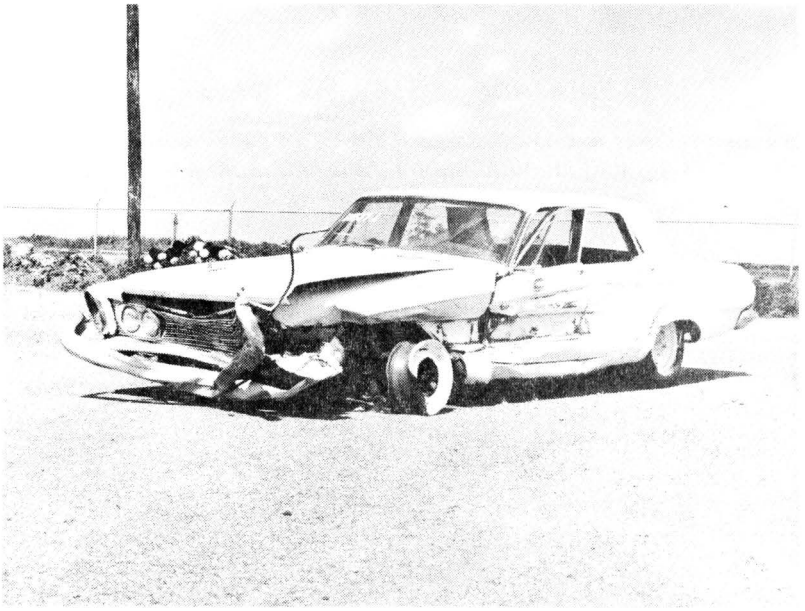

Figure 5 Vehicle After Test (FT-A)

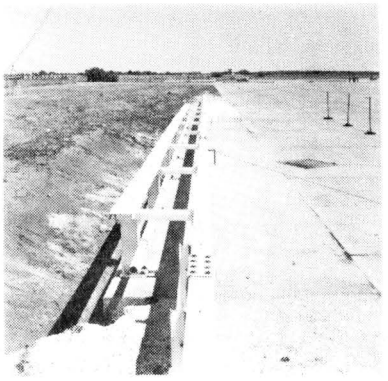

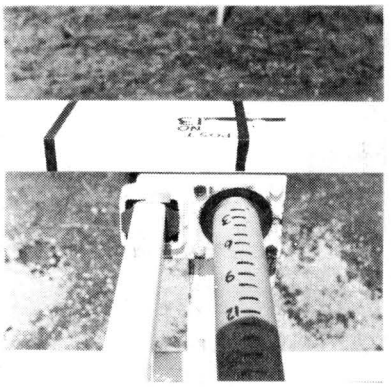

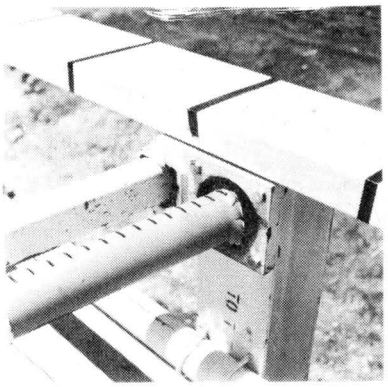

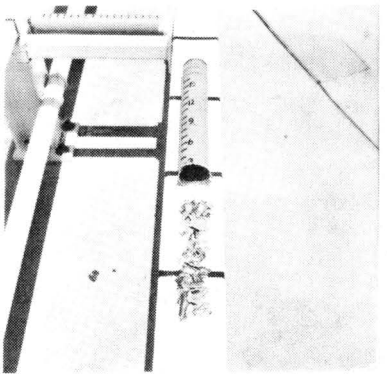

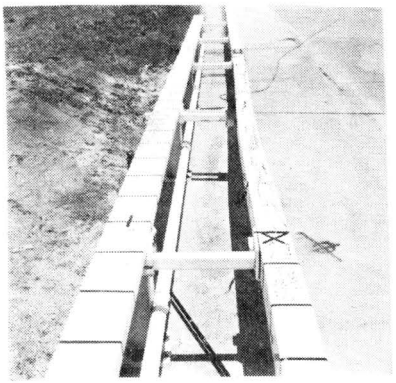

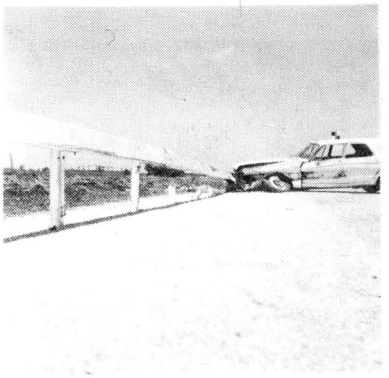

Figure 6 Installation Before and After Test (FT-A)

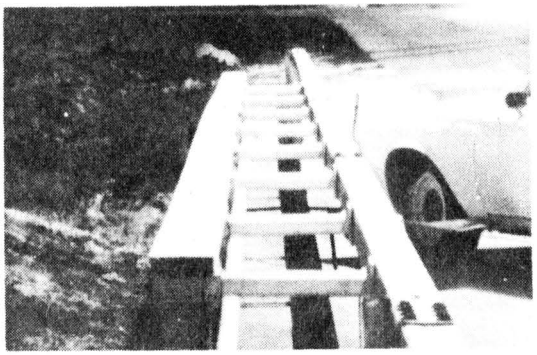

1.

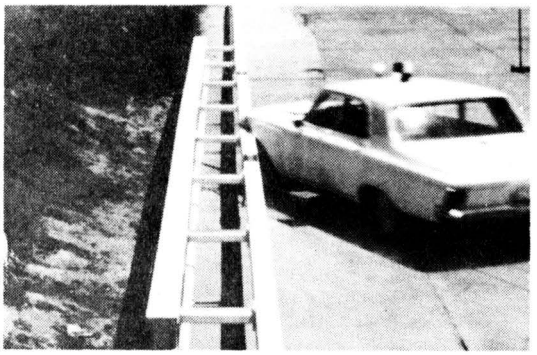

2.

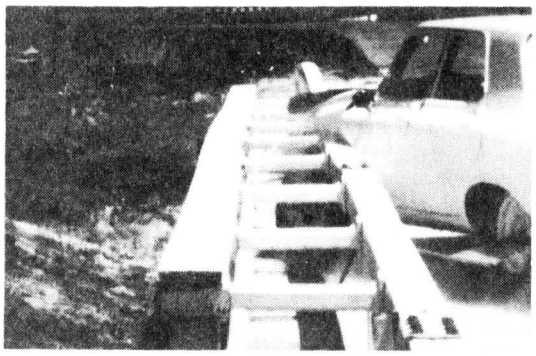

3.

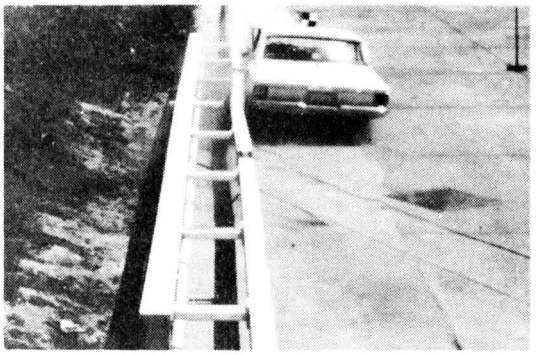

4.

5.

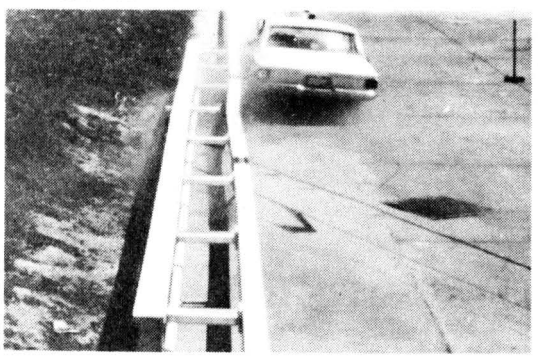

6.

Figure 7 Sequential Photographs of Test (FT-A)

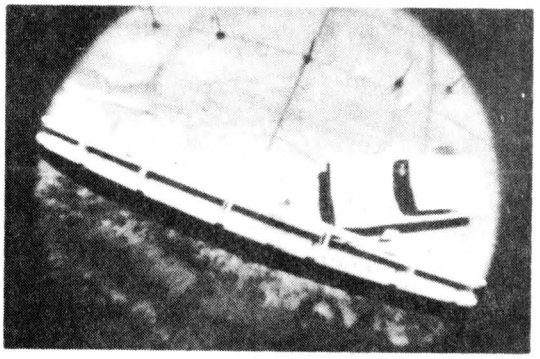

1.

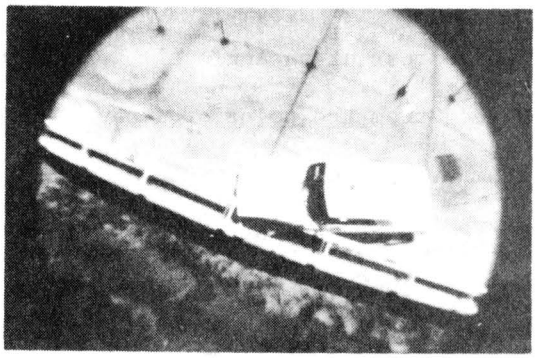

2.

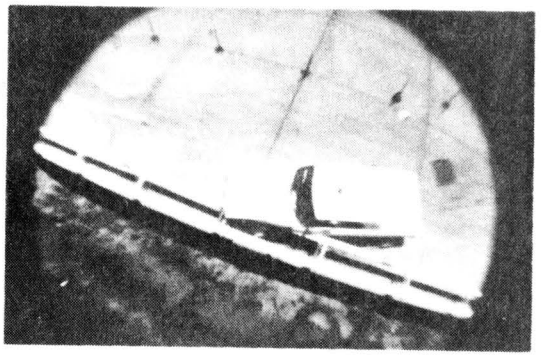

3.

Figure 8 Sequential Photographs of Test (FT-A)

Test FT-B

A heavy vehicle was selected for the second test in the program, a 1959 4-door Oldsmobile weighing 4720 lbs. Impact velocity was 54.8 mph at an angle of 25°.

Figures 9 and 10 show the condition of the test vehicle before and after the test. The point of impact was again chosen at a point on the rail half-way between two posts. After impact, the vehicle left the rail, moved to a position some 5 feet from the original rail position, followed the rail, and then turned back into the guardrail due to left front drag caused by wheel damage. After tearing down four guardrail line posts, the vehicle came to rest at an angle of approximately 45° to the guardrail, some 100 feet from the point of impact. No visible vehicle compartment encroachment was noted.

The simulated bridge deck was cracked as shown in the lower left photograph of Figure 11, but was repaired prior to Test FT-C.

Figure 9 Vehicle Before Test (FT-B)

Figure 10 Vehicle After Test (FT-B)

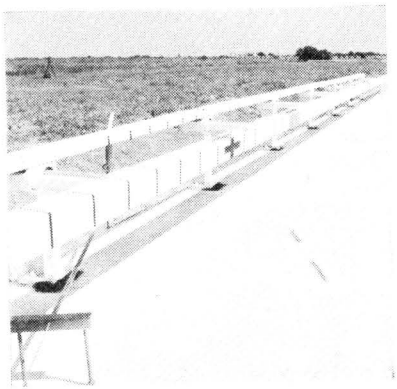

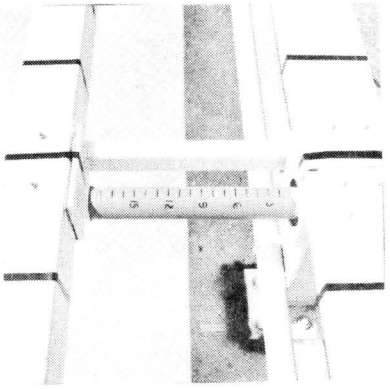

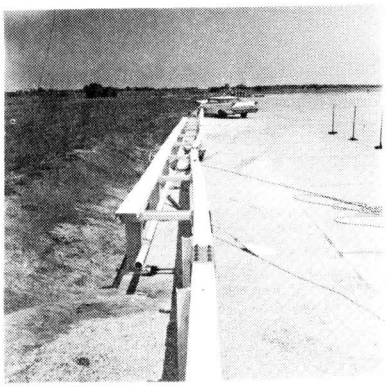

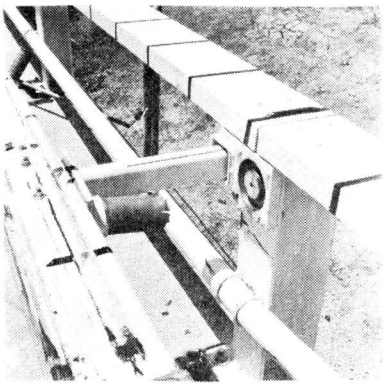

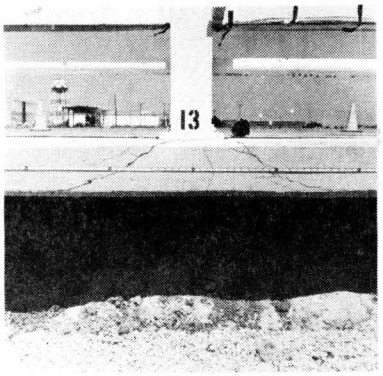

Figure 11 Installation Before and After Test (FT-B)

1.

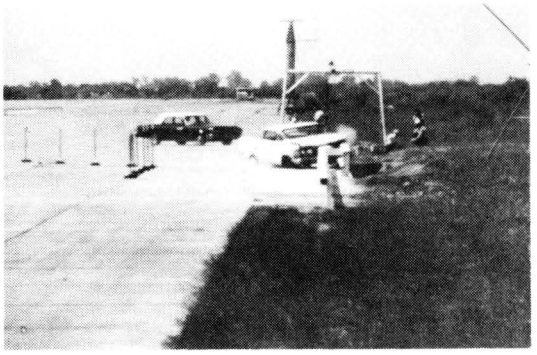

2.

3.

4.

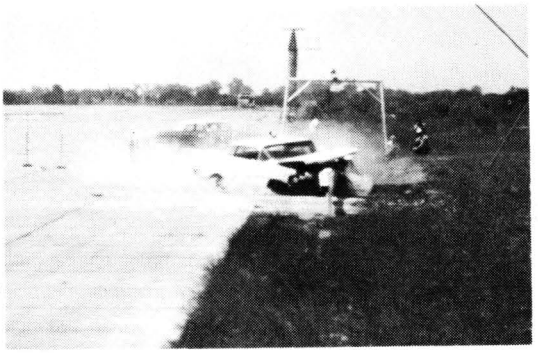

5.

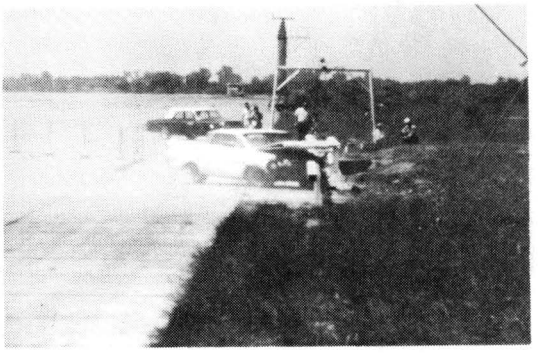

6.

Figure 12 Sequential Photographs of Test (FT-B)

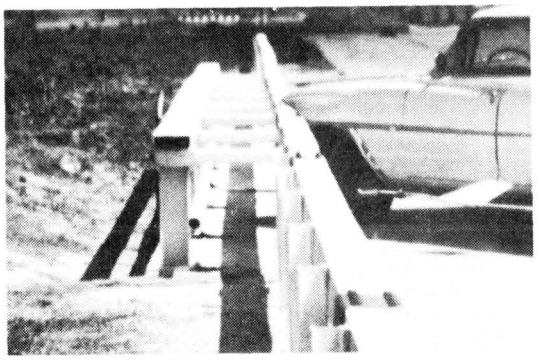

1.

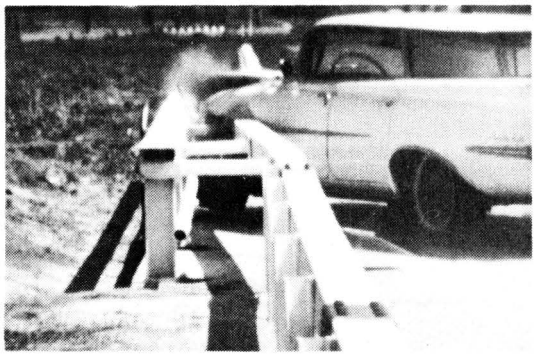

2.

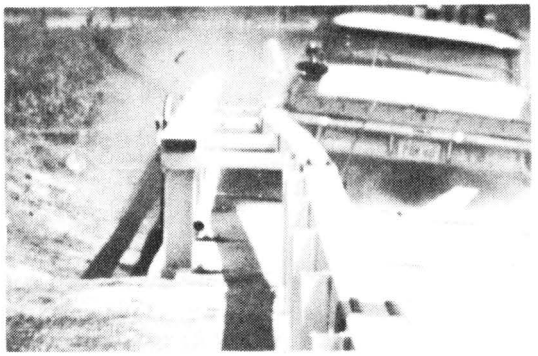

3.

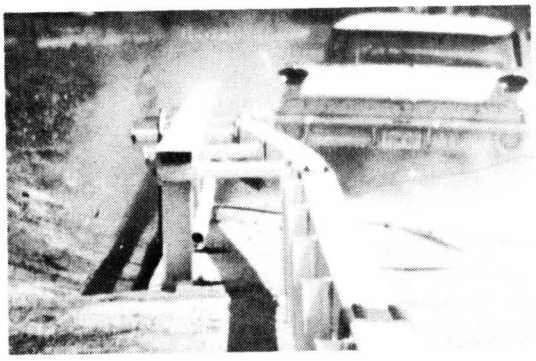

4.

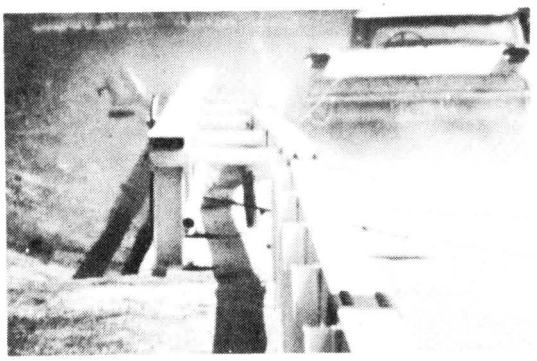

5.

Figure 13 Sequential Photographs of Test (FT-B)

Test FT-C

Since the first two tests involved medium and heavy weight vehicles, a 1560 lb, 1961 Volkswagen was chosen for the third test. The impact angle was 25° and the impact velocity was 46.1 mph. Although 60 mph was desired, the vehicle did not have sufficient power to achieve this in the available acceleration distance.

Vehicle condition before and after the test is shown in Figures 14 and 15. There was no measurable tube activation due to the impact, though one tube was superficially deformed at the die. After impact, the vehicle followed the rail (at a distance of from one to two feet) for some 120 feet, brushed the end of the guardrail in a long left turn, and then came to rest in an open field. Though the left side of the vehicle was dented from front to rear, there was no significant encroachment of the vehicle compartment.

Figure 14 Vehicle Before Test (FT-C)

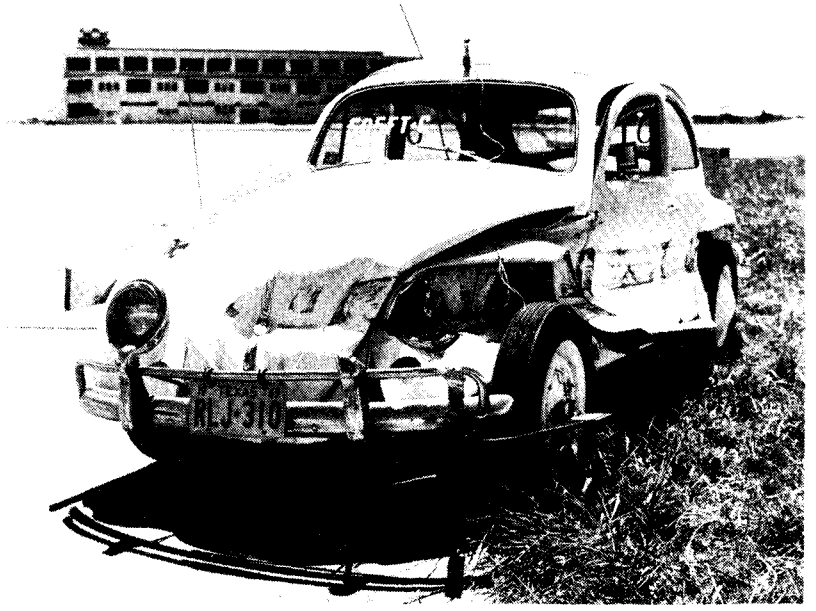

Figure 15 Vehicle After Test (FT-C)

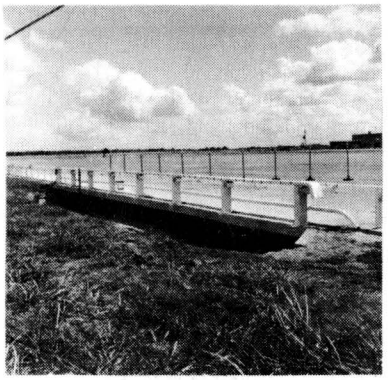

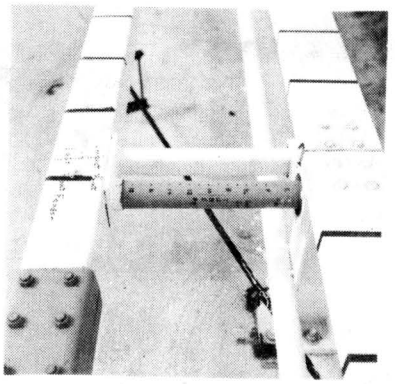

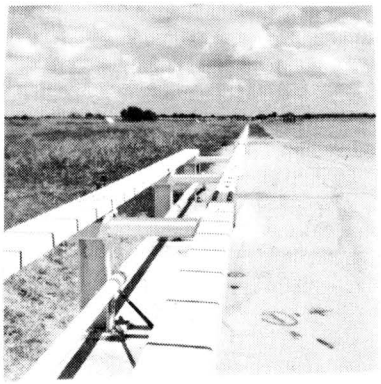

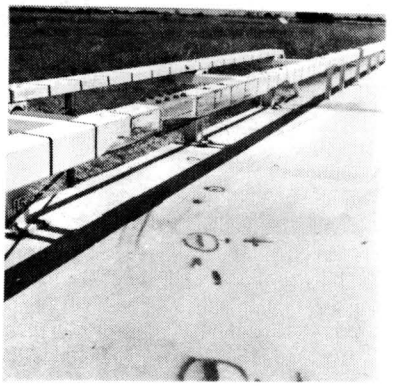

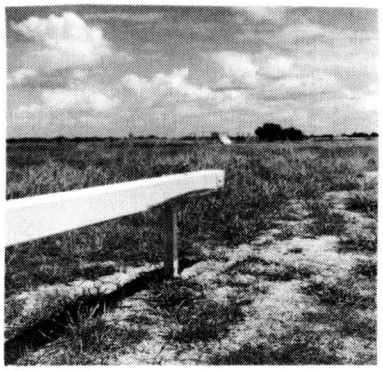

Figure 16 Installation Before and After Test (FT-C)

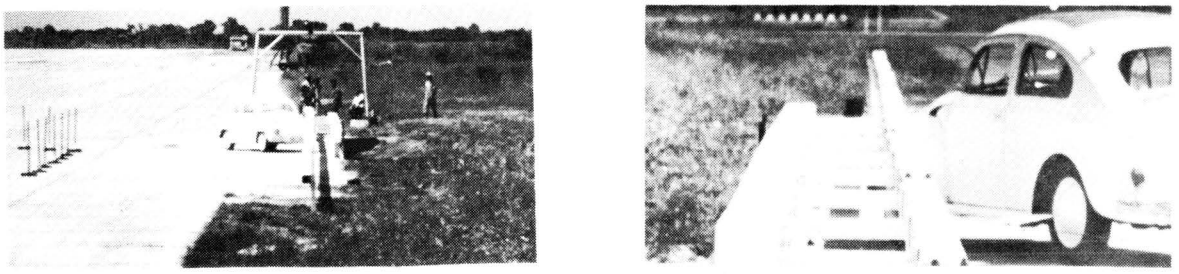

1.

2.

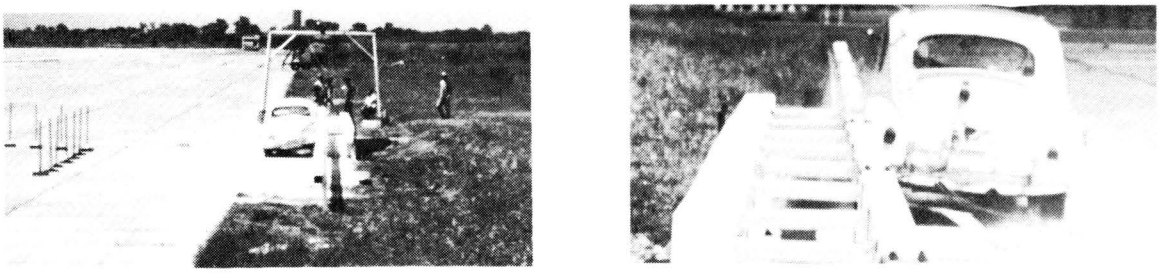

3.

4.

Figure 17 Sequential Photographs of Test (FT-C)

Test FT-D

The fourth and final test in this project was designed to test the transition area between the bridge rail and guardrail. A point fifteen (15) feet upstream from the bridge deck (17 feet from the first bridge rail post) was chosen for the impact point. The test was run on July 8, 1969 with a 3270 lb, 1963 4-door Plymouth similar to the vehicle used in FT-A. Impact velocity was 61.8 mph and the angle of attack was 25°.

The vehicle was successfully redirected though there was considerable damage to the installation and the vehicle. After traveling approximately 80 feet from the point of impact, the vehicle came to rest in the guardrail system just downstream from the bridge. As shown in Figure 21, the outer sheet metal of the left front door was snagged by the rail splice just after impact and was torn off. The inner door panel remained in place, however.

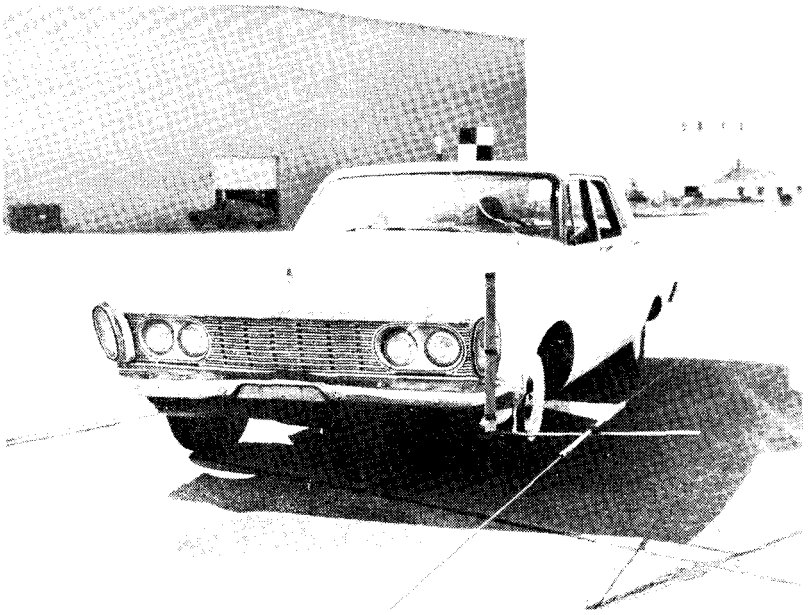

Figure 18 Vehicle Before Test (FT-D)

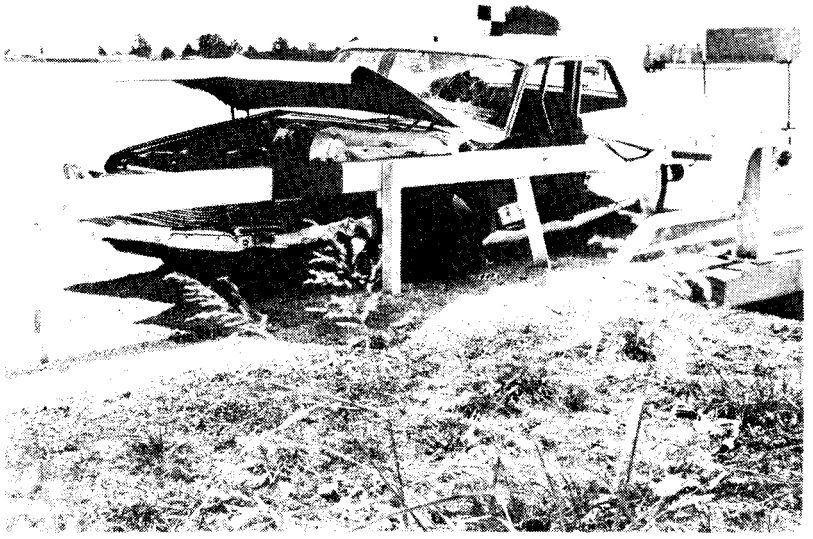

Figure 19 Vehicle After Test (FT-D)

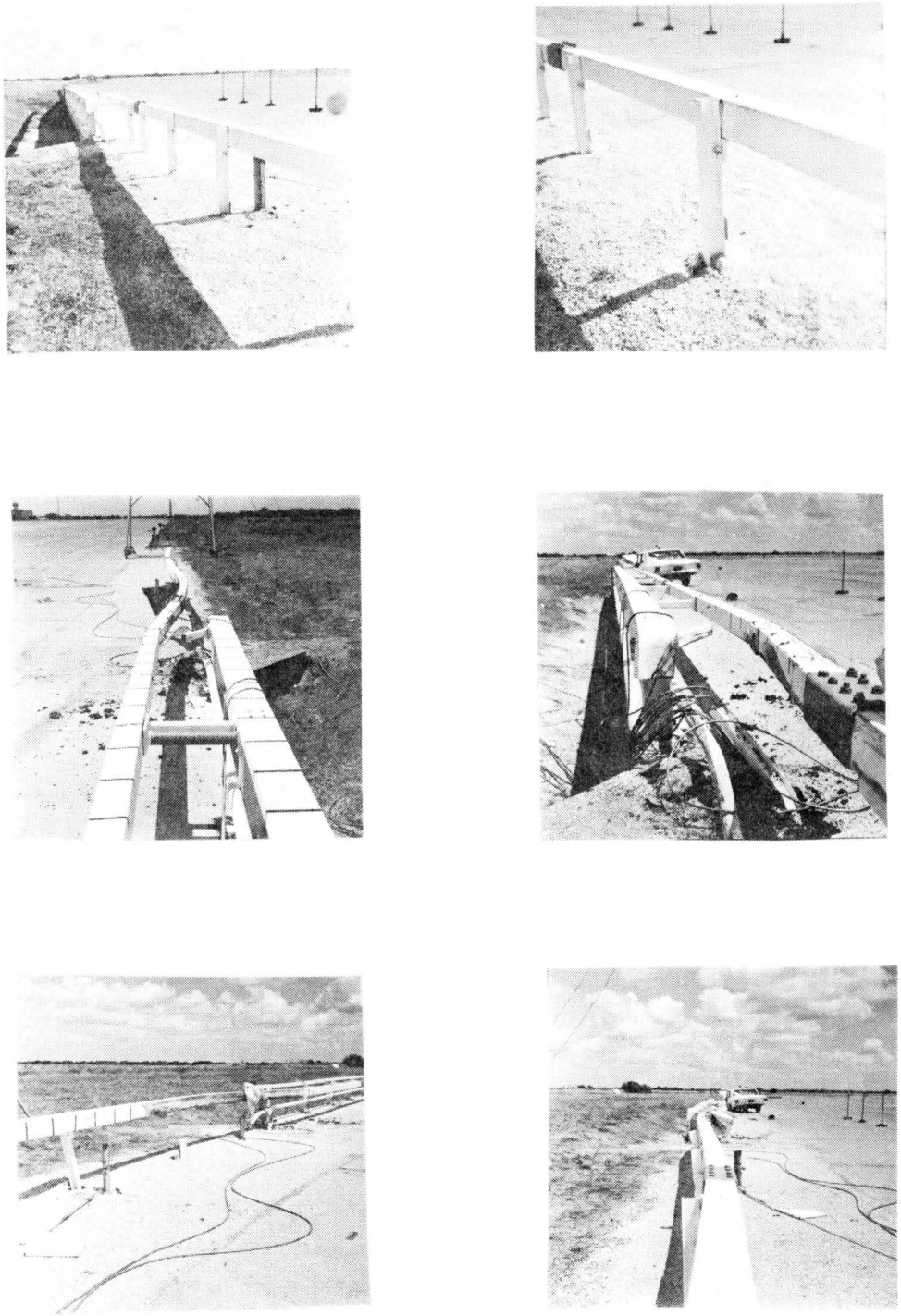

Figure 20 Installation Before and After Test (FT-D)

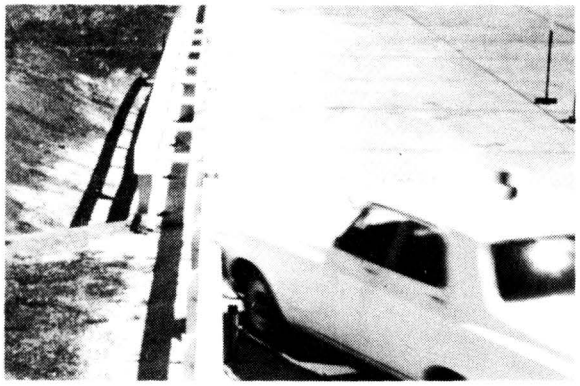

1.

2.

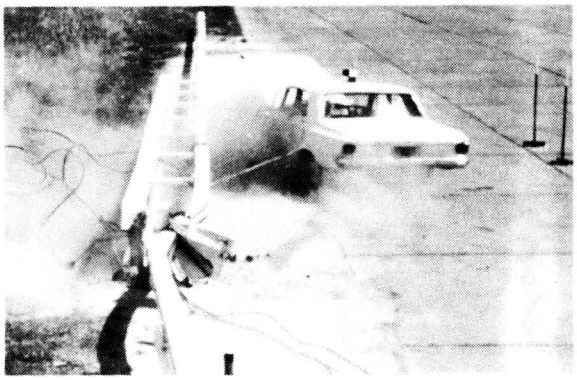

3.

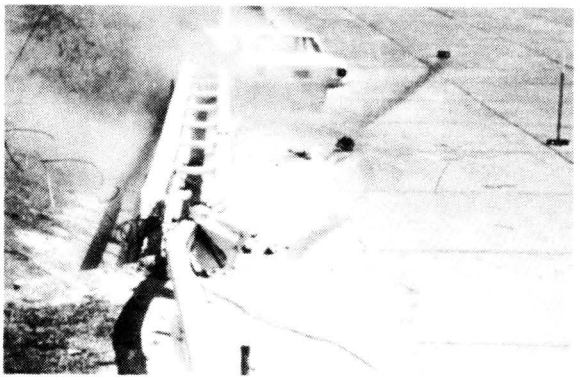

4.

Figure 21 Sequential Photographs of Test (FT-D)

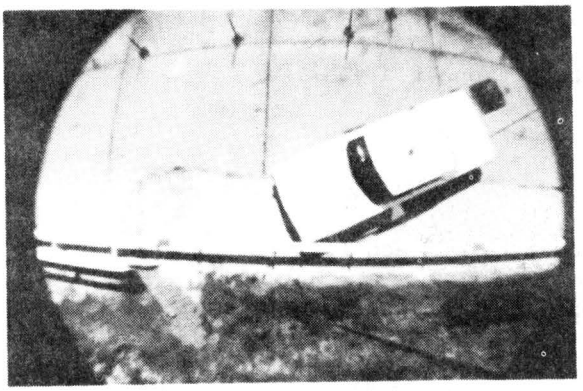

1.

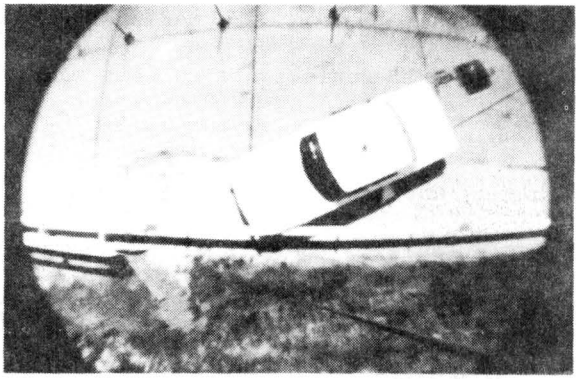

2.

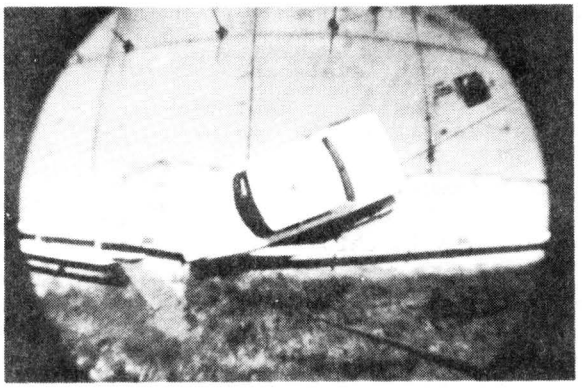

3.

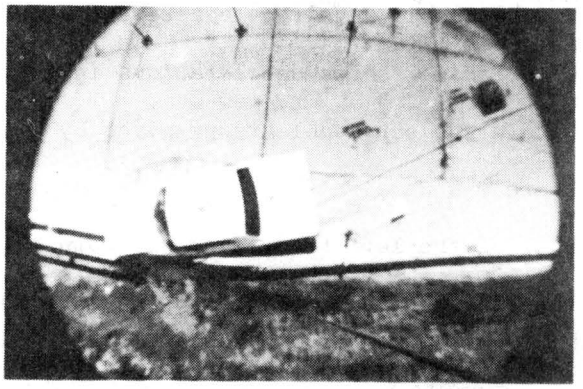

4.

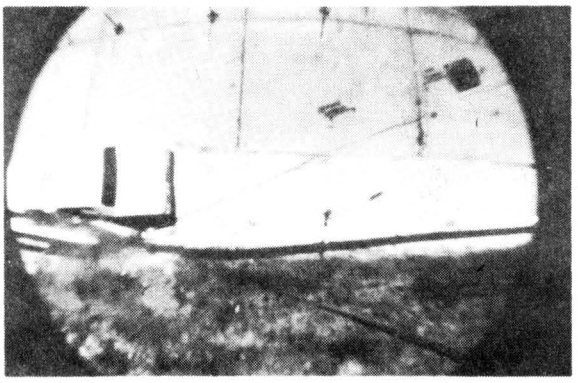

5.

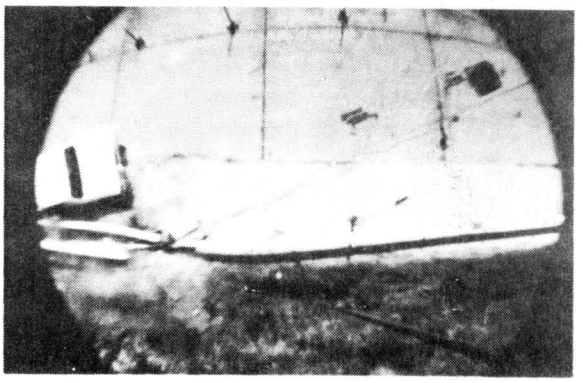

6.

Figure 22 Sequential Photographs of Test (FT-D)

SUMMARY AND CONCLUSIONS

The full-scale tests to determine the interaction of a vehicle and an Energy-Absorbing Type Bridge Rail are summarized in Figure 2, Table 1, and Table 2.

In Table 1, the figures shown indicate how much of each fragmenting tube was used in absorbing the energy at a particular bridge post. In Tests FT-A, B, and C the largest of these deformations is a rough approximation of the maximum deflection of the box beam rail. Approximately 10,000 lbs is required to activate each fragmenting aluminum tube.

Table 2 shows decelerations in g's. All deceleration levels are within the survivable range given by Olson et al[2]. In all of the tests, there was no significant vehicle compartment encroachment, but in FT-D part of the left front door was torn off. In all tests in this series, the vehicles were redirected and came to rest without rolling over. A properly seatbelted, shoulder-harnessed passenger would probably have sustained only minor injuries in each test.

TABLE 1

DEFORMATION OF FRAGMENTING TUBES

(In Inches)

Bridge Post No.	Bridge Tube No.	Test No.			
		FT-A	FT-B	FT-C	FT-D
10	1*	0	1/8"	0	1-1/4"
11	2	0	6"	0	0
12	3	0	14-3/4"	0	0
13	4	2-1/2"	10"	0	0
14	5	5-1/2"	1/8"	0	0
15	6	0	0	0	0
16	7	0	0	0	0
17	8	0	0	0	0

* Tubes are numbered from South to North end of bridge. (Vehicle travels from South to North.)

TABLE 2

AVERAGE VEHICLE DECELERATIONS

(In g's)

Test No.	$\bar{a}_t$*	$\bar{a}_t$**	$\bar{a}_l$***
FT-A	4.5	5.3	2.1
FT-B	3.7	3.7	2.0
FT-C	3.7	4.7	2.0
FT-D	4.5	4.3	3.3

* Average deceleration perpendicular to bridge rail up to maximum penetration. Calculated from photographic measurement of initial velocity and transverse distance vehicle c.g. travels from initial contact to maximum penetration.

** Average deceleration perpendicular to bridge rail up to maximum penetration. Calculated from photographic measurement of initial velocity and bridge rail deflection.[2]

*** Average deceleration along vehicle's longitudinal axis during contact with bridge rail. Calculated from photographic measurement of initial and final velocities, and distance in contact.

SELECTED REFERENCES

1. Woolam, William E. and Garza, Luis R., "Design, Fabrication, and Installation of a Fragmenting-Tube-Type Energy Absorber in Conjunction with a Bridge Rail," Southwest Research Institute, 1969.

2. Olson, R. M., Post, E. R., and McFarland, W. F., "Tentative Service Requirements for Bridge Rail Systems," National Cooperative Highway Research Program Report, Project 12-8, February, 1969.

A P P E N D I X

Photographic and Electronic Data

TABLE A1

TEST 505 FT-A

High Speed Film Data

Time msec.	Displacement ft	Time msec.	Displacement ft
-50.0	- 4.3	(Continued)	
-40.0	- 3.4	200.0	14.9
-30.0	- 2.6	210.0	15.5
-20.0	- 1.7	220.0	16.1
-10.0	- 0.9	230.0	16.7
0 Impact	0	240.0	17.3
10.0	0.9	250.0	17.9
20.0	1.7	260.0	18.5
30.0	2.6	270.0	19.1
40.0	3.4	280.0	19.7
50.0	4.3	290.0	20.3
60.0	5.1	—— Car Leaves Rail ——	
70.0	5.9	300.0	20.9
80.0	6.6	310.0	21.5
90.0	7.4	320.0	22.1
100.0	8.2	330.0	22.7
110.0	9.0	340.0	23.3
120.0	9.7	350.0	23.9
130.0	10.4	360.0	24.5
140.0	11.1	370.0	25.1
150.0	11.7	380.0	25.7
160.0	12.4	390.0	26.4
170.0	13.1	400.0	26.9
180.0	13.6		
190.0	14.2		

TABLE A2

TEST 505 FT-B

High Speed Film Data

Time msec.	Displacement ft	Time msec.	Displacement ft
-61.2	- 4.9	(Continued)	
-51.0	- 4.1	240.5	16.7
-40.8	- 3.2	250.5	17.1
-30.6	- 2.4	260.5	17.7
-20.4	- 1.6	270.5	18.2
-10.2	- 0.8	280.6	18.8
0 Impact	0	290.6	19.3
10.0	0.8	300.6	19.7
20.0	1.6	320.6	20.8
30.1	2.4	340.7	21.8
40.1	3.2	360.7	22.7
50.1	4.0	380.8	23.7
60.1	4.8	400.8	24.6
70.1	5.6	420.8	25.6
80.2	6.3	440.9	26.6
90.2	7.1	460.9	27.5
100.2	7.9	481.0	28.5
110.2	8.6	501.0	29.4
120.2	9.2	521.0	30.4
130.3	10.0	541.1 — Car Leaves Rail	— 31.3
140.3	10.7	561.1	32.3
150.3	11.3	581.2	33.3
160.3	11.9	601.2	34.3
170.3	12.6	621.2	35.2
180.4	13.3	641.3	36.2
190.4	13.9	661.3	37.1
200.4	14.5	681.4	38.0
210.4	15.1	701.4	39.1
220.4	15.6	721.4	40.0
230.5	16.1	741.5	40.9
		761.5	41.9

TABLE A3

TEST 505 FT-C

High Speed Film Data

Time msec.	Displacement ft	Time msec.	Displacement ft
-71.3	- 4.8	(Continued)	
-61.1	- 4.1	203.7	10.0
-50.9	- 3.4	213.8	10.5
-40.7	- 2.8	224.0	10.9
-30.6	- 2.1	234.2	11.4
-20.4	- 1.4	244.4	12.0
-10.2	- 0.6	254.6	12.4
0 Impact	0	264.8	13.0
10.2	0.6	274.9	13.5
20.4	1.3	285.1	13.9
30.6	1.9	295.3	14.5
40.7	2.5	305.5	14.9
50.9	2.9	315.7	15.4
61.1	3.5	325.9	16.0
71.3	3.9	336.0	16.4
81.5	4.4	— Car Leaves Rail —	
91.6	4.9	346.2	16.9
101.8	5.3	356.4	17.4
112.0	5.7	366.6	17.9
122.2	6.2	376.8	18.4
132.4	6.7	387.0	18.9
142.6	7.1	397.1	19.4
152.7	7.6	407.3	19.9
162.9	8.0	417.5	20.3
173.1	8.5	427.7	20.8
183.3	9.0	437.9	21.3
193.5	9.5	448.1	21.8

TABLE A4

TEST 505 FT-D

High Speed Film Data

Time msec.	Displacement ft	Time msec.	Displacement ft
-61.5	- 5.6	(Continued)	
-51.2	- 4.6	304.2	20.8
-41.0	- 3.7	324.5	21.6
-30.7	- 2.8	344.8	22.5
-20.5	- 1.9	365.0	23.2
-10.2	- 0.9	385.3	24.1
0 Impact	0	405.6	24.9
10.1	0.9	425.9	25.7
20.3	1.8	446.2	26.5
30.4	2.7	466.4	27.2
40.6	3.6	486.7	28.0
50.7	4.4	507.0	28.7
60.8	5.3	527.3	29.5
71.0	6.2	547.6	30.3
81.1	7.0	567.8	31.1
91.3	7.8	— Car Leaves Rail —	
101.4	8.8	588.1	31.9
111.5	9.5	608.4	32.6
121.7	10.3	628.7	33.4
131.8	11.1	649.0	34.2
142.0	11.9	669.2	34.9
152.1	12.6	689.5	35.7
162.2	13.4	709.8	36.5
172.4	14.0	730.1	37.3
182.5	14.8	750.4	38.1
192.7	15.3	770.6	38.8
202.8	16.0	790.9	39.7
212.9	16.6	811.2	40.5
223.1	17.1	831.5	41.3
233.2	17.6	851.8	42.0
243.4	18.1	872.0	42.7
263.6	19.0		
283.9	20.0		

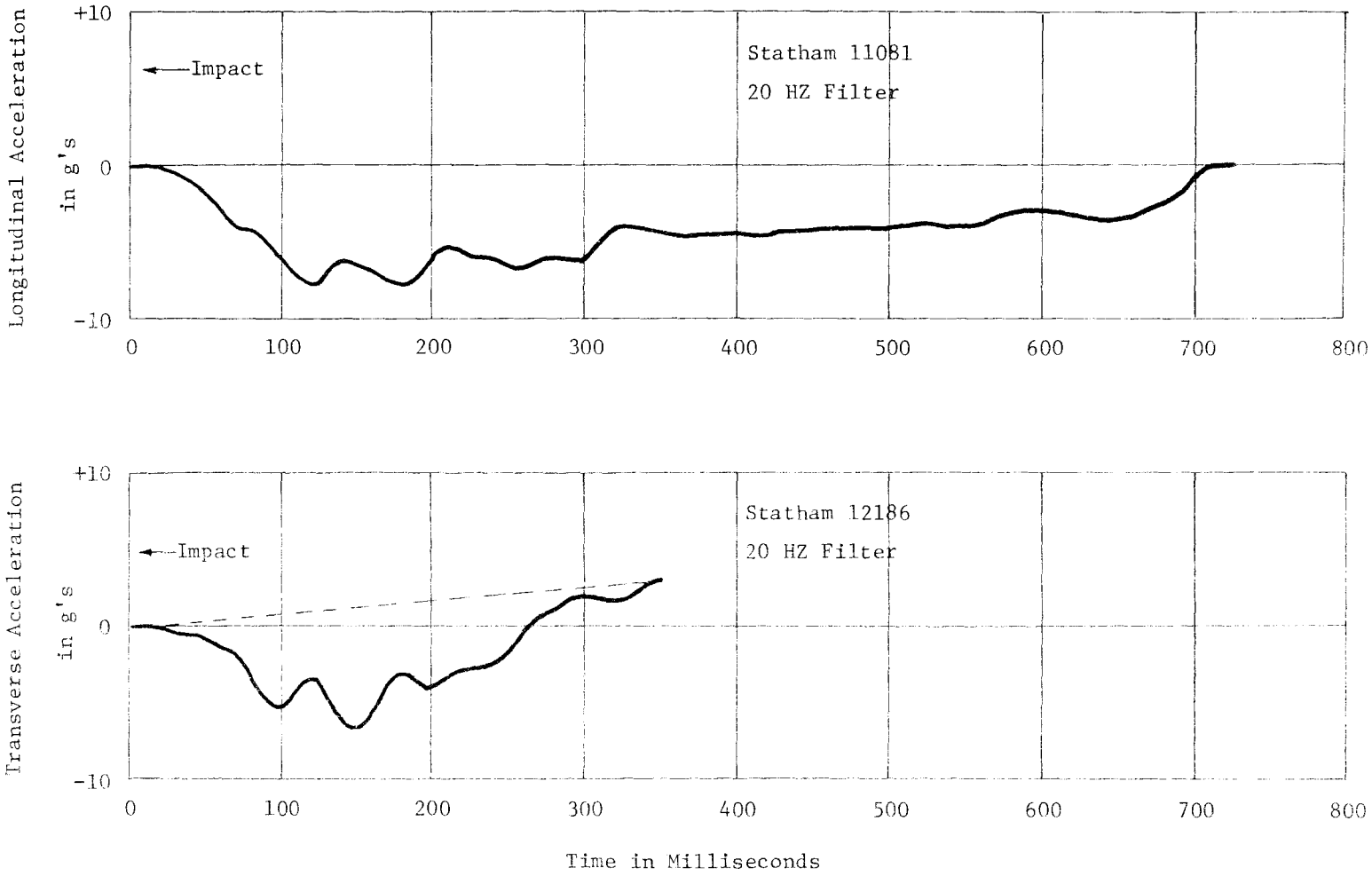
Longitudinal Acceleration
in g's
+10
0
-10
Impact
Statham 11081
20 HZ Filter
0
100
200
300
400
500
600
700
800
Transverse Acceleration
in g's
+10
0
-10
Impact
Statham 12186
20 HZ Filter
0
100
200
300
400
500
600
700
800
Time in Milliseconds

TEST 505 FT-A

Longitudinal Acceleration
in g's
+10
0
-10
← Impact
CFC 1558
20 HZ Filter
0
100
200
300
400
500
600
700
800
Transverse Acceleration
in g's
+10
0
-10
← Impact
Statham 1108l
20 HZ Filter
0
100
200
300
400
500
600
700
800
Time in Milliseconds

TEST 505 FT-B

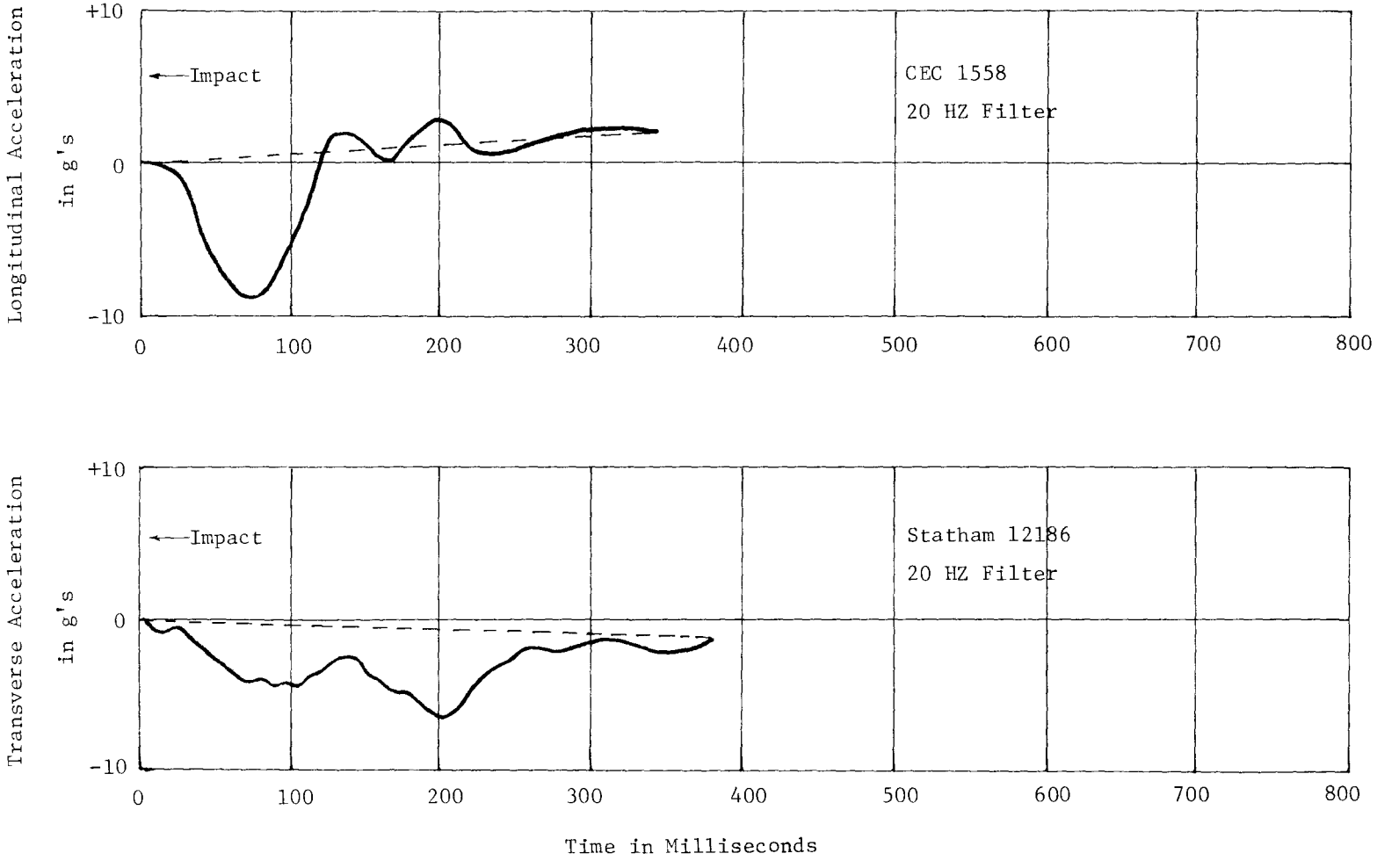
Longitudinal Acceleration
in g's
+10
0
-10
Impact
CEC 1558
20 HZ Filter
0
100
200
300
400
500
600
700
800
Transverse Acceleration
in g's
+10
0
-10
Impact
Statham 12186
20 HZ Filter
0
100
200
300
400
500
600
700
800
Time in Milliseconds

TEST 505 FT-C

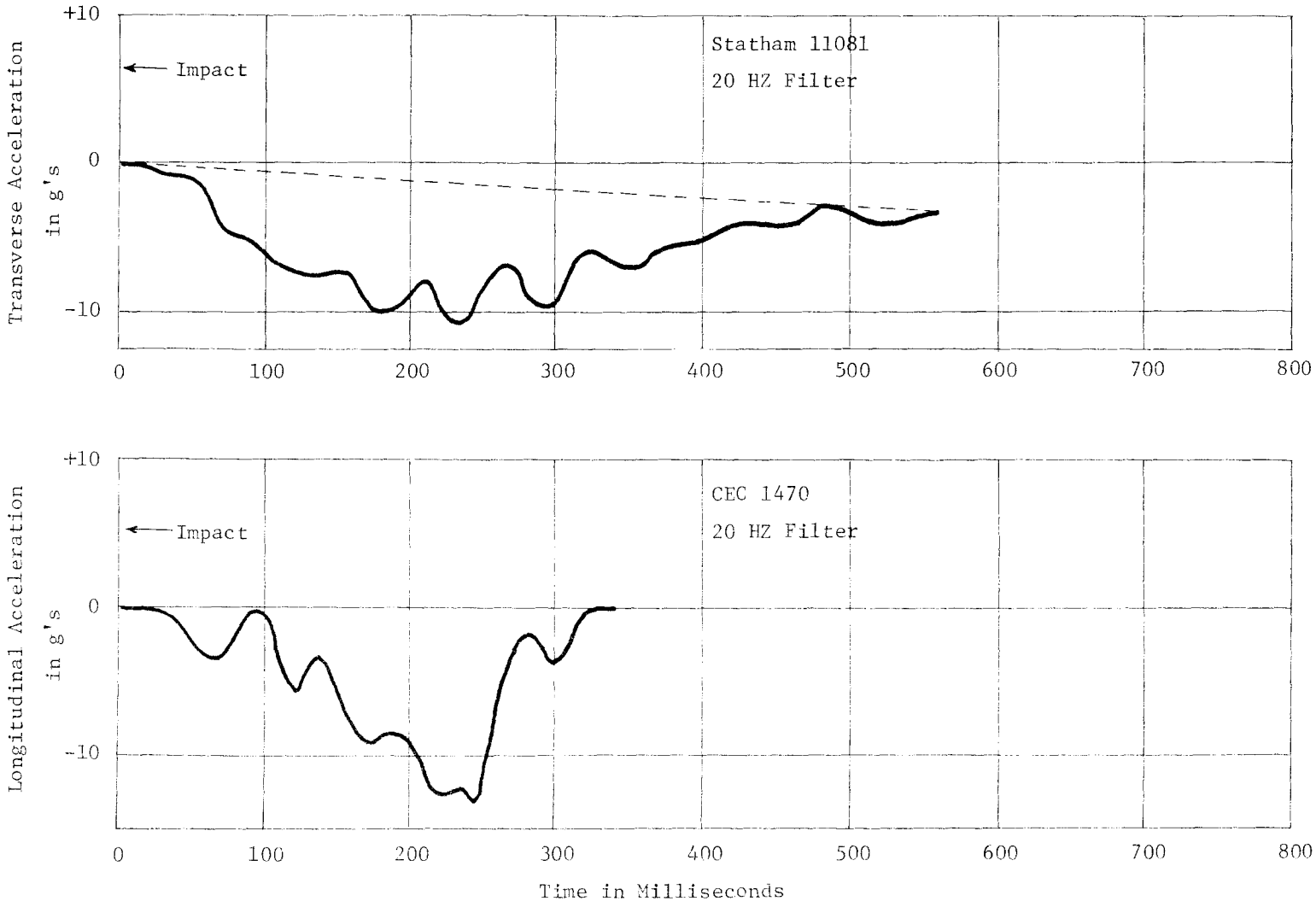
+10
0
-10
Transverse Acceleration
in g's
Impact
Statham 11081
20 HZ Filter
0
100
200
300
400
500
600
700
800
+10
0
-10
Longitudinal Acceleration
in g's
Impact
CEC 1470
20 HZ Filter
0
100
200
300
400
500
600
700
800
Time in Milliseconds

TEST 505 FT-D

TECHNICAL MEMORANDUM 505-9

Texas Transportation Institute
Texas A&M Research Foundation

FEASIBILITY OF LIGHTWEIGHT CELLULAR CONCRETE VEHICLE CRASH CUSHIONS

A Tentative Progress Memorandum on Contract No. CPR-11-5851

U.S. Department of Transportation
Federal Highway Administration
Bureau of Public Roads

by

Don L. Ivey
Associate Research Engineer

Eugene Buth
Assistant Research Engineer

and

T. J. Hirsch
Research Engineer

These crash tests and evaluations were conducted under the Office of Research and Development, Structures and Applied Mechanics Division's Research Program on Structural Systems in Support of Highway Safety (4S Program). The opinions, findings, and conclusions expressed in this report are those of the authors and not necessarily those of the Bureau of Public Roads.

NOTE: For the reader who is interested in gaining a general idea of the value of this particular arresting system and not in the details necessary to document the technical aspects of this study, the authors recommend reading page 2, noting the comparative values of speed and deceleration on page 13, and scanning the photographs in this report.

January 1970

INTRODUCTION

Cellular concrete structures have been proposed as vehicle deceleration devices in a recent feasibility study by Cornell Aeronautical Laboratories[1*]. Three vehicle crash tests have been conducted on a lightweight cellular concrete crash cushion (designed by personnel of the Texas Transportation Institute) with very favorable results. The crash cushion is composed of vermiculite concrete with hollow cardboard tubes (23 inches in diameter) spaced throughout to provide the necessary voids. Lightweight welded wire fabric is used as reinforcement for the vermiculite. The first Concrete Crash Cushion constructed is shown in Figures 1 and 2.

The concrete used for the crash cushions in this study was composed of cement, water, and a commercial grade of vermiculite. This vermiculite aggregate was very uniform in gradation. Vermiculite is a kiln-expanded mica. Since mica is a rock composed of many thin layers, it is subject to high expansion, leaving spaces between these layers. The average size particle is approximately a 1/8 inch cube. On close examination, a single cubical particle looks like a tiny accordian. These small cubes can be compressed to a flat particle by slight pressure. The extreme light weight (per bulk volume) of this aggregate in combination with a high degree of air entrainment produces a very lightweight, low-strength concrete.

---

* Superscript numerals refer to corresponding references at the end of this report.

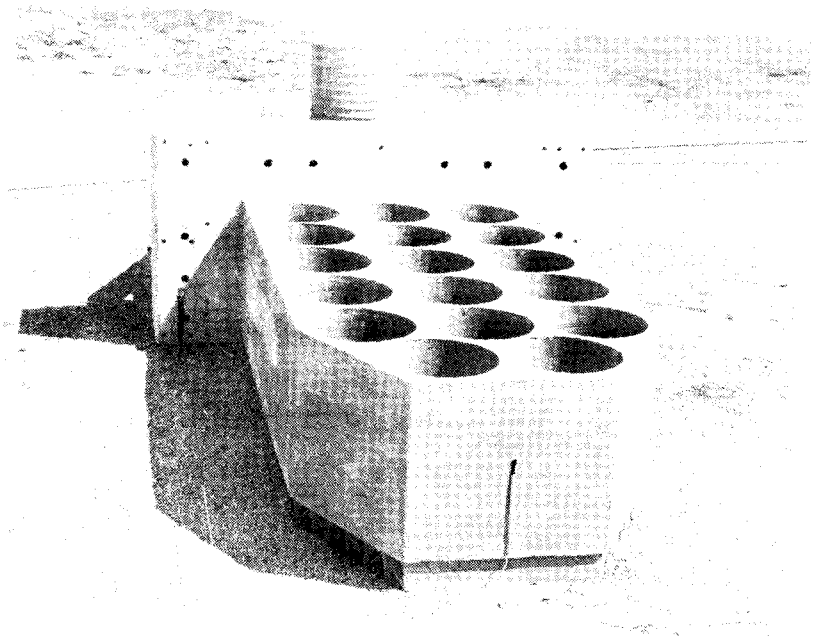

Figure 1. Prototype of Concrete Crash Cushion

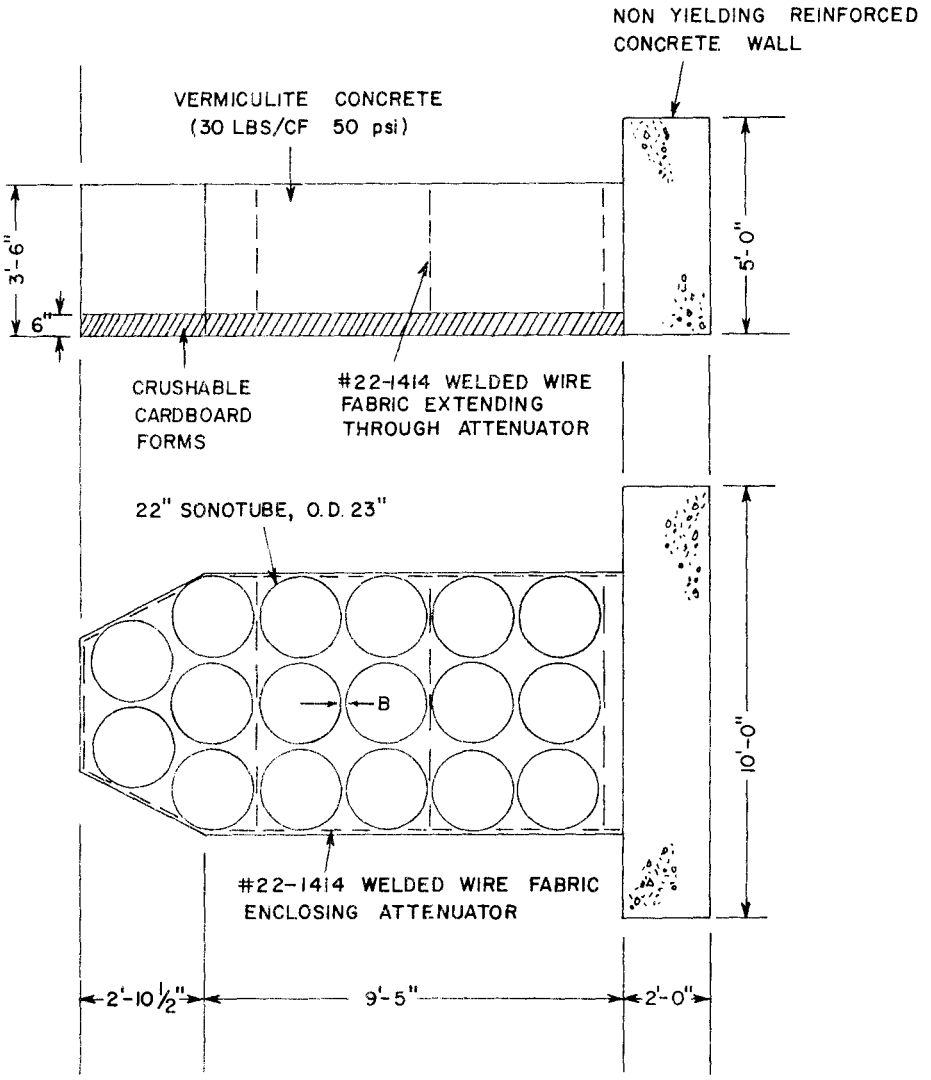

FIGURE 2, CONCRETE CRASH CUSHION, TEST 505V-A

MATERIALS AND CONSTRUCTION

A 1:7 mixture of vermiculite concrete was used in all three crash cushions. Coarse vermiculite aggregate and Type III Cement were used in the cushions for Tests 505V-A and 505V-B. Welded wire fabric (24-1414) reinforcement was placed longitudinally in each side wall and transversely between each row of sonotubes in the 505V-A cushion. In the 505V-B cushion, a layer of this wire fabric was also placed in the top and bottom surfaces. Mixture proportions and properties of the concrete are given in Table 1. Folding cardboard carton forms were used as the bottom form with reinforced 3/4 inch plywood sheets used for the side forms. In Tests 505V-A and 505V-B, the cardboard carton forms remained in place and supported the cushion 6 inches above ground level when installed at the test site. The sonotube spacing was maintained with small wooden blocks.

The cushion for Test 505V-A was cast as a single unit, then transported to the test site and installed. The 505V-B cushion was cast in place at the test site. Precast modules were used in constructing the cushion for Test 505V-C. One of the three-tube modules is shown in Figure 4. The welded wire fabric was placed in all four outside walls of the forms. Using a new fast-setting cement developed by the Portland Cement Association, the forms were removed in less than two hours after casting. This cement was furnished by the Lone Star Cement Corporation and is still in the experimental stage.

TABLE 1

MIXTURE PROPORTIONS AND PROPERTIES OF VERMICULITE CONCRETE

Test	Aggregate	Cement	Water	Wet Unit Wt	Dry Unit Wt	Compressive Strength
505V-A	121.3 lbs/cy 20.2 cf/cy	272 lb/cy 2.9 sacks/cy	607 lb/cy 72.9 gal/cy 25.1 gal/sack	37 pcf	32 pcf @ 12 days	50 psi @ 12 days
505V-B	140 lbs/cy 23.4 cf/cy	312 lb/cy 3.34 sacks/cy	629 lb/cy 75.5 gal/cy 22.6 gal/sack	40 pcf	32 pcf @ 18 days	71 psi @ 13 days
505V-C	150 lbs/cy 23.0 cf/cy	305 lbs/cy 3.24 sacks/cy	645 lb/cy 77.4 gal/cy 23.9 gal/sack	41 pcf average	21 pcf @ 30 days	57 psi @ 30 days

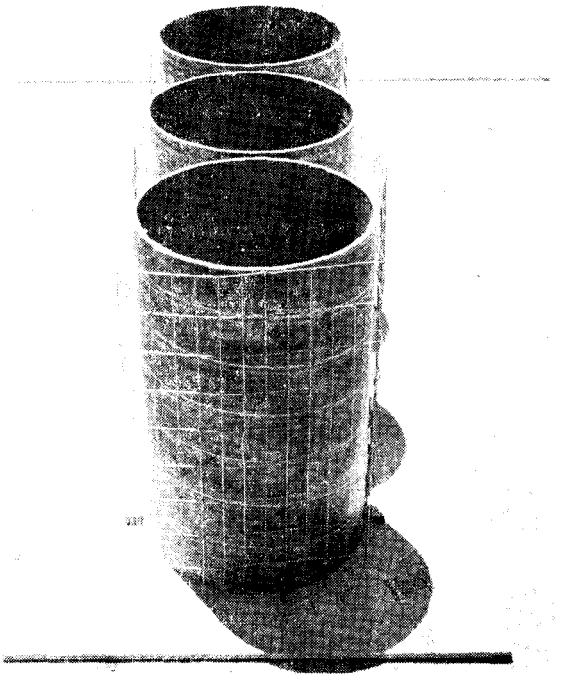

Figure 3, Non-concrete Components of Precast Vermiculite Module

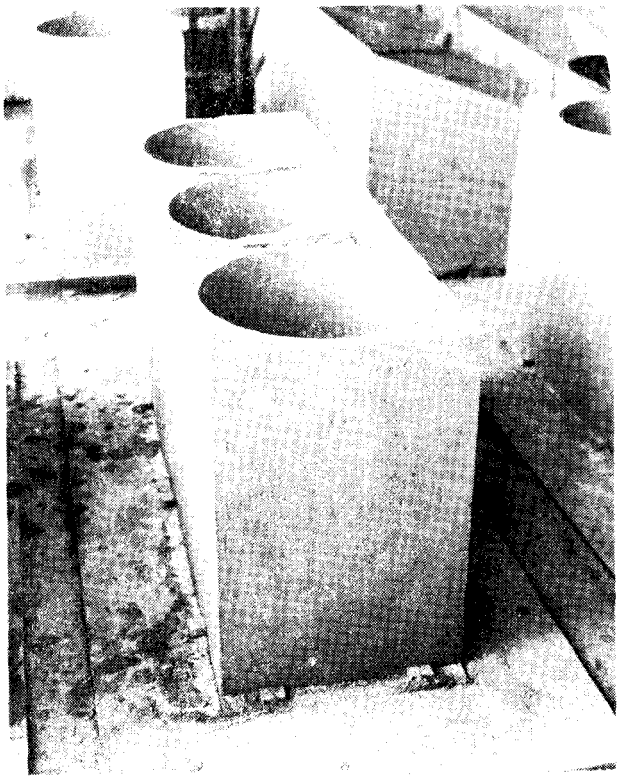

Figure 4, Precast Vermiculite Module

TEST PROGRAM

General

Three full-scale vehicle crash tests of the lightweight cellular concrete crash cushion have been conducted. Electronic accelerometers and an Impact-O-Graph were used in each test to record decelerations. High-speed cameras (500 frames per second) recorded the crash, and analysis of this film gives vehicle displacement and velocity with respect to time. Rough estimates of deceleration over distances of several feet can also be achieved by analysis of the photographic data. Selected photographs of the vehicle and crash cushion before and after each particular test, and sequential photographs of the test in progress are included.

Crash Tests

In Test 505V-A, only one-half of the proposed full-size crash cushion was fabricated. The first 12 feet of the cushion, shown in Figure 1, was subjected to a low-speed test (41 mph) by a 3650 lb vehicle. In Test 505V-B, a full-sized crash cushion (24 feet in length) was cast in place (see Figure 5). In this test, a 3200 lb vehicle impacted the cushion at a velocity of 59 mph. In the third test, 505V-C, the precast modular construction technique was used and the barrier was put together in the field using three-tube and two-tube modules. The design of this cushion is shown by Figure 6. A 4560 lb vehicle traveling 64 mph impacted this crash cushion head on. For comparison purposes, the test of a 3270 lb vehicle traveling 53 mph

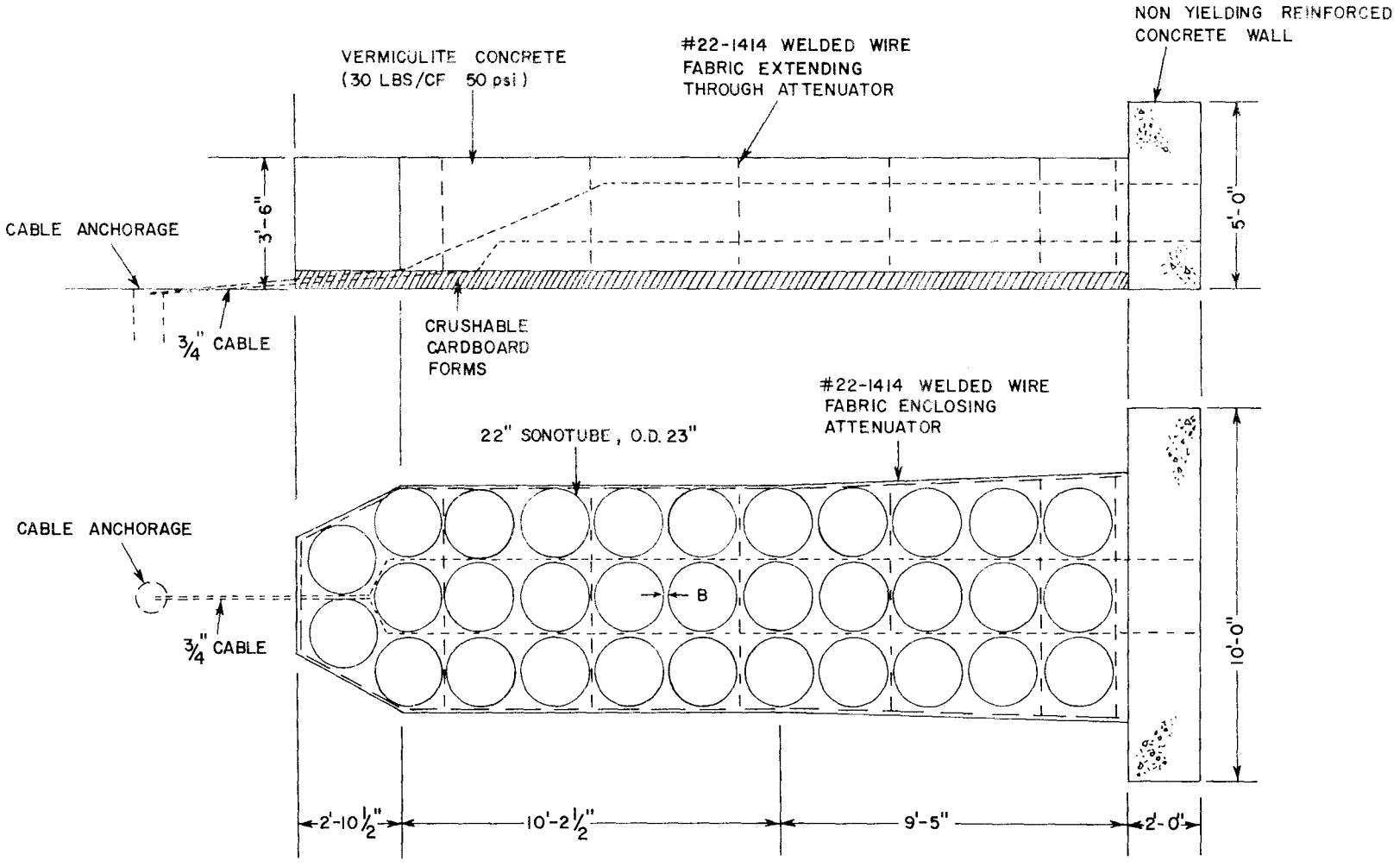

DIMENSION B = 2 IN.

FIGURE 5, CONCRETE CRASH CUSHION, TEST 505V-B

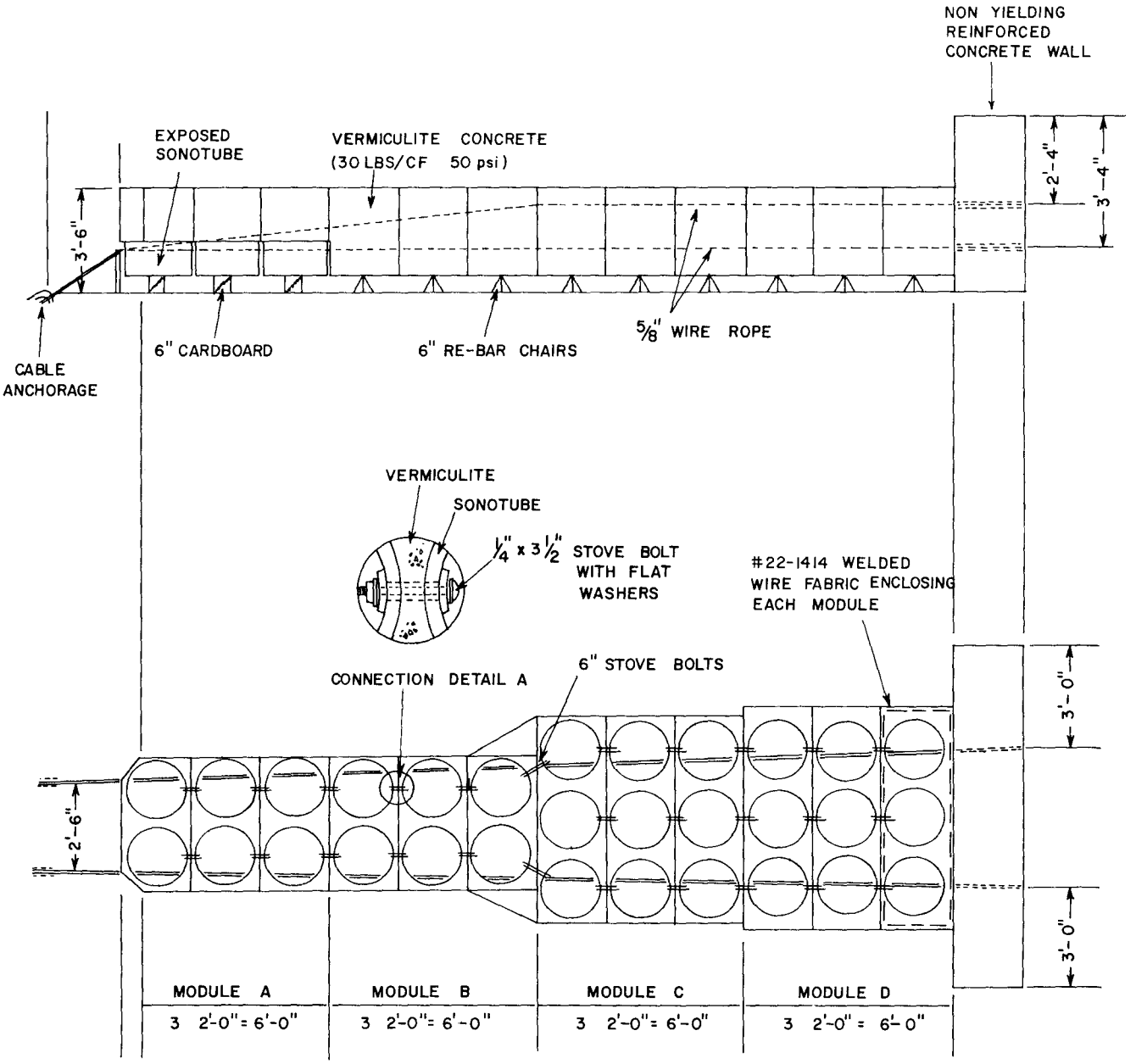

FIGURE 6, CONCRETE CRASH CUSHION, TEST 505V-C

impacting a rigid wall is included. This test is designated 505-IW and is shown in Figure 7.

These four head-on tests are summarized in Table 2. In Test 505V-A (Figures 8 through 14), the 1956 Pontiac was stopped in 9.0 ft with an average barrier force of 23,000 lbs. The average deceleration was 6.3 g's, which is considered an acceptable level. Test 505V-B illustrated the importance of the control of certain parameters in the fabrication of lightweight cellular concrete crash cushions. The compressive strength of the vermiculite concrete was increased to 71 psi and dimension "B" shown in Figure 5 was increased to 2 in. The 24-1414 welded wire fabric was placed in the top and bottom of this barrier to eliminate the tendency of some portions of the barrier to scatter on impact. Due to these differences, the barrier was significantly stiffer than the previous barrier tested and a deceleration level of 10.3 g's was observed (Figures 15 through 21). This corresponds to an average stopping force of approximately 33,000 lbs.

Based on the results of the first two tests, a third barrier, shown in Figure 6, was designed and tested which incorporated estimated stopping forces that varied from 13,000 lbs to 33,000 lbs. The first 12 ft of barrier, with predicted stopping force from 13,000 to 20,000 lbs, would result in the deceleration of a 2,000 lb vehicle traveling 60 mph at a deceleration level slightly less than 10 g's. The next 12 ft of the barrier, with 6 ft at a predicted 25,000 lbs stopping force and 6 ft at 33,000 lbs, would provide the necessary additional stopping force to decelerate a vehicle traveling 60 mph and weighing as much as 4500 lbs. This barrier was tested with a 4560 lb vehicle traveling

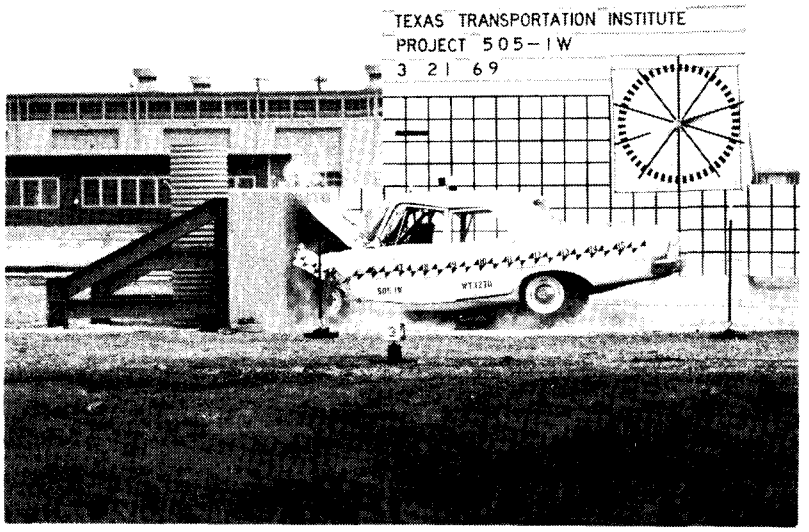

Figure 7, Crash Test 505-IW (Immovable Wall)

TABLE 2

SUMMARY OF TEST DATA

Test No.	505V-A	505V-B	505V-C	505-IW Rigid Wall
Vehicle, Year and Make	1956 Pontiac 4 Door	1963 Dodge 4 Door	1958 Oldsmobile 2 Door	1963 Plymouth 4 Door
Vehicle Weight (W), lbs	3650	3200	4560	3270
Vehicle Velocity (V), fps mph	60.3 41.1	86.2 58.8	93.3 63.6	78.3 53.3
Stopping Distance (D), ft	9.0	11.2	21.4	3.8
Max. Deceleration, g's (longitudinal)	10.5[a]	20.5[a]	10.4[a]	35[a]
Avg. Deceleration, g's (longitudinal)	5.1[a] 6.3[b]	6.6[a*] 10.3[b]	6.5[a] 6.3[b]	25.0[b]
Attenuation Index $AI_{(max)} = \frac{G\ (max.\ test)}{G\ (max.\ rigid)^c}$	0.29	0.39	0.18	0.73
$AI_{(avg)} = \frac{G\ (avg.\ test)}{G\ (avg.\ rigid)^c}$	0.27	0.31	0.17	0.82

[a]Electronic Accelerometer, *Not reliable due to zero shift
[b]Calculated from stopping distance
[c]G (max. rigid) = $0.9V^d$, G (avg. rigid) = $0.574V^d$, V in mph
[d]Emori, Richard I., "Analytical Approach to Automobile Collisions," SAE Paper 680016, Engr. Congress, Detroit, January 8, 1968.

63.6 mph, impacting head on (Figures 22 through 27). The estimated crushing force levels from photographic data show the predicted stopping forces were fairly accurate. The vehicle was stopped in 21.4 ft at an average deceleration of 6.3 g's, which means an average stopping force of 28,700 lbs.

The final test, which was included for comparison purposes (Figures 28 through 34), was that of a vehicle weighing 3270 lbs impacting a rigid wall at 53.3 mph. The average deceleration was 25.0 g's and the stopping distance of the vehicle's center of gravity, c.g., was 3.8 ft. The total vehicle residual crush was 3.3 ft.

A comparison of the severity of these crashes is given in Table 2 by the Attenuation Index. The maximum and average decelerations which would have been experienced by each vehicle had it struck a rigid barrier (for example, Test 505-IW) are calculated using accepted theory[2]. The Attenuation Index is the ratio of the test maximum or average deceleration divided by the rigid barrier maximum or average deceleration, respectively. The theory is an empirical generalization for all types of vehicles based on the particular vehicles tested by Emori, and could not be expected to give accurate decelerations for each vehicle tested. If the theory had accurately predicted the test decelerations, the Attenuation Index shown for this test would have been 1.0. The Attenuation Indices for the three lightweight cellular concrete crash cushion tests show that the impact is approximately 1/4 to 1/3 as severe as it would have been had the vehicle struck a rigid barrier.

In Test 505V-A, only superficial sheet metal damage was sustained by the vehicle. The radiator was not moved with respect to the frame

of the vehicle during the impact. In Test 505V-B, considerably more sheet metal damage was done to the vehicle and the radiator was moved back far enough to encounter the fan blades. However, the vehicle was driven away from the scene of the crash after the fan belt had been removed. In Test 505V-C, again only superficial sheet metal and some bumper damage was sustained. Test 505-IW resulted in the total and irrevocable destruction of the vehicle.

TABLE 3

VEHICLE DEFORMATIONS AND DAMAGES

TEST NO.	VEHICLE DEFORMATION	VEHICLE DAMAGE
505 V-A	Above front bumper and between fenders, 7 in.	Slight damage to right and left front fenders, front bumper arms, gravel shield, grill and hood. Due to defective motor mounts, the motor shifted forward and damaged the radiator.
505 V-B	Entire front was deformed approximately 12 in.	Right and left front fenders, front bumper, bumper arms, grill, hood, radiator, fan, water pump, radiator harness.
505 V-C	Grill and hood 12 in. Right front fender 1 in. Left front fender 6 in. Left front bumper 1 in.	Left front fender, grill, hood, radiator, fan, and bumper arms. Slight damage to right front fender and bumper.
505-IW	Entire front Dynamic - 3.82 ft. Residual - 3.25 ft.	Total.

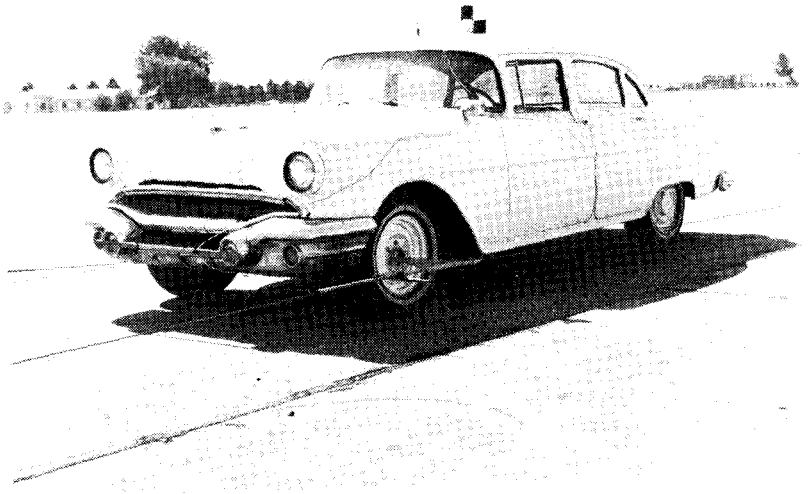

Figure 8, Vehicle Before Test 505V-A

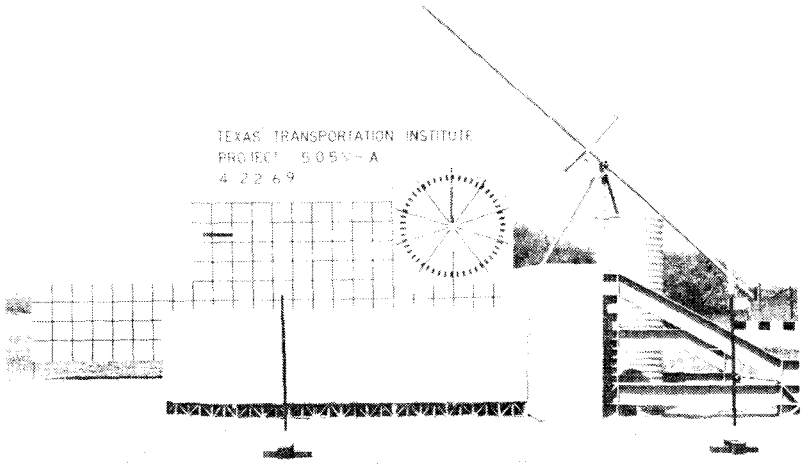

Figure 9, Concrete Crash Cushion Before Test 505V-A

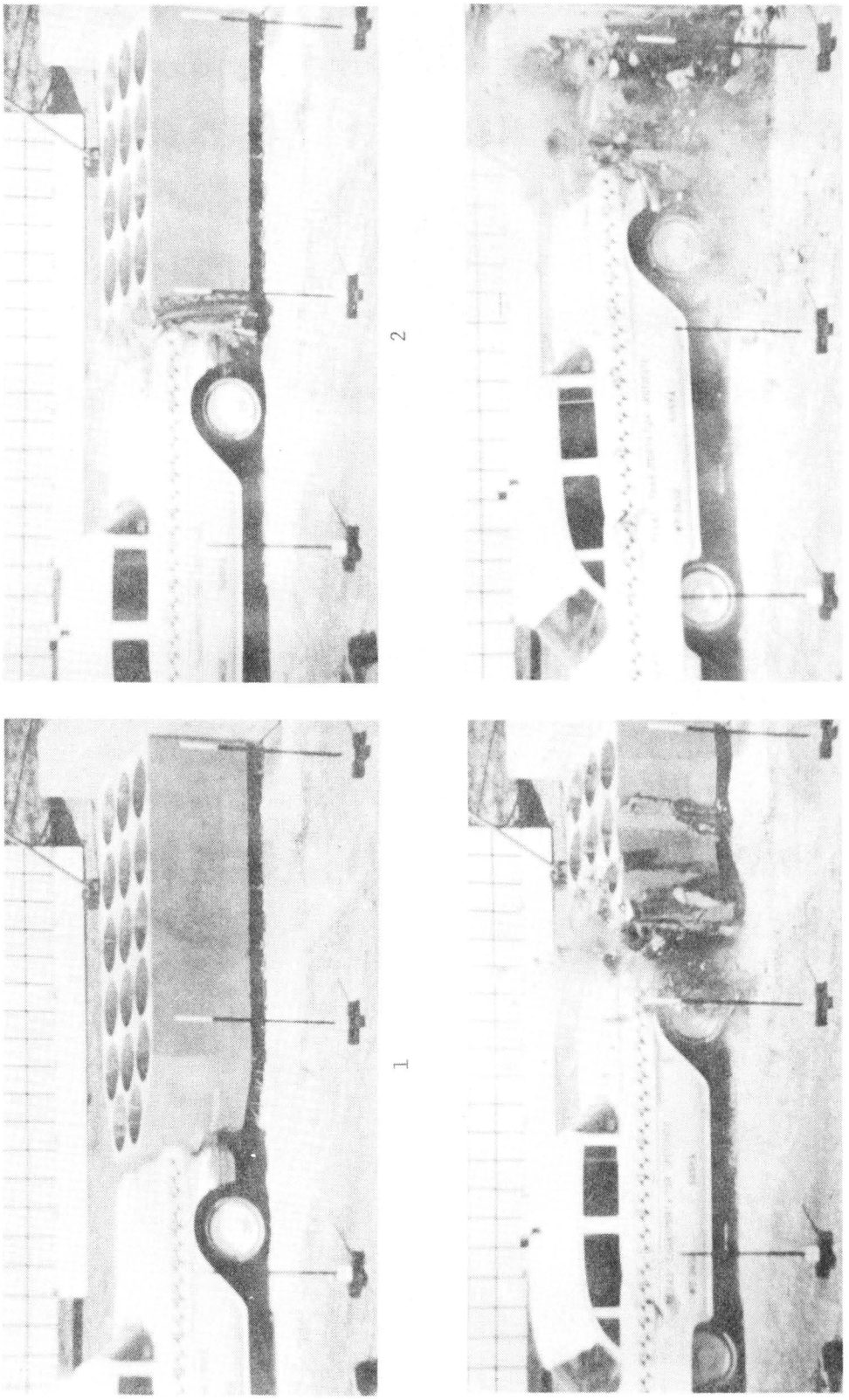

Figure 10, Sequential Photographs of Test 505V-A

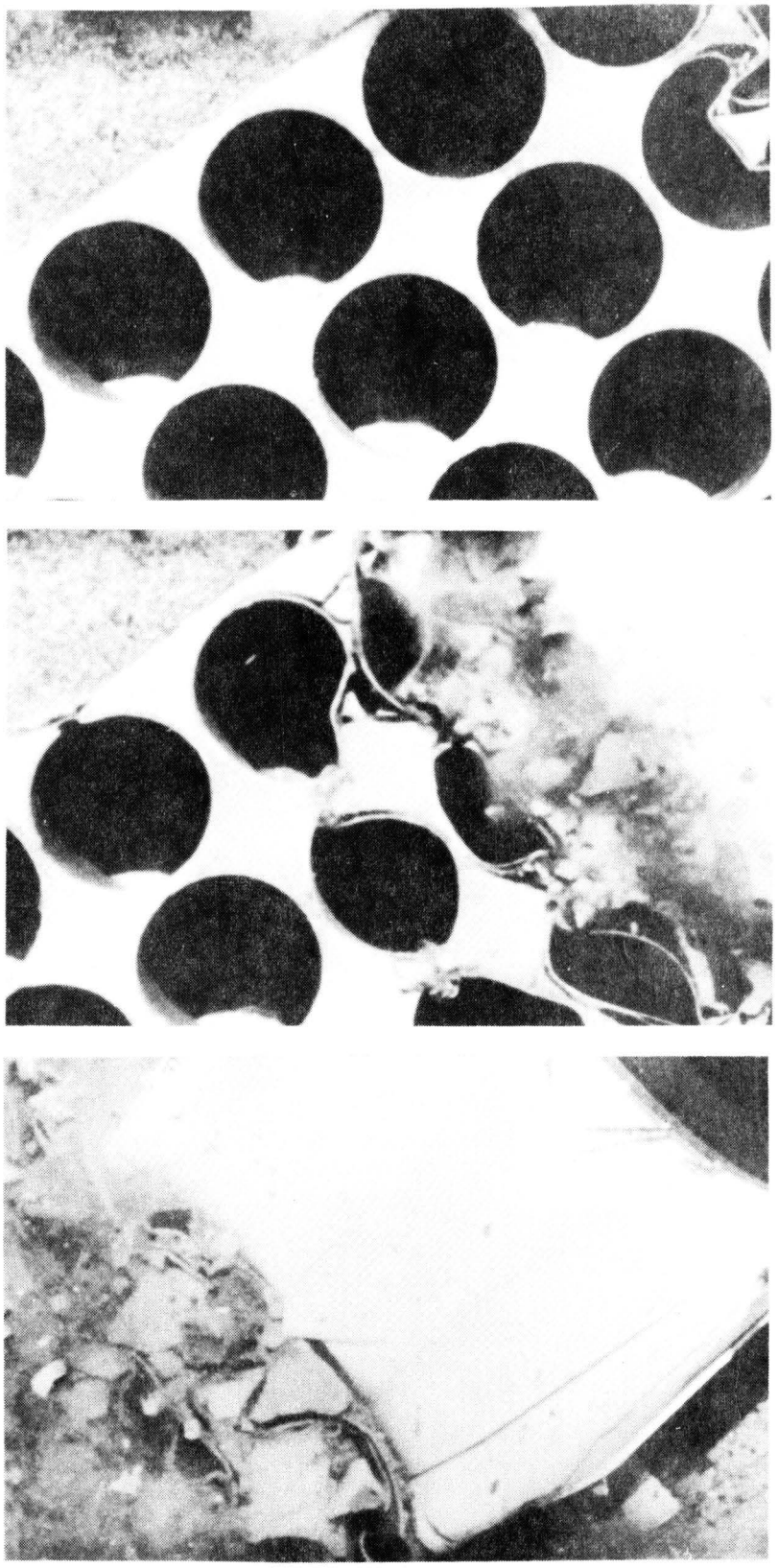

Figure 11, Overhead View of Initial, Intermediate, and Final Crushing Modes During Test 505V-A

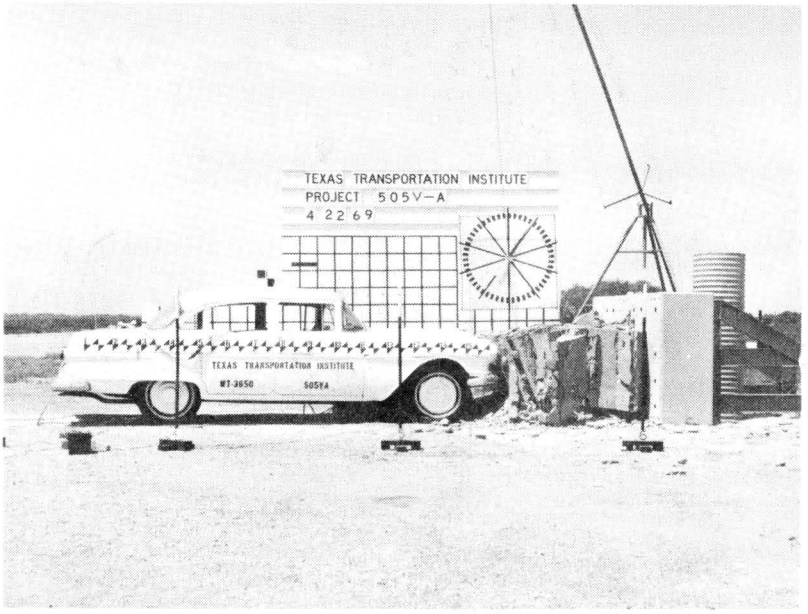

Figure 12, Impact Area After Test 505V-A

Figure 13, Damage to Vehicle in Test 505V-A

Figure 14, Top View of Crash Cushion
After Test 505V-A

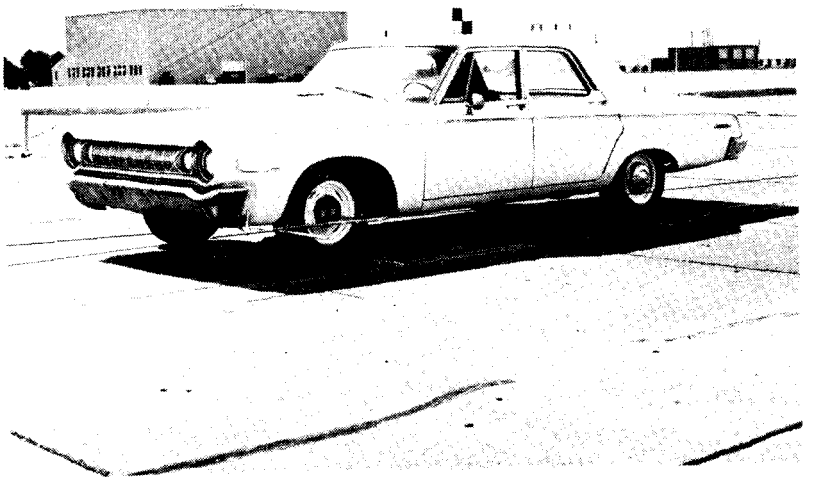

Figure 15, Vehicle Before Test 505V-B

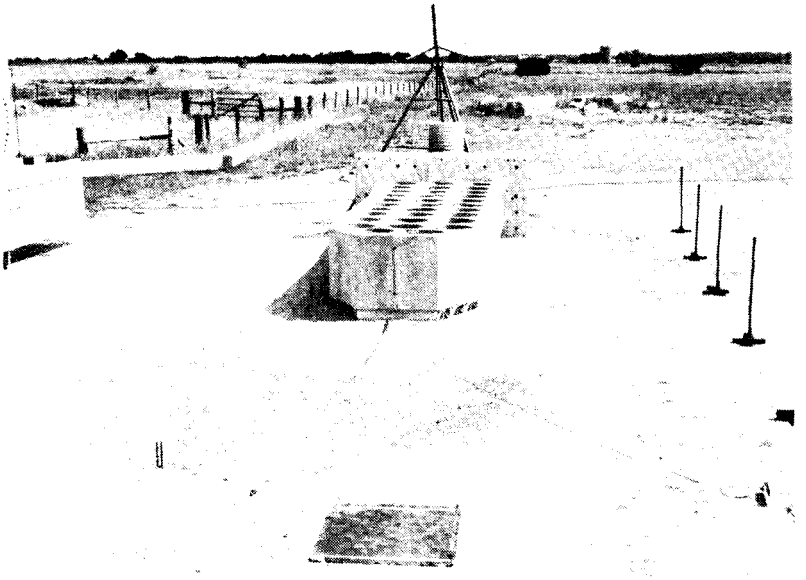

Figure 16, Concrete Crash Cushion Before Test 505V-B

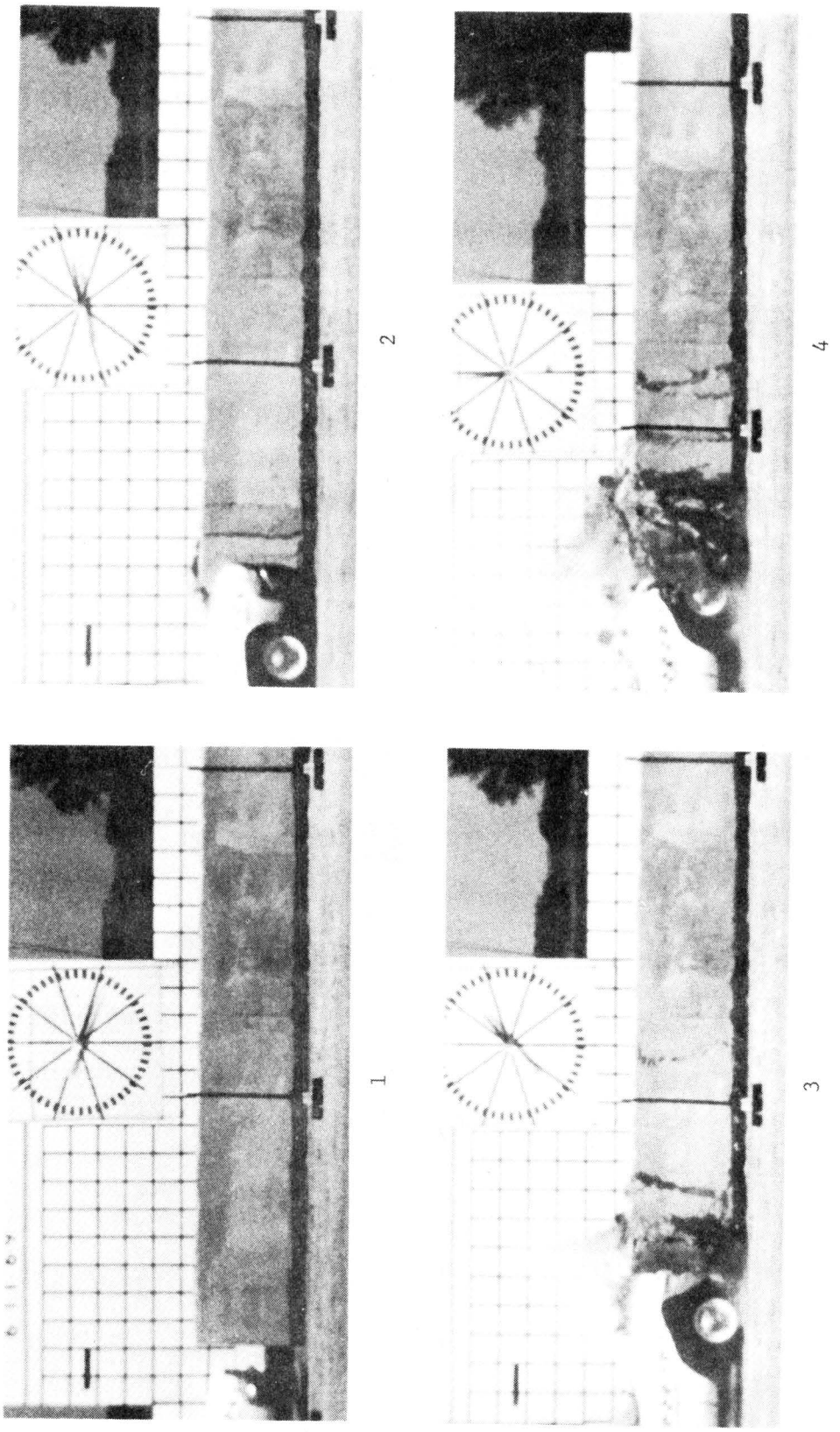

Figure 17, Sequential Photographs of Test 505V-B

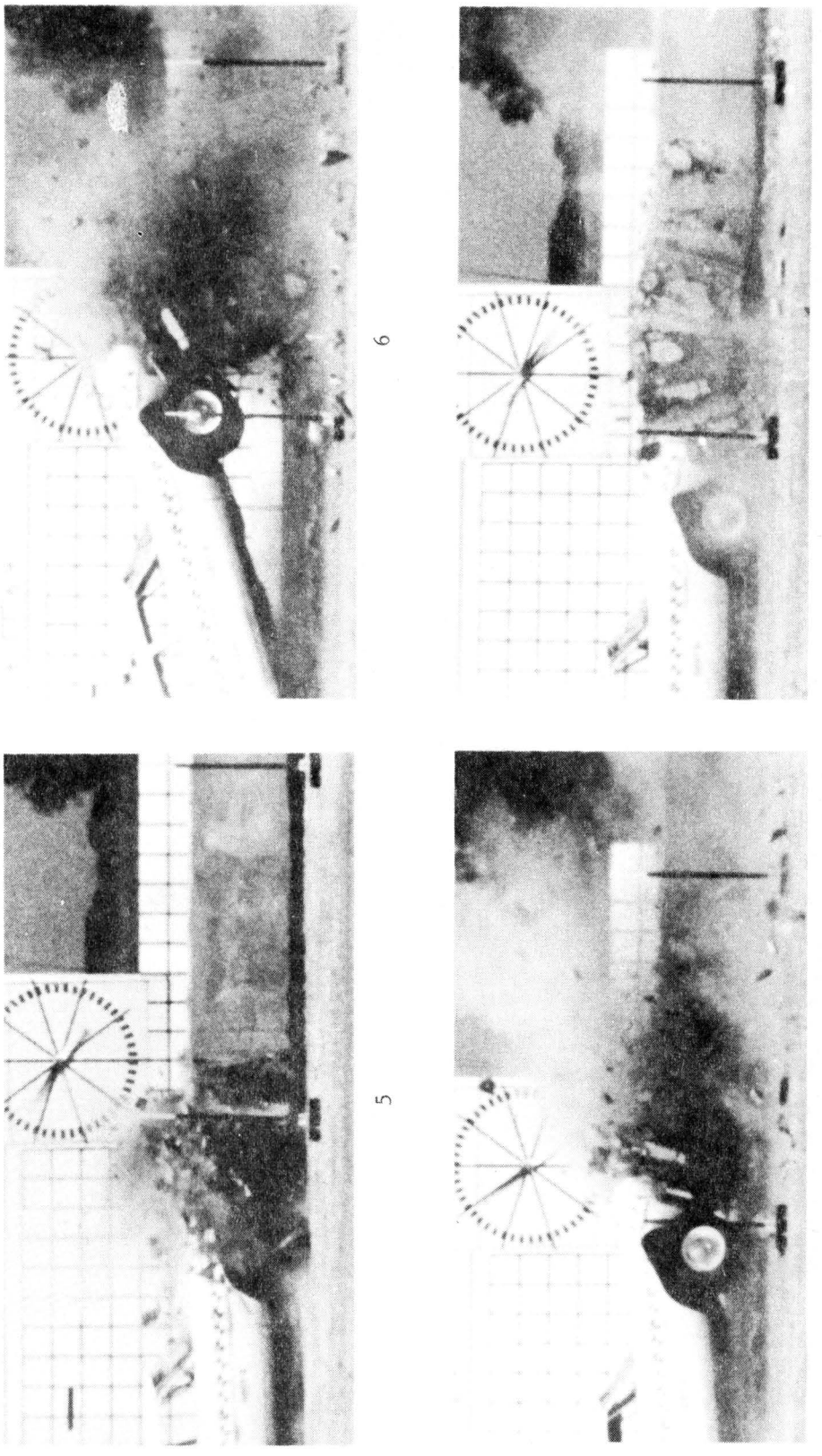

Figure 17, Sequential Photographs of Test 505V-B (Continued)

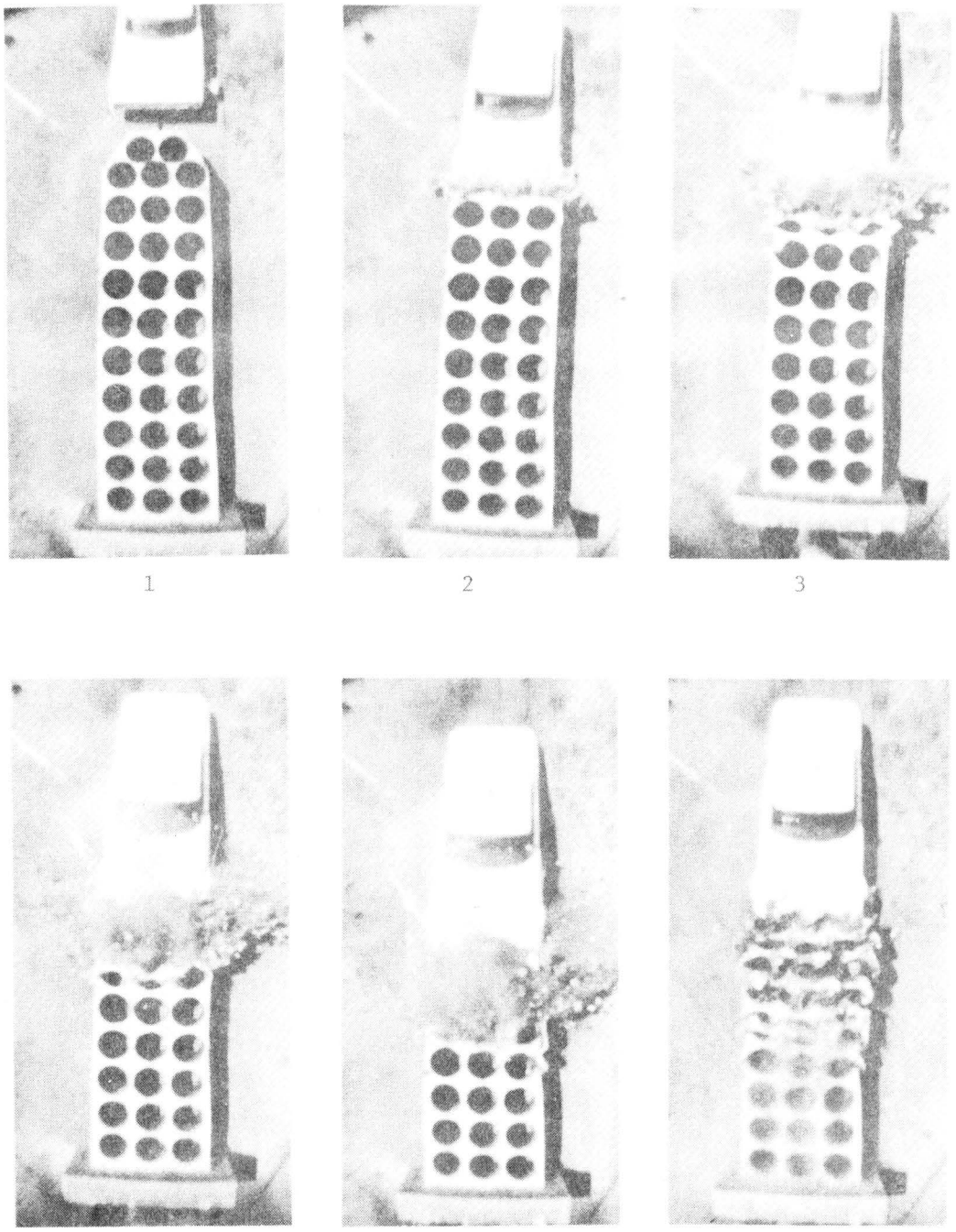

Figure 18, Overhead Sequence Photographs
Of Test 505V-B

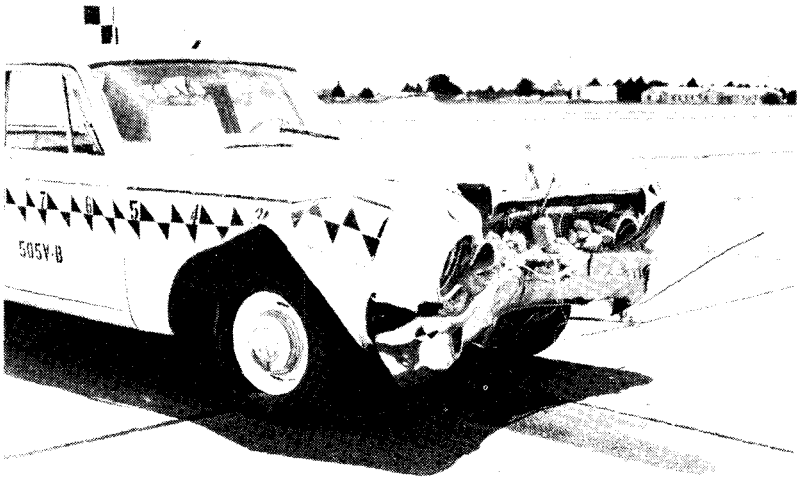

Figure 19, Vehicle After Test 505V-B

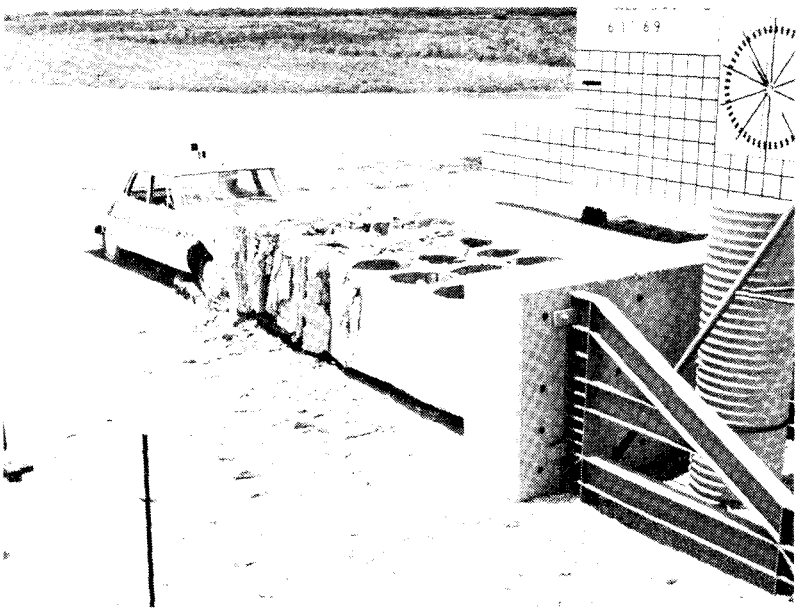

Figure 20, Impact Area After Test 505V-B

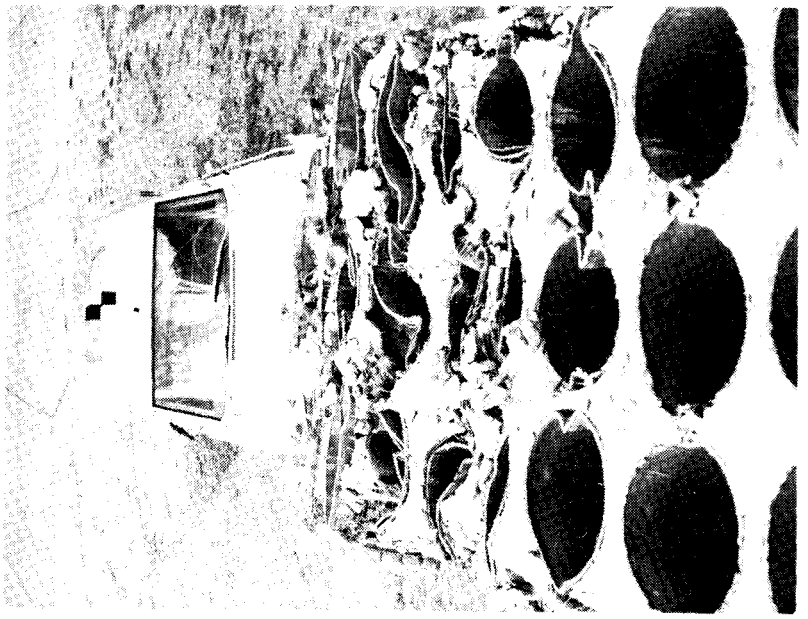

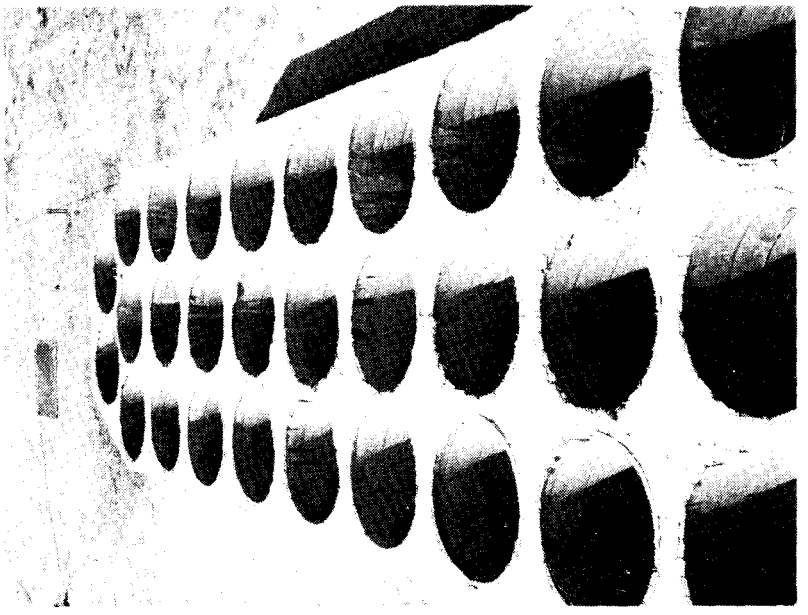

Figure 21, Concrete Crash Cushion Before and After Test 505V-B

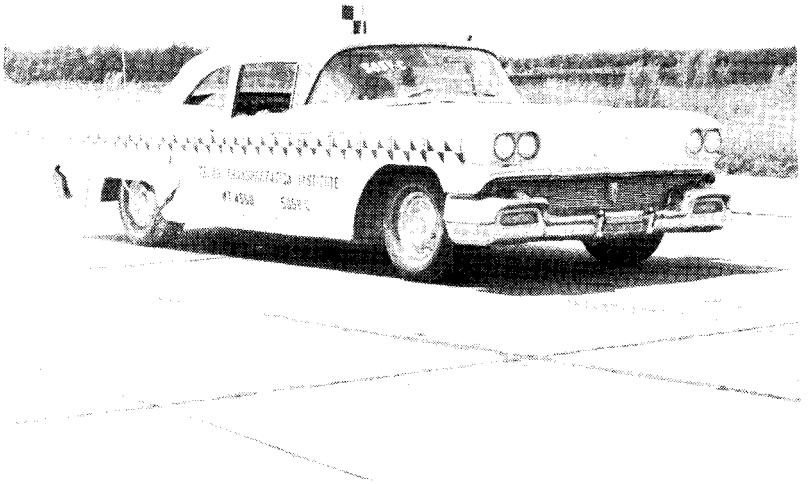

Figure 22, Vehicle Before Crash Test 505V-C

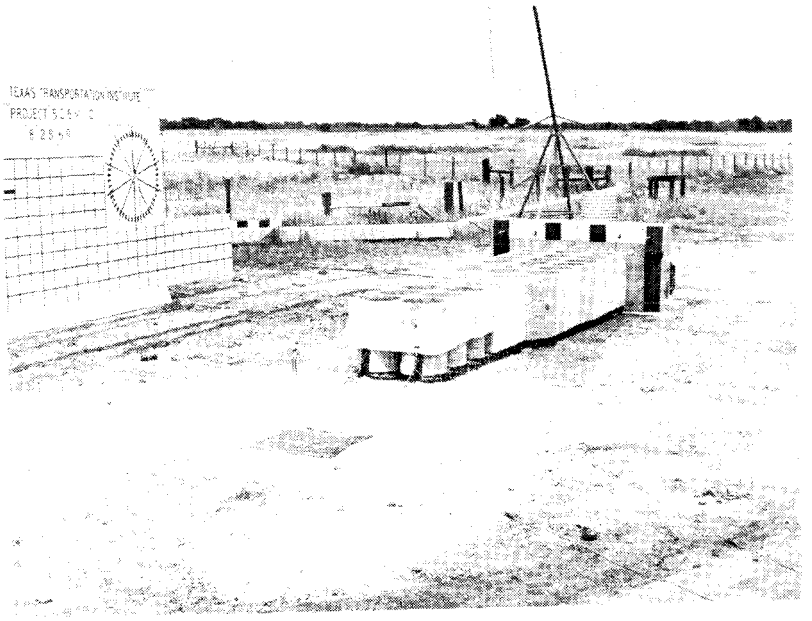

Figure 23, Concrete Crash Cushion Before Test 505V-C

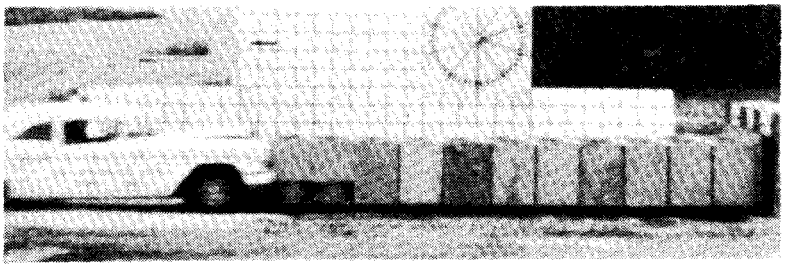

1

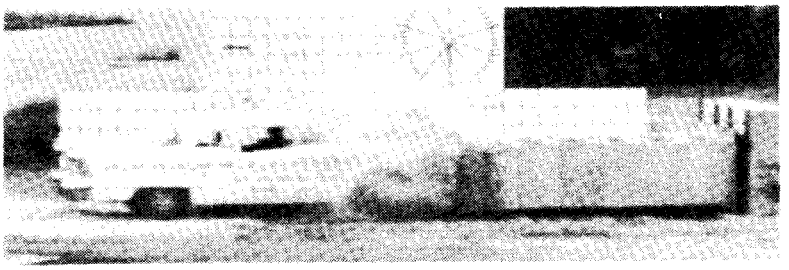

2

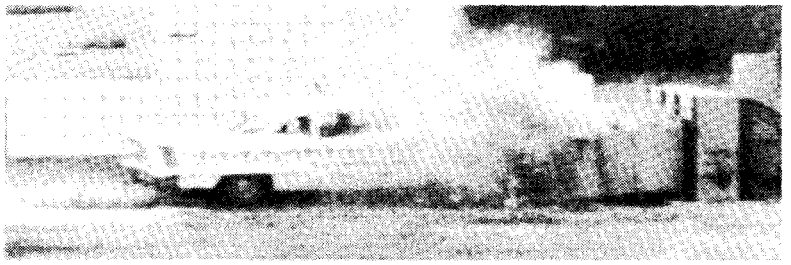

3

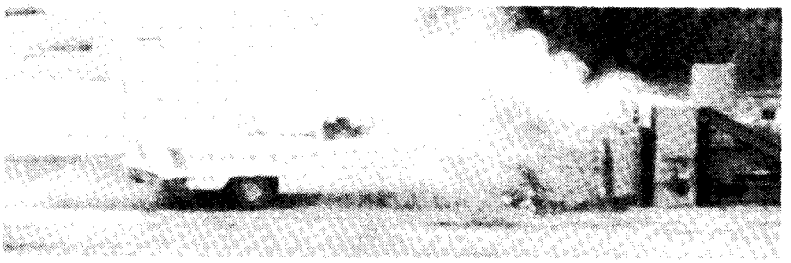

4

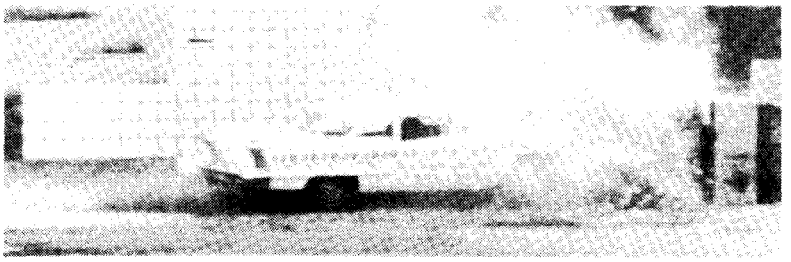

5

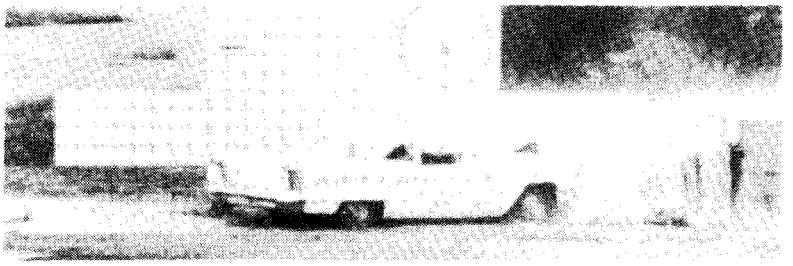

6

Figure 24, Sequential Photographs of Test 505V-C

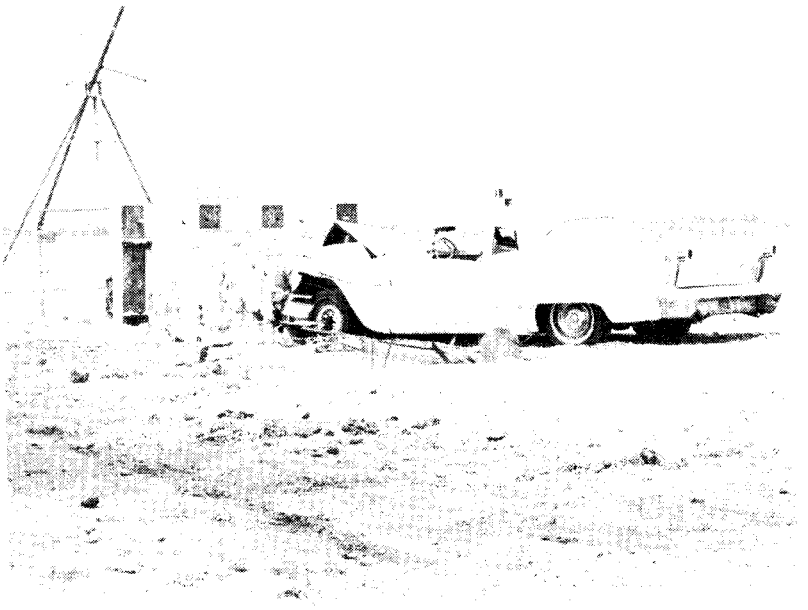

Figure 25, Vehicle After Crash Test (505V-C)

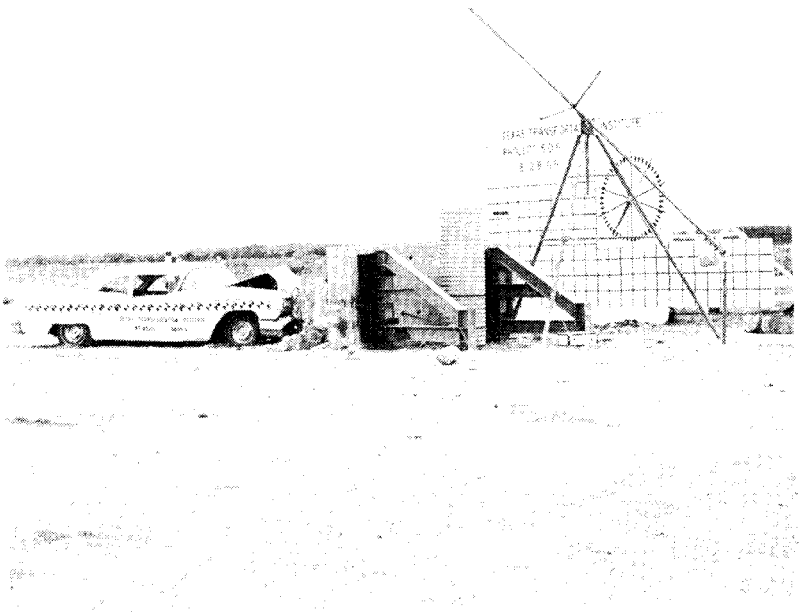

Figure 26, Impact Area After Test (505V-C)

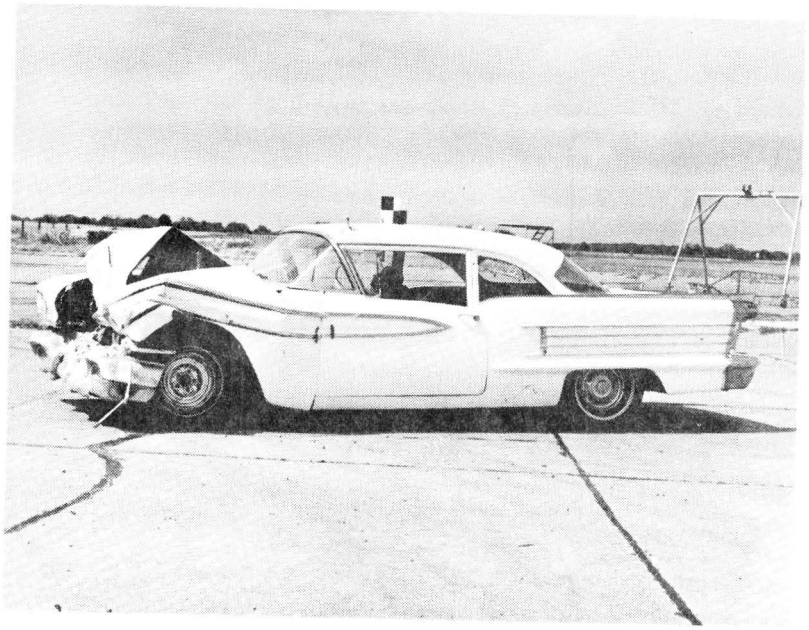

Figure 27, Damage to Vehicle, (505V-C)
Side View

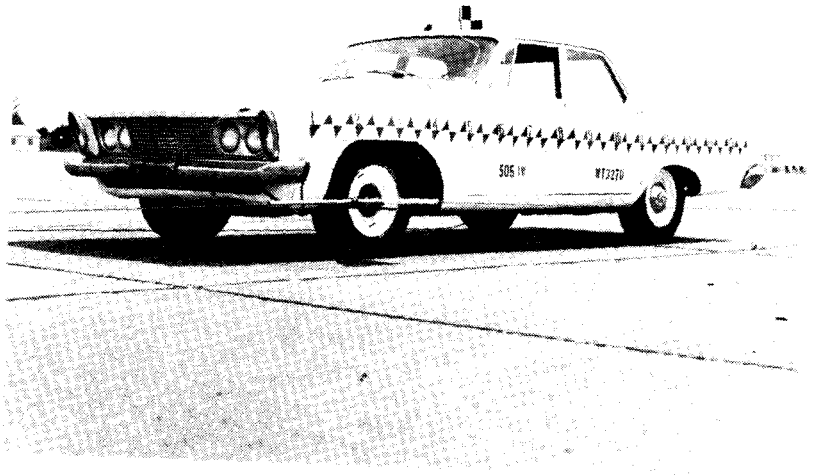

Figure 28, Vehicle Before Crash Test (505-IW)

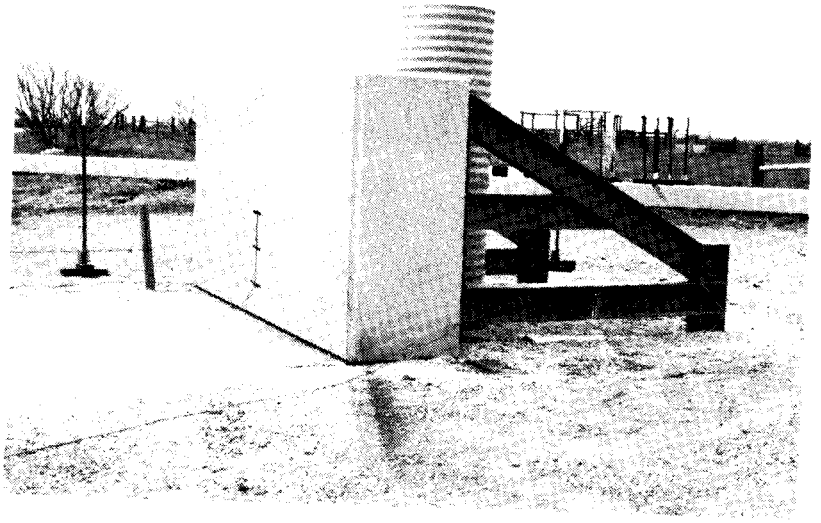

Figure 29, Rigid Barrier Before Test (505-IW)

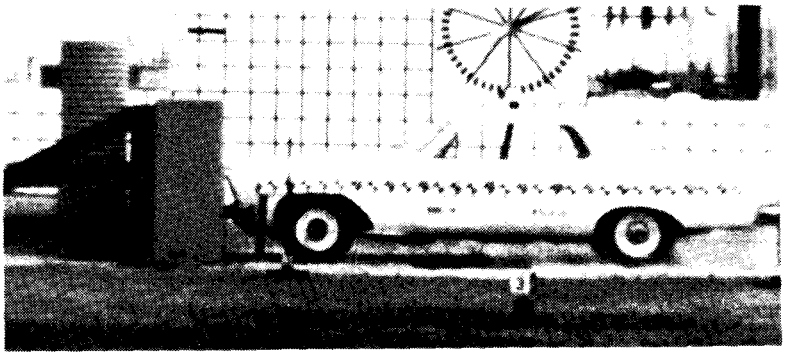

1

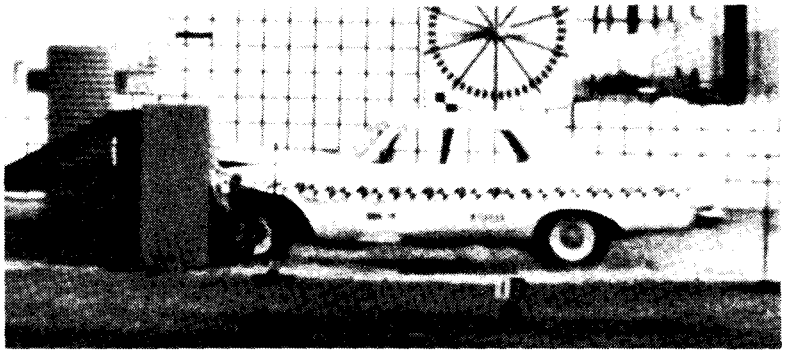

2

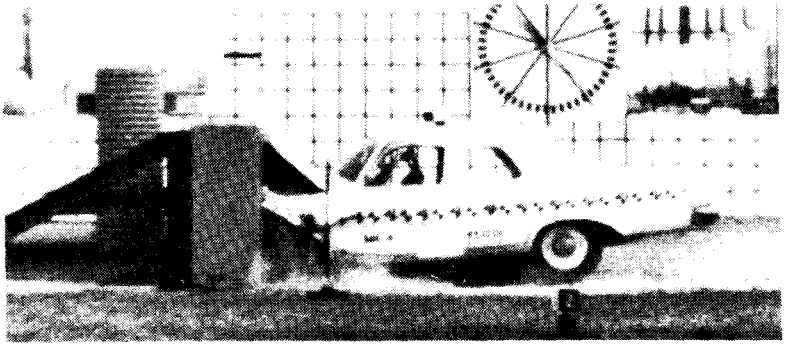

3

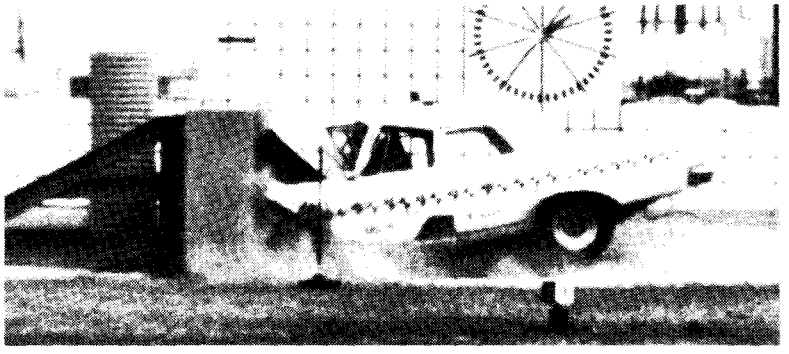

4

Figure 30, Sequential Photographs of Test 505-IW

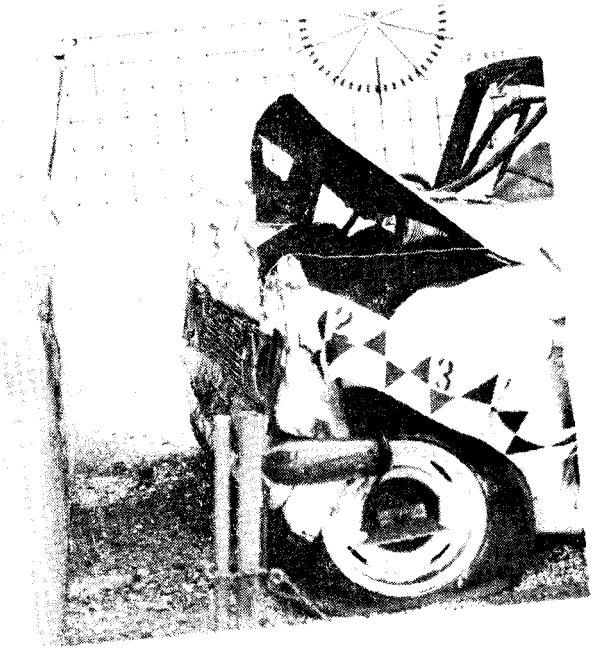

Figure 31. Impact Area After Test (505-IW)

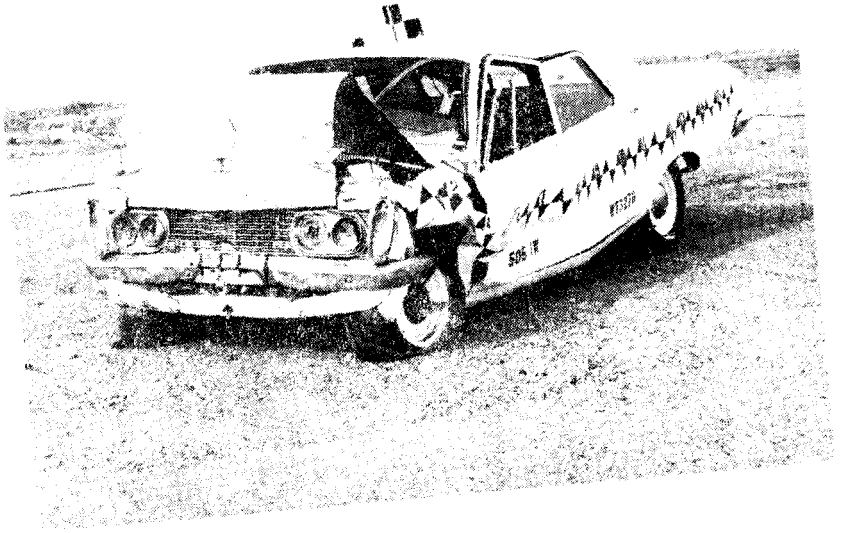

Figure 32. Damage to Vehicle, (505-IW)
Front View

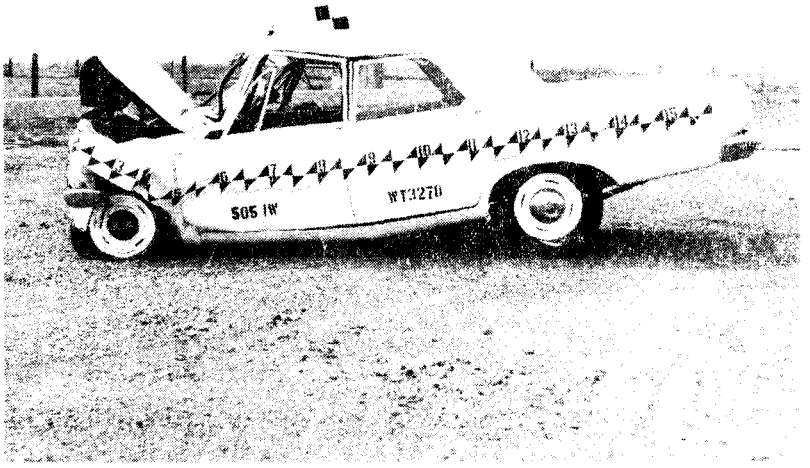

Figure 33, Damage to vehicle, (505-IW)
Side View

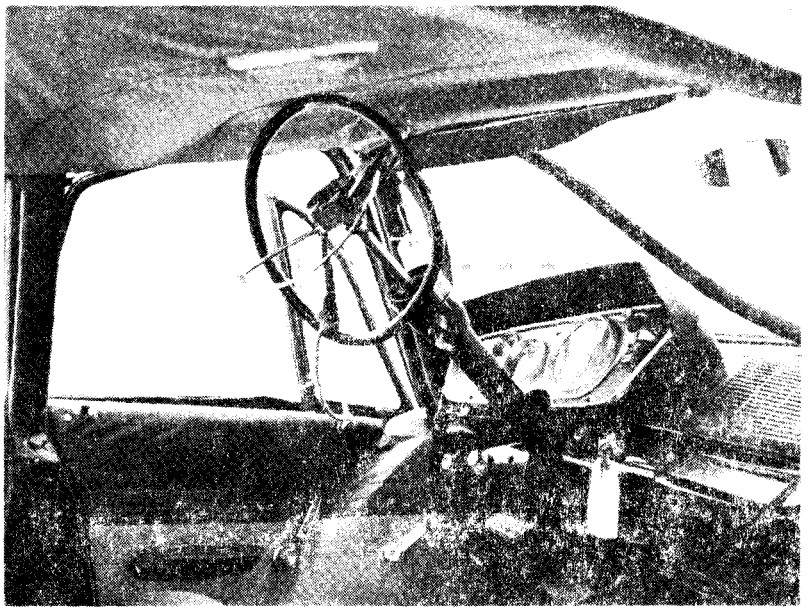

Figure 34, Deformation of Steering Column, Test 505-IW

CONCLUSION

The lightweight cellular concrete crash cushion has been shown to be extremely effective in decelerating a vehicle for the head-on crash condition. Although side angle hits have not been conducted, it is expected that further testing will show the acceptability of this type of impact attenuator for this collision condition. This estimate is based on the acceptable reaction of the Modular Crash Cushion[3] (composed of 55-gallon steel barrels) which functions in a very similar way. All tests show deceleration levels within the tolerance limits of restrained humans. The lightweight cellular concrete crash cushion can be installed by one of two methods by semi-skilled laborers. The formwork can be placed in the field, and a local vermiculite applicator can supply the necessary concrete; or the precast modular construction method can be used. The estimate of cast-in-place construction cost, including all materials and labor, is $800 per installation. Using the modular construction technique, considerable savings should be realized by mass production.

Close quality control should be exercised on the geometry of the attenuator and on the vermiculite concrete. Control of batch proportions and unit weight will give predictable crushing strengths. Replacement of segments of the crash cushion can be easily accomplished after a collision. For a cast-in-place cushion, the crushed material can be removed, that portion of the barrier re-formed, and fresh vermiculite placed in the necessary areas. Fast setting cement will alleviate the problem of curing time. For the precast cushions, the three-tube

modules weigh approximately 250 lbs, and could therefore be handled easily by four men. The modules which have been crushed during a collision can be unbolted, removed, and new modules slipped into place. This refurbishment could be accomplished during a low density traffic period.

REFERENCES

1. Shoemaker, Norris E., "Research and Design of an Impact Absorbing Barrier for Fixed Highway Objects," CAL Report No. VJ-2501-V-1, Cornell Aeronautical Laboratories, Buffalo, June 1968.

2. Emori, Richard I., "Analytical Approach to Automobile Collisions," SAE Paper 680016, Engineering Congress, Detroit, January 8, 1968.

3. Hirsch, T. J., and Ivey, Don L., "Vehicle Impact Attenuation by Modular Crash Cushion," Research Report Number 146-1, Texas Transportation Institute, January 1969.

A P P E N D I X A

Accelerometer Data

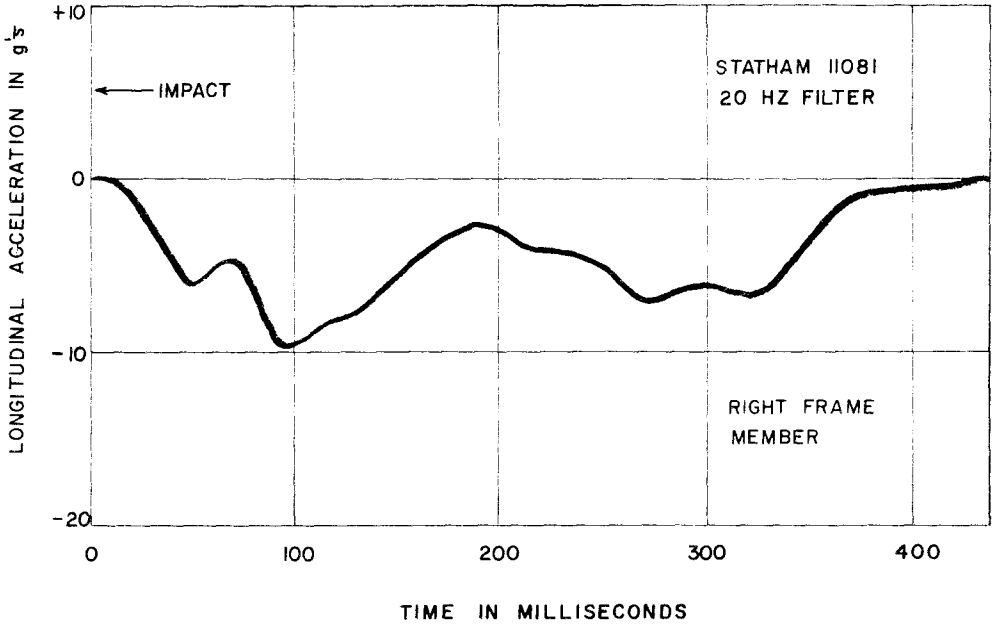

FIGURE A1, LONGITUDINAL ACCELEROMETER DATA, TEST 505V-A

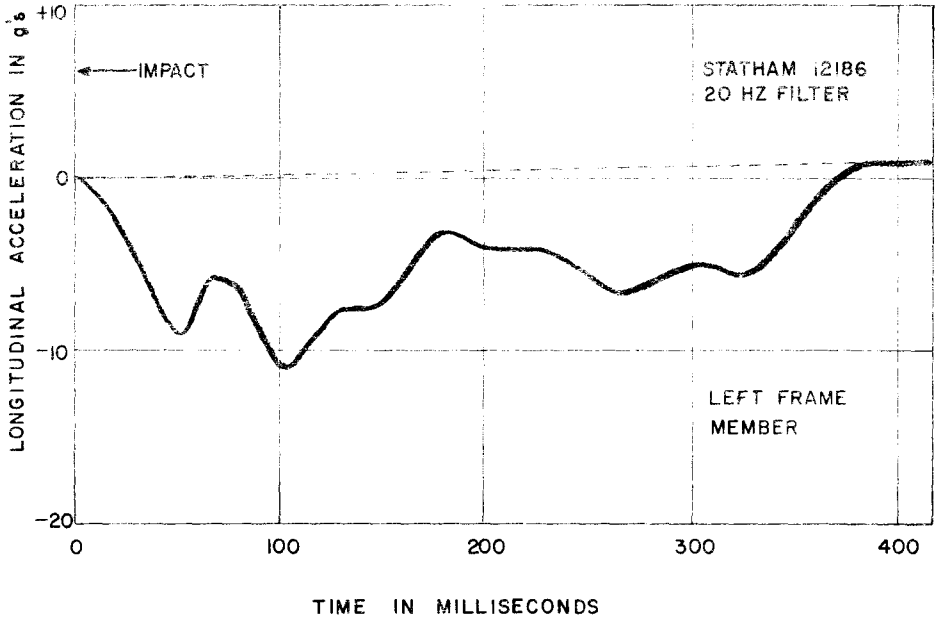

FIGURE A2, LONGITUDINAL ACCELEROMETER DATA, TEST 505V—A

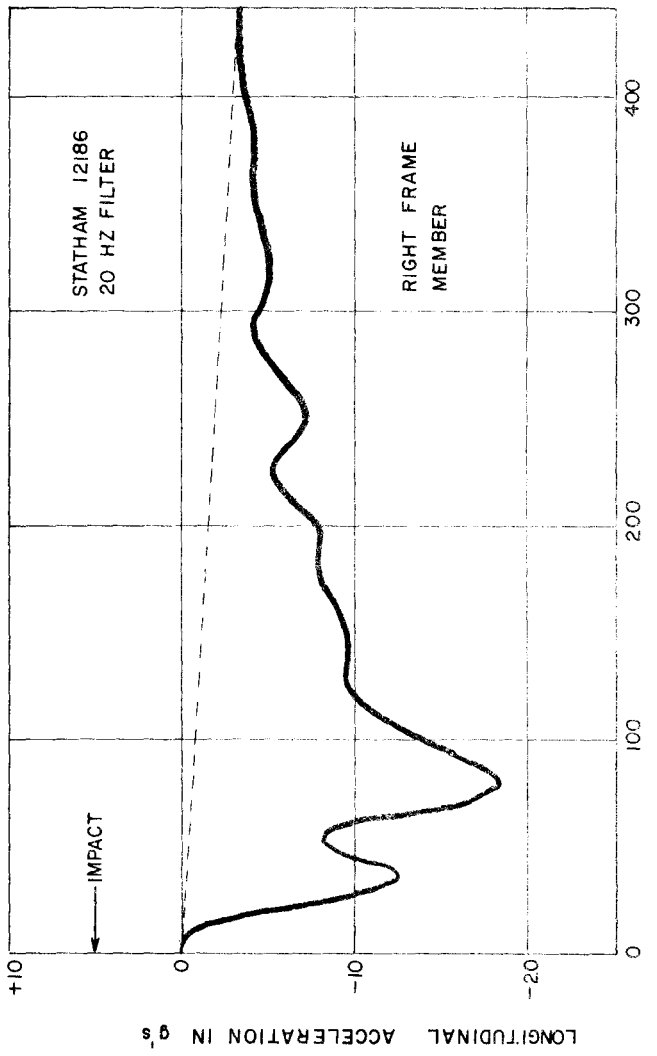

FIGURE A3. LONGITUDINAL ACCELEROMETER DATA, TEST 505V-8

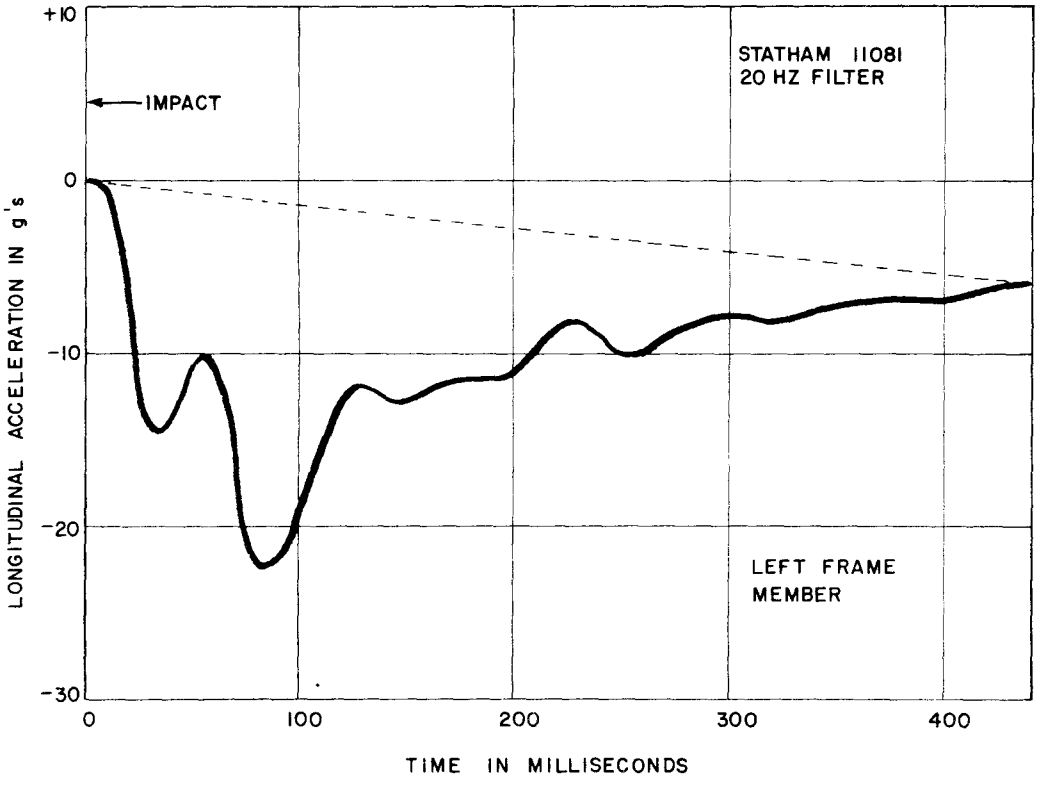

FIGURE A4, LONGITUDINAL ACCELEROMETER DATA, TEST 505V-B

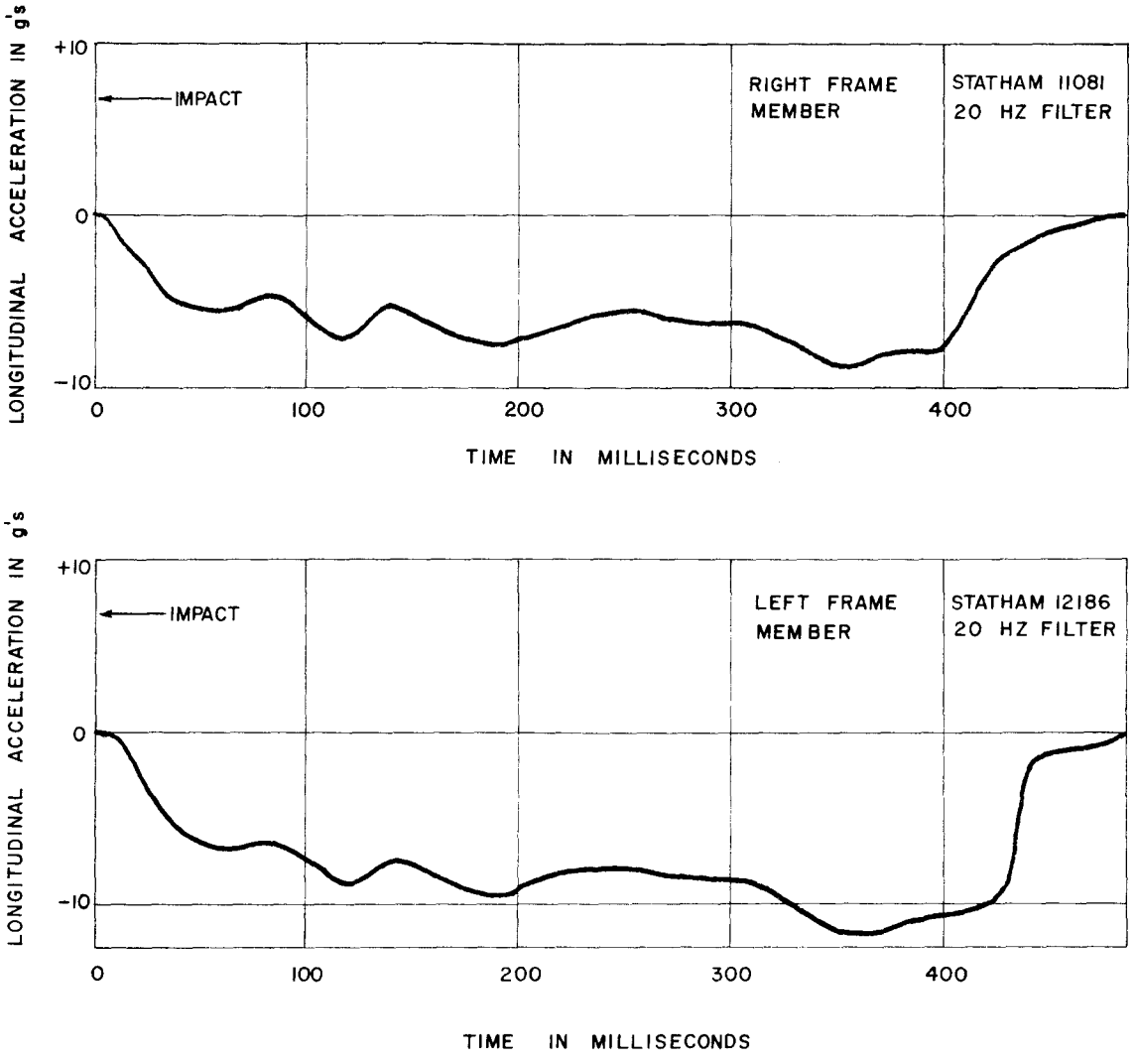

FIGURE A5, LONGITUDINAL ACCELEROMETER DATA, TEST 505V-C

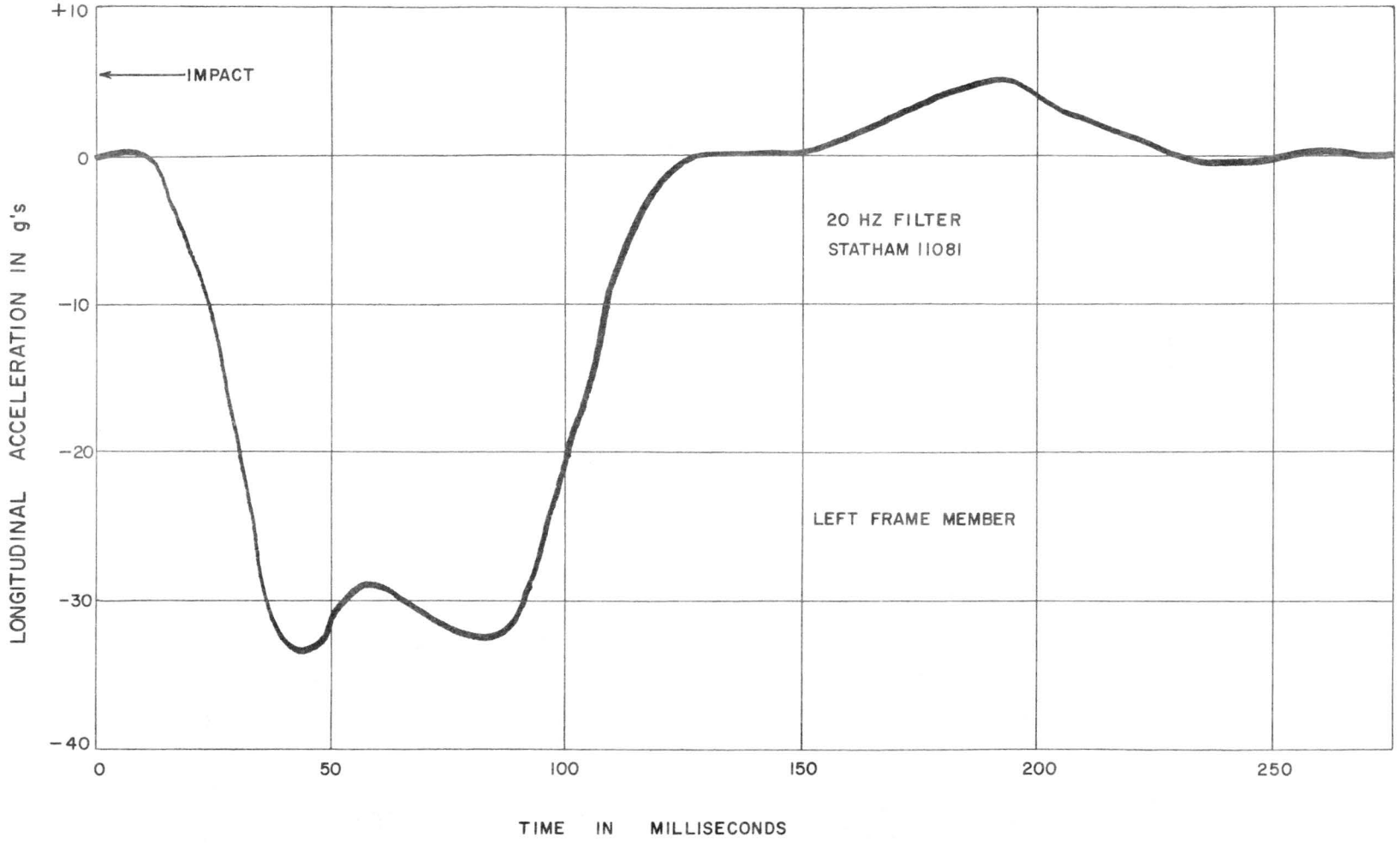

FIGURE A6, LONGITUDINAL ACCELEROMETER DATA, TEST 505 IW

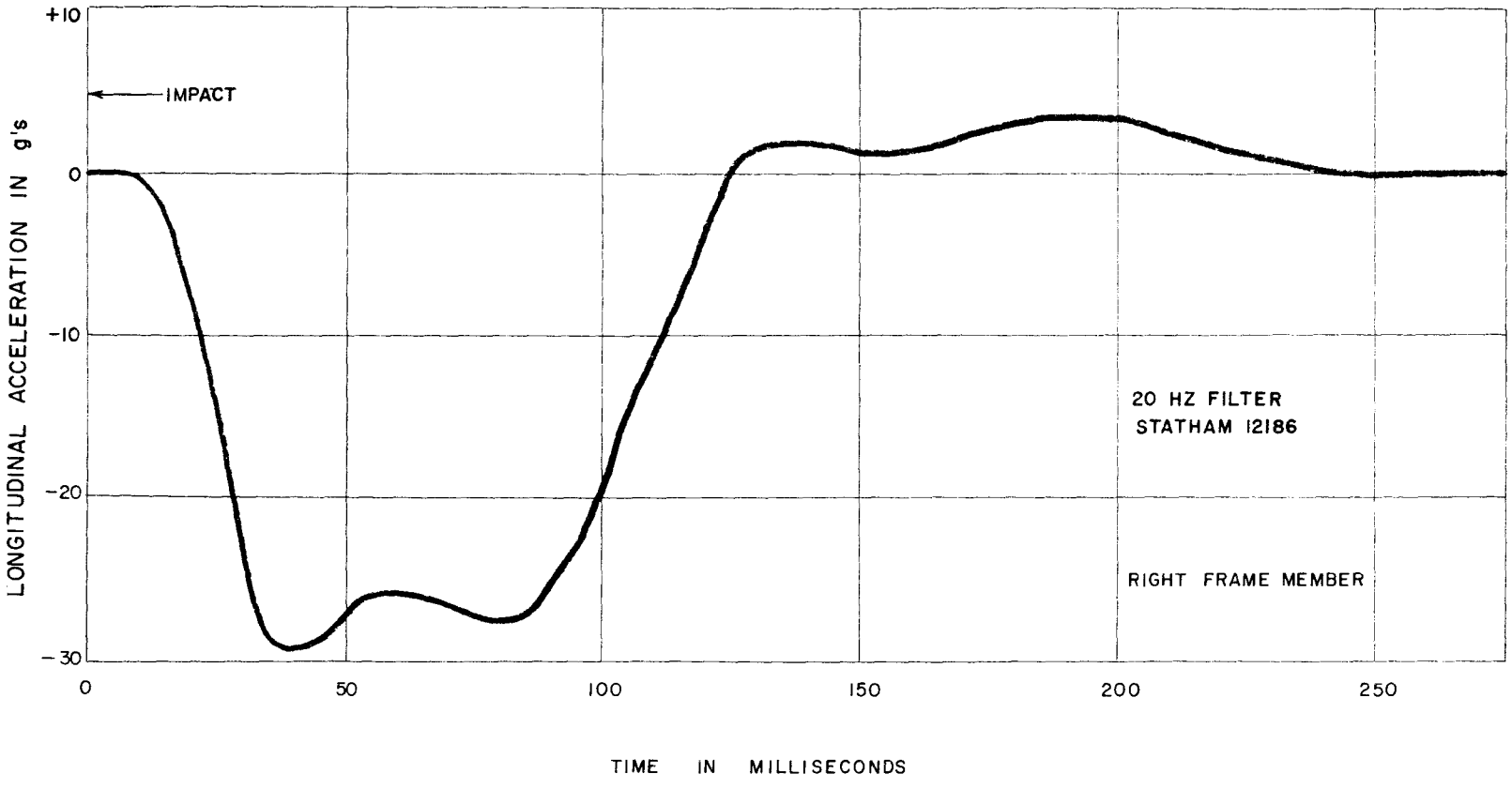

FIGURE A7, LONGITUDINAL ACCELEROMETER DATA, TEST 505 IW

A P P E N D I X B

Photographic Data

TABLE 1B

TEST 505V-A

High-Speed Film Data

Time Milliseconds	Displacement ft	Velocity ft/sec	
-40.60	-2.45		
		59.1	
-30.45	-1.85		
		59.1	60.3 Avg.
-20.30	-1.25		
		62.1	
-10.15	-0.62		
		61.1	
0 Impact	0		
		60.1	
20.30	1.22		
		53.2	
40.60	2.30		
		52.7	
60.90	3.37		
		44.3	
81.20	4.27		
		40.9	
101.50	5.10		
		33.0	
121.80	5.77		
		30.0	
142.10	6.38		
		26.6	
162.40	6.92		
		25.6	
182.70	7.44		
		21.7	
203.00	7.88		
		20.7	
223.30	8.30		
		15.8	
243.60	8.62		
		11.3	
263.90	8.85		
		6.4	
284.20	8.98		
		2.5	
304.50	9.03		
		-2.0	
324.80	8.99		
		-3.9	
345.10	8.91		
		-3.9	

TABLE 1B (Continued)

TEST 505V-A

High-Speed Film Data

Time Milliseconds	Displacement ft	Velocity ft/sec
365.40	8.83	
		-4.4
385.70	8.74	
		-4.4
406.00	8.65	
		-3.9
426.30	8.57	
		-3.4
446.60	8.50	
		-3.4
466.90	8.43	
		-3.9
487.20	8.35	
		-3.0
507.50	8.29	
		-6.4
548.10	8.16	
		-6.4
588.70	8.03	
		-5.9
629.30	7.91	
		-5.5
669.90	7.80	
		-4.4
710.50	7.71	
		-3.4
751.10	7.64	
		-3.9
791.70	7.56	
		-3.1
913.50	7.18	
		+0.6
1035.30	7.25	
		-0.8
1157.10	7.15	
		-0.3
1278.90	7.11	
		+0.2
1400.70	7.14	

TABLE 2B

TEST 505V-B

High-Speed Film Data

Time Milliseconds	Displacement ft	Velocity ft/sec	
-30.15	-2.60		
		88.6	
-20.10	-1.71		
		85.5	86.2
-10.05	-0.85		Avg.
		84.6	
0 Impact	0		
		85.6	
10.05	0.86		
		73.7	
20.10	1.60		
		75.9	
30.15	2.36		
		80.1	
40.20	3.17		
		69.2	
50.25	3.86		
		64.4	
60.30	4.51		
		57.2	
70.35	5.09		
		54.8	
80.40	5.64		
		47.8	
90.45*	6.12		
		42.2	
100.50	6.54		
		41.1	
110.55	6.95		
		37.6	
120.60	7.33		
		34.8	
130.65	7.68		
		32.1	
140.70	8.00		
		30.4	
150.75	8.31		
		29.9	

* Front tires lose contact with ground

TABLE 2B (Continued)

TEST 505V-B

High-Speed Film Data

Time Milliseconds	Displacement ft	Velocity ft/sec
160.80	8.61	
		23.7
180.90	9.09	
		22.3
201.00	9.54	
		17.3
221.10	9.88	
		15.4
241.20	10.19	
		12.4
261.30	10.44	
		10.8
281.40	10.66	
		7.4
301.50	10.81	
		6.9
321.60	10.94	
		5.2
341.70	11.05	
		2.9
361.80	11.11	
		0.9
462.30	11.20	
		-0.4
562.80	11.17	
		-0.9
663.30	11.08	
		-1.8
763.80	10.90	
		-3.0
864.30	10.60	
		-3.9
964.80	10.21	
		-4.7
1065.30	9.73	
		-4.4
1165.80 *	9.29	
		-4.1
1266.30	8.89	
		-2.8
1366.80	8.61	
		-1.9

* Front tires recontact ground

TABLE 2B (Continued)

TEST 505V--B

High-Speed Film Data

Time Milliseconds	Displacement ft	Velocity ft/sec
1467.30	8.42	
		-1.5
1567.80	8.27	
		-0.3
1668.30	8.23	
		+0.3
1768.80	8.26	
		+0.5
1869.30	8.31	
		+0.6
1969.80	8.37	
		+0.8
2070.30	8.45	
		0
2170.80	8.45	

TABLE 3B

TEST 505V-C

High-Speed Film Data

Time Milliseconds	Displacement ft	Velocity ft/sec	
-28.28	-2.64		
		93.1	
-20.20	-1.89		
		92.3	93.3 Avg.
- 8.08	-0.76		
		95.1	
0 Impact	0		
		90.1	
20.20	1.82		
		88.6	
40.40	3.61		
		84.2	
60.60	5.31		
		81.2	
80.80	6.95		
		76.7	
101.00	8.50		
		73.3	
121.20	9.98		
		67.8	
141.40	11.35		
		63.9	
161.60	12.64		
		58.9	
181.80	13.83		
		54.0	
202.00	14.92		
		49.0	
222.20	15.91		
		47.5	
242.40	16.87		
		41.6	
262.60	17.71		
		38.1	
282.80	18.48		
		35.1	
303.00	19.19		
		28.7	
323.20	19.77		
		24.2	
343.40	20.26		
		20.3	

TABLE 3B (Continued)

TEST 505V-C

High-Speed Film Data

Time Milliseconds	Displacement ft	Velocity ft/sec
363.60	20.67	
		14.2
383.80	20.96	
		9.9
404.00	21.16	
		6.2
424.20	21.28	
		3.2
444.40	21.34	
		1.3
464.60	21.37	
		-1.3
666.60	21.10	
		-1.9
868.60	20.73	
		-1.8
1070.60	20.38	
		0.6
1272.60	20.49	
		1.4
1474.60	20.77	
		0
1676.60	20.77	

TABLE 4B

TEST 505-IW

High-Speed Film Data

Time Milliseconds	Displacement ft	Velocity ft/sec	
-19.92	-1.56		
		76.8	
- 9.96	-0.79		78.3
		79.6	Avg.
0 Impact	0		
		72.3	
19.92	1.44		
		55.9	
39.84	2.56		
		40.9	
59.76	3.37		
		17.5	
79.68	3.72		
		4.7	
99.60	3.81		
		-1.4	
119.52	3.78		
		-7.5	
139.44	3.63		
		-8.4	
159.36	3.46		
		-5.8	
179.28	3.35		
		-4.7	
199.20	3.26		
		-2.8	
219.12	3.20		
		-3.1	
239.04	3.14		
		-4.8	
258.96	3.04		
		-5.1	
278.88	2.94		
		-5.9	
298.80	2.82		
		-9.5	
338.64	2.63		
		-9.2	
378.48	2.45		
		-10.1	
418.32	2.25		
		-9.7	
458.16	2.05		
		-9.9	

TABLE 4B (Continued)

TEST 505-IW

High-Speed Film Data

Time Milliseconds	Displacement ft	Velocity ft/sec
498.00	1.86	
		-7.2
537.84	1.71	
		-3.6
577.68	1.64	
		-2.2
617.52	1.60	
		--
657.36	--	
		+3.2
697.20	1.66	
		+3.6
737.04	1.74	
		+4.2
776.88	1.82	
		+3.5
816.72	1.89	
		+3.2
856.56	1.95	
		+1.7
896.40	1.99	
		+1.4
936.24	2.01	

TECHNICAL MEMORANDUM 505-9S

SUPPLEMENT TO 505-9

Texas Transportation Institute
Texas A&M Research Foundation

EVALUATION OF CRASH CUSHIONS
CONSTRUCTION OF LIGHTWEIGHT CELLULAR CONCRETE

A Tentative Progress Memorandum on Contract No. CPR-11-5851

U.S. Department of Transportation
Federal Highway Administration

by

Don L. Ivey
Eugene Buth
T. J. Hirsch
Texas Transportation Institute

and

John G. Viner
Structures and Applied Mechanics Division
Federal Highway Administration

These crash tests and evaluations were conducted under the Office of Research and Development, Structures and Applied Mechanics Division's Research Program on Structural Systems in Support of Highway Safety (4S Program). The opinions, findings, and conclusions expressed in this report are those of the authors and not necessarily those of the Federal Highway Administration.

June 1971

INTRODUCTION

The feasibility of vehicle crash cushions constructed of lightweight cellular concrete was demonstrated by a series of three head-on vehicle impacts on prototype installations. These initial tests were reported in a previous Technical Memorandum[1]*. The concrete crash cushion is one of a group of first generation devices which include the Barrel Crash Cushion, the Fitch Inertia Barrier and the HI-DRO Cell Barrier. The evaluation sequence that has been followed on all of these systems was: (1) Feasibility testing, (2) full-scale head-on testing, and (3) side angle testing. Because of the excellent performance of the concrete cushion in the first three tests conducted, interest was expressed by several states in applying the concept to some of their potentially hazardous areas. A concrete cushion was designed for the State of Florida[2] incorporating the basic cushion which was tested under FHWA's 4S Program (Figure 1, Mod I) and side-fender panels which were previously tested as part of Barrel Crash Cushion designs[3]. The results of two side angle tests of the system which was constructed for Florida (Figure 1, Mod II) were reported to Florida in November 1970.

In consultation with the contract manager for FHWA it was decided that additional tests would be conducted to further evaluate the concrete cushion for both the side angle hit situation and for head-on impacts of small vehicles. Further modifications of the cushion were made prior to the final series of

---

*Superscript numerals refer to corresponding references at the end of this report.

tests which resulted in the design shown as Mod III in Figure 1. The chronological evolution of the Concrete Crash Cushion is illustrated by Figure 1. The most significant concrete cushion designs which have been tested are shown in Figures 2 through 4. This report describes in detail the three tests which were conducted on the Mod III Concrete Crash Cushion.

Appendix B presents the results of a limited scale-model study which was conducted to determine the effects of the dimensions and concrete strength on the static crush strength and energy absorption of the lightweight concrete model.

Appendix C presents the results of a limited study to evaluate the freeze-thaw durability of the vermiculite lightweight concrete used for construction of the crash cushion.

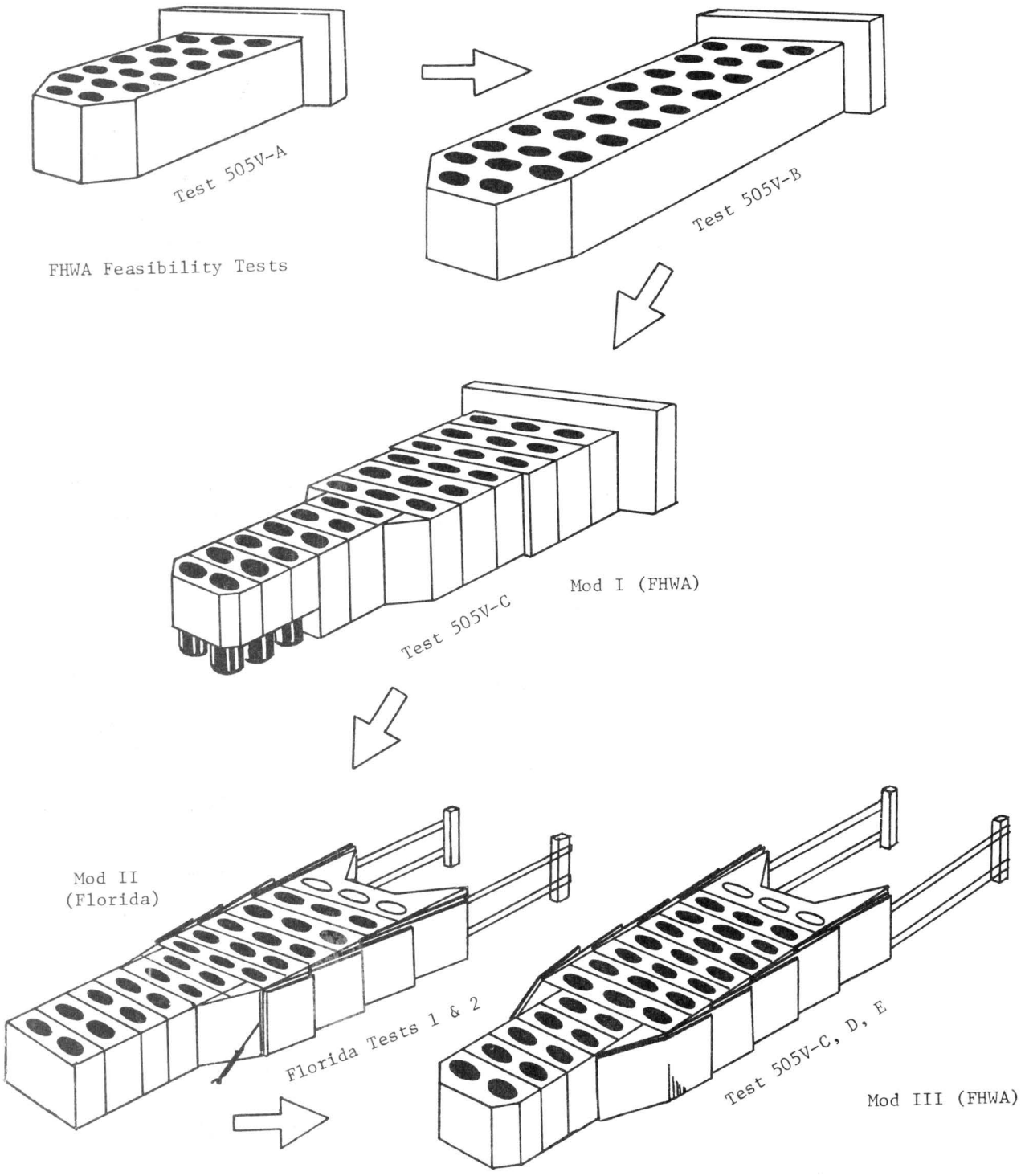

Figure 1, Evolution of Concrete Crash Cushion.

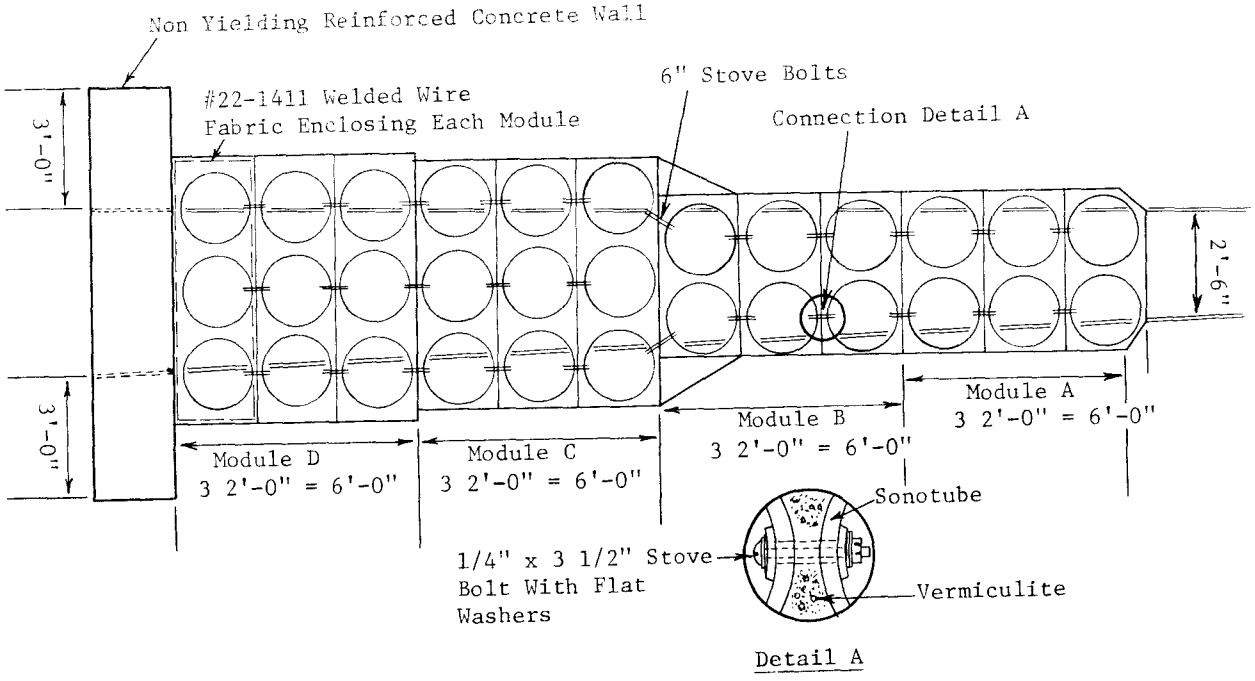

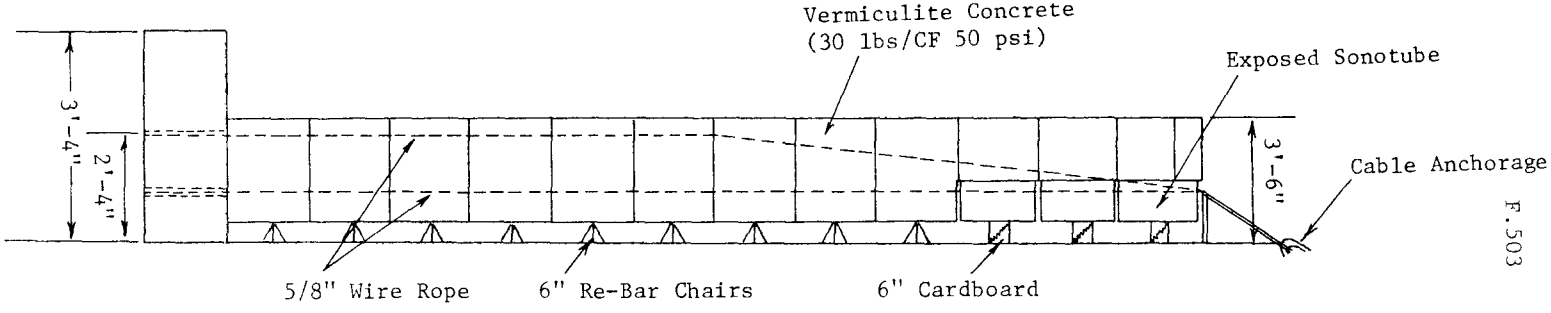

Figure 2, Details of Concrete Crash Cushion (Test 505V-C Mod I).

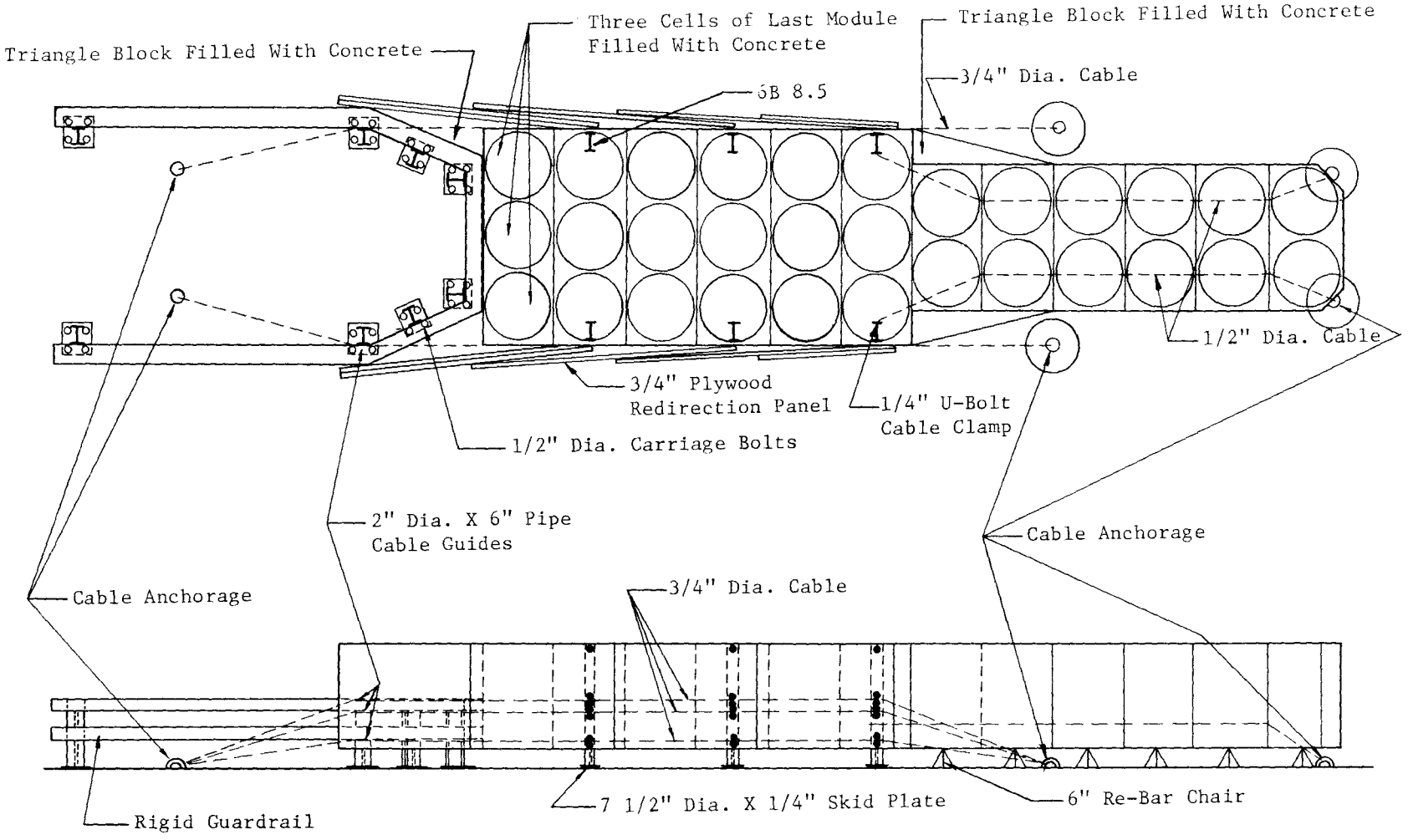

FIGURE 3, Details of Concrete Crash Cushion (Tests FLA-1 & FLA-2)(Mod II).

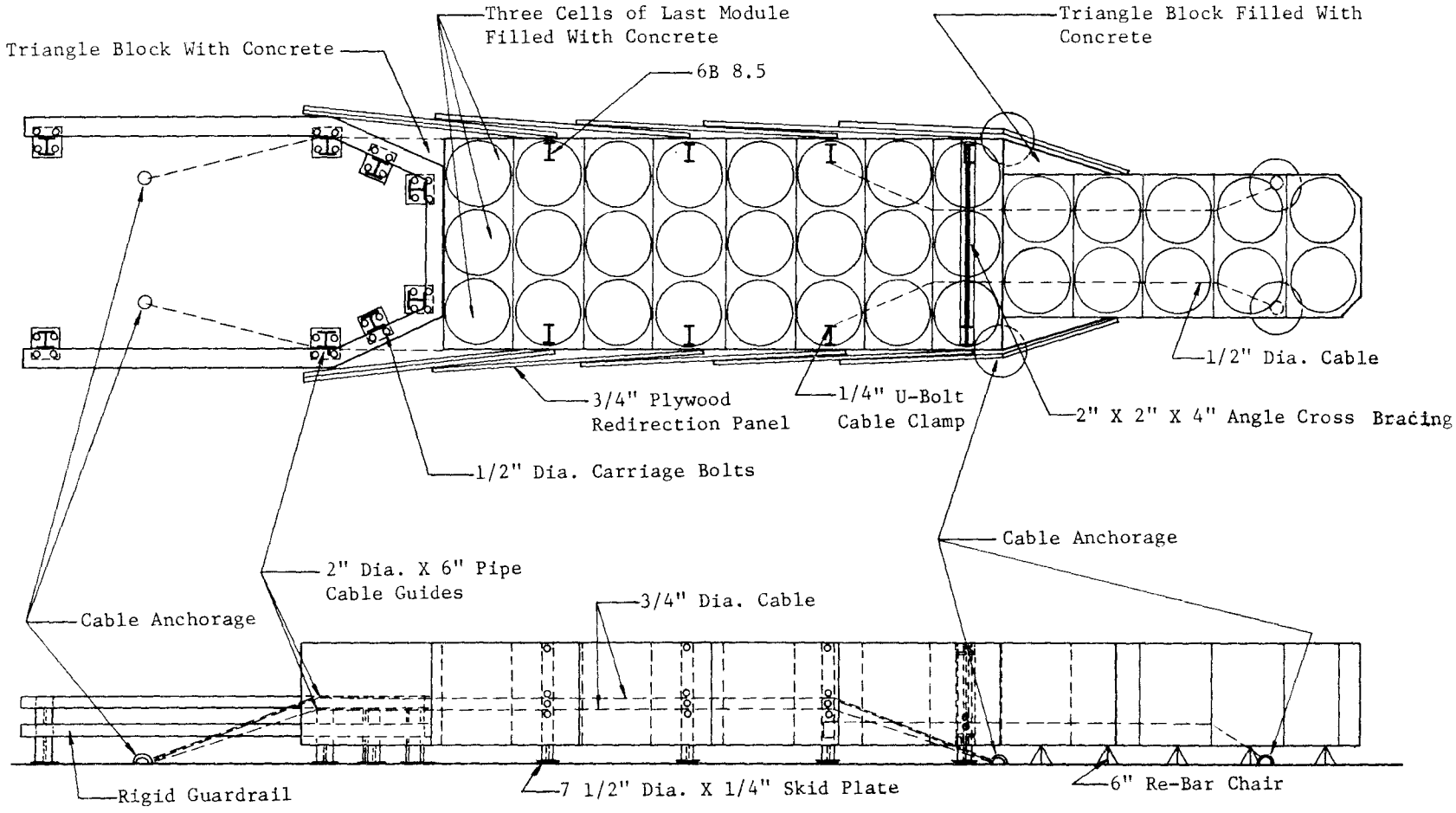

FIGURE 4, Details of Concrete Crash Cushion (505V-D, -E, and -F) (Mod III).

EXPERIMENTAL PROGRAM

General

Three full-scale vehicle crash tests of the Mod III Concrete Crash Cushion which is shown in Figure 4 were conducted in this final test series. These tests were designated 505V-D, -E, and -F respectively. The tests are summarized in Table 1. Properties of the concrete used in the various cushions tested are given in Table 2. Accelerometers and an Impact-O-Graph were used on each test to record vehicle decelerations. All accelerometers were Statham strain gage type and all electronic data was passed through an 80 HZ low-pass filter. High-speed cameras were also used to record the vehicle position and velocity throughout the test. Selected photographs of the vehicle before and after each test and sequential photographs of the test in progress are included.

Test 505V-D

A 1963 Chevrolet weighing 3790 lbs was used in this test. The impact angle was 10° from the longitudinal axis of the cushion and the contact point was 18 feet in advance of the rigid backup rail. The speed at contact was 57.2 mph and speed at loss of contact was 49.6 mph. The average longitudinal deceleration was 1.3 g's. The distance that the vehicle was in contact with the barrier was 20.4 feet over a period of approximately one-third of a second. The vehicle penetrated laterally a maximum distance of about two feet into the barrier and was smoothly redirected. Damage to the vehicle was relatively light as shown in Figure 5. Figure 6 shows that only five modules

TABLE 1

SUMMARY OF TESTS

Factor	Test		
	V-D	V-E	V-F
VEHICLE			
Year	1963	1962	1957
Make	Chevrolet	Chevrolet	Volvo
Weight, lb	3790	3820	2210
ANGLE OF IMPACT, deg	10	20	0
FILM DATA			
Initial Speed, V_1, fps	83.9	87.5	89.7
mph	57.2	59.7	61.2
Final Speed, V_2, fps	72.7	43.9	0
mph	49.6	29.3	0
*Average Deceleration, G_{avg}, g's	1.3	5.6	10.2
Stopping Distance or Contact Distance, S, ft	20.4	16.1	12.2
Time in Contact, sec	0.286	0.235	0.364
ACCELEROMETER DATA			
Longitudinal Deceleration			
Peak g's	6.2	14.7	19.0
Average g's	1.4	4.2	6.4
Time, sec	0.294	0.268	0.446
Transverse Deceleration			
Peak g's	9.8	12.7	--
Average g's	2.4	3.3	--
Time, sec	0.302	0.273	--

*$G_{avg} = (V_1^2 - V_2^2) / 2gS$

TABLE 2

PROPERTIES OF VERMICULITE CONCRETE

Test No.	Average Compressive Strength, psi	Average Unit Weight, pcf
505V-A	50	32
505V-B	71	32
505V-C	57	21
Fla.-1&2	64	22
505V-D,E & F	64	22

were significantly damaged and that the cushion could probably still sustain a head-on impact. The test was considered extremely successful both from the point of view of the safety of vehicle passengers and from the relatively light damage to the vehicle.

Test 505V-E

This test was a 20° side angle impact on the Mod III barrier using a 1962 Chevrolet weighing 3820 lbs. The point of contact was 16 ft in advance of the rigid backup wall. The impact speed was 59.7 mph and speed of the vehicle at loss of contact with the barrier was 29.3 mph. This represented an average deceleration of 5.6 g's in the longitudinal direction. The vehicle was in contact with the cushion for approximately 16 ft. Photographs of this test are shown in Figures 10 through 15. As the vehicle made contact and slid down the side of the cushion, a slight ramping tendency was observed. This interaction finally culminated in the generation of a high roll-initiating force as the vehicle reached the end of the cushion. The vehicle rolled in a counterclockwise direction, when viewed in the direction of vehicle travel; ramped on the rear end of the cushion near the end of the backup wall; traveled beyond the cushion installation, skidding on its left side; rolled clockwise to an upright position; and continued to roll over onto its top. It came to rest approximately 80 ft past the barrier. Although the decelerations which were imparted to the vehicle during its interaction with the cushion were within the range of human tolerance, the roll condition which occurred after the vehicle left the cushion is a very undesirable reaction and is unacceptable from a passenger safety viewpoint.

This is the only test conducted to date, in which an unacceptable reaction of the vehicle resulted. Recommendations are made in the discussion for modification of the barrier to preclude the recurrence of this situation.

Test 505V-F

A 1957 Volvo weighing 2210 lbs was used in this test. The vehicle impacted the cushion head-on at a speed of 61 mph. The average longitudinal deceleration was 10.2 g's, with a peak longitudinal deceleration of 19 g's. The interaction of the vehicle and cushion was considered acceptable and the damage resulting to the vehicle and cushion is shown in Figures 16, 17, and 18.

The decelerations which are imparted to a 2000 lb vehicle can be expected to be approximately twice the decelerations imparted to a 4000 lb vehicle. This is seen by comparing the values given above with the 6.4 average and 10.4 maximum decelerations observed in Test 505V-C[1].

Figure 5 , Vehicle After Test D.

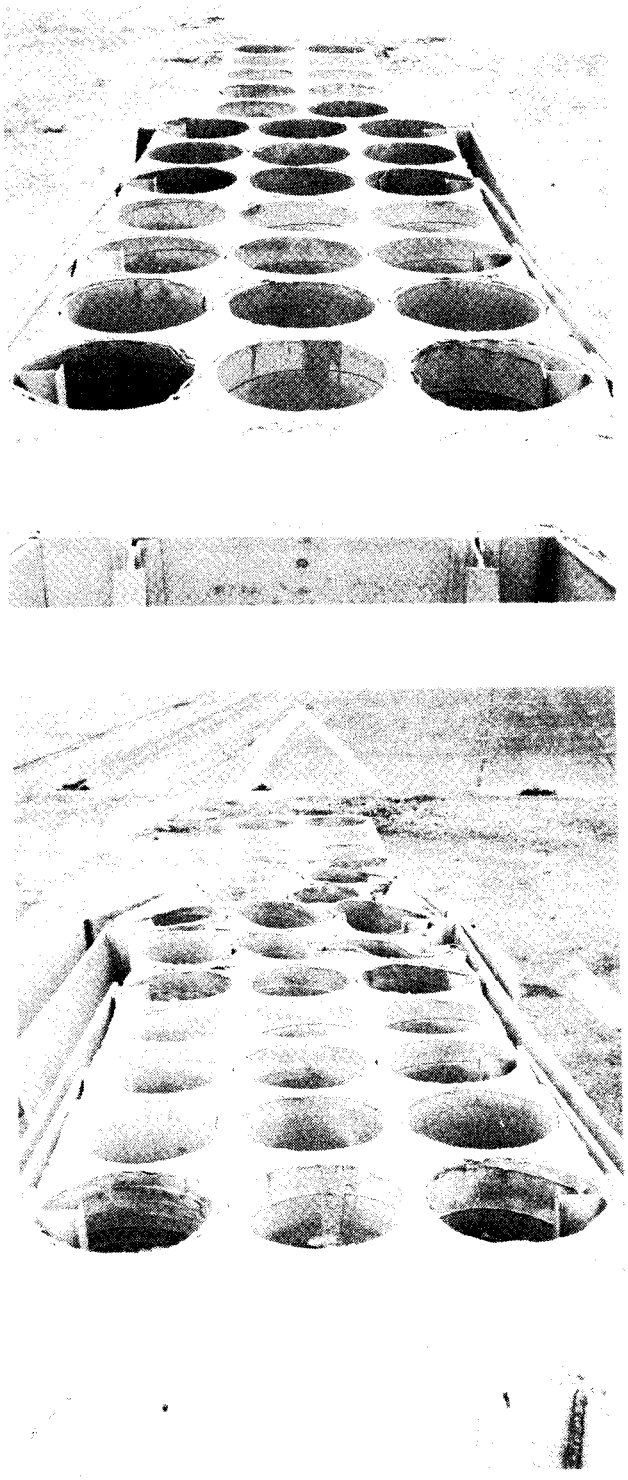

Figure 6, Barrier Before and After Test D (End View).

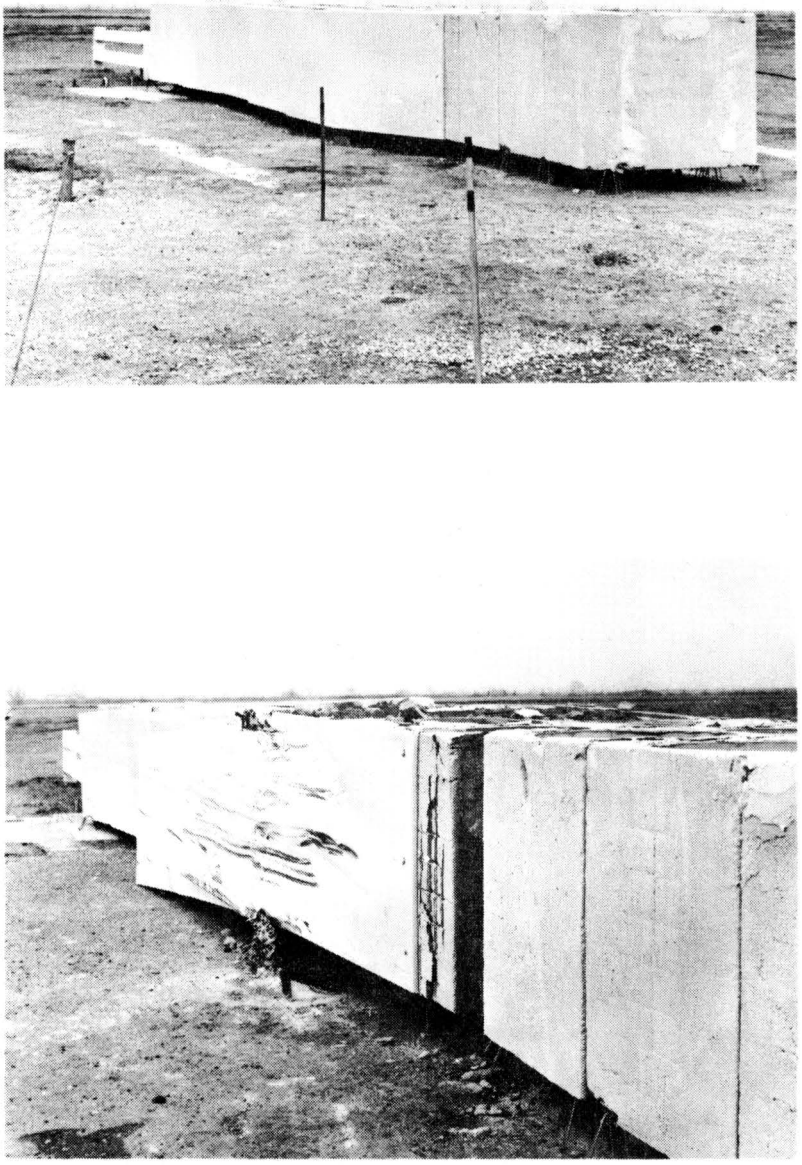

Figure 7, Barrier Before and After Test D (Oblique View).

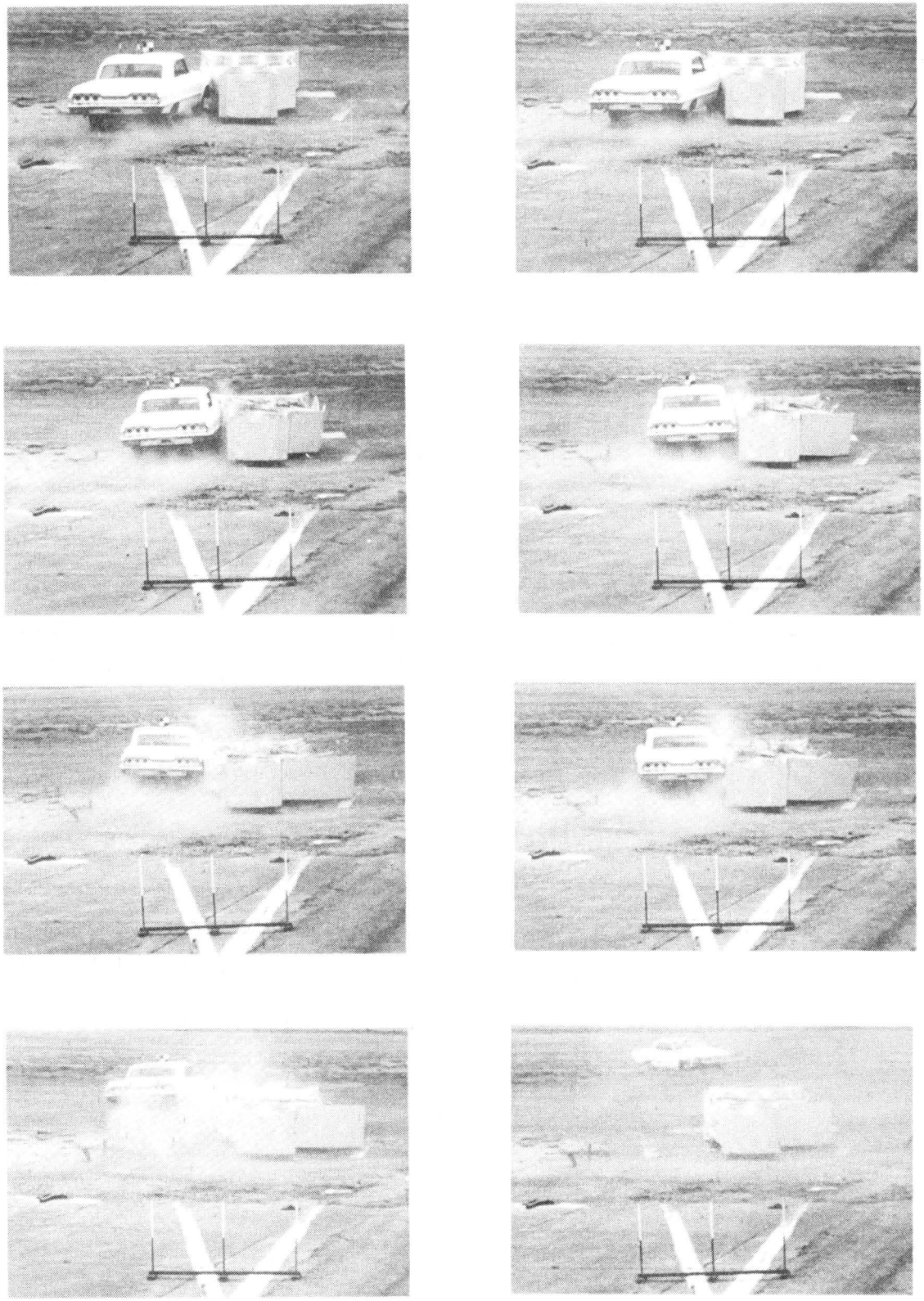

Figure 8, Test D Sequential Photographs (View Parallel With Barrier).

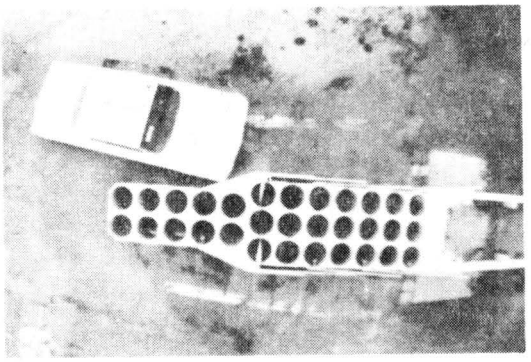

t = 0 sec

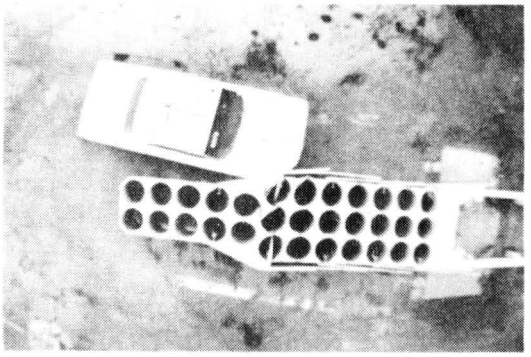

t = 0.046 sec

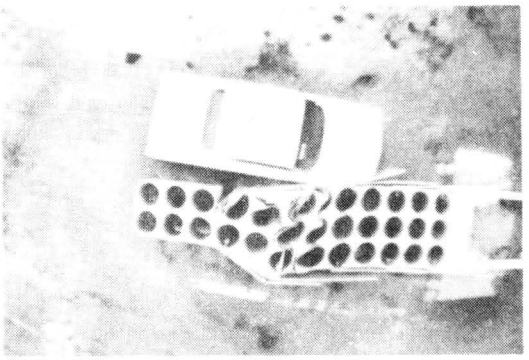

t = 0.112 sec

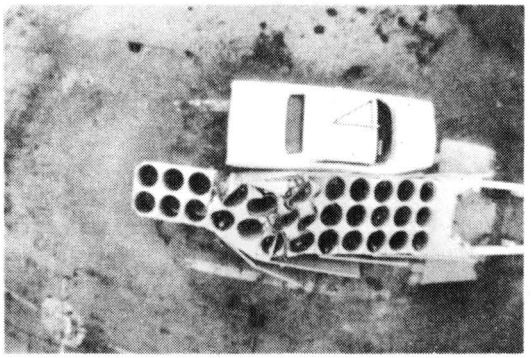

t = 0.199 sec

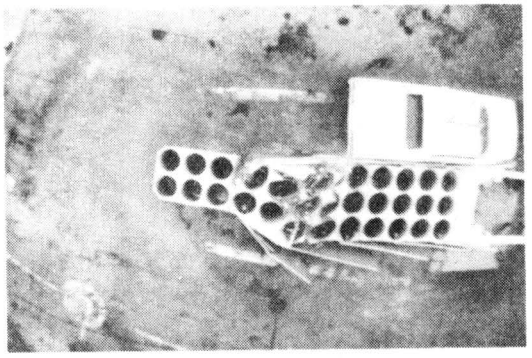

t = 0.306 sec

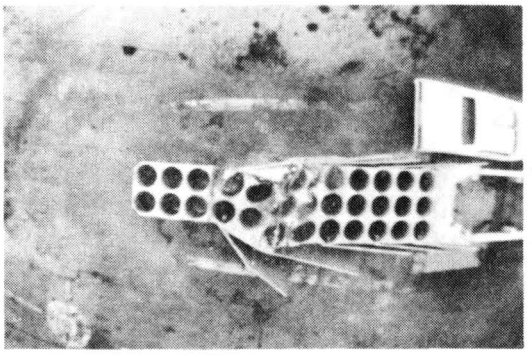

t = 0.429 sec

Figure 9, Test D Sequential Photographs (Overhead View).

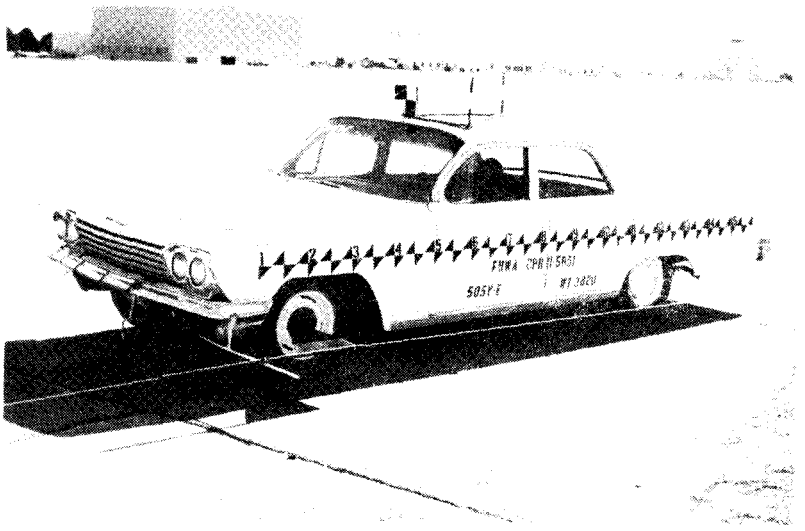

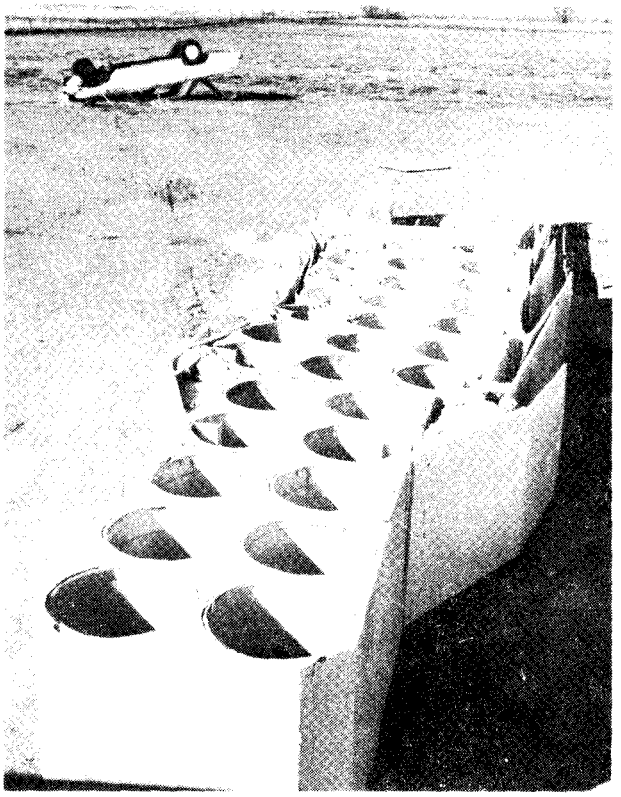

Figure 10, Vehicle Before Test E and in Final Position.

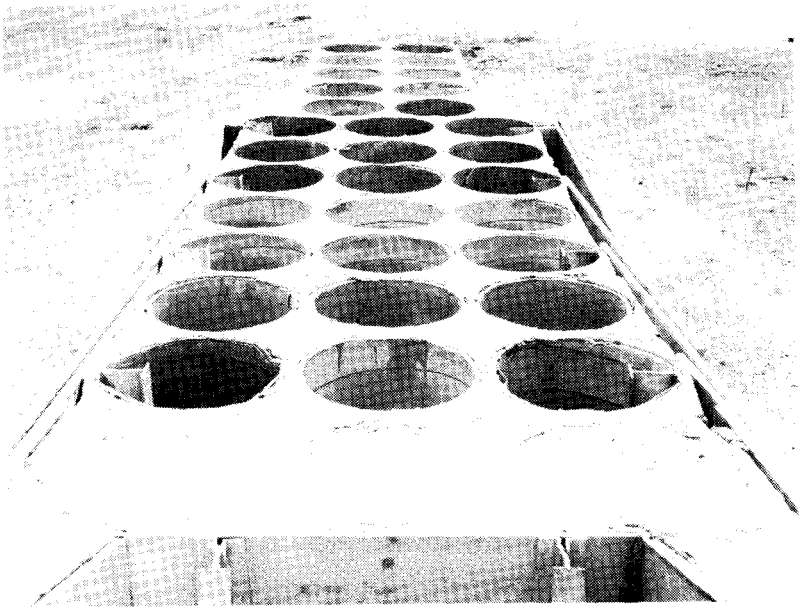

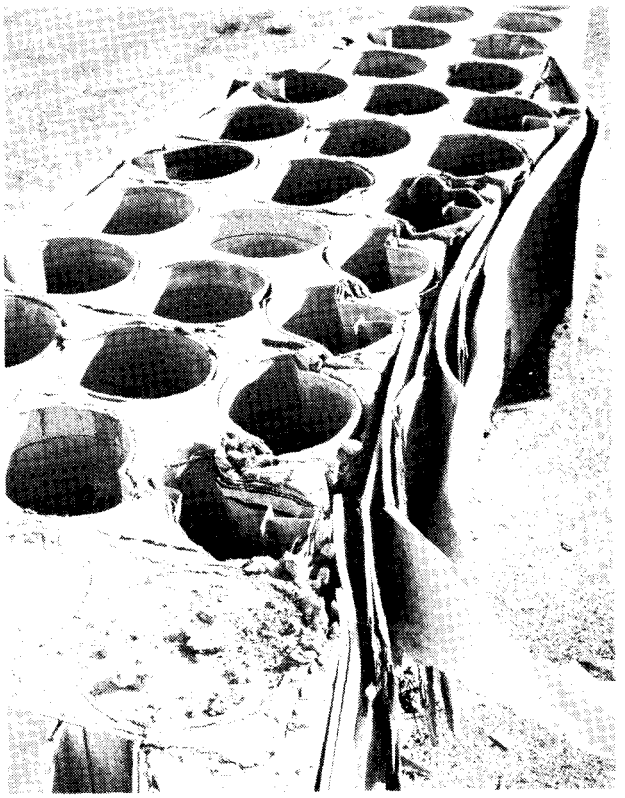

Figure 11, Barrier Before and After Test E.

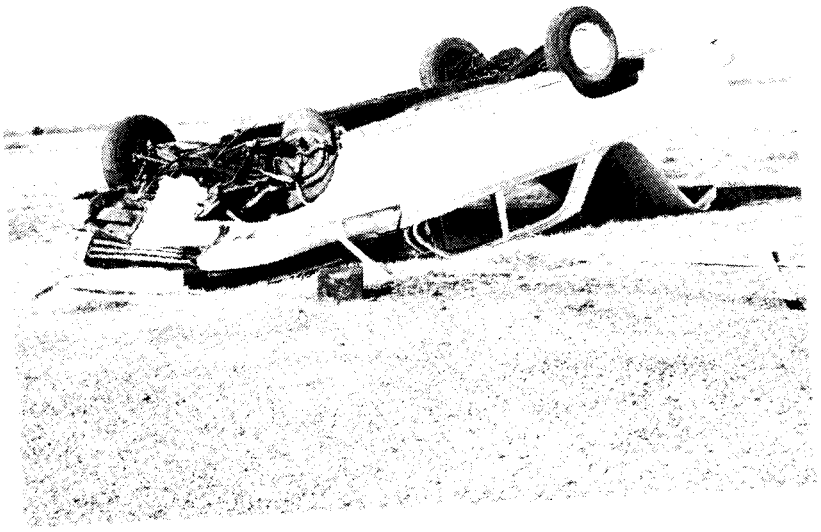

Final Position

After Righting

Figure 12, Vehicle After Test E.

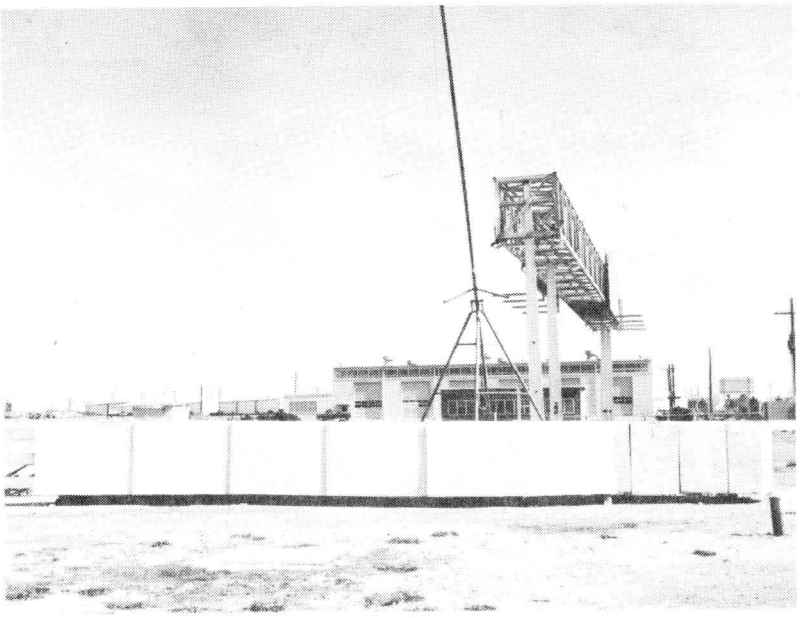

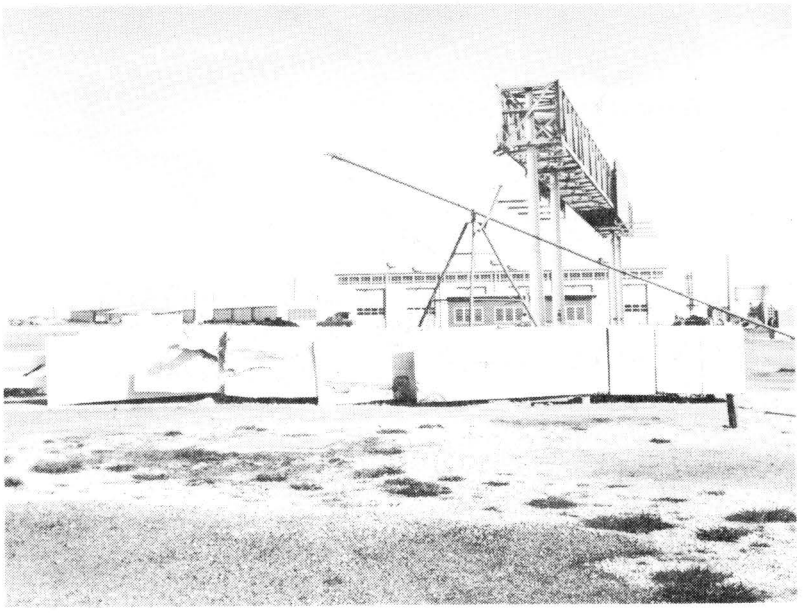

Figure 13. Barrier Before and After Test E (View Perpendicular to Barrier).

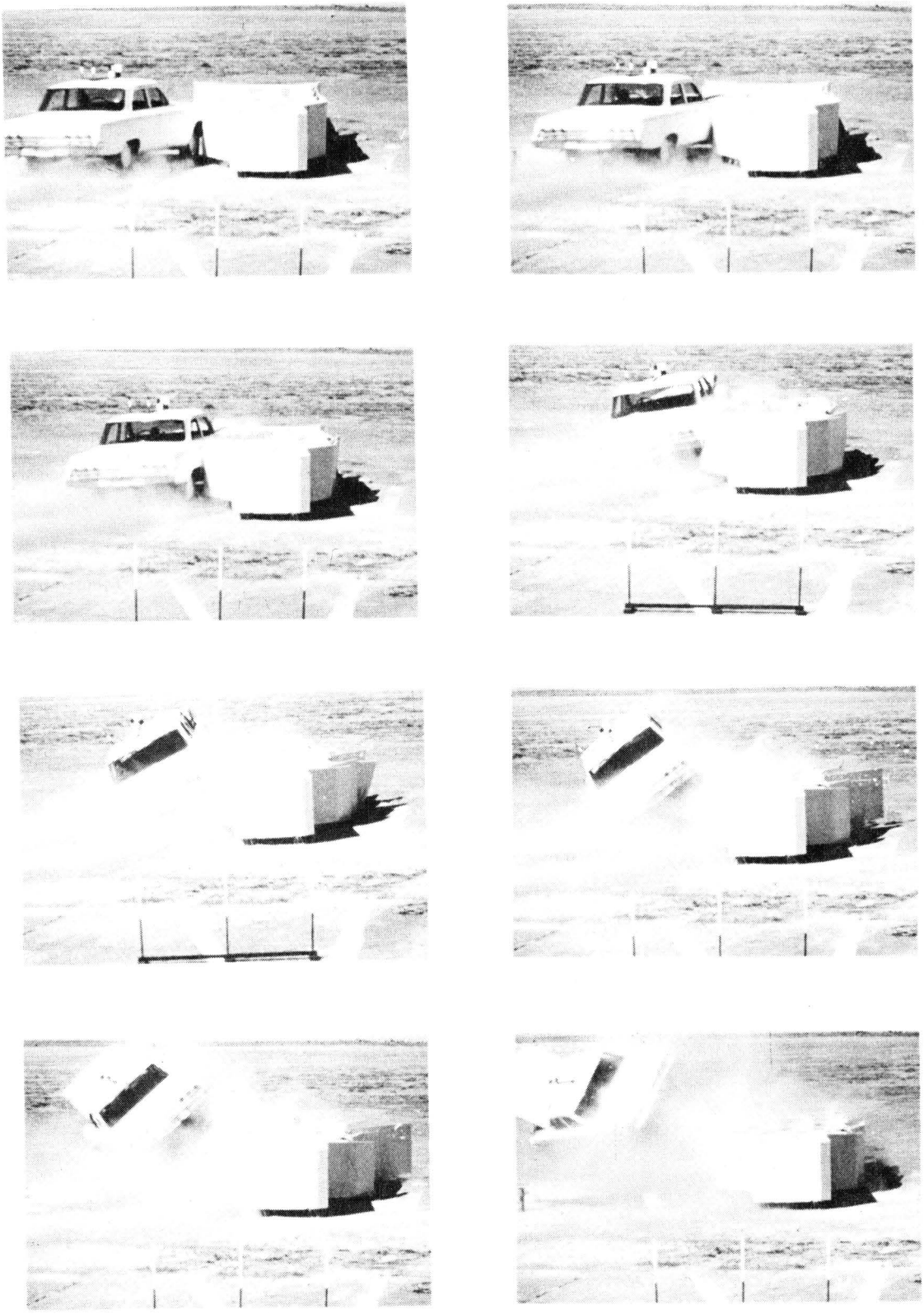

F.520

Figure 14, Test E Sequential Photographs
(View Parallel To Barrier).

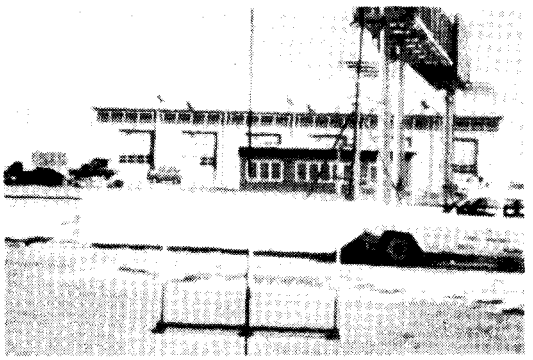

t = 0 sec

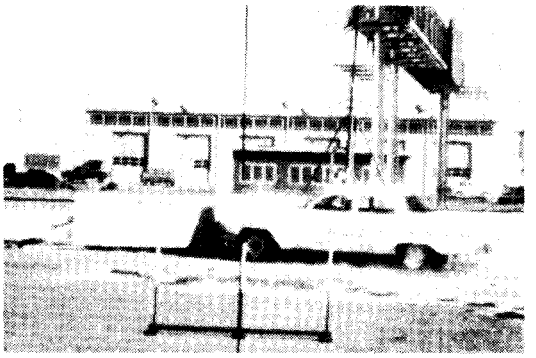

t = 0.104 sec

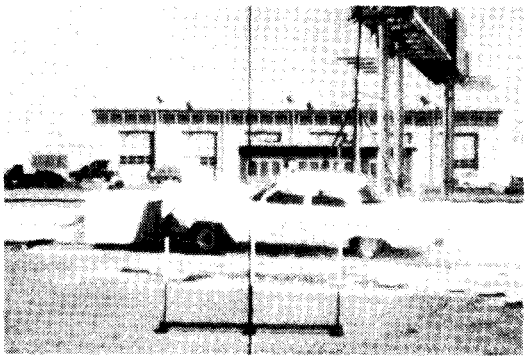

t = 0.153 sec

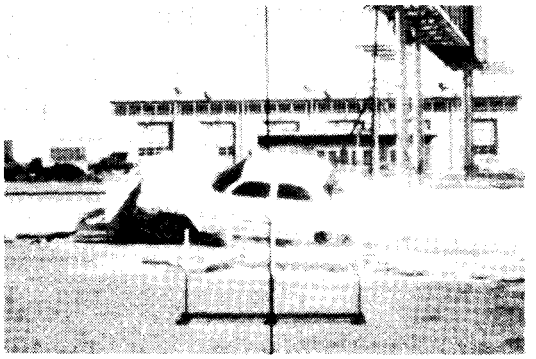

t = 0.213 sec

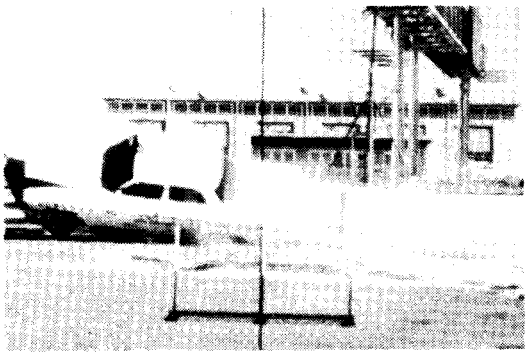

t = 0.351 sec

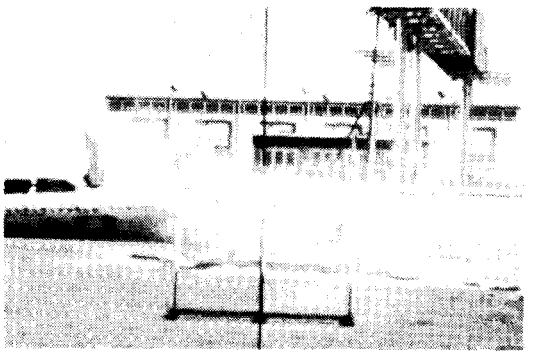

t = 0.536 sec

Figure 15, Test E Sequential Photographs
(View Perpendicular To Barrier).

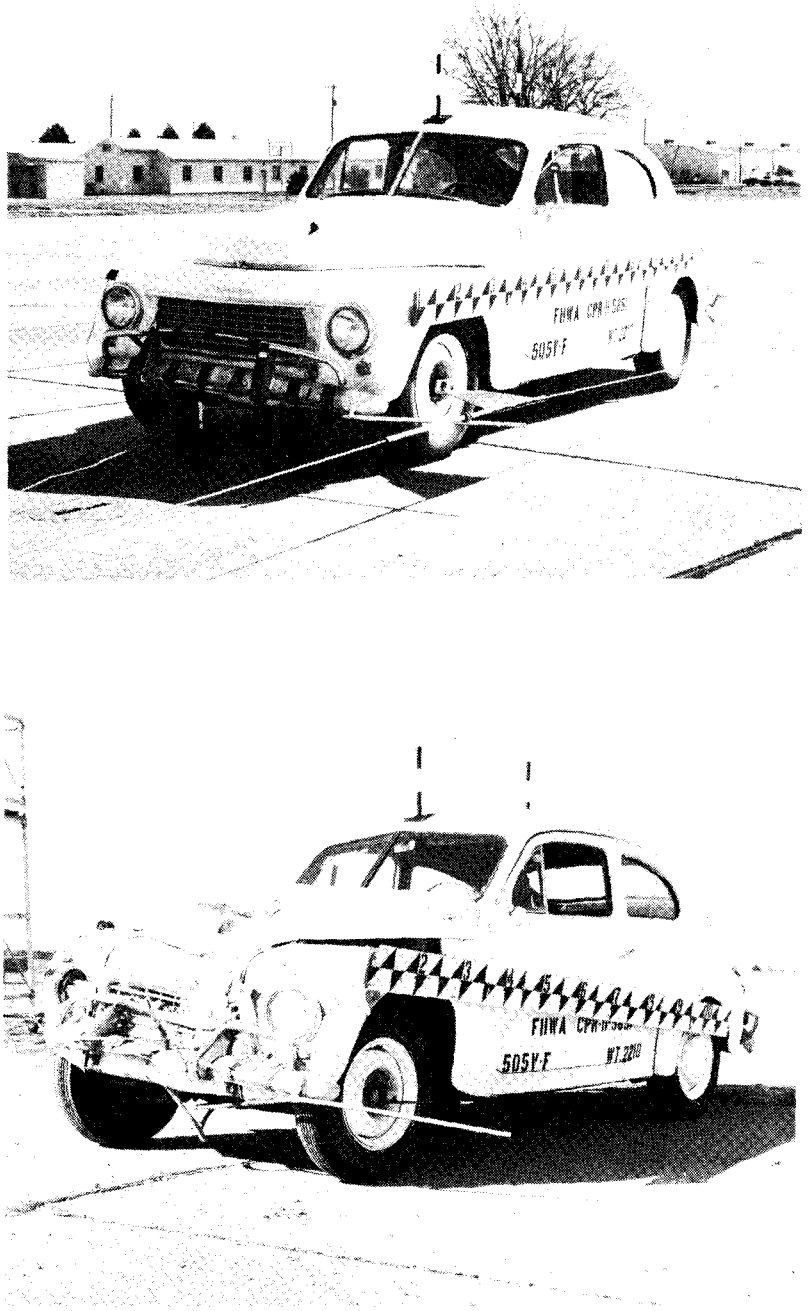

Figure 16, Vehicle Before and After Test F.

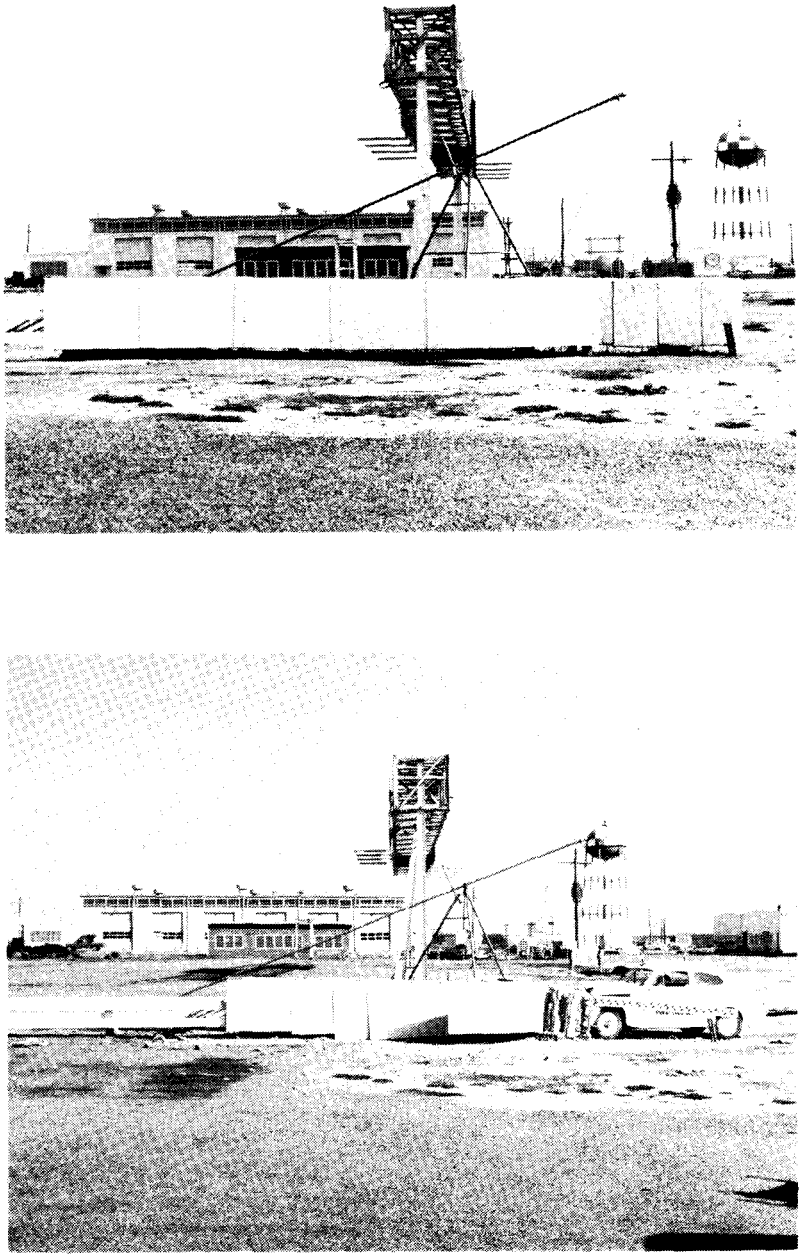

Figure 17. Barrier Before and After Test F
(View Perpendicular to Barrier).

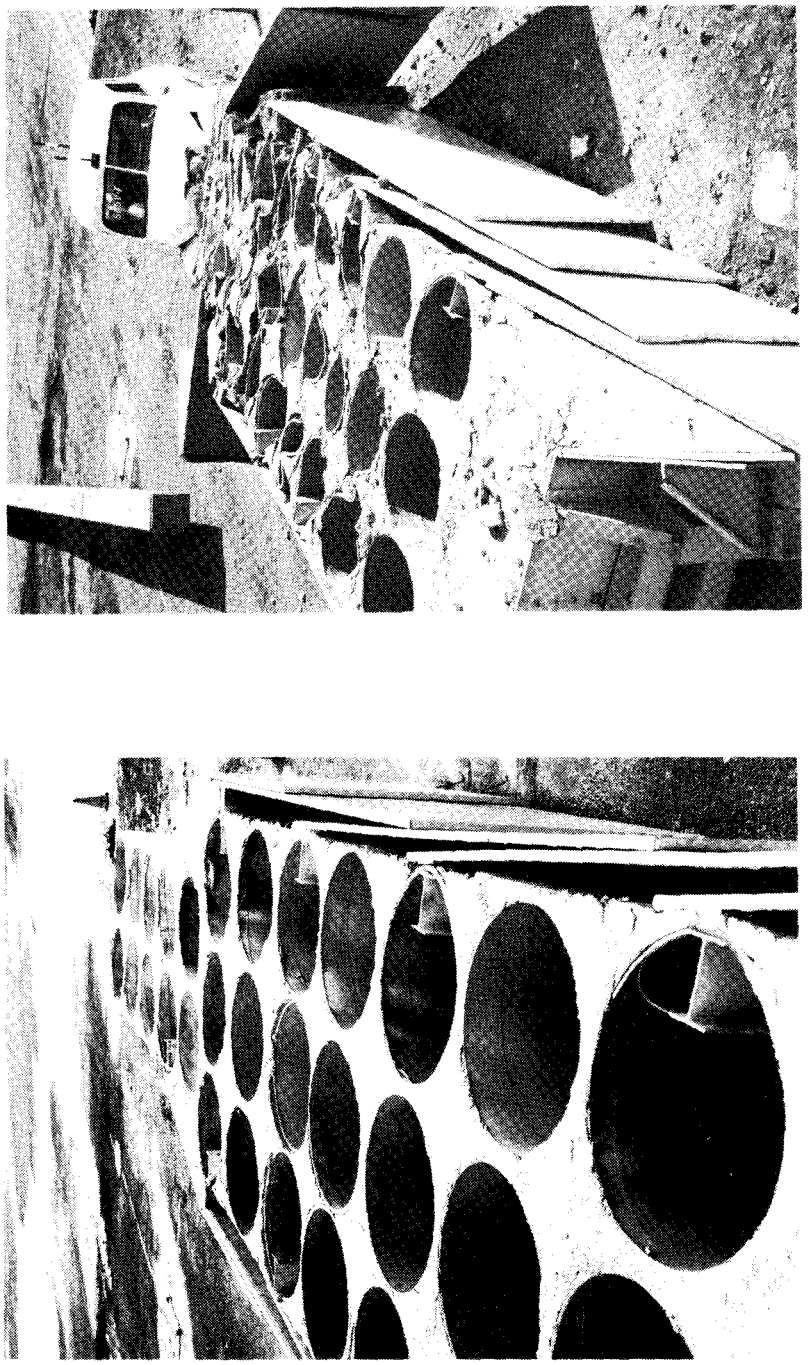

Figure 18, Barrier Before and After Test F (Oblique View).

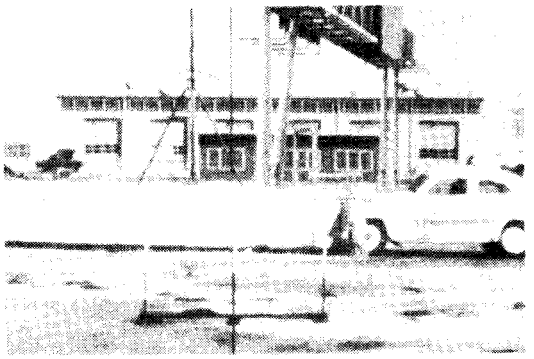

t = 0.023 sec

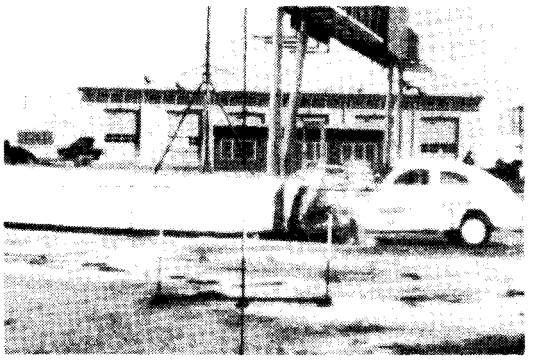

t = 0.054 sec

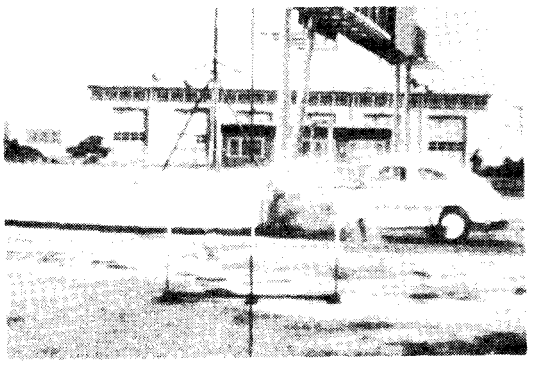

t = 0.085 sec

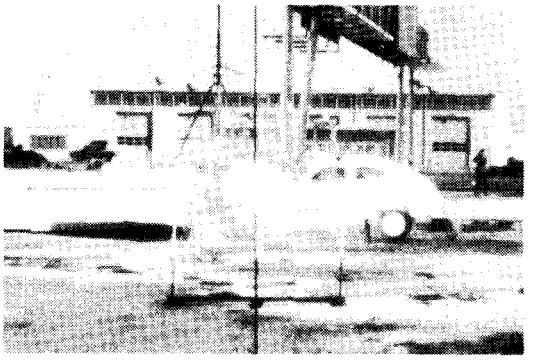

t = 0.208 sec

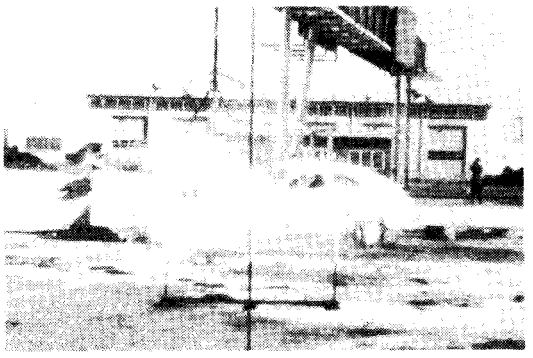

t = 0.309 sec

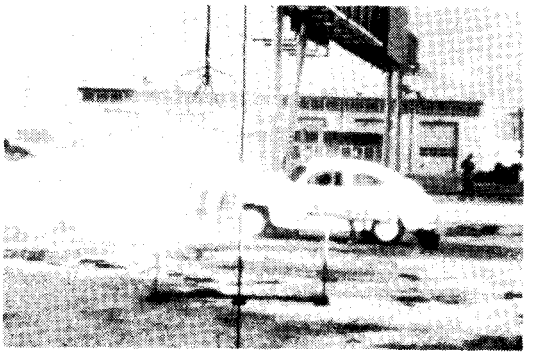

t = 1.712 sec

Figure 19. Test F Sequential Photographs (View Perpendicular To Barrier).

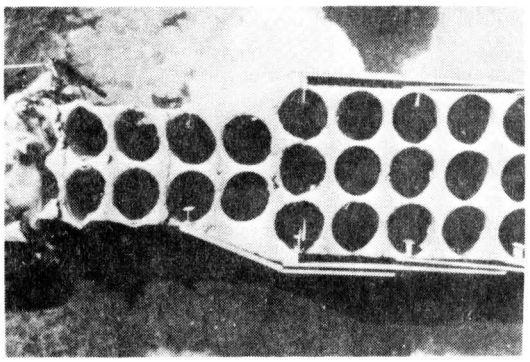

t = 0.031 sec

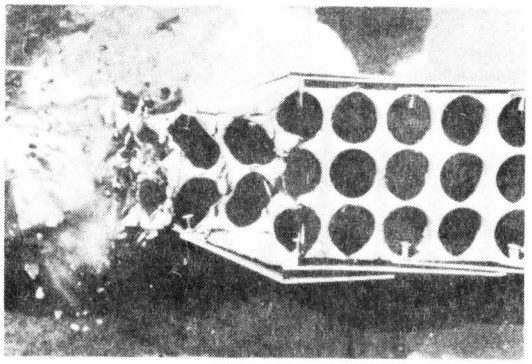

t = 0.064 sec

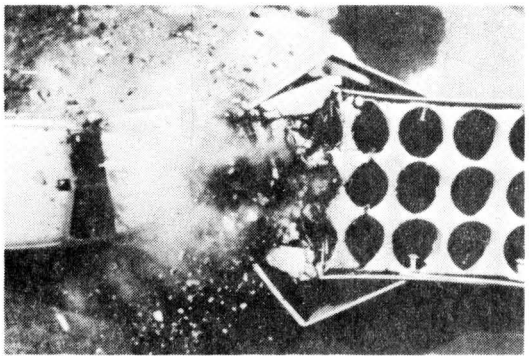

t = 0.130 sec

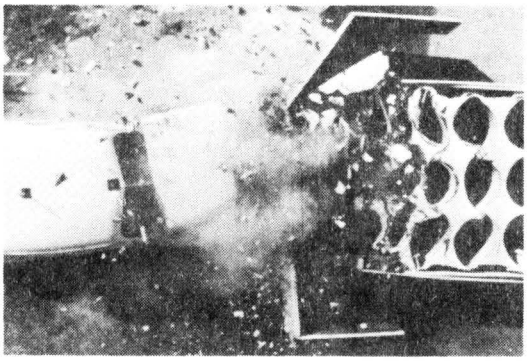

t = 0.199 sec

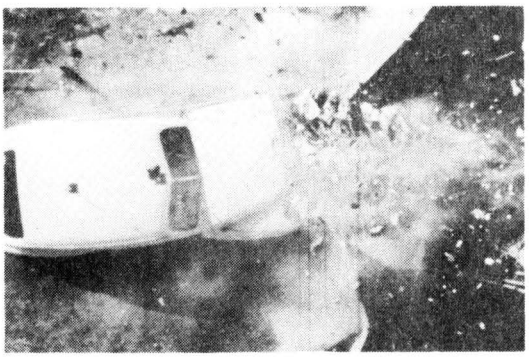

t = 0.380 sec

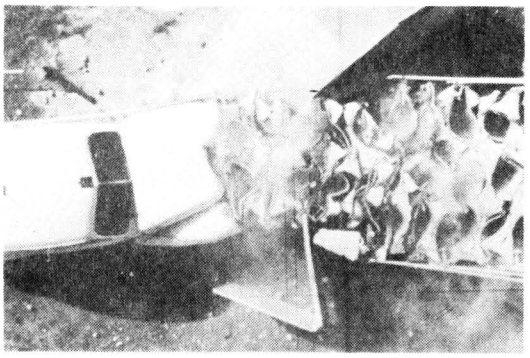

t = 1.480 sec

Figure 20, Test F Sequential Photographs (Overhead View).

DISCUSSION

Of the eight vehicle crash tests that have now been conducted on the concrete crash cushion, all but one have yielded results that appear very favorable from the passenger survivability point of view. The exception to this was the 20°, 59.7 mph, side angle impact of the Mod III cushion (Test 505V-E). In this test the vehicle was subjected to a large moment about the roll axis toward the end of the contact zone. This resulted in a hazardous roll after contact with the cushion was lost and the vehicle came to rest upside down. This tendency in side angle collisions has been noted in other crash tests, such as Test 505R-E[4] and USS Test 1*. In both of these tests, the vehicle contact-wheel appeared to ride up the side panels which resulted in the vehicle becoming airborne as contact with the barrier was lost. The phenomenon observed in Test 505V-E however, appears to be significantly different from that observed in previous tests. From observation of the high-speed test film, it appeared that the following events describe the phenomenon:

1. The vehicle contacts the cushion at the point shown by Figure 15, Photo No. 1, t=0. This point is approximately 16 ft. in advance of the rigid backup wall.
2. The vehicle begins to displace the barrier laterally and slide along the side panels as shown in photos for t=0.104, and t=0.153. There is a slight ramping tendency during this stage, with the

---

*The first test of a series of three tests conducted by United States Steel Corporation, U.S.S. Contract 6339, Texas A&M Research Foundation Project RF 719, March, 1970. No formal publication.

contact side of the vehicle rising approximately one ft as compared to its elevation at contact. This ramping is less severe than noted in the other tests which were referenced, 505R-E and USS Test 1.

3. At t=.213, Figure 15, the vehicle frame appears to be in a state of severe torsion as indicated by the sudden elevation of the right front quadrant of the vehicle. It is at this point, where contact with the last module of the cushion is made, that the severe upward thrust on the right front of the vehicle causes the counterclockwise roll motion. The last module of the Mod II and III cushions is solid vermiculite as compared to the other modules with sonotube openings. The comparative rigidity of this module necessitated one of the following events to occur:

   a) The contact area of the vehicle must be suddenly forced to the outside to pass the rigid module in a relatively violent redirection (barrier force causes a moment about the yaw axis of the vehicle). See Test 1 of the Florida test series[2]. Or,

   b) The contact area of the vehicle must be forced upward to pass over the rigid module resulting in a rolling motion (barrier forces cause a moment about the roll axis of the vehicle). In the slightly elevated position that the right front of the vehicle had achieved in Test 505V-E, the path of least resistance was over the final rigid module.

The question remaining to be answered is why this roll phonomenon occured in Test 505V-E but not in 505V-D or Test 1 of the Florida series. In V-D, the impact angle was only 10° and the vehicle had been almost completely redirected before reaching the solid module. Thus no traumatic force was necessary to get by the rigid portion of the cushion. In Florida Test 1, the impact angle was 20° as in V-E, but the contact point was only six feet in advance of the rigid module. In all other respects the final eight feet of the Florida Mod II cushion was identical to the final eight ft. of the FHWA Mod III cushion. It is hypothesized that the ramping which occured in test V-E was initiated when the vehicle struck the cushion at a point where the cables supporting the redirection panels was low; whereas in Florida Test 1 the cables at the impact point were almost fully elevated. It would therefore appear that the Mod III cushion has a weak point if struck at an angle of 20°, close to where the side panels start. No such weakness was demonstrated by tests on the Mod II cushion since the panels extend out only 11 ft from the rigid backup rail and angle hits in advance of the panels result in an acceptable "pocketing" interaction (see Florida Test 2)[2].

It is believed that this weakness in the Mod III cushion can be overcome by the following design changes: (a.) Replace the solid module at the rear of the Mod III cushion by a standard hollow module and (b.) elevate the side cables at the rear of the cushion 6 in. Item "a" results in reducing the forces imparted to the vehicle at this point

in the interaction and reduces the vehicle reaction necessary to get by the final module. Item "b" results in elevating the vertical position of maximum lateral resistance, and thus reduces the slight ramping tendency which has been noted.

CONCLUSION

The lightweight concrete crash cushion has now shown a capability to perform effectively in decelerating a vehicle for both the head-on and side angle crash conditions*. Seven of eight tests show deceleration levels within the tolerance of restrained humans. Concerning the single test of the Mod III cushion which resulted in an undesirable reaction of the vehicle during a cushion impact, modifications to prevent future reactions of this type are recommended. Since these proposed modifications have not been tested, full-scale tests should be performed before the Mod III barrier is considered for field installations.

The lightweight cellular concrete crash cushion can be installed by semi-skilled laborers using one of two methods. The formwork can be placed in the field, and a local vermiculite applicator can supply the necessary concrete; or the precast modular construction method can be used. The cost per installation compares favorably with that of the barrel crash cushion. Using the modular construction technique, considerable savings should be realized by mass production. Close quality control should be exercised on the geometry of the module and on the vermiculite concrete. Control of batch proportions and unit weight will give predictable crushing strengths. Replacement of segments of the crash cushion after a collision is feasible. For a cast-in-place cushion, the crushed material can be removed, that portion of the barrier reformed, and fresh vermiculite placed in the necessary areas. Fast setting cement will alleviate the problem of curing time. For the precast cushion, the

---

*Design method presented in Appendix B.

three-tube modules weigh approximately 250 lbs and could, therefore, be handled by two men. The modules which have been crushed during a collision can be unbolted, removed, and new modules slipped into place. This refurbishment could be accomplished during a low density traffic period.

The lightweight, low-strength concrete used in these crash cushions exhibits relatively poor durability when subjected to cycles of freezing and thawing if it is allowed to become saturated with water. Several waterproofing agents were tested with limited success as reported in Appendix C. The most certain method of achieving protection has been used by the State of Wisconsin. On two vermiculite cushion installations in Milwaukee, ruberized tarpaulin covers were used to protect the cushions against absorbing water and against the accumulation of ice and snow in the sonotube voids. There has been no durability problem in Wisconsin on the cushions covered in this way.

REFERENCES

1. Ivey, D. L., Buth, E., Hirsch, T. J., "Feasibility of Lightweight Concrete Vehicle Crash Cushions, Highway Research Record No. 306, 1970, pp. 50-57.

2. Ivey, D. L., Buth, E., "Side Angle Collisions with Concrete Vehicle Crash Cushions", Research Report 733, Florida State Department of Transportation, Texas Transportation Institute, November, 1970.

3. Hirsch, T. J., Hayes, G. G., Ivey, D. L., "The Modular Crash Cushion", Technical Memorandum 505-1S, Supplement To 505-1, Texas Transportation Institute, August, 1970.

4. Hayes, G. G., Ivey, D. L., Hirsch, T. J., "Performance of the HI-DRO Cushion Cell Barrier Vehicle-Impact Attenuator", Highway Research Record No. 343, 1971, pp. 93-99.

APPENDIX A

PHOTOGRAPHIC DATA

AND

ACCELEROMETER TRACES

TABLE A1

TEST 505 V-D

High-Speed Film Data

Time (msec)		Displacement (ft)	
-62		-5.2	V_1 = 83.9 fps
-52		-4.3	
-41		-3.4	
-31		-2.6	
-21		-1.7	
-10		-0.9	
0	Impact	0	
9		0.8	
19		1.5	
28		2.3	
38		3.0	
47		3.7	
56		4.4	
66		5.1	
75		5.8	
84		6.4	
94		7.1	
103		7.8	
113		8.4	
122		9.1	
131		9.7	
141		10.4	
150		11.0	
159		11.7	
169		12.3	
178		13.0	
188		13.6	

Time (msec)	Displacement (ft)	
(continued)		
197	14.3	
206	14.9	
216	15.5	
225	16.1	
234	16.7	
244	17.4	
253	18.1	
263	18.8	
272	19.4	
281	20.1	
290	20.8	V_2 = 72.7 fps
300	21.5	
310	22.2	
319	22.8	
329	23.5	
338	24.2	
347	24.9	
356	25.6	
366	26.3	
375	27.0	
385	27.6	
394	28.3	
403	29.0	
413	29.6	
422	30.2	
431	30.9	

TABLE A2

TEST 505 V-E

High-Speed Film Data

Time (msec)		Displacement (ft)	
-40		-3.5	V_1 = 87.5 fps
-30		-2.6	
-20		-1.8	
-10		-0.9	
0	Impact	0	
10		0.8	
20		1.7	
30		2.6	
40		3.5	
50		4.2	
60		5.0	
70		5.8	
80		6.6	
90		7.3	
100		8.1	
110		8.8	
120		9.5	
130		10.2	
140		10.8	
149		11.5	
159		12.1	

Time (msec)	Displacement (ft)	
(continued)		
169	12.7	
179	13.2	
189	13.8	
199	14.3	
209	14.8	
219	15.3	
229	15.8	
239	16.3	V_2 = 43.9 fps
249	16.7	
259	17.2	
269	17.6	
279	18.1	
289	18.5	
299	18.9	
309	19.4	
319	19.8	
339	20.6	
359	21.5	
379	22.3	
399	23.1	

TABLE A3

TEST 505 V-F

High-Speed Film Data

Time (msec)		Displacement (ft)		Time (msec)	Displacement (ft)
-39		-3.5	V_1 = 89.7 fps	(continued)	
-30		-2.7		138	9.0
-20		-1.8		148	9.4
-10		-0.9		167	10.0
0	Impact	0		187	10.5
10		0.9		207	10.9
20		1.8		227	11.2
30		2.6		246	11.5
39		3.4		266	11.8
49		4.1		286	11.9
59		4.8		305	12.1
69		5.4		325	12.2
79		6.1		345	12.2
89		6.7		364	12.2
98		7.2		561	11.6
108		7.7		808	10.8
118		8.2		1302	10.1
128		8.6			

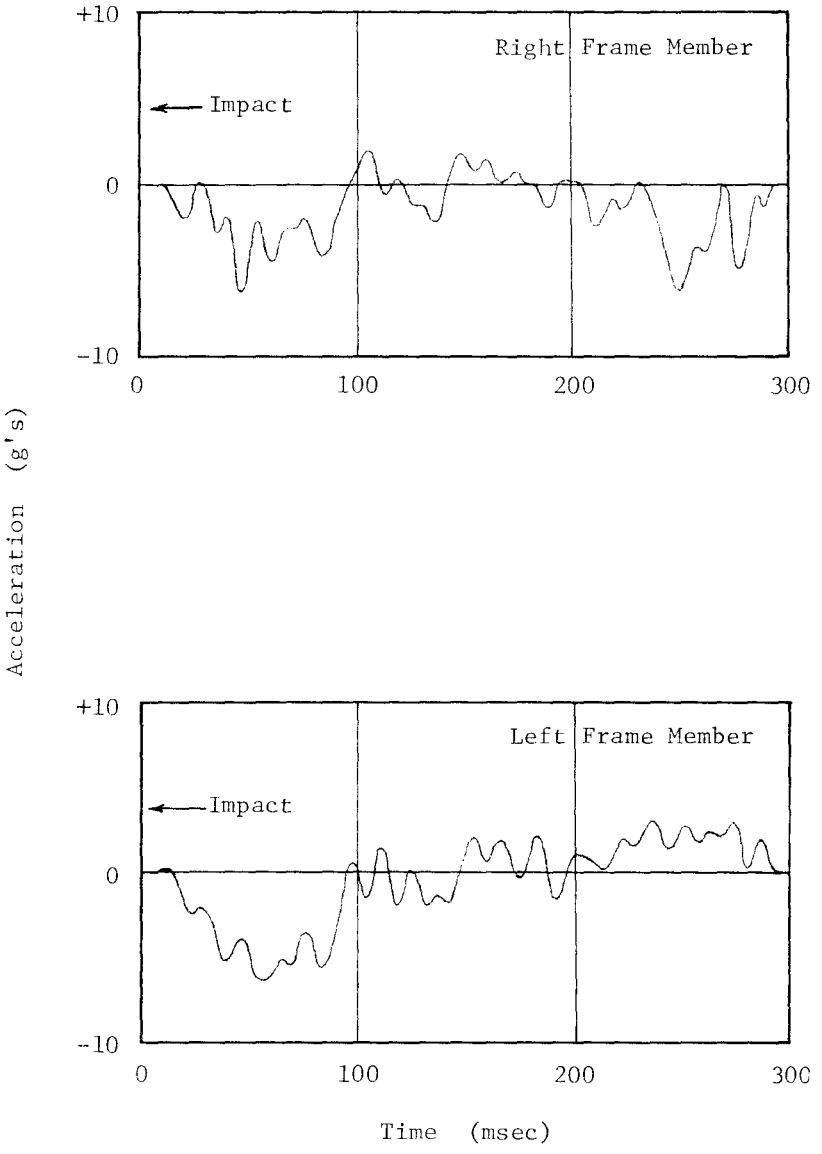

Figure A1 , Longitudinal Accelerometer Data, Test D.

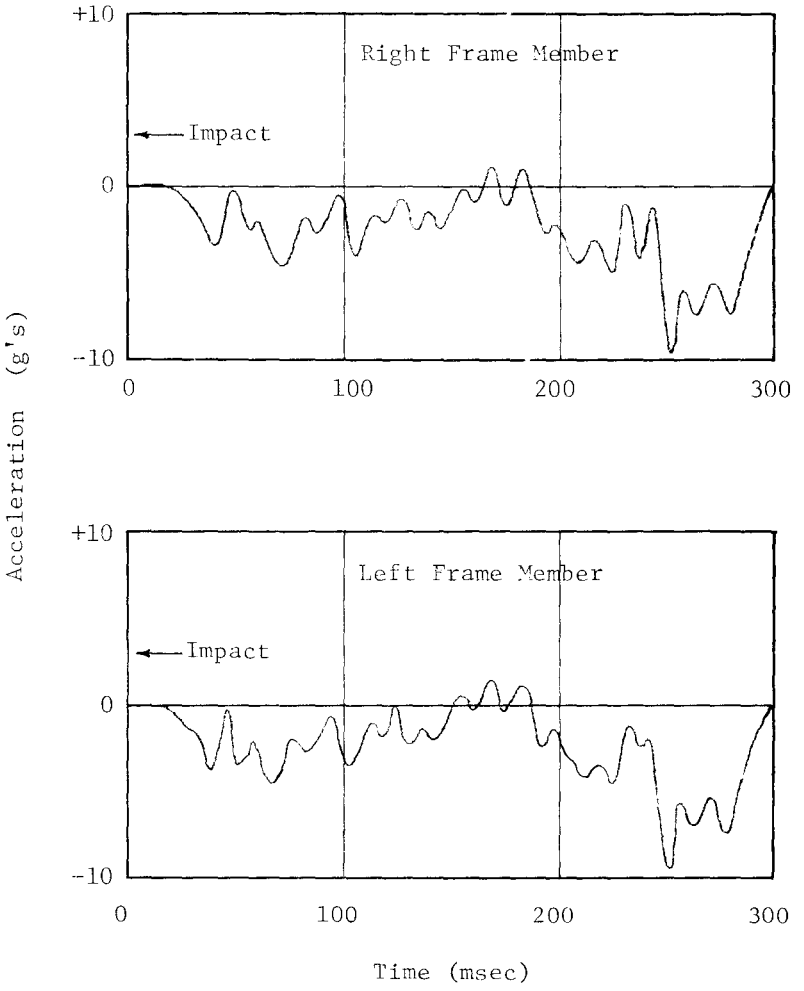

Figure A2, Transverse Accelerometer Data, Test D.

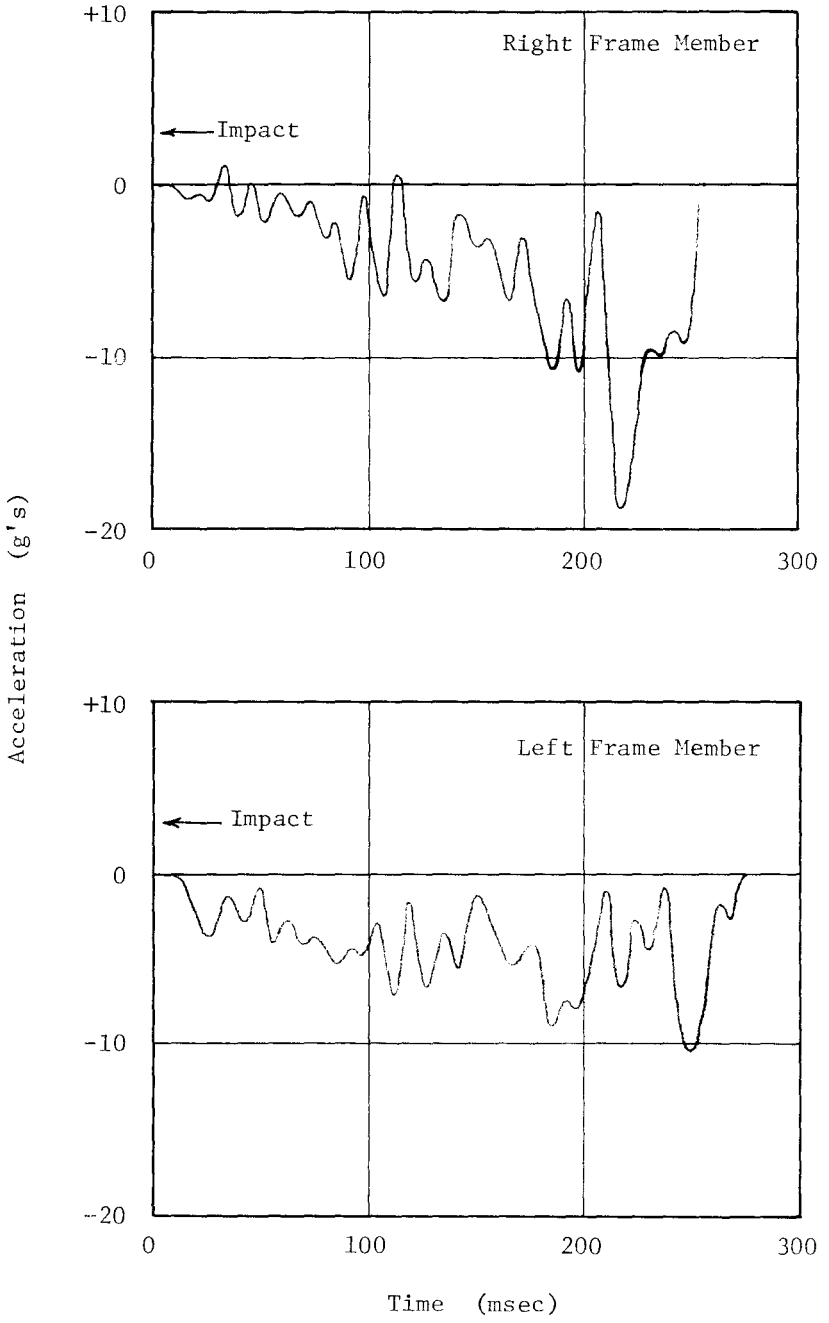

Figure A3, Longitudinal Accelerometer Data, Test E.

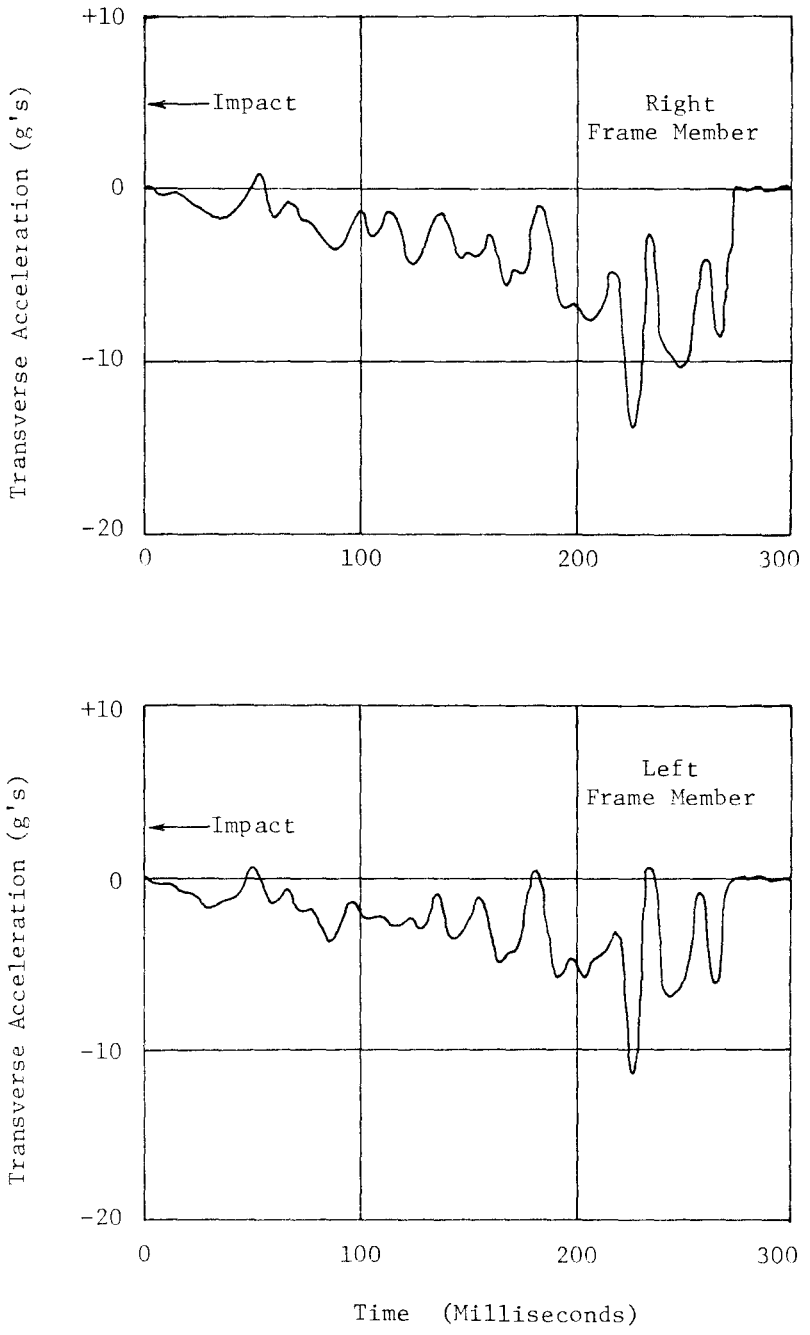

Figure A4 , Transverse Accelerometer Data, Test E

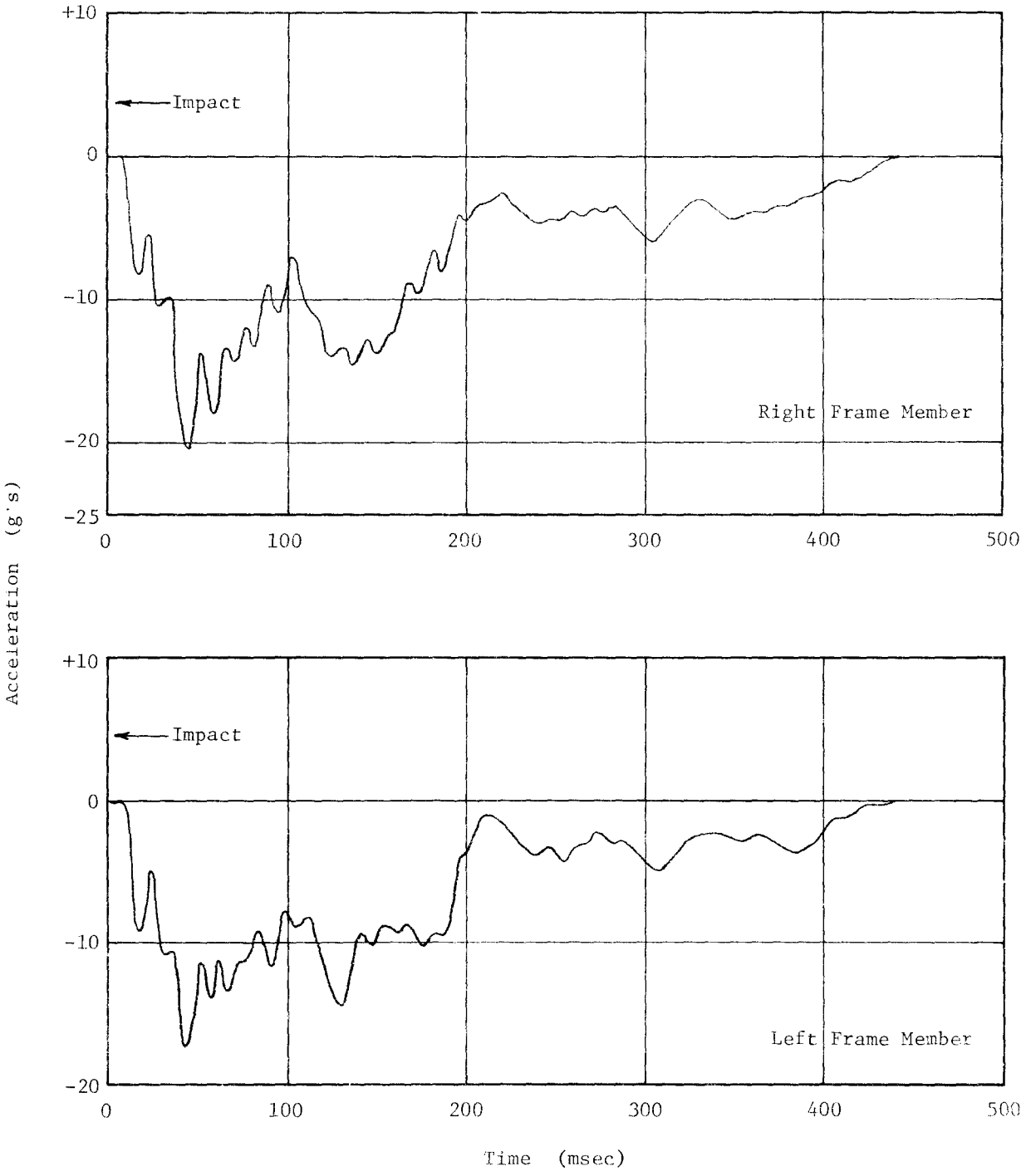

Figure A5, Longitudinal Accelerometer Data, Test F.

APPENDIX E

MODEL STUDY

MODEL ANALYSIS

The following model analysis describes the relationship between the static crushing energy of the full scale vermiculite concrete crash cushion and the static crushing energy of small scale modules.

In the judgment of the writers, the following geometric and material properties are the most important to the relationship between prototype and model. Other factors, which obviously are of some influence to static crushing energy are assumed to be of secondary importance.

Geometric Properties

1) a-(Refer to Figure B1)
2) b-(Refer to Figure B1)
3) h-(Refer to Figure B1)
4) B-(Refer to Figure B1)
5) D-(Refer to Figure B1)
6) t-(Refer to Figure B1)
7) A-Cross sectional area of reinforcement in a module cross section

Material Properties

8) f'_c -static crushing strength of the vermiculite concrete

Structural Property

9) E-static crushing energy of a particular module

In the following development the subscripts p and m refer to prototype and model respectively.

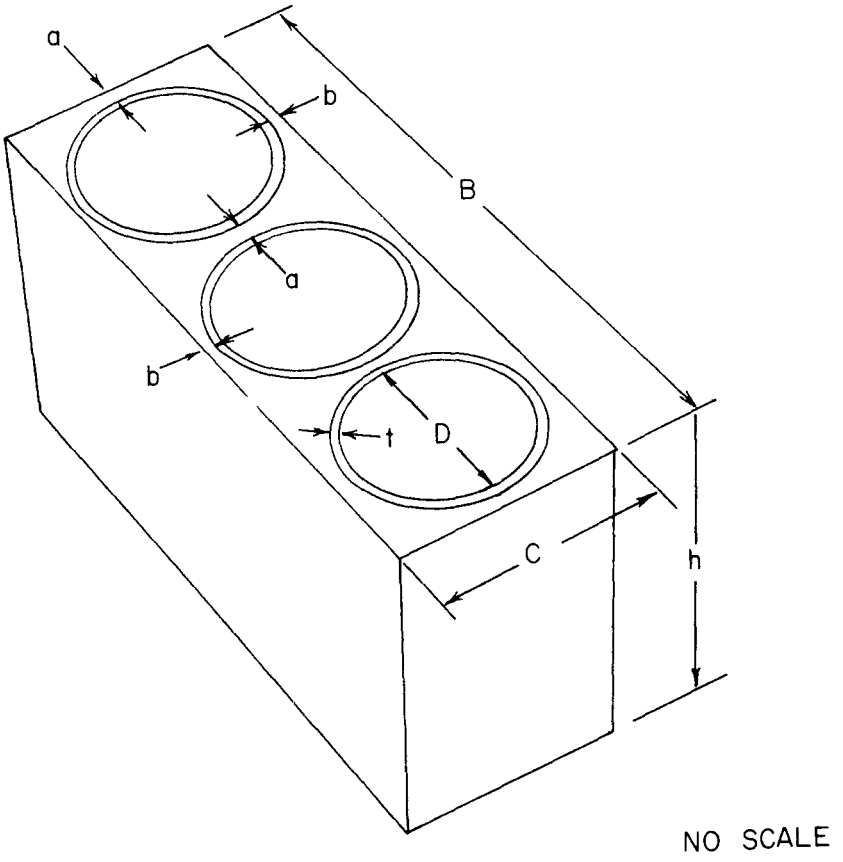

FIGURE BI, MODULE DIMENSIONS

The interrelationship of static crushing strength and the geometric and material properties can be written as follows:

$$E = (\text{A function of}) \ (f'_c, a, b, h, t, B, D, A). \tag{1}$$

Since there are two dimensions involved (force and length) the number of Pi terms necessary to describe this relationship in dimensionless terms is two less than the total number of variables in Eq. 1.

i.e. 9 - 2 = 7 Pi terms

These terms can be chosen and the functional relationship written as:

$$\frac{E}{f'_c \, D^3} = (\text{A function of}) \left\{ \frac{a}{D}, \frac{b}{D}, \frac{h}{D}, \frac{t}{D}, \frac{B}{D}, \& \frac{A}{D^2} \right\}. \tag{2}$$

For the model and the prototype this equation can be expressed as:

$$\frac{E_m}{f'_{c_m} \, D_m^3} = F \left(\frac{a_m}{D_m}, \frac{b_m}{D_m}, \frac{h_m}{D_m}, \frac{t_m}{D_m}, \frac{B_m}{D_m}, \& \frac{A_m}{D_m^2} \right) \tag{3}$$

$$\frac{E_p}{f'_{c_p} \, D_p^3} = F \left(\frac{a_p}{D_p}, \frac{b_p}{D_p}, \frac{h_p}{D_p}, \frac{t_p}{D_p}, \frac{B_p}{D_p}, \& \frac{A_p}{D_p^2} \right). \tag{4}$$

Then if the ratio of D_p to D_m is defined as the modeling factor, the following conditions must be maintained in order for the prediction equation to be valid:

$$a_p = n \, a_m \qquad B_p = n \, B_m$$

$$b_p = n \, b_m \qquad A_p = n^2 \, A_m \, .$$

$$h_p = n \, h_m$$

$$t_p = n \, t_m$$

These equations are found by equating the corresponding Pi terms of Eqs. 3 and 4 and substituting n for the ratio D_p/D_m.

If these conditions are held, then the prediction equation is:

$$\frac{E_m}{f'_{c_m} D_m^3} = \frac{E_p}{f'_{c_p} D_p^3} .$$

Since F'_{c_m} can be made equal to f'_{c_p}, this equation reduces to:

$$E_p = n^3 E_m. \tag{5}$$

Thus if the static energy of a model module is determined by testing, the energy of a prototype would be predicted by Eq. 5.

EXPERIMENTAL PROGRAM

The design concrete mixtures and actual batch data are given in Tables B1 and B2. The schedule of model modules, including the parameters studied, are given in Table B3.

Cardboard molds for standard 6 x 12 in. concrete cylinders were used to simulate the "sonotubes" in the model modules. The forms for the modules (illustrated in Figure B2) were made of plywood. Half-inch hardware cloth with alternate wires removed to obtain the correct amount of cross-sectional area was used for reinforcement (Figure B3). The assembled form is shown in Figure B4, and a model module in Figure B5.

The model modules were tested in a hydraulic universal testing machine as shown in Figure B6. A scale on either end of the loading head was used to determine crushing distance. Figures B7 through B14 and B15 through B18 are sequential photographs of the two module tests.

Several limitations of the experimental design should be noted. First, no attempt was made to scale the strength of the cardboard sonotubes; and second, the loading technique used in the model study did not closely simulate the loading of a vehicle on a prototype.

Batches	Cement Type		Mix Properties		Expected f'c
HE 1 (505V-A)	High Early		Cmt.	2.9 sk	50 psi
			Agg.	5 sk	
			Water	73 gal	
			Admix	1 pt/sk agg.	
			U. Wt.	37 pcf	
HE 2	High Early		Cmt.	5 sk	175 psi
			Agg.	7-1/2 sk	
		1:6	Water	100 gal.	
			Admix	1 pt/sk agg.	
			U. Wt.	50 pcf	
HE 3	High Early		Cmt.	7-1/2 sk	425 psi
			Agg.	7-1/2 sk	
		1:4	Water	98 gal.	
			Admix	1 pt/sk agg.	
			U. Wt.	60 pcf	
RS 1 (505V-C)	Regulated Set		Cmt.	3.25 sk	60 psi
			Agg.	5.76 sk	
			Water	77.5 gal.	
			Air	1 pt/sk agg.	
			U. Wt.	41 pcf	

TABLE B1 DESIGN CONCRETE MIXTURES

BATCH NO.	DATE	CEMENT lbs.	AGGREGATE[1] cu. ft.	WATER lbs.	ADMIX pints	UNIT WEIGHT lbs.	AIR[2] %
RS1	4/30/70	79 1/2	6	168	1 1/2	40.5	35
HE1	5/05/70	54.4	4	121.4	1	42	50
HE2	5/11/70	94	6	166.7	1 1/2	43	50
HE3	5/12/70	141	6	163.3	1 1/2	49	51

[1] 1 sk = 4 cu. ft.

[2] Measured with pressure meter.

TABLE B2, BATCH DATA

VERMICULITE MODEL MODULES

Module	Concrete Batch	Design f'c psi	Actual f'c psi	h^1 inch	B^1 inch	C^1 inch	a^1 inch	b^1 inch
M1	RS1	50	77	9.82	19.7	6.53	0.272	0.136
M2	HE2	175	104	9.82	19.7	6.53	0.272	0.136
M3	HE3	425	220	9.82	19.7	6.53	0.272	0.136
M4	RS1	50	77	9.82	18.85	6.53	0.136	0.136
M5	RS1	50	77	9.82	20.50	6.53	0.545	0.136
M6	RS1	50	77	9.82	6.74	6.53	0.272	0.136
M7	RS1	50	77	9.82	13.20	6.53	0.272	0.136
M8	RS1	50	77	9.82	19.7	6.74	0.272	0.272
M9	RS1	50	77	9.82	19.7	7.30	0.272	0.545

[1]See Figure 1

TABLE B3 MODEL MODULE SPECIFICATIONS

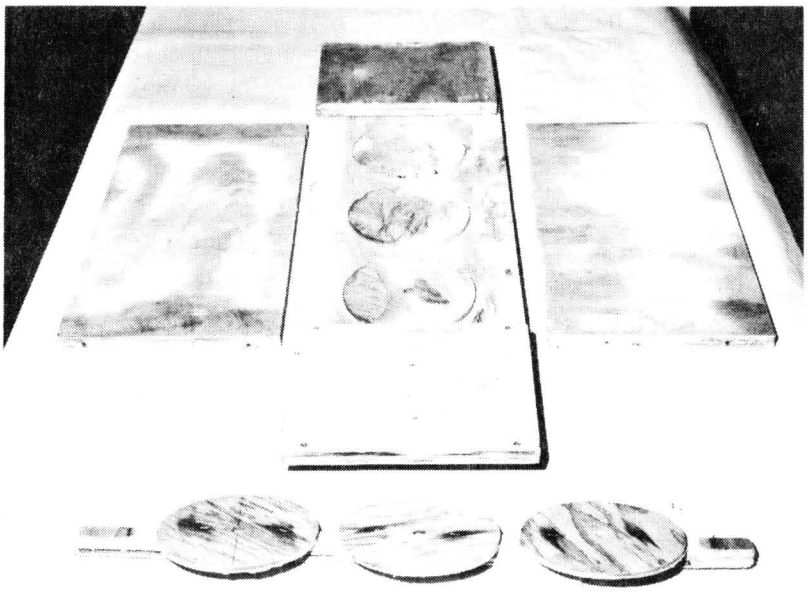

Figure B2

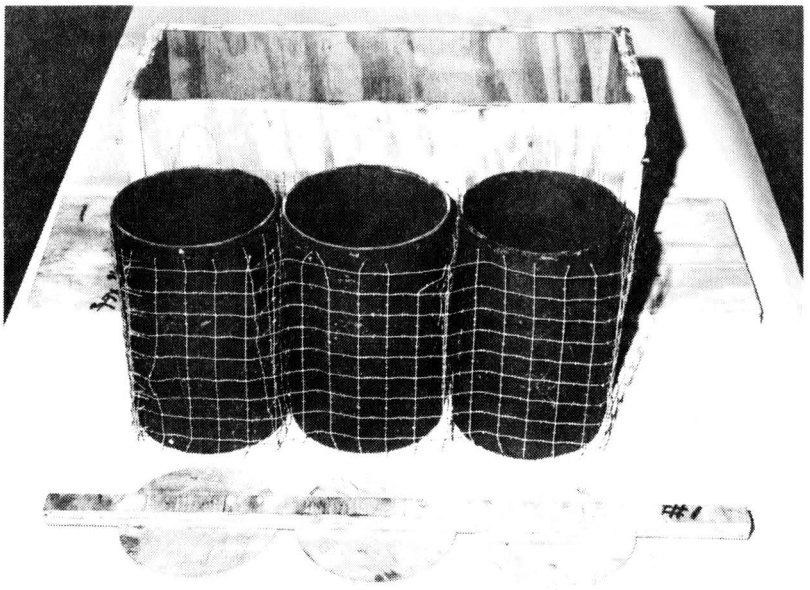

Figure B3

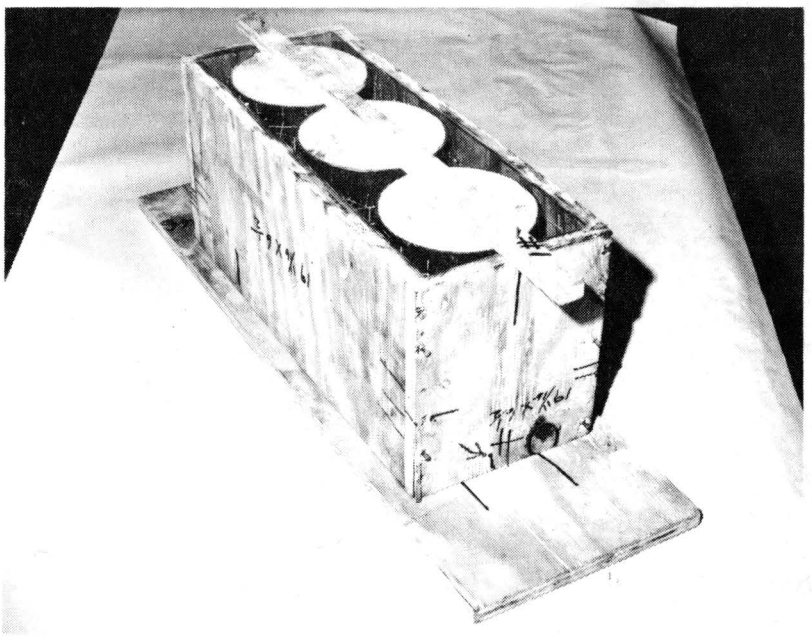

Figure B4

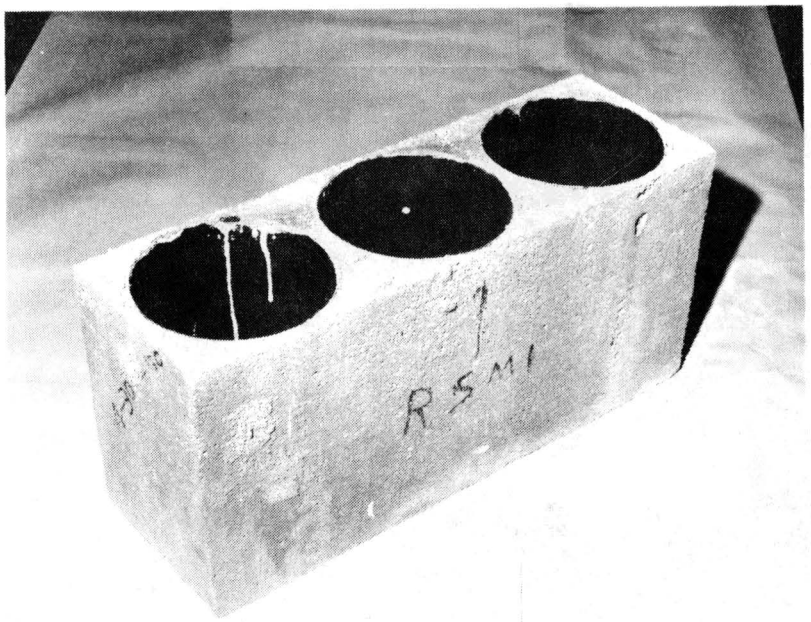

Figure B5

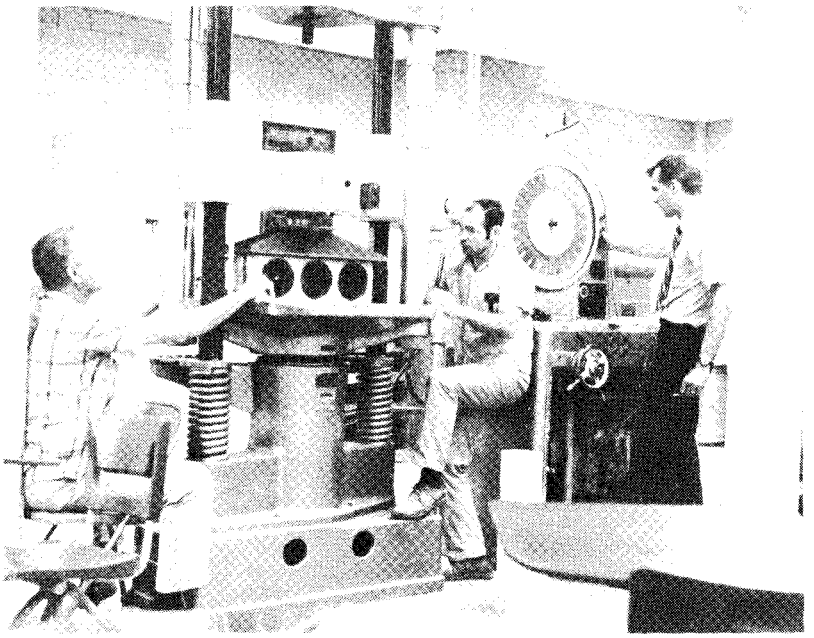

Figure B6

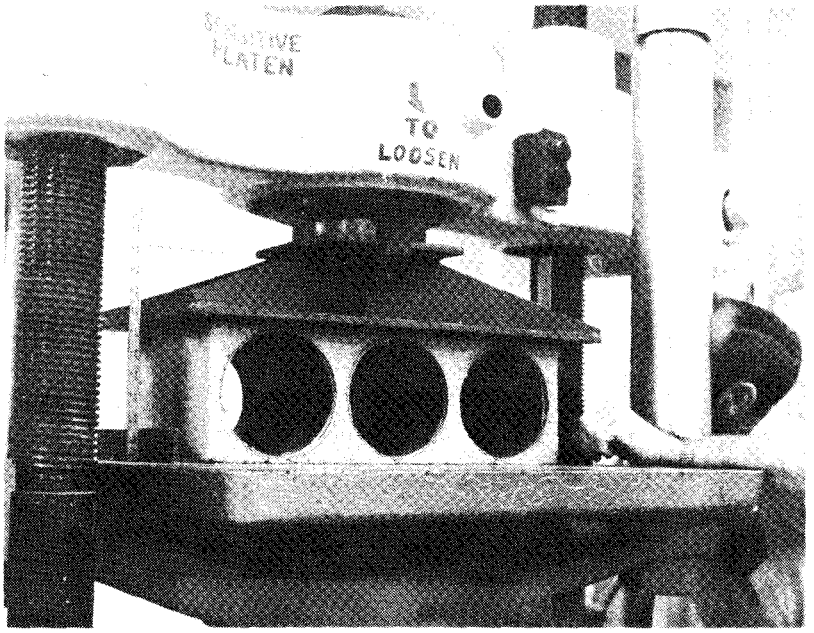

Figure B7

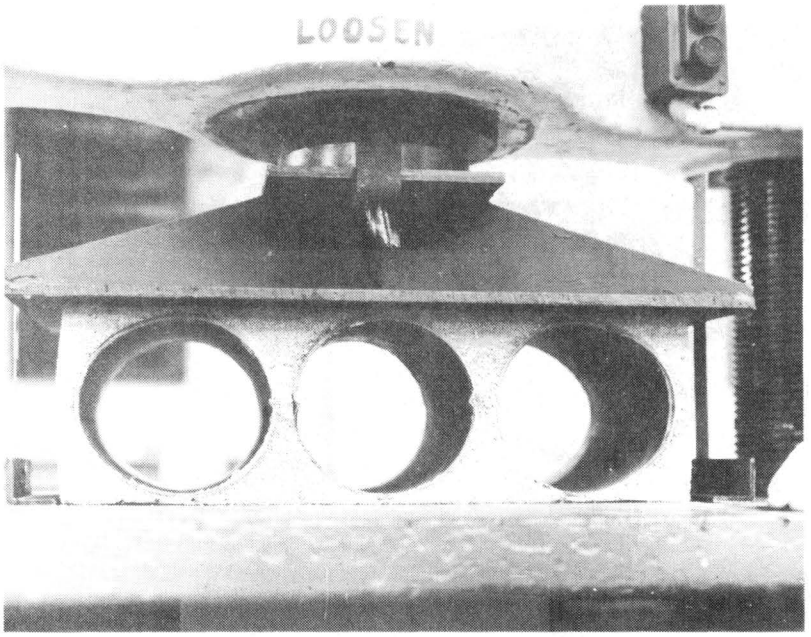

Figure B8

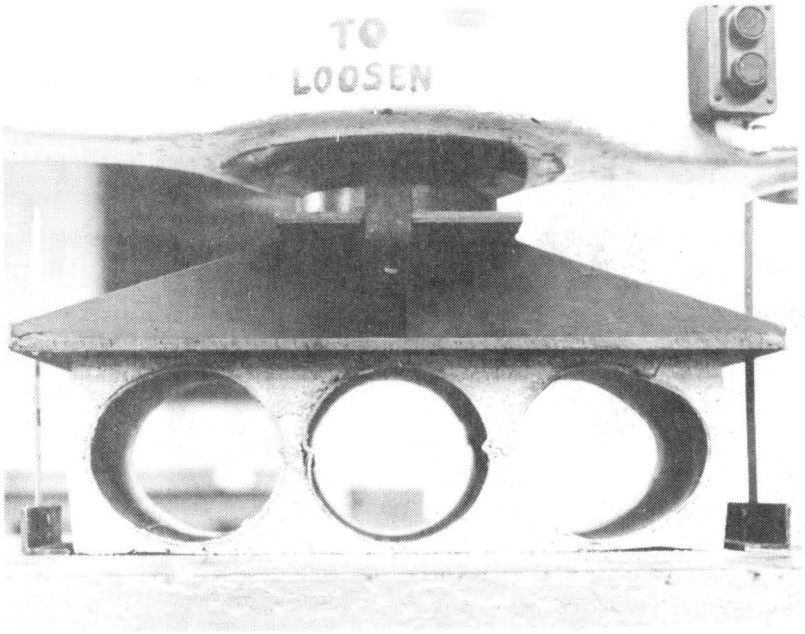

Figure B9

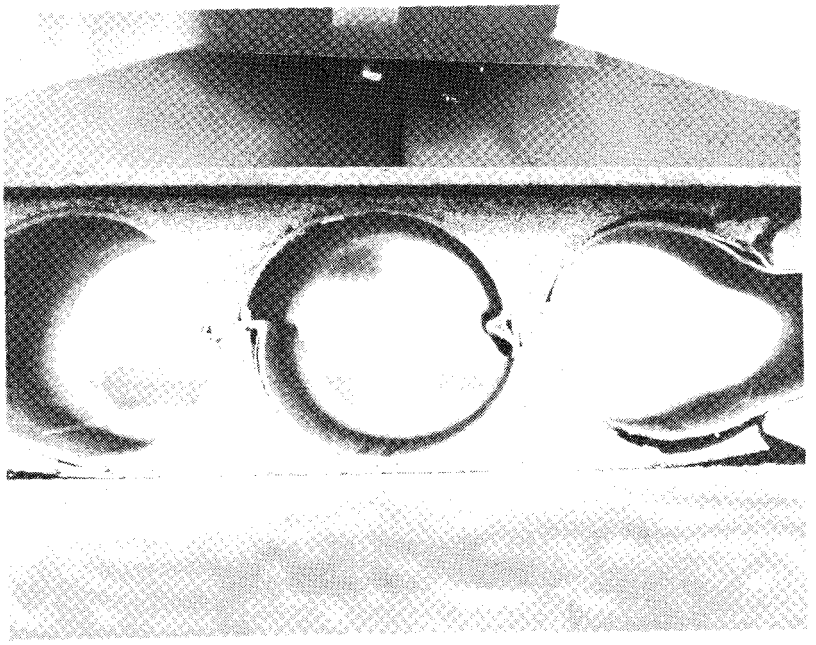

Figure B10

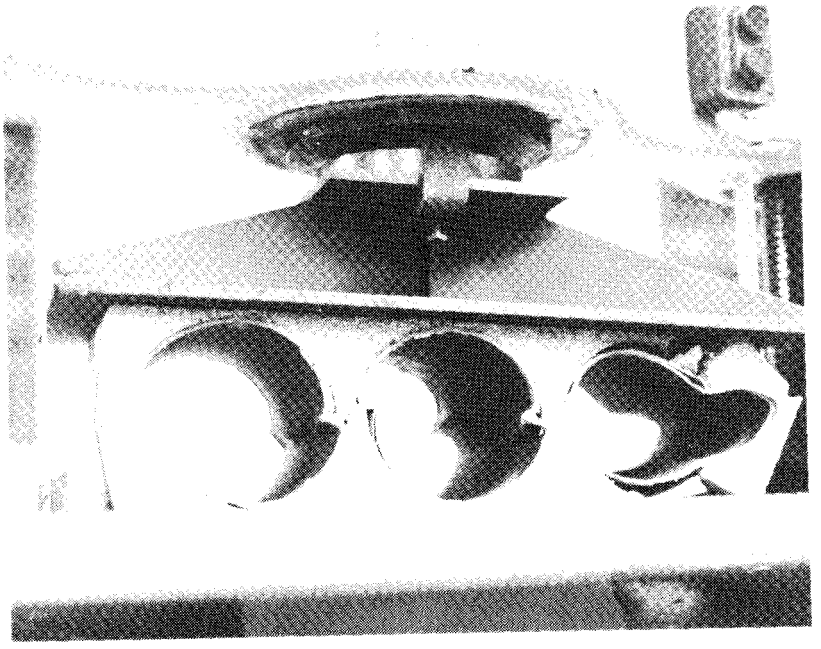

Figure B11

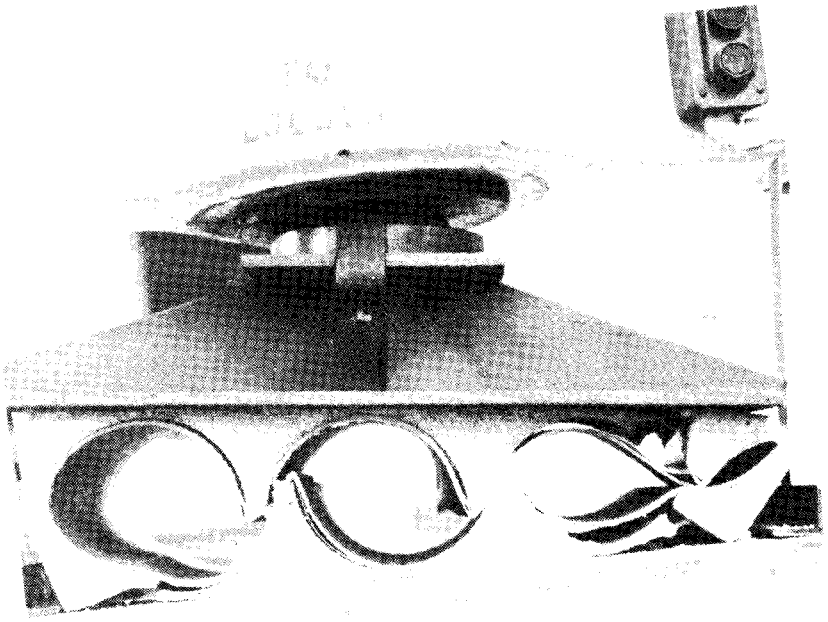

Figure B12

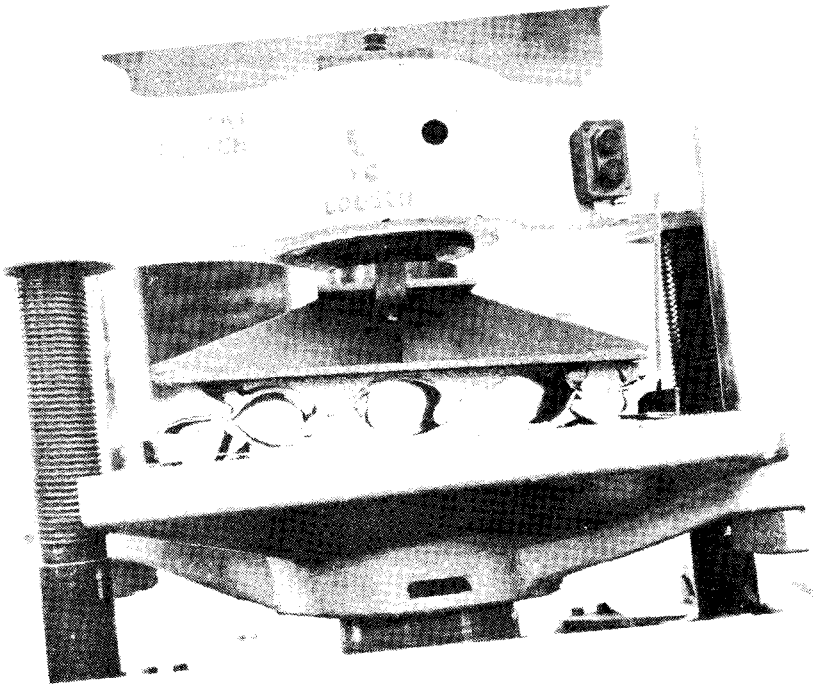

Figure B13

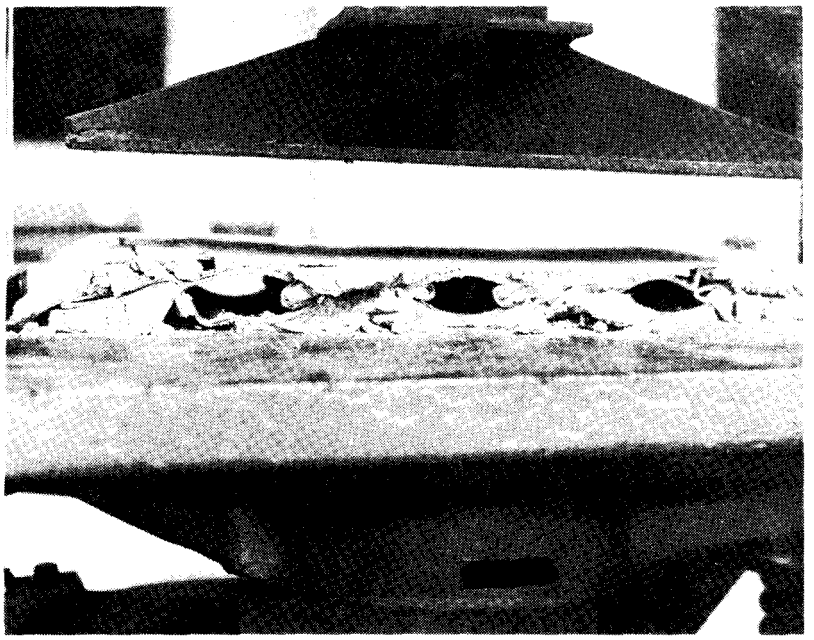

Figure B14

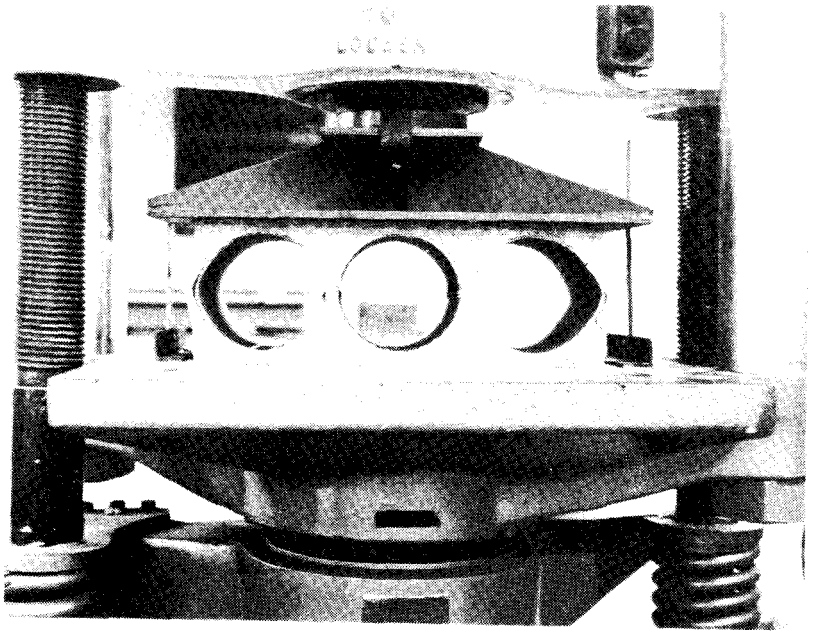

Figure B15

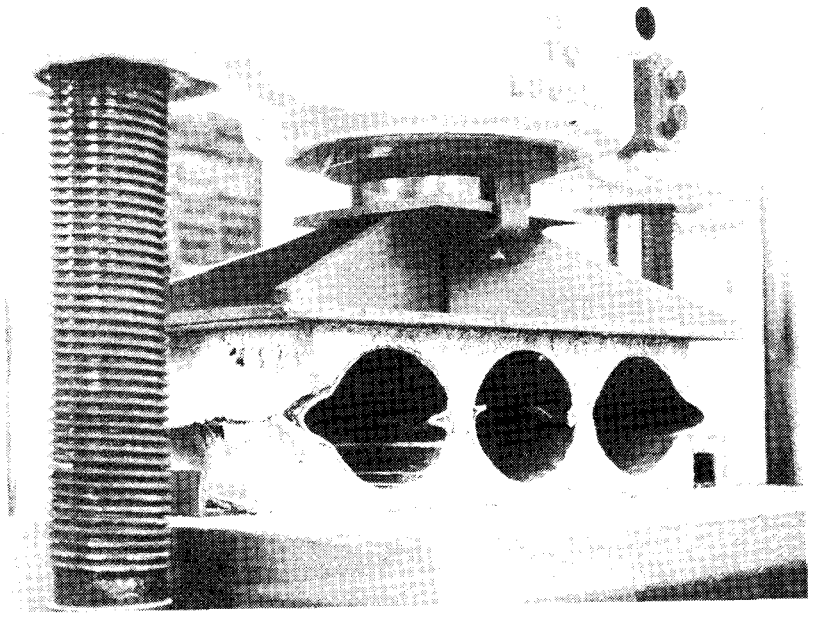

Figure B16

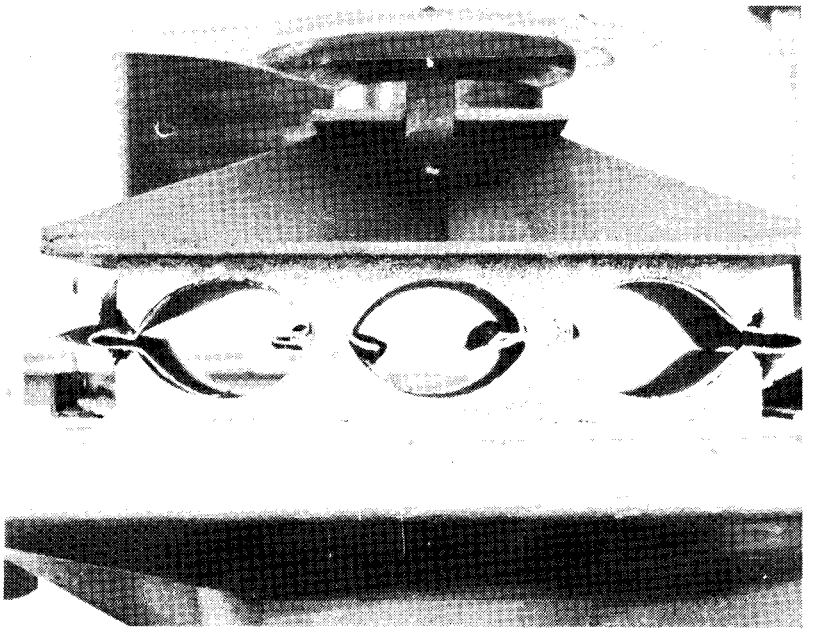

Figure B17

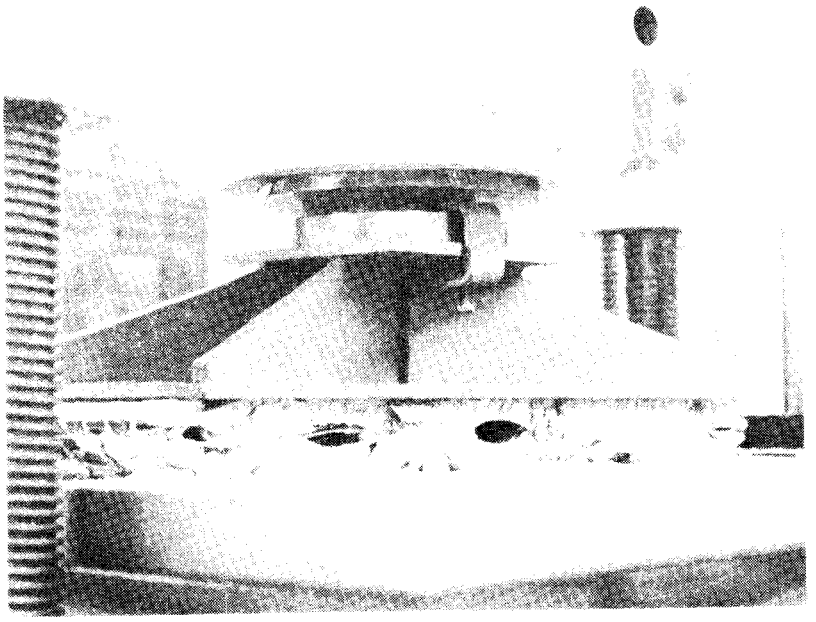

Figure B18

RESULTS

STRENGTH-TIME RELATIONSHIPS

The strength-time relationships for the four concrete mixtures are illustrated in Figure B19. As anticipated, there appears to be little gain in strength after the initial 21 days.

MODEL MODULES

Curves illustrating the relationship between crushing force and distance are shown in Figures B20 through B23. An effective crushing distance of 4.0 in. (crushing ratio = .61) was chosen for these model modules. This number represents a compromise between the point where the energy absorbing capacity of the model module was consumed and the actual crushing ratio observed for prototype cushions.

Figures B24 through B27 show the relative influence of variations in compressive strength and dimensions on the nondimensional energy parameter $E/(f'_c D^3)$. The results are most encouraging in that a rather linear relationship between the energy parameter and the other influential parameters under study is indicated. This lends additional confidence to the use of model analysis to predict prototype behavior in this particular application.

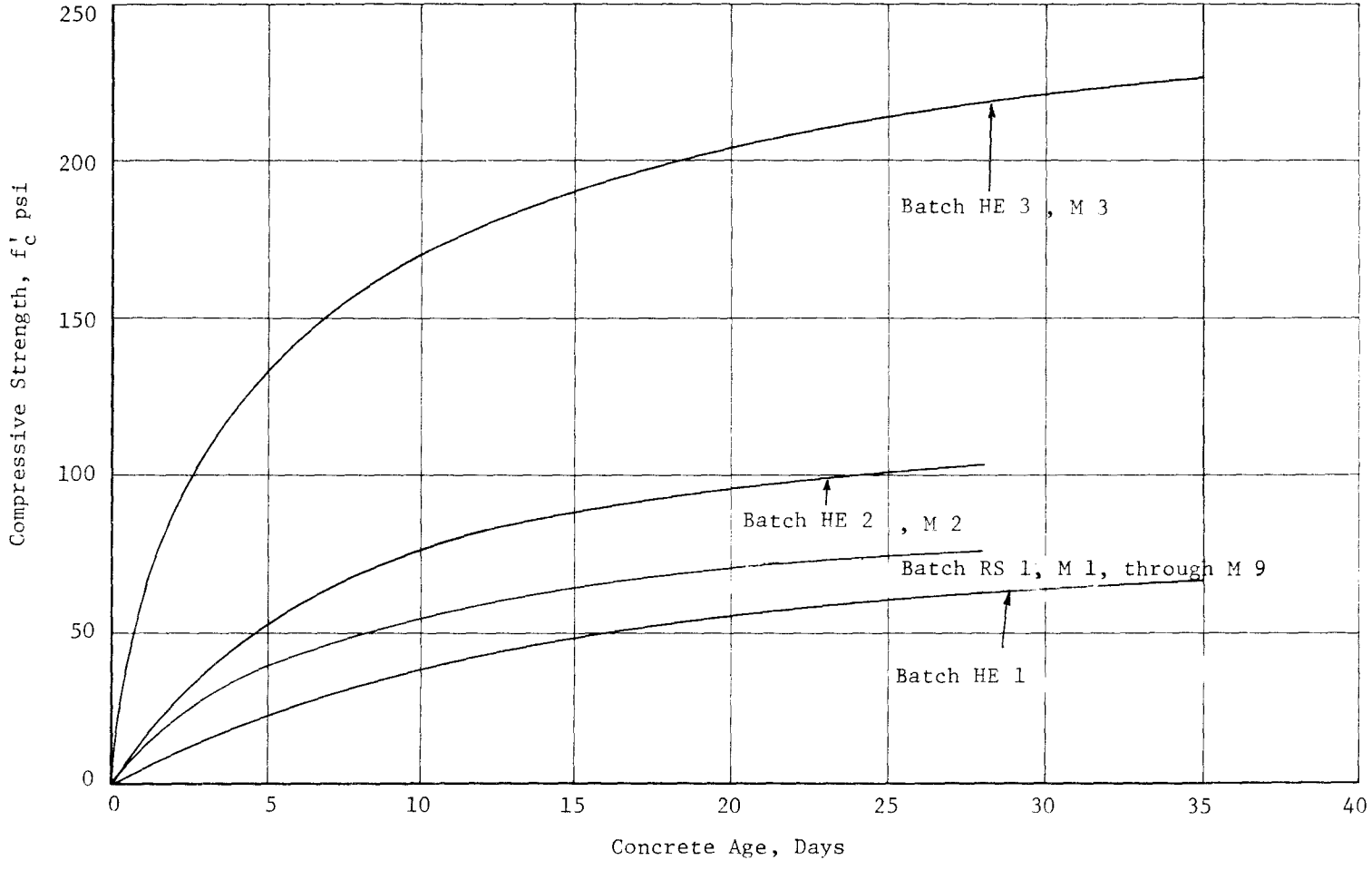

Figure B19 , Concrete Strength Development

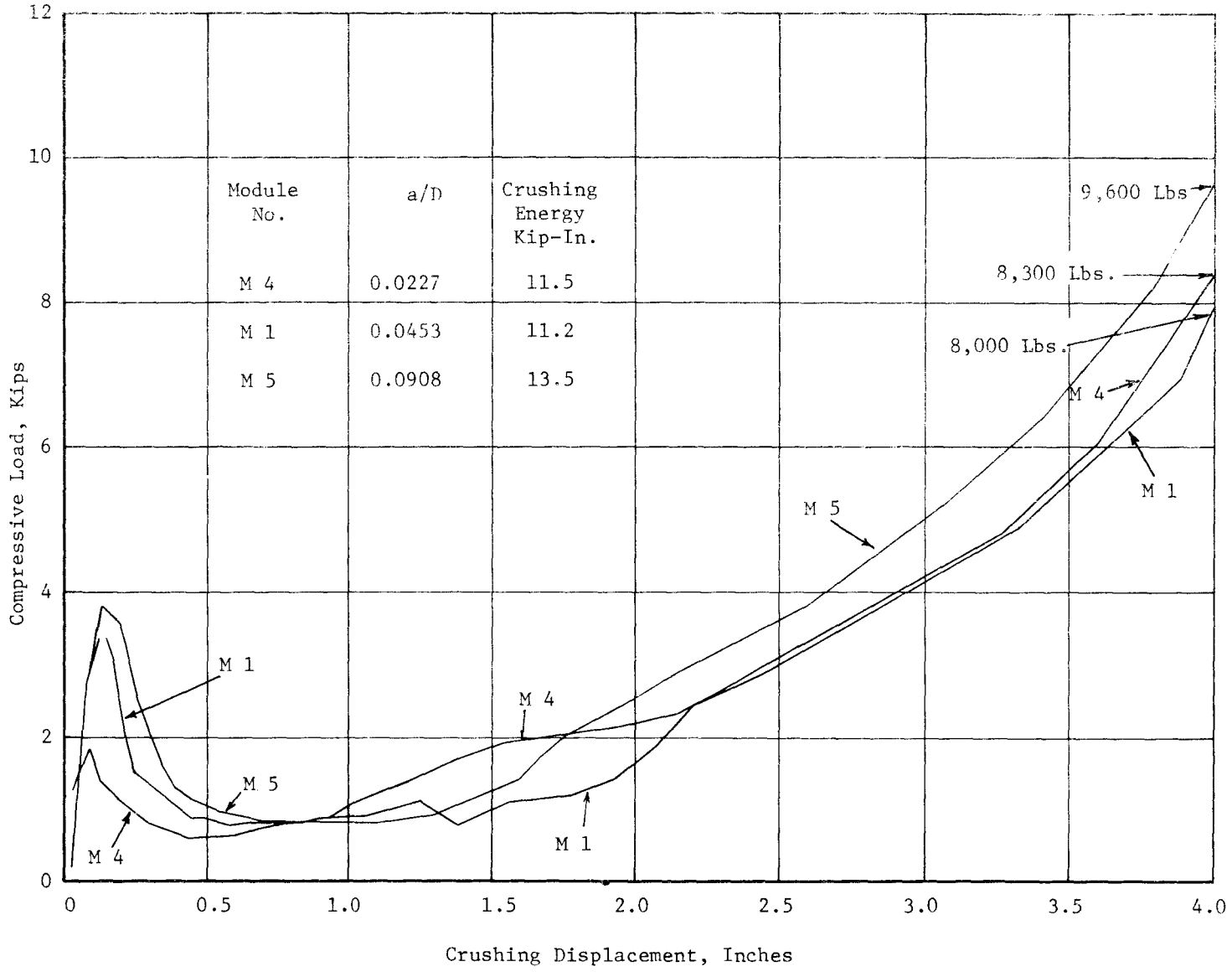

Figure B20 Model Tests For Variation In a/D Ratio

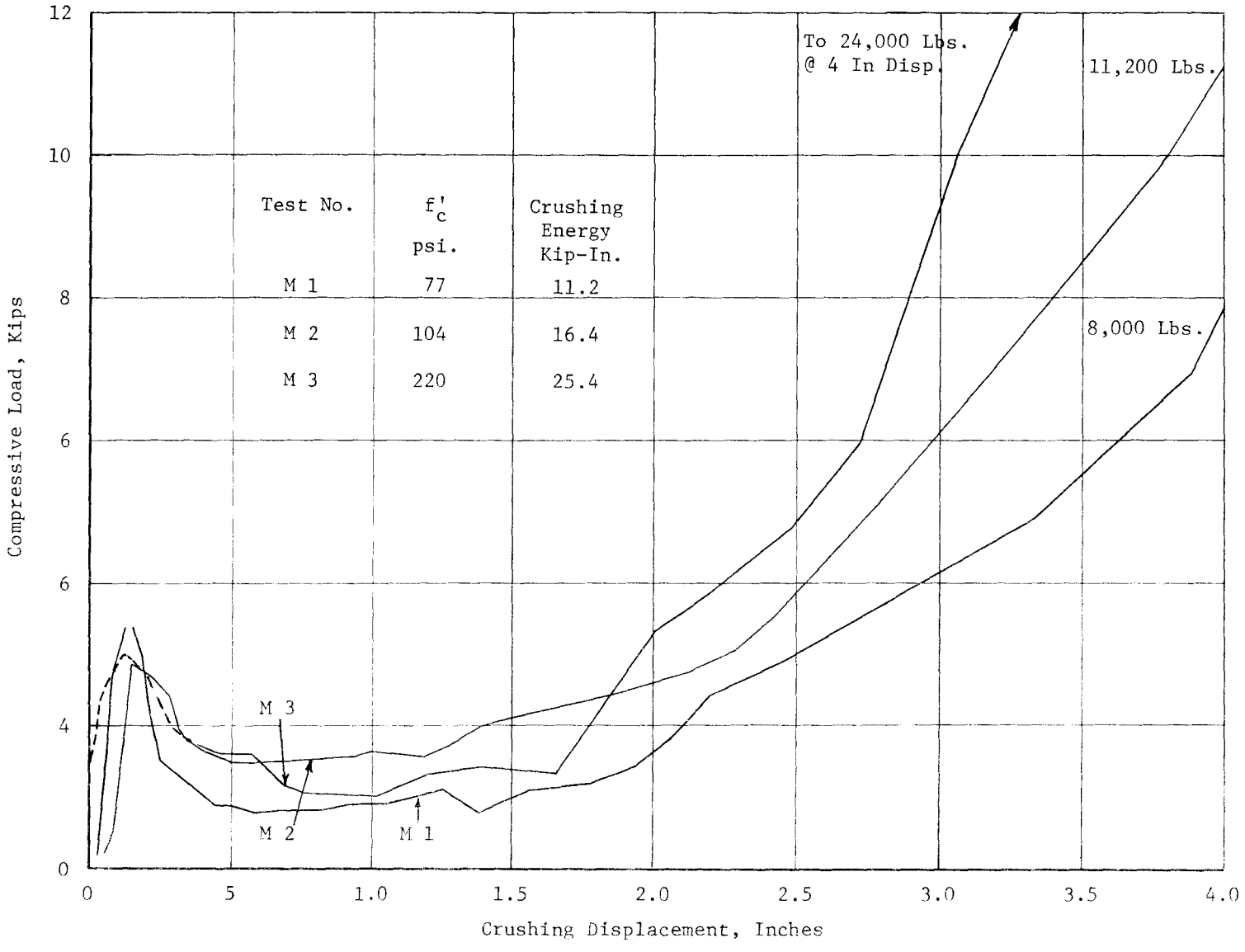

Figure B21, Module Tests For Variations In Compressive Strength

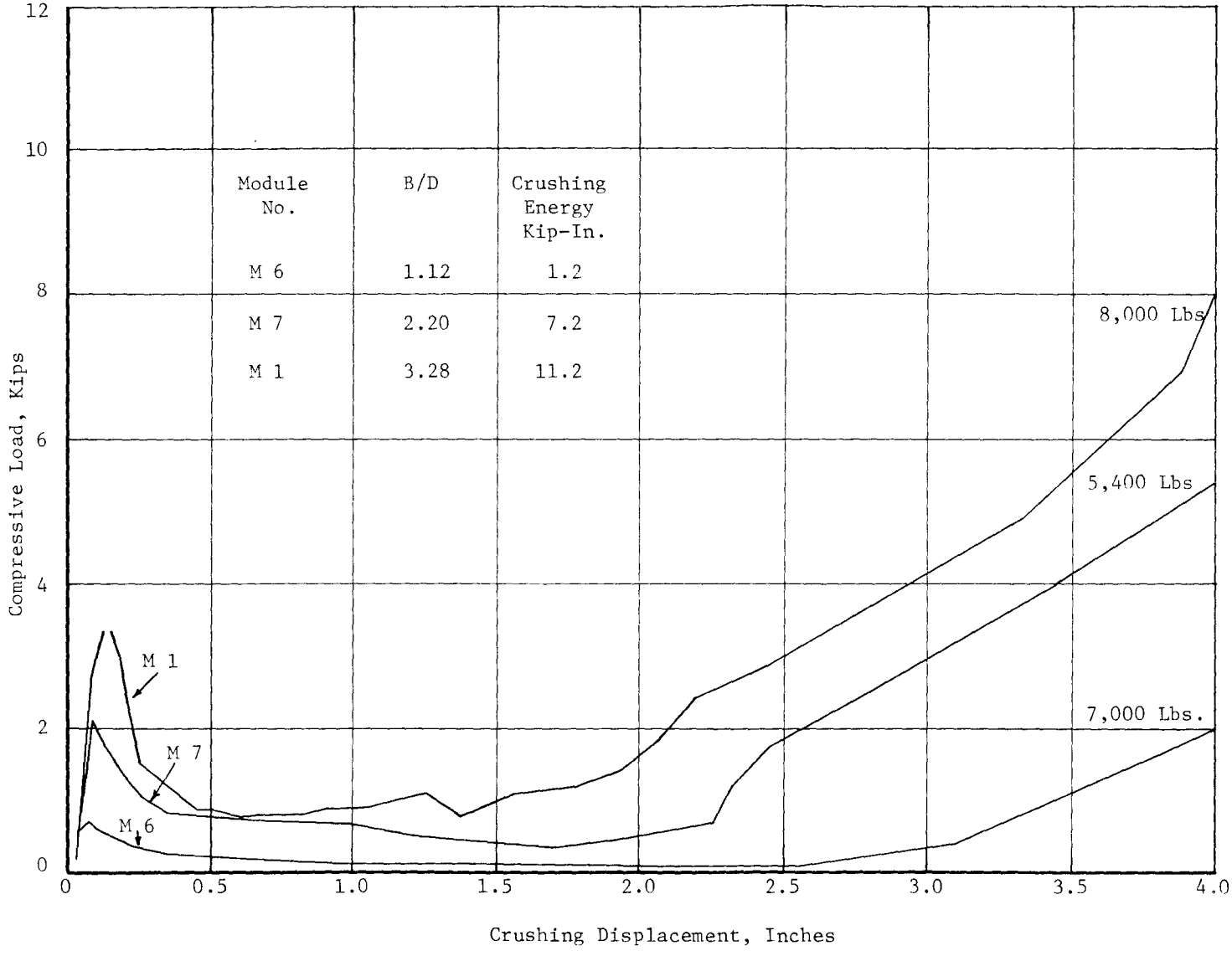

Figure B22 Model Tests For Variation In B/D Ratio

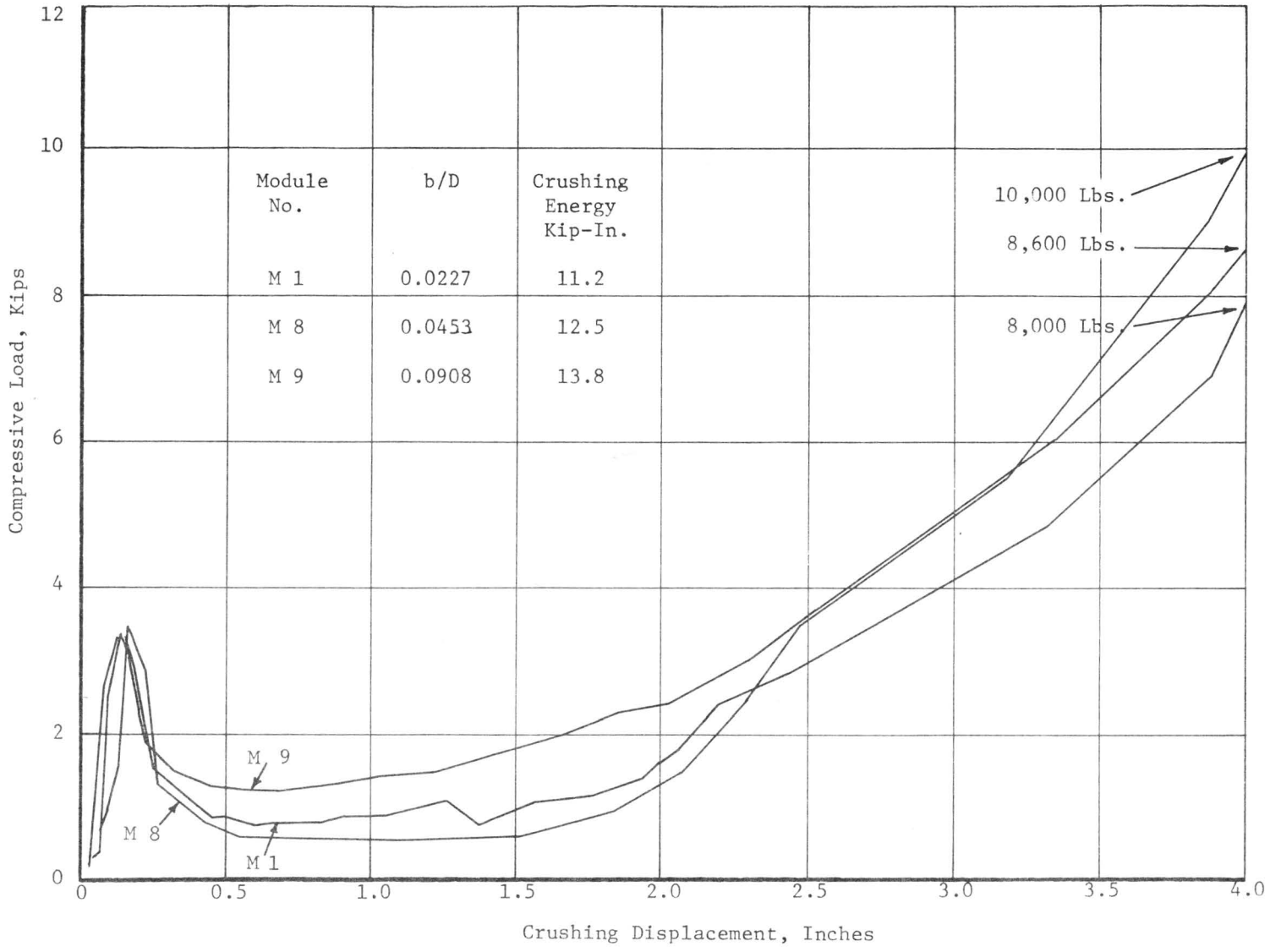

Figure B23, Model Tests For Variation Of b/D Ratio

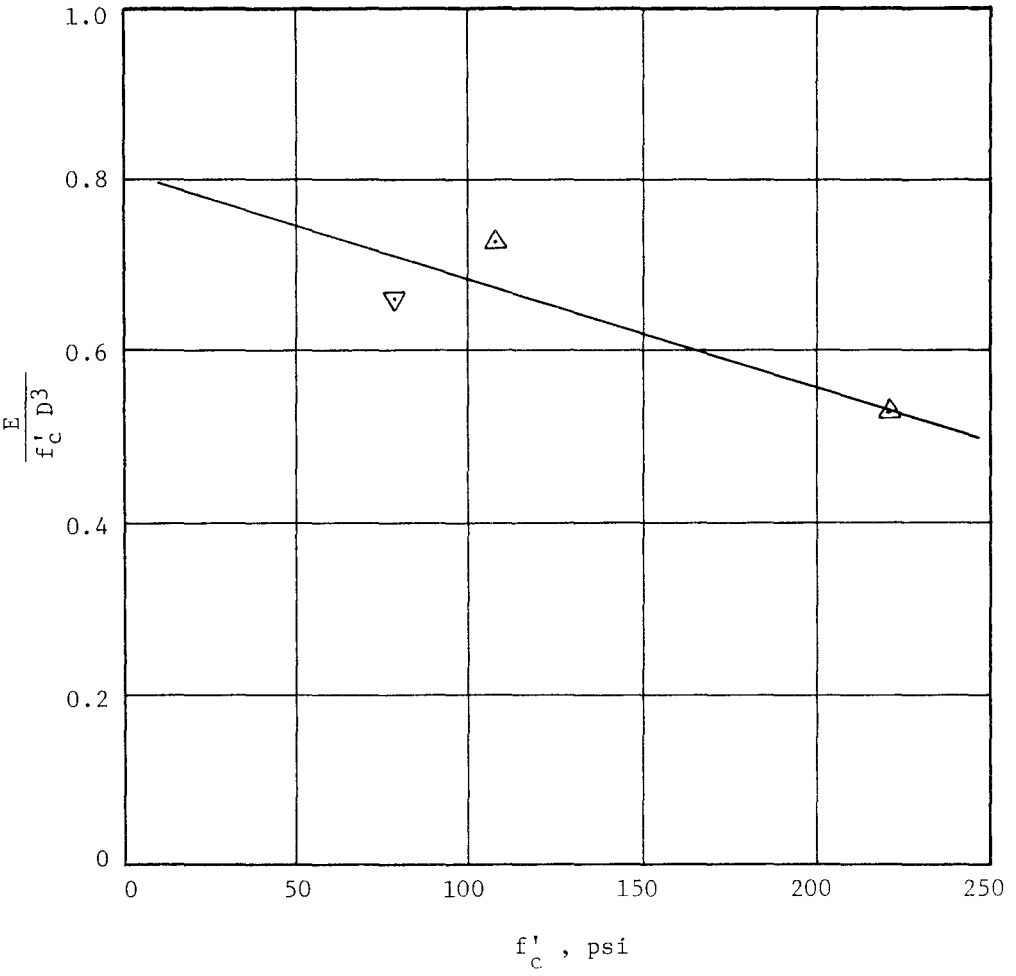

Figure B24, Influence of f'_c

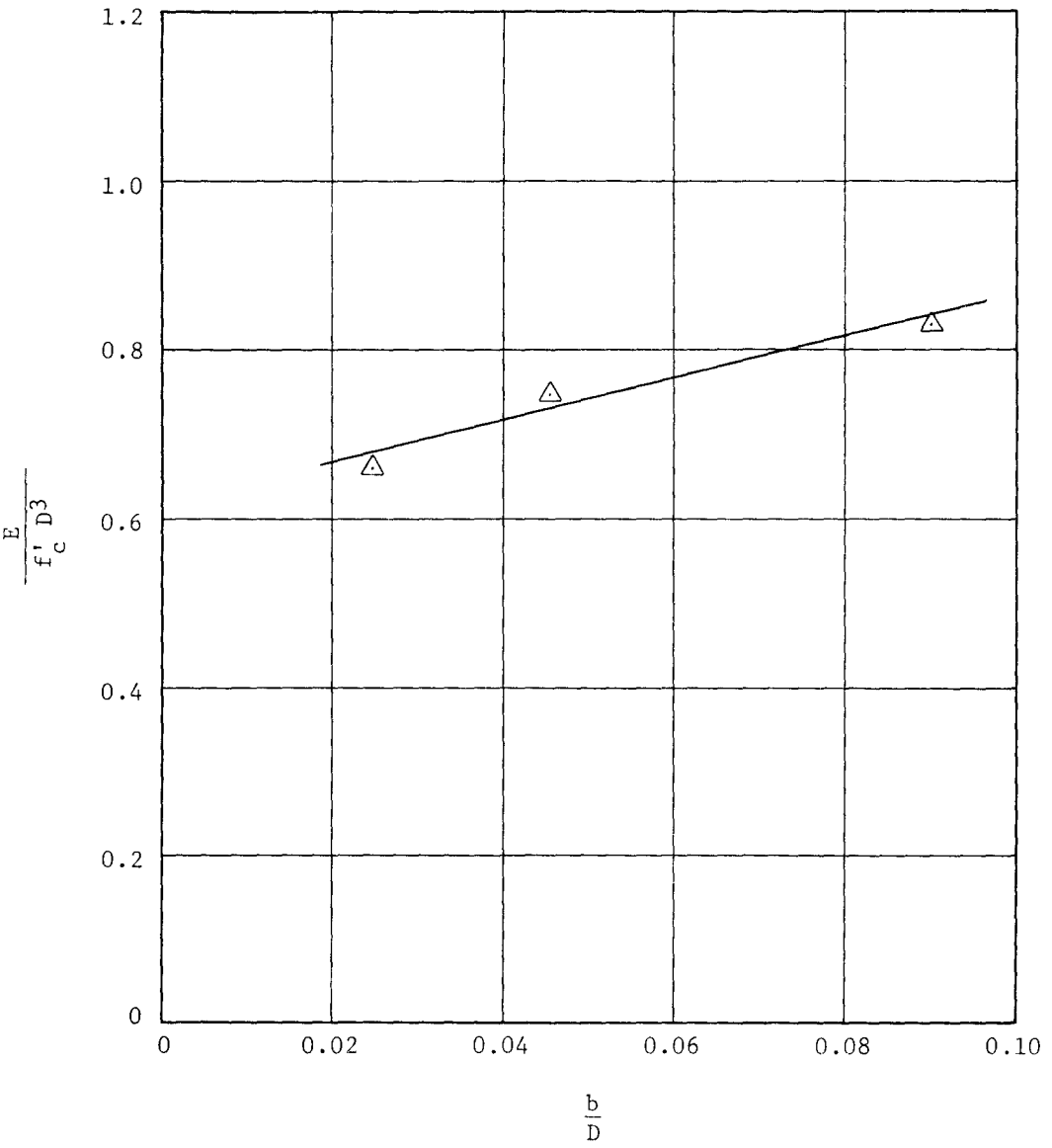

Figure B25, Influence of b/D

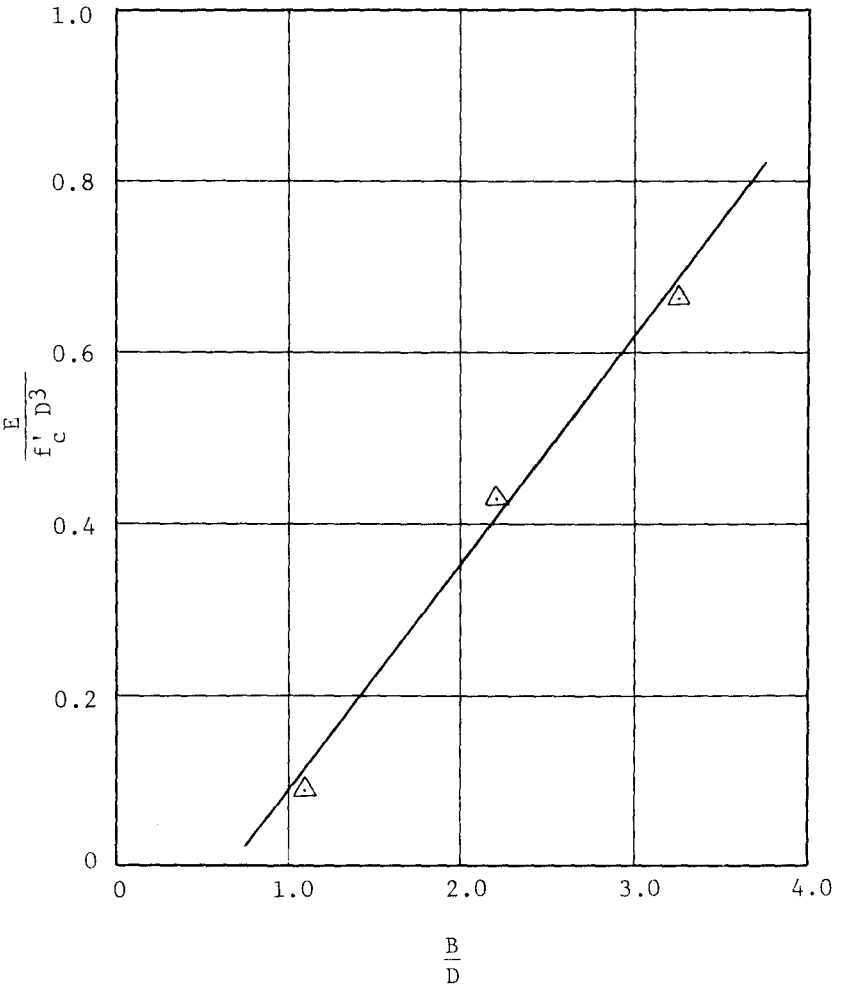

Figure B26 Infulence of B/D

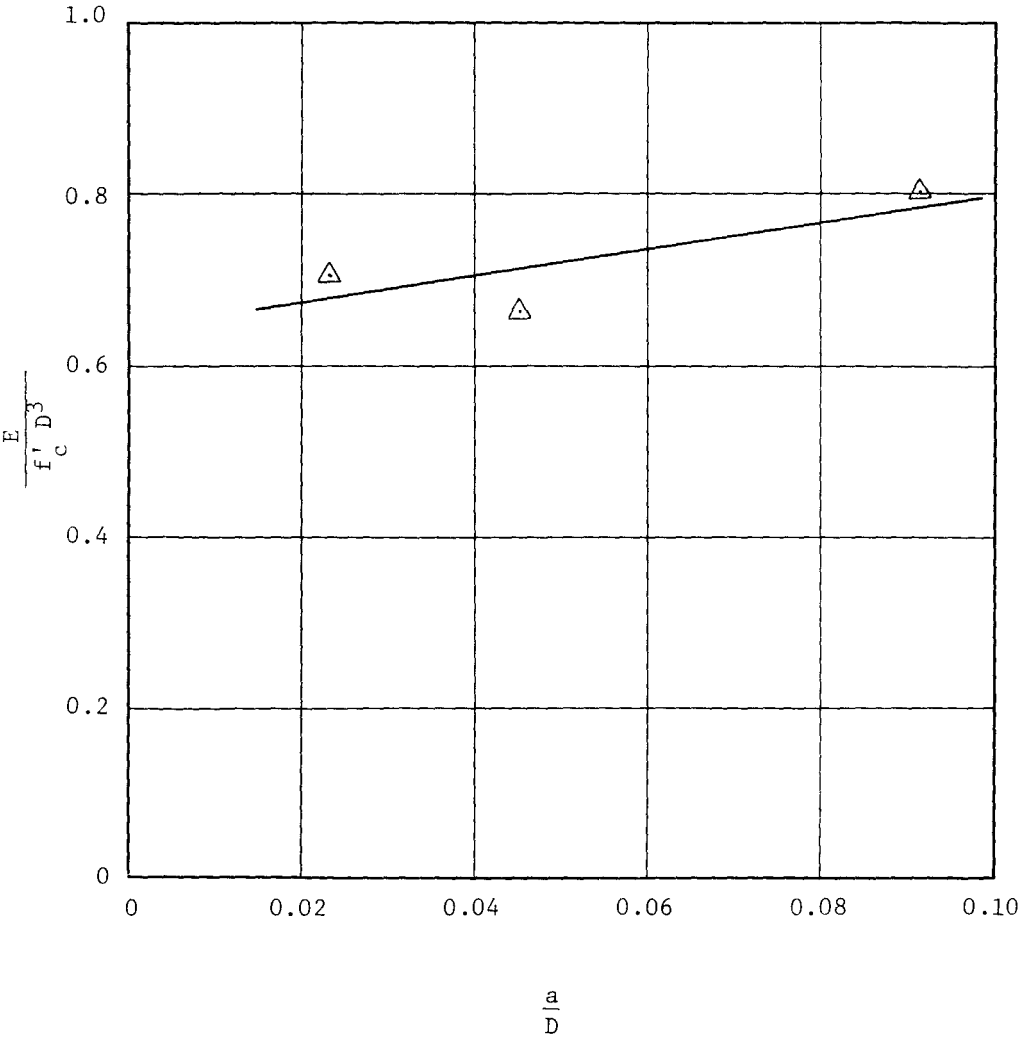

Figure B 27 Influence of a/D

PREDICTIONS WITH MODEL ANALYSIS

The test results from this model study can be used to predict the energy absorbed in the vehicle crash tests if the relationship between the energy absorbed in the dynamic and static conditions can be determined. To do this a comparison will be made between the energy predicted from the model study for the cushions tested in 505V-C and 505V-F and the actual kinetic energy absorbed during these tests. In Figures B28 through B31, the model test data in kip-in. is plotted as a function of the parameters f'_c, B/D, a/D, and b/D. If all model test values are multiplied by the cube of the scale factor and divided by 12, the result will be predicted prototype energy values in kip-ft. These new predicted values are also plotted on these Figures.

It is assumed that in test V-C, the energy absorption capacity of the cushion was exactly used up and that the capacity of this cushion is equal to the kinetic energy of the vehicle immediately before impact (namely 619 kip-ft). The crushing ratio of the modules in this cushion was experimentally determined by dividing the distance the vehicle penetrated the cushion by the original length of the cushion; 21.4 ft./24 ft. = .89. This value is assumed to be the crushing ratio for prototype modules. The predicted energy, on the basis of static model tests, is determined and adjusted for differences in compressive strengths using Figures B28 through B31. For an M7 type module, the

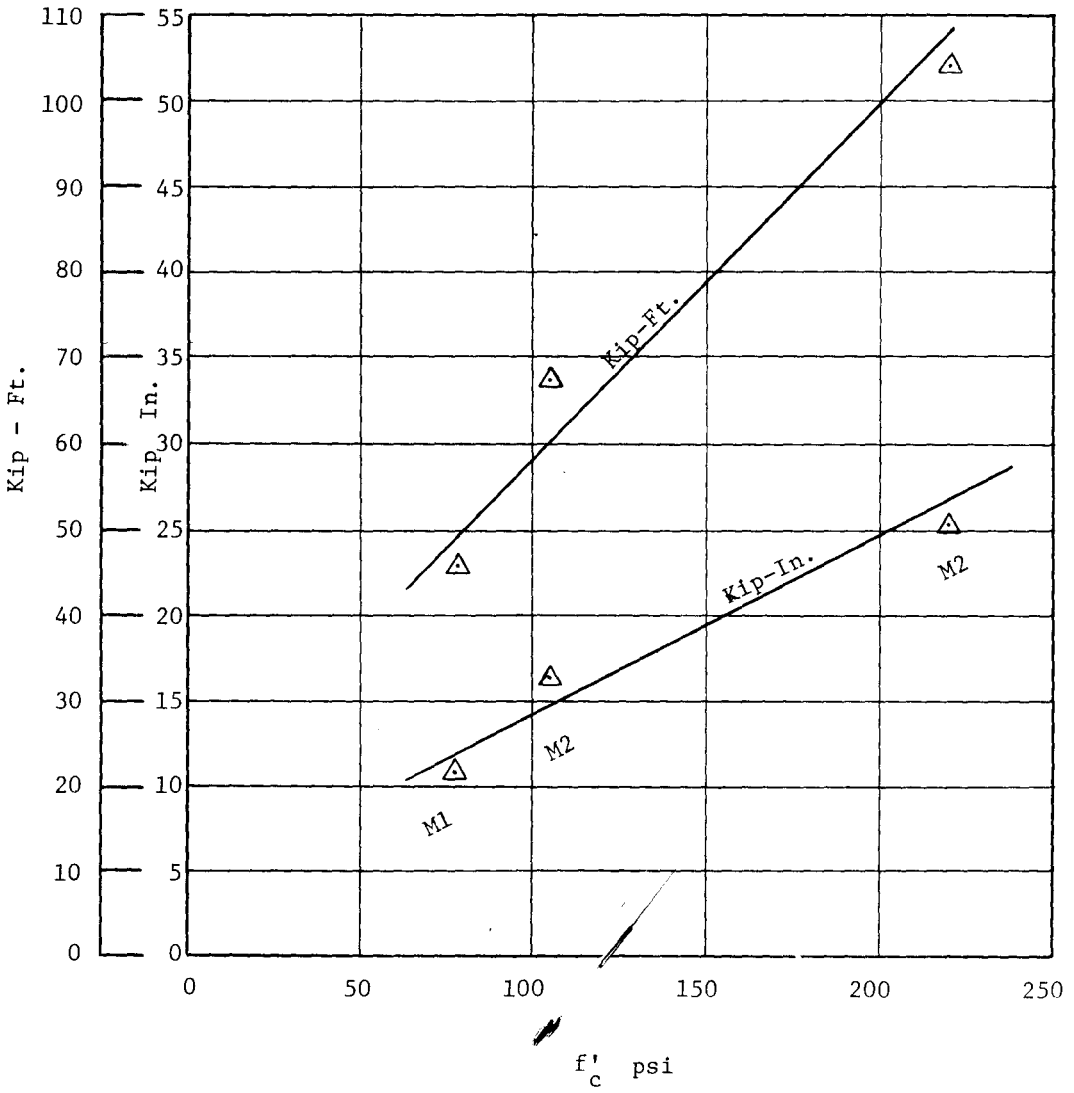
Kip - Ft.
Kip In.
110
100
90
80
70
60
50
40
30
20
10
0
55
50
45
40
35
30
25
20
15
10
5
0
0
50
100
150
200
250
f'c psi
Kip-Ft.
Kip-In.
M1
M2
M2
M2

Figure B28

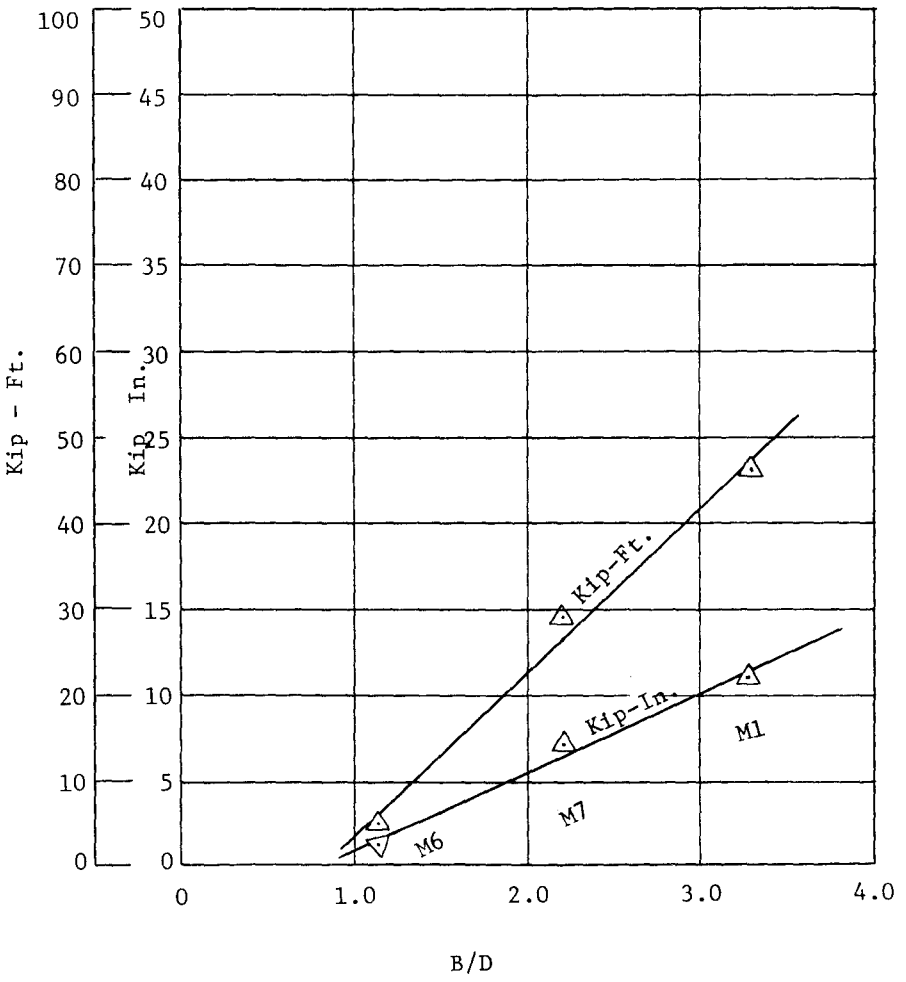
100
90
80
70
60
50
40
30
20
10
0
Kip - Ft.
50
45
40
35
30
25
20
15
10
5
0
Kip In.
0
1.0
2.0
3.0
4.0
B/D
Kip-Ft.
Kip-In.
M1
M7
M6

Figure B29

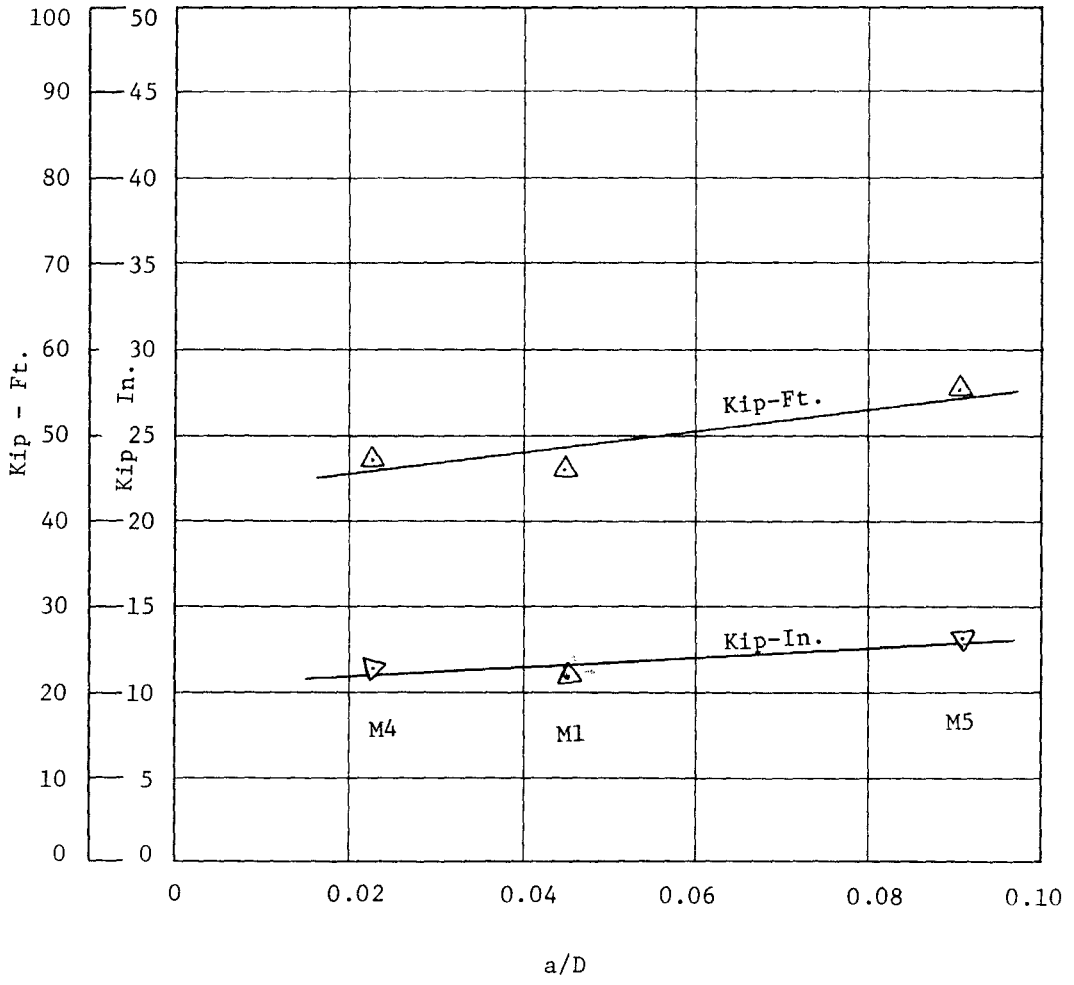
100
90
80
70
60
50
40
30
20
10
0
Kip - Ft.
50
45
40
35
30
25
20
15
10
5
0
Kip - In.
0
0.02
0.04
0.06
0.08
0.10
a/D
Kip-Ft.
Kip-In.
M4
M1
M5

Figure B30

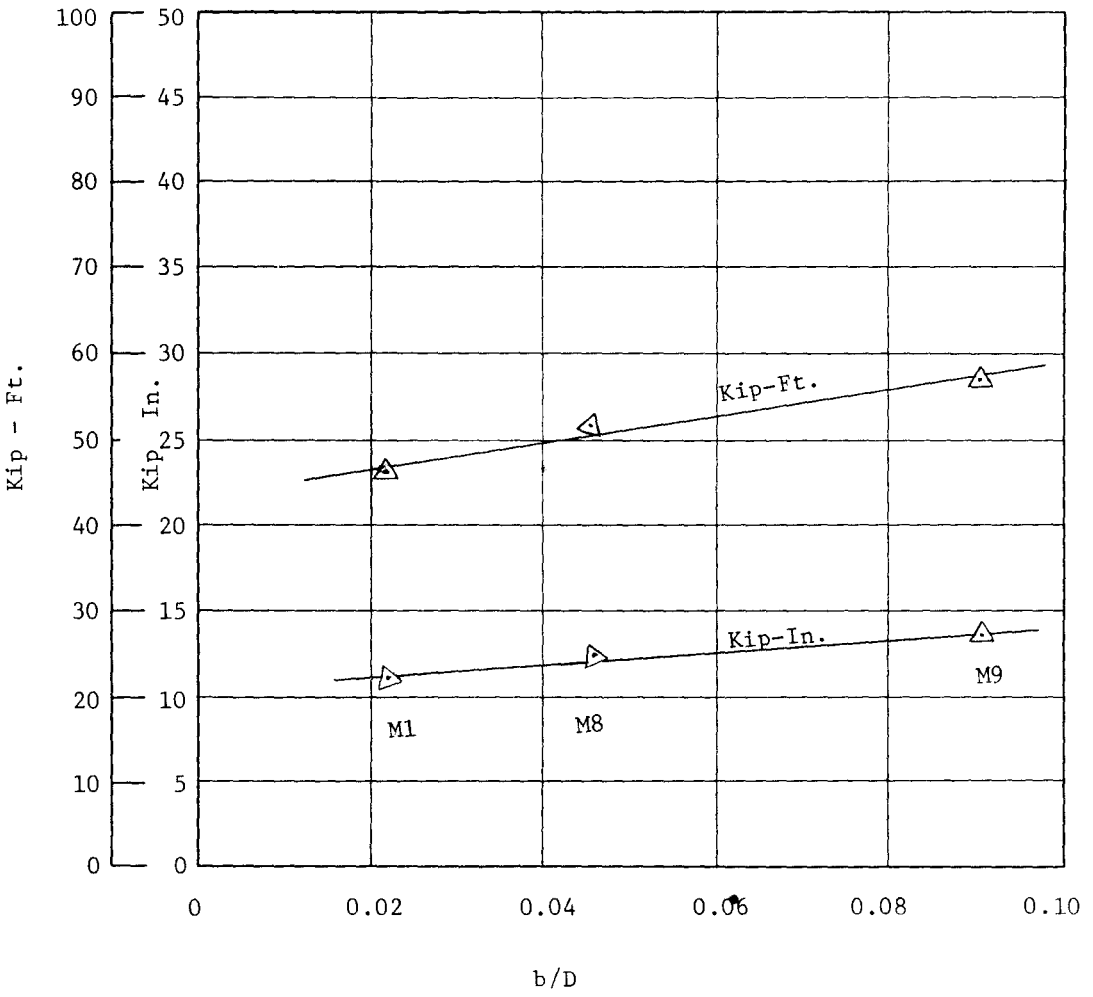
Kip - Ft.
Kip - In.
Kip-Ft.
Kip-In.
M1
M8
M9
b/D
100
90
80
70
60
50
40
30
20
10
0
50
45
40
35
30
25
20
15
10
5
0
0
0.02
0.04
0.06
0.08
0.10

Figure B31

TABLE B4

PREDICTED ENERGY ABSORPTION CAPACITY
FOR 505V-C VERMICULITE CUSHION

505V-C MODULE	CORRESPONDING MODEL MODULE	PREDICTED ENERGY kip-ft.	CUMULATIVE PREDICTED ENERGY
A	2/3 of M7	15.1	15.1
		15.1	30.2
		15.1	45.3
B	M7	22.6	67.9
		22.6	90.5
		22.6	113.1
C	M4	38.5	151.6
		38.5	190.1
		38.5	228.6
D	M1	40.1	268.7
		40.1	308.8
		40.1	348.9

Model Module 2/3 of M7 M7 M4 M1
Prototype Module A B C D

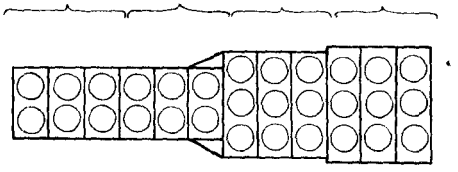

Compressive strength of prototype = 57 psi

TABLE B5

PREDICTED ENERGY ABSORPTION CAPACITY
FOR 505V-F VERMICULITE CUSHION

505V-F MODULE	CORRESPONDING MODEL MODULE	PREDICTED ENERGY kip-ft.	CUMULATIVE PREDICTED ENERGY
A	M7	23.7	23.7
		23.7	47.4
		23.7	71.1
		23.7	94.8
		23.7	118.5
B	M4	40.4	158.9
		40.4	199.3
		40.4	239.7
		40.4	280.1
		40.4	320.5
C	M1	42.0	362.5

Model Module M7 M4 M1
Prototype Module A B C

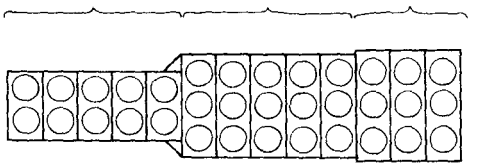

Compressive strength of prototype = 64 psi

energy is 27 kip-ft. from Figure B29. This value is based on the compressive strength of the model modules of 77 psi. To adjust for the prototype compressive strength of 57 psi, Figure B28 is used and the adjustment is: (41/49) (27) = 22.6 kip-ft. Energy values predicted in this manner for the 505V-C cushion are tabulated in Table B4 and for the 505V-F cushion in Table B5.

In test 505 F, the total capacity of the cushion was not consumed. The total penetration into the cushion was 12.2 ft. and some modules were only partially crushed. However, in order to simplify the procedure for predicting the behavior of this cushion, it is assumed that each module was completely crushed (crushing ratio = 0.89) in successive steps beginning at the front of the cushion and proceeding toward the rigid wall until a total crushing distance of 12.2 ft. is reached. This will result in an assumed complete crushing of 12.2/.89 = 13.7 ft. or 6.9 (say 7) modules. The cushion used in this test consisted of 5 modules of M7 type; 5 modules of M4 type and 3 modules of M1 type with the last module filled with vermiculite. The predicted energy absorption of this cushion would then consist of that of five type M7 modules plus two M4 type modules or 199.3 kip-ft.

TABLE B6

COMPARISON OF VEHICLE KINETIC ENERGY
AND PREDICTED STATIC ENERGY ABSORPTION

Test	Kinetic Energy of the vehicle at contact KE=1/2 MV^2 kip-ft.	Predicted Energy Absorption E_p kip-ft.	Ratio KE/E_p
505V-C	619	348.9	1.77
505V-F	277	199.3	1.39
		Average	1.58

DESIGN OF LIGHTWEIGHT CELLULAR CRASH CUSHION USING MODEL PREDICTION RELATIONSHIPS

The problem is to design a lightweight cellular concrete crash cushion which will provide an acceptable deceleration level for a 4500-lb. vehicle traveling 65 mph.

The vehicle kinetic energy is calculated by the following equation:

$$KE = \frac{1}{2} \frac{W}{g} V^2$$

Where

W is the design vehicle weight, 4500 lbs.
g is the acceleration of gravity, 32.2 ft/sec^2
V is the design vehicle velocity, 65 mph. = 95.2 fps.

Thus $KE = \frac{1}{2} \frac{4500}{32.2} (95.2)^2 = 635$ kip-ft

The required stopping distance is determined by the desired average deceleration level (chosen $G_{avg} = 7$) and is calculated as follows:

$$L = \frac{V^2}{2gG_{avg}}$$

$$L = \frac{(95.2)^2}{2(32.2)(7)} = 20.2 \text{ ft.}$$

The problem is then to select a combination of modules that will absorb 635 kip-ft of energy when crushed for a distance of 20 ft. or more. For M4 type modules with a compressive strength of 60 psi, the energy absorption capacity is 39.5 kip-ft. per module. This energy absorption capacity is increased by the average dynamic to static ratio from Table B6 of 1.58; 39.5(1.58) = 62.5 kip-ft. If these modules are used

throughout the cushion, the number of modules required to absorb the energy is:

$$\frac{635}{62.5} = 10.2, \text{ say } 11 \text{ modules}$$

A cushion constructed of 11 modules will be nominally 22 ft. long. For a crushing ratio of 0.89, the crush distance of this tentative cushion will be only 19.6 ft., which is less than the required distance. The crushing distance for a given energy absorption capacity can be increased by substitution of modules with a lower energy absorption capacity. This can be accomplished by partial substitution of M7 type modules with an energy absorption capacity of 27 kip-ft/module when 77 psi concrete is used. The adjustment in energy absorption capacity for a M7 module with 60 psi concrete is obtained from Figure B28 and is 27 kip-ft 42/49 = 22.6 kip-ft. Application of the dynamic to static ratio will yield 22.6(1.58) = 35.7 kip-ft. If five of the M4 type modules are removed from the tentative cushion and replaced with M7 type, the number of M7 modules required is as follows:

Energy required	635 kip-ft.
Six M4 modules	375 kip-ft.
Difference	260 kip-ft.

No. of M7 modules 260/35.7 = 7.3 modules, say 8 modules

The revised cushion design now consists of six M4 and eight M7 type modules which will result in a cushion 28 ft. long. The crushing distance for this cushion is 0.89(28) = 24.9 ft.

A second revision will now be made in an attempt to improve the cushion configuration. Three of the M4 modules are replaced with three

M1 modules. The energy absorption capacity of an M1 module, calculated as before, is 66.3 kip-ft. The design now consists of:

3 M1 modules @ 66.3 kip-ft. = 198.9 kip-ft.

3 M4 modules @ 62.5 kip ft. = 187.5 kip-ft.

7 M7 modules @ 35.7 kip-ft. = 250.0 kip-ft.

Total 636.4 kip-ft.

The crushing distance for this cushion is 0.89(26) = 23 ft.

APPENDIX C

DURABILITY TESTS

OF

VERMICULITE CONCRETE

One of the questions concerning practical application of vermiculite crash cushions is whether this material can withstand exposure to natural environment, particularily in colder regions. The results of a study conducted to obtain some indication of the freezing and thawing durability of vermiculite concretes are reported on the following pages.

EXPERIMENTAL PROGRAM

The properties of the concrete batches tested are listed in Table C1. Three inch by three inch by sixteen inch specimens were cast and sawed in half to result in three inch by three inch by eight inch specimens for testing. Table C2 gives the type of treatment and type of freezing and thawing cycles to which the specimens were subjected. All specimens were moist cured for three days and then cured at 50% relative humidity for at least 25 days before testing.

Household, chest-type freezers were used for the freezing tests. The specimens were out of the freezer about 18 hours and in the freezer about 6 hours during each cycle. The specimens were weighed after each cycle and deterioration was evaluated visually. Deterioration of the specimens was recorded with photographs.

TABLE C1

BATCH DATA

Batch No.	Cement Type	Cement sks/cy	Aggregate cft/cy	Water gal/cy	Wet Unit wt. lbs.	Air %	Compressive Strength, psi
RS1	Regulated Set	3.14	22.3	75.6	40.5	35	77
HE1	High Early Strength	3.27	22.6	83.0	42.0	50	64
HE2	High Early Strength	4.03	24.2	81.5	43.0	50	104
HE3	High Early Strength	5.82	23.2	76.6	49.0	51	220

TABLE C2

SUMMARY OF FREEZING AND THAWING RESULTS

SPECIMEN	TYPE OF TREATMENT	FREEZING & THAWING CYCLES TO FAILURE*	
		Type	Average No.
RS1 BATCH			
16, 16A, 17	None	F & T in water	6
17A, 18, 18A	None	F in air & T in water	11
19, 19A, 20	Two coats of Daracon brushed on	F & T in water	6
20A, 21, 21A	Sprayed one coat of resin**	F & T in water	8
22, 22A	Soaked in linseed oil 24 hours	F & T in water	44
23	Soaked in linseed oil 24 hours	F & T in water	4
23A	Flexible epoxy coating #2	F & T in water	19
24, 24A, 25	Flexible epoxy coating #1	F & T in water	13
HE1 BATCH			
19, 19A, 20	Soaked in Daracon 10 min.	F & T in water	24
20A, 21, 21A	Sprayed two coats of resin**	F & T in water	17
HE2 BATCH			
19, 19A, 20	Soaked in Daracon 10 min.	F & T in water	23
20A, 21, 21A	Sprayed two coats of resin**	F & T in water	32
HE3 BATCH			
19, 19A, 20	Soaked in Daracon 10 min.	F & T in water	35
20A, 21, 21A	Sprayed two coats of resin**	F & T in water	36

*Failure was considered to occur in one of two ways: (1) attrition of the surface to a significant depth (nominally 1/4 inch) and (2) structural cracking of the specimen resulting in separation of the specimen into parts or separation of the protective coating along with a layer of vermiculite from the remainder of the specimen. Failure in all cases was arbitrarily defined by visual inspection.

**A polyester resin normally used in fiberglas reinforced plastic.

RESULTS

Figures C1 through C29 are photographs of the specimens illustrating their condition at the listed number of cycles. The uncoated specimens suffered progressive attrition of the surface without "structural" cracking. The most effective treatment investigated was obtained by soaking the specimens in linseed oil for 24 hours. The two flexible epoxy coating treatments were applied by Perlite Industries Inc. of Midland, Texas.

Specimen RS 23, one of the group soaked in linseed oil for 24 hours prior to freezing and thawing, failed after only four cycles. A single crack formed in the longitudinal direction of the specimen and it separated into two pieces as illustrated in Figure C7. The reason for early failure of this specimen is questioned. The failure was not a classical freeze-thaw type failure and no deterioration other than the single crack was experienced.

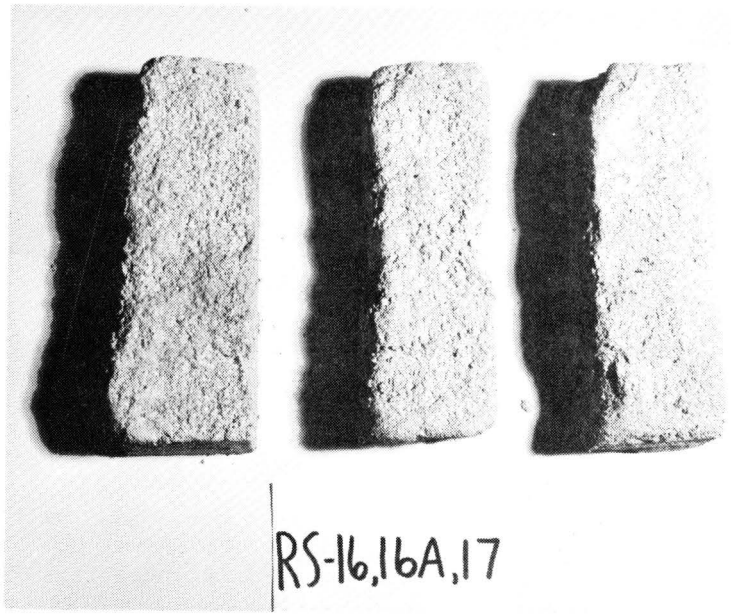

Figure C1 Conditions of specimens RS-16, 16A, 17 after six cycles of freezing and thawing.

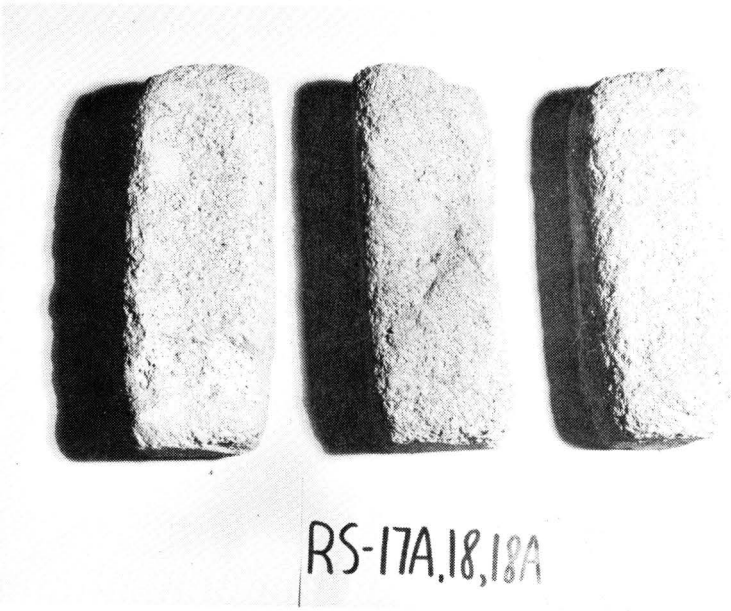

Figure C2 Conditions of specimens RS-17A, 18, 18A after 11 cycles of freezing and thawing.

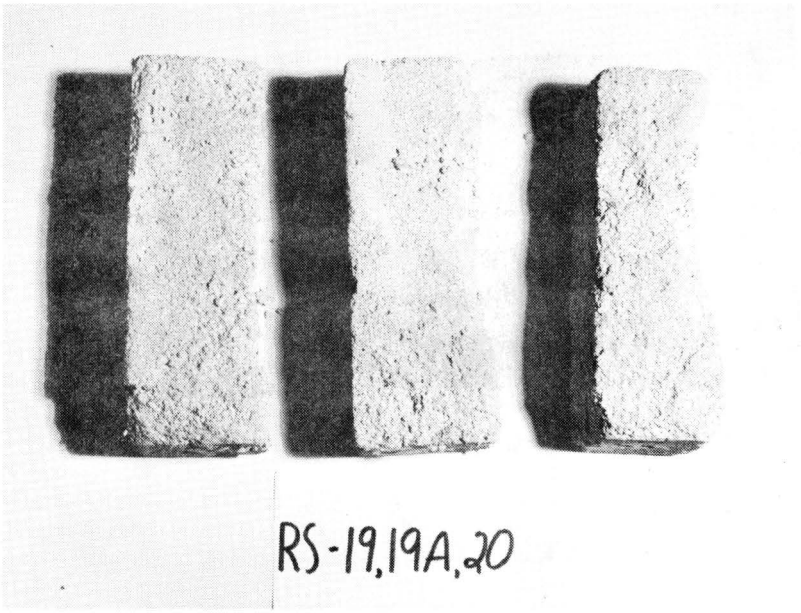

Figure C3 Conditions of specimens RS-19, 19A, 20 after six cycles of freezing and thawing.

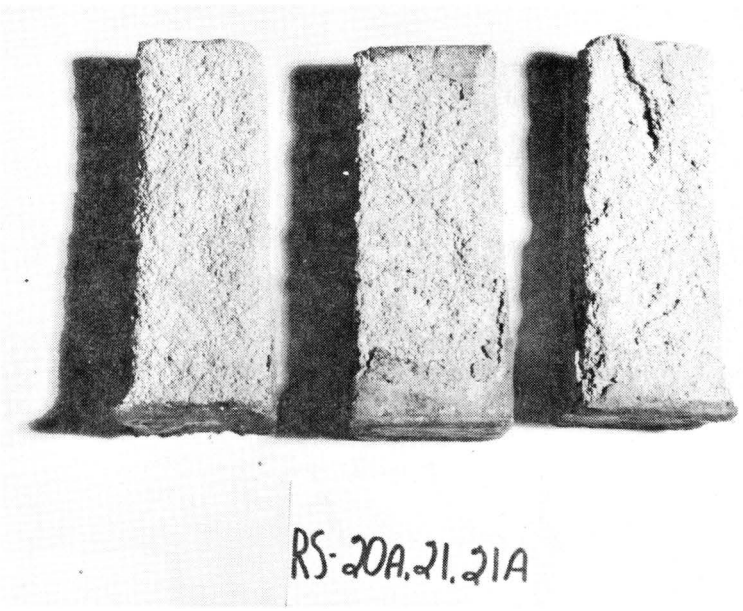

Figure C4 Conditions of specimens RS-20A, 21, 21A after eight cycles of freezing and thawing.

Figure C5 Condition of specimen RS-22 after 44 cycles of freezing and thawing.

Figure C6 Condition of specimen RS-22A after 44 cycles of freezing and thawing.

Figure C7 Conditions of specimens RS-22, 22A after 27 cycles, and RS-23 after 4 cycles of freezing and thawing.

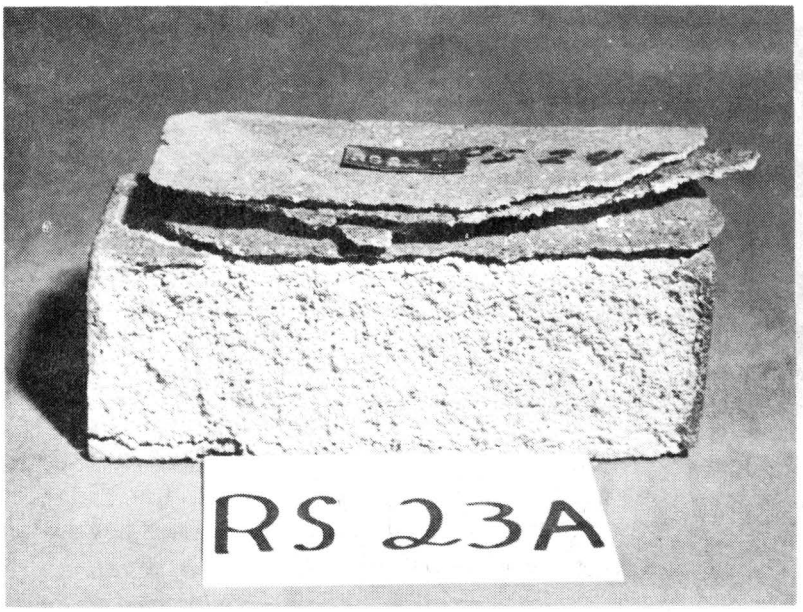

Figure C8 Condition of specimen RS-23A after 19 cycles of freezing and thawing.

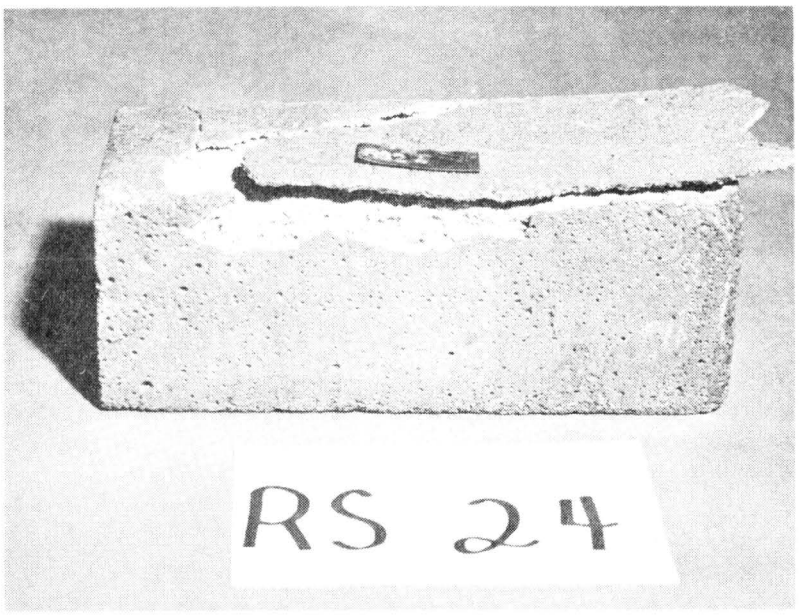

Figure C9 Condition of specimen RS-24 after 14 cycles of freezing and thawing.

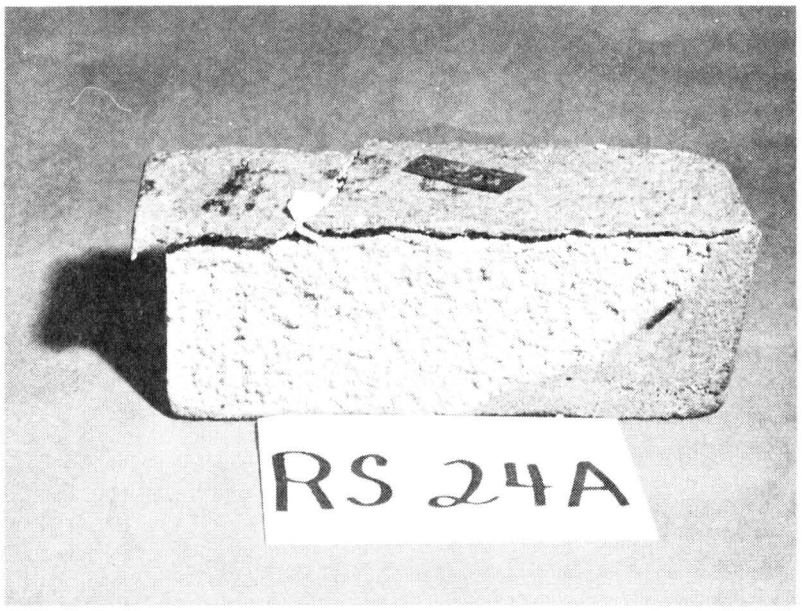

Figure C10 Condition of specimen RS-24A after 16 cycles of freezing and thawing.

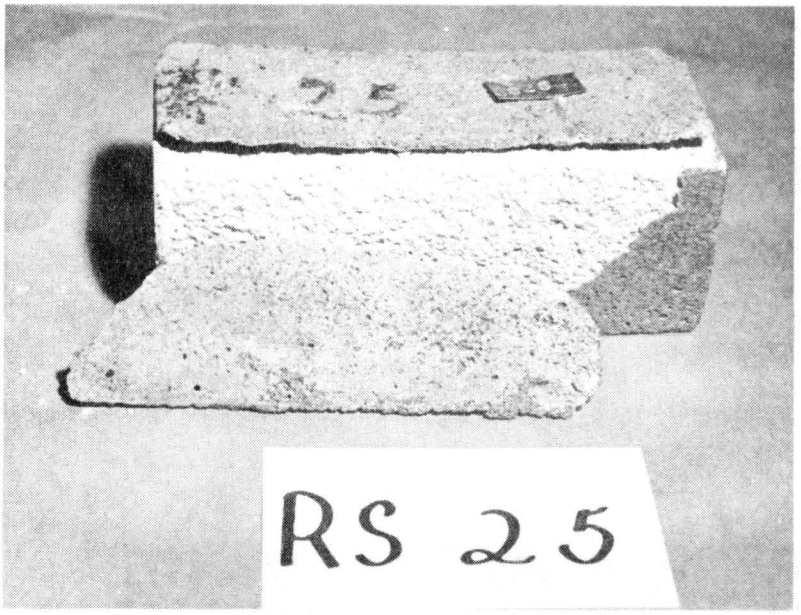

Figure C11 Condition of specimen RS-25 after 8 cycles of freezing and thawing.

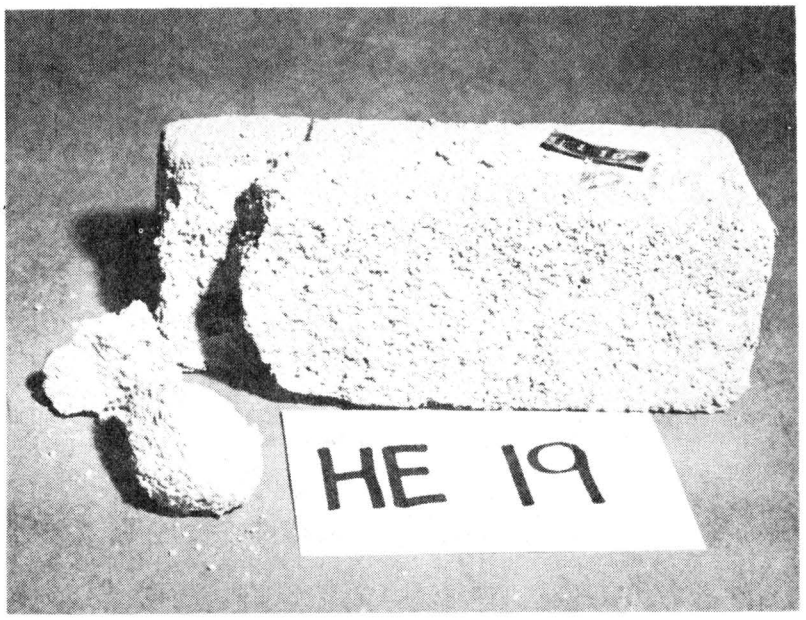

Figure C12 Condition of specimen HE1-19 after 24 cycles of freezing and thawing.

Figure C13 Condition of specimen HE1-19A after 24 cycles of freezing and thawing.

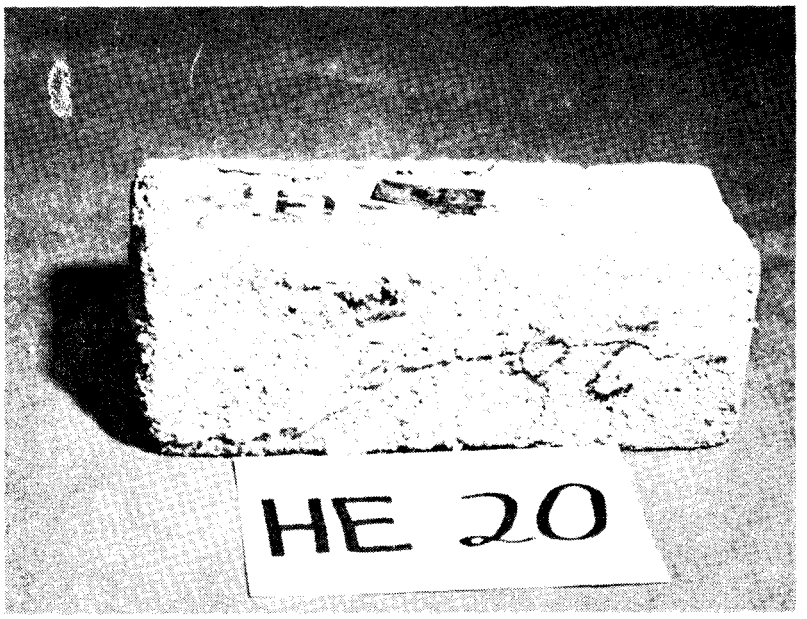

Figure C14 Condition of specimen HE1-20 after 23 cycles of freezing and thawing.

Figure C15 Condition of specimen HE1-20A after 16 cycles of freezing and thawing.

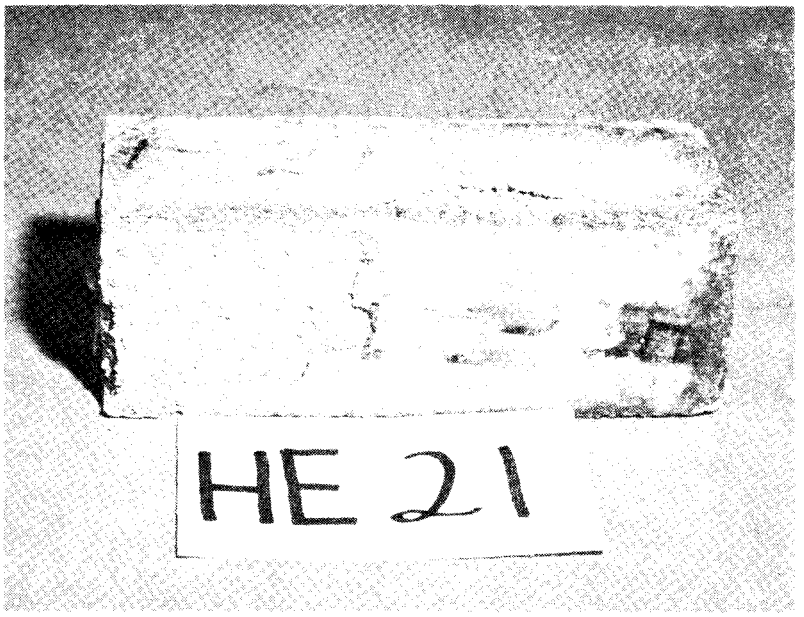

Figure C16 Condition of specimen HE1-21 after 19 cycles of freezing and thawing.

Figure C17 Condition of specimen HE1-21A after 16 cycles of freezing and thawing.

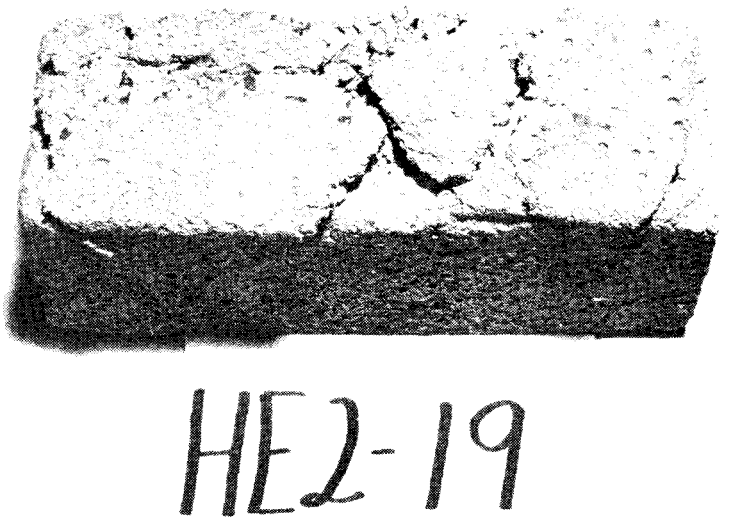

Figure C18 Condition of specimen HE2-19 after 23 cycles of freezing and thawing.

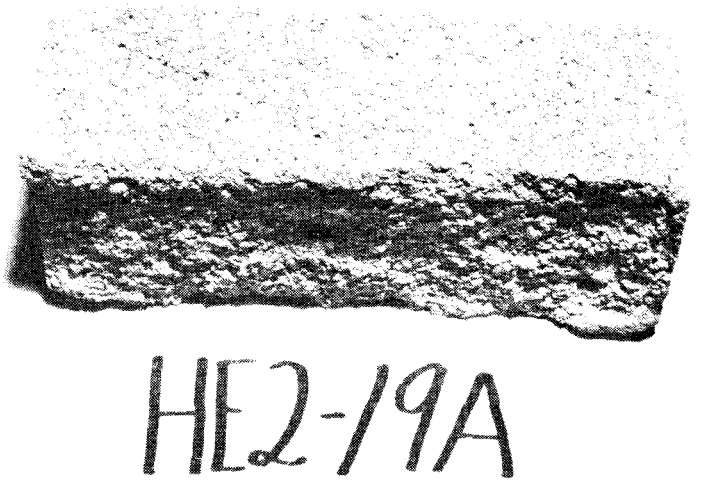

Figure C19 Condition of specimen HE2-19A after 23 cycles of freezing and thawing.

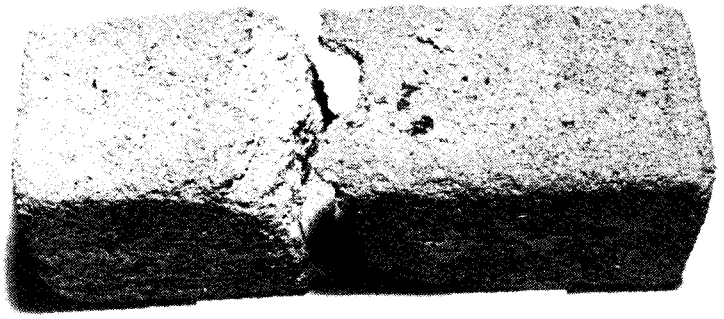

HE2-20

Figure C20 Condition of specimen HE2-20 after 25 cycles of freezing and thawing.

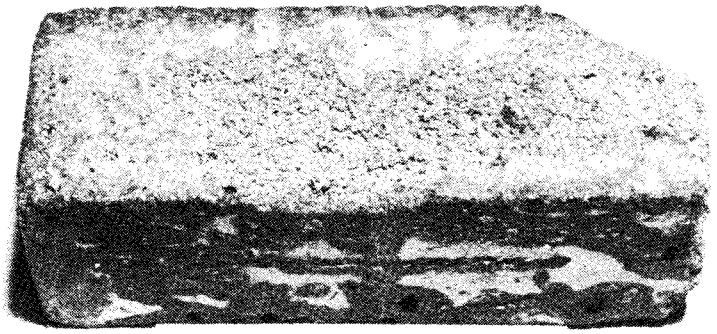

HE2-20A

Figure C21 Condition of specimen HE2-20A after 36 cycles of freezing and thawing.

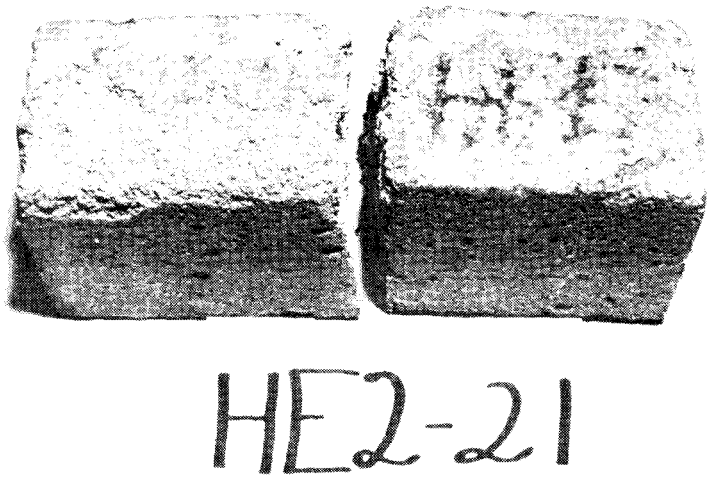

Figure C22 Condition of specimen HE2-21 after 25 cycles of freezing and thawing.

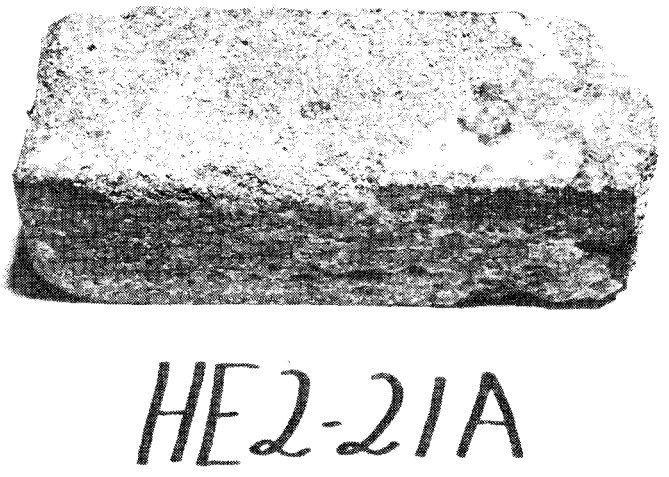

Figure C23 Condition of specimen HE2-21A after 36 cycles of freezing and thawing.

Figure C24 Condition of specimen HE3-19 after 37 cycles of freezing and thawing.

Figure C25 Condition of specimen HE3-19A after 37 cycles of freezing and thawing.

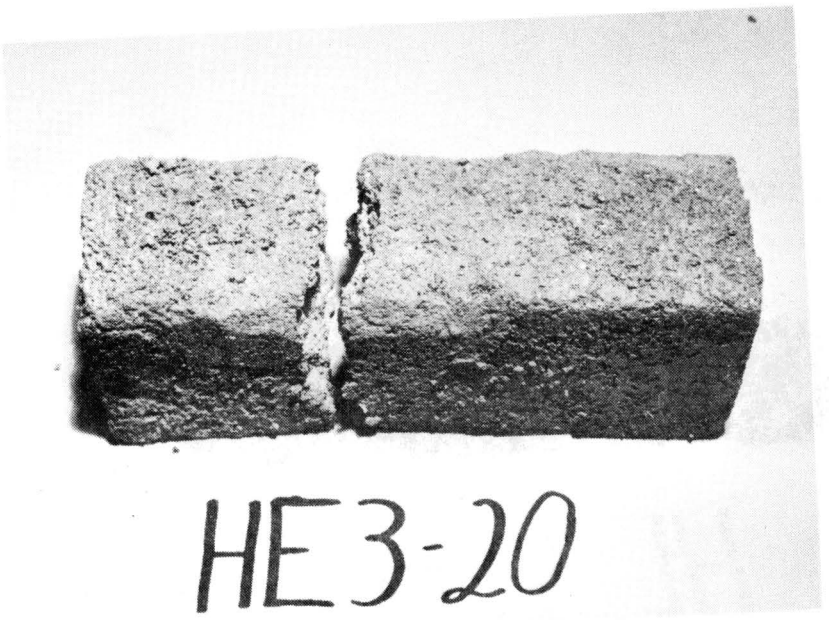

Figure C26 Condition of specimen HE3-20 after 32 cycles of freezing and thawing.

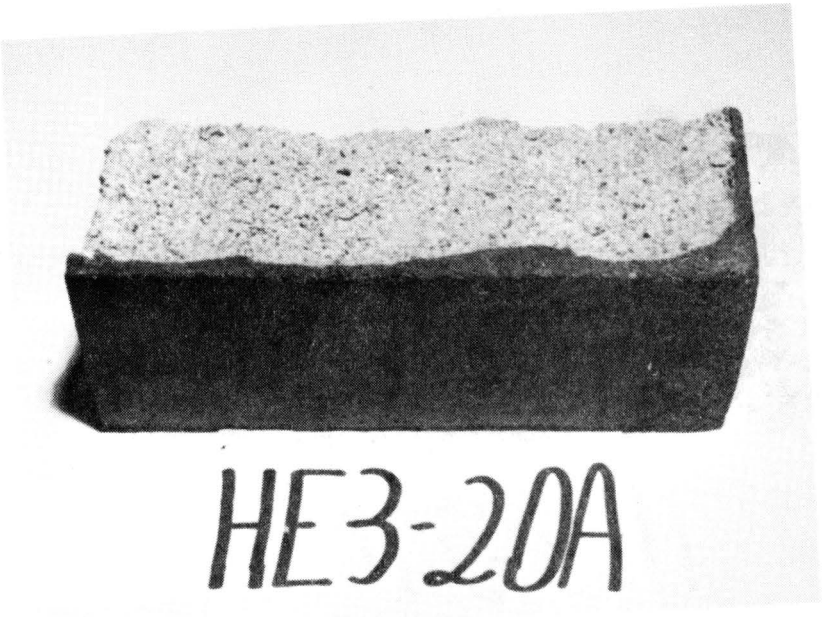

Figure C27 Condition of specimen HE3-20A after 36 cycles of freezing and thawing.

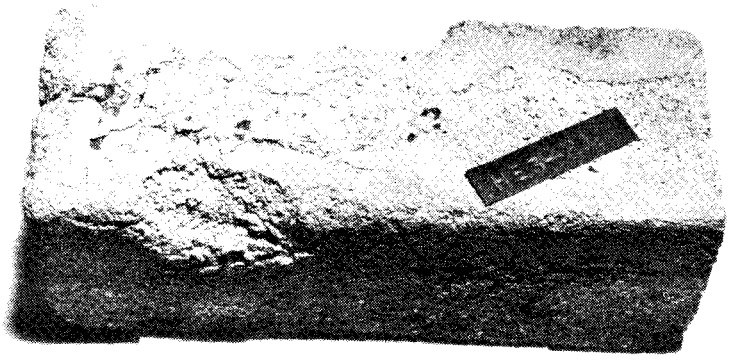

Figure C28 Condition of specimen HE3-21 after 36 cycles of freezing and thawing.

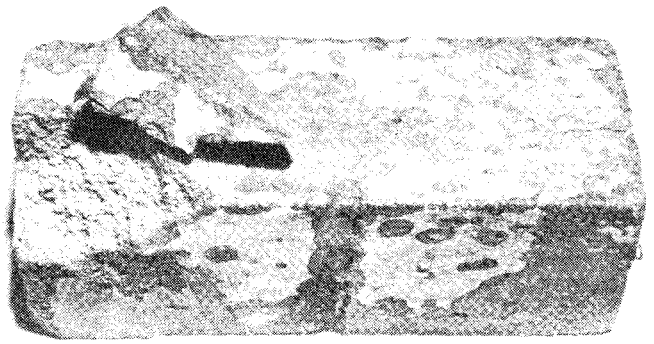

Figure C29 Condition of specimen HE3-21A after 38 cycles of freezing and thawing.

CONCLUSION

The accurate prediction of the durability of a material in a freezing and thawing environment on the basis of laboratory tests has historically been a very difficult or almost impossible task. However some indications of the expected behavior can be obtained from such tests.

The presence of water during both the freezing and the thawing portion of the cycle in these tests represents an exposure condition that is much more severe than one where some drying is allowed. In actual field installations of crash cushions, free drainage occurs and extended periods of exposure to water do not occur. This is beneficial in that the concrete will experience drying periods and the continuous, cumulative saturation of the concrete will be disrupted.

The tests indicate that vermiculite concrete can withstand a significant number of cycles of freezing and thawing even when continousuly exposed to water. All of the protective coatings used were successful, to varying degrees, in inhibiting absorption of water by the concrete and thereby improved the durability. An additional consideration is that deterioration due to freezing and thawing manifests itself by attrition of the surface which can be monitored by visual inspection.

TECHNICAL MEMORANDUM 505-10

Texas Transportation Institute
Texas A&M Research Foundation

TEXAS T1 BRIDGE RAIL SYSTEMS

A Test and Evaluation Report on Contract No. CPR-11-5851

U.S. Department of Transportation
Federal Highway Administration

by

Robert M. Olson, Harry L. Smith

Don L. Ivey, and T. J. Hirsch

These crash tests and evaluations were conducted under the Office of Research and Development, Structures and Applied Mechanics Division's Research Program on Structural Systems in Support of Highway Safety (4S Program). The opinions, findings, and conclusions expressed in this report are those of the authors and not necessarily those of the Federal Highway Administration.

April 1971

SUMMARY OF RESULTS

High speed films were examined to determine the reduction in velocity produced by a collision incident, and to estimate the average total impact force (Average G_{Total}), and its components parallel (Average G_{Long}) and perpendicular (Average G_{Lat}) to the barrier. A discussion of the method of photographic analysis is contained in Appendix A, and the results are tabulated in Table 1. It is recognized that during a collision peak values of unit impact force occur as shown in the accelerometer traces in Appendix B. It is further recognized that such peak values may be two to three or more times the magnitude of the average values presented in this report, and that these peak values may be very significant in the design of barrier systems and connections. The relationship between average loads and peak loads is not resolved in this study. Average values of impact force have been computed and presented in this report and shed some light on the significance of the relationship of the forces parallel and perpendicular to a barrier as shown in Table 1.

Two crash tests (T1-A and T1-B) on a Texas Highway Department T1 Rail show that the system is strong enough to restrain the test vehicles. Vehicle damage was moderate in the lower speed test but severe in the higher speed test. Snagging, which occurred in Tests T1-A and T1-B, accounts for high components of impact force parallel to the railing system and large reduction in velocity. Comparison of the results of these two tests with the test on a modified barrier (T1-D) show that the

	DATA FROM FILMS					COMPUTED RESULTS					
	SPEED*	SPEED**	SPEED	DISPLACEMENT		CHANGE IN SPEED			AVERAGE DECELERATION		
	V_1	V_2	V_3	S_{LAT}	S_{LONG}	(V_1-V_2)	(V_1-V_3)	(V_2-V_3)	G_{LAT}	G_{LONG}	G_{TOTAL}
	(ft/sec)	(ft/sec)	(ft/sec)	(ft)	(ft)	(ft/sec)	(ft/sec)	(ft/sec)	(g's)	(g's)	(g's)
T1-A	65.2	40.2	39.2	2.5	13.1	25.0	26.0	1.0	4.7	2.2	5.2
T1-B	82.7	41.3	39.1	3.5	13.0	41.4	43.6	2.2	5.4	4.7	7.2
T1-C	85.0	61.1	58.3	5.2	15.0	23.9	26.7	2.8	3.9	2.2	4.5
T1-D	90.1	80.4	79.7	3.3	14.5	9.7	10.4	0.7	6.8	0.2	6.8

NOTES:

*V_1 is the speed of the vehicle at impact.

**V_2 is the speed of the vehicle when it becomes parallel to the rail.

V_3 is the speed of the vehicle at loss of contact with the rail.

F_{LAT} = Vehicle weight x G_{LAT}

F_{LONG} = Vehicle weight x G_{LONG}

F_{TOTAL} = Vehicle weight x G_{TOTAL}

$\mu = F_{LONG}/F_{LAT}$

	COMPUTED AVERAGE IMPACT FORCE			
	F_{LAT}	F_{LONG}	F_{TOTAL}	μ
	(lbs.)	(lbs.)	(lbs.)	
T1-A	8,740	4,090	9,670	0.47
T1-B	21,170	18,420	28,220	0.87
T1-C	14,310	8,070	16,520	0.56
T1-D	24,620	720	24,620	0.03

Table 1. Test Data Summary and Analysis

average longitudinal impact force is greatly reduced by eliminating snagging, but the added W-Section makes a stronger system and produces a higher component of force perpendicular to the barrier. An examination of Table 1 shows that the average total deceleration under similar conditions of impact (T1-B and T1-D) are nearly identical. However, the component of force parallel to the barrier is much less and the damage rating is considerably less in a collision with the modified rail system.

Damage Ratings

The National Safety Council published a "Vehicle Damage Scale for Traffic Accident Investigators" in 1968. This damage rating scale, developed in the NSC Traffic Accident Data Project, consists of photographs of automobiles damaged in accidents. Fourteen observers compared the photographs of vehicles damaged in Tests A, B, C and D with the NSC pictures. The results of the comparisons are listed in Table 2.

The letters LFQ and FL in the table refer to the location of the damage as defined in the NSC rating scale. Some observers compared the test vehicle with LFQ (Left Front Quarter) photographs, and others with FL (Front Left) photographs.

Details of individual tests are presented in the following pages, and an evaluation of the several tests is included at the end of the report.

OBSERVER	TEST NUMBER			
	T1-A	T1-B	T1-C	T1-D
1	LFQ-5	LFQ-7	LFQ-4	LFQ-5
2	LFQ-5	FL-7	LFQ-5	LFQ-6
3	FL-5	LFQ-7	LFQ-5	LFQ-5
4	FL-2	LFQ-7	LFQ-4	LFQ-6
5	FL-6	LFQ-7	LFQ-4	LFQ-6
6	LFQ-5	FL-7	LFQ-5	LFQ-4
7	FL-4	FL-7	FL-2	FL-4
8	LFQ-6	FL-3	FL-2	FL-2
9	FL-7	FL-5	FL-3	FL-3
10	LFQ-5	FL-7	FL-4	FD-4
11	LFQ-6	FD-6	LFQ-4	FL-6
12	FL-4	FD-6	FL-4	FD-4
13	LFQ-4	FD-6	LFQ-4	FL-4
14	FL-4	LFQ-7	FL-4	FD-4
AVERAGE (14 Observations)	4.9	6.4	3.9	4.5

Table 2. Vehicle Damage Ratings

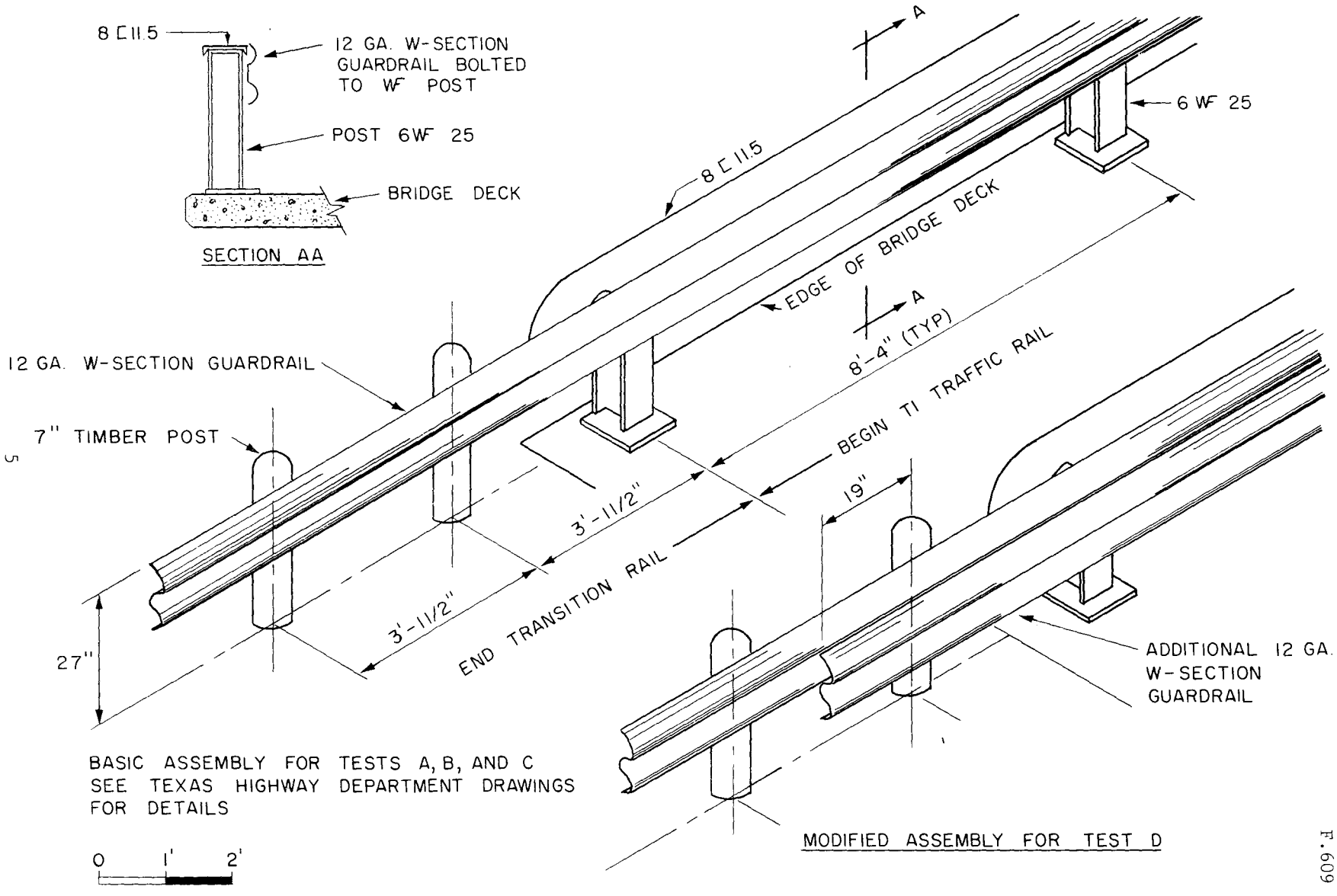

FIGURE 1, TEXAS TI PROTECTIVE BARRIER

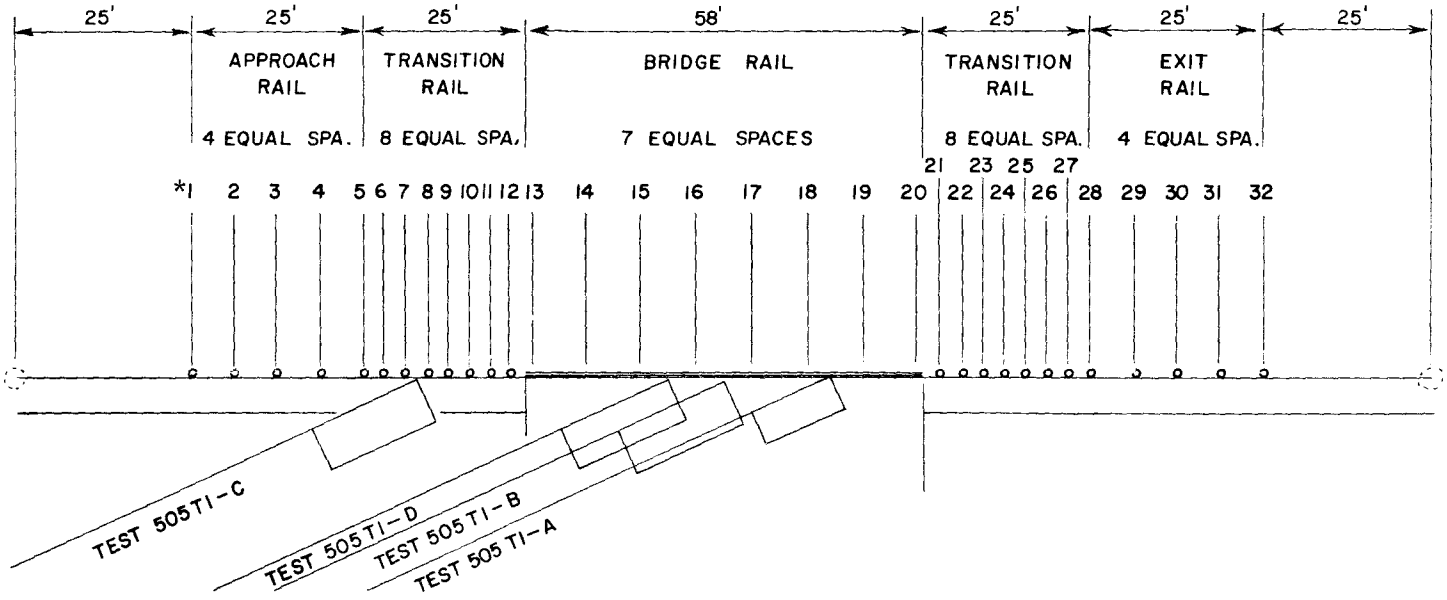

TEST NUMBER	505TI-A**	505TI-B**	505TI-C	505TI-D***
IMPACT ANGLE	25°	25°	25°	25°
VEHICLE WEIGHT (LBS.)	1860	3920	3670	3620
IMPACT VELOCITY (MPH)	44.5	56.4	58.0	61.4

* REFERS TO POST NUMBERS

** STANDARD TI

*** MODIFIED TI

FIGURE 2, SUMMARY OF TESTS.

DETAILS OF INDIVIDUAL TESTS

Test T1-A Results

The 1860 lb. vehicle, traveling 44.5 mph, impacted the bridge rail section at an angle of 25°. Figure 3, the Position-Time Diagram, illustrates this test. The bridge rail contained and redirected the vehicle.

The average total impact force caused by the collision of this lightweight vehicle traveling at moderate speed is estimated to be 9672 lbs. (1860 lbs. x 5.2 g's). The T1 barrier was designed in accordance with the AASHO Standard Specifications for Bridges (1964 Interim Specifications) which produces a rail strong enough to restrain an impact force greater than that applied in this crash test.(1) The 12 gage W-section was deformed at its lower edge during the collision to the extent that the crash vehicle snagged post number 19 (T = 150 msec, approximately) before being redirected by coming into contact with the 11.5 lb. channel. These events in the collision incident caused the vehicle to be slowed from 65.2 fps (44.5 mph) to 39.2 fps (26.7 mph). The average lateral component of impact force is estimated to be 8,740 pounds, and the average longitudinal component of impact force is estimated to be 4,090 pounds. The photographs clearly indicate that the impact attenuation was provided by the vehicle, since the barrier was not displaced during the collision incident.

A damage rating of 4.9 indicates moderate damage to the vehicle.

---

[1] "Interim Specifications for Bridge Railings," American Association of of State Highway Officials, 1964.

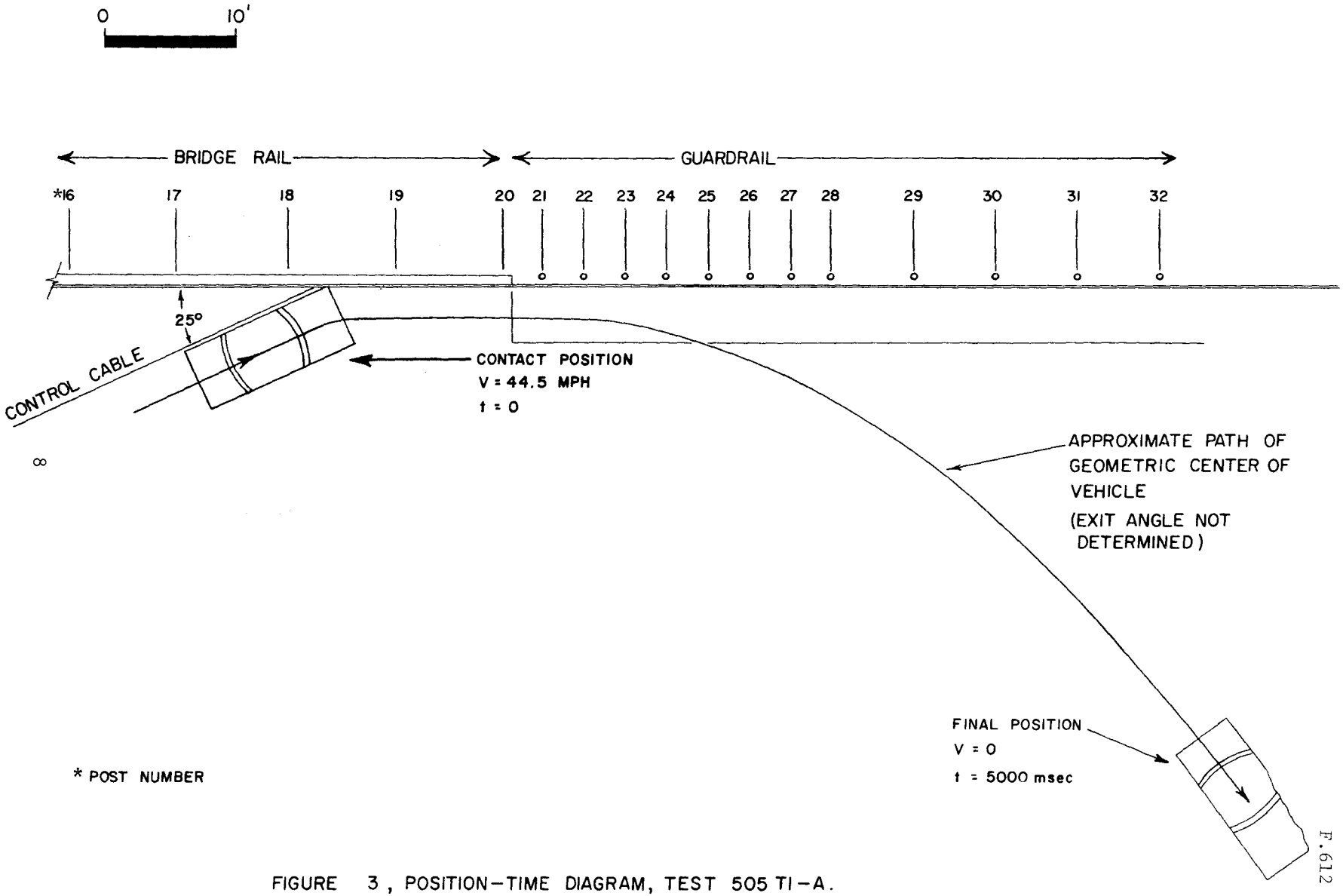

FIGURE 3, POSITION-TIME DIAGRAM, TEST 505 TI-A.

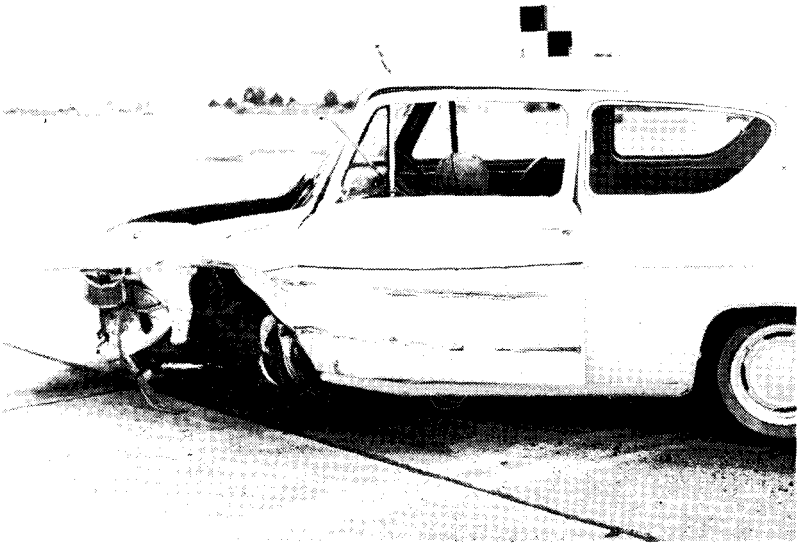

TABLE 3

SUMMARY OF HIGH-SPEED FILM CRASH TEST DATA

Test T1-A

Vehicle Weight = 1860 lb (1958 Anglia, 2-door)

Impact Angle = 25°

Velocity at Impact = 44.5 mph or 65.2 fps

Change in Velocity
During Rail Contact = 17.8 mph or 26.0 fps

Deflection of Barrier: Negligible

Damage to Barrier: Slight

Damage to Vehicle = Moderate (Damage Rating: 4.9)

Probability of Injury
To Unrestrained Occupants: 50%(2)

---

[2]"Tentative Service Requirements For Bridge Rail Systems," NCHRP Report 86, R.M. Olson, E.R. Post, and W.F. McFarland, Highway Research Board, 1970, p. 15.

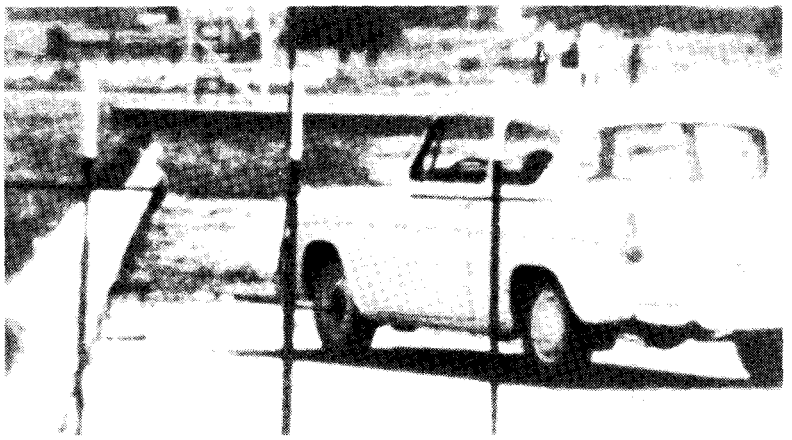

T = -20 msec

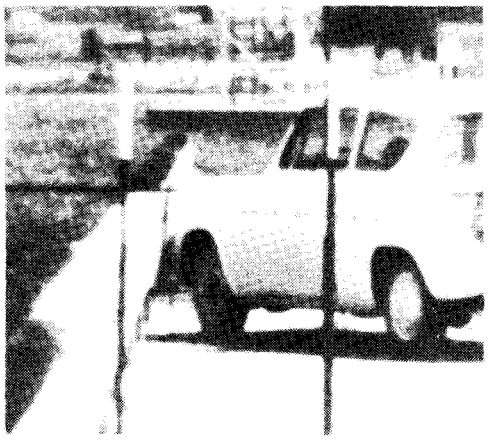

T = 0 msec

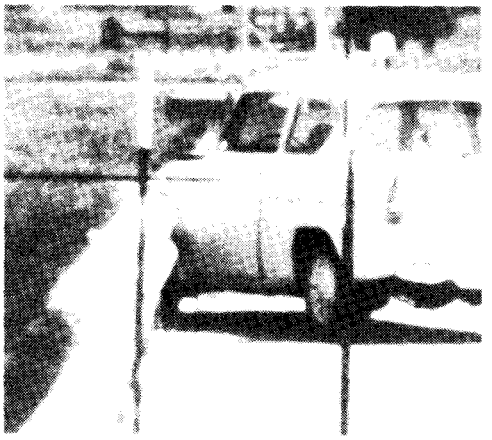

T = 60 msec

T = 120 msec

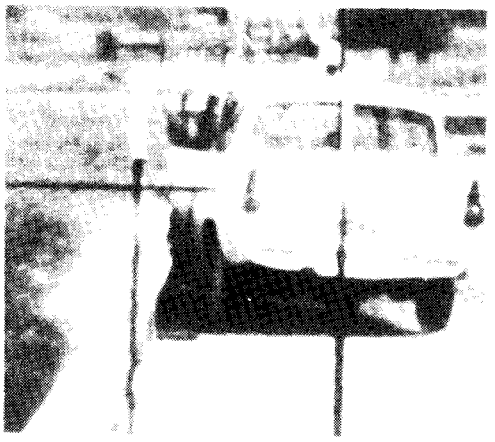

T = 180 msec

Figure 4, Sequential Photographs of Test T1-A.

T = 300 msec

T = 480 msec

T = 680 msec

T = 1680 msec

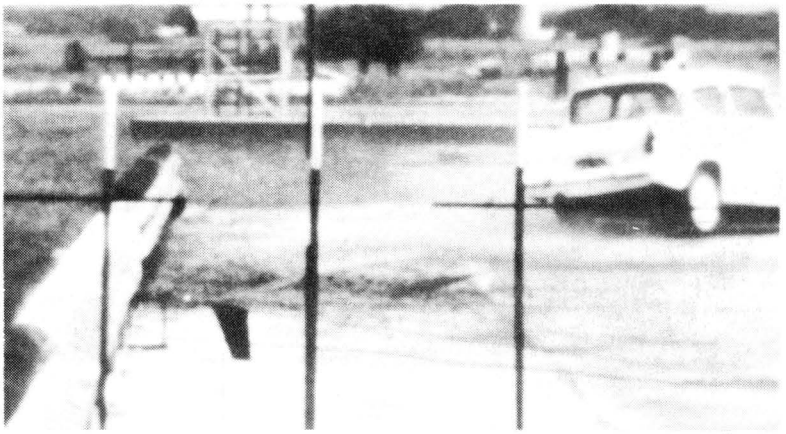

T = 2080 msec

Figure 4 (continued)

Figure 5. Vehicle Before Test T1-A.

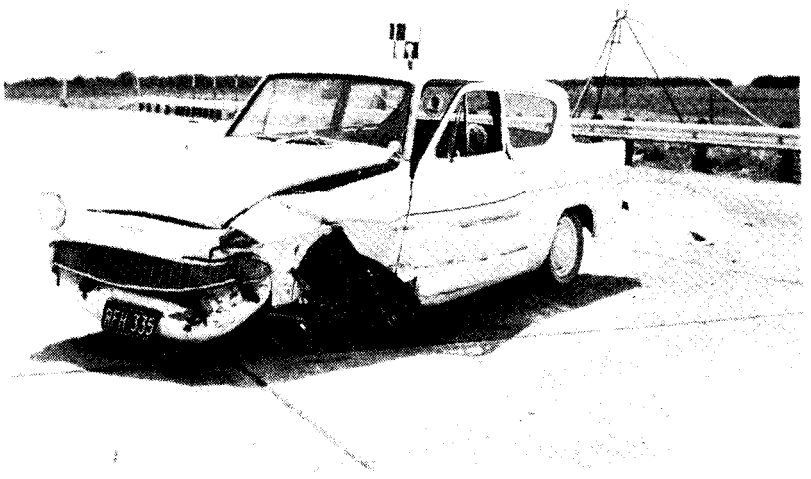

Figure 6. Vehicle After Test T1-A.

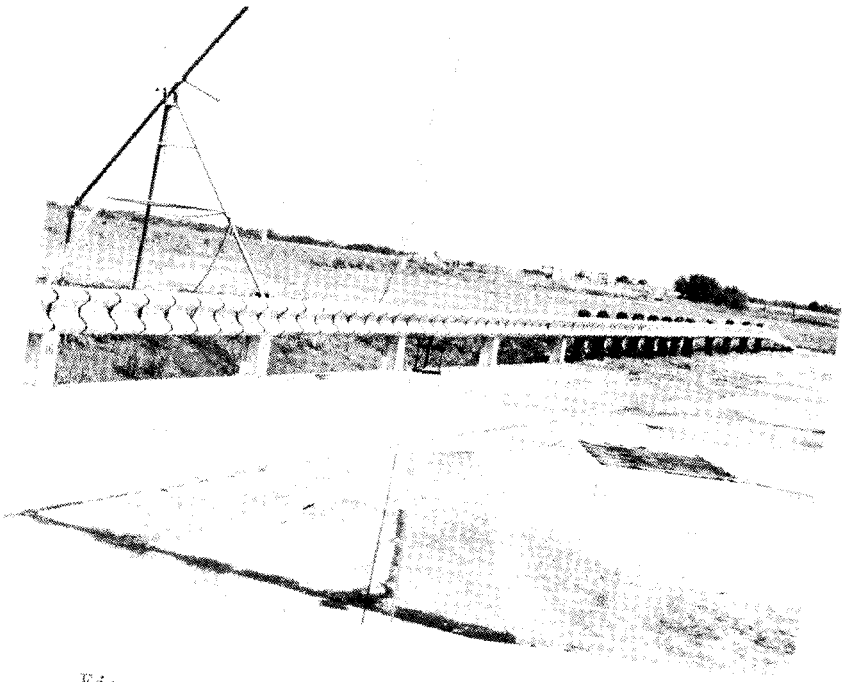

Figure 7, Impact Area Before Test T1-A.

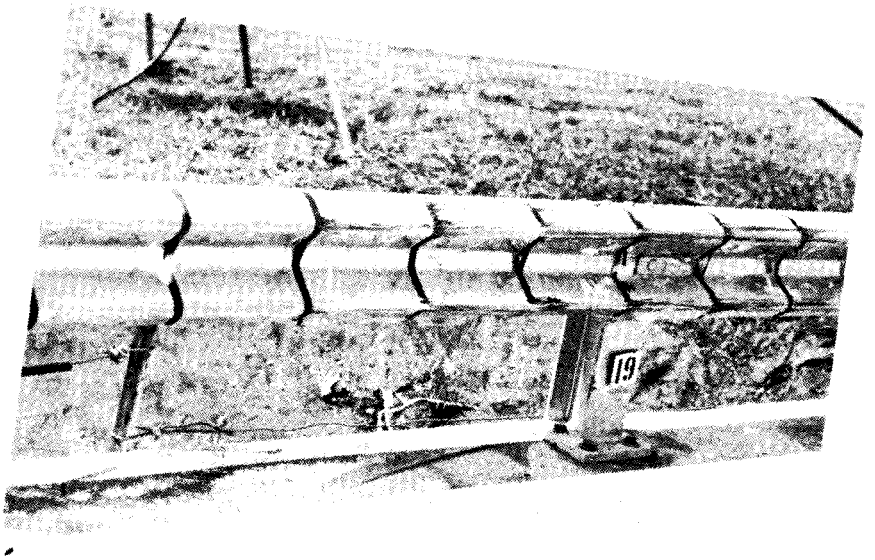

Figure 8, Impact Area After Test T1-A.

Test T1-B Results

The 3920 lb. vehicle contacted the guardrail at a 25° angle while traveling 56.4 mph. The Position-Time Diagram, Figure 9, depicts the vehicle-barrier interaction. Figure 10 shows sequential photographs of the collision.

The average total impact force estimated to be 28,224 lbs. (3920 lbs. x 7.2 g's) indicates that the T1 barrier, designed in accordance with AASHO Standard Specifications for Highway Bridges (1964 Interim Specifications) is strong enough to restrain an impact force greater than that applied in this test.(1) Under the force of impact the 12 gage W-section was deformed into the plastic range and fractured (Figure 14) permitting the crash vehicle to snag post number 17, producing an average longitudinal component of impact force of 18,420 pounds, and an average lateral component of impact force of 21,170 pounds. The average total impact force accounts for the extensive damage to the vehicle (see Figure 12), which provided major portion of the impact attenuation in this collision incident since the barrier displacement was negligible (see Figure 10).

A damage rating of 6.4 is indicative of the severe vehicle damage produced by the collision with this strong system.

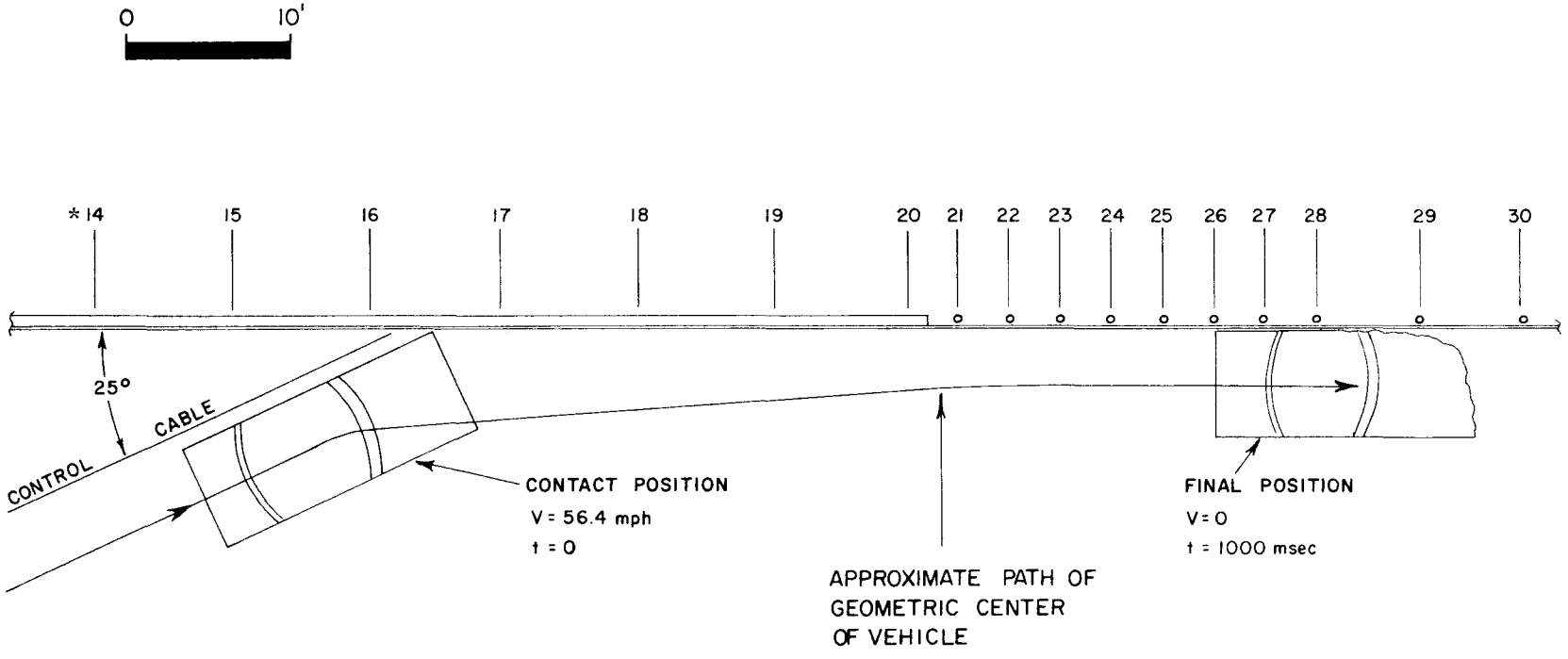

* POST NUMBER

FIGURE 9, POSITION-TIME DIAGRAM, TEST 505 TI-B.

TABLE 4

SUMMARY OF HIGH-SPEED FILM CRASH TEST DATA

Test T1-B

Vehicle Weight = 3920 lb (1961 Ford, 4-door)

Impact Angle = 25°

Velocity at Impact = 56.4 mph or 82.7 fps

Change in Velocity = 29.7 mph or 43.6 fps

Deflection of Barrier: Negligible

Damage to Barrier: Moderate

Damage to Vehicle: Severe (Damage Rating: 6.4)

Probability of Injury
To Unrestrained Occupants: 85%[2]

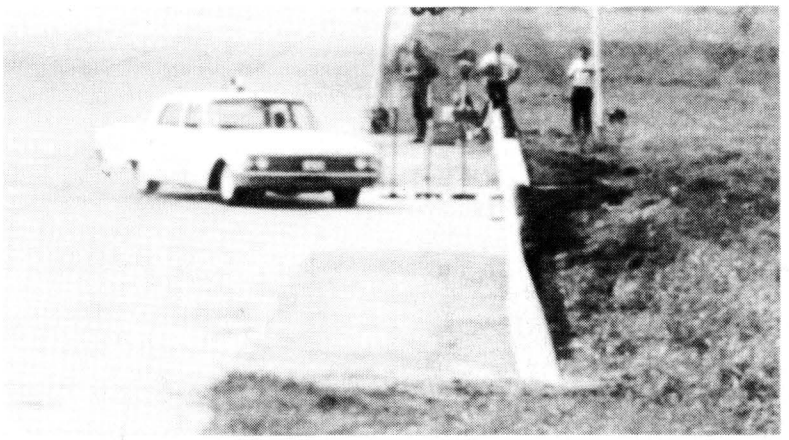

T = -102 msec

T = 0 msec

T = 51 msec

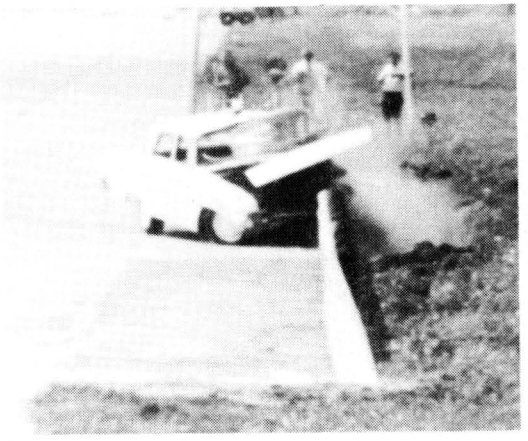

T = 153 msec

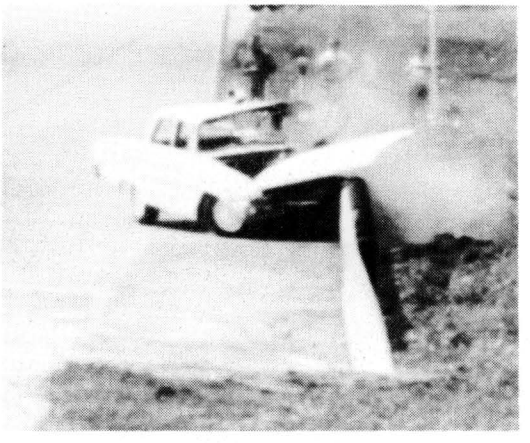

T = 255 msec

Figure 10, Sequential Photographs of Test T1-B.

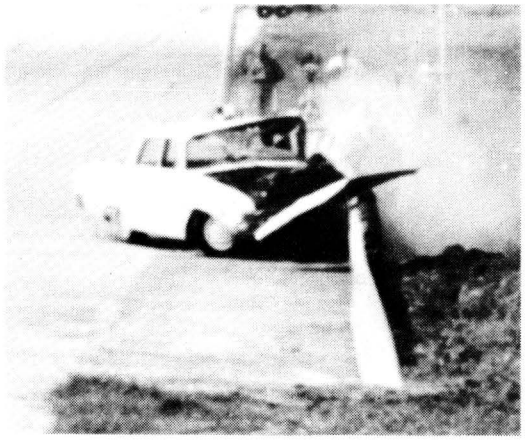

T = 357 msec

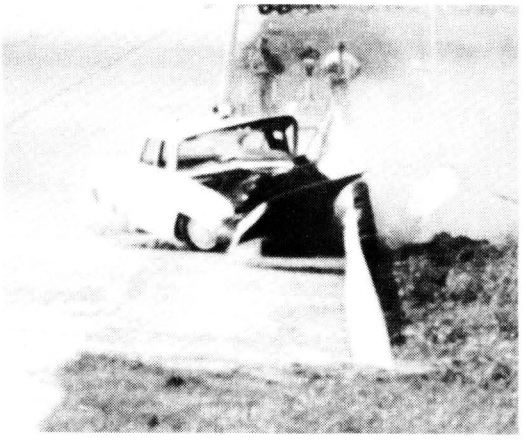

T = 510 msec

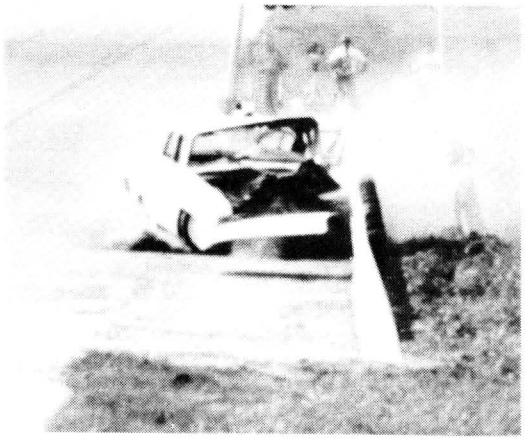

T = 612 msec

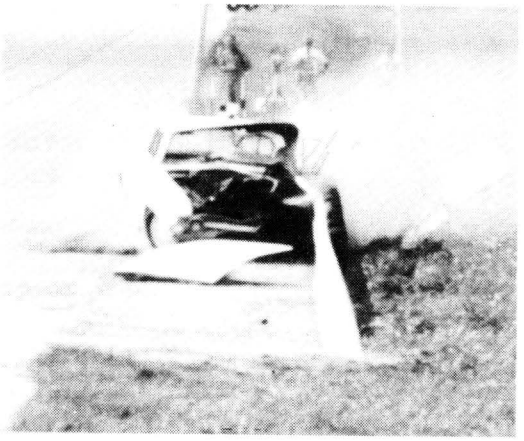

T = 714 msec

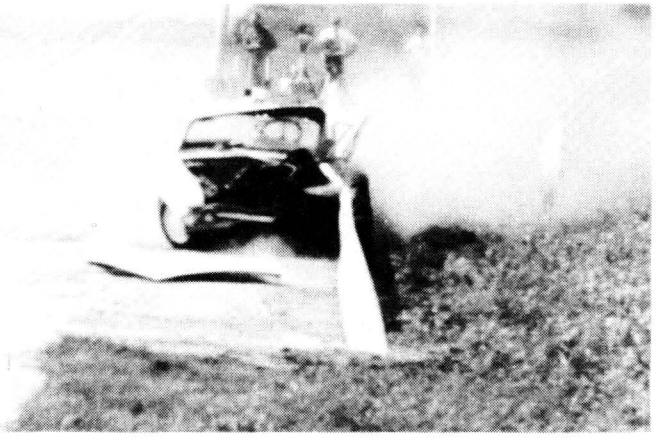

T = 816 msec

Figure 10 (continued)

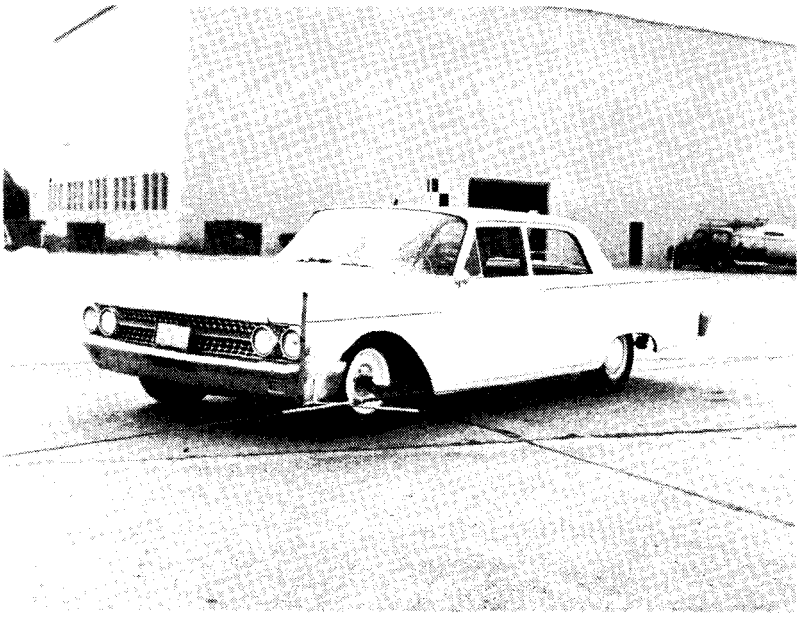

Figure 11, Vehicle Before Test T1-B.

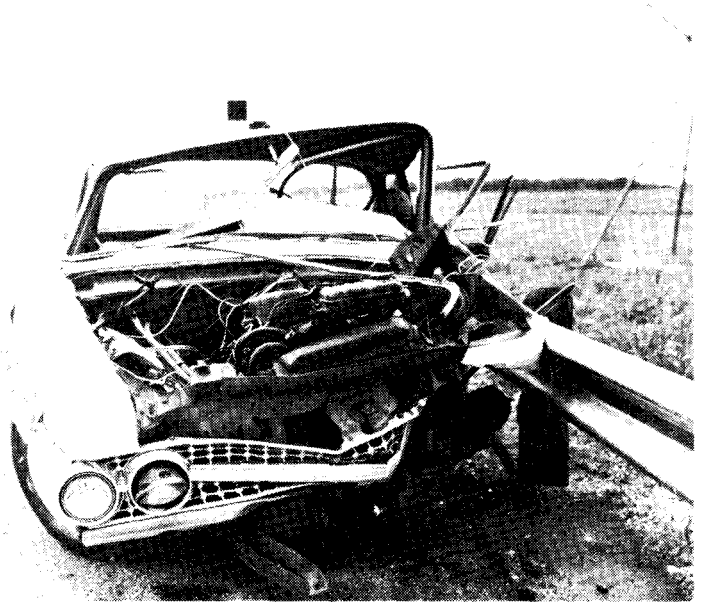

Figure 12, Vehicle After Test T1-B.

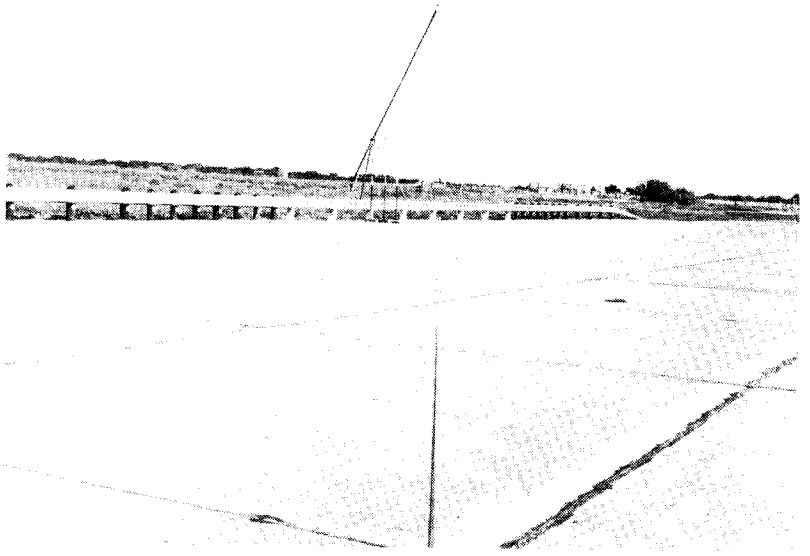

Figure 13, Impact Area Before Test T1-B.

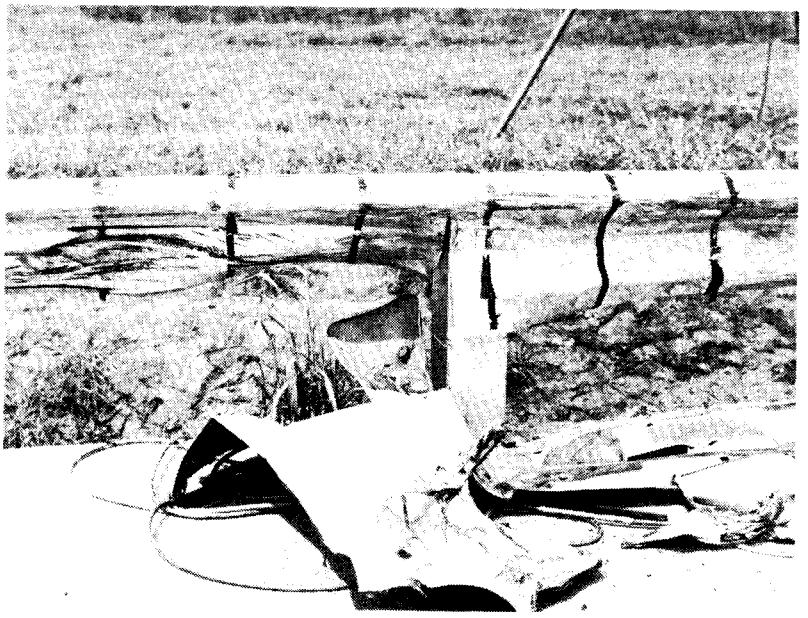

Figure 14, Impact Area After Test T1-B.

Test T1-C Results

A 3670 lb. vehicle traveling 58.0 mph, at an impact angle of 25°, contacted the guardrail 15 ft. in advance of the guardrail-bridge rail interface. The Position-Time Diagram, Figure 15, and the motion picture sequential photographs, Figure 16, given an indication of the behavior of the vehicle and barrier during the interaction. The guardrail contained and redirected the vehicle as intended.

The average total impact force in this test is estimated to be 16,515 lbs. (3670 lbs. x 4.5 g's). The average lateral component of impact force is estimated to be 14,310 lbs., and the average longitudinal component of impact force is estimated to be 8,070 lbs. The barrier is capable of significant lateral displacement as shown in Figure 20 and thus provides impact attenuation capabilities not available in the stronger T1 bridge rail. The average lateral and longitudinal components of impact force are considerably smaller than those estimated for test T1-B. The vehicle weights and speeds were comparable in the two tests, but a 21-inch displacement of the transition rail resulted in a much reduced impact force. Such a force reduction owing to rail displacement was predicted in the final report of an NCHRP study.[2] The transition rail to bridge rail connection was adequate to provide structural continuity between the two systems.

The damage rating of 3.9 indicates moderate damage to the colliding vehicle.

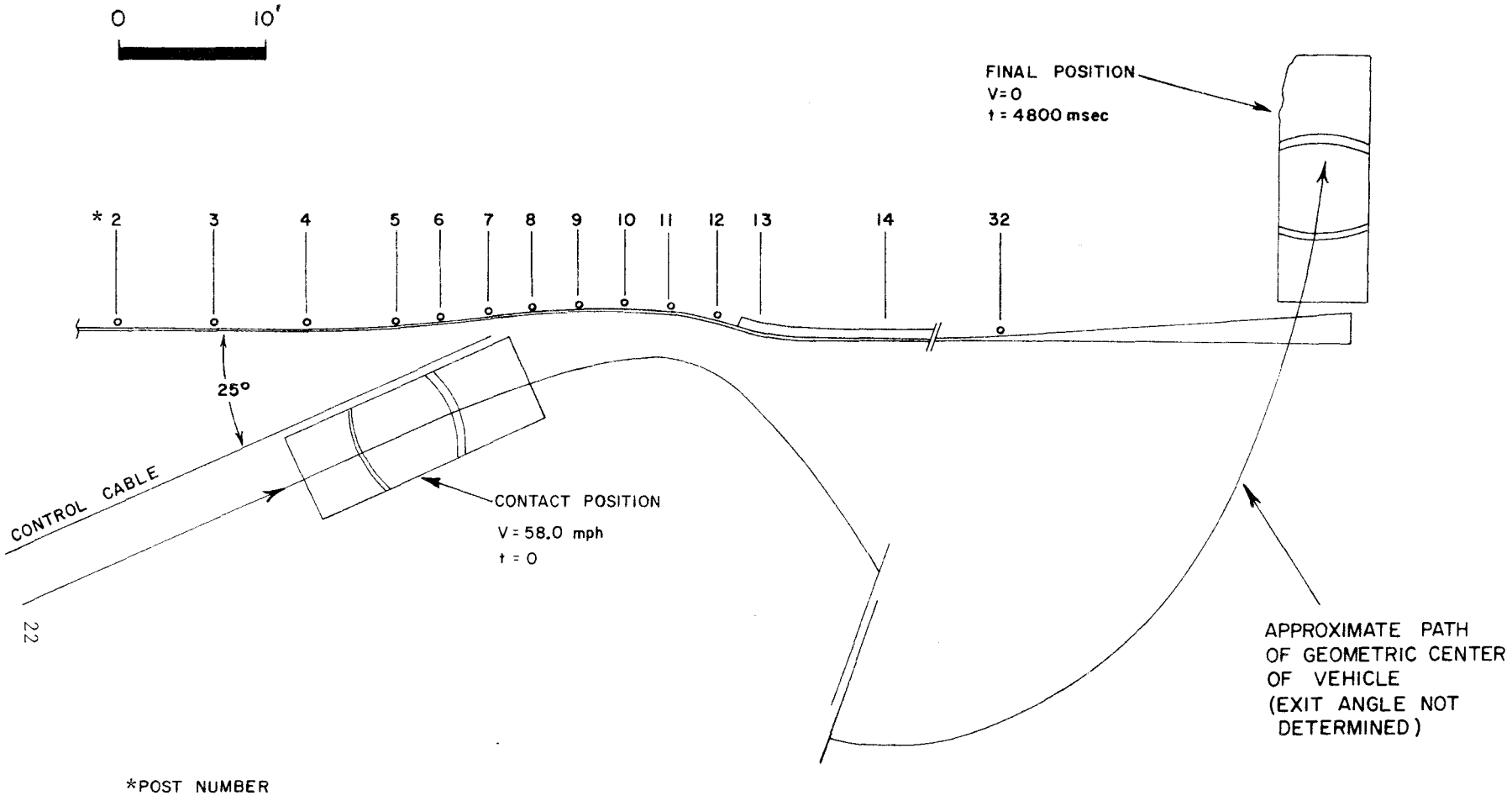

FIGURE 15, POSITION—TIME DIAGRAM, TEST 505 TI-C.

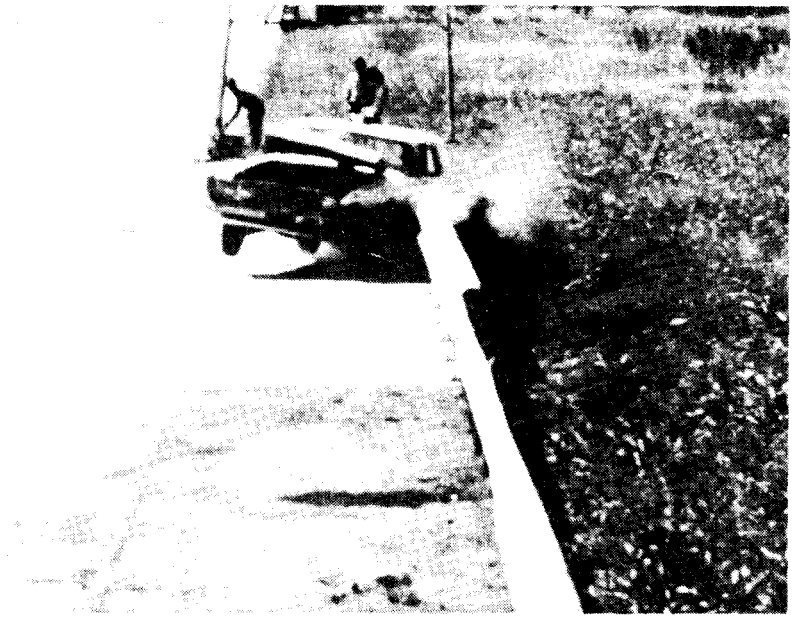

TABLE 5

SUMMARY OF HIGH-SPEED FILM CRASH TEST DATA

Test T1-C

Vehicle Weight = 3670 lb (1965 Plymouth, 4-door)

Impact Angle = 25°

Velocity at Impact = 58.0 mph or 85.0 fps

Change in Velocity = 18.2 mph or 26.7 fps

Deflection of Guardrail: 21 in.

Damage to Guardrail: Moderate

Damage to Vehicle: Moderate (Damage Rating: 3.9)

Probability of Injury
To Unrestrained Occupants: 30%[2]

T = -166 msec

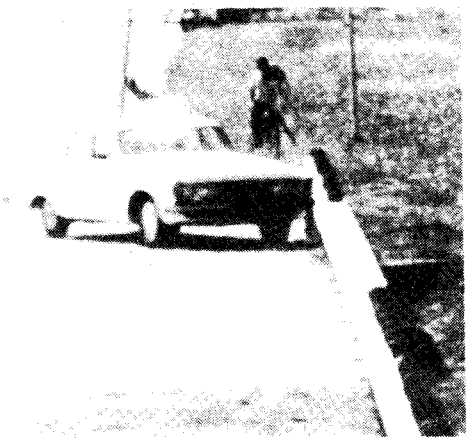

T = 0

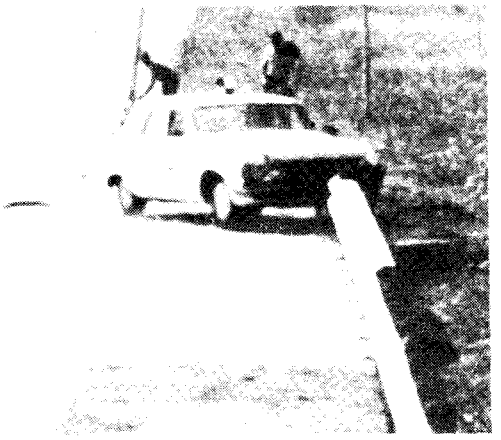

T = 83 msec

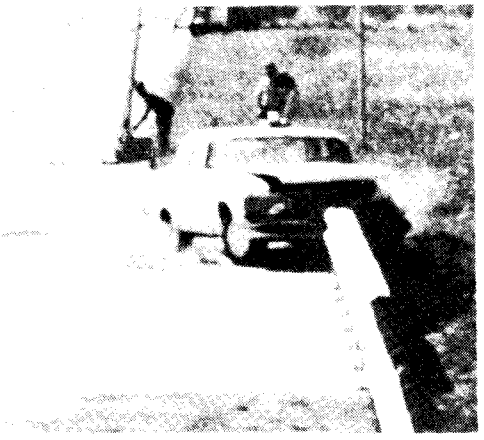

T = 166 msec

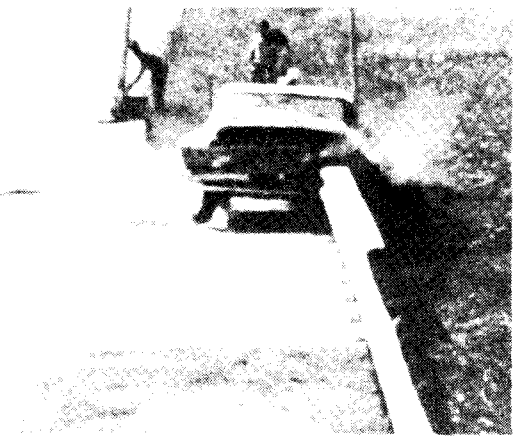

T = 249 msec

Figure 16, Sequential Photographs of Test T1-C.

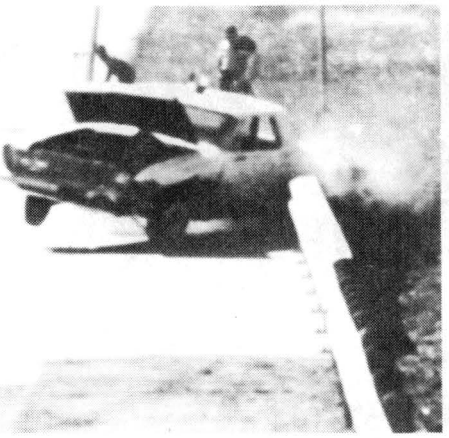

T = 415 msec

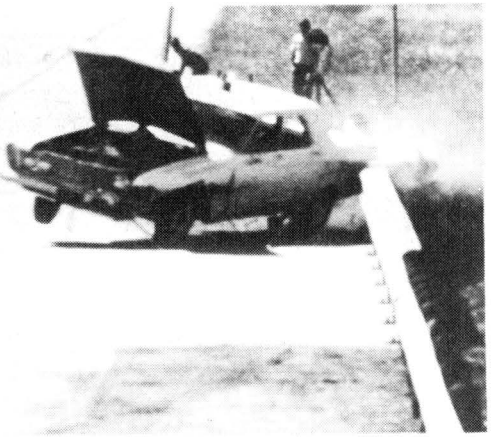

T = 498 msec

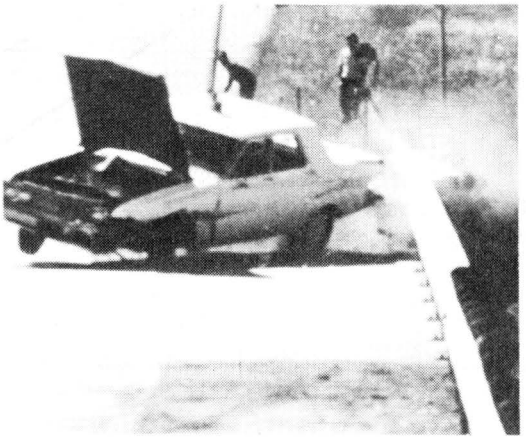

T = 581 msec

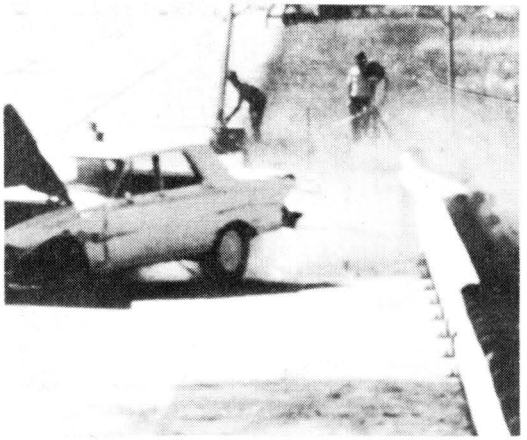

T = 747 msec

T = 830 msec

Figure 16 (continued)

Figure 17, Vehicle Before Test T1-C.

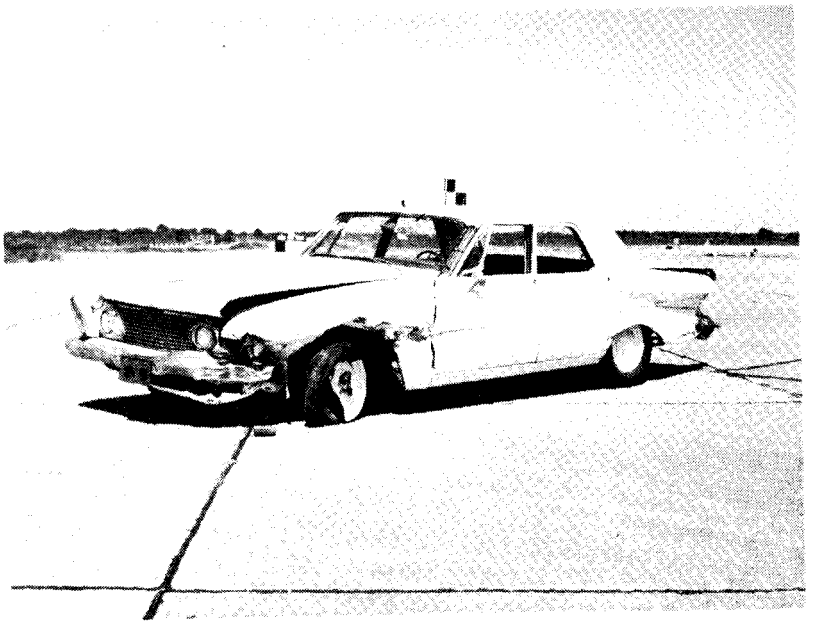

Figure 18, Vehicle After Test T1-C.

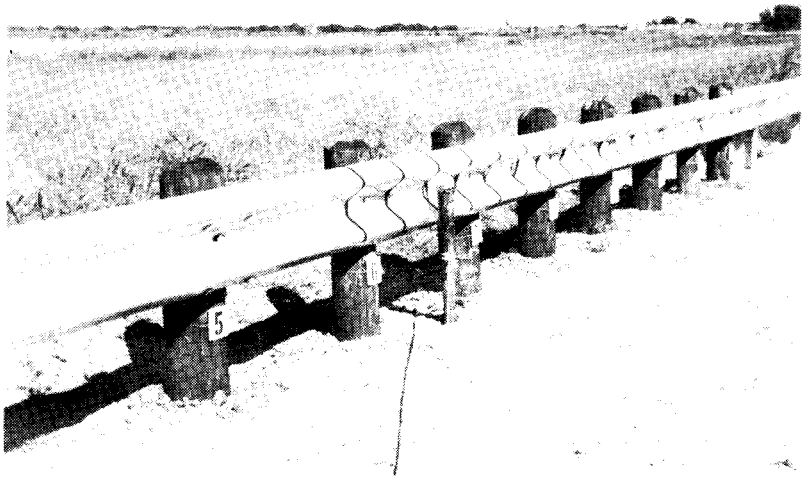

Figure 19, Guardrail Installation Before Test T1-C.

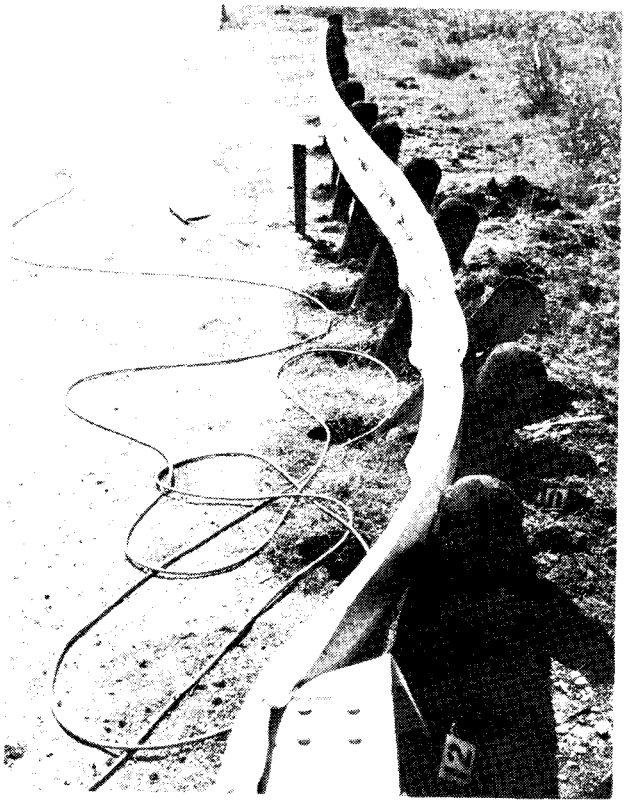

Figure 20, Guardrail Installation After Test T1-C.

Test T1-D Results

The Texas T1 bridge rail was modified for Test T1-D as shown in Figure 1. An overlapping W-section guardrail was added to the bridge rail section of the barrier system. The 3620 lb. vehicle, traveling 61.4 mph collided with the barrier bridge rail section at an angle of 25°. The Position-Time Diagram, Figure 21, and the motion picture sequential photographs, Figure 22, show the vehicle-barrier interaction during the collision. The protective barrier contained and redirected the vehicle.

The average total impact force in this test is estimated to be 24,616 lbs. (3620 lbs. x 6.8 g's). It is apparent that the overlapped 12 gage W-sections provided a stronger system between posts; thus the lateral deceleration component was 26 percent larger than in Test T1-B; however, the longitudinal component was only 4 percent of that produced in Test T1-B. It is significant that the average total g's in these two tests were nearly the same (see Table 1); but the damage rating in the modified rail test was in the moderate range, whereas a severe damage rating resulted in Test T1-B. Elimination of snagging accounts for the reduction in damage, because the longitudinal component of deceleration was reduced to 0.2 g. The average lateral component of impact force is estimated to be 24,620 pounds; however, the average longitudinal component of impact force is estimated to be only 720 pounds.

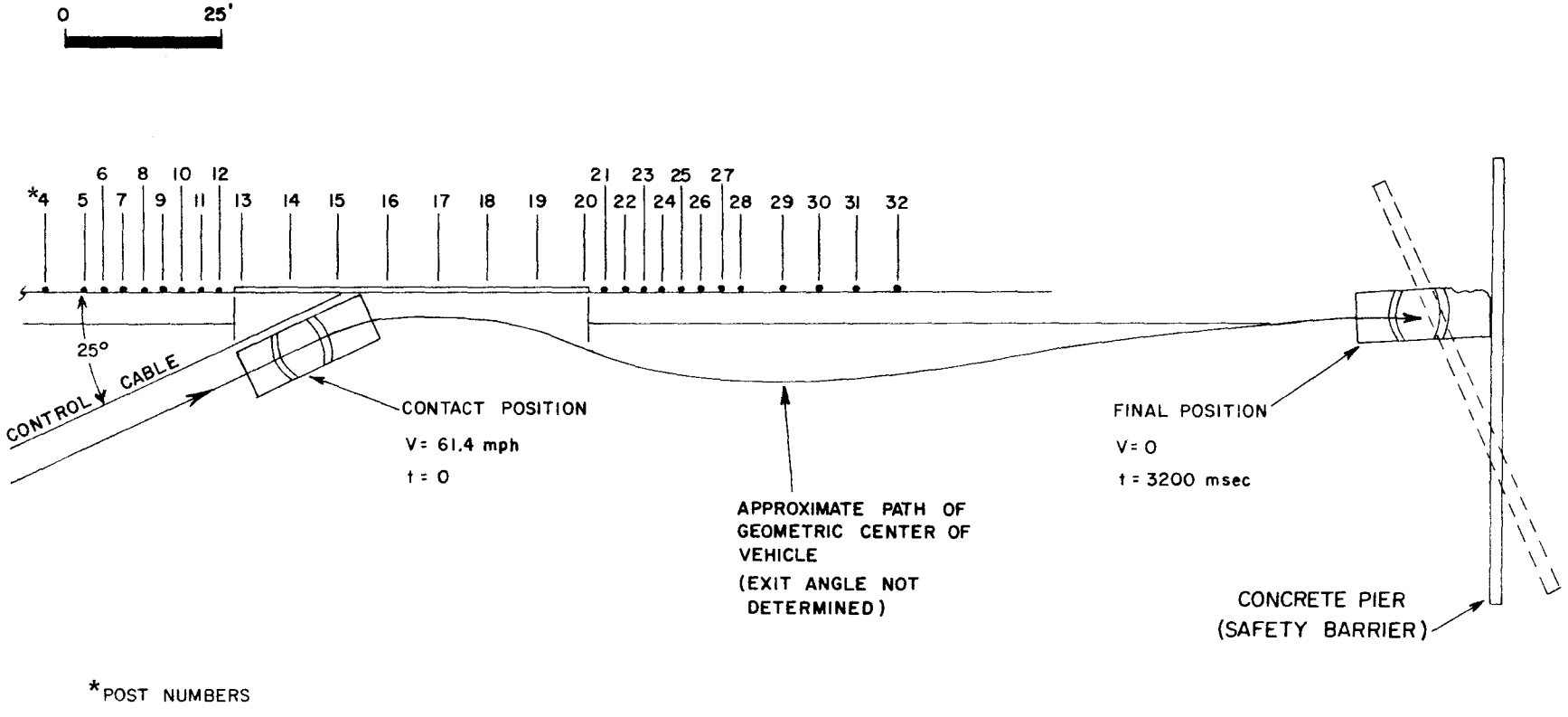

FIGURE 21, POSITION—TIME DIAGRAM, TEST 505 TI-D.

TABLE 6

SUMMARY OF HIGH-SPEED FILM CRASH TEST DATA

Test T1-D

Vehicle Weight = 3620 lb (1964 Dodge, 4-door)

Impact Angle = 25°

Velocity at Impact = 61.4 mph or 90.1 fps

Change in Velocity = 7.1 mph or 10.4 fps

Deflection of Barrier: 2 in.

Damage to Barrier: Slight

Damage to Vehicle: Moderate (Damage Rating: 4.5)

Probability of Injury
To Unrestrained Occupant: 45%(2)

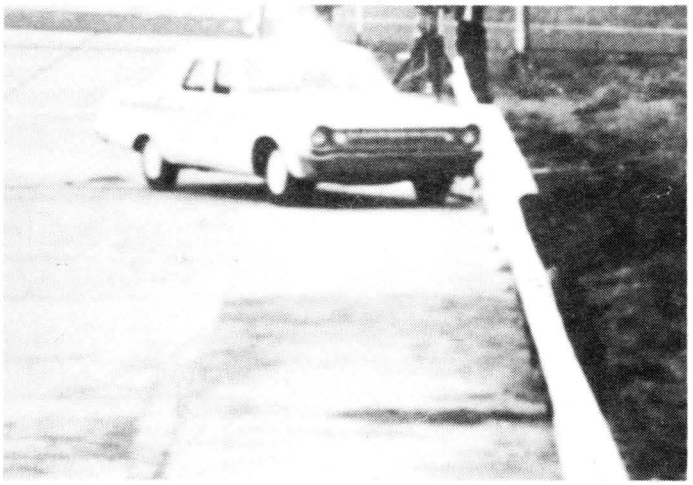

T = 0 msec

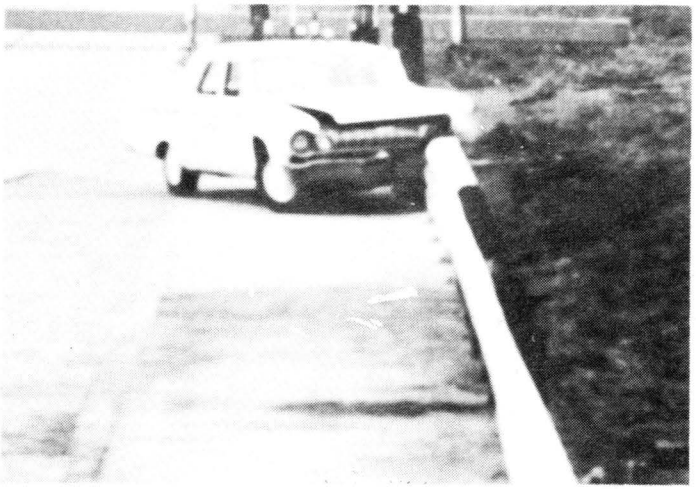

T = 103 msec

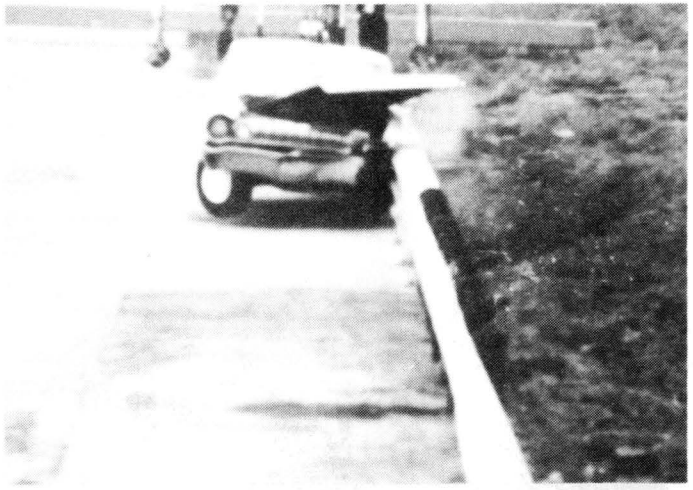

T = 202 msec

T = 400 msec

Figure 22, Sequential Photographs of Test T1-D.

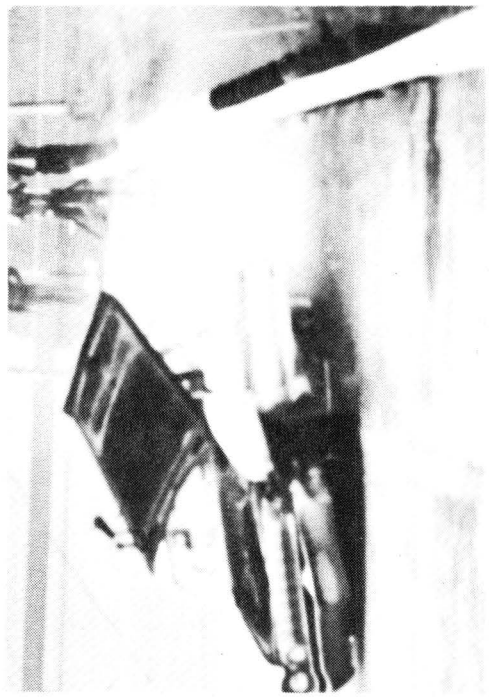

T = 895 msec

T = 1668 msec

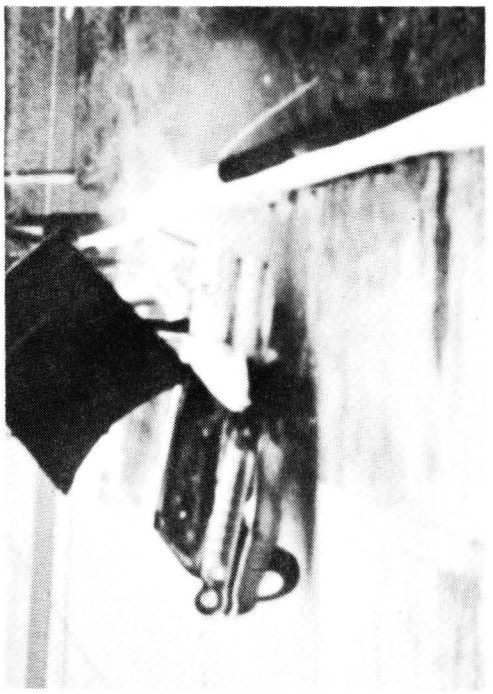

T = 598 msec

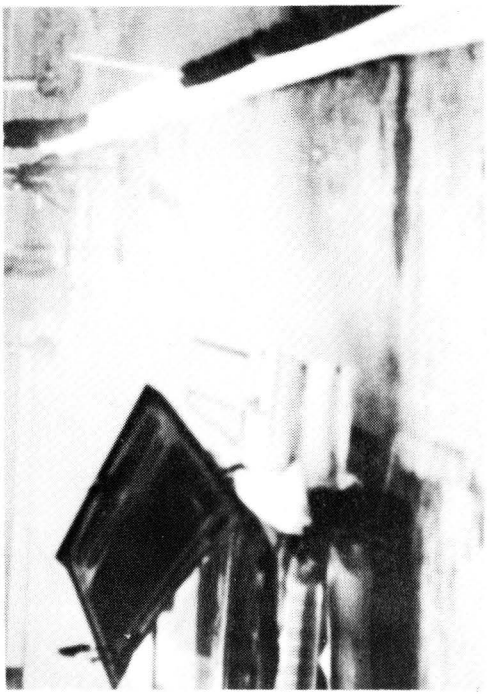

T = 1291 msec

Figure 22 (continued)

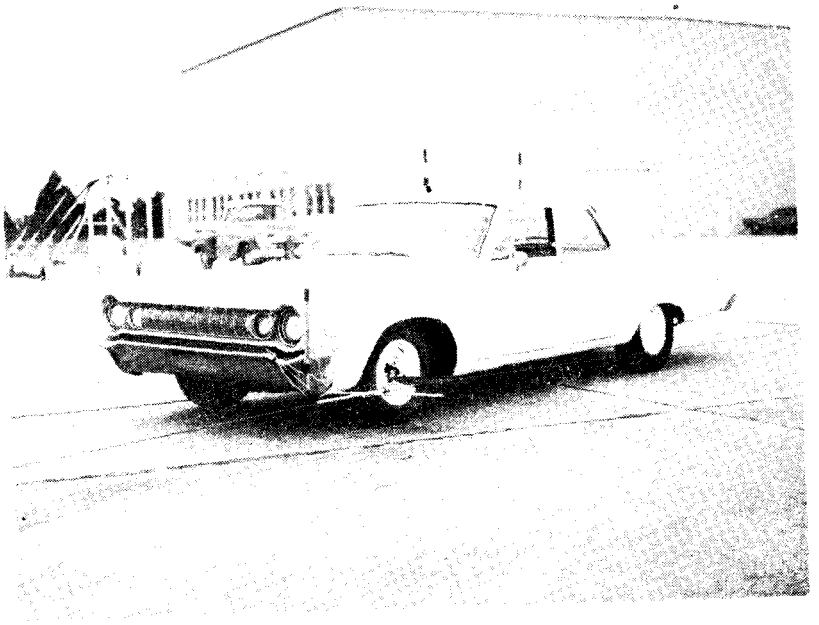

Figure 23, Vehicle Before Test T1-D.

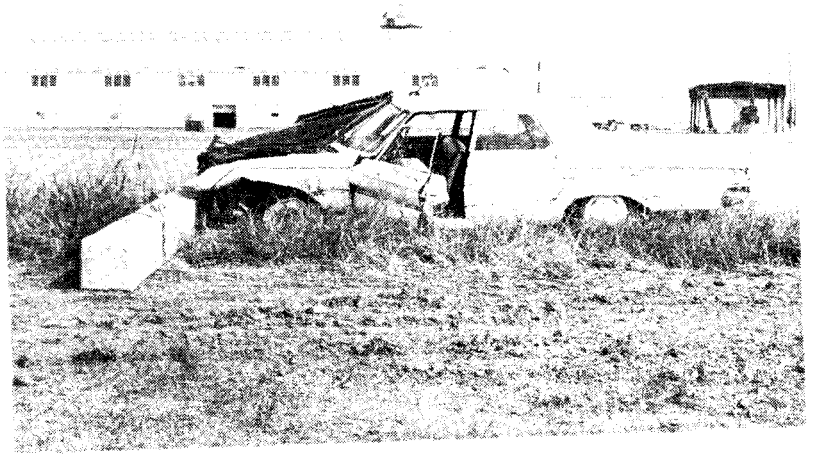

Figure 24, Vehicle After Test T1-D.

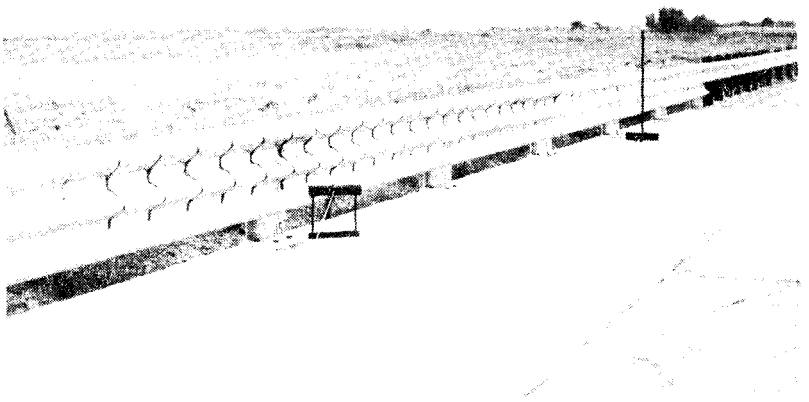

Figure 25, Barrier Before Test T1-D.

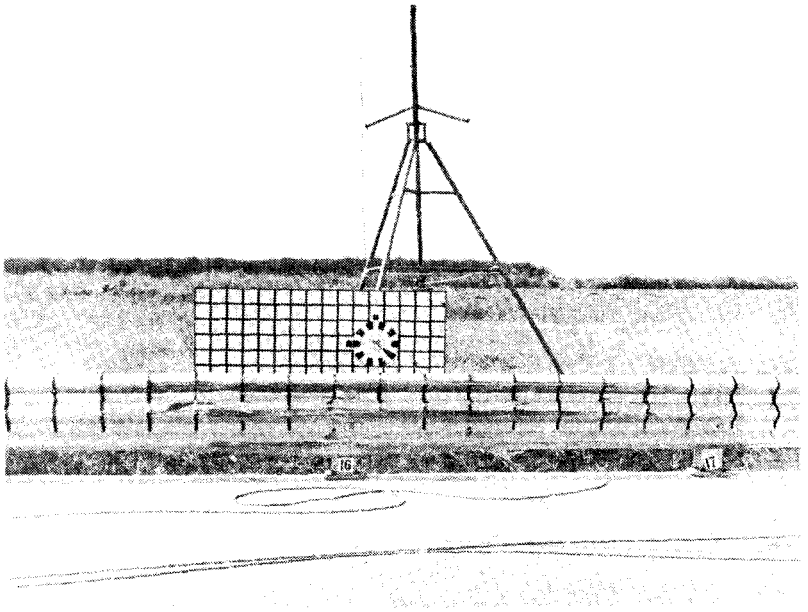

Figure 26, Barrier After Test T1-D.

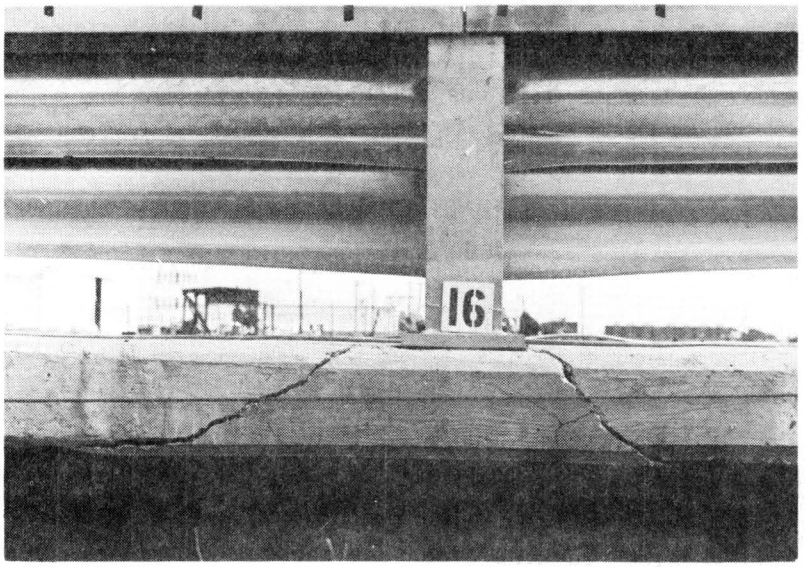

Figure 27, Rail and Slab After Test T1-D.

CONCLUSION AND EVALUATION

In four of four full-scale vehicle crash tests, it was found that the Texas T1 protective barrier is an effective vehicle containment and redirection system. The tests ranged in severity from an 1860 lb vehicle traveling 44.5 mph to a 3670 lb vehicle traveling 58.0 mph. All tests were conducted at an impact angle of 25°. Damage to the bridge rail section of the test barrier was relatively minor. Damage to the transition guardrail section in a single test was extensive. Vehicle damage ranged from moderate to severe. The Texas T1 bridge rail is a rigid system which undergoes negligible lateral displacements during a vehicle collision. The transition rail connection had adequate strength.

On the basis of the tests conducted, it appears that maintenance costs of the T1 Bridge Rail System should be nominal. The usual damage in a high-speed collision consists of localized deformations to the impacted W-section, and cracking of the bridge slab in the pattern shown by Figure 27. The bridge slab cracking appears to be a diagonal tension-type crack which results from the punching shear load generated by the base plate of the bridge rail support post. Although the concrete cracks in the collision area appear to be severe, the structural integrity of the slab is maintained by the steel reinforcement.

It is the opinion of the authors that these cracks may be repaired by placing a lateral load on the support post to force the crack open, grouting the crack with epoxy, and then reversing the lateral load to close the crack. The structural integrity of the bridge rail system does not appear to be damaged significantly by these diagonal tension cracks. Damage to the W-section rail is reduced by adding an additional, partially overlapping, W-section as in the modified T1 test (T1-D).

Tentative service requirements suggested in NCHRP Report 86 are listed below:

1. A bridge rail system must laterally restrain a selected vehicle.
2. A bridge rail system must minimize vehicle decelerations.
3. A bridge rail system must smoothly redirect a colliding vehicle.
4. A bridge rail system must remain intact following a collision.
5. A bridge rail system which serves vehicles and pedestrians must provide protection for vehicle occupants and pedestrians.
6. A bridge rail system must have a compatible approach rail or other device to prevent collisions with the end of the bridge rail system.
7. A bridge rail system must define yet permit adequate visibility.
8. A bridge rail must project inside the face of any required curb.
9. A bridge rail system must be susceptible of quick repair.
10. The foregoing requirements must be met by giving emphasis first to safety, second to economics, and third to aesthetics.

Evaluations of vehicle-barrier interaction on the basis of these service requirements is presented in Table 7. The evaluations were made using information from high-speed films, a National Safety Council damage rating scale, estimates of probable injuries from Figures 7 and 8 of NCHRP Report 86, and examination of the barrier after each test. Safety, economics, and aesthetics (Service Requirement 10) are evaluated in the table by assigning a numerical value for each test. It is recognized that the vehicle weight, speed, and consequently impact force varied widely between tests. The evaluation of each item was made with these facts in mind.

Service Requirement	T-1 Bridge Rail Test T1-A	T-1 Bridge Rail Test T1-B	Transition Rail Test T1-C	Modified T-1 Bridge Rail Test T1-D
1	Adequate lateral restraint is provided by each of these barriers, penetration and vaulting do not occur.			
2	G_{TOTAL} = 5.2 Vehicle Damage Rating: 4.9 Probability of Injury: 50%	G_{TOTAL} = 7.2 Vehicle Damage Rating: 6.4 Probability of Injury: 85%	G_{TOTAL} = 4.5 Vehicle Damage Rating: 3.9 Probability of Injury: 30%	G_{TOTAL} = 6.8 Vehicle Damage Rating: 4.5 Probability of Injury: 45%
3	Good redirection, Slight snagging. See Figure 4	Poor redirection, Severe snagging. See Figure 10	Good redirection. See Figure 16	Fair redirection. See Figure 22
4	Each barrier remained intact following the collision.			
5	Not applicable	Not applicable	Not applicable	Not applicable
6	Yes	Yes	This approach rail is compatible geometrically and has adequate connection to bridge rail.	Yes
7	Each barrier satisfies the requirement for delineation, and does not obstruct driver's sight distance.			
8	No curb	No curb	No curb	No curb
9	No repairs required	Replaced W-section	Replaced posts and W-section	No repairs required
10	SAFETY: 3 ECONOMICS: Vehicle Repair: 2 Barrier Repair: 2 AESTHETICS: 1	SAFETY; 4 ECONOMICS: Vehicle Repair: 4 Barrier Repair: 3 AESTHETICS: 1	SAFETY: 1 ECONOMICS: Vehicle Repair: 1 Barrier Repair: 4 AESTHETICS: 1	SAFETY: 2 ECONOMICS: Vehicle Repair: 3 Barrier Repair: 1 AESTHETICS: 1

Table 7. Evaluation of Barriers Using Tentative Service Requirements

A P P E N D I X A

Photographic Data

PHOTOGRAPHIC DATA

The method employed to compute change in velocity and average deceleration components is defined in Figure A1. The values substituted in the governing equations were taken from data acquired by frame to frame analysis of high-speed films of the collision incident in each test. The data and results from computation are contained in Tables A1, A2, A3, and A4.

Velocities V_1, V_2, and V_3, the directed speeds of the colliding vehicle, were determined by measuring the displacement of some reference mark on the vehicle over an interval of time. V_1 was calculated over a time interval just prior to impact; V_2, when the vehicle became parallel to the rail; and V_3, when the vehicle lost contact with the rail.

The finite increment of displacement, ΔS_{lat}, is computed using Equation (2) in Figure A1. Dimension D_1 is computed using AL and B for each vehicle and the angle θ for each test. Dimension D_2 is estimated from high-speed films obtained from a camera located parallel to the bridge rail.

The distance ΔS_{long} is observed from high-speed film using a camera placed perpendicular to the bridge rail.

The average decelerations perpendicular and parallel to the rail (Average G_{lat} and Average G_{long}) are computed by Equations (3) and (4) shown in Figure A1. The average total deceleration (Average G_{total}) is defined as the vector sum of these components, as shown in Figure A1.

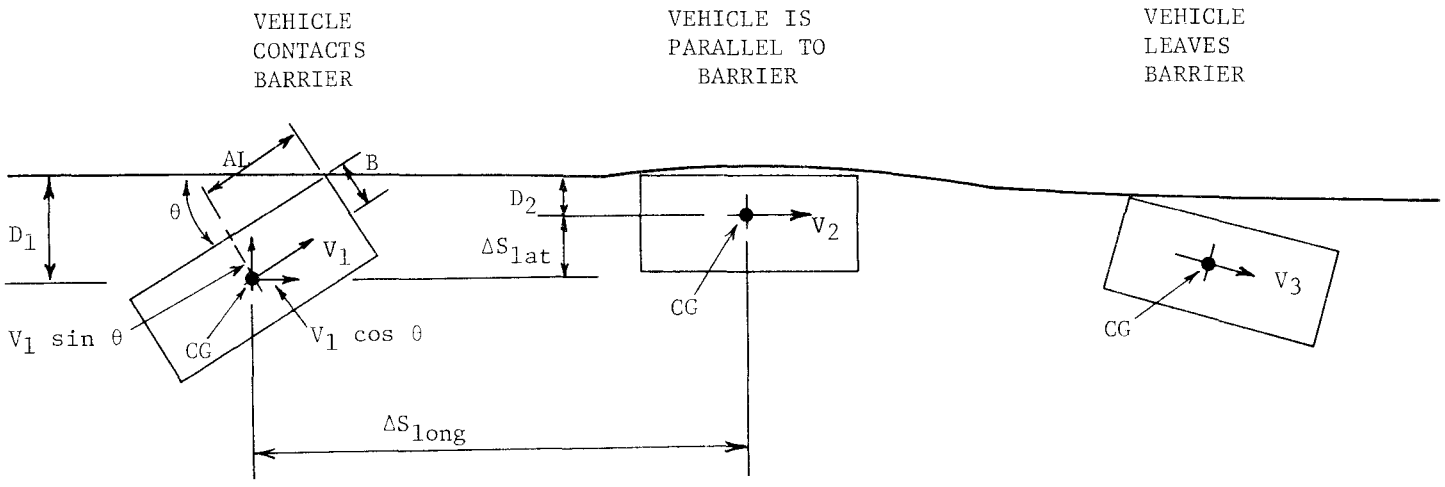

GOVERNING EQUATIONS:

(1) $\Delta V = V_3 - V_1$

(2) $\Delta S_{lat} = D_1 - D_2$

(3) Average $G_{lat} = \dfrac{(V_1 \sin \theta)^2}{2g\Delta S_{lat}}$

(4) Average $G_{long} = \dfrac{(V_1 \cos \theta)^2 - V_2^2}{2g\Delta S_{long}}$

(5) Average $G_{total} = \left[(\text{Avg. } G_{lat})^2 + (\text{Avg. } G_{long})^2\right]^{1/2}$

Figure A1, GEOMETRIC REPRESENTATION OF PHOTOGRAPHIC ANALYSIS

TABLE A1

TEST 505 T1-A

High-Speed Film Data

Time (msec)		Displacement (ft)	
-69		-4.5	V_1 = 65.2 ft/sec
-46		-3.0	
-23		-1.5	
0	Impact	0	
10		0.7	
20		1.3	
31		2.0	
41		2.6	
51		3.3	
61		3.8	
71		4.4	
82		4.9	
92		5.5	
102		5.9	
112		6.4	
122		6.8	
143		7.6	
163		8.4	
184		9.2	
204		10.1	
225		10.9	
245		11.7	
265		12.5	
286		13.4	V_2 = 40.2 ft/sec
306		14.2	
327		15.0	
347		15.9	
367		16.6	
388		17.5	

Time (msec)	Displacement (ft)
(Continued)	
408	18.3
429	19.1
449	19.9
469	20.7
490	21.4
510	22.3
531	23.1
551	23.8
571	24.6
592	25.3
612	26.1
633	26.8
653	27.5
674	28.3
694	29.0
714	29.8
735	30.4
755	31.1
776	31.8
796	32.5
816	33.2
837	33.8
857	34.5
878	35.2
898	35.8
918	36.4
939	37.1
959	37.7

V_3 = 39.2 ft/sec

TABLE A2

TEST 505 T1-B

High-Speed Film Data

Time (msec)		Displacement (ft)	Time (msec)	Displacement (ft)
-81		-6.7	(Continued)	
-71		-5.8	153	11.1
-61		-5.1	163	11.6
-51		-4.2	173	12.0
-41		-3.4	184	12.5
-31		-2.5	194	12.9
-20		-1.7	204	13.4
-10		-0.9	214	13.8
0	Impact	0	224	14.2
10		0.8	234	14.6
20		1.6	245	14.9
31		2.4	255	15.4
41		3.2	265	15.8
51		4.0	275	16.2
61		4.8	286	16.6
71		5.6	306	17.4
82		6.4	326	18.2
92		7.2	347	19.0
102		7.9	367	19.8
112		8.6	388	20.5
122		9.2	408	21.3
133		9.9	428	22.0
143		10.5		

V_1 = 82.7 ft/sec

*V_2 = 41.3 ft/sec

*V_3 = 39.1 ft/sec

*Vehicle snagged post No. 17, and consequently did not become parallel to the rail; sidewise skidding and loss of contact for only a short time interval do not permit determination of these values to the accuracy reported in other tests in this series.

TABLE A3

TEST 505 T1-C

High-Speed Film Data

Time (msec)		Displacement (ft)	
-60		-5.1	V_1 = 85.0 ft/sec
-50		-4.3	
-40		-3.4	
-30		-2.6	
-20		-1.7	
-10		-0.9	
0	Impact	0	
10		0.9	
20		1.7	
30		2.5	
40		3.4	
50		4.2	
60		5.0	
72		5.9	
82		6.7	
92		7.6	
103		8.3	
113		9.2	
123		9.9	
133		10.7	
144		11.4	
154		12.1	
164		12.8	

Time (msec)	Displacement (ft)	
(Continued)		
174	13.6	
184	14.3	
195	15.1	
205	15.7	
215	16.4	
225	17.1	V_2 = 61.1 ft/sec
236	17.8	
246	18.4	
256	19.1	
266	19.7	
277	20.3	
287	20.9	
297	21.5	
308	22.1	
318	22.6	
328	23.3	
338	23.9	
348	24.6	
359	25.2	
369	25.8	
379	26.4	
(Continued)		

Table A3 (Continued)

Test 505 T1-C

Time (msec)	Displacement (ft)	
(Continued)		
390	26.9	
400	27.6	
410	28.2	
420	28.9	
430	29.5	
441	30.2	
451	30.8	
461	31.4	
472	32.0	
482	32.6	
492	33.2	V_3 = 58.3 ft/sec
502	33.8	
512	34.4	
523	35.1	
533	35.7	
543	36.2	
554	36.9	
564	37.4	
574	38.0	
584	38.6	
594	39.2	
605	39.8	

TABLE A4

TEST 505 T1-D

High-Speed Film Data

Time (msec)		Displacement (ft)	
-81		-7.3	
-70		-6.2	
-58		-5.1	
-46		-4.1	
-35		-3.1	
-23		-2.1	
-12		-1.0	
0	Impact	0	V_1 = 90.1 ft/sec
13		1.2	
26		2.3	
39		3.5	
51		4.5	
64		5.6	
77		6.6	
90		7.7	
103		8.7	
116		9.7	
129		10.6	
141		11.7	
154		12.7	
167		13.7	
180		14.7	
193		15.8	
206		16.8	
219		17.8	
231		18.8	
244		19.8	V_2 = 80.4 ft/sec

Time (msec)	Displacement (ft)	
(Continued)		
257	20.8	
270	21.8	
283	22.8	
296	23.9	
309	24.9	
321	25.9	V_3 = 79.7 ft/sec
334	26.9	
347	28.0	
360	28.9	
373	30.0	
386	31.1	
399	32.0	
412	33.1	
424	34.1	
437	35.1	
450	36.1	
463	37.1	
476	38.1	
489	39.1	
502	40.1	
514	41.0	
527	42.1	
540	43.1	
553	44.0	
566	45.0	
579	46.0	

A P P E N D I X B

Accelerometer Data

ACCELEROMETER DATA

An attempt was made to reconcile the data recorded on accelerometers mounted parallel and perpendicular to the longitudinal axis of the colliding vehicle with the data observed from high-speed films of the collision incident. Such reconciliation was not affected during the course of this study. However, the accelerometer traces are included in this appendix for consideration by readers of this report.

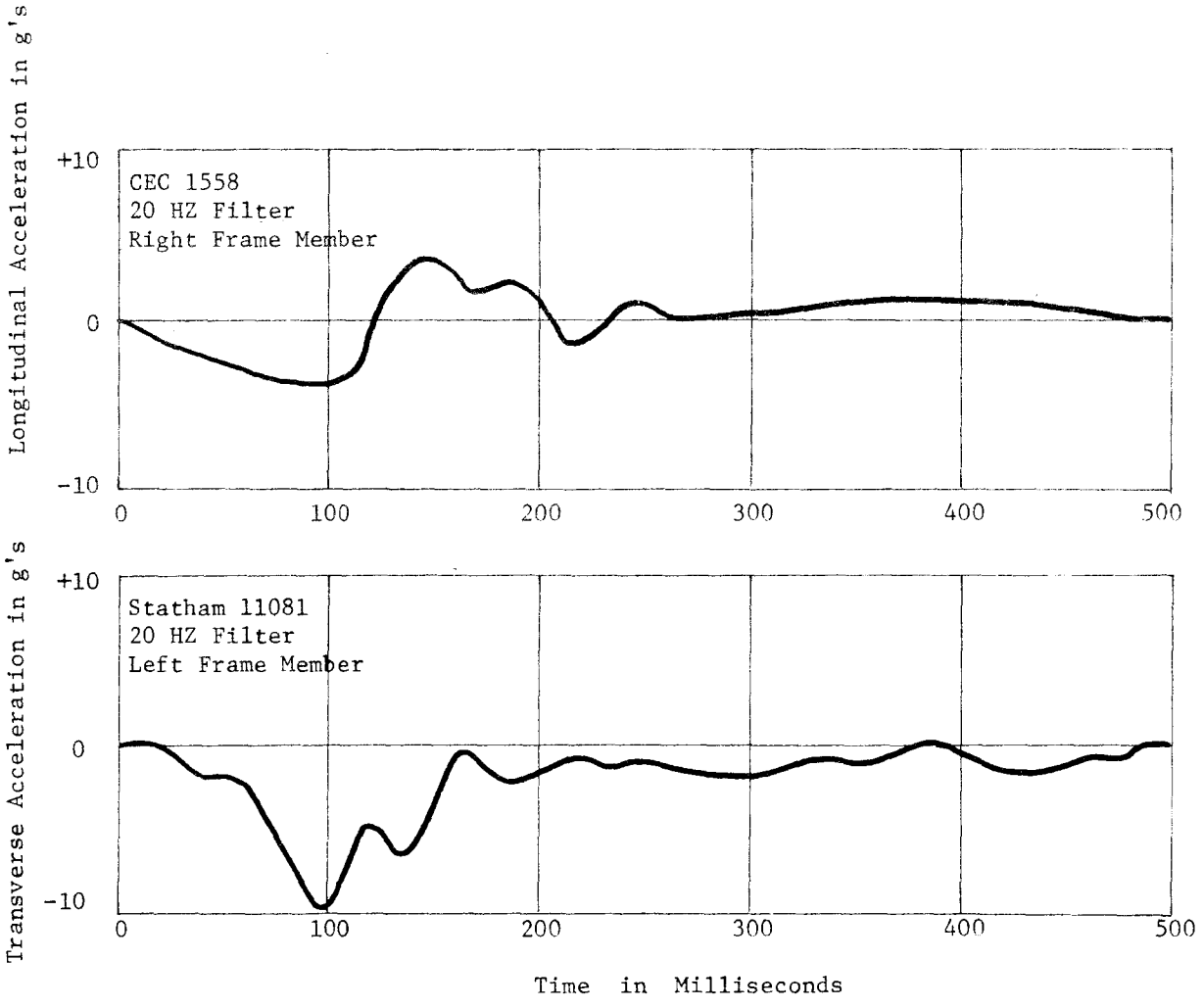

Figure B1, Accelerometer Data, Test 505T1-A.

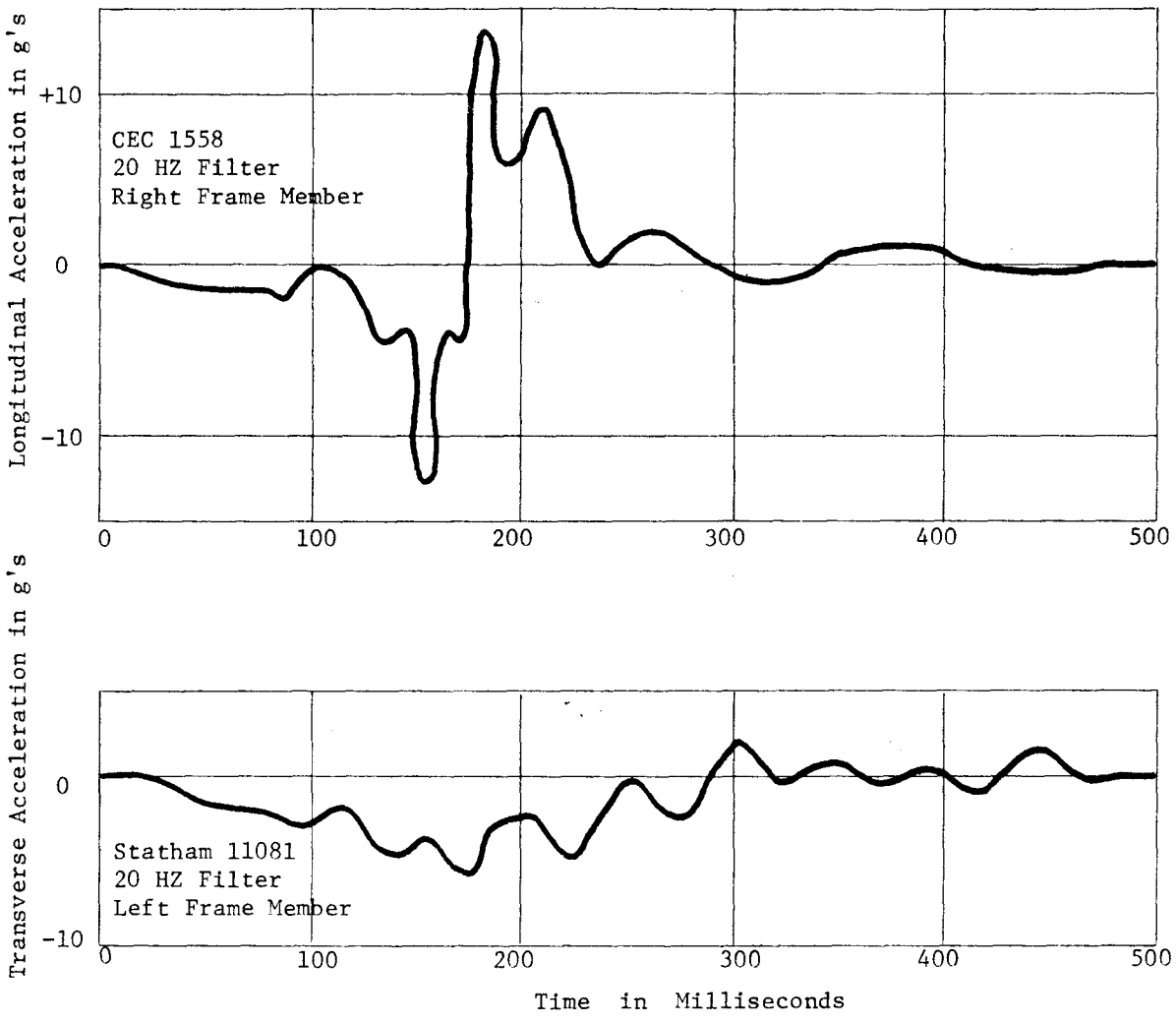

Figure B2, Accelerometer Data, Test 505T1-B.

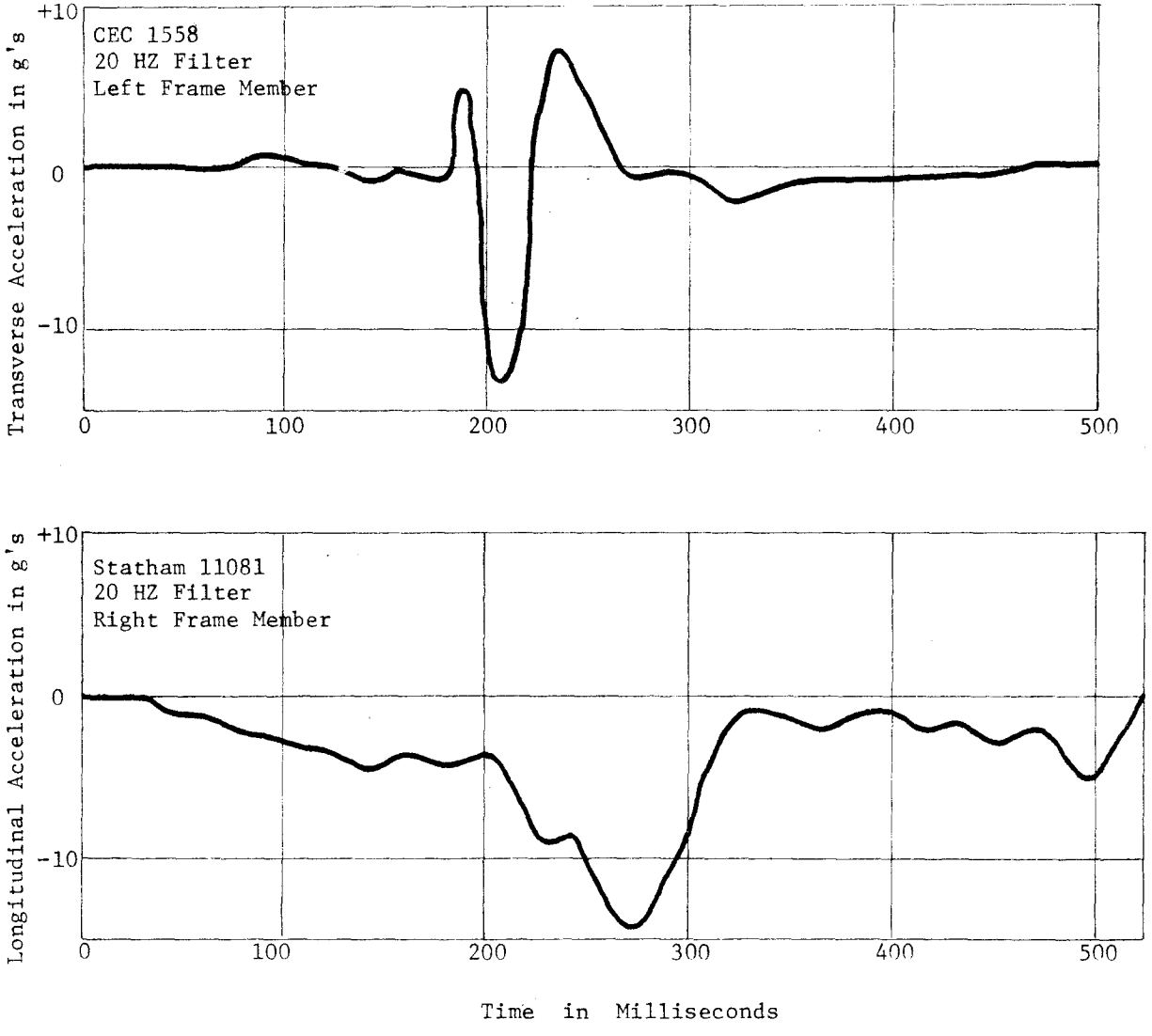

Figure B3, Accelerometer Data, Test 505T1-C.

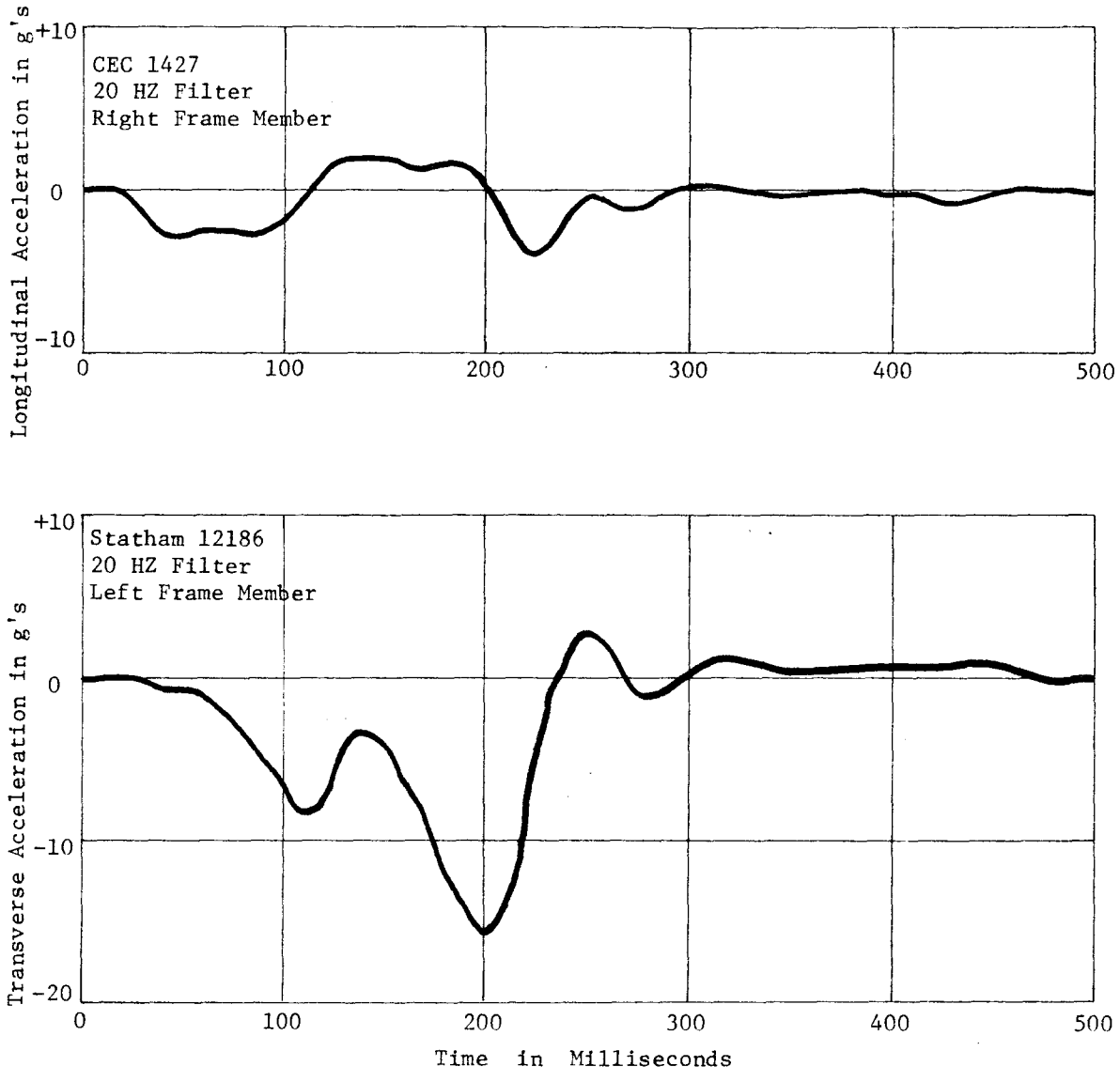

Figure B4, Accelerometer Data, Test 505T1-D.

TECHNICAL MEMORANDUM 505-11

Texas Transportation Institute
Texas A&M Research Foundation

PERFORMANCE OF THE "HI-DRO CUSHION" VEHICLE IMPACT ATTENUATOR

A Test and Evaluation Report on Contract No. CPR-11-5851

U.S. Department of Transportation

Federal Highway Administration

by

Gordon G. Hayes
Physics Research Associate

Don L. Ivey
Associate Research Engineer

and

T. J. Hirsch
Research Engineer

These crash tests and evaluations were conducted under the Office of Research and Development, Structures and Applied Mechanics Division's Research Program on Structural Systems in Support of Highway Safety (4S Program). The opinions, findings, and conclusions expressed in this report are those of the authors and not necessarily those of the Federal Highway Administration.

NOTE: For the reader who is interested in gaining a general idea of the value of this particular arresting system and not in the details necessary to document the technical aspects of this study, the authors recommend reading page 2, noting the comparative values of speed and deceleration on page 10, and scanning the photographs in this report.

August 1970

INTRODUCTION

As part of its 4S Program (Structural Systems in Support of Highway Safety), the Bureau of Public Roads sponsored a series of vehicle crash tests to help evaluate the "HI-DRO Cushion" Vehicle Impact Attenuator. The testing was conducted in September, October, and November of 1969.

The impact attenuator has been analyzed and simulated by digital computer under the direction of Dr. Charles Y. Warner of Brigham Young University under another portion of the 4S Program.[1*] This system is now handled by Energy Absorption Systems, Inc. of Chicago.

The crash cushion consists of an assembly of plastic, water-filled tubes with orifices in the caps. When the Hi-Dro Cell barrier is struck by a vehicle, the water in the tubes is forced out the orifices. This reaction of individual tubes results in a predictable barrier deformation force characteristic. Augmenting the vehicle stopping force is the barrier inertia.

DESCRIPTION OF SYSTEM

The basic unit of the crash cushion is the "HI-DRO CUSHION CELL", which is a hollow cylinder or envelope made of plastic material (see Figure 1). The cap contains orifices through which the water in the cell can be expelled. The "stiffness" of the cell is determined by the orifice areas. These cells were assembled as shown in Figures 2, 3, and 4 for the first three tests.

The 138 cells were divided among eight "bays" separated by diaphragms as shown in Figure 2. The third "bay" from the front was void of cells due to design factors concerning the profile of the acceleration pulse

---

*Superscript numerals refer to corresponding numbers in the Selected References.

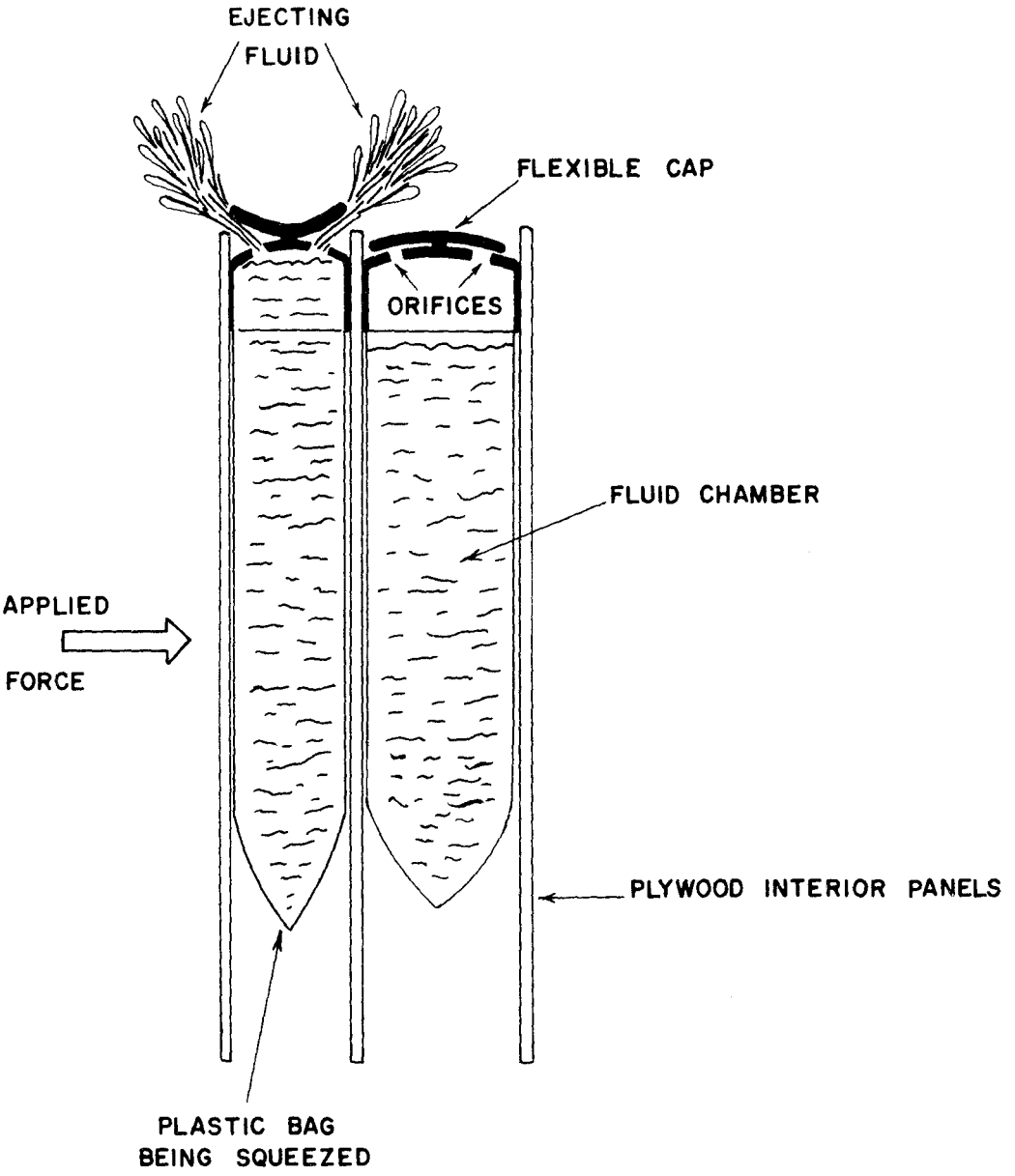

FIGURE 1, FUNCTION OF HI-DRO CELL

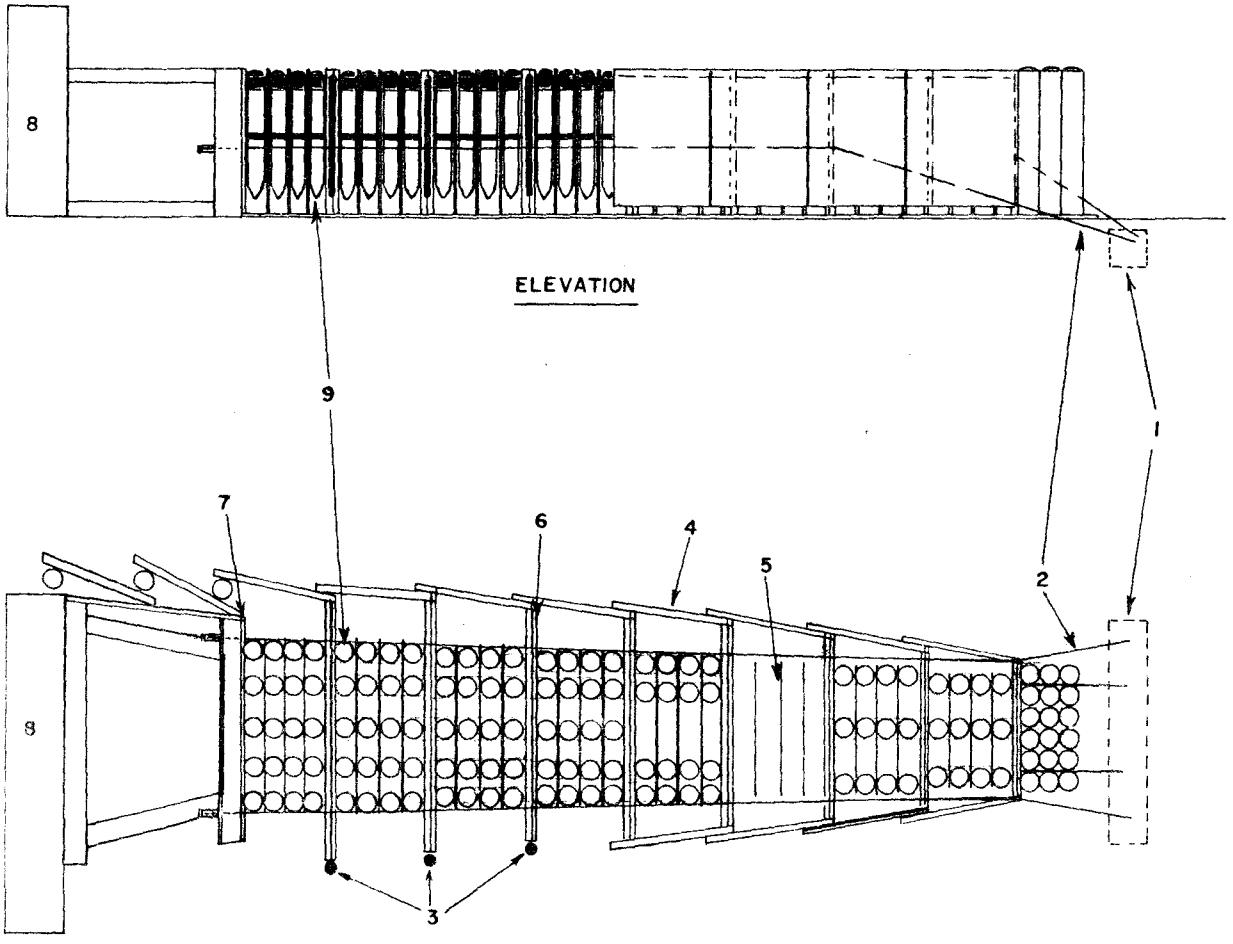

1 FRONT ANCHOR
2 MAIN RESTRAINING CABLES
3 STEEL BARS TO SIMULATE WEIGHT OF SIDE DEFLECTION PANELS
4 DEFLECTION PANELS
5 INTERIOR PANELS (THIS BAY VOID OF CELLS)
6 TRANSVERSE DIAPHRAGMS
7 STEEL BACKUP PLATE
8 RIGID CONCRETE WALL
9 HI-DRO CUSHION CELLS

FIGURE 2, TTI CONFIGURATION OF HI-DRO CELL SANDWICH UNIT

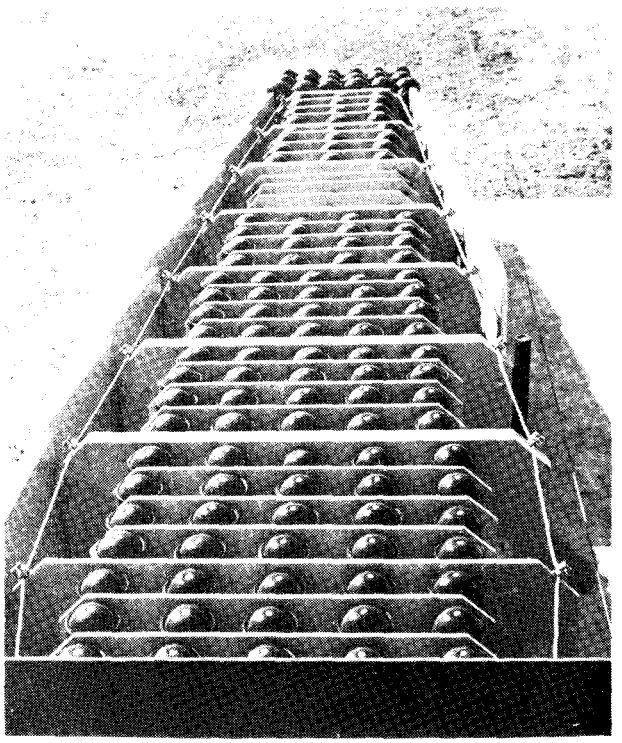

Figure 3. Top View of Barrier.

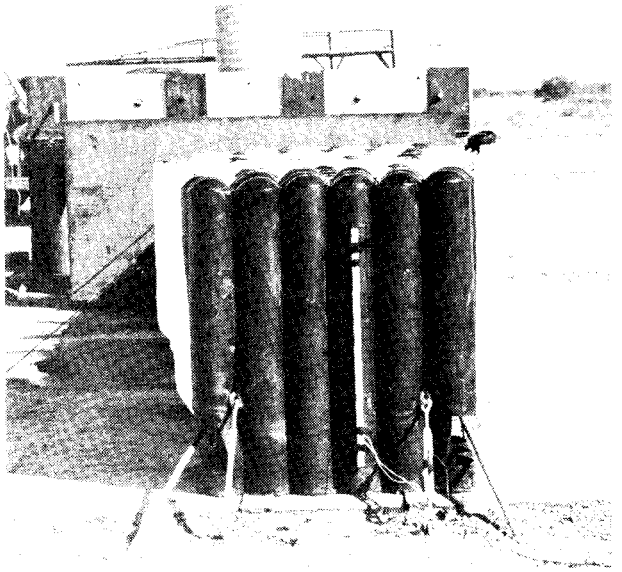

Figure 4. Front of Barrier.

produced during impact.[1] The diaphragms separating the bays were made of 1 1/2 in. fiberglassed plywood. The three diaphragms closest to the rigid barrier each had two 1/4 in. steel plates attached. The rows of cells in each bay were separated by 1/4 in. Duraply interior panels.

The "fish-scale" fender panels were designed to provide redirectional ability during angled impacts while providing minimum interference during head-on crashes. These panels were hinged to the transverse diaphragms, and were made of 1 1/4 in. fiberglassed plywood in the first three tests.

In the final two tests, the five front fender panels on the impacted side were made of fiberglassed Hexcel, which is a lightweight, high-strength, paper material resembling a honeycomb. In addition, the wood portions of the second and third diaphragms from the rear of the attenuator were removed and the 12-gage steel plate in the last diaphragm was eliminated in order to maintain the previous weight distribution after the modified fender panels had been installed. The 7/8 in. diameter restraining cables were increased to 1 in., and the last diaphragm was increased in width to provide a constant diverging side slope. The steel rods on the "off" side of the barrier (item 3 in Figure 2) simulated the weight of deflection panels which were left off in order to avoid modification of the width of the back-up wall.

TEST PROGRAM

The test conditions for the series are shown in Table 1. For the angled tests, the impact point was approximately the rear edge of the first fender panel. The side of the unit diverged from the centerline by 6°09', making an impact angle with the side of the cushion of about 26°.

Four accelerometers were used in each test vehicle, two on each longitudinal frame member. For head-on tests, all were mounted longitudinally, while in the angled tests, one on each side was mounted transversely. In addition, a mechanical Impact-O-Graph was mounted in the vehicle trunk as a secondary source of acceleration data.

An Alderson anthropometric dummy simulated a driver, and was secured by a seat belt attached to a load cell for measuring seat belt force.

Redlakes Hycam cameras, operating at 500 frames per second, recorded the events for time-displacement analysis. A Photosonics camera (500 f.p.s.) was mounted over the barrier looking vertically downward. Much of the event was obscured in this view by the ejected water. Other cameras covered each test for documentary purposes.

Film and accelerometer data are presented in the appendix. The accelerometer traces were obtained through a 20 HZ low-pass active filter to eliminate the effects of vehicle "ringing" and other noise, and to permit consistent analysis of the traces. The original unfiltered data is preserved on magnetic tape.

The initial velocity and stopping distance, or distance in contact, can be measured accurately from the high-speed films, and an average deceleration can be calculated from these values. This average deceleration can be compared with that from the electromechanical accelerometers which also indicate peak g's.

TABLE 1

TEST CONDITIONS

TEST	A	B	C	D	E
Vehicle	1964 VW Sedan	1961 Pontiac Sedan	1963 Pontiac Sedan	1962 Renault Sedan	1964 Dodge Sedan
Weight, lbs	1820	4650	4410	1680	3710
Initial Speed, mph	42	64	54	59	59
Initial Angle with Barrier Centerline, degrees	0	0	20	0	20
Propulsion	Self Powered	Self Powered	Self Powered	Towed	Self Powered

DESCRIPTION OF TESTS

Table 2 summarizes the pertinent test data. In the first test, a Volkswagen sedan weighing 1820 lbs impacted the barrier head-on at 42 mph. The vehicle was stopped in 13.2 ft with an average deceleration of 4.5 g's, and a peak deceleration of 14.6 g's. The vehicle damage was not severe (see Figures 5 through 8).

The second test utilized a Pontiac sedan weighing 4650 lbs, impacting head-on, with an initial speed of 64 mph. The average deceleration over 17.3 ft and 0.340 sec was 7.9 g's, while the maximum deceleration of 13.4 g's was lower than that of the first test (see Figures 9 through 13).

In the third test, a Pontiac sedan weighing 4410 lbs struck the cushion at 54 mph and at an angle of 20° with the barrier centerline. The vehicle had begun to redirect and had rotated approximately 5° when the main restraining cables pulled out of their front anchorage connections. The left front of the vehicle went head-on into the rigid barrier, and the vehicle rolled over on its right side (see Figures 14 through 23).

The cables pulled out of their connectors due to an improper installation procedure. A lead filler was used instead of the more desirable babbitt metal. All cushion units in service are equipped with factory-fabricated cables and connectors. Because of this installation error, this test cannot be judged representative of the performance of the barrier. In spite of this, the films showed a very tolerable average deceleration of 5.8 g's over 16.7 ft and 0.340 sec, while the accelerometers detected a peak of only 14.6 g's.

TABLE 2

SUMMARY OF DATA

TEST	A	B	C	D	E	Rigid Wall
VEHICLE WEIGHT, lbs	1820	4650	4410	1680	3710	3270
ANGLE OF IMPACT, deg	0	0	20	0	20	0
FILM DATA						
Initial Speed, mph	42	64	54	59	59	53
ft/sec	61.6	93.6	79.3	86.3	86.6	78.3
Average Longitudinal Deceleration, g's	4.5	7.9	5.8	7.1	4.9	25.0
Stopping Distance, ft	13.2	17.3	16.7	16.3	19.4*	3.8
Time in Contact, sec	0.740	0.340	0.340	0.580	0.340	0.099
LONGITUDINAL ACCELEROMETER DATA						
Max. Deceleration, g's	14.6	13.4	14.6	15.6	8.9	35.0
Avg. Deceleration, g's	3.1	6.8	5.6	7.3	4.6	18.0
Time, sec	0.46	0.47	0.42	0.29	0.33	0.13
TRANSVERSE ACCELEROMETER DATA						
Max. Deceleration, g's	--	--	5.7	--	9**	--
Avg. Deceleration, g's	--	--	1.1	--	2	--
Time, sec	--	--	0.42	--	0.33	--
ATTENUATION INDEX						
$AI_{(max)} = \frac{G_{max}\ (Test)}{G_{max}\ (rigid\ wall)^{***}}$	0.4	0.2	0.3	0.3	0.2	0.7
$AI_{(avg)} = \frac{G_{avg}\ (Test)}{G_{avg}\ (rigid\ wall)^{***}}$	0.2	0.2	0.2	0.2	0.1	0.7
VEHICLE DEFORMATION, ft	1.04	1.83	3.33	2.33	0.83	3.82

*Distance in contact.
**From Impact-O-Graph (accelerometers malfunctioned)
***G_{max} (calculated from rigid wall impacts) = $0.9V,^2$
G_{avg} (calculated from rigid wall impacts) = $0.574V,^2$
where V = initial speed in mph.

Before the fourth test, the modifications mentioned in the "Description of System" section were made. The vehicle was powered by a towing system which disengaged from the vehicle before impact (see Figures 24 and 25).

In this test a 1680 lb Renault was directed head-on into the cushion at 59 mph. The stopping distance of 16.3 ft gave an average deceleration of 7.1 g's (over 0.580 sec), and the maximum deceleration was 15.6 g's.

The vehicle apparently struck the front of the barrier about one foot off-center and started a yaw and roll motion, finally rolling over on its top after most of the kinetic energy had been absorbed (see Figures 26 through 29).

The final test was another 20° impact. A 3710 lb Dodge sedan traveling at 59 mph was used. This was the only test in which the vehicle left the barrier with significant speed. The average longitudinal deceleration of 4.9 g's was calculated over the distance in contact of 19.4 ft by noting the speeds at the beginning and end of this contact. The maximum deceleration was 8.9 g's. Sequential photographs of the test in progress are shown in Figures 31 and 32.

In this last test, the vehicle began to ramp, or climb up the side of the barrier. It became completely airborne by as much as 1.5 ft for about 20 ft, and upon recontacting the ground rolled over on its left side before coming to rest upright. Examination of vehicle and barrier indicate that a slight contact was made with the upper corner of the rigid steel wall. The path of vehicle contact up the side panels can be seen in Figure 34.

$$G_{avg} = \frac{V^2}{\rho g s} \qquad \frac{(78.3)^2}{(\rho)(32.2)\,3.8} = 25$$

The steel barrier in front of the concrete wall was pulled away from the concrete at the bottom about 6 inches and at the top about 2 inches (see Figures 35 and 36). The restraining cables were fastened to this steel barrier, so this could allow as much as 2 ft of additional localized lateral movement to the cushion.

The damage to the barrier in the head-on tests was relatively minor, usually in the form of torn plastic cells which were easily replaced. The following listing of parts replaced gives an idea of the severity of damage to the barrier in each test:

Test A -- No parts replaced.

Test B -- 25 cartriges replaced, 19 of which were repairable.

Test C -- Failure of anchorages caused damage which necessitated replacement of several fender panels, diaphragms, and interior panels. (Some replacements were made in the course of the previously mentioned modification of the barrier structure.)

Test D -- No parts replaced.

Test E -- Damage to fender panels only. No replacements were made because no further tests were planned.

FIELD EXPERIENCE

One severe collision with a HI-DRO cushion located in New Orleans, Louisiana, has recently been reported.[6]

On April 2, 1970, a vehicle skidded sideways into the barrier on rain-slick pavement at an estimated speed of 70 mph. The driver's side of the vehicle impacted the barrier nose. The driver, who was unrestrained, suffered cuts and bruises, but was treated and released. The vehicle was towed to a garage, and then driven inside. The authors of that report feel that the collision would have undoubtedly been fatal if the impact attenuator had not been there.

CONCLUSION

Pertinent data from a rigid wall test[3] conducted in March of 1969 is included in Table 2 for comparison purposes. This vehicle was a 1963 Plymouth sedan weighing 3270 lbs which was directed head-on into a rigid concrete wall at 53 mph. The vehicle stopped in 3.8 ft (vehicle deformation) with an average deceleration of 25 g's and a peak of 35 g's.

Table 2 also includes a comparison of Attenuation Indices, which are defined as the ratios of decelerations experienced in the cushioned impacts with those calculated for rigid barrier impacts. The values experienced in a rigid wall crash will depend in part on the crush characterisitcs of the impacting vehicle. For this reason the Index for the rigid wall test is not unity. The more attenuation caused by the inclusion of a crash cushion, the smaller will be the Attenuation Index.

The accelerometer traces are shown in the Appendix. Note that the traces usually consist of more than one major peak. One or more of the secondary peaks are related to pressure waves reflecting from the rear of the barrier, while the initial peak is primarily due to inertial forces.[4]

The predictions of the mathematical model developed at Brigham Young University showed very good agreement with the test data for the head-on tests.[1] No predictions were made for the angled tests.

Great design flexibility is possible by varying orifice size and number, arrangement of cells, size of cells used, and amount of fluid in the cells.

The 4S Program of the Federal Highway Administration uses the following criteria for development and testing of protective barriers:[5]

Vehicle weight range	-	2,000 to 4,500 lbs.
Vehicle speed	-	60 mph.
Impact angle	-	Up to 25° as measured from the direction of the roadway.
Average permissible vehicle deceleration	-	12 g's maximum while preventing actual impacting or penetration of the roadside hazard.
Maximum occupant deceleration onset rate	-	500 g's per second.

The observed average deceleration levels were significantly below the 12 g level in all tests. The accelerometer traces showed that the 12 g level was exceeded by peak decelerations no longer than 0.03 seconds except in Test D which was a head-on test of a vehicle weighing less than the minimum weight specifications.

Other tests on this type of barrier have been conducted by Rich Enterprises, California Division of Highways, and Brigham Young University. The results of these tests have, in general, shown acceptable performance of this vehicle impact attenuator.

SELECTED REFERENCES

1. "Development of a Hydraulic-Plastic Barrier for Impact-Energy Absorption." Final report on BPR-DOT Contract No. FH-11-6909. Department of Mechanical Engineering, Brigham Young University.

2. Emori, Richard I., "Analytical Approach to Automobile Collisions." SAE Paper 680016, Engineering Congress, Detroit, January 1968.

3. Ivey, Don L., Buth, Eugene, and Hirsch, T. J., "Feasibility of Lightweight Cellular Concrete Vehicle Crash Cushions." Technical Memorandum 505-9, Texas Transportation Institute, January 1970.

4. Warner, C. Y., "Hydraulic-Plastic Cushions for Attenuation of Roadside Barrier Impacts." *Highway Research Record No. 259.*

5. Tamanini, F. J. and Viner, John G., "Structural Systems in Support of Highway Safety." ASCE Meeting Preprint 930, July 21-25, 1969.

6. Walters, William C. and Bokun, Steve G. Performance Report of the HIDRO Cushion Crash Attenuation Devices, Highway Research Report, Louisiana Department of Highways, June, 1970.

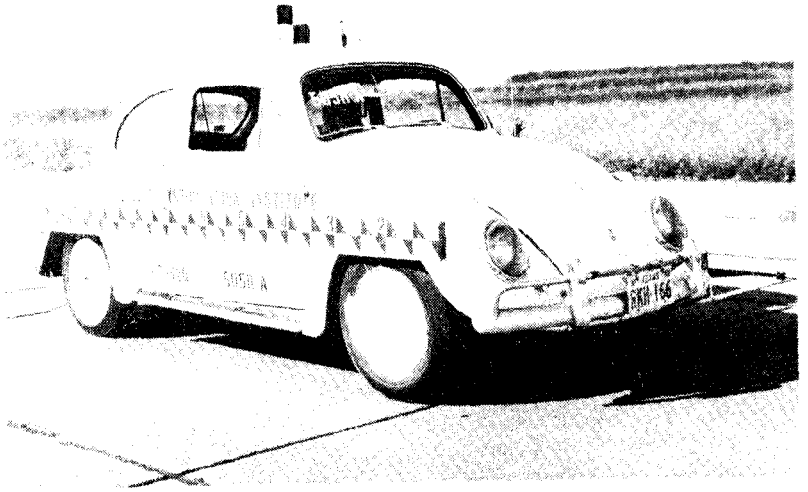

Figure 5, Vehicle Before Test A.

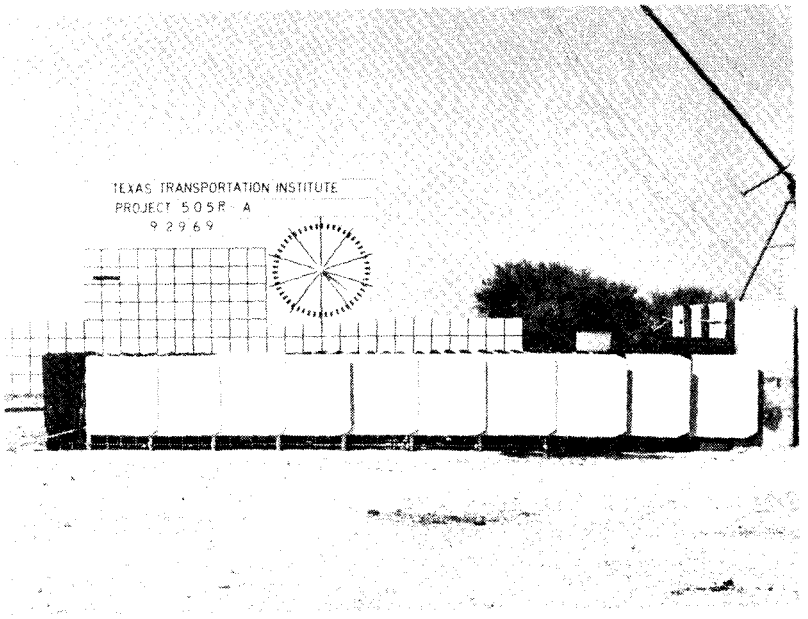

Figure 6, Barrier Before Test A.

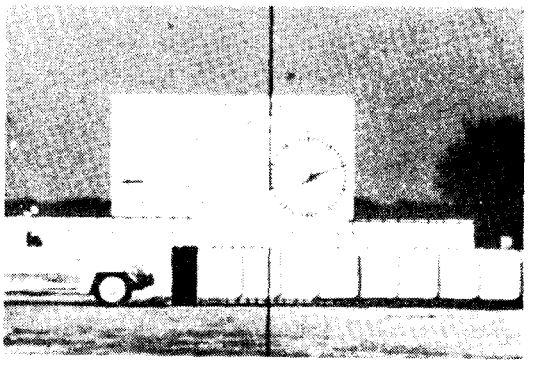

1

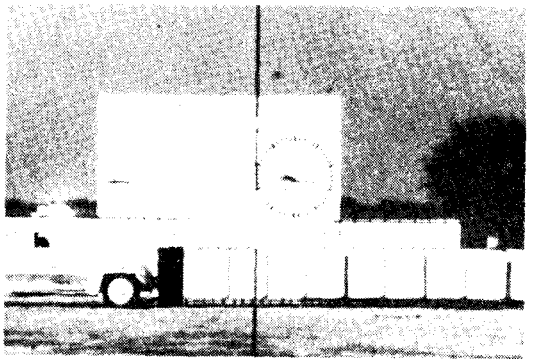

2

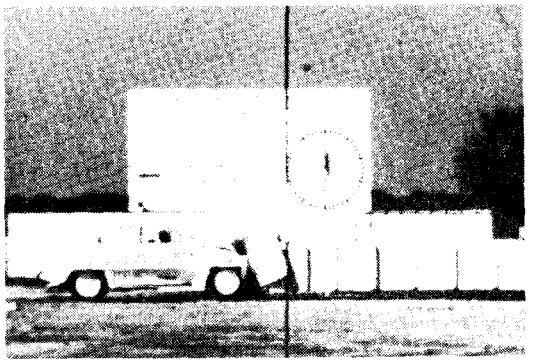

3

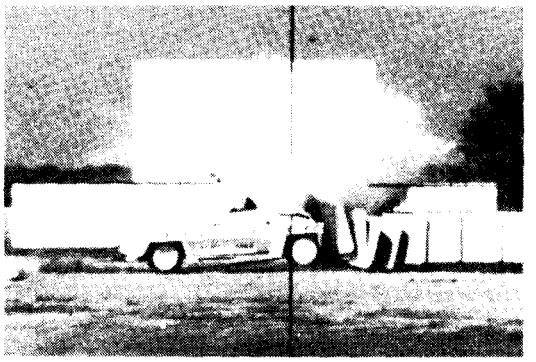

4

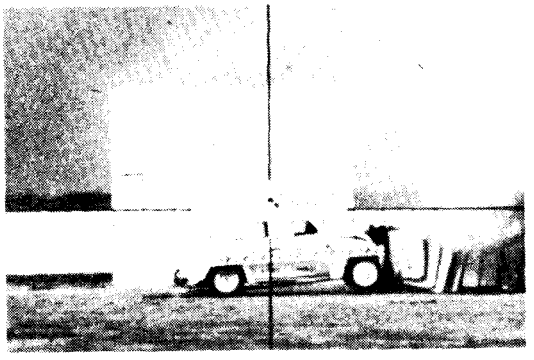

5

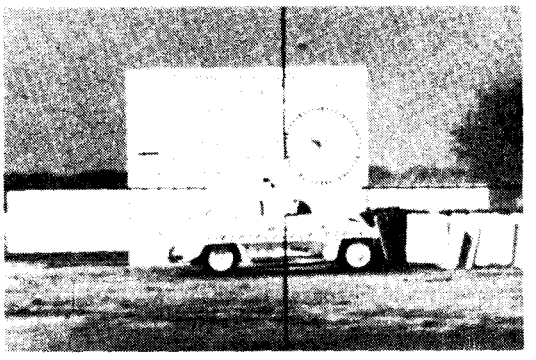

6

Figure 7. Sequential Photographs of Test A.

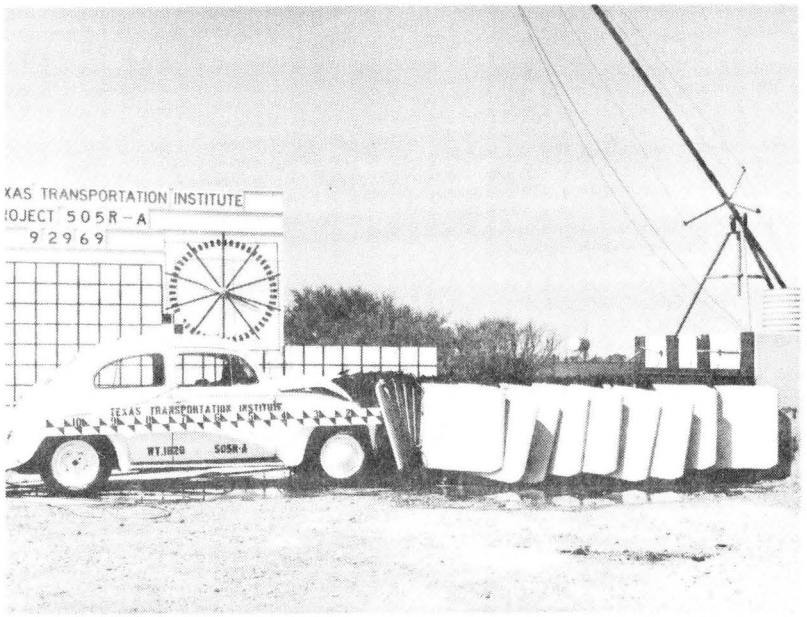

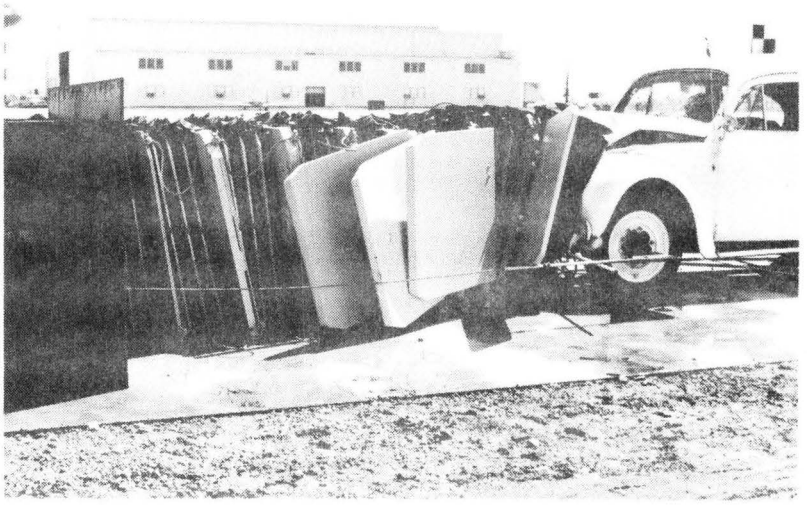

Figure 8, Vehicle and Barrier After Test A.

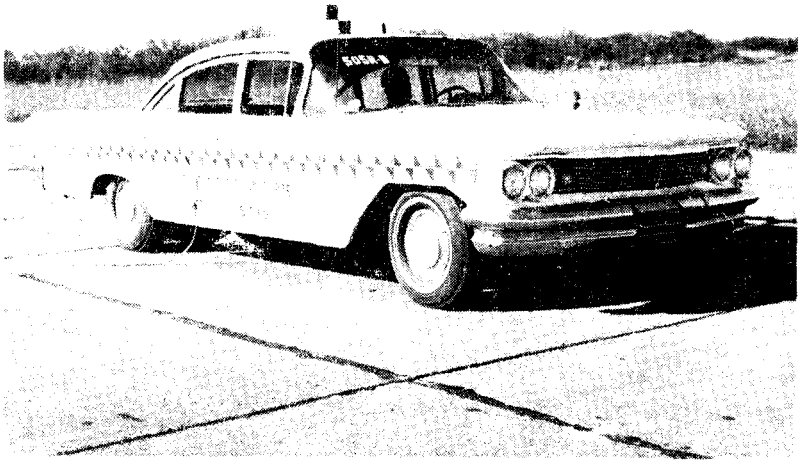

Figure 9, Vehicle Before Test B.

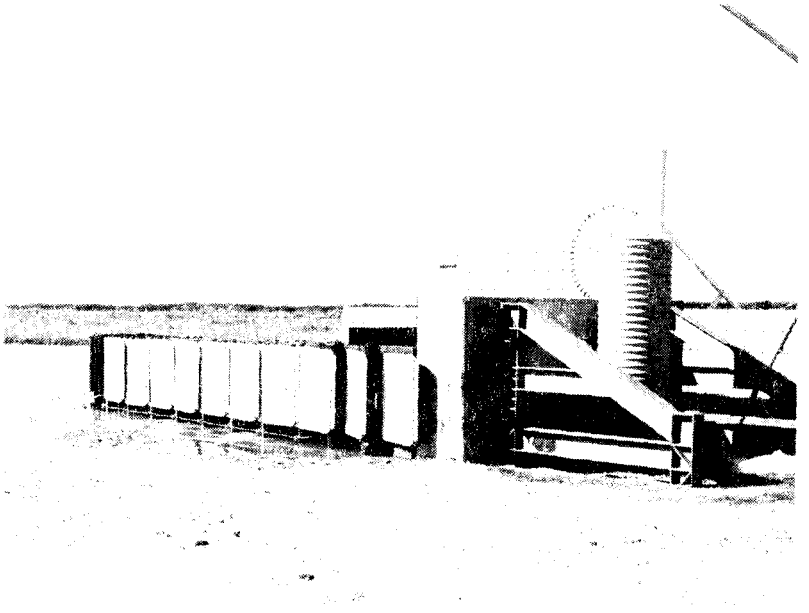

Figure 10, Barrier Before Test B.

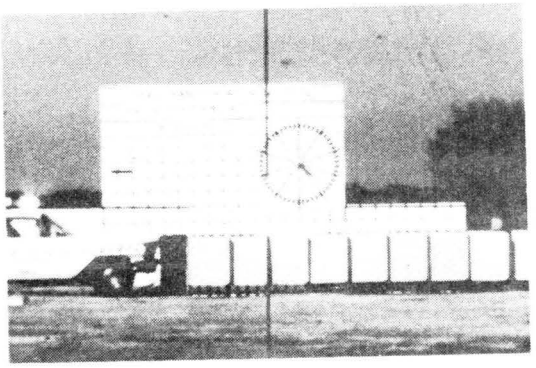

1

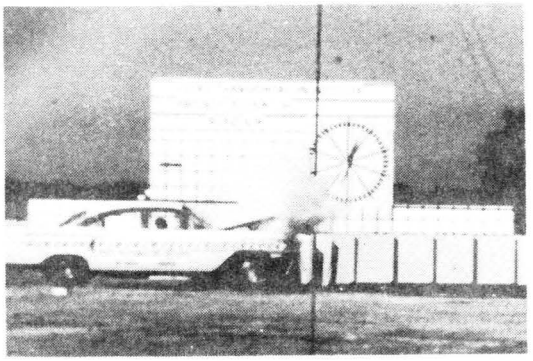

2

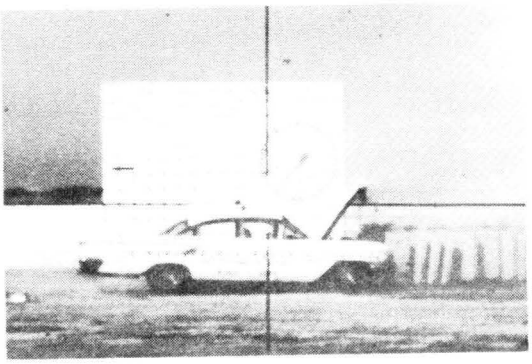

3

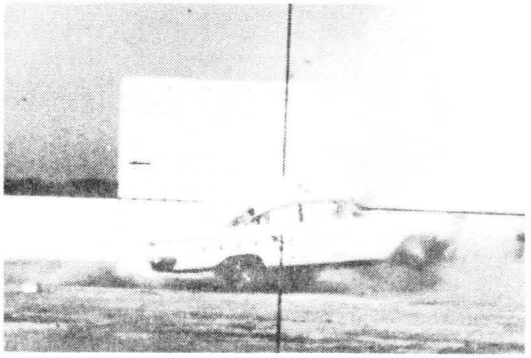

4

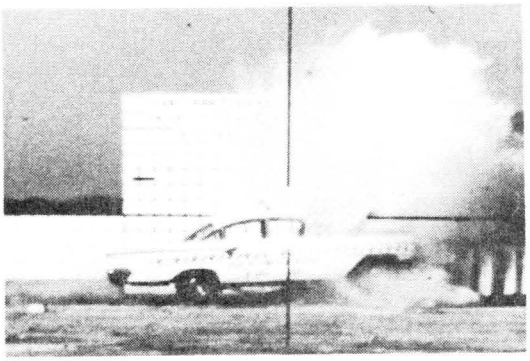

5

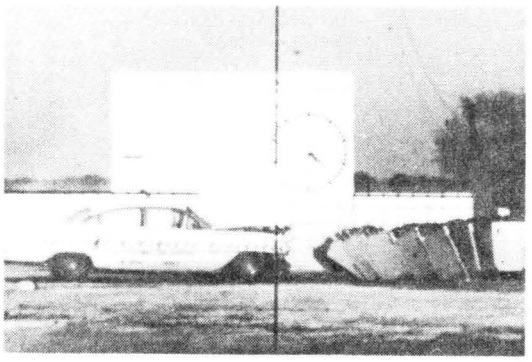

6

Figure 11, Sequential Photographs of Test B.

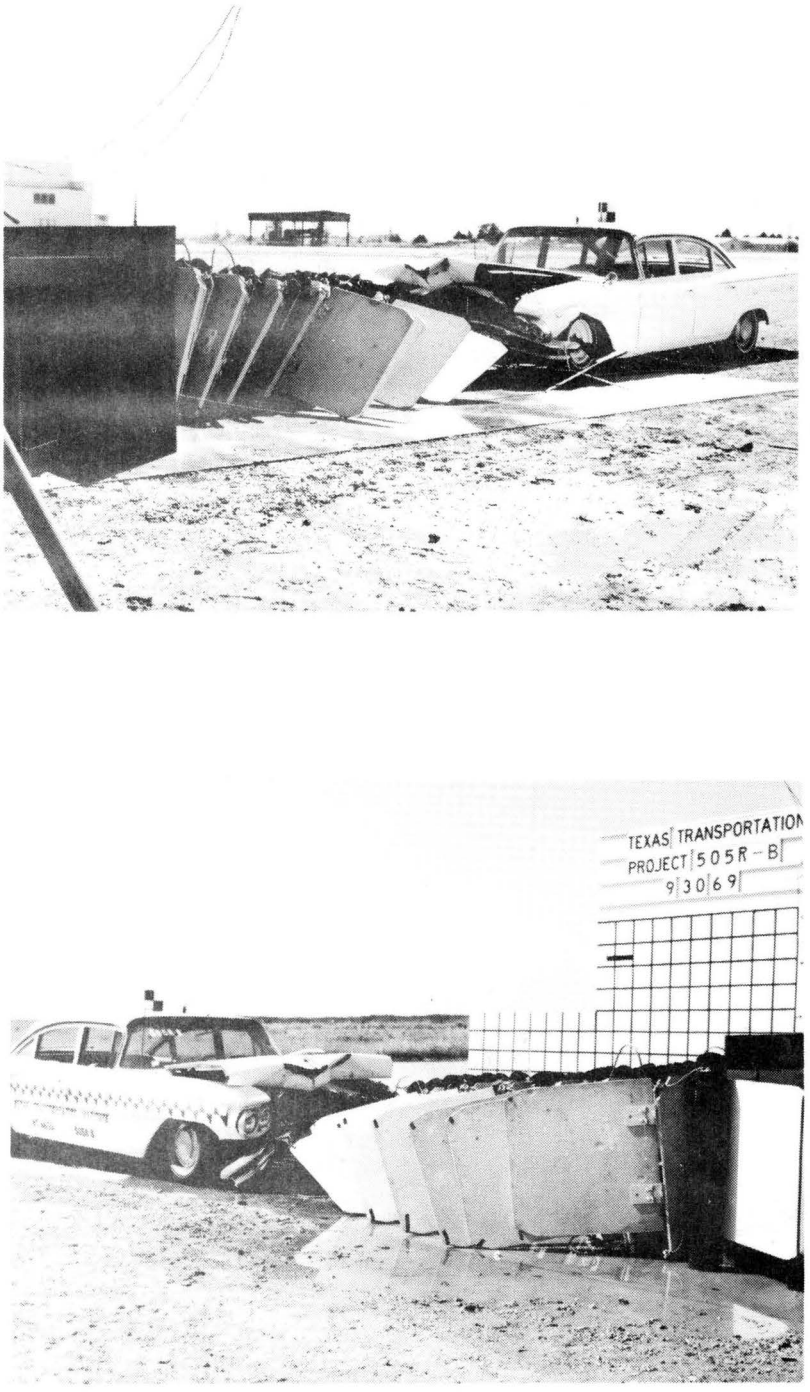

Figure 12. Vehicle and Barrier After Test B.

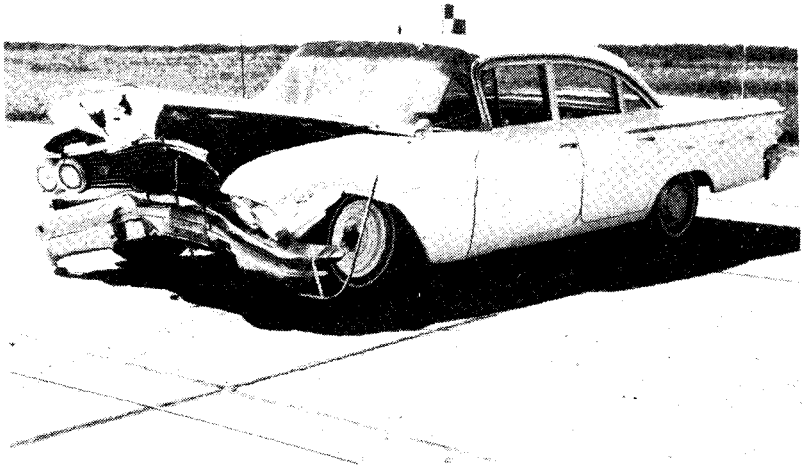

Figure 13. Vehicle After Test B.

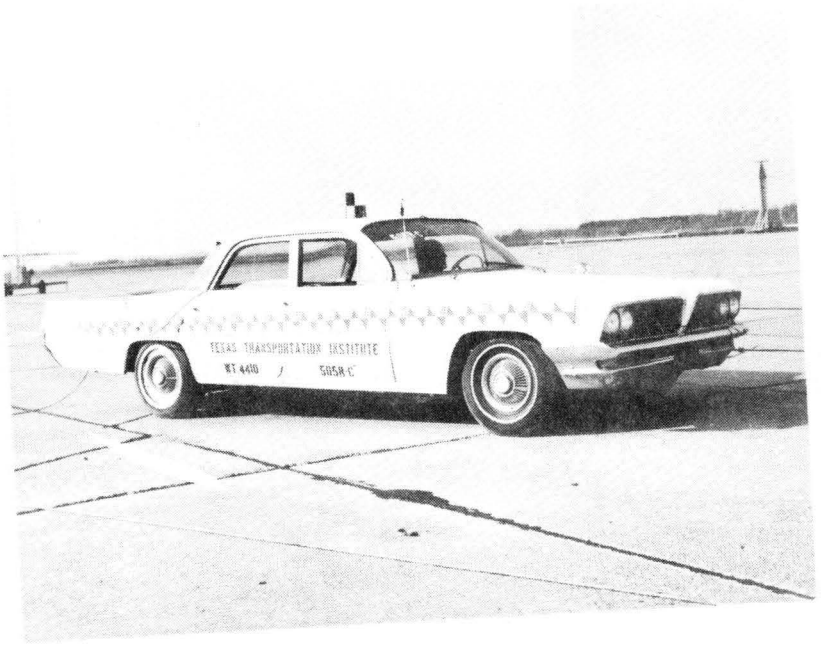

Figure 14, Vehicle Before Test C.

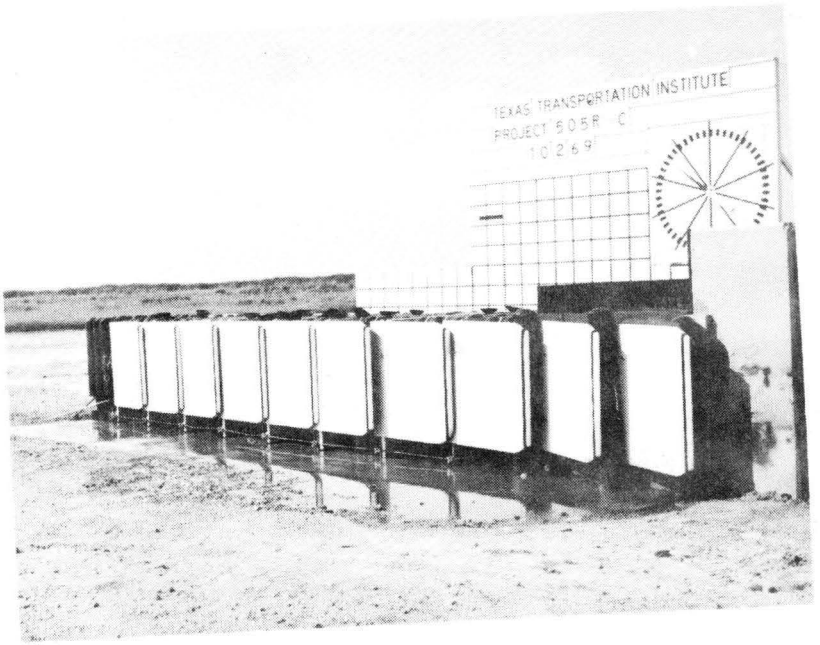

Figure 15, Barrier Before Test C.

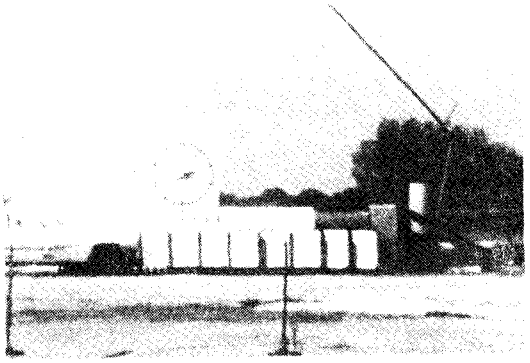

1

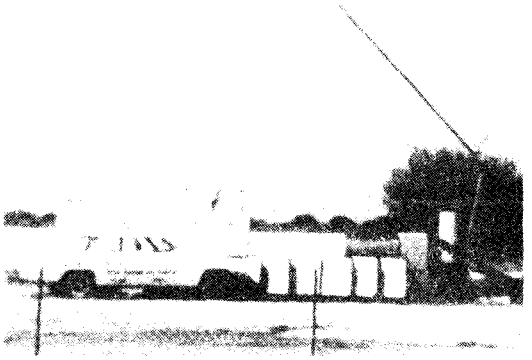

2

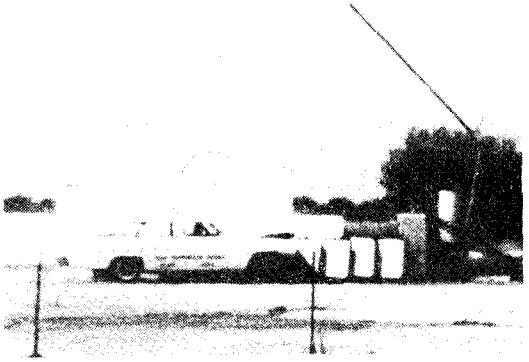

3

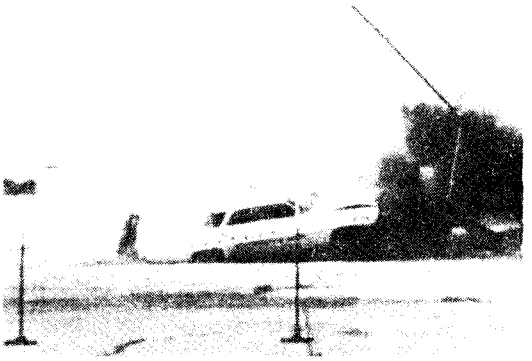

4

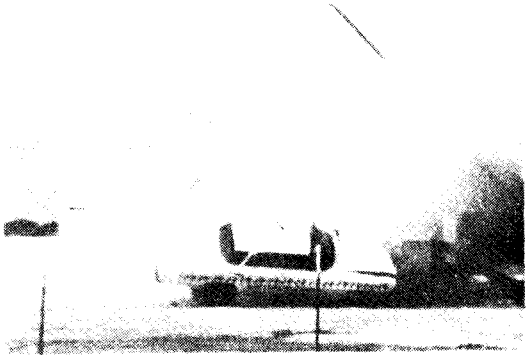

5

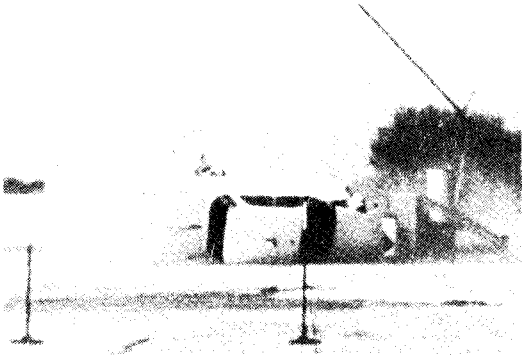

6

Figure 16, Sequential Photographs of Test C.

1

2

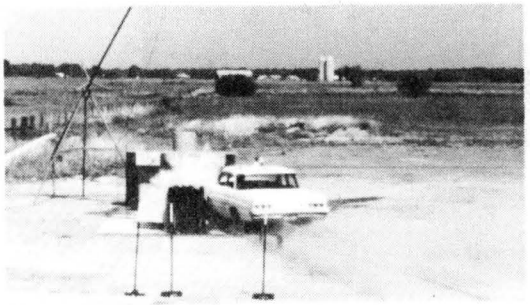

3

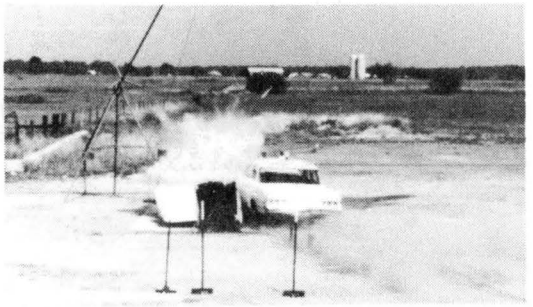

4

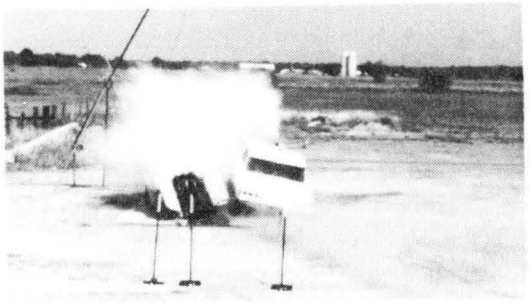

5

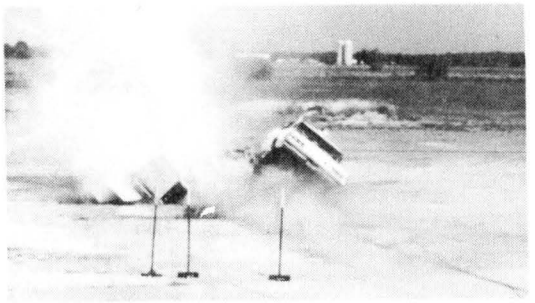

6

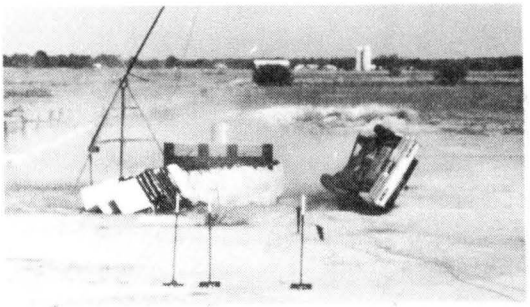

7

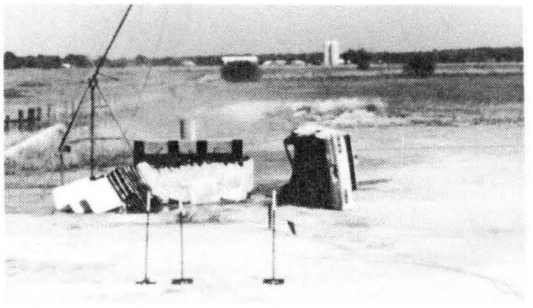

8

Figure 17, Sequential Photographs of Test C.

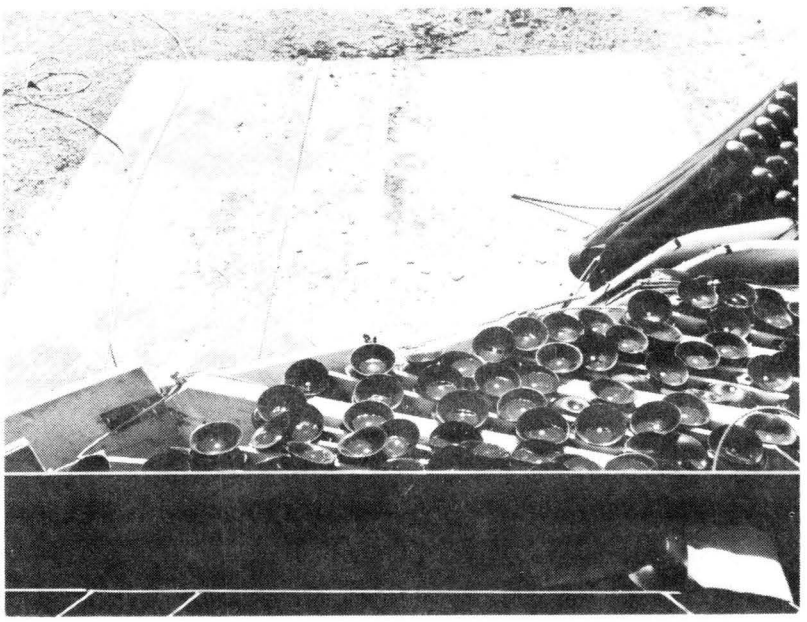

Figure 18, Barrier After Test C.

Figure 19, Vehicle After Test C.

Figure 20, Connection From Which Cable Pulled Free.

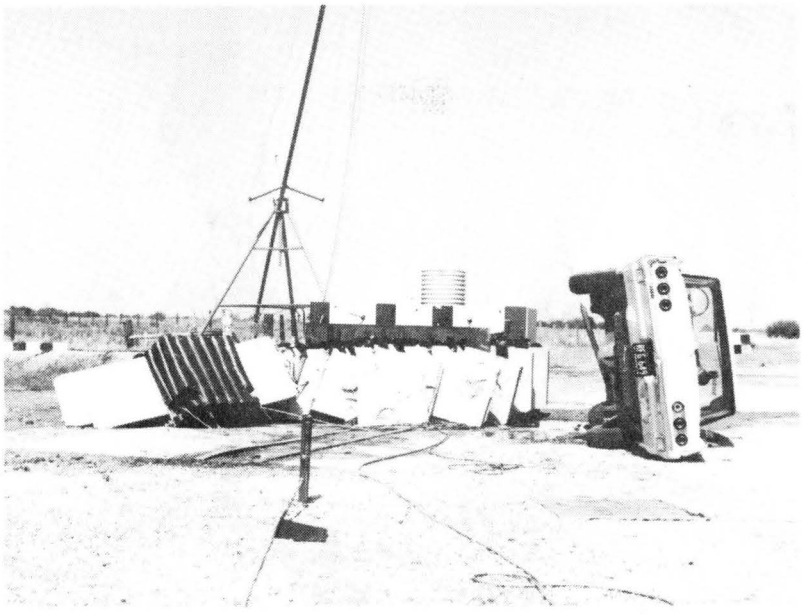

Figure 21, Crash Area After Test C.

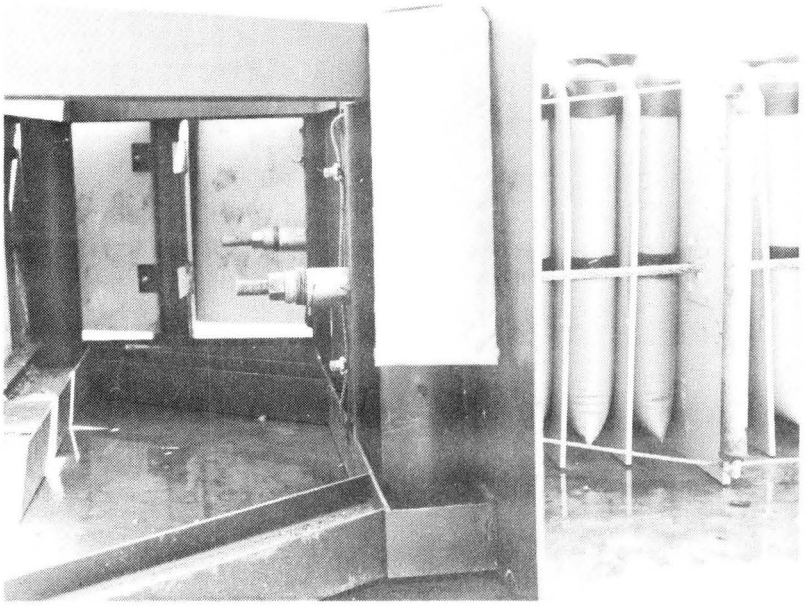

Figure 22, Steel Backup Plate Before Test C, Showing Restraining Cable Connections and Water-filled Tubes.

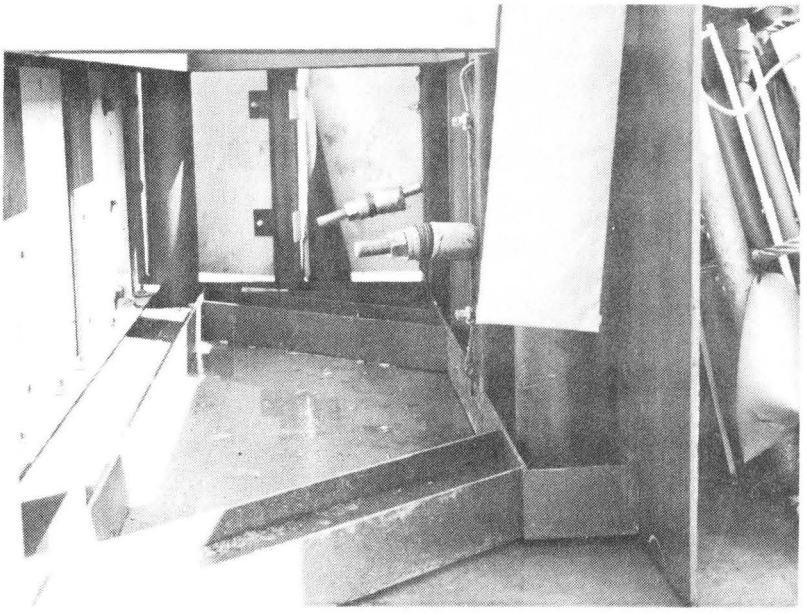

Figure 23, Steel Backup Plate After Test C Showing Loose Cable on Struck Side.

Figure 24, Front of Vehicle Showing Tow Cable (center) and Guidance Cable (right).

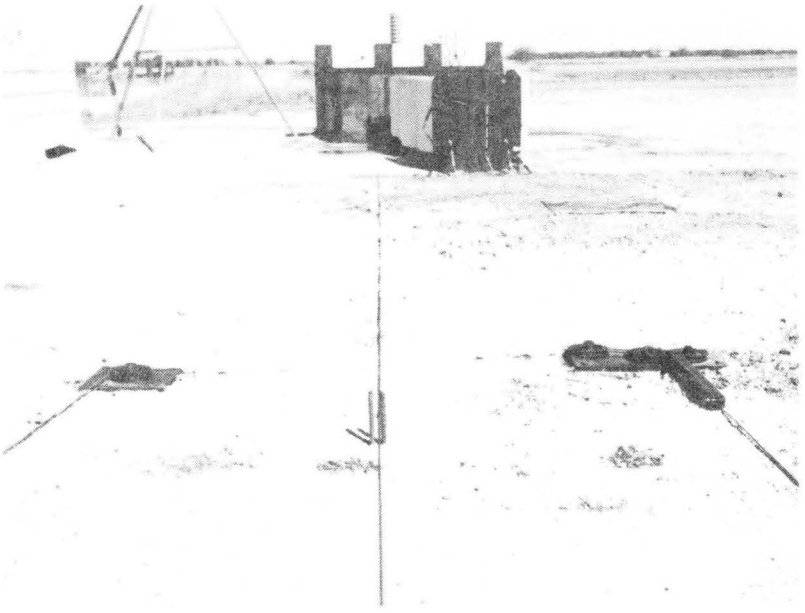

Figure 25, Tow System Pulleys and Guidance Cable for Test D.

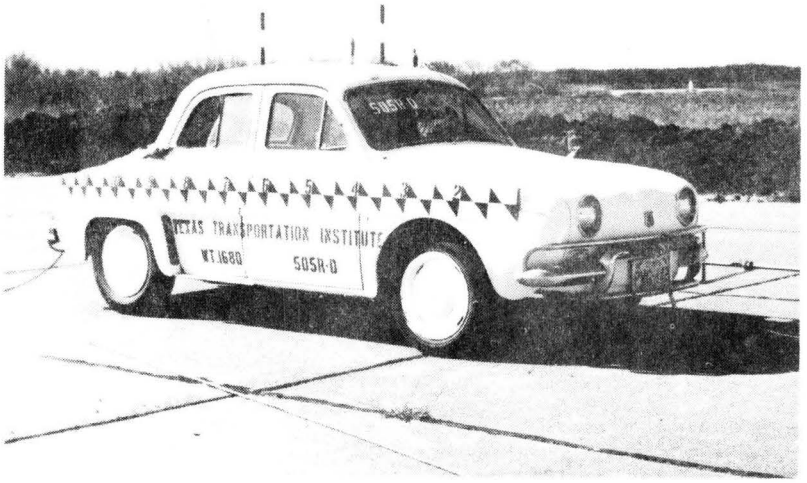

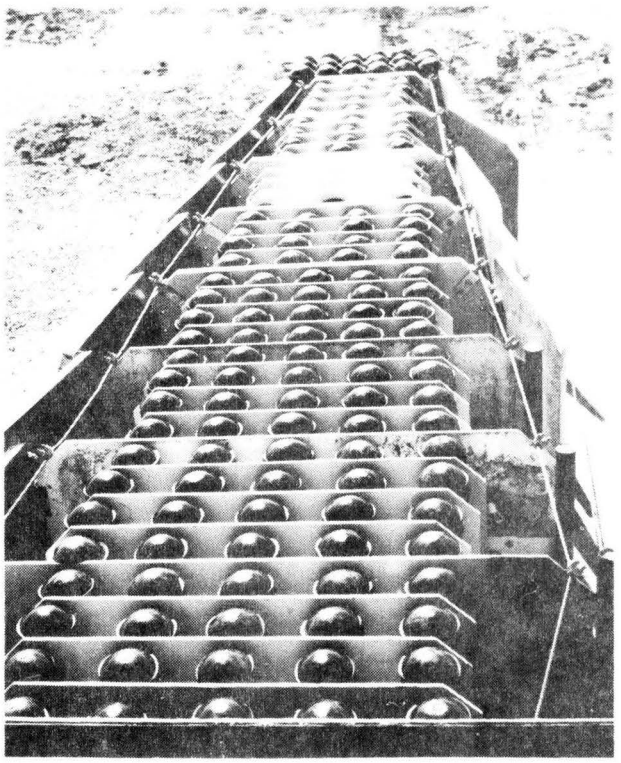

Figure 26, Vehicle and Barrier Before Test D.

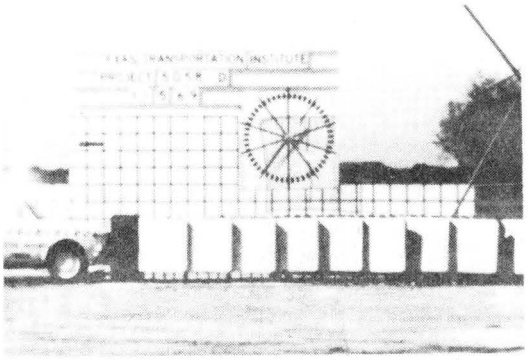

1

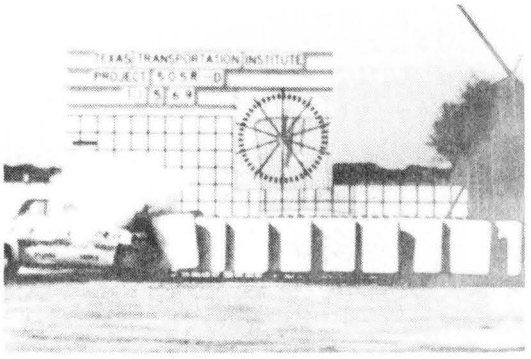

2

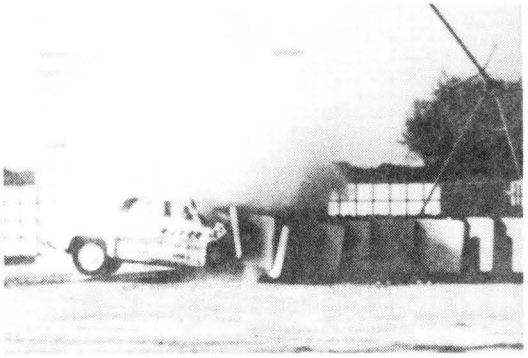

3

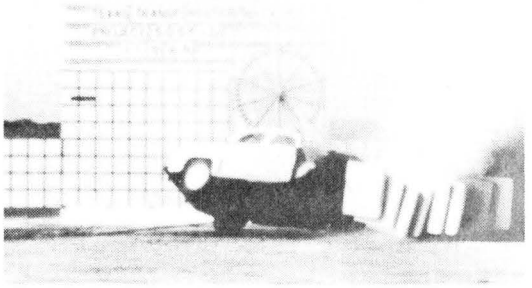

4

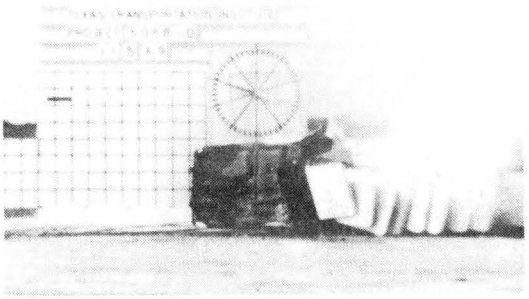

5

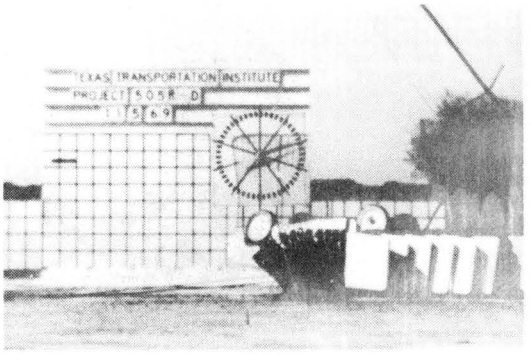

6

Figure 27, Sequential Photographs of Test D.

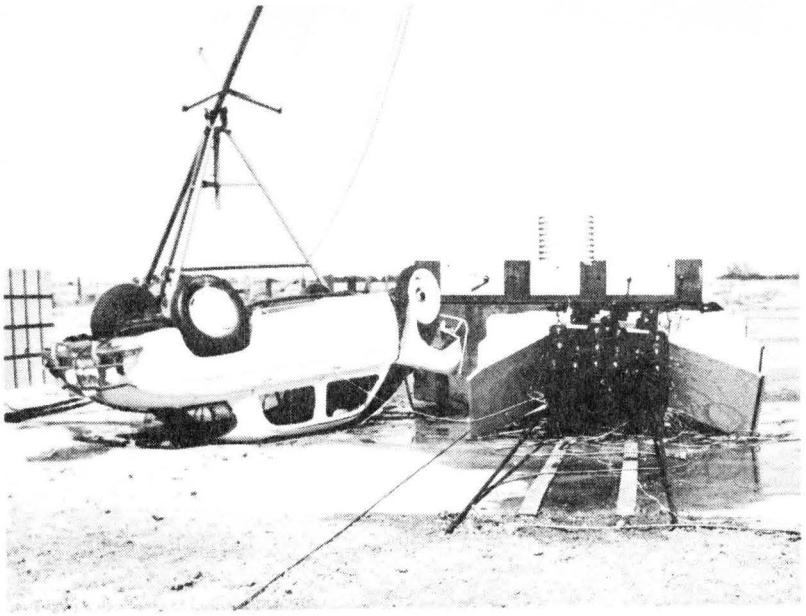

Figure 28, Vehicle and Barrier After Test D.

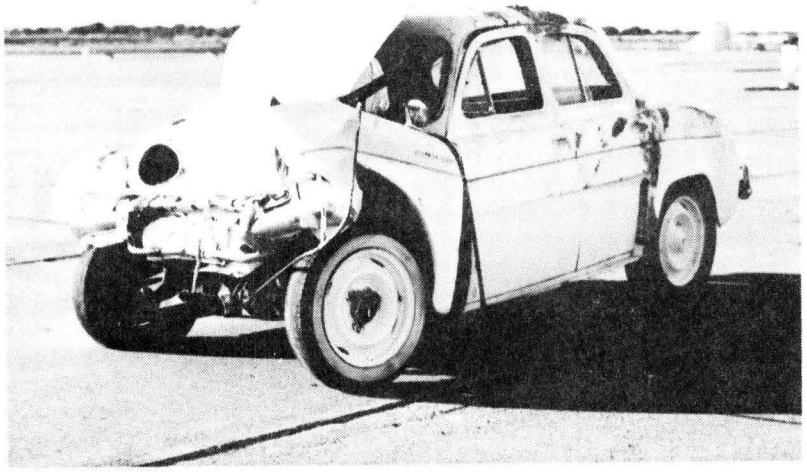

Figure 29, Vehicle After Test D (righted).

Figure 30, Vehicle Before and After Test E.

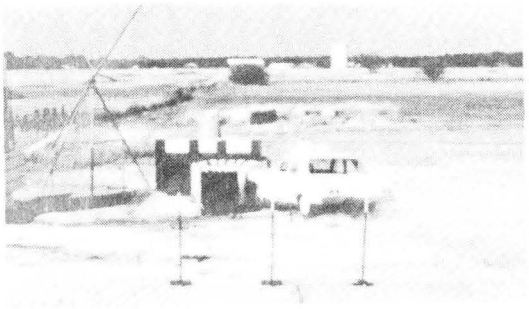

1

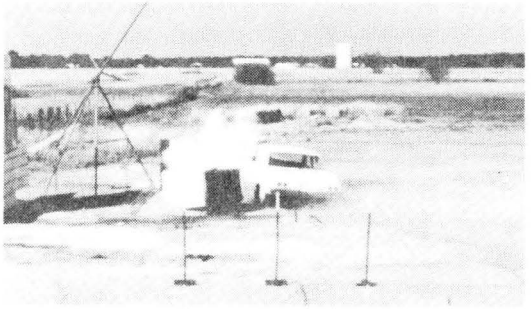

2

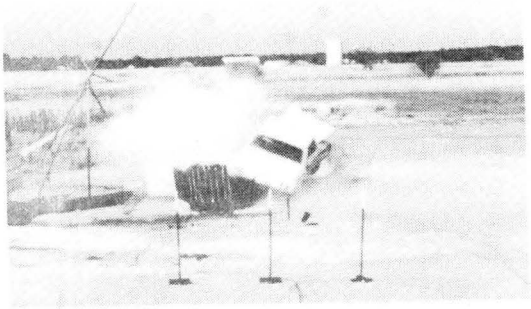

3

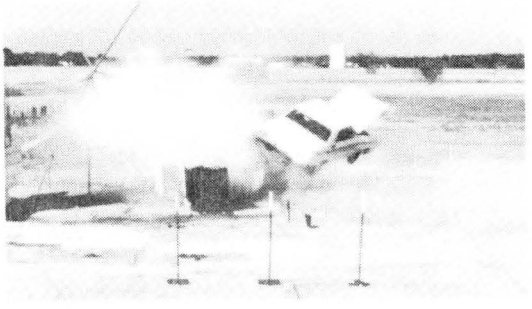

4

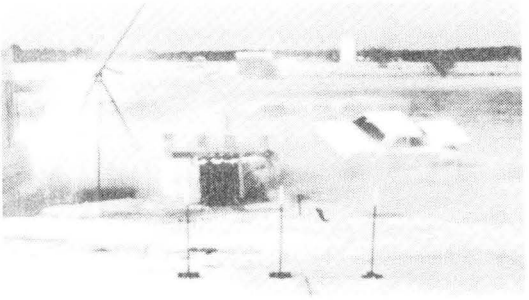

5

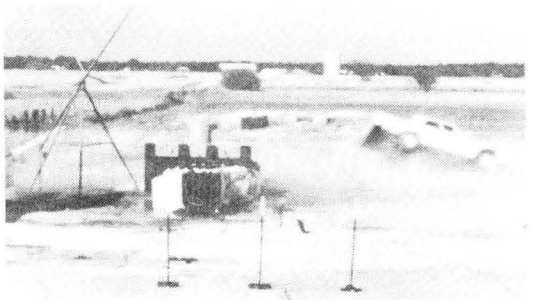

6

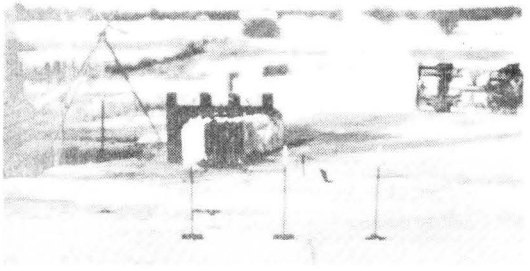

7

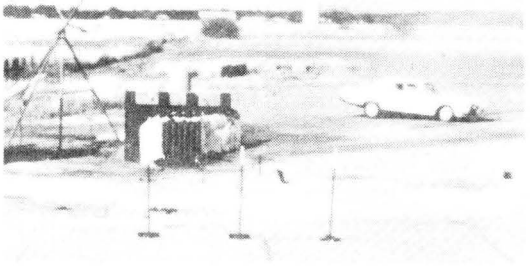

8

Figure 31, Sequential Photographs of Test E.

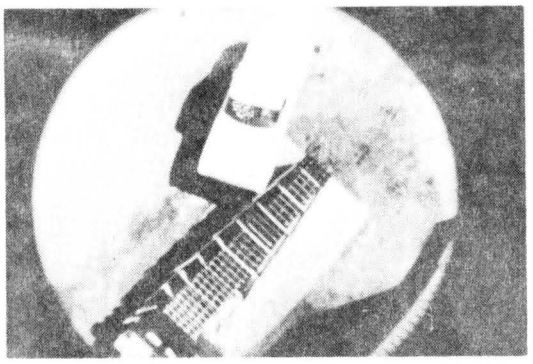

1

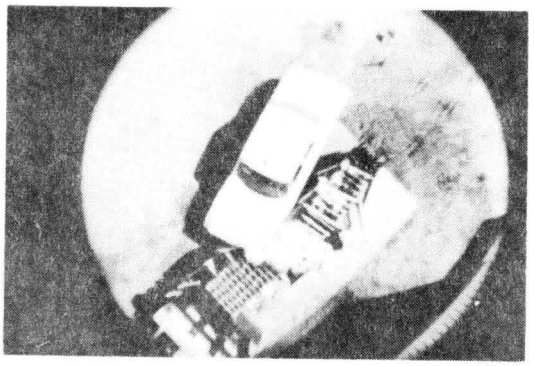

2

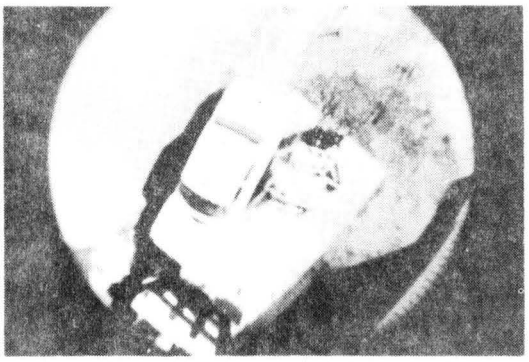

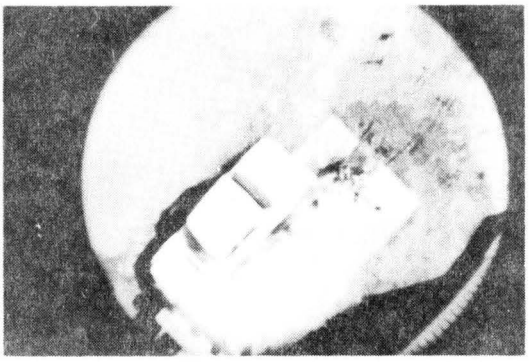

4

5

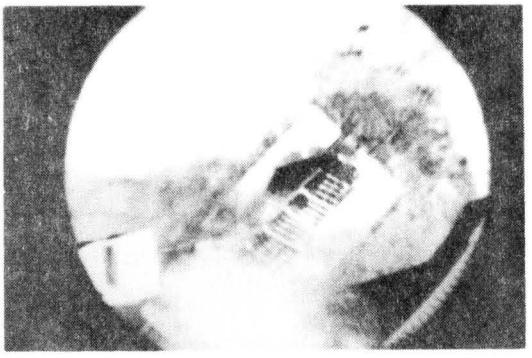

6

Figure 32, Overhead Sequential Photographs of Test E.

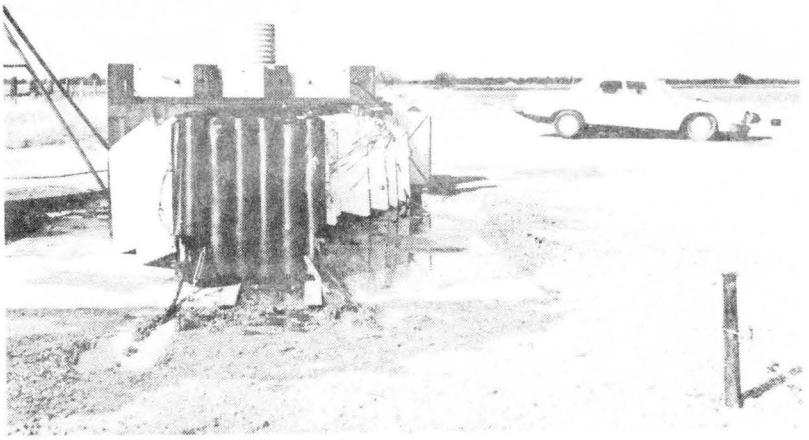

Figure 33, Impact Area After Test E.

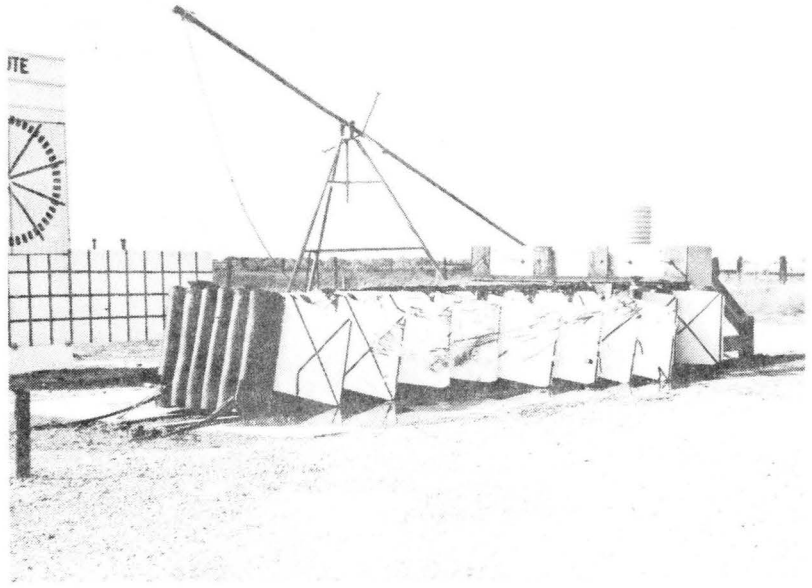

Figure 34, Barrier After Test E.

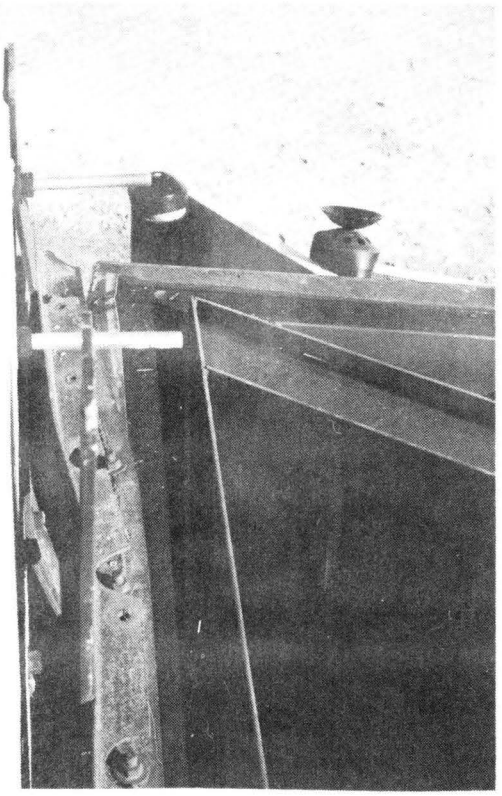

Figure 35, Steel Backup Plate Pulled Away About 2" at the Top.

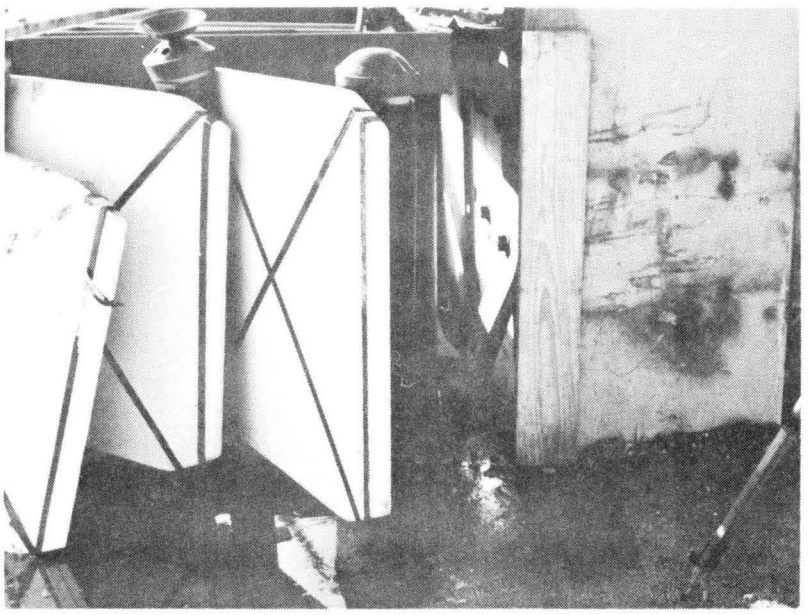

Figure 36, Steel Backup Plate Pulled . Away About 6" at the Bottom.

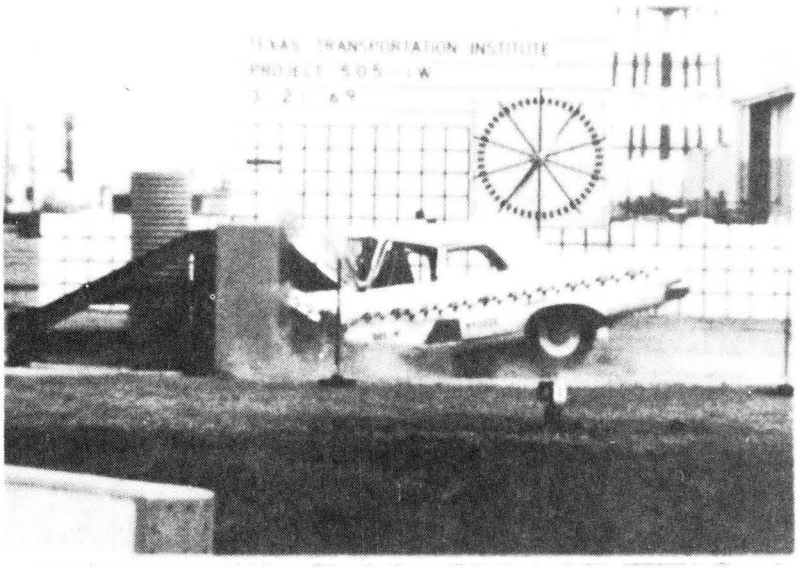

Figure 37, Rigid Wall Crash Test.

APPENDIX

Photographic and Electronic Data

TABLE 3

TEST 505 R-A

High-Speed Film Data

Time (Milliseconds)	Displacement (Feet)	Time (Milliseconds)	Displacement (Feet)
-51.0	-3.1	(continued)	
-40.8	-2.5	367.3	11.1
-30.6	-1.9	408.1	11.5
-20.4	-1.2	448.9	11.8
-10.2	-0.6	489.7	12.2
0 Impact	0	530.6	12.4
20.4	1.3	571.4	12.6
40.8	2.4	612.2	12.8
61.2	3.4	693.8	13.1
81.6	4.3	775.5	13.2
102.0	5.1	857.1	13.1
122.4	5.7	938.8	12.9
142.8	6.4	1020.4	12.7
163.2	7.0	1102.0	12.5
183.6	7.7	1183.7	12.3
204.0	8.2	1265.3	12.2
224.4	8.8	1347.0	12.1
244.8	9.2	1428.6	12.0
285.6	10.0	1510.2	12.0
326.4	10.5		

TABLE 4

TEST 505 R-B

High-Speed Film Data

Time (Milliseconds)	Displacement (Feet)	Time (Milliseconds)	Displacement (Feet)
-40.3	-3.8	(continued)	
-30.2	-2.8	322.6	17.3
-20.2	-1.9	362.9	17.2
-10.1	-0.9	403.2	17.0
0 Impact	0	443.5	16.7
20.2	1.9	483.8	16.3
40.3	3.7	524.2	16.0
60.5	5.3	564.5	15.6
80.6	6.9	604.8	15.2
100.8	8.3	846.7	13.3
121.0	9.7	1048.3	12.1
141.1	10.9	1249.9	11.0
161.3	12.0	1451.5	10.1
181.4	12.9	1653.1	9.3
201.6	13.7	1854.7	8.7
221.8	14.5	2056.3	8.2
241.9	15.3	2257.9	7.9
262.1	16.0	2459.5	7.7
282.2	16.6	2661.1	7.6

TABLE 5

TEST 505 R-C

High-Speed Film Data

Time (Milliseconds)	Displacement (Feet)	Time (Milliseconds)	Displacement (Feet)
-49.0	-3.9	(continued)	
-38.9	-3.1	210.8	13.1
-28.7	-2.4	229.9	13.9
-19.2	-1.6	249.1	14.8
-9.6	-0.8	268.2	15.5
0 Impact	0	287.4	16.0
19.2	1.5	306.6	16.4
38.3	3.0	325.7	16.6
57.5	4.4	344.9	16.7
76.6	5.8	364.0	16.6
95.8	7.1	455.5	16.2
115.0	8.3	547.0	15.8
134.1	9.4	638.5	15.4
153.3	10.4	730.0	15.1
172.4	11.3	821.5	14.9
191.6	12.2	913.0	14.8

TABLE 6

TEST 505 R-D

High-Speed Film Data

Time (Milliseconds)	Displacement (Feet)	Time (Milliseconds)	Displacement (Feet)
-49.5	-4.3	(continued)	
-39.6	-3.4	188.0	10.1
-29.7	-2.6	208.0	10.6
-19.8	-1.7	228.0	10.9
-9.9	-0.9	248.0	11.2
0	0	267.0	11.6
9.9	0.8	287.0	11.9
29.7	2.4	307.0	12.1
49.5	3.9	327.0	12.4
69.3	5.3	366.0	12.9
89.1	6.4	406.0	13.3
109.0	7.3	446.0	13.6
129.0	8.2	505.0	14.1
148.0	8.9	544.0	14.3
168.0	9.5		

TABLE 7

TEST 505 R-E

High-Speed Film Data

Time (Milliseconds)	Displacement (Feet)	Time (Milliseconds)	Displacement (Feet)
-31.6	-2.7	(continued)	
-26.3	-2.3	105.2	8.1
-21.1	-1.8	126.2	9.4
-15.8	-1.4	147.1	10.6
-10.5	-0.9	168.1	11.8
-5.3	-0.5	189.0	12.9
0 Impact	0	210.0	14.0
5.3	0.4	230.9	15.0
10.5	0.9	251.7	16.0
15.8	1.3	272.6	16.8
21.1	1.7	314.1	18.4
31.6	2.6	340.0	19.4
42.1	3.5	365.8	20.3
52.6	4.3	417.2	22.2
63.1	5.1	468.2	24.0
73.6	5.9	518.8	25.9
84.2	6.7	569.2	27.9
94.7	7.4	619.3	29.9

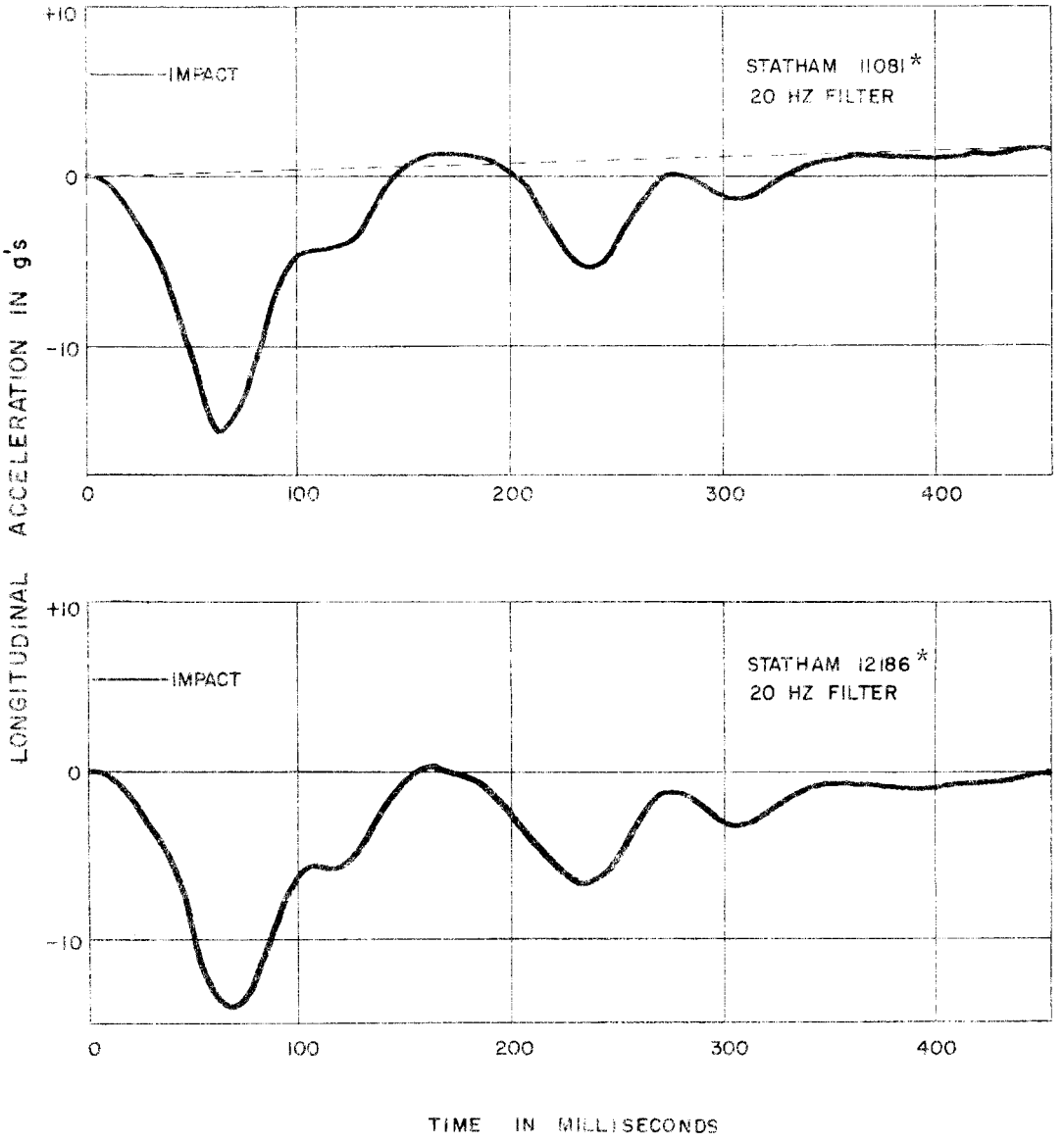

*Typical strain gage accelerometers.

FIGURE 38. LONGITUDINAL ACCELEROMETER DATA, TEST 505R-A

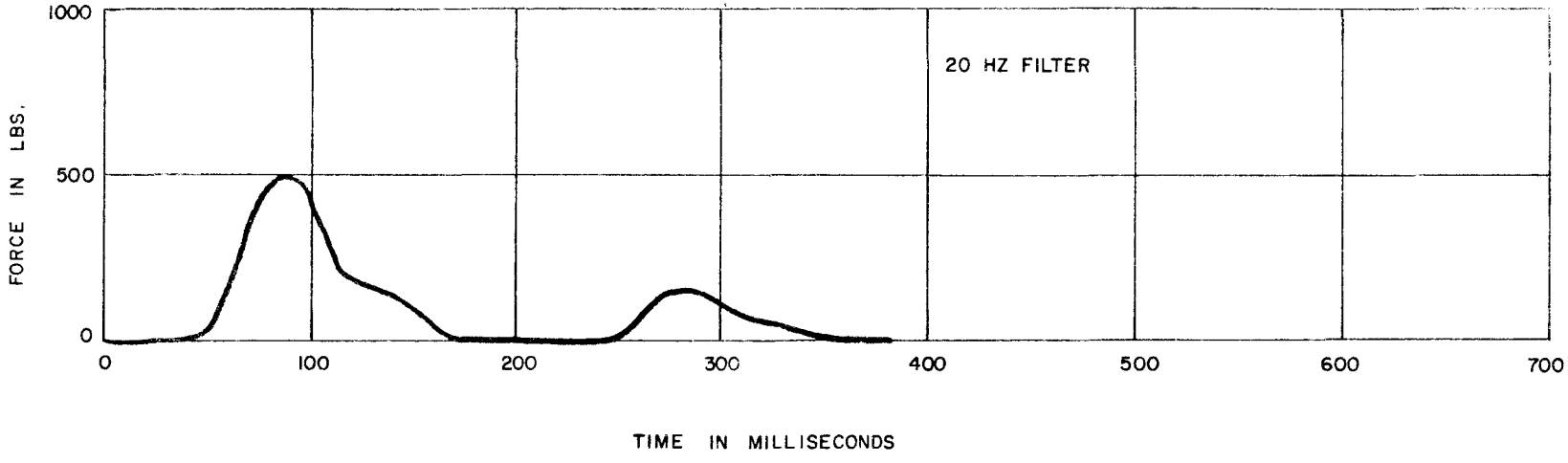

FIGURE 39, DUMMY SEATBELT DATA, TEST 505R-A

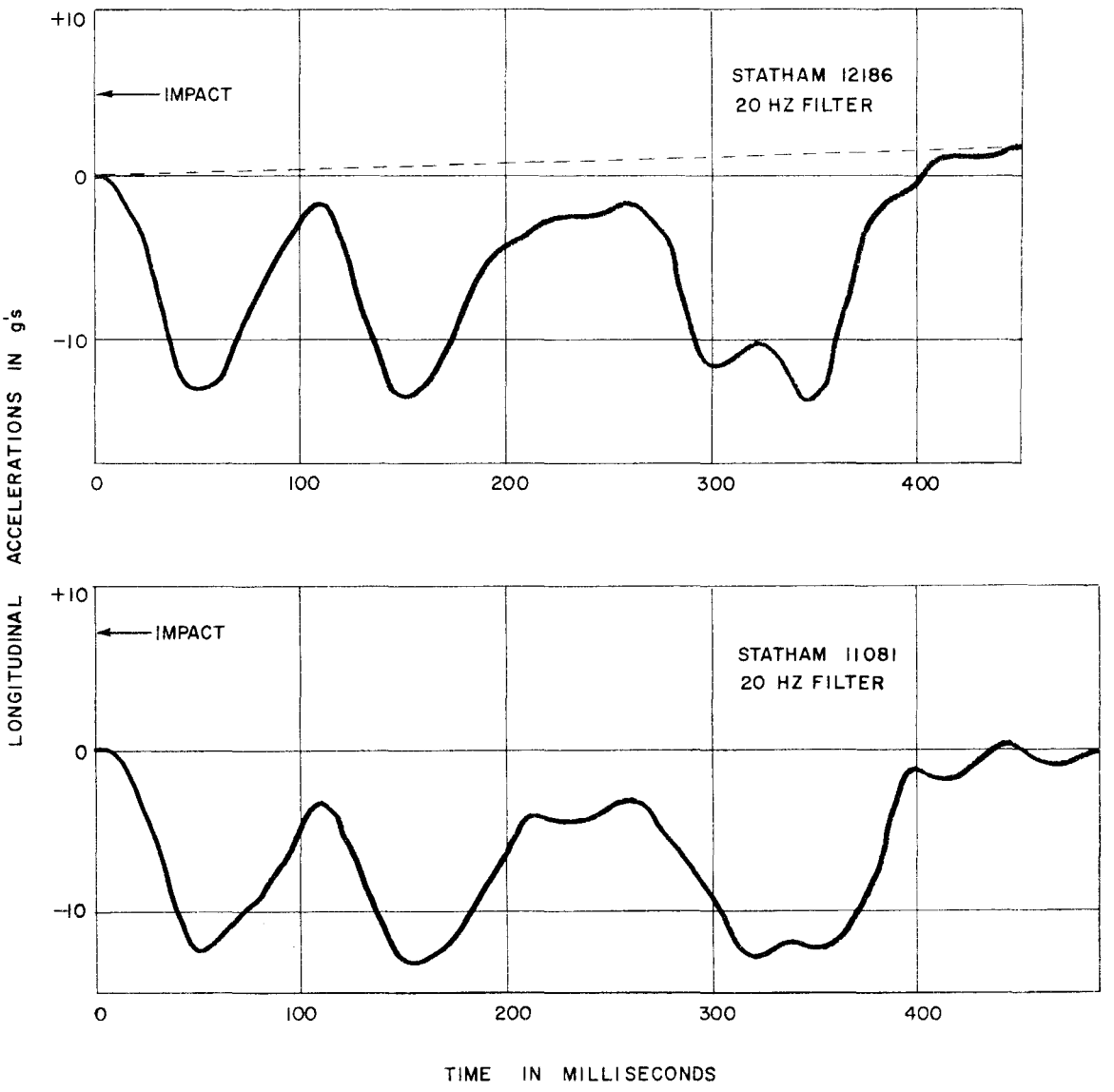

FIGURE 40, LONGITUDINAL ACCELEROMETER DATA, TEST 505R-B

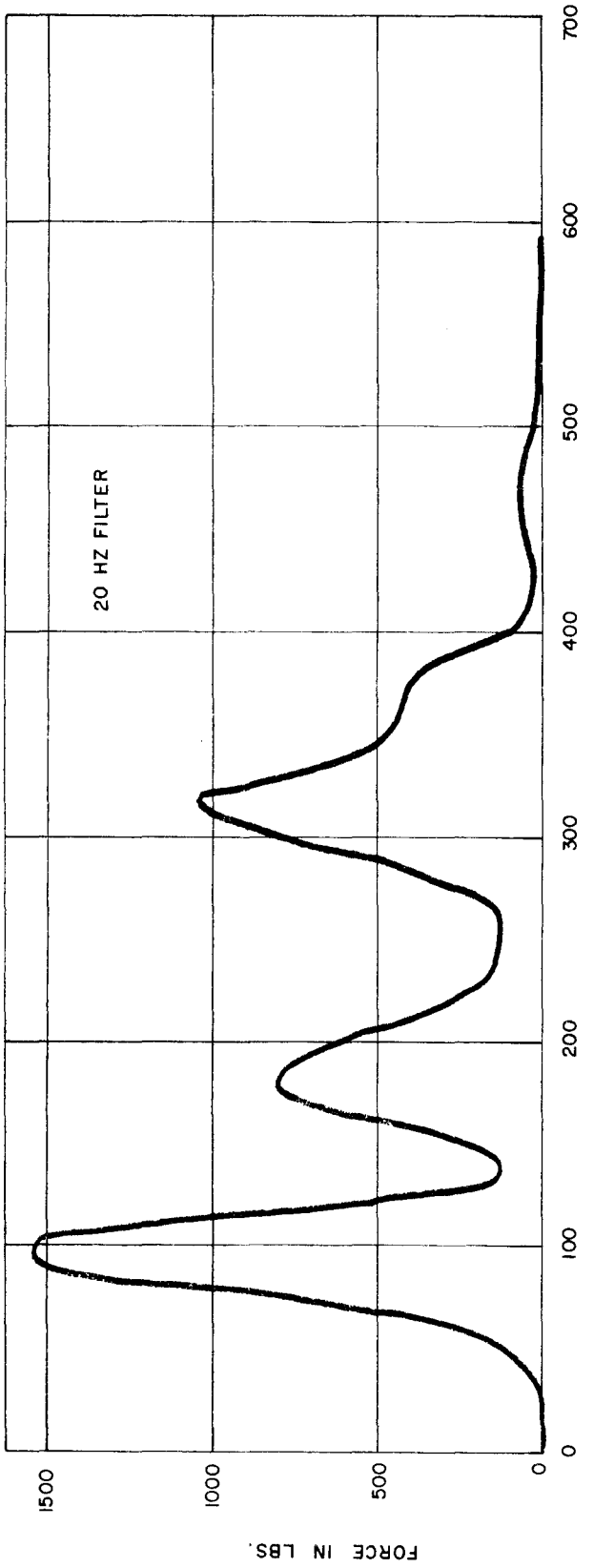

FIGURE 41, DUMMY SEATBELT DATA, TEST 505R-B

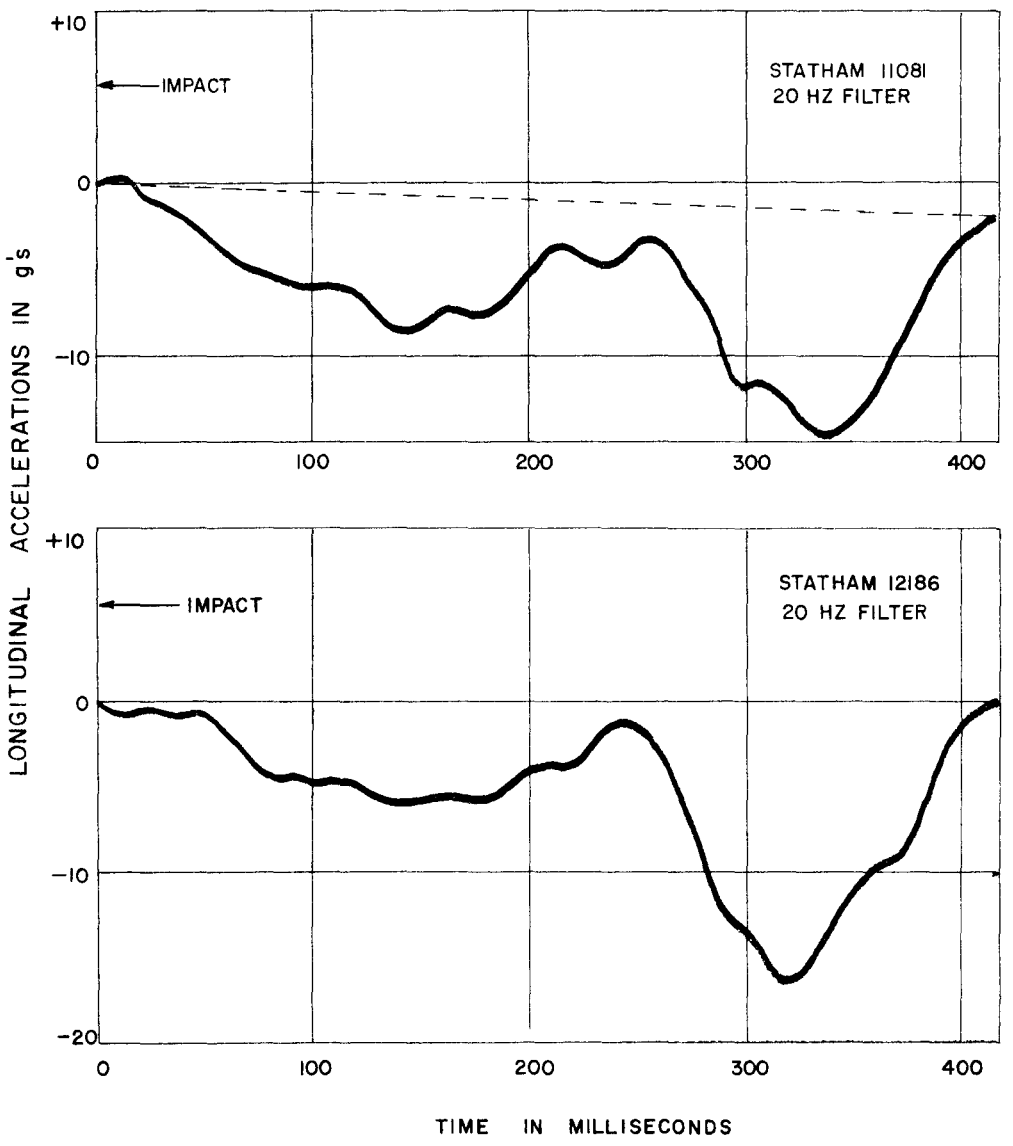

FIGURE 42, LONGITUDINAL ACCELEROMETER DATA, TEST 505R-C

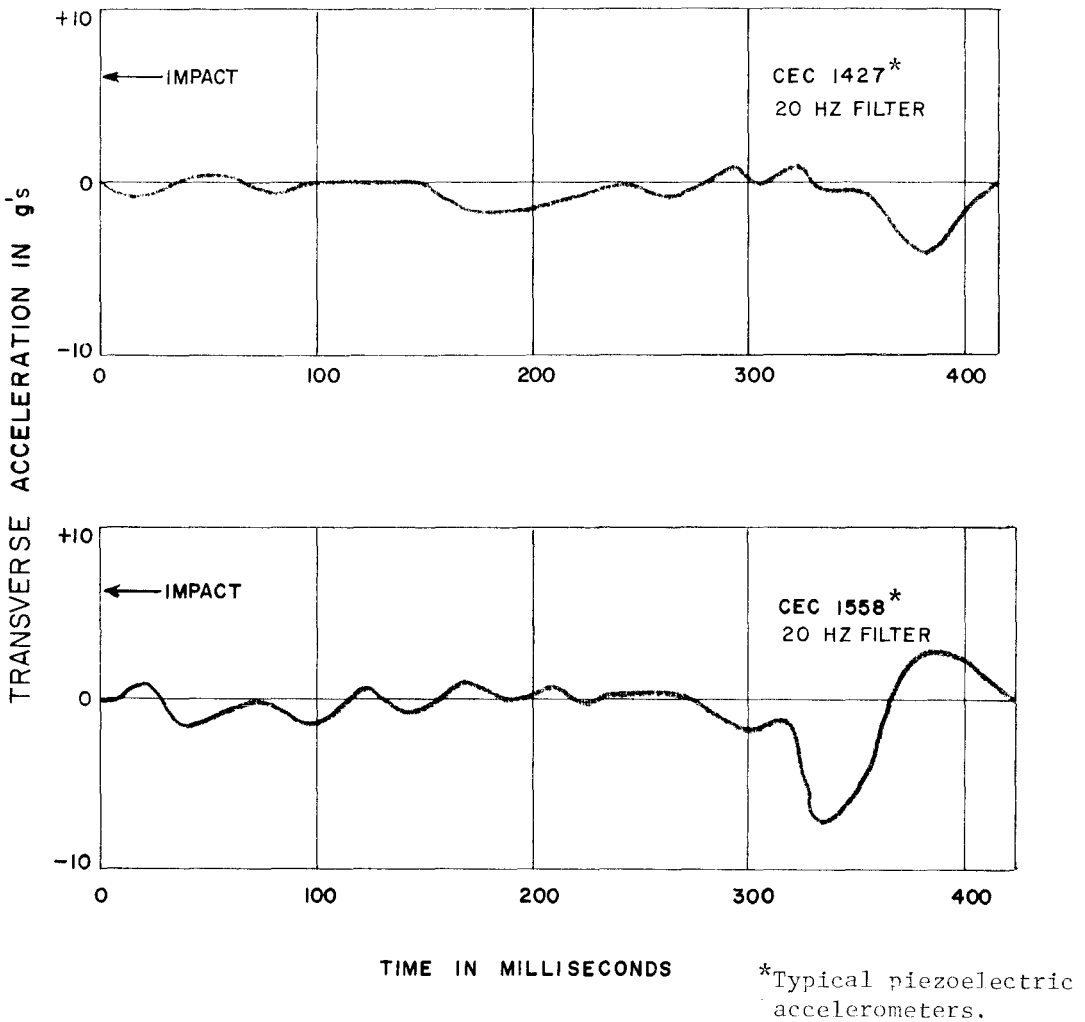

*Typical piezoelectric accelerometers.

FIGURE 43, TRANSVERSE ACCELEROMETER DATA, TEST 505R-C

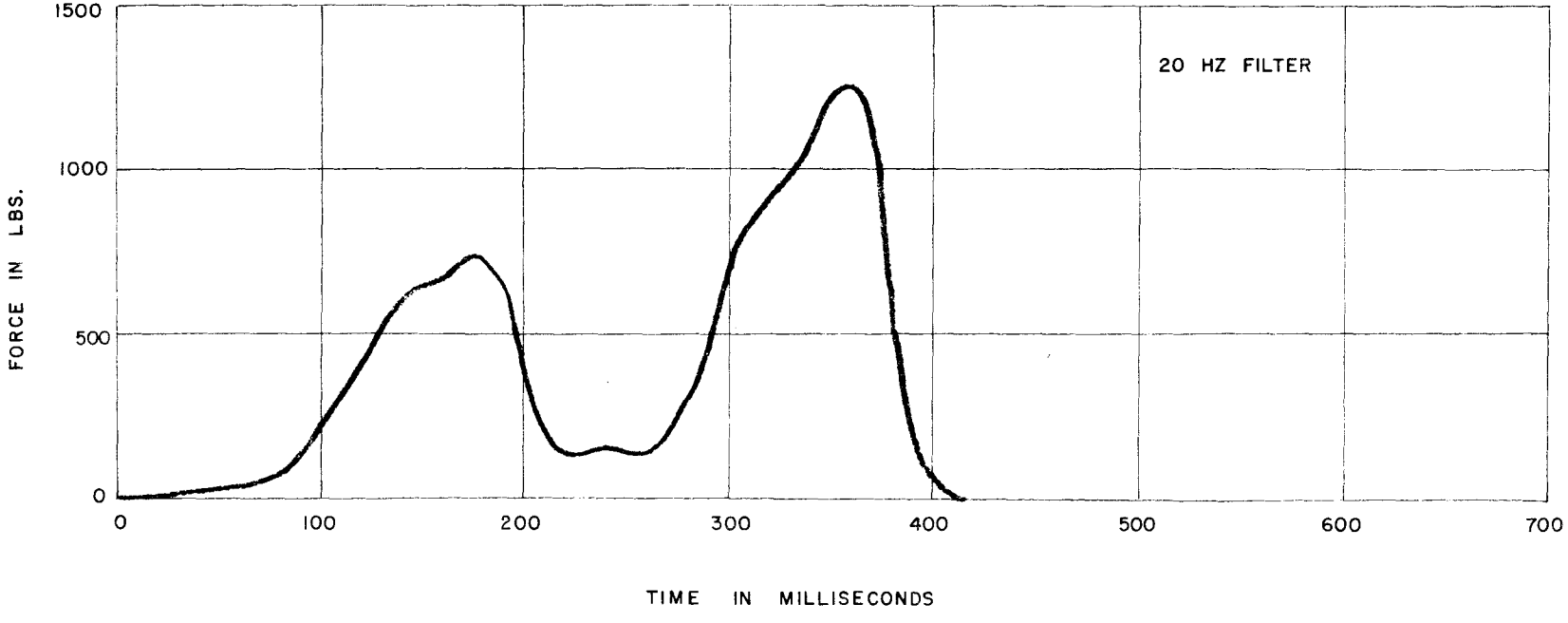

FIGURE 44, DUMMY SEATBELT DATA, TEST 505R-C

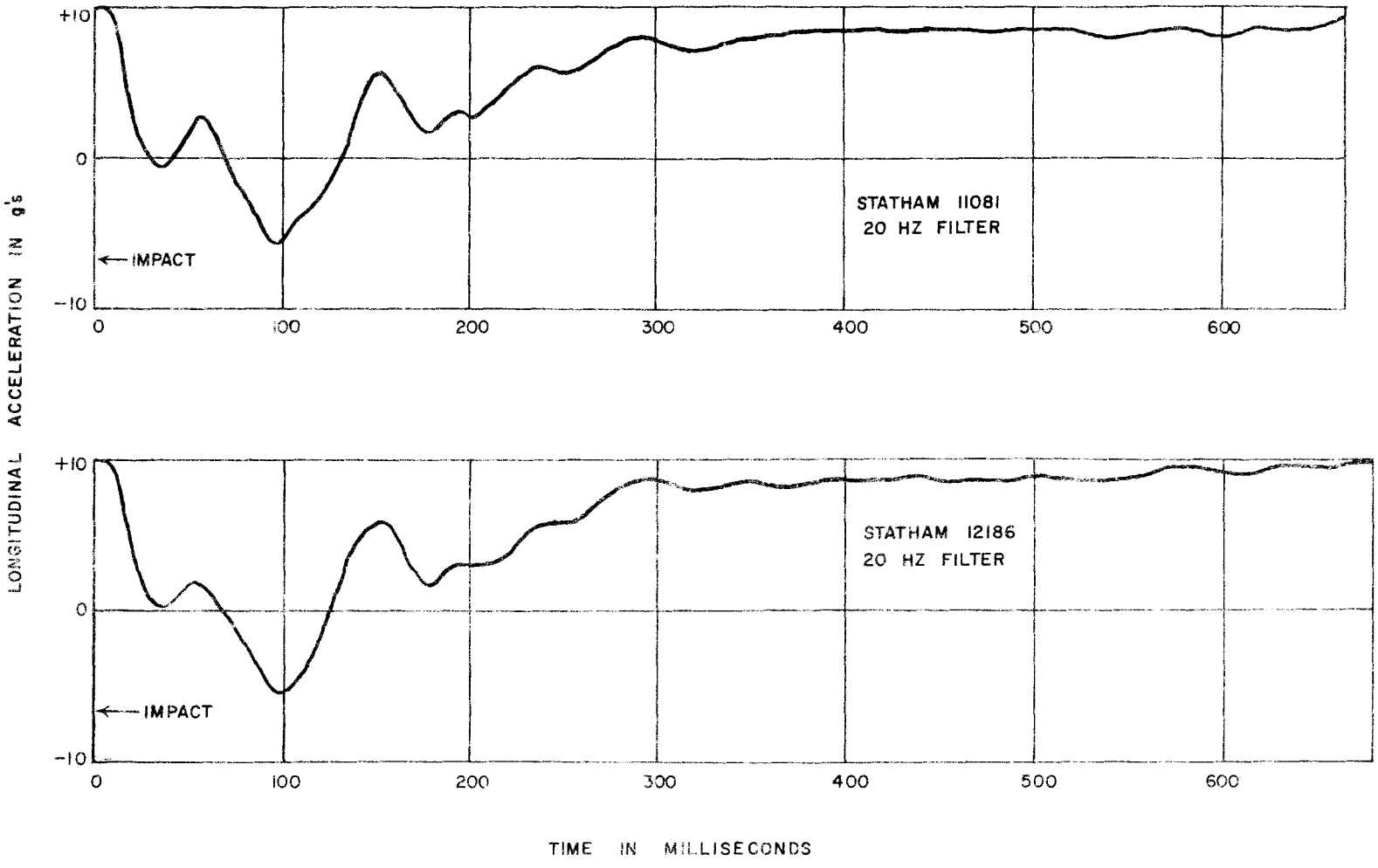

FIGURE 45, LONGITUDINAL ACCELEROMETER DATA, TEST 505R-D

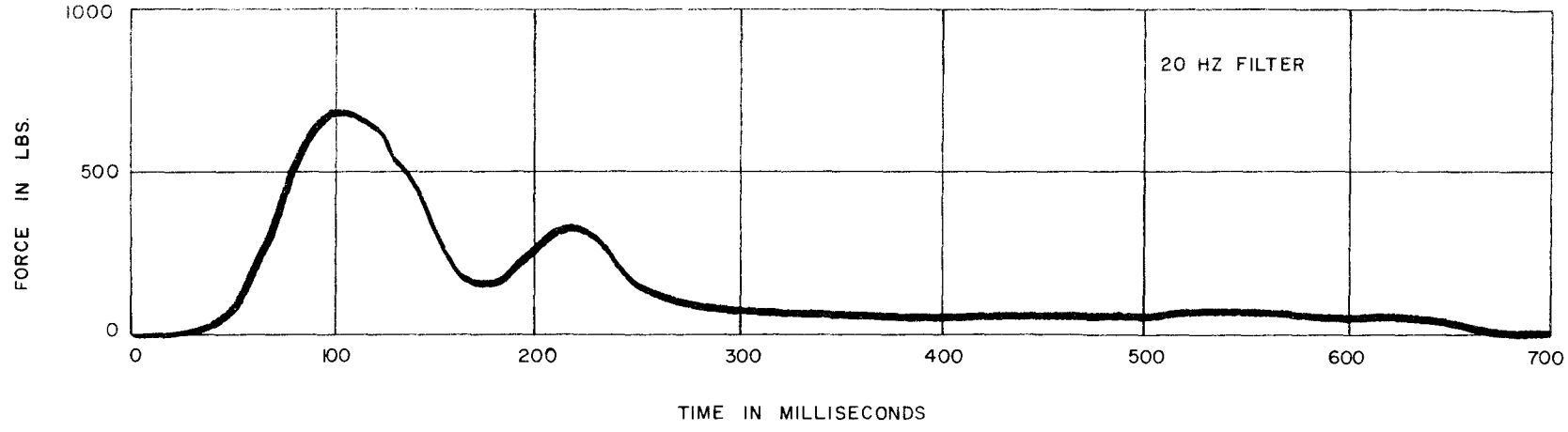

FIGURE 46 , DUMMY SEATBELT DATA, TEST 505R-D

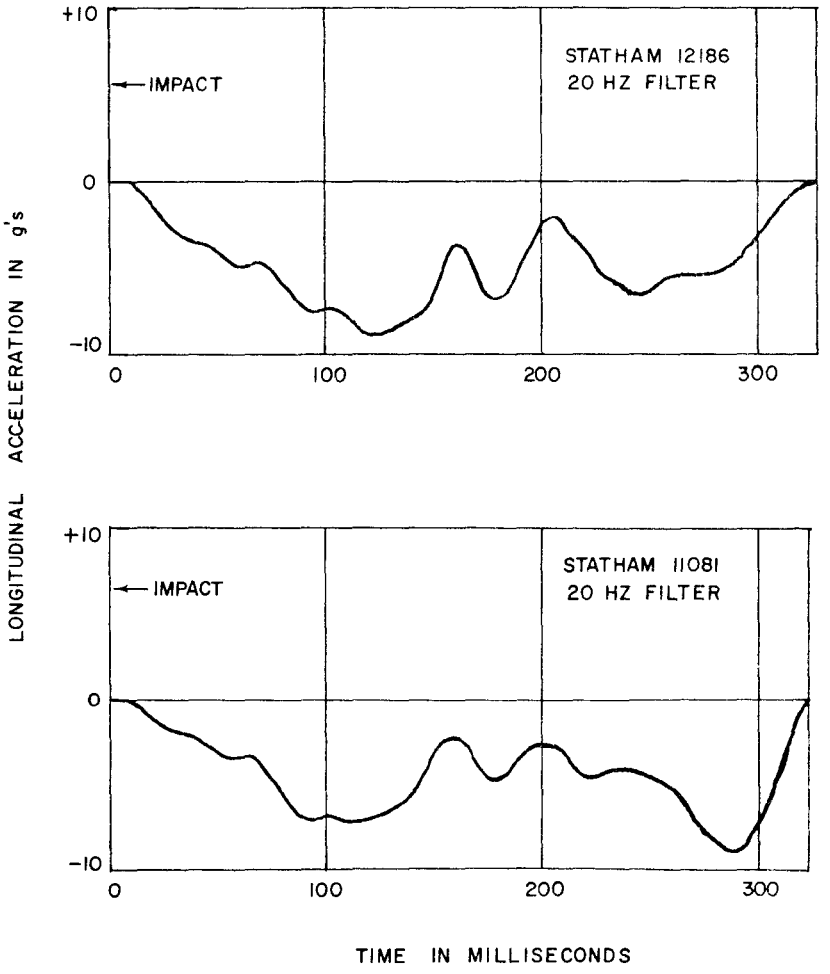

FIGURE 47, LONGITUDINAL ACCELEROMETER DATA, TEST 505R-E

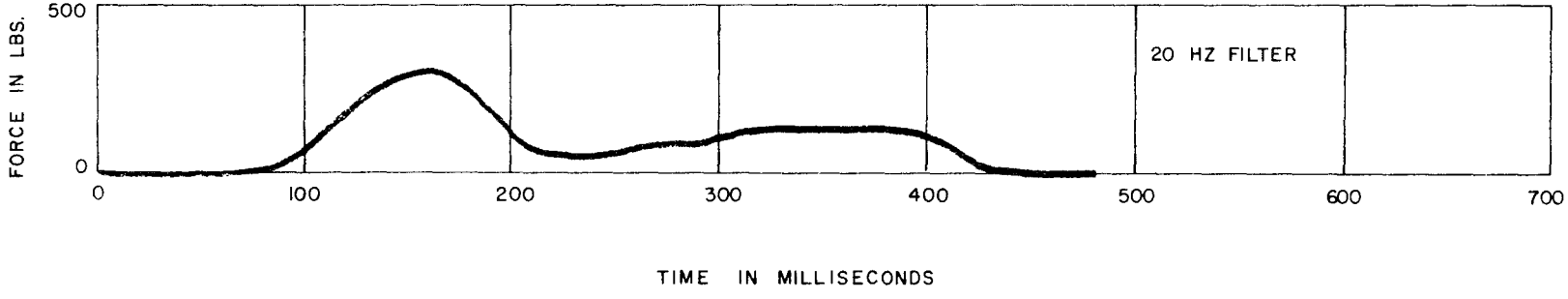

FIGURE 48, DUMMY SEATBELT DATA, TEST 505R-E

TECHNICAL MEMORANDUM 505-12

Texas Transportation Institute
Texas A&M Research Foundation

NEW YORK BOX-BEAM BRIDGE RAIL-GUARDRAIL

A Test And Evaluation Report On Contract No. CPR-11-5851

U.S. Department of Transportation
Federal Highway Administration

by

Arthur J. Stocker
Assistant Research Engineer

Don L. Ivey
Associate Research Engineer

and

T. J. Hirsch
Research Engineer

These crash tests and evaluations were conducted under the Office of Research and Development, Structural and Applied Mechanics Division's Research Program on Structural Systems in Support of Highway Safety (4S Program).

May 1971

INTRODUCTION

Full-scale crash testing remains the most effective way of demonstrating the performance characteristics of a highway barrier system. A number of different tests on guardrail-bridge rail systems have been conducted under the Federal Highway Administration 4S Program, Structural Systems in Support of Highway Safety. As part of this program, two crash tests of a modified New York Box Beam system were conducted. This strong beam-weak post barrier is a modification of a New York Box Beam Guide Rail system which was reported by Malcolm Graham.[1]* The design tested was provided by William C. Burnett of the Department of Transportation of the State of New York.

Tests were conducted with medium weight vehicles at nominal speeds of sixty mph and impact angles of 25°. The first impact was directed into the bridge rail and the second into the transition zone between the guardrail and the bridge rail.

In each test the vehicle was contained and redirected by the barrier rail. Vehicle decelerations were reduced considerably by the deflection characteristics of this barrier and vehicle compartment encroachment was found to be negligible. The barrier performed in a very acceptable manner.

---

*Superscript numbers refer to corresponding numbers in the References.

BARRIER DESCRIPTION

Figures 1 through 6 show details of the basic components of the modified New York Box-Beam Bridge Rail system. A description of the major elements of the strong beam-weak post design is as follows:

Item	Description	Material (ASTM)
Bridge rail	6" x 6" x 3/8" box beam	A500
Bridge rail post	3 I 5.7	A36
Bridge rail post base plate	10" x 9-1/2" x 1"	A36
Guardrail	6" x 6" x 3/16" box beam	A500
Guardrail Post	3 I 5.7	A36
Guardrail post spade	8" x 24" x 1/4" plate	A36
Rail splice plates	Size varies	A36
Bolts--Bridge rail to clip	3/8"	A307
Bolts--Guardrail to clip	3/8"	A307
Bolts--Clip to guardrail post	1/2"	A307
Bolts--Splice plates	3/4"	A325
Bolts--Bridge post base plate to deck	7/8"	A325

MECHANICAL PROPERTIES OF MATERIALS

Material	Tensile (ksi)	Yield Point (ksi min.)	% Elongation (min. on 2")
A 36	58 - 80	36	23%
A 307	60	36	23%
A 325	120	92	N/A 1-1/4" dia.
A 500	Type A - 45 Type B - 58	Type A - 39 Type B - 46	Type A - 25% Type B - 23%

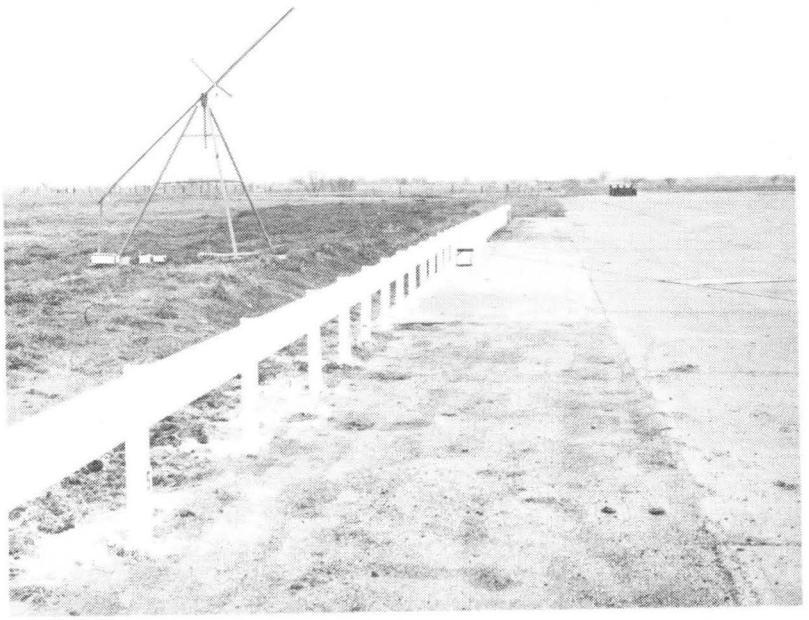

Figure 1, Overall View of Bridge Rail-Guardrail.

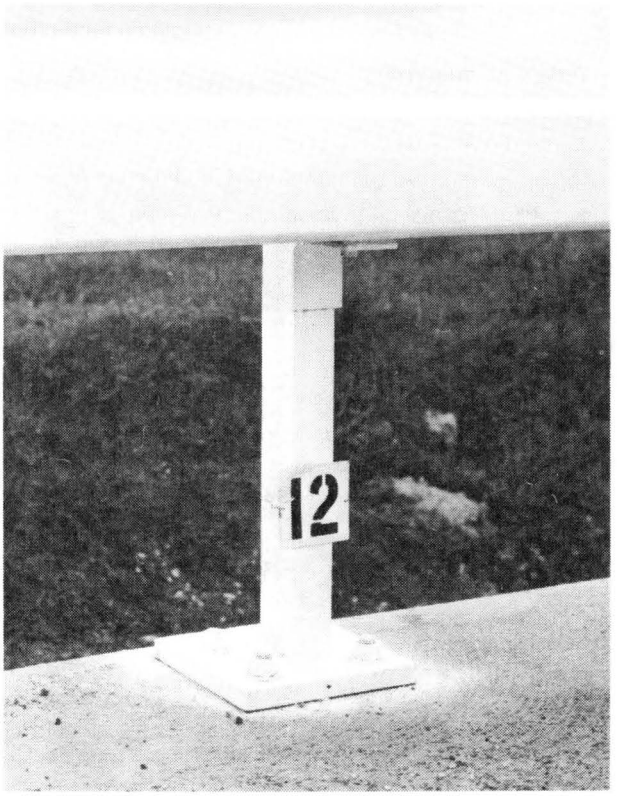

Figure 2, Bridge Post.

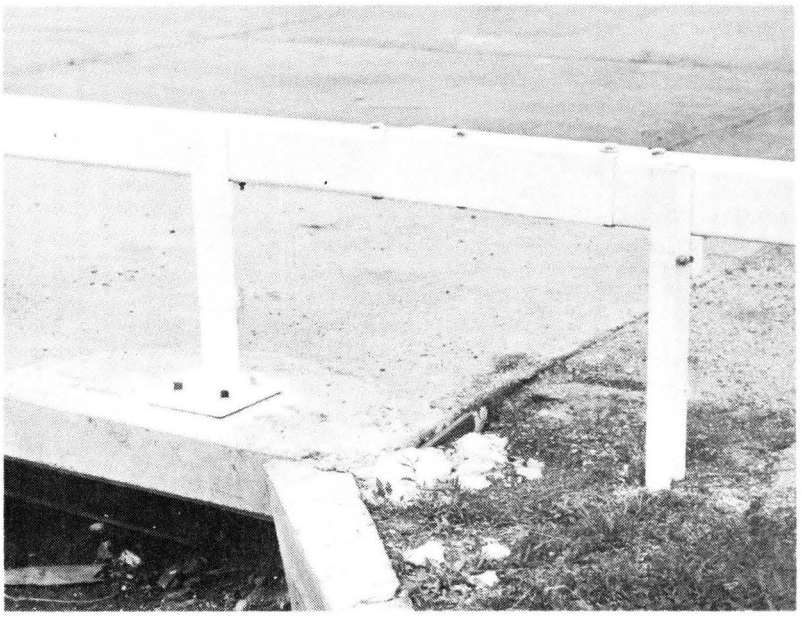

Figure 3, Bridge Rail-Guardrail Transition.

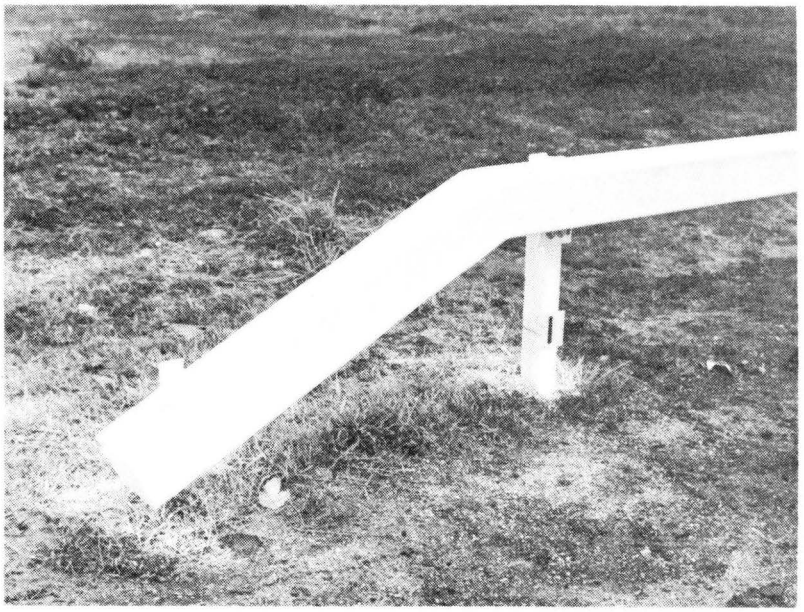

Figure 4, Detail of End Anchorage.

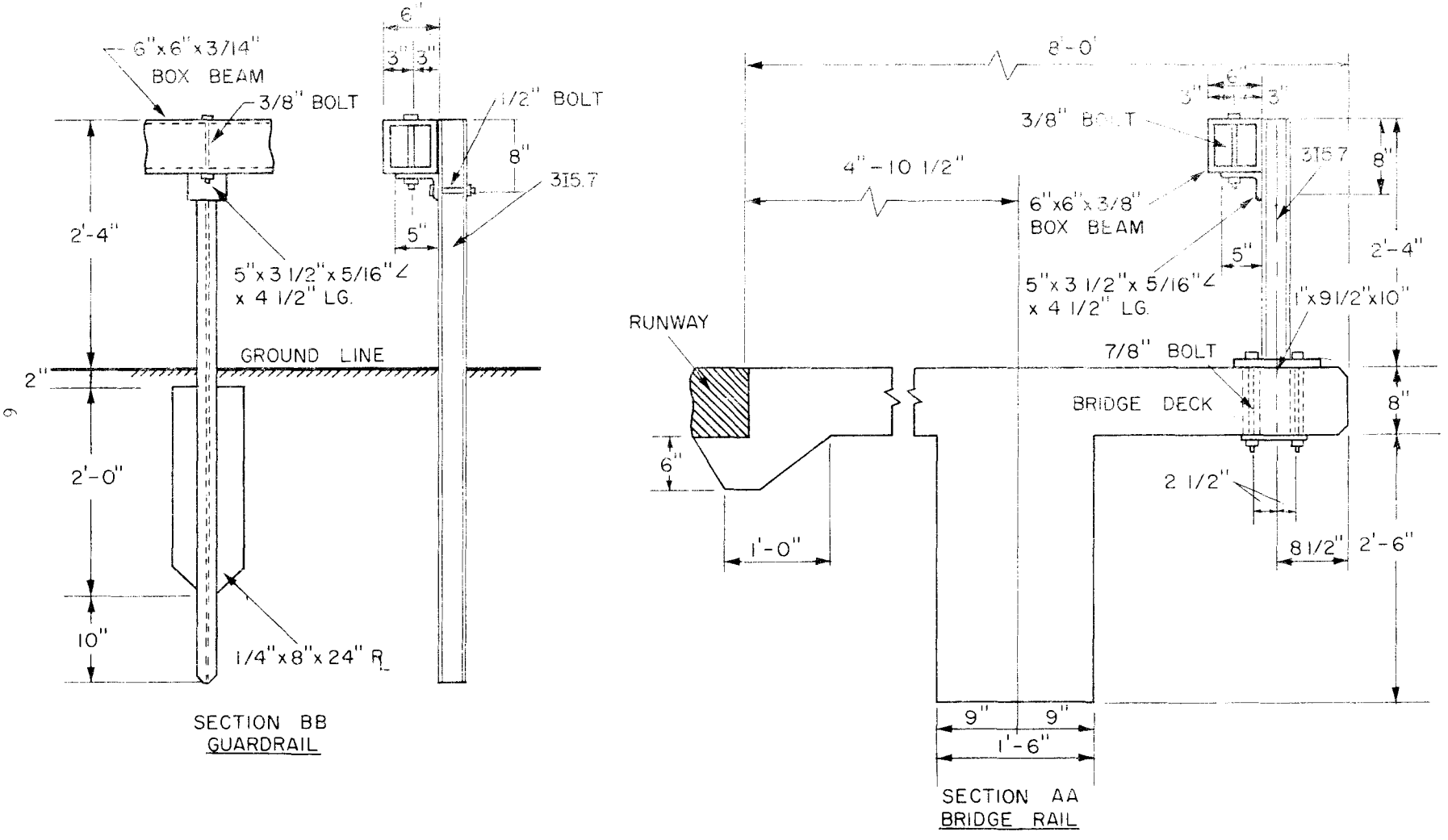

FIGURE 5, BRIDGE RAIL AND GUARDRAIL SECTIONS

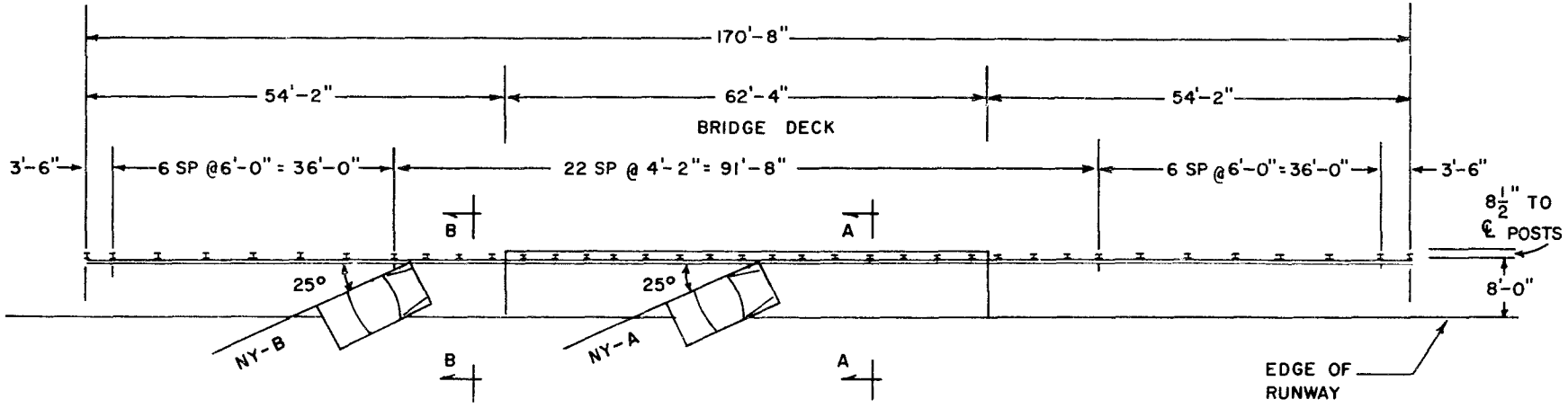

TEST NUMBER	NY—A	NY—B
ANGLE OF APPROACH	25°	25°
VEHICLE WEIGHT	3800 LBS.	3670 LBS.
IMPACT SPEED	55.4 MPH.	57.9 MPH.
INITIAL KINETIC ENERGY (KIP—FT)	389	412

FIGURE 6, BRIDGE RAIL — GUARDRAIL LAYOUT AND TEST SUMMARY

VEHICLE DAMAGE RATINGS

The National Safety Council in 1968 published a report entitled, "Vehicle Damage Scale for Traffic Accident Investigators."[2] The damage rating scale, developed in the NSC Traffic Accident Data Project, consists of photographs of automobiles damaged in accidents. The photographs are classified according to a particular type of impact damage: left front quarter (LFQ), front left (FL), etc. The severity of damage, illustrated by the photographs, is indicated by an arbitrary scale from 1 to 7, with 7 being the most severe.

Ten observers compared the photographs of the damaged vehicles from tests A and B with the NSC pictures. Results of the comparisons are presented below.

Observer	Test NY-A	Test NY-B
1	LFQ-5	LFQ-5
2	FL-4	FD-4
3	LFQ-5	LFQ-5
4	FL-3	FL-5
5	LFQ-5	LFQ-5
6	FL-2	FL-4
7	LFQ-5	LFQ-4
8	FL-3	FL-5
9	LFQ-5	LFQ-7
10	LFQ-4	FL-5
Average of 10 Observations	4.1	4.9

TEST DESCRIPTION

Test NY-A

A 1964, 4-door Dodge weighing 3800 lbs was chosen for the first test which was conducted on March 20, 1970. Speed at impact was 55.4 mph and the angle between the bridge rail and impacting vehicle was 25°. The path of the vehicle's c.g. is depicted graphically in Figure 7. Average longitudinal deceleration calculated from the high-speed films was 1.3 g's. Deceleration perpendicular to the rail, from the high-speed film, was 4.8 g's. (The method used for computing average decelerations is given in Figure 25.)

Approximately 50 ft of bridge rail and guardrail were damaged in the crash and 12 bridge posts and guard posts were destroyed or damaged to some extent.

Vehicle damage is shown in Figure 9, and was rated as 4.1 on the severity index published by the National Safety Council.[2]

Sequential photographs of the crash are shown in Figures 10 and 11. Damage to the guardrail-bridge rail installation is shown in Figures 12, 13, 14, and 15.

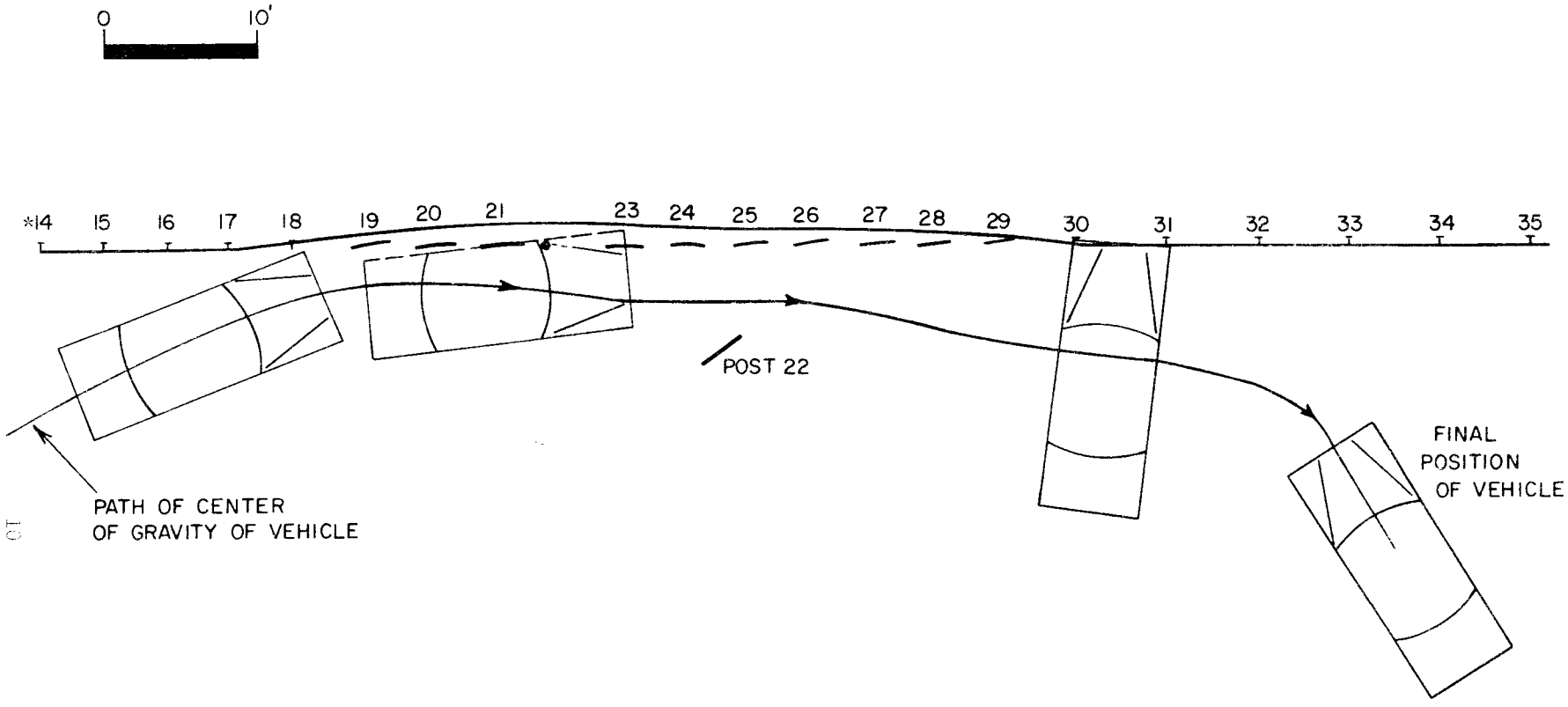

FIGURE 7, PATH OF VEHICLE'S c.g.— TEST 505 NY-A

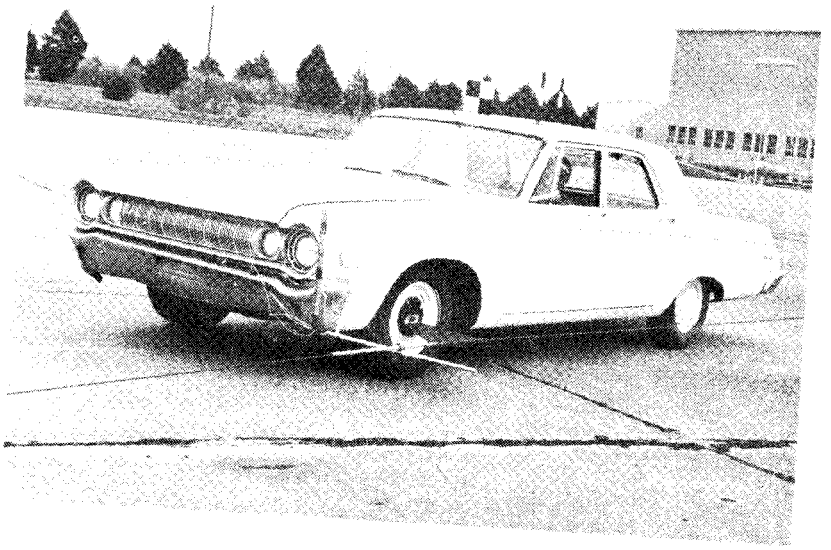

Figure 8, NY-A Vehicle Before Test.

Figure 9, NY-A Vehicle After Test.

1

2

3

4

5

6

Figure 10, Sequence Photographs of Test NY-A (View parallel to bridge rail).

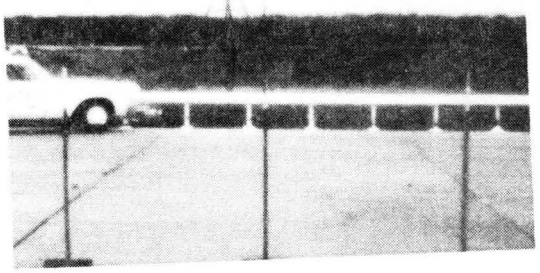

1

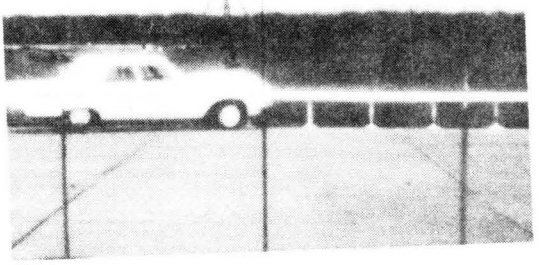

2

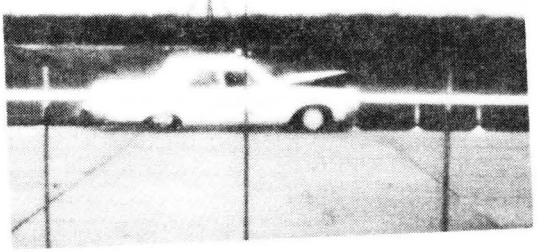

3

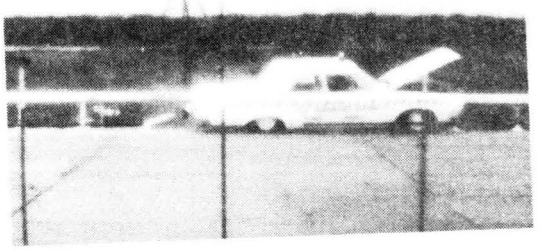

4

5

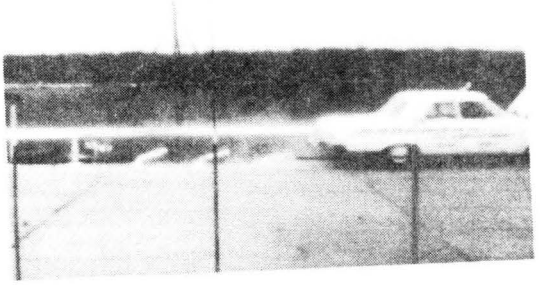

6

Figure 11, Sequence Photographs of Test NY-A (View perpendicular to bridge rail).

Figure 12, Deflection of Bridge Rail-Guardrail in Test NY-A.

Figure 13, Damaged Bridge Posts in Test NY-A.

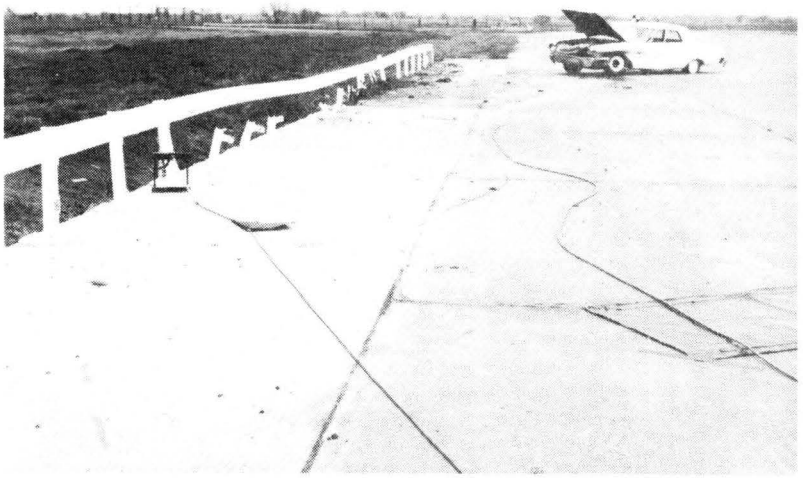

Figure 14, Overall View of Damaged Installation, Test NY-A.

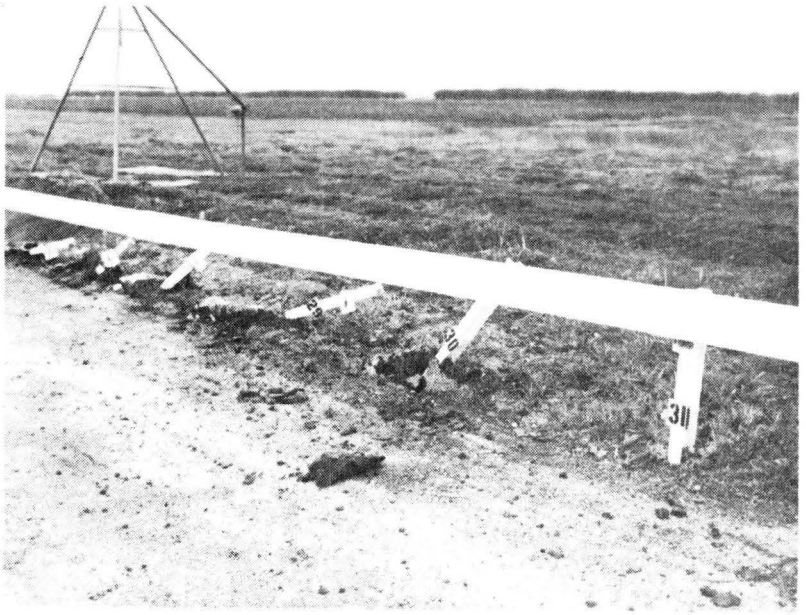

Figure 15, Damaged Guardrail, Test NY-A.

Test NY-B

The second and final test was designed to test the critical point of the guardrail-bridge rail transition. In other barrier systems, potentially hazardous conditions have been observed during collisions at this point. One of the major stimuli for using the continuous box beam in both the guardrail area and the bridge rail area is the fact that a smooth transition in barrier stiffness can be achieved, thus in effect eliminating the potential problem of the transition. It was the opinion of the New York designers that this was a major advantage of the system, and this property was recognized by the Federal Highway Administration.

The test was conducted on April 17, 1970 using a 1964, 4-door Dodge weighing 3670 lbs. The angle between the approach path of the vehicle and the rail was 25° as in the first test. Speed at the time of impact was 57.9 mph. A graphic description of the path of the vehicle's c.g. is provided in Figure 16. Average longitudinal deceleration calculated from film data was 2.1 g's. Average deceleration perpendicular to the bridge rail was calculated from high-speed film as 5.1 g's.

Damage was incurred on approximately 60 ft of the barrier, with some 11 bridge and guard posts bent or broken. Vehicle damage is shown in Figure 18, and was rated as 4.9 on the severity index published by the National Safety Council.[2]

Figures 19 and 20 give two views of the crash with sequential photographs from high-speed film. Figures 21 through 24 show damage to the barrier.

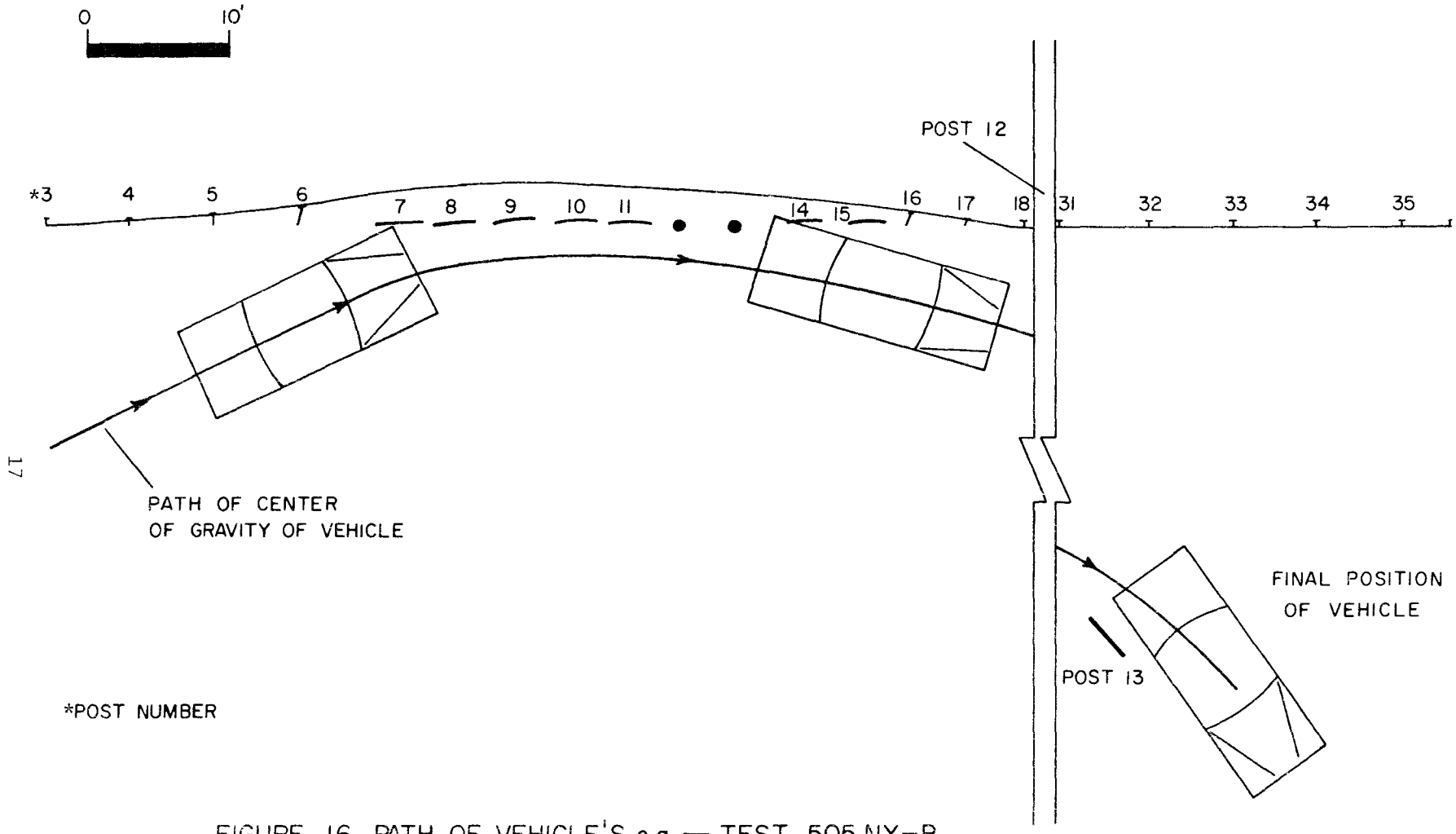

FIGURE 16, PATH OF VEHICLE'S c.g. — TEST 505 NY-B

Figure 17, NY-B Vehicle Before Test.

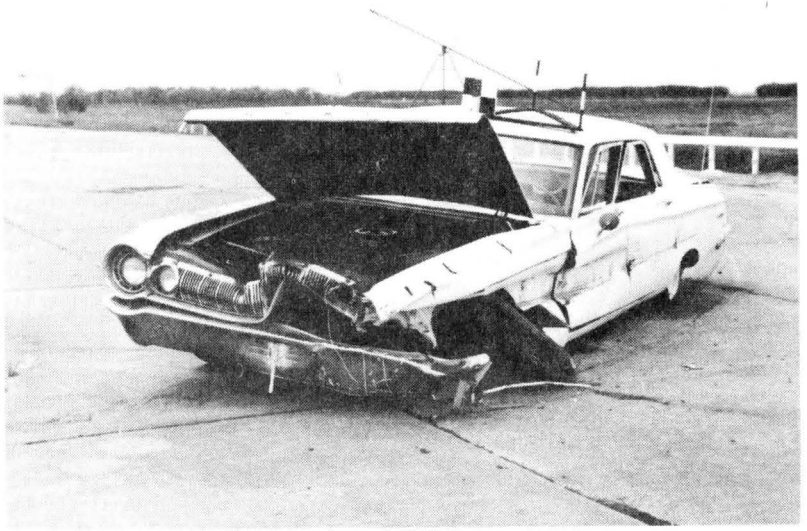

Figure 18, NY-B Vehicle After Test.

1

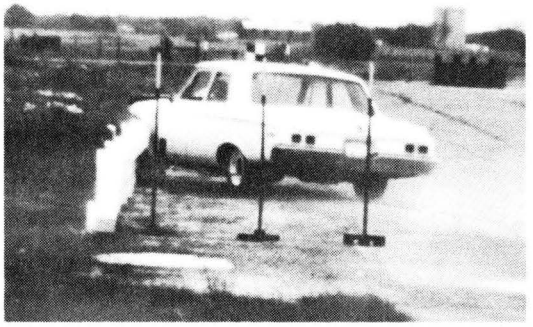

2

3

4

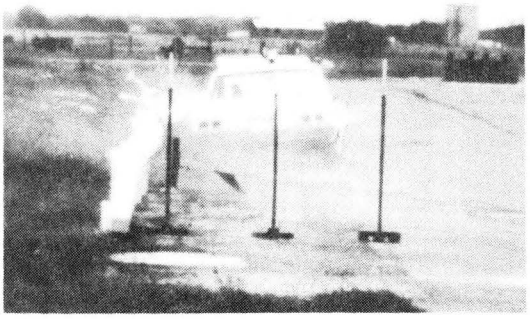

5

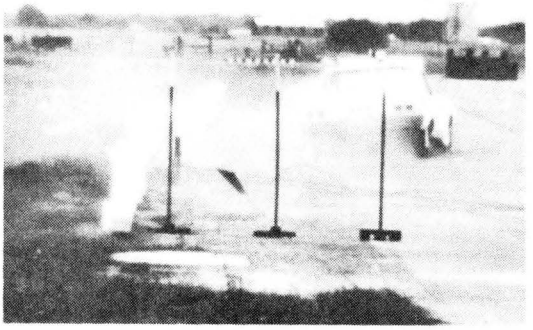

6

Figure 19, Sequence Photographs of Test NY-B
(View parallel to bridge rail).

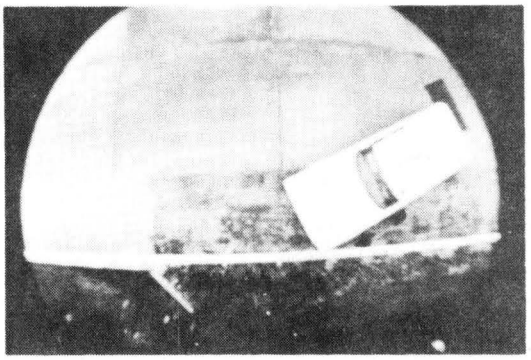

1

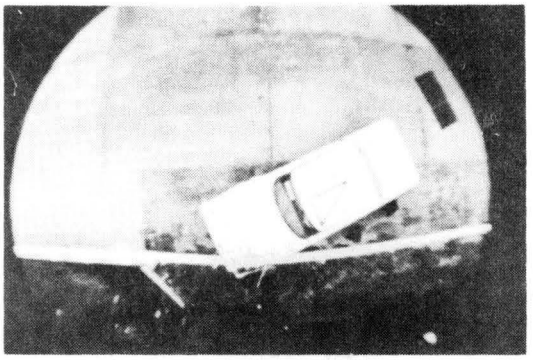

2

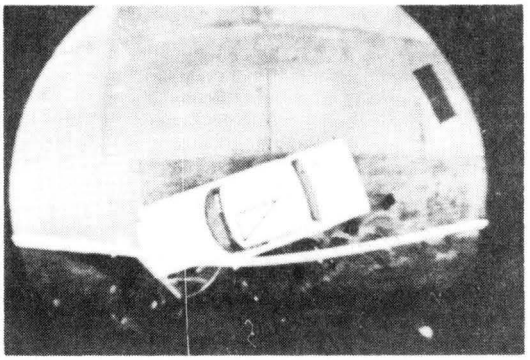

3

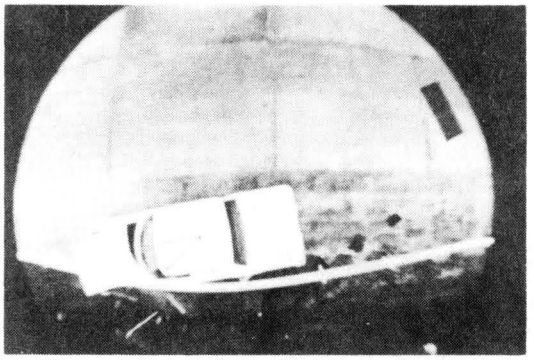

4

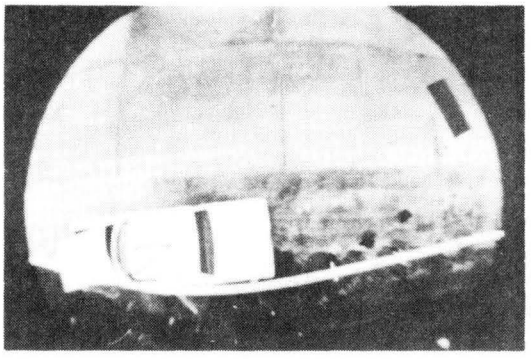

5

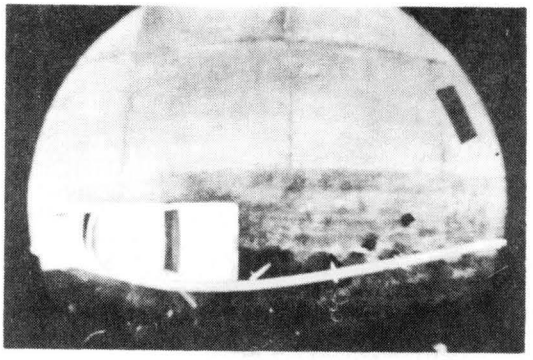

6

Figure 20, Sequence Photographs of Test NY-B (Overhead View).

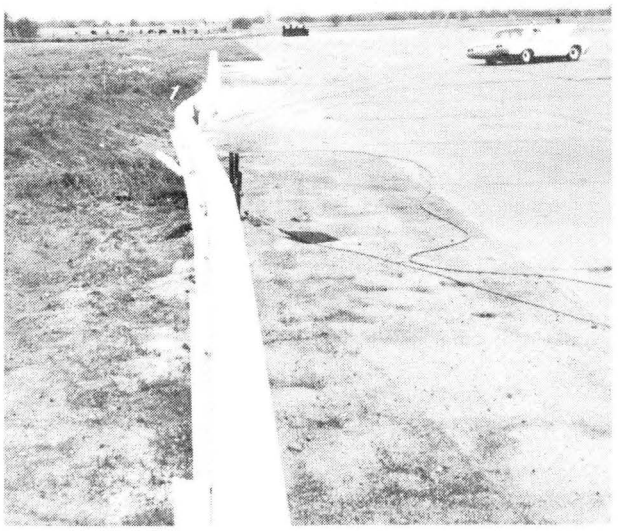

Figure 21, Deflection of Bridge Rail-Guardrail, Test NY-B.

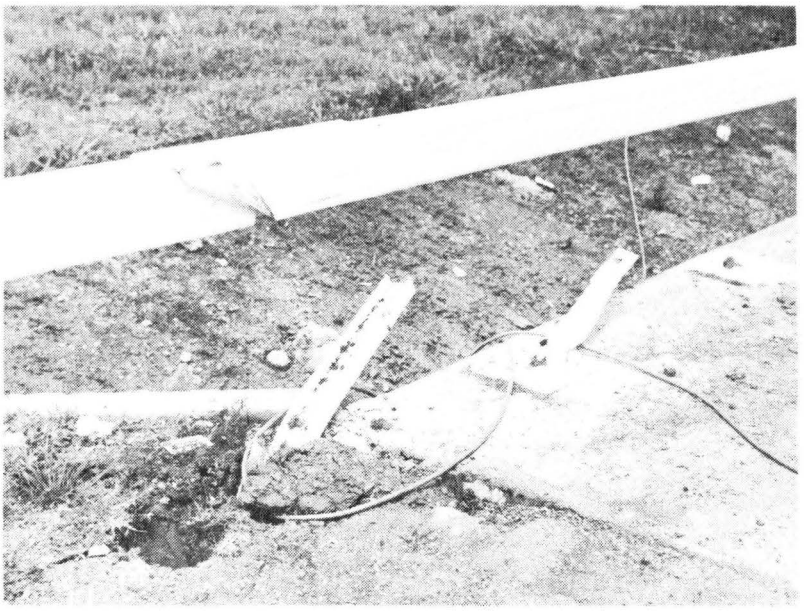

Figure 22, Damage at Bridge Rail-Guardrail Transition, Test NY-B.

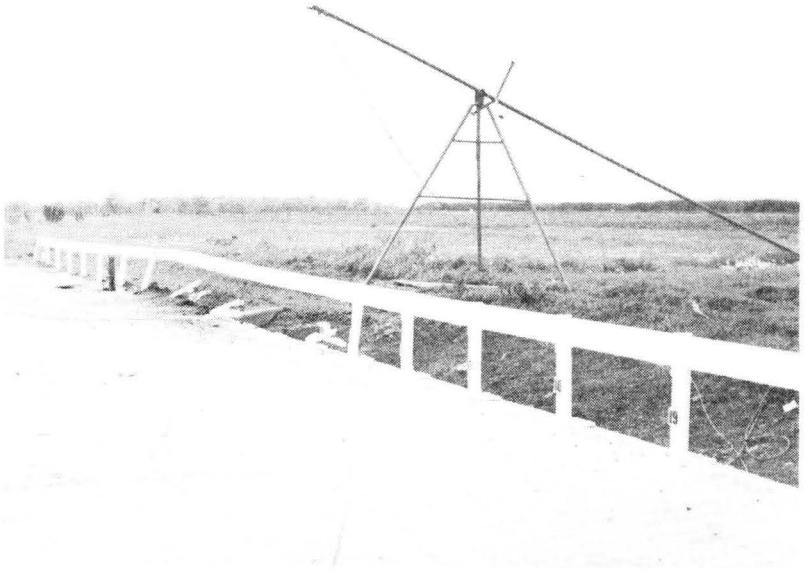

Figure 23, Overall View of Damaged Installation, Test NY-B.

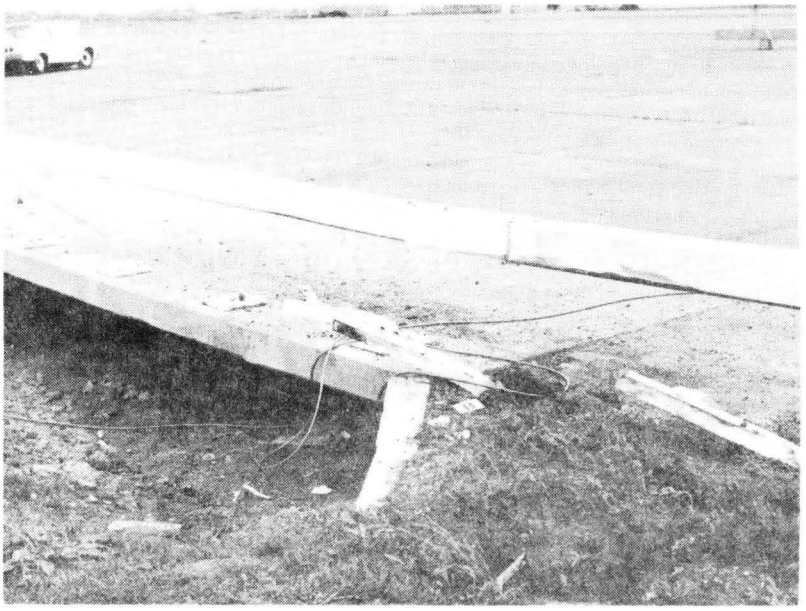

Figure 24, Damaged Bridge Posts, Test NY-B.

PHOTOGRAPHIC DATA

The method employed to compute change in velocity and average deceleration components is defined in Figure 25. The values substituted in the governing equations were taken from data acquired by frame to frame analysis of high-speed films of the collision incident in each test. The data and results from computation are contained in Tables 1, 2 and 3.

Velocities V_1, V_2, and V_3, the directed speeds of the colliding vehicle, were determined by measuring the displacement of some reference mark on the vehicle over an interval of time. V_1 was calculated over a time interval just prior to impact; V_2, when the vehicle became parallel to the rail; and V_3, when the vehicle lost contact with the rail.

The finite increment of displacement, ΔS_{lat}, is computed using Equation (2) in Figure 25. Dimension D_1 is computed using AL and B for each vehicle and the angle θ for each test. Dimension D_2 is estimated from high-speed films obtained from a camera located parallel to the bridge rail.

The distance ΔS_{long} is observed from high-speed film using a camera placed perpendicular to the bridge rail.

The average decelerations perpendicular and parallel to the rail (Average G_{lat} and Average G_{long}) are computed by Equations (3) and (4) shown in Figure 25. The average total deceleration (Average G_{total}) is defined as the vector sum of these components, as shown in Figure 25.

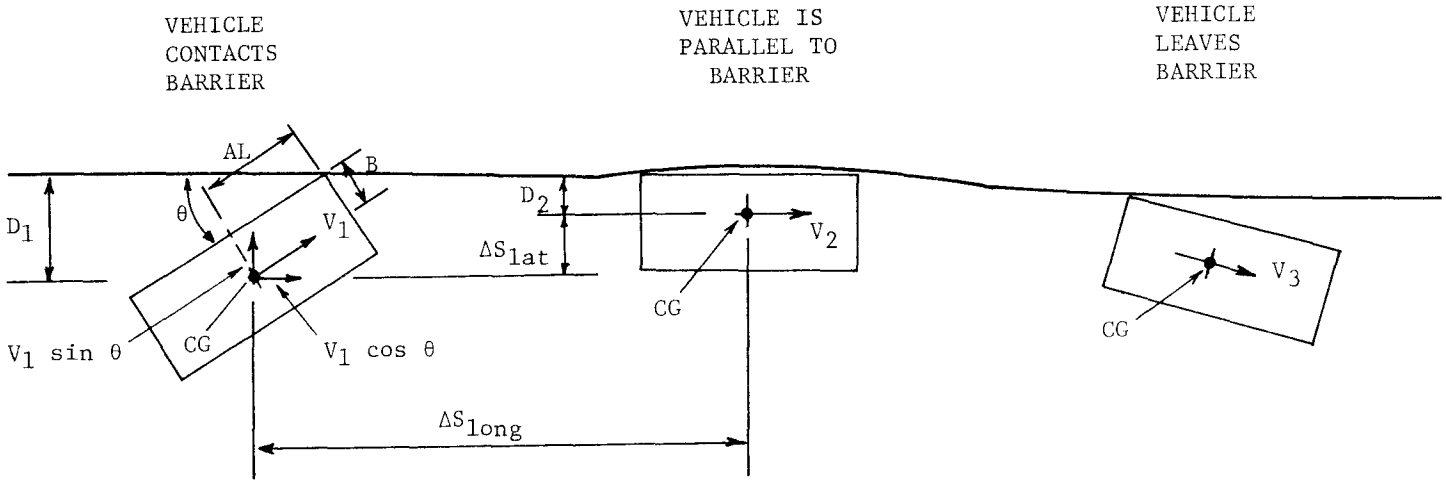

GOVERNING EQUATIONS:

(1) $\Delta V = V_3 - V_1$

(2) $\Delta S_{lat} = D_1 - D_2$

(3) Average $G_{lat} = \dfrac{(V_1 \sin \theta)^2}{2g\Delta S_{lat}}$

(4) Average $G_{long} = \dfrac{(V_1 \cos \theta)^2 - V_2^2}{2g\Delta S_{long}}$

(5) Average $G_{total} = \left[(\text{Avg. } G_{lat})^2 + (\text{Avg. } G_{long})^2\right]^{1/2}$

FIGURE 25, GEOMETRIC REPRESENTATION OF PHOTOGRAPHIC ANALYSIS

TABLE 1

SUMMARY OF TEST DATA

Factor	Test	
	NY-A	NY-B
VEHICLE		
Year	1964	1964
Make	Dodge	Dodge
Weight, lbs	3800	3670
Angle of Impact, deg	25	25
FILM DATA		
Initial Speed (V_1), ft/sec	81.2	85.0
mph	55.4	57.9
Speed at loss of contact (V_3), ft/sec	----*	53.1
mph	----*	36.2
Speed when vehicle is parallel to rail (V_2), ft/sec	60.8**	57.3
mph	41.5**	39.1
ΔS_{long}, ft	21.3**	20.0
ΔS_{lat}, ft	3.9**	3.9
Average G_{long}, g's	1.3	2.1
Average G_{lat}, g's	4.8	5.1
Average G_{total}, g's	5.0	5.5
Maximum Guardrail Deflection, ft	1.5	3.0
Residual Barrier Deformation, ft	0.25	1.25

*No V_3 as defined in Figure 25 due to vehicle spinout.
**Since vehicle never became parallel, these computations were made when the vehicle was at its minimum angle with the rail (5°).

TABLE 2

TEST 505 NY-A

High-Speed Film Data

Time (msec)		Displacement (ft)	
-57		-4.7	
-49		-4.0	
-41		-3.3	V_1 = 81.2 ft/sec
-33		-2.7	
-24		-2.0	
-16		-1.4	
-8		-0.7	
0	Impact	0	
19		1.5	
38		3.1	
57		4.6	
75		6.1	
94		7.5	
113		8.9	
132		10.2	
151		11.4	
170		12.7	

Time (msec)	Displacement (ft)	
(continued)		
189	14.0	
208	15.1	
226	16.4	
245	17.5	
264	18.7	
283	19.9	
302	21.1	
321	22.3	V_2 = 60.8 ft/sec
340	23.4	
358	24.6	
377	25.7	
396	26.8	
415	27.9	
434	29.0	
453	30.1	
472	31.2	

TABLE 3

TEST 505 NY-B

High-Speed Film Data

Time (msec)	Displacement (ft)	Time (msec)	Displacement (ft)
-76	-6.5	(continued)	
-63	-5.4	251	18.4
-51	-4.3	271	19.6
-38	-3.2	290	20.6
-25	-2.2	309	21.8
-13	-1.1	329	22.9
0 Impact	0	348	24.0
13	1.0	367	25.1
25	2.0	387	26.2
38	3.1	406	27.2
51	4.1	425	28.3
63	5.1	445	29.3
76	6.1	464	30.4
89	7.1	483	31.4
101	8.0	503	32.4
114	8.9	522	33.5
127	9.8	541	34.5
139	10.7	561	35.5
155	12.1	580	36.6
174	13.3	599	37.6
193	14.7	618	38.6
213	16.0	638	39.6
232	17.2		

V_1 = 85.0 ft/sec

V_2 = 57.3 ft/sec

V_3 = 53.1 ft/sec

SUMMARY AND CONCLUSIONS

A summary of data obtained in the two tests is given in Table 1. Based on these data and detailed analysis and observation of the high-speed film, the following conclusions are presented:

1. In both tests, the barrier installation performed the basic function of containing and redirecting the vehicle. An excellent transition between guardrail and bridge rail is achieved by this strong beam-weak post system.

2. Vehicle compartment encroachment was negligible in each test.

3. All deceleration levels are within the survivable range given by Olson et al.[3] The deflection of the box-beam acts to reduce the decelerations experienced by passengers and to reduce damage to the vehicle. A properly seat-belted, shoulder-harnessed passenger would probably have sustained only minor injuries in both crashes. The test parameters of 25° and 60 mph are extreme, considering probable accident conditions, and are more in the nature of a "strength" test of the barrier system. Collisions with this barrier at lower angles and speeds should result in a very low probability of passenger injury.

Tentative service requirements suggested in NCHRP Report 86 are listed below:

1. A bridge rail system must laterally restrain a selected vehicle.
2. A bridge rail system must minimize vehicle deceleration.
3. A bridge rail system must smoothly redirect a colliding vehicle.
4. A bridge rail system must remain intact following a collision.
5. A bridge rail system which serves vehicles and pedestrians must provide protection for vehicle occupants and pedestrians.

6. A bridge rail system must have a compatible approach rail or other device to prevent collisions with the end of the bridge rail system.
7. A bridge rail system must define yet permit adequate visibility.
8. A bridge rail must project inside the face of any required curb.
9. A bridge rail system must be susceptible of quick repair.
10. The foregoing requirements must be met by giving emphasis first to safety, second to economics, and third to aesthetics.

Evaluations of vehicle-barrier interaction on the basis of these service requirements are presented in Table 4. The evaluations were made using information from high-speed films, a National Safety Council damage rating scale, estimates of probable injuries from Figures 7 and 8 of NCHRP Report 86[3], and examination of the barrier after each test. Safety, economics, and aesthetics (Service Requirement 10) are evaluated in the table by assigning a numerical value for each test. It is recognized that the vehicle weight, speed, and consequently impact force varied widely between tests. The evaluation of each item was made with these facts in mind.

TABLE 4

EVALUATION OF BARRIERS USING TENTATIVE SERVICE REQUIREMENTS

Service Requirement	New York Box Beam Bridge Rail (Test NY-A)	New York Box Beam Bridge Rail (Test NY-B)
1	Lateral restraint adequate - Penetration and vaulting did not occur.	
2	G_{Total} = 5.0 Vehicle Damage Rating: 4.1 Probability of Injury: 35%	G_{Total} = 5.5 Vehicle Damage Rating: 4.9 Probability of Injury: 40%
3	Good Redirection Slight Snagging	Good Redirection Moderate Snagging
4	Both barriers remained in tact in that box beam held though posts were torn loose.	
5	Not Applicable	Not Applicable
6	Yes	Yes
7	Rail and post system does define yet permits adequate visibility.	
8	No Curb	No Curb
9	Replace 12 Posts Replace Two 25' Rail Sections Quick Repair Possible	Replace 11 Posts Replace Three 25' Rail Sections Quick Repair Possible
10	Safety: 1 Economics: Vehicle Repair: 1 Barrier Repair: 1 Aesthetics: 1	Safety: 2 Economics: Vehicle Repair: 2 Barrier Repair: 2 Aesthetics: 1

REFERENCES

1. Graham, Malcolm D., et al. "New Highway Barriers: The Practical Application of Theoretical Design." Highway Research Record 174, pp. 88-183, 1967.

2. "Vehicle Damage Scale For Traffic Accident Investigators," National Safety Council, TAD Project Technical Bulletin No. 1, 1968.

3. Olson, R. M., Post, E. R., and McFarland, W. F., "Tentative Service Requirements For Bridge Rail Systems," National Cooperative Highway Research Program Report 86, NCHRP Project 12-8, FY '66. Library of Congress Catalogue Number: 70-605165, 1970.

TECHNICAL MEMORANDUM 505-13

Texas Transportation Institute
Texas A&M Research Foundation

IMPACT RESPONSE OF FIFTY-FOOT LUMINAIRE SUPPORT STRUCTURES

A TENTATIVE PROGRESS MEMORANDUM ON CONTRACT CPR-11-5851
U.S. Department of Transportation
Federal Highway Administration
Bureau of Public Roads

by

J. E. Martinez
Assistant Research Engineer

and

T. J. Hirsch
Research Engineer

and

J. J. Jumper
Research Assistant

This memorandum presents the results of mathematical simulation of vehicle collision with fifty-foot luminaire support structures mounted on bases offering low resistances. The work was conducted under the Office of Research and Development, Structures and Applied Mechanics Division, Research Program on Structural Systems in Support of Highway Safety (4S Program). The opinions, findings, and conclusions expressed in this report are those of the authors and not necessarily those of the Bureau of Public Roads.

December 19, 1969

IMPACT RESPONSE OF FIFTY-FOOT LUMINAIRE SUPPORT STRUCTURES

General Background and Problem Description

This report presents the findings of a small parameter study conducted to determine the impact response of luminaire support structures having a mounting height of 50 ft and mounted on frangible breakaway-type bases. Previous studies investigated the behavior of 30 and 40 ft high installations under a variety of conditions and it is felt that the results presented herein will give an insight to the response of taller installations. The inter-relationships of some identifiable parameters can be observed in the typical charts presented in Figs. A1 and A2 in the appendix. These results are for a 40-ft installation and are also presented in Ref. 1.

The study was conducted for an aluminum tapered shaft having dimensions of 12" O. D. (base) x 6.6" O. D. (top) x 43.6' long (.219" wall thickness). The mast arm was taken to have a length of 15 ft and a 75-lb luminaire was assumed. Breakaway base energy levels of 750 ft-lbs and 3000 ft-lbs were considered for the supports. The 750 ft-lb level is typical of a slip-type attachment and the 3000 ft-lb value is typical of some frangible aluminum bases. The vehicular impact speed was varied from 15 mph to 45 mph and vehicular weights of 2000 lbs, 3000 lbs, and 5000 lbs were employed. A central head-on impact was assumed for all cases.

The mathematical model was verified by results obtained from full-scale crash tests and is basically the same one discussed in Ref. 1,

except for minor modifications in the initial part of the motion. The computer coding was rewritten and a more efficient Runge-Kutta numerical integration procedure was employed. Considerable time was spent in optimizing the coding with the net result being a highly efficient computer program capable of solving problems in a minimum amount of computer time.

Discussion of Results

Tables 1 and 2 present the results of the study for supports mounted on bases having 750 ft-lb and 3000 ft-lb base fracture energies. The tabulated information consists of vehicular velocity changes, deceleration rates, vehicle-support contact times, and lateral movement of the luminaire support structure. The lateral movement values represent the maximum translation of the structure, in the direction of the roadway, at the instant the structure initially hits the ground. These values are measured with respect to a coordinate system having its origin at the base of the support and give an indication of where the structure will come to rest. A typical support hitting the ground is shown in Figs. 1 and 2.

The study revealed that for all the cases considered, the vehicular velocity changes and deceleration rates remained within allowable limits. This is based on criteria established in Ref. 2 which considers vehicular velocity changes during impact in excess of 11 mph as hazardous.

Collisions at the slower velocities (15 mph) are characterized by a secondary collision between the falling pole and the car. These cases have the support acquiring just enough kinetic energy to translate a

short distance, strike the ground, and then fall on the vehicle. These collisions can be considered hazardous as the support could strike the passenger compartment area of the vehicle and cause injury to the occupants or strike the vehicle and then come to rest on the roadway, thus creating an unsafe condition for other near-by motorists.

The lateral translations obtained from the study reveal that, excluding the 15 mph collisions, maximum movements of approximately 10.5 ft can be expected. It should be emphasized that these translations are taken at the instant the support strikes the ground and, depending on the impact point and the structure's angular kinetic energy, the maximum translation could conceivably be greater when the structure comes to rest.

Conclusions

From this limited exploratory study, it can be concluded that luminaire support structures of 50-foot mounting heights can be designed to have safe, initial damage-limiting characteristics when bases of low-fracture energies are utilized. Secondary collision characteristics of the severed pole with the impacting vehicle for conditions other than those assumed in this study cannot be acceptably established with any degree of confidence.

Recommendations

The study presented in this report has been conducted for bases offering low resistance and has assumed a central, head-on vehicle impact. The majority of the present 50-ft installations employ bases

having fracture energies greater than those investigated here, and since most collisions are not central, it is believed that a more complete study is required to establish the level of safety of these structures. It is therefore recommended that this basic exploratory investigation be expanded into a more comprehensive study to include greater ranges of the parameters considered herein, angular impacts as well as possibly other parameters, other constructional materials, and secondary collision characteristics.

Vehicle Weight (lbs)	Vehicle Impact Velocity (mph)	Change in Vehicle Velocity (mph)	Average Vehicle Deceleration (g's)	Contact Time (sec)	Support Lateral Movement (ft)	Comments
2000	15	1.70	1.18	0.065	--	Base of support hits in front of vehicle and secondary collision follows
2000	30	1.20	1.08	0.049	10.40(T)	Luminaire hits ground
2000	45	1.30	1.60	0.036	7.96(T)	Luminaire hits ground
3500	15	0.72	0.36	0.091	--	Base hits ground in front of vehicle and secondary collision follows
3500	30	0.55	0.30	0.083	6.86(T)	Top of post hits ground
3500	45	0.50	0.70	0.032	9.13(L)	Luminaire hits ground
5000	15	0.45	0.46	0.045	--	Base of support hits in front of vehicle and secondary collision follows
5000	30	0.30	0.30	0.038	3.65(T)	Top of post hits ground
5000	45	0.34	0.54	0.029	7.48(L)	Luminaire hits ground

(T) Translation of top of post
(L) Translation of luminaire

Table 1. Results for Collisions With 50-Ft. Support Structures Mounted on Bases Having an Energy Level of 750 ft-lbs.

Vehicle Weight (lbs)	Vehicle Impact Velocity (mph)	Change in Vehicle Velocity (mph)	Average Vehicle Deceleration (g's)	Contact Time (sec)	Support Lateral Movement (ft)	Comments
2000	15	6.10	3.80	0.072	--	Base of support hits in front of vehicle and secondary collision follows
2000	30	3.40	3.40	0.046	8.14(T)	Top of post hits ground
2000	45	2.60	3.30	0.036	9.36(T)	Luminaire hits ground
3500	15	4.56	1.96	0.106	--	Base of support hits in front of vehicle and secondary collision follows
3500	30	2.40	1.24	0.088	9.40(T)	Luminaire hits ground
3500	45	1.70	2.10	0.037	4.32(B)	Top of post hits ground
5000	15	2.30	1.50	0.071	--	Base of support hits in front of vehicle and secondary collision follows
5000	30	1.40	1.25	0.050	9.97(T)	Top of post hits ground
5000	45	1.02	1.23	0.038	9.64(L)	Luminaire hits ground

(B) Translation of base of support

Table 2. Results for Collisions With 50-Ft. Support Structures Mounted on Bases Having an Energy Level of 3000 ft-lbs.

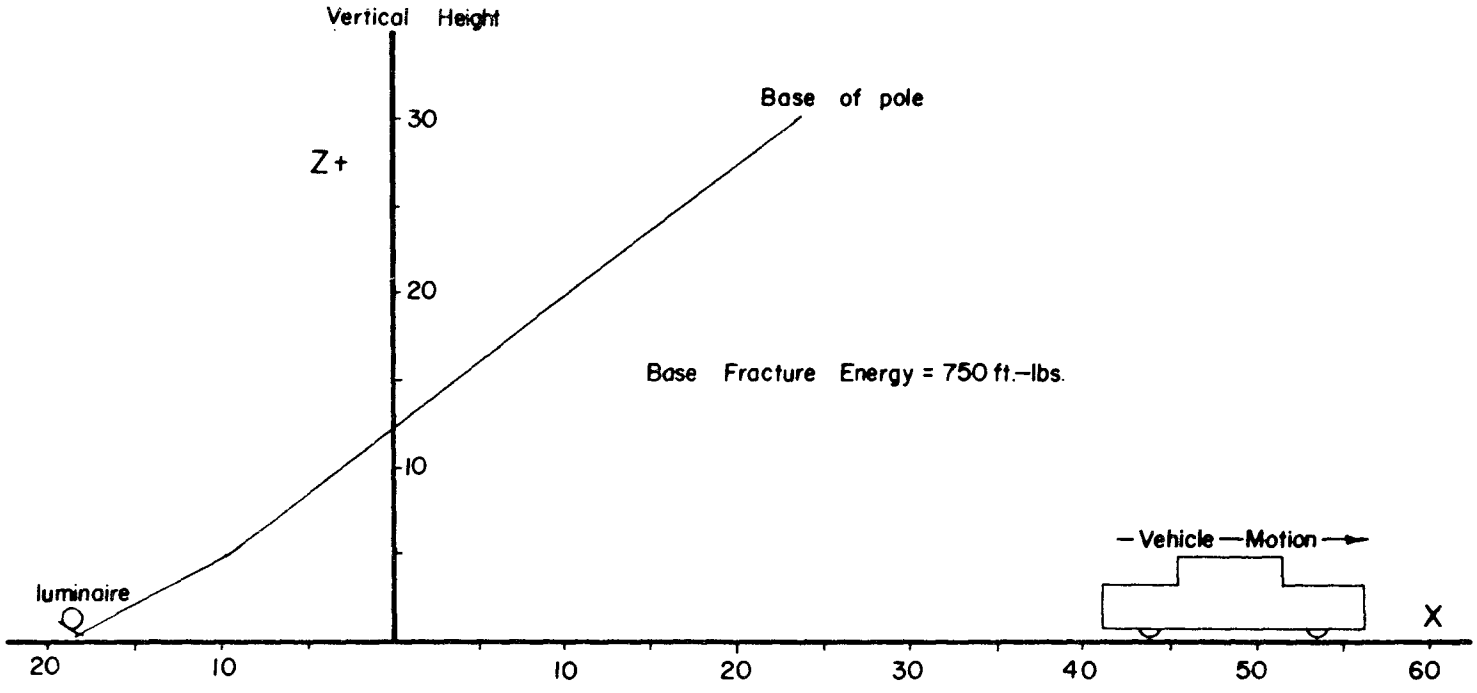

FIGURE·1 IMPACT BY 3500 lbs. VEHICLE TRAVELLING AT 45 mph

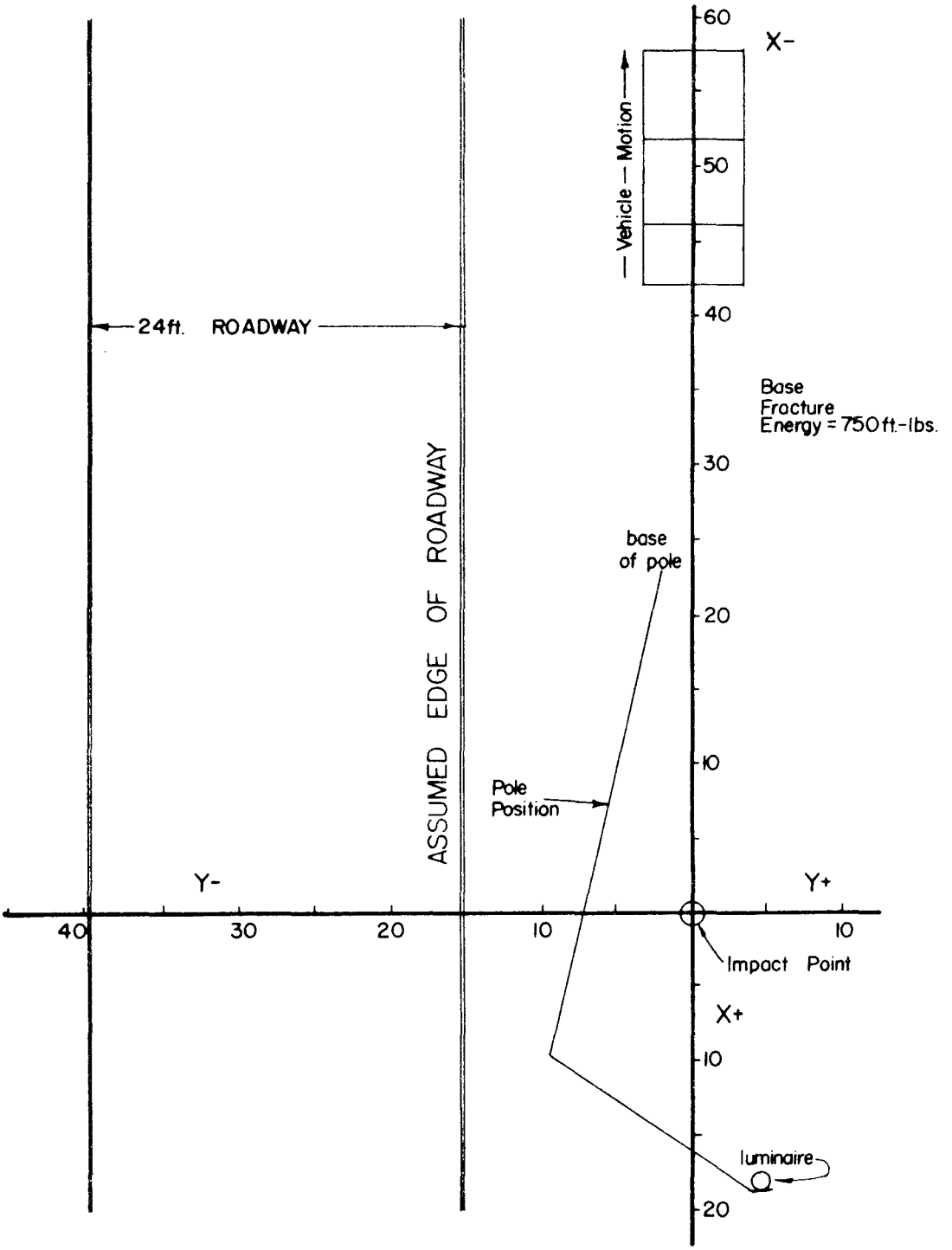

FIGURE·2 IMPACT BY 3500 lbs. VEHICLE TRAVELLING AT 45 mph

APPENDIX A

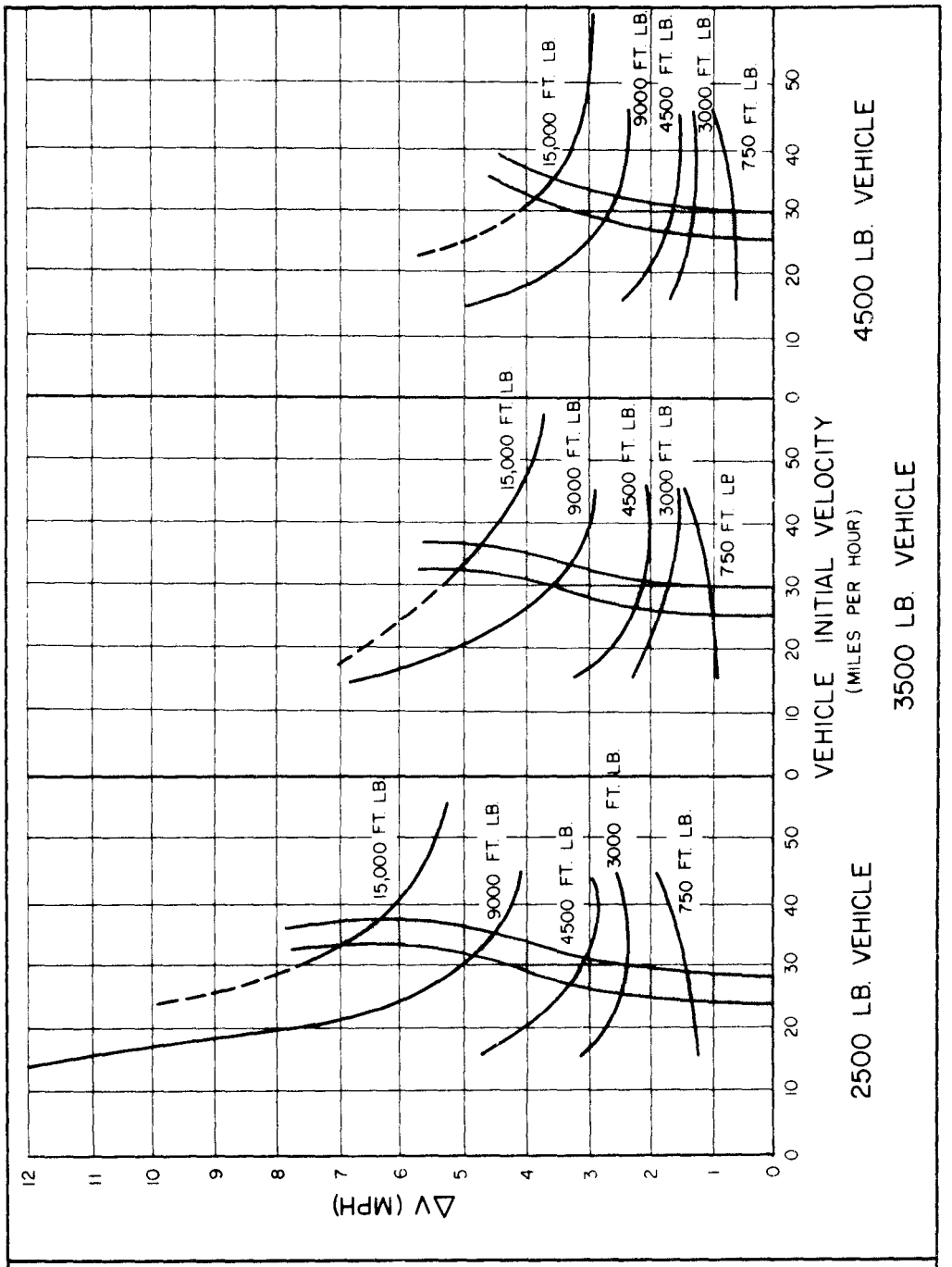

FIGURE A-1 40 FT. M.H. ALUMINUM SUPPORT

FIGURE A-2 40 FT. M.H. STEEL SUPPORT

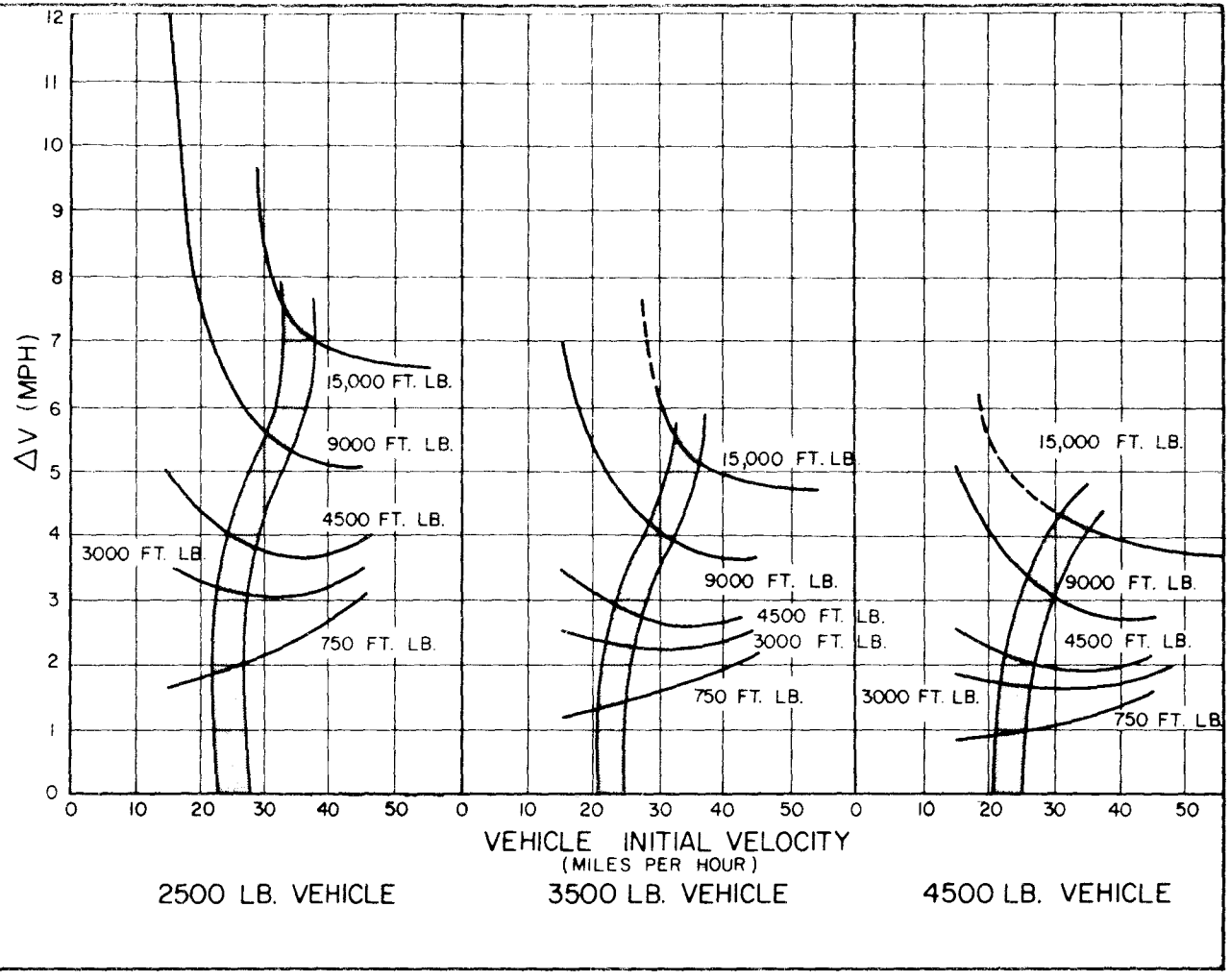

References

1. Edwards, T. C., Martinez, J. E., et al., "Development of Design Criteria for Safer Luminaire Supports," Final Report, NCHRP Project 15-6, Texas Transportation Institute, Texas A&M Research Foundation, Texas A&M University, College Station, Texas.

2. Patrick, L. M., et al., Knee, Chest, and Head Impact Loads, Proceedings of the 11th Stapp Car Crash Conference, Anaheim, California, October 10-11, 1967, p. 116.

TECHNICAL MEMORANDUM 505-14

Texas Transportation Institute
Texas A&M Research Foundation

FIBERGLASS MEDIAN BARRIER

A Test And Evaluation Report On Contract No. CPR-11-5851

U.S. Department of Transportation
Federal Highway Administration

by

G. G. Hayes
Research Associate

M. A. Pittman
Research Associate

and

T. J. Hirsch
Research Engineer

These crash tests and evaluations were conducted under the Office of Research and Development, Structural and Applied Mechanics Division's Research Program on Structural Systems in Support of Highway Safety (4S Program).

May 1971

Introduction

A full-scale vehicle crash test was conducted on a prototype soil-filled fiberglass median barrier designed and fabricated by the Molded Fiberglass Resin Company of Ashtabula, Ohio. The median barrier was previously analyzed and subjected to scale-model tests by IIT Research Institute of Chicago, Illinois.[1,2*] This report presents the results of the single crash test.

*Superscript numerals refer to corresponding numerals in selected references.

Barrier Description

The barrier consists of a fiberglass trough containing fill material. Ten foot sections are bolted together to form the trough. Figure 1 is a drawing of a section of the barrier, while Figures 2, 3, and 4 are photographs of the test installation. A fiberglass guardrail or rubrail is attached to the outside of the barrier to form a vehicle redirectional surface. This rail is shown in Figures 1 and 2. The lower portion of the barrier rests in a 10 in. wide by 11 in. deep trench parallel to the roadway. Pea gravel was used as fill material for the test conducted by TTI. A 150 ft. length of median barrier was installed adjacent to a concrete vehicle-approach area as shown in Figure 4.

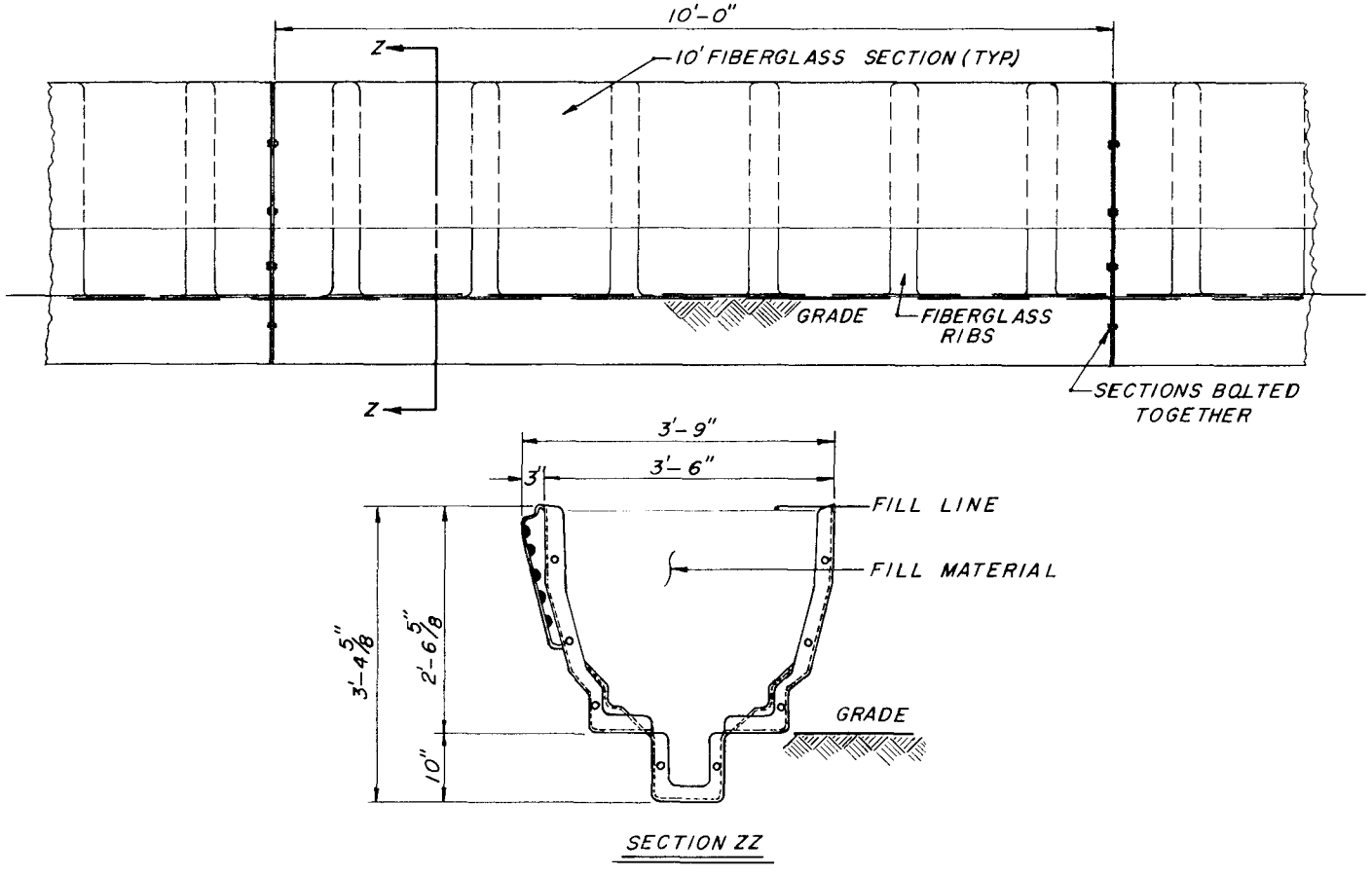

Figure 1 Detail of fiberglass section.

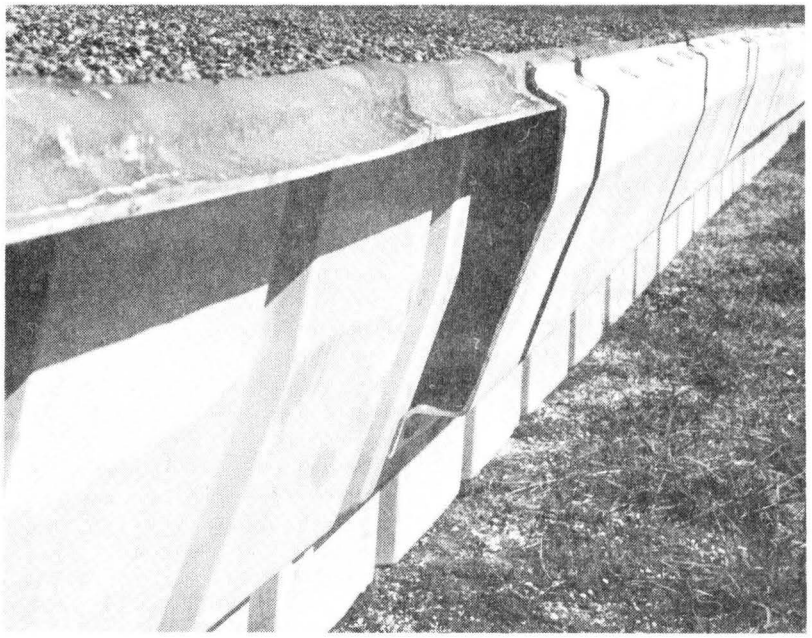

Figure 2 , Ground Level View of Rubrail Bolted To Fiberglass Trough

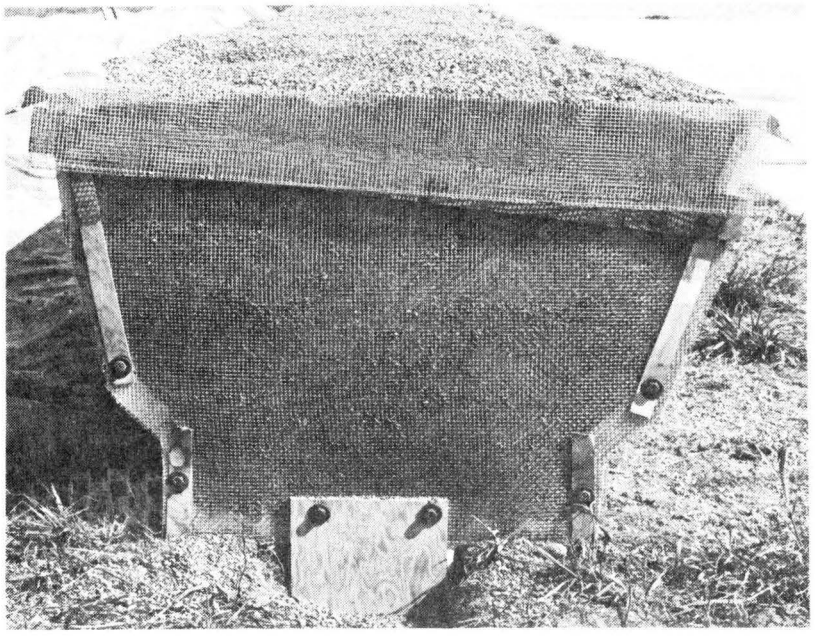

Figure 3 , End View of Fiberglass Median Barrier

Figure 4 , Overhead View of Median Barrier Before Test

INSTRUMENTATION

For this test, four strain gage type accelerometers were mounted on the frame of the vehicle. Two were placed on the left frame member and two on the right frame member. One accelerometer on each frame measured transverse decelerations and the other measured longitudinal decelerations. Longitudinal decelerations represent decelerations toward the rear of the vehicle and transverse decelerations are toward the left of the vehicle. A tri-axial electro-mechanical deceleration device (an Impact-O-Graph) was located on the right rear floorboard of the vehicle.

An Alderson anthropometric dummy, weighing 160 lbs., was placed on the driver's side of the vehicle with a lap belt fastened across the pelvic region. A strain gage load cell was connected to the lap belt to measure the force on the lap belt during impact. The lap belt force trace is shown as a negative force because it represents a rearward force on the dummy.

The signals from the four accelerometers and the load cell were transmitted by telemetry to a ground station where they were recorded on magnetic tape. These data were then passed through an 80 HZ low-pass filter to reduce the effects of "ringing", and then displayed on Visicorder paper.

Four high-speed cameras were used in this test to cover the event. One was placed perpendicular to the barrier; another parallel to the barrier; another perpendicular to the initial path of the vehicle; and the other provided a view from overhead. Each of the high-speed films had timing lights so that elapsed time at any point could be calculated. A stadia board marked in increments of 3 in. on the left side of the vehicle was used in determining distance traveled. These distances were measured on a Vanguard Motion Analyzer.

Initial speed was then computed from the time-displacement data obtained. Two other low-speed cameras, one a panned shot and one a stationary view parallel to the barrier, provided a qualitative coverage of the crash test.

DESCRIPTION OF TEST

A 1966 Chevrolet sedan traveling 54 mph impacted the Fiberglass Barrier at an angle of 25°. The point of impact was 84.5 ft. from the north end of the barrier. The fiberglass trough and rubrail began shattering at 0.046 sec. after impact and allowed the vehicle to penetrate the barrier. The vehicle then ramped and came to a stop astride the barrier (see Figures 5 through 8).

The barrier was damaged severely. Twelve feet of the front wall was completely destroyed, and the back wall collapsed. The vehicle was also damaged extensively, as evidenced by a right front fender residual deformation of 3.1 ft.

A summary of the pertinent data obtained is presented in Table 1. Accelerometers indicated an average longitudinal deceleration of 5.2 g's (average of left and right frame members) over 0.248 sec. and an average transverse deceleration of 2.0 g's (average of left and right frame members) over 0.213 sec.

Time-displacement data from the high-speed films are given in Table 2, and reproductions of the accelerometer and lap belt force traces are shown in Figures 9, 10 and 11. There is some accelerometer activity past the times shown in Figures 9 and 10, but the major decelerations have been included.

1

2

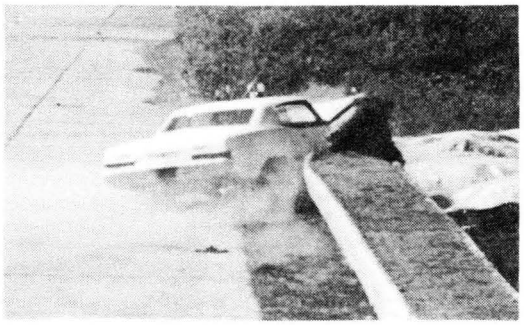

3

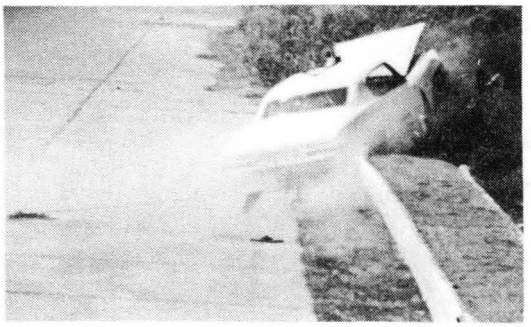

4

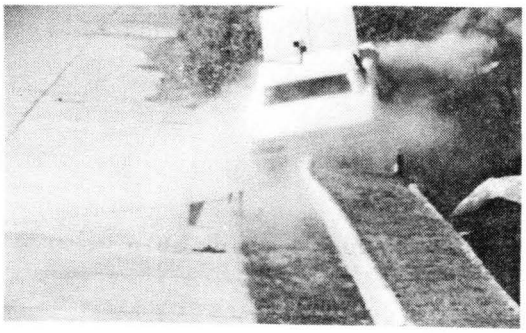

5

6

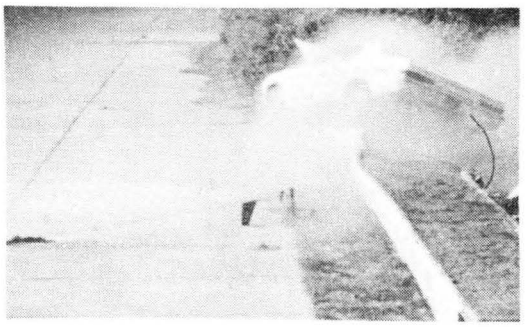

7

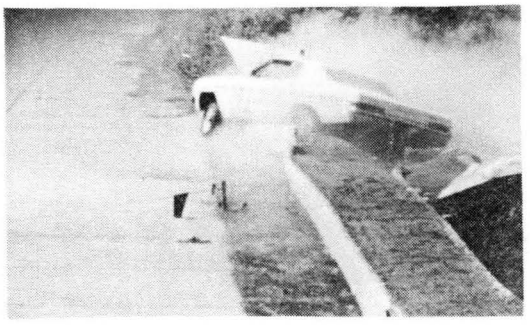

8

Figure 5, Sequential Photographs of Test FG-A (Parallel to Barrier)

T + 0.046 sec.

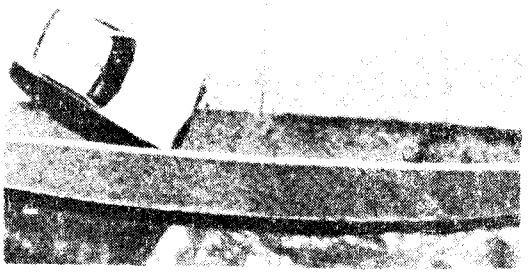

Impact

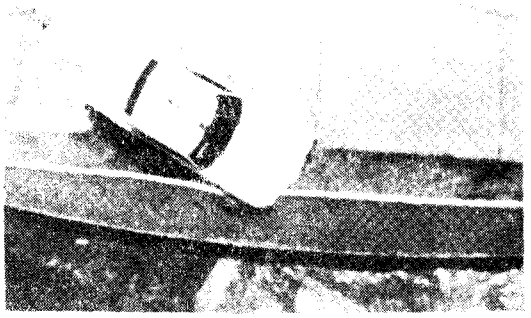

T + 0.054 sec.

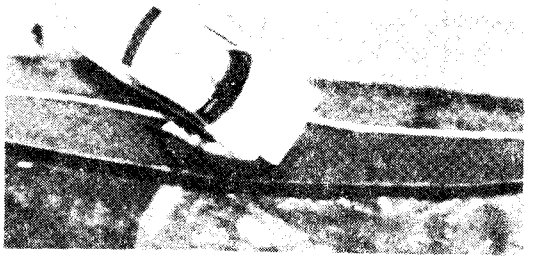

T + 0.120 sec.

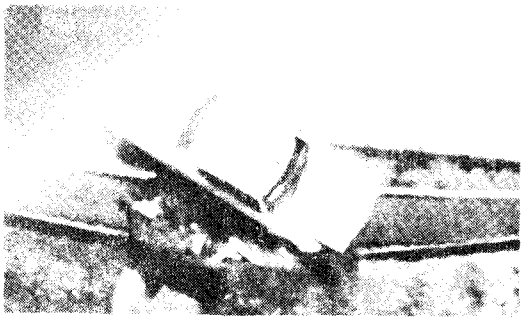

T + 0.262 sec.

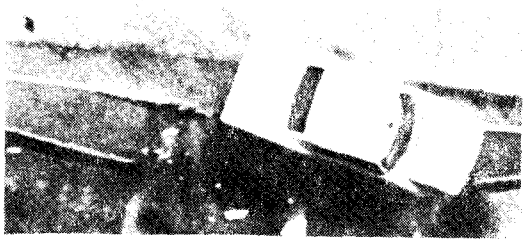

T + 0.391 sec.

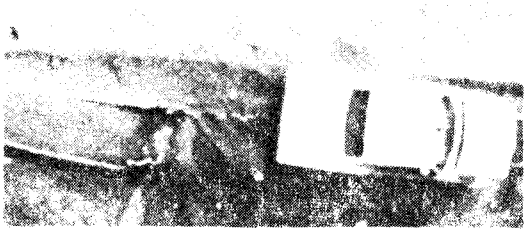

T + 0.663 sec.

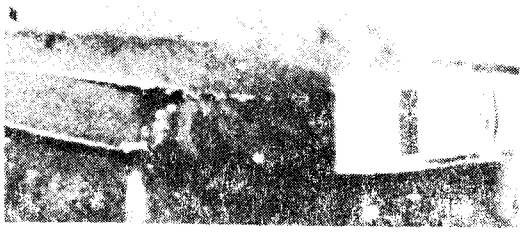

T + 0.834 sec.

Figure 6 , Sequential Photographs of Test FG-A (Overhead View)

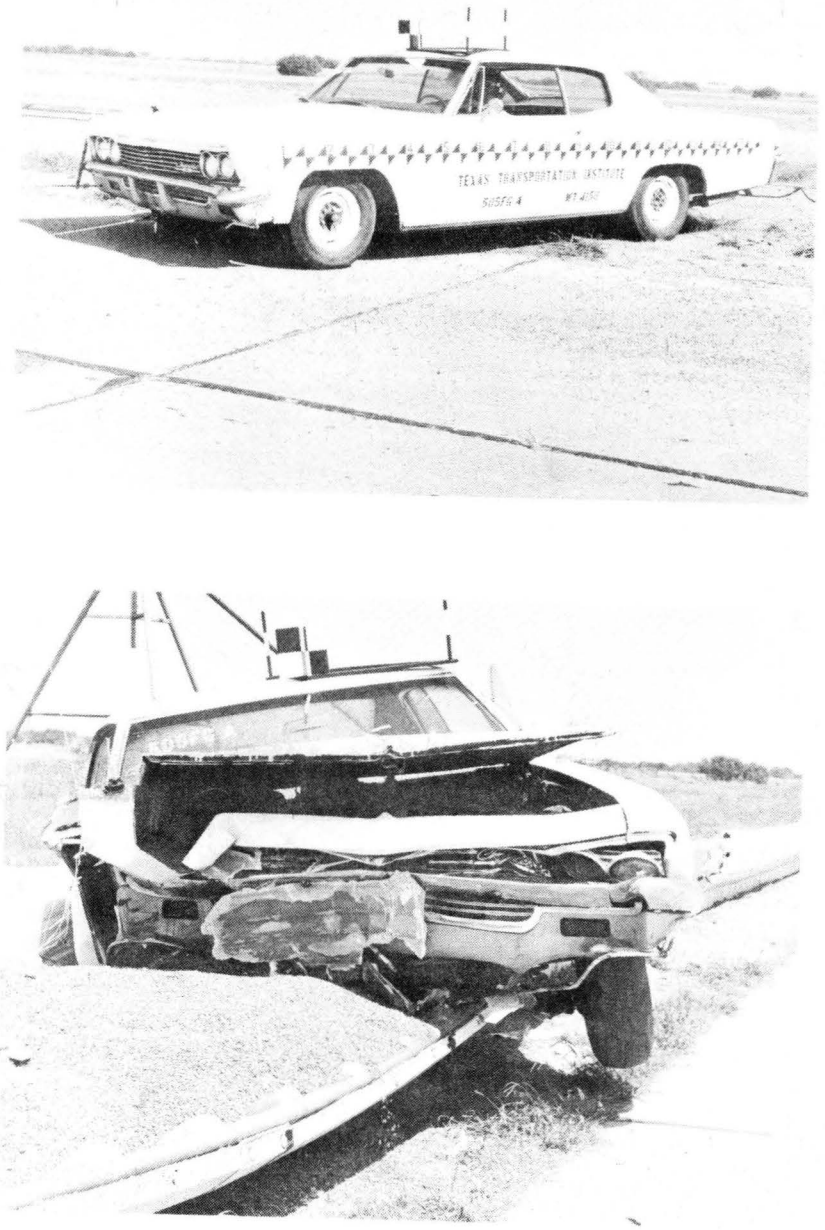

Figure 7 , Vehicle Before and After Test FG-A

Figure 8 , Vehicle and Barrier After Test FC-A

Table 1

TEST 505 FG-A

SUMMARY OF DATA

Vehicle Make: 1966 Chevrolet Caprice

Impact Angle: 25°

Initial Speed: 79.2 ft./sec. or 54.0 mph

Maximum Lateral Penetration of Barrier: 5.3 ft.

Maximum Lateral Displacement of c.g.: 7.8 ft.

Longitudinal Stopping Distance: 38.0 ft.

Avg. Longitudinal Deceleration (computed): 2.6 g's
$(v^2/ 2gs)$

Avg. Deceleration Perpendicular to Barrier (computed): 2.2 g's
$((v \sin \theta)^2/2gs)$

Longitudinal Deceleration:

Accelerometer	Maximum (g's)	Average (g's)
Left Frame Member	12.5	5.4 (over 248 msec)
Right Frame Member	14.8	5.0 (over 248 msec)

Transverse Deceleration:

Accelerometer	Maximum (g's)	Average (g's)
Left Frame Member	8.6	2.4 (over 213 msec)
Right Frame Member	6.7	1.6 (over 213 msec)

Seat Belt:

Maximum force - 591 lb.

Average force - 156 lb. (over 257 msec)

Table 2

TEST 505 FC-A

High-Speed Film Data

Time (milliseconds)	Displacement (feet)	Time (milliseconds)	Displacement (feet)
-50.9	-4.0	137.3	9.6
-38.1	-3.0	145.0	10.0
-25.4	-2.0	152.6	10.4
-12.7	-1.0	165.3	10.9
0 Impact	0	178.0	11.5
7.6	0.6	190.7	12.0
15.3	1.2	203.4	12.5
22.9	1.8	216.2	12.9
30.5	2.4	228.9	13.3
38.1	3.0	241.6	13.8
45.8	3.6	254.3	14.1
53.4	4.1	267.0	14.5
61.0	4.7	279.7	14.9
68.7	5.2	292.4	15.3
76.3	5.8	305.2	15.7
83.9	6.3	330.6	16.4
91.5	6.8	356.0	17.0
99.2	7.4	381.4	17.7
106.8	7.9	406.9	18.3
114.4	8.3	432.3	19.0
122.1	8.8	457.7	19.6
129.7	9.2	483.2	20.2

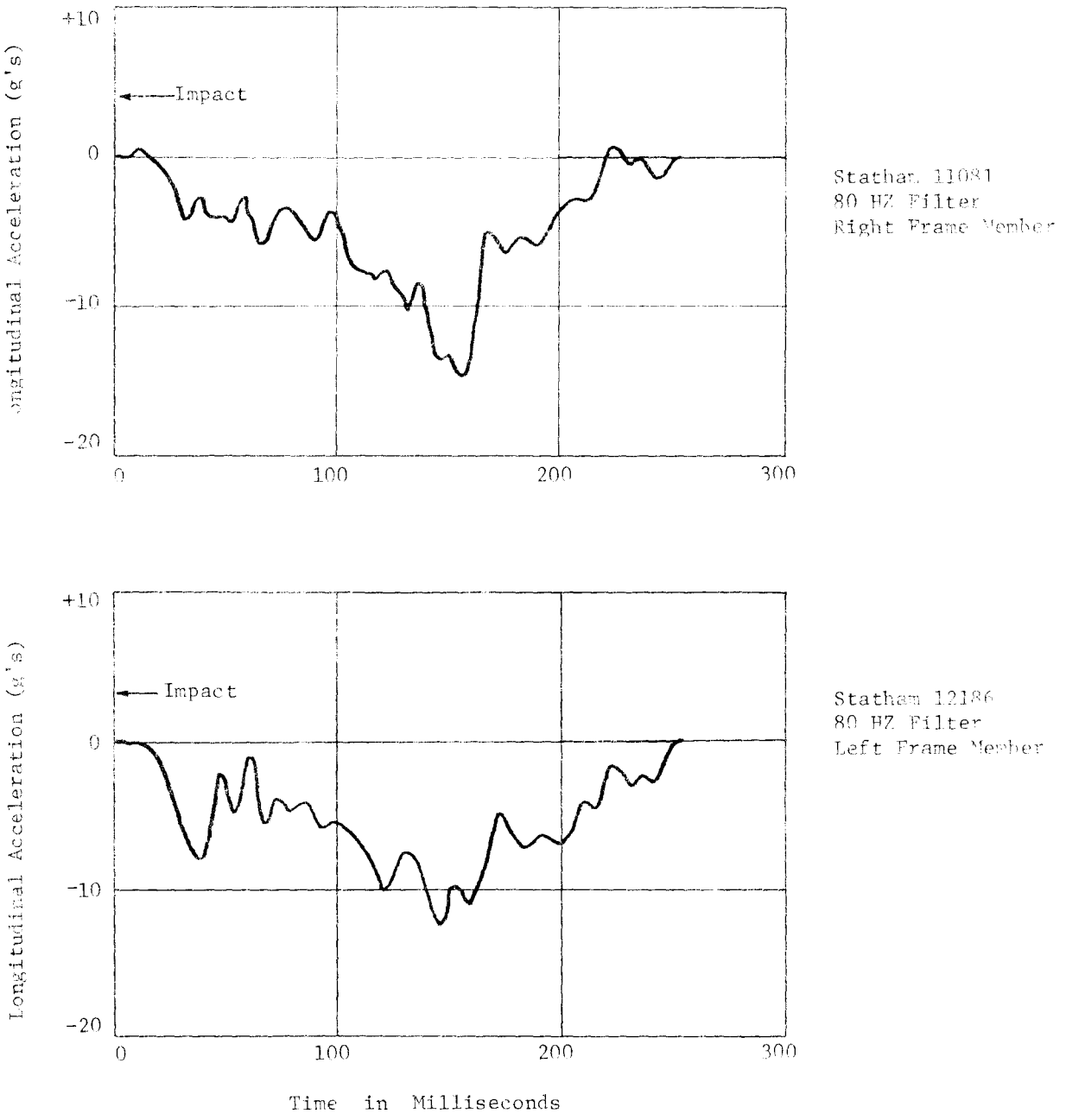

Figure 9 , Longitudinal Accelerometer Data, Test 505 FG-A

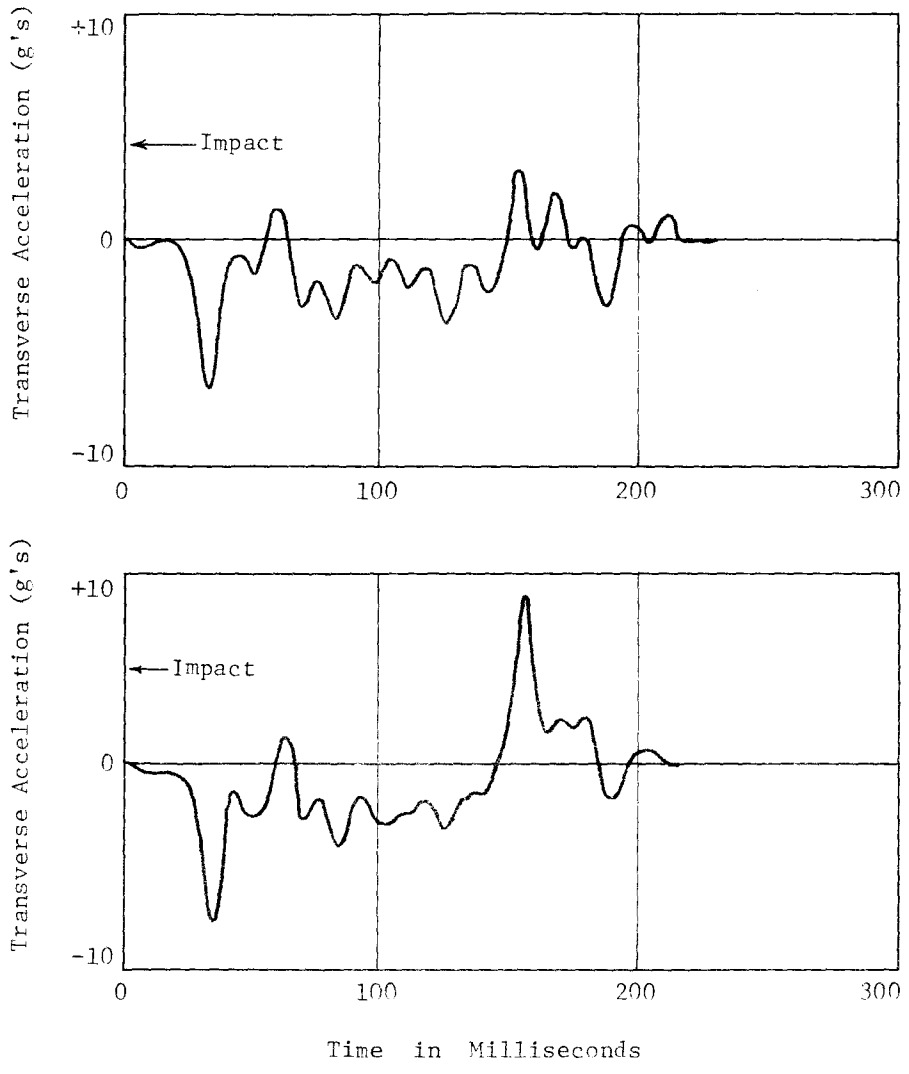

Statham 20
80 HZ Filter
Right Frame Member

Statham 511
80 HZ Filter
Left Frame Member

Figure 10, Transverse Accelerometer Data, Test 505 FG-A

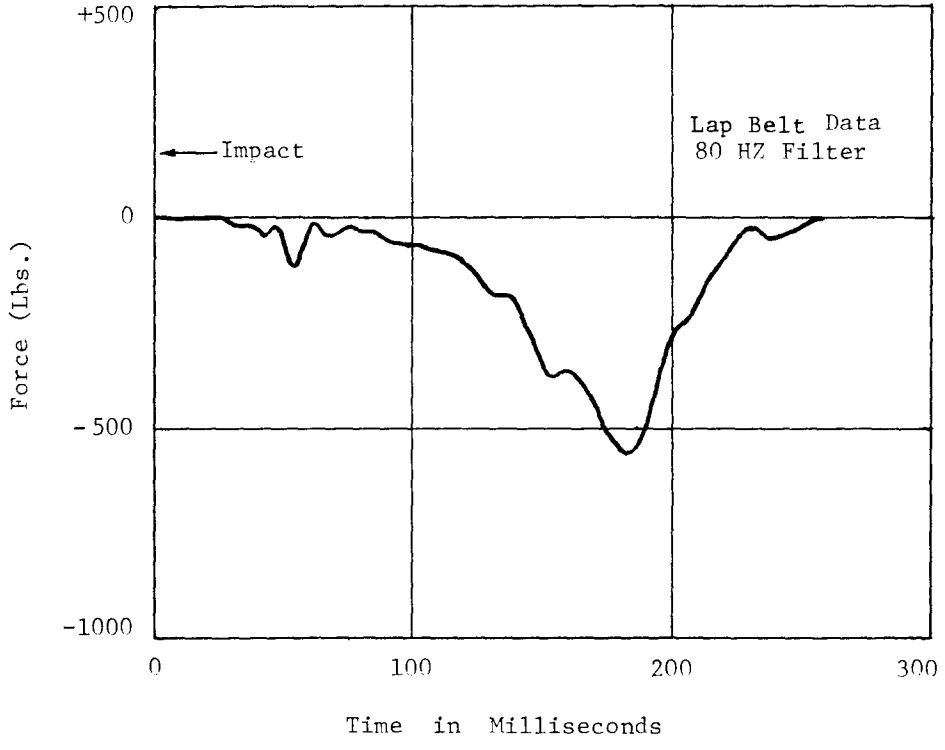

Figure 11, Lap Belt Data, Test 505 FG-A

CONCLUSION

Although the vehicle decelerations observed in this test were tolerable to properly restrained passengers,[3] the median barrier did not redirect the vehicle as intended or desired. The fiberglass barrier lacked strength and roughness to prevent the vehicle from penetrating it. In particular, the barrier contact surfaces and connections could possibly be altered to prevent disintegration of the side of the barrier under vehicular impact. This might be accomplished by replacing the fiberglass guardrail or rubrail with the common metal W-section flexbeam railing. However, this is only speculation and further design modifications would probably be necessary. The bolted connections employed throughout the system appeared to be totally unsatisfactory. Steel bolts in holes in the fiberglass created many areas of high stress concentration which the non-ductile (or brittle) fiberglass could not tolerate.

The fact that most fiberglass lacks ductility (the ability to undergo large plastic deformation) creates many difficult design and fabrication problems for impact resistant structures. Ductile materials generally perform better than brittle materials under impact loads, particularly at connections and in areas of high stress concentration since by yielding, the ductile material can redistribute high stress concentrations.

REFERENCES

1. Nelson, D.N. and Singh, M.M., "Investigation of Soil Filled Median Barriers," Report prepared by ITT Research Institute for the Molded Fiberglass Body Company, March 1969.

2. Rao, P.N., "Investigation of Energy Absorption of Soil Filled Guard Rails," Final report of IIT Research Institute Project D6055 for Molded Fiberglass Resin Company, subcontract P.O. No. L5832 (under Department of Transportation Prime Contract), July 1970.

3. Damon, A., Stoudt, H.W. and McFarland, R.A., "The Human Body in Equipment Design," Harvard University Press, 1966.

TECHNICAL MEMORANDUM 505-15

Texas Transportation Institute
Texas A&M Research Foundation

A HYBRID BARRIER FOR USE AT BRIDGE PIERS IN MEDIANS (MODULAR CRASH CUSHION PLUS CONCRETE MEDIAN BARRIER)

A Test and Evaluation Report on Contract No. CPR-11-5851

U. S. Department of Transportation
Federal Highway Administration

by

G. G. Hayes
D. L. Ivey
T. J. Hirsch
Texas Transportation Institute

and

John C. Viner
Structures and Applied Mechanics Division
Federal Highway Administration

These crash tests and evaluations were conducted under the Office of Research and Development, Structural and Applied Mechanics Division's Research Program on Structural Systems in Support of Highway Safety (4S Program).

June 1971

INTRODUCTION

Bridge piers in the roadway median at highway overpass structures present a rigid object hazard to passing motorists. The probability of injury to occupants of a vehicle which violates the median in the overpass area would be greatly reduced by the addition of an energy absorbing device in front of the outermost bridge piers.

Use of guardrails at such locations is not a wholly satisfactory solution, as a substantial portion of the length of these median installations are end treatments; and all currently available guardrail end treatments are quite hazardous themselves.[1*] The hybrid crash cushion and concrete median barrier discussed in this technical memorandum is one possible alternative to current treatments at these locations.

An impact attenuator which had a compatible transition to a concrete median barrier system was designed, constructed, and tested to evaluate the feasibility of such a design. These evaluation tests consisted of two vehicles directed at angles of 10° and 20° into the side of the system and one vehicle which impacted the crash cushion head-on.

*Superscript numerals refer to corresponding numbers in the selected references.

DESCRIPTION OF BARRIER SYSTEM

Two simulated concrete bridge piers were installed for the tests. The protective installation shown in Figures 1A and 1B was a combination of a shaped concrete median barrier[2] and a variation of the Modular Crash Cushion.[3,4] This cushion was designed by the Structures and Applied Mechanics Division of the Federal Highway Administration with the assistance of the Texas Transportation Institute.

The crash cushion was composed of 55-gallon steel drums with holes in the tops and bottoms to reduce the crush strength. Plywood panels (2 ft high and 4 ft long) covered with sheet metal were attached to the upstream side of the crash cushion adjacent to oncoming traffic to provide a redirection capability for vehicles which strike a glancing blow. These redirectional panels are attached to the drums in a fish-scale fashion and telescope in a head-on collision without altering barrier crush characteristics.

These 2 ft by 4 ft panels were chosen in preference to the 3 ft by 8 ft panel scheme used in earlier development tests[4] and in the demonstration conducted by U. S. Steel in order to minimize the ramping of the vehicle that was noted in these impacts. The 2 ft by 4 ft panel was inspired by Hanson's[5] use of 2 ft by 3 ft panels in the design of a barrier for use in Denver, Colorado. It was felt that the 2 ft high panels, centered on the 2 ft 10-3/4 in. drums would decrease ramping by offering a smaller smooth surface, as the tops and bottoms of the drum would probably lip over the panel edges during impact and retard any ramping

tendency. Also, the lower trailing corners of these 2 ft by 4 ft panels could not scrape against the ground and cause a tendency toward ramping in this fashion.

Steel cables gave the cushion and redirectional penals lateral stability for side impacts. The cables were passed through eye bolts in the support posts so that the drums, support posts, and redirectional panels could slide along the cables during a head-on collision. As shown in Figure 1B, the 3/4 in. wire rope cables were located at the top rolling hoop of the steel drum to encourage a slight downward wedging action (again to decrease ramping tendencies) of the panels under side impact. This feature was suggested by the U. S. Steel demonstration tests conducted by TTI.

As shown in Figure 1A, the downstream treatments differed from the upstream treatments. The two 3/4 in. cables were between the first and second columns of drums in order to eliminate vehicle snagging at the cable anchorage when impacting this downstream side. No plywood redirectional panels were used on the left-hand side in this installation. If panels were used on the left side, they would have to be hinged at their rearward edge to redirect vehicles moving from the rear to front (see Figure 1A). The outside top edge of the concrete median barrier was aligned with the side face of the downstream steel drums so that unnecessary contact with the downstream drums would be avoided.

The concepts for this barrier called for as narrow a barrier as possible in order to allow its use where space is restricted, as well as to offer a smaller target to an errant vehicle, thereby reducing the number of collisions with the barrier. For this reason, the shaped concrete median barrier was selected as an element of the hybrid barrier.

In order to stop impacting vehicles in the 2000 to 4500 lb weight range with acceptable deceleration forces and at the same time avoid an unnecessarily long barrier, previous designs for steel drum crash cushion tests used an increase in the number of drums per row towards the rear of the barrier. This resulted in barrier designs which had four to six drums per row at the rear of the barrier. In these tests, all drums had the same crushing strength (same gage and hole cut-out pattern). This could be referred to as a mono-modular design concept. In order to achieve the desired minimum width for the barrier presented in this report and achieve these same goals, a barrier three drums wide having three different crush strengths was used. Relatively "soft" drums were used on the crash cushion nose, "medium stiff" in the center, and "stiff" drums in the rear of the crash cushion.

The crush characteristics of these drums and the corrugated metal pipe segments used in this design are given in reference 6. It was recognized that the use of two different gage drums with identical hole cut-out patterns could result in confusion in the field. In reference 6 an array of crushing resistances using the same gage of drum but varying the hole cut-out pattern is presented so as to minimize such possible field problems.

The resulting design had the same number of drums in each row permitting the cables to be kept straight in plan view as is desirable and permitting the side of the crash cushion to be aligned parallel to the roadway. This had the advantage of reducing the angle of impact with the side of the barrier in a given collision as compared with the previously discussed design.

The concrete median portion of this barrier is an adaptation of the GM shaped concrete section. In a 63 mph, 25° impact into a 32 in. high New Jersey shaped concrete median barrier reported by Nordlin,[2] portions of the sheet metal of the vehicle lipped over the top of the barrier. As the concept of the hybrid barrier discussed in this report called for a design in which the concrete median section of the barrier could be placed as close as possible to the bridge piers, the concrete median barrier height was increased to 40 in. as shown in Figure 1A. This modified GM shape had an upper face that was 25 in. high with a 3-7/8 in. offset as compared to the 16-7/8 in. height and 2-7/8 in. offset of the standard GM shape. The purpose of this change was primarily for improving barrier performance for collision involving pick-up trucks and heavier vehicles. Evaluation of this aspect of the barrier design was beyond the scope of this investigation.

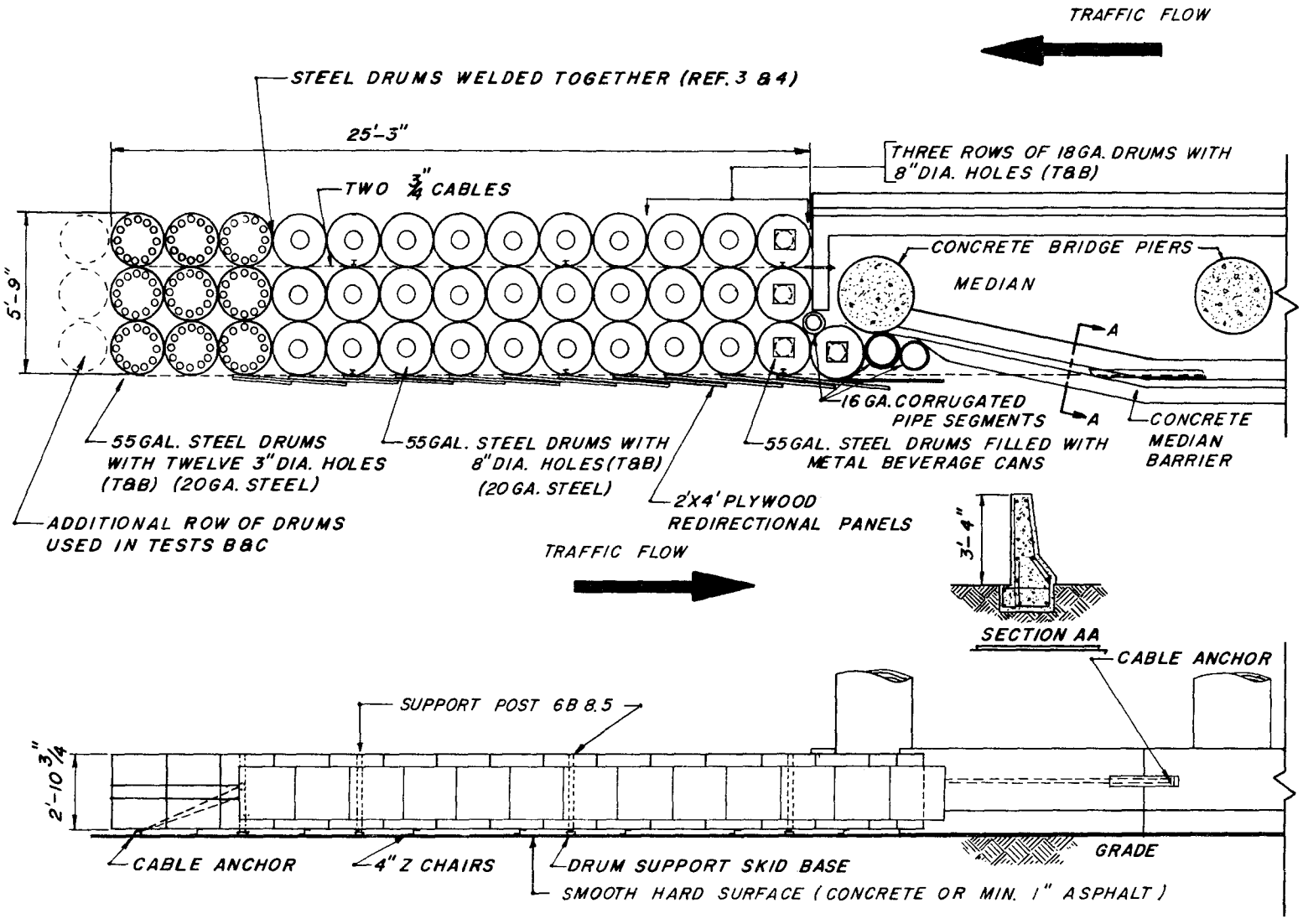

FIGURE IA, CRASH CUSHION – MEDIAN BARRIER SYSTEM

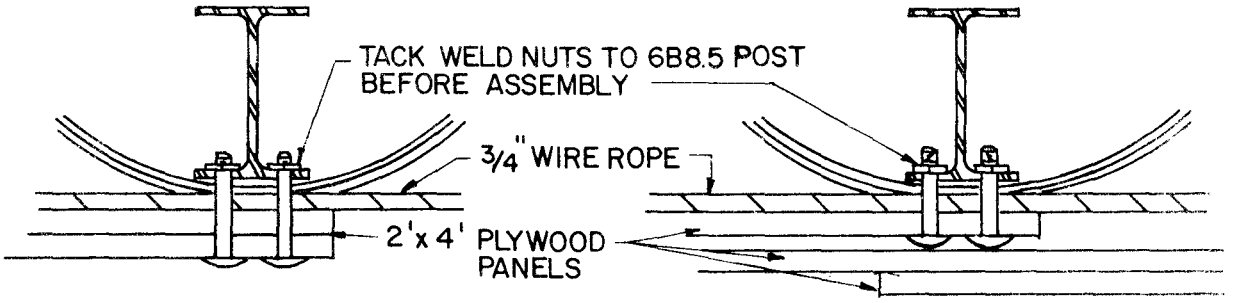

LEAD PANEL ATTACHMENTS

INTERMEDIATE & FINAL ATTACHMENTS

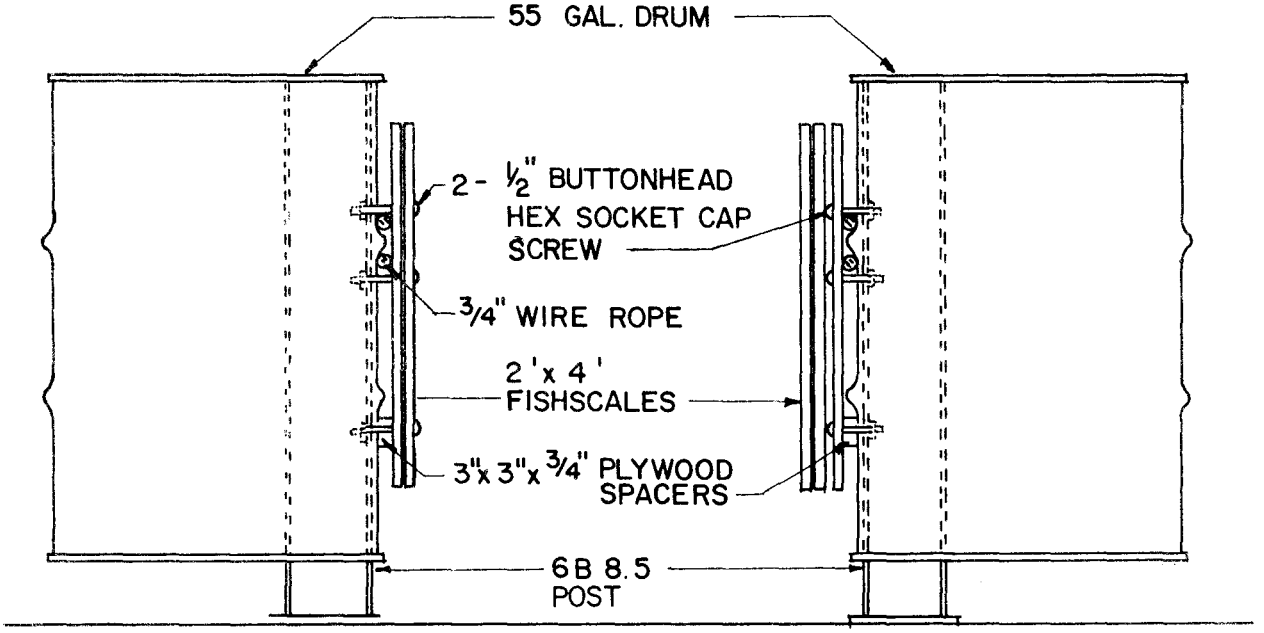

FIGURE 1B DETAIL OF 2' x 4' PLYWOOD REDIRECTION PANELS AND CONNECTION

PHOTOGRAPHIC INSTRUMENTATION

In Tests A and B, four high-speed cameras with a film speed of frames per second were used. One was located perpendicular to the initial path of the vehicle, one parallel to the crash cushion center line, one perpendicular to the crash cushion center line, and one overhead. In Test C, a head-on impact, two cameras were located perpendicular to the crash cushion center line (and vehicle path), and one was mounted overhead. In all tests, three documentary cameras with speeds of 24, 64, and 128 frames per second were used.

The high-speed motion pictures had timing marks on the edge of the film from which film speed, and therefore elapsed time, could be computed. Each test vehicle had a stadia board and several targets on it to facilitate the measurement of vehicle movement. The average speed of the vehicle over a desired interval could then be obtained from the time-displacement determinations shown in the Appendix. These measurements were made along the path of the vehicle. The lateral motion of the vehicle (perpendicular to the crash cushion) was determined from the overhead or end-view cameras.

ELECTROMECHANICAL INSTRUMENTATION

In Tests A and B, transverse and longitudinal accelerometers were mounted on short flanges welded to each longitudinal frame member just behind the front seat. In Test C, only longitudinal accelerometers were included on the vehicle. Throughout this report, longitudinal decelerations indicate accelerations toward the rear of the vehicle and transverse decelerations toward the right of the vehicle. In all tests, an anthropomorphic dummy was secured in the driver's seat by a lap belt connected

to a load cell which sensed lap belt force. In Test C, a head-on impact, biaxial accelerometers were mounted in the head of the dummy. The signals from the various transducers were transmitted by telemetry to a ground station and recorded on magnetic tape. The accelerometer data were passed through an 80 HZ low-pass, active filter to reduce the effects of "ringing". Reproductions of the accelerometer and lap belt traces are included in the Appendix.

DESCRIPTION OF TESTS

Test A

A 4150 lb Ford sedan was directed obliquely into the side of the crash cushion at 56.7 mph. The vehicle's approach path made a 20° angle with the center line of the crash cushion with the impact point selected such that the driver's seat was directed at the center of the front bridge pier. With this impact point, it was thought that maximum barrier deflection would occur in the vicinity of the transition between the crash cushion and the shaped concrete barrier, and thus provide the most meaningful test for this transition for use with the other selected conditions. This caused the left front end of the vehicle to contact the crash cushion at the rear edge of the fifth fender panel from the front as seen in Figure 2. Both the maximum deformation of the crash cushion and the maximum vehicle accelerations occurred at roughly 0.150 sec after impact. The overhead sequential photographs of Figure 3 indicate that the front end of the vehicle was near the bridge pier-median barrier transition at this time as desired. Figure 4 shows sequential photographs from an end view. No elapsed times are shown in the figure because the camera with which the photographs were made does not incorporate timing marks on the film.

The vehicle redirected smoothly. The path of the departing vehicle can be seen in Figure 5, which shows the crash cushion before and after the test. The residual lateral deformation of the side of the crash cushion was 16 in. Seven steel drums and eight fender panels were damaged. Figure 6 shows the vehicle before and after the test. The left

front of the vehicle was deformed 18 in. longitudinally and 16 in. transversely. The damage to the left front wheel caused the vehicle to swerve in an arc to the left after loss of contact with the barrier.

The vehicle deceleration data are shown in Tables 1 and 2. The accelerometers indicated a maximum longitudinal deceleration of 14.4 g's and a maximum transverse deceleration of 10.4 g's. The average longitudinal deceleration was 2.6 g's over 0.46 sec, and the average transverse deceleration was 2.0 g's over 0.46 sec. The average lateral deceleration (from contact until the vehicle was parallel to the barrier center line) calculated from high-speed film over 0.27 sec was about 4 g's.

Test B

In this test, a 3990 lb, 1964 Dodge sedan struck the barrier 10° to the center line at 62.3 mph. The purpose of this test was to evaluate the transition between the crash cushion and the shaped concrete barrier under the 60 mph, 10° test conditions that have caused vehicle ramping and near roll over in previous tests. The crash cushion had been restored to its original condition with the exception of one corrugated steel pipe at the edge of the concrete backup wall which was not replaced. In addition, another row of steel drums was added to the front of the crash cushion (compare Figures 2 and 7). As in Test A, the impact point was selected such that the driver's seat was aimed at the center of the bridge pier.

Figures 8 and 9 are sequential photographs of the test, and Figures 7 and 10 show the barrier before and after the test. The damage to the crash cushion was slight. The redirection was very smooth, with only

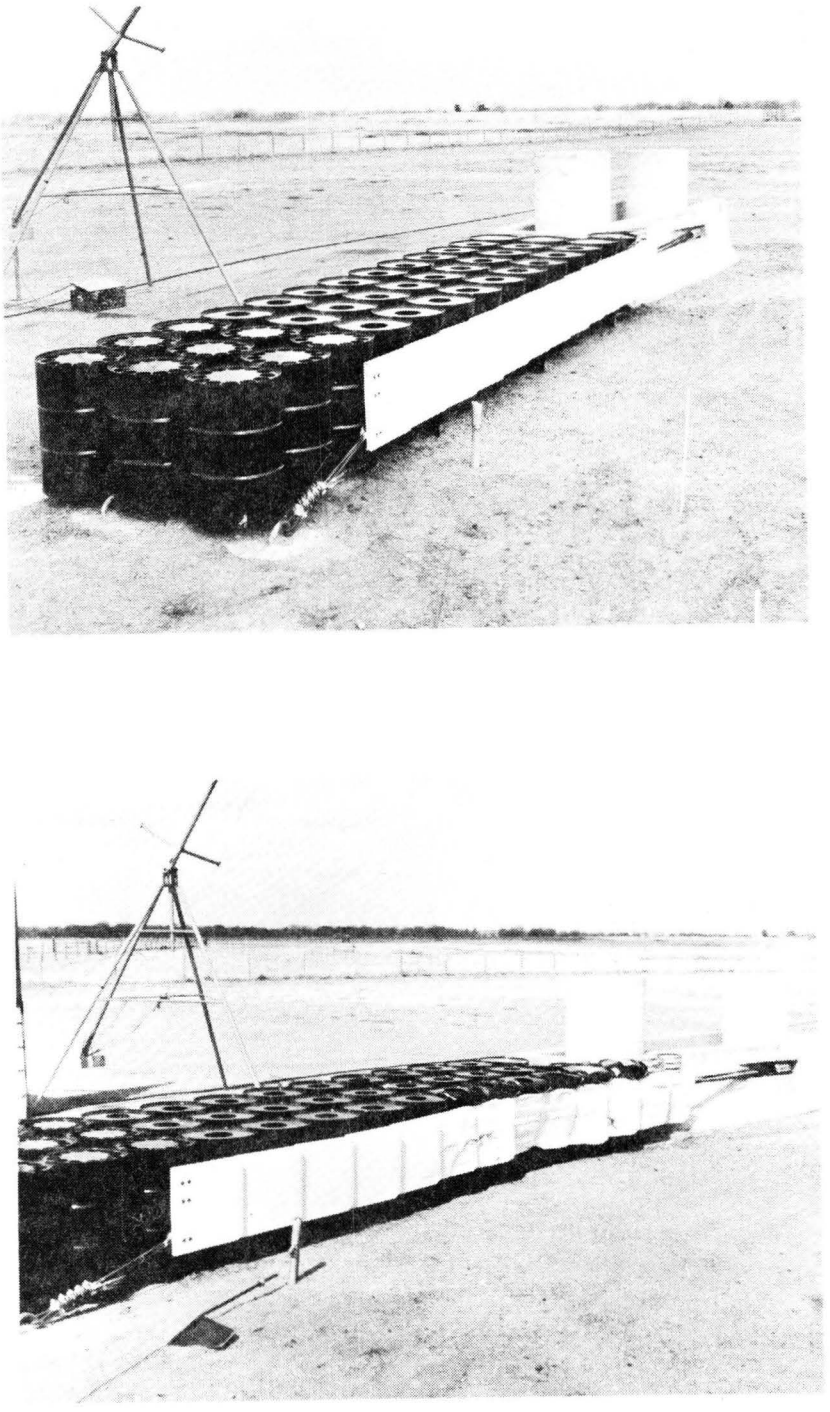

Figure 2 , Barriers Before and After Test A (Oblique View).

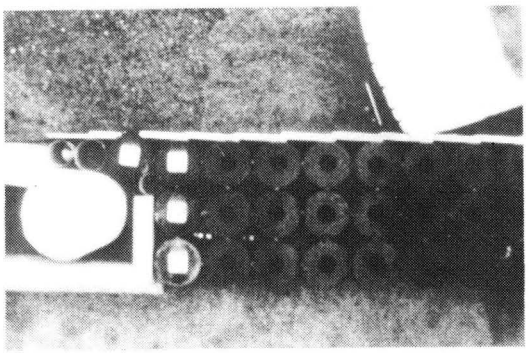

t = 0 sec

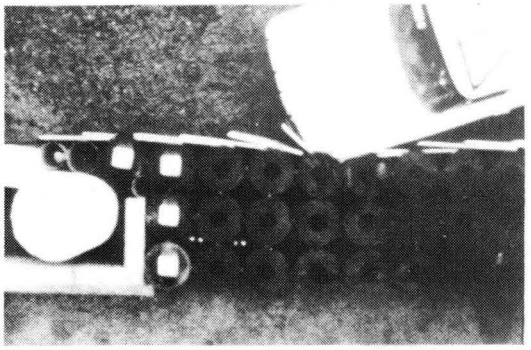

t = 0.046 sec

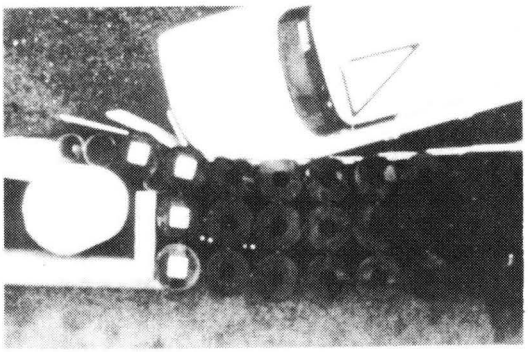

t = 0.113 sec

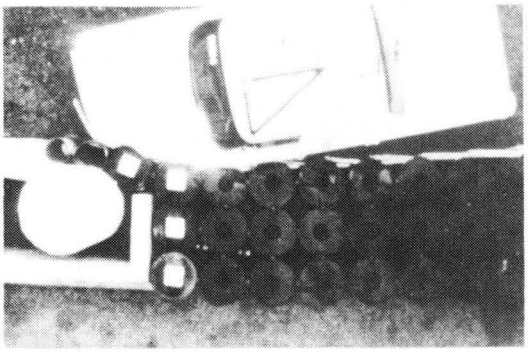

t = 0.167 sec

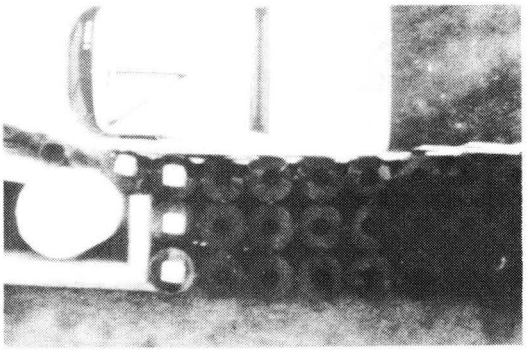

t = 0.256 sec

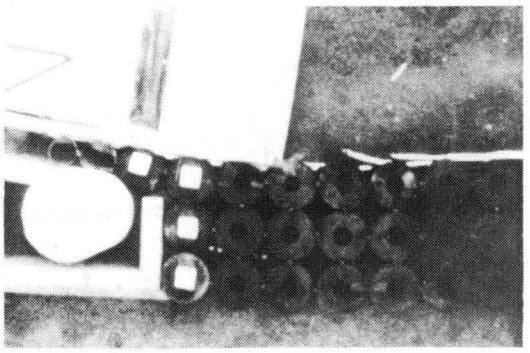

t = 0.346 sec

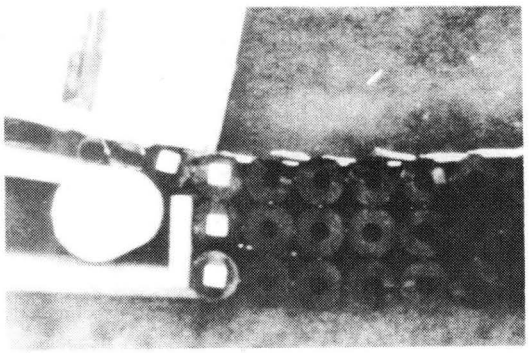

t = 0.421 sec

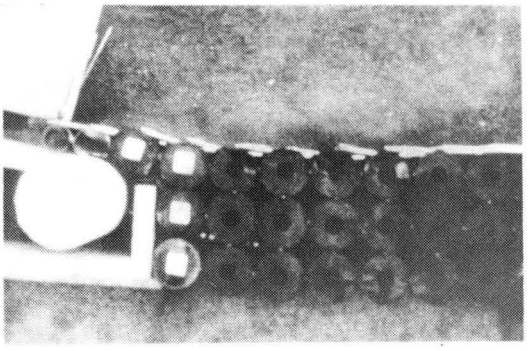

t = 0.515 sec

Figure 3, Test A -- Sequential Photographs (Overhead View).

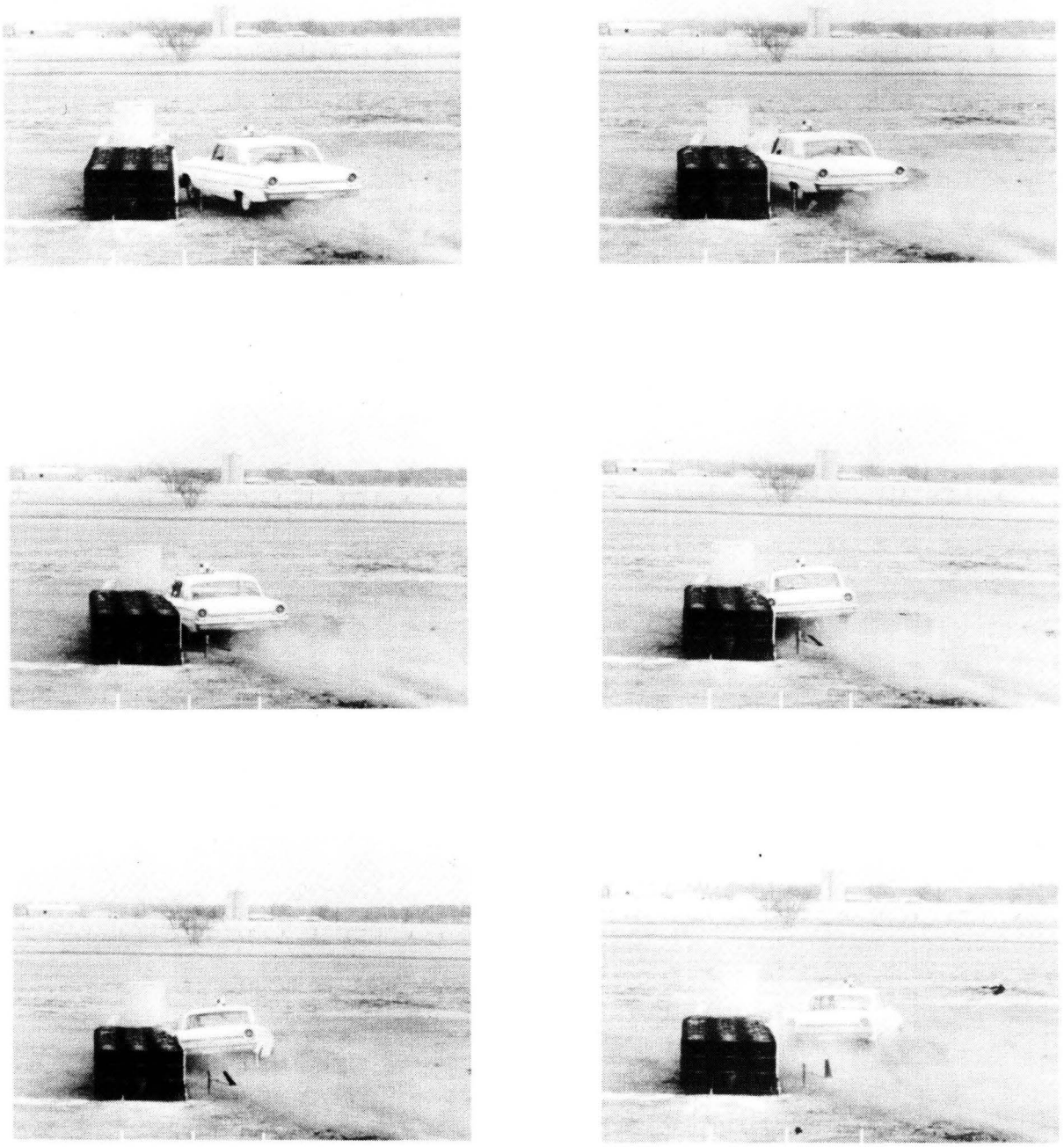

Figure 4 , Test A - - Sequential Photographs
(View Parallel to Barrier).

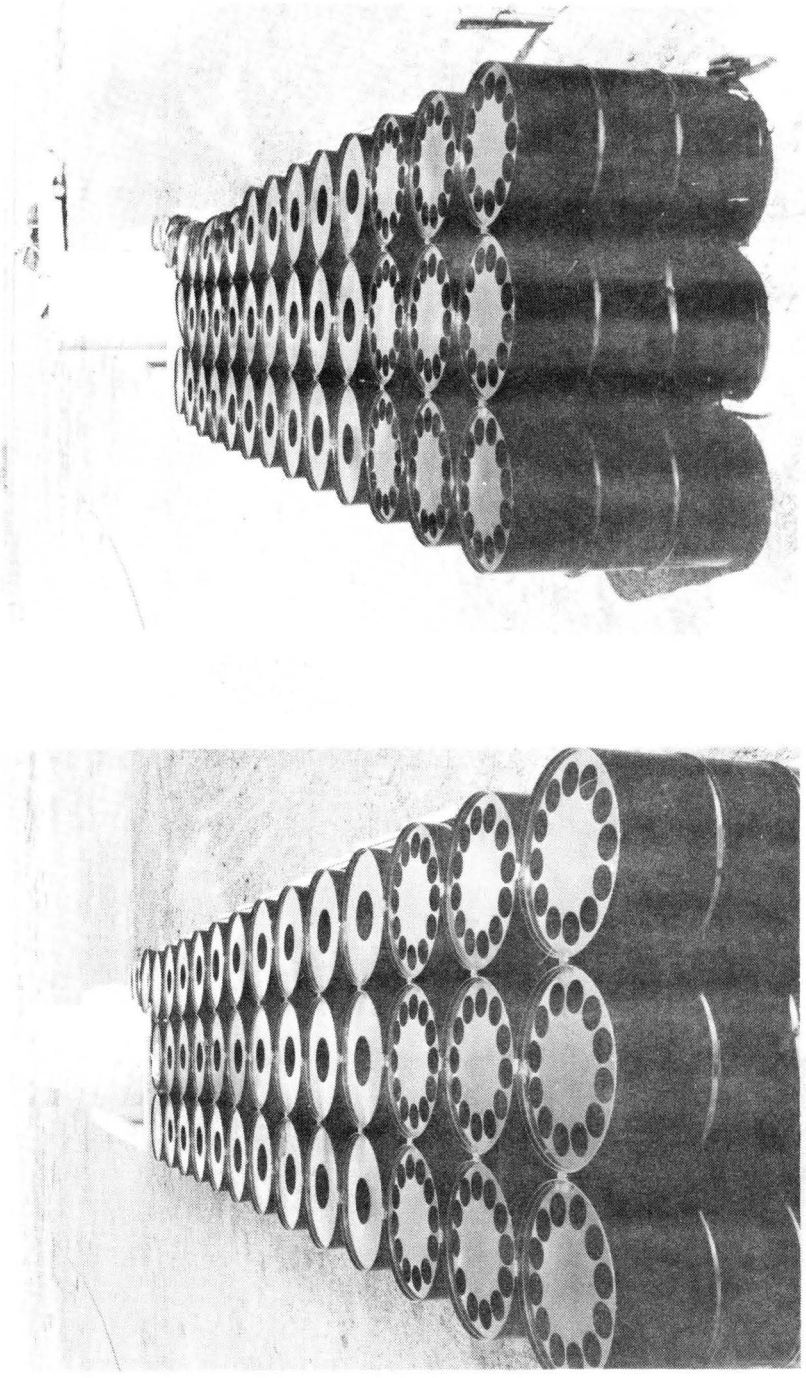

Figure 5 , Barriers Before and After Test A (End View).

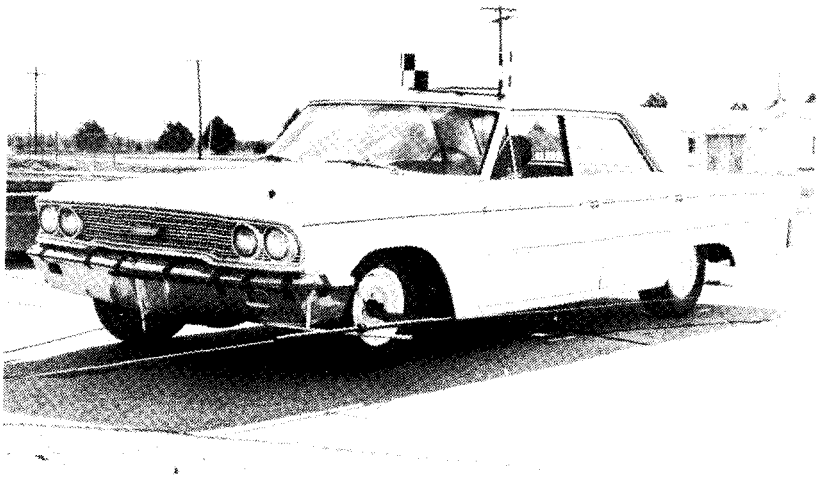

Figure 6 . Vehicle Before and After Test A.

TABLE 1

DATA FROM FILM ANALYSIS

Factor	Test A	Test B	Test C
Vehicle Weight, lbs.	4150	3990	1790
Impact Angle, deg.	20	10	0
Initial Speed, ft/sec	83.1	91.4	81.8
mph	56.7	62.3	55.8
Final Speed, ft/sec	45.6	75.9	0[a]
mph	31.1	51.7	0[a]
Time in Contact, sec	0.513	0.414	0.257[a]
Distance in Contact, ft	29.2	31.9	11.3[a]
Average Longitudinal Deceleration, g's			
Vehicle Parallel to Barrier	4.0[b]	2.5[b]	9.2[a,b]
	3.9[c]	2.4[c]	9.9[c]
Loss of Contact	2.6[b]	1.3[b]	8.9[b,d]
	2.3[c]	1.2[c]	7.8[c,d]
Average Lateral[e] Deceleration, g's			
Vehicle Parallel to Barrier	3.9[b]	3.0[b]	---
	3.2[c]	2.6[c]	---

[a]At end of forward motion in Test C.

[b]Calculated by $(V_i^2 - V_f^2 / 2gD)$; Where V_i = initial speed, V_f = speed at point of interest, D = distance traveled by vehicle's CG, and g = 32.2 ft/sec^2.

[c]Calculated by $(1/g)(\Delta V/\Delta t)$; where ΔV = change in speed of vehicle's CG, and Δt = time interval.

[d]To end of accelerometer traces (0.5 ft. of rebound)

[e]Lateral = perpendicular to barrier centerline.

TABLE 2

DATA FROM ACCELEROMETERS

Factor	Test A	Test B	Test C
Vehicle Weight, lbs	4150	3990	1790
Impact Angle, deg	20	10	0
Maximum Deceleration,[a] g's			
Longitudinal	14.4	3.4	13.8
Transverse	10.4	11.0	--
Average Deceleration,[a] g's			
Longitudinal	2.6	0.8	7.2
Time Interval, sec	.460	.411	.356
Transverse[b]	2.0	2.0	--
Time Interval, sec	.461	.410	--

[a]Values given are averages of right and left accelerometer outputs.

[b]Transverse to vehicle longitudinal axis.

a slight ramping of the left front end of the vehicle observed. The vehicle left the barrier at an angle of about 5° to the center line of the crash cushion, and the tracks of the vehicle as it left the barrier can be seen in Figure 7. The damage to the vehicle is shown in Figure 11. The vehicle was driven away from the site after the test, which indicates, along with the small angle of departure, that a driver could have maintained control after the impact.

From the accelerometer data, the maximum longitudinal deceleration was 3.4 g's and the maximum transverse deceleration was 11.0 g's. The average longitudinal deceleration was 2.5 g's, and the average deceleration perpendicular to the crash cushion was 3.0 g's. These were obtained from the high-speed films to the time of parallelism, 0.19 sec. The average longitudinal and transverse decelerations from the accelerometers over about 0.4 sec were 0.8 and 2.0 g's, respectively.

Test C

In the final test of the series, a 1965 Simca, weighing 1790 lb, struck the crash cushion head-on at 55.8 mph. Unreported accidents or collisions with crash cushions prior to the time have required highway engineers to make frequent inspections and needed repairs. Because of the plywood redirection panels, it was thought that the damage caused by Test B was not severe enough to alter the crash cushion behavior in the planned Test C. Consequently, it was felt desirable to demonstrate this and accordingly, except for painting and reshaping some of the fender panels, the crash cushion was not restored after Test B. At test time, the crash cushion had a bow in it from the last test, the

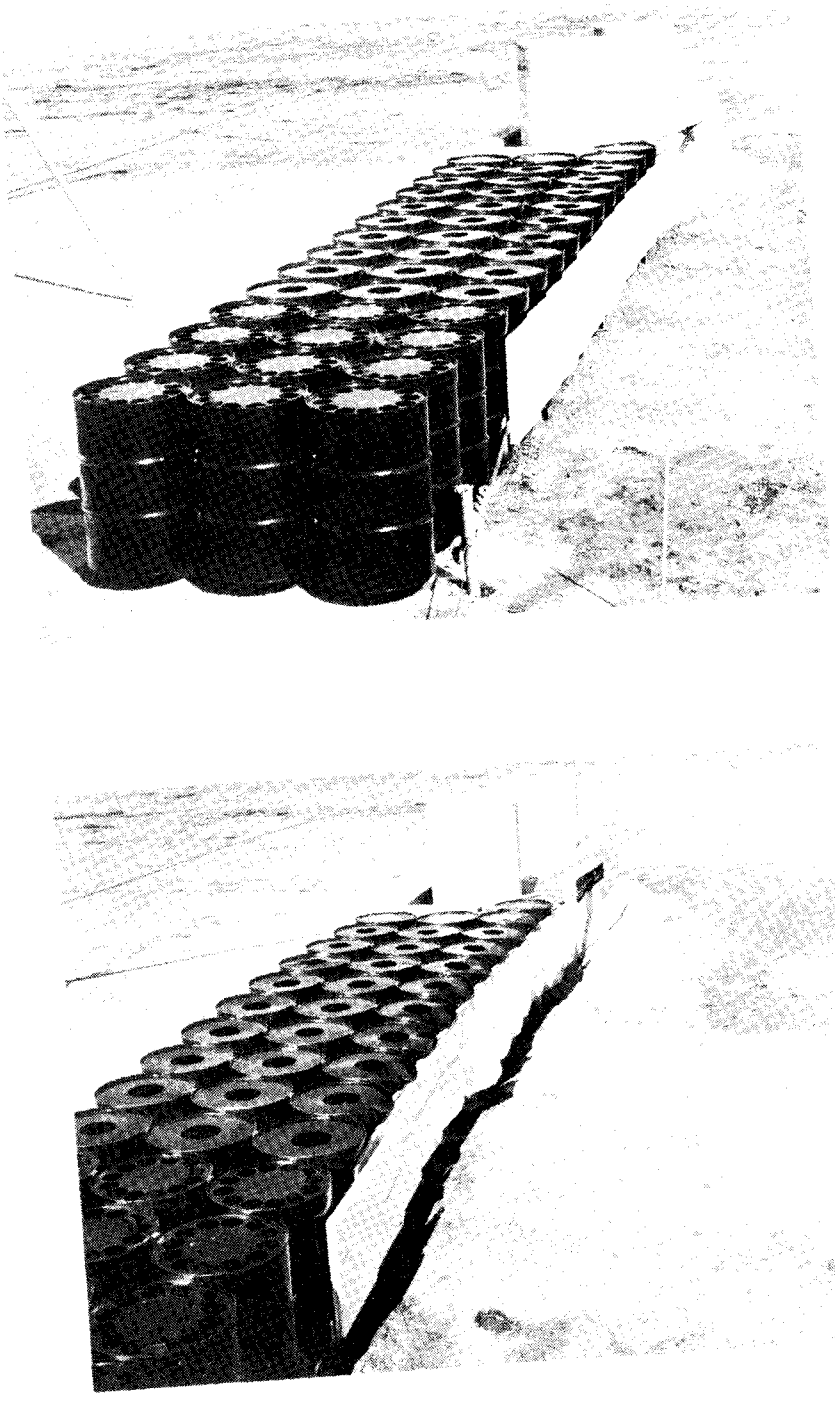

Figure 7. Barriers Before and After Test B (Oblique View).

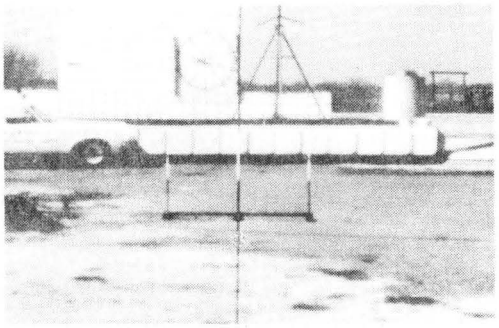

t = 0 sec

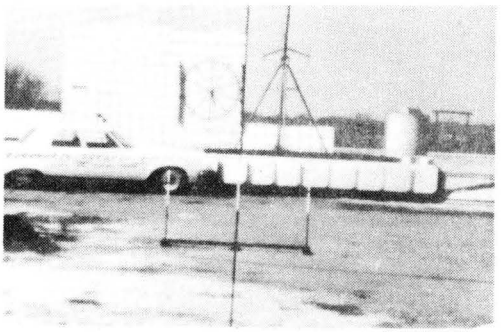

t = 0.061 sec

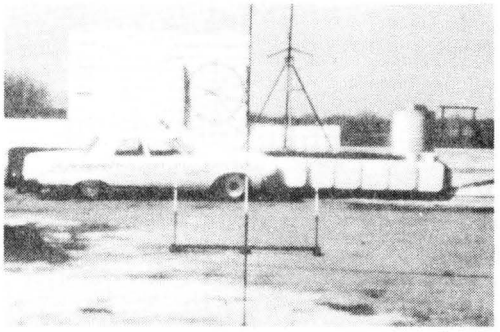

t = 0.108 sec

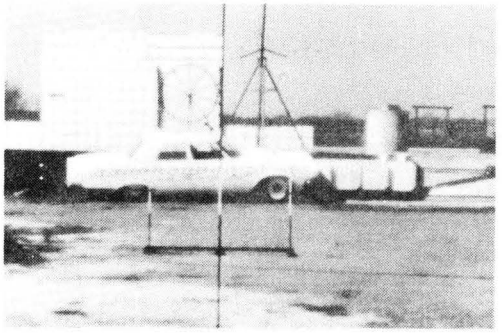

t = 0.169 sec

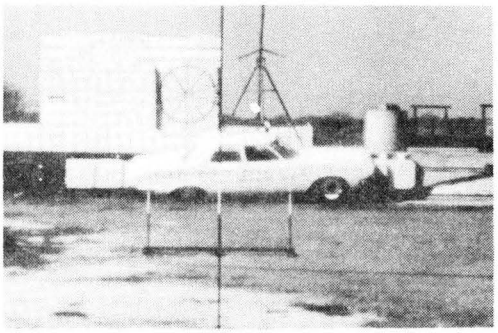

t = 0.220 sec

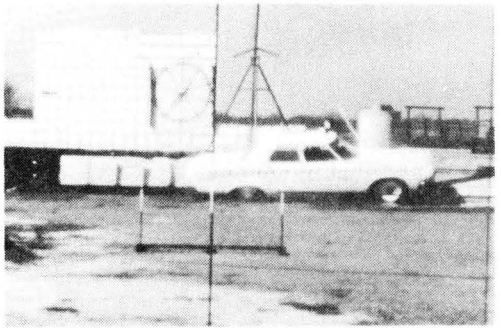

t = 0.281 sec

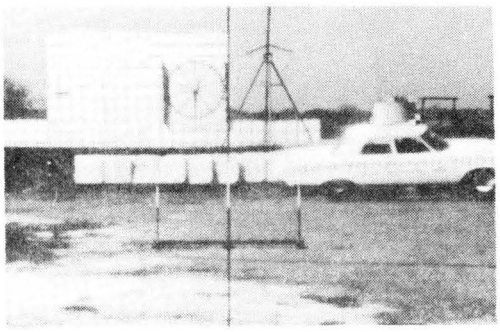

t = 0.350 sec

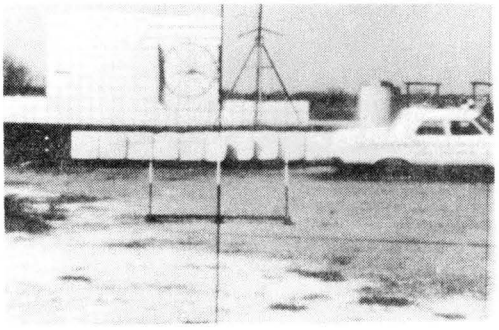

t = 0.413 sec

Figure 8, Test B -- Sequential Photographs (View Perpendicular to Barrier).

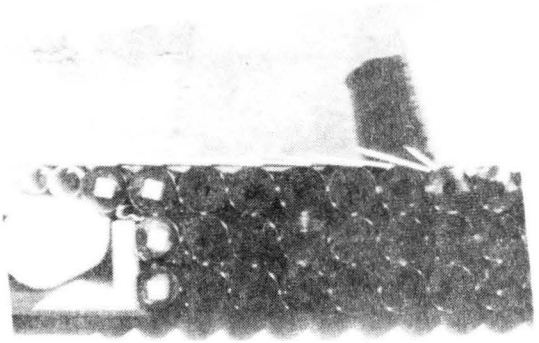

t = 0.051 sec

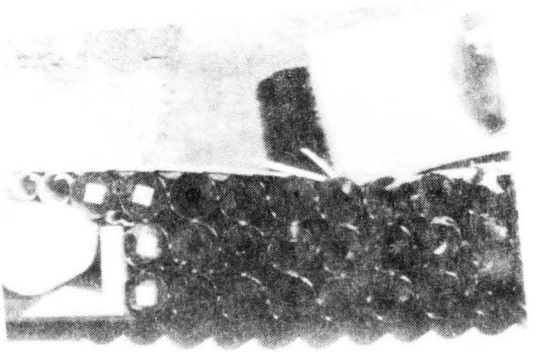

t = 0.091 sec

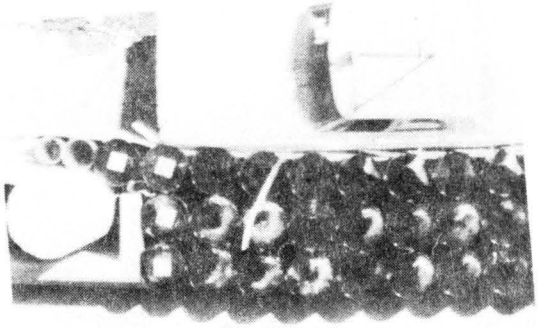

t = 0.182 sec

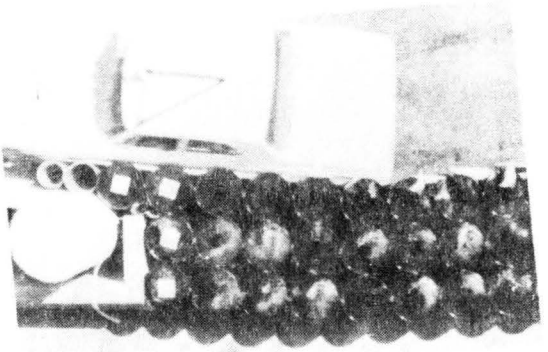

t = 0.283 sec

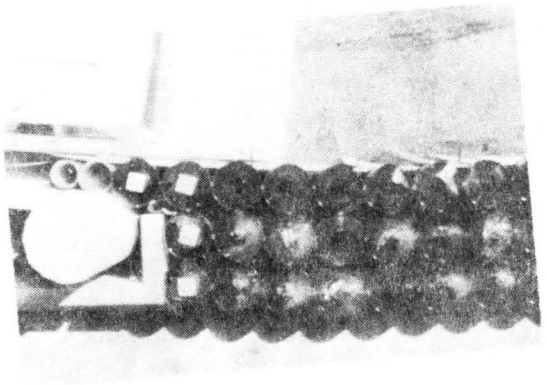

t = 0.354 sec

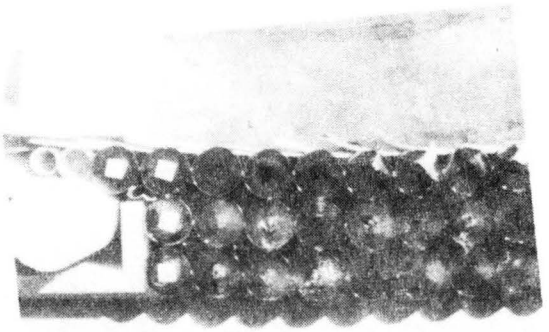

t = 0.414 sec

Figure 9, Test B -- Sequential Photographs (Overhead View).

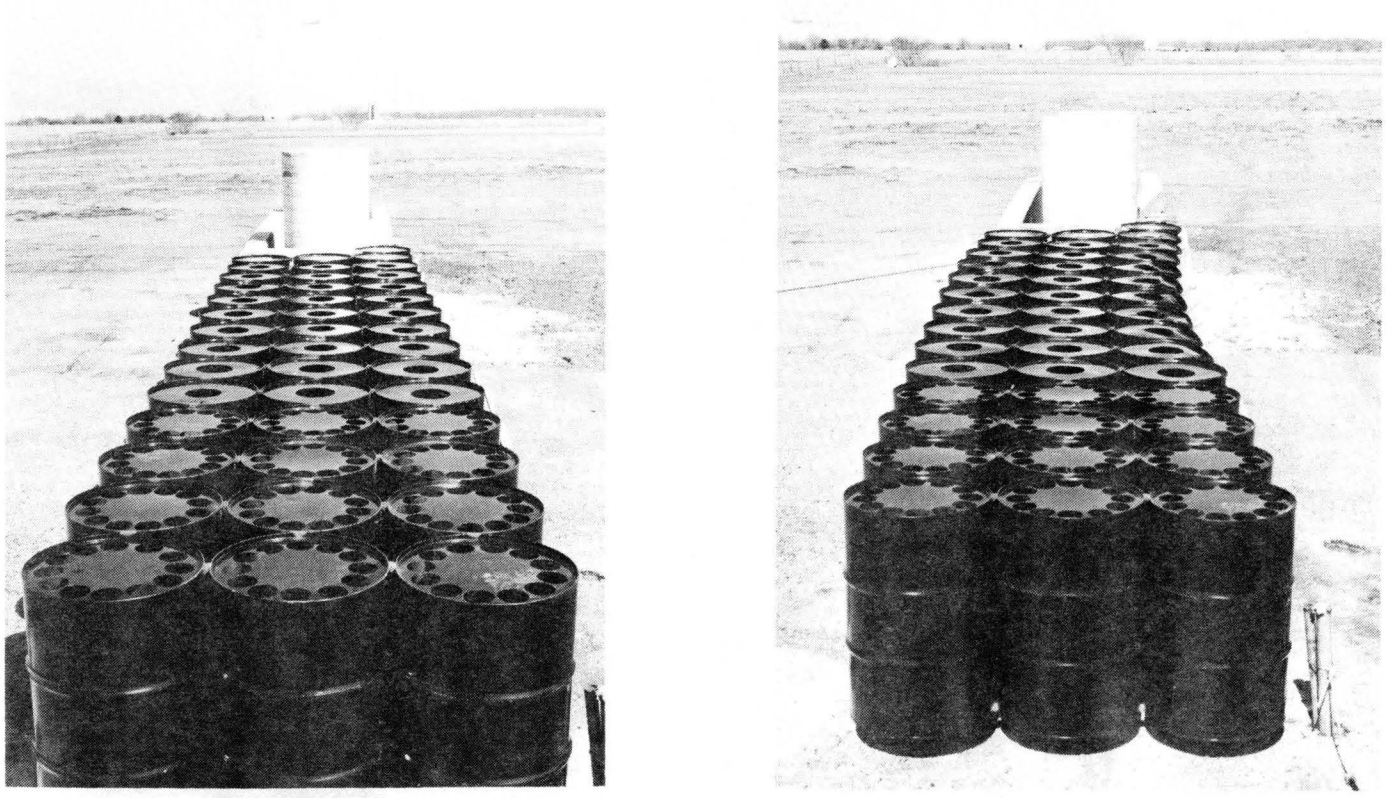

Figure 10, Barriers Before and After Test B (End View).

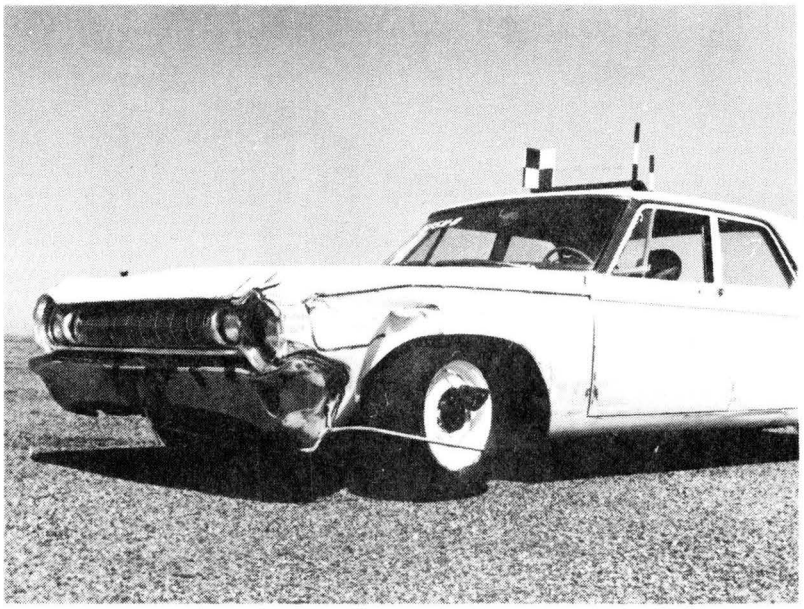

Figure 11, Vehicle Before and After Test B.

maximum deformation being 9 in. The condition of the crash cushion before and after the test is shown in Figure 12. The damaged fender panels can be seen in the first photograph of Figure 13. Figure 14 shows sequential photographs of the test from an overhead camera. The damage to the vehicle can be seen in Figures 15 and 16. The front end of the lightweight, rear-engined vehicle was deformed 11 in. at the bumper level, and the hood (or baggage compartment lid) was pushed back but did not penetrate the windshield.

The vehicle's forward motion stopped in 0.257 sec and 11.3 ft of travel. The average deceleration over this interval, from the films, was 9.2 g's. The vehicle rebounded 1.8 ft. The average deceleration, from the accelerometers, over 0.356 sec was 7.2 g's.

In this test, the resultant from the biaxial accelerometers in the dummy's head was plotted and graphically integrated piece wise to obtain an index to compare to a published injury criterion called the Gadd Severity Index.[7] This index is defined as follows:

$$SI = \int_0^t a^n \, dt$$

where a = acceleration in g's,

t = time in seconds, and

n = an exponent greater than unity.

For head-face impacts whose duration is between 1 and 60 msec[8], the exponent "n" has a value of 2.5; and the upper limit of "Severity Index" for survival is estimated to be about 1000, with moderate injury occurring

at about 700. Caution must be taken in the use and interpretation of the Severity Index for time durations greater than 60 msec such as in this test. For example, Snyder[8] has observed that although we normally are exposed to 1 g all our lives, the formula indicates that a fatal injury would occur in about 16 minutes.

The Severity Index for this test was 176 for the 540 msec event, indicating a low probability of head injury. The photography showed that the dummy's face impacted the upper portion of the steering wheel. However, the chest probably absorbed most of the energy of the torso motion striking the steering column and lower part of the steering wheel. The dashboard of the vehicle was bent outward by the steering column, and the driver's seat was shifted forward (see Figure 17).

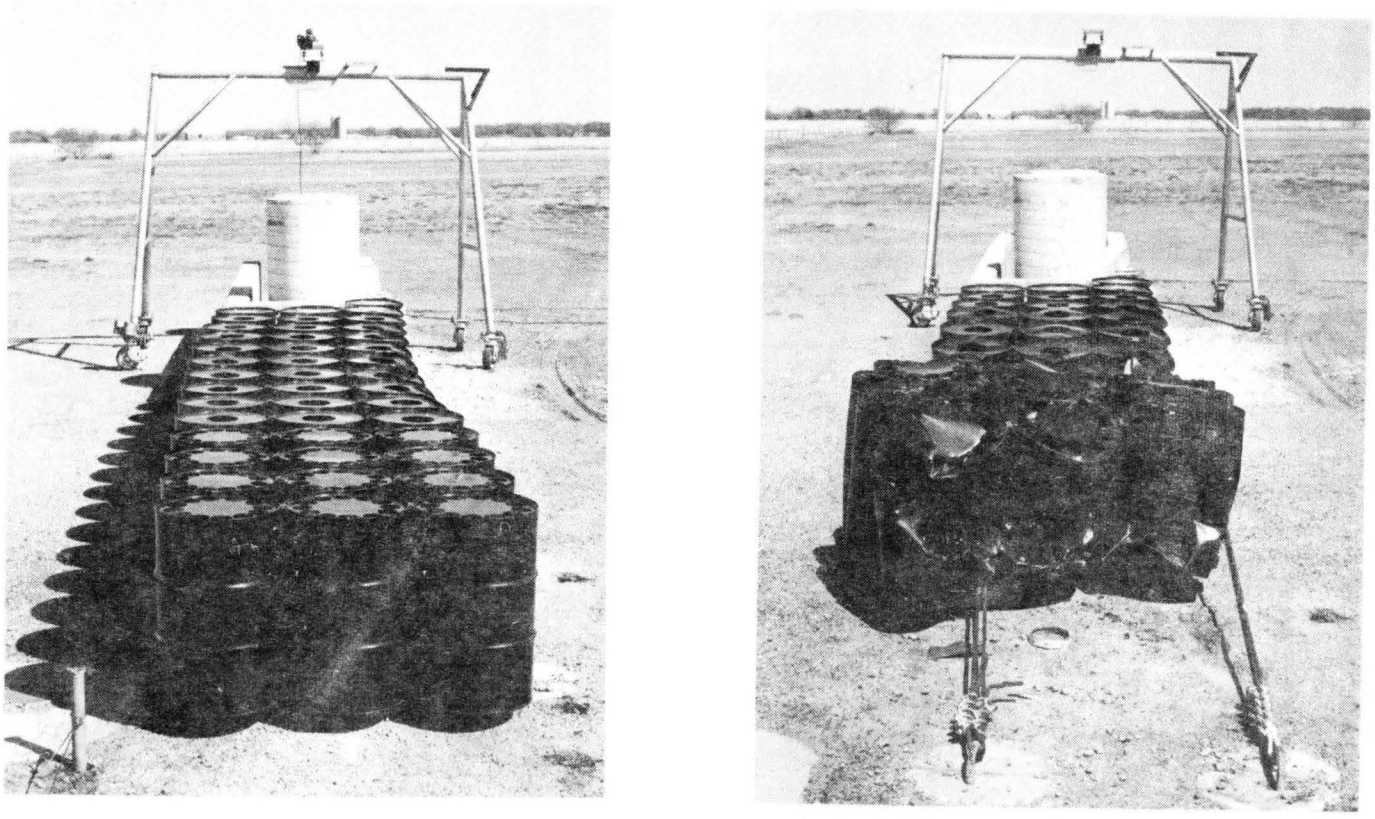

Figure 12 , Barriers Before and After Test C (End View).

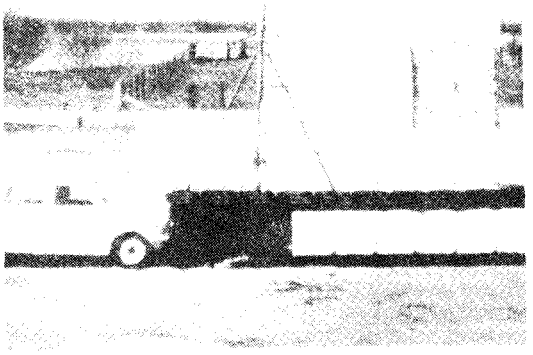

t = 0 sec

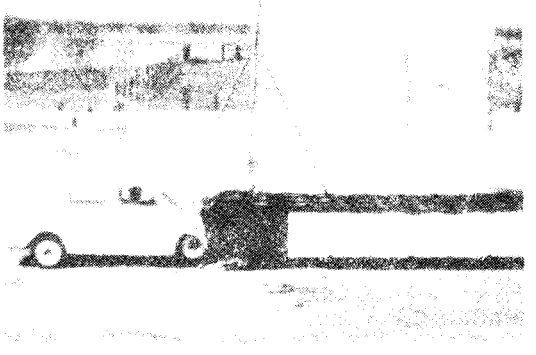

t = 0.047 sec

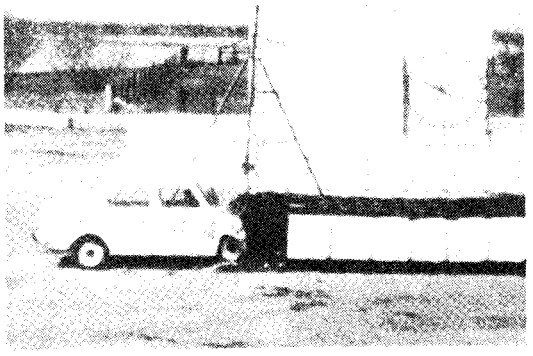

t = 0.084 sec

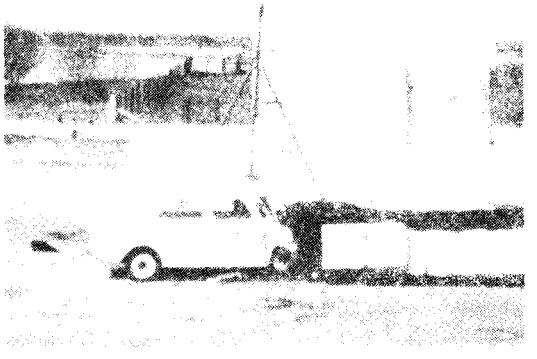

t = 0.133 sec

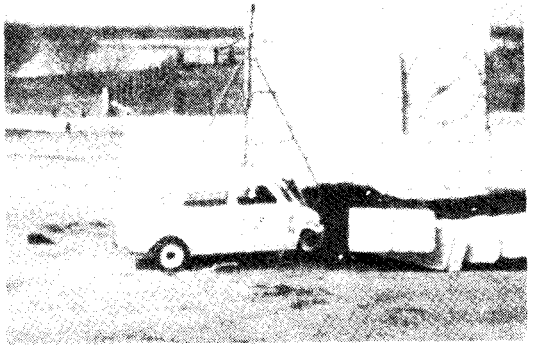

t = 0.186 sec

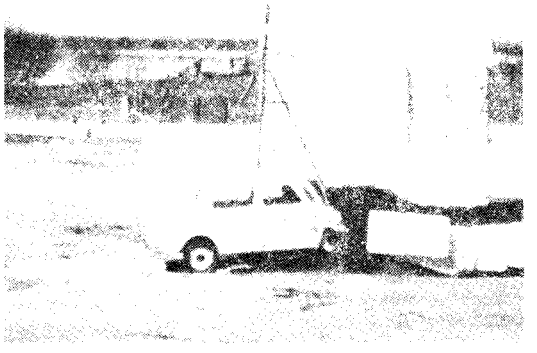

t = 0.271 sec

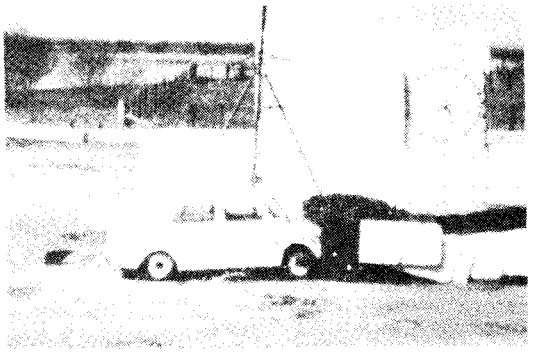

t = 0.646 sec

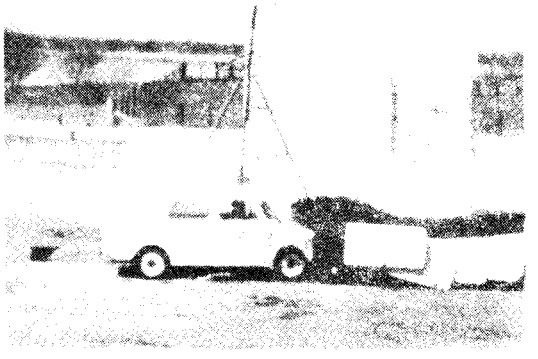

t = 1.250 sec

Figure 13, Test C - - Sequential Photographs (View Perpendicular to Barrier).

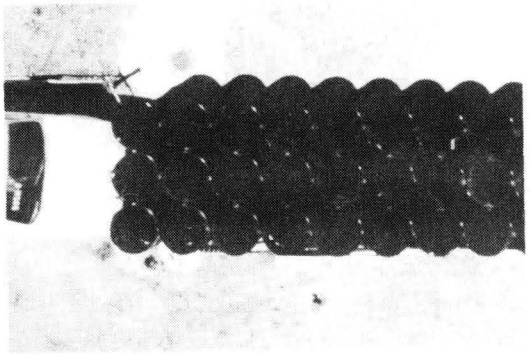

t = 0 sec

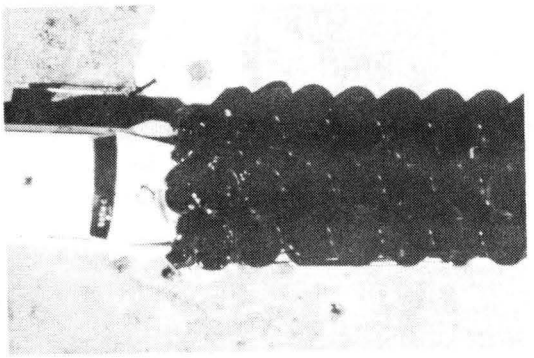

t = 0.036 sec

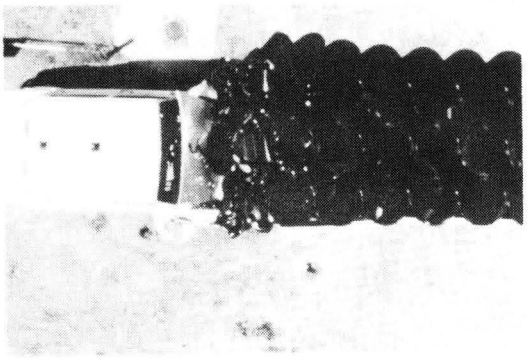

t = 0.088 sec

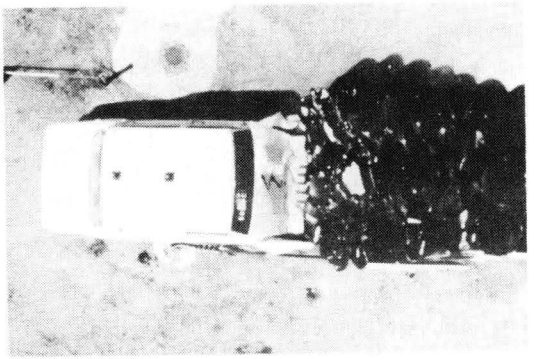

t = 0.165 sec

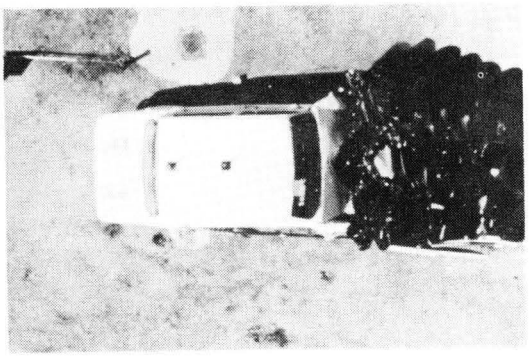

t = 0.277 sec

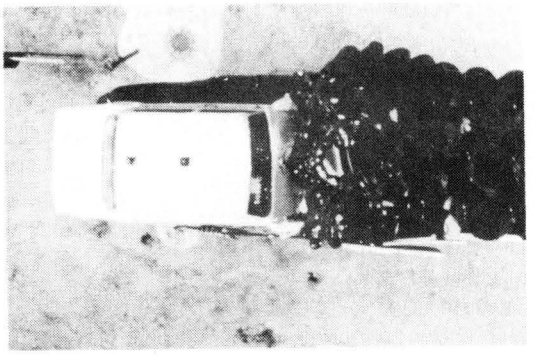

t = 0.690 sec

Figure 14 , Test C - - Sequential Photographs (Overhead View).

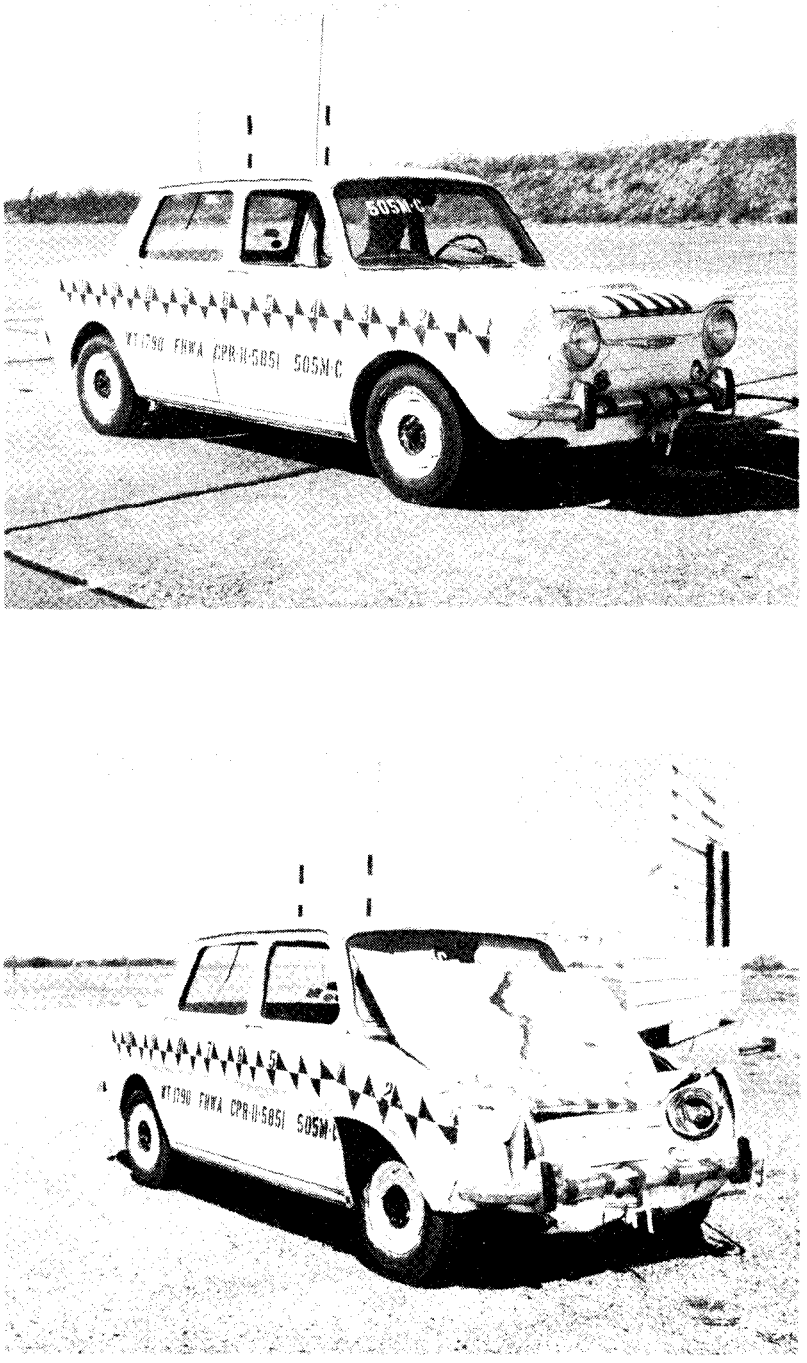

Figure 15. Vehicle Before and After Test C.

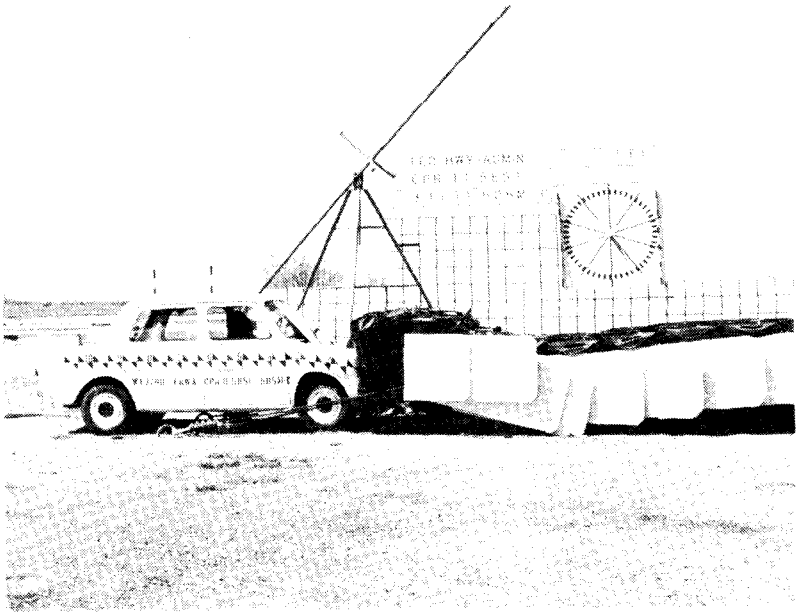

Figure 16, Final Position of Vehicle, Test C.

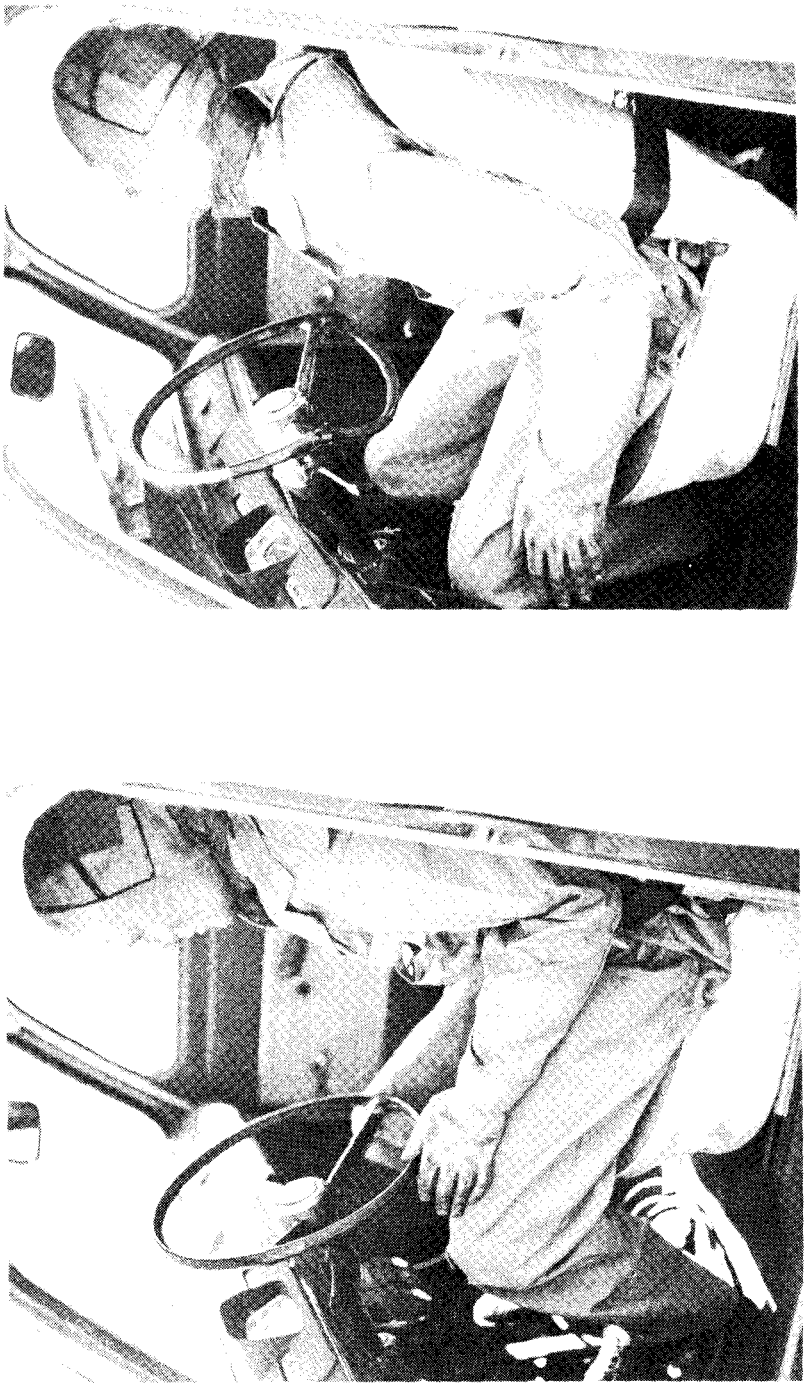

Figure 17. Anthropometric Dummy and Vehicle Interior Before and After Test C.

CONCLUSIONS

1. The Modular Crash Cushion with compatible transition to a concrete median barrier performed comparable to previous Modular Crash Cushions in attenuating a head-on vehicle impact.
2. The crash cushion used in this test series with a compatible transition to a concrete median barrier had sufficient lateral strength to smoothly redirect 4000 lb vehicles impacting the side of the cushion at angles of 10° and 20°, at 60 mph.
3. During angle impacts the vehicles remained relatively stable during and after the redirectional process; and showed no tendency to ramp, overturn, or spin out. The 2 ft high by 4 ft long redirection panels appear far superior to other previously tested redirection panels used on the modular steel drum crash cushion. Accordingly, adaptation of this panel and cable arrangement to other steel drum crash cushion designs should improve their performance.
4. The vehicle decelerations in all tests indicate that a properly restrained passenger would have survived the impacts with little or no injury.[9] This, coupled with the very stable behavior and low departure angles of the vehicles in the angled impact, suggests that a properly restrained driver might have regained control of the redirected vehicles.
5. This barrier design can also be adopted for use at elevated exit ramps by using the cable and panel arrangement of the impacted side of the device, examined in this report, on both sides of the barrier.

6. Use of the information presented in reference 6 will allow the design of a barrier of this type using all 20 gage drums with different crash strengths (hole cut-out patterns) rather than the combination of 18 gage and 20 gage drums used in these tests. This should reduce possible confusion in the field, as for each selected crush resistance a different hole cut-out pattern would be selected.

SELECTED REFERENCES

1. Michie, Jarvis D., Calcote, Lee R., and Bronstad, Maurice E., "Guardrail Performance and Design," Final Report on NCHRP Project 15-1(2), January 1970.

2. Nordlin, Eric F. and Field, Robert N., "Dynamic Tests of Steel Box Beam and Concrete Median Barriers," Highway Research Record No. 222, 1968.

3. Hirsch, T. J., "Barrel Protective Barrier," Technical Memorandum 505-1, Texas Transportation Institute, Texas A&M Research Foundation, a progress memorandum on Contract CPR-11-5851, U. S. Department of Transportation, Federal Highway Administration.

4. Hirsch, T. J., Hayes, G. G., and Ivey, D. L., "The Modular Crash Cushion," Technical Memorandum 505-1S, Supplement to 505-1, Texas Transportation Institute, Texas A&M Research Foundation, a progress memorandum on Contract CPR-11-5851, U. S. Department of Transportation, Federal Highway Administration, August 1970.

5. Hensen, Ronald J., "Energy Absorber Designs for Exit Ramp Gores," Denver Research Institute, an evaluation prepared for a barrier selection for the South Broadway Exit from I-25 southbound, Denver, Colorado.

6. White, M. C., "The Modular Crash Cushion: Design Data from Static Crush Tests of Steel Drums and of Corrugated Steel Pipes," a progress memorandum on Contract CPR-11-5851, U. S. Department of Transportation, Federal Highway Administration, April 1971.

7. Gadd, C. W., "Use of a Weighted-Impulse Criterion for Estimating Injury Hazard," Proceedings of the Tenth Stapp Car Crash Conference, SAE, New York, 1966.

8. Snyder, Richard G., "Human Impact Tolerance," 1970 International Automobile Safety Conference Compendium, Detroit, Michigan, May 13-15, 1970; Brussels, Belgium, June 8-11, 1970, pp. 712-782.

9. Patrick, L. M., et al., "Knee, Chest, and Head Impact Loads," Proceedings of the 11th Stapp Car Crash Conference, Anaheim, California, October 10-11, 1967.

APPENDIX A

TABLE 3

TEST A HIGH-SPEED FILM DATA

Time (sec)		Displacement (ft)
-.064		-5.32
-.051		-4.25
-.038		-3.19
-.026		-2.13
-.013		-1.07
0	Impact	0
.013		1.07
.026		2.11
.038		3.15
.051		4.17
.064		5.18
.077		6.16
.090		7.12
.102		8.05
.115		8.95
.128		9.81
.141		10.63
.154		11.39
.166		12.21
.179		12.96
.192		13.67
.205		14.34
.218		15.01

*V_i = 83.1 ft/sec

Time (sec)	Displacement (ft)
(continued)	
.230	15.64
.243	16.27
.256	16.88
.269	17.51
.282	18.14
.294	18.76
.307	19.40
.320	20.02
.333	20.64
.346	21.26
.358	21.86
.371	22.47
.384	23.09
.397	23.69
.410	24.30
.422	24.89
.435	25.50
.448	26.10
.465	26.98
.484	27.85
.503	28.72
.522	29.59
.541	30.44
.559	31.32
.578	32.17
.597	33.01
.616	33.88

**V_p = 48.5 ft/sec

***V_f = 45.6 ft/sec

*V_i = Speed at impact

**V_p = Speed when vehicle is parallel to barrier

***V_f = Speed at loss of contact

TABLE 4

TEST B HIGH-SPEED FILM DATA

Time (sec)	Displacement (ft)
-.037	-3.38
-.028	-2.53
-.019	-1.71
-.009	-0.86
0 Impact	0
.009	0.80
.019	1.62
.028	2.45
.037	3.26
.047	4.06
.056	4.85
.065	5.63
.075	6.43
.084	7.18
.094	7.94
.103	8.69
.112	9.41
.122	10.16
.131	10.88
.140	11.60
.150	12.35
.159	13.06
.168	13.79
.178	14.52
.187	15.24
.196	15.94
.206	16.66
.215	17.38
.225	18.10

V_i = 91.4 ft/sec

V_p = 76.4 ft/sec

Time (sec)	Displacement (ft)
(continued)	
.234	18.82
.243	19.53
.253	20.23
.262	20.93
.271	21.64
.281	22.34
.290	23.05
.299	23.77
.309	24.46
.318	25.16
.327	25.87
.337	26.57
.354	27.64
.413	31.78
.423	32.51
.433	33.28
.442	34.05
.452	34.76
.462	35.50
.472	36.26

V_f = 75.9 ft/sec

TABLE 5

TEST C HIGH-SPEED FILM DATA

Time (sec)	Displacement (ft)		Time (sec)	Displacement (ft)
-.050	-4.09	V_i = 81.8 ft/sec	(continued)	
-.040	-3.26		.129	8.34
-.030	-2.45		.139	8.79
-.020	-1.63		.158	9.53
-.010	-0.81		.178	10.13
0 Impact	0		.198	10.58
.010	0.83		.218	10.92
.020	1.57		.238	11.15
.030	2.31		.257	11.26
.040	3.05		.337	10.94
.050	3.74		.416	10.34
.059	4.45		.495	9.87
.069	5.09		.574	9.57
.079	5.71		.653	9.47
.089	6.30		.772	9.62
.099	6.85		.891	9.87
.109	7.39		1.010	9.97
.119	7.88		1.129	9.85

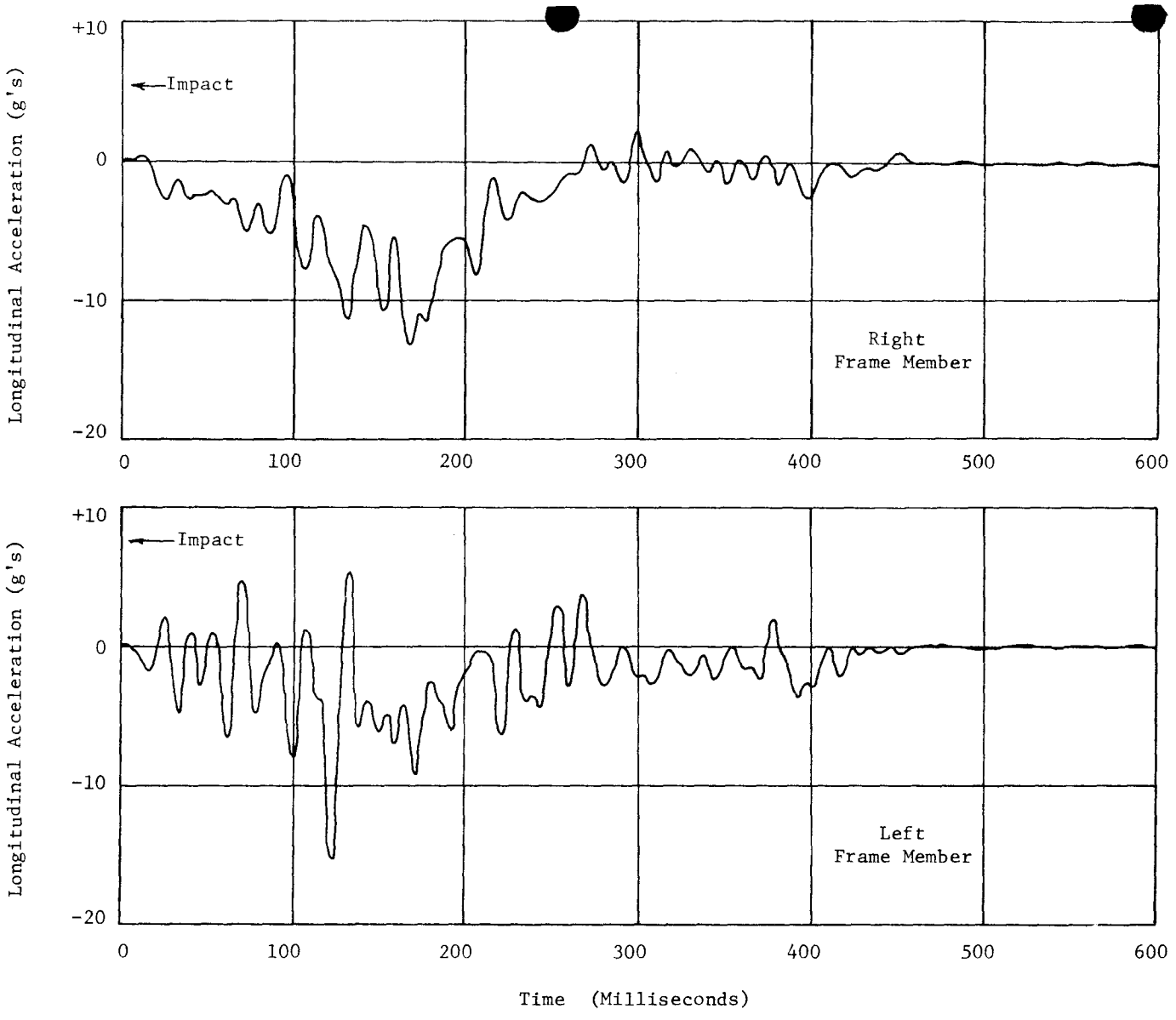

Figure 18, Longitudinal Accelerometer Data, Test A
(80 HZ Low-Pass Filter)

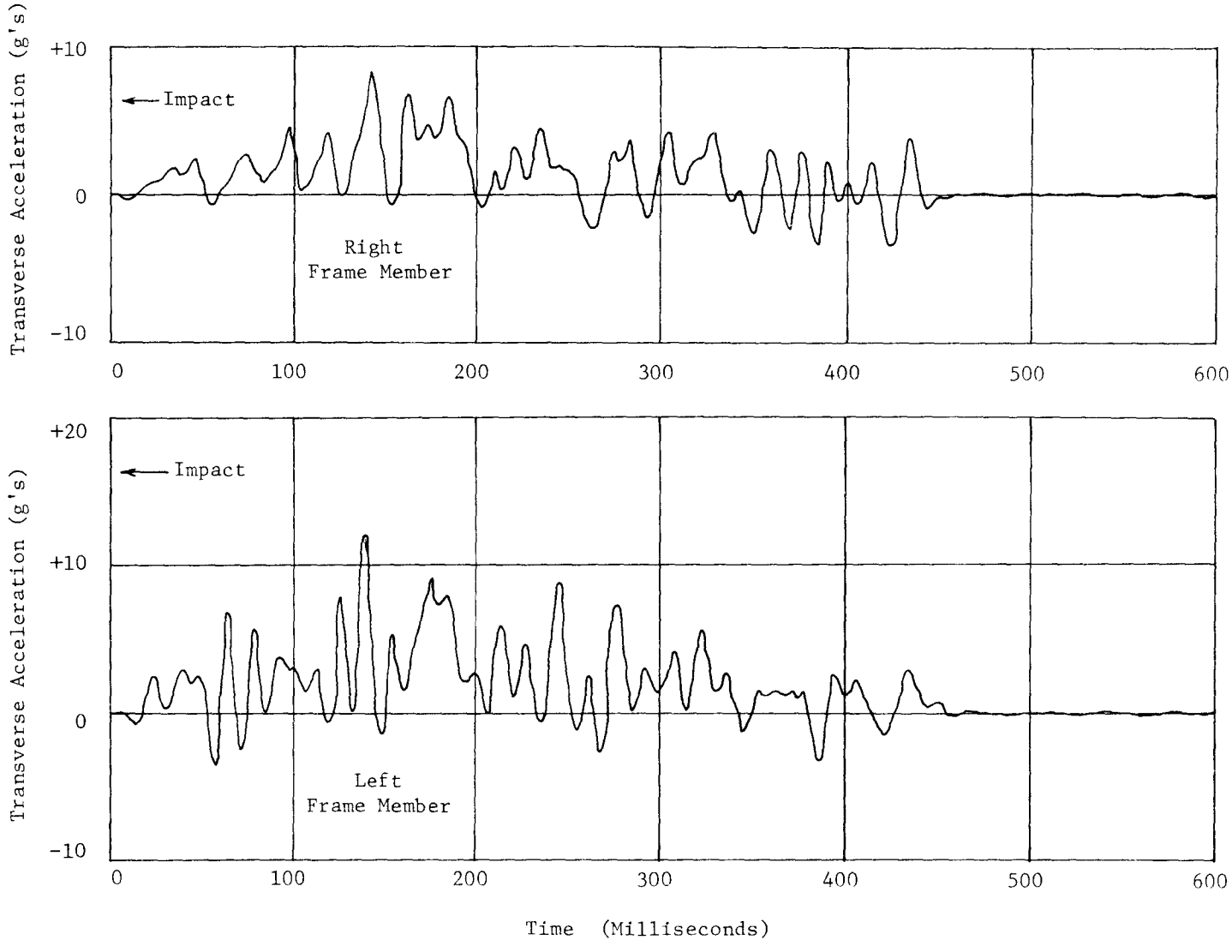

Figure 19, Transverse Accelerometer Data, Test A
(80 HZ Low-Pass Filter)

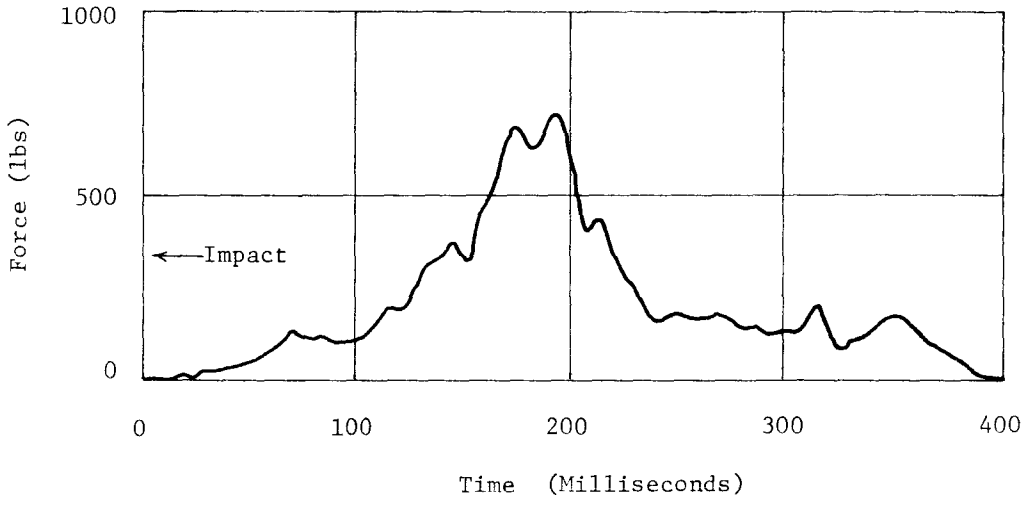

Figure 20, Lap Belt Data, Test A

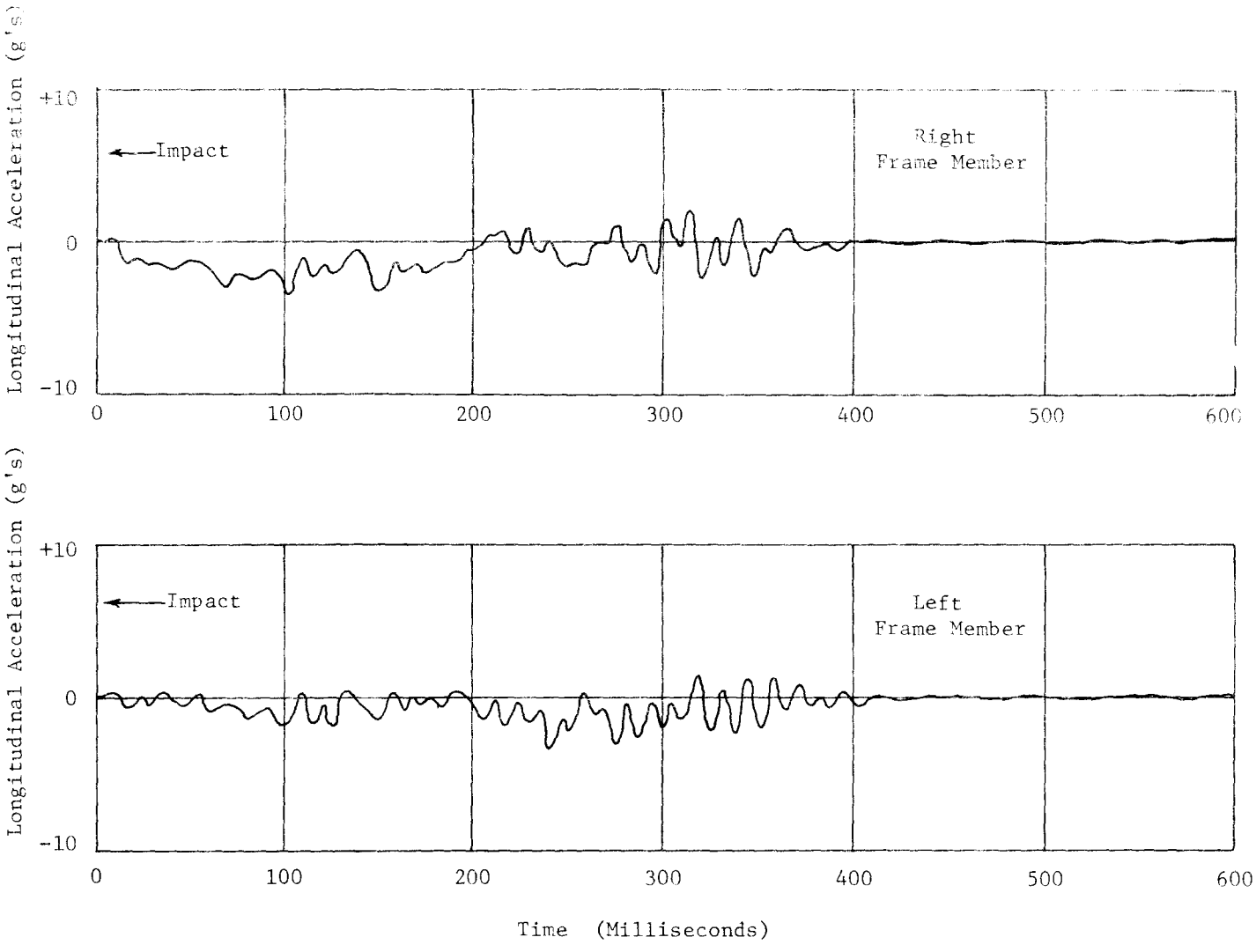

Figure 21, Longitudinal Accelerometer Data, Test B
(80 HZ Low-Pass Filter)

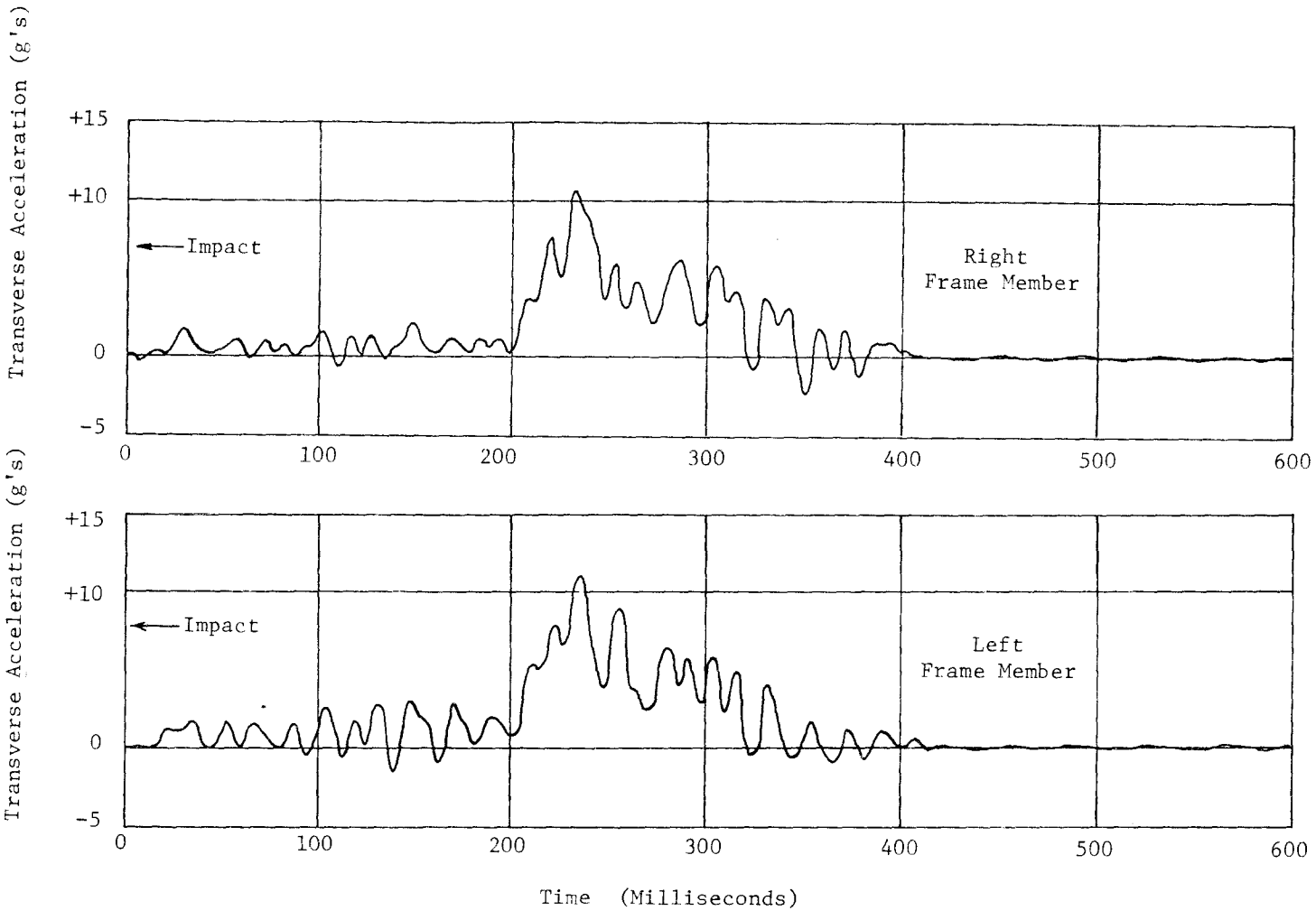

Figure 22, Transverse Accelerometer Data, Test B
(80 HZ Low-Pass Filter)

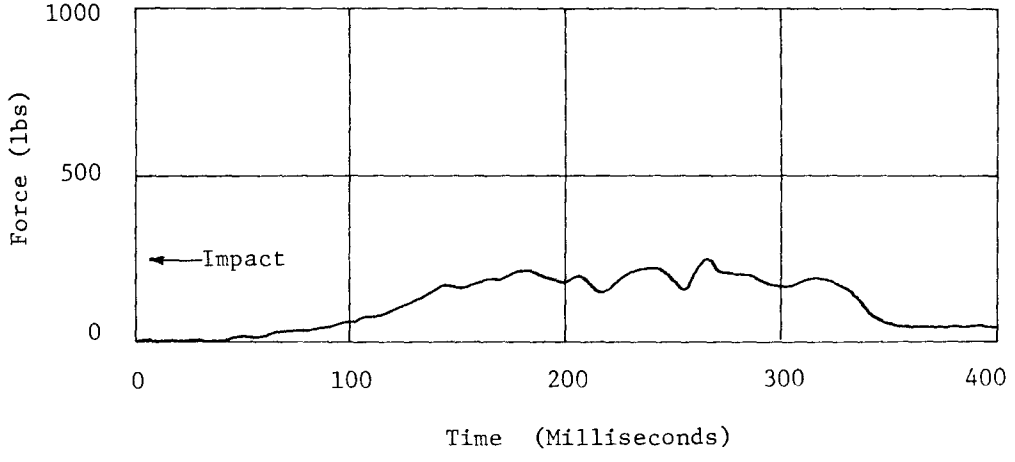

Figure 23, Lap Belt Data, Test B

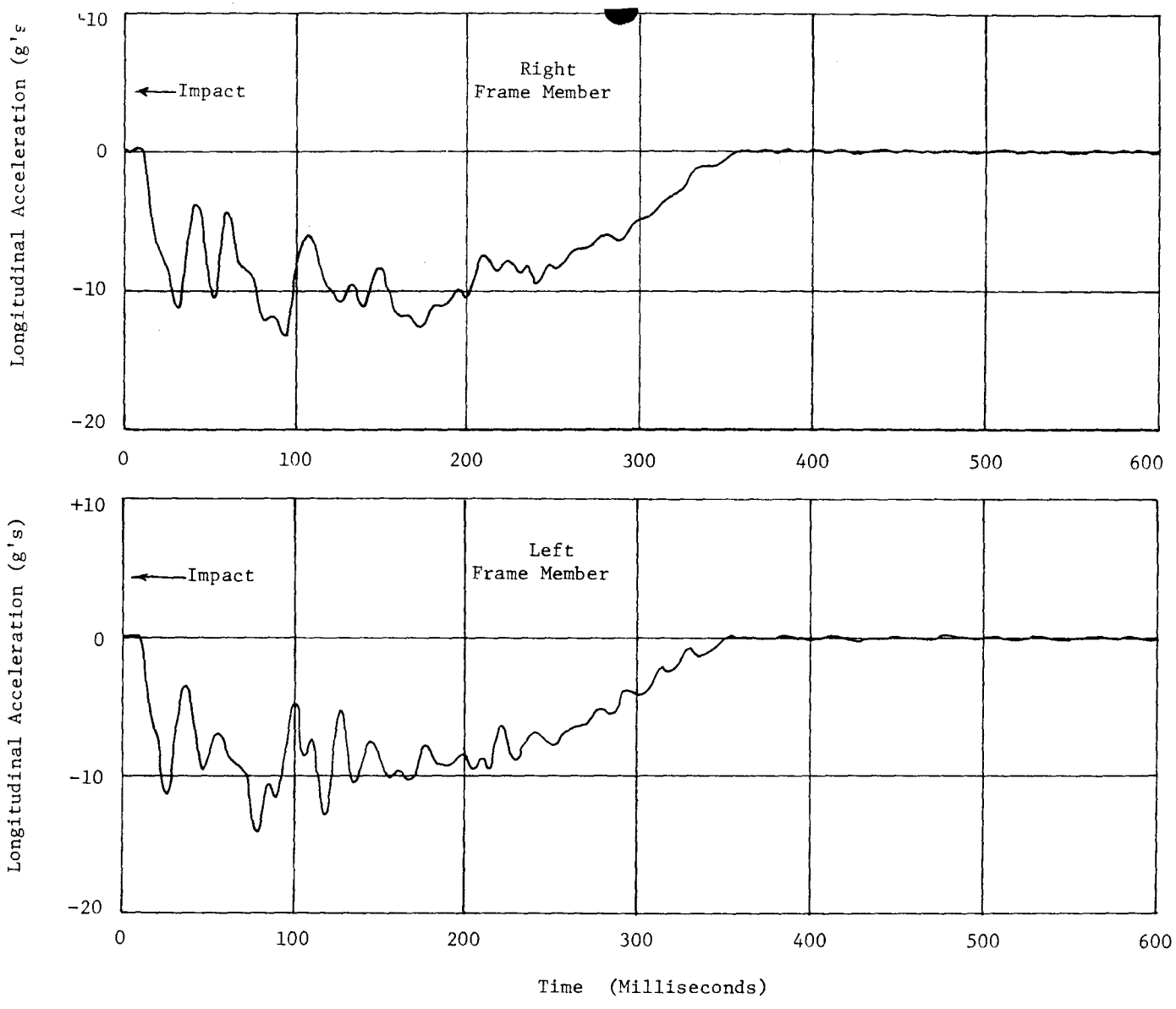

Figure 24, Longitudinal Accelerometer Data, Test C
(80 HZ Low-Pass Filter)

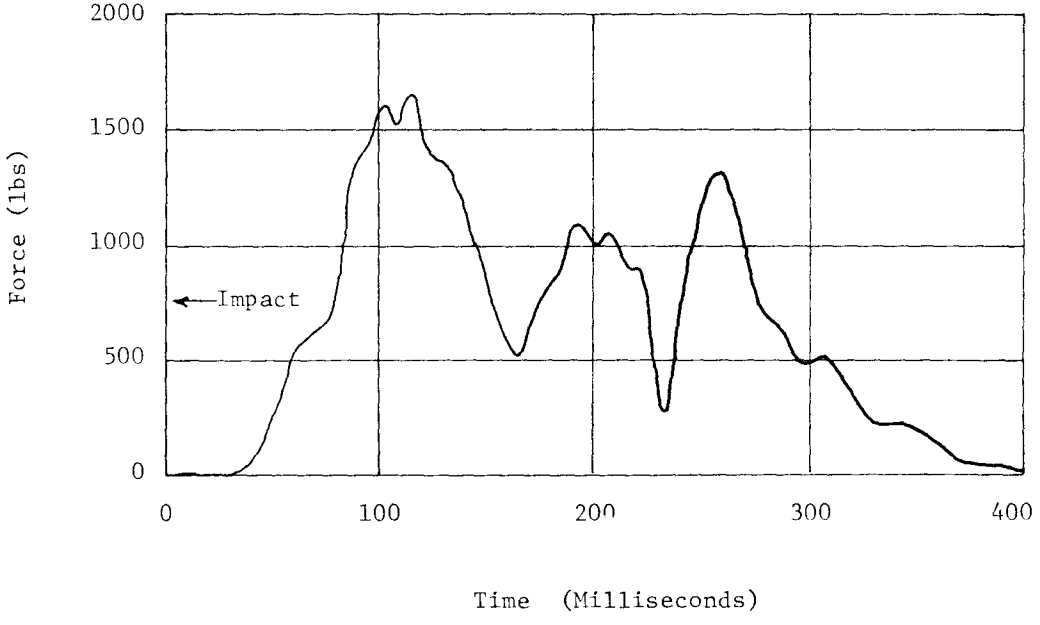

Figure 25, Lap Belt Data, Test C

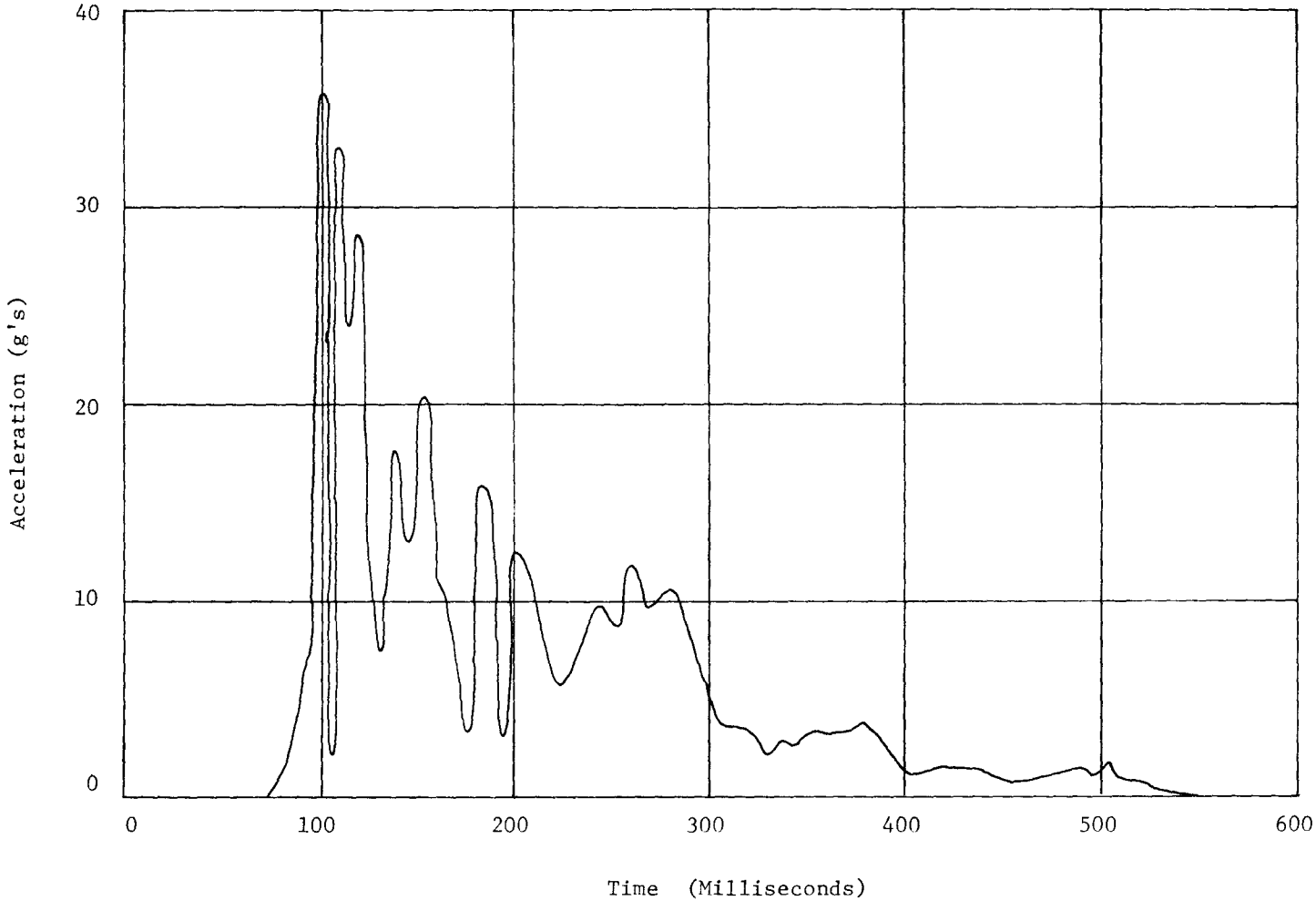

Figure 26 , Resultant Acceleration of Dummy's Head

TECHNICAL MEMORANDUM 505-16

Texas Transportation Institute
Texas A&M Research Foundation

FEASIBILITY OF CONCRETE PIPE CRASH CUSHIONS

A Test And Evaluation Report On Contract No. CPR-11-5851

U.S. Department of Transportation
Federal Highway Administration

by

M. A. Pittman
Research Associate

D. L. Ivey
Research Engineer

and

T. J. Hirsch
Research Engineer

This crash test and evaluation was conducted under the Office of Research and Development, Structural and Applied Mechanics Division's Research Program on Structural Systems in Support of Highway Safety (4S Program).

July 1971

INTRODUCTION

One full-scale vehicle crash test was conducted on a system composed of reinforced concrete sewer pipes embedded 4 ft-3 in. in the soil. This crash cushion is shown in Figures 1 and 3. The results of this crash test are presented in this report.

Pendulum tests were conducted by the Southwest Research Institute (SwRI)[1]* on various transite, vitrified clay, and concrete pipes (see Table 1). The purpose of these tests was to acquire force and energy data; and thereby determine the feasibility of crash cushions constructed of the readily available materials mentioned above. These crash cushions would be economical and easy to install at ground level sites. A reinforced concrete sewer pipe tested by SwRI (30 in. O.D.) was chosen for use in the prototype crash cushion which was built and tested at TTI. The pipes used in the crash cushion and the pipe tested by SwRI had the same dimensions and were embedded in the soil to the same level.

*Superscript numbers refer to corresponding references at the end of this report.

TABLE 1

PIPE DIMENSIONS

(After Michie and Bronstad[1])

Test Number	Material	O.D. (in.)	I.D. (in.)	Length (in.)	Height Above Grade (in.)
1	Transite Class 2400	11.4	10	66	30
2	Transite Class 2400	20.3	18	66	30
3	Vitrified Clay	21.5	17	63	30
4	Concrete Sewer Regular	23.0	18	51	24
5	Concrete Sewer Extra Strong	30.4	24	51	24
6	Concrete Sewer Extra Strong (reinforced)*	30.0	24	75	24

*Reinforcement was 3 x 8-6/8 welded wire fabric. The 8-ga wires were longitudinal, and the 6-ga wires were circumferential.

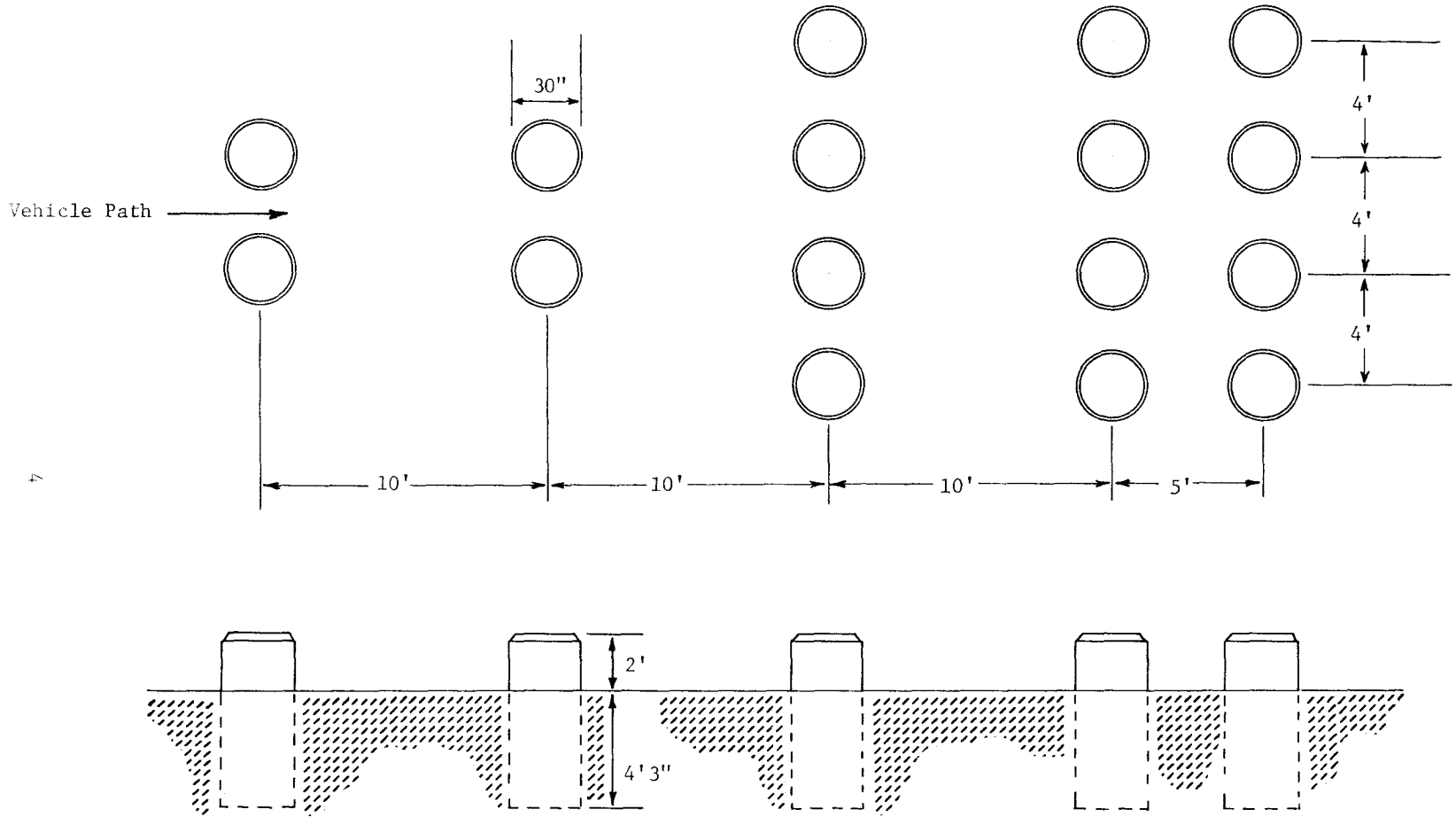

FIGURE 1, CONFIGURATION OF REINFORCED CONCRETE PIPE CRASH CUSHION

DESIGN CONSIDERATIONS

Results of pendulum tests conducted on individual pipes at SwRI are presented in Table 2. The extrapolation of the pendulum test data to a hypothetical vehicle collision was viewed with extreme caution since it was felt that the failure mechanism of a pipe, when subjected to a rigid pendulum impact, would be significantly different from the failure mechanism of the same pipe when impacted by the deformable front end of an automobile. For example, the accelerometer traces which were developed by pendulum tests showed the main pendulum impact deceleration pulse to be very high, with a duration of only 3 to 5 msec. The energy spent in fracturing the pipe was therefore very low and probably not indicative of the energy that would be expended by a vehicle. If the peak force from the pendulum data is used to calculate energy loss in a vehicle crash test, a rather high value is obtained. This is explained in more detail in a later section. For this reason, the use of pendulum data was considered somewhat questionable for the prediction of energy losses during full-scale crash tests.

Lacking a reliable prediction method, the decision was made to conduct a full-scale crash test on a reinforced concrete sewer pipe crash cushion, since it seemed apparent that this pipe would give the highest values of fracture energy. By starting with the highest value, it was assumed that some interpolation could be made in predicting the fracture characteristics of the smaller pipes.

TABLE 2

PENDULUM TEST RESULTS

(After Michie and Bronstad[1])

Test	Impact Velocity (V_I, fps)	Pulse Duration (t, msec)	Fracture Energy (KE, ft-kips)	Velocity Change (ΔV, fps)	Peak Force (kips)
1 Transite	29.3 (20.0 mph)	2.8	1.64	0.44	22.6
2 Transite	29.8 (20.4 mph)	4.2	3.78	0.91	40.7
3 Vitrified Clay	28.1 (19.2 mph)	2.5	5.35	1.34	70.6
4 Concrete	28.4 (19.4 mph)	2.5	5.50	1.39	79.5
5 Concrete	28.6 (19.6 mph)	3.2	6.72	1.71	78.5
6 Reinf. Concrete	29.0 (19.8 mph)	3.8	8.58	2.16	82.8

Pendulum Weight = 2300 lbs

BARRIER DESCRIPTION

Sixteen reinforced concrete sewer pipes were arranged in five rows (3 rows, 4 pipes wide; and 2 rows, 2 pipes wide) as shown in Figure 1. The first 4 rows were 10 ft apart (center to center). The last row was only 5 ft behind the row preceding it. The pipes were spaced 4 ft apart (center to center) laterally. These reinforced concrete pipes had an outside diameter of 30 in. and a length of 75 in. The reinforcement was 3 x 8-6/8 welded wire fabric. The 8-ga. wires were longitudinal, and the 6-ga. wires were circumferential. The pipes were embedded 4 ft 3 in. in the soil and the interior of the pipes was filled with soil to ground level. Details of a single pipe are shown in Figure 2.

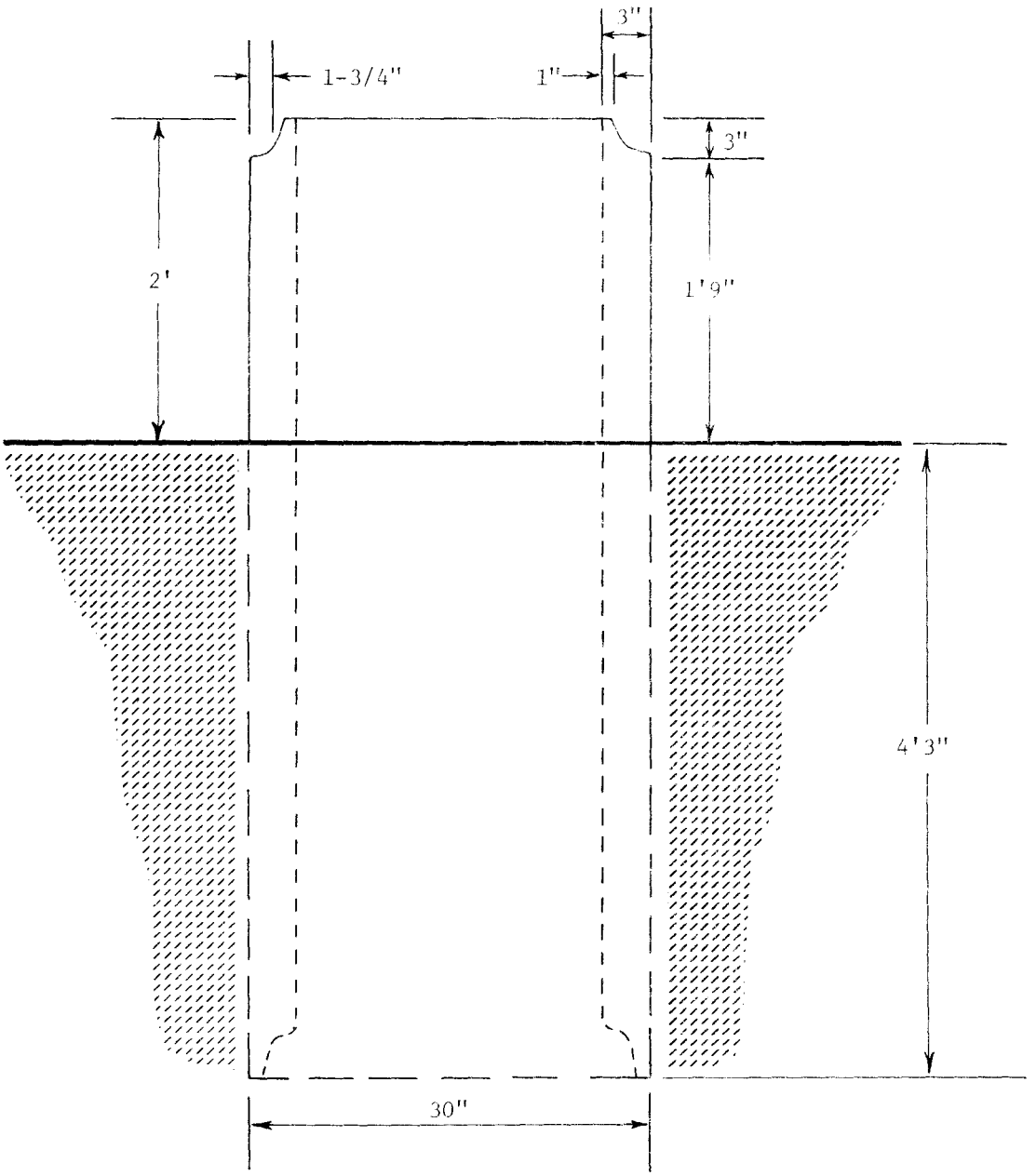

FIGURE 2, DETAILS OF ONE REINFORCED CONCRETE PIPE

INSTRUMENTATION

For this test, two strain-gage-type accelerometers were mounted on the frame of the vehicle, one on the left frame member and one on the right. Both accelerometers measured decelerations along the vehicle's longitudinal axis, i.e. along the path of the vehicle. A tri-axial electromechanical acceleration measuring device (Impact-O-Graph) was located on the right rear floorboard of the vehicle. This device is used as a secondary source of acceleration information.

An Alderson anthropometric dummy, weighing 160 lb, was placed on the driver's side of the vehicle. A lap belt was fastened across the dummy's pelvic region. A strain-gage load cell was connected to the lap belt to measure the force on the lap belt during impact.

The signals from the two accelerometers and the load cell were transmitted by telemetry to a ground station where they were recorded on magnetic tape. These data were then passed through an 80 Hz low-pass filter to reduce the effects of "ringing", and then displayed on Visicorder paper. The Impact-O-Graph records accelerations with a stylus on its own roll of chart paper, and is independent of the other electronic instrumentation.

Two high-speed cameras located perpendicular to the vehicle path were used to record the crash event. Both high-speed films had timing lights so that elapsed time at any point could be calculated. A stadia board marked in 3 in. increments on the right side of the vehicle was used in determining distance traveled. These distances were measured on a Vanguard Motion Analyzer. Initial speed was then computed from the time-displacement data obtained.

TEST DESCRIPTION

A 3950 lb Chevrolet impacted the system head-on at a speed of 40.5 mph. After shattering the two pipes in the first row, the vehicle ramped, became airborne, and finally came to rest on top of the third row of pipes (see Figure 3). The first row of pipes was completely shattered and the soil was disturbed when the pipes began to tilt in the ground (see Figure 4), but the rest of the system remained intact and sustained little damage. Average longitudinal deceleration from the film was 9.2 g's over 4.3 ft of travel and 0.105 sec (accelerometer traces showed no significant longitudinal forces on the vehicle after this time). Although vertical accelerations were obviously significant, they were not determined. Vehicle damage was moderate, with a front-end deformation of 1.3 ft.

A summary of the pertinent data obtained is presented in Table 3. Time-displacement data from the high-speed films are given in Table 4, and reproductions of the accelerometer force traces are shown in Figure 6.

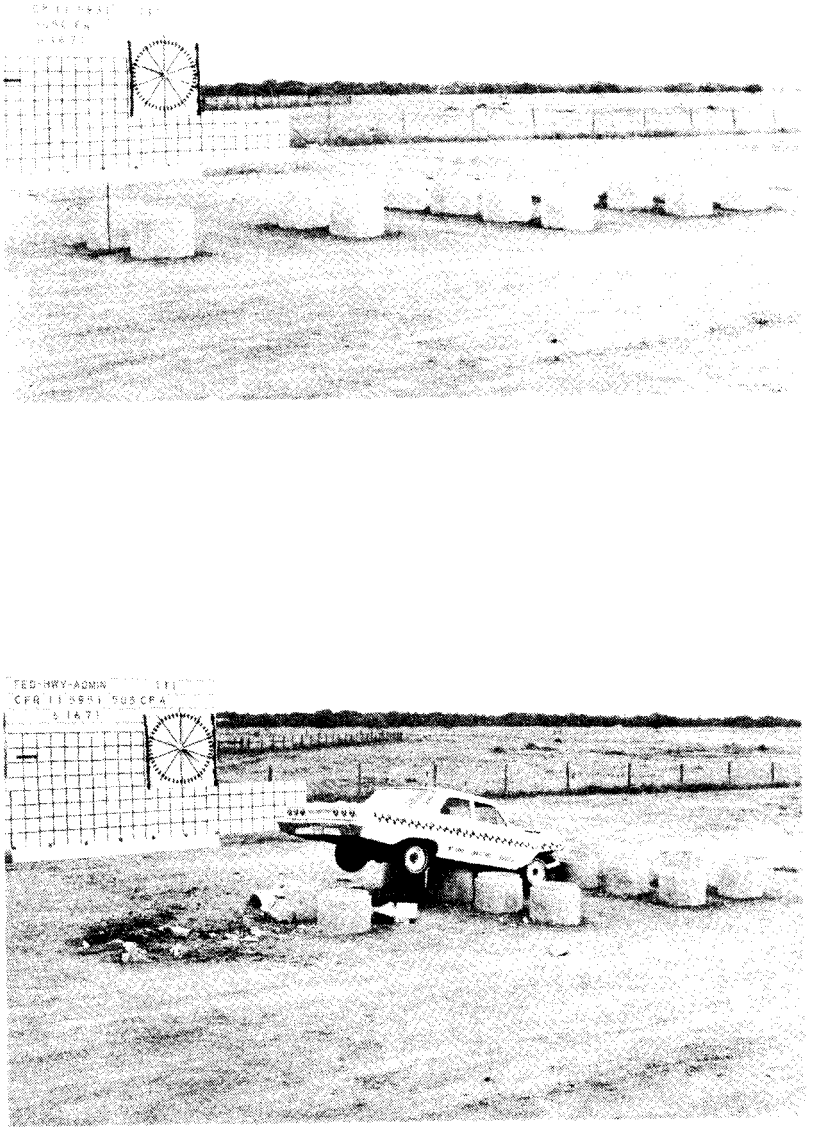

FIGURE 3, BARRIER BEFORE AND AFTER TEST 505 CP-A.

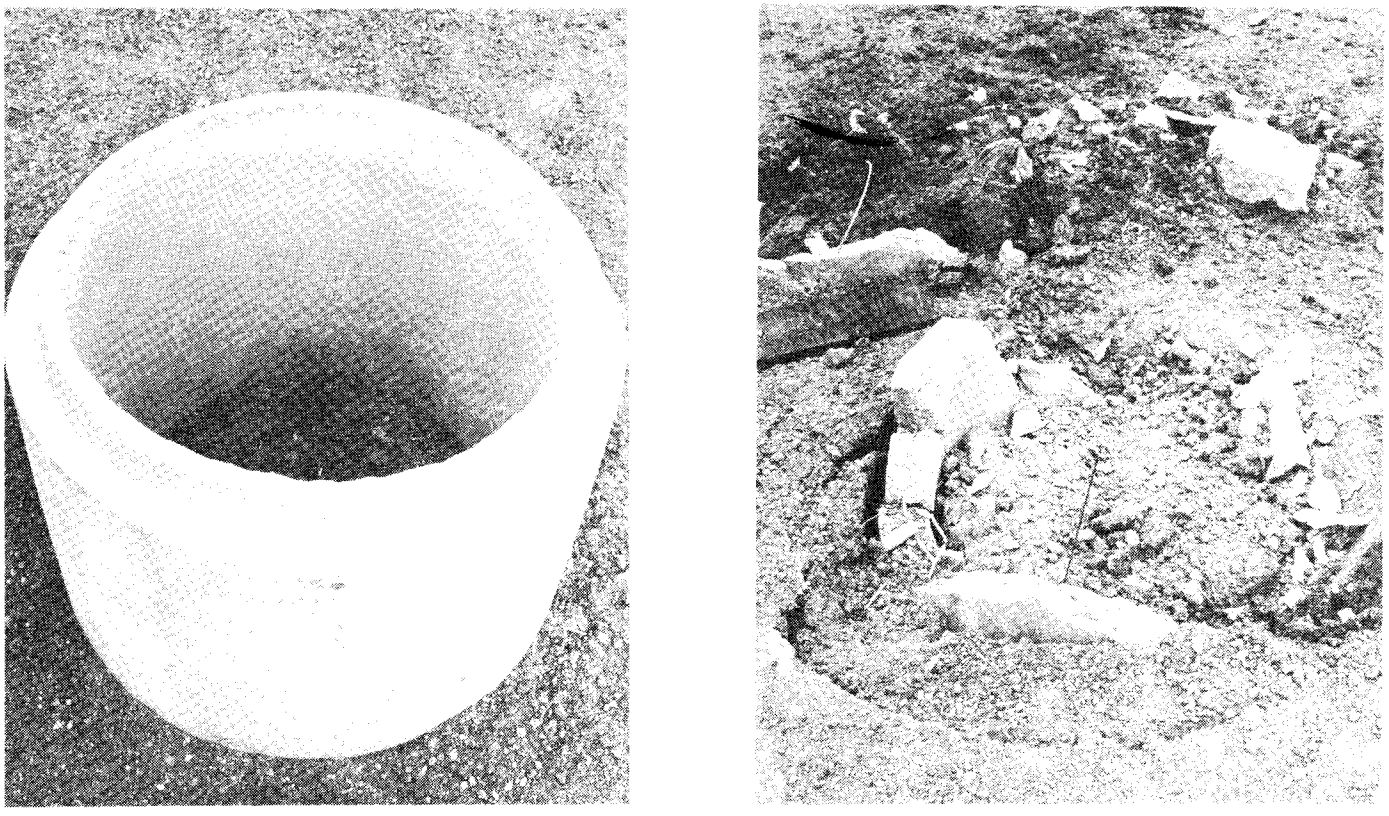

FIGURE 4, CONCRETE PIPE BEFORE AND AFTER TEST 505 CP-A.

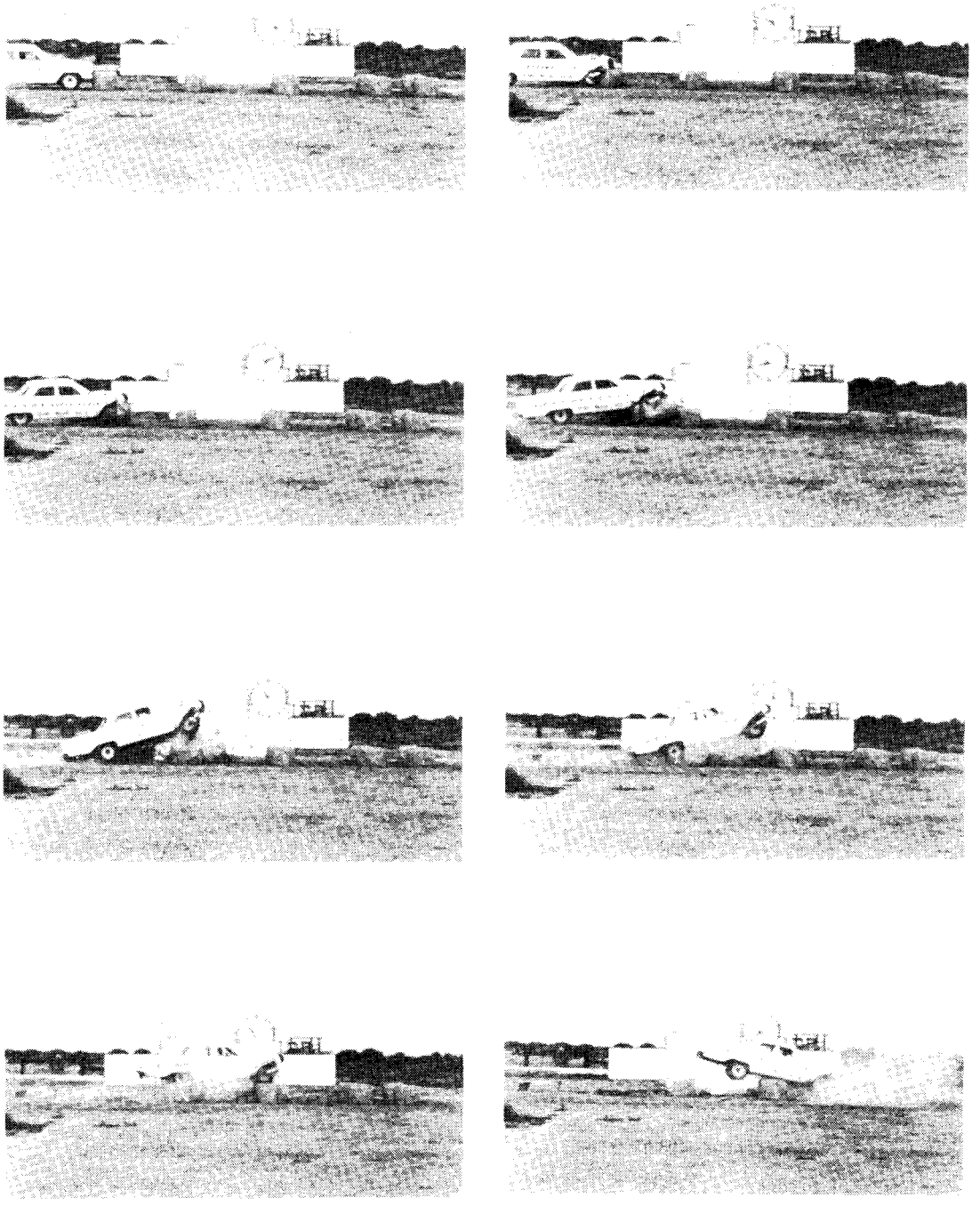

FIGURE 5. SEQUENTIAL PHOTOGRAPHS OF TEST 505 CP-A.
(View Perpendicular To Barrier)

TABLE 3

SUMMARY OF DATA

Test 505 CP-A

VEHICLE

Year	1963
Make	Chevrolet
Weight, lb	3950

FILM DATA

Initial Speed, fps	59.4
mph	40.5
Final Speed,* fps	31.7
mph	21.6
Distance traveled,* ft	4.3
Average Deceleration, g's $(V_i^2 - V_f^2) / 2gS$	9.2
Duration,* sec	0.104
Initial Kinetic Energy, Kip-ft	216.5
Final Kinetic Energy, Kip-ft	61.6

ACCELEROMETER DATA

Maximum Deceleration, g's	20.3**
Average Deceleration, g's	6.8**
Time, sec	0.104

OTHER DATA

Residual Front Deformation, ft	1.3

*Taken when accelerometer pulse goes back to zero.
**Average of right and left frame members.

TABLE 4

HIGH-SPEED FILM DATA

Test 505 CP-A

Time (msec)		Displacement (ft)	
-42		-2.48	V_i = 59.4 fps
-31		-1.86	
-21		-1.30	
-10		-0.68	
0	Impact	0	
21		0.96	
42		2.02	
63		2.85	
84		3.57	
104		4.24	V_f = 31.7 fps
125		4.95	
146		5.63	
167		6.18	
188		6.89	
208		7.52	
229		8.15	
250		8.72	
271		9.26	

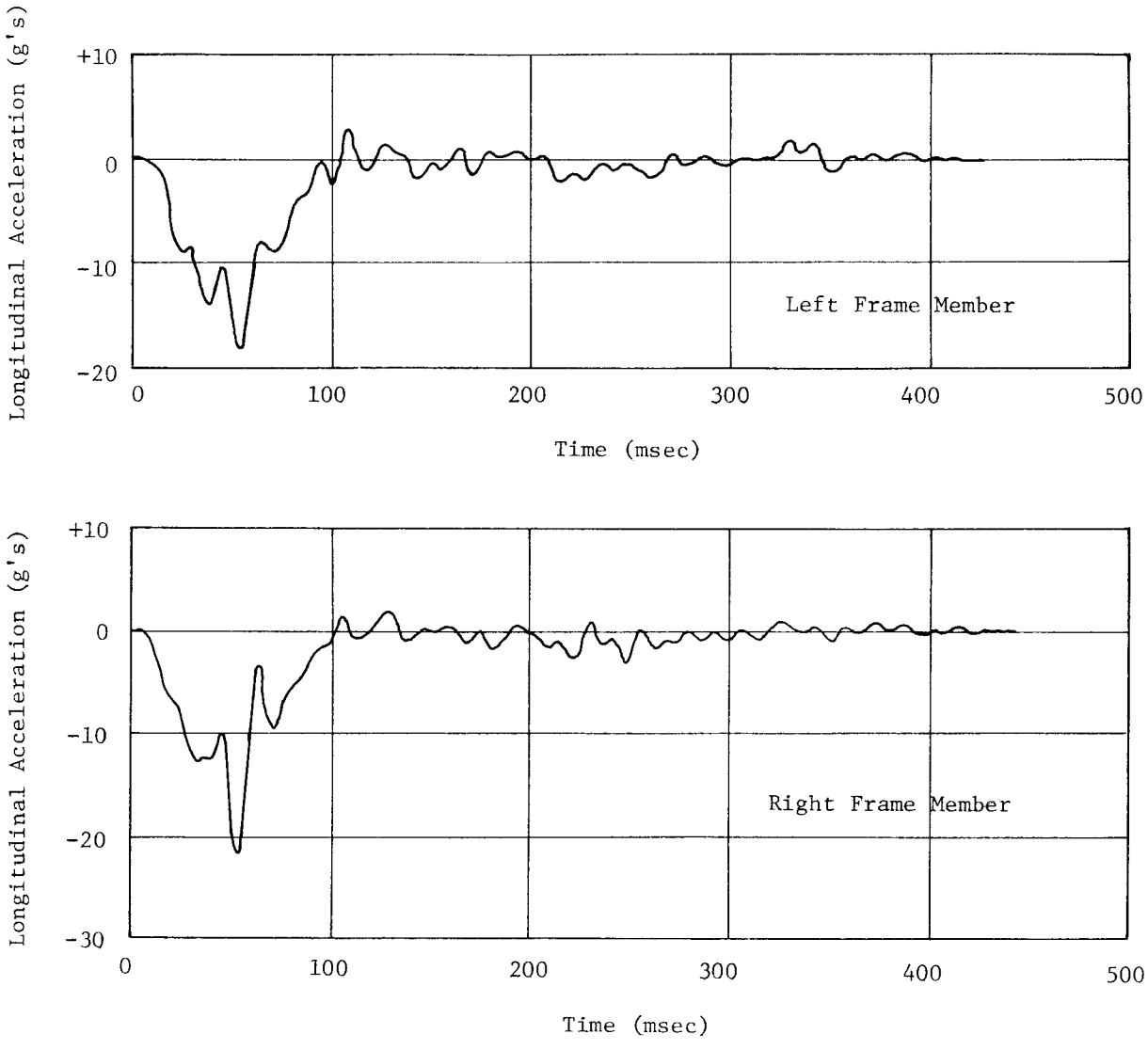

FIGURE 6, ACCELEROMETER DATA, TEST 505 CP-A.

DISCUSSION

As discussed previously, the energy losses during the pendulum tests were much lower than those losses expected in a vehicle crash test. In an effort to gain some insight from the pendulum tests, it was estimated that the impact force during a vehicle collision would vary in direct proportion to the amount of vehicle front end crush, finally reaching the maximum force observed in the pendulum test. The slope of the unit force or acceleration versus crush distance graph is defined as the crushing coefficient. Edwards, et al[2] and Emori[3] have shown that the crushing coefficient of the front end of a vehicle varies from 9 g's/ft* to 12.5 g's/ft**. A crushing coefficient of 10 g's/ft, which is within the above range, was the assumption used in the following computations.† If the weight of an impacting vehicle is 4000 lb, then the crushing coefficient in kips/ft is:

$$10 \text{ g's/ft} \times 4000 \text{ lb} = 40{,}000 \text{ lb/ft} = 40 \text{ kips/ft}.$$

If the pipe fractured under the same maximum force in a vehicle test as it did in a pendulum test (approximately 80 kips), it would be necessary to crush the front end of a 4000 lb vehicle 2 ft:

$$\text{Crushing Distance} = \frac{80 \text{ kips}}{40 \text{ kips/ft}} = 2 \text{ ft}.$$

The total energy expended in crushing the vehicle front end under these assumptions would be the area under the force versus crushing distance curve which is shown in Figure 7. The area under this curve is:

$$E = \frac{F_m \times d}{2} = \frac{80 \text{ kips} \times 2 \text{ ft}}{2} = 80 \text{ kip-ft}.$$

*Based on impacts with rigid poles.
**Based on impacts with flat rigid walls.
†Another reference which was pointed out to the authors at the later date gave a crushing coefficient of 5 g's/ft determined by frontal collision with a 14.5 in. diameter pole. This reference is: McHenry, Ray, et al., Cornell Aeronautical Laboratory, Inc., PB 175 919, pp. 62-68.

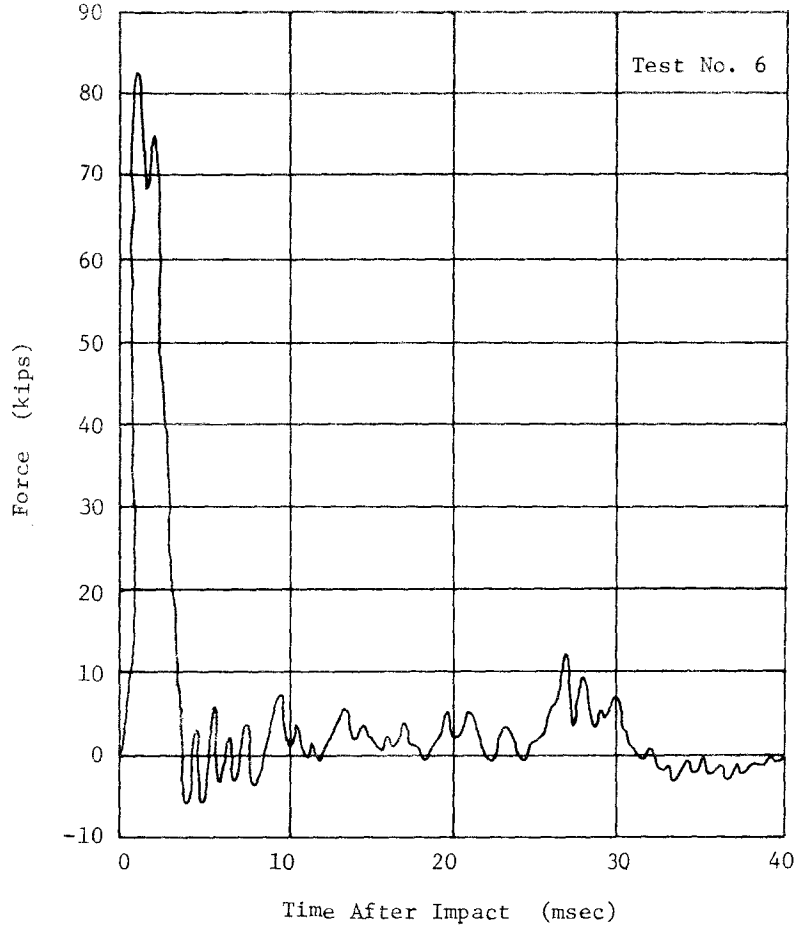

PENDULUM DATA FROM TEST #6
(After Michie and Bronstad[1])

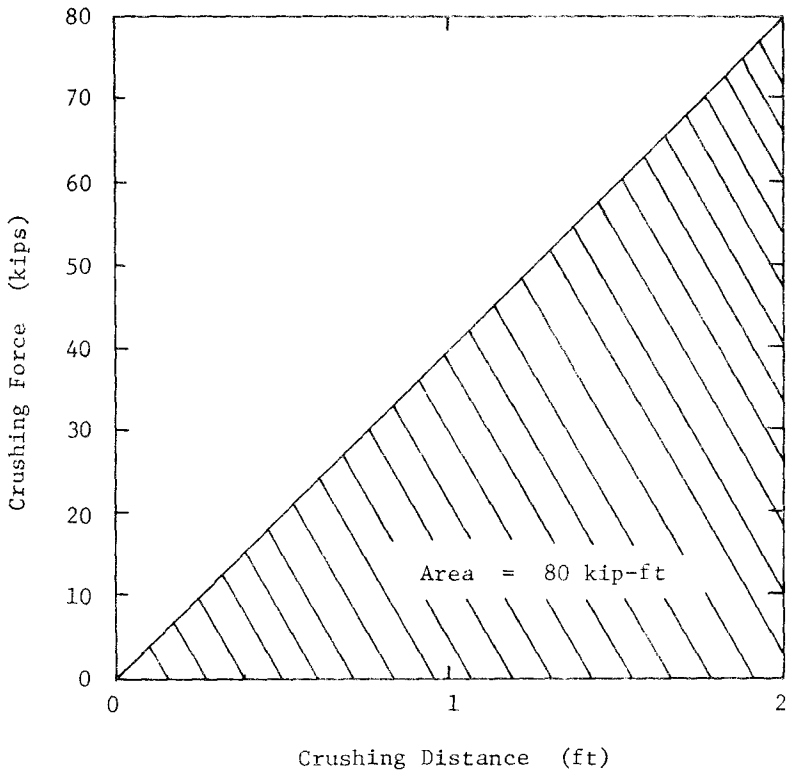

ESTIMATED ENERGY EXPENDED
IN CRUSHING OF VEHICLE FRONT

FIGURE 7

Therefore, during an impact with the first two pipes, it was estimated that the energy lost would be 160 kip-ft.

The following computations show that our original estimate of energy loss due to front end crush was somewhat high. Since the residual front end crush from Table 3 is 1.3 ft, the dynamic crush was estimated to be 1.5 ft. From the above, the maximum force due to each pipe in the first row is:

$$F_m = \text{slope} \times \text{crush distance} = 40 \text{ kips/ft} \times 1.5 \text{ ft} = 60 \text{ kips.}$$

The total vehicle crushing energy loss is:

$$E = \frac{F_m \times d}{2} = \frac{60 \text{ kips} \times 1.5 \text{ ft}}{2} = 45 \text{ kip-ft.}$$

Therefore, for two pipes, the vehicle is expected to absorb 90 kip-ft. The actual energy loss after 4.3 ft of vehicle travel was 155 kip-ft. This leaves 65 kip-ft of energy to be accounted for--in fragmentation and acceleration of pipes, deformation of the soil, abrasion of pipe fragments against the under side of the vehicle, ramping of the vehicle, and inaccuracy in estimating energy losses due to vehicle front end crush.

Another consideration which was felt to be of great significance in the design of a cushion is the fact that the crushing characteristic of the front end of the vehicle does not remain constant, but should increase after each row of pipe is encountered. As the crushing coefficient increases, the pulse duration for each row of pipe should decrease, resulting in a decrease in the energy lost during each new pipe impact. Since severe ramping occurred during impact with the first row of pipes, there was no

indication of the magnitude of the assumed change in the crushing characteristic of the vehicle front end or of the decrease in amount of energy lost during subsequent impacts.

CONCLUSION

Since the reinforced concrete pipe tested gave a maximum deceleration of approximately 20 g's, and an average deceleration of approximately 9 g's, it would be desirable to reduce these deceleration levels in any subsequent tests. A better selection of pipe might be the transite 20 in. O.D. pipe which was used in Test #2 in the report by Michie and Bronstad.[1] This should reduce the deceleration levels to approximately 5 g's average and 10 g's maximum. By reducing the force level developed by each row of pipe, the ramping tendency should also be reduced. Whether or not this ramping tendency can be reduced to a level which would make this type of cushion feasible is a matter of speculation.

It was shown that concrete pipe crash cushions have the capability of absorbing enough kinetic energy to stop a vehicle in a reasonable distance, and thus should be considered a definite possibility for development.

REFERENCES

1. Michie, J. D. and Bronstad, M. E., "Impact Tests Of Nonmetallic Pipe Sections," Report prepared for U.S. Department of Transportation, Federal Highway Administration on DOT Order No. 1-1-1360, April 1971.

2. Edwards, Thomas C., Martinez, J. E., McFarland, William F., and Ross, Hayes E., "Development of Design Criteria For Safer Luminaire Supports," NCHRP Report No. 77, Highway Research Board, 1969.

3. Emori, Richard I., "Analytical Approach to Automobile Collisions," SAE Paper 680016, Engineering Congress, Detroit, January 1968.

TECHNICAL MEMORANDUM 505-17

TEXAS TRANSPORTATION INSTITUTE
TEXAS A&M RESEARCH FOUNDATION

THE MODULAR CRASH CUSHION:

DESIGN DATA FROM

STATIC CRUSH TESTS OF STEEL DRUMS

AND OF CORRUGATED STEEL PIPES

A Tentative Progress Memo on Contract No. CPR-11-5851

U. S. Department of Transportation
Federal Highway Administration

by

M. C. White
Engineering Research Associate

The static crush tests on 20-gage drums and corrugated steel pipe were conducted under the Office of Research and Development, Structures and Applied Mechanics Division's Research Program on Structural Systems in Support of Highway Safety (4S Program); and the used paint drums were tested under Texas HP&R Research Study 2-8-68-146. The United States Steel Corporation furnished the 20-gage drums.

April 1971

INTRODUCTION

The Modular Crash Cushion, after extensive experimental crash testing[1,2,3,4] and as evidenced by field crash data,[4,5] has proven to be a practical, economical, and aesthetically pleasing crash cushion for protecting certain rigid roadside obstacles.

This report presents the calculated static crush energy and the calculated static average load values obtained from the static load versus crush distance test data for two types of modules, 55-gallon steel drums and corrugated steel pipes. The calculated static crush values can be used in the design and construction of modular crash cushions.

OBJECTIVES

The general objective of this study was to obtain crush data for several types of modules which could be used in the design and construction of the modular crash cushion. At present there are two design philosophies for modular crash cushions. One philosophy, called "monomodular",[6] results in a cushion which utilizes only one type of module and has a varying number of modules in succeeding rows to give an increasing crush strength during a head-on collision (Figure 1). The other philosophy, called "polymodular",[8] utilizes several types of modules to achieve the increasing crush strength in succeeding rows of modules while maintaining a constant cushion width (Figure 2).

The specific objective of the tests on used 55-gallon loose-head paint drums (ICC Spec. 17E and 17H) was to determine how they could be modified for use in a "monomodular" crash cushion design.[9] The desired values of static load and energy are listed below and were based on the crush characteristics of the 20-gage drum commonly used in "monomodular" designs:

1. a first peak load between 6000 and 9000 lbs.,
2. an average load of 5000 to 6000 lbs. for 18 inches of crush, and
3. a crush energy of 7500 to 9000 ft.lbs. for 18 inches of crush.

The two types of used paint drums tested were ICC Specification 17H and 17E (MODIFIED). The 17H drum is shown in Figure 5 and the 17E (MODIFIED), a 17E tight-head drum that has been converted to a loose-head drum, is shown in Figure 6.

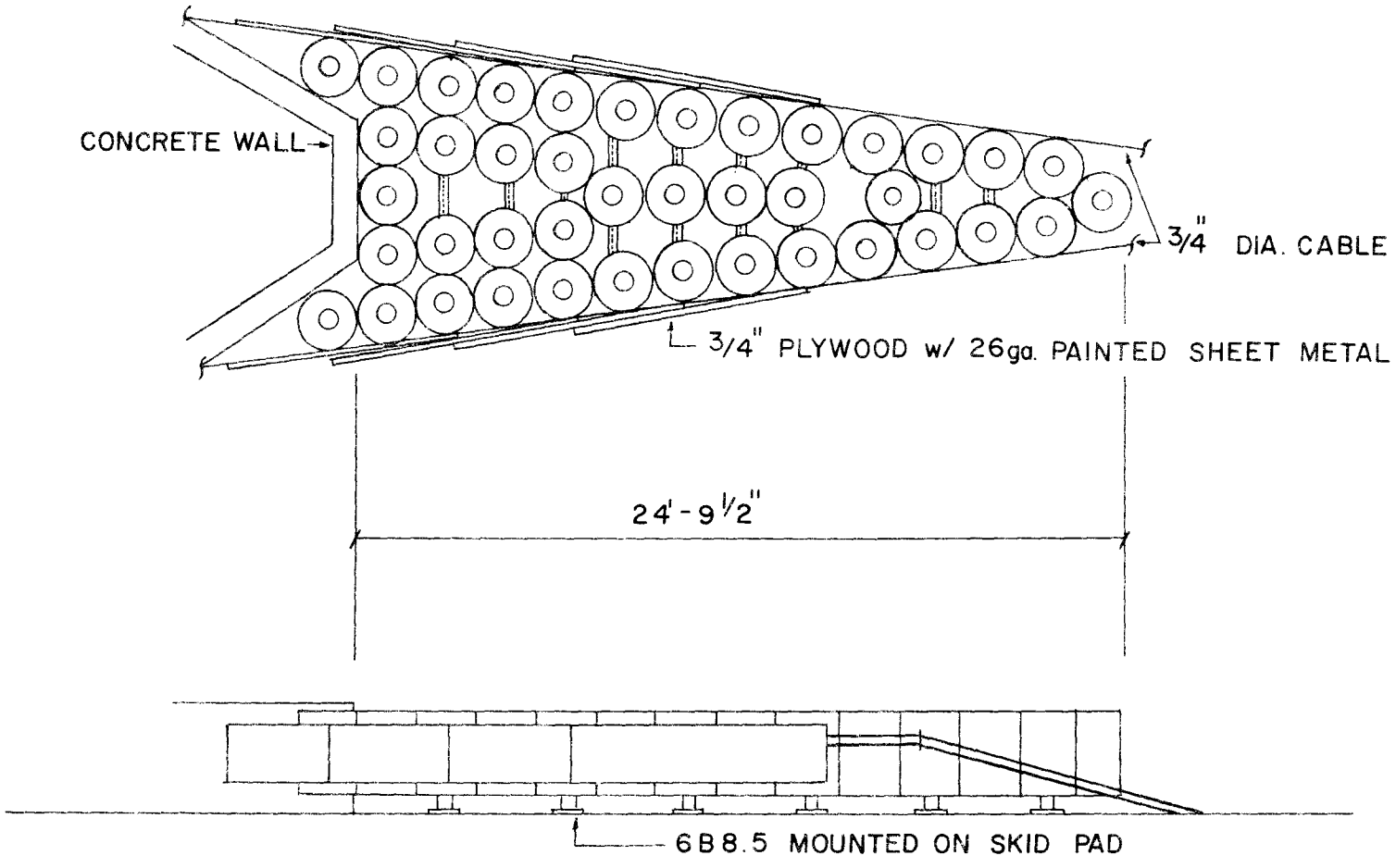

FIGURE I. PLAN AND ELEVATION OF MONOMODULAR CRASH CUSHION WITH PLYWOOD " FISH SCALES "

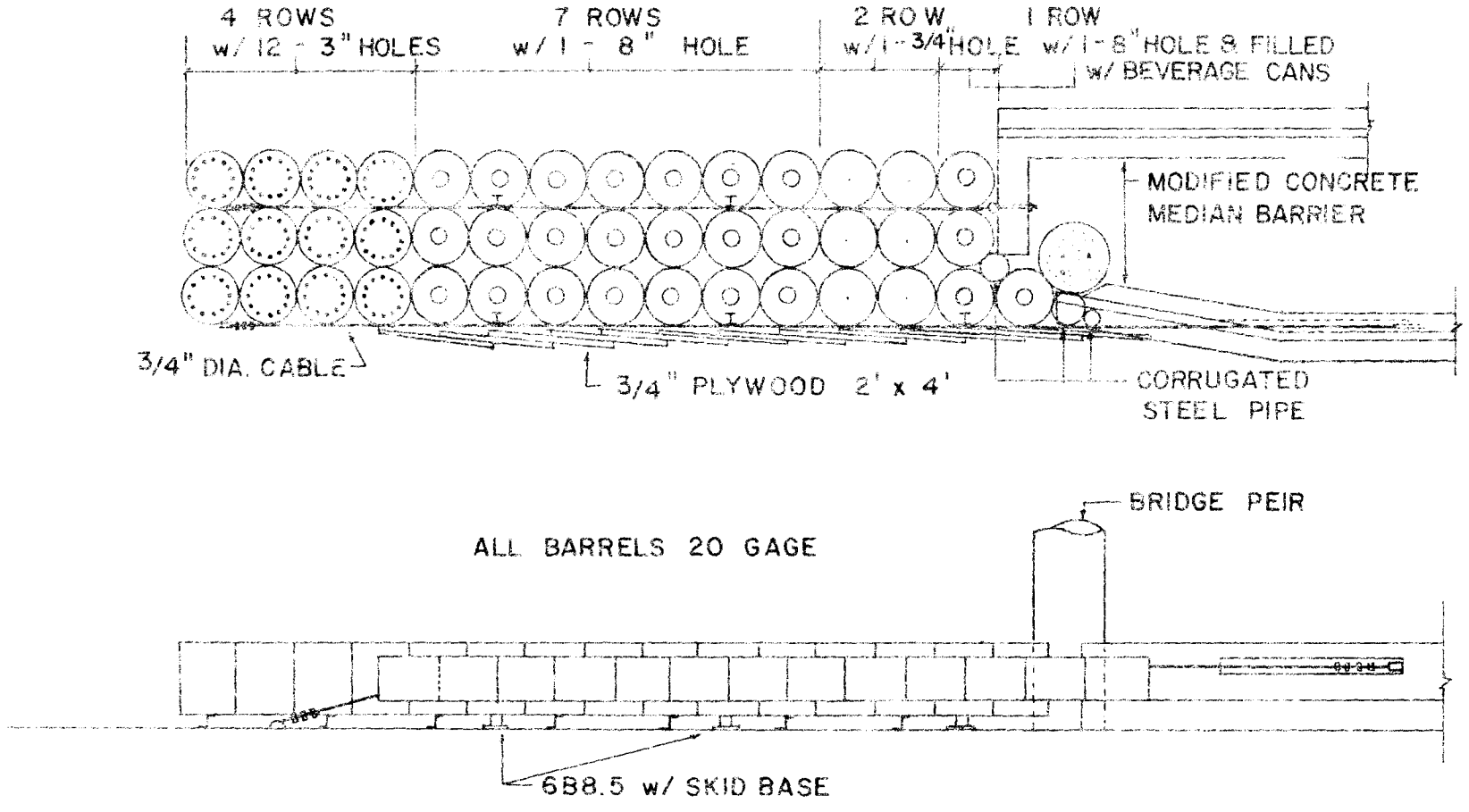

FIGURE 2 PLAN AND ELEVATION OF POLYMODULAR CRASH CUSHION[7]
WITH PLYWOOD " FISH SCALES "

The specific objective of the 20-gage drum tests was to obtain actual static load data for each inch of crush so that the average static load and static crush energy could be calculated and used for "polymodular" crash cushion design. The drums tested were all of 55-gallon capacity, made of 20-gage steel, and of tight-head design with various size cutouts in the head and bottom to give different crush strengths. The five cutout geometries that were tested included twelve 3 inch diameter holes, one 14 inch diameter hole, one 8-1/4 inch diameter hole, one 2-1/4 inch diameter hole, and one 3/4 inch diameter hole as shown in Figure A3 in the Appendix.

The specific objective of the tests on corrugated steel pipe was to obtain data needed for "polymodular" crash cushion designs. The various diameters and gage thicknesses of corrugated steel pipes that were tested are listed in Table 1. These specimens were of lock seam construction with radial corrugations. Specimens of helically wound corrugated pipe were tested but are not included in this report because they did not crush symmetrically (see Figure 3), and were thus deemed unfit for crash cushion use.

TABLE 1. CORRUGATED STEEL PIPE SPECIMENS TESTED

Wall Thickness (ga.)	Nominal Inside Diameter (in.)							
16	36	30	24	21	18	15	12	8
14	36	30	24	21	18	15	12	
12	36	30	24					

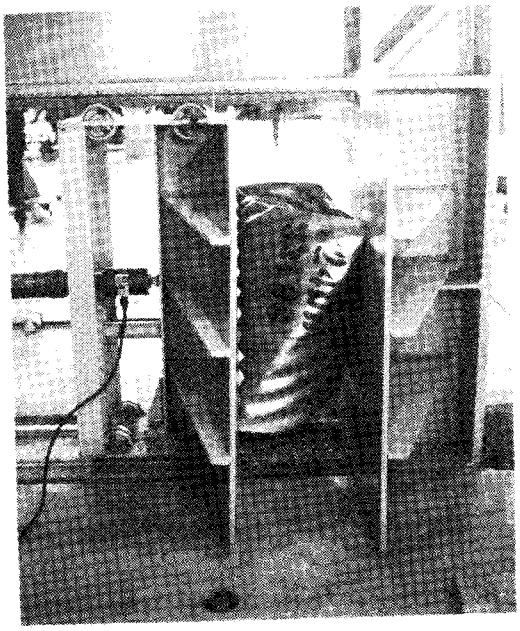

FIGURE 3. UNSYMMETRICAL CRUSHING OF HELICALLY WOUND CORRUGATED STEEL PIPE.

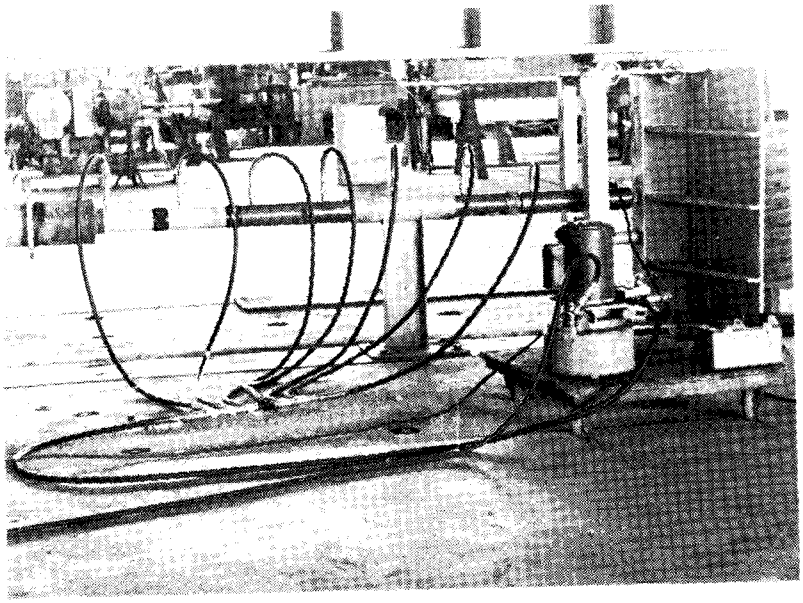

FIGURE 4. MODULE CRUSHER AND APPARATUS.

PROCEDURE

The module crusher is shown in Figure 4. Seven hydraulic cylinders of 40 kip capacity and with a total stroke of 35 inches provided the crush force. A 20 kip capacity transducer was mounted between the cylinders and the movable platen. A digital readout strain indicator was calibrated to read one microstrain per pound load from the load transducer to simplify the data acquisition and reduction. A steel tape secured to the load frame directly above the movable platen and a pointer attached to the movable platen indicated crush distance. Load readings were hand recorded at every inch of crush displacement. An electrically powered, variable flow rate pump provided pressure to the cylinders and was calibrated to advance the movable platen approximately 1/2 inch per minute.

The used paint drums were modified by cutting a 13.5 inch diameter hole in the head and bottom of each drum and welding the loose-heads to the rims with eight equally spaced 1 inch beads (every 9-3/8 inches or 45° spacing). The drums were then placed between the jaws of the crusher as shown in Figures 5 and 6. Figure 7 shows a partly crushed drum, Figure 8 shows a prior guidance setup for movable jaw which allowed cocking of jaw, and Figure 9 shows a drum after 20 inches of crush. Drums with smaller diameter holes were tested but are not included in this report because the crush loads were much too high.

The corrugated steel pipes were placed in the jaws of the crusher with the riveted seam at an approximate 45° angle from the diameter between the points of contact with the jaws. The crushed pipe in

Figure 10 indicates the location of the seam with respect to the plastic hinges that form during the crushing procedure.

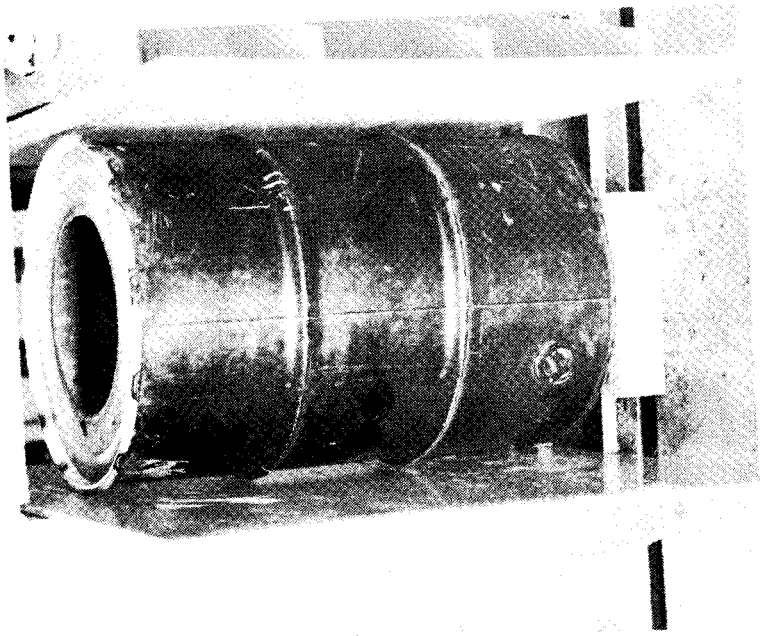

FIGURE 6. ICC SPEC. 17E (MOD.) DRUM WITH 13 1/2" DIA. HOLES.

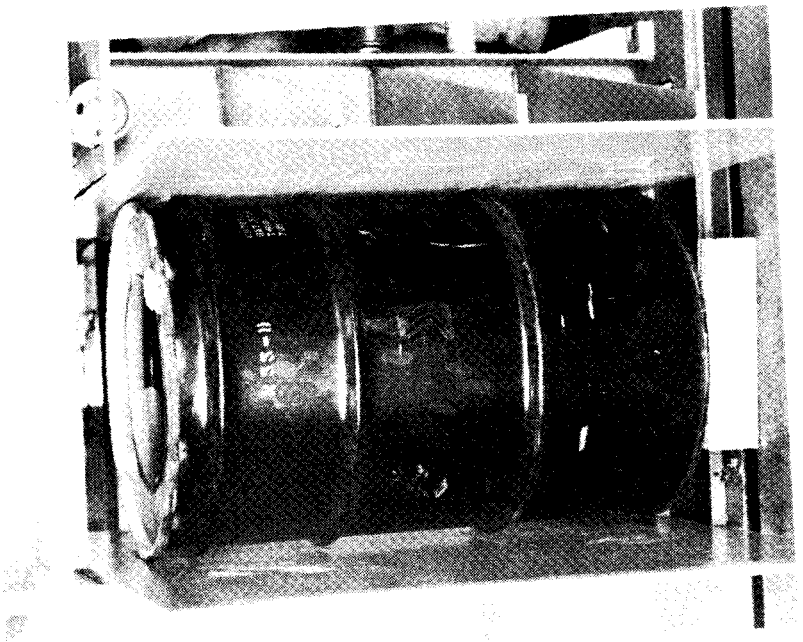

FIGURE 5. ICC SPEC. 17H DRUM WITH 13 1/2" DIA. HOLES.

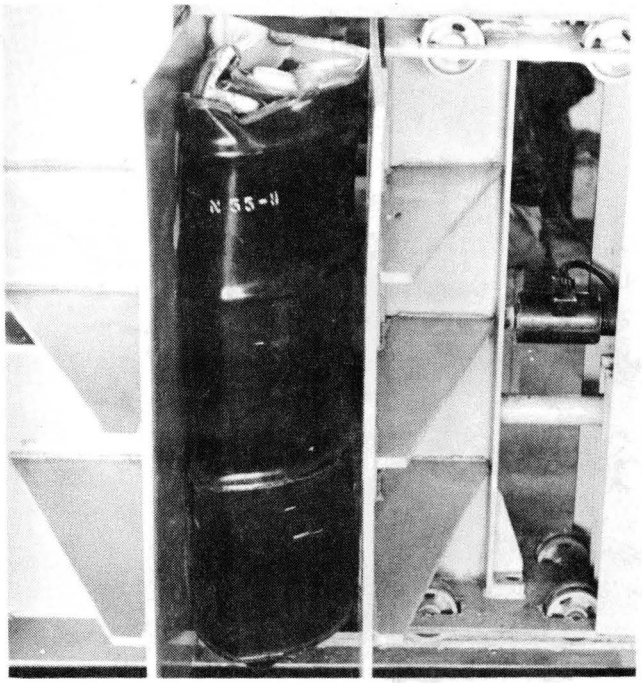

FIGURE 7. PARTIALLY CRUSHED DRUM SHOWING TYPICAL MODE OF FAILURE. NOTE VEE-TRACK WHEELS.

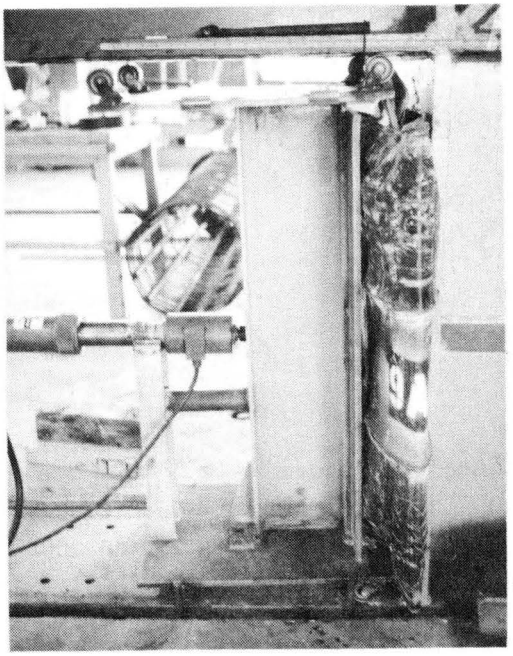

FIGURE 8. PRIOR SETUP AS USED ON TEST OF TWELVE 3" DIAMETER HOLE DRUMS. SEE TABLE A8 IN APPENDIX. NOTE COCKING OF MOVABLE JAW.

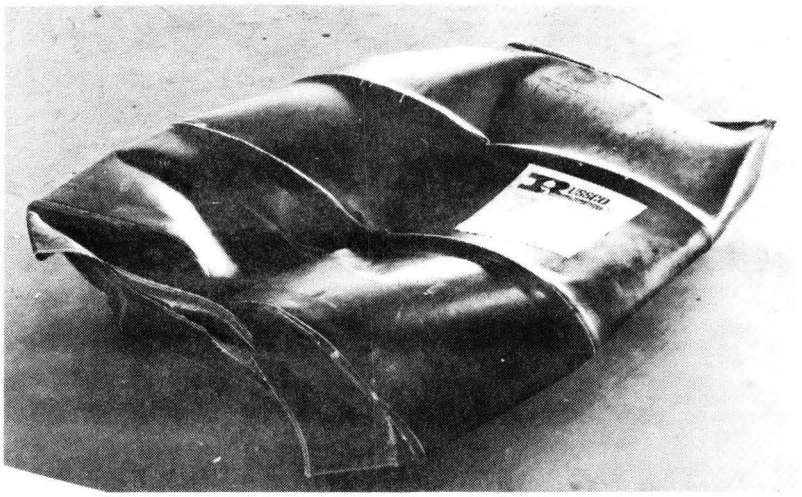

FIGURE 9. DRUM AFTER 20 INCHES OF CRUSH.

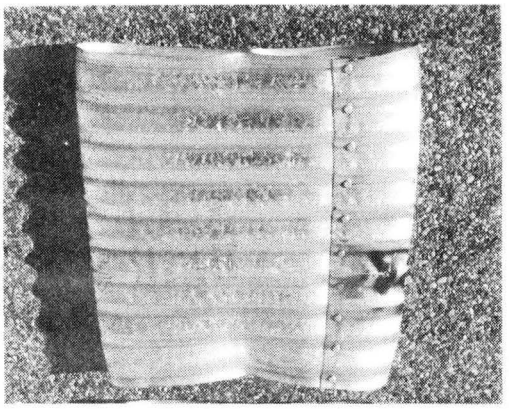

FIGURE 10. FULLY CRUSHED CORRUGATED STEEL PIPE SHOWING LOCATION OF SEAM WITH RESPECT TO PLASTIC HINGES.

RESULTS

A summary of the used paint drum test results and corresponding values of the standard "monomodular" drum (20-gage steel with 8-1/4 inch holes) is shown in Table 2. The test results are well within the ranges desired. The test data are listed in Table A1 and plotted in Figure A1, both in the Appendix.[9]

The 20-gage drum crush tests are summarized in Table 3. The data are listed in Tables A2 through A7 and plotted in Figure A2, both in the Appendix. Any of these drums can be used when the cushion design is based on the "polymodular" philosophy, the 7 inch and the 3-1/4 inch drums being usable in either the "monomodular" or "polymodular" design.

Table A8 in the Appendix presents data for the twelve 3 inch diameter holes in drum top and bottom that were obtained with a less accurate setup than is presently used. Comparing Figures 7 and 8 indicates the old system (Figure 8) allowed cocking of the movable jaw and thus did not give as accurate results as the new system (Figure 7) which provides positive guidance of the movable jaw.

Table 4 presents a summary of crush test results for corrugated steel pipes which can be used for "polymodular" crash cushion design. Tables A8, A9, and A10 list the test data; and Figures A4, A5, and A6 present plots of the data, both in the Appendix.

TABLE 2. SUMMARY OF PAINT DRUM TEST RESULTS[9]

	17H*	17E (MOD)*	STANDARD 20 GAGE** CRASH CUSHION DRUM
First Peak Load	7870 lbs.	6860 lbs.	7510 lbs.
Crush Energy @ 18 inches	8531 ft.lbs.	8267 ft.lbs.	8686 ft.lbs.
Average Load for 18 inches	5687 lbs.	5511 lbs.	5791 lbs.

*With 13.5 in. diam. holes.
**With 8.25 in. diam. holes.

TABLE 3. SUMMARY OF 20 GAGE DRUM TEST RESULTS

Hole Configuration	Crush Energy @ 18 inches (ft.lbs.)	Average Load @ 18 inches (lbs.)
Twelve 3" Dia.	3,007	2,005
One 14" Dia.	4,718	3,145
One 7" Dia.	8,686	5,791
One 8-1/4" Dia.	8,573	5,414
One 2-1/4" Dia.	10,362	6,908
One 3/4" Dia.	11,857	7,905

TABLE 4. SUMMARY OF CRUSH TEST RESULTS FOR CORRUGATED STEEL PIPES 25.5 IN. LONG

Dia. (in.)	Gage	Weight (lbs.)	Crush Distance (in.)	Crush Energy (ft-lbs.)	Avg. Force (lbs.)
8	16	16	6	4,287	8,574
12	16	20	9	5,251	7,001
15	16	25	12	5,779	5,779
18	16	29	15	5,986	4,789
21	16	34	18	6,192	4,128
24	16	40	21	6,021	3,441
30	16	49	27	6,152	2,734
36	16	58	33	7,038	2,559
12	14	24	9	7,848	10,464
15	14	30	12	7,205	7,205
18	14	35	15	8,402	6,722
21	14	41	18	8,262	5,508
24	14	48	21	7,473	4,270
30	14	60	27	8,837	3,928
36	14	72	33	9,884	3,594
24	12	65	21	11,985	6,850
30	12	82	27	12,675	5,633
36	12	99	33	14,077	5,119

CONCLUSIONS AND RECOMMENDATIONS

The used paint drums should perform adequately when used in a "monomodular" crash cushion if a 13.5 inch diameter hole is cut in the head and bottom and the loose head is attached with eight 1 inch welds equally spaced around the rim. It is recommended that the entire cushion be made of all 17H, all 17E (MODIFIED), or all standard 20-gage tight-head drums because of diametral and longitudinal dimension variations between the three types of drums (Figure A2). Also, the bolted connector that spans the rims of adjacent standard tight-head drums will not fit the top rims of either the 17H or 17E (MODIFIED). The bolted connector that joins the bodies of adjacent drums, though, will fit any of the three drums mentioned previously.[9]

The 20-gage drums listed in Table 3 show nominal average load values of 2000, 3000, 5500 (includes 7 inch and 8-1/4 inch diameters) and 8000 lbs. for 18 inches of crush. These drums provide an adequate variety of average loads and crush energies so that the entire 2000 lb. to 4500 lb. range of passenger vehicle weights will encounter a survivable deceleration environment upon impacting a properly design polymodular crash cushion. When designing a polymodular crash cushion it is recommended that the cushion be designed first for a 2000 lb. vehicle; then add rows for a 2750 lb. vehicle, for a 3500 lb. vehicle; and finally for a 4500 lb. vehicle.[8] It is also recommended that the drum with the 8-1/4 inch diameter hole be used in lieu of the drum with the 7 inch diameter hole, whether for a monomodular or polymodular design, because the larger diameter hole allows installation of the

6B8.5 skid post from the top side of the cushion (see Figures 1 and 2) and the load and crush energy are very close to being the same. This also decreases the cost of stocking two different drums of the same capacity.

It should be noted that the average load is not a linear function of hole diameter (mainly due to mode of failure differences), thus it is recommended that only the diameters suggested herein be used. Also, the use of the data in Table A2 is recommended instead of that in Table A8 due to better accuracy.

A "polymodular" crash cushion utilizing only corrugated steel pipes instead of drums has been designed and is presently undergoing experimental crash testing. Corrugated steel pipes have been successfully used as energy dissipators at the rear of the polymodular cushion shown in Figure 2. Also, the corrugated steel pipe data have been used in a preliminary design for an impact attenuating bridge rail.[10]

Thus, the corrugated steel pipe has a proven use as a supplemental energy dissipator in polymodular crash cushions using drums as the primary energy dissipator and shows promise as the primary energy dissipator in a modular crash cushion and in an impact attenuating bridge rail.

REFERENCES

1. Hirsch, T. J., "Barrel Protective Barrier," Technical Memorandum 505-1, Texas Transportation Institute, Texas A&M University, College Station, Texas, July 1968.

2. Hirsch, T. J., Hayes, Gordon, and Ivey, D. L., "The Modular Crash Cushion," Technical Memorandum 505-1S, Texas Transportation Institute, Texas A&M University, College Station, Texas, August 1970.

3. Hirsch, T. J. and Ivey, Don L., "Vehicle Impact Attenuation by Modular Crash Cushion," Research Report No. 146-1, Texas Transportation Institute, Texas A&M University, College Station, Texas, June 1969.

4. Hirsch, T. J., Ivey, D. L., and White, Monroe C., "The Modular Crash Cushion - Research Findings and Field Experience," Special Report 107, Highway Research Board, Washington, D. C., 1970.

5. White, Monroe C., Ivey, Don L., and Hirsch, T. J., "In-Service Experience on Installations of Texas Modular Crash Cushions," Research Report No. 146-2, Texas Transportation Institute, Texas A&M University, College Station, Texas, August 1970.

6. White, Monroe C., Marquis, Eugene L., and Hirsch, T. J., "The Modular Crash Cushion: Design, Fabrication, Installation," a report for the United States Steel Corporation, Texas Transportation Institute, Texas A&M University, College Station, Texas, September 1970, pp. 4-8.

7. Hayes, G. G., Ivey, D. L., Hirsch, T. J., and Viner, J. G., "A Hybrid System to Reduce the Hazard of Bridge Piers in Roadway Medians (Modular Crash Cushion Plus Concrete Median Barrier)," Technical Memorandum 505-15, Texas Transportation Institute, Texas A&M University, College Station, Texas, May 1971.

8. White, Monroe C., "The Modular Crash Cushion," a Master of Science thesis, Texas A&M University, College Station, Texas, to be published August 1971.

9. White, Monroe C., "Crush Tests on Used Paint Drums," A Supplementary Technical Memorandum on Study 2-8-68-146, Texas Transportation Institute, Texas A&M University, College Station, Texas, November 1970.

10. Post, E. R., Olson, R. M., Gunderson, R. H., Cetiner, Ayhan, and Ivey, D. L., "Bridge Rail Service Requirements as a Basis for Design Criteria," Final Report for Highway Research Board, National Cooperative Highway Research Program, National Academy of Sciences, Texas A&M Research Foundation, Texas Transportation Institute, College Station, Texas (unpublished).

APPENDIX

TABLE A1. CRUSH TESTS OF 55 GAL. STEEL LOOSE HEAD DRUMS.
LOOSE HEADS WELDED 1" EVERY 9 3/8" (OR 45°)
13 1/2" DIA. HOLES CUT IN HEAD & BOTTOM TYPES
TESTED: ICC SPEC. 17H & 17E (MOD.)

Crush Distance (inches)	Load (lbs)	
	17E	17H
0	0	0
1	6860	7680
2	6860	7870
3	6710	7300
4	6640	7680
5	5160	4900
6	5540	4260
7	6010	4250
8	5050	4480
9	4360	5160
10	3710	4990
11	3580	5370
12	4240	6270
13	4850	4040
14	6600	4230
15	6530	5020
16	5760	5770
17	6230	8110
18	9030	10,000
19	13,230	12,180
20	17,580	17,010

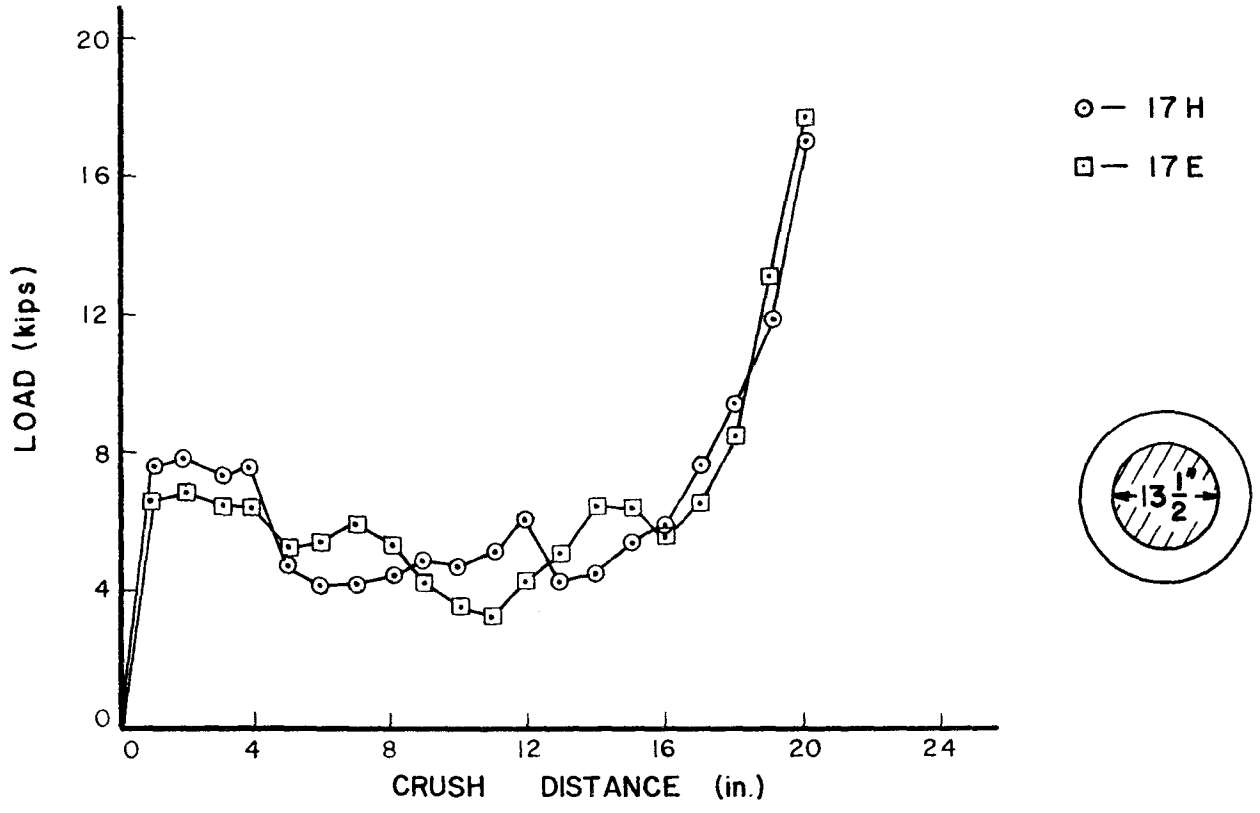

FIGURE A1 LOAD vs. CRUSH DISTANCE FOR USED PAINT DRUMS, I.C.C. SPEC. 17H AND 17E (modified) DRUMS WITH 1- $13\frac{1}{2}$" HOLE

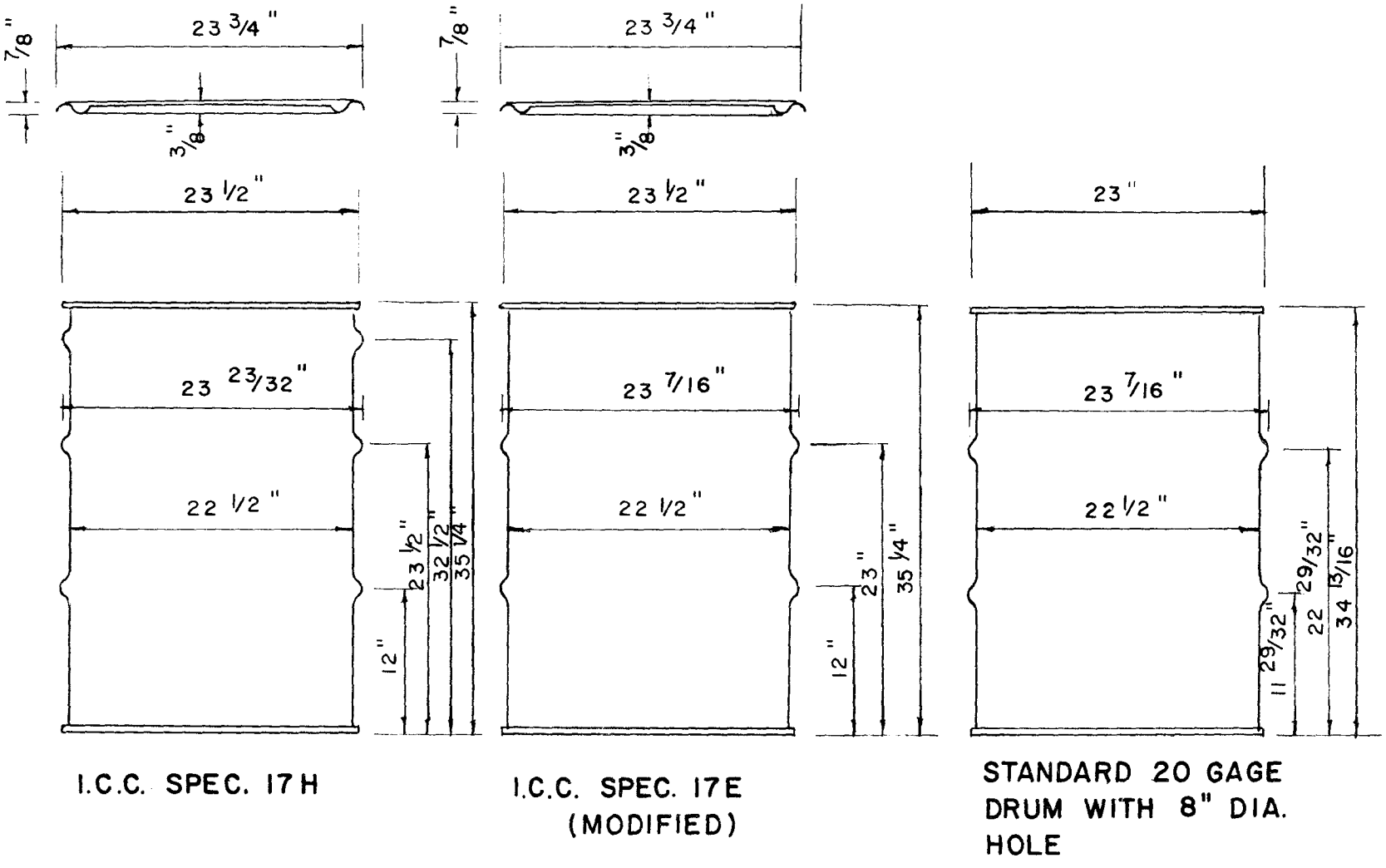

FIGURE A2. DIAMETRAL AND LONGITUDINAL DIMENSIONS OF STANDARD AND USED PAINT DRUMS.

TABLE A2. DRUM CRUSH TESTS
GUAGE - 20; WEIGHT - 32 LBS.
TWELVE 3" HOLES

CRUSH DISTANCE (inches)	ACTUAL LOAD	ENERGY (ft-lbs)	AVERAGE LOAD
0			
1	3,965	165	1,983
2	1,795	203	2,432
3	1,930	560	2,242
4	1,805	716	2,148
5	1,765	865	2,076
6	1,625	1,006	2,012
7	1,585	1,140	1,954
8	1,465	1,267	1,900
9	1,440	1,391	1,855
10	1,435	1,514	1,817
11	1,210	1,625	1,772
12	1,300	1,729	1,729
13	1,290	1,837	1,696
14	1,335	1,947	1,668
15	1,600	2,069	1,655
16	2,900	2,260	1,695
17	4,565	2,575	1,818
18	5,810	3,007	2,005
19	6,920	3,538	2,234
20	8,855	4,195	2,517
21	14,915	5,185	2,963

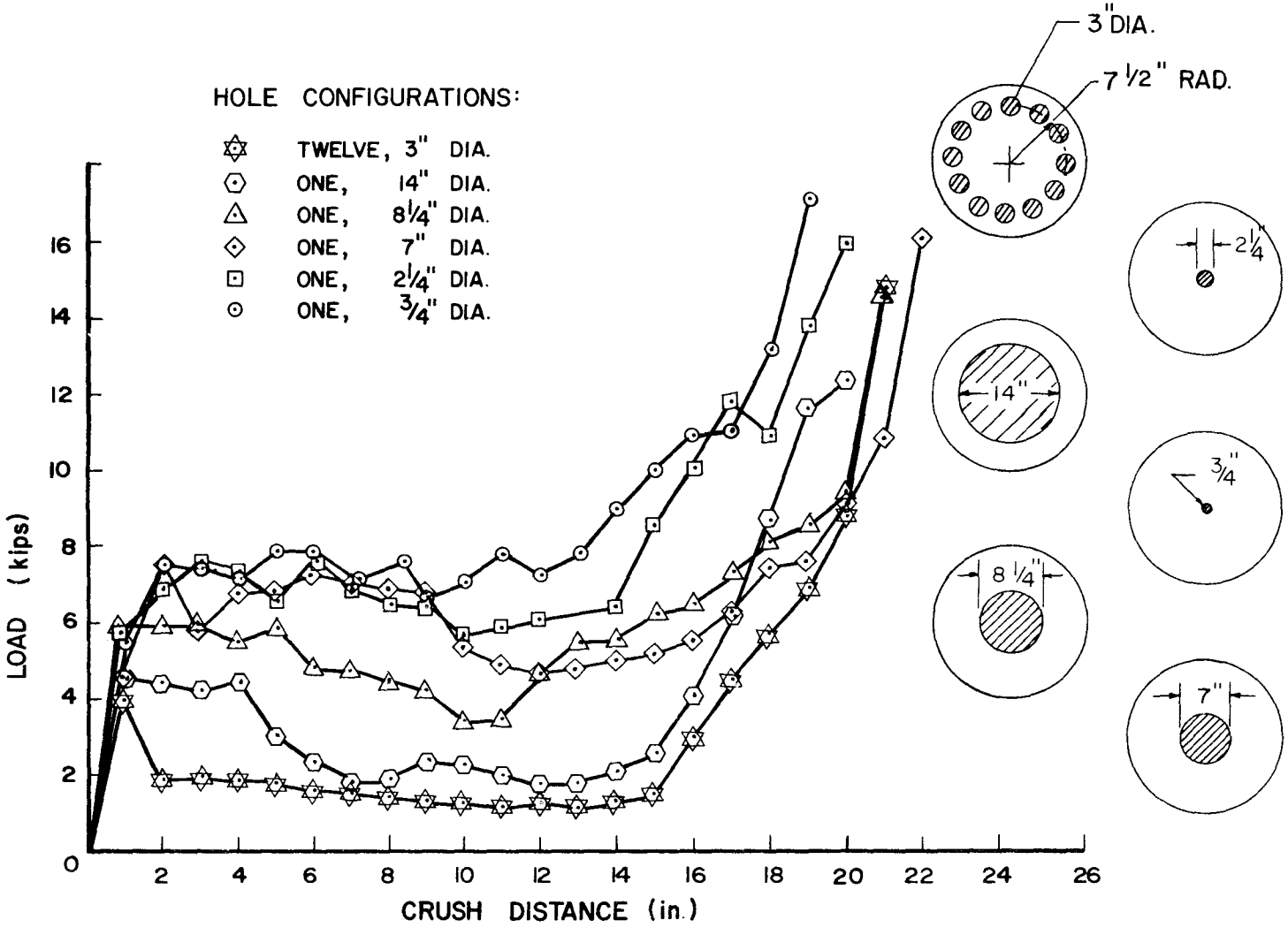

FIGURE A3 LOAD vs CRUSH DISTANCE FOR 20 ga. DRUMS WITH VARIOUS HOLE CONFIGURATIONS

TABLE A 3. DRUM CRUSH TESTS
GAGE - 20; WEIGHT - 32 LBS.
DIA. 14"

CRUSH DISTANCE (inches)	ACTUAL LOAD	ENERGY (ft-lbs)	AVERAGE LOAD
0			
1	4,485	187	2,243
2	4,345	555	3,329
3	4,240	913	3,650
4	4,435	1,274	3,822
5	3,035	1,585	3,805
6	2,455	1,814	3,628
7	1,775	1,990	3,412
8	1,910	2,144	3,216
9	2,445	2,325	3,100
10	2,295	2,525	3,027
11	2,095	2,706	2,952
12	1,650	2,862	2,862
13	1,765	3,004	2,773
14	2,200	3,169	2,717
15	2,680	3,373	2,698
16	4,170	3,658	2,744
17	6,295	4,094	2,890
18	8,680	4,718	3,145
19	11,615	5,564	3,514
20	12,420	6,565	3,939

TABLE A4. DRUM CRUSH TESTS
GAGE - 20; WEIGHT - 33.3 LBS.
ONE 7" HOLE

CRUSH DISTANCE (inches)	ACTUAL LOAD	ENERGY (ft-lbs)	AVERAGE LOAD
0			
1	4,240	177	2,120
2	7,510	666	3,498
3	5,845	1,223	4,891
4	6,645	1,743	5,230
5	6,785	2,303	5,527
6	7,320	2,891	5,781
7	7,010	3,488	5,979
8	6,895	4,067	6,101
9	6,795	4,638	6,184
10	5,370	5,145	6,174
11	4,950	5,575	6,081
12	4,635	5,974	5,974
13	4,660	6,361	5,872
14	5,000	6,764	5,798
15	5,135	7,186	5,749
16	5,520	7,630	5,726
17	6,160	8,117	5,730
18	7,495	8,686	5,791
19	7,680	9,318	5,885
20	9,040	10,015	6,009
21	10,945	10,848	6,199
22	16,020	11,971	6,530

TABLE A5. DRUM CRUSH TESTS
GAGE - 20; WEIGHT - 33.3 LBS.
ONE 8 1/4" HOLE

CRUSH DISTANCE (inches)	ACTUAL LOAD	ENERGY (ft-lbs)	AVERAGE LOAD
0			
1	5,895	246	2,948
2	5,990	741	4,445
3	5,850	1,234	4,935
4	5,530	1,708	5,125
5	5,885	2,184	5,242
6	4,845	2,631	5,262
7	4,800	3,033	5,199
8	4,565	3,423	5,135
9	4,360	3,795	5,060
10	3,515	4,123	4,948
11	3,595	4,419	4,821
12	4,725	4,766	4,766
13	5,525	5,193	4,794
14	5,635	5,658	4,850
15	6,235	6,153	4,922
16	6,385	6,701	5,009
17	7,225	7,246	5,115
18	8,045	7,882	5,255
19	8,530	8,573	5,414
20	9,540	9,326	5,595
21	14,465	10,326	5,900

TABLE A6. DRUM CRUSH TESTS
GAGE - 20; WEIGHT - 33.5 LBS.
ONE 2 1/4" HOLE

CRUSH DISTANCE (inches)	ACTUAL LOAD	ENERGY (ft-lbs)	AVERAGE LOAD
0			
1	5,585	233	2,793
2	7,600	782	4,693
3	7,545	1,413	5,653
4	7,315	2,032	6,097
5	6,560	2,610	6,265
6	7,820	3,210	6,419
7	6,765	3,817	6,544
8	6,465	4,369	6,553
9	6,555	4,911	6,548
10	5,765	5,224	6,510
11	5,905	5,911	6,448
12	6,295	6,419	6,419
13	5,990	6,931	6,398
14	6,445	7,449	6,385
15	8,565	7,806	6,245
16	10,055	8,582	6,436
17	11,895	9,420	6,649
18	10,720	10,362	6,908
19	13,880	11,387	7,192
20	15,965	12,630	7,578
21	25,325	14,351	8,200

TABLE A 7. DRUM CRUSH TESTS
GAGE - 20; WEIGHT - 33.6 LBS.
ONE 3/4" HOLE

CRUSH DISTANCE (inches)	ACTUAL LOAD	ENERGY (ft-lbs)	AVERAGE LOAD
0			
1	5,820	243	2,910
2	6,710	765	4,588
3	7,590	1,360	5,442
4	7,175	1,976	5,927
5	7,910	2,604	6,250
6	7,900	3,263	6,526
7	7,165	3,891	6,670
8	7,640	4,508	6,761
9	6,585	5,100	6,800
10	6,980	5,665	6,799
11	7,915	6,286	6,858
12	7,390	6,924	6,924
13	7,875	7,560	6,978
14	9,030	8,264	7,084
15	9,930	9,054	7,243
16	10,865	9,921	7,441
17	11,185	10,892	7,688
18	13,245	11,857	7,905
19	17,095	13,122	8,287
20	21,600	14,734	8,840

TABLE A8. DRUM CRUSH TESTS
GAGE - 20" WEIGHT - 32 LBS.
TWELVE 3" HOLES

NOTE: This test was performed with test apparatus shown in Figure 8.

CRUSH DISTANCE (inches)	ACTUAL LOAD	ENERGY in lbs.	ENERGY ft-lbs.	AVERAGE LOAD
0				
1	2,425	1,213	101	1,213
2	2,715	3,783	315	1,891
3	2,505	6,393	532	2,131
4	2,595	8,943	745	2,236
5	2,245	11,613	968	2,323
6	2,740	14,355	1,196	2,393
7	2,675	17,063	1,422	2,438
8	2,195	18,583	1,549	2,323
9	2,400	19,966	1,664	2,218
10	2,780	22,556	1,880	2,256
11	2,735	25,314	2,109	2,301
12	2,530	27,946	2,323	2,323
13	2,170	30,296	2,525	2,331
14	2,425	32,594	2,716	2,328
15	2,075	34,844	2,904	2,323
16	2,165	36,964	3,080	2,310
17	2,325	39,209	3,267	2,306
18	2,765	41,754	3,479	2,320
19	3,555	44,914	3,743	2,364
20	4,360	48,871	4,073	2,444
21	6,055	54,079	4,507	2,575
22	13,420	63,816	5,318	2,901

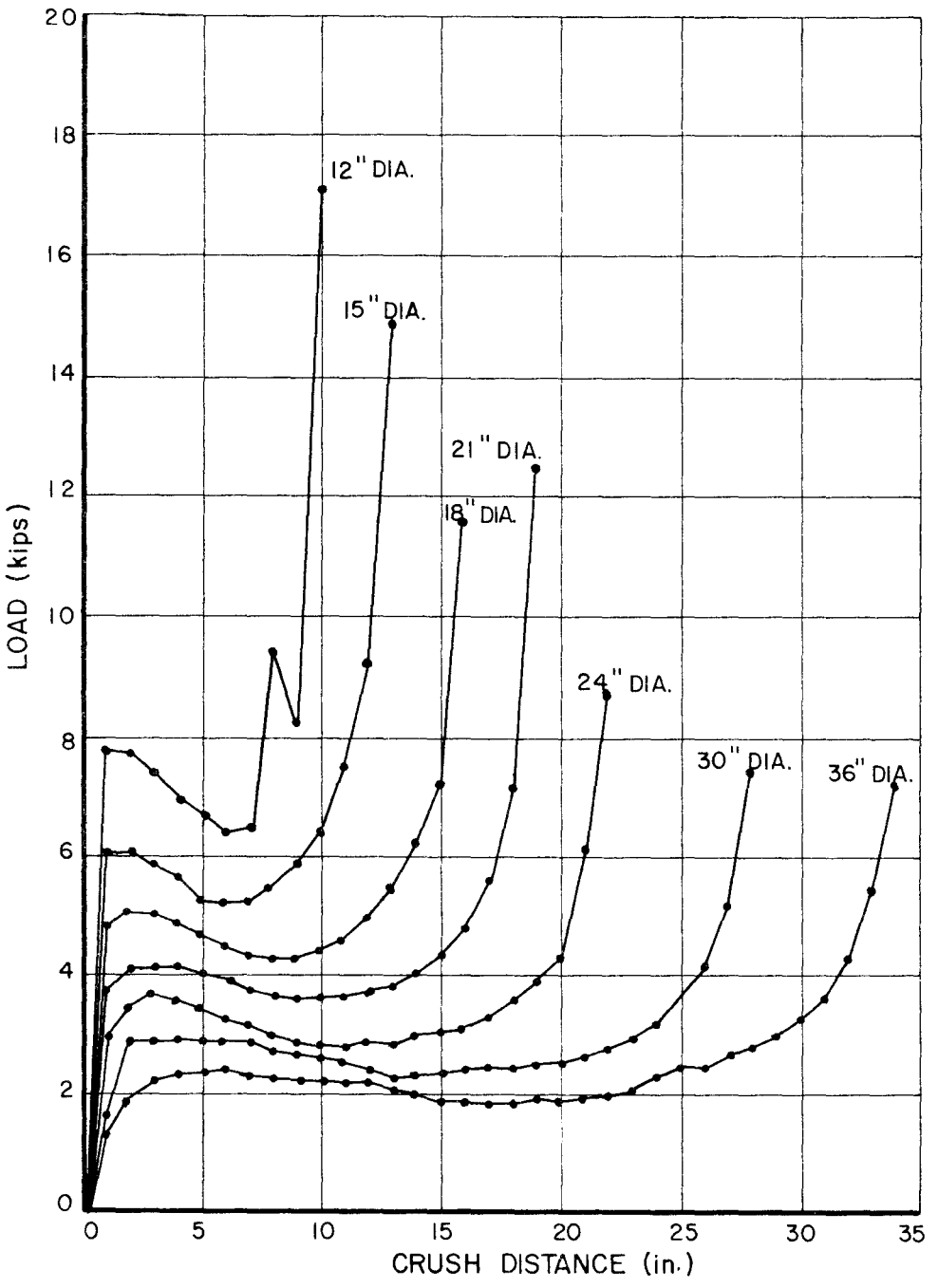

FIGURE A4 LOAD vs. CRUSH DISTANCE 16 ga. CORRUGATED STEEL PIPE OF VARIOUS DIAMETERS & 25.5" lg.

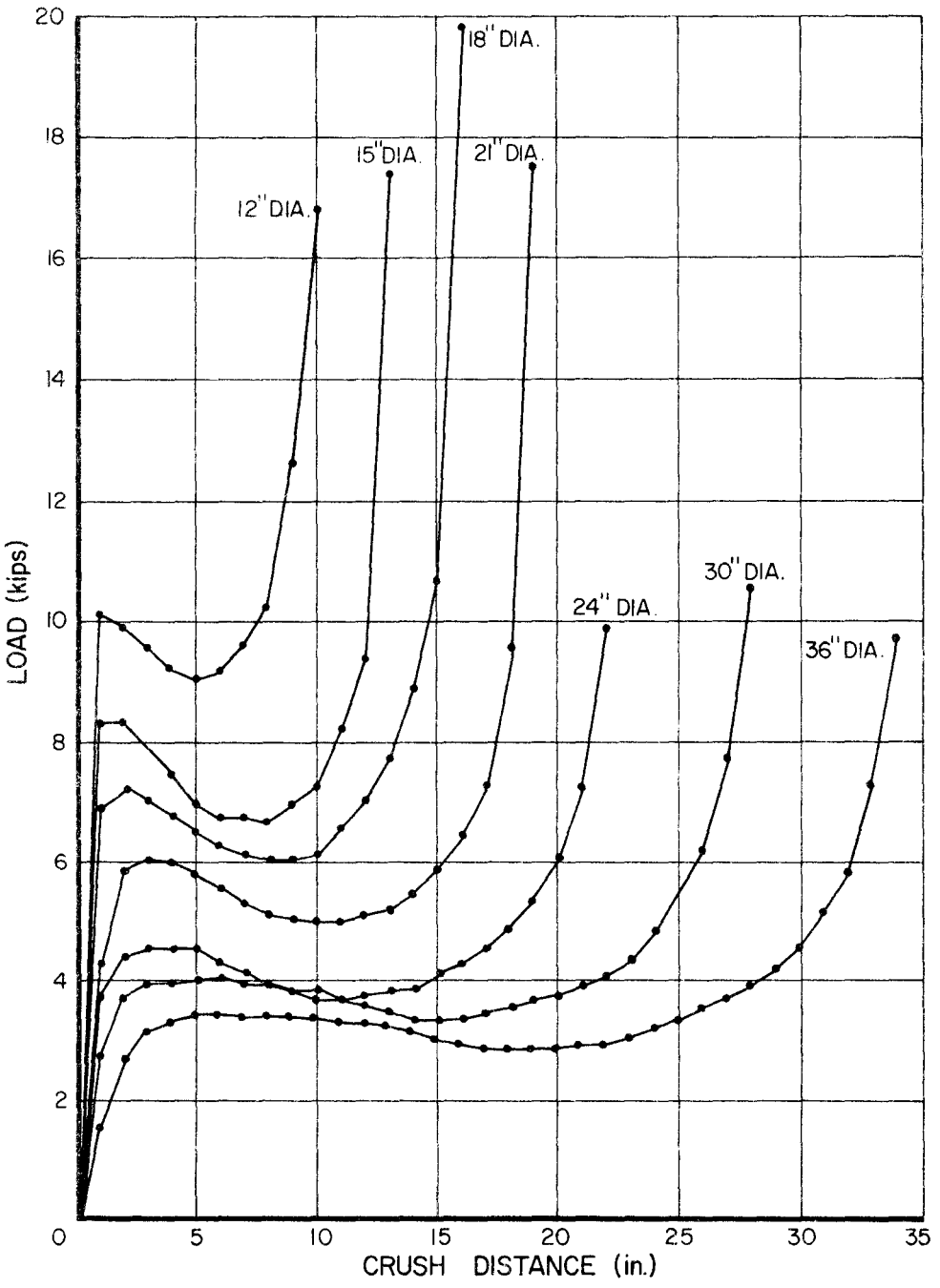

FIGURE A5 LOAD vs. CRUSH DISTANCE FOR 14 ga. CORRUGATED STEEL PIPE OF VARIOUS DIAMETERS & 25.5" lg.

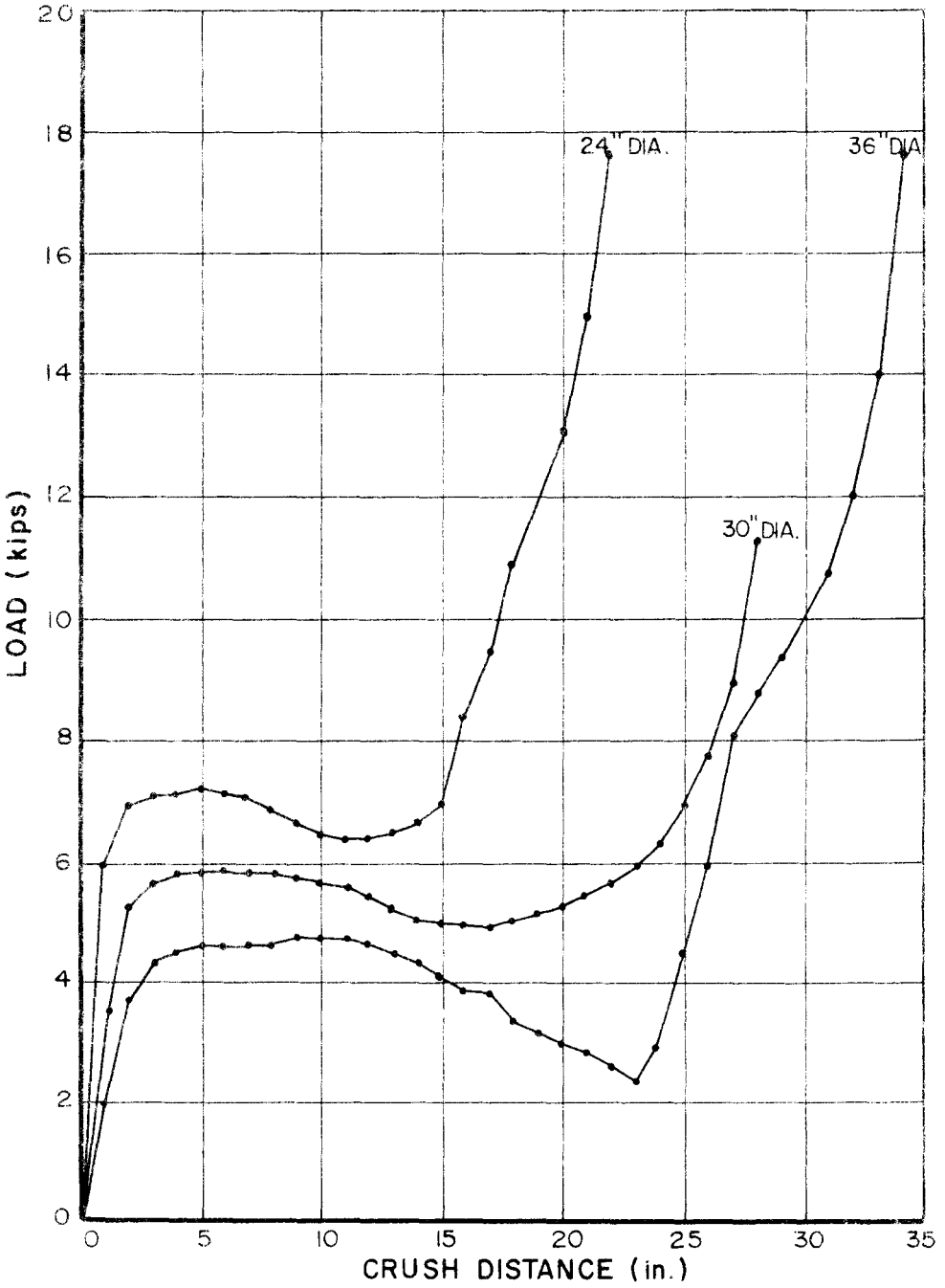

FIGURE A6 LOAD vs. CRUSH DISTANCE FOR 12ga. CORRUGATED STEEL PIPE OF VARIOUS DIAMETERS & 25.5[ksi] lg.

TABLE A9. DATA SHEET FOR CRUSH TESTS OF 16 GAGE CORRUGATED STEEL PIPES

Crush Distance (in.)	Load (lbs)						
	12"ϕ	15"ϕ	18"ϕ	21"ϕ	24"ϕ	30"ϕ	36"ϕ
1	7810	6108	4850	3898	2960	1660	1310
2	7700	6108	5130	4248	3566	2550	1920
3	7380	5954	5058	4248	3665	2800	2240
4	6970	5630	4908	4224	3603	2880	2340
5	6700	5322	4702	4132	3500	2900	2390
6	6380	5262	4520	4000	3298	2880	2400
7	6520	5280	4382	3845	3170	2860	2370
8	9450	5445	4351	3761	3020	2810	2350
9	8200	5893	4354	3690	2922	2720	2310
10	17,160	6432	4452	3722	2861	2620	2280
11		7560	4665	3765	2864	2490	2250
12		9218	5015	3826	2928	2410	2220
13		14,919	5522	3968	2950	2350	2160
14			6308	4186	3023	2360	2040
15			7242	4538	3061	2400	1930
16			11,655	4950	3155	2460	1870
17				5686	3392	2500	1880
18				7264	3608	2540	1870
19				12,618	3930	2600	1910
20					4363	2670	1950
21					6138	2780	1980
22					8720	2900	2050
23						3040	2120
24						3270	2260
25						3550	2380
26						4170	2500
27						5310	2620
28						7430	2830
29							3000
30							3260
31							3610
32							4310
33							5310
34							7210

TABLE A10.DATA SHEET FOR CRUSH TESTS OF
14 GAGE CORRUGATED STEEL PIPES

Crush Distance (in.)	Load (lbs)						
	12"ϕ	15"ϕ	18"ϕ	21"ϕ	24"ϕ	30"ϕ	36"ϕ
1	10,130	8280	6914	4254	3736	2780	1560
2	9910	8370	7234	5870	4407	3770	2640
3	9570	8001	7084	6042	4515	3930	3170
4	9210	7483	6838	5996	4488	3970	3340
5	9060	6990	6554	5837	4467	3990	3400
6	9180	6757	6290	5559	4330	4000	3410
7	9630	6762	6133	5300	4168	3980	3400
8	10,290	6678	6038	5122	3974	3950	3400
9	12,620	6964	6027	5034	3828	3880	3390
10	16,820	7283	6155	5000	3727	3840	3360
11		8209	6540	4996	3708	3720	3330
12		9390	7012	5096	3758	3600	3290
13		17,400	7768	5194	3816	3460	3250
14			8896	5479	3937	3380	3160
15			10,690	5875	4106	3370	3060
16			19,690	6441	4310	3390	2940
17				7305	4573	3450	2870
18				9535	4910	3560	2820
19				17,550	5358	3680	2820
20					6046	3760	2840
21					7065	3890	2880
22					9870	4100	2960
23						4350	3060
24						4800	3170
25						5420	3320
26						6180	3480
27						7680	3670
28						10,550	3880
29							4180
30							4570
31							5100
32							5800
33							7210
34							9760

TABLE A11. DATA SHEET FOR CRUSH TESTS OF 12 GAGE CORRUGATED STEEL PIPES

Crush Distance (in.)	Load (lbs)						
	12"	15"	18"	21"	24"	30"	36"
1					5950	3510	1960
2					6910	5270	3730
3					7060	5670	4320
4					7140	5770	4500
5					7210	5820	4600
6					7170	5840	4600
7					7070	5850	4620
8					6890	5840	4680
9					6670	5780	4710
10					6490	5720	4710
11					6410	5600	4720
12					6400	5440	4660
13					6450	5260	4530
14					6640	5100	4330
15					6950	5030	4110
16					8370	4970	3860
17					9450	4970	3820
18					10,880	5020	3890
19					----	5110	3190
20					13,080	5260	2970
21					14,970	5440	2760
22						5660	2610
23						5900	2390
24						6280	2920
25						6950	4520
26						7700	5980
27						8930	8070
28						11,220	8750
29							9360
30							10,000
31							10,770
32							12,010
33							13,970
34							17,620

TECHNICAL MEMORANDUM 505-18

TEXAS TRANSPORTATION INSTITUTE
TEXAS A&M RESEARCH FOUNDATION

A FEASIBILITY STUDY OF USING CORRUGATED STEEL PIPES IN MODULAR CRASH CUSHIONS

A Tentative Progress Memo on Contract No. CPR-11-5851

U. S. Department of Transportation
Federal Highway Administration

by
Monroe C. White
Engineering Research Associate
Gordon G. Hayes
Physics Research Associate
and
T. J. Hirsch
Research Engineer

The tests reported herein were conducted under the Office of Research and Development, Structures and Applied Mechanics Division's Research Program on Structural Systems in Support of Highway Safety (4S Program).

August, 1971

Introduction

Following the successful implementation of the 55 gallon steel drum modular crash cushion, a study of the feasibility of using other energy absorbing modules was initiated.[1,2*] One possible energy absorbing module is corrugated steel pipe. Corrugated steel pipe with diameters of 12, 15, 18, 21, 24, 30, and 36 inches, of 16, 14, and 12 gage steel with a specimen length of 25.5 inches, were statically crush tested and found to have reasonable static force and crush energy values for use in a modular crash cushion[3] (see Table 1 for summary of static crush force and energy for corrugated steel pipes used in the three tests reported herein).

This multitude of available diameters and thicknesses of corrugated steel pipes encompasses a wide range of static force and crush energy characteristics, thus indicating the use of what is called the polymodular design method. This design method is based on a row-by-row analysis of the force and energy relationships between the vehicle and modular crash cushion, whereas the other simpler design method, called monomodular, involves using energy absorbing modules of the same strength and designing the whole cushion from two vehicle parameters, velocity and weight.[2,4]

Test Descriptions and Objectives

Three experimental crash tests were conducted, two head-on tests and one side-angle test. The first test, CSP-1, was conducted to

---

*Numbered superscripts correspond to like numbers in reference.

determine and to reveal the overall dynamic interaction of the vehicle and cushion during impact. The cushion consisted of fifteen rows of fifteen inch diameter pipes arranged four abreast. The first nine rows were of 16 gage metal and the last six rows were of 14 gage metal as shown in Figure 1.

The second and third tests, CSP-2 and CSP-3, respectively, were conducted on a crash cushion designed for a 2000 lb. to 5000 lb. vehicle weight range and installed in a simulated median in front of simulated bridge piers. The sides of the bridge piers were protected by a modified concrete median barrier. The cushion installation, shown in Figure 2, consisted of one row of two and three rows of three 24 inch diameter 16 gage pipes, five rows of three 24 inch diameter 14 gage pipes, three rows of four 18 inch diameter 16 gage pipes, and five rows of four 18 inch diameter 14 gage pipes. The pipes in the last row and the offset pipes each contained an inner pipe which increased the module stiffness and was intended to protect against angle impacts near the last row and at the transition to the concrete median barrier. The objective of the angle test, CSP-2, was to evaluate the redirection capability of the flexbeam panels installed along the side of the crash cushion. The objective of the head-on test, CSP-3, was to determine if the addition of the flexbeam on the nose and the more numerous and stronger support posts would eliminate the ramping tendency observed in CSP-1.

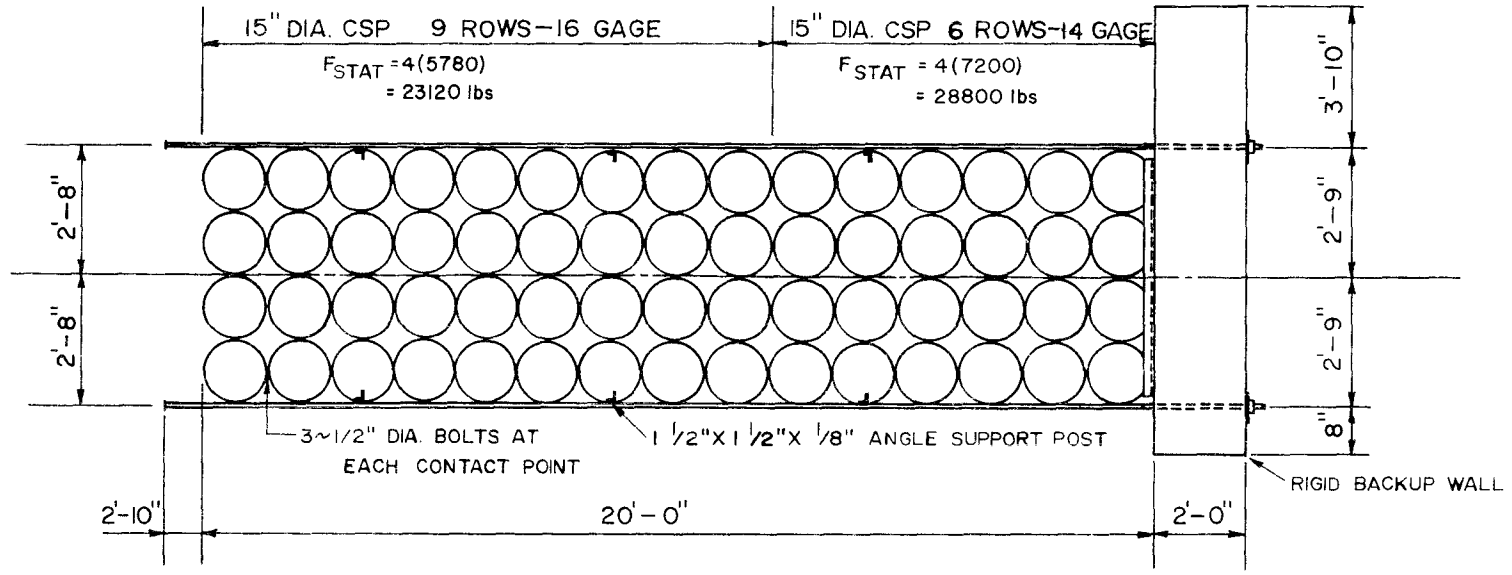

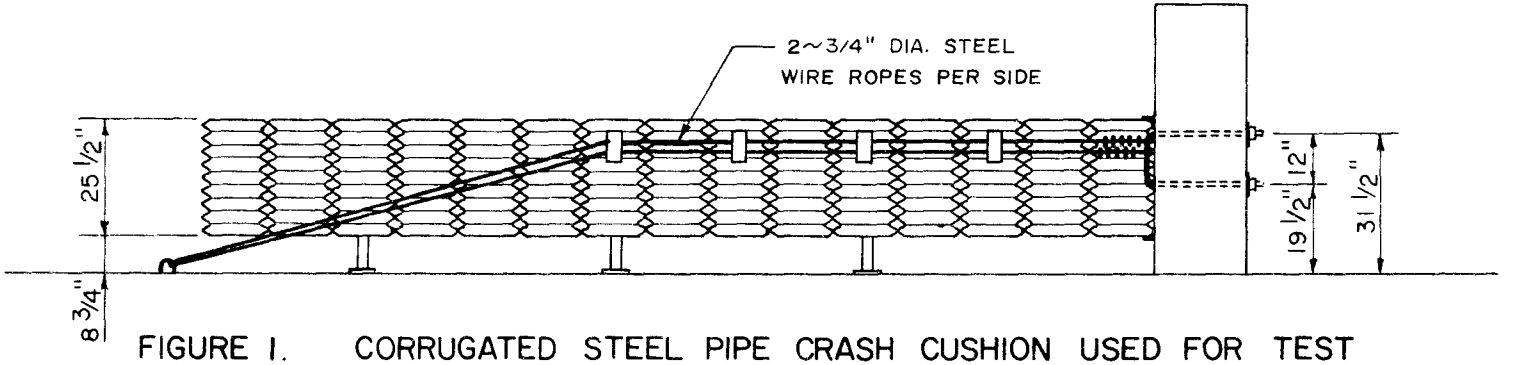

FIGURE 1. CORRUGATED STEEL PIPE CRASH CUSHION USED FOR TEST 505 CSP-1

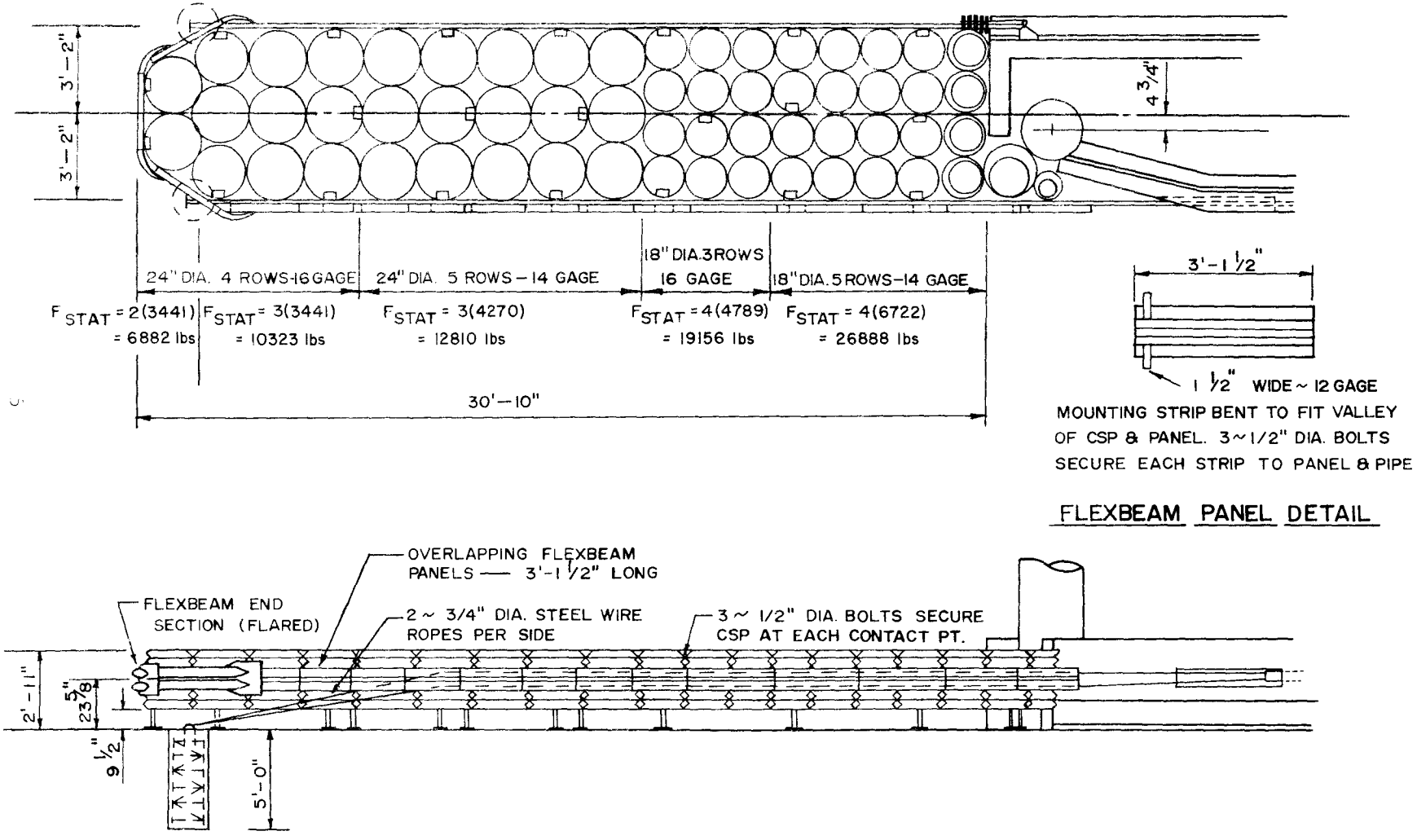

FIGURE 2. CORRUGATED STEEL PIPE CRASH CUSHION USED FOR TESTS 505 CSP - 2 & 3

TABLE 1.

SUMMARY OF STATIC CRUSH TEST
RESULTS FOR CORRUGATED STEEL
PIPES 25.5 IN. LONG

Nominal Inside Diameter (in.)	Wall Thickness (ga.)	Module Weight (lb.)	Crush Distance (in.)	Crush* Energy (ft.-lb.)	Average* Force (lb.)
15	16	25	12	5,780	5,780
15	14	30	12	7,200	7,200
18	16	29	15	5,990	4,790
18	14	35	15	8,400	6,720
24	16	40	21	6,020	3,440
24	14	48	21	7,470	4,270

*Values are rounded off to nearest ten pounds.

Note: Data taken from curves on Figures A11, A12, and A13 in the Appendix.

Experimentation

Test Instrumentation

Photographic instrumentation. Data from high-speed films were used to determine vehicle time-displacement. Vehicle speeds and average decelerations were computed from this data. For an angle test, such as CSP-2, the high-speed film was used to estimate the time when the vehicle was parallel to the barrier and when it had completely lost contact with the barrier.

Each high-speed film had a timing mark placed on it at specific time intervals, usually 1 mark every 0.01 seconds. Thus, elapsed time could be determined. A stadia board placed on the side of the vehicle was used to relate actual distances with apparent distances on the film, so that vehicle displacement along its path could also be determined.

In test CSP-1, three high-speed cameras were used. Two cameras, both running at 250 frames per second, were located perpendicular to the vehicle's path (also perpendicular to the barrier as this was a head-on crash). The third camera, running at 400 frames per second, was placed overhead.

Four cameras, all running at 400 frames per second, were used to photograph test CSP-2. One was perpendicular to the vehicle's path, another parallel to the barrier, a third perpendicular to the barrier, and the last, overhead.

Three high-speed cameras, all running at 400 frames per second, were used in test CSP-3. Two cameras were perpendicular to the vehicle's path (also perpendicular to the barrier). The third was placed on the other side of the barrier at an angle of 115° with respect to the vehicle's path.

Electromechanical instrumentation. Accelerometers placed in the test cars provided a trace of longitudinal and transverse acceleration (g's) versus time for the car axes. In test CSP-2, both longitudinal and transverse accelerometers were used, but in the two head-on tests, CSP-1 and CSP-3, only the longitudinal accelerometers were used. The right longitudinal and right transverse accelerometers were mounted on short flanges which were welded to the right longitudinal frame member just behind the front seat. Similarly, the left longitudinal and left transverse accelerometers are mounted on the left longitudinal frame member. The data recorded from these accelerometers were run through an 80 Hz low pass filter to reduce the "ringing" effect. An Impact-O-Graph, an alternative source of acceleration data, was mounted in the trunk of each test vehicle. In all tests a 160 lb. anthropometric dummy was placed in the driver's seat and secured with a lap belt. A force versus time trace was obtained from a load cell attached to the lap belt. The actual signals produced by all of the electromechanical instruments were transmitted from the car by telemetry and recorded on magnetic tape.

Test Results

Summary of results. Summaries of the analyses of film data and accelerometer data for the three tests are presented in Tables 2 and 3, respectively. The accelerometer traces and seat belt force traces are presented in Figure A1 through A10 in the appendix. The film data are presented in Tables A1, A2, and A3, also in the appendix.

Test CSP-1. The 1964 Dodge weighing 3750 lbs. impacted the barrier head-on at a speed of 58.4 mph. After seven rows of pipes had crushed, the front portion of the barrier pivoted upward at the 8th and 9th rows of pipes. The vehicle ramped upward and became airborne. The first five rows of pipes became detached in a group and rotated through 360° in the air before coming to rest on top of the rear portion of the barrier near the backup wall (see Figure 3). Little vehicle damage resulted (0.5 ft) despite a high peak deceleration of 24 g's noted from the accelerometers. The average deceleration from the accelerometers, however, was only 5.6 g's over 0.316 seconds impact duration. Figure 4 shows sequential photos of the test.

The support posts, instead of sliding as intended, buckled from the high frictional force which apparently resulted from the normal force exerted by the initial tension in the cables.

Since the vehicle ramped and became airborne, the dynamic-to-static force (and energy) ratio can not be accurately determined.

Table 2. DATA FROM FILM ANALYSIS

Factor	Test CSP-1	CSP-2	CSP-3
Vehicle weight, lb.	3750	3810	3880
Impact angle, deg.	0	20	0
Initial speed, ft/sec. (V_i)	85.6	87.7	91.4
mph	58.4	59.8	62.3
Final speed, ft/sec. (V_f)	0	----	0
Total stopping distance, ft (S)	28.7	----	27.2
Total stopping time, sec.	1.528	----	1.167
Average longitudinal deceleration, g's (G)	4.0**	----	4.8**
Speed after contact*, ft/sec. (V_f)	57.1*	65.8	62.5*
mph	39.0*	44.9	42.6*
Time in contact, sec.	0.089	0.344	0.093
Distance in contact, ft. (S)	6.2	23.8	7.4
Average longitudinal deceleration, g's. (G)	10.2**	2.2**	9.3**
Exit angle, degrees	----	7.7	----

* In Tests CSP-1 and CSP-3 the vehicle "ramped" shortly after impact. Data immediately below asterisk applies only during contact before ramping.

** $G = \frac{V_i^2 - V_f^2}{2gS}$ longitudinal acceleration parallel to vehicle path or parallel to side of barrier for redirection tests

Table 3. DATA FROM ACCELEROMETERS

Factor	Test CSP-1	CSP-2	CSP-3
Vehicle weight, lb.	3750	3810	3880
Impact angle, deg.	0	20	0
Maximum deceleration[a], g's.			
Longitudinal	23.0	6.3	19.5
Transverse[b]	----	12.0	----
Average deceleration[a]			
Longitudinal			
Total event, g's.	5.6	1.5	4.3
Time interval, sec.	0.316	0.358	0.521
Before ramping, g's.	7.7	----	6.5
Time interval, sec.	0.100	----	0.100
Transverse[b], g's.	----	3.4	----
Time interval, sec.	----	0.325	----

[a] Values given are averages of right and left accelerometer outputs.

[b] Transverse to vehicle longitudinal axis.

Test CSP-2. A 3810 lb. Plymouth sedan traveling 59.8 mph impacted the barrier at an angle of 20° with respect to the barrier centerline. Dynamic lateral deformation of the barrier started at impact, reaching a maximum of 1.0 ft. in 0.277 sec. as determined from the overhead camera film. The residual lateral deformation of the barrier was 0.4 ft. Damage to the left front quarter of the vehicle was considerable (see Figure 5), with a deformation on the left fender of 1.8 ft. and a deformation of the left side of the bumper of 1.4 ft. Damage to the barrier was much less severe (see Figure 6), consisting of scrapes along the guardrail and pipes and also some crushing of the lower portions of the outside row of pipes. With only minor repair, the barrier was used again for test CSP-3.

The vehicle redirected smoothly, with an average longitudinal deceleration, determined from the accelerometer traces, of 1.5 g's over 0.358 sec. The maximum longitudinal deceleration was 6.3 g's (accelerometer). Average transverse deceleration, also determined from accelerometer traces, was 3.4 g's over 0.325 sec., with a maximum of 12.0 g's. The average longitudinal deceleration, as determined from film, was 2.2 g's over 0.344 sec. The exit angle was 7.7° and the velocity after contact was terminated was 44.9 mph.

Sequential photographs from two different views of the crash may be seen in Figures 7 and 8.

Test CSP-3. Text CSP-3 was a head-on test of the corrugated steel pipe crash cushion. In this test, the barrier was impacted by a 1963 Plymouth sedan weighing 3880 lbs. and traveling 62.3 mph.

Figure 9 shows the vehicle before and after and Figure 10 shows the cushion before and after the collision. The barrier-vehicle interaction was similar to that of test CSP-1, the first head-on test of this series. As in CSP-1, the first rows of the barrier (rows 1-6) were crushed and bent downward, then pivoted upward from a point between the 6th and 7th rows. The front of the vehicle was lifted upward by one of the flexbeam panels which dug into the ground, pushing against the first rows of the barrier (see Figure 11). The vehicle continued to ramp upward, pushing the first four rows of pipes, which had become detached, over the right side of the barrier. The front wheels of the vehicle recontacted the remaining portion of the barrier, then the car started to slide down backwards, with the head end of the vehicle sliding along the support cables. Figure 12 shows the vehicle at rest, suspended by the barrier and support cables. The peak deceleration taken from the accelerometer traces was 19.5 g's. The average longitudinal deceleration, also from accelerometer data, was 4.3 g's over 0.521 sec. (total event) and 5.0 g's over 0.100 sec. (before ramping).

Since the vehicle again ramped and became airborne, the dynamic-to-static force (and energy) ratio cannot be determined.

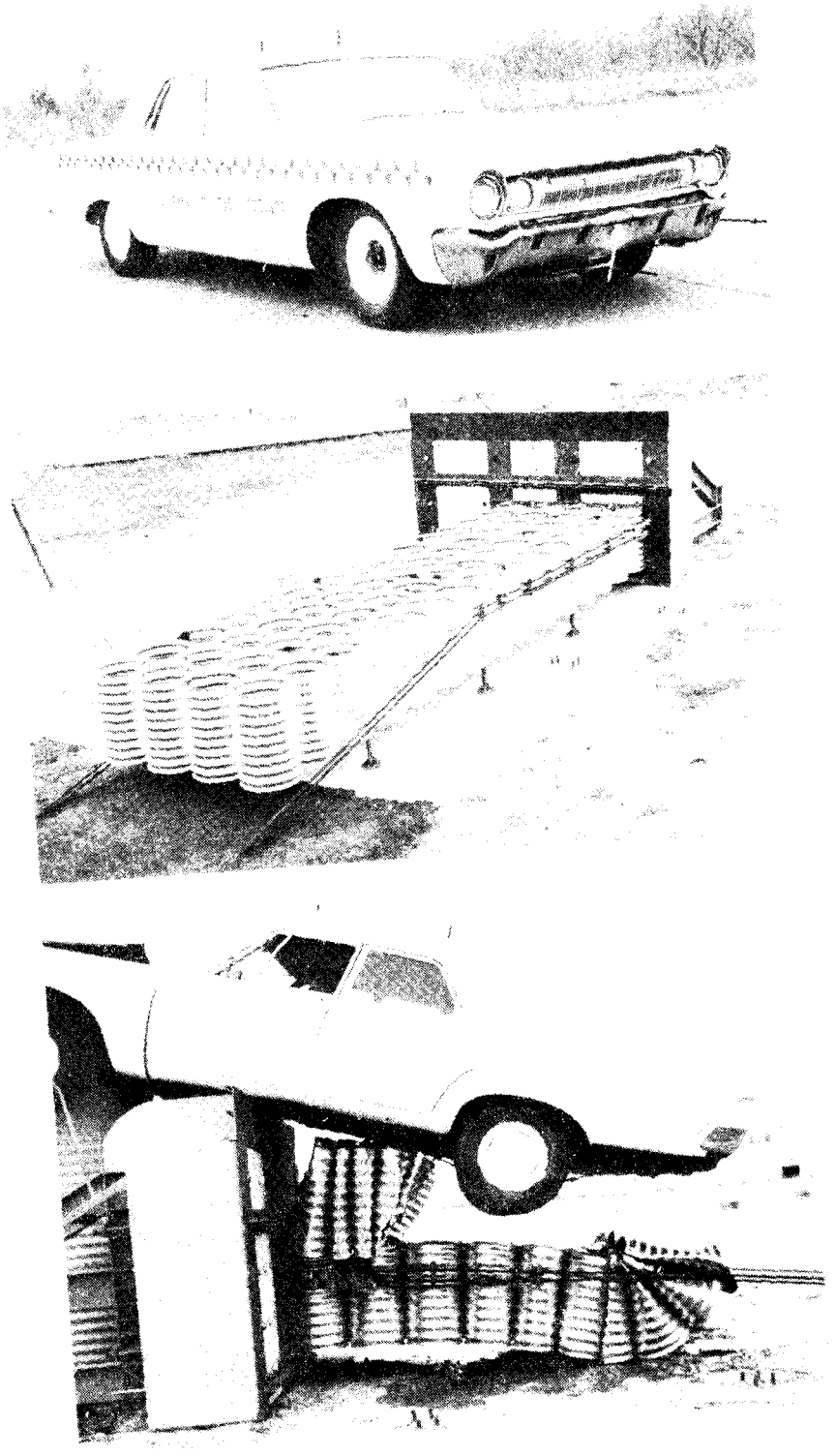

FIGURE 3. Vehicle and station before and after the collision, Test 896F.

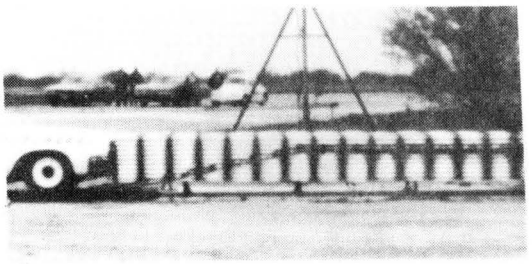

t = 0.000 sec.

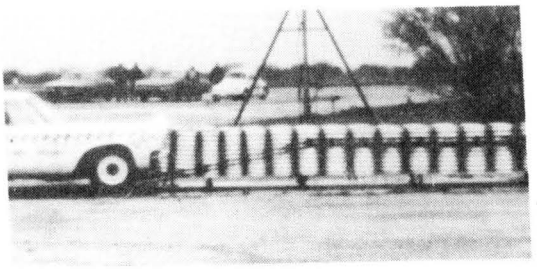

t = 0.038 sec.

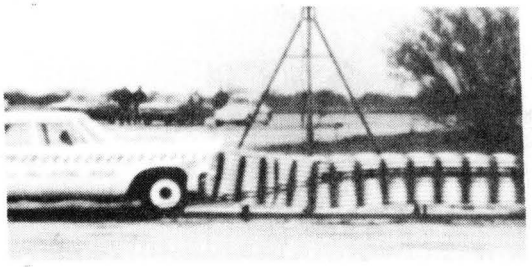

t = 0.072 sec.

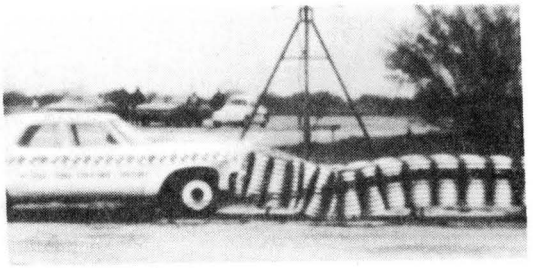

t = 0.098 sec.

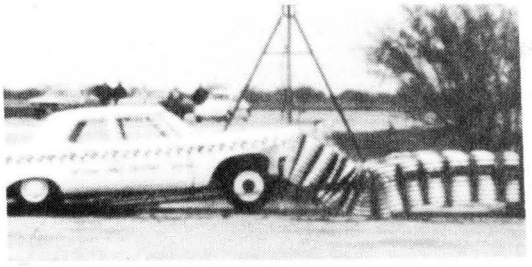

t = 0.163 sec.

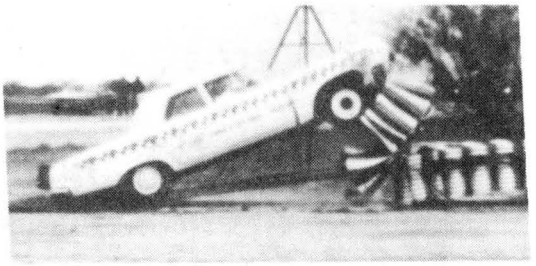

t = 0.310 sec.

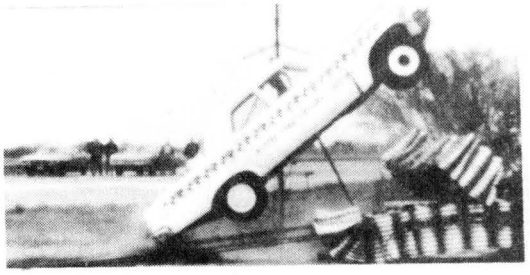

t = 0.553 sec.

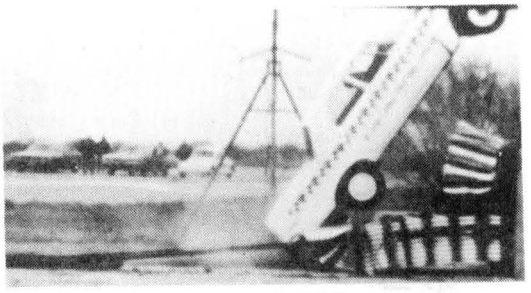

t = 0.807 sec.

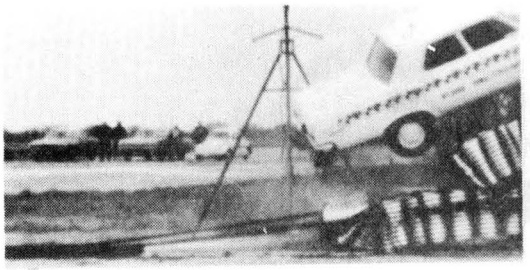

t = 1.174 sec.

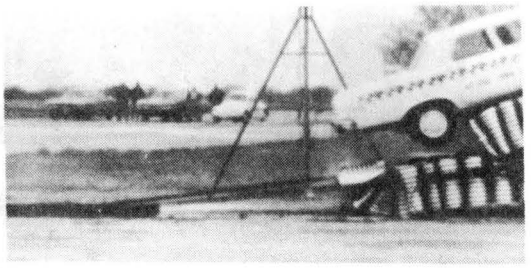

t = 3.438 sec.

FIGURE 4. Sequence Photos of Test CSP-1.

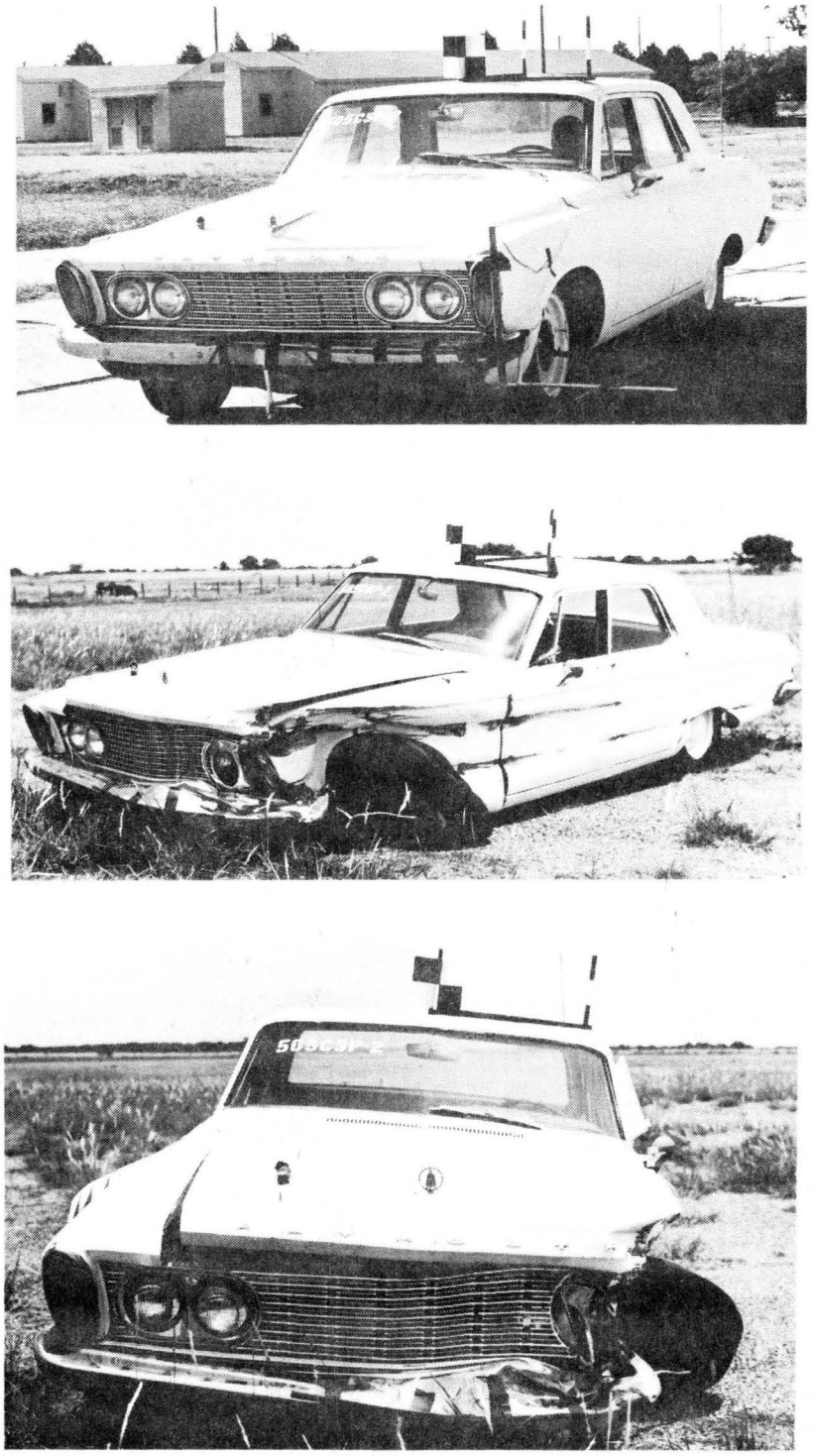

FIGURE 5. Vehicle before and after the collision, Test CSP-2.

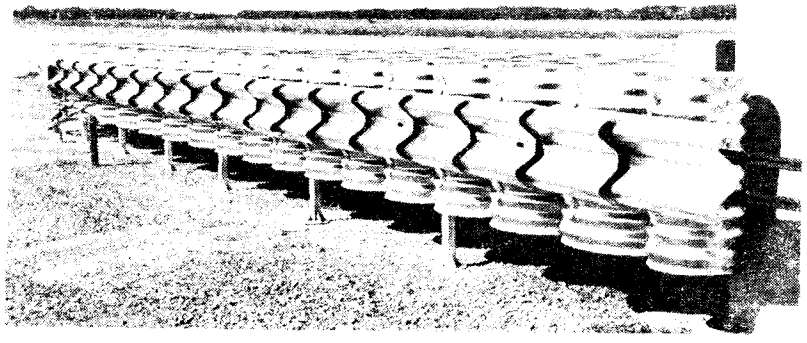

before

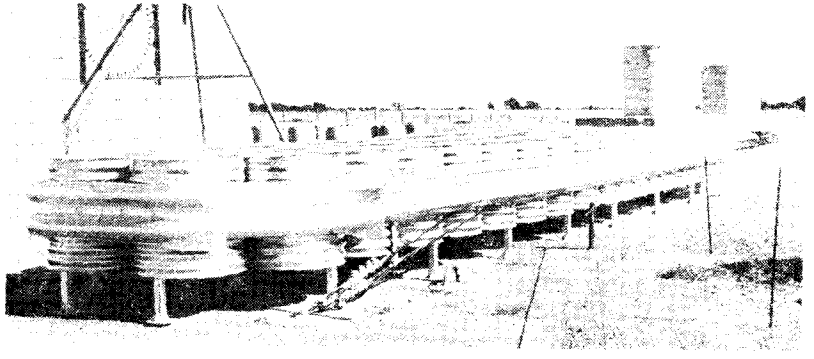

before

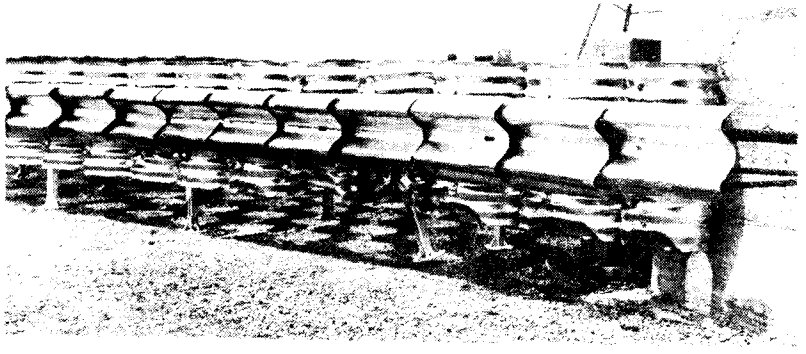

after

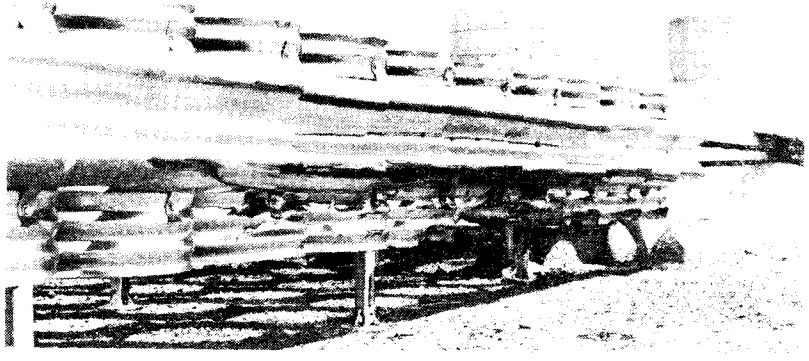

after

FIGURE 6. Two views of cushion before and after the collision, Test CSP-2.

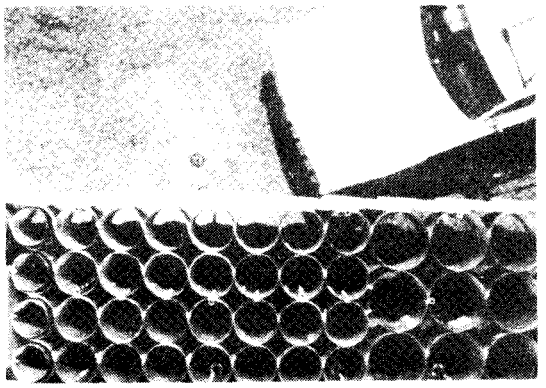

t = 0.000 sec.

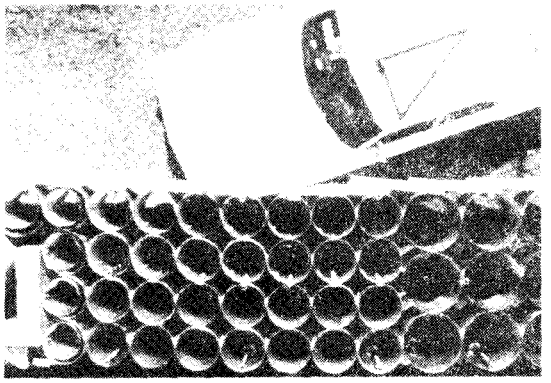

t = 0.064 sec.

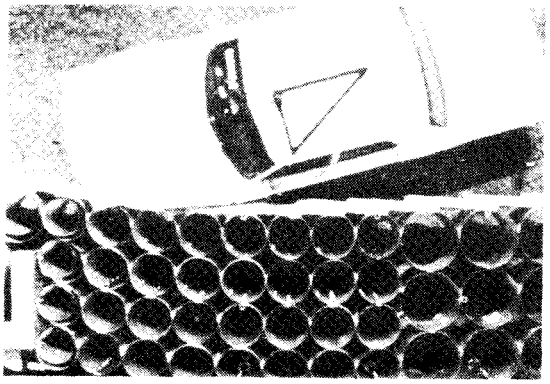

t = 0.106 sec.

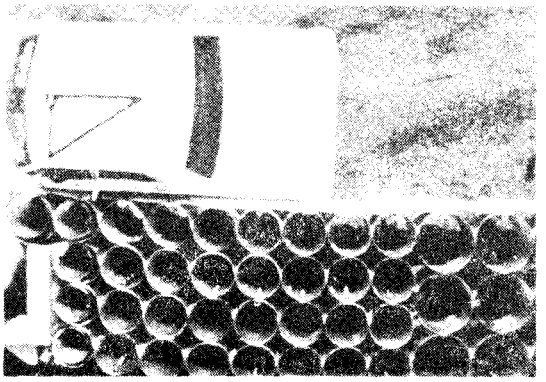

t = 0.217 sec.

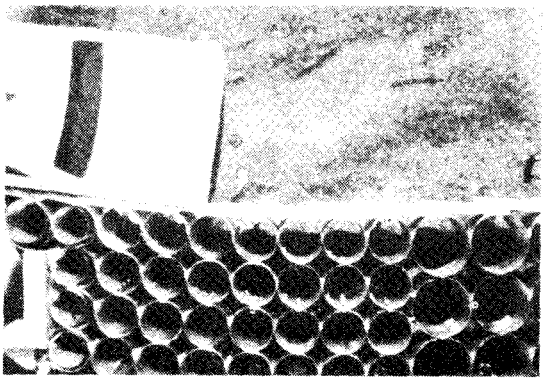

t = 0.277 sec.

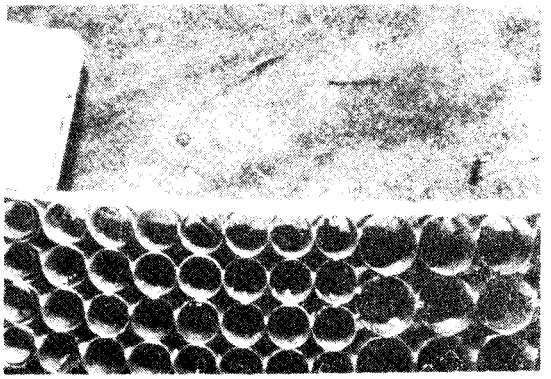

t = 0.328 sec.

FIGURE 7. Overhead sequential photos of Test CSP-2.

t = 0.000 sec.

t = 0.070 sec.

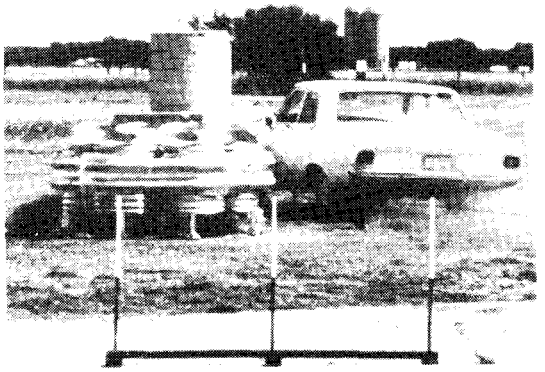

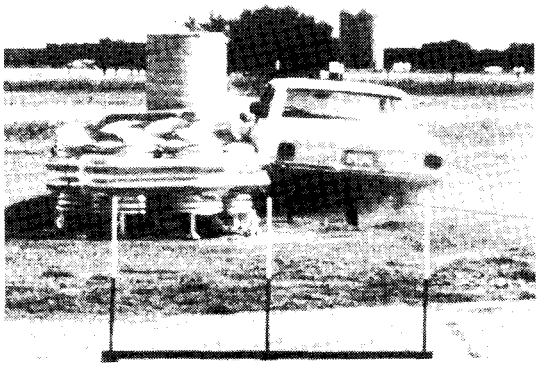

t = 0.171 sec.

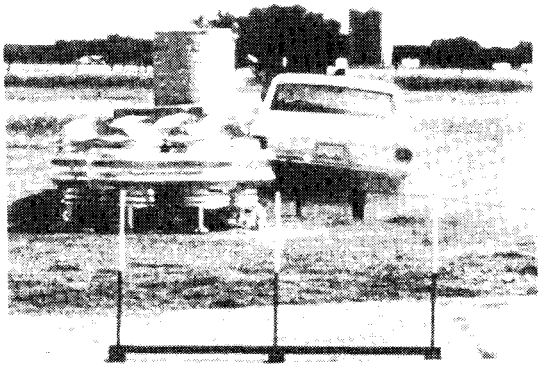

t = 0.217 sec.

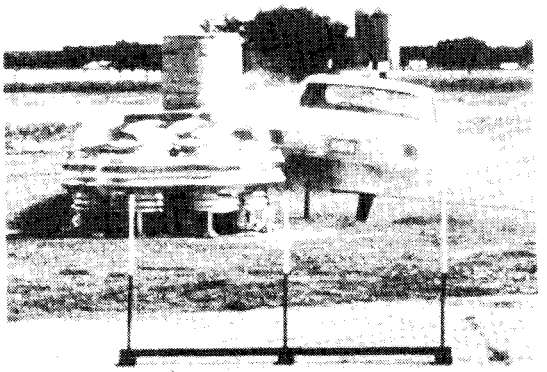

t = 0.344 sec.

FIGURE 8. End view sequential photos of Test CSP-2.

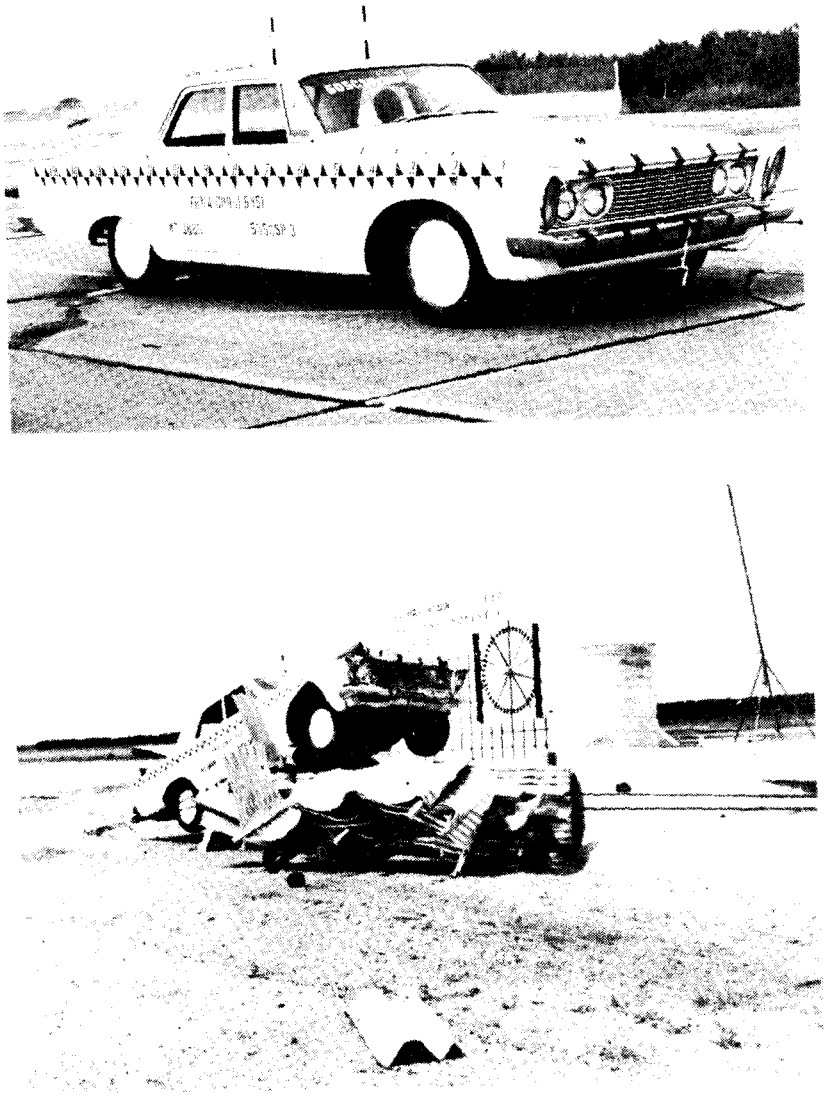

FIGURE 9. Vehicle before and after the collision, Test CSP-3.

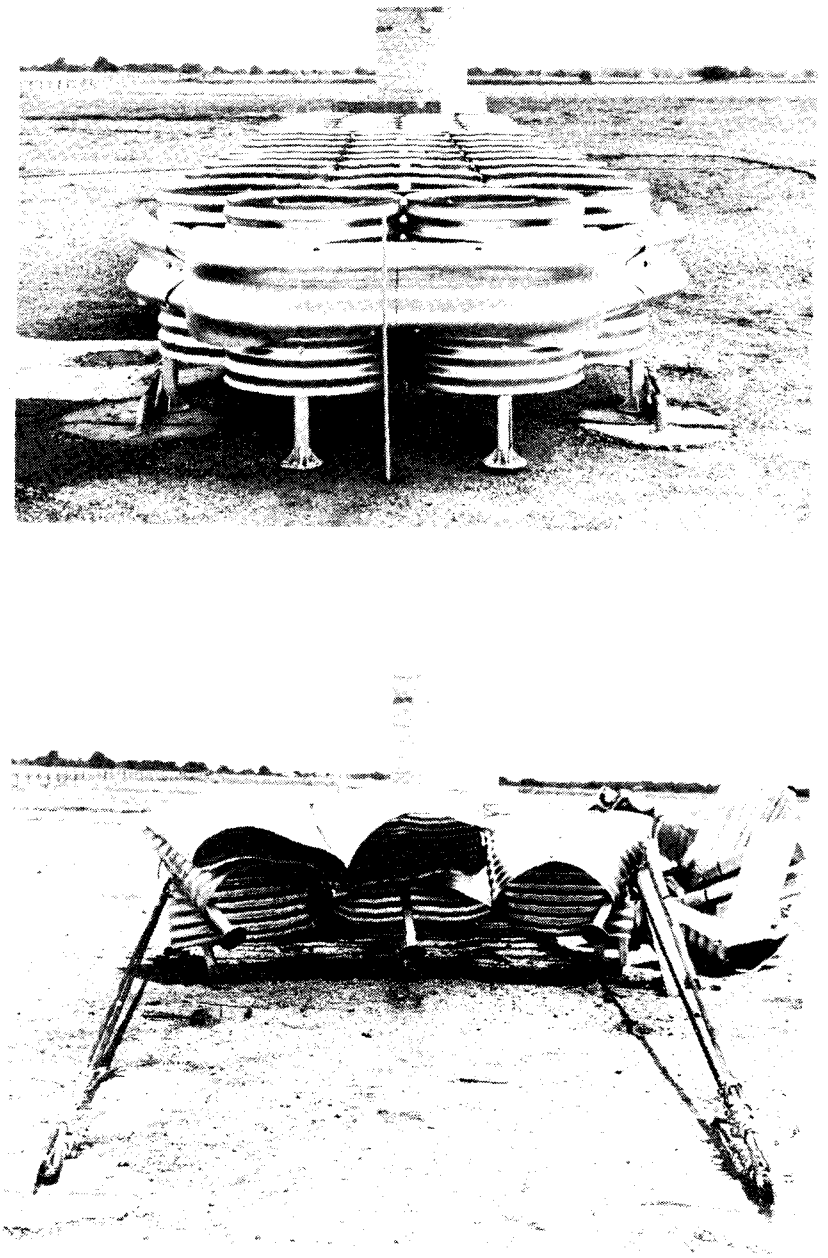

FIGURE 10. Cushion before and after the collision, Test CSP-3.

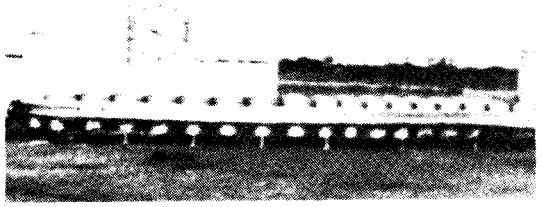

t = 0.000 sec.

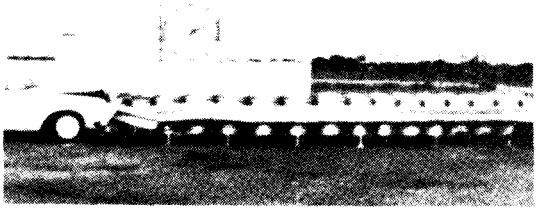

t = 0.052 sec.

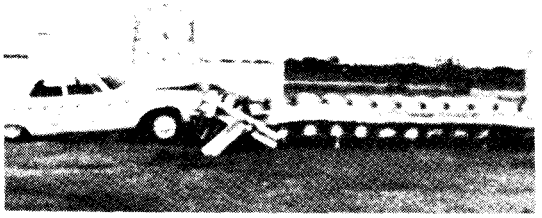

t = 0.169 sec.

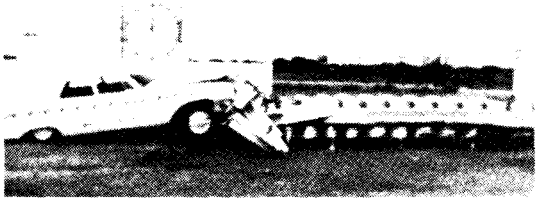

t = 0.227

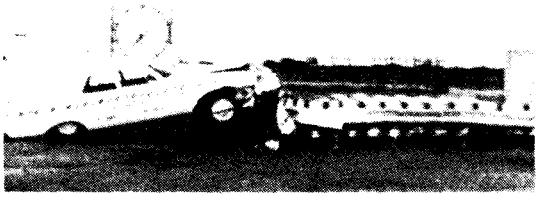

t = 0.284 sec.

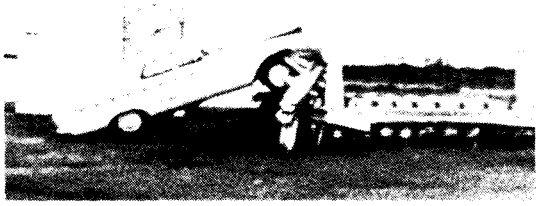

t = 0.415 sec.

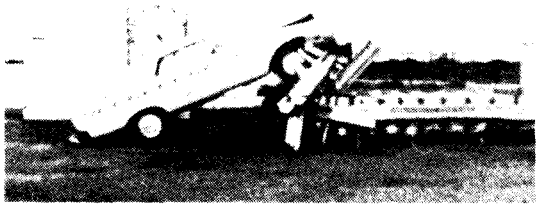

t = 0.458 sec.

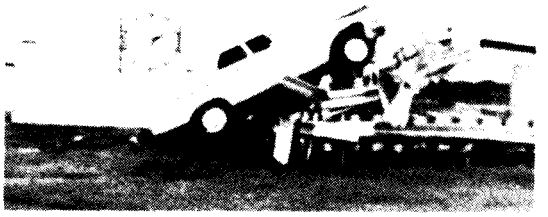

t = 0.649 sec.

FIGURE 11. Sequential photos of Test CSP-3.

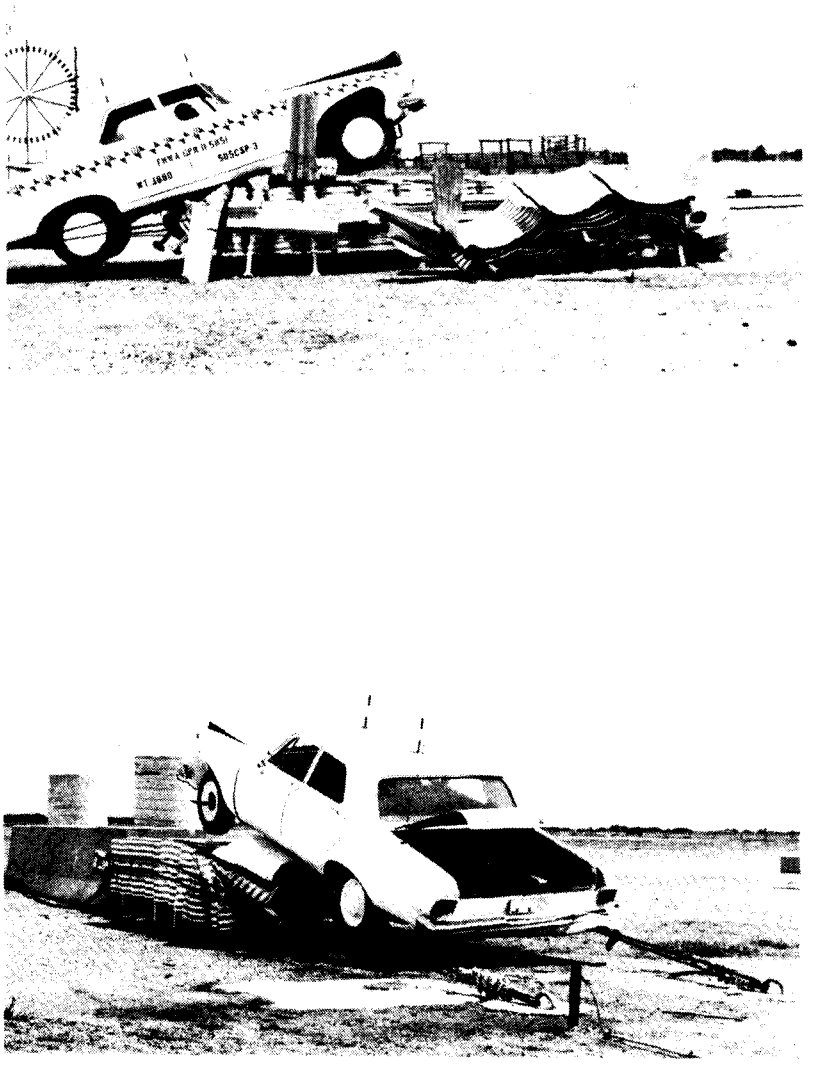

FIGURE 12. Vehicle and cushion after the collision, Test CSP-3.

Conclusions and Recommendations

The corrugated steel pipe crash cushion did not perform as intended during the two head-on tests. From the high speed films of CSP-1 it was surmised that the pipe support legs were insufficiently strong, particularly at the point where the cables angle downward from the horizontal. Also, it is believed that the strength distribution of the pipe contributed to the ramping, i. e., the pipe is weaker at top and bottom and stronger in the midsection, thus tending to deform first at one of the weaker points and allowing the vehicle to ramp. The addition of more and stronger legs, and the flexbeam on the nose and side of the cushion did not prevent ramping in test CSP-3, in fact one of the flexbeam panels aided ramping by digging in the ground and "vaulting" the vehicle upward.

It appears that the strength distribution of the pipe along with the frictional forces on the support legs and the length-to-height ratio of the cushion work in combination during impact to cause a vertical force to be applied to the vehicle, causing it to ramp.

Three changes are suggested below as possible remedies to the ramping problem. They are:

1. Increase the length of the module such that the top and bottom of the pipe will not be in contact with the distributed force from the nose of the impacting vehicle, i. e., the vehicle will feel the more uniform strength distribution of only the midsection of the pipe. This will also decrease the length-to-height ratio. An

alternate to increasing the module length would be to raise the bottom of the cushion to approximately 15 inches above grade.

2. Add dish shaped skid plates to the support posts to decrease frictional forces on the bottom of the cushion, particularly at the post where the cables angle downward.
3. Decrease the initial tension in the cables from the present 4000 to 5000 lbs. down to 500 to 1000 lbs. This will also help to decrease the frictional forces on the bottom of the cushion and perhaps allow the support post to remain upright and also keep the flexbeam panels from digging into the ground.

It is recommended that the above suggestions be investigated before deletion of or implementation of the corrugated steel pipe crash cushion as a viable vehicle impact attenuator.

A reliable experimental value for the dynamic-to-static force (and energy absorption) ratio still remains to be found from further tests where the vehicle does not ramp on head-on impact.

The corrugated steel pipe crash cushion with flexbeam side panels indicated excellent side-deflection behavior in test CSP-2.

In summation, the corrugated steel pipe crash cushion performs well under side impact but needs further investigation to correct the ramping problem during head-on impact.

References

1. White, M. C., Ivey, D. L., and Hirsch, T. J., "In-Service Experience on Installations of Texas Modular Crash Cushions," Research Report 146-2, Texas Transportation Institute, Texas A&M University, College Station, Texas, December, 1969.

2. White, M. C., and Hirsch, T. J., "Highway Crash Cushions," a Special Report for the Federal Highway Administration, Department of Transportation, Texas Transportation Institute, Texas A&M University, College Station, Texas, (pending publication).

3. White, M. C., "The Modular Crash Cushion: Design Data from Static Crush Tests of Steel Drums and of Corrugated Steel Pipes," Technical Memorandum 505-17, Texas Transportation Institute, Texas A&M University, College Station, Texas, April, 1971.

4. White, M. C., "The Polymodular Design Method for Designing Modular Crash Cushions," a Report for United States Steel Metal Products Division, United States Steel Corporation, Pittsburgh, Pennsylvania, (pending publication).

Appendix

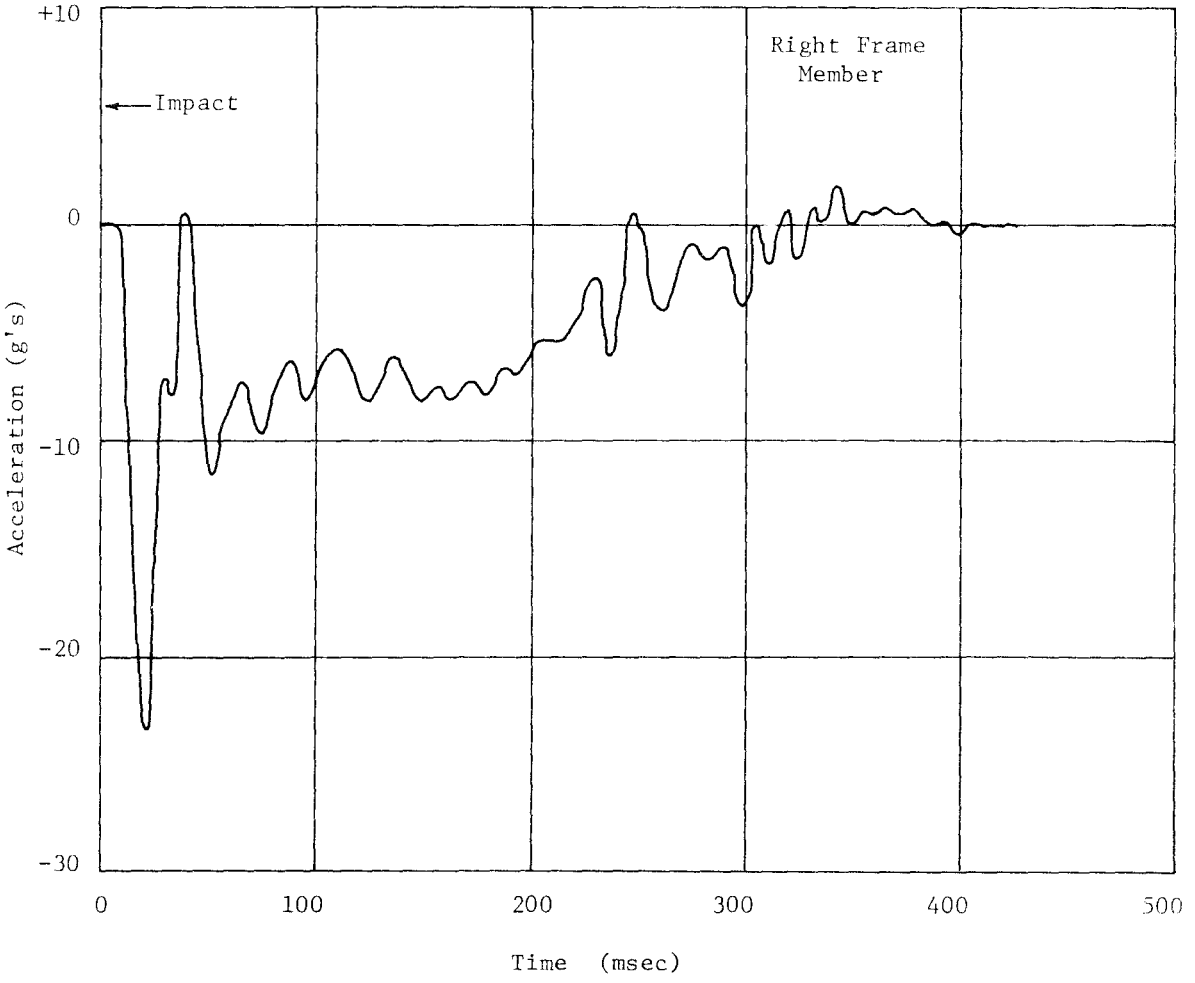

FIGURE A1. LONGITUDINAL ACCELEROMETER DATA, TEST CSP-1
(80 HZ LOW-PASS FILTER)

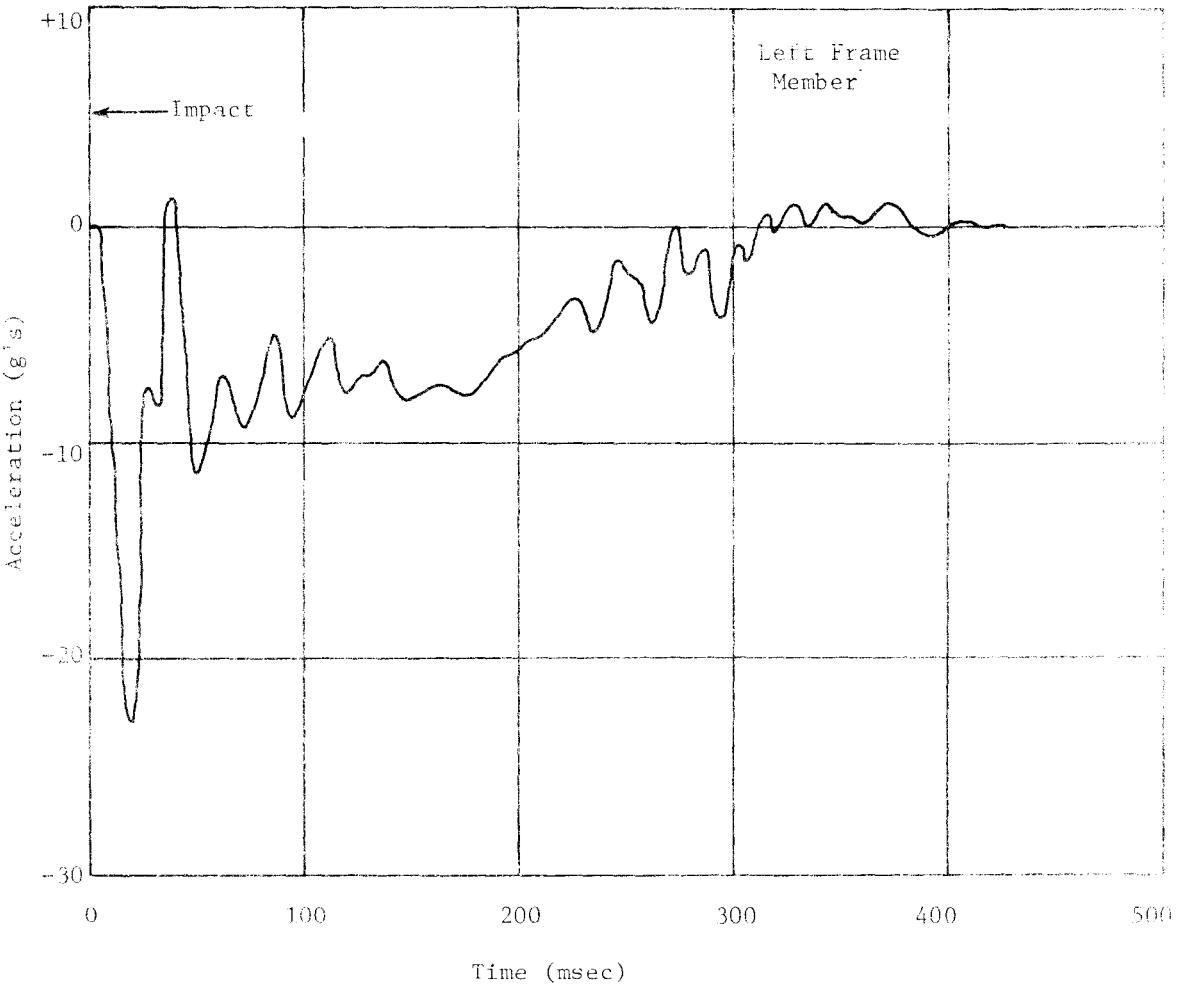

FIGURE A2. LONGITUDINAL ACCELEROMETER DATA, TEST CSP-1 (80 HZ LOW-PASS FILTER)

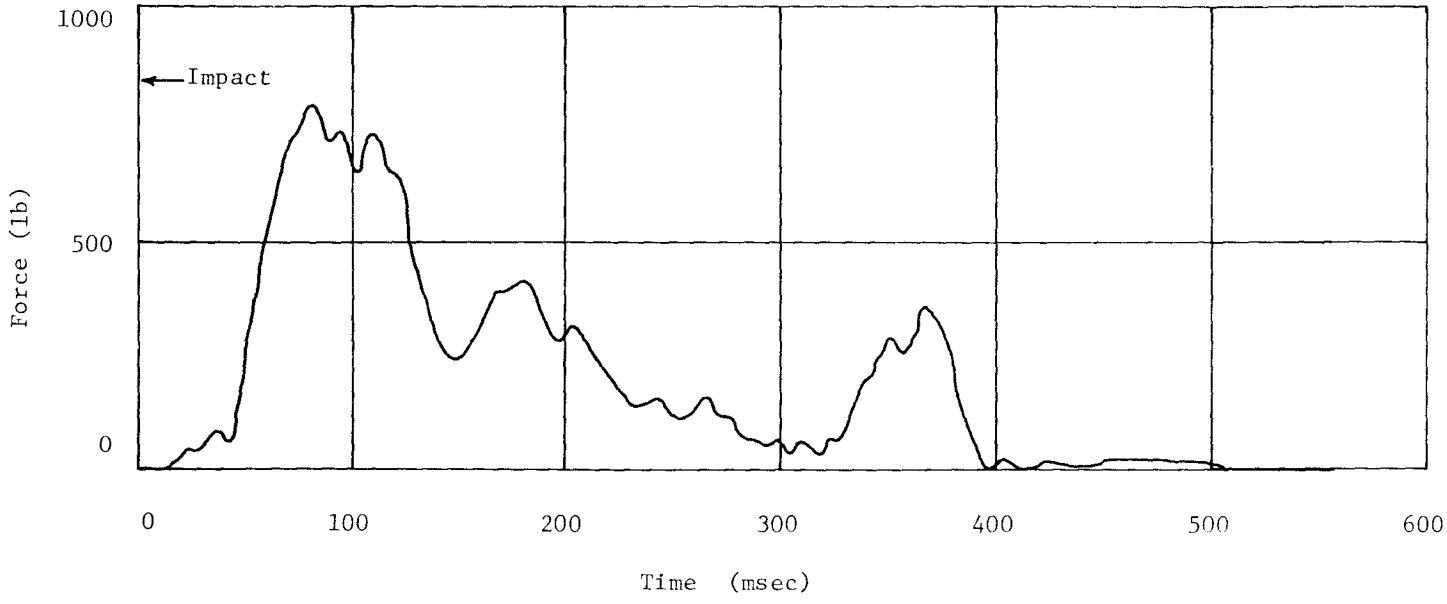

FIGURE A3. LAP BELT DATA, TEST CSP-1
(80 HZ LOW-PASS FILTER)

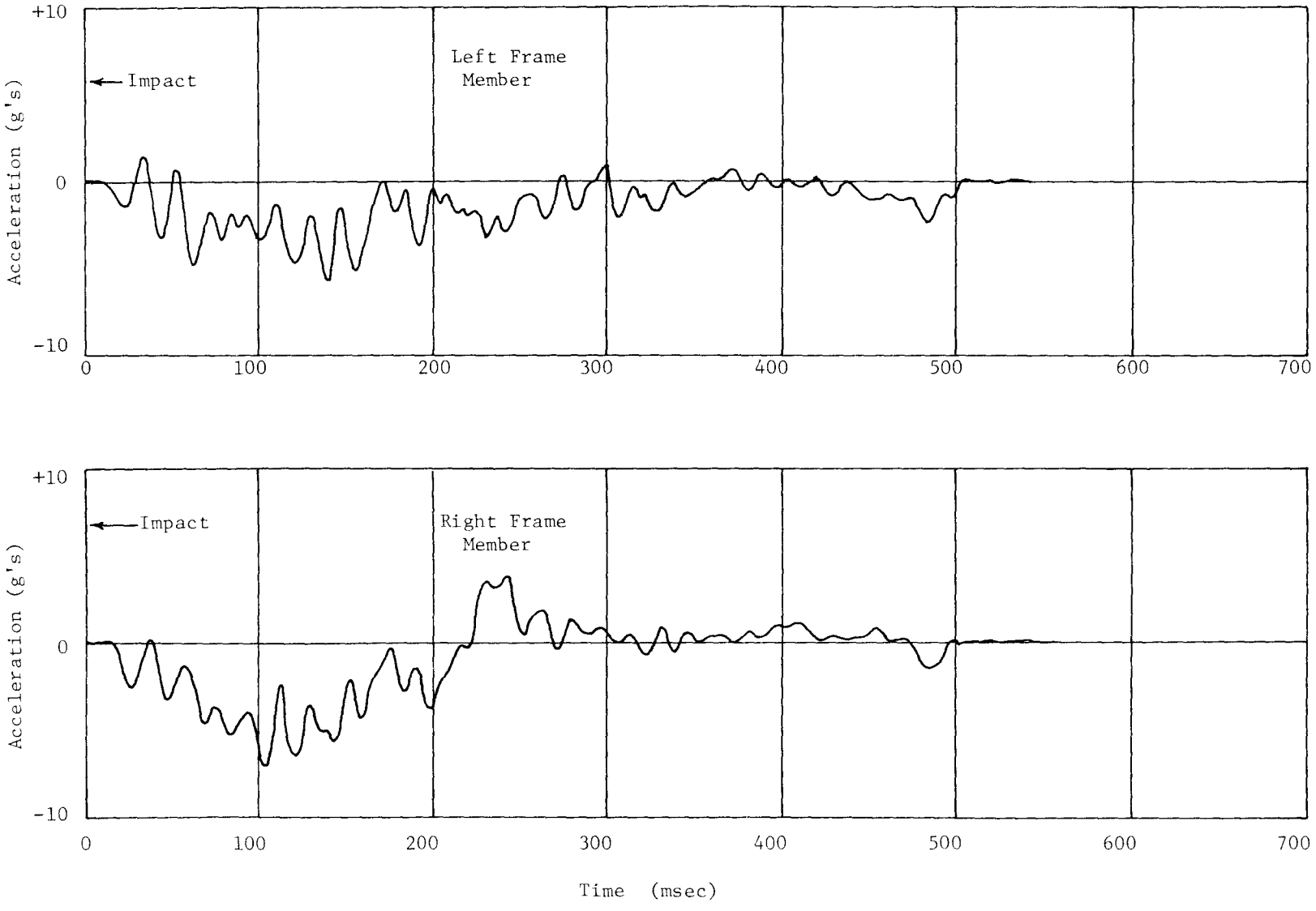

FIGURE A4. LONGITUDINAL ACCELEROMETER DATA, TEST CSP-2
(80 HZ LOW-PASS FILTER)

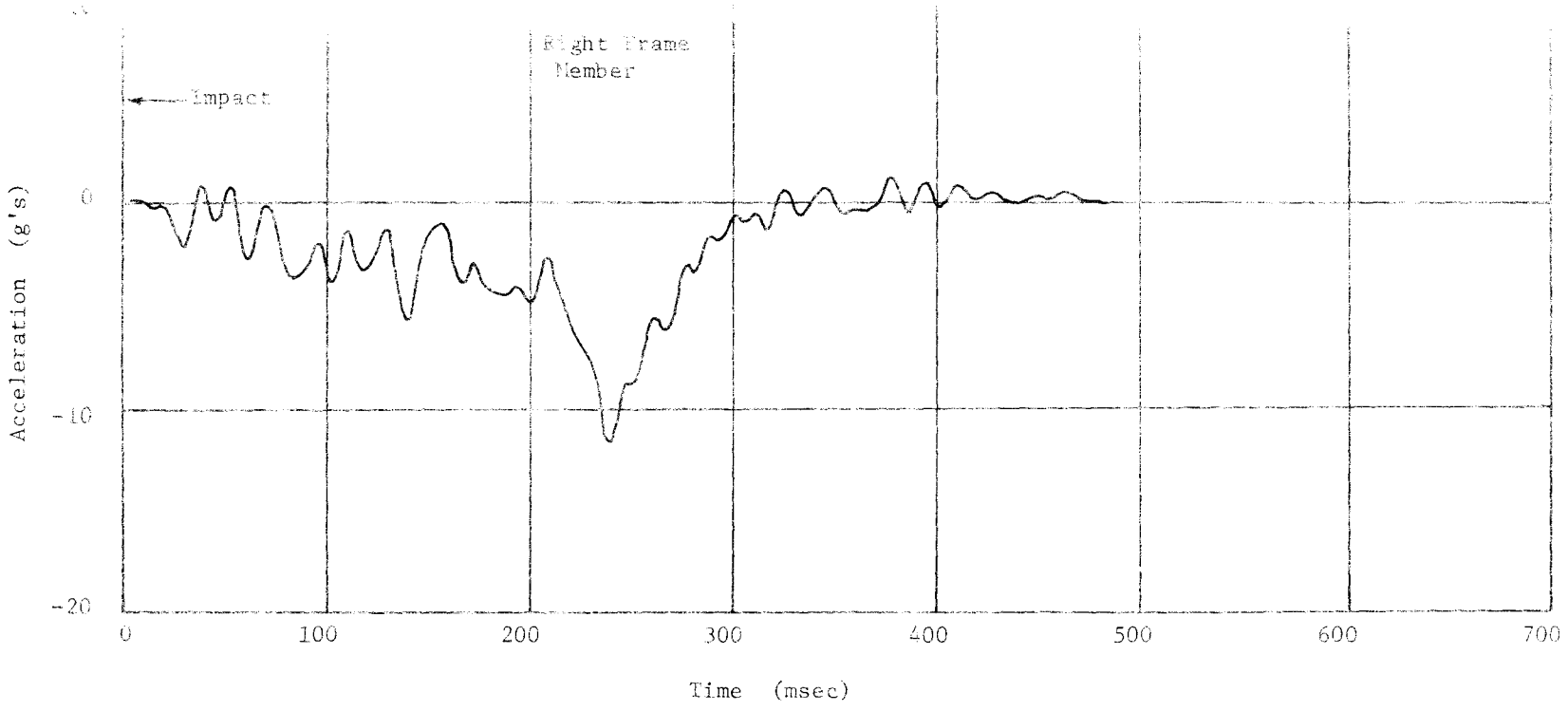

FIGURE A5. TRANSVERSE ACCELEROMETER DATA, TEST CSP-2
(80 HZ LOW-PASS FILTER)

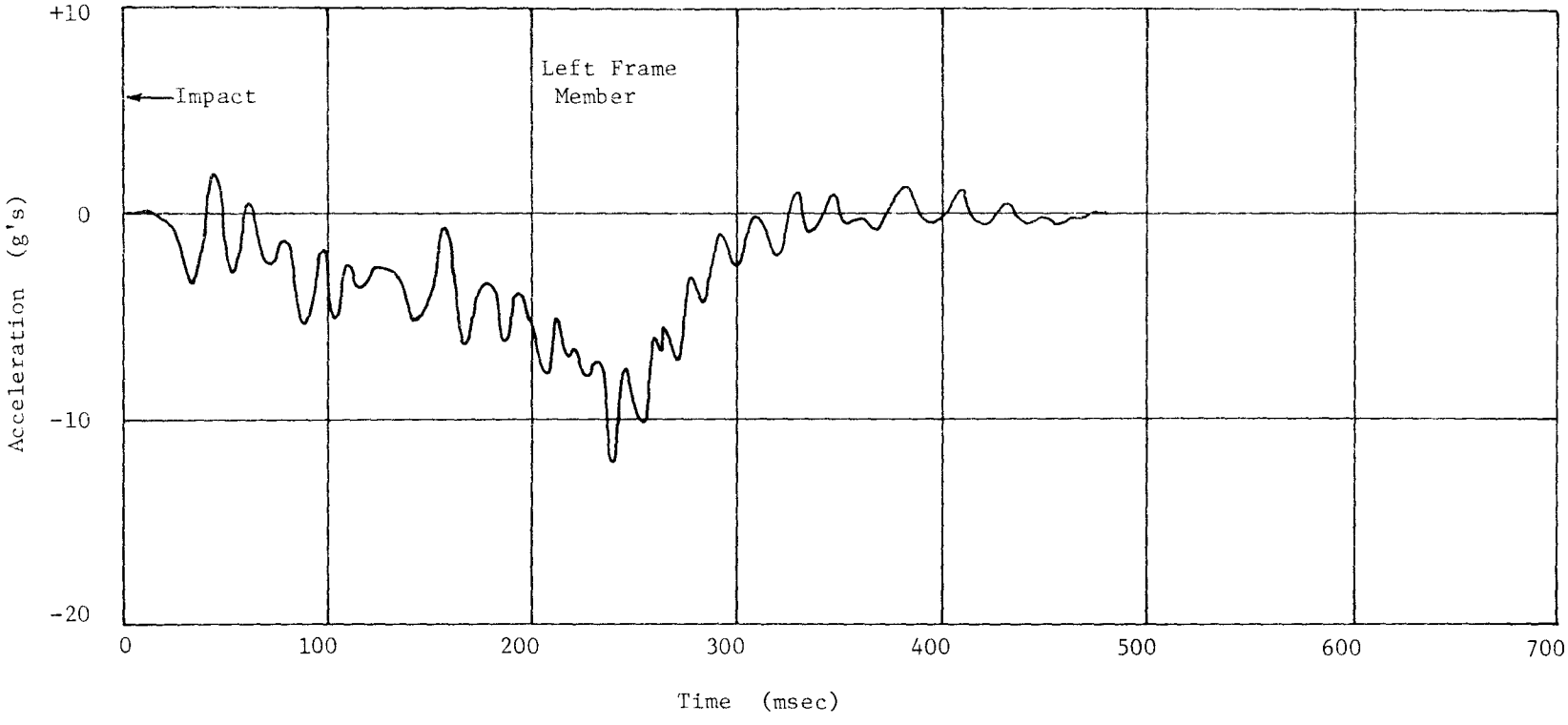

FIGURE A6. TRANSVERSE ACCELEROMETER DATA, TEST CSP-2
(80 HZ LOW-PASS FILTER)

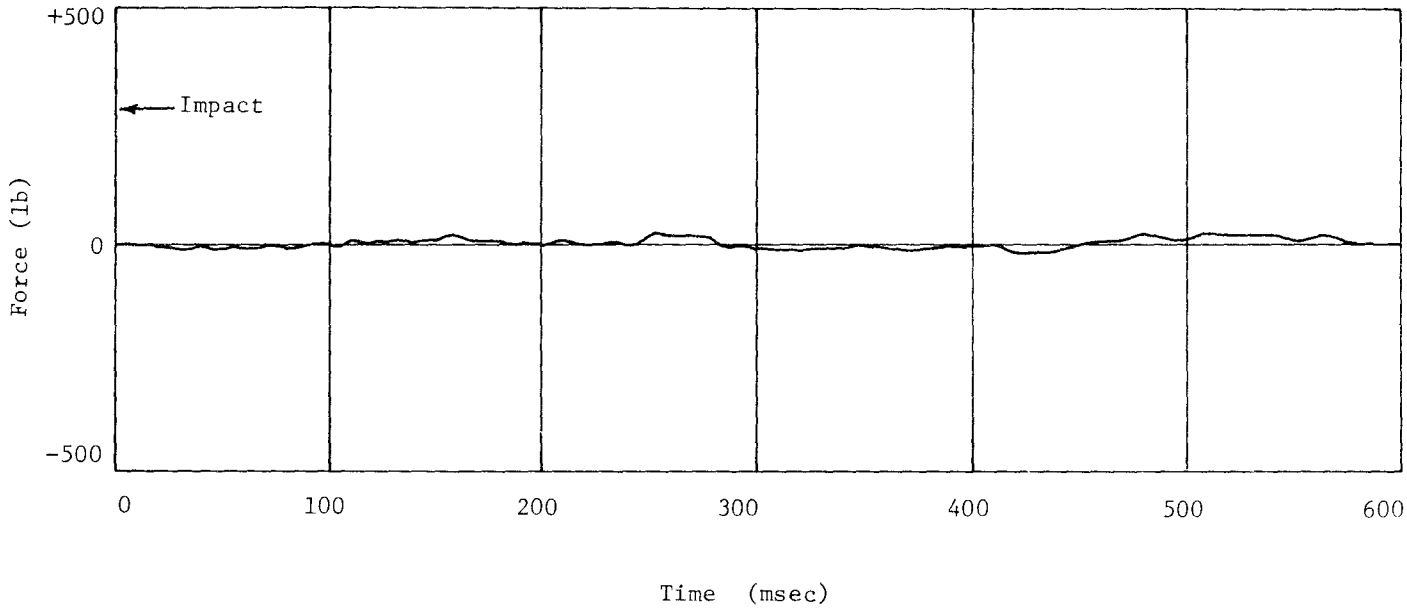

FIGURE A7. LAP BELT DATA, TEST CSP-2
(80 HZ LOW-PASS FILTER)

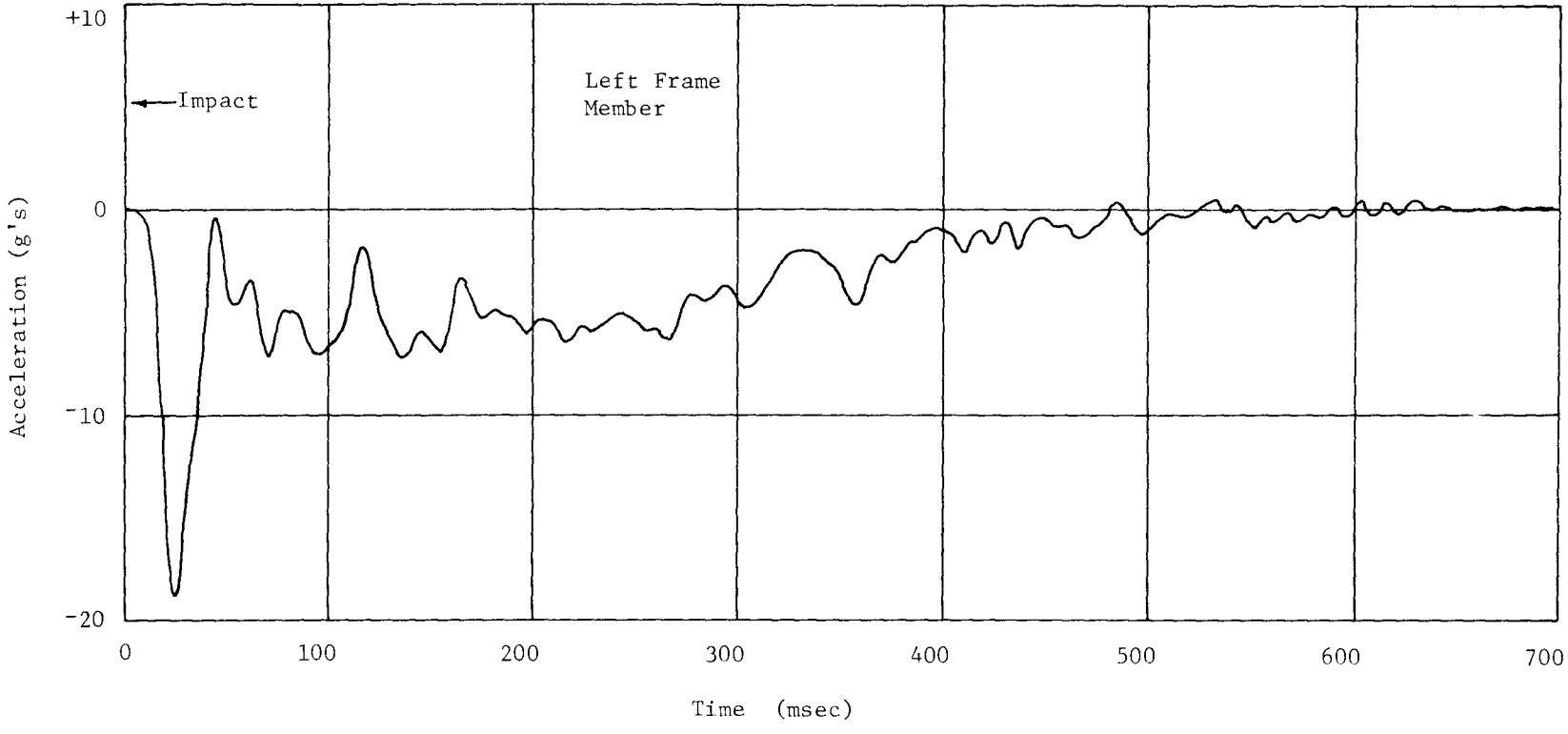

FIGURE A8. LONGITUDINAL ACCELEROMETER DATA, TEST CSP-3
(80 HZ LOW-PASS FILTER)

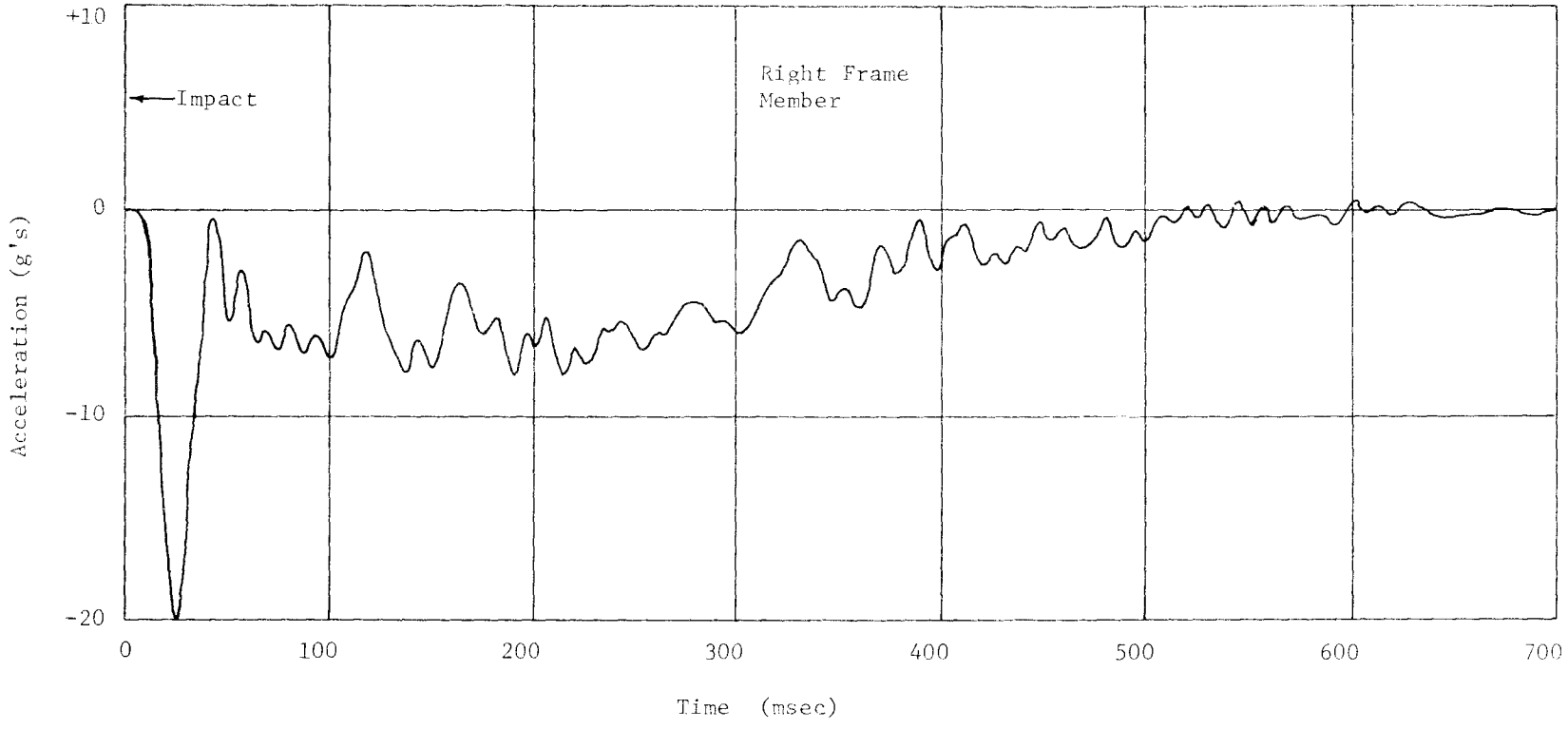

FIGURE A9. LONGITUDINAL ACCELEROMETER DATA, TEST CSP-3
(80 HZ LOW-PASS FILTER)

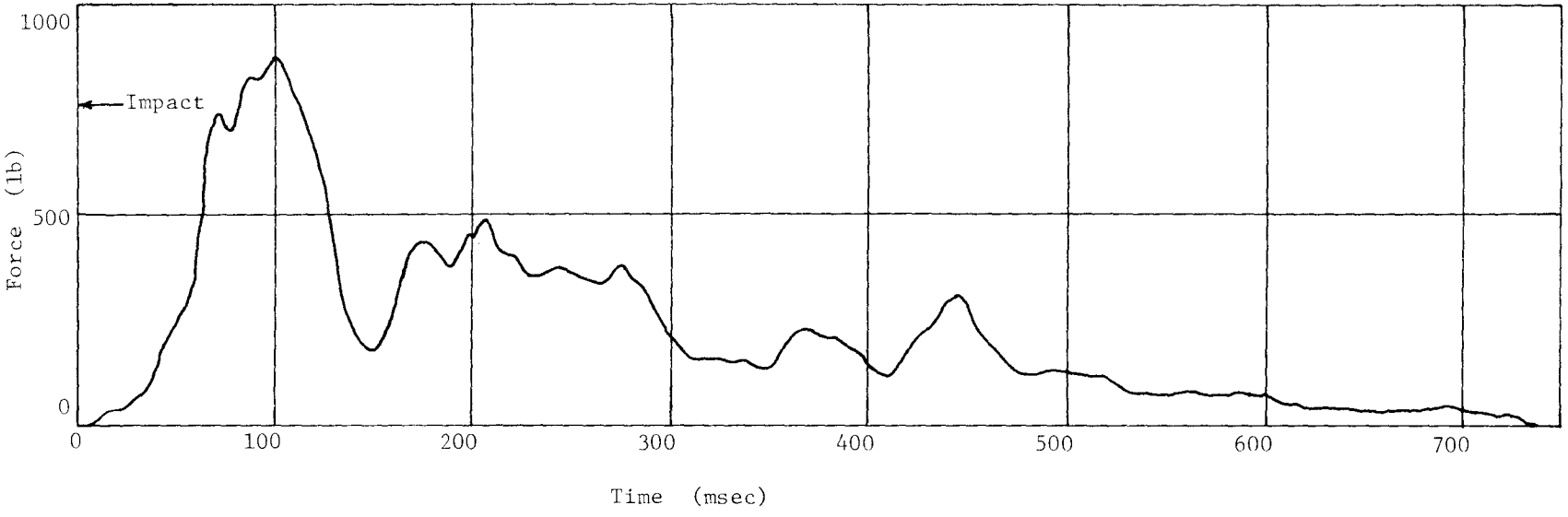

FIGURE A10. LAP BELT DATA, TEST CSP-3
(80 HZ LOW-PASS FILTER)

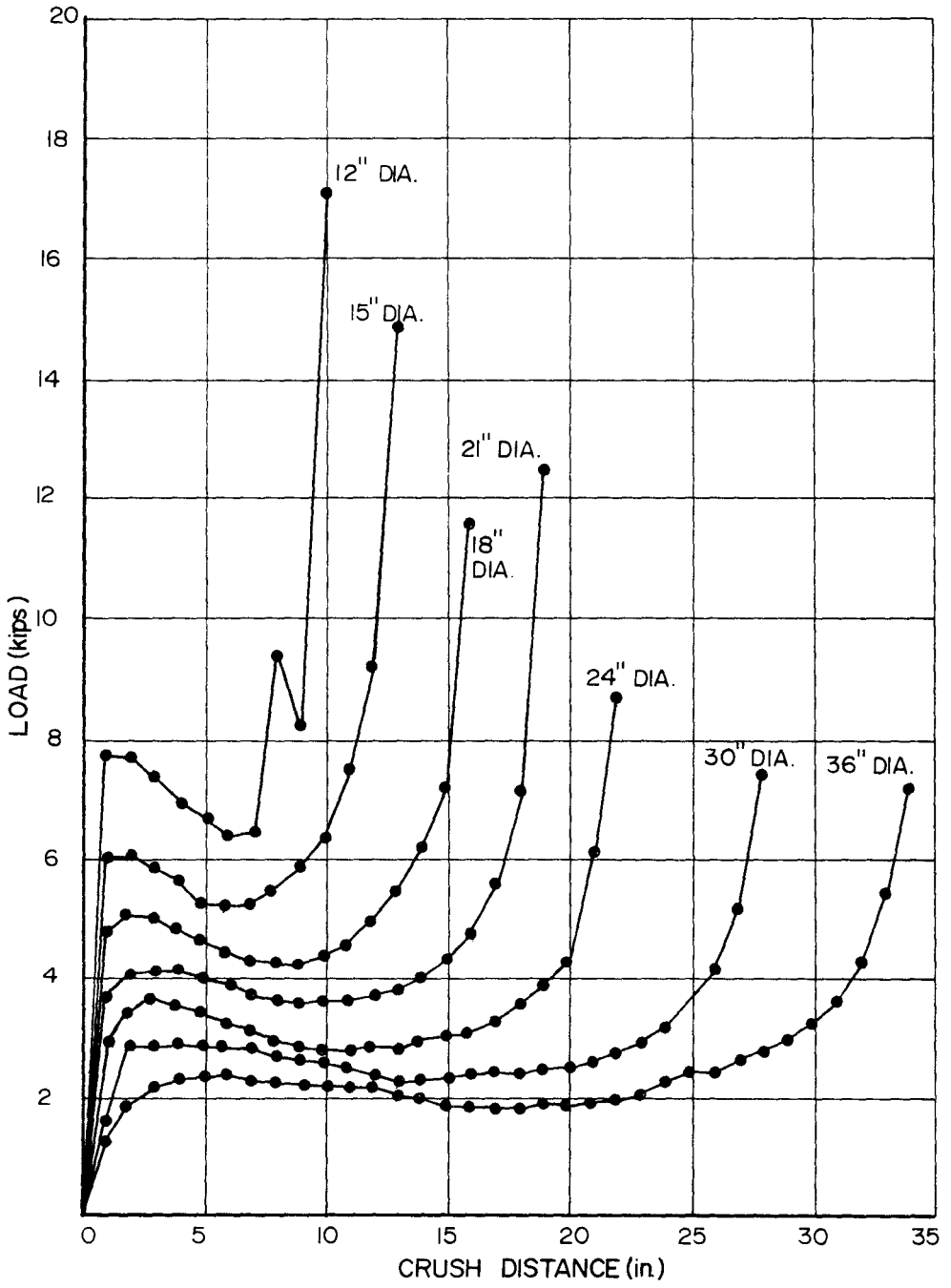

FIGURE A11. LOAD vs. CRUSH DISTANCE 16ga. CORRUGATED STEEL PIPE OF VARIOUS DIAMETERS & 25.5" lg.

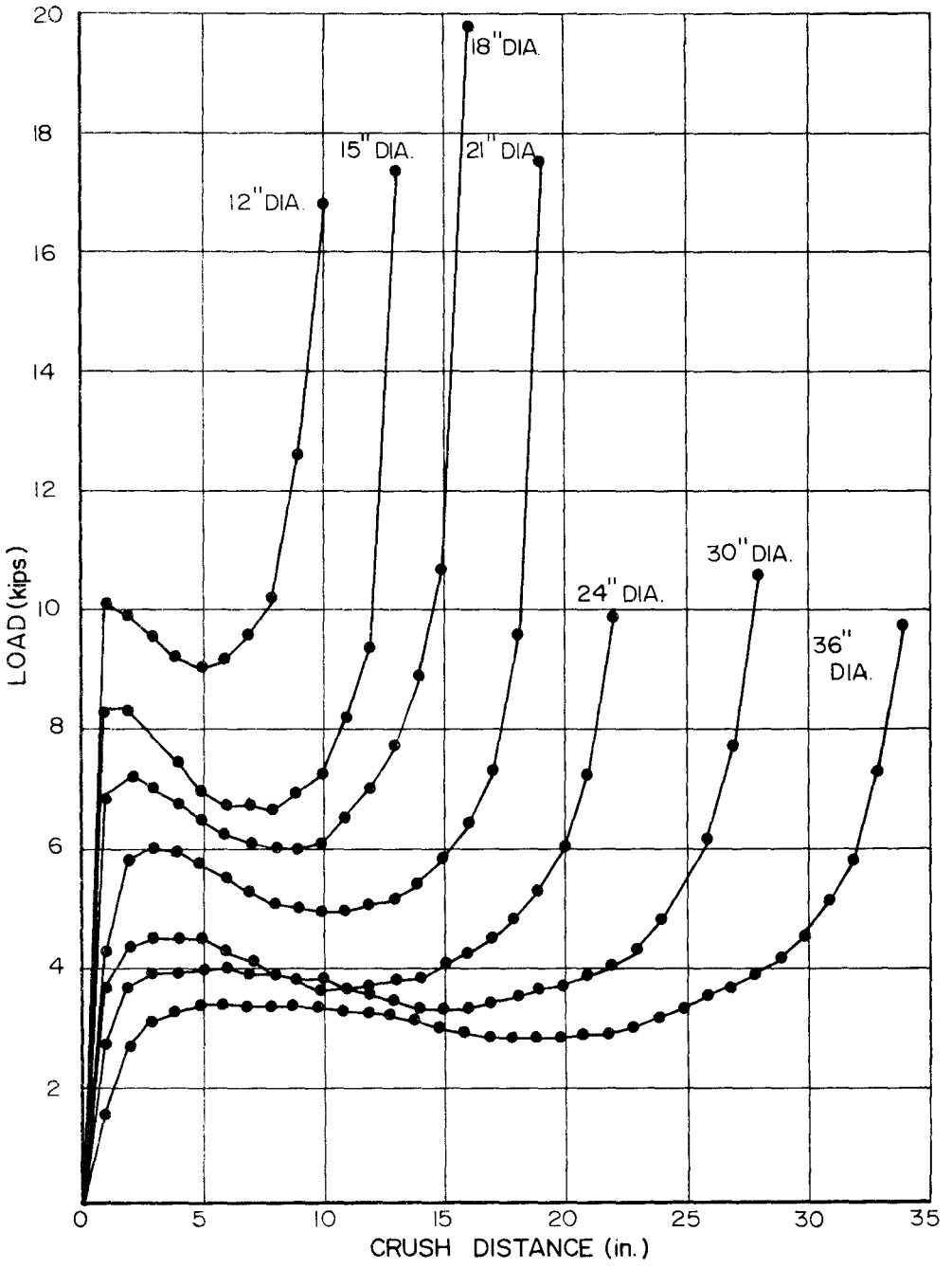

FIGURE A12. LOAD vs. CRUSH DISTANCE FOR 14ga. CORRUGATED STEEL PIPE OF VARIOUS DIAMETERS & 25.5" lg.

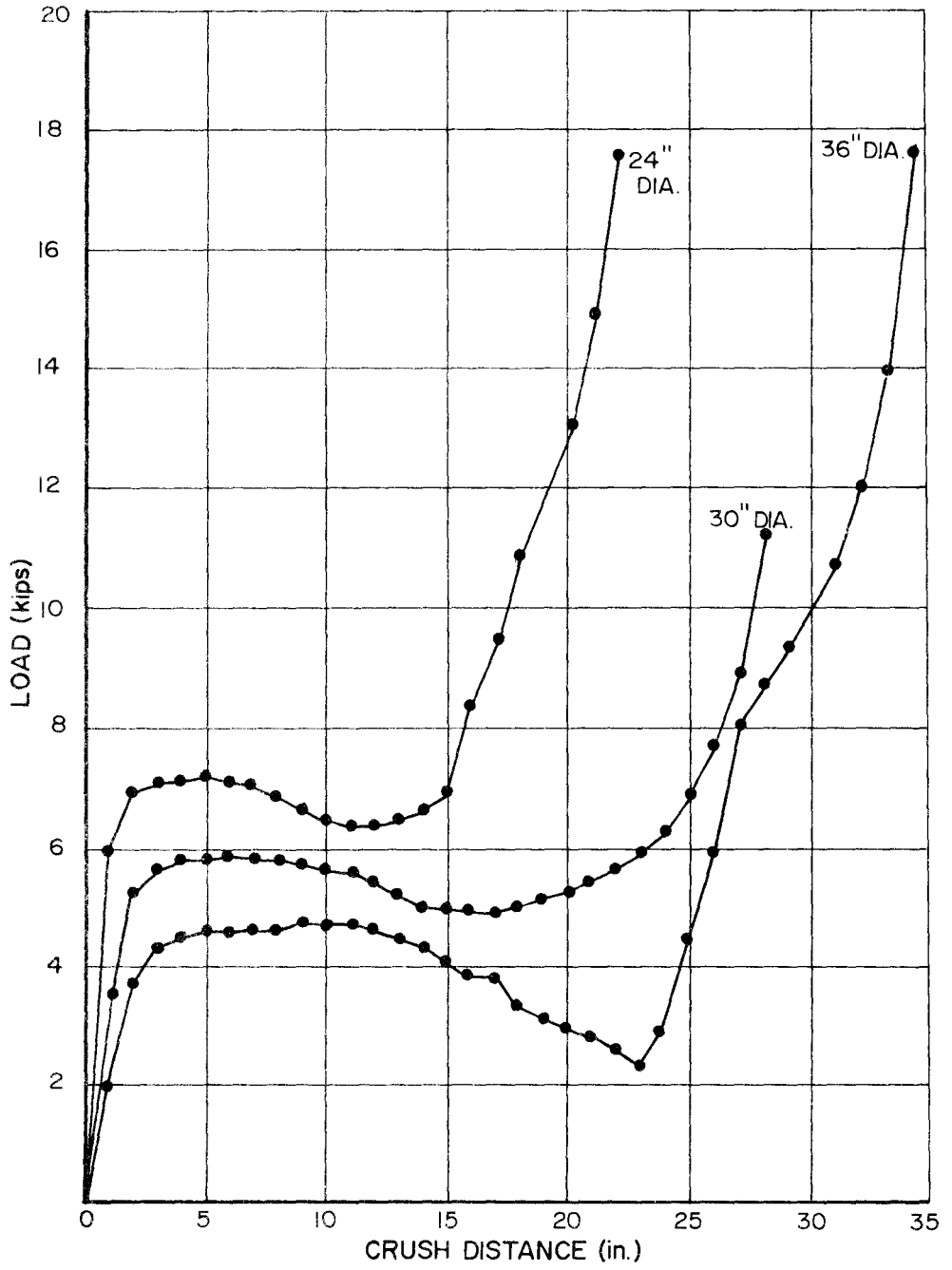

FIGURE A13. LOAD vs. CRUSH DISTANCE FOR 12ga. CORRUGATED STEEL PIPE OF VARIOUS DIAMETERS & 25.5" lg.

TABLE A1.

TEST 505 CSP-1

HIGH-SPEED FILM DATA

Time (milliseconds)		Displacement (feet)	
-52		-4.5	
-45		-3.8	
-37		-3.2	
-30		-2.5	
-22		-1.9	
-15		-1.2	
- 7		-0.6	
0	Impact	0	
7		0.6	
15		1.1	
22		1.7	
30		2.3	
37		2.9	
45		3.4	
52		3.9	
60		4.4	
67		4.9	
74		5.4	
82		5.8	
89		6.2	VEHICLE "RAMPS"
⋮		⋮	
1528		28.7	MAXIMUM FORWARD TRAVEL

TABLE A2.

TEST 505 CSP-2

HIGH-SPEED FILM DATA

Time (milliseconds)		Displacement (feet)	Time (milliseconds)	Displacement (feet)
-76		-6.6	(continued)	
-61		-5.3	168	12.8
-45		-4.0	184	13.8
-30		-2.7	199	14.7
-15		-1.3	224	16.2
0	Impact	0	250	17.7
15		1.3	275	19.3
31		2.6	301	21.0
46		3.9	326	22.6
61		5.2	352	24.3
76		6.4	377	26.0
92		7.6	403	27.7
107		8.7	428	29.3
122		9.8	454	31.0
138		10.9	479	32.7
153		11.9	505	34.3

TABLE A3.

TEST 505 CSP-3

HIGH-SPEED FILM DATA

Time (milliseconds)		Displacement (feet)	
-31		-2.8	
-23		-2.1	
-15		-1.4	
- 8		-0.7	
0	Impact	0	
8		0.7	
15		1.4	
23		2.0	
31		2.7	
39		3.3	
46		3.9	
54		4.5	
62		5.1	
70		5.7	
77		6.3	
85		6.9	
93		7.4	VEHICLE "RAMPS"
⋮		⋮	
1167		27.2	MAXIMUM FORWARD TRAVEL

TECHNICAL MEMORANDUM 505-19

Texas Transportation Institute
Texas A&M Research Foundation

FEASIBILITY STUDY OF VEHICLE CRASH CUSHIONS CONSTRUCTED OF READILY AVAILABLE MATERIALS

A Test And Evaluation Report On Contract No. CPR-11-5851

U.S. Department of Transportation
Federal Highway Administration

by

M. A. Pittman
Research Associate

and

T. J. Hirsch
Research Engineer

These crash tests and evaluations were conducted under the Office of Research and Development, Structural and Applied Mechanics Division's Research Program on Structural Systems in Support of Highway Safety (S Program).

July 1971

INTRODUCTION

During the latter part of 1967, four crash tests were conducted on impact attenuators which were predecessors to the present Modular Crash Cushion[1,2,5*]. Barrier configurations tested ranged from burlap bags filled with empty beverage cans to an arrangement of 55-gallon steel drums filled with empty beverage cans. One of the purposes of this study was to design crash cushions of readily available materials. These barriers were conceived by researchers at the Texas Transportation Institute (TTI) and were tested at the Texas A&M Research Annex in cooperation with the Federal Highway Administration. This report discussed the results of the four tests.

TEST DESCRIPTIONS

In the first test, 505-1A, the barrier consisted of 21 burlap bags filled with empty beverage cans and held together with poultry wire. The bags were arranged as shown in Figure 1. A 3500 lb Ford impacted the barrier head-on at a speed of 22 mph. The vehicle's front end rose off the ground during impact, but the vehicle remained stable. Average longitudinal deceleration was 3.9 g's, with a stopping distance of 6.3 ft. Vehicle damage was very minor, as shown in Figure 2. This test was conducted to investigate the feasibility of using waste metal beverage containers as an energy absorbing material for highway crash cushions. Since some of the burlap bags ruptured and allowed the cans to scatter, it was concluded that the beverage containers should be packaged in a stronger

---

*Superscript numbers refer to corresponding references at the end of this report.

FIGURE 1. BURLAP BAGS FILLED WITH EMPTY BEVERAGE CANS BEFORE TEST 505-1A.

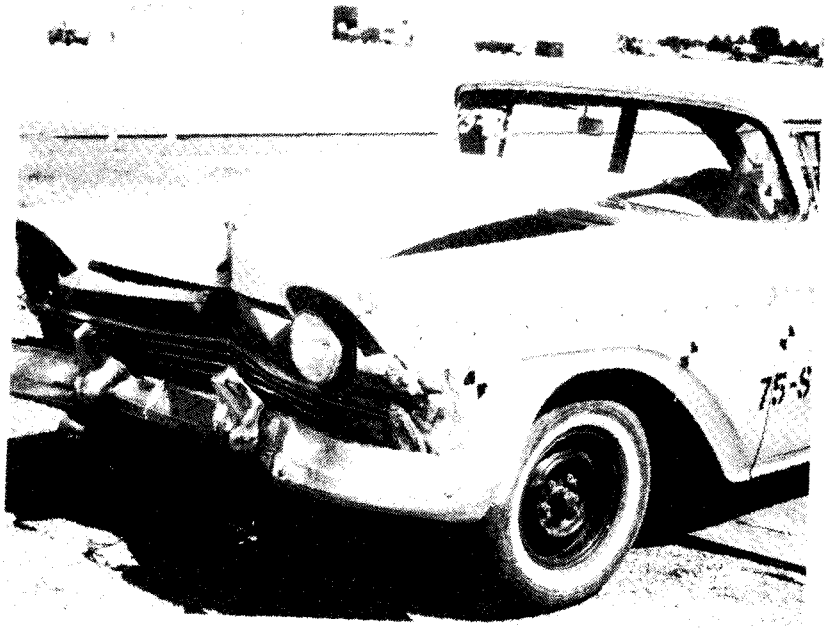

FIGURE 2. VEHICLE AFTER TEST 505-1A.

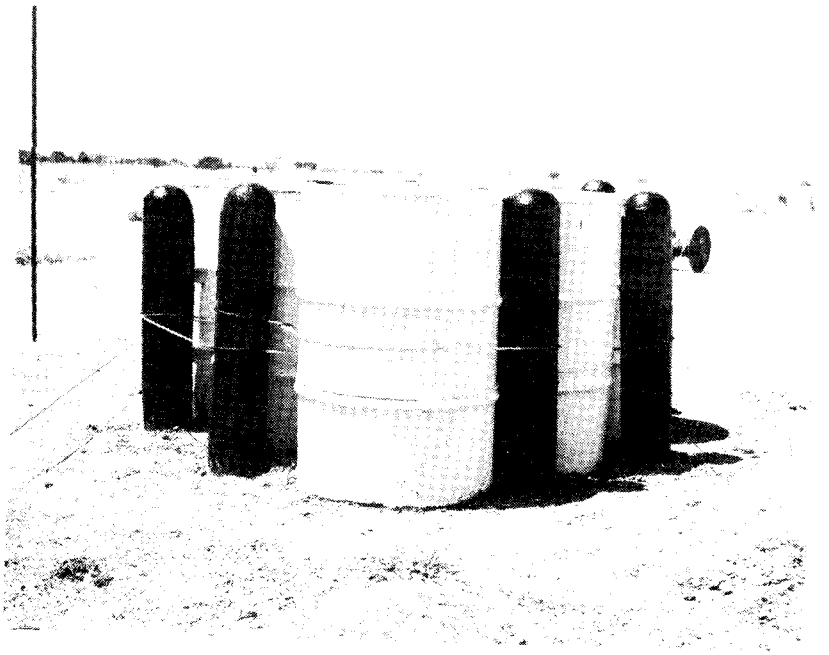

FIGURE 3. EIGHT 55-GALLON STEEL DRUMS FILLED WITH EMPTY BEVERAGE CANS AND ARRANGED BETWEEN TIMBER POSTS BEFORE TEST 505-1B.

FIGURE 4. BARRIER AND VEHICLE AFTER TEST 505-1B.

container so their behavior would be more predictable.

The next configuration tested (505-1B) is shown in Figure 3. Eight 55-gallon steel drums (16 gage steel) filled with empty beverage cans were arranged between seven 7-in. diameter timber posts. These posts were 5.5 ft in length and were embedded in 2.5 ft of soil. A 1/2-in. diameter steel cable was looped around the barrel system in an attempt to hold it together. The initial speed of the 3380 lb vehicle as it impacted the barrier was 63 mph. Shortly after the head-on impact, the vehicle was launched into the air by the timber posts. The vehicle was still moving at a speed of 8 mph after being launched. Thus its change in speed during impact was only 55 mph. The barrels and posts scattered, and the vehicle came to a stop on top of the barrier as shown in Figure 4. The vehicle was damaged considerably. Average longitudinal deceleration was 14.2 g's, with a peak of 40.0 g's. Since the barrels and post were scattered by the vehicle impact and this caused the vehicle to launch and become airborne, it was concluded that such a system should have a rigid backup support. It was felt that the rigid backup support would assure more predictable crushing of the energy absorbing material and provide more stability to the system.

In test 505-1C, fifteen 55-gallon, 16-gage steel drums filled with empty beverage cans were arranged 3 drums wide and 5 drums deep. The barrels were held together by a 1/2-in. diameter cable which was looped around and between them (see Figure 5). The steel drum system was placed against a rigid backup support wall. A 3520 lb Plymouth impacted the barrier head-on at a speed of 59 mph. During contact, the vehicle's front end became slightly airborne, and the barrel system was slightly lifted off the ground. The vehicle received severe damage. Both vehicle

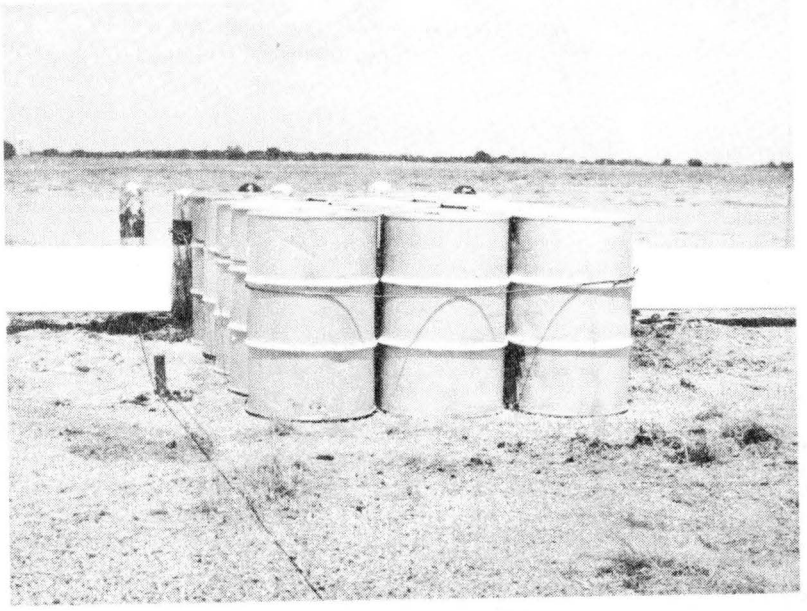

FIGURE 5. FIFTEEN 55-GALLON STEEL DRUMS FILLED WITH EMPTY BEVERAGE CANS BEFORE TEST 505-1C.

FIGURE 6. BARRIER AND VEHICLE AFTER TEST 505-1C.

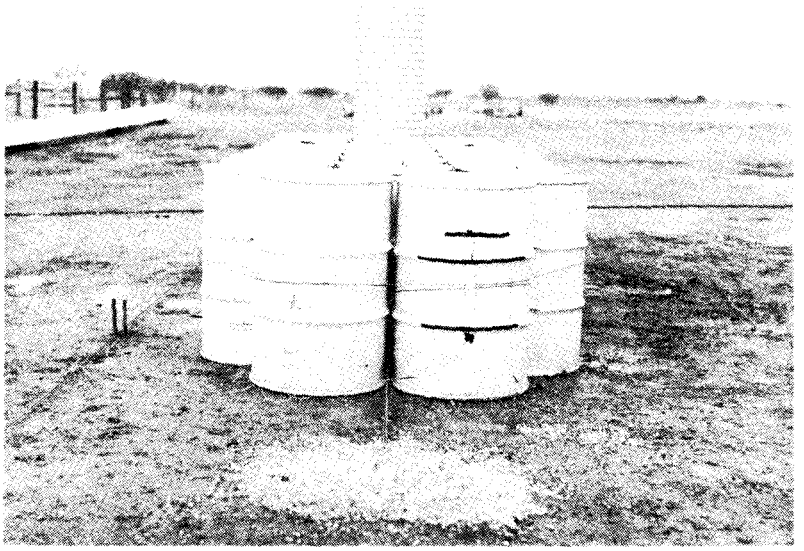

FIGURE 7. TWENTY-NINE 55-GALLON STEEL DRUMS FILLED WITH EMPTY BEVERAGE CANS BEFORE TEST 505-1D.

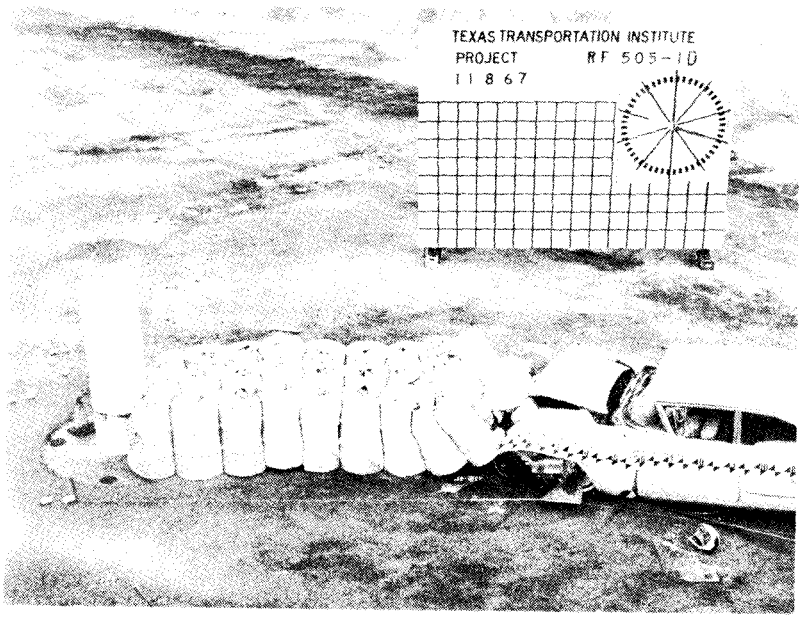

FIGURE 8. BARRIER AND VEHICLE AFTER TEST 505-1D.

and barrier are shown after the test in Figure 6. The average longitudinal deceleration was 14.2 g's over a distance of 7.1 ft. It was concluded that the 10 ft long barrier did not provide sufficient stopping distance. The length of the next barrier tested was increased to 20 ft.

The barrier for the next test (505-1D) consisted of twenty-nine 55-gallon, 16-gage steel drums filled with empty beverage cans placed in front of a simulated bridge pier as shown in Figure 7. There were nine rows, 3 drums wide, and the first row was 2 drums wide. The tops and bottoms of the barrels were welded together and a cable was looped around and threaded through the system. This cushion was hit head-on by a 4480 lb vehicle traveling 67 mph. The front end of the vehicle was lifted slightly off the ground, as were several rows of barrels. The vehicle was stopped after 10.4 ft of travel, with an average longitudinal deceleration of 16.7 g's. The vehicle sustained considerable damage, as shown in Figure 8.

SUMMARY

Table 1 contains a summary of the pertinent data obtained from these early tests. Tables 2 through 5 give the high-speed film data for tests 505-1A through 505-1D.

These four tests clearly indicated that the crushing strength of the barrels had to be decreased and the empty beverage cans removed in order to reduce the impact force levels encountered and to minimize vehicle damage. Static crush tests[1,3,4] were conducted on uncut, 18 and 20-gage, tighthead, 55-gallon steel drums with 4 elliptical holes cut in the top and bottom of the barrel. Results of these static tests indicated the importance of removing some of the metal from the top and bottom of each

drum in order to reduce the crushing strength of the barrel. The uncut barrels generated approximately 3 times as much stopping force as the barrels with the elliptical holes.

Results of full-scale crash tests conducted on modified barrel systems have been very favorable. These tests have been reported previously.[1,2,4,5]

TABLE 1

SUMMARY OF DATA

Factor	Test No.			
	1A	1B	1C	1D
Vehicle Weight, lb	3500	3380	3520	4480
Initial Speed, mph fps	22 33	63 92	59 86	67 98
Change in Speed, mph fps	22 33	55* 80	59 86	67 98
Average Long. Decel., g's ($\Delta V/\Delta Tg$)	3.9	14.2	14.2	16.7
Stopping Distance, ft	6.3	8.5+	7.1	10.4
Time in Contact, sec	0.265	0.177	0.188	0.182

*Vehicle was launched and became airborne while still moving at a speed of 8 mph.

TABLE 2

TEST 505-1A

HIGH-SPEED FILM DATA

Time (msec)		Displacement (ft)
-47		-1.53
-31		-1.02
-16		-0.51
0	Impact	0
16		0.51
31		1.02
47		1.53
78		2.48
109		3.40
140		4.27
172		5.04
203		5.71
234		6.16
265		6.34
296		6.34
328		6.20
484		5.64
640		5.16

TABLE 3

TEST 505-1B

HIGH-SPEED FILM DATA

Time (msec)		Displacement (ft)
-16		-1.50
-14		-1.25
-11		-1.00
- 8		-0.75
- 5		-0.50
- 3		-0.25
0	Impact	0
21		1.75
40		3.25
65		5.00
73		5.50
82		6.00
88		6.25
100		6.75
107		7.00
123		7.50
143		8.00
156		8.25
177		8.50

TABLE 4

TEST 505-1C

HIGH-SPEED FILM DATA

Time (msec)		Displacement (ft)
-44		-3.80
-33		-2.85
-22		-1.90
-11		-0.95
0	Impact	0
11		0.90
22		1.52
33		2.29
44		3.05
55		3.78
66		4.41
78		4.98
89		5.50
100		5.96
111		6.26
122		6.56
133		6.79
144		6.96
155		6.98
166		7.04
177		7.08
188		7.08

TABLE 5

TEST 505-1D

HIGH-SPEED FILM DATA

Time (msec)		Displacement (ft)	Time (msec)	Displacement (ft)
-36		-3.55	(Continued)	
-29		-2.84	87	7.10
-22		-2.13	95	7.53
-15		-1.42	102	7.90
- 7		-0.71	109	8.24
0	Impact	0	116	8.56
7		0.69	124	8.87
15		1.38	131	9.11
22		2.03	138	9.34
29		2.68	146	9.56
36		3.31	153	9.77
44		3.92	160	9.98
51		4.53	167	10.17
58		5.09	175	10.33
66		5.62	182	10.43
73		6.14	189	10.43
80		6.65		

REFERENCES

1. Hirsch, T. J., "Barrel Protective Barrier," Technical Memorandum 505-1, FHWA Contract No. CPR-11-5851, Texas Transportation Institute, Texas A&M Research Foundation, July 1968.

2. Hirsch, T. J., Hayes, Gordon G., and Ivey, Don L., "The Modular Crash Cushion," Technical Memorandum 505-1S, FHWA Contract No. CPR-11-5851, Texas Transportation Institute, Texas A&M Research Foundation, August 1970.

3. White, Monroe C., "The Modular Crash Cushion: Design Data From Static Crush Tests of Steel Drums and of Corrugated Steel Pipes," Technical Memorandum 505-17, FHWA Contract No. CPR-11-5851, Texas Transportation Institute, Texas A&M Research Foundation, April 1971.

4. Hirsch, T. J., and Ivey, Don L., "Vehicle Impact Attenuation by Modular Crash Cushion," Research Report No. 146-1, Texas Highway Dept. HPR Study 2-8-68-146, Texas Transportation Institute, June 1969.

5. Hayes, G. G., Ivey, D. L., Hirsch, T. J., and Viner, J. G., "A Hybrid Barrier for Use at Bridge Piers and Medians," Technical Memorandum 505-15, FHWA Contract No. CPR-11-5851, Texas Transportation Institute, Texas A&M Research Foundation, May 1971.

TECHNICAL MEMORANDUM 505-20

Texas Transportation Institute
Texas A&M Research Foundation

FEASIBILITY OF SNAGGING A VEHICLE WITH HOOK AND CABLE SYSTEM

A Test and Evaluation Report on Contract No. CPR-11-5851

U.S. Department of Transportation
Federal Highway Administration

by

T. J. Hirsch
Research Engineer

and

John G. Viner
Structures and Applied Mechanics Division
Federal Highway Administration

The opinions, findings and conclusions expressed in this report are those of the authors and not necessarily those of the Federal Highway Administration.

These crash tests and evaluations were conducted under the Office of Research and Development, Structural and Applied Mechanics Division's Research Program on Structural Systems in Support of Highway Safety (4S Program).

May 1971

DESCRIPTION OF TESTS

In December of 1967 two tests were conducted to determine if it was feasible to stop a vehicle using a hook and cable system.[1] A steel hook (fabricated from 1.5 in. thick steel plate--see Figures 1 and 2) was welded to the frame of a 1958 Plymouth sedan (see Figure 4). Each end of a 7/8 in. diameter 6 x 19 wire rope 50 ft. long was attached to a Van Zelm Metal Bender (25,000 lb. capacity).[2] The metal benders were attached to steel anchor posts 12 ft. apart as shown in Figures 3 and 4.

The first test was conducted with the vehicle traveling 60 mph and at an angle of 5° from a normal to a line between the anchorage points. The vehicle passed over the cable without snagging it (a clean miss). This happened despite the fact that the steel hook had a ground clearance of only 2.5 in.

For the second test the hook was modified as shown in Figure 1 reducing the hook ground clearance to 1.5 in. The cable was placed in a lazy W position as shown in Figure 3 and blocked up at the center approximately 5 in. off the ground so the vehicle hook could engage it. This configuration was found necessary to prevent the front wheels of the vehicle from depressing the cable to the ground where the vehicle hook could not engage it.

---

1. Magyar, N., "Vehicle Arresting System," Conceptual Studies, Program-Phase "A", Martin Marietta Corp., Baltimore, Maryland, FHWA Contract FH-11-6621, Volume II, September, 1968.

2. Hirsch, T. J., Hayes, G. G., and Ivey, D. L., "Dragnet Vehicle Arresting System," Texas Transportation Institute, February 28, 1969, Technical Memorandum 505-4.

Since the cable was attached to two 25,000 lb. metal benders, the maximum possible stopping force could reach 50,000 lb. Consequently, the frame of the vehicle was reinforced with 3/16 in. thick steel plates in an attempt to strengthen the point where the steel hook was attached (Figures 1 and 6). Previous analysis indicated there was no single point on the vehicle frame capable of resisting forces of 50,000 lb.[1]

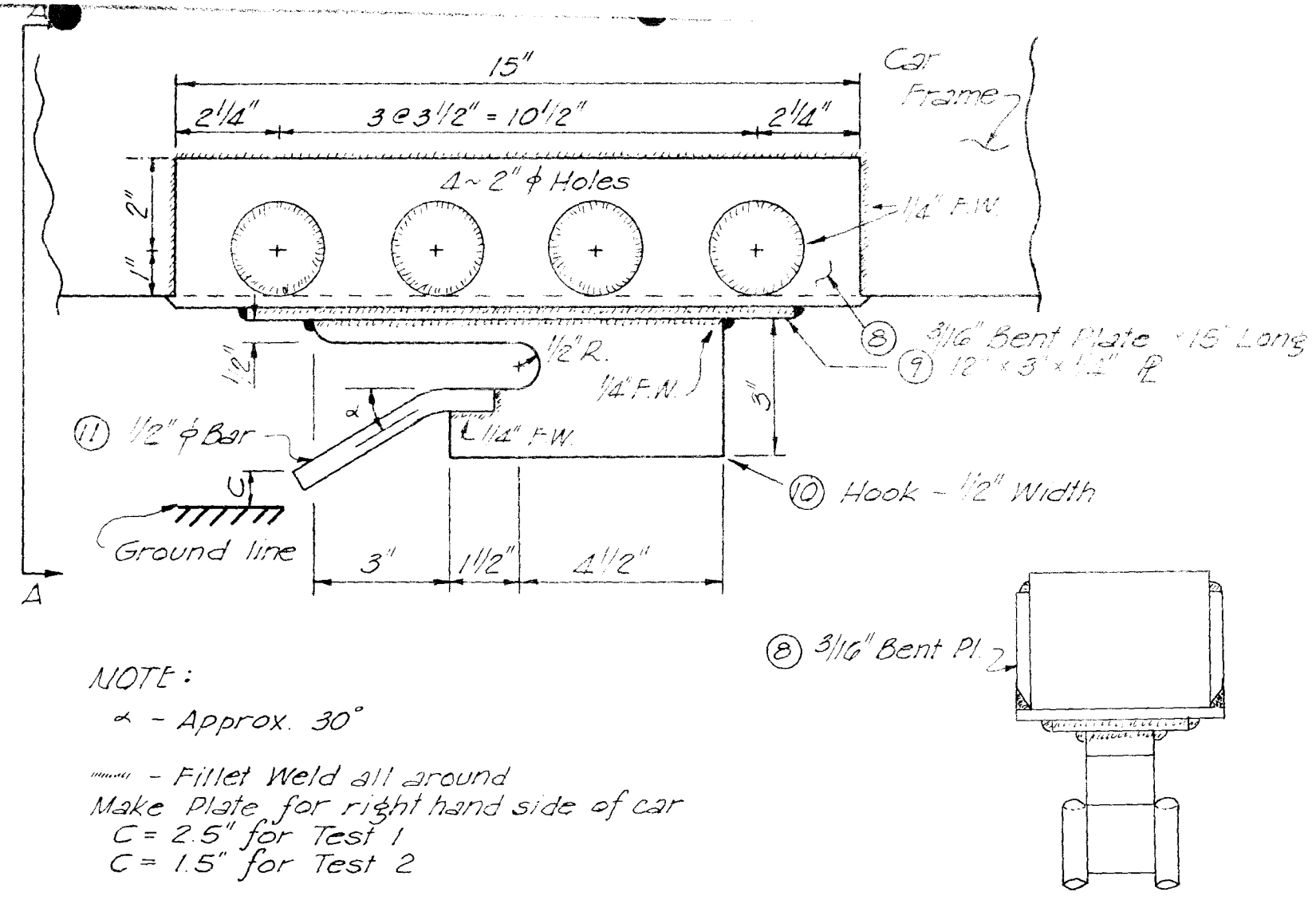

NOTE:

α - Approx. 30°

⌇⌇⌇⌇ - Fillet Weld all around

Make Plate for right hand side of car

C = 2.5" for Test 1

C = 1.5" for Test 2

SECTION A-A

FIGURE 1. HOOK DETAILS

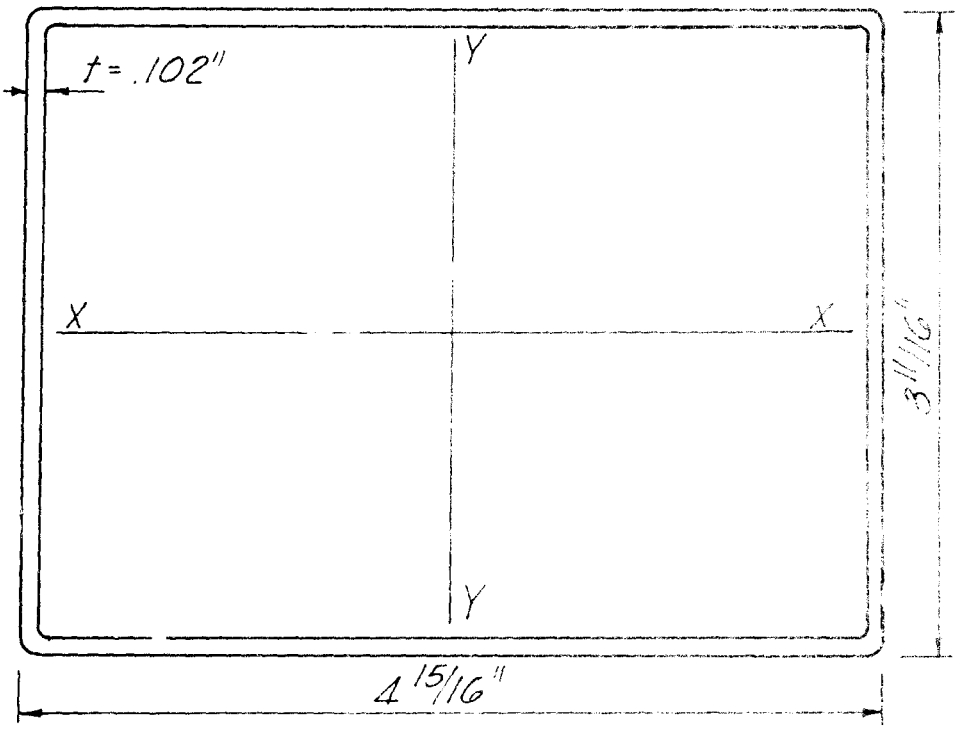

'58 PLYMOUTH FRAME PROPERTIES
(TEST VEHICLE 505-3A 12-6-67)

$I_{x-x} = 2[(4.84)(.102)(1.78)^2 + 1/12(.102)(3.59)^3]$
$= 2[1.56 + 0.39] = 3.90\ in.^4$
$I_{y-y} = 2[(3.59)(.102)(2.42)^2 + 1/12(.102)(4.84)^3]$
$= 2[2.12 + 0.97] = 6.18\ in.^4$
$A = (2)(1.02)(4.84 + 3.59) = 1.72\ in.^2$ Weight 3600 lbs

'67 FORD PROPERTIES
$I_{x-x} = 2.3\ in.^4$ $I_{y-y} = 0.94\ in.^4$ $A = 0.87\ in.^2$ Wt 3800 lbs.

$I_{x-x} = 0.59$
$I_{y-y} = 0.15$
$A = 0.50$
$Wt. = 1.05$

RATIO OF '67 FORD TO '58 PLYMOUTH PROPERTIES

FIGURE 2 - FRAME PROPERTIES OF '58 PLYMOUTH

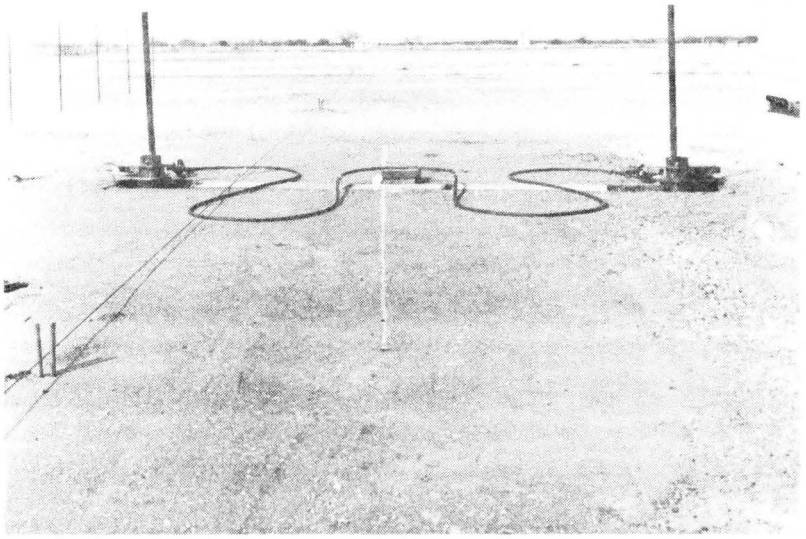

Figure 3: Snag Cable and Metal Benders before Test.
7/8 in. diameter cable 50 ft. long blocked up approximately 5 in. off ground. Metal benders 12 ft. apart.

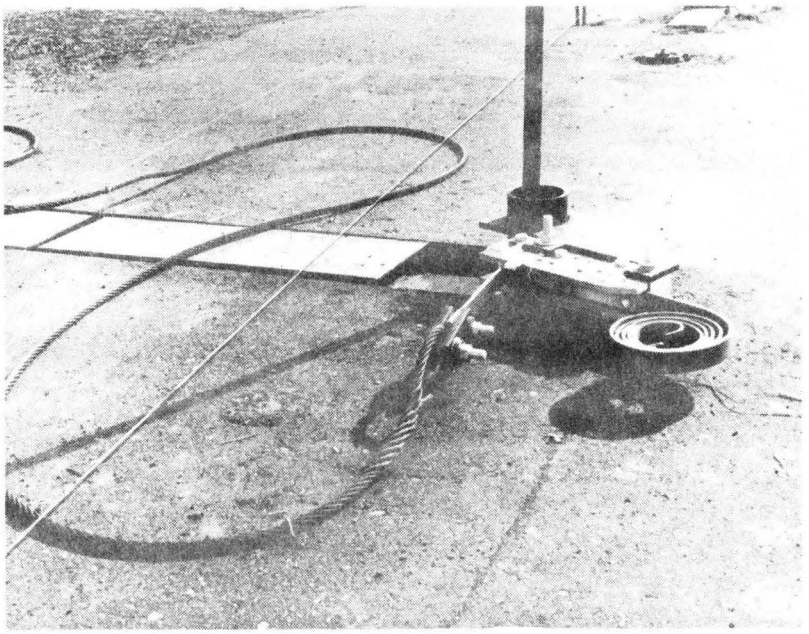

Figure 4: Metal bender with 25,000 lb. metal tape to supply stopping force.

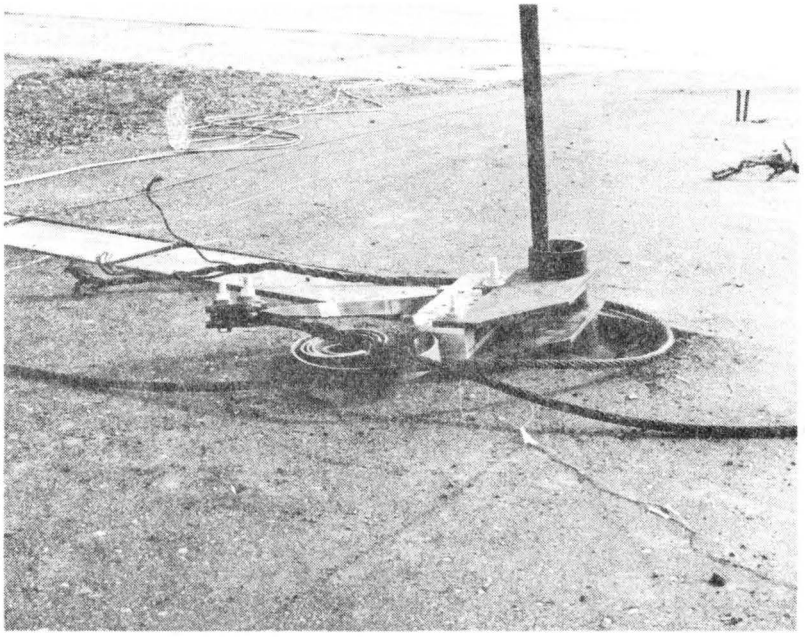

Figure 5: Metal bender and broken cable after test.

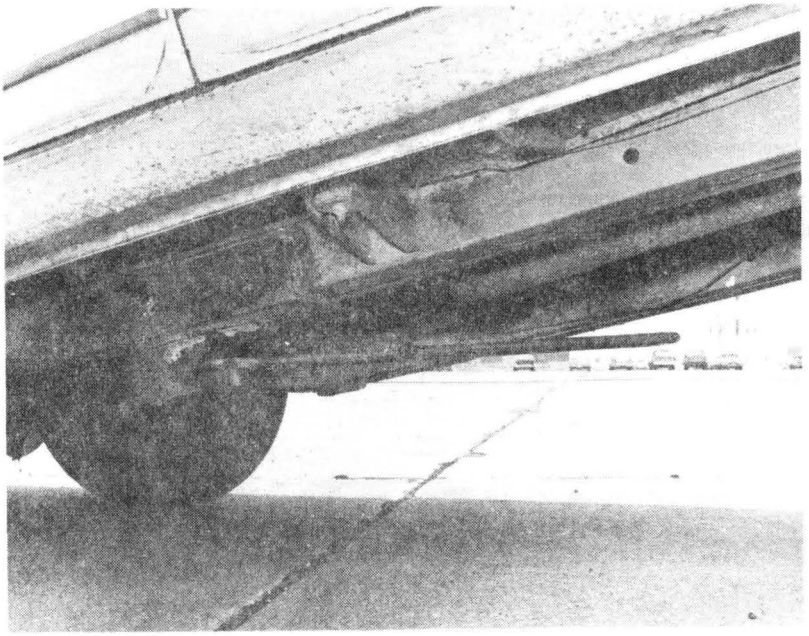

Figure 6 : Snag hook welded to frame of vehicle. Photo taken after test. Vehicle frame bent and several weld fractured.

-.306 sec.

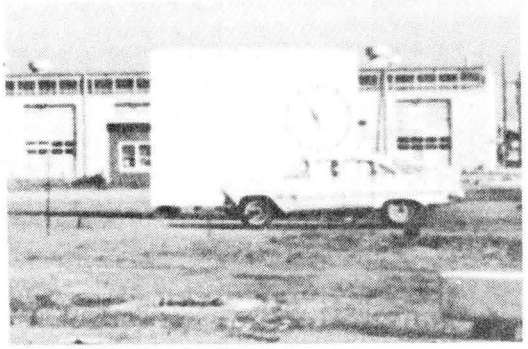

-.020 sec.

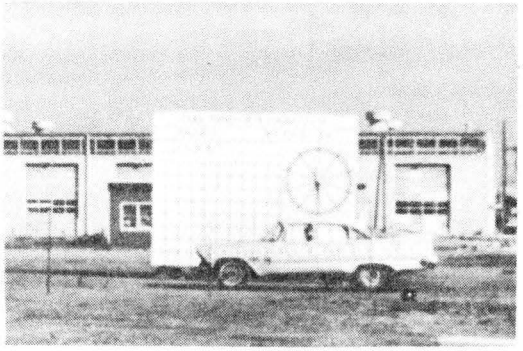

snag .000 sec.

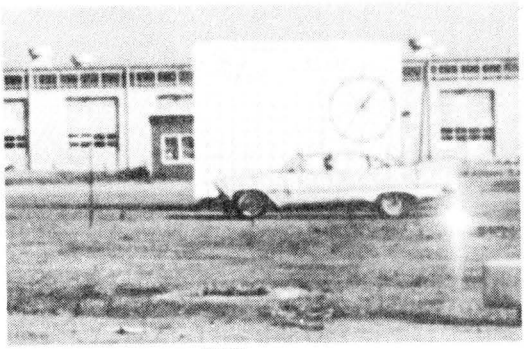

.020 sec.

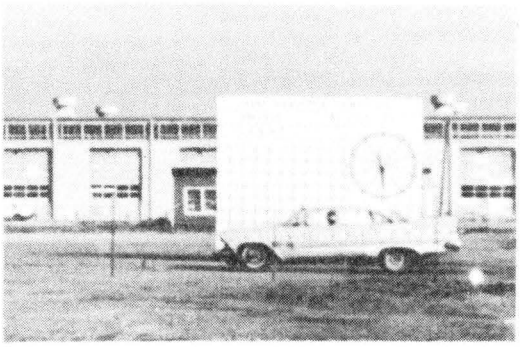

.035 sec.

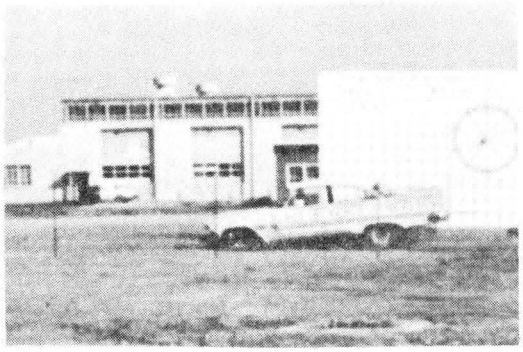

.144 sec.

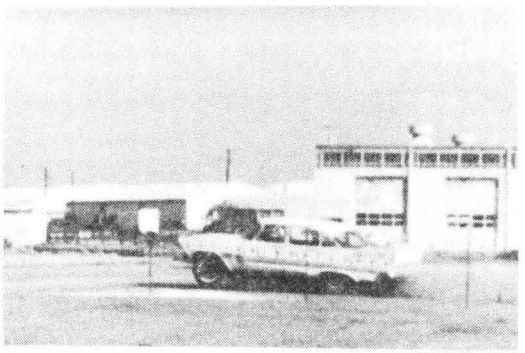

.418 sec.

Figure 7: Sequential Photographs of Test 505-3B.

TEST RESULTS (Second Test)

Figure 7 presents sequential photographs of the vehicle during the test. The 3600 lb. vehicle engaged the cable while traveling at a speed of 57.3 mph at an angle of about 5° from the normal of a line between the two anchorages. The initial engagement occurred at -.286 sec. At 0 sec. (Figure 7 snag) the cable became taut and began exerting the stopping force. At 0.061 sec. the cable broke after slowing the vehicle to 48.8 mph over 4.86 ft. of travel. The average longitudinal deceleration imposed on the vehicle was approximately 6.3 g's as indicated by the data presented in Table 1.

Table 1. Data From Film Analysis
Test 505-3B (Second Test)

Vehicle Weight	3600 lb.
Initial Speed, V_i	57.3 mph (84.1 fps)
Final Speed, F_f (immediately after cable broke)	48.8 mph (71.6 fps)
Time in Contact (T)	0.061 sec.
Distance Vehicle Traveled (S) in contact with cable	4.86 ft.

Average Longitudinal Deceleration

$$\frac{V_i^2 - V_f^2}{2gS} = 6.2 \text{ g's}$$

$$\frac{V_i - V_f}{gT} = 6.4 \text{ g's}$$

Approximately 13.5 in. of tape was pulled out of each metal bender accounting for approximately 56,000 ft.-lb. of energy consumed by the metal benders. The total vehicle kinetic energy was 395,000 ft.-lb. thus only about 15% of the vehicle kinetic energy was consumed by the metal benders.

The cable apparently broke because of the sharp bend it made around the vehicle snagging hook.

The frame of the vehicle was displaced about 2.5 in. relative to the car body during the test. In the three attachment points of the car body to frame forward of the snag hook, the frame was found to be torn on the tension side of the bracket. In the attachment to the rear of the snag hook the attachment bolt was on the verge of pulling loose from the car body. It appeared that the car frame was on the verge of being torn from the car body when the cable failed.

Knowing the tape capacity of the metal benders to be 25,000 lb., a simple analysis indicates the maximum deceleration imposed on the vehicle to be approximately 13.5 g's.

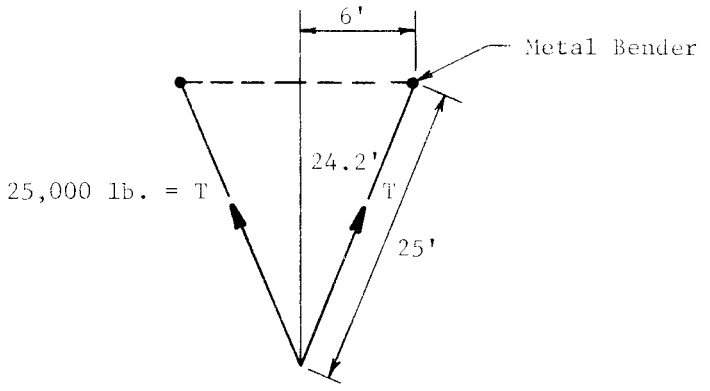

$$\text{Maximum Stopping Force} = 2 \times 25{,}000 \left(\frac{24.2}{25}\right)$$

$$= 48{,}400 \text{ lb.}$$

$$\text{Maximum Deceleration} = \frac{F}{W} = \frac{48{,}400}{3{,}600}$$

$$= 13.5 \text{ g's (computed)}$$

The difference between the computed maximum deceleration of 13.5 g's and the average deceleration of approximately 6.3 g's (determined from film analysis) can be attributed to several things as follows:

1. The vehicle engaged the cable at an angle of about 5°, thus one end of the cable became taut before the other,
2. The 50 ft. length of cable stretched as the force was applied,
3. In analysis of the high speed movie film, it was difficult to determine precisely the time and distance of engagement when the cable broke completely and released the vehicle.

CONCLUSIONS

Analytical studies made forthe Federal Highway Administration by Martin Marietta Corporation [1] indicated that no single point on a standard weight passenger car (1967) is capable of resisting forces of approximately twelve times the weight of the vehicle (12 g's). The experience gained from the full scale test report here support this conclusion.

It is clear that even if substantial lower deceleration forces are used that many practical engineering problems must be resolved before this concept could be employed to stop or arrest errant vehicles leaving the highway.[1] Some of these problems are as follows:

1. Attachment of snagging hook to vehicle needs careful study for strength and desirable location.
2. Cable location and configuration needs careful study.
3. A positive engaging system needs to be developed.
4. Capacity and location of metal bender (or other energy absorber) needs careful study.